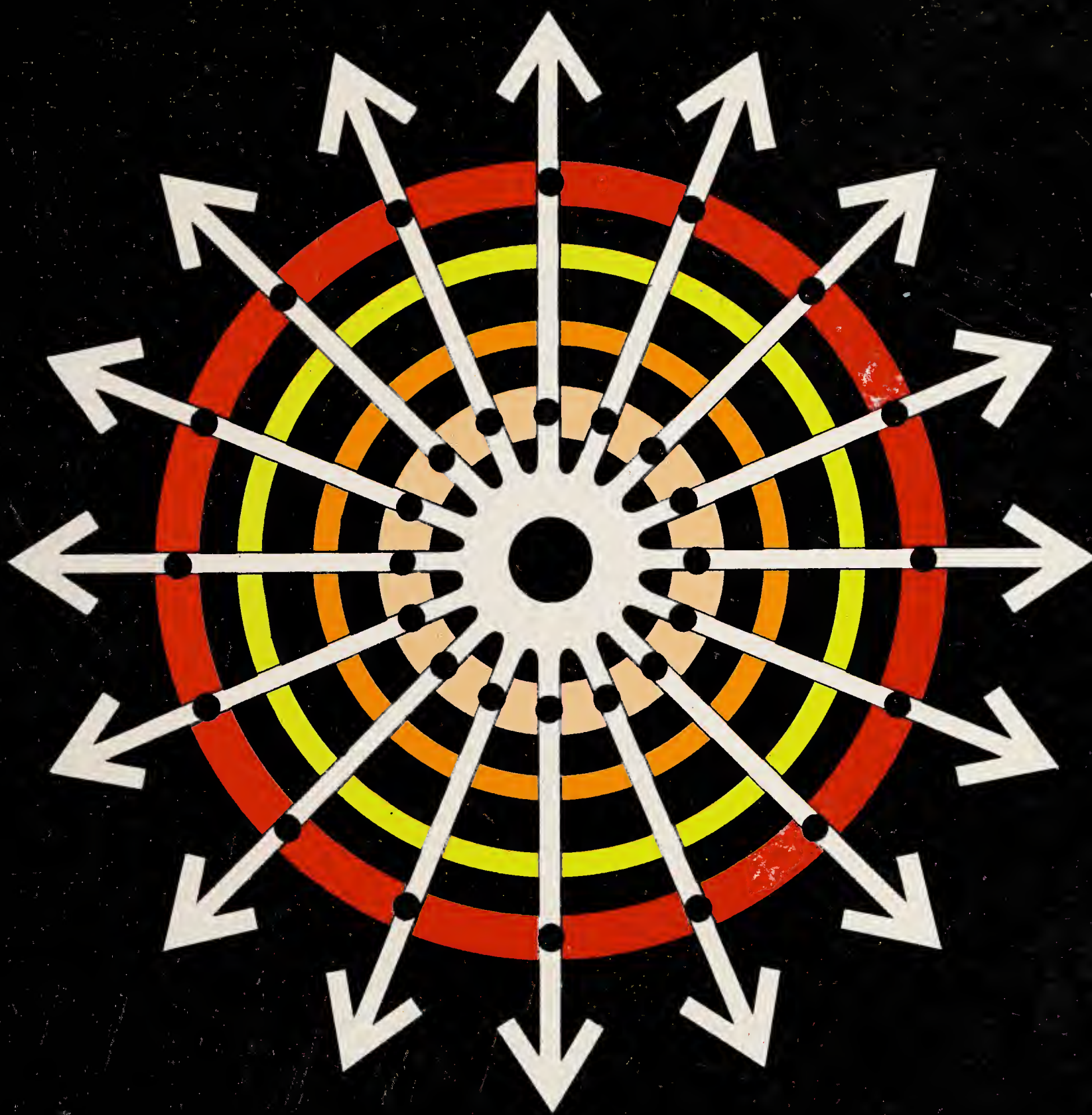


# LASER SPECTROSCOPY AND OTHER TOPICS



G. W. SERIES



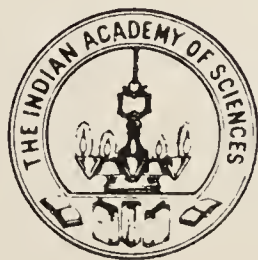
Digitized by the Internet Archive  
in 2018 with funding from  
Public.Resource.Org

<https://archive.org/details/laserspectroscop00unse>



# Laser Spectroscopy and other topics

Selected Papers  
of  
G. W. Series  
Raman Professor, 1982-83



INDIAN ACADEMY OF SCIENCES  
BANGALORE 560 080  
1985

© 1985 INDIAN ACADEMY OF SCIENCES, BANGALORE

The copyright of individual papers rests with the original publishers viz., Royal Society, London; W. H. Freeman and Co., California; The Institute of Physics and Physical Society, London; Academic Press, New York; Taylor & Francis, London; The American Physical Society, New York; North-Holland, Amsterdam; Plenum, New York; Gordon and Breach, New York; Springer-Verlag, Berlin.



## FOREWORD

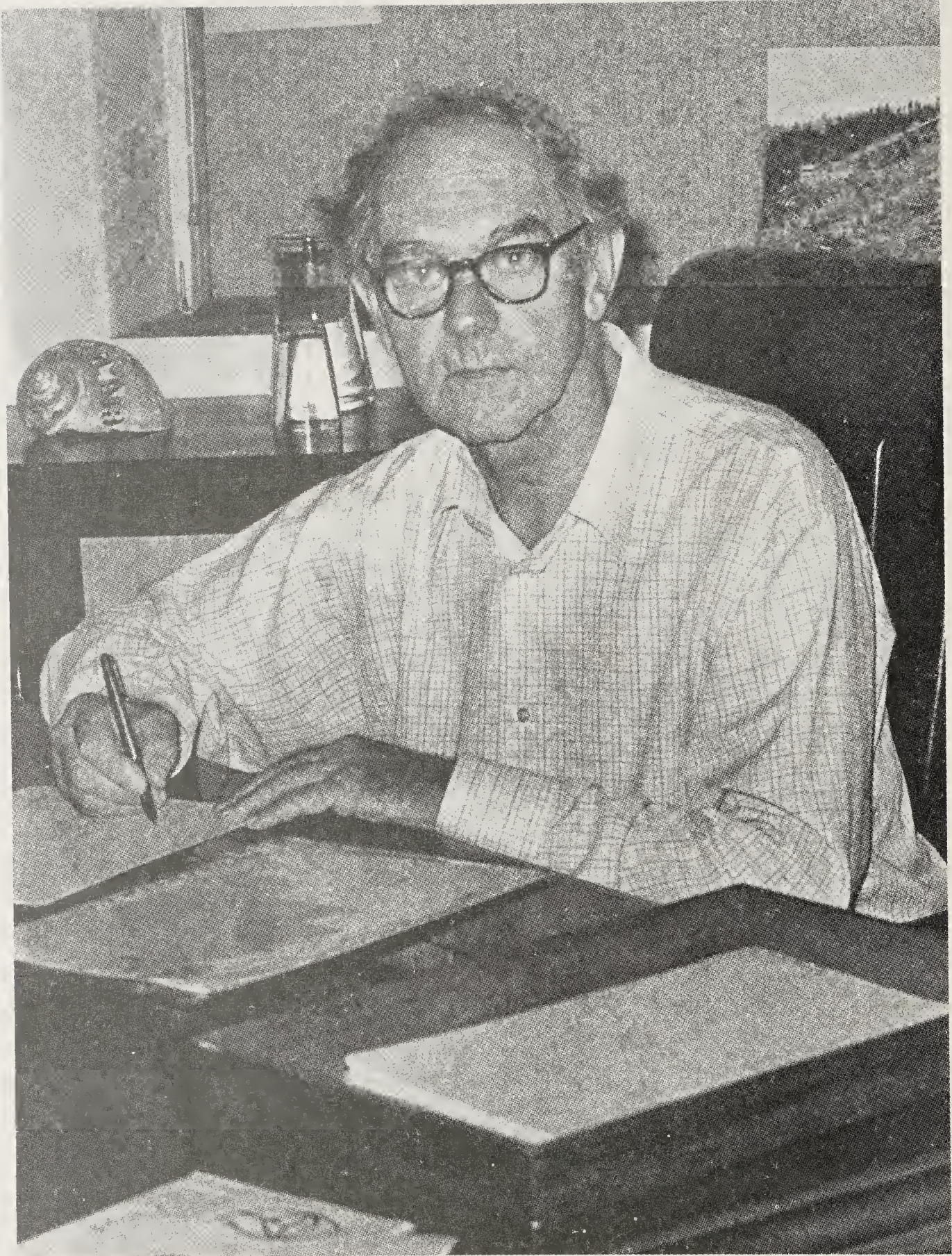
Prof. G. W. Series through his work has influenced greatly, the growth of spectroscopy over the last two to three decades. A pioneer in the field of quantum beat spectroscopy, his optical measurement of the Lamb Shift and the hyperfine structure in atomic hydrogen and his precise determination of one of the most basic constants of physics — the Rydberg Constant — have made him a recognized authority in this field. Anyone who reads his delightful monograph on “The Spectrum of Atomic Hydrogen” will realise what a remarkable teacher he is, and how elegantly he relates the successive formulations of the quantum theory with experimental studies on the simplest of atoms.

Prof. Series visited India as the Raman Professor of the Indian Academy of Sciences (along with his wife Annette) during the winter of 1982. He travelled around India visiting laboratories and lecturing and luring many young scientists into the delights of spectroscopy. This visit deepened and widened the close connections which he already had with many Indian scientists. It is with great pleasure that we bring out this volume of the selected papers of Prof. Series (together with some of the lectures he delivered in India). These illustrate most clearly the major theme of his classic research work, the interaction of radiation with atoms.

We thank the original publishers of these papers and articles for permitting us to reproduce them.

S. Ramaseshan  
President  
Indian Academy of Sciences





Prof. G. W. Series



## BIOGRAPHICAL SKETCH

Prof. G. W. Series, whose selected papers have been reprinted in this volume, was born on 22 February 1920 and received his B.A., M.A. and D. Phil degrees from Oxford University where he worked from 1938 to 1968, with a break of six years during the second world war. His thesis on a classic problem of atomic physics — the spectrum of the hydrogen atom — gave an optical determination of the newly discovered Lamb shift. This work led to a continuing interest in the fundamental atomic constants and in high resolution techniques. In this connection, he was attracted by the Brossel-Bitter experiment in which radio frequency resonance in an excited state was monitored via changes in fluorescent optical radiation, thereby measuring structure far finer than the Doppler width which would have limited a purely optical method. After applying this technique to an excited state of potassium, Prof. Series pioneered the study of light beats in which the coherence between the amplitudes of different Zeeman components (for example) shows itself in modulation of the emitted intensity. In a three-level system, such coherence is naturally expressed in terms of the alignment tensor of which he and his collaborators made a thorough study. Studies of fluorescence with intensity and polarisation-modulated light followed. An important extension of these ideas was the inclusion of propagation effects, i.e. the space varying phase of the optical field. This was achieved by generalising the classical theory of dispersion to include the time-varying alignment of the atoms undergoing resonance.

Prof. Series has proposed and tested the concept of reducing the width of a spectral line by selecting those atoms which ‘live’ longer than the average. After moving to the University of Reading in 1968 he has been interested in the phenomenon of spontaneous emission, and in particular whether the Feynman-Wheeler absorber picture could be applied to provide an alternative to the conventional theory based on vacuum fluctuations. More recent work includes optogalvanic effects and nonlinear spectroscopy with lasers.

The many honours which Prof. Series has received include the Fellowship of the Royal Society (1971) and the Meggers Award and Medal of the Optical Society of America (1982). He visited India in 1982-83 as the Raman Professor of the Indian Academy of Sciences. Audiences all over the country had the benefit of his deep insight into atoms, radiation, and what happens when they meet. His lectures were animated by a strong personal touch. Difficulties, subtleties, and even false trails were clearly brought out and his debt to peers and colleagues generously acknowledged.

The papers assembled in this volume speak for themselves but a few general remarks on their overall significance may not be out of place. According to conventional views at least, atoms and their interaction with radiation are described by quantum mechanics and quantum electrodynamics. However, this bald statement does not by itself bring out the varied phenomena and novel experimental possibilities latent in the subject. The strength and value of this collection lies in the unique record it gives of the growth of this rich field, as seen by one of its founders. The serious student of these papers will see the interplay of theory and experiment, each reinforcing the other. He will realise the value of physical pictures and intermediate, approximate levels of description such as semiclassical radiation theory and

classical dispersion theory, which have played such a crucial role in our understanding of the interaction between matter and light.

Rajaram Nityananda  
Raman Research Institute  
Bangalore



## LIST OF PAPERS REPRODUCED

	<i>Page</i>
<i>I. The Spectrum of Atomic Hydrogen</i>	
1. The fine structure of the hydrogen $\alpha$ line. H. Kuhn and G. W. Series. 1950. <i>Proc. R. Soc. (London)</i> . <b>A202</b> , 127-142.	1
2. The fine structure of the line 4686 Å of singly ionized helium. G. W. Series. 1954. <i>Proc. R. Soc. (London)</i> . <b>A226</b> , 377-392.	19
3. The spectrum of atomic hydrogen. T. W. Hänsch, A. L. Schawlow and G. W. Series. 1979. <i>Sci. Am.</i> <b>240</b> , 94-110.	35
4. Atomic hydrogen and fundamental physical constants. G. W. Series and D. N. Stacey. 1982. <i>Eur. J. Phys.</i> <b>3</b> , 129-135.	51
<i>II. Double Resonance, Level-Crossing and Optical Pumping.</i>	
5. Double resonance measurements of hyperfine structures in potassium. G. J. Ritter and G. W. Series. 1957. <i>Proc. R. Soc. (London)</i> . <b>A238</b> , 473-488.	59
6. Radio-frequency spectroscopy of excited atoms. G. W. Series. 1959. <i>Rep. Progr. Phys.</i> <b>22</b> , 280-328.	75
7. Optical pumping and related topics. G. W. Series. 1979. <i>In Quantum optics</i> . Proc. Tenth Session of Scottish Universities Summer School. (Eds) S.M. Kay and A. Maitland (New York: Academic Press). pp 395-482.	125
8. Thirty years of optical pumping. G. W. Series. 1981. <i>Contemp. Phys.</i> <b>22</b> , 487-509.	213
<i>III. Coherence Spectroscopy and Radiative Interactions</i>	
9. Light beats as indicators of structure in atomic energy levels. J. N. Dodd, W. N. Fox, G. W. Series and M. J. Taylor. 1959. <i>Proc. Phys. Soc.</i> <b>74</b> , 789-791.	237
10. Line shapes in the method of intersecting energy levels. B. P. Kibble and G. W. Series. 1961. <i>Proc. Phys. Soc.</i> <b>78</b> , 70-74.	241
11. Theory of modulation of light in a double resonance experiment. J. N. Dodd and G. W. Series. 1961. <i>Proc. R. Soc. (London)</i> . <b>A263</b> , 353-370.	247
12. The modulation of light in a double resonance experiment. J. N. Dodd, G. W. Series and M. J. Taylor. 1963. <i>Proc. R. Soc. (London)</i> . <b>A273</b> , 41-68.	267
13. Theory of resonance fluorescence excited by modulated or pulsed light. A. Corney and G. W. Series. 1964. <i>Proc. Phys. Soc.</i> <b>83</b> , 207-212.	295
14. Double resonance excited by modulated light. A. Corney and G. W. Series. 1964. <i>Proc. Phys. Soc.</i> <b>83</b> , 213-216.	301
15. Proposal for measuring Lamb shifts by the study of modulated, fluorescent light. G. W. Series. 1964. <i>Phys. Rev.</i> <b>A136</b> , 684-688.	305

16. The forward-scattering of resonance radiation, with special reference to double resonance and level-crossing experiments. A. Corney, B. P. Kibble and G. W. Series 1966. *Proc. R. Soc. (London)* **A293**, 70-93. 311
17. Theory of the modulation of light in optical pumping experiments. G. W. Series. 1966. *Proc. Phys. Soc.* **88**, 957-968 335
18. The transfer of coherence by collisions of  $^3\text{He}$  atoms. R. B. Partidge and G. W. Series. 1966. *Proc. Phys. Soc.* **88**, 983-993. 347
19. Should resonance curves in optical pumping be Doppler-broadened? G. W. Series. 1966. *Proc. Phys. Soc.* **88**, 995-1000. 359
20. The level-crossing effect in resonance fluorescence stimulated by monochromatic light. G. W. Series. 1966. *Proc. Phys. Soc.* **89**, 1017-1020. 365
21. Theory of frequency and polarization modulation in resonance fluorescence. G. W. Series. 1970. *J. Phys.* **B3**, 84-97. 369
22. 'Line crossings' in the forward scattering of resonance radiation. R. Q. Hackett and G. W. Series. 1970. *Opt. Commun.* **2**, 93-96. 383
23. Determination of the hyperfine structure of the level  $3^2\text{P}_{3/2}$  of  $^{23}\text{Na}$  by time-resolved level-crossing spectroscopy. J. S. Deech, P. Hannaford and G. W. Series. 1974. *J. Phys.* **B7**, 1131-1148. 387
24. Time-resolved fluorescence spectroscopy. J. N. Dodd and G. W. Series. 1978. *In Progress in atomic spectroscopy*. Part A (Eds) W. Hanle and H. Kleinpoppen (New York: Plenum) pp. 639-677. 405
25. Collisional and radiative relaxation as an eigenvalue problem. G. W. Series. 1978. *Comments Atom. Mol. Phys.* **7**, 117-121. 445
26. A semi-classical approach to radiation problems. G. W. Series. 1978. *Phys. Rep. (Lamb Festschrift)*. **43**, 3-41. 451
27. Forward scattering and polarization spectroscopy. W. Gawlik and G. W. Series. 1979. *In Proc. IV Int. Conf. laser Spectroscopy*. (Eds) H. Walther and K. W. Rothe (Springer-Verlag) pp. 210-221. 491

#### IV. Laser Spectroscopy

28. Determination of lifetimes and hyperfine structures of the 8, 9 and 10  $^2\text{D}_{3/2}$  states of  $^{133}\text{Cs}$  by quantum-beatspectroscopy. J. S. Deech, R. Luypaert and G. W. Series. 1975. *J. Phys.* **B8**, 1406-1414. 503
29. Optogalvanic detection of atomic alignment. G. W. Series. 1981. *Comments Atom. Mol. Phys.* **10**, 199-201. 513
30. Alignment effects in optogalvanic spectroscopy. P. Hannaford and G. W. Series. 1981. *In Proc. V Int. Conf. Laser Spectroscopy*. (Eds) A. R. W. McKellar, T. Oka and B. P. Stoicheff (Springer-Verlag) pp. 94-102. 517



	<i>Page</i>
31. Observation of level-crossing effects in optogalvanic spectroscopy. P. Hannaford and G. W. Series. 1981. <i>J. Phys.</i> <b>B14</b> , L661-666.	527
32. Multimode saturation resonances in optogalvanic spectroscopy. Application to the determination of Lande $g$ -factors in zirconium. P. Hannaford and G. W. Series. 1982. <i>Opt. Commun.</i> <b>41</b> , 427-430.	533
33. Determination of hyperfine structures in ground and excited atomic levels by level-crossing optogalvanic spectroscopy. Application to $^{89}\text{Y}$ . P. Hannaford and G. W. Series. 1982. <i>Phys. Rev. Lett.</i> <b>48</b> , 1326-1329.	537
34. Laser spectroscopy. G. W. Series. 1984. <i>Contemp. Phys.</i> <b>25</b> , 3-29.	541
<i>V. Pedagogical</i>	
36. Basic quantum mechanics of atomic structures and transitions. G. W. Series. 1983. In <i>Quantum metrology and fundamental physical constants</i> . (Eds). P. H. Cutler and A. A. Lucas (Plenum), Also <i>Proc. NATO Advanced Study Institute</i> Erice, Sicily, Novr 1981, <i>Physics</i> , Ser. B., <b>98</b> , 15-60.	569
<i>VI. Lectures</i>	
37. Ubiquity of $\alpha$ : The fundamental atomic constants. Lecture delivered at Bangalore, India, 3 February 1983.	615



## The fine structure of the hydrogen $\alpha$ line

By H. KUHN AND G. W. SERIES, *Clarendon Laboratory, University of Oxford*

(Communicated by Lord Cherwell, F.R.S.—Received 23 January 1950)

[Plate 12]

A new attempt has been made to resolve spectroscopically the fine structure of the  $\alpha$  line, 6563 Å, of the Balmer series of heavy hydrogen. A deuterium discharge tube, whose walls were partly of copper, was immersed in liquid hydrogen and run at very low current densities. By this means the Doppler width of the individual lines was sufficiently reduced to enable the satellite between the main components of the 'doublet' to be resolved much more completely and to be measured more accurately than was possible before. The spectroscopic resolution was achieved with a Fabry-Perot interferometer of large diameter, mounted internally in a prism spectrograph.

The measurements support the assumption that the  $2S_{\frac{1}{2}}$  term is higher than is predicted by the Dirac theory, and lead to the value  $0.0369 \pm 0.0016$  cm.<sup>-1</sup> for the amount of the shift, in good agreement with the latest value found by Lamb & Retherford from microwave measurements. The relative widths of the main components and the interval between them also provide qualitative evidence for the shift of the  $2S_{\frac{1}{2}}$  term. The intensities of the lines were found to agree approximately with the prediction of the Dirac theory.

The weak line  $2P_{\frac{1}{2}}-3S_{\frac{1}{2}}$  was partly resolved from the neighbouring strong line  $2P_{\frac{3}{2}}-3D_{\frac{3}{2}}$ . The provisional value for the distance between them would indicate that the  $3S_{\frac{1}{2}}$  term is shifted very little, if at all. Further attempts are being made to obtain a more reliable value for this term.

### 1. INTRODUCTION

The structure of the first line of the Balmer series, 6563 Å, has been the object of a large number of investigations and controversies. Most workers confined their attention to the measurement of the wave-number difference of the two main peaks, generally called (1) and (2), comparing it with the prediction of current theories. Though the existence of a third component, (3), between the main peaks, was deduced as early as 1925 by Hansen from an analysis of his photometer tracings, the large Doppler width, due to the small mass of the hydrogen atom, prevented the resolution and measurement of this third component.

The existence of this component was subsequently explained by the introduction of the electron spin into the theory. The combined effect of the spin and relativity corrections in the wave-mechanical theory of the hydrogen atom (Goudsmit & Uhlenbeck 1925; Heisenberg & Jordan 1926; Pauli 1927) led to the same values of the terms as Sommerfeld's theory (1916), but altered their interpretation and the selection rules. Dirac (1928) derived the same results in a more consistent way, and the term 'Dirac theory' will be used in this paper when these results are referred to.

In heavy hydrogen,  $^2\text{H}$ , the fine structure is expected, on theoretical grounds, to be essentially the same as in light hydrogen, but the Doppler width is 1.4 times smaller, and the use of this isotope for investigations of the fine structure made considerable advances possible. The best resolution was obtained by R. C. Williams (1938*a*), whose photometer tracings show a very slight dip between the components (3) and (2). This partial resolution enabled him to make an approximate measurement of the position of the component (3) which, he concluded, was not in the



position predicted by the Dirac theory. The spacing between the main peaks (1) and (2) also disagreed with the prediction of this theory. Pasternack (1938) suggested that these discrepancies could be explained by assuming an upward displacement of the  $2S_{\frac{1}{2}}$  level of about  $0.03 \text{ cm.}^{-1}$  from its theoretical position. The work of other observers (Drinkwater, Richardson & Williams 1940), however, contradicted these results, which were therefore not generally accepted until the shift of the  $2S_{\frac{1}{2}}$  level was confirmed by Lamb & Retherford (1947) using a microwave method based on the metastability of the  $2S_{\frac{1}{2}}$  state. These experiments were carried out with light hydrogen, but deuterium was later found to give the same results.

In most of the previous spectroscopic work, discharge tubes immersed in liquid air had been used. Only one attempt to use liquid hydrogen for cooling a discharge tube appears to have been reported (Heyden 1937), but the resolution was not improved. The application of the atomic beam technique to atomic hydrogen has been discussed and tried (Mack & Barkowsky 1942; Williams 1942), but apparently without success.

In the present investigation of the fine structure of the  $\alpha$  line of deuterium, a specially designed discharge tube with walls partly of copper was immersed in a bath of liquid hydrogen. With the extremely small current densities used, it was found that temperatures of the emitting atoms below  $55^\circ \text{ K}$  were reached, resulting in a considerable improvement in resolution. It was thus possible to measure the position of the third component directly, and it was also found that the component (2) was wider than (1), owing to unresolved structure. Our results prove the reality of the shift of the  $2S_{\frac{1}{2}}$  level and give the amount of this shift to an accuracy of about 5 %.

Previous workers had often found large discrepancies between the observed intensity ratios of the components and the predictions of the theory. In the conditions of the experiments described below, the intensities differ only little from the theoretical values. This fact removes some objections which could be raised against previous work, and indicates that the spectrum observed can be ascribed to unperturbed hydrogen atoms.

The faint component  $2P_{\frac{1}{2}}-3S_{\frac{1}{2}}$  was resolved and its position measured, though not with the same accuracy as for the other components.

## 2. THE LIGHT SOURCE

The design of the discharge tube which was used in the final experiments is shown in figure 1. It consists partly of copper and partly of Pyrex glass, using commercial copper-glass seals. A mixture of helium and heavy hydrogen passed vertically downward through the copper tube *A*, where it was precooled before entering the zone *C* of the cathode glow. It then passed through the short glass tube *G* to the copper section *B*, at the entrance to which a positive column *P* was formed. The light from the latter emerged through the lens *L* and the window *W*. The positive column was only 2 to 3 cm. long. Complications through self-absorption, which often arise in end-on observations, were thus avoided.

The design and operation of the discharge tube were based on the following considerations:

(1) It is clear that the use of copper walls instead of glass walls ensures a considerably greater rate of heat flow into the cooling bath and thus helps to reduce the temperature of the gas. The tendency of metal walls to favour recombination of atoms can be overcome by covering the walls with a thin layer of heavy ice (Wood 1921).

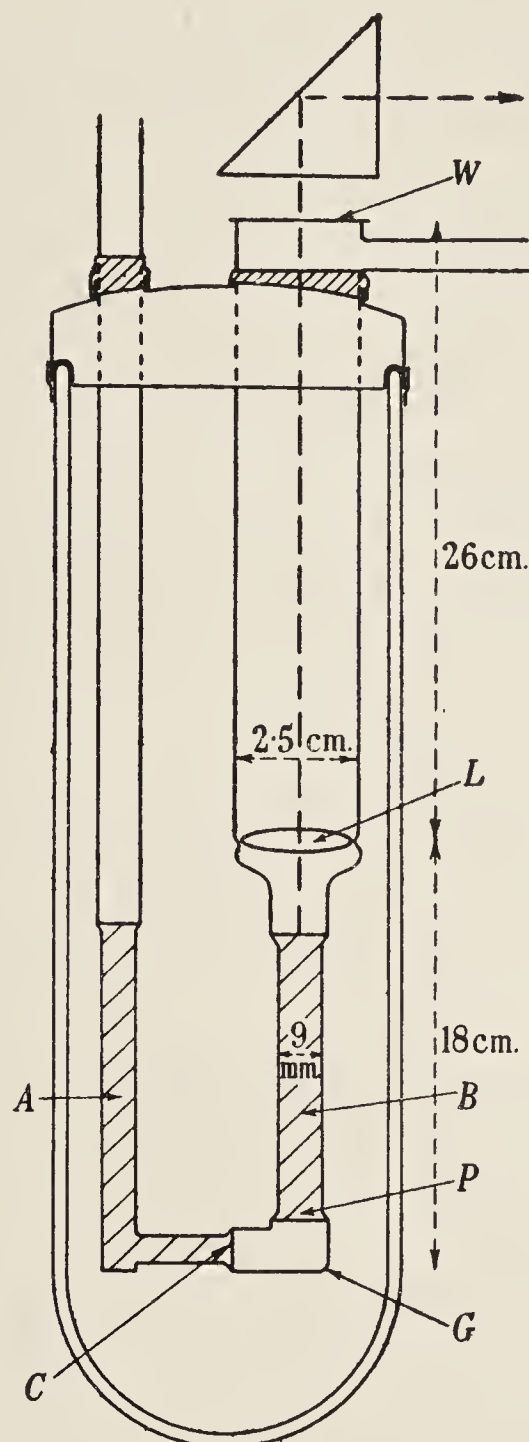


FIGURE 1. Discharge tube.

(2) The hydrogen atoms are formed from molecules by excitation and simultaneous dissociation, and have initially a large amount of kinetic energy. If the density of helium is high enough, collisions with helium atoms will rapidly reduce the temperature of the hydrogen atoms (the mean free path was about  $\frac{1}{100}$  mm. under the normal conditions of the discharge). Most of the hydrogen atoms which are available for excitation will therefore have low temperature. The process of excitation of the atom by electron impact will also impart some kinetic energy to the atom; but an estimate shows that the effect is small and would only become important at temperatures below those reached in the present experiments.



(3) The formation of atoms will be strong in the cathode glow. The gas, when reaching the anode, can thus be expected to contain a certain amount of deuterium in the atomic state. It is difficult to say how far this process of preformation of atoms was actually taking place under the conditions of our experiments.

(4) Wide aperture of the emergent beam of light was essential, in view of the wide aperture of the spectrograph used (see § 3). In order to reconcile this requirement with the necessarily large distance from the positive column to the window, the lens  $L$  was inserted inside the discharge tube.

Before the tube was filled, heavy-water vapour was admitted. When the cooling bath was then applied, a film of heavy ice formed on the walls.

The most favourable values of the pressures of helium and deuterium were found by trial. Too high pressure of deuterium made the molecular spectrum of deuterium appear too strongly, and too high pressure of helium produced  $\text{He}_2$  bands. In most experiments, the pressure of helium was about 1.7, that of deuterium 0.2 mm. Hg, though other pressures were also used. The pressure was measured by means of a sensitive glass gauge of the Bourdon type ('spoon gauge'). A mercury diffusion pump maintained the circulation of the gas mixture, which, before entering the discharge tube, passed through a trap with charcoal, cooled with liquid air.

Figure 1 shows how the discharge tube was fitted into a brass cap which formed the lid of the Dewar vessel containing the liquid hydrogen. The anode limb consisted of a 2.5 cm. wide glass tube, the upper end of which protruded through the metal cap and was closed by a plane window. The clearance between the lens  $L$  and the walls of the glass tube was enough to allow the flow of gas towards the pump.

A connexion from the brass cap to a rotary oil pump allowed the hydrogen bath to be used at low pressure. The temperature of the bath was reduced to 14° K in some experiments.

The voltage applied to the discharge tube in normal running conditions was always below 300 V; the current was varied from 2 to 20 mA, but the 'standard' current used in the exposures on which the final results were based was 5 mA. The current density was then about 7 mA/cm.<sup>2</sup>.

In the earlier stages of the work, a discharge tube of different design was used; the cathode was situated above the anode in the wide, vertical glass tube. It consisted of an aluminium ring almost touching the wall of the tube. The light from the positive column passed through the cathode ring; since an image of the positive column was formed on the slit, no light from the negative glow surrounding the ring was expected to reach the slit. But this method was open to objections and was abandoned in favour of the design described above.

### 3. THE OPTICAL SYSTEM

Liquid hydrogen is a more effective cooling agent than liquid air only if the power input into the discharge tube is exceedingly small. The optical system therefore had to be designed so as to produce the greatest possible intensity of the image for the given, very small, brightness of the source. At the same time, the resolving power had to be great enough to avoid any appreciable loss of the resolution which the



reduced Doppler width allowed. But the resolving power could not be increased by increasing the spacing of the etalon plates, since this would have entailed the overlapping of adjacent orders. A Fabry-Perot interferometer of very large diameter was therefore used, and the silver films were made just thick enough to produce the required, previously calculated, reflectivity. It was combined with a prism spectrograph constructed in the laboratory workshop and designed specially for this purpose.

The focal length of the camera lens of the spectrograph was chosen just large enough to separate, with the available prism, the  $H_{\alpha}$  line from certain adjacent deuterium bands and from the helium red line 6678 Å, with a width of the slit image of 1 mm. A telescope lens of focal length 65 cm. satisfied this condition, in conjunction with a 60° prism, a combination which produced a dispersion of 100 Å/mm. in the red. The height of the prism was 9 cm.

A focal length of 65 cm. is sufficient to produce, with an etalon of spacing 7.67 mm., fringes of a large enough scale for photometric work with plates of medium grain size. Since, further, the size of the available etalon was similar to that of the prism, internal mounting was chosen. The etalon was placed between prism and camera lens. The collimator was a telescope lens of focal length 44 cm.

The image of the source formed on the photographic plate had to be large enough to avoid serious variation of intensity within the fringe pattern. This required a linear magnification of about 3:2. The effective aperture of the beam leaving the source had therefore to be at least  $\frac{3}{2}$  times larger than the effective aperture of the camera lens which was about 1:10. By the device of placing a lens inside the discharge tube, an aperture of 1:6.5 was obtained.

The Fabry-Perot etalon consisted of two plates of fused silica, of diameter 11.5 cm., made by Messrs Adam Hilger Ltd. The spacers were also made of fused silica. An area of diameter 7 cm. was generally used, with the exception of a small portion which had to be masked off. It was found, however, that further reduction of the exposed area improved the resolution slightly.

The plates were silvered by evaporation in a vacuum and had a reflectivity of 91 % and a transmission factor of 5 % for red light. This reflectivity gives a theoretical half-value width of  $\frac{1}{33}$  of an order. With the spacer of 7.67 mm. which was used in most experiments, this corresponds to 0.02 cm.<sup>-1</sup>. Test exposures with cadmium red light showed that the actual resolution was not much below this value.

The spectrograph and interferometer were placed in a room, the temperature of which was thermostatically controlled to within  $\frac{1}{5}$  to  $\frac{1}{10}$ ° C. The discharge tube was set up in the adjacent room; the light entered through a slot in the wall containing a small glass window. Under favourable conditions, this arrangement permitted exposures of several hours, though generally the time of exposure was only 15 to 30 min.

Ilford H.P. 3 plates were mostly used. They proved to be faster, for light of wave-length 6563 Å, than other types of plates tried (Astra VIII, Kodak IHA, Astra VII). Of these, only Astra VII had considerably finer grain, but it was found to require too long exposures.



## 4. THE MEASUREMENT OF THE WAVE-NUMBER DIFFERENCES

Figure 2, plate 12, gives a typical spectrogram taken with the 7.67 mm. spacer. It shows the components (1), (2) and (3) in three different orders.

The main object of this work was the accurate measurement of the spacing between the components (1) and (3), of which one is six times stronger than the other. When the exposure was long enough to make the fainter line clearly visible, the stronger one was over-exposed, even on the comparatively soft plates used (Ilford H.P. 3). Only in a correctly exposed fringe can the setting of the cross-wire in the comparator be expected to give the position of the maximum; in an over-exposed fringe, any slight asymmetry, due to the genuine shape of the line or to instrumental effects, will give rise to systematic differences between the setting and the true maximum. Direct measurement of the distance between the two lines photographed in one single exposure would thus have been liable to serious errors. The following technique was therefore developed: three successive exposures were made on one plate, with times of exposure in the ratio 1:10:1. The distances of the strong fringes (1) and (2) from a reference mark were measured in the first and last exposure, and the distances of the faint fringes, due to component (3), from the same reference mark in the middle exposure. The plate was rejected if the distances measured in the first and third exposure did not agree well enough.

After some preliminary experiments with a glass fibre across the slit, suitable reference marks were ultimately found in the outer fringes which are narrower than those used for the measurement of the fine structure and could therefore be measured very accurately. In the second, longer exposure, the end of the slit which framed the reference fringes was covered during most of the time, and was only uncovered for 1 or 2 min. at the beginning and at the end of the exposure.

The centre of the fringe system can be found directly if fringes on both sides of the centre are visible. Such a setting would, however, have resulted in a considerable sacrifice in the number of orders in which the fine structure could be measured, and fringes on one side only of the centre were usually used. The centre was calculated, in the customary way, from the measured position of the fringes in three orders. This method relies, to some extent, on the validity of the square-root formula for the radii of the fringes, and thus on the absence of distortion in the camera lens. A series of measurements of interference fringes produced with cadmium red light showed that the formula held, in fact, accurately.

Of the two main peaks of the fine structure, that of shorter wave-length, (2), is a blend of two lines of similar intensities (see § 6), and thus not so suitable for measurement and for an analysis of the structure. The wave-number difference of components (3) and (1) was therefore chosen as the principal aim of the measurements. The wave-number difference (2) - (1) was also measured, partly for comparison with results of other workers.

In an attempt to study the possible influence of variations of discharge conditions, especially of the current density and deuterium pressure, a large number of exposures were taken in which these conditions were varied over a wide range.

With increase in the current, the resolution of component (3) decreased, and the



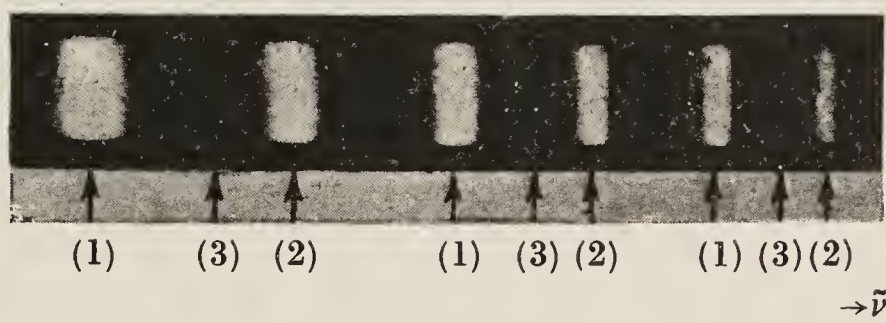


FIGURE 2. Fine structure in three orders, with 7.67 mm. spacer; current 5 mA.

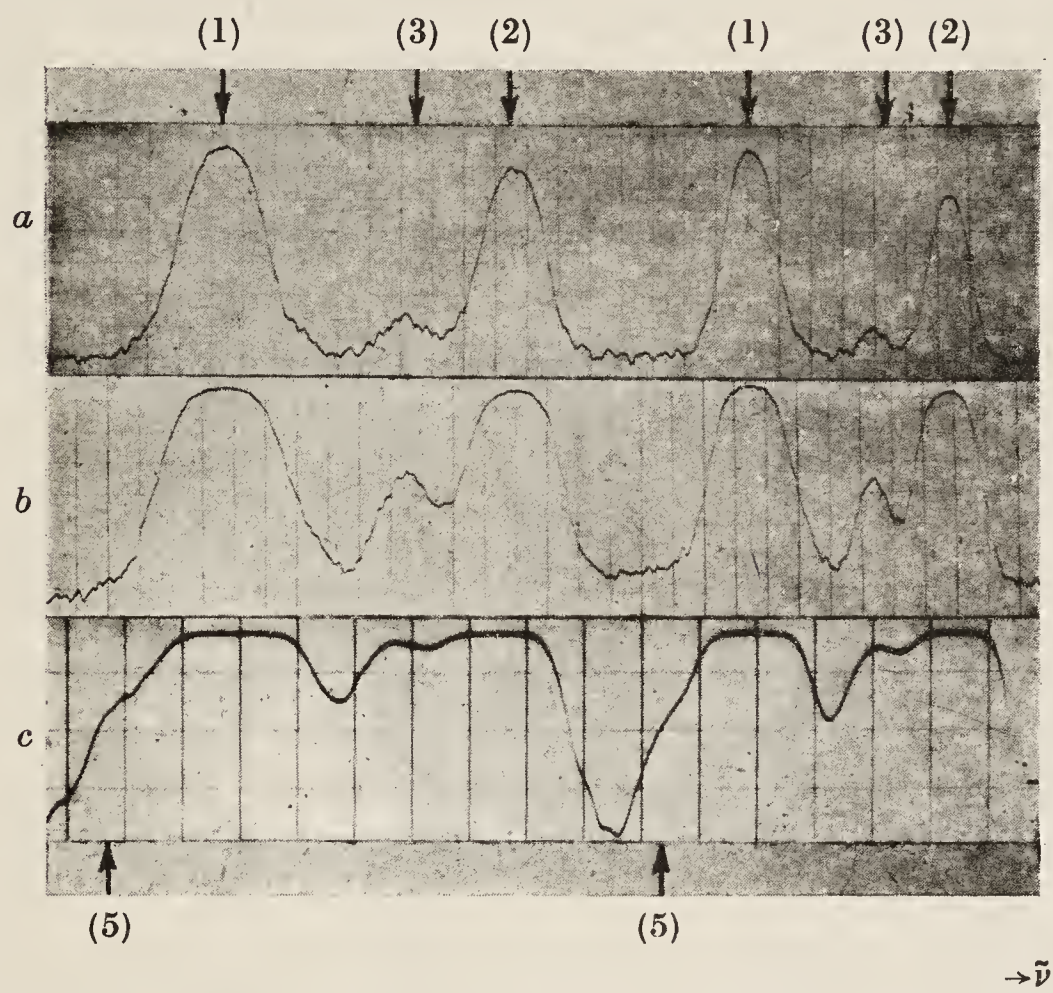


FIGURE 3. Photometer tracings, 7.67 mm. spacer; current 5 mA.  
a, short exposure; b, standard exposure; c, long exposure.

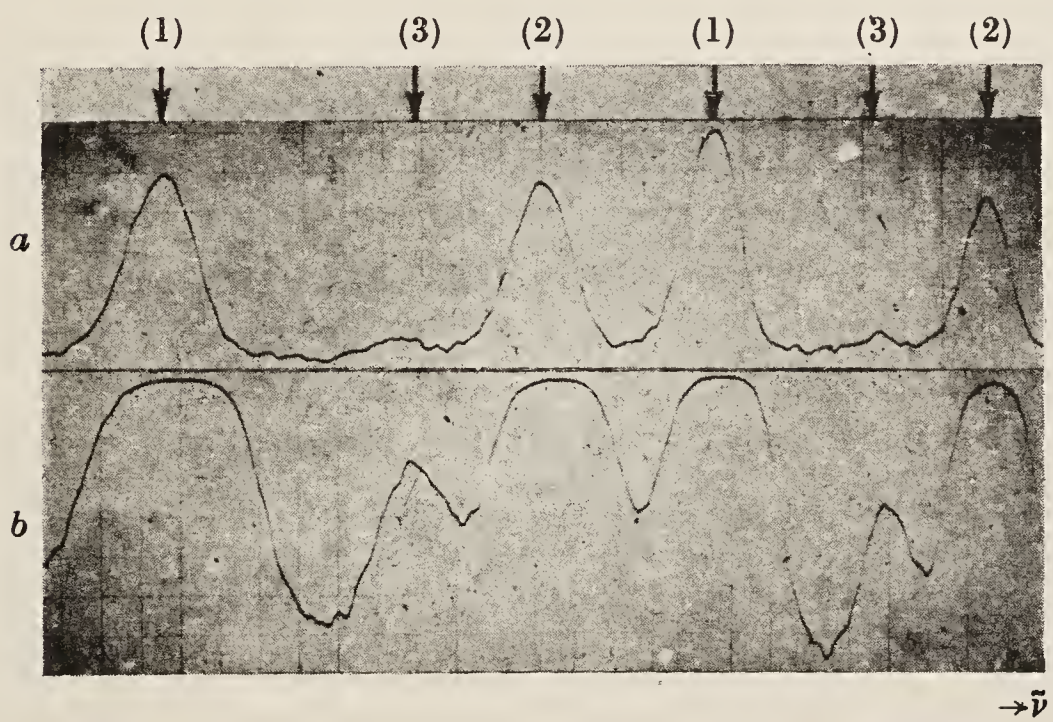


FIGURE 4. Photometer tracings, 10 mm. spacer, cooling bath at 14° K.  
a, current 2 mA; b, current 5 mA.

(Facing p. 132)



measurements became less accurate, but no change in the distances could be observed, as shown in table 1. The number of fringes from which each value has been derived is given in brackets.

In order to test the influence of the variation of the pressure of deuterium, three sets of exposures were taken. In the first, the deuterium pressure was so low that the deuterium  $\alpha$  line appeared weaker than the helium red line, in the second set the deuterium pressure had the standard value of 0.2 mm., whereas in the third it was so high that the helium red line had completely disappeared. The three average values, each taken over six fringes, of the wave-number difference (3) – (1) were 0.188, 0.186 and 0.188  $\text{cm}^{-1}$ , and for the difference (2) – (1), 0.325, 0.324 and 0.323  $\text{cm}^{-1}$ . From these and a number of similar comparisons, it was concluded that a variation of the concentration of deuterium, sufficient to alter considerably the conditions of the discharge, did not affect the position of the components.

TABLE 1. SPACINGS OF COMPONENTS AT DIFFERENT CURRENTS

current (mA)	2-2½	5	10	20
(3) – (1)	0.188 (5)	0.189 (16)	0.189 (6)	0.188 (15) $\text{cm}^{-1}$
(2) – (1)	0.323 (5)	0.322 (16)	0.323 (12)	0.322 (17) $\text{cm}^{-1}$

Comparisons between exposures in which the temperature of the cooling bath was 20 and 14° K respectively, i.e. made with liquid hydrogen at atmospheric and at reduced pressure, also failed to show any significant differences in the measured spacings. At the lower temperature, the lines were noticeably narrower when the current was below 5 mA.

Great attention was paid to the possible influence of traces of light hydrogen which are impossible to exclude in an apparatus containing greased taps. Occasional tests with an etalon of suitably chosen spacing showed that the proportion of light to heavy hydrogen was less than 1:50. With the spacing of 7.67 mm., the component (1) of  $^1\text{H}$  falls well outside the pattern of  $^2\text{H}$ , and component (2) of  $^1\text{H}$  midway between (1) and (3) of  $^2\text{H}$ , well resolved from either. Even a considerably greater amount of light hydrogen than that actually present would therefore not have affected the measurements. The mentioned relative positions of the lines were calculated from the known isotope shift (Williams 1938*b*; Drinkwater *et al.* 1940) and verified in an exposure taken after a splinter of sealing wax had fallen into the discharge tube, as the result of an accident; the lines of  $^1\text{H}$  appeared then in the calculated positions.

Though variations in discharge conditions had no measurable effect on the positions of the lines, the most reliable results were clearly those taken at very low current density, since they give the best resolution and consequently the greatest accuracy of measurement, and are also least likely to be affected by electric fields and other possible causes of error (see § 10). The final values for the positions of the lines were therefore based on a number of exposures taken under 'standard conditions', with a current of 5 mA and with the cooling bath at atmospheric pressure. They are summarized in table 2, where each line represents one plate.



The three orders measured on each plate were produced by light coming from different parts of the cross-section of the discharge tube. No significant difference was found between the averages of the interval (3) – (1) measured in the different orders.

In order to determine accurately the spacing between the etalon plates, the interference fringes produced by the two mercury yellow lines were measured. A mercury lamp containing the pure isotope 198, kindly supplied by the General Electric Company, was used for this purpose. The spacing (multiplied by the refractive index of air) was found as 0.7675 cm.

TABLE 2. WAVE-NUMBER DIFFERENCES OF COMPONENTS IN  $\text{cm}^{-1}$

order counted from centre	...	(3) – (1)			(2) – (1)		
		2	3	4	2	3	4
current 5		0.1864	0.1868	—	0.3210	0.3199	—
mA. 5		0.1879	0.1875	0.1898	—	0.3204	0.3211
	5	0.1876	0.1862	—	0.3215	0.3215	—
	2.5	0.1882	0.1844	—	0.3196	0.3205	—
	5	0.1865	0.1880	0.1867	0.3202	0.3206	0.3221
	5	0.1889	0.1923	0.1859	0.3214	0.3226	0.3218
	5	0.1881	0.1895	0.1882	0.3217	0.3207	0.3223
	5	0.1904	0.1897	0.1888	0.3206	0.3224	0.3206
	5	0.1861	0.1878	0.1858	0.3213	0.3228	0.3213
	5	0.1879	0.1889	0.1875	0.3195	0.3232	0.3229
	5	—	0.1868	—	0.3183	0.3232	0.3196
	5	0.1875	0.1874	0.1874	0.3203	0.3221	0.3219
	5	0.1857	0.1871	0.1866	0.3195	0.3222	0.3215
	5	0.1895	0.1898	—	0.3209	0.3220	0.3236
	5	0.1892	0.1881	0.1923	0.3210	0.3218	0.3210
mean		0.1879	0.1880	0.1879	0.3205	0.3217	0.3216
mean of all orders			0.1879			0.3213	
standard deviation			0.0003			0.0002	

Exposures were also taken with a 10 mm. spacer and gave good agreement with the values of table 2; but the component (2) of light hydrogen fell near the component (3) of deuterium, and very slight errors arising from this overlapping could not be excluded. The measurements were therefore not included in the final average.

In preliminary work, the wave-number difference (2) – (1) was also measured with a 5 mm. spacer, with results in close agreement with those in table 2.

The highest resolution was obtained with a current of 2 mA and a temperature of the bath of  $14^\circ \text{K}$ . It was especially in these exposures that the line (2) appeared noticeably wider than (1). From a tracing such as that shown in figure 4*a*, plate 12, the ratio of the widths was found to be about 1.3. The time of exposure was, however, very long with this low current, and component (3) was therefore not measured under these conditions.

Figure 3, plate 12, shows photometer tracings of spectrograms taken with the 7.67 mm. spacer, at a discharge current of 5 mA. The short exposure (*a*) shows qualitatively the relative intensities of components (1), (2) and (3). In the medium

exposure (b) the component (3) is seen more clearly. It represents the 'standard' conditions of current and exposure as used in most measurements. In the long exposure (c) the components (1), (2) and (3) are over-exposed, and component (5) appears as a hump on the wing of component (1).

Exposures with the 10 mm. spacer, and with the cooling bath at a temperature of 14° K, i.e. with the liquid hydrogen under reduced pressure, are shown in figure 4. The discharge currents were 2 and 5 mA in (a) and (b) respectively.

### 5. MEASUREMENT OF THE INTENSITIES

The spectral sensitivity curve of the Ilford H.P. 3 plate drops very rapidly at the wave-length of  $H_\alpha$ , so that the usual method of calibration by means of white light in conjunction with a spectroscope was not accurate enough. The intensity marks were therefore made with light from a hydrogen discharge tube, from which the red line was selected by a colour filter. Neutral filters, previously calibrated, were used for producing known ratios of intensity. In this way, intensity marks were made on several of the plates on which the fine structure was photographed. The densities were measured both on the recording micro-photometer of the Oxford Observatory and on a non-recording Zeiss micro-photometer.

Line 3 of table 3 gives the measured ratios of the peak intensities of the components (1), (2) and (3). The intensity (1) was chosen as unit.

TABLE 3. RELATIVE INTENSITIES OF THE COMPONENTS

	(1)	(2)	(3)
theoretical, uncorrected	1.0	0.71	0.11
theoretical, corrected	1.0	0.65	0.12
experimental	1.0	0.70	0.18

### 6. THE POSITION OF THE $2S_{\frac{1}{2}}$ TERM

Relativistic quantum mechanics, either in the form of Schrödinger's theory with the inclusion of relativistic and spin corrections, or in the form of Dirac's theory, leads to the following expression for the term values of hydrogen:

$$T_{n,j} = -\frac{R}{n^2} - \frac{R\alpha^2}{n^3} \left( \frac{1}{j + \frac{1}{2}} - \frac{3}{4n} \right).$$

Figure 5a shows the terms with  $n = 2$  and  $n = 3$  plotted according to this formula, with the use of the latest numerical values of the constants  $R_D = 109707 \text{ cm.}^{-1}$  and  $\alpha^2 = 5.3258 \times 10^{-5}$  (Du Mond & Cohen 1949). The intensities of the lines as calculated by Sommerfeld & Unsöld (1926) and Kupper (1928) are given as numbers next to the lines and are roughly indicated by the length of the lines.

Neglecting at first the small effect of the unresolved, weak component (4) and any instrumental corrections, it is clear that the measured distance (3)–(1) is about 0.03 to 0.04  $\text{cm.}^{-1}$  smaller, and the distance (2)–(1) is about 0.007  $\text{cm.}^{-1}$  smaller than the respective theoretical values. The only simple way of explaining these facts is the assumption that the  $2S_{\frac{1}{2}}$  level is about 0.03 to 0.04  $\text{cm.}^{-1}$  above the



$2P_{\frac{1}{2}}$  level, as shown in figure 5*b*. Pasternack (1938) had, in fact, made this assumption on the basis of the results of R. C. Williams (1938*a*). The new fact that component (2) appears wider than (1) on our spectrograms proves independently the qualitative correctness of this assumption. Accepting the fact that  $2P_{\frac{1}{2}} - 2S_{\frac{1}{2}} = x$  is of the assumed order of magnitude, we can now derive an accurate value of  $x$  from an analysis of our measurements.

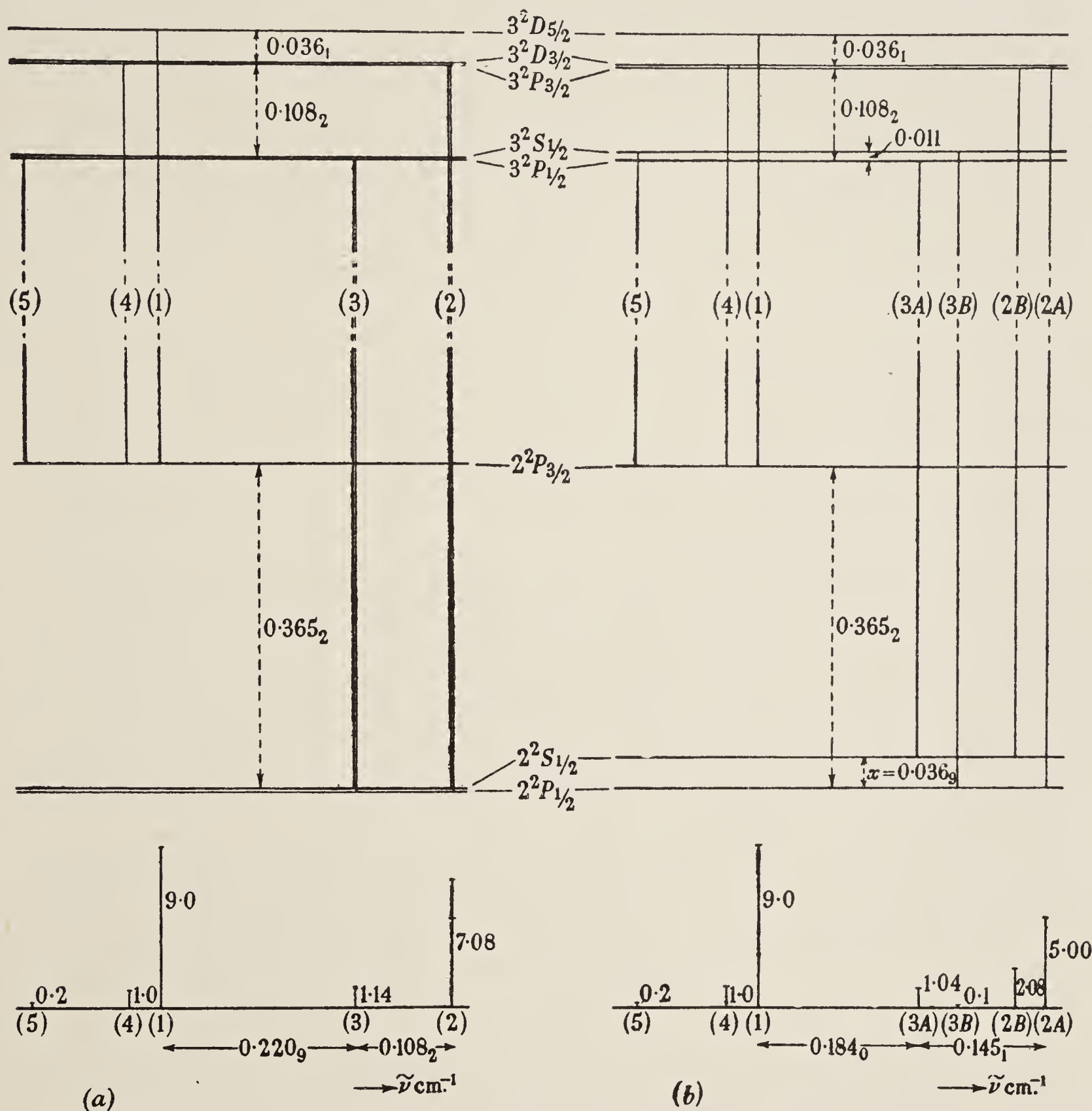


FIGURE 5. Term diagram. *a*, Dirac theory; *b*, showing shifts of S terms.

The intensities of the components in figure 5*b* are derived from the same theory as those in figure 5*a*. There is little doubt that these theoretical results for the intensities apply, even though the term values differ slightly from those given by the theory, if the cause of the difference can be ascribed to an internal effect in the atom, acting as a perturbation having central symmetry. The components (2) and (3) are now split into two subcomponents *A* and *B*. Though these splittings are not

resolved, the ratio of the intensities of the blends (2), (3) and (1 + 4) can be compared with the theoretical values. The first line in table 3 gives the theoretical intensities calculated by adding the subcomponents *A* and *B*. The figures in the second line are based on the same values for the individual components, but the peak intensity of unresolved components has been calculated by superposition of Doppler distribution curves. Some allowance has also been made for instrumental background, with the use of Airy's formula. But this estimate neglects the Doppler width of the strong lines and is therefore certainly too small. On account of this, and other possible sources of error, the values for (2) and especially for (3) in the second line of table 3 are probably rather too low. Comparison with the experimental values in line 3 does not indicate, therefore, any discrepancy outside the possible, rather wide, limits of error. In view of this, it can be assumed that the ratios of the intensities of the unresolved components also agree, at least roughly, with the theoretical values. In the experiments of R. C. Williams (1938*a*), the intensities differed very considerably from the theoretical values.

In figure 5*b*, the position of the term  $3S_{\frac{1}{2}}$  has been assumed somewhat arbitrarily. This term leads to the faint component (3) *B* and therefore only affects a small correction applied to the position of component (3) (see below). The term difference  $3P_{\frac{1}{2}} - 3S_{\frac{1}{2}}$  has been assumed to be about one-third of the difference  $2P_{\frac{1}{2}} - 2S_{\frac{1}{2}}$ . This may be justified either by reference to the new theories of radiation shifts of terms or by the general argument that the whole structure of the level  $n = 3$  is about one-third as wide as that of the level  $n = 2$ .

In comparing the measured wave-number difference of the fringes (3) and (1) with the wave-number difference of the two single lines (3) *A* and (1), two effects have to be considered. (*a*) The peak of (1) will be slightly shifted by the presence of the unresolved, weak satellite (4) and the peak (3) *A* by the unresolved, weak satellite (3) *B*. (*b*) The lines (1) and (2), though well resolved from (3), are considerably stronger than the latter and therefore have a slight influence on its position. Both effects are small, particularly (*b*), and can therefore be estimated by comparatively crude methods.

The only important causes of the finite widths of the fringes are Doppler effect and instrumental broadening. The half-value width of the latter is considerably smaller than the half-value width of the Doppler effect, and the intensity distribution near the maximum will thus differ very little from pure Doppler distribution. The instrumental broadening, however, obeys an entirely different law which causes it to be the predominant effect at great distances from the maximum. The correction (*b*) can therefore be calculated as practically due only to instrumental width. This was done by means of Airy's formula, with the experimentally determined reflectivity of the etalon plates. The result of this calculation was a shift of component (3) by  $0.0005 \text{ cm.}^{-1}$  towards (2).

For the calculation of effect (*a*), the shape of the line was assumed to be that given by pure Doppler effect, but with the use of the experimentally determined half-value width. The influence of instrumental broadening was thus treated as an empirically determined increase of the Doppler width, corresponding to a higher 'effective' temperature. Its value was found from the measured half-value width



$\Delta\nu = 0.078 \text{ cm.}^{-1}$  of component (1). Allowance for the influence of (4) on the width of (1) gave the effective half-value width of a single line as  $0.072 \text{ cm.}^{-1}$ . With the use of this value, it was found that (4) shifts the maximum of (1) by  $0.0020 \text{ cm.}^{-1}$ , and that (3) *B* causes a shift of  $0.0014 \text{ cm.}^{-1}$  of the peak of (3) *A*. When this correction was calculated, a provisional, uncorrected value of the term shift  $x$  had to be used at first, and the resulting, corrected value of  $x$  was used in a second calculation (with very nearly the same result), in a process of successive approximation. Also the assumption of the shift of the term  $3S_{\frac{1}{2}}$  by  $x/3$  enters into this correction. If the latter shift were assumed to be zero, the result would only be changed by  $0.0004 \text{ cm.}^{-1}$ .

From the wave-number difference  $(3) - (1) = 0.2209 \text{ cm.}^{-1}$  in the Dirac term diagram  $[2P_{\frac{1}{2}} - 2P_{\frac{3}{2}} - (3P_{\frac{1}{2}} - 3D_{\frac{3}{2}})]$  and the observed value,  $0.1879 \text{ cm.}^{-1}$  of the distance of the peaks (3) and (1), the shift of the  $2S_{\frac{1}{2}}$  term is found as

$$\begin{aligned} x = 2P_{\frac{1}{2}} - 2S_{\frac{1}{2}} &= 0.2209 - 0.1879 + 0.0020 + 0.0014 + 0.0005 \\ &= 0.0369 \text{ cm.}^{-1}. \end{aligned}$$

#### 7. THE SPACING OF THE MAIN PEAKS (1) AND (2)

If the assumption of the shift of the  $2S_{\frac{1}{2}}$  level is accepted, the component (2) must be regarded as a blend of two lines which are just not resolved and whose intensities are in the ratio 5:2. In a blend of this kind, the position of the maximum will depend quite critically on the individual line shape, and the correction of the type (a) considered in the preceding section will be large. Also in the measurement of a strongly unsymmetrical blend it is doubtful whether the crosswire of the travelling microscope is set on the maximum or the centre of gravity. Since further the position of only one component of the blend, namely, (2) *B*, depends on the position of the level  $2S_{\frac{1}{2}}$ , it is evident that the measurement of the spacing of the peaks (2) and (1) is not an accurate way of determining the position of this level.

In order to test if the measured spacing  $(2) - (1)$  is at least compatible with the value  $0.037 \text{ cm.}^{-1}$  of the term shift, the peak-to-peak distance was calculated from this value with the use of the methods discussed. The result was  $0.323 \text{ cm.}^{-1}$ . The measured value  $0.321$  is very little, but probably significantly, lower. The assumption that the cross-wire was set somewhere between the maximum and the centre of gravity of the blend would account for the difference.

#### 8. THE FAINT COMPONENT (5) AND THE POSITION OF THE TERM $3S_{\frac{1}{2}}$

In very long exposures, a further line appeared next to component (1), towards increasing wave-length. It is due to the transition  $2P_{\frac{1}{2}} - 3S_{\frac{1}{2}}$ . Indications of it have been observed by Heyden (1937) who was, however, not able to resolve it from the 45 times stronger line (1).

On our plates, this line can be distinctly seen and measured with the travelling microscope, but the resolution is not complete, and the photometer tracings (see figure 3c, plate 12) show it only as a hump in the wing of the overexposed line (1),



not as a maximum of intensity. Our measurements of this component (5) which have been briefly reported before (Kuhn & Series 1948), were carried out in the earlier stages of this work, when the technique of measurement was not as good as in the later experiments. Partly for this reason and partly because of incomplete resolution, the results show a large scatter and are to be considered as provisional. As an average of 17 fringes measured in 8 exposures, the distance of component (5) from (1) was found to be  $0.138 \pm 0.006 \text{ cm.}^{-1}$ .

The Dirac term diagram (figure 5a) gives the value  $0.144 \text{ cm.}^{-1}$  for the wave-number difference of these two components. Allowance for the shift of the peak of (1) due to component (4) reduces this value by  $0.002 \text{ cm.}^{-1}$ , and allowance for instrumental intensity distribution of (1) may reduce it further by an amount  $y$ . Any upward displacement  $z$  of the term  $3S_{\frac{1}{2}}$  is then found as

$$z = 0.144 - 0.138 - 0.002 - y = 0.004 - y \pm 0.006 \text{ cm.}^{-1}.$$

Even if  $y$  is assumed to be negligible, our measurements make an upward shift of more than  $0.01 \text{ cm.}^{-1}$  unlikely. It is hoped that further measurements under improved conditions will give a more definite result.

## 9. THE TEMPERATURE OF THE EMITTING ATOMS

An estimate of the temperature of the radiating atoms was made from the half-value width of the line (1), measured on photometer tracings. The width was corrected in two respects, first for the influence of the minor component (4), secondly for the instrumental contribution to the width of the line. The remaining width was treated as a pure Doppler effect, and leads to an upper limit for the temperature, since it includes all the minor causes of broadening, such as hyperfine structure, radiation width, Stark effect and imperfections of the etalon.

The first correction is small and was made by numerical calculation. The second correction was made by means of a formula given by Minkowsky & Bruck (1935). The calculation leads to the value  $55^\circ \text{ K}$  for the temperature under standard discharge conditions. Under the most favourable conditions (lowest current, and the cooling bath at reduced pressure) the value  $40^\circ \text{ K}$  was obtained. Though no great accuracy is claimed for these figures, they show that other causes of broadening, such as Stark effect, must have been comparatively small.

## 10. DISCUSSION OF THE RESULTS

Before the results of this work can be compared with other experiments or with theory, it is necessary to discuss various possible systematic errors, as far as they have not been treated in earlier sections.

(a) *Non-uniform illumination.* A decrease of the illumination of the slit image towards the ends could not be avoided. If the slope of the intensity 'envelope' of the fringes had been too great, it could have displaced the maxima. The good agreement of the values of the interval (3) – (1) derived from different orders proved that this effect was negligible. For the interval (2) – (1), the average for the second



order is slightly different from that for the third and fourth orders. This might well be due to the complex structure of the line (2) which could cause measuring errors depending on the dispersion (see § 7).

(b) *Overlapping effects.* The influence of overlapping lines of light hydrogen was specially investigated and excluded by suitable choice of the spacer, as explained in § 4. The possibility that a faint, unknown line of the molecular deuterium spectrum might cause errors by overlapping has been mentioned by other authors. But the intensities of the molecular and atomic spectra of hydrogen depend on the current density in an entirely different way, and since the measured spacings show no dependence on the current density, this source of error can be excluded. Also the variation of deuterium concentration would have revealed any effect of this kind, for similar reasons. The same argument applies to helium bands which have a much higher excitation potential than hydrogen atomic lines and whose intensity depended on the conditions of the discharge in a different way. Another line which might possibly have overlapped was the helium spark line 6560 Å. Subsidiary experiments, however, showed that even much stronger lines of the helium spark spectrum were very weak under the conditions of our discharge.

Very few actual impurities could persist in a discharge at the temperature of liquid hydrogen, in a gas which was circulated through charcoal cooled with liquid air, and they would have revealed their influence by erratic results.

The use of different spacings of the etalon plates, with perfectly concordant results, was a further safeguard against errors caused by the overlapping of unknown lines.

(c) *Self-absorption.* The term  $2S_{\frac{1}{2}}$  is known to be metastable, and self-absorption might occur in lines connected with this level, namely, (2)*B* and (3)*A*. This would alter the relative intensities and cause a shift in the blend (2). But any shift in the line (3) would be only of the order of magnitude of the correction applied to this line on account of the influence of (3)*B*. No evidence for self-absorption was, in fact, found. The concentration of metastable atoms must certainly increase with current density, but this was found to affect neither the positions nor, as far as could be judged, the intensity ratio of the lines.

Owing to the small energy difference between the metastable state and the state  $2P_{\frac{1}{2}}$ , metastable hydrogen atoms are probably extremely sensitive to impacts. This would account for failure of attempts to prove their existence by self-absorption in discharge tubes (Ornstein, Zernicke & Snoek 1928). In our experiments, with low current densities and the presence of helium, self-absorption would not have been expected.

(d) *Stark effect.* Stark effect in discharges, caused either by the local fields of the ions or by the potential drop in the discharge tube, can have noticeable effects on the spectra of light atoms, especially hydrogen. It would cause broadening, shifts and changes of relative intensities of the lines. Theoretical estimates such as those carried out by Heyden (1937) show that these effects are negligible under the conditions of our discharge. Independently, our experimental results provide direct evidence against any appreciable influence of electric fields; the intensity ratio of the components, which should respond strongly to Stark effects, were found to agree



essentially with theory. Change of current density and of deuterium content strongly affect ion density and potential drop, and neither of these changes was found to affect the position of the lines. Also effects of electric fields would be different in the different parts of the discharge tube, but in fact light coming from different parts of the cross section of the discharge tube gave the same positions of the components. In one experiment, the polarities of the electrodes were exchanged, so that the light was taken from the inside of a hollow cathode; but again, the measurements gave the same results.

(e) *Accuracy of the result.* The shifts of the lines (1) and (3) resulting from the influence of the faint, unresolved components (4) and (3)*B* respectively were estimated on the basis of a half-value width of  $0.072 \text{ cm.}^{-1}$ . If, instead, the half-value width had been assumed as  $0.065$  or  $0.078 \text{ cm.}^{-1}$ , the distance (3) – (2) would have been changed by  $0.0005 \text{ cm.}^{-1}$  in either direction. (These assumptions represent the extreme limits of error in the estimate of the half-value width.) To allow for inaccuracies caused by the simplified method of calculating the corrections, this estimate of error may be doubled. Compared with the resulting value of  $\pm 0.001 \text{ cm.}^{-1}$ , representing the uncertainties in the corrections, the statistical error of the measurements is small. By adding twice the value of the standard deviation ( $2 \times 0.0003 \text{ cm.}^{-1}$ ), we arrive at the estimated limits of error of  $\pm 0.0016$ , and the shift of the term  $2S_{\frac{1}{2}}$  is found as

$$0.0369 \pm 0.0016 \text{ cm.}^{-1}.$$

In a preliminary publication (Kuhn & Series 1948), the value of this shift derived from earlier experiments was reported as  $0.043 \pm 0.006 \text{ cm.}^{-1}$ ; this was in disagreement with the preliminary result of Lamb & Retherford (1947) which was given as  $0.033 \text{ cm.}^{-1}$ . Since then these authors have improved their methods and have given as their final results, for both light and heavy hydrogen,  $0.0354 \pm 0.0002 \text{ cm.}^{-1}$ . Our new lower value agrees with this new raised value of Lamb & Retherford (1949) within the accuracy of our experiments. The difference between our new and our preliminary value, which is just inside the stated limits of error of the latter, is partly due to imperfections in our early technique which led to a much greater statistical error, and partly to the corrections which had not then been investigated.

(f) *Comparison with theory.* At the time when Lamb & Retherford's first results were published, a paper by Bethe (1947) appeared, in which he calculated that the interaction between the atom and the radiation field should result in a term shift of the order of magnitude of that which had been observed. Since then, a number of authors, treating this interaction in different ways, have arrived at a more accurate theoretical value for the shift of the  $2S_{\frac{1}{2}}$  term in hydrogen. Kroll & Lamb (1949) quote the value  $1052 \text{ Mc./sec.}$ , while French & Weisskopf (1949) give  $1051 \text{ Mc./sec.}$ , and indicate that Schwinger's new formulation of quantum electrodynamics gives the same results. This theoretical value ( $0.0351 \text{ cm.}^{-1}$ ) agrees fairly closely with Lamb & Retherford's later value, and with our spectroscopic value, though it is slightly below both. In this comparison, we have neglected the extremely small shifts of the P and D terms to which the theory leads.



The theories predict a shift of the term  $3S_{\frac{1}{2}}$  of  $(\frac{2}{3})^3$  times that of the term  $2S_{\frac{1}{2}}$ , i.e. of 0.0104 cm.<sup>-1</sup>. Our present, provisional, measurement of the term  $3S_{\frac{1}{2}}$  would indicate that the shift is less than this.

The authors wish to thank Professor Lord Cherwell for his interest in the work and Professor F. Simon for the supply of liquid hydrogen. The purchase of the large etalon and other optical equipment was made possible by Professor D. A. Jackson's generous benefactions to the Laboratory.

#### REFERENCES

- Bethe, H. A. 1947 *Phys. Rev.* **72**, 339.  
 Dirac, P. A. M. 1928 *Proc. Roy. Soc. A*, **117**, 610 and **118**, 351.  
 Drinkwater, J. W., Richardson, Sir O. & Williams, W. E. 1940 *Proc. Roy. Soc. A*, **174**, 164.  
 Du Mond, J. W. M. & Cohen, E. R. 1949 *Rev. Mod. Phys.* **21**, 651.  
 French, J. B. & Weisskopf, V. F. 1949 *Phys. Rev.* **75**, 1240.  
 Goudsmit, S. & Uhlenbeck, G. E. 1925 *Naturwissenschaften*, **13**, 953.  
 Hansen, G. 1925 *Ann. Phys., Lpz.*, **78**, 558.  
 Heisenberg, W. & Jordan, P. 1926 *Z. Phys.* **37**, 263.  
 Heyden, M. 1937 *Z. Phys.* **106**, 499.  
 Kroll, N. M. & Lamb, W. E. 1949 *Phys. Rev.* **75**, 388.  
 Kuhn, H. & Series, G. W. 1948 *Nature*, **162**, 373.  
 Kupper, A. 1928 *Ann. Phys., Lpz.*, **86**, 511.  
 Lamb, W. E. & Retherford, R. C. 1947 *Phys. Rev.* **72**, 241.  
 Lamb, W. E. & Retherford, R. C. 1949 *Phys. Rev.* **75**, 1325.  
 Mack, J. E. & Barkowsky, E. C. 1942 *Rev. Mod. Phys.* **14**, 82.  
 Minkowski, R. & Bruck, H. 1935 *Z. Phys.* **95**, 299.  
 Ornstein, L. S., Zernicke, F. & Snoek, J. L. 1928 *Z. Phys.* **47**, 627.  
 Pasternack, S. 1938 *Phys. Rev.* **54**, 1113.  
 Pauli, W. 1927 *Z. Phys.* **43**, 601.  
 Sommerfeld, A. 1916 *Ann. Phys., Lpz.*, **51**, 1.  
 Sommerfeld, A. & Unsöld, A. 1926 *Z. Phys.* **36**, 259.  
 Williams, R. C. 1938*a* *Phys. Rev.* **54**, 558.  
 Williams, R. C. 1938*b* *Phys. Rev.* **54**, 568.  
 Williams, W. E. 1942 *Rev. Mod. Phys.* **14**, 94.  
 Wood, R. W. 1921 *Phil. Mag.* **42**, 729.





# The fine structure of the line 4686 Å of singly ionized helium

BY G. W. SERIES

*Clarendon Laboratory, University of Oxford*

(Communicated by H. G. Kuhn, F.R.S.—Received 14 April 1954)

A liquid-hydrogen-cooled discharge tube similar to that formerly used in the investigation of the fine structure of the  $\alpha$ -line of heavy hydrogen has now been used to reduce the Doppler width of the components of the line  $n = 4 \rightarrow n = 3$  in the spectrum of  $\text{He}^+$ . The resolving power necessary to separate some components was obtained without sacrificing spectral range by using two Fabry-Perot etalons in series mounted externally to a prism spectrograph. For other components a single etalon was used. Eight components were resolved and their separations measured, and a ninth partially resolved. The positions of certain band lines of hydrogen and helium which lie close to the  $\text{He}^+$  complex and overlap it in different orders of interference were also measured.

The relative intensities of the components were broadly in agreement with the relative transition probabilities calculated from the Dirac theory, but some anomalies were observed.

From the measurements it is deduced that some of the energy levels are displaced from the positions predicted by the Dirac theory: the  $3S_{\frac{1}{2}}$  level upwards by  $0.140 \pm 0.005 \text{ cm}^{-1}$ , the  $4S_{\frac{1}{2}}$  level upwards by  $0.056 \pm 0.003 \text{ cm}^{-1}$  and the  $4P_{\frac{1}{2}}$  level downwards by  $0.011 \pm 0.003 \text{ cm}^{-1}$ . These displacements of the  $S_{\frac{1}{2}}$  levels are in good agreement with the predictions of the new theory of quantum electrodynamics, but the theory does not predict a displacement of the  $4P_{\frac{1}{2}}$  level by this amount. The Stark effect could account for part of the discrepancy, but there remains a disagreement with the theory which exceeds the estimated experimental error.

## 1. INTRODUCTION

The main features of the fine structure of the line 4686 Å of  $\text{He}^+$ , first resolved by Paschen (1916, 1927), were at that time interpreted with reference to Sommerfeld's theory of the structure of hydrogen-like ions. Dirac's theory (1928), leading to the formula

$$T_{n,j} = -\frac{RZ^2}{n^2} \left[ 1 + \frac{\alpha^2 Z^2}{n} \left( \frac{1}{j + \frac{1}{2}} - \frac{3}{4n} \right) \right], \quad (1)$$

gave the same energy levels but a different ascription of quantum numbers, and allowed one to calculate the relative transition probabilities of the components. Those details of the structure which were resolved by Paschen were well accounted for also by Dirac's theory, but in recent years the microwave observations of Lamb and others (see Triebwasser, Dayhoff & Lamb 1953, and references there given) on the fine structure of hydrogen, and the optical investigations of Kuhn & Series (1950; see also Series 1951; these papers will be called I and II) have shown beyond doubt that Dirac's theory alone cannot account for the positions of the  $2S$ ,  $2P$  and  $3S$  levels in hydrogen and the  $2S$  level in  $\text{He}^+$ . The experiments are in excellent agreement with the new theory of quantum electrodynamics (Salpeter 1953).

It is therefore a matter of interest to attempt to resolve more components in Paschen's line ( $n = 4 \rightarrow n = 3$ ). Improved resolution has been achieved by Kopfermann, Krüger & Öhlmann (1949), by Hirschberg & Mack (1950) and by Murakawa & Suwa (1952). These workers used liquid-air cooling of the discharge to reduce the Doppler width of the lines and Fabry-Perot etalons to obtain the necessary instrumental resolution. The positions of the  $3S$  and  $4S$  levels derived from their measurements agree with the new theory to within the limits of accuracy of the experiments. An attempt will be described here in which we have improved the resolution further by using liquid hydrogen to cool a discharge run at very low current, and two Fabry-Perot etalons in series, where necessary, to take advantage of the reduced Doppler width and yet avoid overlapping of orders (see § 2). Eight components have been resolved and measured and a ninth partly resolved.

## 2. THE EXPERIMENTAL ARRANGEMENT

The apparatus used was a development of that described in I and II for the investigation of the hydrogen  $\alpha$ -line. The light source was a d.c. discharge in a U-tube cooled by liquid hydrogen and run at very low current, usually 15 mA at 300 V, in order to reduce the Doppler width of the lines. It was necessary, however, to take light from within the hollow cathode in order to obtain sufficient intensity in the spark lines. The cathode was a copper tube 5 cm long and 9 mm in diameter which formed part of the wall of the U-tube (see figure 1 in I). Helium at a pressure of  $\frac{1}{4}$  to  $\frac{1}{2}$  mm of mercury continually circulated over cooled charcoal.

The light was analyzed as in the earlier work by Fabry-Perot etalons of 11.5 cm diameter stopped down to 5 cm. Sometimes one was used, sometimes two in series were used, and a large variety of spacers. In preliminary experiments the etalons were mounted internally in a prism spectrograph, and sometimes a third was placed immediately in front of the spectrograph slit. The function of this etalon, which was provided with very small spacers in the form of slips of mica, was to act as a high-order interference filter in suppressing light scattered from very strong arc lines. Light silvering of the etalon plates (transmission about 25 %) enabled the intensity of this scattered light to be reduced by a factor of 20, while light of wave-length 4686 Å was weakened only by a factor of 2. All the components recorded in this work with the exception of (7) could be photographed on Ilford Zenith plates in 10 h using discharge currents of 15 mA and this arrangement of three etalons in series.



The difficulty of scattered light was overcome more successfully by mounting the main etalons externally; the measurements quoted here were all obtained with this arrangement. Some components could be resolved satisfactorily by the use of one etalon, but for others the greatest allowable plate separation which avoided overlapping of orders provided insufficient resolving power. In these cases two etalons were used in series, their spacers being in the ratio 3:1 or sometimes 2:1 (see II, p. 279). The spacers must be so chosen that fringes of the stronger components in suppressed orders, which may appear as weak ghosts, do not fall too close to the components which are being investigated. This condition fixes the choice of spacer within fairly narrow limits for each component, and it is rarely possible in a complicated, wide pattern to measure more than two or three intervals with any given arrangement. Thus, for example, spacers of  $\frac{1}{16}$  and  $\frac{3}{16}$  in. allow the intervals between components (4), (5*a*), (5*b*) and (6) to be measured, but incompletely suppressed fringes of the strong component (1) fall near (3) (see figures 2 and 3).

A further difficulty which appeared in the course of the work was the suspected presence of weak, foreign lines due to molecular hydrogen. In order to investigate this point it was necessary to use a number of spacers whose lengths were fixed to within very small tolerances.

These unusual demands on the sizes of the spacers were largely met by the use of steel roller bearings. The English and metric sizes up to  $\frac{1}{4}$  in. diameter provide a wide range for selection. It is usually not difficult to select three from a batch of a dozen which are equal in diameter to about 1000 Å; the spring pressure provided by the etalon mount allows the necessary adjustment to be made. These spacers were found to be sufficiently stable for exposures of 10 h or more in a room controlled in temperature to  $\frac{1}{5}^{\circ}$  C. When spacers were needed which could not be found among the standard sizes of roller bearings, it was necessary to make them in the laboratory. The technique of making Invar spacers to close tolerances is described in II (p. 278).

The method of adjustment of two etalons mounted inside a prism spectrograph is also described in II (p. 279). When they are mounted externally it is necessary to use a primary slit which can be imaged in the plane of the spectrograph slit. Slight rotation of the suppressor etalon about a vertical axis allows secondary images of the slit, due to secondary reflexions between the etalons, to be displaced from the primary image. The spectrograph slit passes light from the primary image only (figure 1). Phase adjustment of the etalons is made in the usual way by enclosing one of them in a sealed box and varying the pressure of the air in it. In the present work it was necessary to make this adjustment photographically before every run.

The plates of the resolving etalon were silvered to a reflectivity of 85 to 90 % at  $\lambda$  4700 Å; for the suppressing etalon the figure was about 70 %. These plates allowed the weakest components in the complex to be photographed in 12 to 14 h on special photographic plates (M 1246) having fine grain and high sensitivity, prepared and supplied through the courtesy of Mr Waller of Ilford Ltd. When the resolving etalon alone was used the exposure for the same components was 3 to  $3\frac{1}{2}$  h with the same discharge current, 15 mA.

When the interval between a strong and a weak component was to be measured, e.g. (2)–(3), the technique of using a reference mark described in I (p. 132) was used



again. This technique also permitted a check on the stability of the etalons during the long exposures. The use of the double etalon allowed these intervals to be measured in a different way, for it was sometimes possible to measure from a weak component in an unsuppressed order to a strong component in a partly suppressed order on one and the same exposure. This method is open to objection, for the line

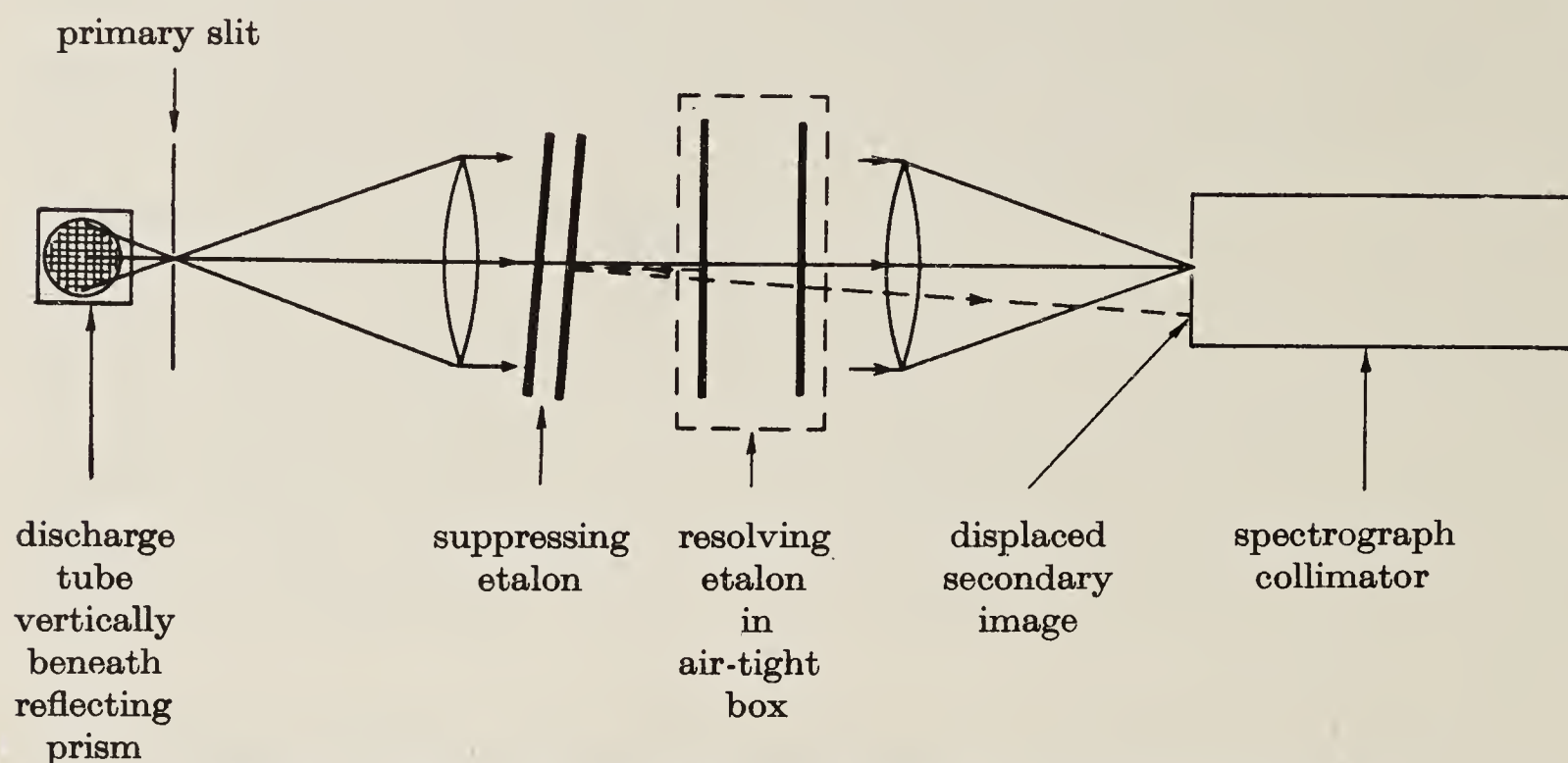


FIGURE 1. External mounting of the double etalon. Horizontal section.

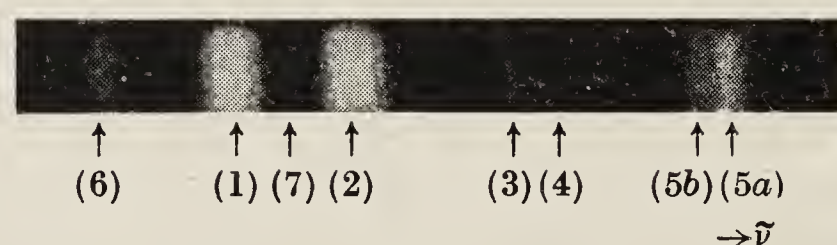


FIGURE 2. Spectrogram showing the fine structure in one order of a double etalon with spacers in the ratio 1:3.

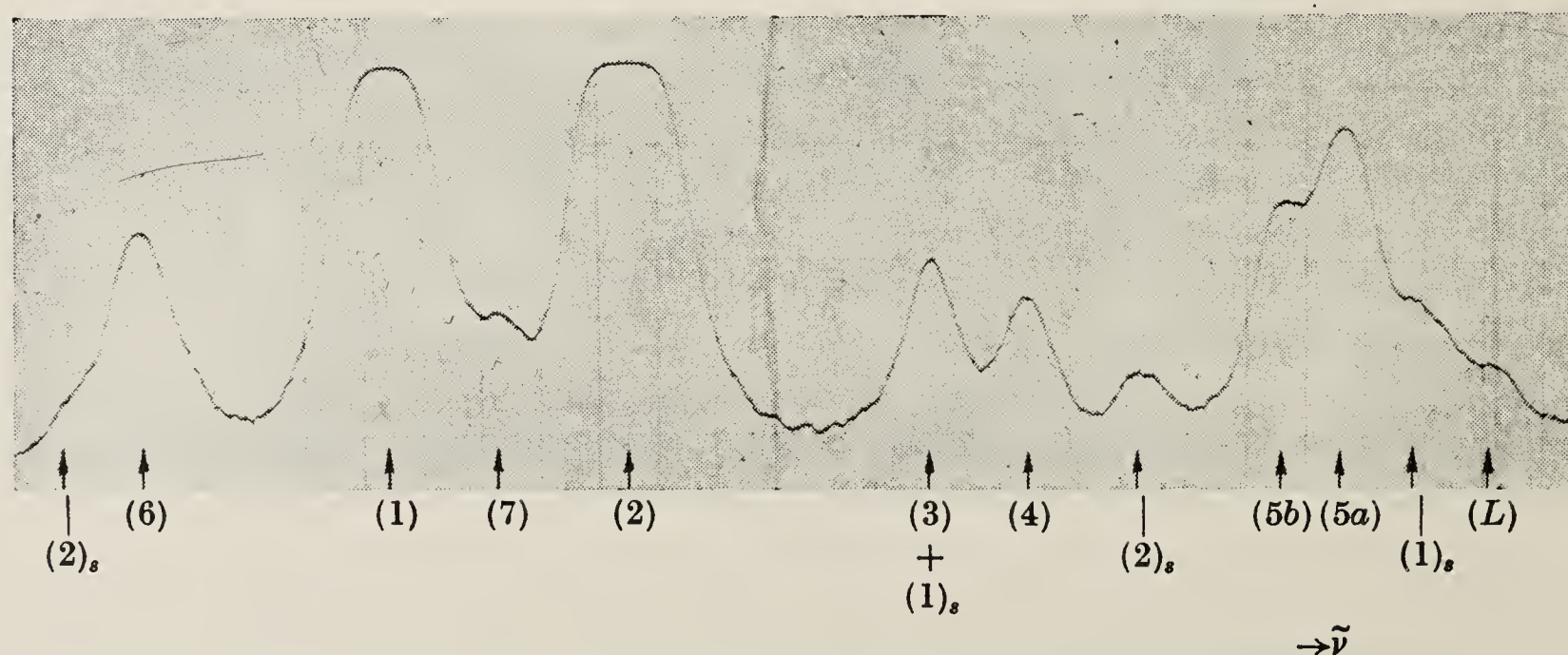


FIGURE 3. Photometer tracing of a spectrogram similar to that of figure 2. Components which appear as fringes of incompletely suppressed orders are marked with the subscript *s*, e.g. (1)<sub>s</sub>. The helium band line identified by Leo is marked (L).



contour of an unsuppressed fringe may differ from that of a suppressed fringe, but it was used occasionally as a check.

Microphotometer tracings were made from some of the plates, but all the measurements were made on the plates themselves.

### 3. MEASUREMENTS

The spectroscopists mentioned in §1 had already achieved partial resolution of the components ( $3P_{\frac{1}{2}}-4D_{\frac{3}{2}}$ ), ( $3S_{\frac{1}{2}}-4P_{\frac{1}{2}}$ ) which, according to the Dirac theory, should coincide. Almost complete resolution was achieved here by using the double etalon with spacers  $\frac{3}{16}$  and  $\frac{1}{16}$  in.; they are labelled (5a) and (5b) in figures 2 and 3. Spectrograms such as figure 2 furnish direct proof of the inadequacy of the Dirac theory. They allow the interval between the components,  $0.139 \text{ cm}^{-1}$ , to be measured to a precision of about 3 % of its value.

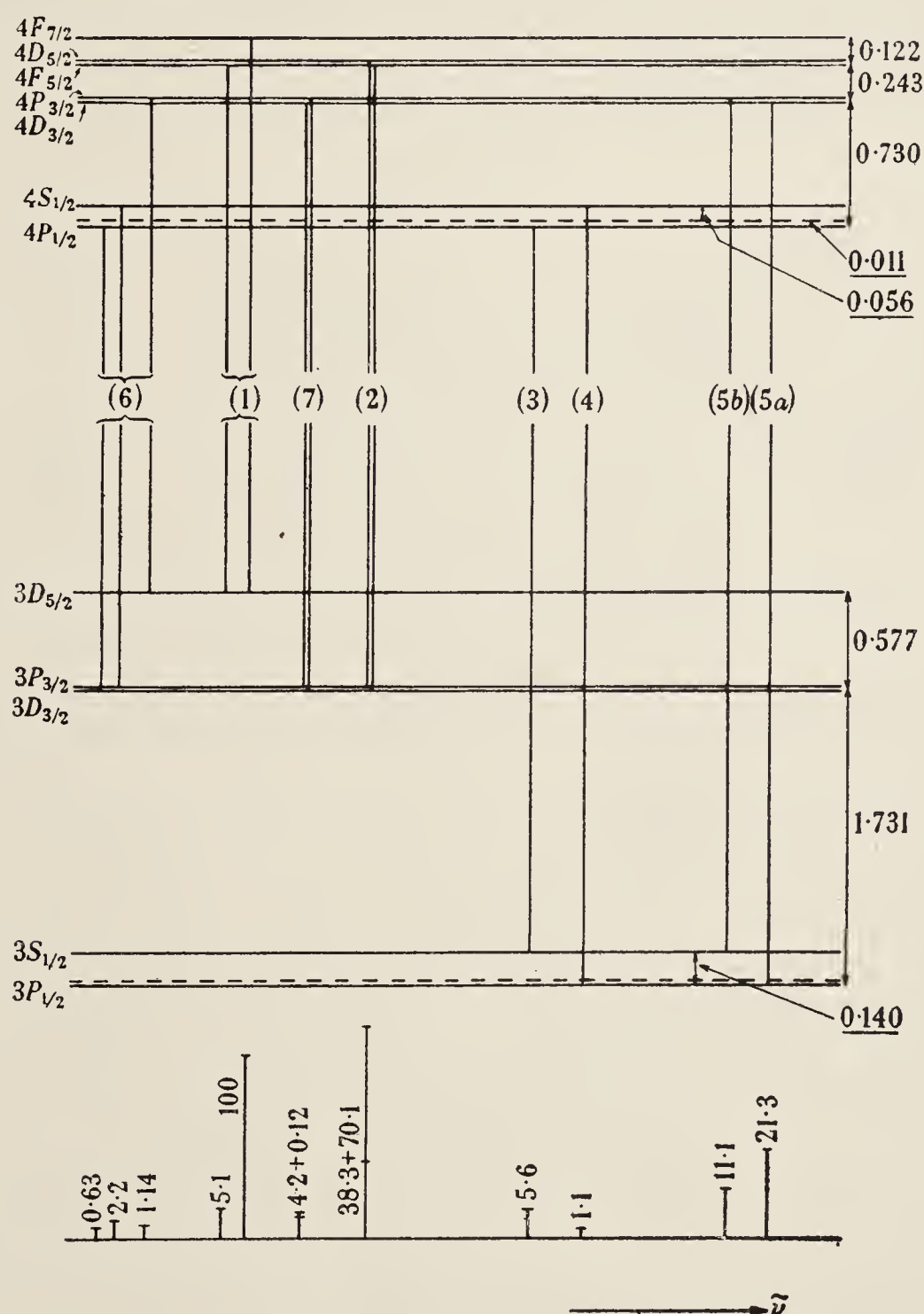


FIGURE 4. Term diagram. Intervals in  $\text{cm}^{-1}$ . The intervals which are not underlined are calculated from the Dirac formula (1), §1 using the latest numerical values of the constants  $R_{\text{H}}$  and  $\alpha$  (Dumond & Cohen 1953). The levels drawn with broken lines are the positions of the  $S_{\frac{1}{2}}$ ,  $P_{\frac{1}{2}}$  levels according to the formula. The intervals which are underlined are displacements deduced from the measurements. The transitions are labelled with relative transition probabilities calculated from the Dirac theory.

TABLE 1. INTERVALS BETWEEN COMPONENTS IN CM<sup>-1</sup>

Table 1A

etalon	interval	mean	no. of fringes	no. of plates
double, 1:3	(5 <i>a</i> )-(5 <i>b</i> ) 0.125*, 0.146, 0.143, 0.144, 0.141, 0.136, 0.141, 0.138	0.139	8	5
wave-number	(5 <i>a</i> )-(4) 0.680*, 0.671, 0.670	0.674	3	2
range in one	(5 <i>a</i> )-(6) 2.411, 2.411, 2.415, 2.406, 2.412, 2.400, 2.412, 2.405	2.409	8	4
order,				
3 × 1.0505 cm <sup>-1</sup>	(5 <i>a</i> )-(7) 1.729*, 1.742, 1.724, 1.723	1.729	4	3
	(5 <i>b</i> )-(4) 0.546*			
	(4)-(6) 1.730*			
	(5 <i>b</i> )-(1)† 1.798*			
	(5 <i>a</i> )-(2)‡ 1.488			
	} used for checks			

The discharge current was usually 10 mA. For values marked \* it was 15 mA.

† Weakly illuminated fringe.

‡ Incompletely suppressed fringe.

Table 1B

etalon	interval	mean	no. of fringes	no. of plates
single 2.004 cm <sup>-1</sup>	(3)-(4) 0.222, 0.204, 0.212, 0.195, 0.212, 0.216, 0.215, 0.205, 0.214, 0.212, 0.212, 0.208, 0.196*, 0.187*, 0.180*, 0.199*, 0.199*	0.205	17	6
hydrogen bands near (3)	(2)-(3) 0.596, 0.601, 0.602, 0.602, 0.615*, 0.603*	0.603	6	3
	(2)-(4) 0.805, 0.803, 0.814, 0.813, 0.818*, 0.817*	0.812	6	3
	(4)-(6) 1.718, 1.748, 1.748, 1.732, 1.733, 1.743, 1.712, 1.732, 1.754, 1.736	1.736	10	5
single 2.004 cm <sup>-1</sup> (circulation through CuO)	(2)-(3) 0.608, 0.600, 0.603, 0.616	0.607	4	2
	(2)-(4) 0.810, 0.818, 0.821, 0.824, 0.807, 0.803	0.814	6	3
single 2.103 cm <sup>-1</sup>	(2)-(3) 0.604, 0.611, 0.609, 0.601	0.606	4	2
hydrogen bands near (3)	(2)-(4) 0.821, 0.830, 0.825, 0.831, 0.818, 0.815, 0.824	0.823	7	3
single 2.040 cm <sup>-1</sup>	(2)-(3) 0.600, 0.602	0.601	2	2
	(2)-(4) 0.803, 0.806	0.805	2	2
hydrogen bands clear of (3) and (4)	(3)-(4) 0.228, 0.226, 0.212, 0.209, 0.191	0.213	5	3
double, 1:2 2 × 1.670 cm <sup>-1</sup>	(2)-(3) 0.599, 0.606, 0.616	0.607	3	2
	(2)-(4) 0.782, 0.799, 0.819	0.800	3	2
	Mean of all plates: (2)-(3):0.605 (2)-(4):0.814 (3)-(4):0.207	} difference 0.209		

The discharge current was usually 15 mA. For values marked \* it was 10 mA.

- Notes. (a) The notes in column 1 refer to the investigations described in §5.
- (b) Values for the interval (3)-(4) are independent of the values for (2)-(3) and (2)-(4). The mean values therefore afford a check on the measurements. The self-consistent intervals (2)-(3), 0.606 cm<sup>-1</sup>; (2)-(4), 0.813 cm<sup>-1</sup>; (3)-(4), 0.207 cm<sup>-1</sup>, are used in the text.
- (c) Values for the interval (4)-(6) show an unusually large scatter, but the mean value 1.736 cm<sup>-1</sup> agrees well with the value 1.735 cm<sup>-1</sup> deduced from table 1A.



Table 1c

etalon	interval	cooling bath	current (mA)		mean	no. of fringes	no. of plates
single, 2.504 cm <sup>-1</sup>	(1)–(2)	liquid air	100	0.452, 0.462, 0.458, 0.456	0.457	4	1
			50	0.455, 0.453, 0.450, 0.455	0.453	4	1
			40	0.449, 0.463, 0.458	0.457	3	1
			30	0.459, 0.447	0.453	2	1
			20	0.462, 0.448, 0.462	0.457	3	1
			15	0.456, 0.455, 0.456	0.456	3	1
			10	0.443, 0.447, 0.455, 0.438, 0.449, 0.456, 0.457	0.449	7	2
single, 2.504 cm <sup>-1</sup>	(1)–(2)	liquid hydrogen	15	0.447, 0.453, 0.450, 0.442, 0.451, 0.452, 0.453, 0.451	0.450	8	2
double, 1:2, 2 × 1.670 cm <sup>-1</sup>	(1)–(2)	liquid air	20	0.451, 0.443, 0.455, 0.449	0.450	4	2
Mean of all fringes: (1)–(2):0.453.							

Mean of all fringes: (1)–(2):0.453.

Table 1D

etalon	interval		mean	no. of fringes	no. of plates	calculated*
double, 1:3, 3 × 0.851 cm <sup>-1</sup>	(5a)–(7)	1.737, 1.739, 1.728, 1.712, 1.728, 1.720, 1.717, 1.710	1.724	8	3	1.729
	(5a)–(3)	0.889, 0.877, 0.882, 0.884, 0.882, 0.874, 0.873	0.880	7	3	0.881
	(5a)–(1)	1.944, 1.944, 1.931, 1.939	1.940†	4	2	1.940

\* Calculated from the mean values of tables 1A to C.

† These distances are measured to a suppressed fringe of (1).

Table 1A records measurements on components (5a) and (5b) and on three other components, (4), (6) and (7), which were resolved in these spectrograms free from incompletely suppressed fringes. The over-exposed components (1) and (2) and the overlapped component (3) were not measured on these plates. They were measured relative to the others and to one another on spectrograms taken with different spacers as indicated in tables 1B to 1D.

The components are interpreted as follows (referring to figure 4):

Component (1) The blend of ( $3D_{\frac{3}{2}}-4F_{\frac{3}{2}}$ ) with ( $3D_{\frac{3}{2}}-4F_{\frac{3}{2}}$ ). These were partly resolved under certain conditions, but the measurements refer to the maximum of the unresolved blend (see §6).

Component (2) The coincident pair ( $3D_{\frac{3}{2}}-4F_{\frac{3}{2}}$ ), ( $3P_{\frac{3}{2}}-4D_{\frac{3}{2}}$ ). No sign of structure was ever observed in (2).

Component (3) ( $3S_{\frac{3}{2}}-4P_{\frac{3}{2}}$ ).

Component (4) ( $3P_{\frac{3}{2}}-4S_{\frac{3}{2}}$ ).

Component (5a) ( $3P_{\frac{3}{2}}-4D_{\frac{3}{2}}$ ).

Component (5b) ( $3S_{\frac{3}{2}}-4P_{\frac{3}{2}}$ ).

Component (6) The blend of ( $3D_{\frac{3}{2}}-4P_{\frac{3}{2}}$ ) and ( $3D_{\frac{3}{2}}-4P_{\frac{3}{2}}$ ) with ( $3P_{\frac{3}{2}}-4S_{\frac{3}{2}}$ ).

Component (7) The coincident pair ( $3P_{\frac{3}{2}}-4D_{\frac{3}{2}}$ ), ( $3D_{\frac{3}{2}}-4P_{\frac{3}{2}}$ ). No sign of structure was ever observed in (7).

The measurements provide a number of cross-checks on the positions of the components. Some of these are shown at the foot of table 1 B and in the fourth and seventh columns of table 1 D. These cross-checks support the estimates of error made in §§7 and 8.

It will be observed that the measurements taken with a single etalon (table 1 B, for example) show a greater scatter than those recorded for double etalons. This reflects the smaller resolving power of the single etalon compared with the double. Nevertheless, the line width of the single etalon was sufficiently small to allow the complete resolution of components (3) and (4).

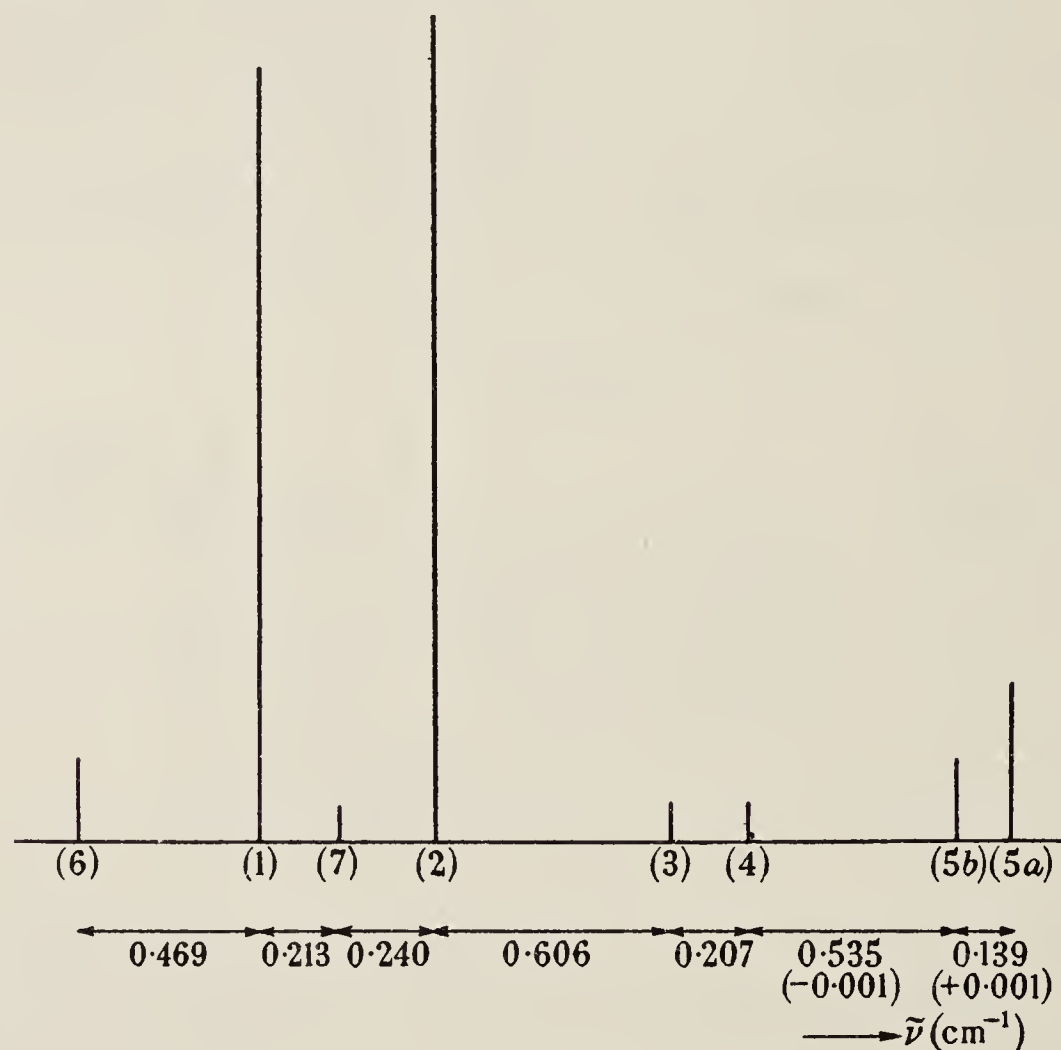


FIGURE 5. Mean values of the intervals between components as deduced from the measurements (see §3). The observed relative intensities are qualitatively indicated by the heights of the lines. The correction (0.001) is shown for component (5b).

For convenience of reference the results are shown diagrammatically in figure 5 in which the intervals were obtained from the mean values of the measurements in the way shown below. It is to be understood that the intervals measured directly are more reliable than those obtained by differences. Thus, for example, the interval (1)–(6) is less reliable than the directly measured interval (4)–(6). The latter is used in §7 when the position of (6) is under discussion.

(5a)–(5b) Table 1 A.

(5b)–(4) (5a)–(4) minus (5a)–(5c) in table 1 A. } Compare (5a)–(3) in table 1 D.

(4)–(3) Table 1 B.

(3)–(2) Table 1 B.

(2)–(7) Mean of (5a)–(7) in tables 1 A and 1 D minus (5a)–(2) above.

(7)–(1) (2)–(1) in table 1 C minus (2)–(7) above.

(1)–(6) (5a)–(6) in table 1 A (compare (4)–(6) in table 1 B) minus (5a)–(1) above.



In the course of the investigation a number of lines due to molecular hydrogen were measured relative to the  $\text{He}^+$  component (1). A line of the band spectrum of helium which falls just outside the  $\text{He}^+$  complex, formerly observed by Paschen (1916) and identified as a band line by Leo (1926) was also observed and measured. This appears to be the line at 4685.318 Å recorded by Curtis & Long (1925). The positions of these lines are given in table 2.

TABLE 2. DISTANCES FROM (1) IN  $\text{cm}^{-1}$  OF FOREIGN LINES

Helium band line: +2.27 (one measurement).

Hydrogen band lines definitely identified: -4.42, +9.03, +24.52.

Hydrogen band lines observed, but not properly resolved from components of  $\text{He}^+$ : +15.76, -19.93.

#### 4. THE INTENSITIES OF THE COMPONENTS

The relative intensities were not measured, but the following conclusions could be drawn from the spectrograms:

(a) Components (1) and (2) were far stronger than any other components. (2) was always slightly stronger than (1).

(b) The intensities of components (5a), (5b), (3) and (7) relative to (1) and to one another were, as far as could be judged, in agreement with the ratios of transition probabilities calculated from the Dirac theory (Kupper 1928; Slack 1928).

(c) Component (4) always appeared as strong as (3), and sometimes a little stronger. It was not possible to relate the variations to any particular feature of the discharge. The intensity of (4) was thus at least five times as great as one would expect from the transition probability.

(d) Component (6) always appeared nearly as strong as (5b). Its intensity was thus approximately five times as great as expected.

It is tempting to associate the anomalous intensities of (4) and (6) with their common upper level,  $4S_{\frac{1}{2}}$ . If, for some reason, this level were overpopulated in the discharge by a factor of 5, then the intensities observed would all be consistent with the transition probabilities calculated from the Dirac theory.

A component which is evidently that which we call (6) appears resolved in the photometer tracing reproduced by Paschen (1927). It appears stronger than the unresolved blend of (3) + (4) and is therefore anomalously strong, as we observed it. On the other hand, Leo also observed this component (1926) and found it to be definitely weaker than (3) + (4). The intensities of the other components observed by these authors in their d.c. discharges are qualitatively in agreement with our observations. In a spectrogram published by Murakawa & Suwa (1952), component (4) appears to be weaker than (3). It appears, therefore, as though the intensities of (4) and (6) may be rather sensitive to the discharge conditions. No information about the intensity of (6) can be obtained from the publications of Kopfermann *et al.* (1949), Hirschberg & Mack (1950) or Murakawa and Suwa (1952).

In this connexion we recall a slight anomaly in the intensity of component (3) (i.e. the blend of  $2P_{\frac{1}{2}}-3S_{\frac{1}{2}}$  with the major constituent  $2S_{\frac{1}{2}}-3P_{\frac{1}{2}}$ ) in the hydrogen  $\alpha$ -line, reported in I, p. 135. The rather wide limits of error in the measurement of



the relative intensities did not certainly indicate a discrepancy with the calculated ratios of transition probabilities, but the measured value was rather high. If the  $3S_{\frac{1}{2}}$  level in the hydrogen discharge had been overpopulated by a factor of about five, the calculated intensity would approach much more closely to the measured value. At the same time, however, the peak of the blend would have been slightly displaced and one would deduce a rather greater value for the shift of the  $2S_{\frac{1}{2}}$  level in hydrogen.

### 5. VALIDITY OF THE MEASUREMENTS

Before we attempt to interpret the measurements in terms of relative positions of energy levels, the results will now be presented of various subsidiary experiments designed to investigate whether the components of the  $\text{He}^+$  complex were being displaced either by foreign lines or by the Stark effect.

#### (a) *Foreign lines*

The possibility of overlapping foreign lines was investigated very fully after an accidental leak of liquid hydrogen from the cooling bath into the discharge in the course of one experiment. When the plate had been developed it was noticed that foreign lines overlapped the line  $4686 \text{ \AA}$ , and these were soon identified as hydrogen band lines. This aroused the suspicion that foreign lines due to molecular hydrogen might be present even under normal conditions, and affecting the measured positions of the helium lines. Hydrogen from tap grease could gain access to the circulating helium; indeed, when the plates were scrutinized it was noticed that  $\text{H}_{\beta}$  appeared faintly on some of them.

A laborious investigation was therefore undertaken to check this point. Hydrogen was deliberately mixed with helium and the positions of the band lines measured relative to the main components of the helium line. Most of the band lines listed by Gale, Monk & Lee (1928) in the neighbourhood were observed and identified by the method of exact fractions. Spacers were then made which would throw the hydrogen band lines clear of the  $\text{He}^+$  components—this was possible since the observed hydrogen lines were not within the helium pattern but several orders away—and these were used to obtain new measurements of the intervals in the helium complex. The positions of components (3) and (4), the weakest resolved components, were particularly investigated.

The interval (2)–(3) proved to be statistically quite insensitive to the choice of spacer although hydrogen band lines, had they been present, would have fallen close to (3) with the spacers indicated in table 1B. The interval (2)–(4) seemed to vary slightly with the spacer, but there was no correlation with the possible presence of a band line near (4). Nor can this fluctuation be correlated with any of the lines recorded in the M.I.T. *Wavelength tables* (1939) of other elements which might have been excited in the discharge (Hg, Cu, Pb), nor with helium band lines. There is no good reason to suppose that it is not a statistical fluctuation.

Finally, some experiments were made in which the circulating gas passed over heated copper oxide before the cooled charcoal. It was hoped by this means to eliminate hydrogen completely from the gas. Traces of  $\text{H}_{\beta}$  still appeared, however,



and it was concluded that tap grease between the charcoal and the discharge was providing hydrogen. The matter was not pursued. The measured intervals remained substantially unaltered in these experiments, and it was concluded, primarily on the basis of the measurements with different spacers, that the suspicions regarding the influence of hydrogen bands had been unjustified.

(b) *The Stark effect*

It is well known that the helium lines are particularly subject to the influence of electric fields. In the present experiments it is necessary to distinguish between the macroscopic fields which sustain the discharge and the microscopic, inter-ionic fields. The former can be estimated but are difficult to change; the latter can be easily changed but are difficult to estimate.

TABLE 3. THE STARK EFFECT. DISPLACEMENTS OF LEVELS  
IN  $\text{cm}^{-1}$  FOR A FIELD OF 150 V/CM

4	$F_{\frac{7}{2}}$	$m_j$		} upwards centre of gravity shift with reference to the transition to $3D_{\frac{3}{2}}$ (component (1)), 0.003
		$\pm \frac{7}{2}$	0	
		$\pm \frac{5}{2}$	+ 0.003	
		$\pm \frac{3}{2}$	+ 0.004	
		$\pm \frac{1}{2}$	+ 0.005	
4	$D, F_{\frac{5}{2}}$	$\pm \frac{5}{2}$	$\pm 0.007$	} symmetrically up and down
		$\pm \frac{3}{2}$	$\pm 0.004$	
		$\pm \frac{1}{2}$	$\pm 0.001$	
4	$P, D_{\frac{3}{2}}$	$\pm \frac{3}{2}$	$\pm 0.013$	} symmetrically up and down
		$\pm \frac{1}{2}$	$\pm 0.004$	
4	$S_{\frac{1}{2}}$	$\pm \frac{1}{2}$	+ 0.009	upwards
4	$P_{\frac{1}{2}}$	$\pm \frac{1}{2}$	− 0.009	downwards
3	$D_{\frac{3}{2}}$	$\pm \frac{5}{2}$	0	
		$\pm \frac{3}{2}$	+ 0.000	
		$\pm \frac{1}{2}$	+ 0.000	
3	$P, D_{\frac{1}{2}}$	$\pm \frac{3}{2}$	$\pm 0.006$	} symmetrically up and down
		$\pm \frac{1}{2}$	$\pm 0.002$	
3	$S_{\frac{1}{2}}$	$\pm \frac{1}{2}$	+ 0.001	upwards
3	$P_{\frac{1}{2}}$	$\pm \frac{1}{2}$	− 0.001	downwards

The theory of the Stark effect enables us to decide which components in the complex are the most sensitive. Various authors have given calculations based on the Dirac term scheme, but we know of no published work which bases the calculations on the modified term scheme. We have therefore performed these calculations and report them in the following paper (Series & Stevens 1954). The numerical results are given in table 3. It turns out that (3) and (4) are the most sensitive components in the complex for displacements which are small compared with the interval ( $4P_{\frac{1}{2}} - 4S_{\frac{1}{2}}$ ), and that (1) is about one-third as sensitive. (2) is relatively insensitive. (5a) and (5b) are about one-ninth as sensitive as (3) and (4). A field of about 150 V/cm would shift (3) and (4) each by  $0.010 \text{ cm}^{-1}$ .

The influence of the microfields may be investigated by changing the current. The size of the cathode in these experiments was such that with the current densities

used it was not completely covered by the discharge. Thus the current, and with it the microfields, could be varied over a considerable range without greatly affecting the voltage, that is, the macrofields.

The consequences of these current variations could most easily be observed on the interval between the strong components (1) and (2), for their resolution is not impaired under the more violent discharge conditions, and liquid-air cooling may be used. A Stark effect would cause the interval to be reduced. Over a range of currents from 10 to 100 mA there was no significant change in this interval (table 1 c). It was concluded that there was no significant Stark effect due to microfields.

On the other hand, it was known that the dark space was about 1 mm and that the discharge was sustained by about 300 V. Using the well-known relation (see, for example, Little & von Engel 1954) that the macroscopic field in the dark space falls linearly, we deduce that the field changes from practically zero at the edge of the glow to 6000 V/cm at the wall. It was therefore quite conceivable that the macroscopic fields would produce a shift in the components, particularly (3) and (4).

Some evidence on this point was provided by experiments in which different parts of the discharge were imaged on the spectrograph slit. This was accomplished in two ways: the first by using lenses of different powers internally in the discharge tube (see figure 1 in I), the second by using a cathode of 23 mm internal diameter instead of the 9 mm normally used. The values  $0.670$ ,  $0.676 \text{ cm}^{-1}$  for the interval (5a)–(4) were obtained in experiments of the former type. Experiments of the latter type were difficult because much larger currents were needed to provide the same current density, and the efficiency of cooling of the gas was impaired, with consequent loss of resolution. For this reason the values  $0.115$  and  $0.122 \text{ cm}^{-1}$  obtained in these experiments for the interval (5a)–(5b) are not reliable, but more confidence can be placed in the values  $0.672$ ,  $0.660$ ,  $0.670 \text{ cm}^{-1}$  for the interval (5a)–(4). These figures may be compared with the mean value of this interval under standard conditions,  $0.674 \text{ cm}^{-1}$ . Now with the wide tube the fringes were formed by light which had come from regions of the discharge far from the walls, that is, away from the region of strong macrofields. Hence one would expect the Stark effect to be reduced. But component (4) moves towards (5a) under a Stark effect, and is one of the most sensitive components. We would expect, therefore, that if (4) were shifted by the Stark effect in the normal discharge, the distance (5a)–(4) would have been increased when the wide tube was used. The observed effect, if real at all, is in the opposite direction. The evidence provided by these experiments, therefore, is that they disclose no trace of Stark effect due to macrofields.

Further remarks on the Stark effect are made in § 8.

## 6. CORRECTIONS AND LINE WIDTHS

With the exception of (5a) and (5b) the resolution of the components was sufficiently complete to avoid the necessity for corrections due to overlapping, but components (1) and (6) are themselves blends and we have to apply small corrections in order to find the positions of their major constituents.

In the case of (5b) the small correction  $0.001 \text{ cm}^{-1}$  to allow for the overlapping of (5a) has been estimated on the basis of a comparison between photometer



tracings and composite Doppler intensity distributions. The comparison enables us to deduce a line width of about  $0.11 \text{ cm}^{-1}$  which, when allowance is made for the instrumental contribution (Minkowski & Bruck 1935), leads to the figure  $110^\circ \text{ K}$  for the temperature of the radiating  $\text{He}^+$  ions in the liquid-hydrogen-cooled discharge at 10 mA. No correction is necessary for (5a) itself.

The minor constituent of (1) was partly resolved under the best conditions of resolution, but the measurements in table 1c represent less favourable conditions. A line width of  $0.16 \text{ cm}^{-1}$ , used in conjunction with the theoretical separation and intensity ratio of the constituents, leads to a correction less than  $0.002 \text{ cm}^{-1}$  for the major constituent.

It is difficult to estimate a reliable correction for component (6) because of the intensity anomaly which, though most probably associated with the level  $4S_{\frac{1}{2}}$ , is not certainly so. If we assume that the constituent ( $3P_{\frac{3}{2}}-4S_{\frac{1}{2}}$ ) is five times too strong and that the other constituents are situated as shown in the term diagram (figure 4), then the line width  $0.16 \text{ cm}^{-1}$  leads to the value  $0.001 \text{ cm}^{-1}$  for the displacement of the maximum of the blend from the position of the major constituent towards shorter wave-lengths.

Component (7) lies almost symmetrically between the much stronger components (1) and (2). It is impossible to estimate a reliable correction, but there is no doubt that it will not be large compared with the statistical errors of measurement.

## 7. INTERPRETATION OF THE MEASUREMENTS

We assume that the term diagram given by the Dirac theory is substantially correct. We then infer from the measurements that some of the energy levels are slightly displaced from the positions predicted by that theory.

On the provisional assumption that the (5a)–(5b) interval is entirely due to the displacement of the  $3S_{\frac{1}{2}}$  or the  $3P_{\frac{1}{2}}$  levels, or both, we arrive at the figure  $(0.139 + 0.001) = 0.140 \text{ cm}^{-1}$  for their separation. But the position of the level  $3P_{\frac{1}{2}}$  relative to  $3P_{\frac{3}{2}}$  may be found from the intervals (5a)–(7) or (4)–(6). These distances,  $1.727$  and  $1.735 \text{ cm}^{-1}$ , when one remembers the small uncertainties associated with components (6) and (7), are very close to the Dirac value  $1.731 \text{ cm}^{-1}$ . We infer that neither  $3P_{\frac{1}{2}}$  nor  $3P_{\frac{3}{2}}$  is appreciably shifted, for it is unlikely that they would both shift by the same amount. Thus the separation between  $3S_{\frac{1}{2}}$  and  $3P_{\frac{1}{2}}$  is interpreted as due to an upward shift of the  $3S_{\frac{1}{2}}$  level.

Again, if we assume that the (5a)–(4) interval,  $0.674 \text{ cm}^{-1}$ , differs from the Dirac value  $0.730 \text{ cm}^{-1}$  solely on account of an upward shift of the  $4S_{\frac{1}{2}}$  level, this must be  $0.056 \text{ cm}^{-1}$ .

The interval (3)–(4) yields information about the relative positions of the  $S_{\frac{1}{2}}$  and  $P_{\frac{1}{2}}$  levels. If neither the  $3P_{\frac{1}{2}}$  nor the  $4P_{\frac{1}{2}}$  level were displaced, the interval (3)–(4) would be the sum of the  $S_{\frac{1}{2}}$  shifts,  $0.140 + 0.056 = 0.196 \text{ cm}^{-1}$ . The measured value is  $0.207 \text{ cm}^{-1}$ . Even an unfavourable combination of errors of measurement would hardly account for the discrepancy. We conclude that either the  $3P_{\frac{1}{2}}$  or the  $4P_{\frac{1}{2}}$  level or both are displaced. The postulate that the  $3P_{\frac{1}{2}}$  level is appreciably displaced is contrary to the reasoning of the last paragraph but one, and would also destroy the agreement between the deduced shift of  $3S_{\frac{1}{2}}$  and the prediction of the theory of



quantum electrodynamics (see §8). On experimental grounds alone it is preferable to postulate that the discrepancy in the (3)–(4) interval is accounted for solely by a downwards displacement of the  $4P_{\frac{1}{2}}$  level. The amount of this displacement is then  $0.207 - (0.140 + 0.056) = 0.011 \text{ cm}^{-1}$ .

There remains component (1) whose distance from (2),  $0.453 \text{ cm}^{-1}$ , compares satisfactorily with the Dirac value  $(0.455 + 0.002) \text{ cm}^{-1}$ , though the measurement is discussed again in §8.

The observations, then, are in good agreement with the Dirac term scheme modified as follows:

- (a) an upward shift of  $3S_{\frac{1}{2}}$  by  $0.140 \pm 0.005 \text{ cm}^{-1}$ ,
- (b) an upward shift of  $4S_{\frac{1}{2}}$  by  $0.056 \pm 0.003 \text{ cm}^{-1}$ ,
- (c) a downward shift of  $4P_{\frac{1}{2}}$  by  $0.011 \pm 0.003 \text{ cm}^{-1}$ .

The figure  $0.005 \text{ cm}^{-1}$  for the error in the  $3S_{\frac{1}{2}}$  level is about 4 times the probable error of the mean of the eight fringes which locate it. Smaller errors are quoted for the other levels since they are determined by measurements on thirty or more fringes.

## 8. COMPARISON WITH THE THEORY OF QUANTUM ELECTRODYNAMICS

The state of the theory at the time of writing is given by Salpeter (1953) and by Baranger, Bethe & Feynman (1953). The calculations to lowest order are based on the formula

$$\Delta_n(P_{\frac{1}{2}} - S_{\frac{1}{2}}) = \frac{8\alpha^3}{3\pi} R \frac{Z^4}{n^3} (B - 2 \ln Z),$$

where  $B$  is a constant which is independent of  $Z$  and is thought to be very insensitive to  $n$ . A number of correction terms increase the value of  $\Delta_2$  for hydrogen by about  $\frac{1}{2} \%$  and lead to excellent agreement with the experimental value. (The latest value is given by Triebwasser *et al.* 1953.) For singly ionized helium the formula (without the correction terms) leads to  $\Delta_3 = 0.137 \text{ cm}^{-1}$  and  $\Delta_4 = 0.058 \text{ cm}^{-1}$ . If one bases the calculation on the value  $14020 \text{ Mc/s}$  obtained experimentally by Lamb & Skinner (1950) for the interval  $\Delta_2$  in  $\text{He}^+$ , and makes use of the relation  $\Delta \propto 1/n^3$ , one finds  $\Delta_3 = 0.139 \text{ cm}^{-1}$  and  $\Delta_4 = 0.058 \text{ cm}^{-1}$ . The predicted shifts for the  $P_{\frac{1}{2}}$  levels alone are very small; we calculate  $0.002 \text{ cm}^{-1}$  for  $3P_{\frac{1}{2}}$  and  $0.001 \text{ cm}^{-1}$  for  $4P_{\frac{1}{2}}$ .

The present measurements are in excellent agreement with the theory for the  $3S_{\frac{1}{2}}$  and  $4S_{\frac{1}{2}}$  levels.

In the case of the  $4P_{\frac{1}{2}}$  level, the disagreement exceeds the estimated experimental error and demands further discussion. We shall consider first the accuracy of the measurements from which we deduce its position, and secondly the possibility of displacement of levels by the Stark effect.

The most direct route to the establishment of its position is from the interval  $4P_{\frac{1}{2}} - (4P_{\frac{3}{2}}, 4D_{\frac{3}{2}})$  which is equal to the difference  $\{(5a) - (3)\} - \{(5a) - (5b) + \text{correction}\}$ . The two distances here measured (see tables 1D and 1A) rely on seven and eight individual values respectively, and in each case the probable error of the mean is less than  $0.002 \text{ cm}^{-1}$ . The Dirac value for this interval,  $0.730 \text{ cm}^{-1}$ , differs from the mean measured value  $0.880 - (0.139 + 0.001) = 0.740 \text{ cm}^{-1}$  by  $0.010 \text{ cm}^{-1}$ , which is



rather large to be attributed to a statistical deviation. We suggest that this difference implies a downward displacement of  $4P_{\frac{1}{2}}$ .

An independent but less direct determination of the position of  $4P_{\frac{1}{2}}$  is from the measurement of the distance (2)–(3) for which the mean value  $0.605 \text{ cm}^{-1}$  (table 1B) depends on nineteen individual measurements with a probable error  $0.0009 \text{ cm}^{-1}$ . If we use the experimental value for the displacement of the  $3S_{\frac{1}{2}}$  level, and assume that the levels associated with component (2) are undisplaced, then we arrive at the value  $(1.731 - 0.140 - 0.730 - y - 0.243) = 0.618 - y \text{ cm}^{-1}$  for the distance (2)–(3), where  $y$  is the downward displacement of the  $4P_{\frac{1}{2}}$  level. Comparison with the measurement yields  $y = 0.013 \text{ cm}^{-1}$ . The use of the theoretical value  $(0.138 - 0.002) \text{ cm}^{-1}$  for the displacement of the  $3S_{\frac{1}{2}}$  level yields  $y = 0.009 \text{ cm}^{-1}$ , a figure which is ten times the probable error of the measurements from which it is obtained.

These two determinations of the position of the level  $4P_{\frac{1}{2}}$  depend essentially on the location of component (3). The statistical error in the measurements which locate (3) is reduced by taking the two determinations together, and by considering also the other checks on the position of (3), e.g.  $(5a) - (3) = \{(5a) - (4)\} + \{(4) - (3)\}$ . The estimated error  $0.003 \text{ cm}^{-1}$  is about 4 times the probable error of 30 distance measurements.

It is therefore very improbable that the discrepancy with theory in the position of the level  $4P_{\frac{1}{2}}$  is to be explained by statistical deviations in the measurements. There are, however, some indications that part of the discrepancy might be explained by a Stark effect in spite of the evidence discussed in §5. We recall that the levels  $4S_{\frac{1}{2}}$  and  $4P_{\frac{1}{2}}$  are the most sensitive levels (table 3) and that (3) and (4) are the most sensitive components. In table 1B the distance (3)–(4) measured with the use of the spacer  $2.004 \text{ cm}^{-1}$  shows signs of a systematic dependence on the current, the values at 10 mA being somewhat lower than those at 15 mA (though this is not supported by the plate on which the distances (2)–(3) and (2)–(4) were measured at 10 mA). Again, though the interval (1)–(2) (table 1C) shows no systematic dependence on current up to 100 mA, it may be significant that the mean value of this interval,  $0.453 \text{ cm}^{-1}$ , is slightly lower than the theoretical value  $0.457 \text{ cm}^{-1}$ , as it would be if there were a small Stark effect. One might also suggest that the intensity anomaly observed in components (4) and (6) might be due to a Stark effect, but since the observed intensities of (3) and (4) are nearly equal, any Stark effect which accounts for the anomaly must at the same time introduce a displacement of  $4S_{\frac{1}{2}}$  and  $4P_{\frac{1}{2}}$  which is at least of the order of magnitude of the unperturbed distance between them. This is quite out of the question.

If there were a Stark effect which increased the separation between (3) and (4) by  $0.010 \text{ cm}^{-1}$ , then this would be made up by the levels  $4S_{\frac{1}{2}}$  and  $4P_{\frac{1}{2}}$  in equal amounts, i.e. by  $0.005 \text{ cm}^{-1}$  each, since the  $3S_{\frac{1}{2}}$  and  $3P_{\frac{1}{2}}$  levels are very insensitive. There would remain a discrepancy with theory of  $0.006 \text{ cm}^{-1}$  for the  $4P_{\frac{1}{2}}$  level, and a discrepancy of  $0.007 \text{ cm}^{-1}$  instead of  $0.002 \text{ cm}^{-1}$  would be introduced for the  $4S_{\frac{1}{2}}$  level. A greater Stark effect might improve the agreement for the  $4P_{\frac{1}{2}}$  level, but would impair it still more for the  $4S_{\frac{1}{2}}$ . The discrepancy remains rather large even when distributed between the two levels in the most favourable way.

We conclude that there is a real discrepancy between the theory and the measurement, and that although the presence of a small Stark effect would improve the agreement, a discrepancy of about six times the probable error of the measurements still remains.

I gratefully express my appreciation of the interest of Dr H. G. Kuhn, F.R.S., in this work at all its stages, and of his constant encouragement. I am indebted to Professor F. E. Simon, F.R.S., for making available the liquid hydrogen, and to Lord Cherwell, F.R.S., for the facilities of the laboratory. Part of the work was done during the tenure of a Nuffield Fellowship.

#### REFERENCES

- Baranger, M., Bethe, H. A. & Feynman, R. P. 1953 *Phys. Rev.* **92**, 482.  
 Curtis, W. E. & Long, R. C. 1925 *Proc. Roy. Soc. A*, **108**, 513.  
 Dirac, P. A. M. 1928 *Proc. Roy. Soc. A*, **117**, 610; **118**, 351.  
 Dumond, J. W. M. & Cohen, E. R. 1953 *Rev. Mod. Phys.* **25**, 691.  
 Gale, H. G., Monk, G. S. & Lee, K. O. 1928 *Astrophys. J.* **67**, 89.  
 Hirschberg, J. G. & Mack, J. E. 1950 *Phys. Rev.* **77**, 745.  
 Kopfermann, H., Krüger, H. & Öhlmann, H. 1949 *Z. Phys.* **126**, 760.  
 Kuhn, H. & Series, G. W. 1950 *Proc. Roy. Soc. A*, **202**, 127 (called 'I').  
 Kupper, A. 1928 *Ann. Phys., Lpz.*, **86**, 511.  
 Lamb, W. E. & Skinner, M. 1950 *Phys. Rev.* **78**, 539.  
 Leo, W. 1926 *Ann. Phys., Lpz.*, **81**, 757.  
 Little, P. F. & von Engel, A. 1954 *Proc. Roy. Soc. A*, **224**, 209.  
 Minkowski, R. & Bruck, H. 1935 *Z. Phys.* **95**, 299.  
 M.I.T. 1939 *Wave-length tables*. New York: Wiley.  
 Murakawa, K. & Suwa, S. 1952 *J. Phys. Soc. Jap.* **7**, 467.  
 Paschen, F. 1916 *Ann. Phys., Lpz.*, **50**, 901.  
 Paschen, F. 1927 *Ann. Phys., Lpz.*, **82**, 689.  
 Salpeter, E. E. 1953 *Phys. Rev.* **89**, 92.  
 Series, G. W. 1951 *Proc. Roy. Soc. A*, **208**, 277 (called 'II').  
 Series, G. W. & Stevens, K. W. H. 1954 *Proc. Roy. Soc. A*, **226**, 393.  
 Slack, F. G. 1928 *Phys. Rev.* **31**, 527.  
 Triebwasser, S., Dayhoff, E. S. & Lamb, W. E. 1953 *Phys. Rev.* **89**, 98.



*Sci. Am.* (1979) **240**, 94-110

# The Spectrum of Atomic Hydrogen

by Theodor W. Hänsch, Arthur L. Schawlow and George W. Series

**SCIENTIFIC  
AMERICAN**

MARCH 1979

VOL 240, NO. 3 PP 94—110



PUBLISHED BY **W. H. FREEMAN AND COMPANY** 660 MARKET STREET, SAN FRANCISCO, CALIFORNIA 94104

Copyright © 1979 by Scientific American, Inc. All rights reserved. Printed in the U.S.A. No part of this offprint may be reproduced by any mechanical, photographic or electronic process, or in the form of a phonographic recording, nor may it be stored in a retrieval system, transmitted or otherwise copied for public or private use without written permission of the publisher. The trademark and tradename "SCIENTIFIC AMERICAN" and the distinctive logo-type pertaining thereto are the sole property of and are registered under the name of, and are used herein under license from, Scientific American, Inc.

# The Spectrum of Atomic Hydrogen

*For almost a century light emitted by the simplest of atoms has been the chief experimental basis for theories of the structure of matter. Exploration of the hydrogen spectrum continues, now aided by lasers*

by Theodor W. Hänsch, Arthur L. Schawlow and George W. Series

The spectrum of the hydrogen atom has proved to be the Rosetta stone of modern physics. Once this pattern of lines had been deciphered much else could also be understood. Most notably, it was largely the effort to explain the spectrum of light emitted by the hydrogen atom that inspired the laws of quantum mechanics. Those laws have since been found to apply not only to the hydrogen atom but also to other atoms, to molecules and to matter in bulk. They are the ultimate foundation of modern chemistry, of solid-state physics and even of applied sciences such as electronics.

The central position of the hydrogen atom in the history of 20th-century physics might seem to suggest that the spectrum has long been known in all its details. That is not so. Only in the past few years have some of the subtler features of the spectrum been resolved, and many others have not yet been observed directly. Measuring the positions of the spectral lines remains today a significant test of the predictions of the quantum theory.

The most recent advances in the analysis of the spectrum can be attributed to a new tool of spectroscopy: the laser. Because the finest details of the spectrum are closely spaced they can be distinguished only by light that is highly monochromatic, or confined to a narrow range of wavelengths. The laser is a source of such light. As a result of some ingenious laboratory technology it has become a spectroscopic instrument of unprecedented resolution.

## The Line Spectrum

When light from a hot filament is dispersed according to wavelength by a prism or a diffraction grating, the result is a continuous fan of colors, but the spectrum from a pure, rarefied gas of atoms or molecules consists of discrete lines. If the spectrum is recorded from light emitted by the gas, it appears as a sequence of bright lines against a dark background. If light is passed through the gas, discrete wavelengths are ab-

sorbed, giving rise to dark lines on a bright background.

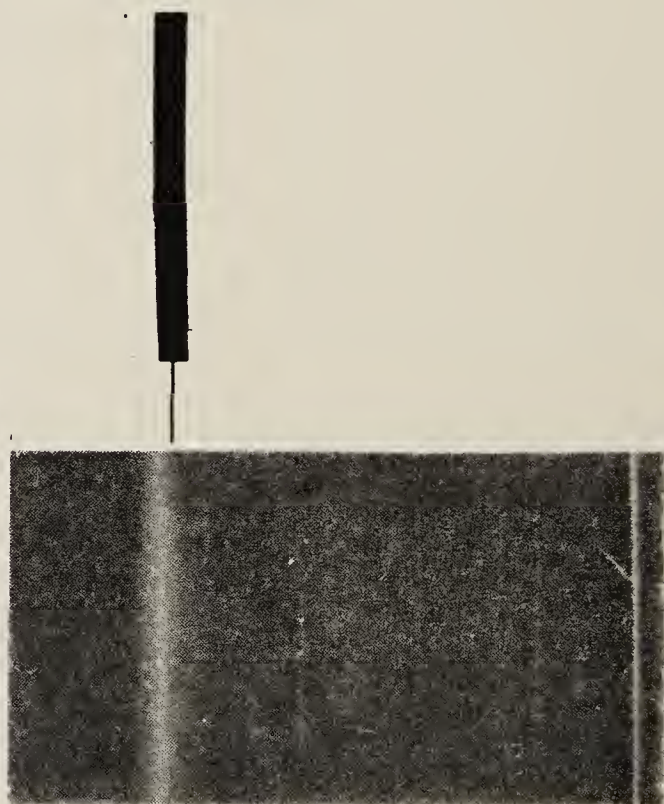
Hydrogen is the simplest of atoms, being made up of a single electron and a nucleus that consists of a single proton, and so it can be expected to have the simplest spectrum. The spectrum is not, however, an easy one to record. The most prominent line was detected in 1853 by Anders Jonas Ångström. (The common unit for measuring wavelengths of light is named for Ångström; one angstrom unit is equal to  $10^{-8}$  centimeter.) In the next two decades three more lines were observed, but the first extended series of atomic-hydrogen lines was found not in the laboratory but in the spectra of stars. In 1881, working with the first photographs of stellar spectra, Sir William Huggins identified 10 lines as being emissions of atomic hydrogen.

It may seem surprising that lines of the hydrogen spectrum were seen in astronomical observations before they were seen in terrestrial experiments. The difficulty in measuring the spectrum in the laboratory is not in detecting the lines but in preparing pure atomic hydrogen. Ordinary hydrogen gas consists of diatomic molecules ( $H_2$ ), which have a spectrum that is much more complicated than the spectrum of the isolated hydrogen atom. Splitting the molecules requires more energy than can be supplied by most thermal excitations, such as a flame. One device that furnishes the energy very effectively is the gas-discharge tube, where electrons accelerated by an applied voltage dissociate the molecules. Over the years means have been discovered for enhancing the atomic spectrum and suppressing the molecular one.

The spectral lines detected by Huggins range in wavelength from the red portion of the visible spectrum to the near ultraviolet. The first two lines are quite far apart, but the subsequent ones come at smoothly decreasing intervals, and those at the shortest wavelengths are bunched closely together. In 1885, working from the astronomical measurements, Johann Jakob Balmer found

that he could account for the positions of all the known lines by applying a simple empirical formula. The entire set of lines has since come to be known as the Balmer series. Another group of lines, the Lyman series, lies in the far ultraviolet, and there are other series at longer wavelengths. Within each series the individual lines are designated by Greek letters, starting with the line of longest wavelength. Thus the bright red line first seen by Ångström is the Balmer-alpha line, the next is the Balmer-beta line and so on. Because of the prominence of the Balmer-alpha line it is sometimes called

BALMER-ALPHA  
6,563



PATTERN OF DISTINCT LINES is formed when the light emitted by hydrogen atoms is dispersed according to wavelength. The lines are those of the Balmer series, and their approximate wavelengths are given in angstrom units (one angstrom is equal to  $10^{-8}$  centimeter). The color photograph was made by Jon Brenneis and one of the authors (Schawlow)



simply the hydrogen-alpha, or H-alpha, line.

In 1889 Johannes Rydberg discovered that the line spectra of many elements, most notably those of the alkali metals, could be fitted by a single empirical formula. A later version of the formula, which is equivalent to Rydberg's equation but more explicit, has the form

$$\frac{1}{\lambda} = R \left[ \frac{1}{(m+b)^2} - \frac{1}{(n+c)^2} \right]$$

Here  $\lambda$  (the Greek letter lambda) is the wavelength of a particular line in an atomic spectrum,  $m$  and  $n$  are numbers that take on successive integer values (1, 2, 3 and so on) and  $R$ ,  $b$  and  $c$  are constants. The values of  $b$  and  $c$  depend on what series of lines is being measured, but  $R$  is the same for all lines of all the elements.  $R$  is now called the Rydberg constant; if the wavelength is expressed in meters,  $R$  has the value  $1.097 \times 10^7$  and the dimensions of reciprocal meters. After Rydberg had checked his formula against a number of spectra he wrote: "I had just finished testing various forms of the function when I heard of Mr. Balmer's communication on the spectral lines of atomic hydrogen. I was delighted to find that his formula is a special case of mine, with the same value of  $R$ , and with  $c = 0$ ." Hence for the

hydrogen atom the equation has a simpler form.

$$\frac{1}{\lambda} = R \left[ \frac{1}{m^2} - \frac{1}{n^2} \right]$$

When the appropriate values of  $m$  and  $n$  are substituted in this formula, it yields the wavelengths of all the lines in the hydrogen spectrum.

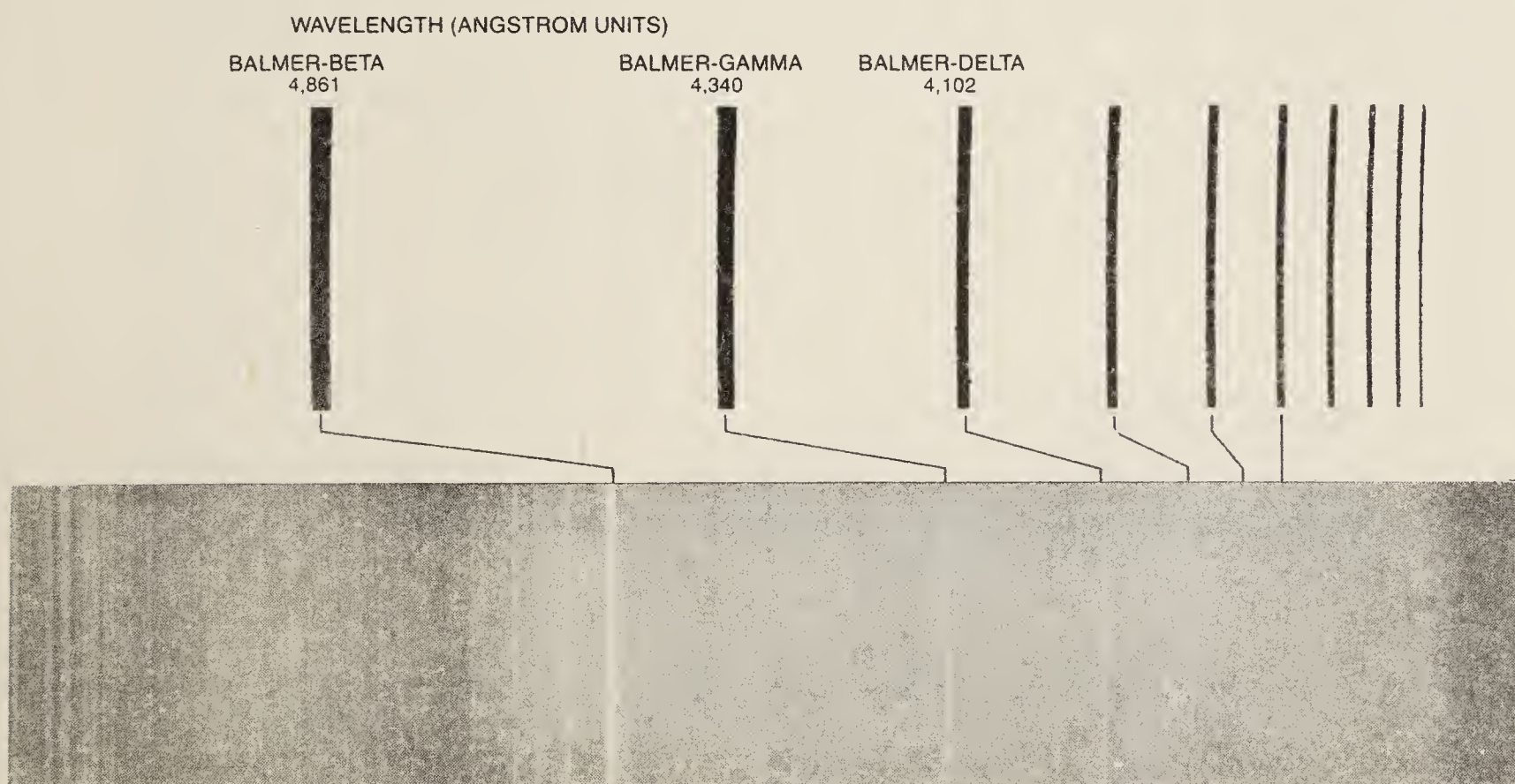
#### Atomic Structure

In 1912 Niels Bohr spent most of the year at the University of Manchester working in the laboratory of Ernest Rutherford, who had just made a vital contribution to the understanding of atomic structure. By then the Balmer and the Rydberg formulas were well known to spectroscopists, and they had been thoroughly tested, but Bohr had never heard of either of them. When he was told of Balmer's equation, he was able to derive it almost immediately from the properties of the hydrogen atom. Abraham Pais and T. D. Lee have reported that Bohr was asked late in his life how he could have escaped knowing of the Balmer formula. He explained that in those days most physicists regarded atomic spectra as being so complicated they were hardly a part of fundamental physics. They were thought

of, he said, as being like the notes of a piano, whose tones depend in a complicated way on the structure of the instrument as a whole.

The reference to musical notes was not an idle one. In the 19th century many investigators had speculated that the light emitted by atoms might be understood by some analogy to the modes of vibration of a solid body. The presence of multiple lines in each series could then be explained by assuming that the first line was the fundamental mode and the rest were overtones, or harmonics. No optical spectrum could be resolved into a fundamental frequency and its overtones, however, and so more direct examination of the atom itself was undertaken.

Rutherford's contribution was the demonstration that the atom is not a solid body but rather consists of a small, dense, positively charged nucleus and the requisite number of negatively charged electrons to form a stable and electrically neutral system. Bohr undertook to explain the spectra of atoms in the context of this model. In doing so he risked the ridicule of his contemporaries by hypothesizing that within the atom the established laws of physics do not apply. Those laws predicted that any bound electron would radiate away all its energy and fall into the nucleus. Bohr



in the latter's laboratory at Stanford University. The black-and-white spectrum was recorded in 1927 by Gerhard Herzberg, who was then at the Darmstadt Technical University in Germany. The intervals between the lines are different in the two photographs because Brenneis and Schawlow dispersed the light with a diffraction grating, whereas Herzberg employed a prism; the prism introduces a distortion because the refractive index of glass is a nonlinear function of wavelength. In both cases the source of the spectrum was a gas-dis-

charge tube in which hydrogen molecules ( $H_2$ ) are dissociated into atoms by an electric potential. In the color photograph the yellow and green bands and the continuous blue background at the right are not part of the atomic-hydrogen spectrum but result from molecular contaminants in the discharge tube. Herzberg eliminated such contamination by cooling the tube in liquid nitrogen. Lines to the right of Balmer-delta, which appear white or light blue in the color photograph, are actually in the ultraviolet region of the electromagnetic spectrum.



is exceptionally troublesome for hydrogen, whose atoms are lighter than any others and therefore move faster. At room temperature the fractional line width is about 12 parts per million. The speed of the atoms, and hence the line width, is proportional to the square root of the absolute temperature. The line width can be reduced by a factor of three or four by cooling the hydrogen discharge lamp from room temperature (300 degrees Kelvin) to the temperature of liquid hydrogen (20 degrees K).

### The Lamb Shift

In the 1930's several investigators tried to resolve the fine structure of hydrogen more completely in order to test the predictions of the Dirac theory. By then it was possible to examine the spectrum of deuterium, the hydrogen isotope with a mass twice that of ordinary hydrogen. The width of a spectral line varies inversely as the square root of the atomic mass, and so the width is reduced in a deuterium spectrum by a factor of about 1.4. Even so, no additional components of the Balmer-alpha line were resolved, and the third component was still not completely separated from its stronger neighbor.

In the course of these investigations, however, some observers reported small discrepancies between the measured spectra and the predictions of the Dirac theory. Of particular interest was the pair of fine-structure levels  $2S_{1/2}$  and  $2P_{1/2}$ . These levels differ in orbital angular momentum and therefore in the average geometrical distribution of the electron, but they have the same total angular momentum and the Dirac theory predicts they should lie at the same energy. Thus although they are distinct

states, they should not give rise to any splitting in the spectrum. Simon Pasternack interpreted experiments carried out by Robley C. Williams and by William V. Houston and his colleagues as showing that the  $2S_{1/2}$  and  $2P_{1/2}$  levels do not exactly coincide. Others, however, disagreed.

The question was settled in 1947 in a brilliant experiment conducted by Willis E. Lamb, Jr. and Robert C. Retherford. They found that the  $2S_{1/2}$  level was shifted upward with respect to the  $2P_{1/2}$  level by about 1,060 megahertz, or millions of cycles per second. Compared with the frequency of the Balmer-alpha line, which is about 450,000 gigahertz (billions of cycles per second), that is a shift in the position of the  $2S_{1/2}$  component by a factor of little more than two parts per million.

Lamb and Retherford did not attempt to resolve the two components in the optical spectrum. Instead they employed radio-frequency energy to stimulate a direct transition between the  $2P_{1/2}$  and the  $2S_{1/2}$  levels. The frequency of the radio waves is 500,000 times lower than the frequency of the Balmer-alpha line; since the Doppler broadening of the line is reduced by the same factor, it could be neglected entirely. This small splitting of the energy levels is now called the Lamb shift.

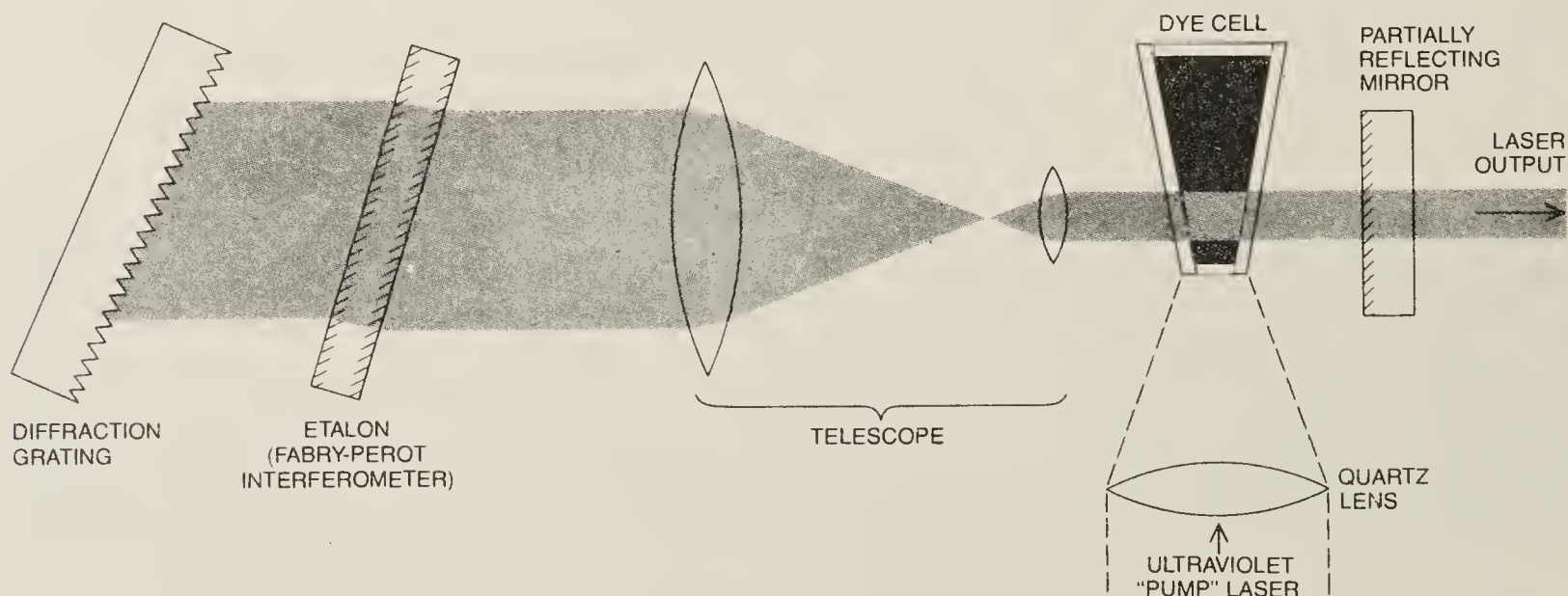
The need to supply an explanation for the Lamb shift inspired another fundamental revision of physical theory, introduced by Richard P. Feynman, Julian Schwinger and Sin-itiro Tomonaga. Their point of departure was the novel idea that the electrons observed in experiments may differ in certain properties, such as mass and charge, from the hypothetical "bare" electron that is imagined to exist in an empty universe.

This difference, which had previously been ignored, can alter the properties of an electron in a bound system. The theory that results from these ideas is called quantum electrodynamics.

In quantum electrodynamics the Lamb shift arises from an interaction between the electron and "zero-point fluctuations" of the electromagnetic field. Such fluctuations, which are always present, cause the electron to jitter about, so that it perceives the nucleus as being somewhat smeared out in space. The result is a seeming alteration of the force between the two particles when they are close together. Because the electron spends more time near the nucleus in the  $S$  state than it does in the  $P$  state, the energy of the  $S$  state is slightly increased.

This model of the hydrogen atom has a further complication. If the electron is regarded as a pointlike particle, it can respond to fluctuations of infinitely high frequency, which have infinite energy. The infinities are avoided, and so is the need to answer questions about the size and structure of the electron, by comparing an electron bound in an atom with a hypothetical bare electron. The small measured energy is found by subtraction. Such calculations are complex, but the predictions of the theory are exceedingly accurate. Indeed, quantum electrodynamics is the most precise theory ever devised, and no discrepancies with experiment have been found.

The fine-structure splitting of various energy levels of the hydrogen atom has been revealed in considerable detail through measurements at radio frequencies. At the same time improved spectroscopic methods have led to precise determinations of the Rydberg constant from measurements of the wavelength



**DYE LASER** emits light that can be confined to a narrow range of wavelengths but can also be tuned over a broad range. The laser medium is a fluorescent dye that emits light with a wide and essentially continuous spectrum when the dye is "pumped" by another laser. From this broad emission band a much narrower interval of wavelengths is selected for amplification by an optical cavity that is tuned to resonate at a particular frequency. Coarse tuning is provided by

a diffraction grating, which disperses the light so that only selected wavelengths are reflected back into the dye cell. An etalon further narrows the bandwidth by passing only those wavelengths that interfere constructively during many internal reflections. A telescope in the cavity spreads the beam so that many grooves of the grating are illuminated. The monochromatic but tunable light has been employed in spectroscopic measurements that eliminate Doppler broadening.



of one component of the Balmer-alpha line. Bryan P. Kibble, William R. C. Rowley, Raymond E. Shawyer and one of us (Series) employed a light source cooled in liquid helium to determine the Rydberg constant to a precision of better than one part in 10 million. Even the Lamb shift was observed in 1948 by one of us (Series), and similar shifts were measured in ionized helium by one of us (Series), by Gerhard Herzberg and by Frederick L. Roesler. The accuracy of the optical experiments, however, does not approach that of the radio-frequency methods.

### Width of Spectral Lines

Although these experiments have been highly successful, the hydrogen atom is such a fundamental testing ground for the laws of physics that it is important to probe deeper as new techniques become available. For now the most promising approach is to improve the resolution of measured spectra; it is resolution that limits the sharpness of observed spectral lines and thereby limits the precision with which their wavelengths can be determined.

The earliest spectroscopic studies of atoms were limited by the resolution of the instrument itself, which was simply a prism or a diffraction grating, a glass plate ruled with many closely spaced lines. The grating has the effect of dispersing light by reflecting different wavelengths through different angles. If the entire visible spectrum is dispersed through, say, 15 degrees, then some components of the Balmer-alpha line might be separated by less than .05 second of arc.

With the application of interferometers to the examination of spectral lines the intrinsic instrumental limitation was removed. The interferometer invented by Michelson and another type devised by the French opticians Charles Fabry and Alfred Perot are sensitive instruments for comparing two wavelengths. They are capable of distinguishing two sharp peaks that differ in frequency by one gigahertz or less. Interferometers fail to fully separate the several components of the Balmer lines not because the instruments are inadequate but because the components themselves are not sharp. Each component is distributed over a range of wavelengths that is often greater than the spacing between the components.

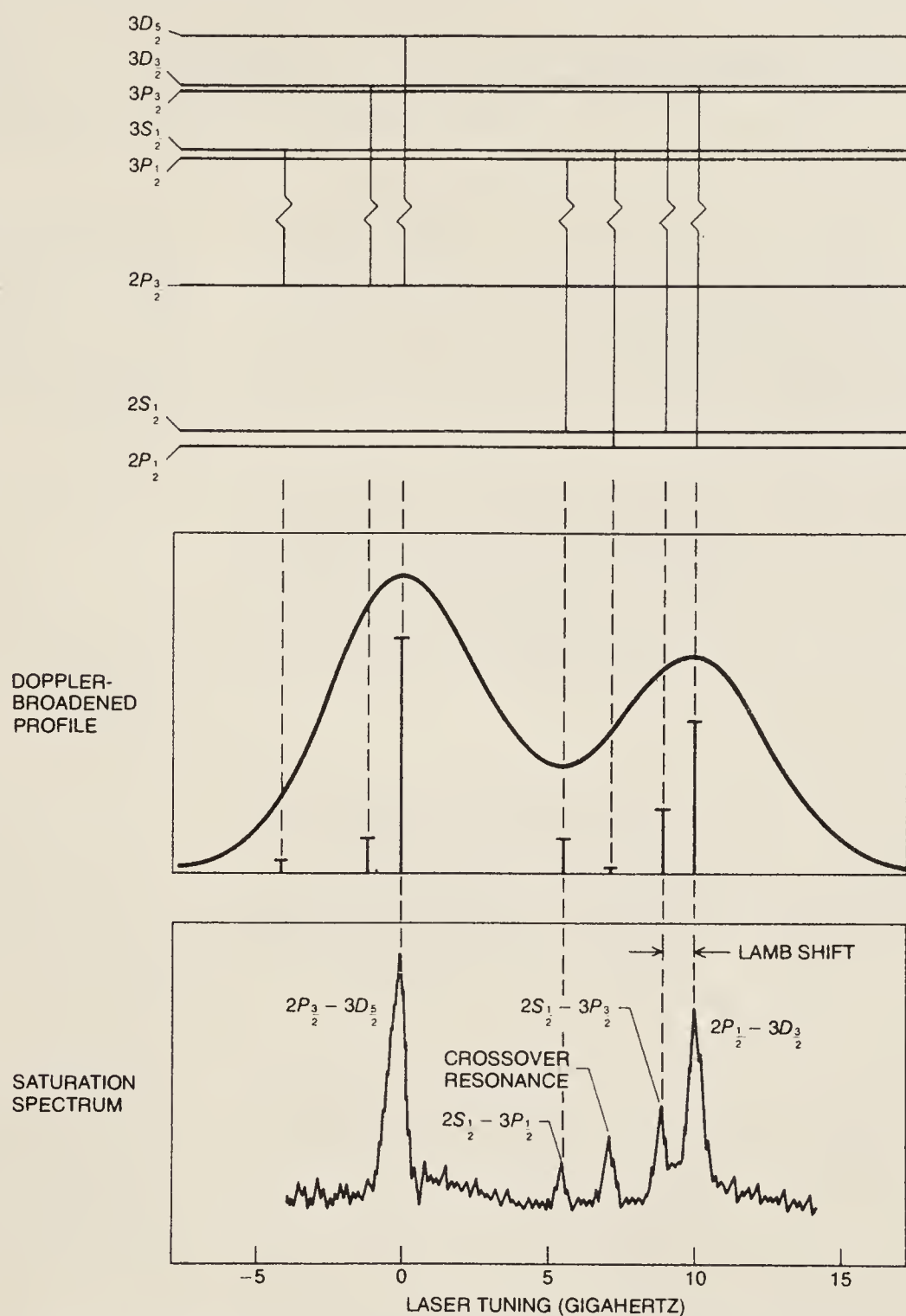
A part of the broadening is the "natural" width of the spectral line. Even under the best possible circumstances of observation no component of a spectrum can ever be absolutely monochromatic. This limitation stems from the fact that the "stationary states" of an atom are not truly stationary. Atoms do, in fact, radiate energy after a finite lapse of time. This is simply to say that excited states do eventually decay.

The natural line width sets an ultimate limit on spectroscopic resolution, but until recently the limit has seldom been approached. That is because the lines are broadened to a much greater extent by another effect: the Doppler shifting of frequencies as a result of the motion of the atoms.

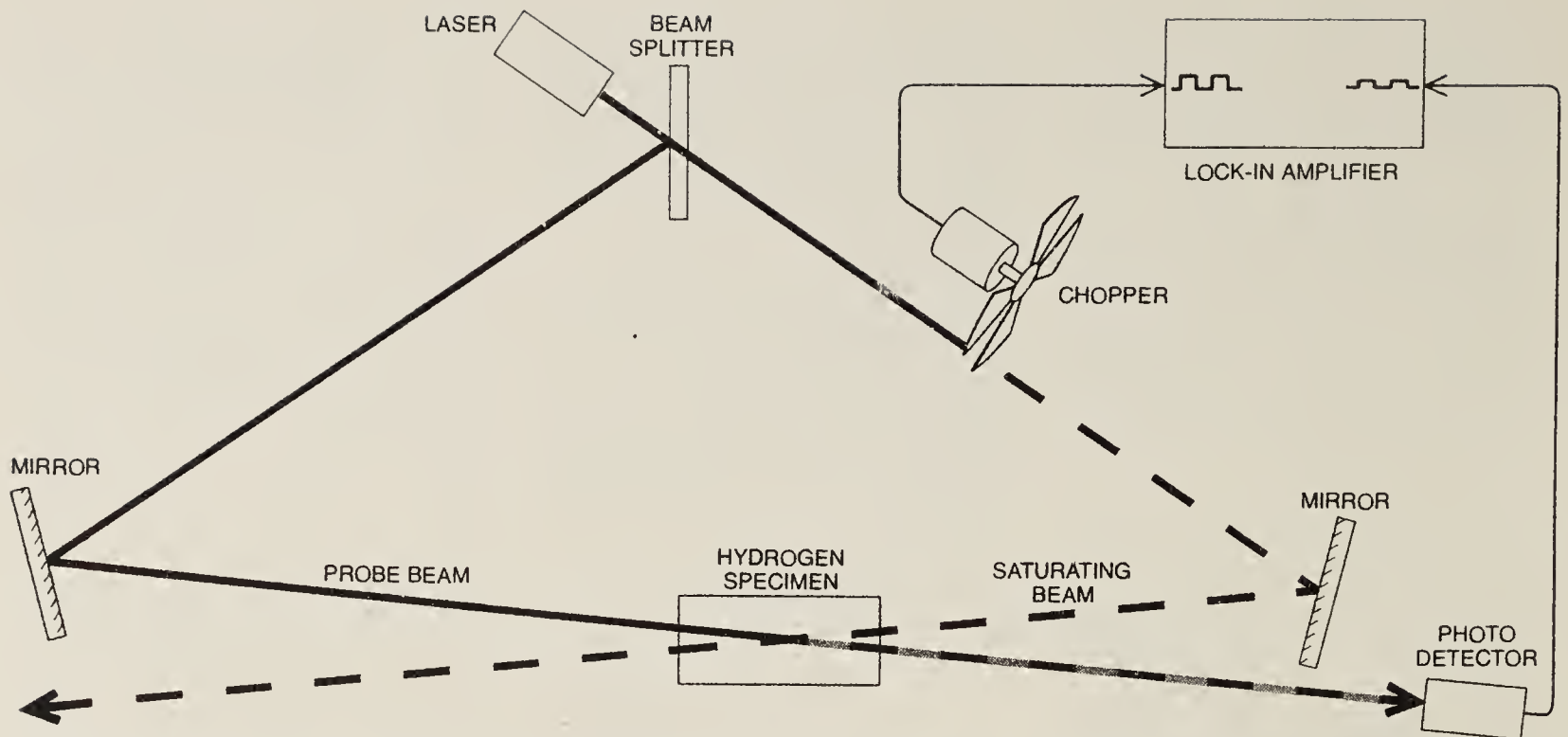
One method of greatly reducing Doppler broadening is to measure the spectrum not of a gas but of a collimated atomic beam. Such a beam can be created by allowing the atoms of a gas to escape from a vessel through a series of pinhole openings. All the atoms that can pass through the holes will be moving in

the same direction, and so light crossing the beam at right angles to the beam will show only small Doppler shifts. The number of atoms in the beam, however, declines as the collimation improves. Moreover it is not always possible to prepare a beam of atoms in the necessary state. To study the Balmer spectrum of hydrogen by absorption, for example, the atoms must be in the  $n = 2$  state; such atoms cannot be formed into beams dense enough for conventional spectroscopic measurements.

The techniques of laser spectroscopy introduced since about 1970 have significantly improved resolution because

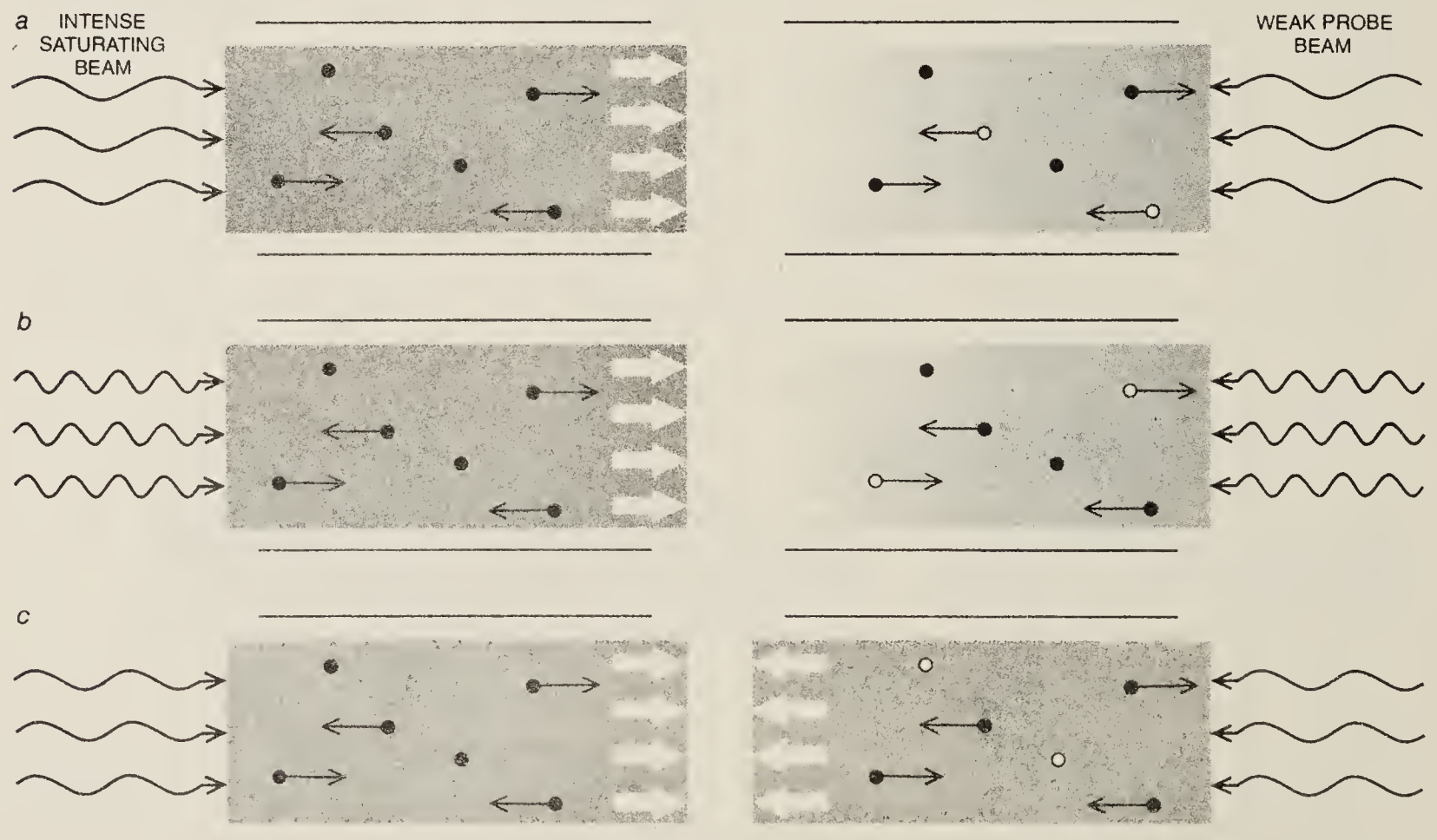


**BALMER-ALPHA LINE** is resolved into a series of sharp peaks by saturation spectroscopy. Theoretical calculations indicate that the line has seven components resulting from fine-structure splittings and the Lamb shift but ignoring the hyperfine structure of much smaller scale. In a Doppler-broadened profile of the line only two components can be distinguished. By examining only those atoms that have no Doppler shift saturation spectroscopy clearly resolves four components. (A fifth peak midway between two other peaks is an artifact called a crossover resonance.) Frequency scale measures tuning of the laser from an arbitrary starting point.



**SATURATION SPECTROSCOPY** suppresses Doppler broadening by labeling a group of atoms that happen to have no component of motion along the optical axis. The light from a dye laser is split into an intense saturating beam and a weaker probe beam, which pass through a specimen of atomic hydrogen in opposite directions. The saturating beam is strong enough to reduce significantly the population of atoms in the state capable of absorbing the laser wavelength: the beam bleaches a path through the gas. The probe beam therefore

encounters a smaller absorption and registers a higher intensity at the detector. The two beams can interact in this way, however, only when they are both absorbed by the same atoms in the gas, and that can happen only when they are both tuned to the wavelength of atoms that have no Doppler shift. In practice the saturating beam is interrupted by a mechanical "chopper," and enhancement in the transmission of the probe beam is detected by tuning the laser through a range of wavelengths and searching for a signal at the chopping frequency.



**COUNTERPROPAGATING BEAMS** from a tunable dye laser undergo opposite Doppler shifts. When the frequency of the saturating beam (measured in the laboratory frame of reference) is below that of some selected component of the spectrum (a), only atoms moving to the left can absorb the light, because their motion shifts the frequency into resonance with the atomic transition. The probe beam, with the same frequency, is absorbed only by atoms moving to the right, and so it is not affected by the saturating beam. When the laser frequency is above that of the spectral component (b), the saturating

beam is absorbed by atoms moving to the right and the probe beam by atoms moving to the left, which are again different groups of atoms. Only when the laser frequency matches the atomic-transition frequency (c) do the two beams interact with the same atoms: those atoms that are effectively standing still. The probe beam then finds that the atoms that might have absorbed it are unable to do so because they have already absorbed radiation from the saturating beam. Transmission of the probe beam therefore increases. Only the component of motion that is directed along the optical axis is depicted.



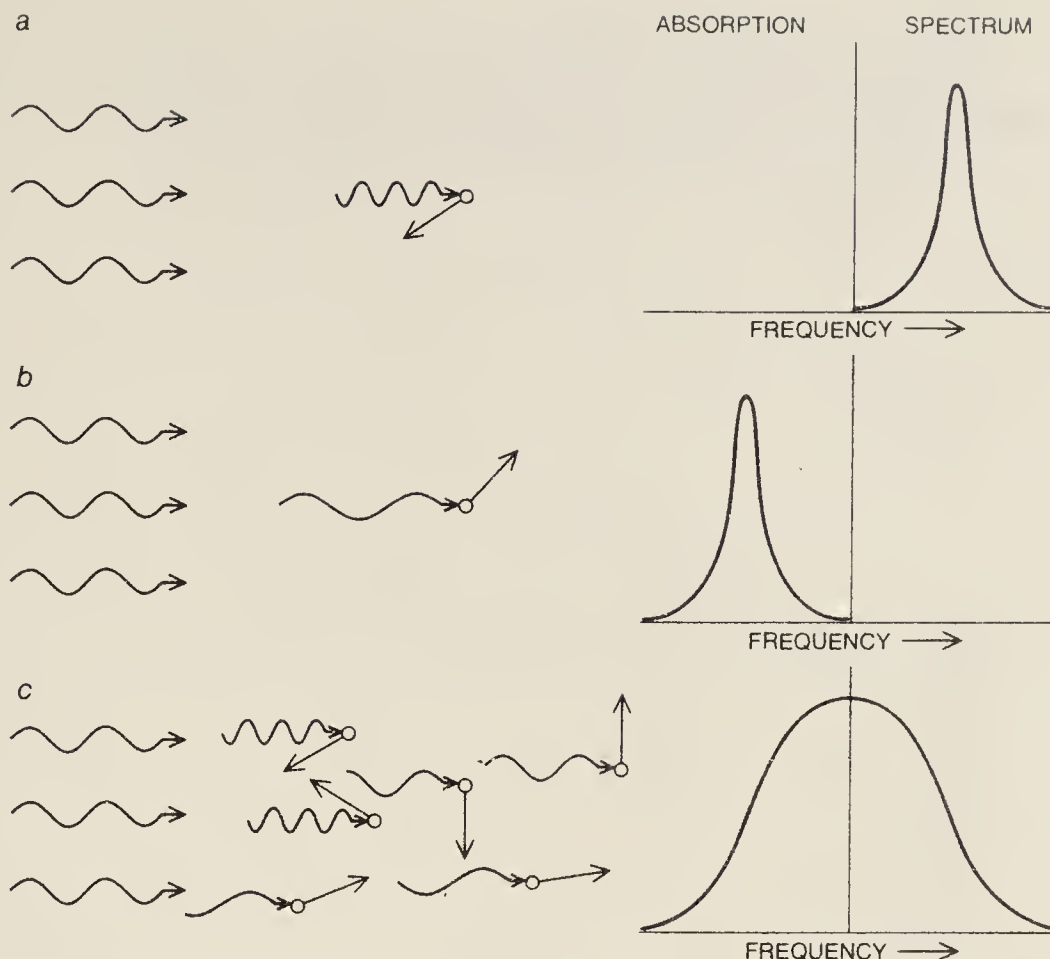
ognized that the electron can acquire angular momentum not only by orbiting the nucleus but also by spinning on its axis. The concept of electron spin was introduced by George Uhlenbeck and Samuel A. Goudsmit to explain measurements of the spectra of alkali-metal atoms. By including electron spin in the theory it was possible to predict with reasonable accuracy not only the wavelengths of the spectral lines but also their intensities; that had not been true for the Bohr-Sommerfeld theory. In 1928 the concept of spin for the electron—and also for the proton and the neutron—was given a more secure foundation when P. A. M. Dirac found a new way of constructing a theory of quantum mechanics that is also consistent with the special theory of relativity. In the Dirac theory electron spin appears as a natural consequence of the basic equations rather than as a special postulate. The magnitude of the spin angular momentum is  $1/2 \hbar/2\pi$ .

### Fine Structure

The relativistic quantum mechanics of Dirac predicts the structure of the hydrogen spectrum in great detail. As in earlier theories each basic energy level is designated by an integer,  $n$ , which is called the principal quantum number. For the lowest energy level (the ground state of the atom)  $n$  is equal to 1, for the first excited state  $n$  is equal to 2 and so on. These integers are the same ones that appear in Rydberg's formula for the spectral lines.

The basic lines of the spectrum—ignoring for the moment any splitting into finer components—are generated by transitions between states that have different principal quantum numbers. The Balmer-alpha line, for example, results from transitions between the states  $n = 2$  and  $n = 3$ . If a hydrogen atom falls from  $n = 3$  to  $n = 2$ , it emits light at the wavelength of the Balmer-alpha line; if the atom then absorbs a quantum of light at the same wavelength, it makes the opposite transition, from  $n = 2$  to  $n = 3$ . All the lines in a series share a common lower state. The transitions that give rise to the Balmer series connect states with principal quantum numbers of 2 and 3, 2 and 4, 2 and 5 and so on. In the Lyman series all the transitions begin at the state  $n = 1$ .

The basic lines of the hydrogen spectrum reflect the dominant interaction in the hydrogen atom: the electrostatic attraction between the nucleus and the electron. The splitting of each line reflects subsidiary interactions, relativistic effects and magnetic effects. The magnetic effects come about because the spinning electron, acting as a magnet, is subjected to a magnetic field attributable to the effective motion of the charged nucleus around the electron. This splitting is called the fine structure



**DOPPLER BROADENING** obscures many details of the hydrogen spectrum by smearing each narrow component over a band of wavelengths. Because the atoms of a gas have random velocities, at any given moment some are moving toward a source of light and others are moving away from it. For an atom moving toward the source (a) the light appears to have a higher frequency (or shorter wavelength) than it does in the laboratory frame of reference. For an atom moving away (b) the frequency is shifted down. As a result of these Doppler effects the measured frequency of a spectral component is different for atoms that have different velocities. The absorption profile for all the atoms in the gas (c) is not a sharp peak but a broad curve.

of the spectrum. Because the nucleus itself also has spin and acts as a magnet, it interacts with the magnetic field arising from the motion of the electron's charge and also from the proximity of the electron's magnetic field. These magnetic interactions are on a still smaller scale, and the corresponding splittings of the spectral lines are called the hyperfine structure.

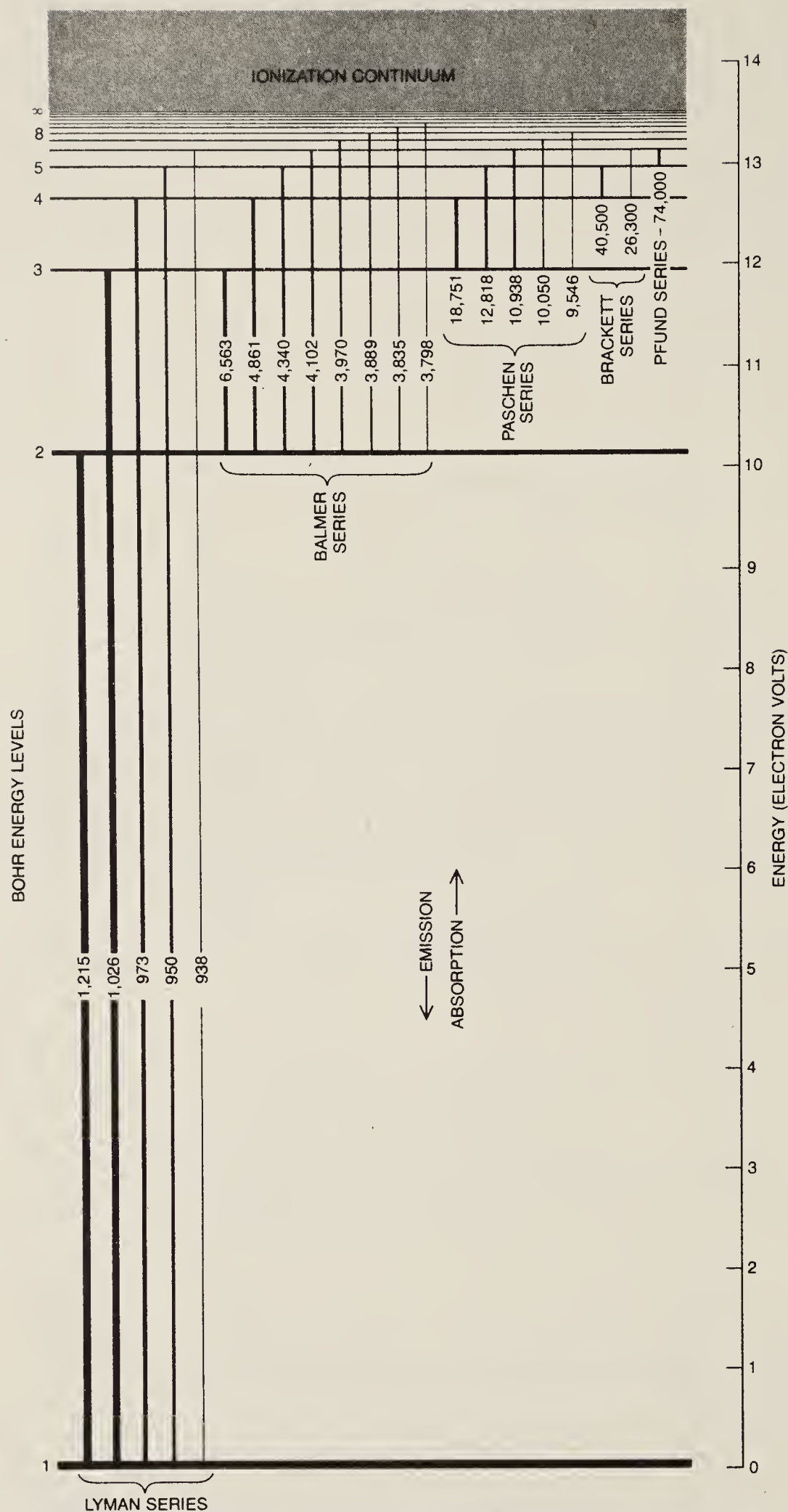
A system of classification has been developed for the fine and hyperfine energy levels, which specifies the magnitudes of the various angular momenta (orbital, electron-spin, nuclear-spin and total) in a stationary state. The principal quantum number, which corresponds to the Bohr energy level, is given by one of the integers in the sequence beginning 1, 2, 3... To this number is appended a letter, such as *S*, *P*, *D* or *F*, which is related to the orbital angular momentum; the letters stand for integers in the series beginning 0, 1, 2, 3... A third symbol, which for the hydrogen atom is always a fraction such as  $1/2$ ,  $3/2$  or  $5/2$ , is related to the sum of the orbital and spin angular momenta. If an analysis is subtle enough to reveal the hyperfine structure (an interaction that depends on the magnetic properties of the nucleus), a fourth label, represented by the symbol *F*, is also needed. It is related to the sum of the orbital, electron-spin and nu-

clear-spin momenta. Generally, stationary states that differ in any label have different energies, although that is not always the case.

The fine structure splits the  $n = 2$  state of the hydrogen atom into three sublevels and the  $n = 3$  state into five sublevels. A simple tabulation of the possible combinations of these levels implies that there could be 15 components of the Balmer-alpha line. Actually several of these transitions are forbidden by conservation laws, and the Dirac theory predicts that the line should have seven components. At the time Dirac proposed his theory experimenters could clearly recognize only two components, although in 1925 G. Hansen detected a third component as a broadening on the side of one of the others.

The factor limiting the resolution of the lines was (and still is) Doppler broadening caused by the thermal motions of the atoms. Because of the Doppler effect the light emitted by an atom appears to be shifted to a higher frequency if the atom is approaching the observer and to a lower frequency if the atom is receding. Atoms in an ordinary light source move in all directions, and so the emitted light is broadened in wavelength by the ratio  $v/c$ , where  $v$  is the average speed of the atoms and  $c$  is the velocity of light. The broadening





**TRANSITIONS BETWEEN STATES** of the hydrogen atom give rise to the line spectrum. Each state is designated by an integer, called the principal quantum number of the corresponding Bohr energy level. When an atom changes from one state to another, the difference in energy appears as a quantum of radiation. The energy of the quantum is directly proportional to the frequency of the radiation and inversely proportional to the wavelength. Absorption of radiation stimulates a transition to a state of higher energy; an atom falling to a state of lower energy emits radiation. The spectrum is organized into series of lines that share a lower level. Wavelengths are given in angstroms; the relative intensity of the lines is indicated by thickness.

4

proposed that an atom could exist in a state where the energy of the electron was not dissipated: a stationary state. Light is emitted or absorbed, he suggested, only when an electron moves from one stationary state to another. The frequency of the light is determined by the difference in energy between the two states, according to the quantum principle introduced by Max Planck. The frequency is found by dividing the energy difference by Planck's constant, which is designated  $h$ .

In Bohr's model the Balmer and the Rydberg formulas have an obvious physical interpretation. The expression  $(1/m^2 - 1/n^2)$  is proportional to the difference in energy between two states of the atom; the integers  $m$  and  $n$  label the states themselves. Bohr did more than just explain this empirical equation, however; he went on to evaluate the Rydberg constant in terms of three fundamental quantities, the electric charge of the electron,  $e$ , the mass of the electron,  $m$ , and Planck's constant,  $h$ . If for the sake of simplicity the nucleus of an atom is assumed to be infinitely massive, then the Rydberg constant is given by the equation

$$R = \frac{2\pi^2 me^4}{h^2}$$

Later refinements have complicated Rydberg's empirical formula for the wavelengths of spectral lines, and so the Rydberg constant is now defined as this combination of  $m$ ,  $e$  and  $h$ .

Bohr imagined that the electrons in an atom follow circular orbits. In calculating the energy of the stationary states he began with the assumption that for orbits of very large diameter the frequency of the emitted light should correspond to the frequency of the orbiting electron, which was a prediction of classical physics. This "correspondence principle" led to the intriguing conclusion that for a stationary state designated by the integer  $n$  the angular momentum of the orbiting electron is equal to  $nh/2\pi$ . Hence the angular momentum, like the energy, can change only in discrete steps. This "quantization" of the angular momentum is of fundamental significance: without it the atom could radiate at any frequency and the state would no longer be stationary.

### Quantum Mechanics

The Bohr atom was a great conceptual advance over earlier theories, but it soon proved inadequate to explain the observed features of atomic spectra, even those of the simplest spectrum, that of hydrogen. Indeed, one detail of the hydrogen spectrum that the Bohr theory could not account for had been known for 20 years when the model was constructed. In 1892 A. A. Michelson had employed the interferometer he had



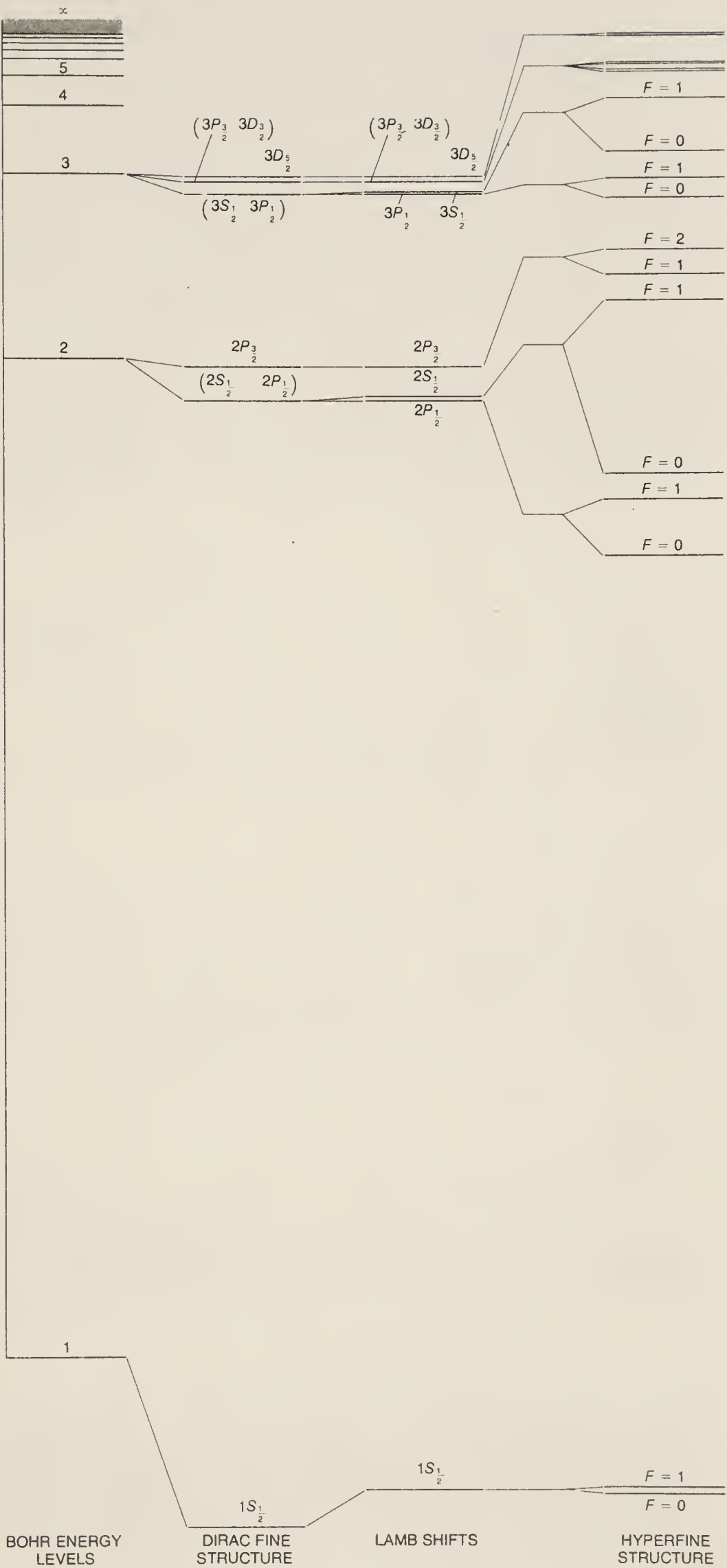
invented to examine the shapes of individual spectral lines, that is, their variation in intensity as a function of wavelength. He had found that the Balmer-alpha line is not a single line at all but rather has two components, separated in wavelength by .14 angstrom.

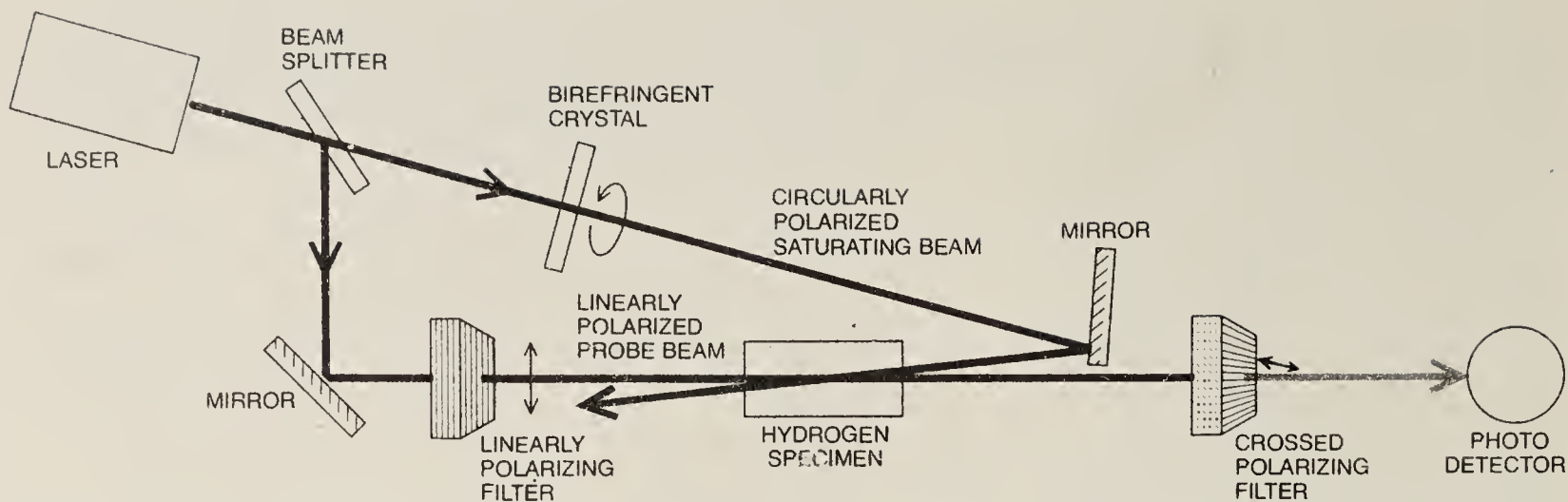
Bohr suggested that the splitting of the Balmer-alpha line might be explained if the electron's orbit in the hydrogen atom is not circular but elliptical. A correction to the orbital motion required by the special theory of relativity would then split each stationary state into a group of states. A more comprehensive discussion of this idea was subsequently presented by Arnold Sommerfeld, who deduced the observed splitting from the calculated properties of the orbits. In his calculation he introduced an important dimensionless number called the fine-structure constant, equal to  $2\pi e^2/hc$ . The numerical value of this constant, about  $1/137$ , has been a source of speculation for physicists ever since.

A more satisfactory treatment of the line splitting was not possible until quantum mechanics was introduced in the 1920's. Two formulations of quantum mechanics were devised, one by Erwin Schrödinger and the other by Werner Heisenberg and Max Born; they were soon found to be mathematically equivalent. An essential idea in both formulations was that the motion of an electron cannot be defined precisely but must be described in terms of probabilities. Both theories predicted the Bohr energy levels of the hydrogen atom, and hence the same wavelengths of the spectral lines, and the predictions could be extended to more complicated atomic systems. Again relativistic corrections had to be introduced in order to explain the splitting of the hydrogen lines.

By the 1920's, however, better measurements of the shape of lines in the hydrogen spectrum were available, and it soon became plain that a further adjustment to the theory was needed. The adjustment was made when it was rec-

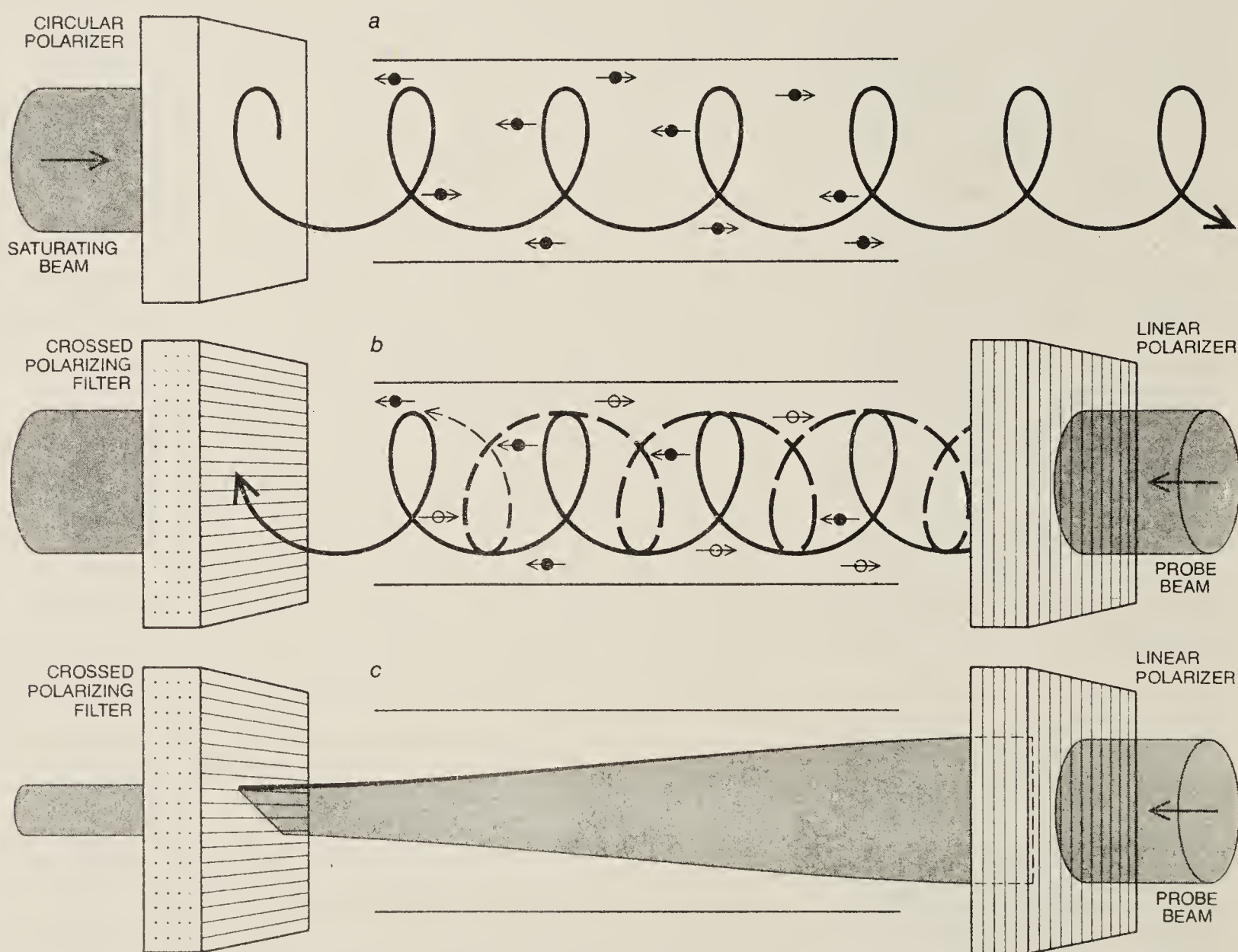
**SPLITTING OF ENERGY LEVELS** results mainly from relativistic and magnetic interactions related to angular momenta in the atom. The single electron of a hydrogen atom can have both orbital and spin angular momentum, and the various possible combinations of these quantities generally have different energies. As a result the Bohr energy levels are split into components called the fine structure of the levels. A subtle effect called the Lamb shift displaces certain of the fine-structure components, creating additional splittings. Finally, the interaction of the electron's magnetic moment with that of the nucleus gives rise to a hyperfine structure. The fine structure and the Lamb shifts are shown here at a larger scale than the Bohr levels, and the hyperfine splittings of the second and third Bohr levels are shown at still greater magnification.





**POLARIZATION SPECTROSCOPY** exploits the fact that small changes in the polarization of light can be detected more easily than small changes in intensity. The output of a laser is again split into two beams, but the saturating beam is given a circular polarization and the probe beam a linear polarization. Because the probe beam encounters crossed polarizing filters very little of it can reach the detector un-

less the hydrogen gas can in some way rotate the beam's plane of polarization. Such a rotation can be introduced by the circularly polarized saturating beam, but only if the two beams interact with the same population of atoms. In this way atoms that happen to be stationary at a given moment are singled out, as in saturation spectroscopy, by the ability to interact with light waves moving in opposite directions.



**CHANGE IN THE POLARIZATION** of a probe beam is induced by the prior passage of a saturating beam. Because the saturating beam is circularly polarized it is selectively absorbed by atoms that have a particular orientation (a), and those atoms are thereby removed from the population of atoms that can absorb radiation at the laser wavelength. Most of the remaining atoms have the opposite orientation. The linearly polarized probe beam can be regarded as a combination of two circularly polarized waves that have the opposite sense of rota-

tion but equal intensity (b). When the probe beam passes through the specimen, one of the circularly polarized components is more strongly absorbed because the atoms have a prevailing orientation. The selective absorption of one circularly polarized component changes the polarization of the remaining light (c), and so a portion of the probe beam can penetrate the analyzing filter. The change in polarization can take place, however, only if the two beams are absorbed by the same population of atoms, namely those that have no Doppler shift.



they include methods for eliminating Doppler broadening. Three such methods will be discussed here. Two of them work by selecting for observation only those atoms in a gas whose component of motion along the optical axis happens to be zero. The third method allows all the atoms in a gas to contribute to a measurement, but it eliminates velocity broadening by arranging two Doppler shifts in opposite directions.

### The Tunable Dye Laser

Lasers provide light of unequalled brightness, directionality and spectral purity. The early lasers, however, could emit light at only a few discrete wavelengths, determined by the spectral lines of the active atoms or ions. Such an instrument is of use in spectroscopy only if the transition to be observed happens to coincide with one of the available laser lines.

In 1966 Peter Sorokin of the Thomas J. Watson Research Center of the International Business Machines Corporation and independently Fritz Schafer of the University of Marburg discovered that liquid solutions of certain fluorescent organic molecules can serve as the medium for a laser with a broad and continuous band of wavelengths. The organic molecules are dyes, which by nature have intense absorption bands; that is why they are strongly colored. In the laser the dye molecules are "pumped," or driven to an excited state, by an intense external light source, such as another laser.

Although the dye laser is capable of amplifying light over a wide range of wavelengths, it was soon learned that a particular wavelength could be selected by designing an optical resonator that will allow only the chosen wavelength to pass repeatedly through the amplifying dye cell. In 1970 one of us (Hänsch) devised a simple pulsed dye laser of high spectral purity. The dye, enclosed in a glass cell, was pumped by pulses of ultraviolet radiation from a nitrogen laser. The resonator consisted of a partially reflecting glass plate at one end of the laser and a diffraction grating at the other. The grating disperses the light emitted by the dye, with the result that only a narrow range of wavelengths is reflected back along the optical axis. A telescope in the laser cavity expands the beam before it strikes the grating, so that many grooves are illuminated with well-collimated light. The line width of the laser is further reduced by inserting a tilted Fabry-Perot interferometer into the cavity. The interferometer is made up of two partially reflecting surfaces whose spacing is precisely controlled; the type of interferometer placed in the laser resonator is called an etalon, and it consists of a single glass plate whose two parallel surfaces are coated with partially reflecting layers. Light waves with dif-

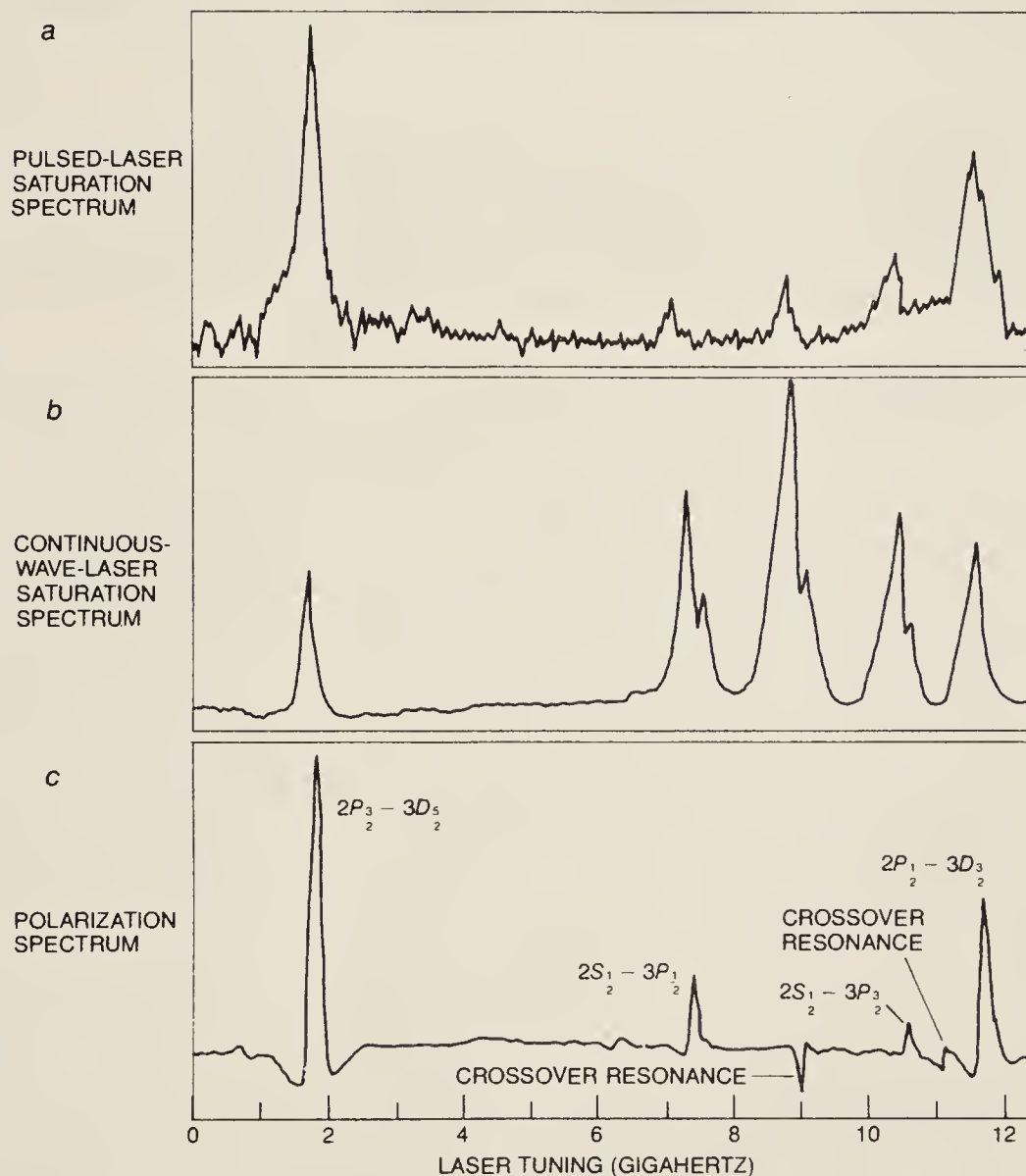
ferent wavelengths take slightly different paths through the etalon. As a result of multiple internal reflections some wavelengths interfere destructively and are extinguished, whereas other wavelengths interfere constructively and are reinforced.

The line width of this laser is a few thousandths of an angstrom, or about one part per million, which is comparable to the resolution of the largest grating spectrographs. The width can be further reduced by a factor of 100 or so by a second Fabry-Perot interferometer outside the laser cavity, which acts as a passive filter. Although at any given setting the light is highly monochromatic, the laser can be tuned over the full range of the dye absorption profile. Gross tuning can be accomplished by changing the angle of the diffraction grating or of the etalon. Finer adjustments can be made by enclosing the grating and

the etalon in an airtight chamber and altering the pressure, which changes the index of refraction of the enclosed gas.

### Saturation Spectroscopy

There is an ultimate limitation on the wavelength resolution of any pulsed laser. The precision with which the wavelength can be known is determined by the number of cycles available for measurement, and hence by the length of the pulse. Narrower lines require a continuous-wave laser. In 1970 Otis G. Peterson, Sam A. Tuccio and Benjamin B. Snavely of the Eastman Kodak Research Laboratories demonstrated the first continuous-wave tunable dye laser. Its principles of operation were the same as those for the pulsed dye laser, but the dye solution was made to flow rapidly in order to avoid overheating. Highly refined continuous-wave dye lasers are



**HIGHER-RESOLUTION SPECTRUM** of the Balmer-alpha line was recorded by polarization spectroscopy. For comparison saturation spectrum shown on page 9 is repeated at the top and an improved saturation spectrum, made with a continuous-wave laser instead of a pulsed one, is given in the middle. In the polarization spectrum no additional components can be detected, but the four peaks that are resolved are much sharper. The two small peaks between the tall outer ones (excluding crossover resonances) have a measured width of about 35 megahertz, almost 10 times narrower than corresponding lines in the pulsed saturation spectrum. The polarization spectrum has an unusual appearance (it makes excursions below the background level as well as above it) because the graph records not the intensity of transmitted light but the rate of change in intensity as the laser is scanned through its frequency range.



now available commercially. In several laboratories line widths as small as a few parts in  $10^{12}$  have been achieved through electronic stabilization of the laser frequency.

Given a source of light that is monochromatic but tunable, an absorption spectrum can be measured by passing the light through a sample of the gas and scanning continuously through the frequencies surrounding a line in the spec-

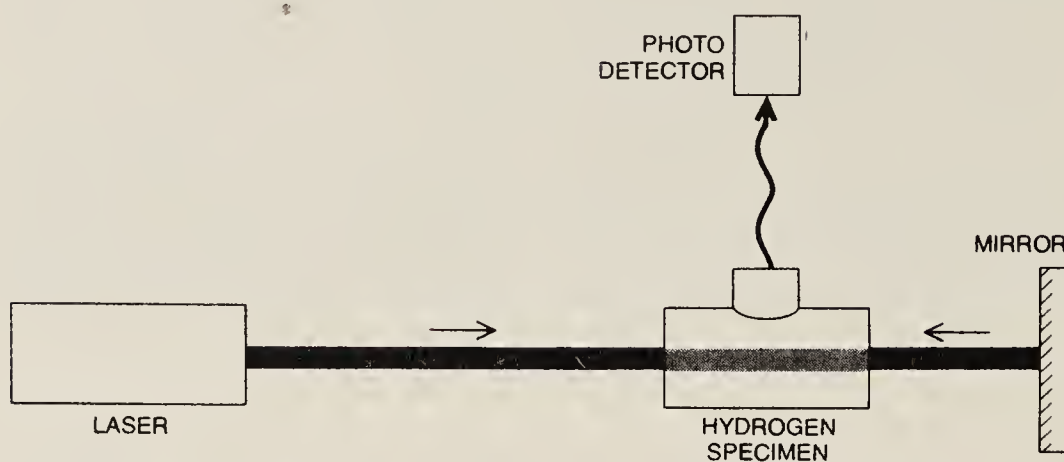
trum. The intensity of the transmitted light can be monitored by a photoelectric detector, which should reveal a dip at the wavelength of each component of the line. This scheme, however, would merely measure the Doppler-broadened profile of the line. To take full advantage of the potential resolution of the laser some means must be found for eliminating Doppler shifts.

One such method has been given the

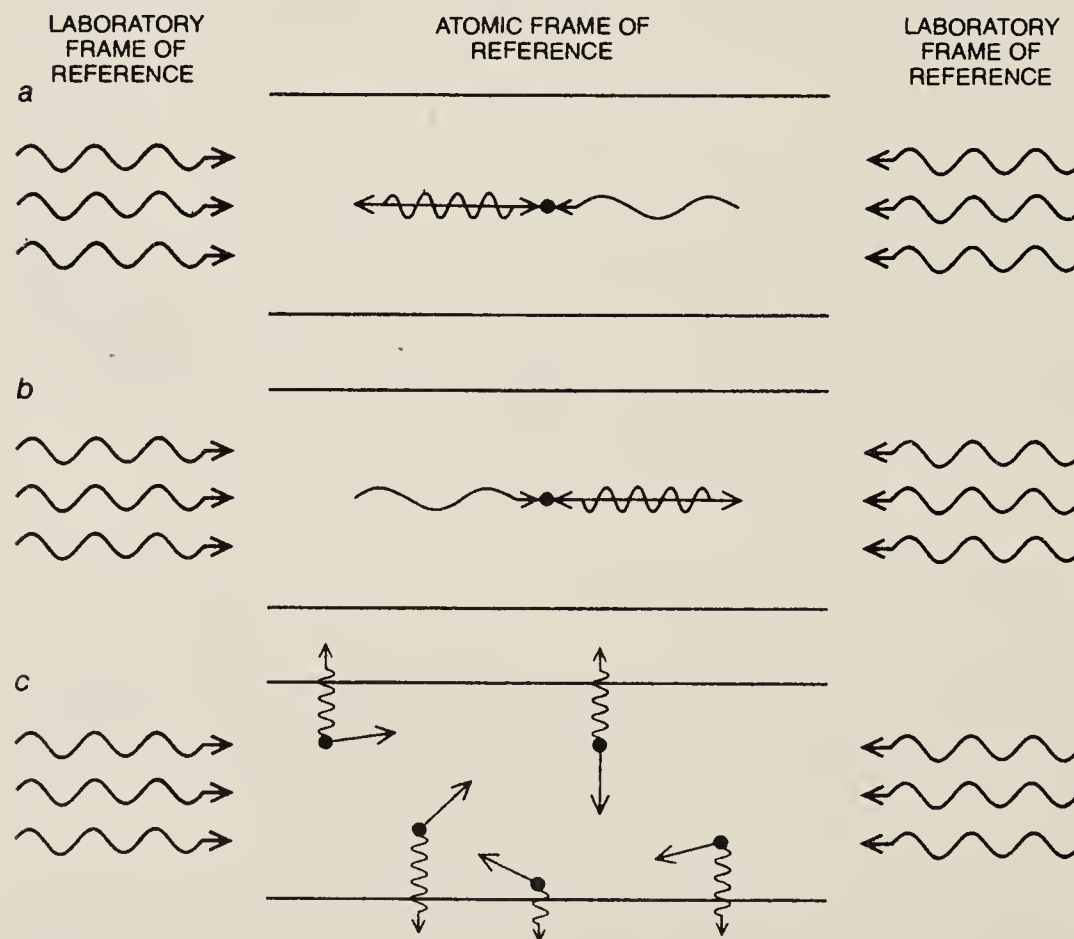
name saturation spectroscopy. It depends for its operation on two properties of laser light: small line width and high intensity. When an atom absorbs a quantum of light, it is excited to a higher energy level and is thereby temporarily removed from the population of absorbing atoms. In an intense beam of light the atoms of a gas may absorb quanta faster than they can return to their original state. As a result the population of absorbing atoms is substantially depleted. The light bleaches a path through the gas, and a second beam of the same wavelength would find the absorbance of the gas reduced.

Lamb was the first to recognize the potential of this effect for high-resolution spectroscopy. He pointed out that the two waves traveling in opposite directions inside a laser could work together to saturate the absorption of a particular class of atoms in the active medium of the laser. Assuming that the line width of the light is narrow enough, it must always interact only with those atoms whose motion shifts the wavelength into resonance with a component of the atomic spectrum. If the frequency of the light is lower than that of the line component, for example, then both waves in the cavity will interact with atoms moving toward them, and these will be different atoms for the two oppositely directed beams. There is one tuning of the laser, however, for which both beams interact with the same atoms: the tuning that corresponds to the exact wavelength of the spectral component, where the atoms that can absorb the light are those standing still or moving transversely to the optical axis. When the laser is tuned to this wavelength, the population of atoms in the absorbing state is depleted and the output of the laser declines. This "Lamb dip" was first observed by Ross A. McFarlane, William R. Bennett, Jr., and Lamb. It was employed for high-resolution spectroscopy by Abraham Szöke and Ali Javan of the Massachusetts Institute of Technology, but it has proved to be of limited utility. Only the laser transitions themselves can be studied, or molecular lines that happen to coincide with gas-laser wavelengths, and any gas to be examined must be placed inside the delicate resonator of a continuous-wave laser.

In 1970 Christian Bordé of the University of Paris and independently one of us (Hänsch) devised a technique for measuring saturation spectra outside the laser resonator. The light of a tunable laser is split into an intense saturating beam and a weaker probe beam. The two beams are then made to traverse the same path through a gas cell, but in opposite directions. If the laser is detuned slightly from the frequency of an atomic transition, then the two beams interact with different atoms and the saturating beam has no effect on the absorption of the probe beam. When the laser is tuned



**TWO-PHOTON SPECTROSCOPY** does not select atoms without a Doppler shift but instead cancels the Doppler shifts of all the atoms in a gas. The dye laser is tuned to a frequency exactly half that of a selected atomic transition. The beam passes through the specimen and then is reflected back on itself, creating a field of standing waves. Atoms in the gas can make the selected transition by simultaneously absorbing two photons, or quanta of light, coming from opposite directions and therefore having opposite Doppler shifts. The excited states created in this way decay to some lower energy level, emitting photons that can be detected and counted.



**OPPOSITE DOPPLER SHIFTS CANCEL** in two-photon spectroscopy. An atom moving to the left (a) sees the wave coming from the left shifted to a higher frequency, but the frequency of the wave coming from the right is shifted down by an equal amount. For an atom moving to the right (b) the frequency shifts are the opposite of these. A stationary atom perceives no Doppler shifts. Regardless of the atom's velocity the sum of the two frequencies is constant and equal to twice the laser frequency (measured in the laboratory frame of reference). All the atoms can therefore absorb two photons (c) and afterward reradiate at some higher frequency.



so that it is absorbed by stationary atoms, however, the saturating beam depletes the population of atoms in the selected state and the probe beam experiences a smaller absorption. In effect the saturating beam labels all the atoms that happen to have a zero component of motion along the optical axis and ignores all others.

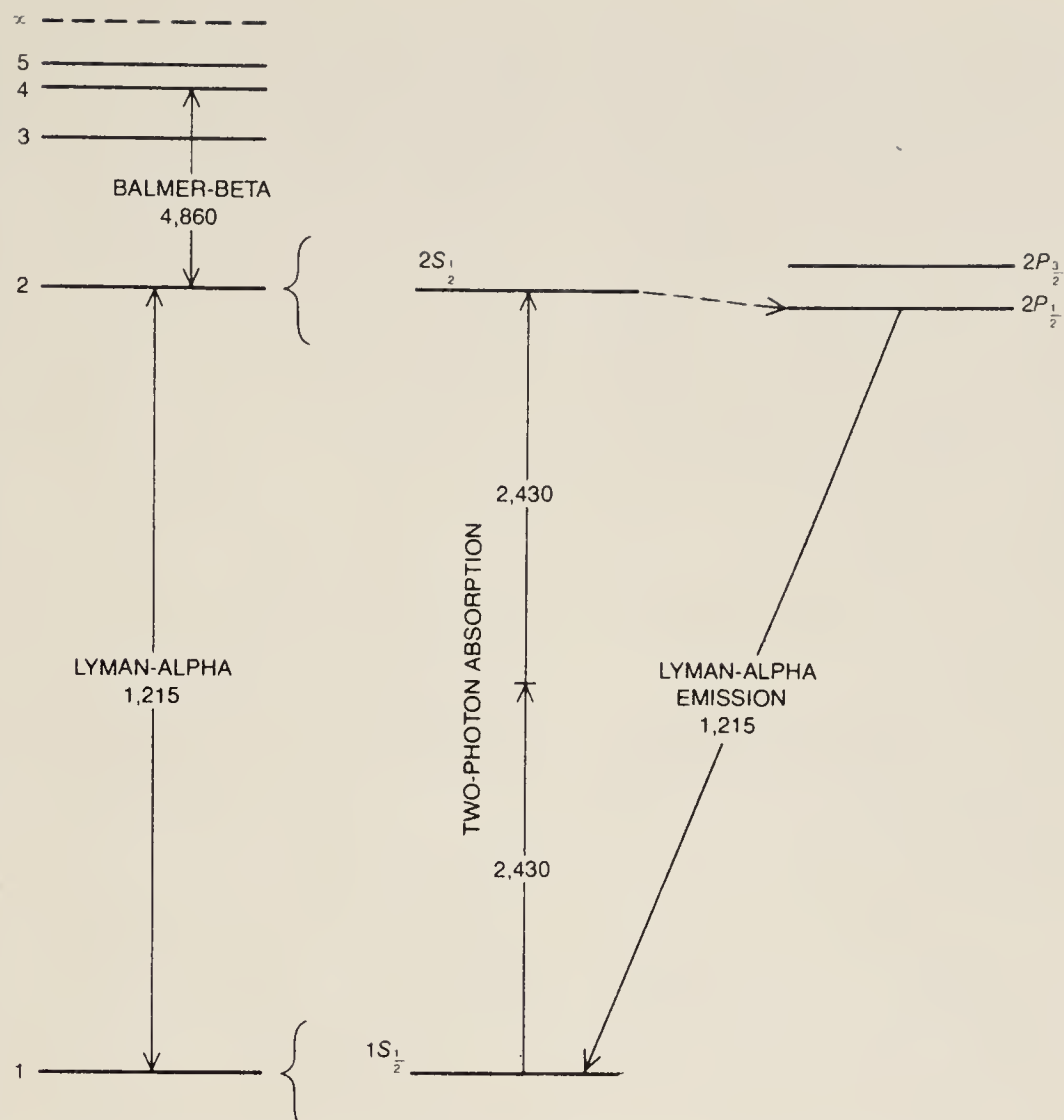
In practice the change in absorption is small and is easily obscured by noise. In order to help distinguish the signal from the background, the saturating beam is chopped, or interrupted at a known frequency, whereas the probe beam is allowed to operate continuously. The signal can then be detected by examining the amplitude of the probe beam for any modulation at the chopping frequency.

Two of us (Hänsch and Schawlow) with Issa S. Shahin, who was then a graduate student at Stanford University, examined the Balmer-alpha line by this method. The hydrogen atoms were excited to the absorbing  $n = 2$  level in a low-pressure gas-discharge tube. The two light beams from a pulsed dye laser were passed through a section of the discharge plasma about 15 centimeters long, where they showed an absorption of about 50 percent.

Of the seven fine-structure components expected theoretically, four were visible, the two strongest ones being resolved far more sharply than in any previous spectrum. What is more, the Lamb shift that splits the  $2S_{1/2}$  and  $2P_{1/2}$  levels was directly observed for the first time in the optical absorption spectrum.

The saturation spectrum also included a fifth peak, but it was a spurious one, called a crossover resonance, which appears midway between any two transitions that share the same upper or lower level. When the laser is tuned to the frequency midway between these two line components, atoms moving in one direction can absorb the saturating beam, and atoms moving the other way can absorb the probe beam. As a result the absorption is saturated not by stationary atoms but by two classes of moving ones.

The sharpness of the peaks in the saturation spectrum suggested that the Rydberg constant could be determined with improved accuracy by measuring the absolute wavelength of one fine-structure component. Such a measurement was undertaken by a group of workers at Stanford led by one of us (Hänsch) and including in particular Munir Nayfeh. The component chosen was the  $2P_{3/2}$ -to- $3D_{5/2}$  transition, which is the strongest one, the one with the smallest unresolved hyperfine splitting and the one least perturbed by the electric field of the discharge tube. It was first necessary to examine the effects on the line position of variations in gas pressure in current and voltage in the discharge tube and in laser intensity, and to correct



**GROUND, OR LOWEST, STATE OF HYDROGEN** can be reached only through transitions whose wavelengths are in the vacuum-ultraviolet region of the electromagnetic spectrum; such transitions can be observed more conveniently by two-photon spectroscopy than by any other technique. The Lyman-alpha line, a transition from  $n = 1$  to  $n = 2$ , has a wavelength of 1,215 angstroms, and radiation at twice this wavelength, or 2,430 angstroms, is required for two-photon spectroscopy. Even the latter wavelength is inaccessible to dye lasers and must be generated by doubling the frequency (or halving the wavelength) of a laser tuned to 4,860 angstroms. The frequency doubling is accomplished by a crystal that under intense illumination emits the second harmonic of the incident frequency. The original laser wavelength (4,860 angstroms) happens to correspond closely to the wavelength of the Balmer-beta line. Absorption of two photons in atomic hydrogen stimulates only the  $1S_{1/2}$ -to- $2S_{1/2}$  transition. The excited atom is converted by weak encounters with other atoms to a  $2P_{1/2}$  state, from which it returns to the ground state by emitting a photon having a wavelength of 1,215 angstroms.

for any systematic errors. In order to measure the absolute position of the line rather than the interval between two lines an accurate reference length was needed. The chosen standard was a helium-neon laser whose frequency was electronically locked to a particular hyperfine component of an absorption line of molecular iodine vapor; this line was also defined by saturation spectroscopy. The wavelength of the stabilized helium-neon laser was known accurately in terms of the international standard of length, which is a spectral line of krypton emitted under defined conditions. The data were evaluated in 1974. The result,  $R = 10,973,731.43 \pm .10$  reciprocal meters, was more accurate than the best previous value by a factor of almost 10.

A related method of Doppler-free spectroscopy was introduced in 1976 by Carl Wieman, a graduate student at Stanford working with one of us

(Hänsch). By exploiting the fact that small changes in the polarization of light can be detected more easily than changes in intensity, the technique achieves greatly improved sensitivity. Fewer atoms can be observed at lower laser intensity, thereby avoiding systematic line shifts and line broadening.

#### Polarization Spectroscopy

As in saturation spectroscopy, the laser light is divided into two beams, one more intense than the other, which traverse the sample in opposite directions. In this case, however, the weaker, probe beam sees the gas sample placed between crossed polarizing filters, so that little light reaches the detector as long as the sample does not change the polarization of the probe. The saturating beam acts on the sample to bring about such changes. It can do so because it is first passed through a quarter-wave plate, a



piece of birefringent material cut and polished so that it gives light a circular polarization. Light is said to be circularly polarized when the electric field rotates (either clockwise or counterclockwise) rather than oscillates in a plane as it does in linearly polarized light.

The probability that an atom will absorb circularly polarized light depends on the orientation of the atom's angular momentum with respect to the rotating field. Initially the orientation of the atoms is random, but the saturating beam depletes the gas of atoms that are oriented so as to absorb light of one circular polarization, leaving an excess of atoms with the opposite sense of rotation. When the probe beam, which is linearly polarized, passes through the same region of gas, the oriented atoms can alter its propagation.

A linearly polarized wave can be regarded as a superposition of two circularly polarized waves of equal intensity, one wave rotating clockwise and the other counterclockwise. When this beam passes through the gas, it encounters atoms that tend to absorb only one of its circularly polarized components, thereby attenuating it and leaving the other component the stronger. As a result when the probe beam emerges from the gas, it is elliptically polarized, and the axis of the ellipse is rotated from the plane of the original linear polarization. The beam has therefore acquired a component that can pass through the crossed polarizing filter. All of this can happen, however, only if the saturating beam and the probe beam interact with the same atoms, namely those that have no Doppler shift.

No light comes through the crossed

polarizing filter if the two beams interact with different sets of atoms, and so there is essentially no background signal. Hence real peaks in the spectrum are not easily obscured by noise or by intensity fluctuations of the laser. When the signal is very small, it is often advantageous to uncross the polarizing filters slightly. The detector then registers a finite background signal, which can either increase or decrease, depending on the direction in which the plane of polarization is rotated.

John Goldsmith, a graduate student at Stanford, Erhard Weber, who was at Stanford on leave from the University of Heidelberg, and one of us (Hänsch) have recently obtained an improved spectrum of the Balmer-alpha line by laser polarization spectroscopy. The saturating and probe beams were generated by a low-power, continuous-wave dye laser with a bandwidth of less than one megahertz.

The spectrum was recorded in the form of a derivative, a mathematical function that measures the rate of change in the probe-beam intensity as the laser is tuned through a band of frequencies. In the polarization spectrum the two largest peaks are sharper than they were in the earlier measurement by saturation spectroscopy, and three smaller components are narrower still. The line width for these components is about 35 megahertz, almost 10 times sharper than in the previous measurement. These three components all represent transitions that begin in the long-lived  $2S_{1/2}$  state, and each of them is known to be split into two hyperfine components separated by some 178 megahertz. It would seem that the hyper-

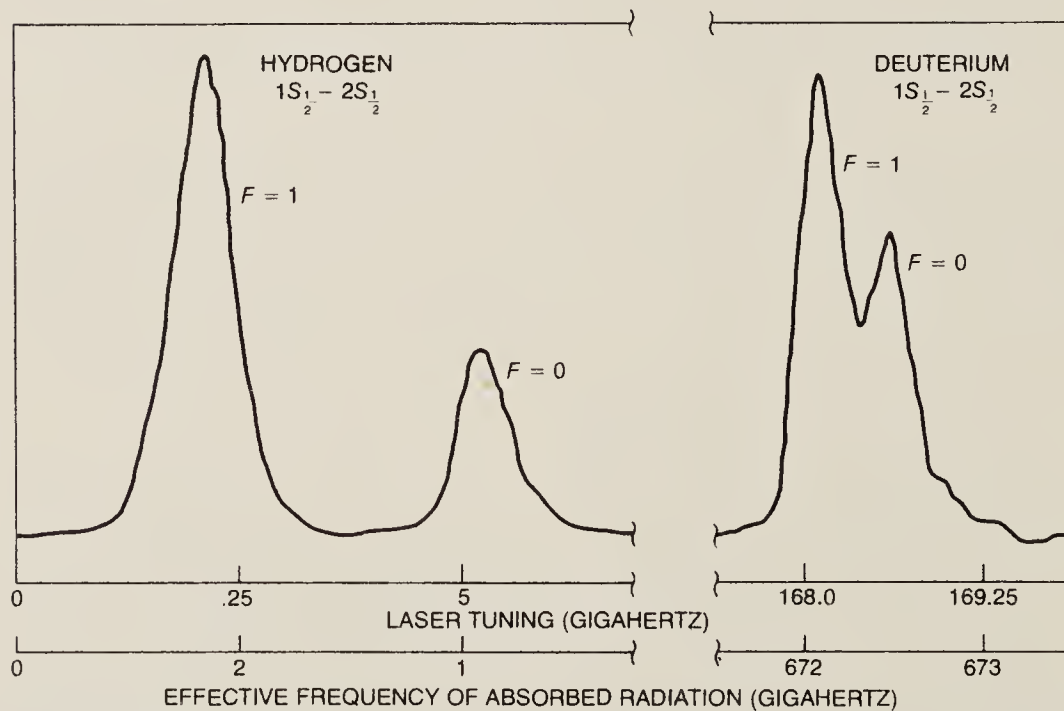
fine splitting should be clearly resolved, but only single peaks are observed. The explanation of this discrepancy is that in each case one of the hyperfine states has a net angular momentum of zero and cannot be polarized. Thus each of the observed peaks is not an unresolved mixture of two transitions but is a single hyperfine component.

The  $2S_{1/2}$ -to- $2P_{1/2}$  component was chosen for a new absolute wavelength measurement, again calibrated against the iodine reference line as a standard of length. The new value of the Rydberg constant derived from this measurement is  $R = 10,973,731.476 \pm .032$  reciprocal meters. The measurement is almost three times as accurate as the previous one, and it places the Rydberg constant among the most precisely known of all fundamental constants. Only the speed of light and the ratio of the magnetic moments of the electron and the proton have been determined with comparable precision.

### Two-Photon Spectroscopy

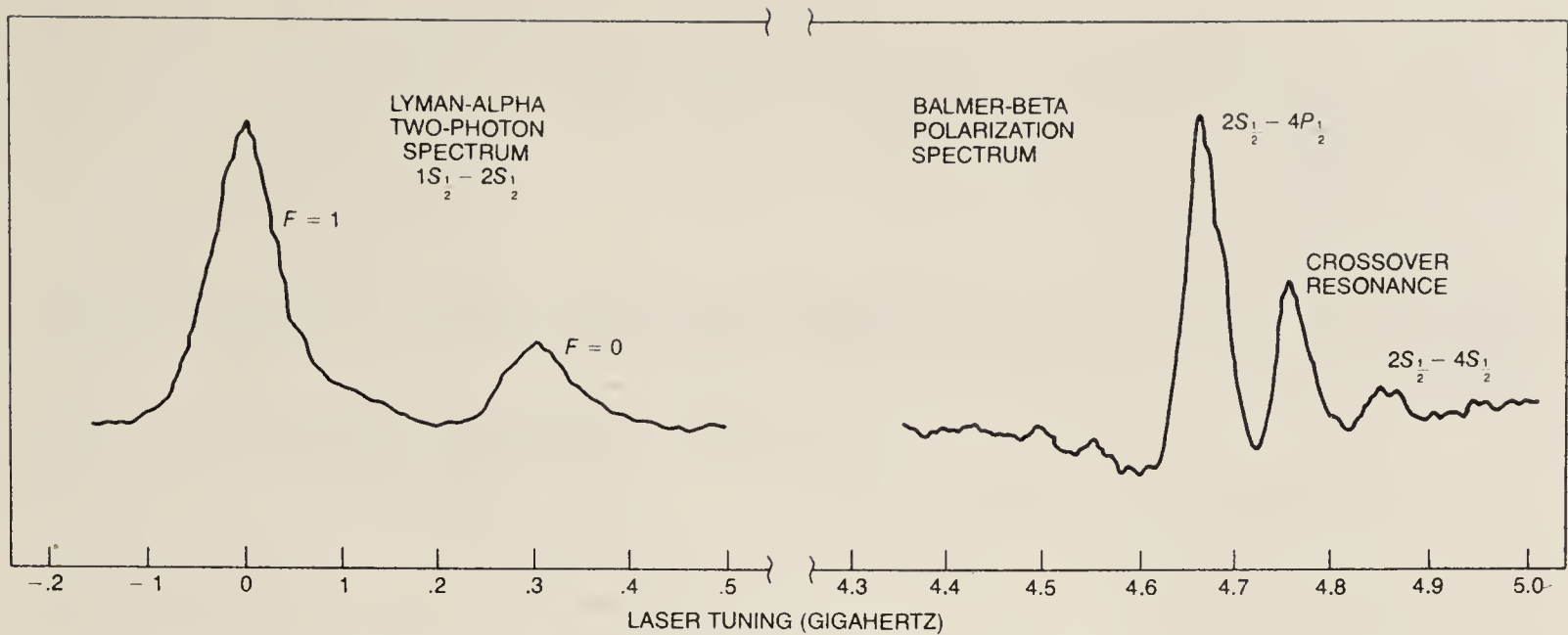
These methods provide convenient access to the lines of the Balmer series, those generated by transitions between the  $n = 2$  energy level and higher levels. Other states cannot be reached as readily. One of particular importance is the  $S_{1/2}$  state with  $n = 1$ , which is the ground state of the hydrogen atom. Even the nearest group of states, those with  $n = 2$ , is so far above the ground state that the wavelength of the corresponding line, which is designated Lyman-alpha, falls in the vacuum-ultraviolet region of the electromagnetic spectrum. Precision spectroscopy is particularly difficult at those short wavelengths, which are far beyond the range of the dye laser.

With intense lasers, however, the difficulties of vacuum-ultraviolet spectroscopy can be avoided by exciting each atom with two photons, which together provide the necessary excitation energy. The probability of an atom's absorbing two photons simultaneously is generally rather small, but it grows with the square of the light intensity. Two-photon spectroscopy is of particular interest for hydrogen because Doppler broadening can be avoided by an ingenious method first suggested in 1970 by L. S. Vasilenko, V. P. Chebotayev and A. V. Shishaev of the Institute of Thermophysics at Novosibirsk in the U.S.S.R. The method was first demonstrated in 1974 by three groups of investigators working independently. Instead of the laser beam's being split into two components the beam is reflected back on itself by a mirror, so that waves moving to the right and to the left travel along the same axis. The gas cell is placed in the standing-wave field that results from this superposition. The laser is then tuned to a frequency exactly half that



**HYPERFINE STRUCTURE** of the  $1S_{1/2}$ -to- $2S_{1/2}$  transition was resolved by two-photon spectroscopy both in normal hydrogen and in deuterium. Transitions between the two hyperfine levels in hydrogen are responsible for the radiation at a wavelength of 21 centimeters observed by radio astronomers. The natural width of the components is probably very small, perhaps as little as one hertz; here they are resolved to within about 100 megahertz. The shift between hydrogen and deuterium is caused mainly by the difference in the mass of the nuclei.





**SIMULTANEOUS MEASUREMENT** of the  $1S_{1/2}$ -to- $2S_{1/2}$  transition and the Balmer-beta line was employed to determine the magnitude of the Lamb shift for the  $1S_{1/2}$  state of hydrogen. The Balmer-beta line was measured by polarization spectroscopy at the fundamental wavelength of the laser, 4,860 angstroms. The frequency-doubled output of the same laser was simultaneously employed to record a two-photon spectrum of the  $1S_{1/2}$ -to- $2S_{1/2}$  transition

at an effective wavelength of 1,215 angstroms. If the Bohr energy levels were exact, the two transitions would be observed at the same laser tuning, but the splittings of the energy levels introduce a small discrepancy. From the measured difference in the laser tunings for the two lines, the magnitude of the  $1S_{1/2}$  Lamb shift was calculated with a precision 50 times greater than that of other measurements. Value for hydrogen was found to be  $8,161 \pm 29$  megahertz.

of a selected atomic transition. At the proper frequency each atom in the gas can simultaneously absorb two photons coming from opposite directions.

Suppose an atom moving along the optical axis in the standing-wave field encounters two photons approaching from opposite directions. One of the photons is Doppler-shifted toward the blue, meaning higher frequencies, but the other photon is shifted toward the red by an equal amount. For a stationary atom both photons have the same energy. In all cases the total energy or frequency of the two absorbed photons is constant, regardless of the velocity of the atom. As long as the laser frequency is detuned slightly from half the transition frequency none of the atoms can absorb the two counterpropagating photons. (There is a small background signal, however, from moving atoms that absorb two photons propagating in the same direction.) When the laser wavelength matches the atomic transition, a sharp increase is observed in the number of excited atoms. The Doppler-free signal is strongly enhanced because all the atoms in the sample can contribute to it rather than just those that happen to be stationary. In this respect the method differs fundamentally from both saturation spectroscopy and polarization spectroscopy in which a population of atoms that are free of Doppler shifts is selected. In Doppler-free two-photon spectroscopy one Doppler shift is made to compensate for another.

A two-photon transition of particular interest is the transition from the  $1S_{1/2}$  state to the  $2S_{1/2}$  state. Because the latter state is a very long-lived one the line is expected to be extraordinarily narrow.

Theoretical estimates suggest a natural line width of about one hertz, or less than one part in  $10^{15}$ , which would make the transition one of the narrowest resonances known in any physical system. The  $1S_{1/2}$  state is in itself interesting because its Lamb shift is the largest one predicted by quantum electrodynamics. An atom at the energy level  $n = 1$  cannot have orbital angular momentum, and so there is no nearby  $P$  state from which the magnitude of the shift can be determined. The shift is simply a displacement of the  $1S_{1/2}$  energy level from the position it would have in the absence of quantum-electrodynamical effects. The magnitude of the shift can be determined only by an absolute measurement of some spectral component, such as the  $1S_{1/2}$ -to- $2S_{1/2}$  transition.

A two-photon excitation of this transition was first observed in 1974 by Siu Au Lee, Wieman and others at Stanford. The Lyman-alpha line has a wavelength of 1,215 angstroms; a photon with half this energy corresponds to a wavelength of 2,430 angstroms, which is still in the ultraviolet and beyond the reach of tunable dye lasers. The Stanford workers therefore employed a dye laser operating at 4,860 angstroms, or twice the required wavelength. The intense light from this source was shined on a crystal that served as a frequency doubler. Because of the high intensity of the applied electromagnetic field the crystal not only reradiated light at the original frequency but also was driven to emit overtones, including the second harmonic, at 2,430 angstroms. About 2 percent of the energy appeared at this wavelength.

The frequency-doubled ultraviolet radiation was reflected by a mirror to

form a standing wave inside a low-pressure gas-discharge tube. Hydrogen atoms that absorbed two photons returned to the ground state by emitting a single, far-ultraviolet photon at a wavelength of 1,215 angstroms. These photons escaped through a window at the side of the chamber and were detected by a photomultiplier.

The  $1S_{1/2}$ -to- $2S_{1/2}$  transitions of both hydrogen and deuterium were measured with this system. Each of these lines has a large hyperfine splitting, which is well resolved in the two-photon spectra. Transitions between the two hyperfine states in hydrogen are responsible for the 21-centimeter radiation that is an important signal in radio astronomy. There is also a large splitting between the hydrogen lines and the deuterium lines, caused chiefly by the difference in nuclear mass. This isotope shift was determined to an accuracy 1,000 times better than earlier measurements. A further improvement by a factor of 10 could provide a new value for the important ratio of electron mass to proton mass.

The greatest interest in the  $1S_{1/2}$  state is in the determination of the ground-state Lamb shift. In the 1950's Herzberg, who was then at the Yerkes Observatory of the University of Chicago, was able to detect the shift, but he measured its value to a precision of only about 14 percent. Two-photon spectroscopy provided an opportunity for a far more accurate determination.

The most straightforward approach to measuring the Lamb shift would be to determine the absolute wavelength of the  $1S_{1/2}$ -to- $2S_{1/2}$  transition, but the value of the Lamb shift calculated from



that wavelength also depends on an assumed value of the Rydberg constant. The Stanford group found a better method, exploiting a peculiar but not accidental coincidence: the fundamental wavelength of the dye laser, namely 4,860 angstroms, nearly coincides with the Balmer-beta line. If Bohr's formula were correct, the correspondence would be exact: the interval from  $n = 1$  to  $n = 2$  (Lyman-alpha) would be just four times the interval from  $n = 2$  to  $n = 4$  (Balmer-beta). Actually the levels are split and shifted somewhat by relativistic and quantum-electrodynamical corrections. The corrections for the  $n = 2$  and  $n = 4$  levels are known with great precision, however, and so a comparison of the two transitions can determine the ground-state Lamb shift.

Three such measurements have been carried out by the Stanford group, the most recent and the most accurate one by Wieman. The Balmer-beta reference line was observed by polarization spectroscopy, while the same laser simultaneously measured the Lyman-alpha line by two-photon spectroscopy. The Balmer-beta spectrum not only resolved the fine-structure components of the line but also revealed the splitting of these components in the weak axial electric field of the gas-discharge tube. In principle the ground-state Lamb shift could be determined by measuring the difference between the Balmer line and the  $1S$ -to- $2S$  line and then comparing the result with the predictions of the Dirac theory. Known corrections would be applied to the positions of the  $n = 2$  and  $n = 4$  levels; any remaining difference would be attributed to the Lamb shift of the  $1S$  state. In practice it was not quite as easy as that, because allowance had to be made for possible systematic errors and imprecisions in the apparatus. The result eventually derived was  $8,161 \pm 29$  megahertz. The experiment is still far short of the accuracy of the theoretic-

cal calculations, which give a value of  $8,149.43 \pm .08$  megahertz, but it represents a significant step beyond Herzberg's earlier measurement.

### Higher Resolution

Many formidable obstacles would have to be overcome in order to approach the one-hertz natural line width of the  $1S_{1/2}$ -to- $2S_{1/2}$  transition. It would not be enough to further reduce the bandwidth of the laser, because there are several other sources of line broadening. One of them is a second-order Doppler shift, a consequence of the special theory of relativity. An atom that is moving appears to oscillate slower than one at rest, so that the moving atom effectively has a lower resonant frequency no matter what the direction of motion is. The counterpropagating beams of two-photon spectroscopy cannot cancel this shift, which should amount to about 50 kilohertz for hydrogen atoms at room temperature.

Another source of line broadening is the finite transit time of a moving atom in the laser beam. Because a moving atom is exposed to the laser light only briefly, even the light from a continuous-wave laser is perceived by the atom as a pulse, whose short duration limits the potential resolution of the spectrum. In principle both effects could be reduced by slowing the atoms, or in other words by cooling the gas. In this regard it is encouraging that Daniel Kleppner of M.I.T. has recently shown that atomic hydrogen can be cooled to the temperature of liquid helium (4.2 degrees K.) without condensing, even though diatomic hydrogen molecules condense at 20 degrees K. Two of us (Schawlow and Hänsch) have recently pointed out that laser light itself might cool a gas to a low temperature. This may seem paradoxical, since an intense light usually sup-

plies heat, but it must be recalled that laser light, being coherent, represents a state of low entropy, or low disorder. A state of low entropy can be made to yield a low temperature.

Several laboratories are now attempting to apply the technique of two-photon spectroscopy to the  $1S_{1/2}$ -to- $2S_{1/2}$  transition of positronium, a hydrogen-like "atom" made up of an electron and its antiparticle, the positron. The properties of this exotic atom are predicted with great precision by quantum electrodynamics, and there is no need to apply corrections for the structure of the nucleus. The experiment is difficult, however, because positronium has a lifetime of only about 140 nanoseconds.

The hydrogen atom has been a focus of attention for almost a century, but the information embodied in this simple system of particles is by no means exhausted. Recent unified field theories, such as those of Steven Weinberg of Harvard University and Abdus Salam of the Imperial College of Science and Technology, predict subtle effects in hydrogen and other atoms that might be observed as small changes in the polarization of emitted or absorbed light. The changes are so small that there is some question of whether they can even be detected, but several groups of investigators are now attempting to measure them accurately enough to test the theories. As the technology of coherent light sources evolves it seems safe to predict that the exploration of the hydrogen spectrum will continue for decades. So far all the recent findings tend to confirm the predictions of theory. It is worth remembering, however, that several major upheavals in 20th-century physics were instigated by the discovery of minute discrepancies between theory and observation in this very spectrum. The hydrogen atom may hold surprises yet to come. On the other hand, perhaps the greatest surprise would be none at all.

### The Authors

**THEODOR W. HÄNSCH**, **ARTHUR L. SCHAWLOW** and **GEORGE W. SERIES** have utilized lasers for high-resolution optical studies of simple atoms. Hänsch is professor of physics at Stanford University. A native of West Germany, he was educated at the University of Heidelberg, which gave him his Ph.D. in physics *summa cum laude* in 1969. The following year he went to Stanford as a NATO Fellow, and in 1972 he joined the faculty. From 1973 to 1975 Hänsch was an Alfred P. Sloan Research Fellow. Schawlow is J. G. Jackson—C. J. Wood Professor of Physics at Stanford. Born in upstate New York, he received his Ph.D. from the University of Toronto in 1949. After two years as a postdoctoral fellow and research associate at Columbia Univer-

sity he became a research physicist at Bell Laboratories. He has been on the Stanford faculty since 1961. He was co-author with Charles H. Townes of the first paper describing the laser. In 1977 Schawlow was awarded the third Marconi International Fellowship, which was presented in Stockholm by the king of Sweden. Series is professor of physics at the University of Reading. He studied at the University of Oxford, where he obtained his Ph.D. in atomic spectroscopy. He then became lecturer in physics at Oxford, moving to Reading in 1969. Series is a Fellow of the Royal Society.

### Bibliography

**THE SPECTRUM OF ATOMIC HYDROGEN.** G. W. Series. Oxford University Press, 1957.

**ATOMIC SPECTRA.** W. R. Hindmarsh. Pergamon Press, 1967.

**OPTICAL RESOLUTION OF THE LAMB SHIFT IN ATOMIC HYDROGEN BY LASER SATURATION SPECTROSCOPY.** T. W. Hänsch, I. S. Shahin and A. L. Schawlow in *Nature Physical Science*, Vol. 235, No. 56, pages 63–65; January 24, 1972.

**AN EXPERIMENTAL DETERMINATION OF THE RYDBERG CONSTANT.** B. P. Kibble, W. R. C. Rowley, R. E. Shawyer and G. W. Series in *Journal of Physics B*, Vol. 6, pages 1079–1089; June, 1973.

**HYDROGEN  $1S$ - $2S$  ISOTOPE SHIFT AND  $1S$  LAMB SHIFT MEASURED BY LASER SPECTROSCOPY.** S. A. Lee, R. Wallenstein and T. W. Hänsch in *Physical Review Letters*, Vol. 35, No. 19, pages 1262–1266; November 10, 1975.



# Atomic hydrogen and fundamental physical constants

G W Series†§ and D N Stacey‡

† 4 Sandfield Road, Oxford, UK

‡ Clarendon Laboratory, Oxford, UK

Received 28 July 1982, in final form 6 September 1982

**Abstract** We describe techniques which allow the study, in undergraduate laboratories, of the spectrum of atomic hydrogen. The Rydberg constant, the electron-proton mass ratio, and the fine-structure constant are evaluated from the measurements. The key to the series of experiments is a discharge tube in which atomic lines dominate over the molecular lines.

**Résumé** Nous décrivons des techniques qui permettent l'étude du spectre de l'hydrogène atomique par des étudiants. La constante de Rydberg, le rapport entre la masse de l'électron et celle du proton, et la constante de structure fine sont déterminés à partir des mesures. L'élément essentiel pour la réalisation de cette série d'expériences est une source dans laquelle les raies atomiques dominent sur les raies moléculaires.

## 1. Introduction

The importance of atomic hydrogen and its spectrum in physics and in the teaching of physics surely needs no emphasis. But what may not be widely appreciated is that experimental study of the spectrum is beset with difficulties. Nevertheless, with some preparation on the part of the supervisor, the gross structure and some of the finer details may be investigated in the undergraduate laboratory to the point where students may obtain for themselves experimental values of the Rydberg constant, the ratio of electron mass to that of the proton, and the fine-structure constant. We describe a set of experiments which, in reaching these objectives, introduces the students to basic techniques of high and low resolution spectroscopy, and allows them to interpret the spectrum in the light of fundamental theory of atomic structure. The Rydberg constant is derived from measurements of the wavelengths of lines in the visible spectrum, the Balmer series, determined with reference to spectroscopic standards by the use of a diffraction grating. The electron-proton mass ratio is calculated from measured values of the spectroscopic isotope shift between hydrogen and deuterium, resolved by means of a Fabry-Perot etalon. The fine-structure constant is found from measurements of the doublet structure in the Balmer lines, again using interferometric techniques.

§ Until recently at J J Thomson Laboratory, University of Reading, UK

## 2. The light source

A difficulty encountered in any investigation of the atomic spectrum of hydrogen lies in the design of a suitable light source. Problems to be solved are: (i) how to suppress the molecular spectrum in favour of the atomic; and (ii) how to deal with the rapid absorption of gas by the walls of the tube and the electrodes. A third problem which arises in connection with the resolution of the doublet structure is how to reduce the Doppler broadening of the components of the fine structure. This last problem has hindered progress in research. In the most recent investigations (Amin *et al* 1981) highly-refined laser techniques were used in conjunction with a highly-collimated atomic beam. To read an account of this work and to gain some appreciation of it would not be beyond the scope of an able undergraduate after completing this set of experiments.

Lasers are not necessary for the experiments described here. Fortunately a type of light source described by Marcle (1960) overcomes the first two problems mentioned above. The reduction of Doppler broadening requires a modification of this, or a different design.

The Marcle source is essentially a Geissler tube using electrodes of pure copper (oxygen-free, high conductivity grade), with a side-tube containing a very concentrated solution of sodium hydroxide. The side-tube provides a reservoir of hydrogen as water at a vapour pressure dependent on the concentration. Atomic hydrogen is liberated in the



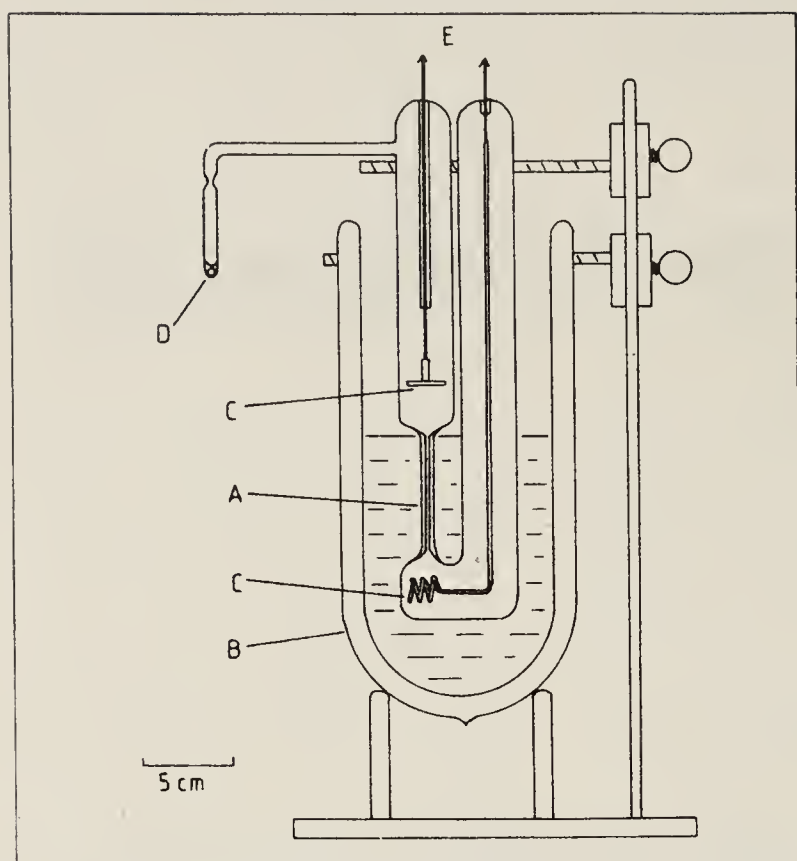


**Figure 1** Hydrogen discharge tube which can be cooled with liquid nitrogen (a modified form of the tube described by Marcley 1960). A, capillary tube, 1 mm bore, from which the light is taken. The liquid nitrogen level should be maintained near the top of the capillary. B, Dewar vessel containing liquid nitrogen, an unsilvered strip permits the radiation to escape. C, copper or aluminium electrodes. D, side-arm containing very concentrated solution of NaOH. E, to power supply, about 3000 V<sub>rms</sub>, with series resistor to limit current to below 20 mA.

discharge by dissociation of the water vapour, and the copper electrodes take care of the oxygen. A convenient power supply is a transformer providing about 3000 V<sub>rms</sub> and 20 mA. It is recommended that a resistor be placed in series with the discharge tube to limit the current to a little below this value.

Marcley gives a detailed drawing of the tube and gives instructions for filling. We follow his procedure, except that we use a diffusion-pumped high vacuum system rather than a simple rotary pump, and fill from a reservoir of H<sub>2</sub>O or a mixture of H<sub>2</sub>O and D<sub>2</sub>O depending on our requirements. Our experience confirms Marcley's claim of a useful life of 1500 h or more; our students are still working with some tubes filled six years ago. We have found pure aluminium a satisfactory alternative to copper as an electrode material.

For the measurement of fine structure, it is desirable to reduce Doppler broadening (see §5). At one time, we used an ordinary Geissler tube with its capillary region immersed in liquid nitrogen. The tube had a ballast volume connected to it to retard the drop in pressure due to absorption of gas.

Recently, however, we have introduced a modified Marcley tube (figure 1) which allows the discharge to be cooled. The capillary region is immersed in liquid nitrogen contained in a Dewar vessel which has an unsilvered strip to allow the radiation to escape. The modified version also operates satisfactorily without the coolant.

### 3. The Rydberg constant

With the discharge tube described in §2 the Balmer series is readily displayed by a grating spectrometer. Whether the observations be visual, photographic or photoelectric is a matter for local decision. The first four members of the series can be seen easily with the eye, while with care ten or more can be photographed (see figure 2). Whatever method is used the important feature is that the positions of the lines are to be measured and reduced to wavenumbers by a standard spectroscopic technique. One possibility is to determine the grating space by reference to some spectral line which is taken as a secondary standard. The green line of mercury (18 307 cm<sup>-1</sup>) is convenient for this purpose. An alternative technique is to make use of helium lines in the visible spectrum (they span the red to the violet; mercury can also be used, although the red lines are rather weak) as secondary standards to determine the constants in an empirical dispersion equation, or to determine corrections if the constants are over-determined. This affords experience in least-squares analysis.

From the wavenumbers  $\tilde{\nu}_n$  the Rydberg constant  $R$  is obtained by use of the equations

$$\tilde{\nu}_n = R(1/4 - 1/n^2), \quad n = 3, 4, 5 \dots \quad (1)$$

Strictly speaking, the Rydberg so determined is that appropriate to the isotope present in the discharge tube rather than  $R_\infty = (me^4/4\pi\hbar^3c)(1/4\pi\epsilon_0)^2$  which is the expression appropriate to a nucleus of infinite mass. It is possible to measure with enough precision to distinguish between  $R_\infty$ ,  $R_H$  and  $R_D$  even with experiments based on a small diffraction grating (see table 1). However, this 'nuclear mass effect' is more appropriately studied interferometrically (see §4).

Our manuscript for this experiment written for the students refers to Balmer's formula for this series,  $\lambda_n = 3645.6 n^2/(n^2 - 4) \text{ \AA}$ , to Bohr's expression for the energy levels,  $E_n = R\hbar c/n^2$  ( $R$  in units of  $2\pi \times$  number of waves per unit length), and to the fact that Schrödinger's equation for the hydrogen atom uncorrected for relativistic effects such as electron spin and with  $V = -e^2/4\pi\epsilon_0 r$  gives the same expression for energy eigenvalues as does Bohr's theory.

An example of the Balmer spectrum photographed from a tube containing H<sub>2</sub>O and D<sub>2</sub>O with a simple grating spectrograph is shown in figure 2.



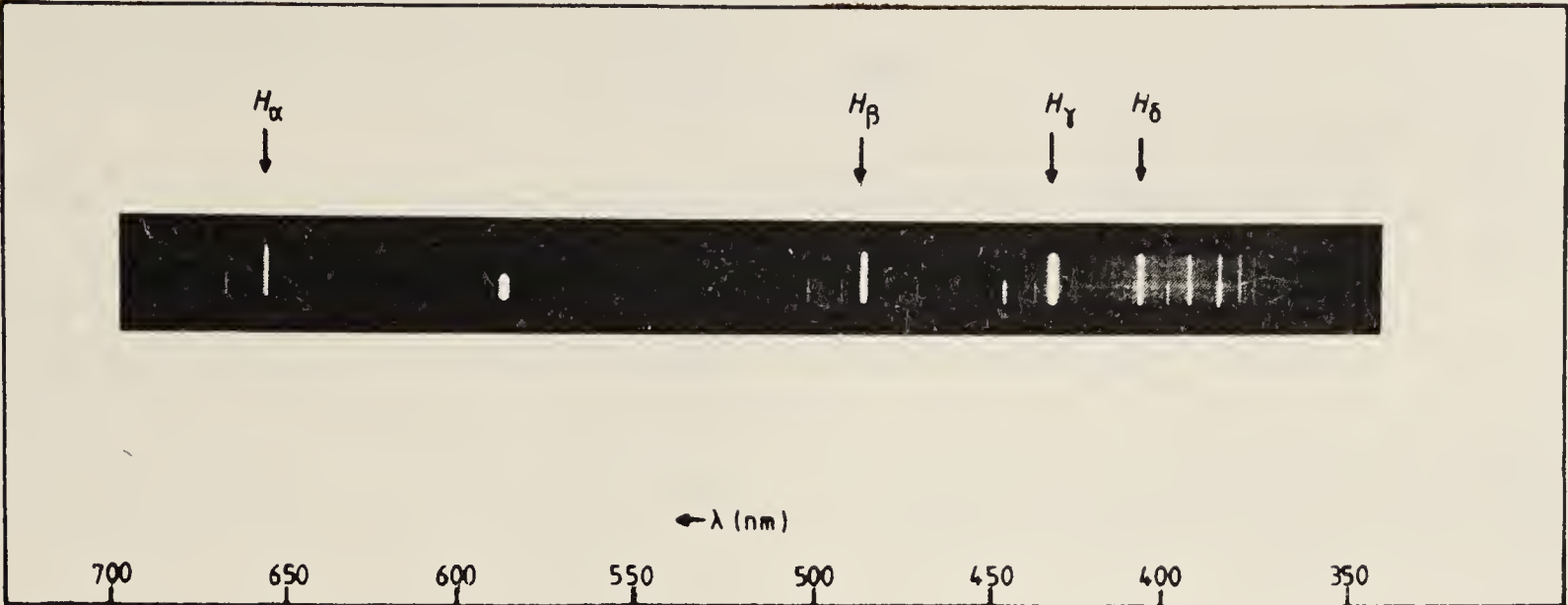


**Figure 2** Photograph of the Balmer series from a Marcle tube filled with a mixture of H<sub>2</sub>O and D<sub>2</sub>O. It is the first order ‘normal’ spectrum of a 45 cm grating spectrograph, so that the dispersion is almost linear ( $d\lambda/dx \approx 4 \text{ nm/mm}$  on the original photograph). The lower series members need an exposure time of typically about 30 s; this photograph was exposed for 45 min with a blue filter to bring out the higher members. The calibration spectrum was obtained from a helium Geissler tube; only half the slit was illuminated by this source to allow the hydrogen and helium spectra to be distinguished.

The atomic lines are dominant, but weak molecular lines are to be seen. The helium spectrum has been superposed for calibration; only half the slit was illuminated by the helium lamp, allowing the lines to be distinguished from those of hydrogen. Doubling of several of the lines due to isotopic structure is not clearly visible in the reproduction but can be seen in the original photograph.

Table 1 shows a set of wavenumbers determined from this photograph. The value of  $R$  (in fact the mean of  $R_H$  and  $R_D$ ) obtained from a least-squares analysis of these results is  $109\,696(5) \text{ cm}^{-1}$

4. The electron–proton mass ratio

4.1. Experimental details

This ratio is obtained from an interferometric determination of the isotope shift between the lines of hydrogen and deuterium, photographed from a Marcle discharge tube with a D<sub>2</sub>O–H<sub>2</sub>O mixture. One aims to generate the lines of each isotope with roughly equal intensity, although there is an advantage in having one set of lines rather stronger than the other, for then one can determine which lines belong to which isotope.

Rather than fill a tube with a mixture of isotopes one can use different tubes, one for each isotope, and a beam splitter to reflect the light from one lamp into the optical train aligned for the other. An important technical point emerges here: if the two beams do not follow the same path through the interferometer, spurious displacements between the two sets of fringes may occur.

In our experiments, we use a Fabry–Perot etalon with 25 mm plates and a spacer of about 0.5 mm giving a free spectral range of  $10 \text{ cm}^{-1}$  (see §4.2) Our spacers are made from a metal annulus. (The fine structure (§5) is more than an order of magnitude smaller than the isotopic structure and is typically not resolved with a free spectral range of this magnitude.) No great demands are made on the reflectivity of the coatings to achieve resolution

**Table 1** Wavenumbers ( $\text{cm}^{-1}$ ) of the Balmer lines. Results obtained from measurements of the photograph shown in figure 2. The second column gives the mean wavenumber of a hydrogen–deuterium pair; the uncertainty in each case is about  $\pm 2 \text{ cm}^{-1}$ . The third column gives the measured isotope shift  $\Delta\tilde{\nu}(\text{D} - \text{H})$ ; the over-exposure needed to bring out the higher series members made it unmeasurable for  $n = 4, 5$  and  $6$ . The known values are given for comparison with these measurements and with the more accurate results obtained interferometrically (§4 and §5).

$n$	$\nu$	$\Delta\tilde{\nu}(\text{D} - \text{H})$	
		Measured	Actual value
3	15234.1	4.7	4.145
4	20565.4	—	5.60
5	23032.5	—	6.27
6	24375.1	—	6.64
7	25184.0	8.3	6.86
8	25711.8	7.5	7.00
9	26069.6	7.9	7.10
10	26325.7	—	—
11	26519.6	—	—

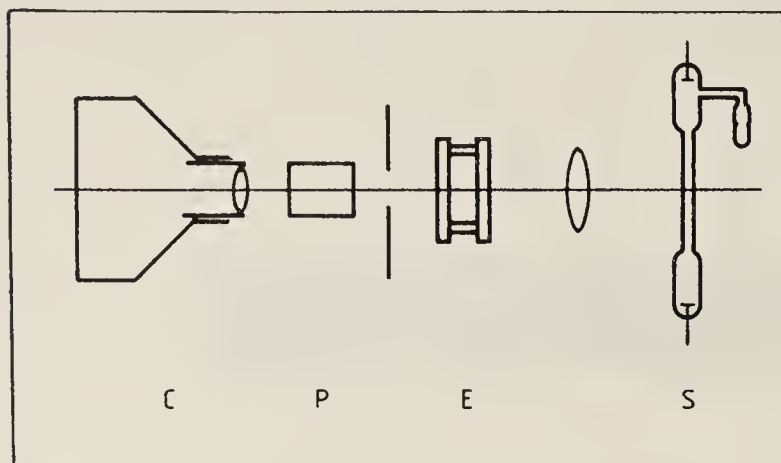


**Figure 3** A simple optical system to enable the isotope shift in  $H_\alpha$ ,  $H_\beta$  and  $H_\gamma$  to be recorded photographically. S, source; P, direct-vision prism; E, etalon, C, camera.

of the isotopic structure, but they need to be broad-band because of the wavelength range to be covered. We provide aluminium-coated plates with reflectivity of about 85% in the green.

With the Marcle lamps the atomic lines are sufficiently strong against the molecular background to be isolated with interference filters, or even gelatin-dye filters. The optical system is then extremely simple; the interferometer is placed in the collimated beam from the discharge tube and the Haidinger fringes focused by a lens onto a photographic emulsion.

Instead of filters we have used a compound (direct-vision) prism, having an unobstructed area a little larger than the aperture of the etalon plates and a dispersion of about 0.04 rad between the red and violet. This optical system is shown in figure 3. With a camera lens of about 25 cm focal length, this provides a separation of about 9 mm between  $H_\alpha$  and  $H_\gamma$ , which is sufficient to separate the images of the discharge tube formed by the light of the first three Balmer lines (see figure 4). The

optical train is now effectively a spectrograph, with the discharge tube taking the place of the slit of the collimator.

#### 4.2. Theory

To the accuracy the student can be expected to achieve in this experiment, say 0.5%, the isotope shift for hydrogen can be assumed to be entirely due to the difference in nuclear masses. Other effects, due to the nuclear volume and quantum electrodynamic corrections, for example, are quite negligible at this level.

The isotope shift is easily found from equation (1). We have

$$R_H = R_\infty(1 + m/M_H)^{-1} \approx R_\infty(1 - m/M_H),$$

with a similar expression for  $R_D$ . Hence

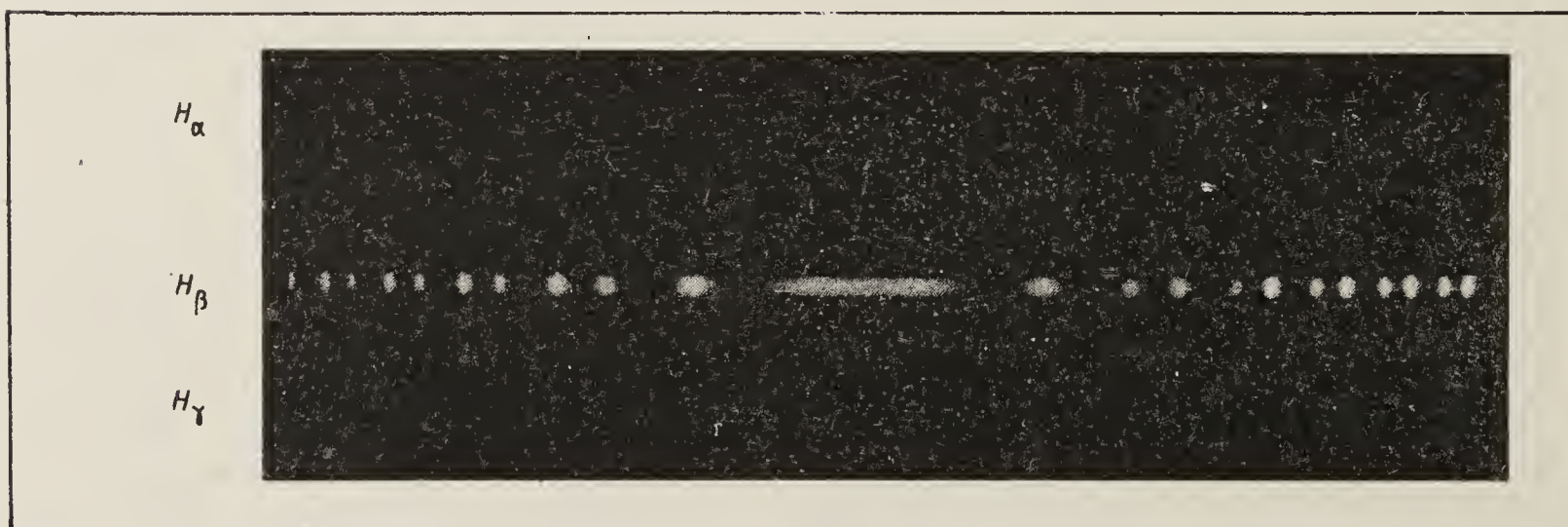
$$\frac{R_D - R_H}{R_\infty} \approx m \left( \frac{1}{M_H} - \frac{1}{M_D} \right).$$

Now  $M_H$  is equal to  $M_D/2$  to better than 1 part in  $10^3$ , so for the present purposes we may write

$$\frac{R_D - R_H}{R_\infty} \approx \frac{1}{2} \left( \frac{m}{M_H} \right).$$

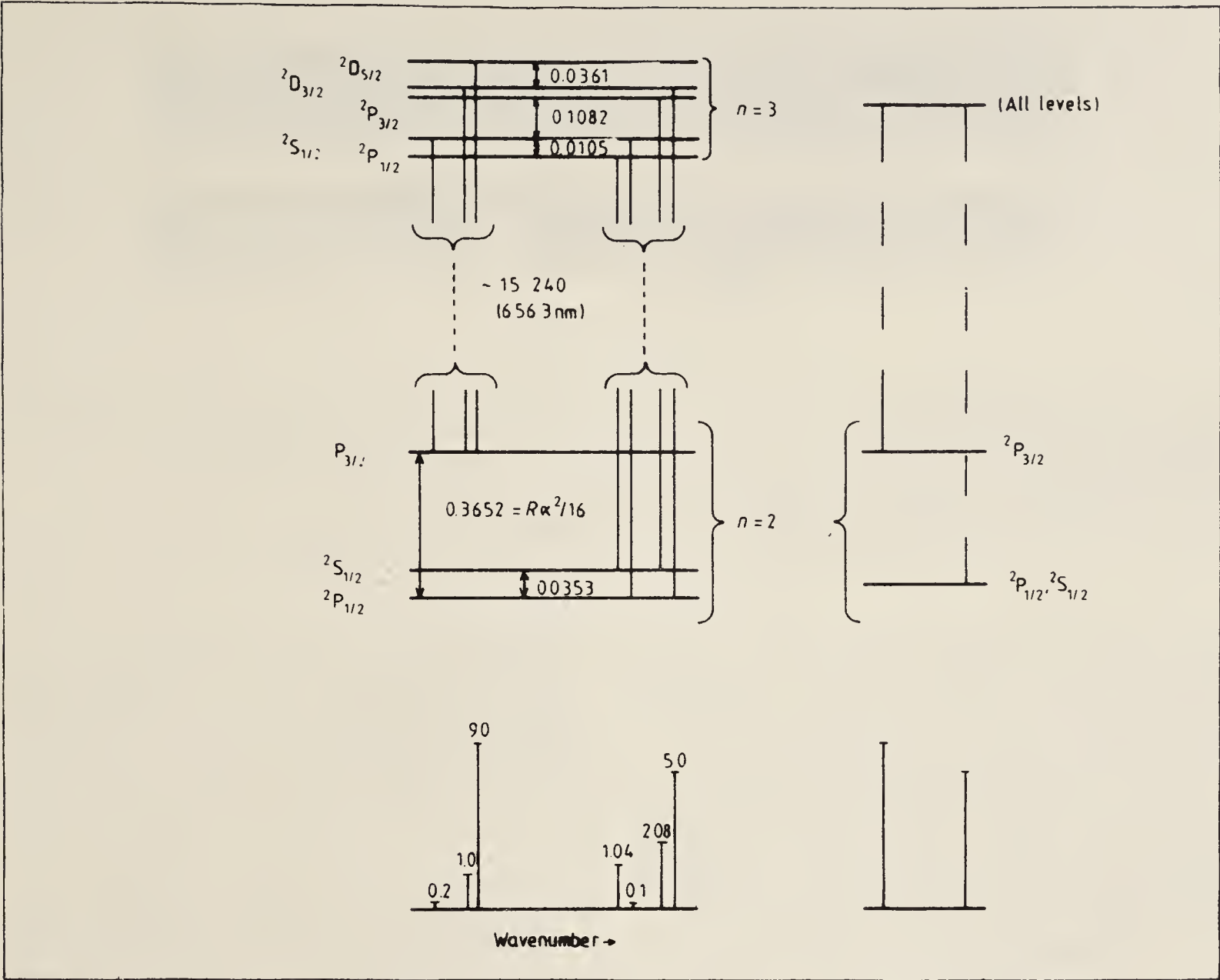
Hence, for any line,  $\Delta\tilde{\nu}/\tilde{\nu} \approx \frac{1}{2}m/M_H$ , and the student can determine a value for the mass ratio from any member of the Balmer series. The isotope shifts of the first few members are given for reference in table 1.

Figure 4 shows the isotopic structure in  $H_\alpha$ ,  $H_\beta$  and  $H_\gamma$ , photographed using the system shown in figure 3. The results obtained from the measurements are in table 2. It can be seen that  $10 \text{ cm}^{-1}$  is a convenient free spectral range to study these structures.



**Figure 4** Photograph of the isotopic structure in  $H_\alpha$ ,  $H_\beta$  and  $H_\gamma$  obtained with the apparatus shown in figure 3. The etalon spacing was 0.513 mm. On the original photograph the images of the discharge tube, crossed by fringes, were 40 mm long. Measurement of the fringes gives the results shown in table 2.





**Figure 5** Fine structure in  $H_\alpha$ . The energy levels with  $n = 2$  and  $3$  are shown with the transitions between them. The simplified diagram shows an approximate interpretation of the doublet structure which can be resolved using the apparatus described in §5. This gives a value of the fine-structure constant to a precision of about 10%. The intervals are in  $\text{cm}^{-1}$ .

**5. The fine-structure constant**

The spectral lines of hydrogen have a fine structure which is more complicated than, for example, the doublet structure of the sodium lines. The complication is attributable to the particular functional form of the field of the nucleus acting on the electron, the Coulomb field, which results in a near-degeneracy of orbital states belonging to the same principal quantum number. In consequence, transitions between different spectroscopic multiplets ( $nl \rightarrow n'l'$ ) overlap, for given  $n$  and  $n'$ . The fine structure of Balmer- $\alpha$  ( $n = 3$ ,  $n' = 2$ ) is shown in figure 5. The overlapping multiplets are (3s-2p), (3p-2s), (3d-2p). Hyperfine structure is not shown in figure 5. It exists and has been measured but it is well below the limit of resolution with the experimental techniques described here.

No simple formula describes the structure shown in figure 5; even the Dirac theory omits important quantum electrodynamic effects. Fortunately, we need not concern ourselves here with detailed

theoretical expressions for the structure, since some of the terms go beyond the level of an undergraduate course and in any case the structure cannot be completely resolved with simple equipment on account of the overlapping of components caused by Doppler broadening. Nevertheless, the partially-resolved structure has a certain simplicity

**Table 2** Isotope shifts in the Balmer lines. Results obtained from measurements of the photograph shown in figure 4. The electron-proton mass ratio  $m/M_H$  is derived as explained in the text. A more accurate value can be found from photographs taken with a larger etalon spacing as described in §5.

$n$	$\Delta\tilde{\nu}(\text{D} - \text{H}) (\text{cm}^{-1})$	$m/M_H$
3	4.13(3)	1/1845(13)
4	5.65(6)	1/1820(20)
5	6.30(4)	1/1829(12)

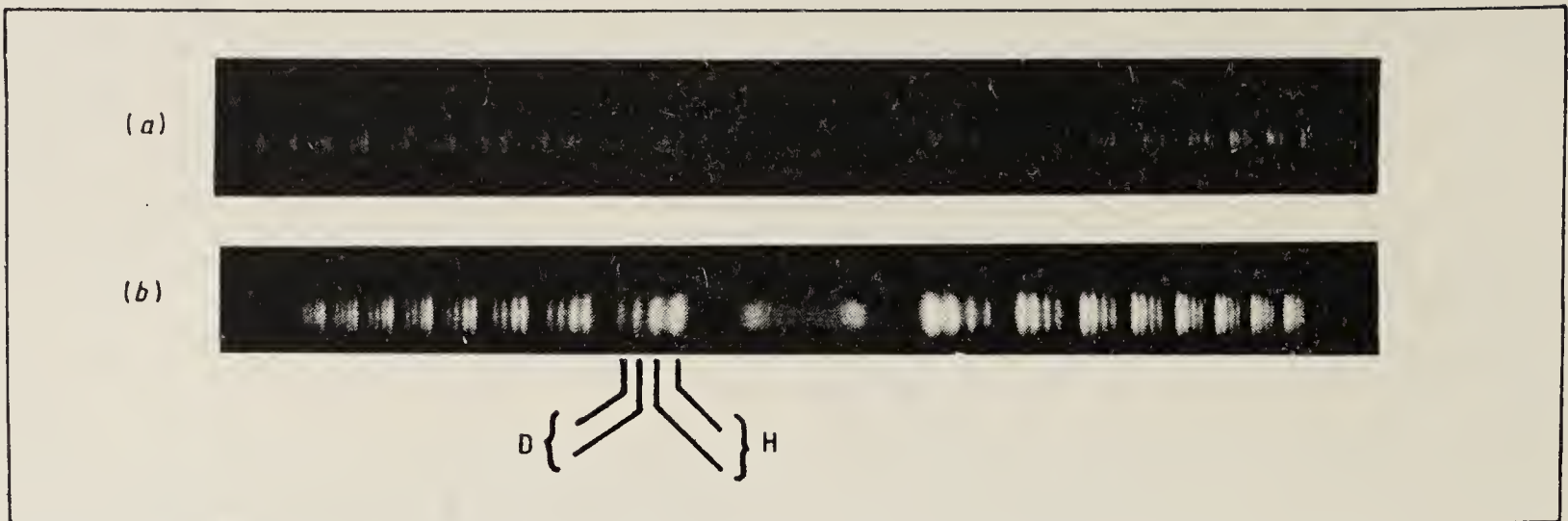


**Figure 6** (a) Photograph of the doublet structure in  $H_\alpha$  and  $D_\alpha$  obtained with an uncooled source. The etalon spacing is 2.865 mm. The resolution is poorer in the lighter isotope, due to the greater Doppler width. (b) Photograph with a liquid-nitrogen cooled source. The improvement in resolution allows the doublet structure to be measured for both isotopes. The results are given in the text. The isotope shift can be measured from either (a) or (b); a value from the latter is also given in the text.

which allows the fine-structure constant  $\alpha$  to be determined to an accuracy of about 10% of its value (we recall that  $\alpha$  is a measure of relativistic effects and is given by  $(e^2/\hbar c) (1/4\pi\epsilon_0)$ ).

It will be noticed that the transitions fall into two groups in which the dominant splitting is the  $2(^2P_{1/2} - ^2P_{3/2})$  interval,  $\delta$ , due almost entirely to spin-orbit interaction. The theoretical expression for this interval, which a student can be expected to understand (see for example, Woodgate 1980) is

$$\delta = (E_{2,1/2} - E_{2,3/2})/\hbar c = R\alpha^2/16.$$

(We have disregarded very small contributions from quantum electrodynamic shifts of these P levels.)

Experimentally, one can resolve a doublet, each member of which is a blend. To a first approximation one can determine  $\alpha$  by equating the measured doublet interval to the theoretical  $^2P_{1/2} - ^2P_{3/2}$  interval. A better value for  $\alpha$  can be obtained by correcting the theoretical expression to allow for the unresolved structure within each component of the doublet. However, this requires the student to take on trust a great deal of information which he has no way of checking for himself; the other intervals involved, the widths of the lines, and the relative intensities of the components. On balance we prefer to avoid this loss of simplicity but interested students can of course improve their results for  $\alpha$  if the additional analysis involved appeals to them.

The optical arrangement illustrated in figure 3 is convenient for this stage of the investigation, except that the prism should be replaced by a filter if a cooled tube is employed. Useful observations can in any case only be made on  $H_\alpha$  (the Doppler widths of the other lines are too large) and the cooled tube gives overlapping images due to scat-

tered light if other lines are not filtered out.

It is instructive to carry out the experiment with a source containing both hydrogen and deuterium to illustrate the limitations imposed by the Doppler width. The hydrogen and deuterium fringe systems need to be clearly separated, the best resolution being obtained with the largest interferometric free spectral range consistent with this requirement. We have found a spacing of 2.9 mm a convenient value. With a plate reflectivity 90% or higher, the width of the instrumental line profile for monochromatic light is less than  $0.06 \text{ cm}^{-1}$  and does not seriously limit the resolution. This reflectivity is best achieved with multilayer dielectric coatings; silver can be used but needs replacing within a few months if kept in an ordinary laboratory atmosphere. Figure 6(a) shows a photograph taken using an uncooled source. The inferior resolution of the doublet due to hydrogen compared with that due to deuterium is readily observable on the original photograph (the Doppler widths at room temperature are  $0.19 \text{ cm}^{-1}$  and  $0.13 \text{ cm}^{-1}$  respectively). With a cooled source (figure 6(b)) both sets of fringes are well resolved.

Photographs of the type shown in figure 6 may also be used for determination of the isotope shift. Adjacent doublets of  $H_\alpha$  and  $D_\alpha$  do not belong to the same order, but the fractional order may be determined by measurement and the integral order difference may be found from the results of the experiment described in §4. This illustrates an important point concerning measurements with a Fabry-Perot etalon; results should always be obtained if possible with more than one spacing, first to enable the relative order numbers of the various components present to be established uniquely and secondly as a check against systematic error.

Measurement of the photograph shown in figure



6(b) gave the following results:

$$\delta = 0.348(3) \text{ cm}^{-1}(\text{H}_\alpha) \quad 0.326(5) \text{ cm}^{-1}(\text{D}_\alpha).$$

The quoted error is entirely statistical; as explained earlier, these measurements give only an approximate value of the  $2p^2P_{1/2,3/2}$  fine structure interval. The line-shape dependence of the measured splitting is apparent from the difference in the results for hydrogen and deuterium. We obtain

$$\alpha^2 \approx 4.91 \times 10^{-5} \quad \alpha \approx 1/143.$$

The isotope shift  $\text{D}_\alpha - \text{H}_\alpha$  is found to be  $4.151(6) \text{ cm}^{-1}$ , the uncertainties due to statistical spread and to measurement of the etalon spacing give comparable contributions to the quoted error. From this shift we obtain

$$m/M_H = 1/1836(3).$$

The interferometric experiments described in §4 and §5 are generally carried out by students in the third or late second year of their course. They do not normally combine their results with those from the grating experiment, which is usually performed much earlier. However, it is interesting to do so since it is then possible to obtain a value for  $R_\infty$  based only on measurements which the student can carry out for himself. The simple expressions in §4.2, together with the results for  $(R_H + R_D)/2$  and  $m/M_H$  given above lead to the value

$$R_\infty = 109\,739(5) \text{ cm}^{-1}.$$

This and the other results obtained in the experiments described can be compared with the data in the appendix taken from the literature.

#### Acknowledgments

We wish to acknowledge the contributions made over the years by many of our colleagues in the Clarendon Laboratory to the development of the experiments described here. Valuable technical assistance has been provided by Mr B E Coates, who has been generally responsible for the experiments. He produced the cooled version of the Marcley tube and has constructed and filled all our hydrogen and deuterium sources. Mr C W Goodwin has maintained a continuous supply of high quality etalon coatings.

#### Appendix

Some recent results reported in the literature are:

$$m/M_H = 1/1836.15300(25)^a$$

$$\alpha = 1/137.036007(11)^b$$

$$R_\infty = 109\,737.31521(11)^c \text{ cm}^{-1}$$

$$\Delta\tilde{\nu}(\text{D}_\alpha - \text{H}_\alpha) = 4.144931(2)^c \text{ cm}^{-1}$$

<sup>a</sup> Van Dyck and Schwinberg (1981).

<sup>b</sup> Cohen (1980).

<sup>c</sup> Amin *et al* (1981).

#### References

- Amin S R, Caldwell C D and Lichten W 1981 *Phys. Rev. Lett.* **47** 1234–8
- Cohen E R 1980 in *Atomic Masses and Fundamental Constants* ed. J A Nolen and W Benenson (New York: Plenum) vol 6 p 525
- Marcley R G 1960 *Am. J. Phys.* **28** 35–8
- Van Dyck Jr R S and Schwinberg P B 1981 *Phys. Rev. Lett.* **47** 395–8
- Woodgate G K 1980 *Elementary Atomic Structure* 2nd edn (Oxford: Oxford University Press) pp 61–9





## Double resonance measurements of hyperfine structures in potassium

BY G. J. RITTER AND G. W. SERIES

*The Clarendon Laboratory, University of Oxford*

(Communicated by H. G. Kuhn, F.R.S.—Received 8 June 1956—

Revised 23 August 1956)

Radio-frequency magnetic resonances have been studied between the states of the atomic level  $5^2P_{\frac{1}{2}}$ , excited in a coarse atomic beam of potassium by optical resonance radiation. The resonances were detected by observing changes in the intensity of the scattered resonance radiation. Hyperfine structure was observed in the Paschen-Back region, and in magnetic fields down to zero. Values of  $a$  and  $b$ , the magnetic dipole and electric quadrupole interaction constants, derived independently from measurements in the strong and zero field regions, are in agreement. The values  $a = 1.97 \pm 0.1$  Mc/s,  $b = 1.7 \pm 0.3$  Mc/s have been obtained for the interaction constants of  $^{39}\text{K}$ . Double quantum transitions between hyperfine structure levels were observed in zero field. The nuclear magnetic moment derived from  $a$  agrees with molecular beam magnetic resonance measurements; the nuclear electric quadrupole moment derived from  $b$  is  $0.11_3 \pm 0.02 \times 10^{-24}$  cm<sup>2</sup>.

Hyperfine structure was also observed in the level  $5^2P_{\frac{3}{2}}$ . A preliminary value for the  $a$  factor is  $9.3 \pm 0.5$  Mc/s.

### INTRODUCTION

The hyperfine structure of the ground state of potassium, which was measured to high precision by Kusch, Millman & Rabi (1940), does not allow a determination of the nuclear electric quadrupole moment, since the electronic angular momentum quantum number  $J$  is  $\frac{1}{2}$ . Optical measurements of the hyperfine structure of the ground and excited states are limited by the Doppler width of the lines which, even under the favourable conditions of atomic beam spectroscopy (Jackson & Kuhn 1938) did not allow resolution of the hyperfine structure of any level having  $J > \frac{1}{2}$ .

The line width in the 'double-resonance' method, first suggested by Brossel & Kastler (1949) and explored by Brossel & Bitter (1952), is limited only by the natural width of the energy levels; the Doppler width, being proportional to the frequency which is actually measured, is completely negligible. This method, therefore, offered the possibility of the resolution of hyperfine structure in some excited state having  $J > \frac{1}{2}$ , and of determining the nuclear electric quadrupole moment.

The magnitude of the hyperfine structure in potassium is exceptionally small because of the small nuclear magnetic moment and the small value of  $(1/r^3)$ . Numerical estimates indicated that in the first excited  $P_{\frac{3}{2}}$  level the  $a$  factor would be about 5 Mc/s, while the double resonance line width would be at least 12 Mc/s. The second  $P_{\frac{3}{2}}$  level, ( $5^2P_{\frac{3}{2}}$ ), however, has a much weaker transition probability to the ground level and the natural width is smaller than the hyperfine structure. An experiment was, therefore, designed to investigate the hyperfine structure of the level  $5^2P_{\frac{3}{2}}$ . A brief report has already been published (Ritter & Series 1955).

The experimental method may be understood from figure 1, which shows the Zeeman components of the ground level and of the level  $5^2P_{\frac{3}{2}}$ . For the moment we ignore the hyperfine structure and notice that optical radiation of wavelength

4044 Å will excite the states  $|\pm \frac{3}{2}\rangle, |\pm \frac{1}{2}\rangle$  of  $5^2P_{3/2}$  (the states are distinguished by their quantum number  $M_J$ ), but that these states will be populated unequally unless the exciting radiation is isotropic. In particular, if the exciting radiation is polarized with the electric vector parallel to an applied magnetic field ( $\pi$  excitation,  $\Delta M_J = 0$ ), the states  $|\pm \frac{1}{2}\rangle$  alone are populated. Decay to the ground level may be by emission of  $\pi$  ( $\Delta M_J = 0$ ) or of  $\sigma$  ( $\Delta M_J = \pm 1$ ) radiation. If, however, some of the excited atoms in the states  $|\pm \frac{1}{2}\rangle$  are transferred to  $|\pm \frac{3}{2}\rangle$  by some process, they can decay by emission of  $\sigma$  light only. An increase in the amount of  $\sigma$  radiation is thus an indication of a change of orientation of the excited atoms.

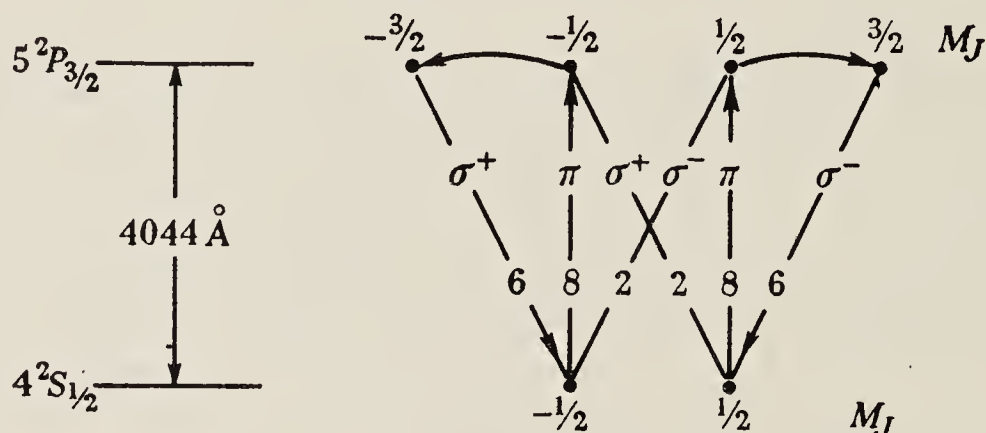


FIGURE 1. Optical and radio-frequency transitions, ignoring the hyperfine structure. The relative intensities are marked for optical excitation in a direction perpendicular to a magnetic field.

The change of orientation may be induced by the magnetic component of a radio-frequency field rotating at the frequency of the Larmor precession of the atoms in a steady magnetic field. The experiment is then a paramagnetic resonance experiment performed on excited atoms. Resonance is detected, not by measuring changes in the power absorbed in a resonant circuit, but by observing changes in the intensity of the optical radiation in some fixed direction, which may be that of the steady magnetic field, in which direction one sees  $\sigma$  light only.

The transitions  $\Delta M_J = \pm 1$  occur at the same frequency. A symmetrical hyperfine structure is found in these transitions taken together if the magnetic field is strong enough to decouple  $I$  and  $J$  completely; at smaller fields the structure is asymmetrical, and in zero field, transitions occur between the hyperfine structure levels themselves.

Radio-frequency resonances in the strong, intermediate and zero field regions are described in § 4*a*, *b* and *c*. In § 4*d* are described experiments in which the state of polarization of the exciting radiation was altered. Resonances in the  $P_{3/2}$  level were detected.

## 2. THEORETICAL

### (a) Theory of the energy levels

The experiments have been interpreted with reference to the following Hamiltonian, which represents the energy of the atom in the absence of the radio-frequency field:

$$\mathcal{H} = a\mathbf{I} \cdot \mathbf{J} + \frac{b}{2I(2I-1)J(2J-1)} [3(\mathbf{I} \cdot \mathbf{J})^2 + \frac{3}{2}(\mathbf{I} \cdot \mathbf{J}) - I(I+1)J(J+1)] + \beta g_J \mathbf{J} \cdot \mathbf{H} + \beta_N g_I \mathbf{I} \cdot \mathbf{H}. \quad (1)$$



In this expression,  $a$  is the magnetic dipole interaction constant of the hyperfine structure, and  $b$  is the electric quadrupole interaction constant. The last two terms represent the interaction with an external steady field  $H$  of the electronic and nuclear magnetic moments respectively, and of these we ignore the latter since its magnitude is very small compared with the line width in the experiments.  $\beta$  and  $\beta_N$  are the Bohr and nuclear magnetons respectively.

$a$  and  $b$  are determined from the experiments. The value of  $a$  derived from the known value of the magnetic moment and the Goudsmit formula is, for comparison,

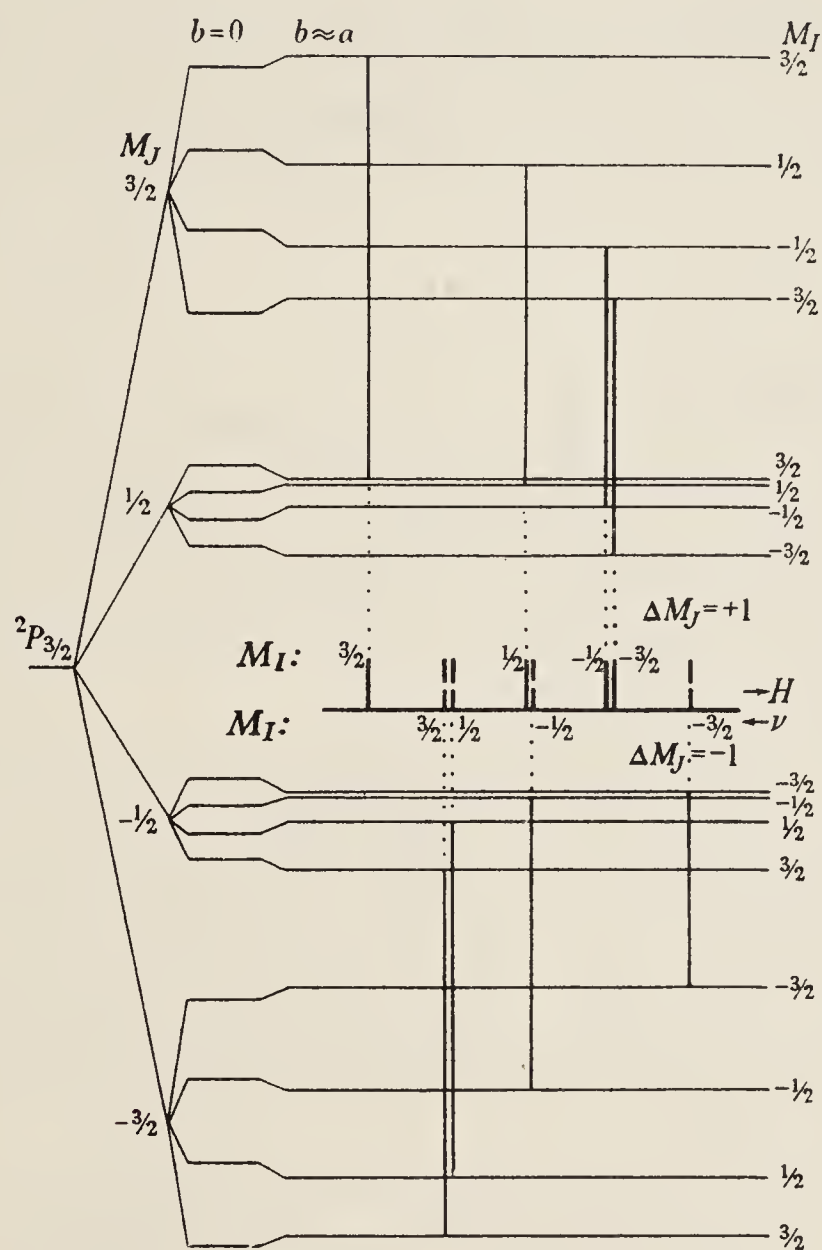


FIGURE 2. Energy levels and radio-frequency transitions in a 'strong' magnetic field.

about 1.9 Mc/s. From  $b$ , or more reliably from  $b/a$  (see Davis, Feld, Zabel & Zacharias 1949), the nuclear electric quadrupole moment  $Q$  can be calculated.

The energy levels in strong field derived from the above Hamiltonian are given by

$$W_{M_J, M_I} = GM_J + aM_J M_I + (b/36) [3M_J^2 - 15/4] [3M_I^2 - 15/4], \quad (2)$$

where  $G = g_J \beta H$ ;  $M_J = \pm \frac{3}{2}, \pm \frac{1}{2}$ ;  $M_I = \pm \frac{3}{2}, \pm \frac{1}{2}$  (see Kopfermann 1956, where the weak field formulae may also be found). Figure 2 shows a plot of the strong field levels in which  $b$  has been taken approximately equal to  $a$ , and in which the transitions allowed by the selection rules  $\Delta M_J = \pm 1$ ,  $\Delta M_I = 0$  have been drawn. All of these have equal intensity. Transitions between  $M_J = \pm \frac{1}{2}$  presumably also take place, but are not observed under excitation by  $\pi$  light since these two states

are equally populated. Small corrections calculated by second-order perturbation theory were applied to (2) to allow for incomplete decoupling of  $I$  and  $J$ .

Two lines, namely,  $|\frac{3}{2}, \frac{3}{2}\rangle - |\frac{1}{2}, \frac{3}{2}\rangle$  and  $|\frac{1}{2}, -\frac{3}{2}\rangle - |-\frac{3}{2}, -\frac{3}{2}\rangle$  (in the  $|M_J, M_I\rangle$  notation) could be located in intermediate fields. The energy levels concerned come from the linear and quadratic factors into which, among others, the secular equation factorizes. Solution of these equations yields the following result for the frequencies of the transitions

$$h\nu = \pm \frac{(3a+b)}{2} + \frac{G}{2} + \sqrt{\left\{\left(\frac{3a+b}{2}\right)^2 + \left(\frac{G}{2}\right)^2\right\}},$$

where the positive sign applies to the first-named transition above. The difference in frequency between these two lines, at constant field, is  $(3a+b)$ .

In intermediate fields transitions according to the selection rules  $\Delta M_J = \pm 1$ ,  $\Delta M_I = \mp 1$  were observed when the radio-frequency magnetic field was parallel to the steady field.

#### (b) *Theory of the radio-frequency transitions*

The approximations usually made in the theory (see, for example, Ramsey 1956) are not all valid here. In particular, the perturbation introduced by the radio-frequency field, which is necessarily of the order of magnitude of the natural width of the levels, is in some of these experiments comparable with the resonance frequency. The latter may not then be the same as the frequency interval between the unperturbed levels. A complication in the case of the experiments at zero field is that the levels themselves are degenerate.

We have attempted to make estimates of the necessary corrections and find that at the lower frequencies they become comparable with the frequency itself. On the other hand, these resonance frequencies taken uncorrected are concordant with the high-frequency results where the correction is negligible. This suggests that our estimates of the corrections are pessimistic. In the absence of a complete theory of the transition process, we therefore make the following assumption in interpreting our results: *the resonance frequencies are not appreciably different from the frequency differences between the levels.*

A complete theory should take account of the further point that the line width is comparable with the hyperfine structure. Under perturbation by a radio-frequency field the coupling between electron and nucleus may then be weakened, even when the frequency is considerably larger than the line width.\* To this effect we attribute the fact that the observed strong field patterns showed signs of more complete de-coupling than was expected.

#### (c) *Multiple quantum jumps*

Transitions have been observed on a number of occasions between states  $|M\rangle$ ,  $|M+n\rangle$  when the intervening  $(n-1)$  states are unequally spaced (see, for example, Kusch 1956). Such lines are predicted (Salwen 1955) to be narrower than the single quantum jumps in the ratio  $1/n$ , and their intensities are more strongly dependent on the radio-frequency field strength. We interpret some of our resonances in zero field as double quantum jumps.

\* We are indebted to Professor V. F. Weisskopf for a discussion of this point.



## 3. EXPERIMENTAL

The apparatus, shown schematically in figure 3, comprises a light source, a resonance bulb and its associated coils, and detecting equipment.

(a) *The light source*

This was a hollow cathode tube similar to that described by Kelly, Kuhn & Pery (1954), but larger. The cathode cavity, of diameter about 12 mm, allowed a normal type of discharge at a current of 250 mA. Both electrodes were water-cooled. The potassium spectrum was strongly excited from metallic potassium in the cavity, while the spectrum of the carrier gas, neon, was largely suppressed by a filter of ammoniated copper sulphate solution. The essential condition that the potassium resonance lines 4044 and 4047 Å should not show self-reversal was checked by interferometric examination.

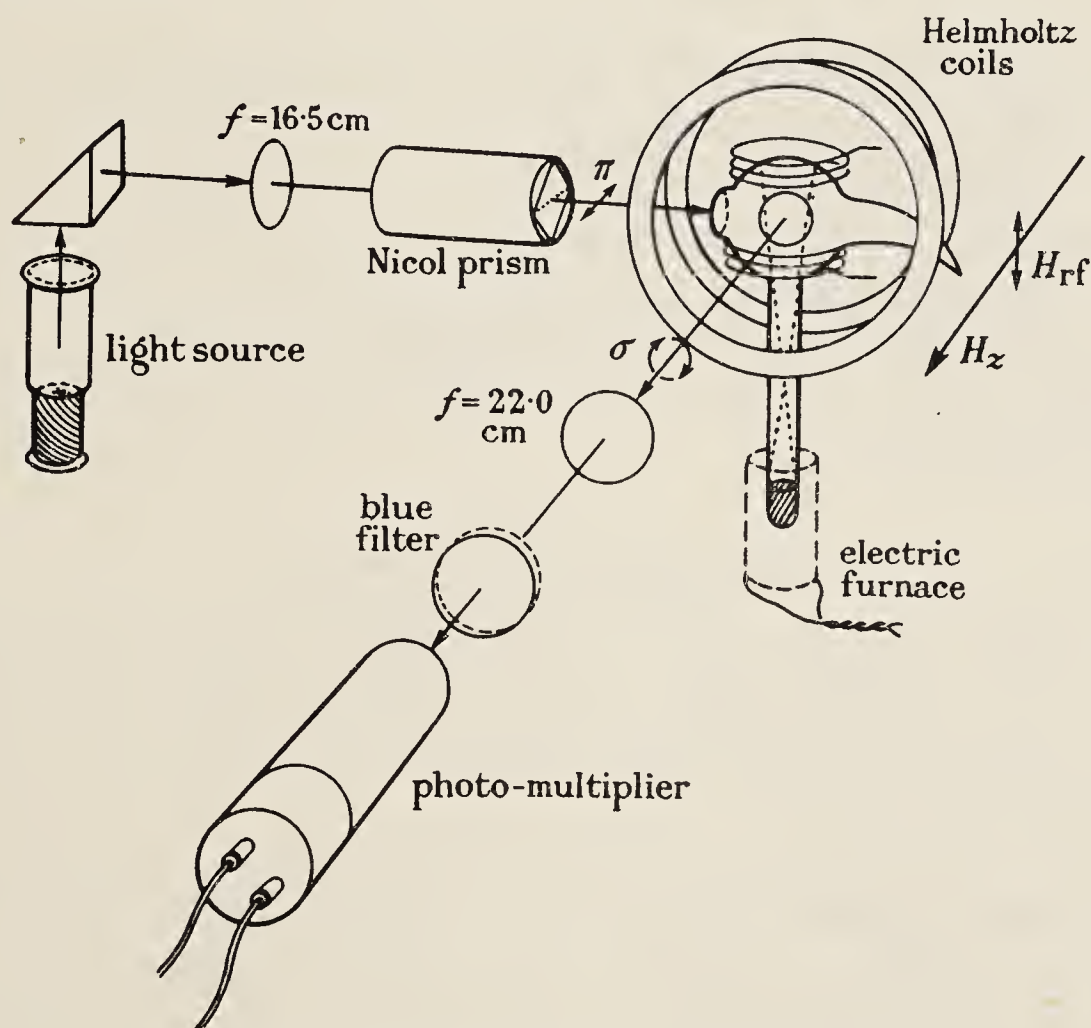


FIGURE 3. The experimental arrangement.

In the main experiments the exciting radiation was plane polarized (by means of a Nicol prism) with its electric vector parallel to the magnetic field in the resonance bulb. This arrangement gives the largest signal. Other arrangements are described in § 4 (d).

(b) *The resonance bulb*

In view of the desirability of avoiding collisions in the potassium vapour which would compete with the radio-frequency field in reorienting the atoms, and in view of the ease with which an atomic beam of potassium can be arranged, it was decided to illuminate with the resonance radiation a coarsely collimated atomic beam traversing a glass bulb, as shown in figure 3. The potassium was distilled into the

beam tube under vacuum, and continuously pumped during experiments. It is not, however, necessary to use an atomic beam. After we had heard of the work of Krüger and his colleagues (Althoff 1955; Meyer-Berkhout 1955) on rubidium and caesium, in which the metal is sealed off in a tube and heated by a stream of hot air, we obtained a signal from potassium in the same way. The beam method was used in obtaining the results presented here

Helmholtz coils of about 25 cm diameter and 500 turns each were sufficient to provide the steady magnetic fields that were used. The field was sufficiently uniform over the illuminated region. The radio-frequency field was provided by means of a smaller pair of coils of two or three turns each and 9 cm diameter which approximately fulfilled the Helmholtz condition. The coils formed part of a resonant circuit which was excited by means of one of a number of oscillators capable of providing 2 or 3 A in the coils.

#### *(c) The detecting equipment*

The illuminated region of the resonance bulb was imaged by a lens of large aperture onto the cathode of a photomultiplier tube, Du Mont type 6292, placed to receive the resonance radiation scattered in a direction at right angles to the incident light. A phase-sensitive detecting system was employed. The signal modulation necessary for this was achieved by adding to the steady magnetic field a small component alternating at about 60 c/s, provided by a small rotary converter. The photomultiplier signal, amplified and rectified by the detector, was applied to a recording milliammeter.

#### *(d) The experimental method*

Apart from the work in zero field, the frequency in a given experiment was kept constant and the magnetic field varied uniformly and continuously through resonance. Calibration marks at fixed values of the field were made on the recorder chart by an auxiliary pen.

The detecting system records only the change in signal corresponding to a small oscillation of the field about a mean value. Consequently, the recorder plots the differentiated curve of signal against magnetic field, not the resonance curve itself. This was an advantage in the present experiments in that, although the resonance curve turned out to be an unresolved blend of eight hyperfine structure components (see figure 4), the slight inflexions in the envelope of the curve showed up as well-resolved minima in the differentiated curve. This allowed easy recognition of structure which might otherwise have been missed.

The resonance curves in zero field might, in principle, have been obtained in a similar way by taking curves when the applied field was very weak, and extrapolating the lines back to zero field. This was not possible in the present case because even the small modulating field was not a small field in relation to the hyperfine structure. The modulation was therefore applied to the radio-frequency field itself and monitored by display on an oscillograph. The recorded signal then indicated the difference between switching the oscillator on and off (100 % modulation), and the resonance curves were plotted point by point as a function of frequency.



Since the width of the lines in these experiments was never smaller than 3 % of the applied frequency, there was no point in attempting to measure either the frequency or the field to high precision. Frequencies were measured to about 0.1 % by means of a crystal wavemeter, and the magnetic fields were calculated from the measured currents in the coils to an accuracy of 0.1 G. Large Helmholtz coils were used to balance out the stray field in the neighbourhood of the resonance bulb for the zero field experiments.

#### 4. RESULTS

(a)

##### (i) High field experiments

The resonance curves obtained at about 41 Mc/s, in fields of 20 to 25 G were almost symmetrical. No signal could be obtained at this frequency when the r.f. and steady fields were parallel.

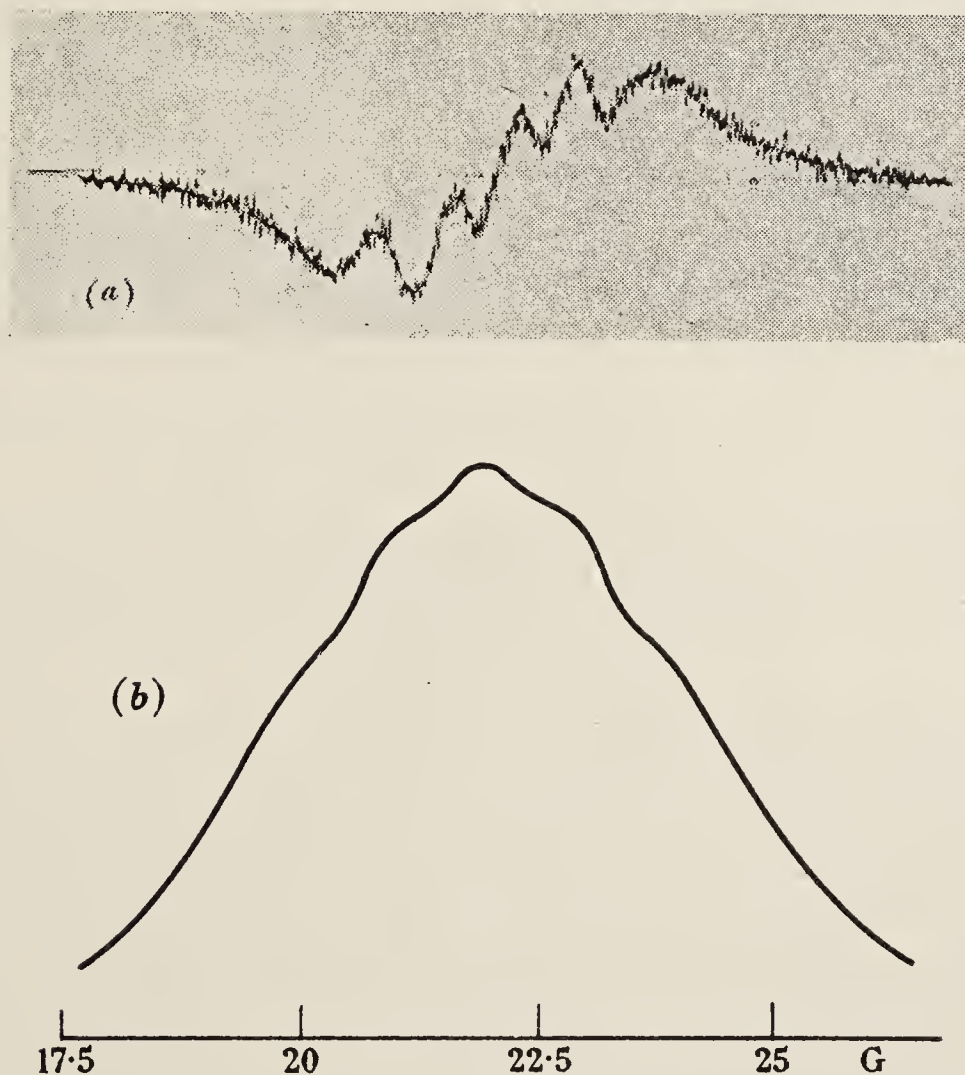


FIGURE 4 (a) Differentiated resonance curve obtained at 41.5 Mc/s.  
(b) The experimental curve integrated.

Figure 4 shows the recorder tracing of a differentiated resonance curve, and also the curve derived from it by geometrical integration. The main features of figure 4b are obtained from the formula (2) if we set  $b \approx a$ , as in figure 2.

Resonances at this frequency were investigated with values of the r.f. field strength varying by a factor greater than 2. No great changes in the pattern were observed, although the curves at the higher field strengths were more symmetrical. Those curves obtained at the lowest r.f. field which gave an appreciable signal were used for detailed comparison with formula (2).

Figure 5 shows a smoothed experimental curve obtained at a low r.f. field strength, and, for comparison, an attempted reconstruction based on formula (2). The correction terms, which make the pattern asymmetrical, have been included. The values  $a = 2.0$  Mc/s,  $b = 1.8$  Mc/s,  $\delta = 1.5$  Mc/s and a line shape given by the formula

$$I = I_0 \frac{\delta^2}{(\nu - \nu_0)^2 + \delta^2}$$

(Ramsey 1956) were used. The agreement is tolerably good, but the reconstructed curve is less symmetrical, as was the case with all the reconstructions that were tried.

The presence of  $^{41}\text{K}$ , present in its natural abundance of about 1 part in 14, is of little consequence in these attempted reconstructions. It can be taken into account if we assume a provisional value of  $b$ , since the ratio  $Q_{41}/Q_{39}$  has been measured (Lee, Fabricand, Carlson & Rabi 1953).

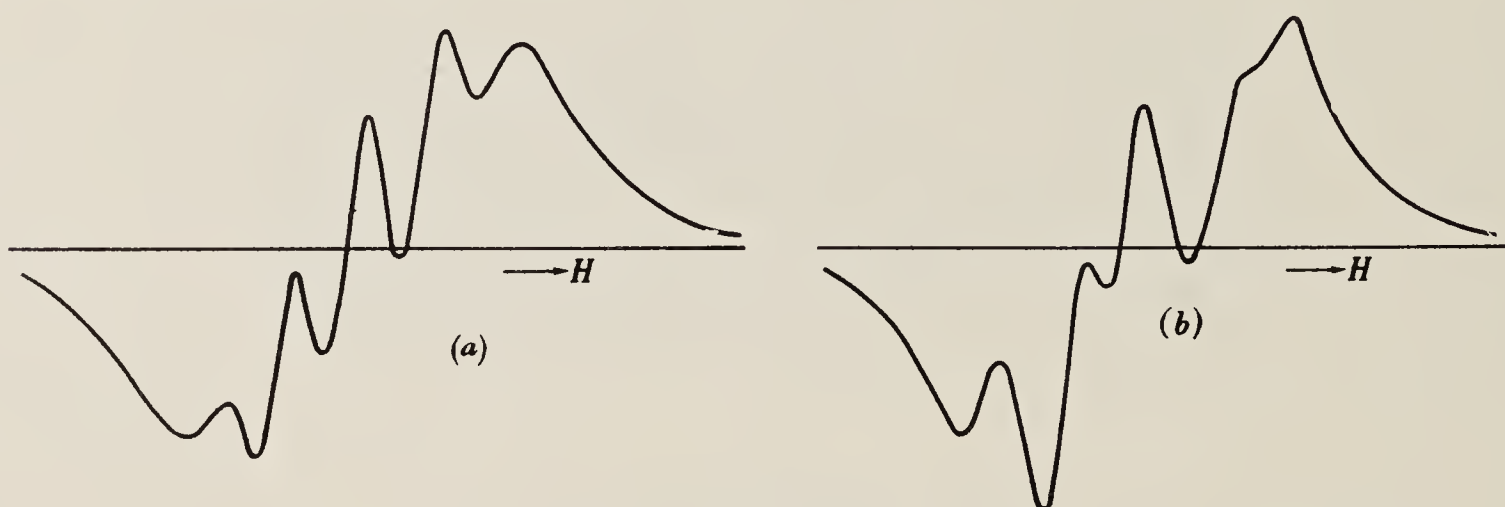


FIGURE 5. (a) Experimental curve at low radio-frequency field strength. (b) Reconstruction based on formula (2) and additional correction terms, with  $a = 2.0$  Mc/s,  $b = 1.8$  Mc/s, and  $\delta = 1.5$  Mc/s.

Of greater concern is the possible occurrence of  $\Delta M_J = \pm 2$  transitions. Their presence with a relative intensity of 10 to 15 % would affect the reconstruction of the experimental curves on the basis of  $\Delta M_J = \pm 1$  transitions. Their presence with greater intensity would cause loss of resolution, since the lines would fall between the  $\Delta M_J = \pm 1$  lines. On theoretical grounds we expect them to be weak since the intervals between levels with the same  $M_J$  are not exactly equal (see Ramsey 1956).

Complete symmetry of the pattern implies complete decoupling of  $I$  and  $J$ . The degree of decoupling appears to depend on the r.f. field strength, and therefore on the line width. A possible explanation of this effect is given in § 2b.

A study of the way in which the components are grouped allows one to fix limits to the ratio  $b/a$  without appealing to their absolute values. We find  $b/a = 1.0 \pm 0.25$ . If now one converts the separation in gauss between the outermost lines into frequency units by means of the value of  $g_J$  derived from the centre of the pattern (allowing for the small correction terms), one obtains the value  $a = 1.94 \pm 0.18$  Mc/s. The value  $1.34 \pm 0.02$  is found for  $g_J$ , which agrees with the theoretical value 1.33.

$a$  and  $b$  may be determined in a different way by using the intervals between the outer pair and the inner pair of the 'five' lines, treating the latter as blends. These intervals may be obtained without a full reconstruction of the pattern by observing



that the lines are located, to a good approximation, at points half-way between the maxima and minima of the experimental curves. These points showed no systematic movement at different r.f. fields, apart from a slight increase in the separation of the outermost lines at the higher fields. This method yields the values

$$a = 1.99 \pm 0.10 \text{ Mc/s}, \quad |b| = 1.8 \pm 0.4 \text{ Mc/s}.$$

The sign of  $b$  relative to  $a$  cannot be derived from these curves.

(ii) *Separated resonances in high fields*

We have so far not distinguished between right and left circularly polarized light. If reference is made to figure 1, it will be noticed that the r.f. transitions  $M_J = \frac{1}{2} \rightarrow \frac{3}{2}$  are accompanied by an increase in  $\sigma^-$  light, and  $M_J = -\frac{1}{2} \rightarrow -\frac{3}{2}$  by an increase in  $\sigma^+$  light. It is therefore possible in principle to separate the two sets of hyperfine structure lines. This is particularly significant in that it allows the determination of the sign of  $b$  relative to  $a$ .

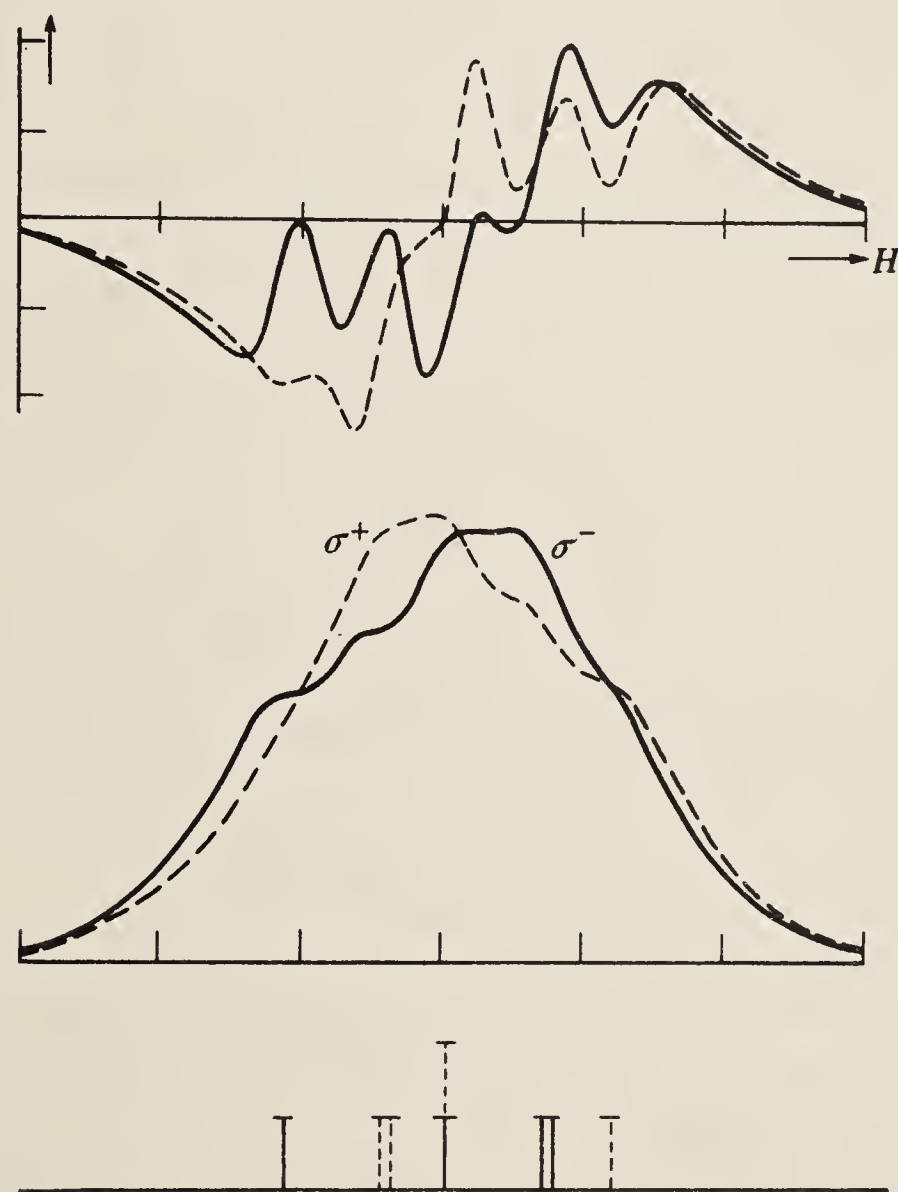


FIGURE 6. Separated resonance curves obtained at 41.5 Mc/s.  
(The integrated curves are shown below.)

Figure 6 shows the resonance curves obtained at 41.5 Mc/s when a suitably orientated mica quarter-wave plate and Nicol prism were inserted in front of the photomultiplier. Clearly, some separation of right and left circularly polarized light has been achieved. Attempts to explain the incompleteness of the separation in terms of strain in the glass of the absorption bulb, or the finite aperture for reception

of the resonance radiation were unsuccessful. The incomplete separation was ultimately attributed to secondary scattering of light inside the absorption bulb.

The pattern marked  $\sigma^-$  was obtained by selecting light polarized in the same sense as the current in the coils, and therefore corresponds to a change in  $M_J$  of  $-1$  in emission, i.e. it corresponds to r.f. transitions from  $M_J = +\frac{1}{2}$  to  $+\frac{3}{2}$ . Now the hyperfine structure of these transitions is asymmetrical and depends on the sign of  $b$  relative to  $a$ . The structure (as a function of field) is shown in the figure by the solid lines for the case when  $b$  and  $a$  have the same sign. The dotted lines show approximately the positions of the components when  $b$  is opposite in sign to  $a$ . (Actually, the dotted lines show the transitions from  $M_J = -\frac{1}{2}$  to  $-\frac{3}{2}$  when  $b$  and  $a$  have the same sign, and are displaced only by the correction terms from the transitions between the positive values of  $M_J$  when  $b/a$  is negative.)

If we allow for the fact that the separation of the patterns is incomplete, there is no difficulty in identifying the  $\sigma^-$  curve with the solid lines, i.e. the alternative in which  $b$  and  $a$  have the same sign.

The following independent methods confirm that  $b/a$  is positive:

(i) It will be observed that the resolution at the peak of the integrated curves of figure 6 is better in the case of  $\sigma^-$  than of  $\sigma^+$ . The difference is on account of the incomplete decoupling of  $I$  and  $J$ , and appears in a calculation of the correction terms, which lead to a better separation of the components of the transition  $M_J = +\frac{1}{2} \rightarrow +\frac{3}{2}$  than of  $M_J = -\frac{1}{2} \rightarrow -\frac{3}{2}$ . This allows us to identify the curve marked  $\sigma^-$  with transitions between the positive values of  $M_J$  without knowing the sense of rotation of the light, and again implies that  $b$  and  $a$  have the same sign.

(ii) The same identification of resonance curves with transitions can be made by comparing curves taken at 19 Mc/s, at which frequency it was possible to observe signals with the r.f. field both parallel and perpendicular to the steady field. The identification is made without appealing to the experimental arrangement which determines the sense of rotation of the light. Details are given by Ritter (1955).

(iii) The measurements at zero and intermediate fields, discussed in the next sections, lead to the conclusion that  $b$  and  $a$  have the same sign.

#### (b) Zero field experiments

The frequency range covered in these experiments was from 0.5 to 8.5 Mc/s. There was considerable practical difficulty in keeping the r.f. field constant while the frequency was being varied over a resonance line, since the line widths were a large fraction of the absolute frequency.

A line at 7.5 Mc/s was excited by r.f. currents smaller than had been used in the high field experiments. Lines at 1.4 and 5.1 Mc/s, on the other hand, could not be excited unless the current was at least twice as great. The lower frequency lines were distinctly narrower than the other. Figure 7 shows the 1.4 and 7.5 Mc/s resonance curves obtained on separate runs. The frequency scale is the same in both cases, but the ordinates are arbitrary.

The widths of these lines can only be determined approximately. They are about 2 and 1 Mc/s for the broad and narrow lines, respectively. For comparison, the reconstructed high field pattern in figure 5 (b) is based on a line width of 3 Mc/s. It



is reasonable that the zero field line at 7.5 Mc/s should be narrower than this since smaller r.f. fields were used in exciting it, but the lines at 1.4 and 5.1 Mc/s are abnormally narrow. On experimental grounds we interpret them as double quantum transitions. We shall show that, on this hypothesis, values of  $a$  and  $b$  may be obtained which are consistent with the values derived from the high field experiments. All questions of displacements of the levels by the r.f. field will be ignored for the time being.

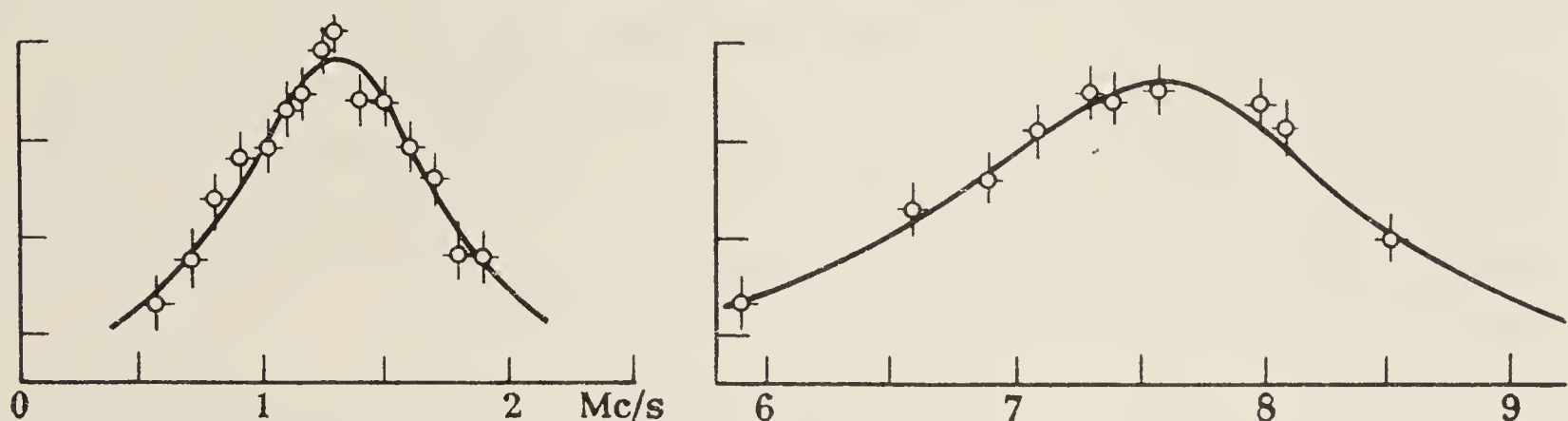


FIGURE 7. Resonance curves in zero magnetic field.

The intervals between the hyperfine structure levels  $F = 3, 2, 1$  and  $0$  are, respectively,  $(3a + b)$ ,  $(2a - b)$ ,  $(a - b)$ , (Kopfermann 1956). We interpret the line at 7.5 Mc/s as the transition 3-2, the line at 5.1 Mc/s as the double transition 3-1, and the line at 1.4 Mc/s as the double transition 2-0. We then have

$$(3a + b) = 7.5,$$

$$(3a + b) + (2a - b) = 2 \times 5.1,$$

$$(2a - b) + (a - b) = 2 \times 1.4.$$

These equations taken in pairs yield for  $a$  and  $b$  the values 2.04, 1.38; 2.04, 1.66; 1.98, 1.57 Mc/s respectively. The experimental uncertainty of about one-tenth of a line width in locating the peaks leads to uncertainties,  $\pm 0.05$  Mc/s for  $a$  and  $\pm 0.15$  Mc/s for  $b$ . The equations are self-consistent, and consistent with the results of the last section to within the stated accuracy. We use for the zero field results the values

$$a = 2.02 \pm 0.05 \text{ Mc/s}, \quad b = 1.54 \pm 0.15 \text{ Mc/s}.$$

It is natural to enquire whether the single quantum transitions 2-1 and 1-0, and the triple quantum transition 3-0 might not also be observed.

We have searched for the 2-1 transition in the region of 2.4 Mc/s, and have obtained signals which might be traces of this line. Theoretical estimates of its intensity are very unreliable because of our lack of understanding of the r.f. transition process.

We have also searched for the 2-1 transition under circumstances in which we aim at populating the 2 level by radio-frequency transitions from the 3 level simultaneously with the optical excitation. In these experiments an extra oscillator, working at a fixed frequency near 7.5 Mc/s, is used to excite an independent set of coils round the resonance bulb. The 2-1 resonance is then explored in the ordinary



way. Indications of the line have been found in these experiments, about which it is hoped to publish more in due course.

The 1-0 transition would occur at about 0.4 Mc/s. It is clearly pointless to search for such a transition when the line width would be 2 to 3 Mc/s, and the states completely mixed by the r.f. perturbation.

No indications have been found of the triple quantum transition 3-0, presumably because the r.f. fields have been insufficiently strong.

### (c) *Intermediate field experiments*

The resonance radiation scattered by atoms in intermediate fields possesses properties which we have so far not discussed. Its intensity in a given direction varies with the magnetic field, quite apart from the presence of r.f. fields. The reason for this lies in the mixing of states which takes place in intermediate fields, and the anisotropic transition probabilities for excitation and decay.

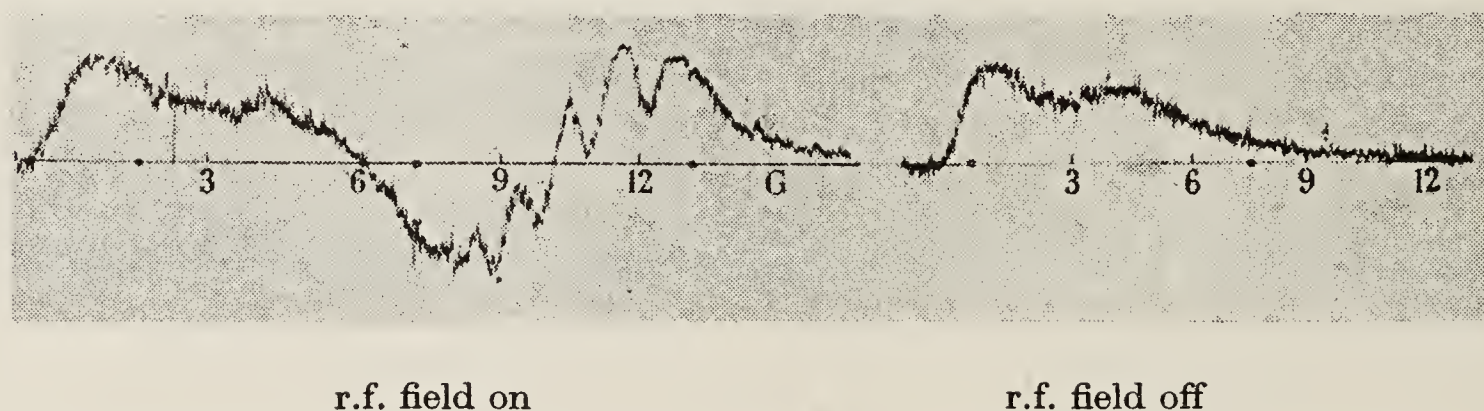


FIGURE 8. Signal as a function of field in the intermediate field region, with and without a radio-frequency field at 19 Mc/s.

The intensity as a function of field depends in a complicated way on the hyperfine structure of the ground and excited states. It is closely related to the degree of polarization of the resonance radiation, measurements of which have been used in order to deduce the hyperfine structure (Ellet & Heydenberg 1934). We have made no attempts to use our measurements of these intensity variations to deduce the hyperfine structure, since the method is so insensitive to the values of  $a$  and  $b$ . It was necessary, however, to take account of the phenomenon because it provided a variable background signal which had to be subtracted from our resonance curves. Figure 8 shows the signal as a function of field up to about 15 G, with and without an r.f. field at 19 Mc/s.

Resonance curves were taken through the intermediate field region at frequencies from 5.1 Mc/s. The asymmetrical curves obtained have not been analyzed in detail. It is, however, possible to locate the outermost, high-field component of the hyperfine structure in all these curves, and the innermost, low-field component on some of them. These components correspond to the transitions  $|\frac{1}{2}, -\frac{3}{2}\rangle - |-\frac{3}{2}, -\frac{3}{2}\rangle$  and  $|\frac{3}{2}, \frac{3}{2}\rangle - |\frac{1}{2}, \frac{3}{2}\rangle$  respectively, for which the frequencies can be calculated rigorously (§ 2a).

A comparison of the observed and calculated positions of these components shows good, but not perfect agreement. The crosses in figure 9 show the experimental points; the lines show the calculated relationship based on the theoretical value



of  $g_J$  and the value 7.75 Mc/s for  $(3a + b)$ . This value is derived from the overall width of the high-field curves. (The zero field value 7.5 Mc/s might equally well have been used without affecting the conclusions.) The systematic discrepancy at lower frequencies lies outside the experimental error. It is likely that the explanation lies in the superficial way in which we have treated the transition process.

The theoretical expression for the interval between the components at a given field is  $(3a + b)$ , where  $a$  and  $b$  have their algebraic values. The experimental value, 7.5 Mc/s, agrees sufficiently closely with the interval 7.75 Mc/s between the outermost lines in strong fields whose separation is  $(3|a| + |b|)$ . This is further evidence that  $a$  and  $b$  have the same sign.

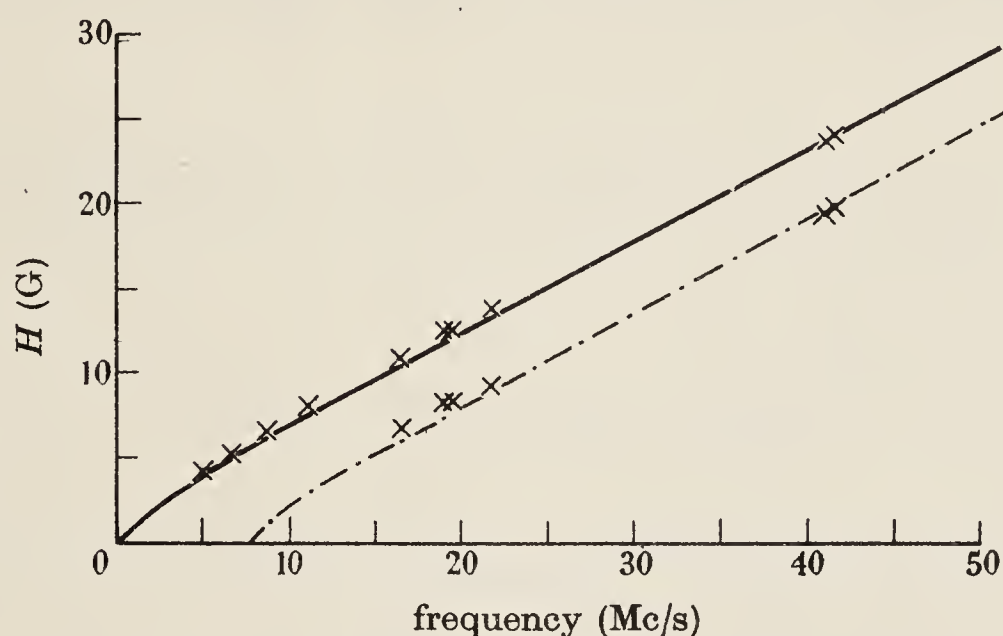


FIGURE 9. Field as a function of frequency for the components  $|-\frac{1}{2}, -\frac{3}{2}\rangle - |-\frac{3}{2}, -\frac{3}{2}\rangle$  (solid line) and  $|\frac{1}{2}, \frac{3}{2}\rangle - |\frac{3}{2}, \frac{3}{2}\rangle$  (broken line). The lines are calculated, the crosses are experimental points.

#### (d) Related experiments

##### (i) Excitation by $\sigma$ , and by unpolarized light

Inspection of figure 1 shows that the desired inequality in the populations of the excited states can be achieved not only by using  $\pi$ , but also (less efficiently) by  $\sigma$  excitation, and by unpolarized light. These methods were tried, using light incident at right angles to the magnetic field, and plane-polarized perpendicular to the field in the case of  $\sigma$  excitation. As expected,  $\sigma$  excitation gave a signal in the negative direction compared with  $\pi$  excitation, while natural light gave a signal in the same sense as with  $\pi$  excitation.

##### (ii) The $P_{\frac{1}{2}}$ level

In the former experiments there is complete symmetry between  $\pm |M_J\rangle$ . The possibility of a signal arises from the fact that the excited level contains  $|\frac{3}{2}\rangle$  and  $|\frac{1}{2}\rangle$ , whereas the ground level contains only  $|\frac{1}{2}\rangle$  states. The method therefore fails for the excited  $P_{\frac{1}{2}}$  level. It is for this reason that we have been able to ignore this level in our discussion of the experiments so far, although the resonance radiation scattered from it contributes to the background light seen by the photo-multiplier.

Excitation by  $\sigma^+$  or by  $\sigma^-$  light alone, on the other hand, will populate the  $+$  and  $-$  states unequally, both in the  $P_{\frac{3}{2}}$  and in the  $P_{\frac{1}{2}}$  levels. This method therefore makes

possible the investigation of the  $P_{\frac{1}{2}}$  level, which is of interest in that it furnishes a value of the  $a$  factor for comparison with the related constant of the  $P_{\frac{3}{2}}$  level.

Exploratory experiments of this type were undertaken. The only changes in the experimental arrangement were that the magnetic field was directed at  $45^\circ$  to both incident and scattered light (a sacrifice of efficiency to convenience), and that the beams were polarized and analyzed in elliptical polarization.

In order to obtain the desired signals it was necessary to work at high r.f. field strengths and to use a large amplitude for the 60 c/s magnetic field which modulated the signal. For this reason, the structure in the  $P_{\frac{3}{2}}$  resonance was lost. Figure 10 shows extra lines which appeared at 41.5 Mc/s away from the  $P_{\frac{3}{2}}$  resonances, and which can satisfactorily be interpreted as  $P_{\frac{1}{2}}$  resonances.

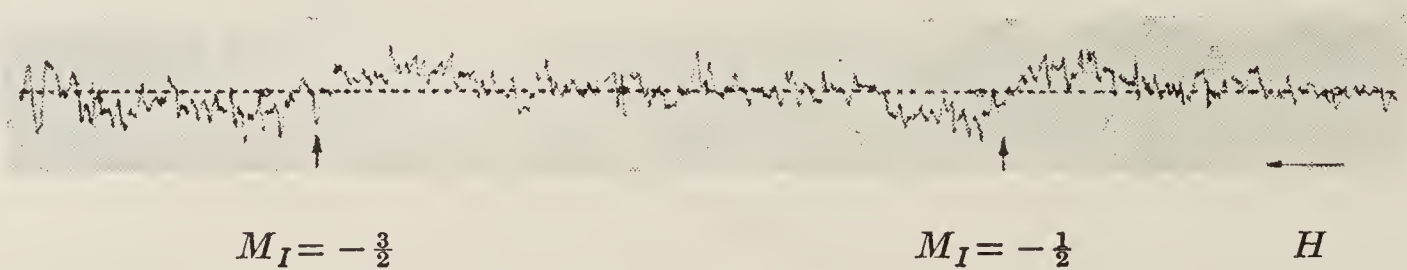


FIGURE 10. Resonances in the  $P_{\frac{1}{2}}$  level.

Of the four unequally spaced hyperfine structure components of the  $P_{\frac{1}{2}}$  resonance, it was expected (from calculations based on an estimated  $a$  factor) that two would overlap the  $P_{\frac{3}{2}}$  pattern. The lines in figure 10 are interpreted as the remaining two, namely those in which  $M_I$  (which does not change in the transition) is equal to  $-\frac{1}{2}$  and  $-\frac{3}{2}$ .

Although the value of the magnetic field was only approximately known, its ratio for these two lines could be measured to about 1 %. It is possible to use this value, together with the frequency at which the lines were observed, to derive  $a_{\frac{1}{2}}$ . We make use of the well-known formulae (see Ramsey 1956) which give the position of the  $P_{\frac{1}{2}}$  lines in intermediate fields, and obtain the relation

$$k^2 - k \frac{(3h^2 - 2h + 3)}{2(1 - h^2)} - 1 = 0,$$

in which  $k = (\text{frequency})/a_{\frac{1}{2}}$  and  $h$  is the ratio of the magnetic fields. Putting in the experimental values  $h = 1.12/1.43$ , frequency = 41.5 Mc/s we arrive at  $a_{\frac{1}{2}} = 9.29$  Mc/s with a precision of about 5 %. Comparing  $1/5 (a_{\frac{1}{2}}) = 1.86 \pm 0.1$  Mc/s with the values of  $a_{\frac{3}{2}}$  quoted in 4 (a) and (b) we find no disagreement.

### (iii) The ground level $S_{\frac{1}{2}}$

In principle r.f. resonances in the ground level might have produced signals with this experimental arrangement. The possibility was excluded that the lines described in the last paragraph arose from the ground level.

### (iv) Transitions $\Delta M_J = \pm 2$

A feature of the experiments with elliptically polarized light was the occurrence of an exceptionally strong signal at a field strength about one-half that at which the



ordinary  $P_{\frac{3}{2}}$  resonance occurred. This can be explained in terms of single quantum transitions in the  $P_{\frac{3}{2}}$  level, in which  $M_J$  changes by  $\pm 2$  and  $M_I$  by  $\mp 1$ . Such transitions are allowed when  $I$  and  $J$  are incompletely decoupled, although the transition probability is smaller than that for the  $\Delta M_J = \pm 1$  transitions by the factor which measures the impurity of the states in the  $|M_J, M_I\rangle$  representation—a factor of about 1/100 in our experiments. Structure was observed in these resonances in agreement with this interpretation. The large signal strength of the  $\Delta M_J = \pm 2$  transitions is a consequence of the very large difference in population between  $|\frac{3}{2}\rangle$  and  $|\frac{1}{2}\rangle$ , for  $\sigma^-$  light populates  $|\frac{3}{2}\rangle$  and  $|\frac{1}{2}\rangle$ , but not  $|\frac{1}{2}\rangle$ . Since the relative signal strengths were of the order 10, it follows that the relative populations of  $|\frac{1}{2}\rangle$  and  $|\frac{3}{2}\rangle$  must have been of the order 1000:1.

## 5. DISCUSSION OF THE RESULTS

### (a) Evaluation of the nuclear moments

In §2(b) we have given reasons for treating with reserve measurements of resonance frequencies when these are comparable with the line width. These considerations apply especially to the measurements in zero field, to which we therefore attach less weight than to the high field observations. The two sets of measurements are, nevertheless, in agreement to within the stated errors.

From the high-field experiments we have, by treating the experimental curves in two different ways,

$$(i) \quad a = 1.94 \pm 0.18 \text{ Mc/s}, \quad b/a = 1.0 \pm 0.25$$

$$(ii) \quad a = 1.99 \pm 0.10 \text{ Mc/s}, \quad b = 1.8 \pm 0.4 \text{ Mc/s}$$

and from the zero-field experiments

$$a = 2.02 \pm 0.05 \text{ Mc/s}, \quad b = 1.54 \pm 0.15 \text{ Mc/s},$$

with the supporting values  $(3a + b) = 7.5 \text{ Mc/s}$  from the experiments at intermediate fields and  $1/5$ .  $(a_{P_{\frac{1}{2}}}) = 1.86 \pm 0.1 \text{ Mc/s}$  from the measurements of  $P_{\frac{1}{2}}$  resonances.

We take as final values

$$a = 1.97 \pm 0.1 \text{ Mc/s}, \quad b = 1.7 \pm 0.3 \text{ Mc/s}, \quad b/a > 0.75.$$

This value of  $a$ , substituted in the Goudsmit formula, yields  $\mu_I = 0.40 \pm 0.02$  nuclear magneton, to be compared with the molecular beam magnetic resonance value (Kusch *et al.* 1939), 0.391 nuclear magneton.

The nuclear electric quadrupole moment  $Q$  is calculated from the relation (Davis *et al.* 1949)

$$Q = \frac{8b}{3a} \left( \frac{\beta}{e} \right)^2 \frac{\mu_I}{I} \frac{m}{M} = +0.113 \pm 0.02 \times 10^{-24} \text{ cm}^2.$$

This value refers to the more abundant isotope  $^{39}\text{K}$ . The ratio  $Q(^{41}\text{K})/(Q^{39}\text{K})$  has been found by Lee *et al.* (1953) to be  $1.220 \pm 0.002$ . We have made no corrections of the type discussed by Sternheimer (1954).

### (b) The factor $g_J$

The experimental value  $1.34 \pm 0.002$  compares satisfactorily with the theoretical value 1.33.

(c) *The lifetime of the  $5^2P$  term*

A systematic investigation of the width of the resonance lines as a function of r.f. field was not attempted. A lower limit to the lifetime derived from the quoted line widths is  $1.5 \times 10^{-7}$  sec.

We are grateful to Professor Lord Cherwell, F.R.S., for making available to us the facilities of the Clarendon Laboratory. Dr H. Kuhn, F.R.S. and Dr B. Bleaney, F.R.S., have given us much encouragement and helpful advice, for which we here express our thanks. One of us (G.J.R.) is indebted to the Rhodes Trust for a Scholarship.

## REFERENCES

- Althoff, K. 1955 *Z. Phys.* **141**, 35.  
 Brossel, J. & Bitter, F. 1952 *Phys. Rev.* **86**, 308.  
 Brossel, J. & Kastler, A. 1949 *C.R. Acad. Sci., Paris*, **229**, 1213.  
 Davis, L., Feld, B. T., Zabel, C. W. & Zacharias, J. R. 1949 *Phys. Rev.* **76**, 1076.  
 Ellet, A. & Heydenberg, N. P. 1934 *Phys. Rev.* **46**, 583.  
 Jackson, A. A. & Kuhn, H. 1938 *Proc. Roy. Soc. A*, **165**, 303.  
 Kelly, F. M., Kuhn, H. & Pery, A. 1954 *Proc. Phys. Soc. A*, **67**, 450.  
 Kopfermann, H. 1956 *Kernmomente*, 2nd ed. Frankfurt am Main: Akademische Verlagsgesellschaft.  
 Kusch, P. 1956 *Phys. Rev.* **101**, 627.  
 Kusch, P., Millman, S. & Rabi, I. I. 1939 *Phys. Rev.* **55**, 1176.  
 Kusch, P., Millman, S. & Rabi, I. I. 1940 *Phys. Rev.* **57**, 765.  
 Lee, C. E., Fabricand, B. P., Carlson, R. C. & Rabi, I. I. 1953 *Phys. Rev.* **91**, 1935.  
 Meyer-Berkhout, U. 1955 *Z. Phys.* **141**, 185.  
 Ramsey, N. F. 1956 *Molecular beams*. Oxford University Press.  
 Ritter, G. J. 1955 Thesis, University of Oxford.  
 Ritter, G. J. & Series, G. W. 1955 *Proc. Phys. Soc. A*, **68**, 450.  
 Salwen, H. 1955 *Phys. Rev.* **99**, 1274.  
 Sternheimer, R. 1954 *Phys. Rev.* **95**, 736.



# RADIO-FREQUENCY SPECTROSCOPY OF EXCITED ATOMS

By G. W. SERIES  
Clarendon Laboratory, Oxford

## CONTENTS

	PAGE
§ 1. Introduction .....	280
1.1. Precision of measurement .....	280
1.2. Stimulated transitions and conditions of observation .....	281
1.3. Types of experiment .....	282
§ 2. Time-independent theory .....	285
2.1. Stationary state theory of hyperfine structure .....	285
2.2. Calculation of the nuclear moments .....	287
§ 3. Time-dependent theory .....	289
3.1. Simple model for the radio-frequency transitions .....	289
3.2. Violation of the simplifying assumptions .....	291
3.3. Multiplicity of energy levels .....	292
3.4. Finite life of excited states .....	294
3.5. Transitions between excited states in the vicinity of other states .....	297
3.6. Quanta of different kinds .....	298
§ 4. Double resonance experiments .....	299
4.1. Resonance radiation .....	299
4.2. Spatial distribution of resonance radiation: classical model...	300
4.3. Intensity and polarization of resonance radiation: quantum theory .....	301
4.4. Double resonance experiments in magnetic fields .....	305
4.5. Double resonance experiments in zero magnetic field .....	311
4.6. Excitation by unpolarized light in zero magnetic field .....	314
4.7. Double resonance measurements of isotope shifts .....	316
4.8. Detection by coincidence of photons in cascade .....	317
§ 5. Excitation by electron impact .....	317
5.1. Selective excitation of different states within a given term .....	319
5.2. Selective excitation of different terms .....	321
§ 6. Atomic beam experiments .....	323
§ 7. Table of measurements .....	325
Acknowledgments .....	327
References .....	327

*Abstract.* Radio-frequency and optical spectroscopy are compared. Standard results in the theory of hyperfine structure are quoted. The excitation of atoms and the detection of radio-frequency resonances are discussed quantitatively. Experiments are described in which the techniques of 'double resonance', electron impact, and atomic beams are used. A table of measurements is given.

## § 1. INTRODUCTION

### 1.1. Precision of Measurement

EXCITED states of atoms have conventionally been studied by optical spectroscopy. In the analysis of a set of close-lying energy levels such as Zeeman or hyperfine structure components interferometric techniques are extremely powerful. The limit to the precision of such work lies not in the apparatus—the Fabry-Pérot interferometer, for example, is capable of whatever

resolving power may be required—but rather in the line width of the radiation under investigation. The most important cause of line broadening in high resolution spectroscopy is the Doppler effect, which leads to half-intensity line widths of order of magnitude  $0.02 \text{ cm}^{-1}$  (600 Mc/s). (A considerable reduction on this figure is achieved in atomic beam light sources.)

This limitation in the study of close energy levels is not fundamental, but arises merely through the very high frequency of optical radiation: it will be recalled that the Doppler width is proportional to the frequency which is actually observed. A great increase in precision is to be expected if the intervals between energy levels are investigated directly, rather than through the intermediacy of other, very remote, levels.

This report will be concerned with such direct measurements, made in the radio- and microwave-frequency regions. We shall often use the term ‘radio-frequency’ alone to cover also the microwave range.

The high precision characteristic of measurements of ground levels is not to be expected in the radio-frequency spectroscopy of excited states because of the finite lifetimes of the atoms. A typical lifetime of  $10^{-8}$  sec implies a broadened energy level and a half-intensity line width of about 30 Mc/s (both levels contribute to the width). The gain in precision of measurement over optical methods is nevertheless very considerable, as these order-of-magnitude figures imply.

In using the term ‘excited states’ in this report, we exclude metastable states when the radio-frequency transition is between a pair of metastables. Among the experiments which, for this reason, we ignore are those of Heberle, Reich and Kusch (1956) on the hyperfine structure of the  $2^2\text{S}_{1/2}$  levels in hydrogen and deuterium, those of Novick and Commins (1958) on the same structure in helium 3, and those of Drake, Lurio, Hughes and White (1958) on the  $g_J$  values of the  $^3\text{S}_1$  level of helium and the  $^3\text{P}_2$  levels of neon and argon. We include experiments in which only one of the participating states is metastable.

### 1.2. Stimulated Transitions and Conditions of Observation

The very large factor ( $\sim 10^6$ ) between typical optical and radio frequencies implies a factor of the order of  $10^{18}$  in the ratio of the probabilities of spontaneous transitions in the two regions. Thus, while optical spectroscopy relies on the spontaneous decay of excited states, radio-frequency spectroscopy must concern itself with stimulated transitions. Electric dipole and magnetic dipole transitions have been investigated.

The method of detection of transitions in most of the experiments we shall describe requires, in consequence of the equality of transition probabilities forward and backward between a given pair of states, the prior establishment of a difference of population between them. The various methods by which this is accomplished are discussed below.

A further condition for the observation of resonances is that the radio-frequency field must be sufficiently strong to induce transitions before the excited atoms decay. This implies that the matrix elements of  $\mathbf{p} \cdot \mathbf{E}$  ( $\boldsymbol{\mu} \cdot \mathbf{H}$ ) between the given pair of states be of the order of  $\hbar/\tau$ , where  $\mathbf{P}$  ( $\boldsymbol{\mu}$ ) is the electric (magnetic) dipole moment,  $\tau$  is the lifetime of the initially excited state, and  $\mathbf{E}$  ( $\mathbf{H}$ ) is the requisite field strength.



An important difference between electric and magnetic dipole transitions is that the former are much stronger. An estimate of the order of magnitude is obtained by comparing the interaction energies of the two types of dipole, of atomic magnitudes, in electric and magnetic fields of comparable strength. The transition probabilities are in the ratio

$$\frac{\mathbf{p} \cdot \mathbf{E}}{\boldsymbol{\mu} \cdot \mathbf{H}} = \frac{ea_0}{e\hbar/2mc} = 2/\alpha \simeq 300$$

where we have used e.s.u. for the electric dipole and e.m.u. for the magnetic, and set the magnitudes of the fields equal in e.s.u. and e.m.u. respectively;  $a_0$  is the Bohr radius and  $\alpha$  the fine structure constant.

### 1.3. *Types of Experiment*

We shall classify the experiments on excited states by the means which they employ to achieve differences in population, and by their methods of detection of radio-frequency resonance.

#### 1.3.1. *The attainment of differences in population.*

Our starting point will be an assembly of atoms in statistical equilibrium in the ground states. We ignore population differences, if any, which are a consequence of the Boltzmann distribution. Convenient means of excitation are by optical resonance radiation and by electron impact.

Isotropic, unpolarized resonance radiation, uniform in intensity over the region of absorption, results in populations which are in statistical equilibrium, and are therefore of no interest to us. Similarly, the excitation of a set of close-lying atomic energy levels by electrons in a gas discharge is generally characterized by statistical equilibrium at some (high) electron temperature.

Population differences may be induced by resonance radiation which is either non-isotropic, or polarized, or restricted in frequency range, or by any combination of these. Similarly, population differences may be induced by controlled electron bombardment, or in gas discharges in which for some reason statistical equilibrium is not maintained. § 4 of this Report is concerned with excitation by resonance radiation, § 5 with excitation by electron impact.

#### (i) *Excitation by resonance radiation.*

Polarized resonance radiation was used by Brossel and Bitter (1952) in their pioneer 'double resonance' experiment which is described in § 4.4.1. Readers who are unfamiliar with the subject may find it helpful to refer now to this concrete example. The later sub-sections describe the developments which have taken place in this type of experiment. Measurements of Zeeman splittings, hyperfine structures, isotope shifts and lifetimes of excited states have been made.

Unpolarized resonance radiation was used by Rabi and his collaborators in atomic beam experiments designed to measure hyperfine structures in excited states of the alkali metals. The illuminated atoms were not in statistical equilibrium. This work is described in § 6.

(ii) *Excitation by electron bombardment.*

Controlled electron bombardment was used in the first successful radio-frequency experiment on excited states, that of Lamb and Retherford on the  $2^2S_{1/2}-2^2P_{1/2}$  interval in atomic hydrogen. We shall not describe this celebrated experiment here, since it has already been described in these Reports (Lamb 1951). Details of the experiment and its interpretation have been published in a set of six papers (Lamb 1952, Lamb and Retherford 1950, 1951, 1952, Dayhoff, Triebwasser and Lamb 1953, Triebwasser, Dayhoff and Lamb 1953). Lamb's 1951 Report describes also the first version of a similar experiment on the analogous level in  $\text{He}^+$ . We shall describe later versions of this experiment in § 5.2, which also treats other experiments on hydrogen and helium, mainly by Lamb and his collaborators.

The object of these experiments was to make precise measurements of structures in atoms simple enough to be amenable to calculations of very high accuracy. 'Lamb shifts' were discovered and measured in the spectra of hydrogen and ionized helium. Accurate values were obtained for the intervals between triplet levels in neutral helium. In this report we shall not treat the theoretical aspects of the work. A non-specialist account confined to one-electron spectra has recently been published (Series 1957).

Controlled electron bombardment has been used also in experiments which developed naturally from the double resonance experiments. These are described in § 5.1. The technique holds promise of being more versatile than excitation by resonance radiation in that a greater variety of excited states is accessible.

A number of interesting variants on these two methods of excitation have been tried, to which reference will be made in later sections.

1.3.2. *Methods of detection.*

We first consider, quite generally, two different methods for the detection of transitions which have been stimulated by radio-frequency fields:

(a) Measurements on the radiation field itself. This is the technique used in nuclear and paramagnetic resonance experiments in which one looks for changes of energy in the stimulating electrical circuit, at the rate of one radio-frequency quantum for each atomic transition. The same limiting sensitivity is obtained by observing changes of phase in the electrical circuit.

(b) Observation of some secondary change consequent upon the radio-frequency transition. Since an amount of energy much larger than a radio-frequency quantum may be available per atomic transition, this is potentially a much more sensitive technique than the former.

We shall be exclusively concerned with the detection of resonances by secondary effects. Self-evidently, one might make use of the optical (or other short wavelength) radiation emitted in the decay of the excited state. The major part of this report deals with the detection of radio-frequency resonances through the optical radiation. Other methods of detection are used in the atomic beam experiments.

(i) *Detection by changes in intensity or polarization of the emitted optical radiation.*

The optical radiation with which one is concerned is electric dipole. If, therefore, the radio-frequency transition changes the electric dipole matrix



element between the excited and ground states, then the transition can be detected by a change in the total intensity of light radiated in decay. It is clear that electric dipole radio-frequency transitions will have the required property. On this basis radio-frequency resonances were detected in the experiment on  $\text{He}^+$  of Lamb and Skinner (1950) and its recent refinements, and in related experiments on one-electron spectra (§ 5.2).

The change in total intensity is generally of less interest than the change in intensity in some particular direction. Magnetic dipole transitions can bring about such changes, though they do not change the total intensity of the light (unless the atomic spin-orbit coupling is strong). Their effect is to re-orient the atom, and thus to alter the spatial distribution of its (anisotropic) radiation.

Magnetic dipole transitions are formally represented as causing changes in the polarization of the emitted light: indeed, more detailed information about the excited states is sometimes obtainable by examination of the polarization, as well as of the intensity changes. It is, however, worth noticing that magnetic dipole transitions in excited states can often be detected with no polarizing equipment at all.

The experiments of Lamb and his colleagues on the (two-electron) spectrum of neutral helium (§ 5.1.3) make use of changes in intensity of the optical radiation in a given direction to detect magnetic dipole transitions.

In 'double resonance' experiments (§ 4) changes in the intensity or polarization of the fluorescent radiation are used to detect magnetic dipole transitions.

(ii) *Detection by other changes in the optical radiation.*

We shall mention three further possibilities for detection in double resonance experiments which, so far as we are aware, have not yet been exploited in experiments on excited states. They are the measurement of optical dispersion, of the Faraday effect, and of amplitude modulation of the fluorescent light.

Dispersion of optical radiation arises through interference between the primary beam and light scattered in the forward direction. The effects are large near a resonance line. Radio-frequency resonance between excited states, since it causes a re-distribution of the scattered light, should induce a change in refractive index of the scattering vapour.

The Faraday effect is proportional to the difference in refractive indices for  $\sigma^+$  and  $\sigma^-$  light. The amount of the Faraday rotation should therefore change when the refractive indices change at radio-frequency resonance. An effect of this sort has been observed to accompany paramagnetic resonance in the ground state of a  $\text{Cr}^{3+}$  ion in a crystal (Wesemeyer and Daniels 1958). Differences in population were in this case obtained by cooling the crystal in liquid helium.

The third possibility is a consequence of the mixing of states which radio-frequency resonance brings about. Since, under the influence of the radio-frequency field, the state of an excited atom becomes a mixture of the original eigenstates, there will exist definite phase relationships between the scattered light from different levels. The frequencies of these components will differ by the radio frequency itself, so that interference between them will result in modulation at the radio frequency of the amplitude of the scattered light. Experiments

on these lines are in progress. The effect is related to a phenomenon predicted by Dehmelt (1957) and observed by Bell and Bloom (1957) in the ground state of sodium.

(iii) *Detection by other secondary effects.*

In atomic beam experiments radio-frequency transitions are detected by changes in the number of atoms which reach a detector. Types of detector are various: in Lamb's experiments on the  $n = 2$  levels in hydrogen the detector consisted of a cold tungsten plate with the property of liberating electrons when struck by metastable hydrogen atoms; in Rabi's experiments on excited levels of alkali metals the detector consisted of a hot tungsten wire which stripped electrons off the alkali atoms and liberated them as ions. In both cases the radio-frequency transition is followed by some very much more energetic change in the detector.

As we have already remarked, we shall not describe Lamb's experiment in this report. We mention it in this introductory section for the sake of completeness. Rabi's experiments are described in § 6.

## § 2. TIME-INDEPENDENT THEORY

The small energy of radio-frequency quanta limits the application of these techniques to the measurement of hyperfine intervals, apart from a few important special cases in which multiplet intervals are abnormally small, in particular, in the spectra of hydrogen, helium and ionized helium.

For the sake of convenient reference we shall give a few standard results in the theory of hyperfine structure in atomic spectra. Further details may be found in the book by Kopfermann (1958). We shall not discuss the theory of the special cases of multiplet structure.

We shall limit ourselves in § 2 to stationary state (time-independent) theory. In § 3 we discuss transition processes (time-dependent).

### 2.1. Stationary State Theory of Hyperfine Structure

The following Hamiltonian function is generally used to represent the magnetic dipole and electric quadrupole interactions in an atom under a uniform external magnetic field  $\mathbf{H}$ :

$$\mathcal{H} = A\mathbf{I} \cdot \mathbf{J} + \frac{B}{2I(2I-1)J(2J-1)} [3(\mathbf{I} \cdot \mathbf{J})^2 + \frac{3}{2}(\mathbf{I} \cdot \mathbf{J}) - I(I+1)J(J+1)] \\ + g_J \beta \mathbf{J} \cdot \mathbf{H} - g_I \frac{m}{M} \beta \mathbf{I} \cdot \mathbf{H}. \quad \dots\dots(1)$$

In this equation  $\mathbf{I}$  and  $\mathbf{J}$  are operators, having eigenvalues  $[I(I+1)]^{1/2}$  and  $[J(J+1)]^{1/2}$  respectively in units  $\hbar$ , which represent the nuclear and electronic angular momenta.  $A$  and  $B$  are constants proportional to the nuclear magnetic dipole and electric quadrupole moments, respectively. (The term in  $B$  does not apply unless both  $J$  and  $I$  are greater than  $\frac{1}{2}$ );  $g_J$  and  $g_I$  are the electronic and nuclear  $g$ -factors,  $\beta$  the Bohr magneton, and  $m/M$  the electron/proton mass ratio. The positive sign of the term  $g_J \beta \mathbf{J} \cdot \mathbf{H}$  comes from the negative sign of the interaction energy,  $-\boldsymbol{\mu}_J \cdot \mathbf{H}$  coupled with the substitution  $\boldsymbol{\mu}_J = -g_J \beta \mathbf{J}$  which takes



account of the negative charge on the electron. On the other hand, since the nucleus is positively charged we define  $g_I$  through  $\mu_I = g_I \beta \mathbf{I} m / M$ , so that the last term in (1) has a negative sign.

From (1) the hyperfine energy can be deduced in terms of the constants  $A$  and  $B$ , which are then determined by comparison with experiment. Values for the nuclear magnetic dipole and electric quadrupole moments are subsequently obtained under various simplifying assumptions.

### 2.1.1. Zero magnetic field.

We choose a representation in which  $F$  ( $\mathbf{F} = \mathbf{I} + \mathbf{J}$ ) is a good quantum number. The energy of the level  $F$  is then found to be

$$W(F) = \frac{1}{2}AC + \frac{B}{I(2I-1)J(2J-1)} \left[ \frac{3}{8}C(C+1) - \frac{1}{2}I(I+1)J(J+1) \right], \quad \dots\dots(2)$$

where  $C \equiv F(F+1) - I(I+1) - J(J+1)$ .

As an example of the working out of this formula, we quote the hyperfine structure intervals for a nucleus of spin  $I = \frac{3}{2}$  in interaction with electronic spins  $J = \frac{1}{2}$  and  $J = \frac{3}{2}$ :

$$\begin{aligned} \text{(i) } J = \frac{1}{2} \quad W_2 - W_1 &= 2A \\ \text{(ii) } J = \frac{3}{2} \quad W_3 - W_2 &= 3A + B \\ &W_2 - W_1 = 2A - B \\ &W_1 - W_0 = A - B. \end{aligned}$$

### 2.1.2. Weak magnetic field.

In a magnetic field the terms  $g_J \beta \mathbf{J} \cdot \mathbf{H}$  and  $g_I \beta \mathbf{I} \cdot \mathbf{H} m / M$  introduce energy additional to the value of  $W(F)$  given by (2). Under the approximation  $g_J \beta H \ll A, B$  the additional energy is

$$\Delta W(F, m_F) = g_F \beta \mathbf{F} \cdot \mathbf{H} = g_F \beta m_F H \quad \dots\dots(3)$$

where

$$g_F = g_J \left[ \frac{F(F+1) + J(J+1) - I(I+1)}{2F(F+1)} \right] - g_I \frac{m}{M} \left[ \frac{F(F+1) + I(I+1) - J(J+1)}{2F(F+1)} \right]$$

and  $m_F$  takes the  $2F+1$  values  $F, F-1 \dots -F$ .

The second term in the equation for  $g_F$  is three orders of magnitude smaller than the first. Its effect on  $\Delta W$  is generally small compared with the natural width of the energy levels of excited states.

### 2.1.3. Strong magnetic field.

Under the approximation  $g_J \beta H (= G) \gg A, B$  we may again give a simple expression for the energy in the representation in which  $m_J$  and  $m_I$  are good quantum numbers:

$$\begin{aligned} W(m_J, m_I) &= G \left( m_J - \frac{g_I m}{g_J M} m_I \right) + A m_J m_I \\ &+ \frac{B}{4I(2I-1)J(2J-1)} [3m_J^2 - J(J+1)] [3m_I^2 - I(I+1)]. \end{aligned} \quad \dots\dots(4)$$

Again, the term in  $g_I m/M$  may often be neglected.

The order of magnitude of the most important correction terms, which may be evaluated by standard perturbation theory, is  $A^2, B^2/G$ .

#### 2.1.4. Magnetic fields of intermediate strength.

The secular equation whose solution yields the general result may always be arranged so that it factorizes into a set of equations whose first member is linear, and the others of progressively higher order in the energy. If either  $I$  or  $J$  does not exceed  $\frac{1}{2}$ , no equation of order higher than quadratic appears. The solution for  $J = \frac{1}{2}$ ,  $I$  arbitrary, is

$$W(\pm \frac{1}{2}, m_I) = -\frac{1}{4}A - (m_I \pm \frac{1}{2})g_I \frac{m}{M}\beta H \\ \pm \frac{1}{2}[A^2(I + \frac{1}{2})^2 + 2AG'(m_I \pm \frac{1}{2}) + G'^2]^{1/2} \dots\dots(5)$$

where

$$G' = \left(g_J + g_I \frac{m}{M}\right)\beta H.$$

### 2.2. Calculation of the Nuclear Moments

The constants  $A$  and  $B$  express the interaction of the nucleus with all the electrons. Under an approximation which is very good for the magnetic dipole, but rather crude for the electric quadrupole interaction, the contributions from closed shells are generally ignored in the preliminary calculation. More refined calculations have been made by Sternheimer (1954).

Individual electrons outside closed shells each contribute to  $A$  and  $B$  in a way which depends on their coupling. Contributions from individual electrons are vectorially additive. Details, for certain configurations of two electrons, are given by Kopfermann (1958). We shall quote the results for a one-electron system specified by orbital and total angular momentum quantum numbers  $l$  and  $j$ . Following Kopfermann, we use  $a, b$ , to denote the interaction constants for individual electrons.

#### 2.2.1. The nuclear gyromagnetic ratio $g_I$ .

For an s-electron ( $l = 0$ ,  $j = \frac{1}{2}$ ) one finds

$$g_I = a_{1/2} \frac{3n_0^3}{8R_\infty \alpha^2 Z Z_0^2 (1 - d\sigma/dn)} \dots\dots(6)$$

apart from certain correction terms of order unity.  $Z$  is the nuclear charge,  $Z_0$  the 'outer' nuclear charge (1 for a neutral atom, 2 for single ionization, etc.),  $R_\infty$  the Rydberg constant,  $\alpha$  the fine structure constant, and  $n_0$  the effective principal quantum number defined by  $(T/RZ_0^2)^{1/2}$ , where  $T$  is the term value (measured from the ionization limit).  $\sigma$  is the quantum defect  $n - n_0$ .

For  $l \neq 0$ , both  $a$  and  $b$  are proportional to the mean value of  $1/r^3$ , where  $r$  is the electron-nuclear distance. Uncertainty in the value of this quantity can be eliminated by the introduction of  $\delta$ , the fine structure doublet splitting, since



$\overline{1/r^3}$  also enters into a calculation of this interval. We then find, for either of the factors  $a_j = a_{l \pm 1/2}$ ,

$$g_I = a_j \frac{Z_i(l + \frac{1}{2})j(j+1)}{\delta l(l+1)} \quad (l \neq 0), \quad \dots\dots(7)$$

apart from corrections of order unity as before.  $Z_i$  is the 'inner' nuclear charge whose value is approximately the true nuclear charge  $Z$  diminished by 4 for a p-electron and by 11 for a d-electron. A more exact definition is contained in Casimir's expression (1936) for the doublet fine structure,

$$\delta = R_\infty \alpha^2 \frac{dn_0}{dn} \frac{Z_o^2 Z_i^2}{n_0^3 l(l+1)} \mathcal{R} \quad \dots\dots(8)$$

in which  $n$  is the true principal quantum number and  $\mathcal{R}$  a relativistic correction.

Corrections to these expressions for  $g_I$  arise when one takes account of the finite size of the nucleus and the distribution of magnetic moment within it, and also when one introduces relativistic wave functions into the theory. These corrections also are discussed by Kopfermann.

Equation (7) implies that a simple relation exists between the two  $a$  factors. It is

$$a_{l+1/2} = \left( \frac{2l-1}{2l+3} \right) a_{l-1/2}, \quad \dots\dots(9)$$

apart from relativistic corrections. Deviations from this relation of about 14% have been found in rubidium, for example (Senitzky and Rabi 1956). They can be understood on the basis that the allocation of a single quantum state  $(n, l)$  to each electron is only an approximation. A consequence of allowing that a small fraction of some other configuration may be mixed with a particular configuration is to alter the  $a$  factors: the fractional change in  $a_{l+1/2}$  is not necessarily the same as that in  $a_{l-1/2}$ . On these lines Phillips (1956) has given a reasonable explanation of the discrepancy in rubidium.

Deviations from (9) are also to be expected when the uncertainty of measurement is less than  $a^2/\delta$ , for when this quantity is significant the perturbation between the doublet levels  $j = l \pm \frac{1}{2}$  is significant. An especially interesting case arises in  $Li II$  where  $a$  and  $\delta$  are the same order of magnitude (Güttinger and Pauli 1931, Gray 1933).

The case of small perturbations has been discussed by Clendenin (1954).

### 2.2.2. The nuclear electric quadrupole moment $Q$ .

In the relation between  $b$  and  $Q$  it is again desirable to eliminate  $\overline{1/r^3}$  in favour of some directly measurable quantity. This can be done either by introducing one of the  $a$  factors ( $a_{l \pm 1/2}$ ), together with  $g_I$  (determined by some other method), or by introducing, as before,  $\delta$  and  $Z_i$ .

Then we find, by the one substitution

$$Q = \frac{b}{a} \left( \frac{\beta}{e} \right)^2 g_I \frac{m}{M} \frac{4l(l+1)}{j(2j-1)}, \quad \dots\dots(10)$$

and by the other,

$$Q = \frac{b}{\delta} \left( \frac{\beta}{e} \right)^2 Z_i \frac{(2l+1)(2j+2)}{2j-1}, \quad \dots\dots(11)$$

where we have omitted relativistic corrections of order unity.  $\beta$  is the Bohr magneton and  $e$  the electronic charge.

Taking (10) and (9) we have a third relation between  $b$  and  $Q$ .

These three relations do not always give consistent results. Acute discrepancies in gallium and other elements have been discussed by Koster (1952), and may be understood on the basis of configuration mixing. The relation (11) appears to be the most reliable.

To the value of  $Q$  computed as above from interactions with the outer electrons one must make a correction in consequence of the polarization of the inner core of electrons by the nucleus, by which the electric field gradient at the nucleus is altered. The change is proportional to  $Q$ . The necessary corrections may be 10% or more. Sternheimer (1954) has made detailed calculations of this effect. Polarization of the core affects also the relation between  $a$  and  $g_I$ .

### § 3. TIME-DEPENDENT THEORY

The interaction between an atom of magnetic moment  $\mu$  and a magnetic field of amplitude  $\mathbf{H}_1$  which rotates in the  $xy$  plane with angular frequency  $\omega$  is expressed by the addition to the Hamiltonian (1) of a term

$$\begin{aligned}\mathcal{H}(t) &= -\mu \cdot \mathbf{H}_1(t) = -\mu \cdot (H_1 \cos \omega t \mathbf{i} - H_1 \sin \omega t \mathbf{j}) \\ &= -\frac{1}{2}H_1[\mu_+ e^{i\omega t} + \mu_- e^{-i\omega t}], \quad \dots\dots(12)\end{aligned}$$

where  $\mu_{\pm} = \mu_x \pm i\mu_y$ .

The magnetic interaction is taken as an example: the argument also covers electrical interactions, in which case we shall use the symbols  $\mathbf{p}$  and  $\mathbf{E}_1$ .

There will generally exist in the atom energy eigenstates between which the matrix elements of  $\mu \cdot \mathbf{H}_1$  or  $\mathbf{p} \cdot \mathbf{E}_1$  are not zero. The time-dependent perturbation  $\mathcal{H}(t)$  will induce transitions to and fro between such states. We are interested in the transition probability as a function of the frequency and of the matrix elements of the perturbation; we may then derive the form of the resonance curve.

The analysis of this problem expressed in its simplest term is well known. It is given, for example, by Ramsey (1956), where references to the literature may be found. The standard solution, which we quote in § 3.1, is obtained under certain assumptions which are not rigorously valid in the experiments we are concerned with. From this solution, nevertheless, it is easy to obtain the equation of the resonance curve for magnetic dipole transitions between an isolated pair of excited states (§ 3.4.1). Experimental observations are normally interpreted with reference to this equation. The case of electric dipole transitions is treated rather differently (§ 3.4.3).

We normally face more complicated situations than an isolated pair of excited states. In the later sub-sections we shall discuss the attempts which have been made to meet these actual situations.

#### 3.1. Simple Model for the Radio-frequency Transitions

We consider two energy eigenstates of an atomic system,  $p$  and  $q$ , of energies  $W_p$  and  $W_q$ . We define  $\omega_0 = (W_q - W_p)/\hbar$ . It is to be noticed that in order to specify  $p$  and  $q$  we must select an axis of quantization. For the purposes of the



following analysis, the axis of quantization will be the  $z$  axis of the rotating field, though it need not necessarily be so.

We now consider the effect on the atomic system of the perturbation  $-\boldsymbol{\mu} \cdot \mathbf{H}_1(t)$ ,  $(-\mathbf{p} \cdot \mathbf{E}_1(t))$ . We shall need the elements of the perturbation matrix

$$\begin{aligned}\langle p | \mathcal{H}(t) | q \rangle &= - \int \psi_p^* (\tfrac{1}{2} H_1 \mu_+ e^{i\omega t}) \psi_q d\tau = -\hbar \tfrac{1}{2} b_{pq} e^{i\omega t}, \\ \langle q | \mathcal{H}(t) | p \rangle &= - \int \psi_q^* (\tfrac{1}{2} H_1 \mu_- e^{-i\omega t}) \psi_p d\tau = -\hbar \tfrac{1}{2} b_{qp} e^{-i\omega t}. \quad \dots\dots(13)\end{aligned}$$

The magnetic moment  $\boldsymbol{\mu} = \boldsymbol{\mu}_L + \boldsymbol{\mu}_S + \boldsymbol{\mu}_I$ . We shall ignore the nuclear component and write  $\boldsymbol{\mu} \simeq \boldsymbol{\mu}_L + \boldsymbol{\mu}_S$ , whose matrix elements are the same as those of  $\boldsymbol{\mu}_J = -g_J \beta \mathbf{J}$  between states in which  $J$  does not change, that is, for all transitions between Zeeman and hyperfine-structure components. Matrix elements of  $\boldsymbol{\mu}_L + \boldsymbol{\mu}_S$  between states which differ in  $J$  are given by Lamb (1957). If  $J$  does not change, the quantities  $b_{pq}, b_{qp}$  are equal to the matrix elements of  $J_{\pm} = (J_x \pm iJ_y)$  multiplied by  $g_J \beta H_1 / \hbar = \gamma_J H_1$ .

In the solution of the problem the following restrictive assumptions are now made: (i) neither  $p$  nor  $q$  interacts with any other state, (ii) the diagonal elements  $b_{pp}, b_{qq}$  are zero. (This is automatically satisfied in our case, since  $H_1(t)$  has no component along the  $z$ -axis.) An expression can now be deduced rigorously for the probability  $P_{pq}(t)$  that an atom, initially in state  $p$ , will be in state  $q$  after time  $t$ . We find

$$P_{pq}(t) = \frac{|b_{pq}|^2}{(\omega_0 - \omega)^2 + |b_{pq}|^2} \sin^2 \left\{ \tfrac{1}{2} [(\omega_0 - \omega)^2 + |b_{pq}|^2]^{1/2} t \right\}. \quad \dots\dots(14)$$

(In the similar, but not identical expression first given by Rabi (1937), the states  $p$  and  $q$  are defined with reference to a rotating axis of quantization.)

The expression (14) forms the basis of all radio-frequency resonance curves. It will be noticed that the first factor on the right-hand side describes a curve with a maximum at  $\omega = \omega_0$  and a width at half intensity of  $2|b_{pq}|$ . The expression for  $P_{pq}(t)$  is still a good approximation near resonance when assumption (ii) is violated, provided that  $b_{pp}, b_{qq} \ll \hbar\omega_0$ .

From (14) we readily deduce the relative probabilities of radio-frequency transitions. For at resonance ( $\omega = \omega_0$ ), and in a time such that the  $\sin^2(\dots)t$  term is still small, we have

$$P_{pq}(t) = \sin^2 \tfrac{1}{2} |b_{pq}| t \rightarrow (\tfrac{1}{2} |b_{pq}| t)^2 \quad \dots\dots(15)$$

so that transition probabilities are proportional to the squares of the matrix elements of the perturbation. The probabilities of different atomic transitions in a given radio-frequency field  $H_1(t)$  are thus proportional to the squares of the matrix elements of  $J_{\pm}$ . All non-vanishing matrix elements of  $J$  in the representations  $(F, m_F)$  and  $(J, m_J)$  are given below. The formulae may be found in Condon and Shortley

(1951), pp. 63, 65, 66.

$$\begin{aligned}\langle J, m_J | J_z | J, m_J \rangle &= m_J \\ \langle J, m_J \pm 1 | J_{\pm} | J, m_J \rangle &= [(J \mp m_J)(J \pm m_J + 1)]^{1/2}, \quad \dots\dots(16a)\end{aligned}$$

$$\begin{aligned}\langle F, m_F | J_z | F, m_F \rangle &= A m_F \\ \langle F, m_F | J_{\pm} | F, m_F \mp 1 \rangle &= A[(F \pm m_F)(F \mp m_F + 1)]^{1/2} \\ A &= \frac{J(J+1) - I(I+1) + F(F+1)}{2F(F+1)}, \quad \dots\dots(16b)\end{aligned}$$

$$\begin{aligned}\langle F, m_F | J_z | F+1, m_F \rangle &= B[(F+1)^2 - m_F^2]^{1/2} \\ \langle F, m_F | J_{\pm} | F+1, m_F \mp 1 \rangle &= \pm B[(F \mp m_F + 1)(F \mp m_F + 2)]^{1/2} \\ B &= \left[ \frac{(F+1-J+I)(F+1+J-I)(J+I+2+F)(J+I-F)}{4(F+1)^2(2F+1)(2F+3)} \right]^{1/2}, \quad \dots\dots(16c)\end{aligned}$$

$$\begin{aligned}\langle F, m_F | J_z | F-1, m_F \rangle &= C[F^2 - m_F^2]^{1/2} \\ \langle F, m_F | J_{\pm} | F-1, m_F \mp 1 \rangle &= \mp C[(F \pm m_F)(F \pm m_F - 1)]^{1/2} \\ C &= \left[ \frac{(F-J+I)(F+J-I)(J+I+1+F)(J+I+1-F)}{4F^2(2F-1)(2F+1)} \right]^{1/2}. \quad \dots\dots(16d)\end{aligned}$$

Certain matrix elements for the case of intermediate field strengths are given by Torrey (1941).

It will be noticed that  $J_z$  has certain non-vanishing matrix elements. If, therefore, there is a field component  $H_{1z}(t)$  along the axis of quantization, the diagonal elements of the perturbation,  $b_{pp}, b_{qq}$  do not vanish.

The existence of matrix elements of  $J$  is expressed by the following selection rules for magnetic dipole transitions between states of the same  $J$ :

$$\Delta F = 0, \pm 1; \quad \Delta m_F = 0, \pm 1 \quad \text{for the } (F, m_F) \text{ representation};$$

$$\Delta m_J = 0, \pm 1; \quad \Delta m_I = 0 \quad \text{for the } (m_J, m_I) \text{ representation.}$$

Transitions  $\Delta J = \pm 1$  are also allowed by magnetic dipole interaction.

The transitions  $\Delta m_I = 0, \pm 1; \Delta m_J = 0$ , which are allowed if the nuclear magnetic moment is not neglected, are weaker by the factor  $(\mu_I/\mu_J)^2$ .

The matrix elements of the electric dipole moment depend on an evaluation of the radial integrals  $\int R_p^* r R_q dr$  which, for hydrogen wave functions, are tabulated by Condon and Shortley (1951), p. 133. The selection rules are identical with the well-known rules for spontaneous electric dipole transitions.

### 3.2. Violation of the Simplifying Assumptions

In experiments on excited states the assumptions under which equation (14) is derived may be violated in a variety of ways. First, in virtue of the spontaneous emission of radiation, the excited states are connected with remote states. We shall see in § 3.4 how the introduction of decay constants allows a satisfactory treatment of this situation, and generally leads to familiar Lorentz-type expressions for the resonance curve.



The restrictive conditions are again violated if the excited states  $p$  and  $q$  are connected by the perturbation with other excited states in the vicinity. If the frequency separations are exactly equal a rigorous generalization of equation (14) may be given (§ 3.3.1). Approximate solutions (§ 3.3.2) have been found for the general case of unequal intervals. The application of these results to magnetic dipole transitions between excited states is straightforward (§ 3.4.1). Certain particular cases where the intervals are unequal (or the states are perturbed by other fields) have been examined in detail (§ 3.5).

Violation of the condition that the diagonal elements of the perturbation matrix be small can usually be avoided by arranging that the radio-frequency field be at right angles to the axis of quantization, but it is sometimes of interest to use other geometries. In the exploration of  $\Delta m_F = 0$  transitions between weak field hyperfine levels, for example, the condition can easily be violated. No theoretical analysis of this case has come to our notice.

In § 3.6 we shall mention the situation in which the radio-frequency field is composed of several types of quanta. The most common case is met when an oscillating rather than a rotating field is used to induce transitions, which is the usual practice. An oscillating field comprises a mixture of right- and left-handed circularly polarized quanta of the same frequency. The superposition of fields of different frequency is also of interest.

### 3.3. *Multiplicity of Energy Levels*

#### 3.3.1. *Equally spaced energy levels.*

The groups of states  $(F, m_F)$  (or  $(J, m_J)$ ) include more than two if  $F$  (or  $J$ ) is greater than  $\frac{1}{2}$ . In sufficiently weak magnetic fields the energy levels are equally spaced. Through the interaction of several radio-frequency quanta transitions may be induced between any pair of the group. Majorana's well-known solution for the probability of a transition (taken from Ramsey 1956, p. 154) is

$$P(F, m, m', t) = (F-m)!(F+m)!(F-m')!(F+m')!(\sin \frac{1}{2}\alpha)^{4F} \\ \times \left[ \sum_r \frac{(-1)^r (\cot \frac{1}{2}\alpha)^{m+m'+2r}}{(F-m-r)!(F-m'-r)!(m+m'+r)!r!} \right] \dots\dots(17)$$

in which the summation index  $r$  may assume all values for which no argument of a factorial becomes negative, and in which  $\alpha$  is defined by the equation

$$\sin^2 \frac{1}{2}\alpha = P(\frac{1}{2}, \frac{1}{2}, -\frac{1}{2}, t),$$

i.e. the function  $P_{pq}$  of equation (14) with

$$\omega_0 = (W_q - W_p)/\hbar = (g_F \beta H_0)/\hbar = \gamma_F H_0$$

and

$$|b_{pq}|^2 = (\gamma_F H_1)^2.$$

It is to be noticed that the probability of a single quantum transition ( $m - m' = \pm 1$ ) is dependent on whether there exist other values of  $m$  within the group. Multiple quantum transitions are not simply represented as the product of successive single transitions. For small values of  $\gamma H_1 t$  the probability of a  $k$ -quantum transition is proportional to  $(\gamma H_1)^{2k}$ .

## 3.3.2. Unequally spaced energy levels.

We consider groups of energy levels whose unequal spacing may arise through the onset of  $I, J$  (or  $L, S$ ) decoupling, or because they belong to different values of  $F$  in hyperfine structures, or for some other reason. The common feature is that the different members of the group are interconnected by the perturbing field. Transitions  $m \rightarrow m \pm k$ , ( $k$  integral), may be induced through the intervention of  $k$  equal quanta. Conservation of angular momentum between the radiation field and the atom is thus assured. Conservation of energy requires that

$$W_q - W_p = k\hbar\omega_0.$$

When  $k > 1$ , the process is described as the simultaneous interaction of  $k$  quanta, rather than as  $k$  successive interactions. A number of authors (Besset, Horowitz, Messiah and Winter 1954, Winter 1955, Salwen 1955, Hack 1956) have treated the problem theoretically.

The main features disclosed by these analyses are :

(i) The transition probability is generally given by expressions similar to  $P_{pq}$  (equation (14)).

(ii) The resonance line width is of the order  $\delta/k$ , where  $\delta$  is the width appropriate to single-quantum transitions. It is easy to understand this; for if  $k$  quanta act simultaneously, we shall find  $(e^{i\omega t})^k$  in the perturbation operator, and the resonance denominator  $[(k\omega - \omega_{pq})^2 + |b_{pq}|^2 + (1/T)^2]^{-1}$  (see eqn (18)) will be proportional to  $[(\omega - \omega_0)^2 + |b_{pq}|^2/k^2 + 1/T^2 k^2]^{-1}$ , where  $\omega_0 = \omega_{pq}/k = (W_q - W_p)/k\hbar$ .

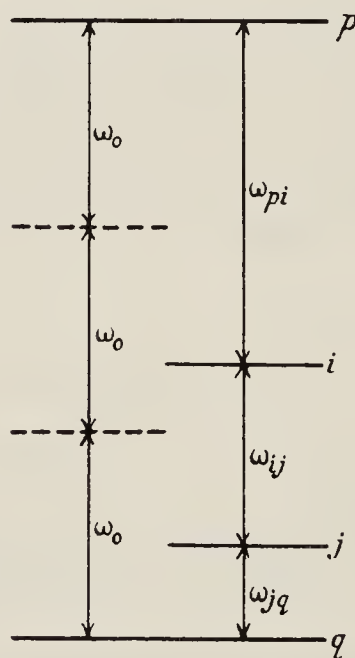


Figure 1. Multiple quantum resonances between unequally spaced levels.

The half-intensity width therefore tends to  $2/Tk$  when  $b_{pq}$  is small, instead of to  $2/T$ .

(iii) The resonant frequency  $\omega^*$  differs from  $\omega_0 = (W_p - W_q)/k\hbar$ . Analytical expressions (Salwen 1955, p. 1284) for the amount of the shift may be understood on the basis of time-independent perturbation theory in which the effect of the radio-frequency field (to first order) has been taken into account by shifting all the levels by the amount  $m\omega_0$  and by allowing perturbation between levels which differ by 1 in  $m$ . Intervals between such levels are reduced by the amount  $\omega_0$ .



Thus, for example, if  $p, i, j, q$  is a set of states whose  $m$ -values decrease successively by 1, their separations, for the present purpose, become

$$\Delta_{pi} = \omega_{pi} - \omega_0, \quad \Delta_{ij} = \omega_{ij} - \omega_0, \quad \Delta_{jq} = \omega_{jq} - \omega_0.$$

Then if  $\frac{1}{2}b_{pi}$  is the matrix element of the perturbation between states  $p$  and  $i$ , a second order perturbation treatment introduces an upward shift of  $p$  by  $|b_{pi}|^2/4\Delta_{pi}$  and a downward shift of  $q$  by  $|b_{jq}|^2/4\Delta_{jq}$ . (Since  $\Delta_{jq}$  is numerically negative in the figure,  $q$  is displaced upwards.)

Subject to the usual approximations of perturbation theory ( $b \ll \Delta$ ), we find the frequency shift

$$\omega^* - \omega_0 = \frac{1}{k} \left[ \frac{|b_{pi}|^2}{4\Delta_{pi}} + \frac{|b_{jq}|^2}{4\Delta_{jq}} \right]$$

to which the general formulae reduce in our example.

(iv) The intensity of a  $k$ -quantum transition under the above approximation is, in our example, proportional to  $[|b_{pi}| |b_{ij}| |b_{jq}| / (\omega_0 - \omega_{qi})(\omega_0 - \omega_{qj})]^2$ : the significant feature of this expression is the proportionality (through the  $b$ ) to the  $2k$ th power of the radio-frequency field. This is true also in the general case. The higher quantum transitions show a strong dependence on the perturbing field strength.

Multiple quantum transitions have been observed on several occasions in experiments on excited states (Althoff 1955, Ritter and Series 1957). Kusch (1956) undertook a systematic study of these transitions in the ground state of  $^{39}\text{K}$ , and found the theory well substantiated for amplitudes of the radio-frequency field which gave a maximum probability of transition. The discrepancies in line width which he found at higher amplitudes can probably be explained by a more detailed analysis of the variation in space of the radio-frequency field (Barrat and Winter 1956).

### 3.4. Finite Life of Excited States

A thorough analysis of the effect of distant states to which decay is possible would entail a solution of the time-dependent wave equation embracing all the states and radiation fields concerned. This we shall not attempt. We represent the effect of distant states in a phenomenological way by introducing constants  $\gamma$  for exponential decay,  $n_i = n_0 e^{-\gamma t}$ . The 'lifetime' of the state,  $T = 1/\gamma$ .

We shall see that  $T$  enters into expressions for the form of the resonance curve, the width of which may be used to determine  $T$ . The cases of magnetic and electric dipole transitions need to be treated differently, since in the one case all the excited states have the same decay constant, while in the other they do not.

The finite lifetime sets a lower limit to the radio-frequency field strength required to induce a transition (§ 1.2). On the other hand, the stimulation of transitions itself artificially shortens the lifetime of the states, so that the width of the resonance curve is a function of  $T$  and of the matrix elements  $b$ .

Rather complicated effects are to be expected if  $T$  is comparable with the precession time of atomic interactions, the hyperfine structure, for example. It is to be expected in this case that the electron-nuclear coupling would be reduced, so that the peak of a radio-frequency resonance curve for a hyperfine interval



would not exactly correspond with the frequency interval given by the stationary state theory. We understand that the problem has been considered by Serber (1956).

In the following sections the radio frequencies are much larger than the reciprocal lifetimes  $\gamma$ , but a case is cited (§ 3.5) where a perturbing level lies within the distance  $\gamma$  of an excited level.

### 3.4.1. Magnetic dipole transitions between excited states.

Following Brossel and Bitter (1952), we consider the simple case of transitions between a pair of isolated states which have the same lifetime  $T$ . We use equation (14) for  $P_{pq}$ , the probability of transition in time  $t$ . The signal  $\Delta S_{pq}$  will be some change, usually in the intensity of a beam of light, consequent upon the transition  $p \rightarrow q$ . Now, of  $N_p$  atoms excited and brought under the influence of the radio-frequency field at time  $t_1$ , a number  $\{N_p \exp[-(t-t_1)/T]\} P_{pq}(t-t_1)$  survive to time  $t > t_1$  and, having been transferred to state  $q$ , contribute to the signal. The simplicity of this expression rests on the fact that both  $p$  and  $q$  decay at the same rate. We need to integrate it for all  $t_1$  from  $-\infty$  to  $t$ . Thus

$$\begin{aligned} \Delta S_{pq} &\propto \int_{-\infty}^t \exp\left[-\frac{(t-t_1)}{T}\right] \frac{|b_{pq}|^2}{(\omega - \omega_0)^2 + |b_{pq}|^2} \sin^2\left[\frac{1}{2}\{(\omega - \omega_0)^2 + |b_{pq}|^2\}^{1/2}(t-t_1)\right] dt_1 \\ &\propto \frac{|b_{pq}|^2}{(\omega - \omega_0)^2 + (1/T)^2 + |b_{pq}|^2}. \end{aligned} \quad \dots\dots(18)$$

In the case of a multiplicity of equally spaced levels, the Majorana formula (17) is used instead of  $P_{pq}$ .

Careful experimental studies of line profiles made by Brossel and his colleagues (Brossel and Bitter 1952, Guiochon, Blamont and Brossel 1956) have confirmed the form of equation (18). It has been extensively used in the determination of  $T$  through the relation

$$(\frac{1}{2}\delta\omega)^2 = |b_{pq}|^2 + (1/T)^2 \quad \dots\dots(19)$$

which gives the line width  $\delta\omega$  between points of half-intensity. In so far as  $|b_{pq}|^2 (\propto H_1^2)$  is usually not known absolutely,  $T$  is determined by extrapolation to zero radio-frequency field strengths.

### 3.4.2. Coherence times.

$T$  (equation (18)) was interpreted as the lifetime of the excited atoms until the Paris group discovered that its value depended on whether multiple scattering of photons was taking place in the resonance chamber (§ 4.4.2). It is now interpreted as a 'coherence time' which tends to a constant value  $\tau$ , the true lifetime, as the atomic density in the vapour is reduced to the point at which multiple scattering ceases.

A theoretical analysis of the relation between  $T$  and  $\tau$  has been outlined (Barrat 1958) and a detailed publication is promised. The problem is stated in terms of the probability amplitudes  $a_p(t)$ ,  $a_q(t)$  for the states  $p$  and  $q$ . There will be definite phase relations between the  $a_p(t)$  and  $a_q(t)$  for the emitting and absorbing atoms, and there arises the possibility of interference phenomena. An analysis



which describes the emitting or absorbing atom as being definitely in one or other of the states  $p, q$  (i.e. in terms of  $|a_p|^2, |a_q|^2$ ), would not disclose the interference effects.

The problem is enlightened by considering the following experiment (Barrat and Brossel 1958). Two separate vessels A and B containing mercury vapour at low pressure (single scattering) are placed in the same steady magnetic field  $H_0$  and the same radio-frequency magnetic field. Vapour in A is excited by resonance radiation from a lamp: the fluorescent radiation from A excites the vapour in B. The fluorescent radiation from B is studied to detect radio-frequency resonances in B. It is found that the details of the resonance curve are quite different from the case of single scattering: in particular,  $T_B > \tau$ . If now a polarizer be inserted between A and B the characteristics of the resonance curve are those of single scattering.

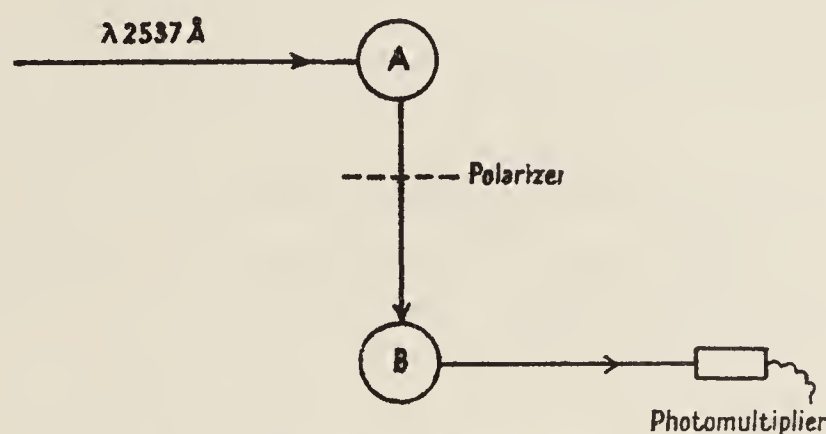


Figure 2. Double scattering of resonance radiation (schematic).

The interpretation of this experiment in the terms proposed above is that, since the atoms are in the same fields, the probability amplitudes  $a(t)$  of an exciting atom in A and an excited atom in B develop at the same rate. The phase relations between the  $a(t)$  of the atom in A are passed on to the atom in B via the resonance radiation. The coherence time of the excited states is then greater than that of either atom:  $T_B > \tau$ . With insertion of the polarizer one determines the probability that the photons which pass will have a given polarization, but sacrifices any coherence which existed between different polarizations (Dirac 1947, Ch. I). The phase relations between the emitting atom in A and the excited atom in B become uncorrelated. The measured lifetime will be that of the atom in B.

### 3.4.3. Electric dipole transitions between excited states.

If electric dipole transitions are allowed between a pair of excited states  $p$  and  $q$ , these will in general decay at different rates. For this reason the treatment of the last section is inapplicable.

We are not aware of any treatment which is valid when the radio-frequency perturbation is not small compared with the natural width of the energy levels. In the case when the perturbation is small, the results of the quantum theory of radiation may be applied (Weisskopf and Wigner 1930, Heitler 1954, p. 186).

Let  $\gamma_p, \gamma_q$  be the decay constants, and let  $\gamma_q > \gamma_p$ . Let  $S_0$  be the energy flux per unit area of radiation of angular frequency  $\omega$ , whose electric vector is parallel to a unit vector  $\mathbf{e}$ . Then  $\gamma_\omega$ , the probability per unit time of a stimulated transition,

may be expressed :

$$\gamma_{\omega} = \left( \frac{2\pi e^2 S_0}{c\hbar^2} \right) (\gamma_p + \gamma_q) \frac{|r_{pq}|^2}{(\omega - \omega_0)^2 + \frac{1}{4}(\gamma_p + \gamma_q)^2} \dots\dots\dots(20)$$

where  $r_{pq}$  is the matrix element of  $\mathbf{e} \cdot \mathbf{r}$  between states  $p$  and  $q$ ,  $\mathbf{r}$  having its usual significance, the sum of the coordinate vectors of the atomic electrons. This expression for  $\gamma_{\omega}$  gives the form of the resonance curve for an isolated pair of excited states, under the approximation that the perturbation is small compared with  $\gamma_p$  or  $\gamma_q$ .

Equation (20) has been derived by Lamb (Lamb and Retherford 1950, Appendix II, Lamb 1952, section L) from the equations of time-dependent perturbation theory (for the particular case that  $\gamma_p \simeq 0$ ) under the approximation that the perturbation is small compared with  $\gamma_q$ .

### 3.5. Transitions between Excited States in the vicinity of other States

Two cases have been investigated in detail. In both cases magnetic dipole transitions were investigated between states  $p$  and  $q$ , one of which was perturbed by a third state. In the one case the perturbation was by the radio-frequency magnetic field, in the other by a static electric field.

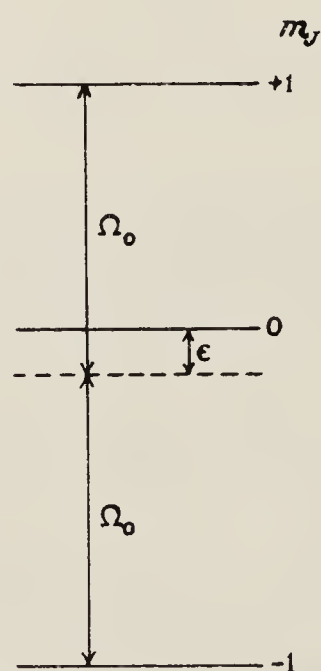


Figure 3. Combined Zeeman and Stark effects in the level  $^3P_1$ .

The first case (Blamont and Winter 1957, Blamont 1957) concerns the states  $m_J = 0, \pm 1$  of the level  $^3P_1$  of mercury. The three energy levels are unequally spaced under the influence of static electric and magnetic fields. The Bohr frequencies  $(W_q - W_p)/\hbar$  are  $\Omega_0 \pm \epsilon$ . Blamont and Winter calculate rigorously an expression for the form of the resonance curve, and find excellent agreement with experiment. The positions of the two maxima depend on the radio-frequency field  $H_1$ , as one would anticipate from the arguments of § 3.3.2. The perturbation formulae lead to the shifts  $\pm(\gamma H_1)^2/4\epsilon$  (matrix element:  $\gamma H_1/\sqrt{2}$ ;  $\Delta = 2\epsilon$ ). Blamont and Winter quote  $\pm 4(\gamma H_1)^2/\epsilon$ , but this is evidently a misprint, since Blamont's article quotes  $\pm(\gamma H_1)^2/4\epsilon$ , in agreement with the perturbation formula.



In the second case (Lamb 1952, p. 271, Lamb and Wilcox 1958) magnetic dipole transitions are investigated between the states  $m_J = \pm \frac{1}{2}(\alpha \text{ and } \beta)$  of the level  $^2S_{1/2}$  of atomic hydrogen. These are both metastable. The perturbing state is  $^2P_{1/2}$ ,  $m_J = \frac{1}{2}$  (e). At about 575 gauss, the states  $\beta$  and e have the same energy. The perturbation between them,  $V$ , arises from the electric field which is a consequence of the motion of the atoms through the magnetic field. Under ordinary time-independent theory, the perturbation between  $\beta$  and e would be such that they would never in fact cross: at the field where they would have crossed, each state should be a 50 : 50 mixture of pure S and P state. An entirely different conclusion is reached when one takes account of the different decay constants of  $\beta$  and e.

If  $|V| \leq \frac{1}{4}\gamma$ , where  $\gamma$  is the decay constant of the P state,  $\beta$  and e do in fact cross, and largely retain their S and P characters. Moreover, the point of intersection does not depend on the perturbation  $V$ . Hence the peak of the resonance curve is unshifted, and the curve itself is far narrower than would correspond to sharing of the decay constant of state e.

### 3.6. *Quanta of Different Kinds*

In the foregoing sections we restricted the argument to a uniformly rotating magnetic or electric field. In actual experiments it is usual to employ an oscillating field  $H_1 \cos \omega t$  which corresponds to the superposition of two fields rotating in opposite directions.

The sense of rotation which is effective in inducing the required transition depends on the sign of  $W_q - W_p$  relative to  $m_q - m_p$ , which, in the magnetic case, depends on the sign of the  $g$ -factor. The sense of rotation which stimulates absorption of energy also stimulates emission. The opposite sense stimulates neither. We refer to the 'resonant' and 'anti-resonant' components of the oscillating field.

It was first calculated by Bloch and Siegert (1940) that the anti-resonant component causes the peak of the resonance curve to be displaced to higher frequencies from  $\omega_0 = (W_q - W_p)/\hbar$  by the amount  $|b_{pq}|^2/4\omega_0$ , where  $\frac{1}{2}b_{pq}$ , as before, is the matrix element of the perturbation (see equation (13)). In applying this relation it is to be understood that the amplitude of the oscillating field is twice that of the rotating field.  $H_1$  in these formulae is the amplitude of the rotating component. The Bloch-Siegert correction is sometimes significant in experiments on excited states.

Ramsey (1955) has shown that if rotating fields of several frequencies  $\omega_1, \dots, \omega_i \dots$  are present simultaneously, the peak of the resonance curve at  $\omega_1$  near  $\omega_0$  is shifted as before by the amount  $\omega_1 - \omega_0 = |b_i|^2/2(\omega_0 - \omega_i)$  for each  $\omega_i$ , provided that  $|b_1| \dots |b_i| \dots \ll \omega_0 - \omega_i$ . This expression includes the Bloch-Siegert case  $\omega_i = -\omega_0$ .

A type of multiple quantum transition, different from that discussed in § 3.3.2, has been investigated by Brossel, Margerie and Winter (1955). Transitions between a given pair of states are induced by the simultaneous action of radio-frequency fields of different frequencies  $\omega$  and  $\omega'$ . The various possibilities are governed by the equation

$$f\omega + g\omega' = \omega_0,$$

where  $f$  and  $g$  are positive or negative integers.

Conservation of angular momentum is satisfied by the selection of photons of appropriate polarization. The radio-frequency field must have a component along the axis of quantization as well as perpendicular to it, so that there exist  $\sigma^+$ ,  $\sigma^-$  and  $\pi$  photons having 1,  $-1$ , and 0 units of angular momentum respectively, in the direction of the axis. An atomic transition  $\Delta m = +1$ , for example, may then be stimulated by the absorption of one photon,  $\sigma^+$ ; or two,  $\sigma^+$  and  $\pi$ ; or three,  $\sigma^+$ ,  $\sigma^-$  and  $\pi$ ; etc. (figure 4).

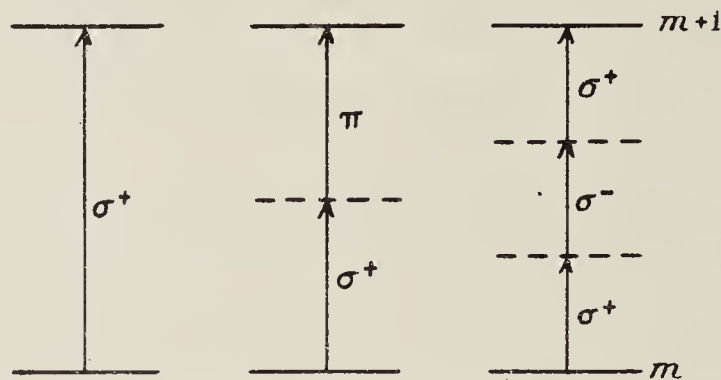


Figure 4. Simultaneous action of quanta of different kinds

One finds for these resonances the same features as in the case of multiple quantum transitions treated earlier (§ 3.3.2), namely, Lorentz line shape, reduction in line width according to the number of quanta participating, intensity proportional to  $|b|^{2f}|b'|^{2g}$  and shift of the peak of the resonance curve. These shifts can be quite large. They are given by the expression

$$\Omega - \omega_0 = \frac{|b|^2}{2(\Omega - \omega)} + \frac{|b|^2}{2(\Omega + \omega)} + \frac{|b'|^2}{2(\Omega - \omega')} + \frac{|b'|^2}{2(\Omega + \omega')} \quad \dots\dots(21)$$

where  $\Omega = f\omega + g\omega'$  at resonance,  $\omega_0 = (W_q - W_p)/\hbar$  and  $\frac{1}{2}b, \frac{1}{2}b'$  are the matrix elements as defined in equation (13) for the two radio-frequency fields which together induce the transition  $\Delta m = +1$ . The formula is deduced for linear radio-frequency fields. It is valid so long as one of the quantities  $|b|^2/(\Omega - \omega) \dots$  is small compared with  $\Omega$ . Terms with zero in the denominator are to be discounted.

Although there may be components of the radio-frequency field along the axis, the matrix elements into which these enter are zero, and they do not appear in equation (21).

In an experiment on sodium in the ground level, Brossel, Margerie and Winter (1955) observed shifts of resonance peaks which agreed well with the predictions of (21).

## § 4. DOUBLE RESONANCE EXPERIMENTS

### 4.1. Resonance Radiation

The phenomena of optical resonance radiation attracted a great deal of attention in the nineteen-twenties and thirties. Wood's early experiments with sodium vapour were followed by quantitative studies of the dependence of the intensity and polarization of the fluorescent radiation on such variables as the vapour pressure of the fluorescent substance, the pressure of foreign gases, the presence of magnetic fields, the geometry of the absorption bulb, and the spectral distribution of the exciting radiation.



It will be recalled that essential conditions for the observation of resonance radiation are low vapour pressure of the substance concerned ( $< 1$  micron of mercury) and illumination by light whose frequency corresponds exactly with an allowed transition in the substance, normally from the ground level. This light may, but need not, originate from a lamp containing the particular substance. Self-reversal in the light source must be avoided. Low pressure of foreign gas in the resonance vessel is usually desirable, but is not always essential. Resonance radiation has been observed in many substances, although most work has been done on sodium and mercury. An excellent account of the subject from the experimental point of view is to be found in the textbook by Mitchell and Zemansky (1934). A shorter account is given by Pringsheim (1949). The quantum theory of resonance radiation is presented in Heitler's book (1954).

In studying the literature of the early nineteen-thirties it is to be remembered that the theory of atomic hyperfine structure was in its infancy. Some of the experiments on the polarization of resonance radiation, for example, which were difficult to interpret at the time, are immediately explicable in terms of nuclear spin.

Of particular importance in connection with double resonance work is an understanding of the distribution in space of resonance radiation, and its polarization. While quantum mechanical calculations are necessary for detailed studies, a model based on classical physics can be very helpful. This we next consider. With its aid we realize, for example, the important practical point that the angular size of light cones can be quite large before the efficiency of double resonance experiments is seriously impaired.

#### 4.2. *Spatial Distribution of Resonance Radiation : Classical Model*

We first represent the atom by an isotropic electric oscillator. Let this be excited by a polarized electromagnetic wave travelling in a particular direction. The oscillator will be stimulated to radiate with the anisotropic distribution characteristic of a dipole.

An external magnetic field will, in general, exert a couple on the oscillating dipole, and the resulting precessional motion will cause a re-distribution of the scattered radiation. But in the important special case of a field parallel to the axis of the dipole there will be no couple, no precession and no change in the scattered radiation.

We wish now to examine the effect of an additional magnetic field, rotating in a plane perpendicular to the static field. We consider the special case cited above. Resolve the oscillating electric dipole into two opposed circular currents, that is, two oppositely directed magnetic dipoles. We endow these with angular momenta parallel to the dipole moments, so that the two angular momenta are also opposed. The magnetic dipoles now precess in the same sense about the static field. If the additional magnetic field rotates at the precessional frequency and in the correct sense, there will occur energy exchanges between the dipoles and the rotating field: that is to say, the dipoles may change their direction with respect to the static field. In this way the rotating magnetic field can bring about a re-distribution of the radiation from the oscillator, and resonance between the rotating field and the precession of the atom may thereby be detected.

In an actual atom the spin-orbit or hyperfine structure interactions may exert couples on the oscillator, which is then no longer isotropic. The distribution of radiation is different in this case, but the possibility still exists of changing the distribution by means of a rotating magnetic field of the correct frequency. This may be the precessional frequency in an external field, as before, or it may be any of the precessional frequencies associated with the spin-orbit or hyperfine structure interactions in zero field.

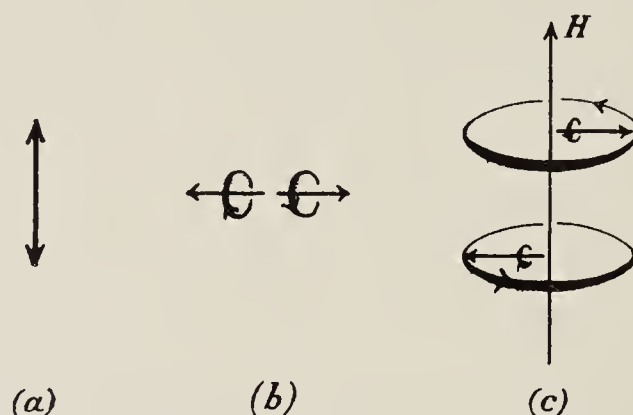


Figure 5. Resolution of an oscillating electric dipole: (a) oscillating electric dipole; (b) equivalent pair of spinning magnetic dipoles; (c) precession of the magnetic dipoles in a static field  $H$ .

#### 4.3. Intensity and Polarization of Resonance Radiation: Quantum Theory

For many purposes it is satisfactory to treat the process of resonance fluorescence as the succession of two independent processes, excitation and decay. This treatment we shall shortly illustrate. It is inadequate when the natural width of the levels is comparable with the distance between them, for then the possibility arises of interference between excitations to different states. The case has been discussed by Hawkins (1955) and by Serber (1956). When the levels are well separated the interference effects are negligible, and the simple treatment suffices.

Knowledge of the probability for excitation to a particular level demands in principle a calculation of the matrix elements of the electric dipole moment. Absolute calculations are generally quite impracticable: we use instead the measured  $f$ -value of the transition, which gives the total cross section for excitation, and the angular factors in the matrix elements, which give the distribution between different states.

The  $f$ -value (oscillator strength) of an atomic transition is a measure of the ability of an atom to absorb radiant energy relative to the ability of a classical oscillating electron. It is in fact connected with the probability for spontaneous decay of the excited level  $A_{kj}$  by the relation

$$f_{jk} = \frac{mc\lambda_{kj}^2}{8\pi^2 e^2} \frac{g_k}{g_j} A_{kj} = 1.51 \frac{g_k}{g_j} \lambda_{kj}^2 A_{kj} \quad (\lambda_{kj} \text{ in cm})$$

where  $g_k, g_j$  are the statistical weights of the levels  $k, j$ .

The integrated cross section for absorption of radiation by a classical oscillating electron is a universal constant,  $\pi e^2/mc$ . We therefore have, for absorption by a transition of oscillator strength  $f$ ,

$$\int \sigma_\nu d\nu = \pi e^2 f / mc \quad \dots\dots(22)$$



where  $\sigma_\nu$  is the cross section at frequency  $\nu$ . If the atoms are illuminated by  $n_\nu d\nu$  photons/cm<sup>2</sup> sec in the spectral range  $d\nu$ , the number of photons/sec absorbed per atom will be

$$\int n_\nu \sigma_\nu d\nu = n_\nu \pi e^2 f / mc = 2.64 \times 10^{-2} n_\nu f \quad \dots\dots(23)$$

if  $n_\nu$  is a constant over the absorption region. Values of  $f$  are to be found in Landolt-Börnstein's tables (1950).

We now quote the relative probabilities,  $A(J, m_J; J', m_J')$ , for transitions between different states.  $f$  will embrace a group of such transitions.

$$\begin{aligned} A[J, m_J; J, (m_J \pm 1)] &: A_{J, J}(J \pm m_J + 1)(J \mp m_J) \\ A[J, m_J; J, m_J] &: 2A_{J, J} m_J^2 \\ A[J, m_J; (J+1), (m_J \pm 1)] &: A_{J, J+1}(J \pm m_J + 1)(J \pm m_J + 2) \\ A[J, m_J; (J+1), m_J] &: 2A_{J, J+1}(J + m_J + 1)(J - m_J + 1). \end{aligned} \quad \dots\dots(24a)$$

In using the formulae for calculating the intensity of light in absorption or emission, it is to be noticed that the spatial distribution of  $\pi$  light ( $\Delta m = 0$ ) is different from that of  $\sigma$  light ( $\Delta m = \pm 1$ ). For this reason, when the intensities of  $\pi$  and  $\sigma$  light are being compared for a direction at right angles to the axis of quantization, the transition probabilities for  $\sigma$  light (given below) are to be multiplied by  $\frac{1}{2}$ . It will be noticed that the totals of  $\pi$  light and of  $\sigma$  light in this direction are always equal.

For the Zeeman components in hyperfine structure we use the above formulae with  $J, m_J$  substituted by  $F, m_F$ . The coefficients  $A_{F, F}$ ,  $A_{F, F+1}$  are then related as follows:

for  $J \rightarrow J$ ,

$$\begin{aligned} A_{F, F} &= A_{J, J} \left\{ \frac{J(J+1) + F(F+1) - I(I+1)^2}{F(F+1)} (2F+1) \right\} \\ A_{F, F+1} &= A_{J, J} \left\{ \frac{(J+F+I+2)(J-F-I-1)(J-F+I)(J+F-I+1)}{(F+1)} \right\}; \end{aligned}$$

for  $J \rightarrow J+1$ ,

$$\begin{aligned} A_{F, F} &= A_{J, J+1} \left\{ \frac{(J+F+I+2)(J+F-I+1)(J-F+I+1)(J-F-I)}{F(F+1)} (2F+1) \right\} \\ A_{F, F+1} &= A_{J, J+1} \left\{ \frac{(J+F+I+3)(J+F+I+2)(J+F-I+2)(J+F-I+1)}{(F+1)} \right\}. \end{aligned} \quad \dots\dots(24b)$$

These formulae have been gathered from the book by Condon and Shortley (1951, pp. 63, 238, 387, 424).

The formulae cannot be used for hyperfine structure if the atom is in a magnetic field which is strong for the excited, and weak for the ground level. In this case each ground state ( $F, m_F$ ) is treated as a sum of states ( $J, m_J; I, m_I$ ) with probability amplitudes which are conveniently given by Condon and Shortley, p. 73.

By way of example, we now apply the formulae to the resonance line of mercury,  $6^1S_0 - 6^3P_1$ ,  $\lambda 2537\text{\AA}$ . The cases  $I = 0$  (even isotopes) and  $I = \frac{1}{2}$  ( $^{199}\text{Hg}$ ) are illustrated in figure 6, where the numbers which break the transition lines are ratios of transition probabilities,  $A(J, m_J; J', m_J')$  or  $A(F, m_F; F', m_F')$ .

Normally, all the ground states of a given isotope will be equally populated (apart from the possibility of a very small Boltzmann factor, which we ignore).

We examine first the effect of illumination whose frequency distribution is uniform over the whole of the absorption region.

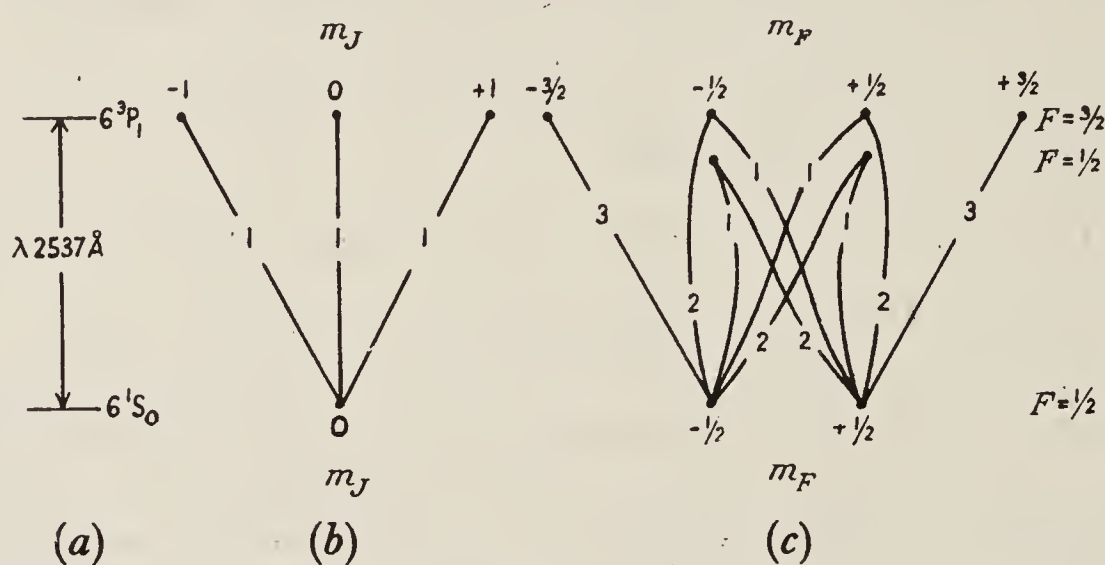


Figure 6. Transition probabilities in the resonance line of mercury: (b) even isotopes:  $I = 0$ . (c)  $^{199}\text{Hg}$ :  $I = \frac{1}{2}$ .

Relative intensities for observation perpendicular to the axis of quantization are obtained by introducing the factor  $\frac{1}{2}$  for the transitions  $\Delta m = \pm 1$ .

The relative populations of the excited states will then be the sums, for each state, of the excitation probabilities for the given type of exciting radiation (bearing in mind the factor  $\frac{1}{2}$  for  $\sigma$  radiation where appropriate). Thus, for excitation in a direction perpendicular to the axis of quantization, we find the following distribution of population.

Excitation by	even isotopes			$^{199}\text{Hg}$					
	$J = 1$			$F = \frac{3}{2}$				$F = \frac{1}{2}$	
	$-1$	$0$	$+1$	$-\frac{3}{2}$	$-\frac{1}{2}$	$+\frac{1}{2}$	$+\frac{3}{2}$	$-\frac{1}{2}$	$+\frac{1}{2}$
	$-1$	$0$	$+1$	$-\frac{3}{2}$	$-\frac{1}{2}$	$+\frac{1}{2}$	$+\frac{3}{2}$	$-\frac{1}{2}$	$+\frac{1}{2}$
$\pi$ light	0	1	0	0	2	2	0	1	1
$\sigma^-$ light	$\frac{1}{2}$	0	0	$\frac{3}{2}$	$\frac{1}{2}$	0	0	1	0
$\sigma^+$ light	0	0	$\frac{1}{2}$	0	0	$\frac{1}{2}$	$\frac{3}{2}$	0	1
natural light	$\frac{1}{2}$	1	$\frac{1}{2}$	$\frac{3}{2}$	$\frac{5}{2}$	$\frac{5}{2}$	$\frac{3}{2}$	2	2

The examples bring out the following facts, which are true generally:

(i) When the values of  $J$  (or  $F$ ) differ between the ground and excited levels, population differences may be induced by light of any polarization, or by natural light. Differences are most pronounced when  $\pi$  light is used.

(ii) When the values of  $J$  (or  $F$ ) are the same in the excited as in the ground level, population differences are induced only by  $\sigma^-$  or  $\sigma^+$  illumination.

It may be verified that isotropic excitation by natural light results in equal population of all the excited states.



We now consider the case when the exciting radiation is non-uniform in frequency distribution, for example, when the hyperfine structure is partially resolved in the light from a source. The transition probabilities are now to be multiplied by the relative intensities of the light in the difference regions of absorption. The result is that the excited states can be unequally populated, even when the illumination is isotropic and unpolarized. We consider a particular example in § 4.6.

The populations  $N_e$  of the excited states having been found, the quantities

$$S_{\sigma+} = \sum_e N_e A_{\sigma+}, \quad S_{\sigma-} = \sum_e N_e A_{\sigma-}, \quad S_{\pi} = \sum_e N_e A_{\pi}$$

give the total amounts of  $\sigma^+$ ,  $\sigma^-$  and  $\pi$  components in the fluorescent light. Proper account must be taken of the spatial distribution, as mentioned above.

Detection of radio-frequency resonances in the excited states rests on changes which take place in  $S_{\sigma+}$ ,  $S_{\sigma-}$  and  $S_{\pi}$  when the  $N_e$  are re-distributed. The changes  $\Delta S$  can be calculated from the formulae of § 3.

Changes in  $S$  can occur in other ways, for example, if the atoms undergo collisions which re-orient them before they decay. As we shall see later, states with  $J = 0$  are less sensitive than others to such collisions.

The smallest signal which can be detected depends on the sources of noise in the experiment. Frequently, the most important source is the shot noise in the emission of electrons from the cathode of a photomultiplier. In this case we can calculate the signal to noise ratio as follows:

Let  $i_s$  be the primary current at the cathode of the photomultiplier due to the fluorescent light  $S$ . Stray light may contribute a further current  $i_0$ . The shot noise is constituted by the random fluctuations in the  $n$  electrons which, in observation time  $\tau$ , constitute the current  $i = i_s + i_0$ . The r.m.s. noise current  $i_n$ , averaged for time  $\tau$ , is the current associated with  $n^{1/2}$  electrons, i.e.

$$i_n = n^{1/2} e / \tau = (ie / \tau)^{1/2}, \quad \text{since } i = ne / \tau.$$

The signal current  $i_{\Delta S}$ , is  $(\Delta S / S) i_s = \beta i_s$ . Thus

$$\frac{i_{\Delta S}}{i_n} = \frac{\beta i_s}{(ie / \tau)^{1/2}}. \quad \dots\dots(25)$$

The fraction  $\beta$  depends only on the relative populations  $N_e$ , the radio-frequency transition probabilities, and the relative probabilities for decay. It does not depend on the spectral density of the exciting radiation, provided this is uniform over the region of absorption. Nor does  $\beta$  depend on the  $f$ -value, or on the density of absorbing atoms  $N_a$ .

$i_s$ , on the other hand, depends on  $n_\nu f$  and  $N_a$ , also on the fraction of the fluorescent light which is received by the photomultiplier  $\phi$  and on the efficiency of the photocathode  $\eta$ . For if, as in equation (23),  $n_\nu d\nu$  is the number of photons per  $\text{cm}^2$  in the spectral range  $d\nu$ , then the number of atoms excited per second is  $(\pi e^2 / mc) n_\nu f N_a l$ , provided that the vapour is optically thin, where  $l$  is the length of vapour column of  $N_a$  atoms per  $\text{cm}^3$ . We then have  $i_s = (\pi e^3 / mc) n_\nu f N_a l \phi \eta$ .

## 4.4. Double Resonance Experiments in Magnetic Fields

We now give brief accounts of experiments which have been performed.

## 4.4.1. The experiment of Brossel and Bitter.

The 'double resonance' method was introduced by Brossel and Bitter (1952), following the prediction of Brossel and Kastler (1949). The excited level  $6^3P_1$  of mercury was studied in a magnetic field.  $\pi$  excitation with the resonance line  $\lambda 2537\text{\AA}$  was chosen, i.e. the light was incident on the resonance cell at right angles to the magnetic field, and was polarized with its electric vector parallel to the field.

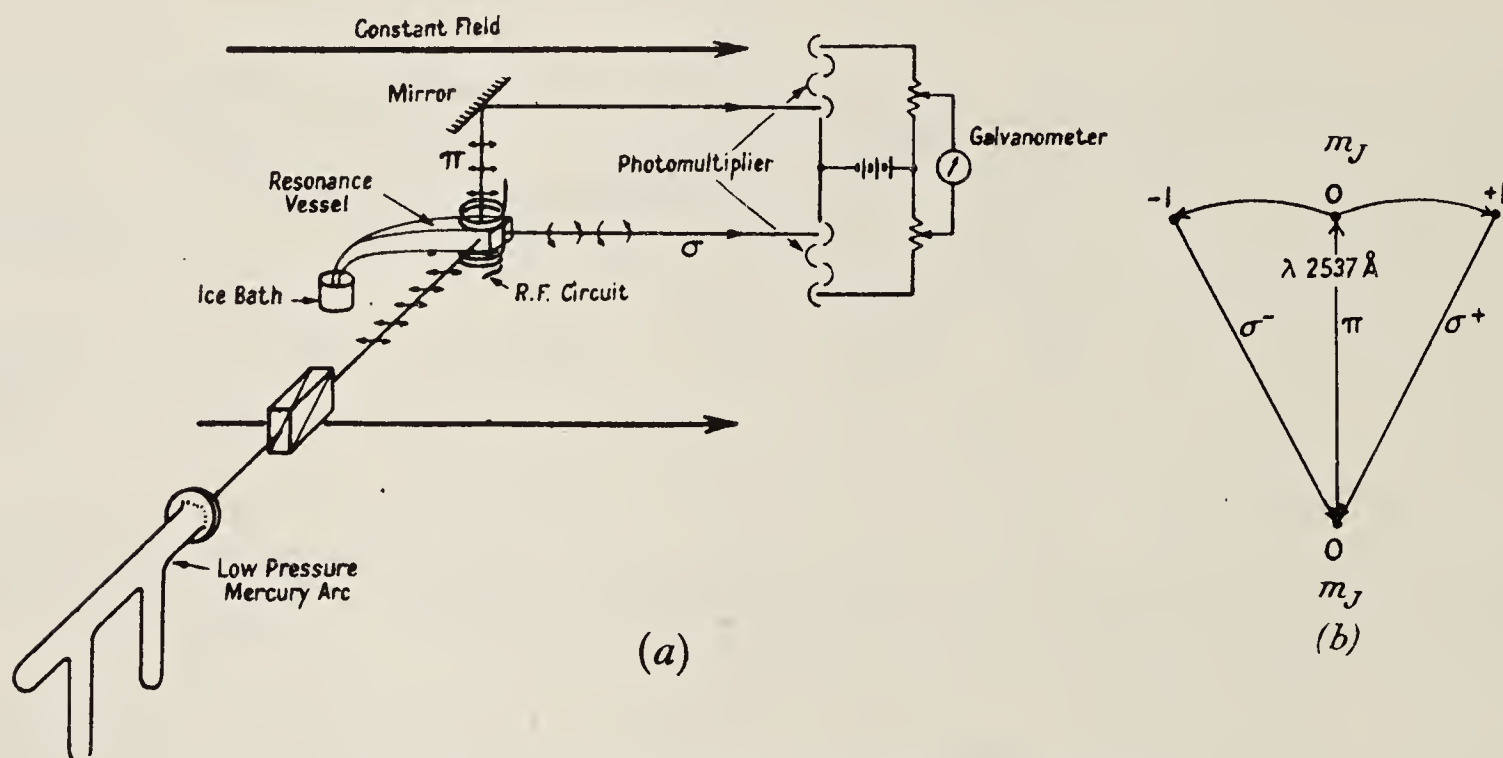


Figure 7. The experiment of Brossel and Bitter.

Under this excitation the state  $m_J = 0$  alone is excited. The radio-frequency magnetic field at fixed frequency  $\nu$  was applied by a coil surrounding the resonance vessel, and the 'static' magnetic field varied through the resonant value  $H_0$  given by  $h\nu = g_J \beta H_0$ . It is clear from figure 7(b) that radio-frequency resonance will be accompanied by an increase in  $\sigma$ , and a decrease in  $\pi$  light. These changes were detected by photomultipliers which received light in the direction of, and perpendicular to, the field, respectively. The currents were set in opposition in order to compensate fluctuations in the light source, and at the same time to double the signal. The difference current was observed on a galvanometer.

Brossel and Bitter studied in detail the line shape of the radio-frequency resonances, and in particular its dependence on the radio-frequency field strength. As is shown in § 3.4.1 it is possible by extrapolation to obtain a line width, and hence a time, which was interpreted as the lifetime of the atoms. Further studies, described in the next section have revealed that the 'coherence time' obtained in this way is not identical with the lifetime but is asymptotic to it at low vapour pressures.

Figure 8(a) shows a set of resonance curves obtained with various amplitudes of radio-frequency field. The double peaked curves obtained at the higher field strengths are predicted by the Majorana formula (equation (17)), which is appropriate to this case.



Figure 8(b) demonstrates displacement of the resonances by the Bloch–Siegert effect (§ 3.6).

From their measurements Brossel and Bitter deduced the value

$$g_J = 1.4838 \pm 0.0004$$

for the level  $6^3P_1$  in mercury. The significance of the experiment lies not so much in this determination as in the demonstration of the feasibility of the method. From this work has stemmed the investigation not only of other excited states, but also of the widening and important field of ‘optical pumping’.

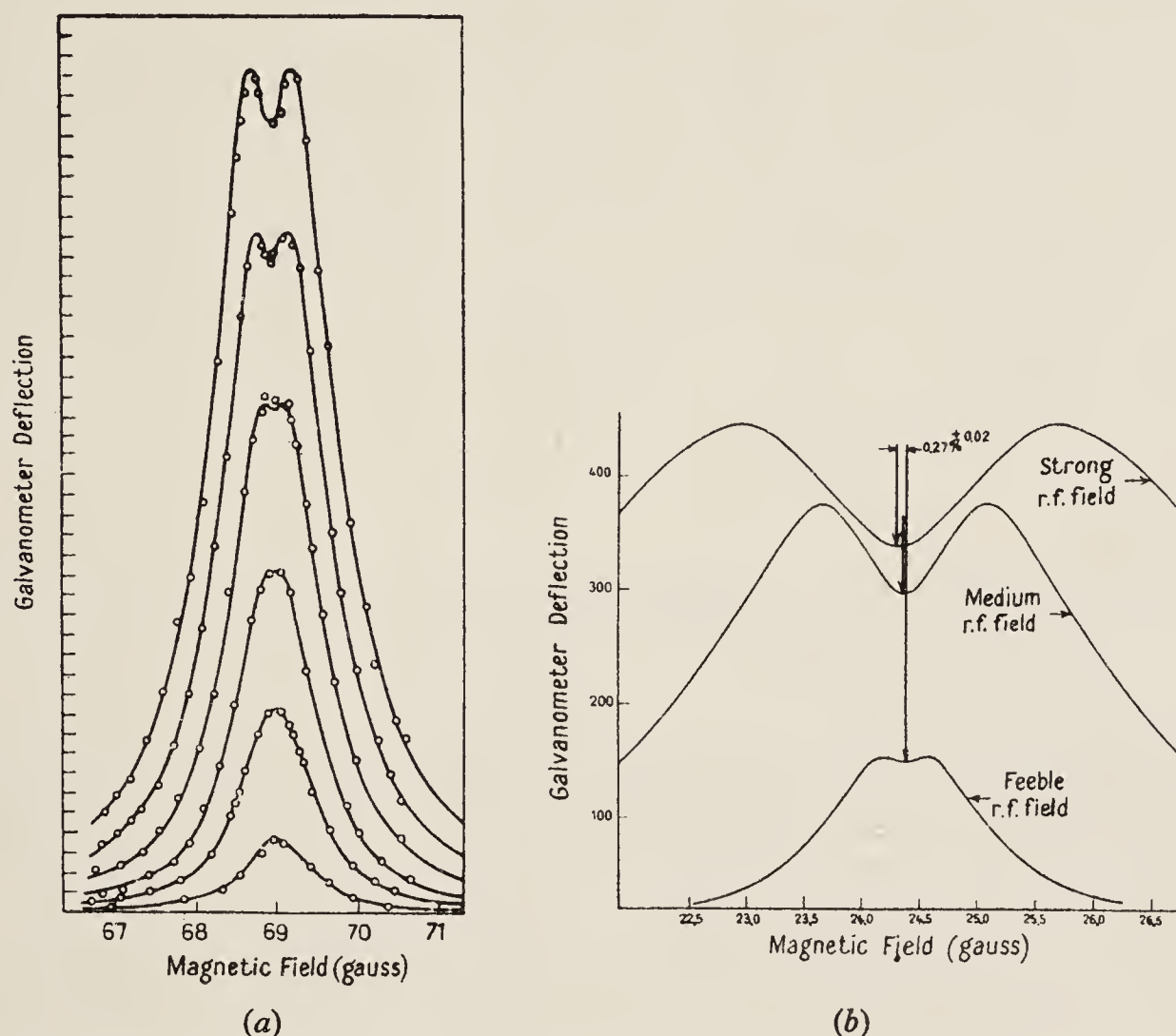


Figure 8. Resonance curves obtained by Brossel and Bitter: (a) resonances at different r.f. field strengths; (b) the Bloch–Siegert effect.

#### 4.4.2. Further studies of excited states in mercury.

Blamont and Brossel (1956) studied the Stark effect of the level  $6^3P_1$  in mercury. The experimental arrangement resembled that of Brossel and Bitter, with the addition of a pair of plane electrodes in the vapour for the establishment of static electric fields of the order of  $50 \text{ kv cm}^{-1}$ . The difficulty of finding electrodes which could be used in a region of strong radio-frequency fields was overcome by using a semiconductor coated on to Pyrex (Blamont 1957).

In contrast with the Zeeman effect, the Stark effect is independent of the sign of  $m_J$  (or  $m_F$ ). The intervals between  $m_J = 0$  and  $\pm 1$ , therefore, which are equal under a magnetic field alone, become unequal when an electric field is simultaneously applied (figure 9(a)): the single peak  $\nu_0$  (figure 9(b)), which denotes two coincident radio-frequency resonances, separates into its two components  $\nu_1$  and  $\nu_2$ . The interpretation of these curves is not quite straightforward, since

doubling of the peak can occur even when there is no electric field if the radio-frequency field is strong enough (see figure 8). Blamont's detailed theory of the line shape (1957, see also § 3.5) is well supported by the measurements.

Guiochon, Blamont and Brossel (1956, 1957) also Boutron, Barrat and Brossel (1957) observed and studied an unexpected narrowing of the radio-frequency resonances with increase in vapour pressure of the mercury. One would expect that the shorter mean free path associated with higher vapour pressures would shorten the lifetimes of the excited atoms and lead to wider radio-frequency resonances, but this is contrary to their observations. They describe the times

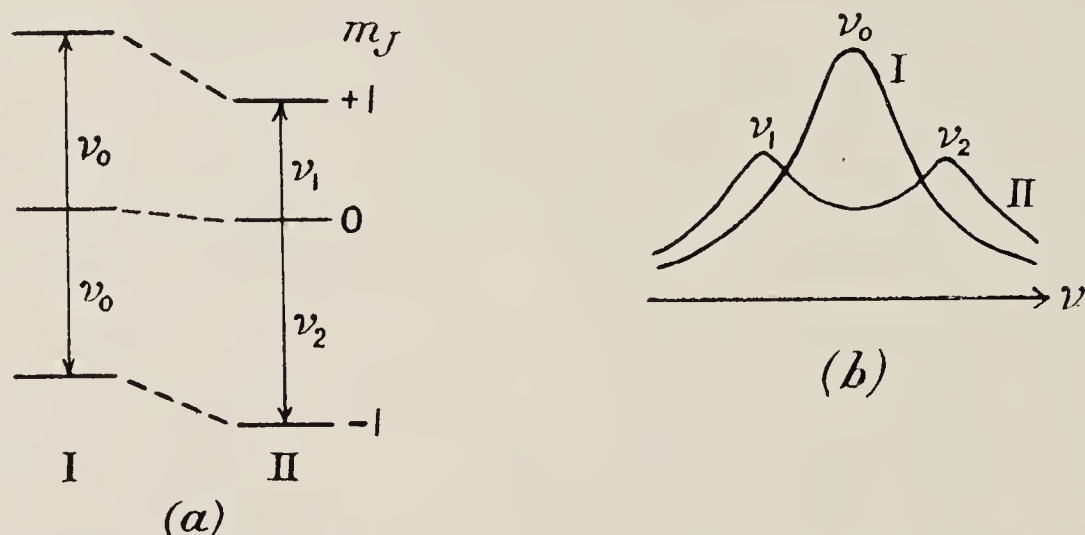


Figure 9. Combined Zeeman and Stark effects in the level  $3P_1$ : (a) energy levels; (b) resonance curves, (I) magnetic field, (II) magnetic and electric fields.

obtained for the line widths as 'coherence times' rather than as atomic lifetimes, and relate the longer 'coherence times' to multiple scattering of photons which takes place when the vapour pressure is increased. The phenomenon is discussed in § 3.4.2. Guiochon *et al.* support their interpretation of line narrowing by numerous measurements of coherence times as a function of vapour pressure in specimens of mercury of different isotopic composition: an increase in the number of atoms of a different sort will not lead to increased scattering. Measurements of 'lifetimes' by the classical methods of depolarization of resonance radiation in magnetic fields lead to 'coherence times' in agreement with the values obtained from double resonance experiments (Barrat 1957). The true lifetime of the level  $6^3P_1$  of mercury they find to be  $1.18 \times 10^{-7}$  sec.

The level  $7^3S_1$  of mercury has been studied by Brossel and Julienne (1956). It is possible to excite this level stepwise by the illumination of mercury vapour with radiation  $2537\text{\AA}$  and  $4358\text{\AA}$  simultaneously, but the yield of doubly excited atoms is rather poor. Far greater yields are obtained by making use of the metastability of the level  $6^3P_0$ , to which atoms in the  $6^3P_1$  level are transferred by collision with molecular nitrogen. Excitation to  $7^3S_1$  is achieved by illumination with radiation  $4046\text{\AA}$  rather than  $4358\text{\AA}$ .

Brossel and Julienne therefore added nitrogen at a pressure of several millimetres of mercury to the absorption vessel containing mercury vapour. The exciting radiations, wavelengths  $2537\text{\AA}$  and  $4046\text{\AA}$  from a mercury lamp, were unpolarized, but directed along the applied magnetic field, corresponding therefore to  $\sigma$  excitation. Radio-frequency resonance was detected by changes in the



intensity of the  $\sigma$  and  $\pi$  components of the emitted radiation  $4358\text{\AA}$ . Resonance peaks at about 53 gauss were observed at a frequency of 148 Mc/s.

Two points are of particular interest in this work: One is the successful application of a radio-frequency magnetic field of high intensity and high frequency (about 4 gauss at 150 Mc/s) to a gas at several millimetres pressure without the stimulation of an ordinary discharge. This was accomplished by arranging that the radio-frequency magnetic field in the resonance vessel was uniform, and almost entirely free of the electric field. These conditions were established at the short-circuited end of a tuned Lecher wire system formed from flat metal strip. The

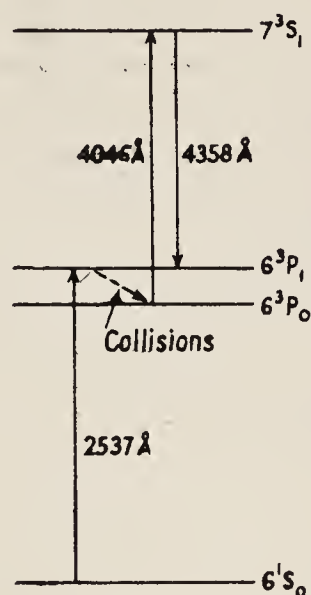


Figure 10. Stepwise excitation from the metastable level in mercury.

second point of interest is that the  $7^3S_1$  states were able to survive in the presence of the nitrogen. The line width of the resonance curves published by Brossel and Julienne is about 20 gauss, corresponding to a time of about  $3 \times 10^{-9}$  sec, which gives the order of magnitude of the lifetime. Attempts are now being made to investigate how the pressure of nitrogen affects the line width.

Kastler, Brossel and their pupils have applied double resonance techniques in the process known as 'optical pumping' to sodium in particular, and have studied in great detail the phenomena of multiple quantum transitions discussed in § 3.3.2 of this report. Since these experiments are concerned with the ground states they will not be described here. They form part of the subject matter of Kastler's Holweck Lecture (1954) and of a number of papers given at the Magnetic Resonance Conference in Paris in 1958 (Kastler 1958) where further references may be found.

Bogle, Dodd and Maclean (1957) have studied the level  $6^3P_1$  of mercury with a view to determining the hyperfine structure coupling constants of the odd isotopes. The levels  $F = \frac{3}{2}$ ,  $F = \frac{1}{2}$  are separated in zero field by about 20 000 Mc/s. In a magnetic field of 2–3 kilogauss the Zeeman components are separated by intervals of about 4000 Mc/s, but these are no longer equal (figure 11), since the electron–nuclear coupling is beginning to break down. From the differences, the hyperfine structure coupling constant can be deduced.

The method of illumination and detection resembled that of Brossel's work, but whereas Brossel and his colleagues used frequencies in the range of conventional high-frequency oscillators, Bogle *et al.* worked at 4250 Mc/s with klystron

and waveguide techniques. A resonance cavity of size appropriate to the wavelength, about 7 cm, allowed the insertion of a fused quartz resonance cell of reasonable dimensions.

Of the two microwave resonances observed, one was interpreted as the single resonance expected from the even isotopes (this occurred at the  $g_J$ -value measured by Brossel and Bitter) and the other as one of the four resonances expected from the isotope 199. The hyperfine structure  $A$ -factor was determined with a precision to about 2%, and agrees with optical determinations of higher precision. As the authors point out, greater accuracy could be obtained by working at higher fields where the Back-Goudsmit effect is more pronounced.

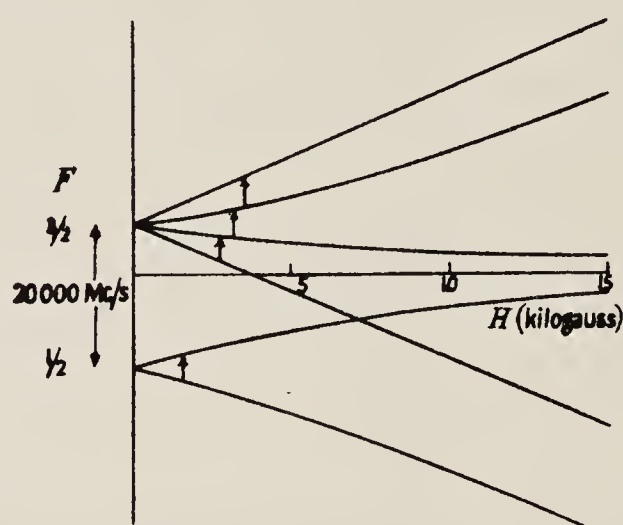


Figure 11. Zeeman effect in the hyperfine structure of the level  $^3P_1$  of  $^{199}\text{Hg}$  ( $I = \frac{1}{2}$ ).

#### 4.4.3. Excited states in potassium and sodium: non-zero fields.

Ritter and Series (1957) observed resonances in the second excited P levels of potassium,  $5P_{3/2}$  and  $5P_{1/2}$ . The experimental features are more conveniently deferred to the next section on resonances in zero field. Here we wish to describe the work in non-zero fields.

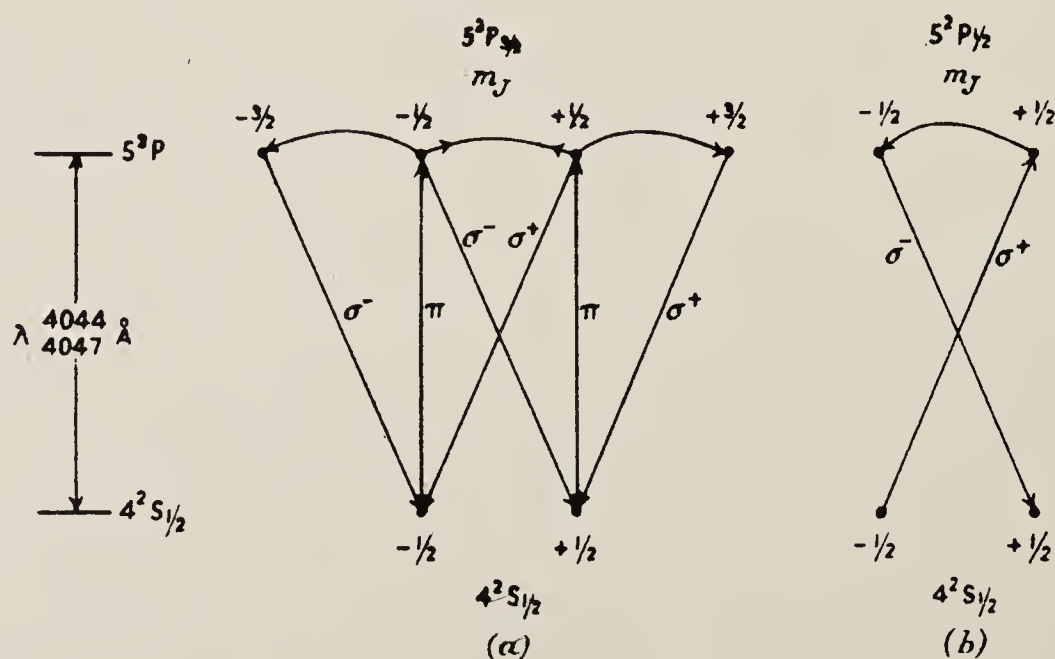


Figure 12. Double resonance in the term  $5^2P$  of potassium: (a)  $5^2P_{3/2}$ : excitation by  $\pi$ , detection by  $\sigma$  radiation; (b)  $5^2P_{1/2}$ : excitation by  $\sigma^+$ , detection by  $\sigma^-$  radiation. For (c), (d), (e) see overleaf.



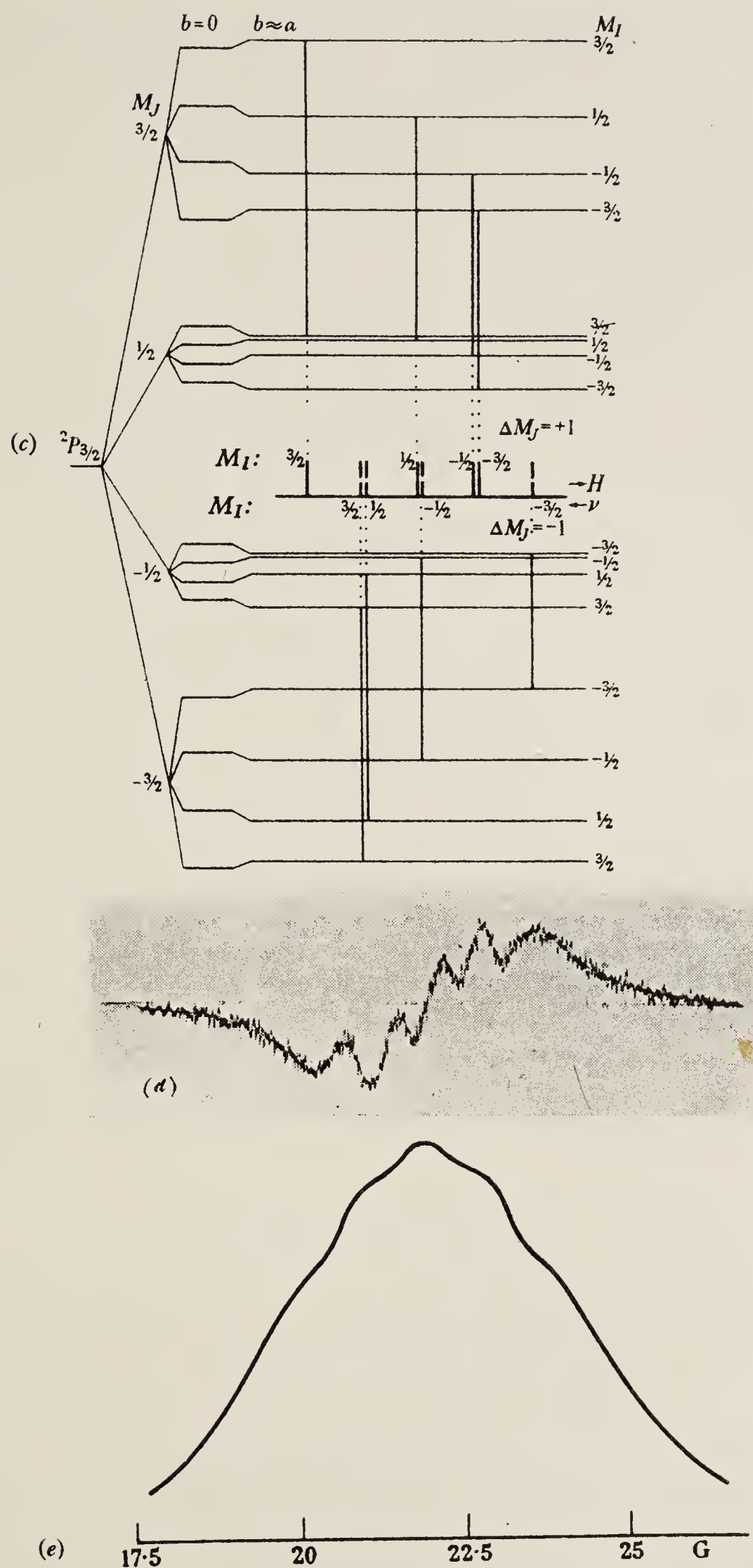


Figure 12 (contd.). Double resonance in the term  $5^2P$  of potassium: (c) hyperfine structure of  $^2P_{3/2}$  in a 'strong' magnetic field; (d) experimental curve showing hyperfine structure in  $5^2P_{3/2}$ ; the phase-sensitive method of detection displays a differentiated resonance curve; (e) the experimental curve integrated.

The magnitude of the hyperfine structure in these levels is exceptionally small, so that in magnetic fields of 25 gauss the electron–nuclear interaction in the  $P_{3/2}$  level is almost entirely broken down. At these fields, under excitation by  $\pi$  light, magnetic resonance curves were obtained in  $\sigma^+$  and  $\sigma^-$  light, combined and separately. The curves show hyperfine structure from which the interaction constants and nuclear moments were deduced.

These resonances in the  $P_{3/2}$  level were observed also at weaker magnetic fields where the  $I$ – $J$  interaction was only partially broken down. It was possible to plot the position of two components over the whole range of magnetic fields from strong to zero. Comparison of the results with the stationary-state theory of the excited level (§ 2.1) showed good, but not perfect agreement. Particularly noticeable was that the degree of decoupling of  $I$  and  $J$  was affected by the strength of the radio-frequency field. This effect could possibly find an explanation in the terms proposed in the last paragraph but one of the introductory § 3.4.

The  $P_{1/2}$  level was studied by means of  $\sigma^+$  light in excitation,  $\sigma^-$  in decay. (When  $J$  does not change between the ground and excited levels,  $\pi$  light and undifferentiated  $\sigma$  light are ineffective in double resonance experiments.) Discrimination by Nicol prism and quarter-wave plate between the two senses of rotation requires a non-vanishing component of magnetic field along the light paths. Resonances in the  $P_{1/2}$  level were detected by Ritter and Series in experiments which were regarded as exploratory.

The experimental values of the hyperfine coupling constants refer to the more abundant isotope,  $^{39}\text{K}$ . The values of  $a_{3/2}$  and  $b_{3/2}$  agreed with those derived from zero field measurements. Values of the nuclear magnetic moment calculated from  $a_{3/2}$  and  $a_{1/2}$  agreed with more precise nuclear resonance measurements. The nuclear electric quadrupole moment was calculated from  $b_{3/2}$  (§ 2.2).

Dodd (private communication) has measured hyperfine structure in the level  $3^2P_{3/2}$  in sodium in magnetic fields about 2300 gauss, at a frequency about 4250 Mc/s. The apparatus was similar to that used in the study of the level  $6^3P_1$  in mercury (§ 4.4.2). The values of the coupling constants are substantially in agreement with those obtained by Sagalyn (1954) and by Perl, Rabi and Senitzky (1955) in zero magnetic fields, but  $b$  is determined unequivocally. Details of the work will be published shortly.

#### 4.5. Double Resonance in Zero Magnetic Field

##### 4.5.1. General principles.

The application of the method to cases of zero magnetic field needs a little further discussion, for here the Zeeman components of a particular level are not separated in energy. Estimates of relative intensity based on the simple approach of § 4.3 are no longer reliable. This is generally not a serious matter if one is interested primarily in the frequency intervals between hyperfine components. Magnetic dipole radio-frequency resonances still take place according to the selection rules

$$\Delta F = 0, \pm 1; \Delta m_F = 0, \pm 1,$$

and are detectable by the techniques we have described.

Since there will always be other levels in the vicinity of the particular pair one is investigating, estimates should be made according to the principles of § 3.3.2



of shifts in the resonance frequency. These will usually be a small fraction of the line width provided the latter is small compared with the resonant frequency. When this condition is not satisfied it will frequently be found that the approximations required by the perturbation treatment are not valid. More theoretical work is required before the fullest information can be obtained from these double resonance measurements. In the meantime, the deduced interaction constants are usually quoted with rather less precision than would be possible if one had a better understanding of the resonance process.

The effect of small stray fields needs to be considered in zero-field experiments. This we now examine.

In a field which is strictly zero the axis of quantization for energy eigenstates is determined with reference to the polarization of the light beam: plane polarized light is termed  $\pi$  if the axis is parallel to the electric vector,  $\sigma$  if perpendicular; for circularly polarized light the axis is in the direction of propagation of the light. This terminology is consistent with the selection rules  $\Delta m = 0, \pm 1$  for  $\pi$  and  $\sigma$  radiation, respectively. Let the states be labelled  $(F, m_F)$  with respect to the axis  $z$  so determined.

If a field is now established in a direction  $z'$  different from  $z$ , the states  $(F, m_F)$  are no longer energy eigenstates. The useful representation for the purpose of measuring energy intervals is  $(F', m'_F)$  with reference to  $z'$ , and in this representation each state is a mixture of the states  $(F, m_F)$ . The population distribution in  $(F', m'_F)$  is quite different from that in  $(F, m_F)$ . Consequently a double resonance experiment designed on the basis of the  $(F, m_F)$  representation may fail entirely.

The transition from the one representation to the other is not quite sudden if the states have a finite lifetime. For if the atoms decay before they have executed a significant precession in the  $z'$  field, the direction  $z'$  is to that extent imprecisely defined for the atom. We deduce, therefore, that a stray field  $H'$  can be tolerated provided that

$$g_F \beta H' < 1/\tau$$

where  $\tau$  is the lifetime of the state, i.e. the separation of the Zeeman components must not exceed the natural width of the energy levels.

For ordinary excited levels, the requirement of a sufficiently small field is not severe: a lifetime of  $5 \times 10^{-8}$  sec, for example, corresponds to a natural width of about 3 Mc/s, and (for  $g_F = 1$ ) to a magnetic field of about 2 gauss. In such a case the earth's field need not be compensated. For metastable states, on the other hand, the earth's field may be uncomfortably great. In experiments on the level  $4^3P_1$  in zinc, for example ( $\tau \simeq 3 \times 10^{-5}$  sec), Böckman, Krüger and Recknagel (1957) report that they were obliged to reduce stray fields to about 0.05 gauss.

#### 4.5.2. Experiments.

A number of authors have performed these experiments with the principal object of measuring hyperfine structures and determining nuclear electric quadrupole moments in elements where they were not known. The quadrupole interaction is only measurable in levels for which  $J > \frac{1}{2}$ : the  $P_{3/2}$  levels of the alkalis, therefore, lend themselves to such determinations. In the first excited  $P_{3/2}$  levels the ratio of natural width to hyperfine structure is less favourable than in the second, consequently more work has been done on the second excited levels. For these

levels, however, the oscillator strengths are smaller than in the first by a factor of about 100. This affects the strength of the exciting radiation in the light source and the cross section for excitation, with consequent reduction in the intensity of the fluorescent light.

The following levels have been investigated :

sodium-23 (ground level $3^2S_{1/2}$ ) :	$3^2P_{3/2}$ : Sagalyn (1954)
	$4^2P_{3/2}$ : Krüger (1958)
potassium-39 (ground level $4^2S_{1/2}$ ) :	$5^2P_{3/2}$ : Ritter and Series (1957)
rubidium-85 and 87 (ground level $5^2S_{1/2}$ ) :	$6^2P_{3/2}$ : Meyer-Berkhout (1955)
caesium-133 (ground level $6^2S_{1/2}$ ) :	$7^2P_{3/2}$ : Althoff (1955)
	$7^2P_{1/2}$ : Bucka (1958) (see § 4.6)
zinc-67 (ground level $4^1S_0$ ) :	$4^3P_1$ : Böckman, Krüger and Recknagel (1957)

The experiments are not sufficiently different to justify separate discussion. Light from the source (figure 13) is polarized and focused on to the resonance

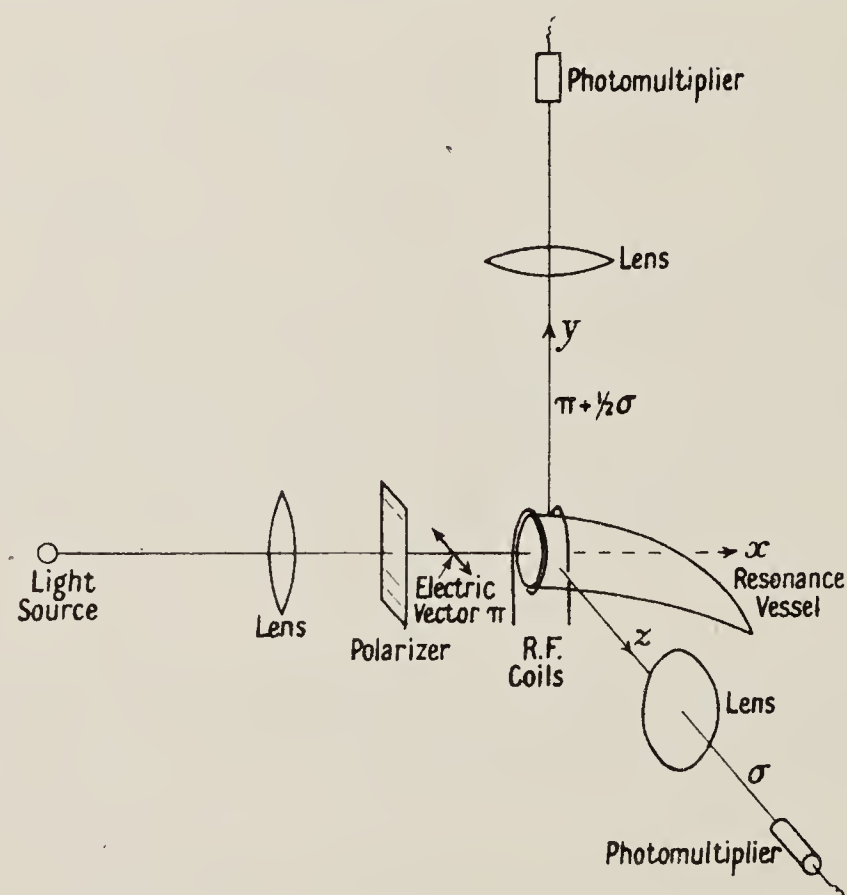


Figure 13. Double resonance in zero magnetic field.

vessel, which itself is focused on to a photomultiplier. In most cases the resonance vessel is horn-shaped for the avoidance of back-reflected light from its walls. The glass, or other material, need not be of particularly high optical quality since good image formation is not necessary. Radio-frequency currents of several amperes are usually required in the coils, and this frequently causes an objectionable gas discharge in the resonance vessel. Partly for this reason most workers have found it necessary to free their samples from foreign gas, either by getters, or by careful re-distillation before sealing in, or by the continuous pumping of a crude atomic beam. When sealed-in samples have been used, the temperature must be controlled in order to establish the necessary vapour pressure. Streams of hot air are often adequate.



Foreign gas is harmful also in its disorientation of excited states through collisions. Second excited states seem particularly sensitive to foreign gas; on the other hand polarized resonance radiation has been observed from the first excited state in sodium in the presence of foreign gases at pressures of several tenths of a millimetre of mercury (Brossel, Margerie and Kastler 1955). S states are especially stable against disorienting collisions.

With the geometrical arrangement of figure 13 the  $z$  direction is the axis of quantization. A photomultiplier in this direction receives  $\sigma$  light only. A photomultiplier in the  $y$  direction receives a mixture of  $\pi$  and  $\sigma$  light, and might be

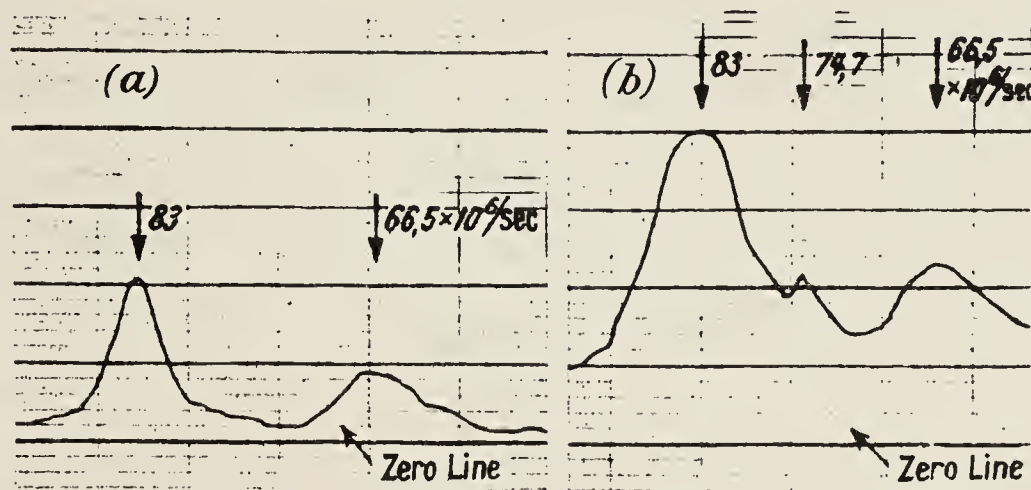


Figure 14. Resonances in the level  $7^2P_{3/2}$  of  $^{133}\text{Cs}$  (Althoff 1955): (a)  $(F=5) \rightarrow (F=4)$  (83 Mc/s) and  $(F=4) \rightarrow (F=3)$  (66.5 Mc/s); (b) double quantum jump  $(F=5) \rightarrow (F=3)$  ( $2 \times 74.7$  Mc/s).

preceded by an analyser to transmit the  $\pi$  light only. The  $y$  and  $z$  signals are sometimes opposed for elimination of spurious changes and for doubling of the effect, but it is often sufficient to use one signal only.

Whereas it is convenient when examining resonances in non-zero fields to fix the radio frequency and obtain the resonances by varying the field, it is necessary to vary the frequency in zero-field experiments. The width of the resonance curves is often an appreciable fraction of the frequency of the peak: the radio-frequency field strength must be monitored over the range.

In figure 13 the radio-frequency field, since it is in the  $x$  direction, induces transitions  $\Delta m = \pm 1$ . The  $y$  direction serves equally well for  $\Delta m = \pm 1$ . The transitions  $\Delta m = 0$  are induced when the radio-frequency field is in the  $z$  direction.

The transitions  $\Delta m_F = 0, \pm 1$  between a given pair of hyperfine levels  $F, F+1$  coincide when the magnetic field is zero or very weak. The radio-frequency spectrum normally corresponds to the intervals between the hyperfine levels  $F, F+1, F+2, \dots$ . Double quantum jumps  $\Delta F = \pm 2$  are not infrequent (figure 14): indeed, they are to be expected if the resonance line width is comparable with the frequency intervals, for then the radio-frequency perturbation is sufficiently strong to favour the double quantum transition (§ 3.3.2).

#### 4.6. Excitation by Unpolarized Light in Zero Magnetic Field

In the following method, due to Bucka (1955, 1956, 1958), double resonance experiments may be performed in zero magnetic field with unpolarized light incident isotropically, or from some limited cone.

A simple example will illustrate the principle. Consider the transition between the ground level  $J = 0$  and an excited level  $J = 1$  of a substance for which  $I = \frac{1}{2}$  (figure 15). Let the two hyperfine components be resolved in a light source: their intensities will be in the ratio 2 : 1.

Now if atoms in the ground level were excited by isotropic radiation of uniform spectral distribution, all the excited states would be equally occupied. Irradiation from the given light source, on the other hand, will over-populate by the factor 2 all the states which belong to  $F = \frac{3}{2}$  compared with those of  $F = \frac{1}{2}$ . Radio-frequency resonances between  $F = \frac{3}{2}$  and  $F = \frac{1}{2}$  will result in a re-distribution of population.

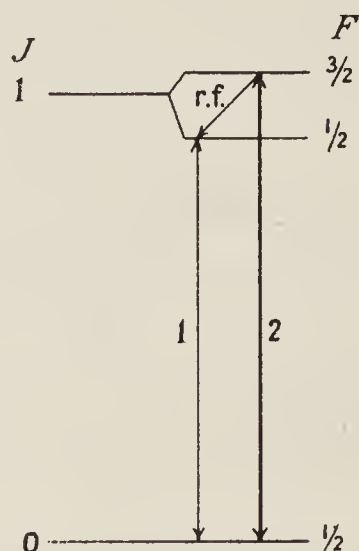


Figure 15. Transition probabilities in hyperfine structure, summed over the  $2F+1$  states of each level.

Detection of the radio-frequency resonances raises another problem, since all the hyperfine states decay with equal probability. Redistribution of population changes the relative intensity of the hyperfine components, but not the total intensity. Bucka converts the relative change into an absolute change by making use of the phenomenon of self-absorption. For the stronger component is more strongly absorbed: consequently transmission of the fluorescent light through vapour of the substance concerned will discriminate between the two components. The final result will be that at radio-frequency resonance some atoms will be transferred to the levels which give rise to the more weakly absorbed light; consequently the total amount of light which emerges from the absorbing vapour will increase.

Bucka (1958) applied the method successfully to the level  $7^2P_{1/2}$  of caesium-133. The situation is rather more complicated than in our example:  $J = \frac{1}{2}$  in the ground and the excited level, and  $I = \frac{7}{2}$ . The hyperfine interval ( $F = 3$ )–( $F = 4$ ) in the ground level is greater than the Doppler width of the optical radiation  $6^2S_{1/2}$ – $7^2P_{1/2}$  (4555Å); that in the excited level is smaller. The line 4555Å is therefore partially resolved into two hyperfine components whose intensities are in the ratio 9 : 7.

The vessel in which the preferential self-absorption was to take place was the same in which the atoms were excited. Bucka detected a radio-frequency resonance between  $F = 4$  and  $F = 3$  of the level  $7^2P_{1/2}$  at  $400.8 \pm 1$  Mc/s, with a signal to noise ratio of 2 or 3 : 1.



#### 4.7. Double Resonance Measurements of Isotope Shifts

In a mixture of isotopes of different nuclear spin, each isotope is characterized by particular values of  $\gamma_F = \omega_0/H_0$  for the various hyperfine transitions, so that by correctly choosing the magnetic field and the frequency in a double resonance experiment, a given isotope will respond independently of others of different  $\gamma_F$  when the mixture is suitably illuminated. All isotopes having  $I = 0$  ( $\gamma_F = \gamma_J$ ) will respond together. Suppose now that the light source provides radiation of infinitely narrow spectral range of variable, known, frequency. As the frequency is swept over the atomic resonance line one will observe a double resonance signal whose width will be the Doppler width for absorption of optical radiation in the resonance vessel. Let the magnetic field at the resonance vessel be changed to correspond to the  $\gamma_F$  of a different isotope, and again let the frequency of the light source be varied. Owing to the spectroscopic isotope shift, light of different frequency will be required to excite the second isotope. In this way one will obtain resonance curves for each isotope plotted on one extended frequency scale, that of the exciting radiation. The isotope shifts for the particular atomic transition may then be read off, subject to a correction for Zeeman displacements in the resonance vessel.

In an actual experiment the radiation from the light source will be Doppler-broadened, and the width of the double resonance line will be some combination of the Doppler widths of light source and resonance vessel. The double resonance method is then at a disadvantage compared with high resolution optical spectroscopy. On the other hand, the new technique is able to differentiate between isotopes in a mixture and for this reason may prove powerful in cases where the use of enriched isotopes in optical work is inconvenient or impossible.

Sagalyn, Melissinos and Bitter (1958) applied the technique to the measurement of isotope shifts in the line  $\lambda 2537\text{\AA}$  of mercury, a case in which optical measurements have not been made with enriched isotopes. A note by Melissinos (1959) has subsequently appeared, quoting measurements made on a very small sample of radioactive mercury-197. The variation in frequency of the light source was accomplished by making use of the Zeeman effect in the line  $\lambda 2537\text{\AA}$  emitted by a mercury-198 lamp. One of the  $\sigma$  components was isolated from the light emitted parallel to the magnetic field, variation of which up to 50 kilogauss provided a frequency range of  $10^5$  Mc/s ( $3\text{ cm}^{-1}$ ). The isotope shifts were thus measured as a function of this magnetic field, called the 'scanning field'.

The 'splitting field', used to select a particular isotope in the resonance vessel, was of the order of 10 kilogauss, which was sufficient to cause some departure from 'weak field' splittings. Different transitions in one and the same isotope were therefore recorded separately since only that microwave resonance is detected for which the 'splitting field' is correctly matched to the 'splitting frequency'. This microwave frequency was about 3000 Mc/s.

It is clear that the technique demands a preliminary study of the microwave resonance frequencies for each transition in each isotope. The line width in these preliminary experiments is that of ordinary double resonance experiments. The information gained allows the determination of  $g$ -factors and hyperfine structure constants. In the work of Sagalyn *et al.* this information is quoted for the

mercury isotopes 199 and 201 with a precision to about 15 Mc/s. The precision of the isotope shift measurements is to about 100 Mc/s.

#### 4.8. Detection by Coincidence of Photons in Cascade

The following experiment proposed by Bradley (1956) is not strictly double resonance, but we include it in this section because of its close relationship.

The level  $\beta$  ( $J = \frac{1}{2}$ ), we suppose, is populated from  $\alpha$  with the emission of photons  $\lambda_1$ , and itself decays to  $\gamma$  with the emission of photons  $\lambda_2$  (figure 16). Suppose we have detectors sensitive only to  $\sigma^+$  photons of wavelengths  $\lambda_1, \lambda_2$  respectively, and that we examine these detectors for coincidences. We expect only accidental coincidences unless radio-frequency transitions are taking place in the level  $\beta$ . A rise in the coincidence rate indicates radio-frequency resonance.

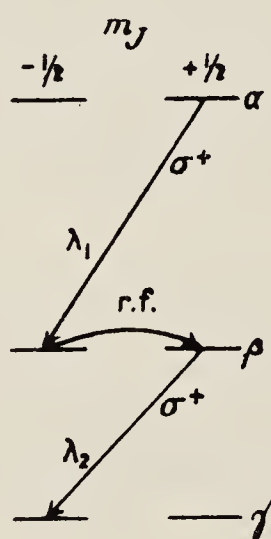


Figure 16. Photons in cascade.

Significant coincidences must occur in a time of the order of the lifetime of the level. The longer this time, the greater the possibility of accidental coincidences. Hence the signal-to-noise ratio is more favourable for levels with shorter lifetimes.

The execution of the experiment has proved to be rather difficult. No results have been published.

### § 5. EXCITATION BY ELECTRON IMPACT

As in the sections on excitation by resonance radiation, we treat the processes of excitation, radio-frequency resonance, and decay as independent processes. The two latter have already been discussed in §§ 3 and 4.3. We here briefly consider the process of excitation and the establishment of differences of population between excited states.

Let  $N_a$  be the particle density in the ground state. We suppose  $N_a$  so low that, under electron bombardment, only single encounters need be considered. Let  $\sigma_e$  be the cross section for excitation to a particular state, so that the rate of excitation is proportional to  $N_a \sigma_e$ . The equilibrium populations  $N_e$  in the excited states are determined by the equations  $N_a \sigma_e \propto N_e \gamma_e$ , where the  $\gamma_e$  are the decay constants of the excited states. Differences in the  $N_e$  clearly depend on differences in the  $\sigma_e$ , or in the  $\gamma_e$ , or in both.



We now distinguish

- (a) states between which magnetic dipole transitions are allowed, from
- (b) states between which electric dipole transitions are allowed.

The next three paragraphs and § 5.1 refer to class (a); the following paragraph and § 5.2 refer to class (b).

Members of class (a) belong to a given *term*. Under Russell–Saunders coupling they will have  $L$  and  $S$  in common, but may differ in  $J$ , or  $m_J$ , or  $F$ , or  $m_F$ . They decay at the same rate,  $\gamma_e$ . The establishment of differences in population therefore depends on differences in the  $\sigma_e$ .

It has been established in a number of cases that radiation, resulting from bombardment of atoms by a uni-directional beam of electrons whose energy is a little greater than the excitation potential of a particular term, is polarized. This implies unequal population of the states  $m_J$  or  $m_F$  which belong to that term, which is the condition required for radio-frequency resonances. Cases which are of interest to us are :

- (i) Selective excitation of the states  $m_J$  which belong to a given  $J$ .
- (ii) Selective excitation of the states  $m_F$  which belong to a given hyperfine level  $F$ , and of the different  $F$  which belong to a given  $J$ .
- (iii) Selective excitation of the levels  $J$  (groups of  $m_J$ ) of the term.

Cases (i) and (ii) are exemplified in §§ 5.1.1 and 5.1.2; case (iii) is exemplified in § 5.1.3.

The theoretical treatment of the selective excitation of different states is at the present time very inadequate. A recent, brief discussion has been given by Lamb (1957). A further contribution has been made by Baranger and Gerjuoy (1958). In an important respect (polarization at the threshold of excitation) the theoretical prediction is precisely contrary to experimental findings. Notwithstanding the theoretical uncertainty, it is helpful to know that the population disparities of different states can be quite marked (20–40%), and are functions of the energy of the electrons. That polarization should arise from a uni-directional beam of electrons whose energy is just above the threshold for excitation is not at all surprising.

Members of class (b) belong to different *terms*. Under Russell–Saunders coupling they generally differ in  $L$ . Their decay constants are different, and their cross sections for excitation are different. Both absolute and relative cross sections for excitation to different terms (generally summed over the states which belong to that term) have been measured and calculated in many cases. A comprehensive account, from the experimental point of view, has been given by Massey and Burhop (1952).

It is characteristic of class (a) that radio-frequency resonance results in a change in the polarization and spatial distribution of the decay radiation, but not in its total intensity. Resonances in class (b) result in changes in the total intensity of some particular *multiplet* (i.e. the totality of the transitions between two terms).

An estimate of the signal to noise ratio in a typical experiment can be made as follows (Lamb 1957):

The number of excitations per second to the level in question is  $(I/e)\sigma N_a l$ , where  $I/e$  is the number of electrons per second in the beam,  $\sigma$  is the cross section for excitation, and  $l$  is the length of vapour column of density  $N_a$  atoms/cm<sup>3</sup>.

This quantity will also be the number of photons emitted per second, and corresponds to the quantity  $S$  at the end of § 4.3. The primary photocurrent  $i_s$  is then  $I\sigma N_a l \phi \eta$ , where  $\phi$  represents the fraction of light collected by the photomultiplier, and  $\eta$  the efficiency of the cathode. At radio-frequency resonance,  $S$  changes by the amount  $\Delta S$ .

The fraction  $\beta = \Delta S/S$  is estimated as in § 3 on the basis of an assumed population distribution  $N_e$ . It is in principle independent of all the parameters mentioned in the last paragraph.

Equation (25) of § 4.3 now gives the signal to noise ratio.

### 5.1. Selective Excitation of different States within a given Term

#### 5.1.1. Detection by decay radiation.

Pebay-Peyroula, Brossel and Kastler have observed magnetic dipole resonances in mercury (1957) and in sodium (private communication).

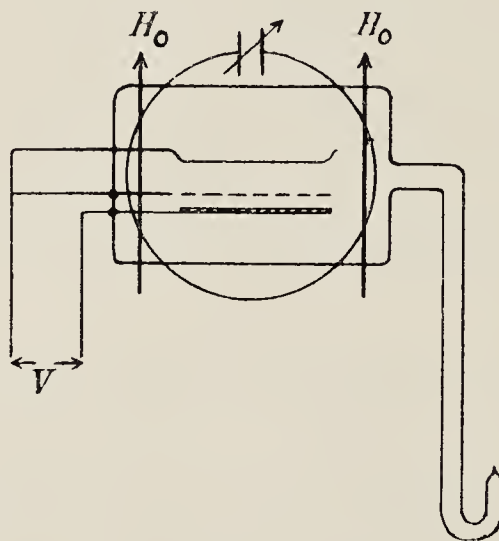


Figure 17. Excitation of mercury vapour by electron impact.

Mercury atoms at a vapour pressure determined by the temperature of the drop of mercury in the side-arm are excited in the space between the grid and plate (figure 17) by an electron beam travelling in the direction of a steady magnetic field  $H_0$ . Preferential excitation of certain states takes place, and the emitted light is polarized. Different spectrum lines are examined separately by a simple monochromator, or by filters. The excitation vessel lies within a radio-frequency coil or microwave cavity, and atomic resonances are indicated by changes in the polarization of the spectrum lines.

Experiments are usually performed at a fixed value of the frequency, and resonance curves displayed as a function of magnetic field. Interpretation of the experiments is thus a question of allocating to the atomic levels the  $g$ -values at which resonance peaks occur. This is not always a simple matter, since atomic resonances affect the polarization and intensity not only of those spectral lines which appear in primary decay, but also of those lines which appear in consequence of cascade processes. Thus, resonances in the level  $7^3P_2$  of mercury were detected in the optical radiation  $7^3S_1-6^3P_2$ ,  $7^3S_1-6^3P_1$  and  $7^3S_1-6^3P_0$ , evidently on account of the primary decay  $7^3P_2-7^3S_1$ . Experiments with isotopes of different nuclear spin, since they show resonances at different  $g_F$  values, assist in the interpretation.



An important detail of technique of the French group is that the distance between grid and plate is kept sufficiently short (about 4 mm) to prevent a complete cyclotron revolution of the electrons in the magnetic field  $H_0$ , otherwise very strong changes of intensity occur at the cyclotron resonance frequency.

Published measurements include the lifetime and  $g_J$ -values of the levels  $5^1D_2$ ,  $6^3F_4$  and  $7^3P_2$  in mercury, also the hyperfine structure of the level  $6^3F_4$  of isotopes 199 and 201.

Measurements of hyperfine structure in the levels  $3^2D$ ,  $4^2D$  and  $5^2D$  of sodium are being made.

### 5.1.2. Detection by absorption of optical radiation.

Dehmelt (1956) observed resonances between the states  $m_J = 0, \pm 1, \pm 2$  of the level  $6^3P_2$  in mercury. This level is metastable, and the experiment, strictly speaking, falls outside the scope of this review. We include it, nevertheless, on account of its similarity to the other work we have described.

Excitation in mercury vapour at room temperature ( $\simeq 1\mu$  vapour pressure) was by an electron current of 200 mA from a plane cathode. The states  $m_J = 0, \pm 1$  were excited in preference to  $\pm 2$ . The magnetic field, about 8.3 gauss, separated the energy levels by equal intervals of about 17.2 Mc/s.

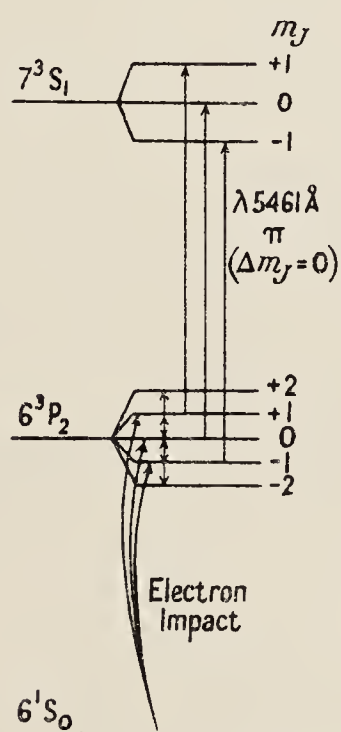


Figure 18. Detection of radio-frequency resonances in the level  $6^3P_2$  by their effect on the absorption of  $\lambda 5461\text{\AA}$ .

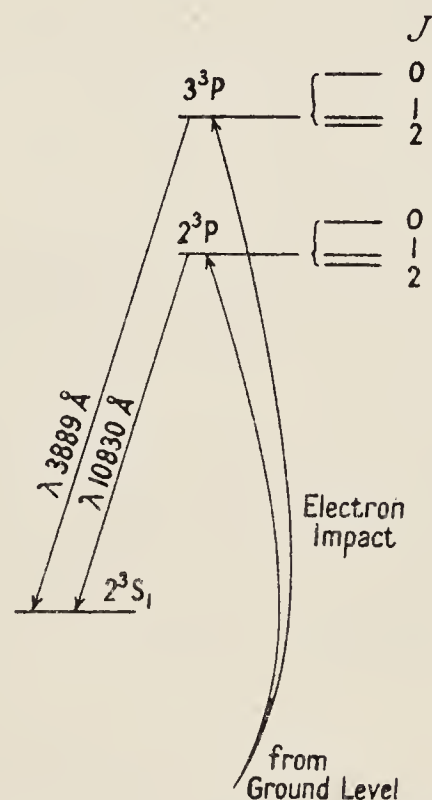


Figure 19. Excitation and decay of  $^3P$  levels in helium.

Particular interest attaches to the method of detection of radio-frequency resonances, which was by absorption of the polarized optical radiation  $\lambda 5461\text{\AA}$ . Under the optical selection rule  $\Delta m_J = 0$ , the consequence of radio-frequency resonances which depletes the states  $0, \pm 1$  in favour of  $\pm 2$  is a reduction in the amount of light absorbed. Since the level is metastable, only small radio-frequency fields are needed. Dehmelt shows a resonance about 0.1 gauss wide obtained under a radio-frequency field of about 12 milligauss.

Dehmelt's absorption technique, together with the 'magnetic scanning' technique of Sagalyn *et al.* (1958, § 3.7) is being applied by Bradley (private communication) to the study of resonances in the level  $^3P_2$  of  $^{198}\text{Hg}$ ,  $^{200}\text{Hg}$ ,  $^{202}\text{Hg}$ ,  $^{199}\text{Hg}$  and  $^{201}\text{Hg}$ ; in the case of the odd isotopes the hyperfine structure is seen. Natural mercury is used in the excitation vessel: the selected isotope is excited by adjusting the magnetic field at the  $^{198}\text{Hg}$  light source to provide a Zeeman component of the correct optical frequency.

### 5.1.3. *Excited states of helium.*

The multiplet intervals  $2^3P_2-2^3P_1$ ,  $3^3P_1-3^3P_0$  and  $3^3P_2-3^3P_1$  in helium were measured by Lamb and Maiman (1957) and Wieder and Lamb (1957) by the techniques we have outlined.

At a pressure of up to 20 microns, helium in sealed-off tubes was excited by electron currents up to  $500\mu\text{A}$ . In decay to the metastable level  $2^3S_1$  the levels  $3^3P$  and  $2^3P$  emit radiation of wavelength 3889 and 10 830Å respectively. These radiations were used to detect magnetic dipole microwave resonances in the regions of 980 Mc/s and 7000 Mc/s, and 1600 Mc/s respectively. These frequencies are not themselves the triplet intervals, but measurement of the magnetic fields at which resonances take place allows deduction of the zero-field intervals.

The excitation region of the helium tube was inserted into a resonant cavity at a place where the radio-frequency magnetic field was strong. While the cavities were designed to observe primarily either  $\pi$  or  $\sigma$  radio-frequency transitions ( $H_{\text{rf}}$  parallel or perpendicular to  $H_0$ , respectively), there were usually sufficient amounts of perpendicular components of  $H_{\text{rf}}$  for the observation of both types of transition in a given apparatus.

Detection of the  $2^3P$  resonances through changes in the intensity in a particular direction of  $\lambda 10\,830\text{\AA}$  could only be accomplished by very careful elimination of stray light from the infra-red-sensitive photomultiplier. The use of a time constant of 150 seconds in the detection system indicates the weakness of the signal and the need for careful control of all the variables of the experiment.

We have indicated that the object of this work was the accurate measurement of intervals in spectra sufficiently simple to be amenable to calculation. The resonant frequencies were determined to a precision better than 1 Mc/s. Lamb (1957) discusses the theoretical problem.

## 5.2. *Selective Excitation of Different Terms*

We here discuss three different experiments: that of Novick, Lipworth and Yergin (1955), also Lipworth and Novick (1957) which followed the exploratory experiment by Lamb and Skinner (1950) on  $n = 2$  in singly ionized helium; that of Lamb and Sanders (1956) on  $n = 3$  in hydrogen; and that of Series and Fox (1958) on  $n = 4$  in singly ionized helium. The object of each of these experiments is the measurement of Lamb shifts, that is, the relative positions of the S and P levels for a given value of the principal quantum number  $n$  in a one-electron spectrum. The experiments have in common the detection of radio-frequency electric dipole transitions by 'optical' means, and the excitation of the various levels by electron impact. In each experiment differences exist in the cross section for excitation to the pair of levels concerned: more significantly, the decay



constants of the levels are different, so that the equilibrium concentrations in the excited states are different. The first two experiments use controlled excitation by a beam of electrons, and the third, a gas discharge.

### 5.2.1. Singly ionized helium : $n = 2$ .

The method of detection of the radio-frequency transitions  $2^2S_{1/2}-2^2P_{1/2}$  in this experiment is based on the entirely different probabilities for decay from these excited levels.  $2^2S_{1/2}$  is metastable: its decay to the ground state of the ion,  $1^2S_{1/2}$ , is forbidden for electric dipole radiation.  $2^2P_{1/2}$ , on the other hand, decays very rapidly with the emission of radiation at  $304\text{\AA}$  (41 ev). This is detected by photoelectric emission at the platinum cathode of an Allen-type electron multiplier. An increase in the current signifies radio-frequency resonance.

The radio-frequency transition is induced in a resonant microwave cavity in which the ions have been excited from helium atoms in their ground state. The signal radiation is accompanied by a large and variable background which arises from shortlived states of the ion. This difficulty was met by Novick, Lipworth and Yergin (1955) by a pulse technique, wherein observation of the radio-frequency signal was delayed by a quarter of a microsecond after application of a pulse of exciting electrons. Lipworth and Novick (1957) used an improved method of phase detection in which, using radio-frequency amplitude modulation, they observe on two different channels the signals 'r.f. on' and 'r.f. off'. By difference and normalization they eliminate the effect of the background, and further, by observing at two different levels of radio-frequency power, they can compensate for changes in the efficiency of the detector.

A very thorough study of the line shape and the effects of possible perturbations allows these authors to quote for the measured interval the value  $14\,040.2 \pm 4.5$  Mc/s. The natural width of the observed resonance is about 1600 Mc/s.

### 5.2.2. Hydrogen : $n = 3$ .

The level  $3^2S_{1/2}$  decays more slowly than  $3^2P_{1/2}$  or  $3^2P_{3/2}$ , and is populated more densely under electron excitation from the ground state of (molecular) hydrogen,

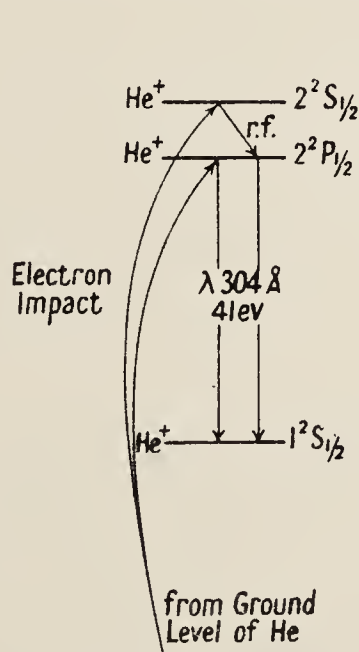


Figure 20. Excitation and decay of  $2^2S_{1/2}$  and  $2^2P_{1/2}$  in ionized helium.

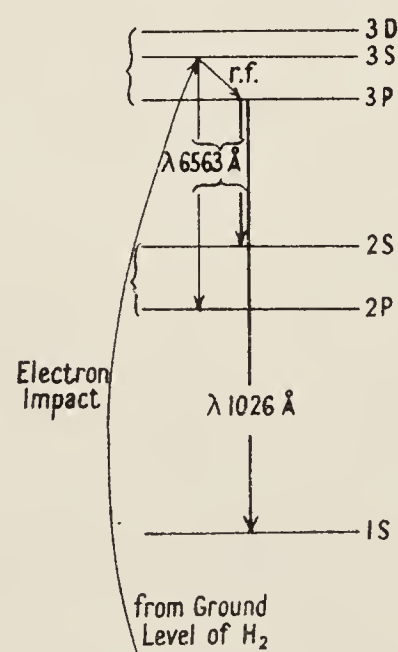


Figure 21. Excitation of 3S in atomic hydrogen, and its decay by different routes.

so that there exists the possibility of observing radio-frequency resonances between it and either of the  $^2P$  levels. For our present argument, the direction of spin is immaterial; we will refer to the S and P terms.

Both 3S and 3P radiate components of the line  $H_\alpha$ ,  $\lambda 6563\text{\AA}$ , in their decay to 2P and 3S respectively, but 3P can decay also to 1S, radiating the Lyman  $\beta$  line,  $\lambda 1026\text{\AA}$ . Transfer of atoms from 3S to 3P therefore changes the total intensity of the  $H_\alpha$  complex, and this change is used to indicate radio-frequency resonance.

Lamb and Sanders (1956) used an interference filter to isolate  $H_\alpha$  from the light emitted on bombardment by electrons of hydrogen at a pressure of about one micron. The glass envelope was situated inside a parallel plate transmission line for application of radio-frequency fields at about 3000 and 500 Mc/s. Resonances were displayed as a function of magnetic field.

A more detailed account of this experiment is in course of preparation (see Lamb and Wilcox 1958).

### 5.2.3. Singly ionized helium : $n = 4$ .

The method of detection in this experiment is similar to that described above, but the ions are excited in a gas discharge rather than by controlled electron bombardment. Normal conditions in a gas discharge are such that there exists statistical equilibrium between the electrons and a set of close-lying energy levels: equality of population obtains between the atomic states. In consequence, the relative intensities of the spectral lines which derive from these states are in the ratio of the transition probabilities for spontaneous decay. In optical investigation of the components of the He II line  $\lambda 4686\text{\AA}$ , ( $n = 4 \rightarrow n = 3$ ), Series (1954) and Herzberg (1956) noticed intensity anomalies which they ascribed to over-population of the level  $4^2S_{1/2}$ . Herzberg further found that the anomaly depended on the pressure of helium, and on the discharge current, and interpreted the effect in terms of the relative magnitudes of the lifetimes of the levels and the mean time between collisions with electrons. Lifetimes in excited states of ionized helium are abnormally short. If the atoms decay before they collide, statistical equilibrium will not be established.

If we accept the over-population of the level  $4^2S_{1/2}$  as a fact, we are in a position to detect radio-frequency transitions to either of the 4P levels by observation of changes in intensity of the radiation  $4686\text{\AA}$ . The term diagram is essentially that of figure 21, with appropriate changes of the principal quantum numbers and of the intervals. Series and Fox (1958) are exploring the possibilities of this experiment. A monochromator is used to separate  $\lambda 4686\text{\AA}$  from the very strong radiations in the helium spectrum which accompany it, and a further interferometric resolution which will allow the partial isolation of those components affected by the radio-frequency resonance is also being attempted.

The ions in a gas discharge are clearly subject to stronger electric fields, and are therefore more likely to be perturbed than would be the case under controlled electron bombardment at low density. It is doubtful, however, whether the latter method of excitation would give sufficient intensity.

## § 6. ATOMIC BEAM EXPERIMENTS

In a common form of apparatus for detecting magnetic resonances in atomic beams (see, for example, Ramsey 1956), atoms in the ground states are sorted



according to their magnetic moments and therefore their  $m_J$  values in strong fields. Those atoms are detected whose  $m_J$  value changes in the experimental region, which is generally termed 'the  $C$  field'.

Changes in  $m_J$  may be brought about through the excitation of atoms by optical resonance radiation, and their subsequent decay. The time for this process is short compared with the time of flight of atoms through the  $C$  field, so that changes at the detector occur merely by illuminating the beam in the  $C$  field.

If, further, radio-frequency fields cause the excited atoms to undergo transitions, there will result further changes in the ground states, and further changes at the detector. This is the basis of the radio-frequency spectroscopy of excited atoms by atomic beam techniques.

Excited state resonances, compared with those obtained from beams of atoms in ground states, are much broader and much weaker. The breadth is of course due to the small lifetime of the excited states, which, in a typical case is about 1000 times shorter than the time of flight of an atom through the  $C$  field. The relative weakness is a consequence not only of the smaller number of excited atoms, but also of the complicated route through which changes of  $m_J$  take place.

As in experiments on ground states, the  $C$  field need not be sufficiently strong to make  $m_J$  a good quantum number. The  $m_J$  value of a state  $(F, m_F)$  for the purposes of atomic beam experiments is that of the pure state  $(m_J, m_I)$  to which  $(F, m_F)$  tends as the field is increased adiabatically. Resonances between ground states cannot normally be detected unless this value of  $m_J$  changes in the  $C$  field. In contrast, a change in  $m_J$  is not a necessary condition for the detection of resonances between excited states. For, as we have remarked, a change in  $m_J$  in the ground states may accompany the process of optical excitation and decay. Such changes may still occur when a radio-frequency transition is induced between excited states which do not differ in  $m_J$ . Radio-frequency transitions between excited states whose values of  $m_J$  are the same or different will generally result in a redistribution of the decaying atoms between the different ground states, and hence in changes in the signal.

Rabi and his colleagues have by these means measured hyperfine structures in the levels  $3^2P_{3/2}$  and  $2^2P_{1/2}$  of  $^{23}\text{Na}$  (Perl, Rabi and Senitzky 1955), in  $5^2P_{3/2}$  and  $2^2P_{1/2}$  of  $^{85}\text{Rb}$  and in  $5^2P_{3/2}$  of  $^{87}\text{Rb}$  (Senitzky and Rabi 1956), and in  $4^2P_{3/2}$  and  $2^2P_{1/2}$  of  $^{39}\text{K}$  (Buck and Rabi 1957), and from their measurements have deduced the nuclear electric quadrupole moments.

The first paper of this series describes the method in detail. The experiments differ in details of technique rather than of principle, and we shall not discuss them separately.

Generally, the steady magnetic field in the  $C$  region was so small that the Zeeman components belonging to a given hyperfine level  $F$  were closer than the natural width of the levels. Transitions  $\Delta F = \pm 1$  were observed: the Zeeman components were quite unresolved. In each case the resonance curves were fitted to a formula of the Lorentz type, and the positions of the peaks used to determine the hyperfine structure interaction constants.

It is most valuable to have measurements on the hyperfine structures of the alkali metals by the quite independent techniques of atomic beam and double

resonance. The measurements up to the present time are largely complementary in that the atomic beam work has been restricted to the first excited states while double resonance measurements have been made mainly on second excited states (§ 4.5.2). There is no reason why double resonance measurements should not also be made on first excited states; this has been done for sodium: the reason for the choice of second excited states is that the hyperfine structures, though smaller, are larger in relation to line width. On the other hand, resonance radiation from the second, is very much weaker than from the first excited states so that the signals are weaker. Nevertheless, the signal to noise ratio in these double resonance experiments is quite as good as that in the atomic beam experiments on first excited states. The scope of the atomic beam work could conceivably be extended by electron bombardment of the beam in the  $C$  field, if that were technically feasible.

### § 7. TABLE OF MEASUREMENTS

The following measurements have been made by means of the techniques described in the preceding sections:

#### (a) $g_J$ -values and lifetimes.

Element	Level	$g_J$	( $\times 10^7$ sec)	Reference
Hg	6s6p $^3P_1$	$1.4838 \pm 0.0004$	$1.18(\pm 0.01)$	} Brossel & Bitter (1952) Boutron <i>et al.</i> (1957)
Hg	6s7s $^3S_1$	( $\simeq 1.9$ )	—	
Hg	6s6f $^3F_4$	$1.2477 \pm 0.0004$	$4.50 \pm 0.12$	} Brossel & Julienne (1956)
Hg	6s7p $^3P_2$	$1.4402 \pm 0.0007$	$2.10 \pm 0.07$	
Hg	5d <sup>9</sup> 6s <sup>2</sup> 6p $^1D_2$	$1.1203 \pm 0.0003$	$16.0 \pm 0.16$	
Na	4p $^2P_{3/2}$	—	0.9†	} Krüger & Scheffler (1958)
	3p $^2P_{3/2}$	$1.3341(\pm 0.0005)$	$\simeq 0.15$	
K	5p $^2P_{3/2}$	$1.34 \pm 0.02$	$\geq 1.5$	} Dodd (private communication)
Rb	6p $^2P_{3/2}$	—	1.0	
Cs	7p $^2P_{3/2}$	—	$\geq 1.6$	Ritter & Series (1956) Meyer-Berkhout (1955) Althoff (1955)

† The value  $7.9 \times 10^{-7}$  sec quoted in the reference is clearly a misprint.

#### (b) Hyperfine structure coupling constants.

(Values in brackets are either given with reserve, or have been estimated from the authors' measurements.)

Element (Isotope)	I	Level	Coupling constants (Mc/s)	$Q(\times 10^{24})$ cm <sup>2</sup>	Reference
<sup>23</sup> Na	3/2	3p $^2P$	$a_{3/2} : 19.5 \pm 0.6$ $b : 2.4 \pm 1.4$	$0.1 \pm 0.06$	} Sagalyn (1954)
		3p $^2P$	$a_{3/2} : 19.06 \pm 0.36$ $b : (2.58 \pm 0.3)$ $a_{1/2} : 94.45 \pm 0.5$	$(0.100 \pm 0.011)$	
			$a_{3/2} : 19.0(\pm 0.5)$ $b : 2.3(\pm 0.3)$		} Perl, Rabi & Senitzky (1955)
		4p $^2P$	(awaiting publication)	$0.13 \pm 0.04$	} Dodd, J. N. (private communication)
		3, 4, 5d $^2D$	(awaiting publication)		
					Krüger & Scheffler (1958) Pebay <i>et al.</i> (1957)



Element (Isotope)	I	Level	Coupling constants (Mc/s)	$Q(\times 10^{24}) \text{ cm}^2$	Reference
$^{39}\text{K}$	3/2	4p $^2\text{P}$	$a_{1/2}$ : (estimated) $b$ : $2.8 \pm 0.8$ $a_{1/2}$ : $28.85 \pm 0.3$	$0.11 \pm 0.02$	} Buck & Rabi (1957)
		5p $^2\text{P}$	$a_{1/2}$ : $1.97 \pm 0.1$ $b$ : $1.7 \pm 0.3$ $a_{1/2}$ : $(9.3 \pm 0.5)$		
$^{85}\text{Rb}$	5/2	5p $^2\text{P}$	$a_{1/2}$ : $25.3 \pm 0.2$ $b$ : $24.4 \pm 1.3$ $a_{1/2}$ : $120.7 \pm 1.0$	$0.27 \pm 0.02$	} Senitzky & Rabi (1956)
		6p $^2\text{P}$	$a_{1/2}$ : $8.16 \pm 0.06$ $b$ : $8.40 \pm 0.4$		
$^{87}\text{Rb}$	3/2	5p $^2\text{P}$	$a_{1/2}$ : $85.8 \pm 0.7$ $b$ : $11.8 \pm 0.6$ $a_{1/2}$ : $409 \pm 4$	$0.13 \pm 0.01$	} Senitzky & Rabi (1956)
		6p $^2\text{P}$	$a_{1/2}$ : $27.63 \pm 0.1$ $b$ : $4.06 \pm 0.2$		
$^{133}\text{Cs}$	7/2	7p $^2\text{P}$	$a_{1/2}$ : $16.60 \pm 0.01$ $b$ : $-0.11 \pm 0.08$ $a_{1/2}$ : $100.2 \pm 0.25$	$-0.003 \pm 0.002$	} Althoff (1955) Bucka (1958)
$^{67}\text{Zn}$	5/2	4s4p $^3\text{P}_1$	A : $632.3 \pm 0.15$ B : $-19.4 \pm 0.15$	$+0.18 \pm 0.02$	} Böckman <i>et al.</i> (1957)
$^{199}\text{Hg}$	1/2	6s6p $^3\text{P}_1$	A : $14910 \pm 420$ $14733.5 \pm 15$		} Bogle <i>et al.</i> (1957) Sagalyn <i>et al.</i> (1958)
		6s6f $^3\text{F}_4$	A : $1255 \pm 20$		
$^{201}\text{Hg}$	3/2	6s6p $^3\text{P}_1$	A : $-5437 \pm 15$ B : $-35.4 \pm 2.4$	$(0.58 \pm 0.18)$	} Sagalyn <i>et al.</i> (1958)
		6s6f $^3\text{F}_4$	A : $(520 \pm 25)$ B : $(\approx 0)$		
$^{197}\text{Hg}$	1/2	6s6p $^3\text{P}_1$	A : $15934 \pm 30$		} Pebay <i>et al.</i> (1957) Melissinos (1959)

(c) *Isotope shifts, relative to the isotope 198, in the line 2537Å. ( $6s^2^1\text{S}_0 - 6s\ 6p\ ^3\text{P}_1$ ) of mercury (Sagalyn *et al.* 1958, Melissinos 1959).*

Isotope	204	202	200	198	201	201	199	197
$\dagger F$ (level $^3\text{P}_1$ ) (odd isotopes)					5/2	3/2	3/2	
Shift (Mc/s)	-15560	-10160	-4680	0	-14720	-660	+6900	+2730

The precision of measurement is to  $\pm 100$  Mc/s.

$\dagger$  It is not necessary to specify the  $F$  value of the level  $^1\text{S}_0$  since the hyperfine structure intervals are zero when  $J = 0$ .

(d) *Multiplet intervals in one- and two-electron spectra.*

Spectrum	Transition	Interval (Mc/s)	Reference
H	$3(^2\text{P}_{1/2} - ^2\text{S}_{1/2})$	$315 \pm 1$	Lamb & Sanders (1956)
He <sup>+</sup>	$2(^2\text{P}_{1/2} - ^2\text{S}_{1/2})$	$14040.2 \pm 4.5$	Lipworth & Novick (1957)
He	$1s\ 2p(^3\text{P}_2 - ^3\text{P}_1)$	$2291.72 \pm 0.36$	Wieder & Lamb (1957)
He	$1s\ 3p(^3\text{P}_2 - ^3\text{P}_1)$	$658.55 \pm 0.15$	Wieder & Lamb (1957)
He	$1s\ 3p(^3\text{P}_1 - ^3\text{P}_0)$	$8113.78 \pm 0.22$	Wieder & Lamb (1957)

(e) *Stark effect of the level  $6^3\text{P}_1$  in mercury. (Blamont and Brossel 1956, Blamont 1957.)*

For electric fields  $X$  between 10 and 70 kv cm<sup>-1</sup> the difference  $\Delta E$  between the displacements of the energy levels  $m_J = 0$  and  $m_J = \pm 1$  is given by  $\Delta E = (21.3 \pm 0.5 \text{ Mc/s})X^2$  where  $X$  is measured in units of 10<sup>5</sup> v cm<sup>-1</sup>.

## ACKNOWLEDGMENTS

To my colleagues in the Clarendon Laboratory I am very grateful for numerous stimulating discussions, and for their comments on the original manuscript of this paper. M. Kastler, M. Brossel and their colleagues in Paris have generously amplified in private discussions their numerous publications. For their help, and for permission to publish figures, I am most grateful. I wish also to thank Professor Krüger for permission to publish figures, and for stimulating discussions, and Professor Bradley and Dr. Dodd for making available unpublished material.

## REFERENCES

- ALTHOFF, K., 1955, *Z. Phys.*, **141**, 33.  
 BARANGER, E., and GERJUOY, E., 1958, *Proc. Phys. Soc.*, **72**, 326.  
 BARRAT, J. P., 1957, *C.R. Acad. Sci., Paris*, **244**, 2785; 1958, *J. Phys. Radium*, **19**, 858.\*  
 BARRAT, J. P., and WINTER, J., 1956, *J. Phys. Radium*, **17**, 833.  
 BELL, W., and BLOOM, A., 1957, *Phys. Rev.*, **107**, 1559.  
 BESSET, C., HOROWITZ, J., MESSIAH, A., and WINTER, J., 1954, *J. Phys. Radium*, **15**, 251.  
 BLAMONT, J. E., 1957, *Ann. Phys., Paris*, **2**, 551.  
 BLAMONT, J. E., and BROSSEL, J., 1956, *C.R. Acad. Sci., Paris*, **243**, 2038.  
 BLAMONT, J. E., and WINTER, J. M., 1957, *C.R. Acad. Sci., Paris*, **244**, 332.  
 BLOCH, F., and SIEGERT, A., 1940, *Phys. Rev.*, **57**, 522.  
 BÖCKMAN, K., KRÜGER, H., and RECKNAGEL, E., 1957, *Ann. Phys., Lpz.*, **20**, 250.  
 BOGLE, G. S., DODD, J. N., and MCLEAN, W. L., 1957, *Proc. Phys. Soc. B*, **70**, 796.  
 BOUTRON, F., BARRAT, J. P., and BROSSEL, J., 1957, *C.R. Acad. Sci., Paris*, **245**, 2250.  
 BRADLEY, L. C., 1956, *Phys. Rev.*, **102**, 293.  
 BROSSEL, J., and BITTER, F., 1952, *Phys. Rev.*, **86**, 308.  
 BROSSEL, J., and JULIENNE, C., 1956, *C.R. Acad. Sci., Paris*, **242**, 2117.  
 BROSSEL, J., and KASTLER, A., 1949, *C.R. Acad. Sci., Paris*, **229**, 1213.  
 BROSSEL, J., MARGERIE, J., and KASTLER, A., 1955, *C.R. Acad. Sci., Paris*, **241**, 865.  
 BROSSEL, J., MARGERIE, J., and WINTER, J., 1955, *C.R. Acad. Sci., Paris*, **241**, 556, 600.  
 BUCK, P., and RABI, I. I., 1957, *Phys. Rev.*, **107**, 1291.  
 BUCKA, H., 1955, *Z. Phys.*, **141**, 49; 1956, *Naturwissenschaften*, **43**, 371; 1958, *Z. Phys.*, **151**, 328.  
 CASIMIR, H., 1936, *On the Interaction between Atomic Nuclei and Electrons* (Haarlem, Holland: Teylers Tweede Genootschap).  
 CLENDENIN, W., 1954, *Phys. Rev.*, **94**, 1590.  
 CONDON, E. U., and SHORTLEY, G. H., 1951, *Theory of Atomic Spectra* (Cambridge: University Press).  
 DAYHOFF, E. S., TRIEBWASSER, S., and LAMB, W. E., 1953, *Phys. Rev.*, **89**, 106.  
 DEHMELT, H. G., 1956, *Phys. Rev.*, **103**, 1125; 1957, *Ibid.*, **105**, 1924.  
 DIRAC, P. A. M., 1947, *The Principles of Quantum Mechanics*, 3rd Edn. (Oxford: University Press).  
 DRAKE, C., LURIO, A., HUGHES, V. W., and WHITE, J. A., 1958, *Bull. Amer. Phys. Soc.*, Ser. II, **3**, 7.  
 GRAY, N. M., 1933, *Phys. Rev.*, **44**, 570.  
 GUIOCHON, M. A., BLAMONT, J. E., and BROSSEL, J., 1956, *C.R. Acad. Sci., Paris*, **243**, 1859; 1957, *J. Phys. Radium*, **18**, 99.  
 GÜTTINGER, P., and PAULI, W., 1931, *Z. Phys.*, **67**, 743.  
 HACK, M. N., 1956, *Phys. Rev.*, **104**, 84.  
 HAWKINS, W. B., 1955, *Phys. Rev.*, **98**, 478.



- HEBERLE, J. W., REICH, H. A., and KUSCH, P., 1956, *Phys. Rev.*, **101**, 612, **104**, 1585.
- HEITLER, W., 1954, *Quantum Theory of Radiation*, 3rd Edn. (Oxford : Clarendon Press).
- HERZBERG, G., 1956, *Z. Phys.*, **146**, 269.
- KASTLER, A., 1954, *Proc. Phys. Soc., A*, **67**, 853 ; 1956, *J. Opt. Soc. Amer.*, **47**, 460 ; 1958, *J. Phys. Radium*, **19**, 797.\*
- KOPFERMANN, H., 1958, *Nuclear Moments* (New York : Academic Press Inc.) (English version by Schneider, E. E.).
- KOSTER, G., 1952, *Phys. Rev.*, **86**, 148.
- KRÜGER, H., and SCHEFFLER, K., 1958, *J. Phys. Radium*, **19**, 854.\* A more complete paper will appear in *Z. Phys.*
- KUSCH, P., 1956, *Phys. Rev.*, **101**, 627.
- LAMB, W. E., 1951, *Rep. Progr. Phys.*, **14**, 23 (London : Physical Society) ; 1952, *Phys. Rev.*, **85**, 259 ; 1957, *Ibid.*, **105**, 559.
- LAMB, W. E., and MAIMAN, T. H., 1957, *Phys. Rev.*, **105**, 573.
- LAMB, W. E., and RETHERFORD, R. C., 1950, *Phys. Rev.*, **79**, 549 ; 1951, *Ibid.*, **81**, 222 ; 1952, *Ibid.*, **86**, 1014.
- LAMB, W. E., and SANDERS, T. M., 1956, *Phys. Rev.*, **103**, 313.
- LAMB, W. E., and SKINNER, M., 1950, *Phys. Rev.*, **78**, 539.
- LAMB, W. E., and WILCOX, L., 1958, *J. Phys. Radium*, **19**, 801\* ; *Phys. Rev.*, in the press.
- LANDOLT-BÖRNSTEIN, 1950, *Zahlenwerte und Funktionen*, 6th Edn., 1/1, 260 (Berlin : Springer-Verlag).
- LIPWORTH, E., and NOVICK, R., 1957, *Phys. Rev.*, **108**, 1434.
- MASSEY, H. S. W., and BURHOP, E. H. S., 1952, *Electronic and Ionic Impact Phenomena* (Oxford : University Press).
- MELISSINOS, A. C., 1959, *Bull. Amer. Phys. Soc.*, **4**, 11.
- MEYER-BERKHOUT, U., 1955, *Z. Phys.*, **141**, 185.
- MITCHELL, A. C. G., and ZEMANSKY, M. W., 1934, *Resonance Radiation and Excited Atoms* (Cambridge : University Press).
- NOVICK, R., and COMMINS, E., 1958, *Phys. Rev.*, **111**, 822.
- NOVICK, R., LIPWORTH, E., and YERGIN, P. F., 1955, *Phys. Rev.*, **100**, 1153.
- PEBAY-PEYROULA, J.-C., BROSSEL, J., and KASTLER, A., 1957, *C.R. Acad. Sci., Paris*, **244**, 57, **245**, 840.
- PERL, M. L., RABI, I. I., and SENITZKY, B., 1955, *Phys. Rev.*, **98**, 611.
- PHILLIPS, M., 1956, *Phys. Rev.*, **103**, 322.
- PRINGSHEIM, P., 1949, *Fluorescence and Phosphorescence* (London : Interscience Publishers).
- RABI, I. I., 1937, *Phys. Rev.*, **51**, 652.
- RAMSEY, N. F., 1955, *Phys. Rev.*, **100**, 1191 ; 1956, *Molecular Beams* (Oxford : University Press).
- RITTER, G. J., and SERIES, G. W., 1957, *Proc. Roy. Soc. A*, **238**, 473.
- SAGALYN, P. L., 1954, *Phys. Rev.*, **94**, 885.
- SAGALYN, P. L., MELISSINOS, A. C., and BITTER, F., 1958, *Phys. Rev.*, **109**, 375.
- SALWEN, H., 1955, *Phys. Rev.*, **99**, 1274.
- SENITZKY, B., and RABI, I. I., 1956, *Phys. Rev.*, **103**, 315.
- SERBER, R., 1956, *Special Technical Report of Columbia Radiation Laboratory*.
- SERIES, G. W., 1954, *Proc. Roy. Soc. A*, **226**, 377 ; 1957, *Spectrum of Atomic Hydrogen* (Oxford : University Press).
- SERIES, G. W., and FOX, W. N., 1958, *J. Phys. Radium*, **19**, 850.\*
- STERNHEIMER, R. M., 1954, *Phys. Rev.*, **95**, 736 and earlier papers there cited.
- TORREY, H. C., 1941, *Phys. Rev.*, **59**, 293.
- TRIEBWASSER, S., DAYHOFF, E. S., and LAMB, W. E., 1953, *Phys. Rev.*, **89**, 98.
- WEISSKOPF, V. F., and WIGNER, E. P., 1930, *Z. Phys.*, **63**, 54, **65**, 18.
- WESEMAYER, H., and DANIELS, J., 1958, *Canad. J. Phys.*, **36**, 405.
- WIEDER, I., and LAMB, W. E., 1957, *Phys. Rev.*, **107**, 125.
- WINTER, J., 1955, *C.R. Acad. Sci., Paris*, **241**, 375, 600.

\* These papers were read at the Magnetic Resonance Conference in Paris in July 1958.





# Optical Pumping and Related Topics

G. W. SERIES

## I. A PRELIMINARY SURVEY

### 1. INTRODUCTION

We propose to give an account of work which is commonly included under the titles:

- (i) optical-radio frequency double resonance experiments,
- (ii) level-crossing experiments,
- (iii) optical pumping experiments.

For the most part, such experiments have been performed on free atoms, and the results that have been obtained are of interest in atomic spectroscopy in particular, and in atomic physics more widely, but the methods have also been applied to molecules and to ions in solids.

The experiments have in common that all the techniques are based on the interaction of light with the atoms, either in absorption or in emission or both. There are close connections with experiments in which electrons are used for excitation.

The light fields we encounter are weak: we shall not be concerned with non-linear effects, nor shall we be concerned with the statistical properties of the fields.

Historically, the experiment which introduced this whole field of work was the optical radio-frequency double resonance experiment of Brossel and Bitter.<sup>(1)</sup> This showed how it was possible to apply to excited atoms the techniques of magnetic resonance which had already been worked out for atoms in their ground states (atomic beam resonance methods).

We shall find it convenient to take the Brossel-Bitter experiment as our starting point, then to discuss level-crossing experiments, and then optical pumping. This is not the historical development. In the first section we shall aim to introduce the whole field, by discussing at length some simple examples. In later sections we shall take up subtle points and elaborate on techniques used in other experiments of the same types.

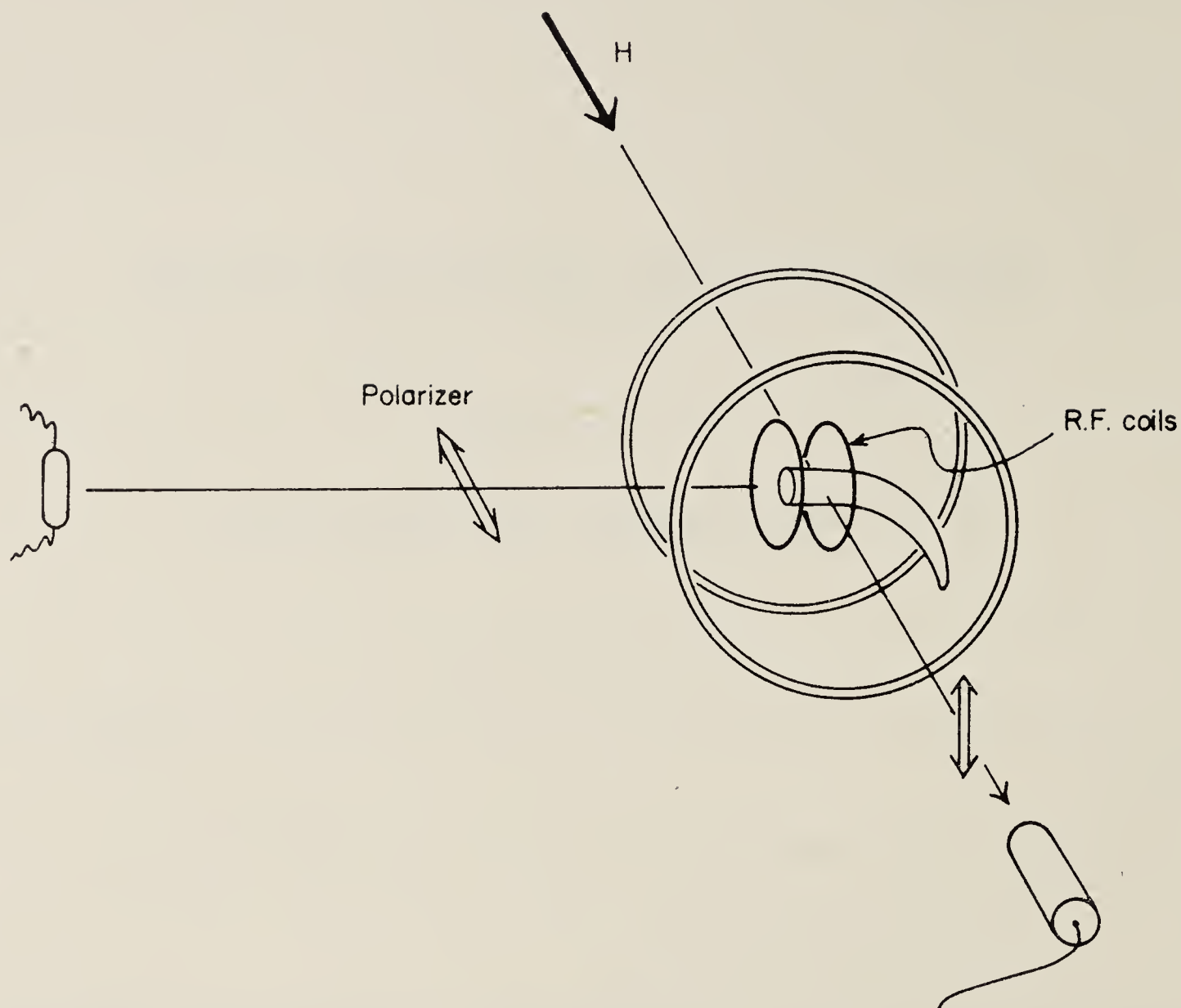


FIG. 1a. Schematic apparatus for performing the Brossel-Bitter experiment.

## 2. THE BROSSSEL-BITTER EXPERIMENT

The Brossel-Bitter experiment measured the Zeeman splitting of the excited state  $6s6p\ ^3P_1$  in mercury by magnetic resonance. The atoms are present in the form of a vapour at very low pressure in the horn-shaped vessel and irradiated by light from a mercury lamp (Fig. 1a). They undergo the process known as resonance fluorescence which can be described (crudely, but well enough for our immediate purpose) as the absorption of a photon, followed by the emission of a photon. The atoms remain in the excited state for a time determined by the probability of spontaneous emission (Einstein coefficient  $A$ ). The mean lifetime is  $\tau = A^{-1}$ . This is the time available for the magnetic resonance transition.

In order to secure an unequal distribution of atoms over excited states  $m$  (Fig. 1b) the incident light is polarized. Magnetic resonance is stimulated by an oscillating magnetic field  $H_1 \cos \omega_0 t$  produced by a current in the coils shown in Fig. 1a. The oscillating field is at right angles to the static field  $H$  which produces the splitting of levels shown in Fig. 1b. This geometrical arrangement stimulates transitions  $\Delta m = \pm 1$ .



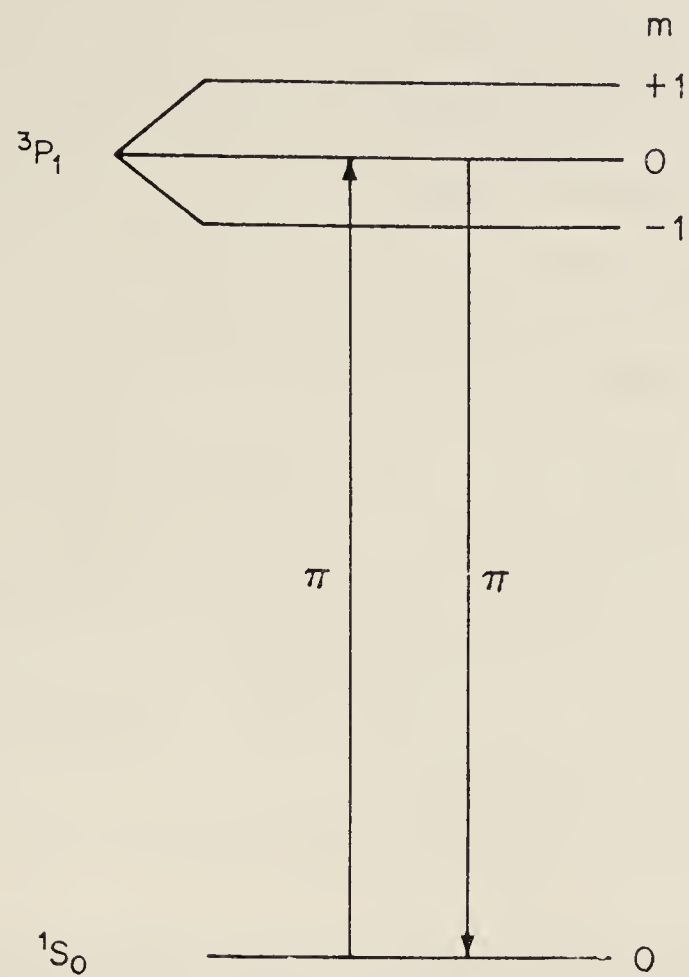


FIG. 1b. Resonance fluorescence in mercury stimulated by  $\pi$ -polarized light.

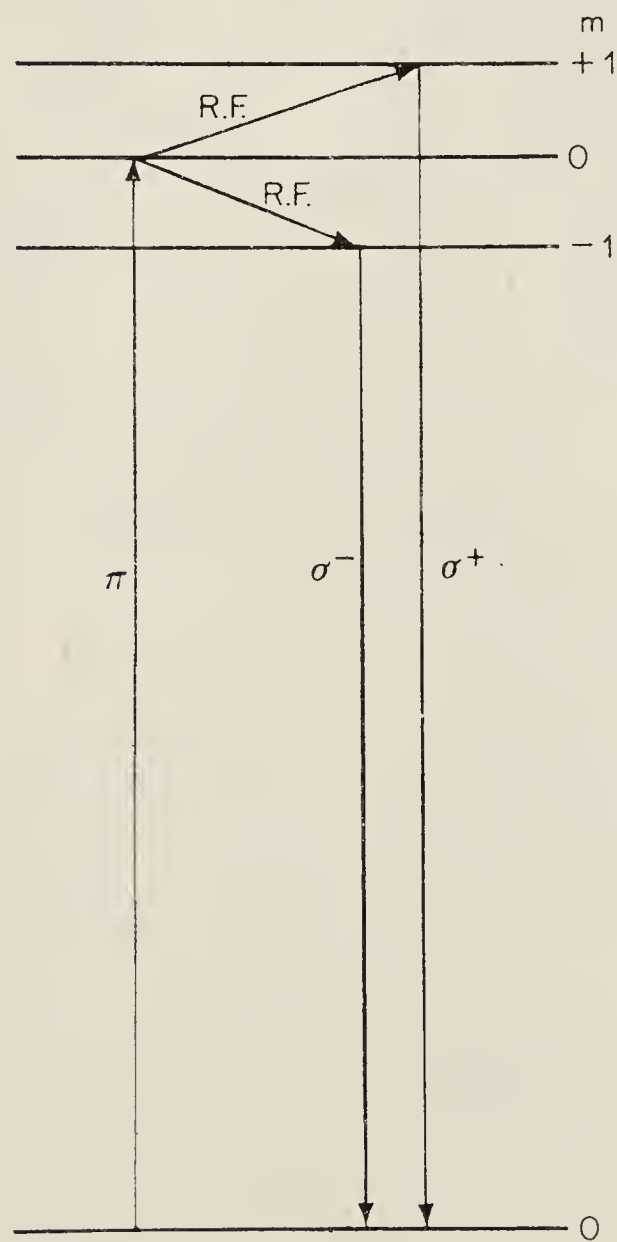


FIG. 1c. Change of polarization of fluorescent light resulting from radio-frequency transitions.

Atoms undergo these transitions:

- (a) if the amplitude  $H_1$  is sufficiently strong, and
- (b) if the frequency  $\omega_0$  is sufficiently close to the splitting in the field  $H$ .

The resonance is detected by making use of the profound effect which the transitions have on the polarization of the emitted light: compare Figs. 1b and 1c, and notice how, as a result of a transition, the polarization is changed from  $\pi$  to  $\sigma$ . These have different spatial distributions. A photomultiplier in a fixed position registers the change. Thus the absorption or emission of a quantum of energy at the radio-frequency determines the polarization of an emitted quantum of vastly greater energy at the optical frequency. That is why this optical method of detection is so much more efficient, when one comes to consider questions of signal-to-noise ratio, than a direct measurement of the absorption of radio-frequency energy.

Figure 2 is an oscilloscope display of a Brossel–Bitter resonance. It was

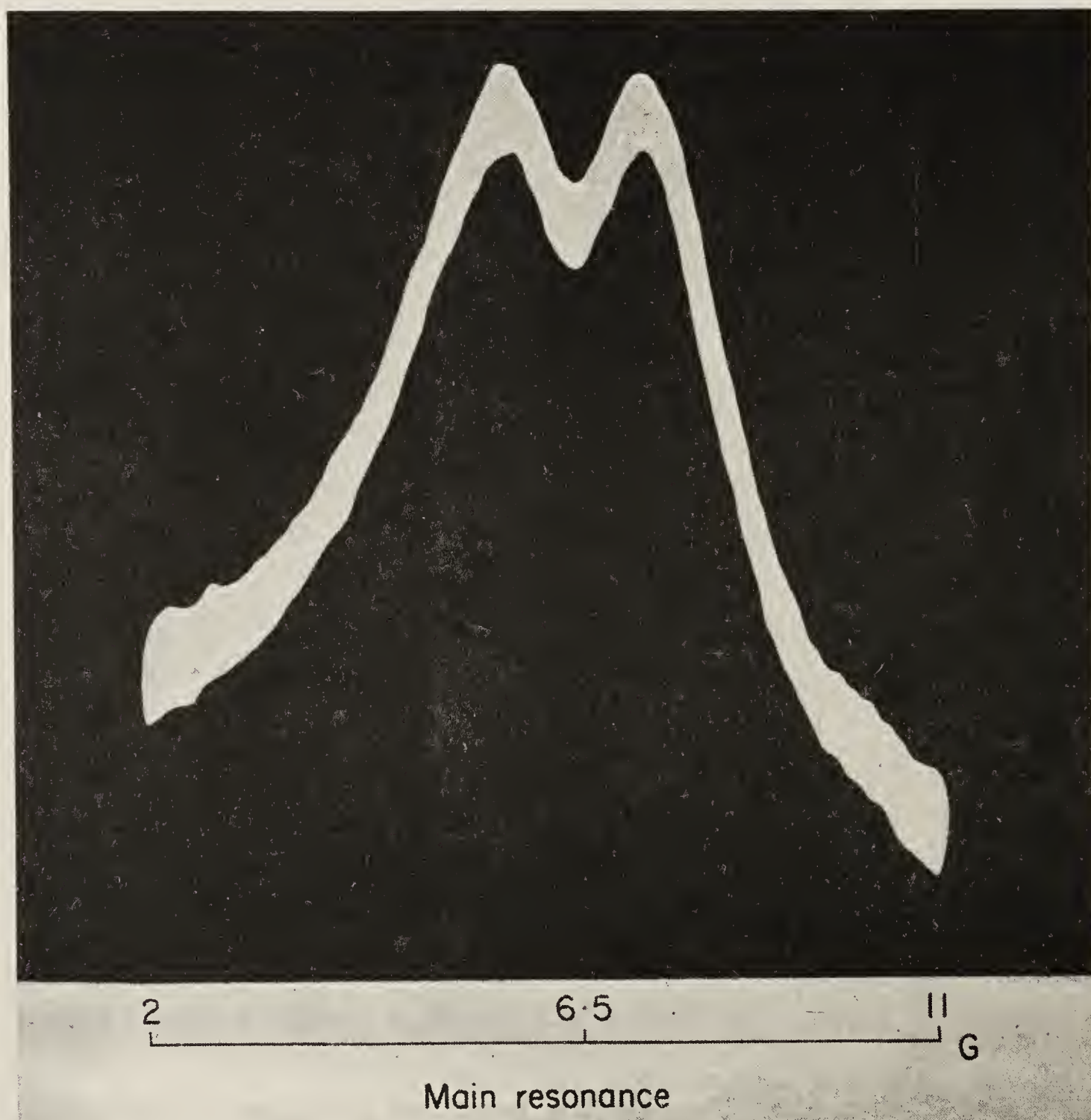


FIG. 2. Double resonance signal in the  $6^3P_1$  state of mercury.



obtained by keeping the frequency fixed at about 6 MHz and sweeping the magnetic field through the resonance region. It is worth noticing that this curve was obtained with very simple methods of detection: wideband amplification of the voltage developed across a resistor in the output of the photomultiplier.

The curve is double-peaked because the transitions  $\Delta m = \pm 1$  are closely coupled. It is similar to the resonance curve of two over-coupled resonant circuits. The curve becomes single peaked when the radio-frequency field strength is reduced.

We shall shortly show how the shape of such resonance curves can be calculated. First, we make some remarks on the properties of the oscillating field required to stimulate the resonances. Our considerations here are not limited to the Brossel–Bitter experiment in particular; we have in mind this type of experiment in general.

## 2.1 AMPLITUDE OF OSCILLATING FIELD

It is important to consider what amplitude of radio-frequency field is necessary to induce transitions. A classical interpretation of magnetic resonance suggests that the field should be strong enough for the excited atom to precess through an angle of about one radian within its lifetime,  $\tau$ . Recalling that the precessional velocity in the field  $H_1$  is  $\gamma H_1$ , where  $\gamma$  is the gyromagnetic ratio, we have for the required condition

$$(\gamma H_1) \tau \approx 1 \text{ rad.} \quad (1)$$

More formally, we find the factor  $\langle J, M | J_x \pm iJ_y | J, M \mp 1 \rangle$  on the left-hand side. Using typical values for  $\tau$  ( $10^{-8}$  sec) and a value of  $\gamma$  corresponding to the Bohr magneton (1.4 MHz/G) we arrive at  $H_1 \approx 10$  G. Actually, this is an over-estimate because we can detect changes of angle smaller than 1 rad, but it is clear we must think in terms of amplitudes of the order of a few gauss. Moreover, in order that the Zeeman levels be non-degenerate, we must think in terms of frequencies of the order of  $10^8$  rad sec $^{-1}$ , i.e., in the range 10–100 MHz.

Clearly, in order to drive such a resonance we need high frequency oscillators with power amplifiers. These requirements stem immediately from the fact that we are dealing with excited states. At a later stage, when we come to consider resonances in the ground states, we shall find that the longer lifetimes allow the use of fields of the order of milligauss, and that kilocycle frequencies are often appropriate.

The use of high power, high frequency fields in studying resonances in excited states often raises technical problems which we shall discuss later.

## 2.2. WIDTH OF RESONANCE CURVES

An important characteristic of a resonance curve is its width. In the present case we can derive a minimum figure for the width by thinking in terms of Fourier transforms. The time available for the oscillating field to interact with the atom is limited by the mean lifetime of the excited state, hence the width of the resonance must be of order  $\tau^{-1}$ . In quantum terms the point to notice is that the excited energy levels of Fig. 1b are broadened by radiation damping, so that the width of a resonance between a pair of levels cannot be less than the sum of their widths,  $2\Gamma = 2\tau^{-1}$ .

This is a minimum width. It may be increased by radio-frequency power broadening (shortening of the lifetime through transitions induced by the oscillating field) or by inhomogeneous static fields. The latter is not a serious problem for excited state resonances, though it is for ground states.

Of course, a precise definition of the width of a resonance curve rests upon knowledge of the profile.

## 2.3. ANALYTICAL EXPRESSION FOR THE LINE PROFILE

The following is a version of the calculation given by Brossel and Bitter. In the interests of simplicity, let us make the system effectively two-level by supposing that we are detecting the light through a circular polarizer ( $\sigma^+$ ) in front of the photomultiplier. Then we are concerned only with transitions 0 to +1.

Suppose an atom is excited at time  $t_0$ . (This is the "pulse" approximation. It is valid if the spectral distribution of the exciting light is much greater than the natural width of the excited states. We shall frequently use this approximation, and discuss it in a later section).

Let  $P(t, t_0)$  be the probability that, at time  $t$ , the atom has made a transition. This can be calculated from the theory of magnetic resonance. The result is

$$P(t, t_0) = (b^2/p^2) \sin^2 \frac{1}{2} p(t - t_0), \quad (2)$$

where

$$b = \gamma H_1; \quad p = \gamma[(H - H_0)^2 + H_1^2]^{\frac{1}{2}}; \quad H_0 = \omega_0/\gamma;$$

$H$  is the static field and  $H_{r.f.} = 2H_1 \cos \omega_0 t$  the oscillating field. (Only one rotating component of  $H_{r.f.}$  is effective: we are ignoring the counter-rotating component).

The probability that the atom has survived in the interval  $(t - t_0)$  is  $\exp[-\Gamma(t - t_0)]$ , where  $\Gamma$  is the decay constant for the excited states (the same for both). To find the probability of emission of a photon of different polarization, eqn (2) must be multiplied by this exponential factor.

If atoms are excited at the uniform rate  $R$ , the number excited in time  $dt_0$  is  $R dt_0$ . Hence, finally, if the atoms are excited independently of one another,



the steady-state intensity of light reaching the detector is

$$\begin{aligned}
 I(H) &\propto \int_0^t (b^2/p^2) \sin^2 \frac{1}{2} p(t-t_0) \exp[-\Gamma(t-t_0)] dt_0 \\
 &\propto b^2/(p^2 + \Gamma^2) \\
 &= (\gamma H_1)^2 / \{ \Gamma^2 + [\gamma(H-H_0)]^2 + (\gamma H_1)^2 \}
 \end{aligned} \tag{3}$$

This is a Lorentzian curve of full width at half-intensity,  $2[H_1^2 + (\Gamma/\gamma)^2]^{\frac{1}{2}}$ . As  $H_1$  tends to 0 the width tends to  $2\Gamma$  (in radians  $\text{sec}^{-1}$ ). The power-broadening is thus quantitatively expressed.

In Brossel and Bitter's paper the probability  $P(t, t_0)$  of equation (2) is replaced by the more complicated expression representing a transition out of the state 0, leading to a more complicated version of (3).

#### 2.4. DOUBLE RESONANCE LINE WIDTH COMPARED WITH OPTICAL LINE WIDTH

The quantitative remarks we made earlier about line widths are borne out by these calculations and exemplified by Fig. 2. The line width of a few gauss in that figure corresponds to a frequency of the order of 1 MHz and a lifetime of order  $10^{-7}$  sec. This line width should be compared with the line width in optical studies of the Zeeman effect—typically, several hundred gauss. The Brossel–Bitter experiment therefore allows the measurement of Zeeman intervals in excited states with a precision orders of magnitude better than optical measurements.

The method is not limited to the measurement of Zeeman intervals. We shall indicate in the next section how it has been applied to determine hyperfine structures.

### 3. DOUBLE RESONANCE METHOD: HYPERFINE STRUCTURES

The basis of the double resonance method is to make use of the changes of polarization of fluorescent light which result from magnetic resonance transitions  $\Delta M = \pm 1$ . This selection rule stems from the existence of matrix elements of the  $(x-y)$  component of the magnetic moment operator

$$\hat{\mu} = (\beta/\hbar)(\hat{L} + 2\hat{S}).$$

In the Brossel–Bitter experiment the states were the eigenstates  $|M\rangle$  of  $\hat{J}_z = \hat{L}_z + 2\hat{S}_z$  and  $\hat{\mu}_{xy}$  has non-vanishing matrix elements between these states. The static magnetic field was used only to remove the degeneracy of the  $|M\rangle$ .

In an atom having hyperfine structure with weak field quantum numbers  $F, M_F$ , the operator  $\hat{\mu}_{xy}$  has matrix elements between states  $|F, M_F\rangle$  and

$|F', M_F \pm 1\rangle$ , where  $F' - F = 0, \pm 1$ . The polarization of the light is determined by the value of  $M_F$ , irrespective of whether levels of different  $M_F$  are degenerate. Hence, the double resonance method may be applied to measure hyperfine intervals in zero field ( $F' - F = \pm 1$ ). It is also, of course, still applicable in fields strong enough to decouple  $I$  and  $J$ , and in intermediate fields. We shall illustrate this by reference to an experiment of Ritter and Series<sup>(2)</sup> on an excited state of potassium.

### 3.1. HYPERFINE RESONANCES IN ZERO FIELD

The apparatus is shown in Fig. 3. It is, in essentials, the same as that used by Brossel and Bitter, but differs in points of experimental technique. Most significant is that the potassium is introduced into the resonance region in the form of a crude atomic beam. The use of a hollow cathode light source is also noteworthy.

The excited states of interest here were the second excited  $P$  states  $5^2P_{3/2}$  whose hyperfine structure allows a determination of the nuclear electric quadrupole moment. The level scheme is shown in Fig. 4a. A blue filter eliminates

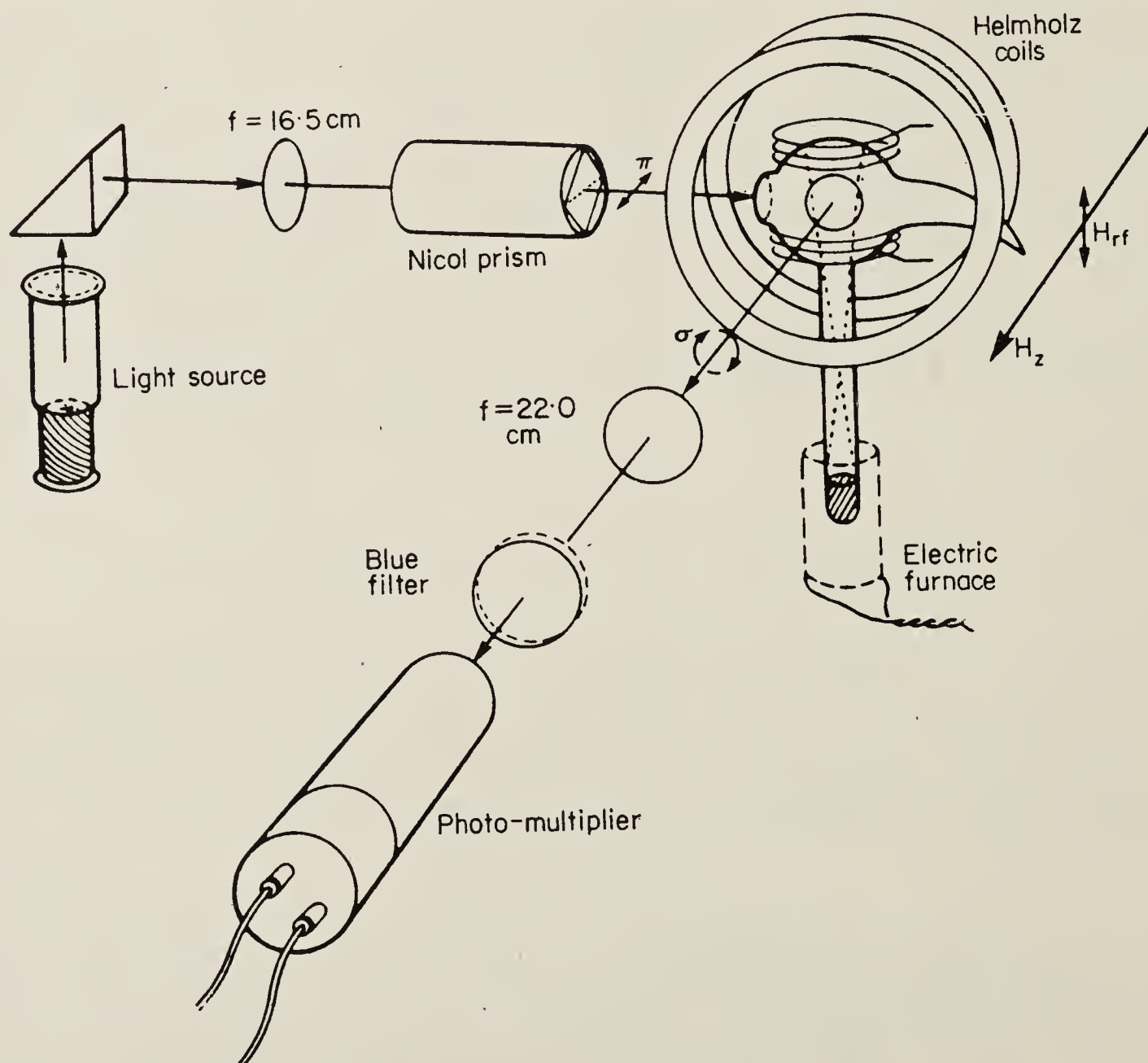


FIG. 3. Double resonance experiment to study the hyperfine structure of  $5^2P_{3/2}$  of potassium. (After Ritter and Series.<sup>(2)</sup>)



the much stronger fluorescence from the  $4^2P$  states. Fluorescence from  $5^2P_{1/2}$  passes the filter but its intensity is unchanged by the magnetic resonance unless circular polarizers are used (see later).

The hyperfine structure of  $5^2P_{3/2}$  is shown in Fig. 4b. Magnetic resonance curves obtained by varying the frequency while keeping the amplitude  $H_1$  fixed are shown in Fig. 5. The interpretation of these curves is not easy without

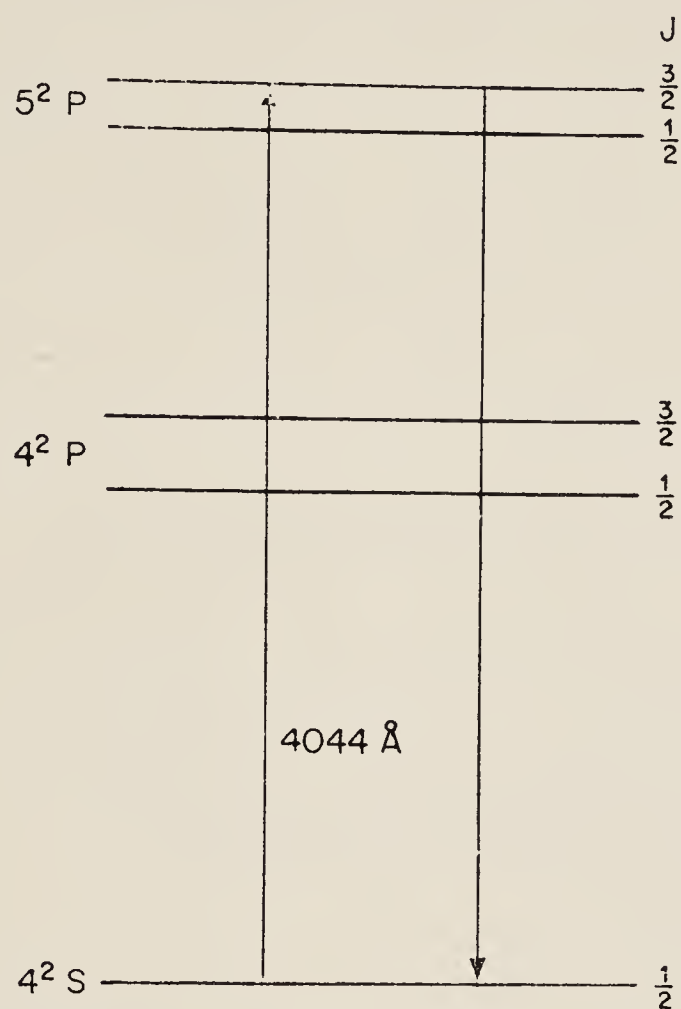


FIG. 4a. Resonance fluorescence of the second excited state in potassium.

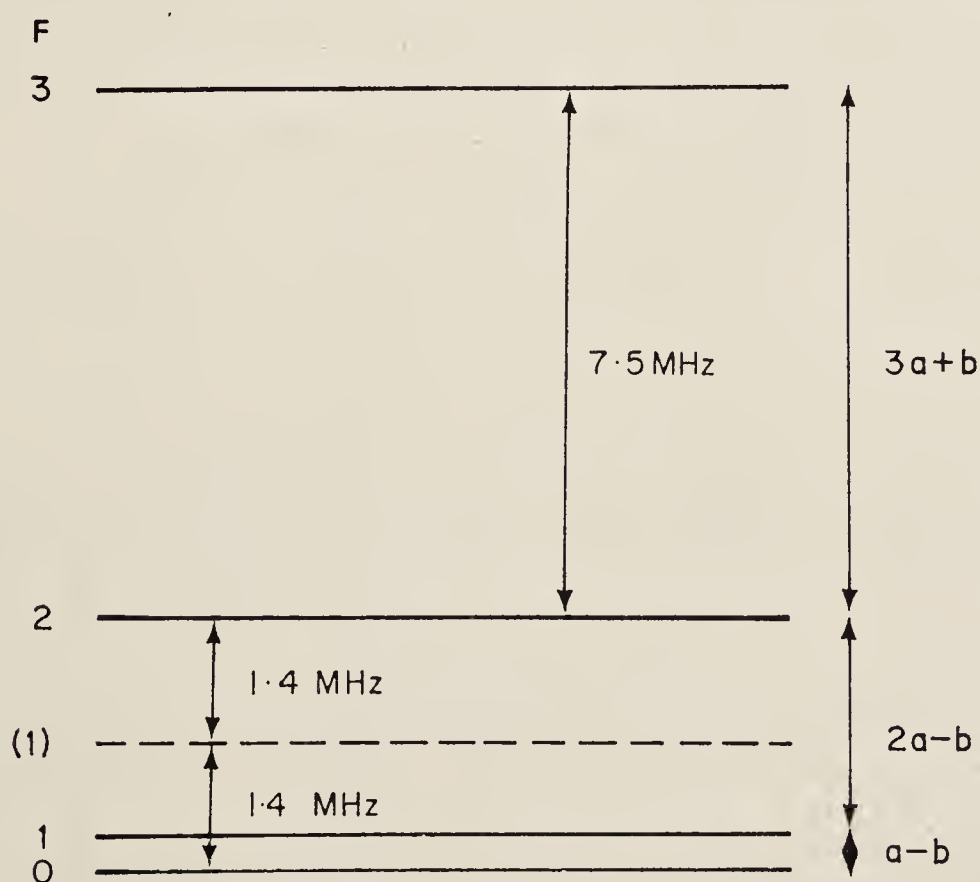


FIG. 4b. Hyperfine structure of  $5^2P_{3/2}$ , showing the double resonance transitions.

additional information (based partly on the known h.f.s. of the ground state and partly on analysis of double resonance curves in strong magnetic fields). With this information one can be confident that the curve at 7.5 MHz represents the complex of transitions between the various  $M_F$  levels belonging to  $F = 3$  and  $F = 2$ . Notice that the width of the line at half intensity is about 2 MHz.

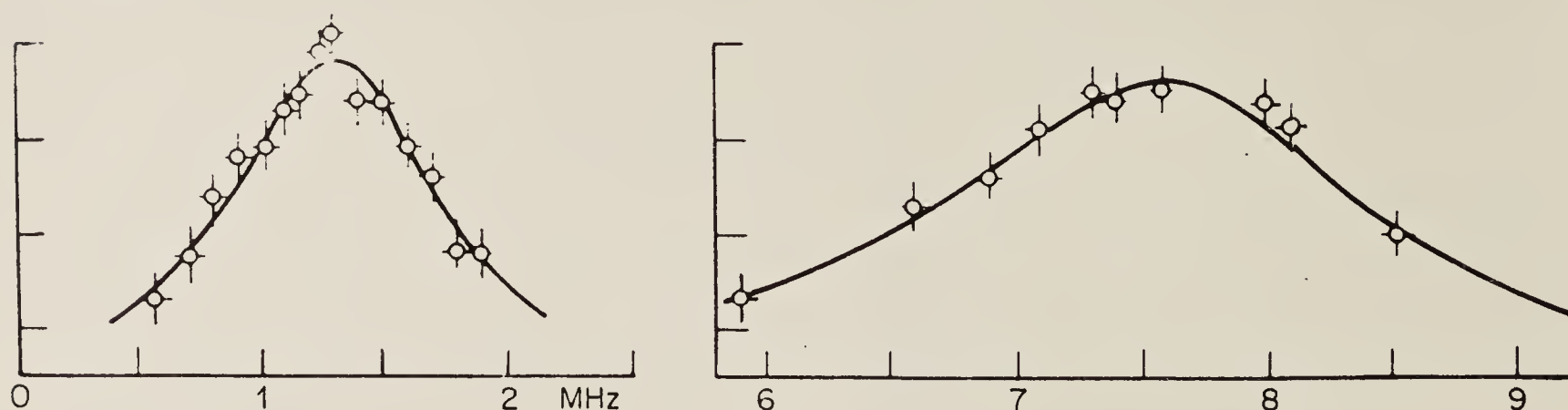


FIG. 5. Experimental curves corresponding to the transitions marked in Fig. 4b. (After Ritter and Series.<sup>(2)</sup>)

The resonance curve at 1.4 MHz is obviously narrower and its interpretation is not immediately obvious. It is, in fact, identified by its width and position as a double-quantum transition between the levels  $F = 0$  and 2. Such transitions are found when the separate resonances 0–1 and 1–2 overlap and the r.f. field is sufficiently strong. We shall discuss these multiple-quantum resonances later.

### 3.2. HYPERFINE STRUCTURE OF RESONANCES IN STRONG FIELD

“Strong field” is, of course, a relative term. The fact that 25 G is a strong field in this context (decouples  $I$  and  $J$ ) emphasises the smallness of the hyperfine structures which the method is capable of measuring.

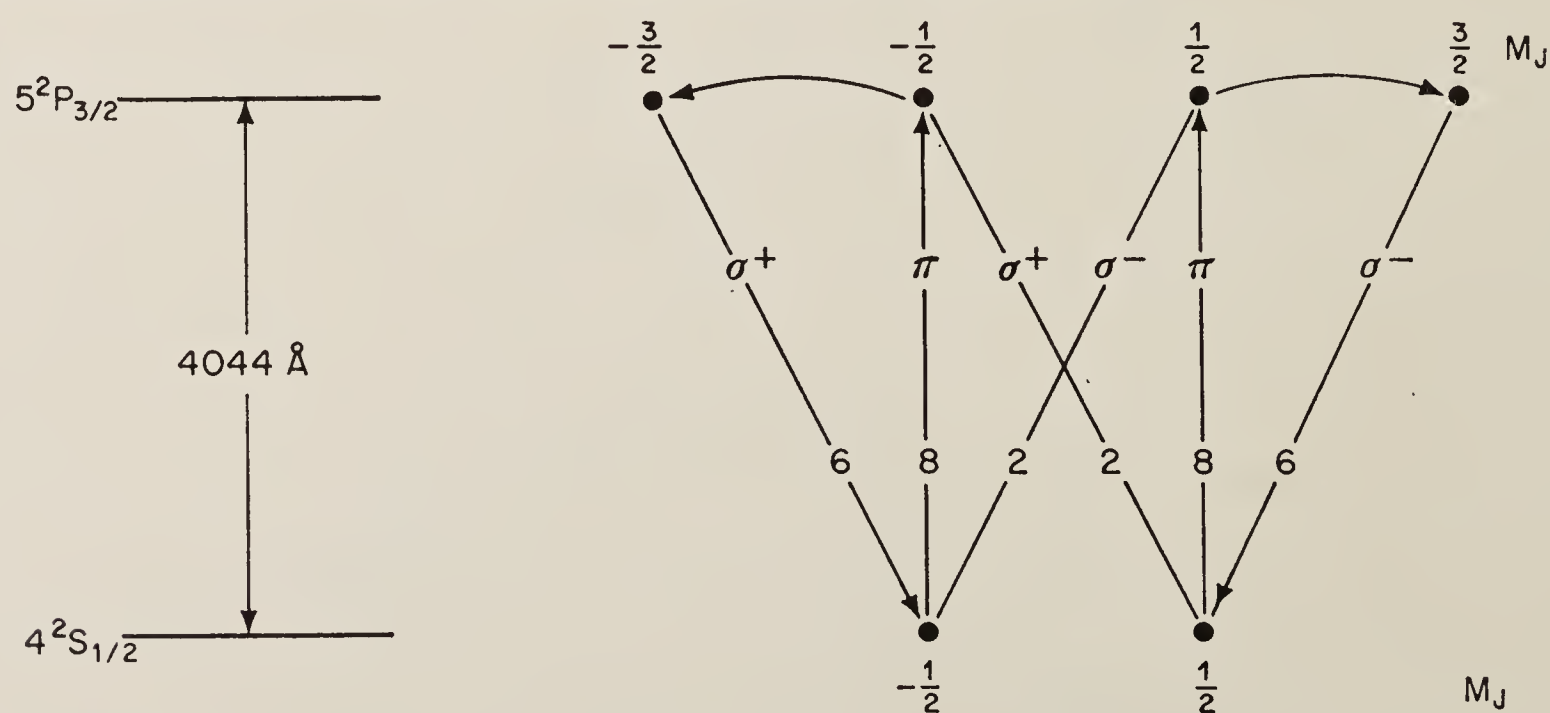


FIG. 6. Fine structure of the transition  $4^2S_{1/2} - 5^2P_{3/2}$  showing Zeeman components and relative transition probabilities. (After Ritter and Series.<sup>(2)</sup>)



With  $I$  and  $J$  decoupled, both the optical and the radio-frequency interactions are with the electron, leaving the orientation of the nucleus unchanged. The interactions, showing the changes in  $M_J$ , are indicated in Fig. 6. The resonances corresponding to transitions between the four values of  $M_J$  would

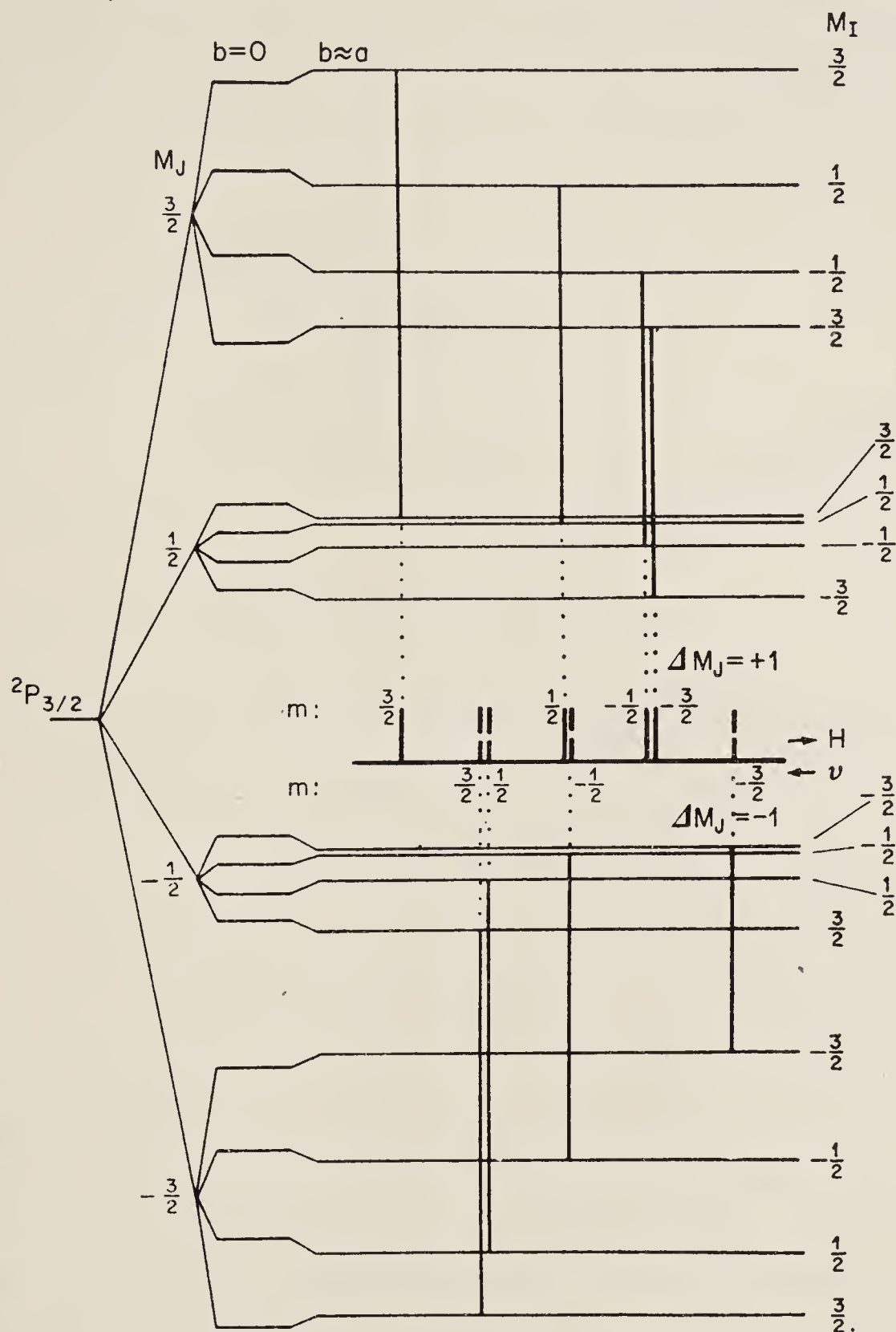


FIG. 7. Hyperfine structure of Zeeman components of  $5^2P_{3/2}$  showing the radio-frequency transitions detectable by the experimental arrangement shown in Fig. 3. The figure has been drawn for a value of the electric quadrupole coupling constant  $b$  approximately equal to that of the magnetic dipole constant  $a$ . (After Ritter and Series.<sup>(2)</sup>)

be coincident were it not for the hyperfine coupling which produces the splittings indicated in Fig. 7.

The corresponding resonance curve is shown in Fig. 8. The frequency was fixed at 41 MHz and the curve obtained by varying the magnetic field. A low-frequency modulation was added to the field in order to allow phase-sensitive

detection. The curve is therefore the derivative of the true resonance curve. The structure is hyperfine structure. Analysis of this curve allowed the determination of the hyperfine interaction constants—magnetic dipole and electric quadrupole.

A recent analysis (Pegg<sup>(3)</sup>) has shown that the quadrupole constant obtained from these curves was seriously in error owing to perturbation of the resonances by the strong radio-frequency fields. These perturbations will be discussed in a later section.

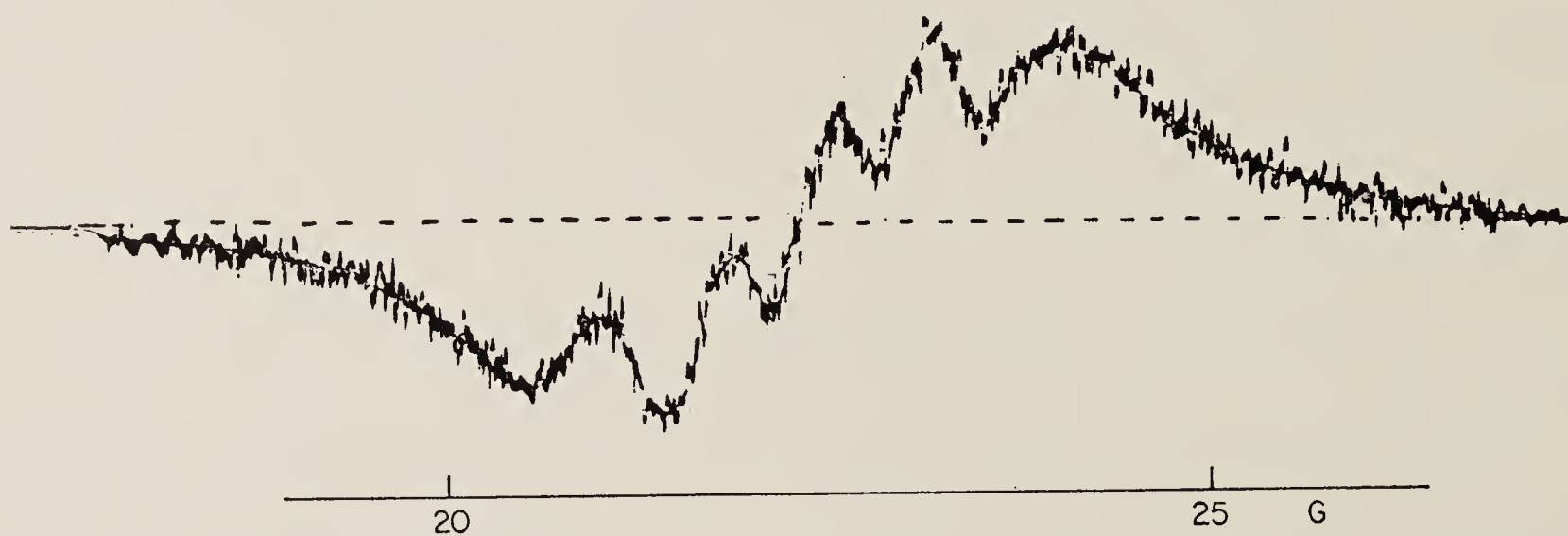


FIG. 8. Experimental resonance curve at 41 MHz (derivative curve). The structure represents the eight incompletely resolved transitions shown in Fig. 7. (After Ritter and Series.<sup>(2)</sup>)

### 3.3. BACKGROUND SIGNAL

In Fig. 9 are compared two signals, one obtained with an oscillating field at 19 MHz and the other with this field turned off. In the first curve the magnetic resonance with hyperfine structure is seen, as in Fig. 8, but a background signal is present which the second curve shows to be independent of the radio-frequency field. There are two contributions to this background signal:

(i) It occurs in the region where the  $I$ – $J$  coupling is being broken down. In this region the atomic wave functions are field-dependent, and the optical transition probabilities are also field-dependent. (In the early days of resonance fluorescence, attempts were made to determine nuclear spins by measuring these changes: Heydenburg *et al.*<sup>(4)</sup>)

(ii) In this region (and also near zero field) there are degeneracies of energy levels. This gives rise to interference effects which are now known as level-crossing and anti-crossing effects. (The changes of intensity in Fig. 9 are due to anti-crossings because  $\pi$  radiation was used to excite the fluorescence). These interference effects form the basis of what has proved to be a most important spectroscopic technique. They were not recognised when the experiments on potassium were performed: the changes of intensity were ascribed to the effect (i). Recent studies (Schmieder *et al.*<sup>(5)</sup>) of level-



crossing effects in these hyperfine states of potassium have led to values of the coupling constants free from the error introduced by the strong radio-frequency fields.

The next sections will be devoted to these interference effects.

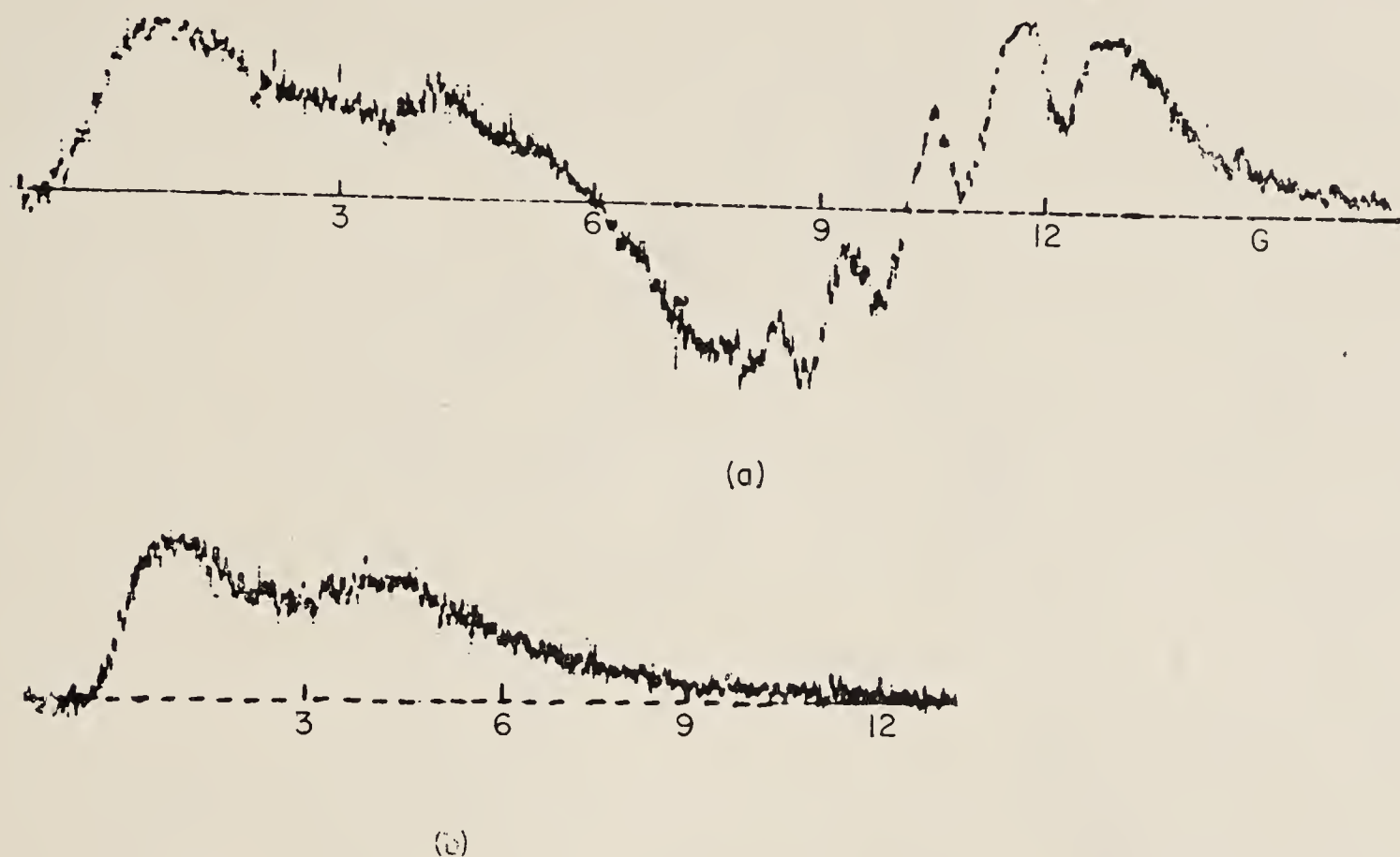


FIG. 9. Fluorescence signal in the range 0–15 G. (After Ritter and Series.<sup>(2)</sup>)

a. With radio-frequency field at 19 MHz.

b. With no radio-frequency field.

#### 4. LEVEL-CROSSINGS

##### 4.1. THE PHENOMENON

First, I should like to show the phenomenon and indicate its usefulness, and then discuss its interpretation.

A sketch showing the essential parts of the apparatus, can be seen in Fig. 10. There is no radio-frequency field. Notice that the exciting light is linearly polarized perpendicular to the magnetic field, and that the fluorescent light (consisting in this case of two circularly polarized components emitted along the direction of  $H$ ) is taken through a linear analyser before reaching the photomultiplier. I emphasise that, for the exciting light and for the fluorescent light we are using one mode of polarization (linear polarizers), but that two different atomic transitions are involved ( $\Delta M = \pm 1$ ), both in excitation and in decay.

The experiment is performed by recording the intensity of fluorescent light as a function of magnetic field. Figures 11a and 11b show results for fluorescence from an excited state of thallium ( $(6s^26d)^2D_{3/2}$ ).<sup>(6)</sup> In this particular

experiment, low-frequency modulation of the magnetic field was used for phase-sensitive detection, so the figures show  $\partial I/\partial H$ .

In Fig. 11a you see strong changes of the intensity in the neighbourhood of zero field. In 11b you see changes at higher fields. These are superimposed on

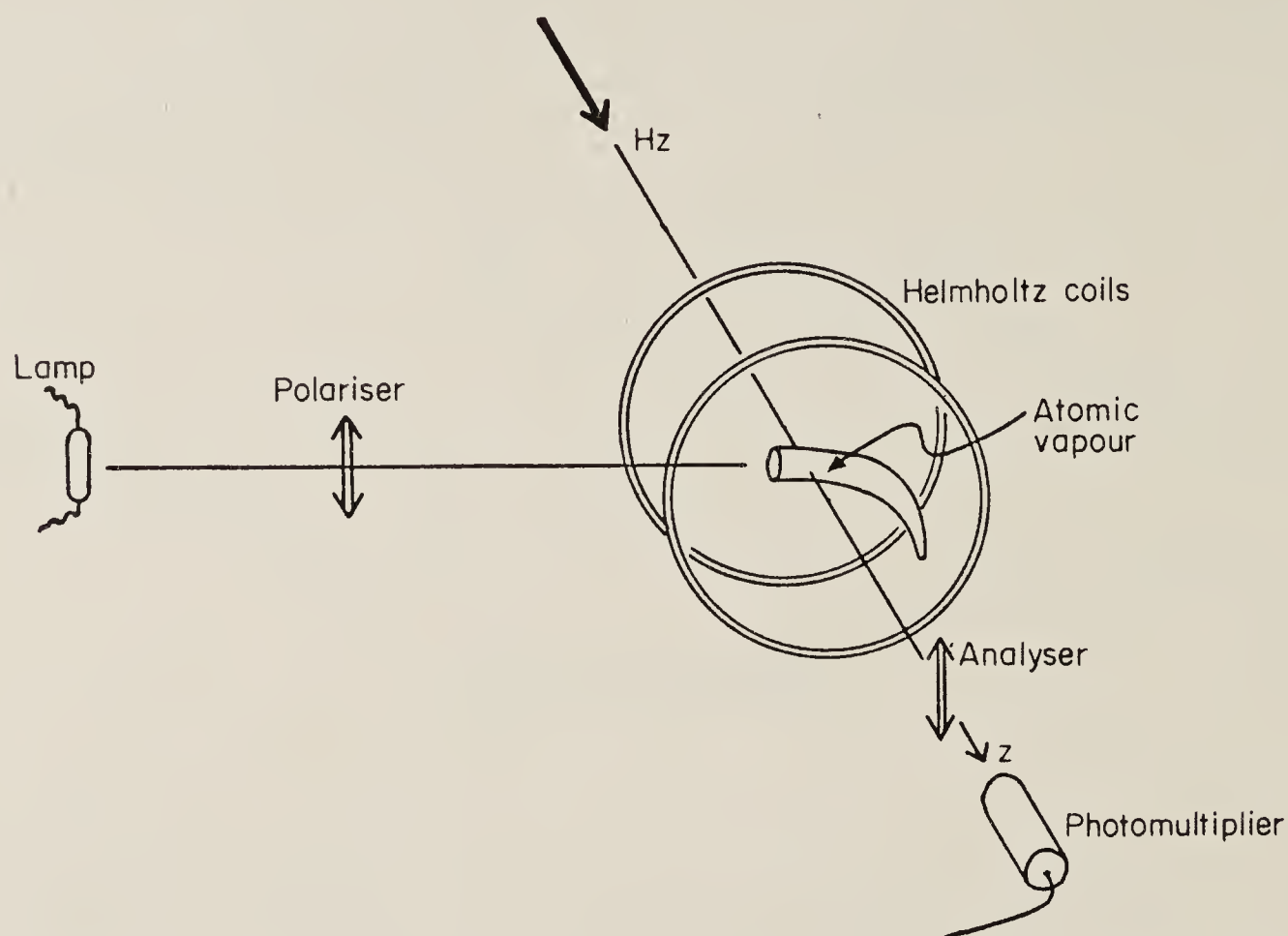


FIG. 10. Geometrical arrangement for studying the level-crossing phenomenon

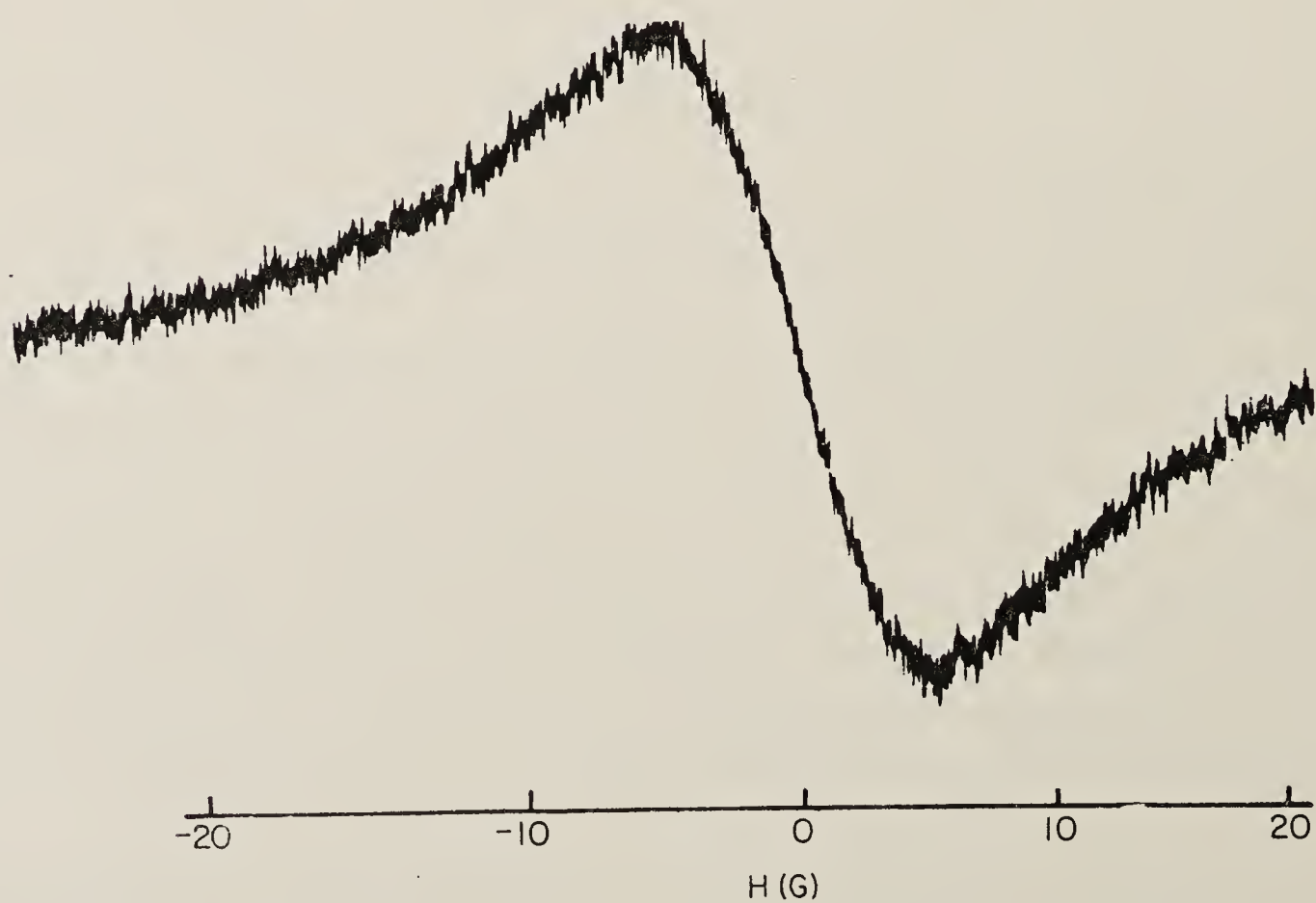


FIG. 11a. Resonance fluorescence from  $(6s^26d) {}^2D_{3/2}$  state of thallium in the vicinity of zero magnetic field. (After Gough and Series.<sup>(6)</sup>)



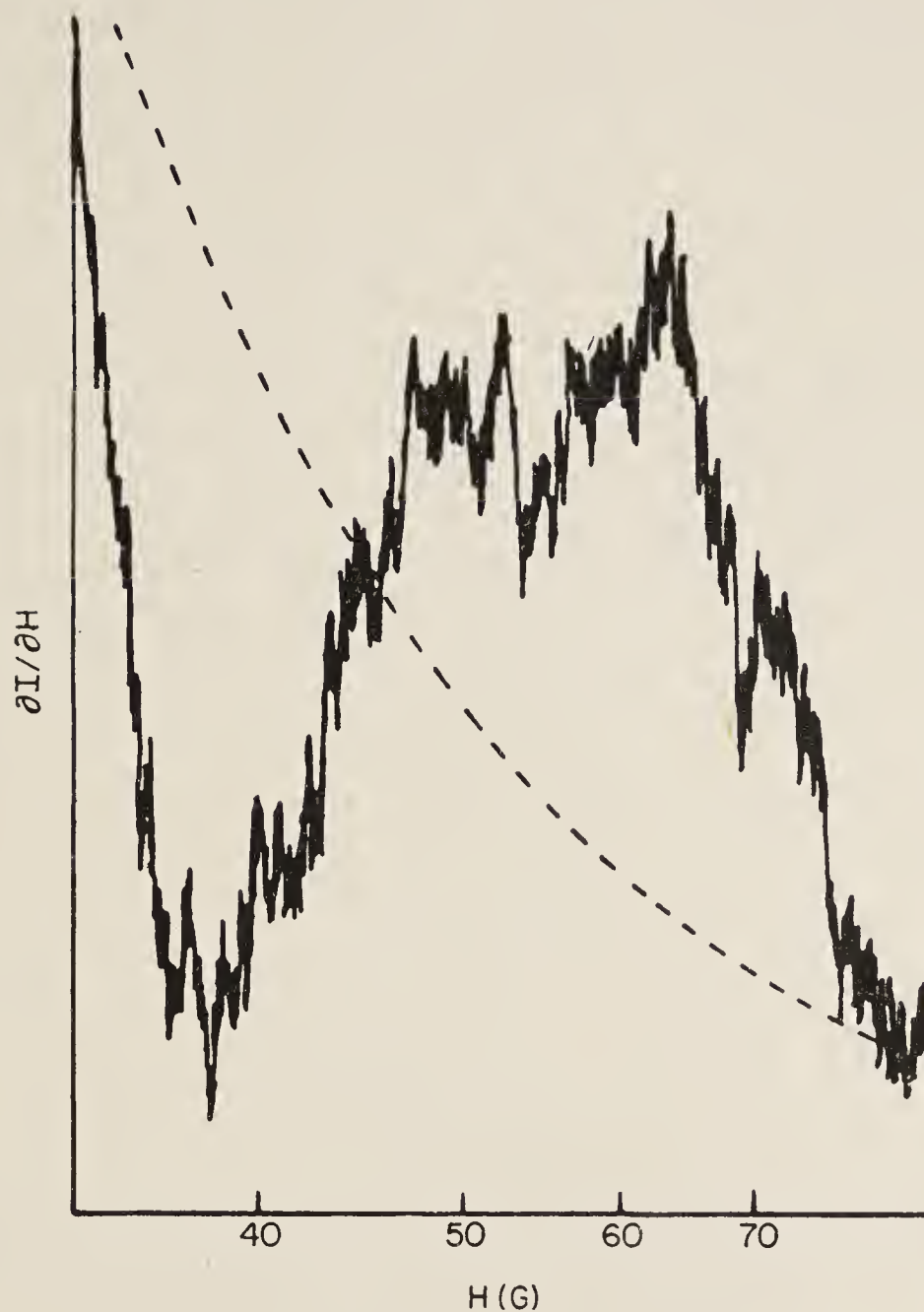


FIG. 11b. The signal extended to higher values of magnetic field. The sensitivity has been increased. The broken line shows the tail of the curve of Fig. 11a. (After Gough and Series.<sup>(6)</sup>)

the tail of the zero-field curve which is shown by the broken line, and the gain has been substantially increased.

Now look at the energy level diagram, Fig. 12, and notice that energy levels having  $\Delta M = 2$  intersect at zero field and at two other places in finite fields. The degeneracy of levels is held to be responsible for the changes in intensity of the fluorescent light. Experimentally, one measures the value of the magnetic field at the centre of the anomaly and calculates the hyperfine constants with the help of the Breit-Rabi formula.

Measurement of the line width is also important. This is generally done for the anomaly at zero field. One can easily calculate the mean lifetime of the excited state from the measured line width.

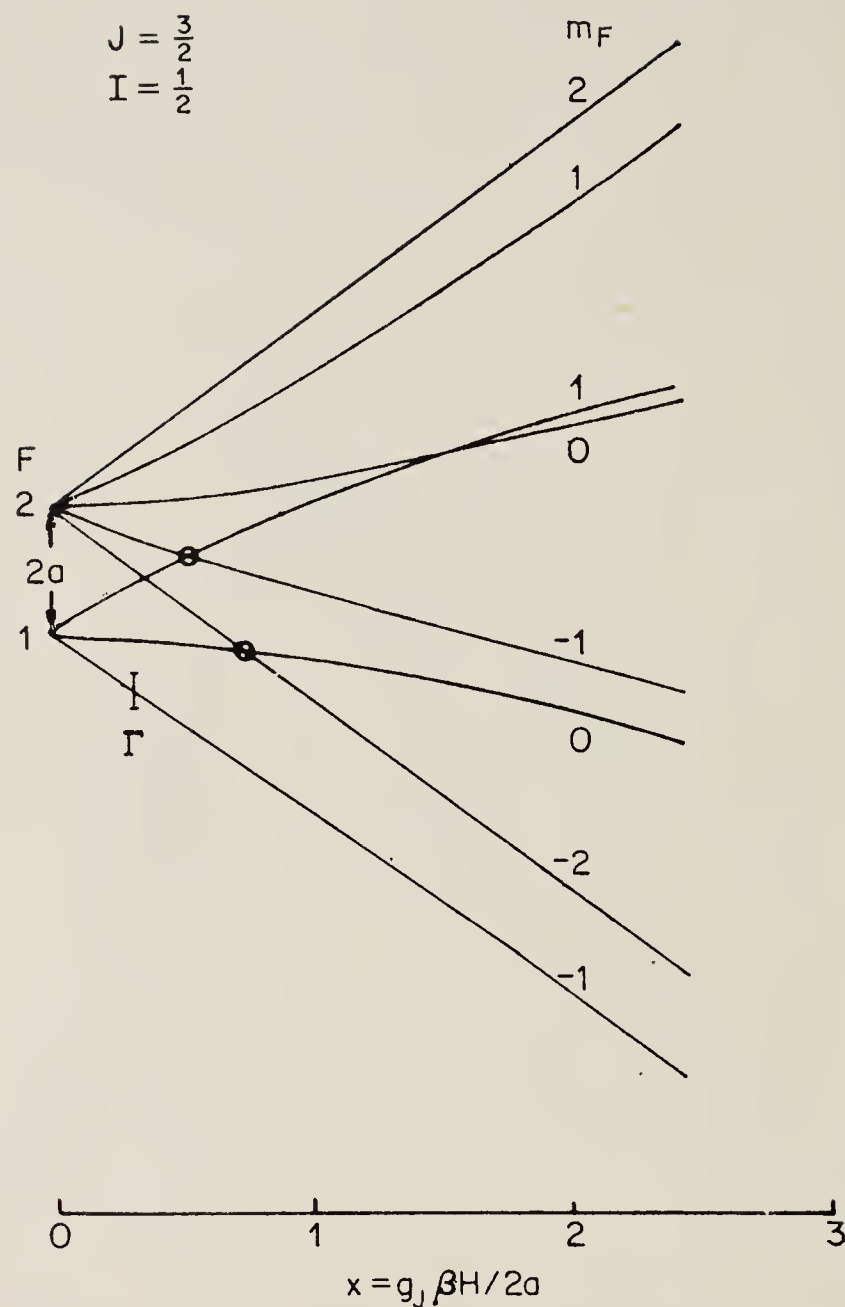


FIG. 12. Decoupling of hyperfine structure by the magnetic field. The vertical bar marked  $\Gamma$  represents the radiation width of the levels.  $a$  is the magnetic dipole constant. The signals of Fig. 11b are attributed to the intersections of levels marked with circles. (After Gough and Series.<sup>(6)</sup>)

#### 4.2. INTERPRETATION OF THE PHENOMENON

It is essentially an interference phenomenon. When the levels are degenerate and under the geometrical conditions specified above, the atoms are excited coherently in two modes and by virtue of this, can radiate coherently in two modes. The interference results in a redistribution in space of the fluorescent light, compared with the distribution when the modes are excited incoherently. The decay rate of the atoms is unaffected: there is no change in the intensity of the fluorescent radiation integrated over space. Notice that the redistribution of light is attributable here to interference whereas in the double resonance experiments it was attributable to the radio-frequency field.

The possibilities for interference are apparent from Fig. 13. The important points are: for the atoms—one initial state, one final state, two intermediate states; for the light—coherence in the incident beam and at the detector.

We can write simple equations based on the notion of pulse excitation which we used before. Suppose an atom is excited at time  $t_0$  by a pulse of polarized



light which allows transitions from a common initial state  $|g\rangle$  to either of two excited states  $|\alpha\rangle$  or  $|\beta\rangle$ . The wave functions for  $|\alpha\rangle$  and  $|\beta\rangle$  develop according to  $\exp -i(k_i - \frac{1}{2}i\Gamma_i)(t - t_0)$  ( $i = \alpha, \beta$ ), where  $k_i$  is the eigenfrequency and  $\Gamma_i$  the damping constant. In many applications (for example, in cases of hyperfine structure), we have  $\Gamma_\alpha = \Gamma_\beta$ . The state vector at time  $t$  for those atoms excited at  $t_0$  is (to within a constant),

$$|t, t_0\rangle = \sum_{i=\alpha, \beta} P_{ig} \exp -i(k_i - \frac{1}{2}i\Gamma) (t - t_0) |i\rangle, \quad (4)$$

where  $P_{ig}$  is the (time-independent) matrix element of the electric dipole operator between the ground and excited state. (This is written as a plausible equation: it can be justified in a number of ways.) The intensity of the light emitted at time  $t$  in such a direction and polarization as to reach the detector will be proportional to  $|\langle f|P'|t, t_0\rangle|^2$ . Thus

$$\begin{aligned} I(t, t_0) \propto & [|P'_{f\alpha} P_{\alpha g}|^2 + |P'_{f\beta} P_{\beta g}|^2] \exp -\Gamma(t - t_0) \\ & + P'_{f\alpha} P_{\alpha g} P'_{\beta f} P_{\beta g} \exp -i(\delta - i\Gamma)(t - t_0) \\ & + \text{complex conjugate}, \end{aligned} \quad (5)$$

where  $\delta = k_\alpha - k_\beta$ .

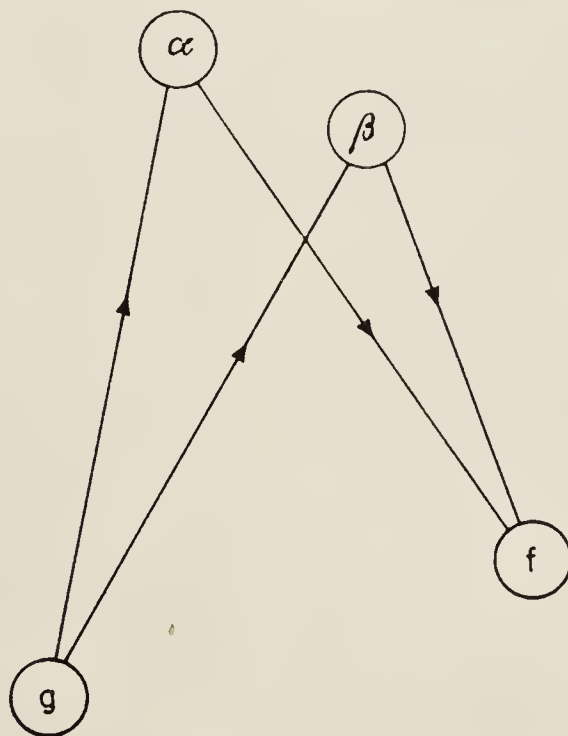


FIG. 13. Resonance fluorescence by two paths from initial state  $g$  to final state  $f$ .

In a steady-state experiment we integrate, as before, over  $t_0$  from 0 to  $t$  and obtain

$$I \propto \frac{(C_1^2 + C_2^2)}{\Gamma} + A \frac{\Gamma}{\Gamma^2 + \delta^2} + B \frac{\delta}{\Gamma^2 + \delta^2} \quad (6)$$



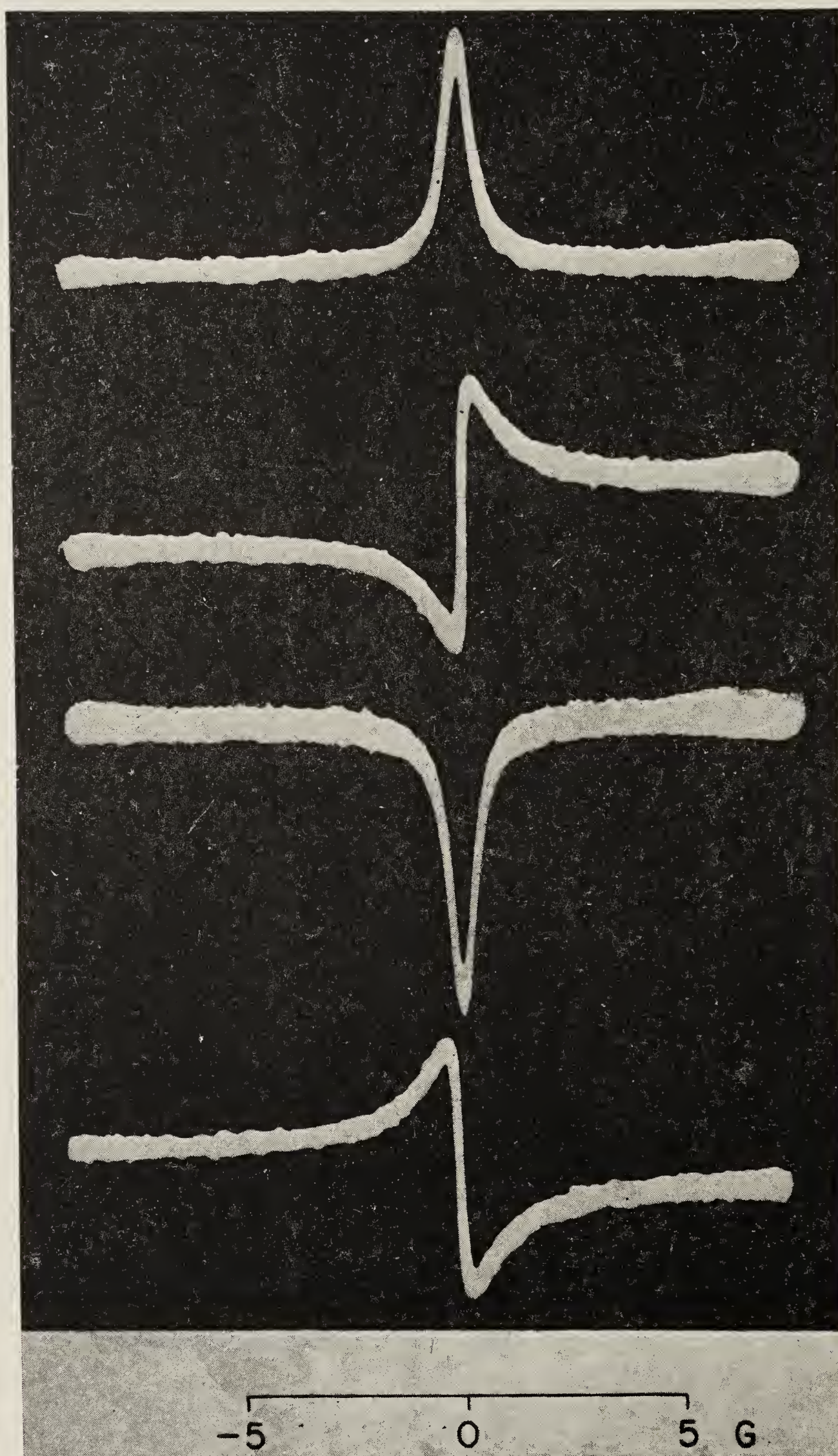


FIG. 14. Zero field level-crossing signals (Hanle effect) for  $6^3P_1$  in mercury. The four curves correspond to rotation of a polarizer in successive steps of  $\pi/4$ . (After Kibble and Series.<sup>(7)</sup>)



where  $C_1 = |P'_{f\alpha} P_{\alpha g}|$ ,  $C_2 = |P'_{f\beta} P_{\beta g}|$ , and  $A + iB = P'_{f\alpha} P_{\alpha g} P'_{\beta f} P_{\beta g}$ . (7)

The first term of (6) is a constant. The second and third are Lorentzian bell-shaped and dispersion functions of  $\delta$ . These are the interference terms, which vanish when  $\delta \gg \Gamma$ . By suitable orientation of polarizer and analyzer one can make either  $A$  or  $B$  vanish. These results are illustrated in Fig. 14,<sup>(7)</sup> which shows a set of experimental curves obtained for the zero-field level-crossing in  $6^3P_1$  states in mercury—the states studied in the Brossel–Bitter experiment.

#### 4.3. DETERMINATION OF LIFETIME

The width at half intensity (the bell-shaped curve) and the distance between the peak and the dip (dispersion curve) is equal to  $2\Gamma$ . For the mean lifetime,  $\tau$ , we have

$$\tau(\text{sec}) = \Gamma^{-1}(\text{radians per sec})^{-1} \quad (8)$$

The method of studying the zero-field level-crossings is, in principle, very attractive for the determination of lifetimes because the sole perturbation on the atoms is the incident light, which is a negligible effect in comparison with spontaneous emission. But in practice there are a number of difficulties:

- (i) admixture of the bell-shaped and dispersion curves,
- (ii) multiple scattering of resonance radiation. This leads to an anomalous narrowing of the curves called “coherence narrowing”
- (iii) distortions caused by non-uniform spectral distribution of the incident light.

We shall discuss these problems in a later section. In practice, the method can be applied to measure lifetimes to a precision of 1 % in favourable cases.

#### 5. ANTICROSSINGS

There is nothing in the above analysis which requires the levels to be of different  $M$ —the interference terms still exist if the levels have the same value of  $M$ . But, in time-independent perturbation theory, “levels of the same  $M$  never cross”. If we are considering the breakdown of  $I$ – $J$  coupling, for example, the hyperfine interaction  $a\mathbf{I} \cdot \mathbf{J}$ , which has non-vanishing matrix elements between states of the same value of  $M = (M_I + M_J)$ , causes repulsion of such levels. Nevertheless, a pair may approach one another to within their natural width, and in this case the interference effect is not negligible. Such a situation is called an “anticrossing”.<sup>(8)</sup>

In the region of an anticrossing the wave functions of the perturbing states are changing rapidly. For this reason it is easier to base an analysis on the unperturbed states, say  $|a\rangle$  and  $|b\rangle$ . The optical matrix elements to  $|a\rangle$  and  $|b\rangle$  vary only slowly through the anticrossing. Calculation of the change in

intensity of the fluorescent light shows that the interference effect has its greatest value when either  $|a\rangle$  or  $|b\rangle$  alone are populated. The interference signal has the analytical form  $|2V|^2/(\gamma^2 + \delta^2 + |2V|^2)$ , where  $|2V|$  is the interval between the levels at their closest approach (a measure of the perturbation energy). This expression should be compared with eqn (3) which describes a double resonance curve. The two have exactly the same form. An anticrossing signal is the same as a double resonance signal, but in the one case the perturbation is internal ( $|2V|$ ), and in the other, external ( $\gamma H_1$ ). (See Fig. 15)

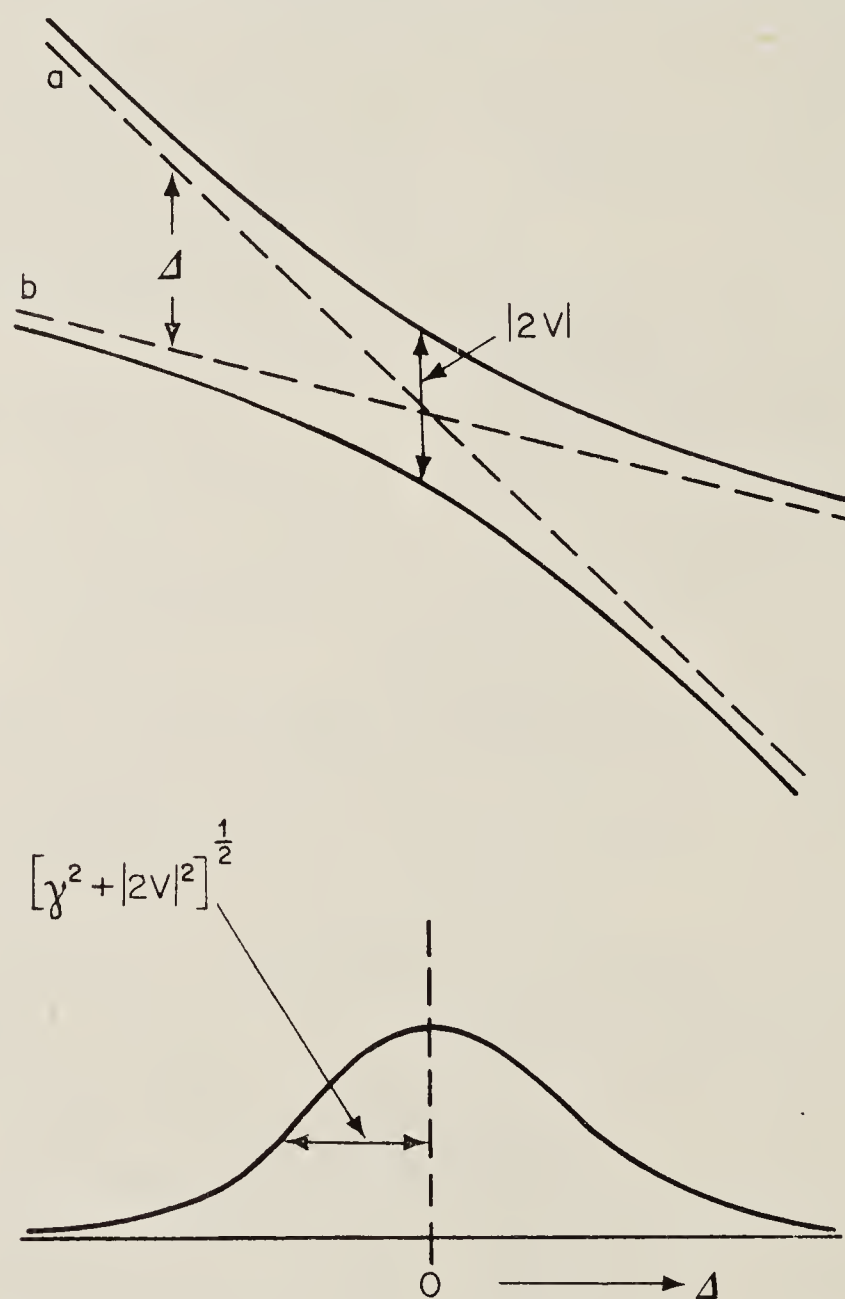


FIG. 15. An “anti-crossing” of energy levels and the corresponding fluorescence signal whose analytical form is given in the text. Here,  $\gamma$  is the damping constant.

It is to be noticed that anticrossing signals are broader than crossing signals, and are not suitable for the measurement of lifetimes. On the other hand, they can be analysed to yield the hyperfine interaction constants.

## 6. GROUND STATES: OPTICAL PUMPING

We have described methods which allow the study of excited states of atoms. To complete our preliminary review we describe some typical experiments in which the ground states of atoms are the focus of interest. Therefore we must choose as a suitable substance one whose atoms have structure in the ground



states. (The even isotopes of mercury, which served as an example before, have a ground state without structure.)

The alkalis have the required structure. Rubidium serves as an excellent example because its vapour pressure at ordinary room temperatures is about right for the experiments we shall describe.

### 6.1. THE PUMPING PROCESS

Consider an assembly of atoms which have undergone resonance fluorescence by anisotropic excitation followed by spontaneous emission, which is an isotropic perturbation. In principle, we have injected anisotropy into the system; that is, we have altered the distribution of atoms over the ground states. We have, therefore, prepared the system for magnetic resonance experiments.

Points of detail will emerge by considering a simple experiment. (See Fig. 16) The bulb contains rubidium vapour at a pressure of about  $10^{-6}$  torr. (It

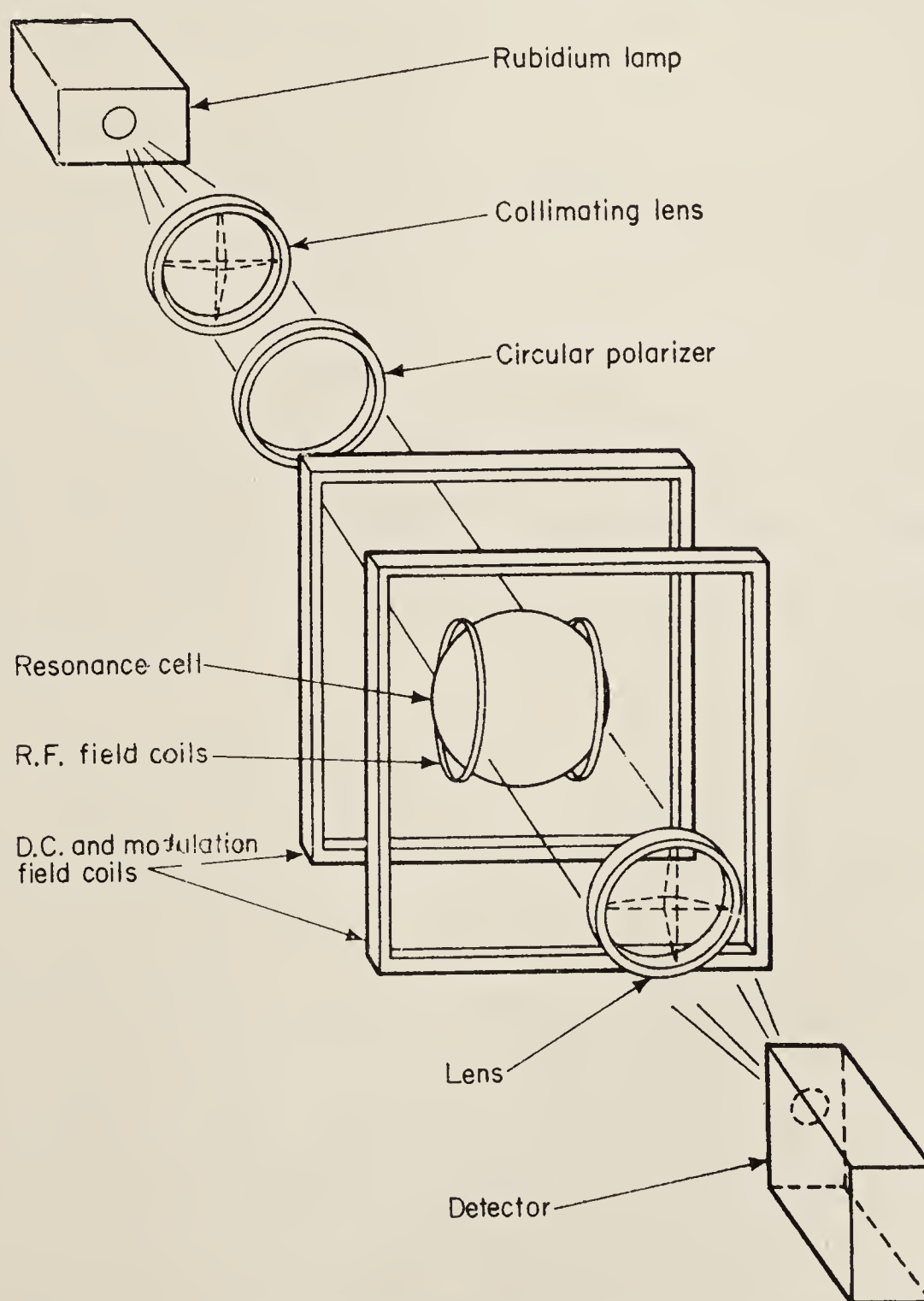


FIG. 16. Apparatus for studying optical pumping in rubidium.

also contains a noble gas at a pressure of a few torr for a reason we shall shortly explain). It is illuminated with light from a rubidium lamp which passes through a circular polarizer. The mounting allows a magnetic field to be applied in the direction of the incident light, and also enables this direction to be aligned with the Earth's field, since this is by no means to be ignored.

The optical transitions are indicated in Figs. 17a and b which, for the sake of simplicity, ignore hyperfine structure. It is clear that, if the atoms are excited by  $\sigma^+$  light and decay by spontaneous emission without any other perturbation, the net result of one cycle will be to transfer atoms from the ground

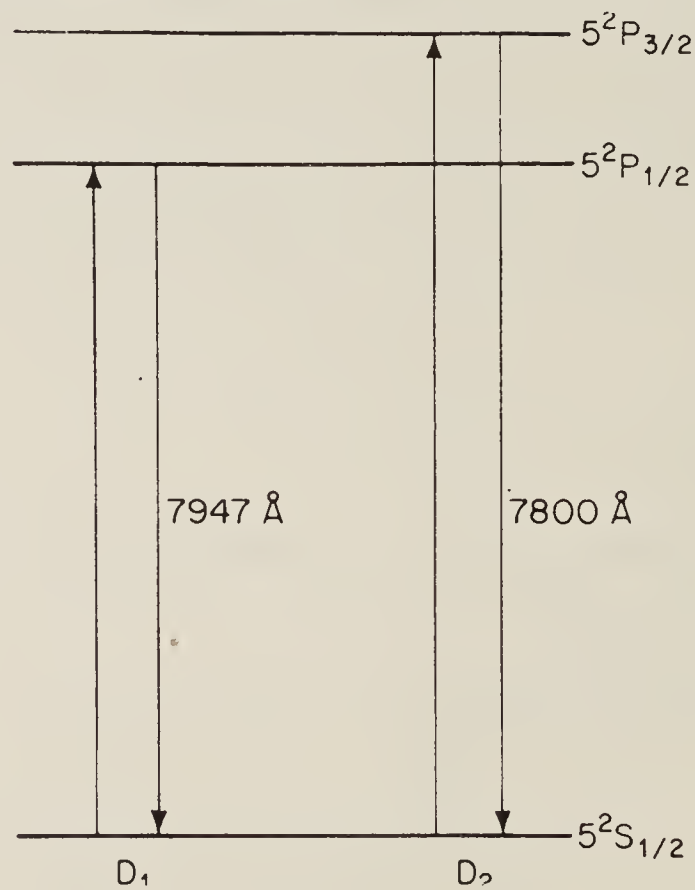


FIG. 17a. Resonance fluorescence of the principal doublet in rubidium.

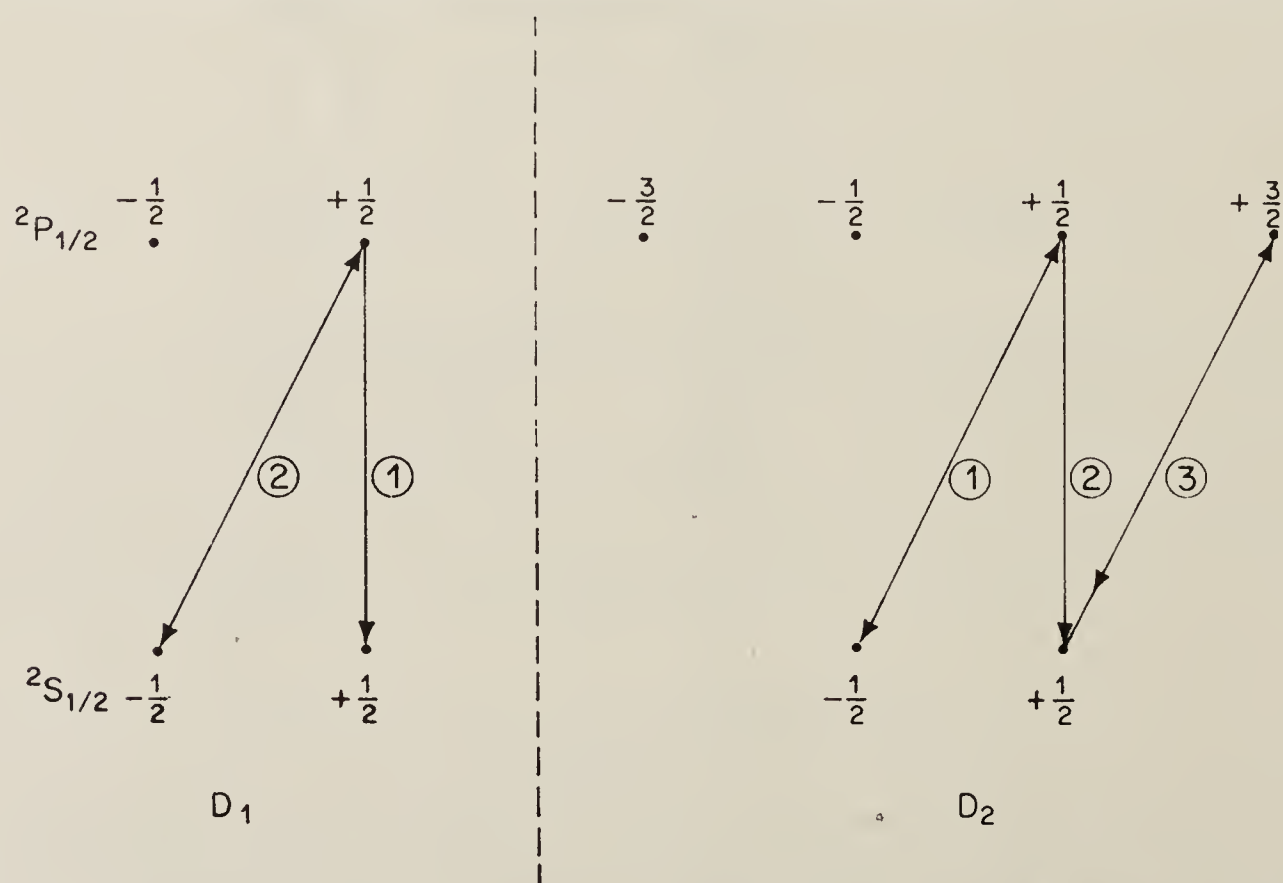


FIG. 17b. Transitions induced by excitation with circularly polarized light. The numbers indicate relative transition probabilities.



state  $|- \frac{1}{2}\rangle$  into  $|+ \frac{1}{2}\rangle$ . This may be expressed quantitatively. Starting from equal populations of the two states, the  $D_1$  light alone will produce a 20:40 mixture, while the  $D_2$  light alone will produce a 10:50 mixture. The two effects are additive. (We shall reconsider this point when we investigate the effect of the noble gas.)

## 6.2. RADIO-FREQUENCY RESONANCE

Having established a difference of population, we can now contemplate a resonance experiment. Coils, as shown in Fig. 16, provide an oscillating field at right angles to the direction of the light beam. The required field amplitude is only of the order of milligauss, since the atoms have lifetimes of the order of milliseconds (we discuss this below). The frequency may be of the order of kHz if we are studying transitions between Zeeman components, or of the order of  $10$  to  $10^3$  MHz if we are studying hyperfine transitions. Signal generators will frequently provide enough power.

## 6.3 MONITORING THE RESONANCES

The r.f. field alters the populations of the levels, and this may be detected

- (i) by its effect on the fluorescent light (but this method will not be applicable if the bulb contains a gas), or
- (ii) by its effect on the absorption coefficient of the vapour.

This latter method has been most commonly used, and is illustrated in Fig. 16. The same light which does the pumping also monitors the resonance. Reference to Fig. 17 shows that the amount of circularly polarized light absorbed depends on the distribution of atoms between the ground states. The resonance is indicated by changes in the current of the photocell placed behind the resonance vessel.

## 6.4. DISCUSSION OF THE RESONANCES

Fig. 18 is an oscilloscope trace of resonances obtained with apparatus of this sort. It is rather a crude picture, but it brings out important points. Notice the following:

- (i) stray fields have been compensated to about 2 mG. The only remaining field is the longitudinal field shown on the scale;
- (ii) R.f. frequency: 5 kHz. Amplitude: a few mG;
- (iii) there is a peak at zero field which needs to be explained;
- (iv) resonances at  $\pm 10.7$  mG are due to  $^{85}\text{Rb}$ , at  $\pm 7.0$  mG due to  $^{87}\text{Rb}$ ; (natural abundances 72 %, 28 %; nuclear spins 5/2, 3/2;  $g_F$ , 1/3, 1/2; respectively);

- (v) resonance line-widths are  $\sim 2$  mG ( $^{85}\text{Rb}$ )  $\sim 1$  kHz, so that  $\tau \sim 10^{-4}$  sec (assuming the line is homogeneously broadened);
- (vi) the small wiggles are due to pick-up from the mains, showing that the time for traversing the sweep was of the order of seconds. This is necessary in order to avoid distorting the resonances, and emphasises the relatively large value of  $\tau$ .

Consider point (iii). Near zero field the energy levels are degenerate or near-degenerate. There are stray transverse static fields and also transverse, low-frequency oscillating fields from the electrical mains. These can stimulate a resonance at zero frequency (or 50 Hz). These stray fields can account for the peak at zero field.

Some conceptual difficulty may still remain. While it is easy to use quantum labels  $M_F$  for non-degenerate levels, and to understand transitions between them, can one still use such language when the levels are degenerate? The answer is yes, for one can choose a quantum axis arbitrarily, and describe any experiment thereby, provided one takes proper account of the perturbations. Here, we choose an axis along the light beam and describe the optical transitions with reference to that axis. We notice that the magnetic field may be skew to the axis and we use a formalism which takes account of that, namely, magnetic resonance transitions at zero frequency. We could equally well

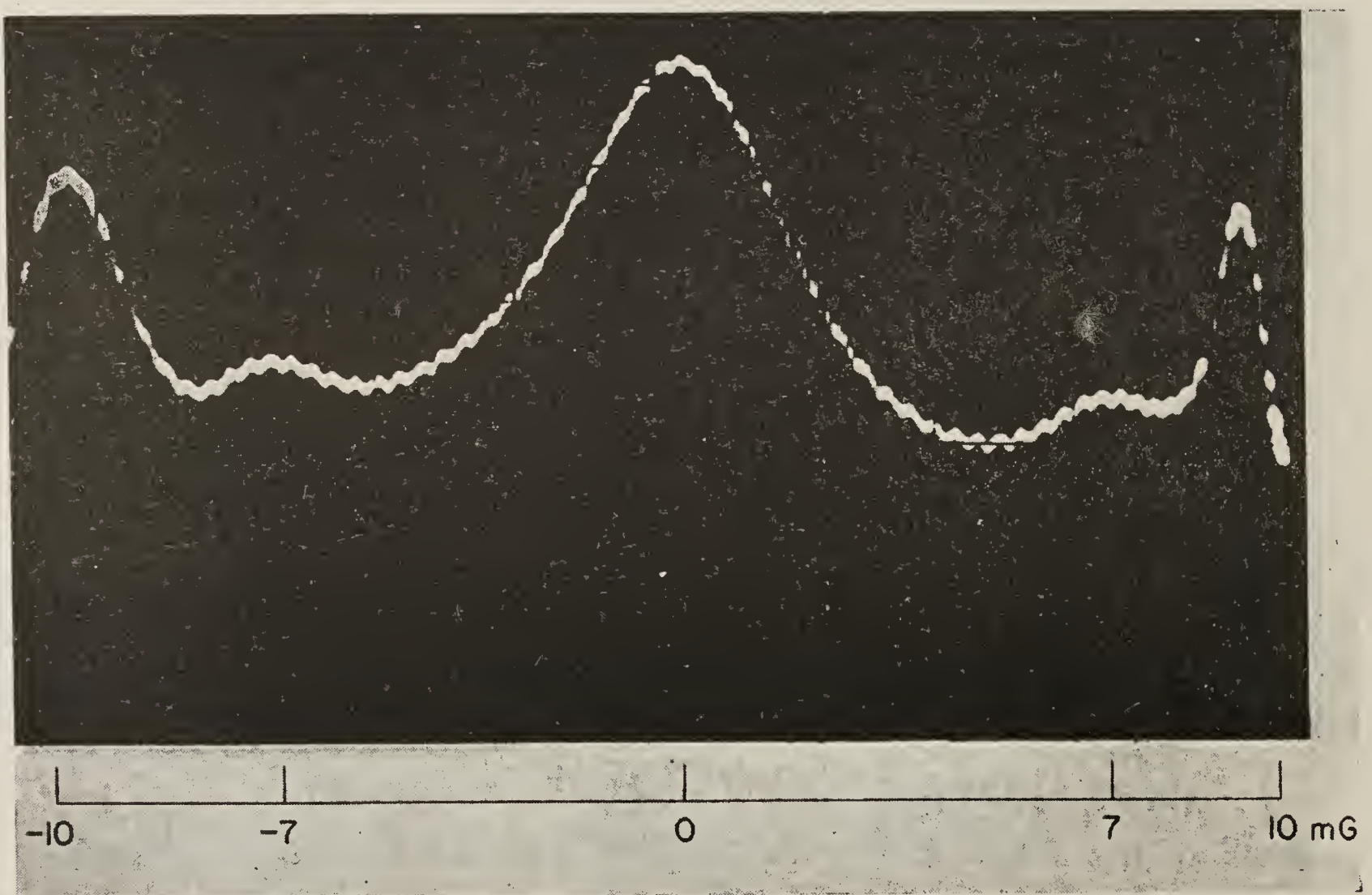


FIG. 18. Oscillogram demonstrating radio-frequency resonances in the ground state of rubidium studied by optical pumping. Resonances at  $\pm 7$  mG correspond to  $^{87}\text{Rb}$ ; those at  $\pm 10.7$  mG to  $^{85}\text{Rb}$ ; for other features see text.



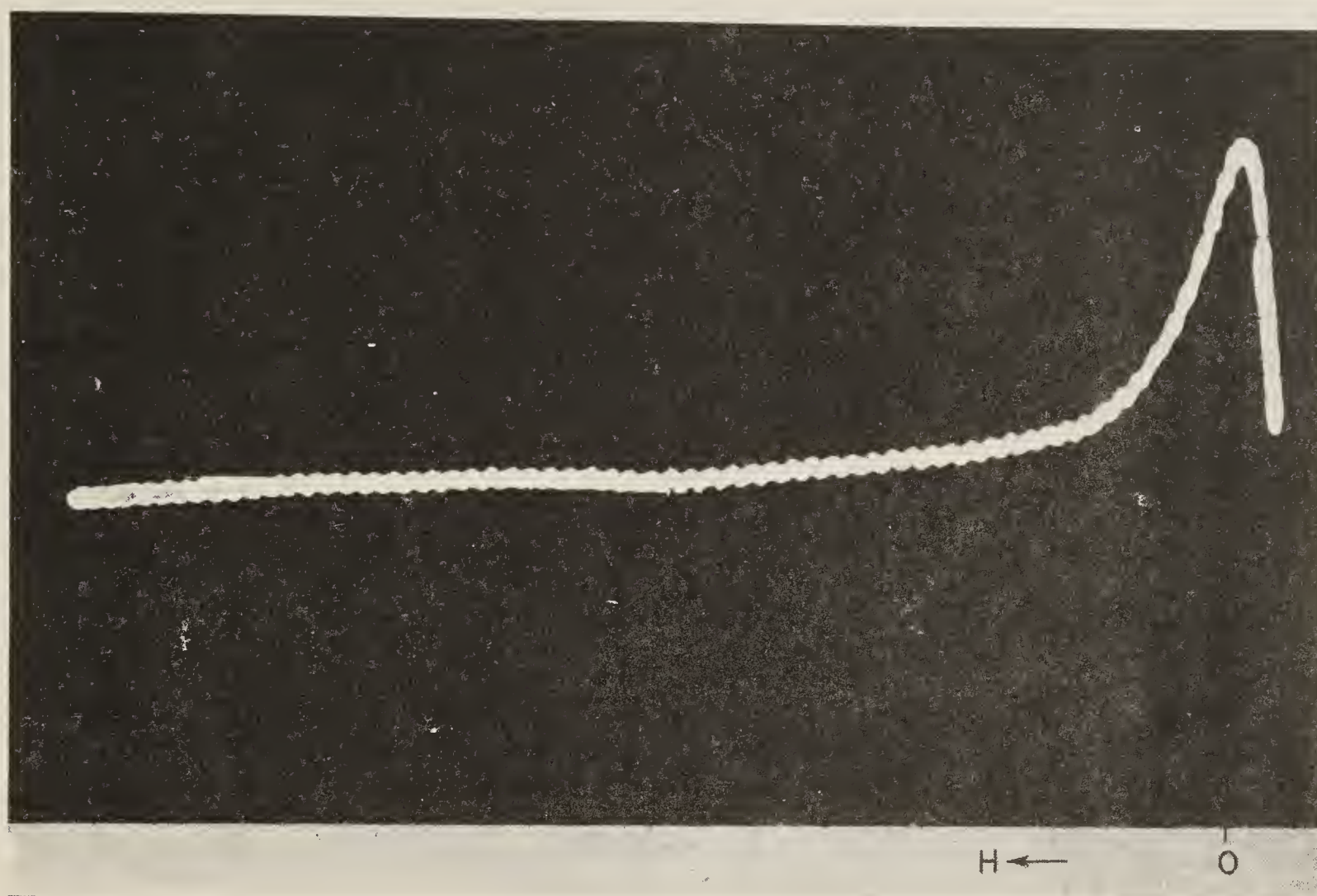


FIG 19a. Optical pumping signal in rubidium. No r-f field.

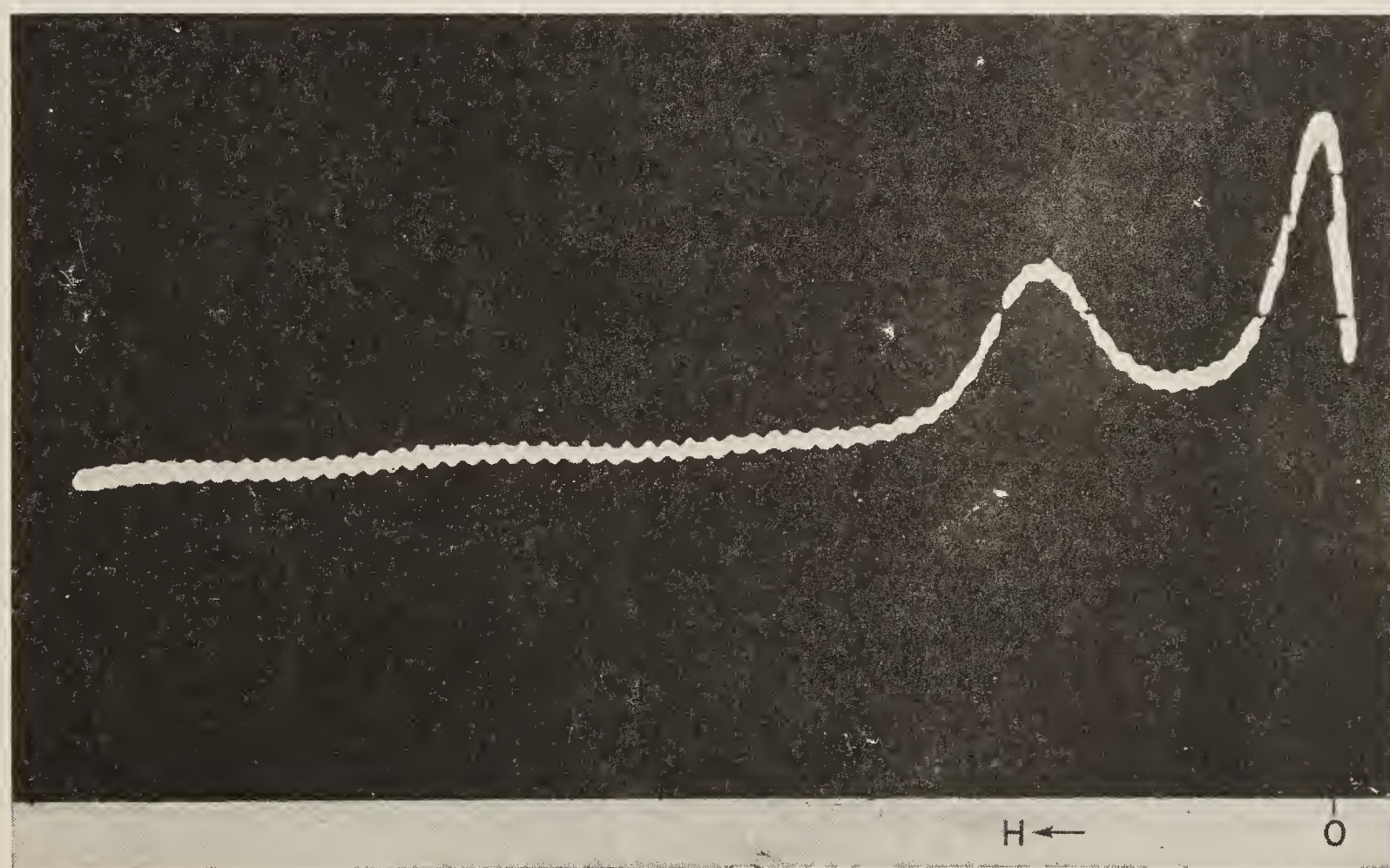


Fig. 19b. Resonance at a frequency of 3 kHz.



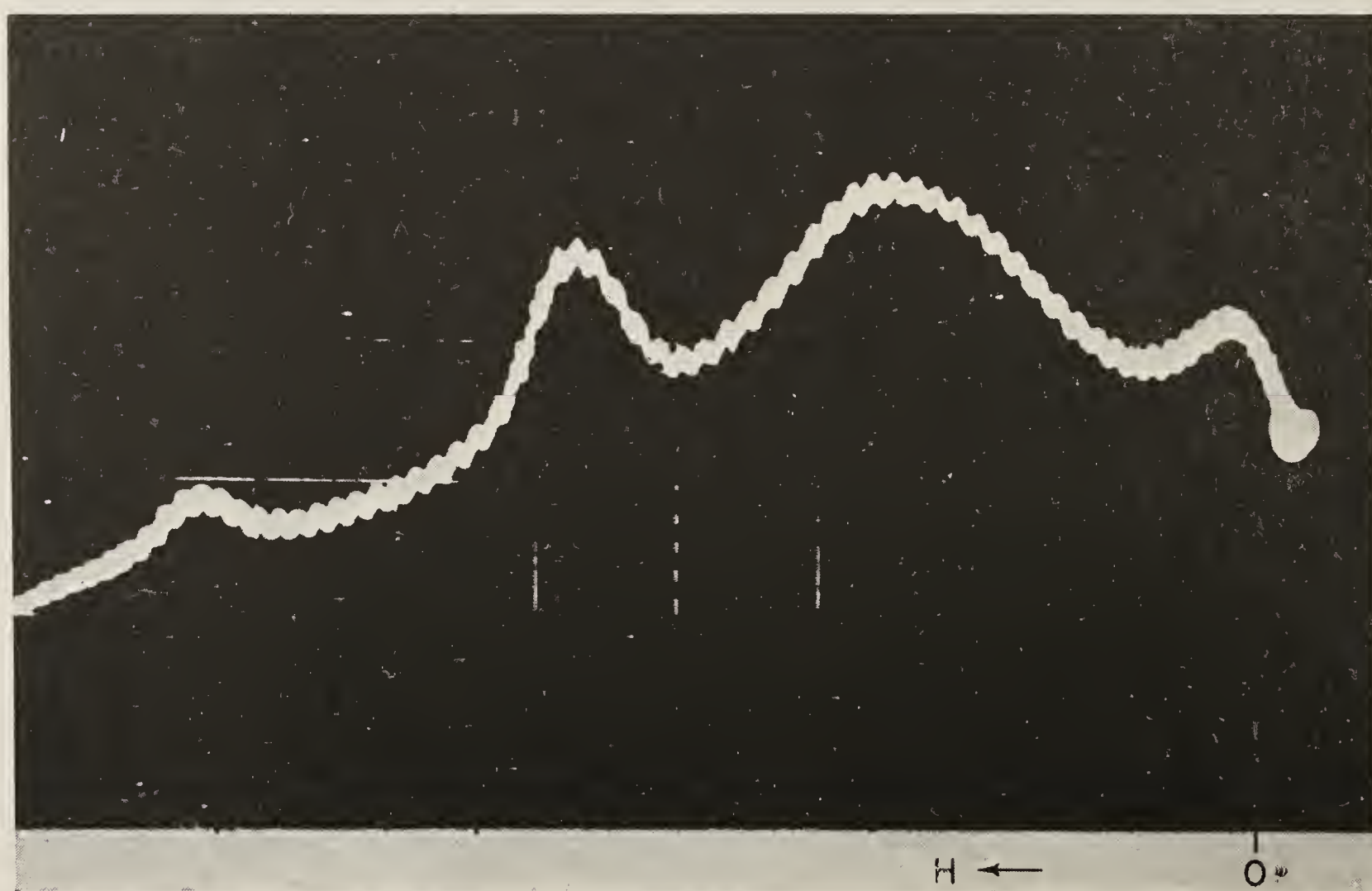
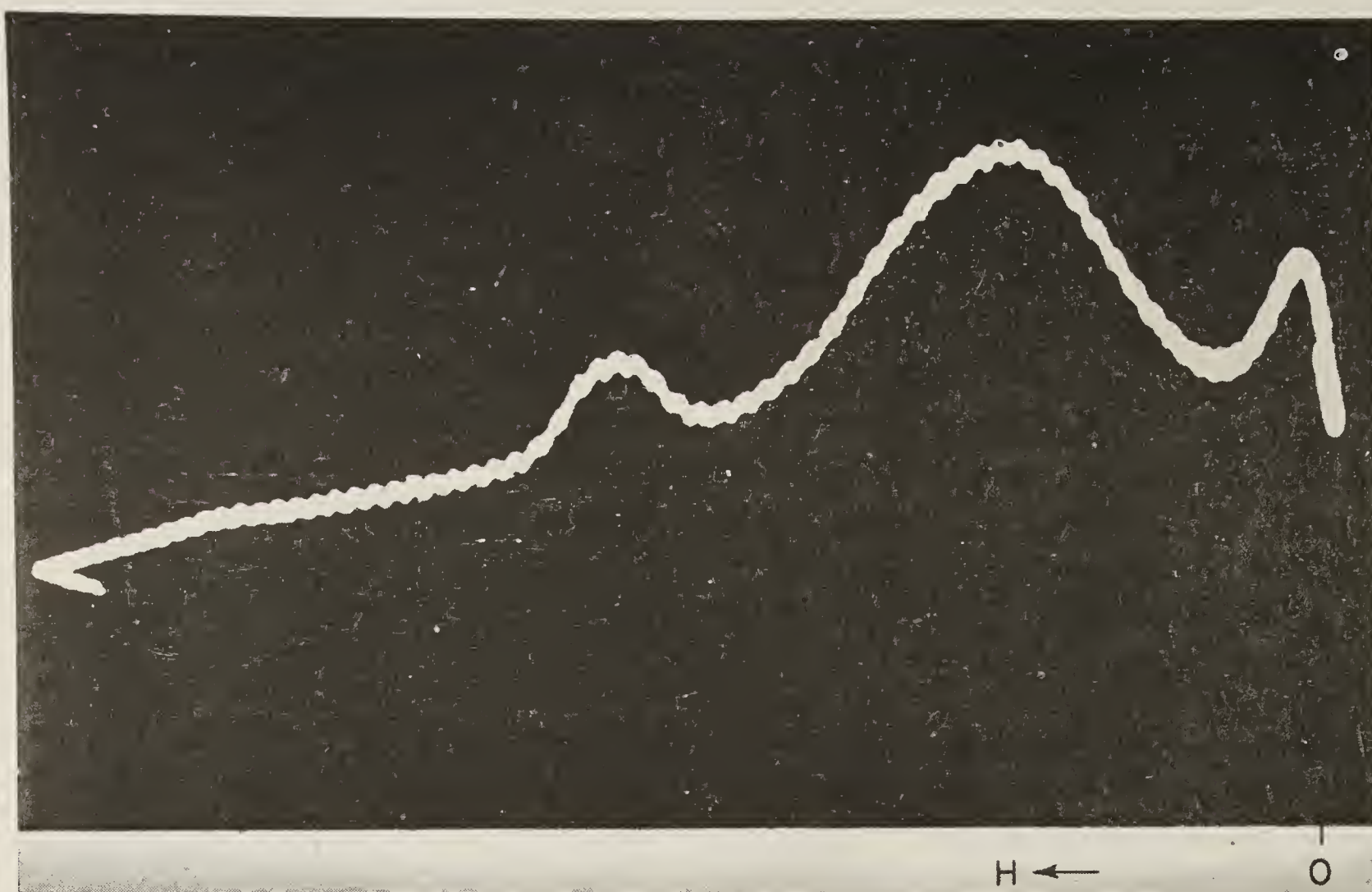


FIG. 19 c, d. The effect of increasing r-f power: resonances at multiples of the field  $H_0$ .



describe these transitions by writing equations for rotating the axis from the longitudinal to the skew direction. Alternatively, we might choose an axis in the skew direction and describe the optical transitions with reference to such an axis, but we would have to remember that, on account of the degeneracy, there may be coherence between different optical transitions.

The fields of work opened by resonances such as shown in Fig. 18 are:

- (a) precision measurement of  $g$ -values of atoms in ground states, (and, correspondingly, of hyperfine intervals);
- (b) measurement of nuclear spins. (The values of  $g_F$  may be determined from the measurements. Then, if  $g_J$  is known,  $I$  may be deduced);
- (c) precision magnetometry and atomic clocks;
- (d) studies of relaxation processes by measurement of the line width under different conditions. We shall elaborate on this.

### 6.5. MULTIPLE QUANTUM RESONANCES

We now illustrate in Fig. 19 an effect which can arise very easily in ground state optical pumping experiments, and can lead to mistaken identification of resonances. This is the occurrence of what appear to be harmonic resonances.

The magnetic field sweep is the same as in Fig. 18, but the zero has been displaced to the right. The radio-frequency has been reduced from 5 to 3 kHz. The figures a, b, c, d are taken with increasing r.f. power, starting from zero. Curve (a) is the zero-field resonance. In (b) is seen the resonance of  $^{85}\text{Rb}$ , as in Fig. 18 but at a field  $H_0$  about 6.4 mG. The resonance of  $^{87}\text{Rb}$  is unresolved.

Increasing r.f. power, Figs. 19 (c) and (d), brings up resonances at approximately  $2H_0$  and  $3H_0$ . (They are not exactly at integral multiples of  $H_0$ , but the small displacements are not our present concern). These might have been due to harmonics in the oscillator, but this possibility was excluded. They are

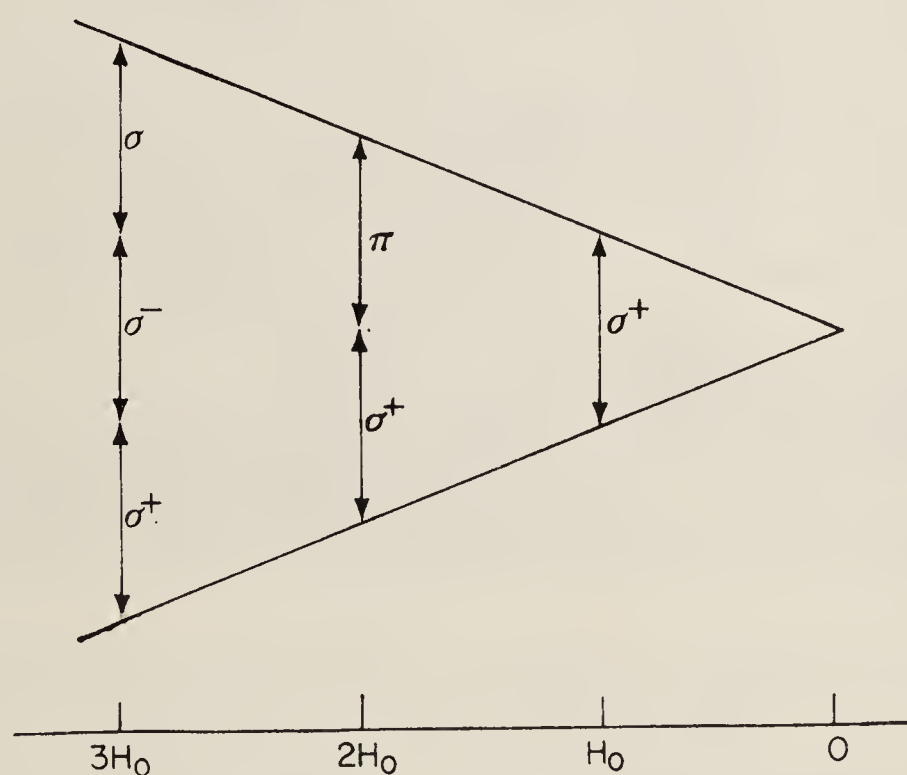


FIG. 20. The resonances interpreted as multiple quantum transitions.

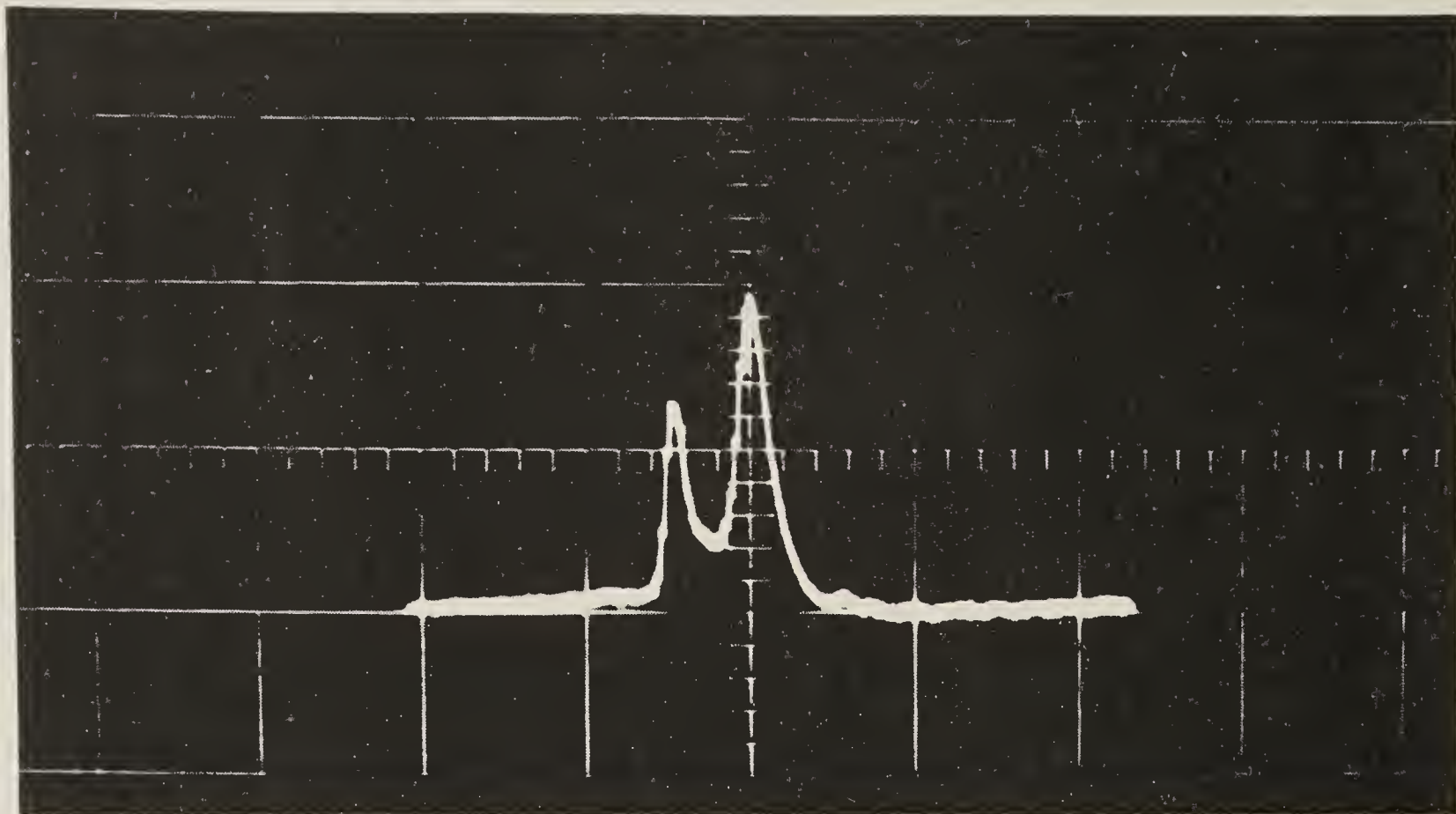


FIG. 21a. Resonance at 5 kHz produced by rotating field. (The zero field signal is also present).

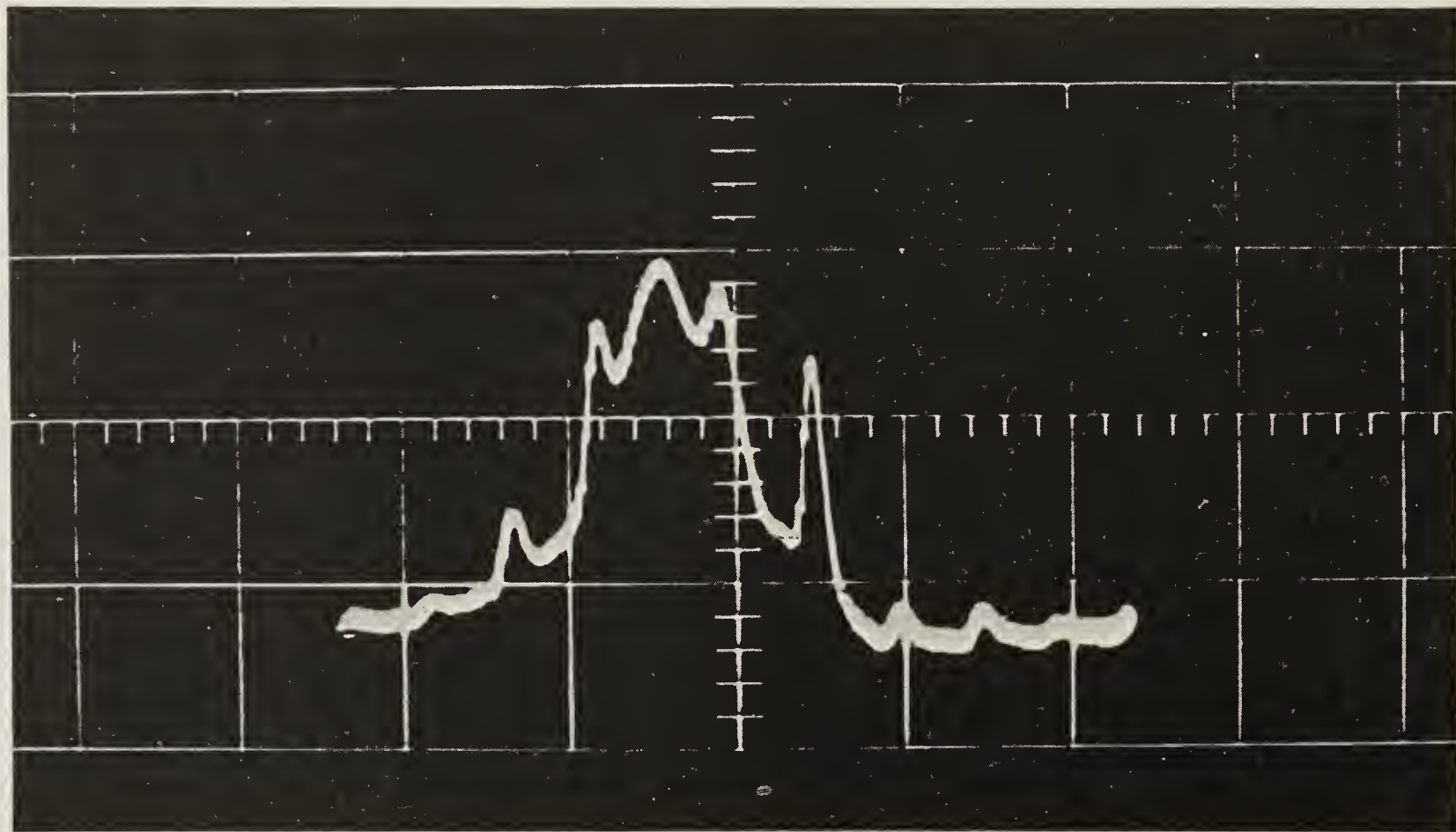


FIG. 21b. Effect of increasing r-f power. The dominant resonance is undisplaced but greatly broadened. Numerous subsidiary resonances appear; the zero field signal is displaced slightly to the left (see Fig. 42).



interpreted as multiple quantum transitions between a pair of levels having  $\Delta M = \pm 1$ , and require for their interpretation the existence of components of the r.f. field *other than* the rotating field which is responsible for the primary resonance at  $H_0(\sigma^+ : \Delta M = \pm 1 \text{ in absorption})$ .

Figure 20 shows how a component of the oscillating field parallel to the static field ( $\pi : \Delta M = 0$ ), combined with  $\sigma^+(\Delta M = \pm 1)$ , can satisfy the conservation of energy and of angular momentum at a field  $2H_0$ , while the counter-rotating component  $\sigma^-(\Delta M = -1 \text{ in absorption})$  can combine with  $2\sigma^+$  to satisfy the conservation laws at  $3H_0$ .

In Fig. 21a. is a resonance curve taken with an arrangement of coils designed to produce a rotating field ( $\sigma^+$  alone). The frequency is now 5 kHz and zero field has been shifted to the centre. The zero field resonance is seen as well as the resonance at about 10 mG due to the rotating field. This should be compared with Fig. 18 where the resonances appear on both sides of zero because an oscillating field was used.

In Fig. 21b. the r.f. field strength has been greatly increased. A variety of resonances appear at fields up to  $5H_0$  on the left and  $4H_0$  on the right. These are due to small  $\sigma^-$  and  $\pi$  components arising from the non-uniform field of the coils, and acting with the  $\sigma^+$  component to generate the resonances.

These multiple quantum transitions should not be confused with the multiple quantum transitions described above (Section 3.1 and Fig. 4b). In the present case we have transitions between atomic eigenstates induced by different components of the r.f. fields, acting coherently. In the former case we had transitions via non-resonant intermediate states of the atom induced by one particular component of the field.

These multiple quantum transitions have been studied by a number of authors.<sup>(9, 10)</sup>

## 6.6. WIDTH OF RESONANCE CURVES: RELAXATION TIMES

We have been concerned with the *occurrence* of resonances. We now return to the question of their *width*.

One might expect the width to be determined by the inverse of the time of flight of atoms across a resonance cell ( $\sim 10^{-4}$  sec, for example). In fact, resonance curves are frequently studied whose width corresponds to times of the order of 1 sec. This is generally achieved by using *wall coatings* or *buffer gases*. The important fact is that, in many cases of interest, it is possible for atoms to undergo many thousands of collisions either with gas molecules, or with the coated wall, without losing their orientation. This is generally true for atoms whose ground states are *S* states (such as the alkalis). Their orientation arises from the electron and nuclear spin, but the spherical symmetry of the distribution of charge isolates the spins from the effects of collision.

Substances chosen for wall coatings are chemically inert materials such as

paraffin hydrocarbons. Similarly, noble gases at pressures from a few torr up to atmospheres are used for buffer gases.

### 6.7. PUMPING CYCLE WITH BUFFER GASES

The use of buffer gases has important consequences for the mechanism of the pumping process, since excited states (which will be  $P$  states if the ground states are  $S$ ) are not inert under collisions with buffer gases. When the pressure of the gas is raised to the point where the time between disorienting collisions is comparable with the radiative lifetime of the pumped atoms, the changes of population induced by optical pumping are radically changed. The situation is usually analysed by assuming that collisions result in the random orientation of excited atoms—equal population of the states  $|M_F\rangle$  or  $|M_J\rangle$ . This is an oversimplification, but it gives useful qualitative results.

If all excited states are equally populated and decay at the same rate, then all the ground states are replenished at the same rate (whatever the coupling scheme). It follows that differences of population between ground states can only be established through different rates of excitation and this raises a difficulty when the ground states are  $S$  states. The intensity sum rules guarantee that if the absorption from an  $S$  state is summed over a multiplet (e.g.  $S_{1/2}$  to  $P_{1/2}$  and  $P_{3/2}$ ), the transition rates from all components of the ground state are equal. (This may be verified by adding the transition probabilities in Fig. 17). Therefore, in order to achieve differences of population one must have light whose spectral distribution over the fine structure components is non-uniform. This is commonly achieved by the use of interference filters or absorption cells. Under some conditions the required change of spectral profile occurs as the pumping light traverses the vapour in the resonance vessel.

### 6.8. HYPERFINE PUMPING

Hyperfine pumping is another variant of the optical pumping method which relies on non-uniform spectral distribution of the pumping light. Suppose the hyperfine components in an absorption line are optically resolvable (resonance lines of rubidium, for example), it is then sometimes possible to find a lamp (often an isotope of the same element) whose spectrum covers the hyperfine components unequally ( $^{85}\text{Rb}$  (lamp) and  $^{87}\text{Rb}$  (sample)). In such a case, light of any polarization will produce an inequality of population between hyperfine states of the ground level. The hyperfine intervals in zero field can now be studied by magnetic resonance, just as for the excited states. The relaxation mechanisms for hyperfine transitions may be different from those for Zeeman transitions. The intensities of the resonances are a measure of  $\langle \mathbf{I} \cdot \mathbf{J} \rangle$ .

### 6.9. SPIN EXCHANGE

We have described how atoms can be oriented by light. An important exten-



sion of the technique due to Dehmelt was the discovery that atoms of one species can be oriented through collisions with atoms of another species which themselves have been oriented by light. Thus, for example, with a mixture of sodium and rubidium vapours in a vessel, the sodium can be oriented by illuminating the bulb with rubidium light. Moreover, r.f. resonances in the sodium may be monitored with the rubidium light because the sodium atoms which have interacted with the radio-frequency field themselves interact with the rubidium atoms.

An important application of this spin-exchange technique is in the study of substances which cannot themselves be oriented by light, or for which there are technical difficulties. Among the substances so studied are atomic hydrogen (and its isotopes) and free electrons.

#### 6.10. METASTABILITY EXCHANGE

Closely related to spin-exchange is metastability-exchange, first studied by Colegrove *et al.*<sup>(11)</sup> We shall illustrate this and the following sections by reference to the experiments of Greenhow.<sup>(12)</sup>

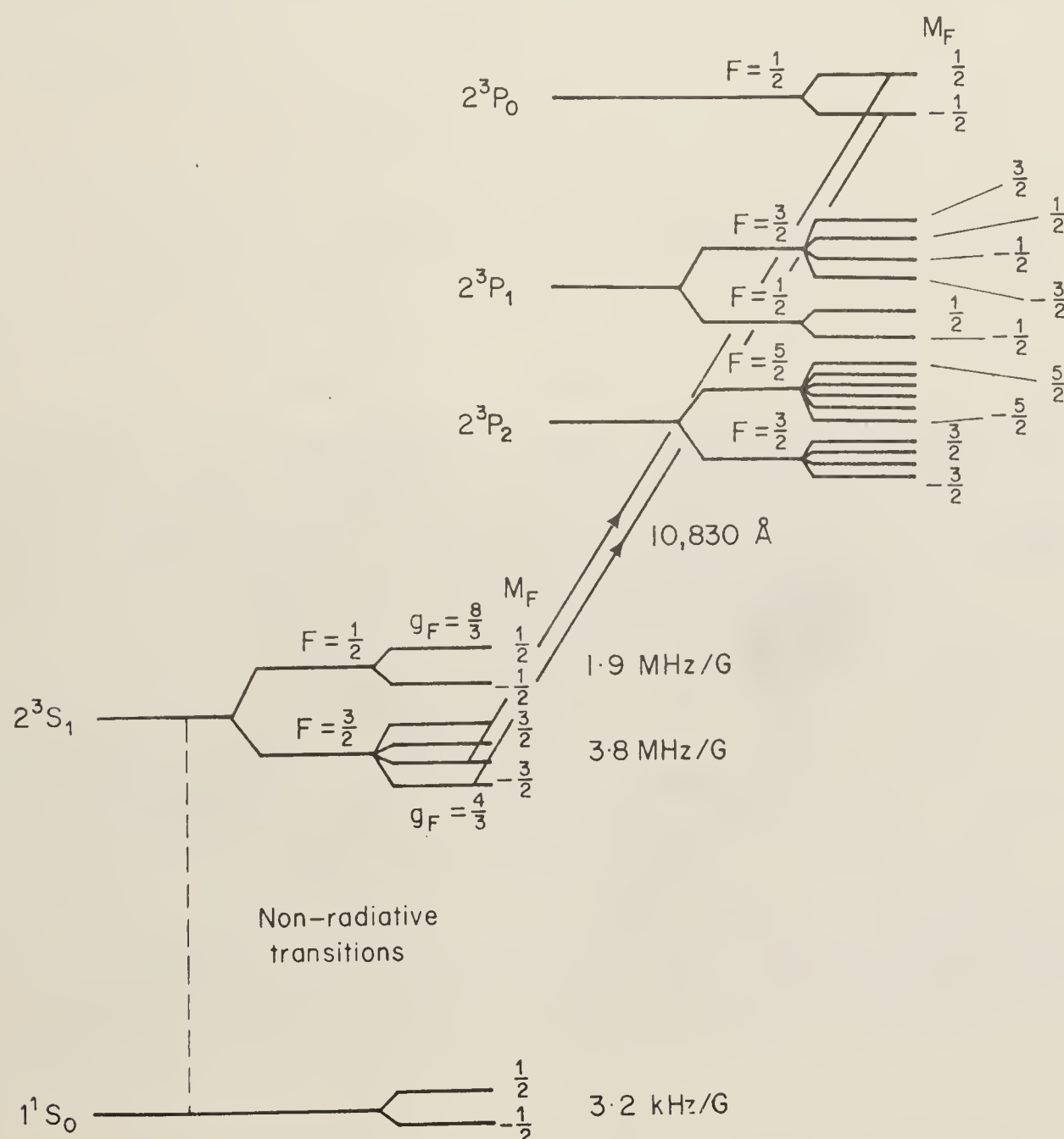


FIG. 22. Term diagram of  $^3\text{He}$  showing optical pumping from the metastable state  $2^3S_1$ .

Optical pumping is performed from the metastable state  $2^3S_1$  which is populated (with random orientation) in a discharge in helium gas at a pressure of a few torr (see Fig. 22). Illumination with circularly polarized light at 10,830 Å or 3889 Å from a helium lamp produces polarization of the metastable atoms through the intermediacy of the excited states  $2^3P$  or  $3^3P$  respectively. The polarization is reflected in the population of the hyperfine states of  $2^3S_1$ , and if the  $I$ - $J$  coupling is not broken down by an external field, the nuclei will also be polarized. When these metastable atoms collide with the much more numerous atoms in the ground state,  $1^1S_0$ , there is a probability that the excitation energy will be transferred without affecting the nuclear polarization. Such collisions establish a nuclear polarization in the ground state.



FIG. 23a. Nuclear resonance at a frequency of 1 kHz in the ground state of  $^3\text{He}$  (this curve was taken with modulated light: see Section III 6.3).  
(After Partridge and Series. *Proc. phys. Soc.* **88**, 983 (1966).)

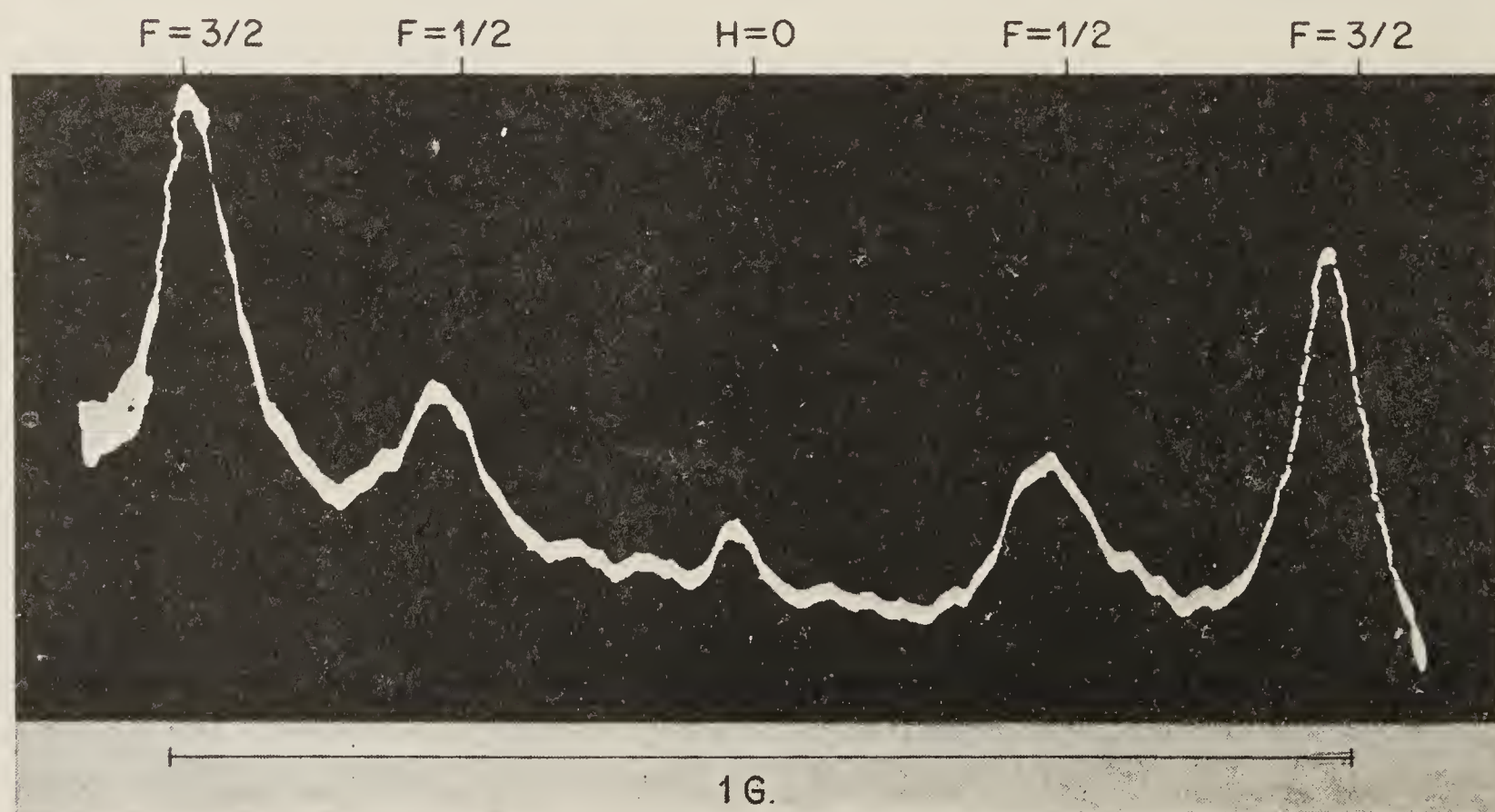


FIG. 23b. Resonances at 1 MHz in the metastable state. It is to be noticed that the line width is nearly two orders of magnitude greater than in (a).



It should be appreciated that this nuclear polarization is in a state in which the electronic angular momentum is zero: the magnetic moment of the atoms resides solely in the nuclear magnetisation. (For the metastable states, the electronic angular momentum is non-zero).

$^3\text{He}$  atoms in their ground states have extremely long relaxation times. (Ten hours has recently been measured by Cohen-Tannoudji *et al.*<sup>(13)</sup>). In the gas discharge, relaxation times are of the order of minutes. The resonances and the relaxation times can be studied by measuring the absorption of light by the metastable atoms, though these are not the only methods available.

Figure 23a shows a nuclear resonance in  $^3\text{He}$  at a frequency of 1 kHz. (Actually, this curve was taken with modulated light, but it demonstrates the characteristics of the resonance). The  $g$ -factor, about  $2.3 \times 10^{-3}$ , shows that it is a *nuclear* resonance.

For comparison, Fig. 23b shows a set of resonances, also monitored by absorption of light by the metastable atoms, where the applied frequency is 1 MHz. The resonances occur at values of the field about  $\frac{1}{4}$  and  $\frac{1}{2}$  G respectively, whereas that in Fig. 23a is at about  $\frac{1}{3}$  G. Yet the frequencies in the two cases differ by a factor  $10^3$ . The resonances in (23b) are Zeeman resonances in the hyperfine states  $F = 1/2$  and  $3/2$  of  $2^3S_1$ , where the  $g$ -factors,  $8/3$  and  $4/3$ , are of electronic magnitude.

## 7. RELAXATION PROCESSES

In many applications of optical pumping it is of interest to study relaxation processes, for this gives information about the interactions between the optically pumped material and the collision partners. Methods available are static methods (e.g., measurement of resonance line width) and the study of transients. The number of time constants required to interpret the measurements depends on the complexity of the system and the symmetry of the environment. For a spin- $\frac{1}{2}$  system in an anisotropic environment two times are sufficient: the longitudinal ( $T_1$ ) and transverse ( $T_2$ ) relaxation times which are familiar from the Bloch equations of magnetic resonance.

The relaxation times will often be measured in a situation where the optical pumping process itself contributes to the relaxation: atoms are suddenly perturbed, either by optical excitation, or by collisions, according to the mechanism of pumping. The time constants measured will then be functions of the mechanism. These times we call  $\tau_1$  and  $\tau_2$ . They are related to  $T_1$  and  $T_2$  by equations of the form

$$\frac{1}{\tau_1} = \frac{1}{T_1} + \frac{K_\alpha}{T_\alpha} + \dots$$

$$\frac{1}{\tau_2} = \frac{1}{T_2} + \frac{K'_\alpha}{T_\alpha} + \dots$$

where  $T_\alpha \dots$  are time constants for the pumping mechanisms, and  $K_\alpha, K'_\alpha \dots$  are numerical constants depending on these mechanisms.

We give examples of the measurement of  $\tau_1$ ,  $T_1$  and  $\tau_2$ .

### 7.1 RELAXATION WITH THE PUMPING LIGHT: $\tau_1$

Interpose a shutter between the pumping lamp and the cell. Suddenly withdraw the shutter and record the exponential change of intensity towards its equilibrium value (Fig. 24a). The time constant is  $\tau_1$ .

### 7.2. RELAXATION IN THE DARK: $T_1$

When equilibrium has been reached, interpose the shutter for a definite time  $(t_1 - t_0)$ . During this time the sample has relaxed in the dark with time constant  $T_1$ . On removal of the shutter one obtains again the pumping curve ( $\tau_1$ ), but the initial point gives the polarization after the lapse of time  $(t_1 - t_0)$ . From the locus of these points (Fig. 24b) one obtains  $T_1$ .<sup>(14)</sup>

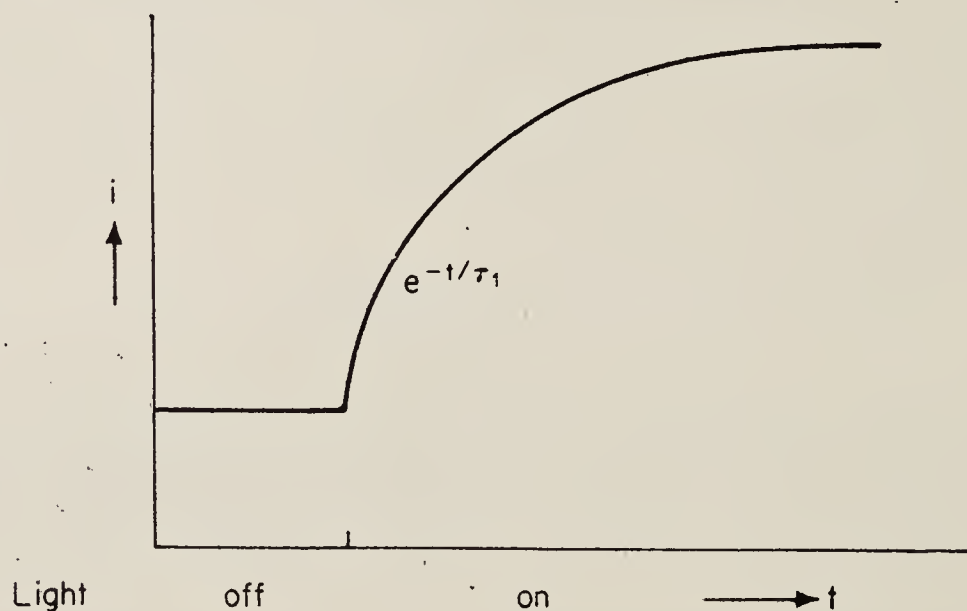


FIG. 24a. Exponential growth of optical pumping signal. (Time constant  $\tau_1$ ).

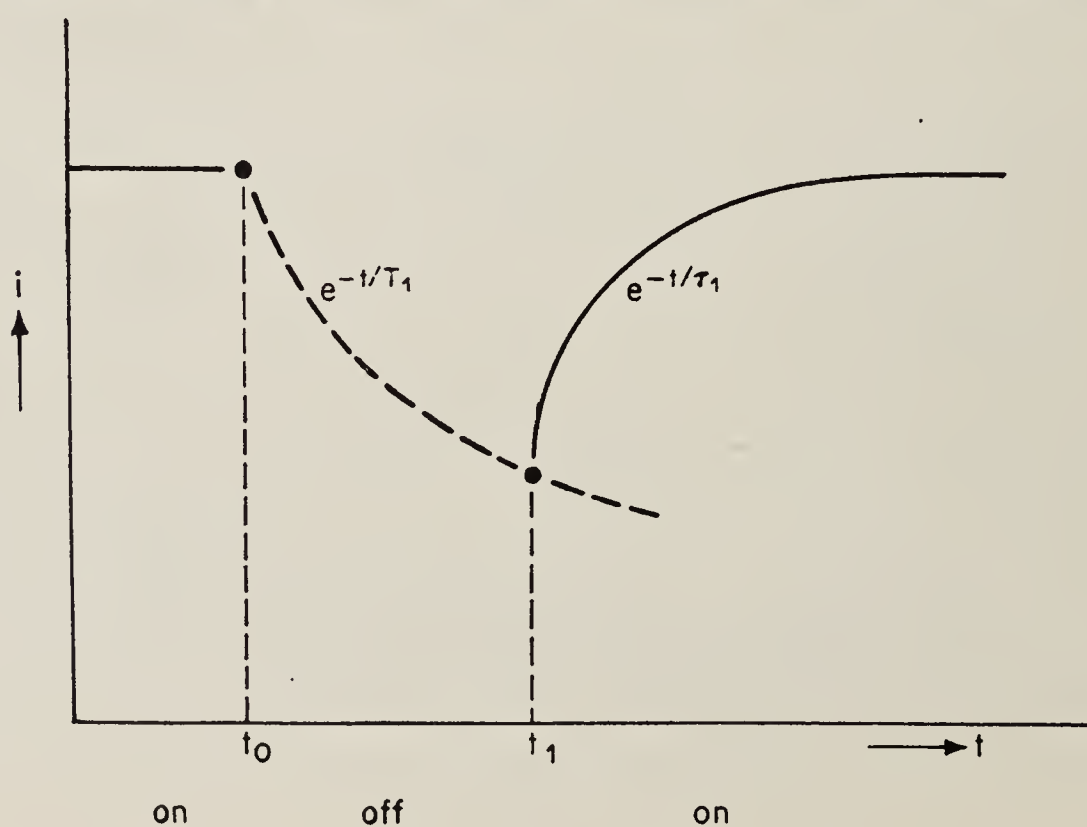
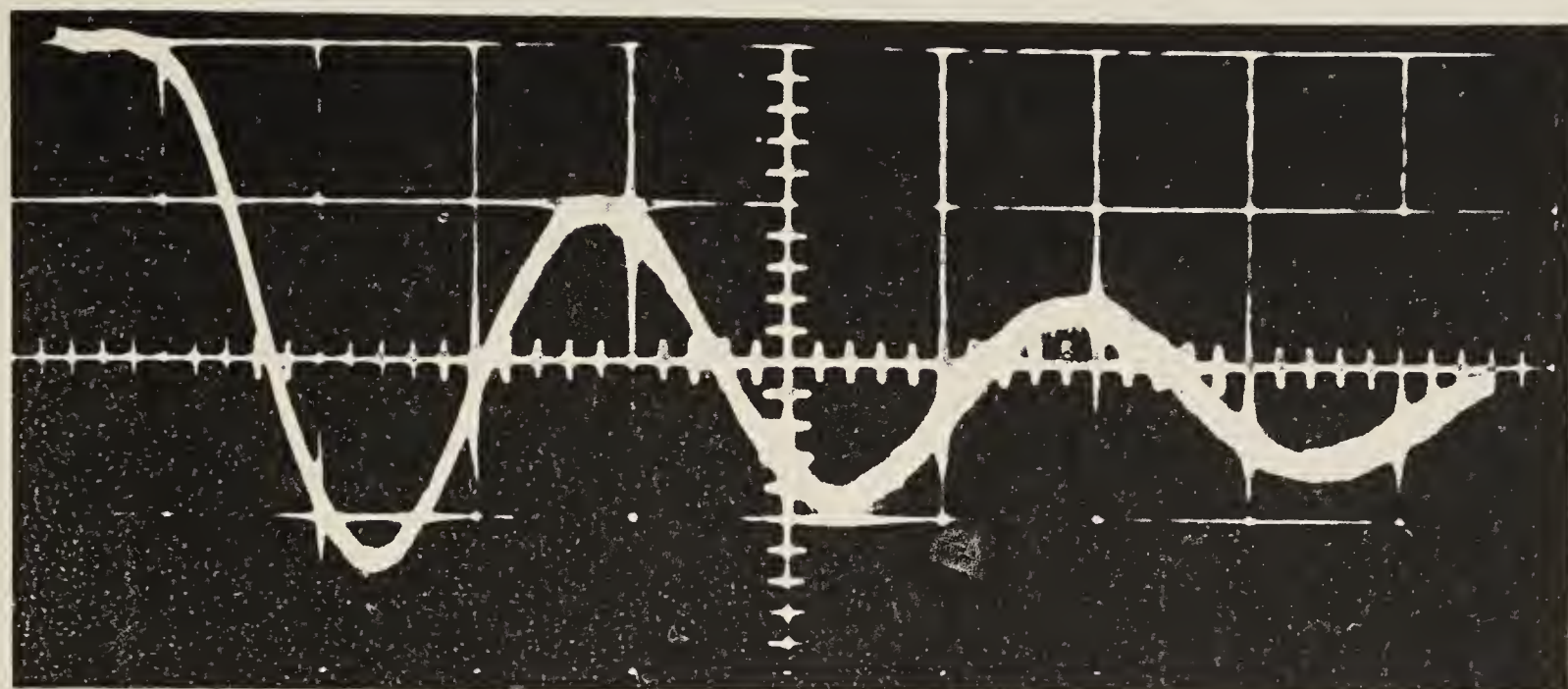


FIG. 24b. To illustrate the method of obtaining points on the curve for relaxation in the dark. (Time constant  $T_1$ ).





40 msec

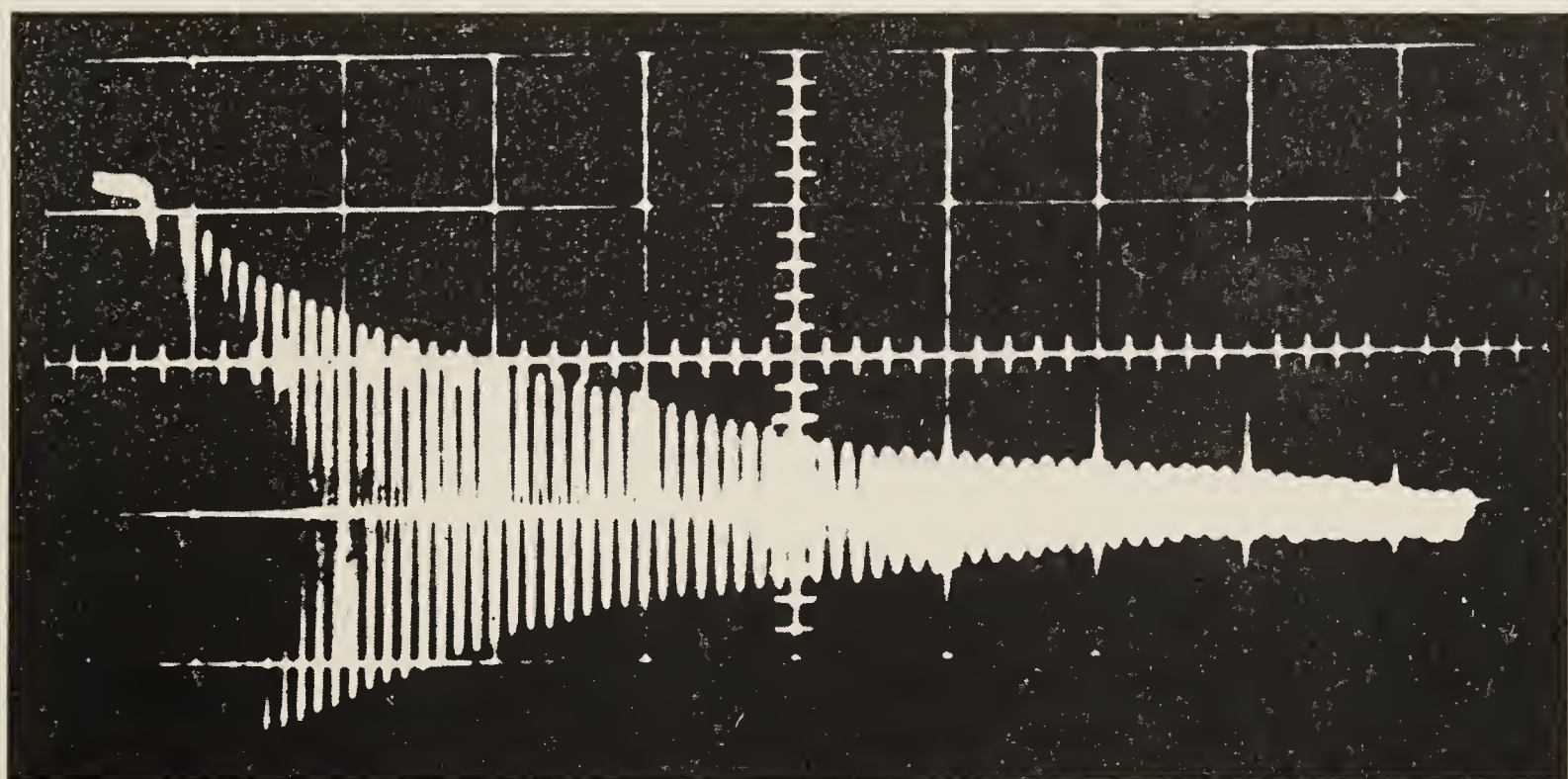
40 msec

Nutation at resonance

$$\omega_1 / 2\pi = 17 \text{ Hz}$$

$$\theta = 85 \text{ msec}$$

FIG. 25. Nutation at resonance of  $^3\text{He}$  in the ground state.  
a. Weak r.f. field.



40 msec

40 msec

Nutation at resonance

$$\omega_1 / 2\pi = 375 \text{ Hz}$$

$$\theta = 64 \text{ msec}$$

b. Stronger r.f. field.

The time constants for relaxation can be obtained from the damping of these curves.



### 7.3. MONITORING LAMP

An alternative procedure is to use separate lamps for pumping and monitoring. The latter should be weak enough so that its pumping and relaxing effect is negligible. If such a lamp is used the indirect technique described above is unnecessary. The relaxation curve ( $T_1$ ) can be observed directly.

### 7.4. NUTATION: MEASUREMENT OF $\tau_2$

The transverse relaxation can be studied by observing the nutation as in Fig. 25. The sample is pumped to equilibrium and the r.f. field, previously adjusted to the resonance frequency, is suddenly switched on. The longitudinal magnetization nutates—i.e., precesses round the effective field which is rotating in the  $x$ - $y$  plane (classical picture of magnetic resonance). This nutation is damped at the rate  $\theta^{-1} = \frac{1}{2}(\tau_1^{-1} + \tau_2^{-1})$ .

Figures 25a and b relate to  $^3\text{He}$  pumped by the process of metastability exchange and monitored via the metastable state. The relaxation time constants in these examples are 64 and 85 msec. The frequency of nutation, 375 Hz in the one case and 17 Hz in the other, is, at resonance, proportional to the r.f. field strength, and measurement of this frequency is a good method for determining this field strength.

## 8. FREQUENCY SHIFTS

Associated with the relaxation processes we have mentioned are dispersive effects which may be manifested as frequency shifts. Thus, there is a frequency shift which arises from the irradiation of atoms by light, and one which arises through collisions between the optically pumped atoms and buffer gases. It will be appreciated that such shifts may give rise to serious errors in the precision spectroscopy to which optical pumping lends itself. On the other hand, the shifts allow a study of interaction processes.

### 8.1. PRESSURE SHIFTS

Figure 26 shows the shift of the zero-field resonance line of  $^{133}\text{Cs}$  as a function of pressure of foreign gas. It will be noticed that both positive and negative shifts occur. With an appropriate mixture of gases, the shift may be eliminated.

### 8.2. LIGHT SHIFTS

Figure 27 shows the shift of the Zeeman resonance,  $M_I = \frac{1}{2} \rightarrow -\frac{1}{2}$ , in the ground state of  $^{199}\text{Hg}$ . The central curve is the resonance obtained under ordinary optical pumping conditions (irradiation with circularly polarized  $^{199}\text{Hg}$  resonance radiation). The curves on either side show the displacement



obtained by irradiating the vapour in addition with  $\sigma^+$  or  $\sigma^-$  light from a different isotope,  $^{201}\text{Hg}$ .

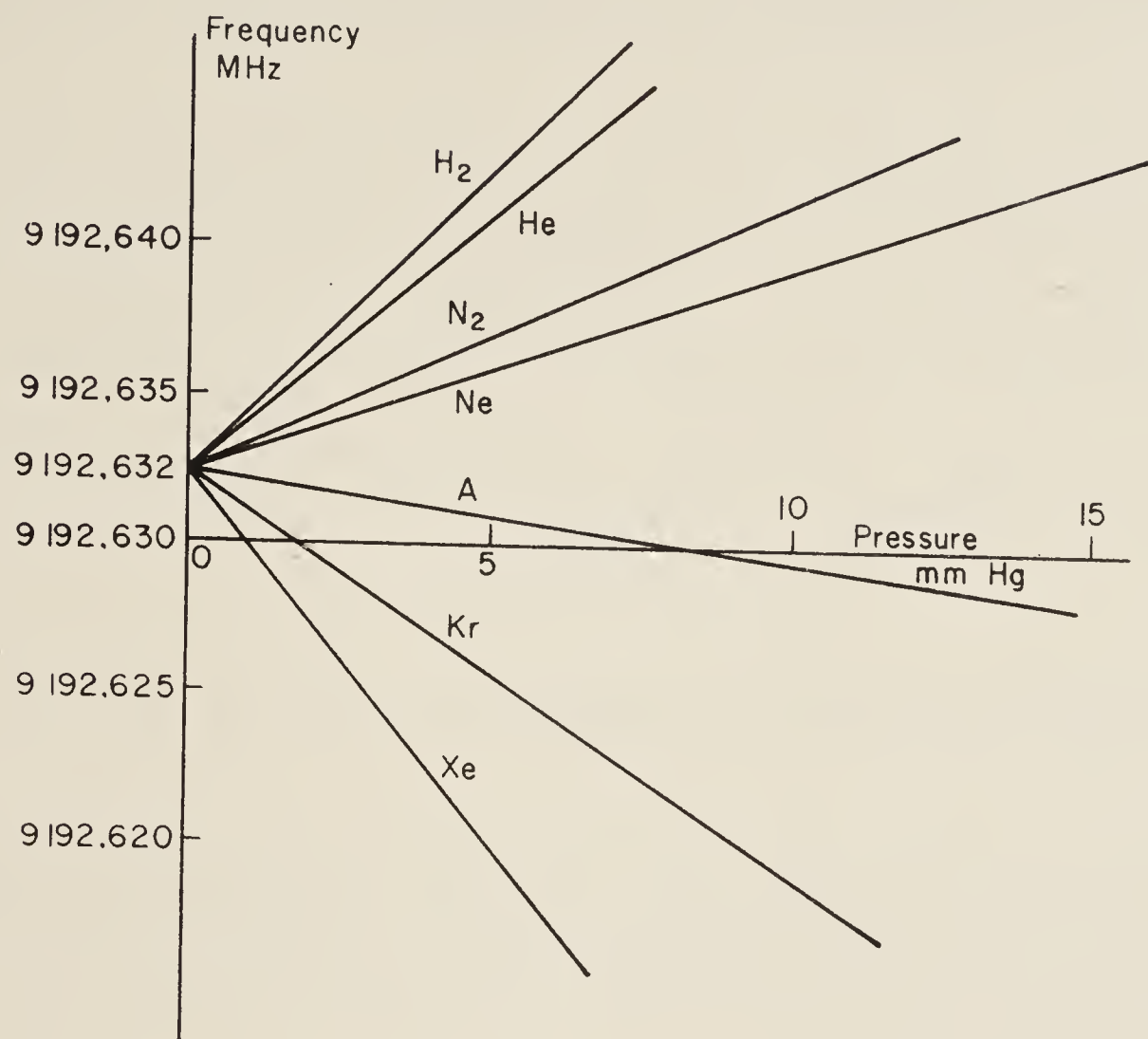


FIG. 26. Pressure shift of zero field hyperfine resonance line of  $^{133}\text{Cs}$  for different buffer gases. (After Arditi and Carver.<sup>(83)</sup>)

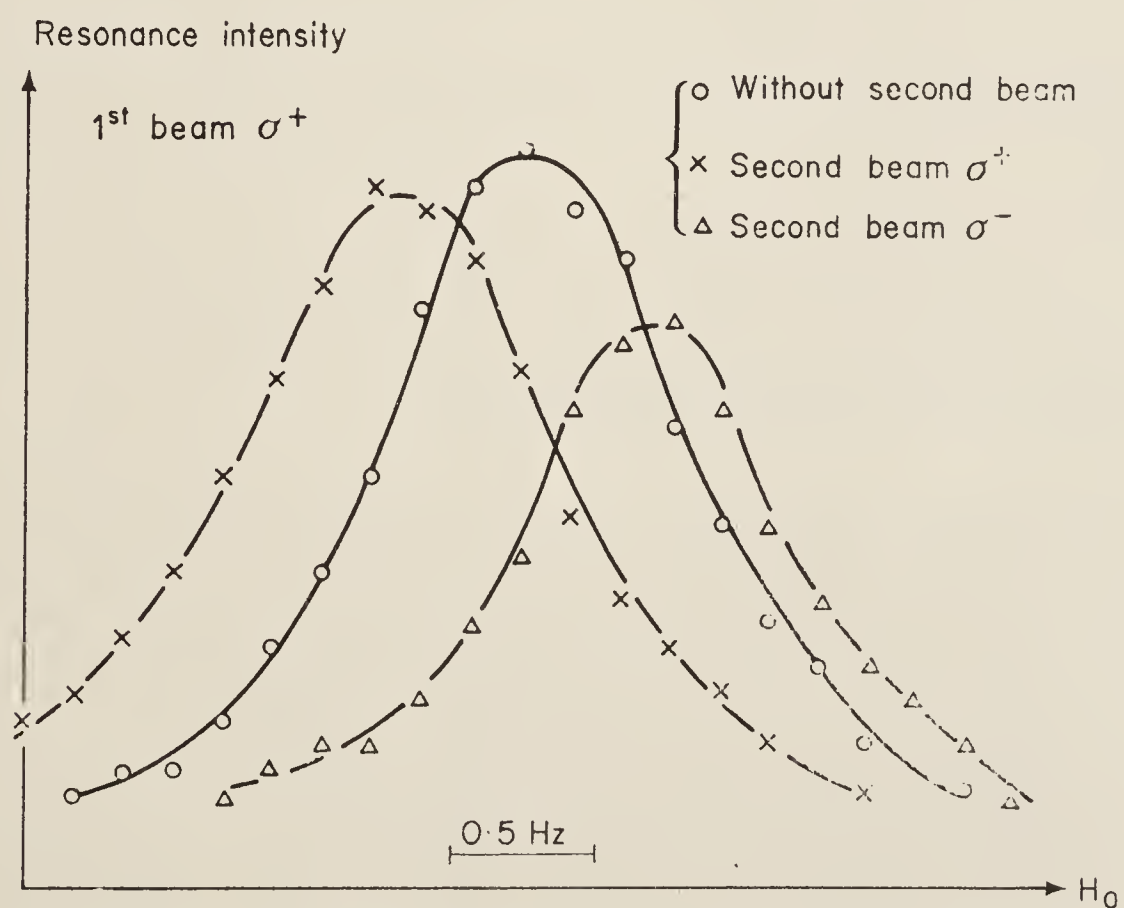


FIG. 27. Resonance curves in the ground state of  $^{199}\text{Hg}$  demonstrating light shifts. (After Cohen-Tannoudji.<sup>(82)</sup>)

One chooses light from a different isotope because the spectral components of  $^{201}\text{Hg}$  do not coincide with the absorption region of  $^{199}\text{Hg}$ . The significance of this is the following. The dispersion curve which is associated with

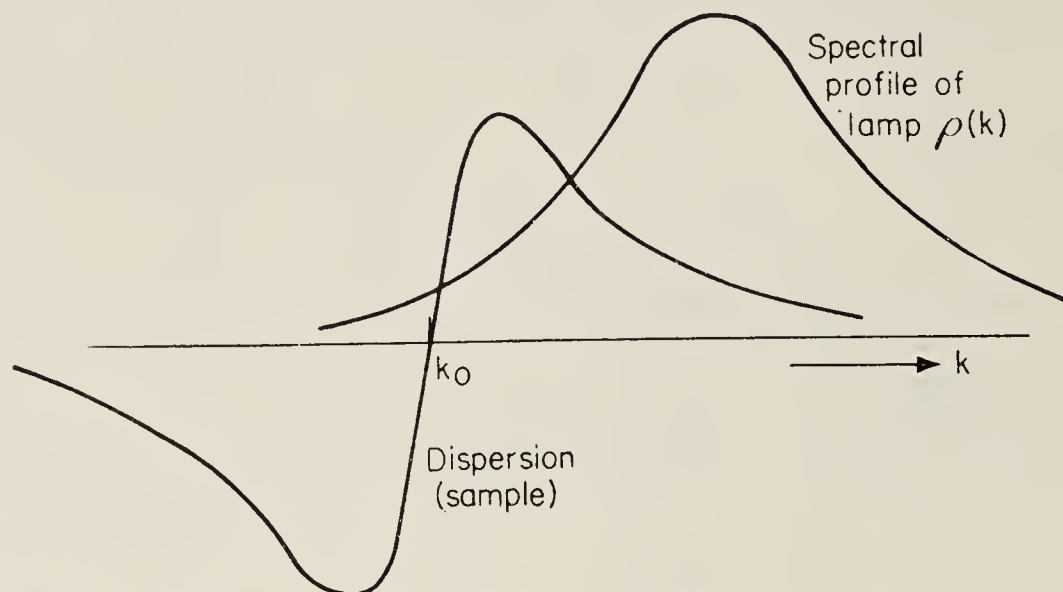


FIG. 28. The light shift is obtained by folding the spectral profile of the lamp with the dispersion curve of the sample (Section I.8.3).

absorption is antisymmetrical about the mid-point. The displacement of the energy level is given by folding the spectrum of the lamp with the dispersion curve and integrating over frequencies (Fig. 28). The result is zero if the lamp spectrum is symmetrical with respect to the absorption, but non-zero if it is asymmetrical.

The displacements seen in Fig. 27 are not the total displacements of the levels, but the *differential* displacements between the levels  $M_I = \frac{1}{2}$  and  $-\frac{1}{2}$ .

It might appear that light shifts could be avoided by using, for irradiation of a sample, only light from the corresponding lamp, but this is not necessarily true. The spectra of pumping lamps are rarely simple lines which fall symmetrically across the absorption spectrum of the sample. Any structure in the lamp which might arise, for example, from hyperfine or isotope effects, is potentially a source of light shifts. On the other hand, the shifts themselves are small, and of significance only in precision measurements.

### 8.3. SEMI-CLASSICAL INTERPRETATION OF LIGHT SHIFTS AND RELAXATION

A detailed account of the optical pumping cycle has been given by Barrat and Cohen-Tannoudji.<sup>(15)</sup> But the following semiclassical interpretation of light shifts and relaxation, due to Pancharatnam,<sup>(16)</sup> is helpful.

The energy acquired by an atom of polarizability  $\alpha$  in an electric field  $E$  is  $-\frac{1}{2}\alpha E^2$ . This holds also for an oscillatory field. For the complex oscillatory field  $E_k \exp -ikt$  we have  $\alpha_k = (e^2/2mk_0)f/(k_0 - k - \frac{1}{2}i\Gamma)$ , where  $k_0$  is a resonance frequency,  $\Gamma$  the corresponding damping constant, and  $f$  the oscillator strength.



The (complex) energy of interaction with radiation of energy density  $\rho(k)$  is

$$\Delta W = - \sum_k \alpha_k |E_k|^2 = -2\pi \int_0^\infty \alpha_k \rho(k) dk. \quad (9)$$

If we give this classical expression a quantum interpretation, the real part of  $\Delta W/\hbar$  gives a level shift  $\delta$  and the imaginary part, the damping due to the incident field. (This is the damping constant for the amplitude: the damping constant for the energy,  $\Gamma'$ , is twice this value).  $\Gamma'$  should be distinguished from  $\Gamma$ , which is the damping constant for spontaneous emission from the excited state.

For the simple case of a transition between states  $|a\rangle$  and  $|b\rangle$ , we have

$$f_{ba} = (2m/\hbar e^2) k_0 |P_{ba}|^2 \quad (10)$$

and 
$$\alpha_{ba} = |P_{ba}|^2 / \hbar (k_0 - k - \frac{1}{2}i\Gamma), \quad (11)$$

where  $P_{ba}$  is the matrix element of the electric dipole operator. Thus

$$\delta = \frac{-2\pi |P_{ba}|^2}{\hbar^2} \int_0^\infty \rho(k) \frac{(k_0 - k)}{(k_0 - k)^2 + (\frac{1}{2}\Gamma)^2} dk \quad (12)$$

and

$$\Gamma' = \frac{4\pi |P_{ba}|^2}{\hbar^2} \int_0^\infty \rho(k) \frac{\frac{1}{2}\Gamma}{(k_0 - k)^2 + (\frac{1}{2}\Gamma)^2} dk, \quad (13)$$

which are essentially the formulae derived by Barrat and Cohen-Tannoudji, illustrated in Fig. 28.

## 9. LEVEL-CROSSING IN GROUND STATES

An essential ingredient of the level-crossing effects in excited states (Section 4) was the preparation of atoms in superposition states. This is the condition we must look for if we wish to study level-crossing effects in ground states.

It can be achieved in the following way. Suppose we set up an optical pumping experiment to produce a polarized system. This can be done by illuminating a sample with circularly polarized light in zero field (Fig. 29).

If the system is space-quantized with reference to the direction of the light ( $Ox$ ), there exists a population difference between the states, but there is no correlation between them. However, if we space-quantize with respect to another direction ( $Oz$ ), each of the new states is to be expressed as a superposition of the former states, so that optical pumping along  $Ox$  has produced a superposition of states defined with reference to  $Oz$ .

If now a magnetic field is applied along  $Oz$ , the states defined with respect to  $Oz$  are energy eigenstates. They are degenerate in zero field, but the field removes the degeneracy. This is precisely the level-crossing situation we met in Section 4.

It remains to monitor the effect of removing the degeneracy. This is done by measuring the absorption of the pumping beam in the system. (It may also be done by using a separate, weak beam in the  $Oy$  direction, or by measuring the fluorescent light). One can obtain curves similar to the level-crossing curves of Fig. 14, for example, but of width corresponding to the relaxation time in the ground state.

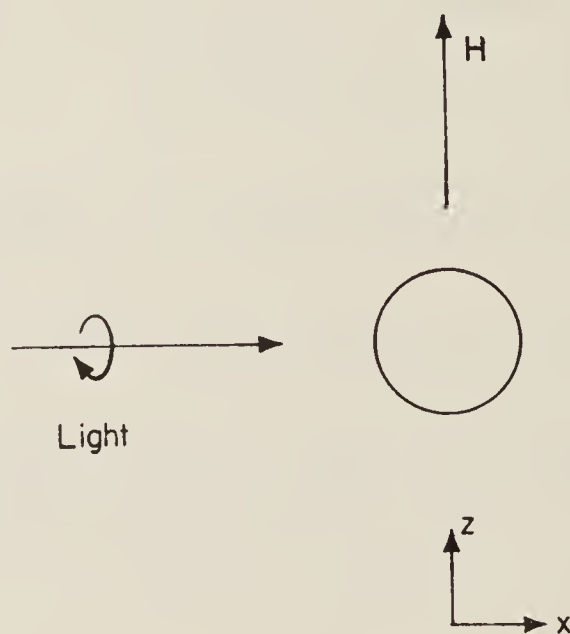


FIG. 29. Geometrical arrangement for studying the Hanle effect in absorption.

The situation we have just analysed in terms of superposition states and interference effects is sometimes described in terms of the transverse magnetisation of the system. The pumping beam creates a magnetisation along  $Ox$ . If a field  $H$  exists, the magnetisation precesses around  $Oz$ . Since different atoms are brought into the field at different times, the net magnetisation is spread out like a fan in the  $x$ - $y$  plane. Between the extreme situations—(a)  $H = 0$ ; magnetisation along  $Ox$ , and (b)  $H \gg (\gamma\tau)^{-1}$ ; magnetism uniformly spread in the  $x$ - $y$  plane—is the transition region which is precisely the region where the degenerate Zeeman levels are becoming resolved—the level-crossing region.

#### 10. DESCRIPTION OF OPTICAL PUMPING IN TERMS OF IRREDUCIBLE SPHERICAL TENSOR OPERATORS

It should be remarked, in conclusion, that a description of the interaction of atoms with light in terms of magnetisation, though often extremely illuminating, is not capable of representing all the phenomena. It can represent only



those phenomena which can be analysed in terms of spherical tensors of multipole order 1. Optical interactions by electric dipole transitions can also monitor atomic properties described by tensors of multipole order 2, for which the appropriate model is a precessing and pulsating ellipsoid. Such a model has been described by Pancharatnam. The limitation to order 2 stems from the selection rule  $\Delta M = \pm 1$  for electric dipole transitions, and may be understood with reference to Fig. 13. Tensors of higher multipole can, in principle, be monitored by transitions of higher multipole or by dipole transitions with more intermediate steps.

It is becoming increasingly common to analyse optical pumping experiments by means of irreducible spherical tensor operators, but no account of this work will be given in this chapter.<sup>(17, 18, 19)</sup>

## II. EXPERIMENTAL DETAILS AND POINTS OF TECHNIQUE

We describe here further experimental details and points of technique.

### 1. EXPERIMENTAL DETAILS

#### 1.1. THE SAMPLE

Two methods are in common use for containing the sample, sealed-off cells and crude atomic beams.

##### *a. Sealed-off cells*

Pyrex or silica cells are commonly used, of linear dimensions between 1 and 5 cm. Spherical or cuboid shapes are used. Sometimes the cells are extended in the form of a horn for a light trap. Good optical quality is not essential.

The vapour under study is normally at a pressure of the order of  $10^{-5}$  or  $10^{-6}$  torr.

Details of the application of wall coatings have been given by Bouchiat and Brossel.<sup>(20)</sup>

The vapour pressure of the sample is commonly controlled by the use of a side arm and thermostat. Special methods have been used for reactive materials. (See, for example, Minguzzi *et al.*<sup>(21)</sup>)

When foreign gases are used in optical pumping experiments a wide range of pressures varying from, say,  $10^{-2}$  torr up to pressures of the order of 1 atmosphere may be used. (Optical pumping of rubidium in argon buffer gas at pressures up to 30 atmospheres has recently been reported.<sup>(22)</sup> It is important to take account of the broadening and displacement of the absorption lines of the sample when high pressures of foreign gas are used.)



*b. Atomic beams*

The sample is used in the form of a beam when there is reason to fear contamination in sealed-off cells, or when it is desired to study materials which cannot conveniently be maintained as a vapour in quartz vessels. The object of the beam is not to secure collimation. Beams have been used in all-glass systems,<sup>(2)</sup> or in metal systems with windows.<sup>(23)</sup>

## 1.2. LIGHT SOURCES

The main requirements are that the light sources should be stable and produce a high flux in the spectral absorption region of the sample. In practically all cases this has been achieved by using a lamp whose output is a line rather than a continuous spectrum. The energy density per unit spectral range is generally insufficient in sources with a continuous spectrum. Notwithstanding this, optical pumping with white light has been performed under circumstances when the absorption line was strongly pressure-broadened,<sup>(22)</sup> and resonance fluorescence from metastable states of neon using sunlight is described by Wood in his book on Physical Optics.<sup>(24)</sup> While certain accidental coincidences of spectral lines sometimes allow the optical pumping of one element by a lamp made from another, it is most common to use in the lamp the same element that is to be studied in the sample. Use is frequently made of separated isotopes to secure differential pumping of hyperfine or Zeeman components. Very little use has been made of lasers in this field.

Insofar as the sample needs to be irradiated by light which can be absorbed by atoms in their ground or in metastable states, it follows that the spectral lines emitted by lamps of the same element are very commonly self-reversed. That is to say, the outer layers of vapour in the lamp may absorb from the broadened spectral line emitted from the core of the lamp, just those regions in the middle of the spectral profile which are needed in the sample. Much effort has gone into the production of lamps free of self-reversal though it should be appreciated that a high degree of self-reversal can be tolerated, provided there is still sufficient energy at the centre of the spectral line. Thus, many forms of commercial sodium lamp show a high degree of self-reversal in their spectrum but have nevertheless often been used for optical pumping.

The disadvantage in irradiating the sample with a large flux of light outside its absorption region (as is the case when a strongly self-reversed lamp is used) is that the stray light scattered from the walls of the resonance vessel is unnecessarily increased. This is objectionable since the main source of noise in optical pumping experiments is normally photoelectric shot noise.

The different types of lamp which have been successfully used in optical pumping experiments include hollow cathode lamps, (internal electrodes) and sealed off electrodeless lamps excited by radio-frequency or microwave oscillators. A discussion of light sources in general has been given by Budick,



Novick and Lurio.<sup>(25)</sup> Bell *et al.*,<sup>(26)</sup> describe the production of small but effective alkali metal lamps. Efficient alkali metal lamps of larger surface area have been described by Atkinson, *et al.*,<sup>(27)</sup> Burling and Czajkowski<sup>(28)</sup> and by Berdowski *et al.*<sup>(29)</sup> The lamp described in the latter paper is suitable for use in high magnetic fields.

Hollow cathode lamps of advanced design, carrying high current and allowing the application of high magnetic fields, are being used at Heidelberg by Otten and zu Putlitz.<sup>(30)</sup>

When sealed-off lamps are prepared for excitation by microwave sources the cells are normally flattened in order to reduce self-reversal. A typical capsule much used by the group in Paris is about 2 cm in diameter and 1 mm thick. Such capsules are placed near an antenna from a microwave oscillator which may typically be a magnetron delivering 100 watts at 2.5 GHz, (such units are

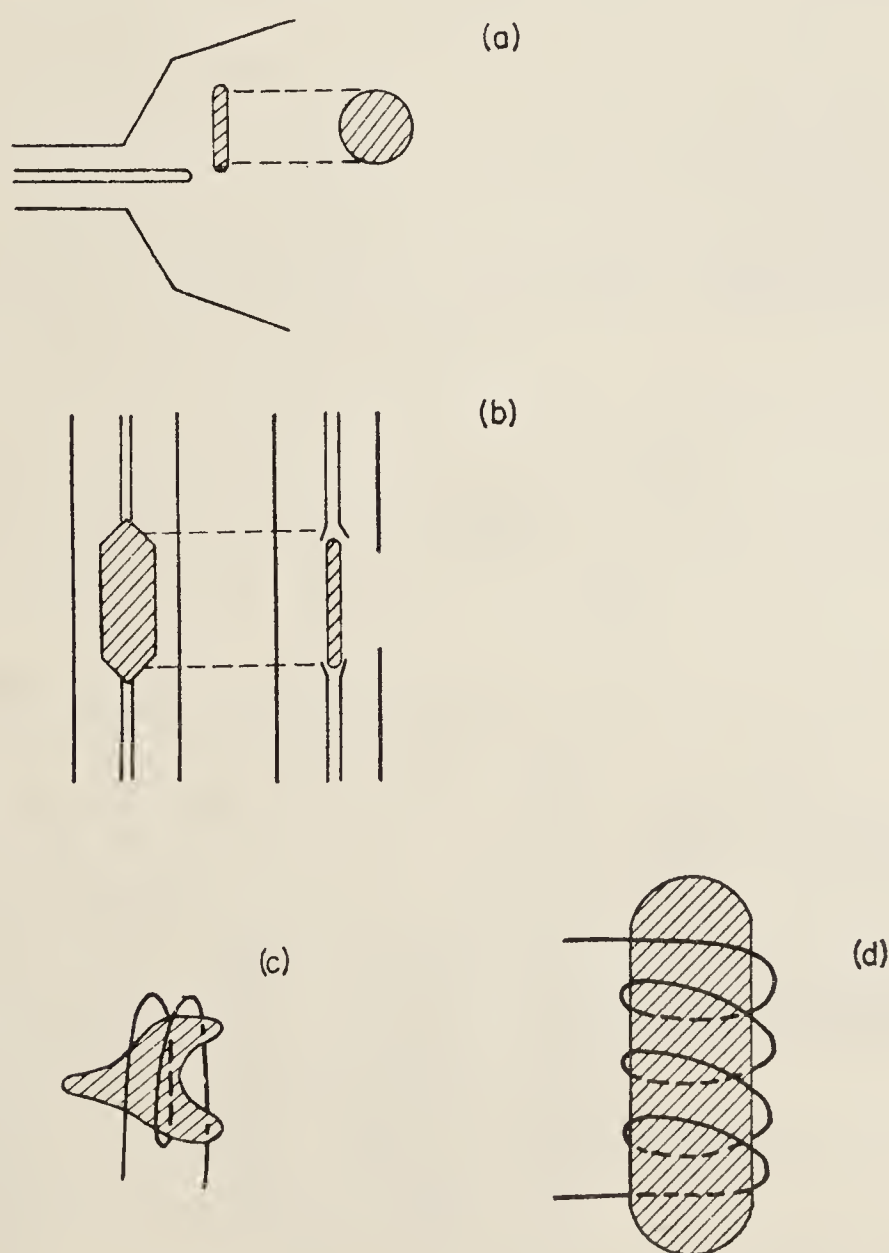


FIG. 30. Some typical light sources: sealed-off cells.

- a. Disc excited by antenna from microwave oscillator.
- b. Flattened cylinder forming part of co-axial line.
- c. Cylinder with re-entrant window in coil of oscillator at about 100 MHz.
- d. Cylinder in coil of oscillator at about 10 MHz.

produced for medical purposes). Alternatively, if the capsules are prepared in the form of a squashed cylinder a few centimeters long and a millimeter thick they may be incorporated as part of the central conductor in a co-axial line driven by a similar oscillator. Capsules used for these purposes will contain a noble gas at a pressure of about 1 torr together with the material whose spectrum is to be excited. It is sometimes necessary to provide a thermostat so that the pressure of the vapour may be controlled independently of the current in the lamp.

A microwave-excited lamp suitable for exciting calcium and magnesium ions has been described by Smith and Gallagher.<sup>(31)</sup> (See Fig. 31).

### 1.3. MAGNETIC FIELDS

It is rarely necessary in optical pumping experiments to use high magnetic fields; the requirements are generally to produce relatively small magnetic fields of high homogeneity. The amount of non-homogeneity which can be tolerated depends on the line width of the resonance being explored. For zero field level-crossing experiments in excited states, for example, where typical line widths might be of the order of a few gauss, stray fields in the laboratory are often a significant perturbation. For optical pumping experiments in ground states it is essential to compensate stray fields. This is commonly done

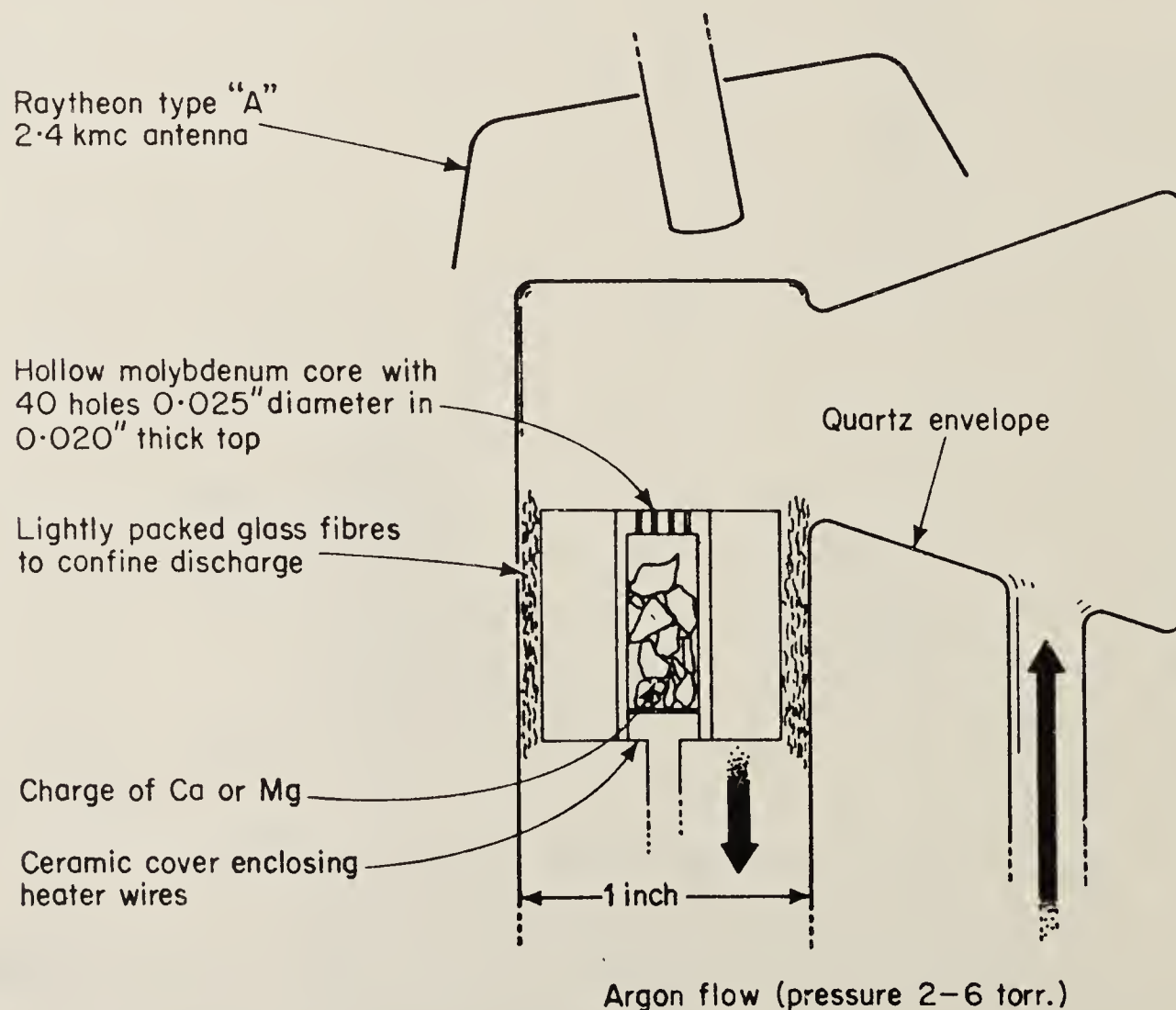


FIG. 31. Flow lamp excited by microwave antenna. (After Smith and Gallagher.<sup>(31)</sup>)



with orthogonal pairs of Helmholtz coils of diameter of the order of 30 cm. Difficulties in obtaining circular formers of this size may be avoided by winding rectangular coils with formers made of channelled material.

The design of coils and solenoids to produce uniform magnetic fields has been discussed by Garrett<sup>(32)</sup> and Franzen.<sup>(33)</sup>

It is possible without too much difficulty to reduce stray static magnetic fields to a few milligauss by the use of large Helmholtz coils. Oscillatory magnetic fields (at the frequency of the A-C mains) are commonly present in the laboratory with amplitude about 2 mG. Attempts to compensate such fields by servo-mechanisms have been rather unsuccessful. More commonly these stray fields have been reduced by shielding.

In a recent experiment Dupont-Roc *et al.*<sup>(34)</sup> studied resonances of width about 1  $\mu$ G for which the sample was enclosed within four concentric cylinders of Mu-metal.

#### 1.4. DETECTORS

Photocells and photomultipliers are commonly used together with electric amplification and recording, although in some of the early work sensitive galvanometers were used very successfully. Many investigations have been successfully performed with a single photodetector. This is possible only when one can rely on the stability of the lamp.

Compensation for drifts in the lamp can often be effected by taking fluorescent light into two photodetectors in such positions that the two signals are in opposite senses. By the use of an optical bridge or by some other arrangement, the signal can be doubled and the effects of drifts eliminated to a first approximation.

In simple cases level-crossing and double resonance signals can be a substantial fraction of the total fluorescent light. In such cases the signal can be displayed on an oscilloscope with wide-band amplification. More commonly narrow band methods of detection are used to rescue the signal from noise: a typical system would use phase sensitive detection with time constants of a few seconds, but in the more complicated cases which are currently being studied the signal is a very small fraction of the fluorescent light and signal averaging methods are increasingly being used.

A novel method of detection, applicable to short-lived radioactive elements, is described in a later section (II 6.4).

#### 1.5. FILTERS AND POLARIZERS

It has been explained that optical pumping is sometimes more advantageously carried out by filtering some of the components of the light from the lamp. Interference filters are commonly used to separate the alkali doublets, for

example. Lyot (polarization) filters are also used for this purpose. Hyperfine components can sometimes be suppressed by introducing into the pumping beam a cell of a different isotope of the element concerned, to act as a differential absorber.

Sheet polarizers (linear and circular) are often adequate but there are occasions when more complete polarization is required and in such circumstances crystal polarizers are used. While one-beam polarizers (e.g. Glan prisms) are attractive, greater aperture can be achieved with two-beam prisms (e.g. Rochon). The unwanted beam is focussed and rejected by a stop.

## 2. SPECTRUM OF THE LAMP

Our analysis, in Section I, of double resonance and level-crossing experiments was based on the assumption that the spectrum of the lamp was uniform across the whole of the absorption region of the sample. There are occasions when this approximation is no longer valid, in particular when the absorption spectrum is being shifted by the application of magnetic fields. In such cases the profile of the resonances may be distorted. This is particularly serious when line profiles are being studied with a view to measuring lifetimes. The resonance line profiles may then be calculated by an analysis based on resolution of the spectrum of the lamp into its Fourier components. The signal due to monochromatic components interacting with stationary atoms is then to be integrated over the spectrum of the lamp and the Doppler absorption profile of the sample.<sup>(35, 36)</sup>

## 3. EXCITATION BY ELECTRONS AND OTHER PARTICLES

There are sometimes advantages to be gained by exciting atoms with electrons or other particles rather than by light. So long as some departure from the statistical population of excited states can be achieved by such methods of excitation, radio-frequency resonance and level-crossing phenomena can be monitored by changes in the fluorescent light.

### 3.1. ELECTRONS

Electron excitation has been developed particularly by Pebay-Peyroula and his colleagues.<sup>(37)</sup> An account of recent work in this field is given in the Proceedings of a Conference held recently in Grenoble.<sup>(38)</sup>

A greater variety of excited states can be reached by electron excitation as compared with optical excitation, but there are two major difficulties in the use of electrons. One is that the fluorescence being detected is often affected



by decay from higher levels in cascade. The other is that the electron trajectories are perturbed by the applied magnetic fields which by the nature of the experiments are required to be varied. Very pronounced resonance effects occur when the cyclotron frequencies of the electrons in the static field approach the frequency of the oscillating field. In order to avoid these effects it is arranged, where possible, that the electrons should travel parallel to the static field and that the path length should be such that off-axis electrons are unable to perform a complete cycle of cyclotron motion in the course of their flight.

Level-crossing experiments require that the electron beam be transverse to the magnetic field (this is a symmetry requirement corresponding to the optical arrangement in which the incident light is polarized at right angles to the magnetic field). Here the deflection of the beam by the magnetic field is particularly serious. The change in deflection as the field is varied gives rise to distortion of the level-crossing line shape.

While most experiments with electron excitation have been performed with a heated filament as a source of electrons, some recent work has been performed in sealed-off vessels where the electrons have been generated in a gas discharge at low pressure. The vessel is placed between condenser plates at the end of Lecher wires. The motion of the electrons under these circumstances is dominantly an oscillation, perpendicular to the plates.<sup>(39)</sup>

### 3.2. HEAVY PARTICLES

The use of heavy particles rather than electrons reduces by many orders of magnitude the difficulties connected with the deviation of electrons by the applied magnetic fields. Level-crossing experiments in helium excited by  $H_2^+$  have been successfully carried out by Kaul.<sup>(40)</sup> A quantitative study of the polarization of fluorescent light from helium excited by protons has been made by Krause and Soltysik.<sup>(41)</sup>

Selective excitation can also be achieved in beams of fast particles which have traversed a thin foil.

## 4. COHERENCE NARROWING, PRESSURE BROADENING AND DEPOLARIZATION

Our discussions of double resonance and level-crossing experiments have hitherto supposed that the signals correspond to the single scattering of light by atoms. If the vapour pressure is low enough the experimental results do, in fact, correspond to single scattering, but as the vapour pressure is increased the light in the resonance vessel may undergo multiple scattering. The first consequence of this is that the light becomes depolarized with consequent loss of signal. But strong signals may nevertheless still be obtained and it is found that, contrary to expectations, the resonance curves and level-crossing curves

become narrower with increase of vapour pressure. As the pressure is increased still further the curves begin to broaden owing to the reduction in lifetime of the excited atoms through collisions.

The narrowing was discovered by the group in Paris and interpreted by them as a consequence of the coherent diffusion of light through the vapour. The phenomenon is called "coherence narrowing". A detailed experimental and theoretical study was made by Barrat.<sup>(42)</sup> It has since been discovered that the coherence narrowing is accompanied by a shift in the magnetic resonance frequencies.<sup>(43, 43a, 44)</sup>

It is necessary to be aware of the phenomenon of coherence narrowing when experiments are undertaken to determine the lifetime of excited states from level-crossing curves. Such curves are taken at a range of vapour pressures and the width, plotted as a function of atomic density, extrapolated to zero density. The broadening at higher vapour pressures allows a study of interatomic interactions. (See, for example, Happer and Saloman<sup>(17)</sup>; Omont and Meunier.<sup>(18)</sup>)

## 5. COMPARISON OF DOUBLE RESONANCE AND LEVEL-CROSSING EXPERIMENTS: MODULATION TECHNIQUES

While double resonance experiments have been extensively applied in studies of excited atoms, they suffer from serious disadvantages which arise from the need to use a strong oscillating field on the sample.

- (i) It is not always a simple matter to achieve the necessary amplitude of magnetic field at the high frequencies required.
- (ii) The oscillating field perturbs the resonances in two ways; first by broadening them and secondly by shifting their positions. (See Section IV).
- (iii) The strong oscillating fields sometimes set up gas discharges in the resonance vessels and the light from such discharges, though weak, is sometimes sufficient to swamp the fluorescent light.

For these reasons level-crossing experiments are to be preferred. The sole external perturbation on the excited atoms is then simply the beam of light used for excitation. Level-crossing experiments can give values for lifetimes of excited states accurate to 1 or 2% in favourable cases. Measurements to this precision demand a careful study of the line profile, which is of the pure Lorentzian shape only for certain well-defined geometrical conditions. The use of finite light cones may introduce some mixture of the dispersion shape—a point which must be carefully studied.



Measurements of the position of level-crossing curves yield values for the hyperfine interaction constant which are fundamentally limited only by the natural width of energy levels. However, calculation of these interaction constants from the measured magnetic fields at which the level-crossing signals are found depends on a knowledge of the  $g_J$ -factor of the states, and if this is not known from optical measurements it must be determined by a double resonance experiment. Indeed, the determination of  $g_J$ -factors is now the most important application of the double resonance method.

An alternative to the double resonance method presents itself in the use of modulated light. If a level-crossing experiment is performed with modulated light the level-crossing signals are displaced to the position where the modulation frequency matches the interval between the levels.<sup>(45)</sup> From the measured fields and frequencies the  $g$ -value can be deduced. This is a type of double resonance experiment which requires no oscillatory field to be applied to the sample. The curves obtained are identical with level-crossing curves—that is to say they suffer neither from radio-frequency broadening nor from displacement of the resonances. The technical difficulties are now transferred to the means of modulating the light. Because of these difficulties the method has not been widely applied. It has, however, been used to verify the physical reality of the frequency diagram—a representation of combinations of the nutational and precessional frequencies in the motion of atoms under oscillating fields (See Section III). The frequency diagram for the excited  $^3P_1$  state of mercury has been explored in this way.<sup>(46,47)</sup>

## 6. SOME TYPICAL RESULTS AND SOME RECENT APPLICATIONS OF OPTICAL PUMPING, DOUBLE RESONANCE AND LEVEL-CROSSING TECHNIQUES

No attempt will be made here to give a complete account of work in this field. Some recent compilations have been made by zu Putlitz,<sup>(48)</sup> by Budick,<sup>(49)</sup> and Major.<sup>(50)</sup> The experiments described in the following sections have been chosen to illustrate a variety of applications.

### 6.1. HYPERFINE STRUCTURE OF HYDROGEN

As an example of the application of optical pumping to measure quantities of fundamental importance in atomic physics, the series of experiments by Pipkin and his colleagues<sup>(51)</sup> on the hyperfine structure of hydrogen, deuterium and tritium may be cited. The measurements of the hyperfine intervals were made to a precision of a few hertz, the intervals themselves being of the order of  $10^9$  Hz. Knowledge of these intervals is of the greatest importance in verifying theories of atomic structure and radiation interactions and in determining the value of the fine structure constant.



## 6.2. PRECISION MEASUREMENT OF ATOMIC $g$ -FACTORS

As an example of more recent precision measurements in optical pumping we refer to the work of White *et al.*<sup>(52)</sup> on the  $g$ -factor ratios for free rubidium atoms. Precision measurements of such quantities were formerly made by the methods of atomic beam resonance spectroscopy. Optical pumping methods offer an alternative technique. In the work of White *et al.* the ratios  $g_I/g_J$  were measured for  $^{85}\text{Rb}$  and  $^{87}\text{Rb}$  to a few parts per million and the ratios  $g_J(^{87}\text{Rb})/g_J(^{85}\text{Rb})$  to a precision of a few parts in  $10^9$ . These results were obtained from evacuated wall-coated cells. Distortion of the Lorentzian line shape was found for cells filled with buffer gases. The results were corrected for shifts arising from the pumping light.

## 6.3. RELAXATION STUDIES BY OPTICAL PUMPING

An extended series of experiments on the relaxation of optically pumped rubidium has been carried out by Mme Bouchiat. A recent report<sup>(20)</sup> gives an account of the relaxation of rubidium on paraffin coated walls. The results are compatible with other measurements on the interaction of rubidium atoms with buffer gases.

## 6.4. DETECTION OF OPTICAL PUMPING BY RADIOACTIVE EMISSION

A variation of the optical pumping method has recently been used to find the nuclear spins and moments of certain short-lived radioactive isotopes.<sup>(53)</sup> It is applicable to isotopes which can be produced by the bombardment of a gas by particles from an accelerator and whose lifetime is short enough for them to decay before they have had time to diffuse through the gas to the walls of the containing vessel.

The isotopes produced in this way are polarized by circularly polarized light, either directly or through spin-exchange. Their polarization is monitored by measuring the asymmetry in the  $\beta$ -emission. The polarization is destroyed by a radio-frequency field at resonance with the Zeeman or hyperfine intervals and the signal is detected by a change in the counting rate.

## 6.5. LEVEL-CROSSING EXPERIMENTS ON HYDROGEN

The fine structure of excited states of atomic hydrogen is no less important than the hyperfine structure in atomic physics. By the application of magnetic fields of a few thousand gauss the spin-orbit coupling is broken down and Zeeman levels of  $2P_{3/2}$  intersect those of  $2P_{1/2}$ . A measurement of the crossing point allows a determination of the  $P_{1/2} - P_{3/2}$  interval and of the fine structure constant. A level-crossing experiment to determine these quantities was recently reported by Metcalf *et al.*<sup>(54)</sup> Similar studies have also been undertaken by Fontana and colleagues.<sup>(55,56)</sup> The sharpness of the resonances is less than



in the measurement of hyperfine structure because it is limited by the short lifetime of the excited  $P$ -states. The fine structure constant is determined to a precision of about one part in  $10^5$ .

#### 6.6. LEVEL-CROSSING EXPERIMENT ON MANGANESE

An example of an experiment in which a weak signal from a complicated structure was analysed to determine the hyperfine structure is the level-crossing experiment of Handrich *et al.*,<sup>(57)</sup> on the MnI spectrum. The modulation necessary for phase sensitive detection was achieved by rotating a polarizer in the fluorescent beam. The signal was retrieved from noise by the use of an Enhancetron.

#### 6.7. HYPERFINE STRUCTURE OF EXCITED ATOMS

As an example of a recent application of double resonance methods to the measurement of a hyperfine structure, we cite the work of Feiertag and zu Putlitz.<sup>(58)</sup> This study of the  $7^2P_{1/2}$  term of  $^{85}\text{Rb}$  was of value in assessing the contribution of core polarization to the magnetic hyperfine structure.

#### 6.8. MEASUREMENT OF $g_J$ -FACTORS OF EXCITED STATES

The structure of levels of excited atoms is of interest not only from the point of view of hyperfine structure but also because measurements of  $g_J$ -values allow one to assess the degree of breakdown of  $L$ - $S$  coupling, for example, and to determine whether or not configuration interaction needs to be taken into account. In this context the double resonance method was used by Ma *et al.*,<sup>(59)</sup> to measure the  $g$ -factors of low-lying  $^3P_1$  states of strontium and barium. The  $g$ -factors were measured to a precision of a few parts in  $10^5$ .

### 7. APPLICATION OF OPTICAL METHODS TO MOLECULES AND IONS IN SOLIDS

We conclude this section with a brief reference to work on systems other than atoms.

#### 7.1. MOLECULES

A detailed analysis of the possibilities for molecular level-crossing spectroscopy has been given by Zare.<sup>(60)</sup> Crosley and Zare<sup>(61)</sup> applied this method to nitric oxide. The width of the zero field level-crossing curve for the state investigated was about 0.4 G, but this cannot be interpreted as a lifetime until the  $g$ -value is known. A double resonance experiment on the same state allowed the determination of the  $g$ -factor and hence the lifetime.<sup>(62)</sup>

In the case of molecules far more than in atoms, accidental coincidences of wavelength allow the excitation of the molecule by line radiation from a lamp of a different substance.

## 7.2. PARAMAGNETIC IONS IN SOLIDS

As an example of the application to ions in solids, we refer to a recent paper by Imbusch *et al.*<sup>(63)</sup> on excited states of  $V^{2+}$  and  $Mn^{4+}$  in  $Al_2O_3$ . This work allowed the measurement of hyperfine structure and spin-lattice relaxation of excited ionic states. References to earlier work in this field are given in the paper. More recently it has been shown by Chase<sup>(64)</sup> that double resonance applied to excited states of ions leads to modulation in the fluorescent light, just as in the case of free atoms.

# III RADIO-FREQUENCY INTERACTIONS

## (a) COHERENCE AND OPTICAL MONITORING

### 1. DISTINCTION BETWEEN OPTICAL FIELDS AND RADIO-FREQUENCY FIELDS

There is an important distinction to be drawn between the interaction of atoms with fields of extended spectral range (broad-band) on the one hand and of sharp frequency on the other. In the context of optical pumping experiments the interactions with light (including spontaneous emission) come under the former heading and with radio-frequency fields under the latter. For broad-band interactions the transition probabilities are independent of time and the absorption and emission processes can be represented by exponentials. Such processes are called "rate processes". In the Einstein treatment of the interaction of radiation with atoms, absorption, stimulated emission and spontaneous emission are treated as rate processes. For monochromatic fields on the other hand the transition probabilities are time-dependent, leading to a sinusoidal oscillation of population between two states connected by the perturbation. This sinusoidal oscillation is formally called nutation, but in the context of magnetic resonance one commonly speaks of spin-flipping. It is important to recognise the existence of two distinct frequencies in the context of magnetic resonance: the driving frequency whose phase is determined by the phase of the laboratory oscillator, and the nutational or spin-flip frequency for which the phase depends on the moment at which the system is introduced into the field and which in steady state experiments is a random variable.



It is, of course, possible to obtain the result for fields of extended spectral range by integrating over the results for monochromatic fields. It is not difficult to show analytically—and, indeed, the conclusion is very plausible—that the response of the system is exponential rather than sinusoidal if the amplitude of the initial state (in the interaction representation) does not change appreciably in the coherence time (reciprocal of the spectral range) of the exciting radiation. From this result one may deduce the following condition for the exponential response: the spectral range of the exciting radiation must be greater than the perturbation (measured in frequency units) applied to the final state of the transition. This perturbation may be that which arises from the exciting field itself or it may be some other perturbation such as an additional relaxing process.

## 2. MONOCHROMATIC FIELDS: SEMICLASSICAL OR QUANTIZED FIELD TREATMENT?

In the semiclassical treatment one describes the field classically and the matter quantum mechanically. The field variables are treated as ordinary algebraic quantities (*c*-numbers) in the analysis, but operators are used to describe dynamical variables of the atoms.

In the quantum field theory the radiation is quantized as well as the matter and the field variables are operators. The state functions are functions both of the field and of the matter.

The important difference between the two approaches lies in the treatment of the spontaneous emission. This needs no special consideration in the quantized field method, but needs supplementary assumptions in the semi-classical method. We shall state these assumptions in due course when we need to use them. All we need at the moment is to know under what circumstances the two treatments are equivalent.

They are equivalent (if properly formulated) when spontaneous emission can be ignored. This is ordinarily true in magnetic resonance or in other situations when the field is monochromatic and the mean photon-number is large compared with unity, for in this case the probability for spontaneous emission is much less than the probabilities for absorption and stimulated emission. This is an example of the normal condition under which quantum theory goes over into classical theory, namely that the contemplated change in a quantum number (in this case the photon-number) is large in comparison with the value of that number. But it is worth noticing that the quantized field and semiclassical theories are also equivalent for absorption processes treated by first order perturbation theory even when the optical fields are weak, (mean photon-number per mode much less than unity) for when one is dealing with absorption the possibility of spontaneous emission is irrelevant.

In the quantized field theory, as normally written, the basis states are energy eigenstates of the system (atoms+optical field), and the radio-frequency field is treated classically. In a recent formulation, Cohen-Tannoudji and Haroche<sup>(65)</sup> have taken (atoms+radio-frequency field) as the closed system whose energy eigenstates form the basis states. Time-dependence is treated by using superposition states.

In the semiclassical theory, time dependences, both of the optical and radio-frequency fields, appear as  $c$ -numbers, and it is very easy to follow phase factors from the fields to the atomic wave function and back to the fields.

We shall use the semi-classical treatment in this account. Detailed analyses will be restricted to studies of the radio-frequency interactions. We shall avoid difficulties connected with spontaneous emission by making use of the “pulse approximation”, and we shall generally use the pulse approximation also in dealing with the absorption of light.

### 3. MONOCHROMATIC FIELDS: SEMICLASSICAL TREATMENT

Two cases can be solved exactly:

- (i) rotating field in the plane perpendicular to a static field.
- (ii) field oscillating parallel to a static field (provided that the atomic coupling is not broken).

The methods of solution are different for these two cases. We shall treat the first fairly thoroughly and the second briefly, in Section III.7. We shall be thinking of magnetic fields, though much of the work will be applicable to electric fields also.

#### 3.1. A FIELD ROTATING IN THE PLANE PERPENDICULAR TO A STATIC FIELD

(This is the standard arrangement for magnetic resonance. The problem and its solution are well known but we wish to establish a notation and to derive some results for reference.)

$$\text{Let the field be } H\mathbf{k} + H_1 (\cos \omega_0 t \mathbf{i} + \sin \omega_0 t \mathbf{j}), \quad (14)$$

where  $\mathbf{i}, \mathbf{j}, \mathbf{k}$  form a set of Cartesian unit vectors. Let us write for the Hamiltonian of the system  $\mathcal{H}_0 + \mathcal{H}_1$ , where  $\mathcal{H}_0$  includes all time independent and isotropic interactions in addition to the interaction with the static field  $H$  and  $\mathcal{H}_1$  describes the interaction with the transverse field  $H_1$ .

The method of solution is:

- (i) make a transformation to eliminate the time dependence;
- (ii) integrate the equation of motion and write in the time development;



(iii) Diagonalize the transformed Hamiltonian;

(iv) transform back to the initial frame.

This sequence of operations yields the operator which gives the development in time of the state vector or density matrix of the atomic system (time-displacement operator). The matrix elements of the operator are easily found and the transition probabilities readily obtained.

Let us study the steps (i) to (iv) in turn and then apply the method to a simple case.

(i) The operator which removes the time dependence is  $\exp(i/\hbar) J_z \omega_0 t$  where  $J_z$  is the operator representing the component of angular momentum  $J$  along the direction of the static magnetic field ( $z$ -axis). As is well known this operator transforms the Hamiltonian  $\mathcal{H}_0 + \mathcal{H}_1$  to

$$\mathcal{H}' = \mathcal{H}_0 + \mathcal{H}_1' - \omega_0 J_z, \quad (15)$$

where  $\mathcal{H}_1' = \exp[(i/\hbar)J_z \omega_0 t] \mathcal{H}_1 \exp[-(i/\hbar)J_z \omega_0 t]$ .

We shall apply this transformation first at the particular time  $t = t_0$  at which the atoms begin to experience the field, and secondly at the later time  $t$  at which we sample the system. For a simple spin system the transformation is equivalent to changing the field given by eqn (14) to the effective field

$$\mathbf{H}_{\text{eff}} = (H - \omega_0/\gamma)\mathbf{k} + H_1 \mathbf{i} \quad (16)$$

( $\gamma$  is the gyromagnetic ratio).

(ii) The equation of motion is

$$i\hbar \frac{\partial}{\partial t} |'t\rangle = \mathcal{H}' |'t\rangle, \quad (17)$$

where  $|'t\rangle$  is the state vector at time  $t$  in the transformed frame. Since  $\mathcal{H}'$  is independent of time the equation integrates to

$$|'t\rangle = \exp[-(i/\hbar)\mathcal{H}'(t-t_0)]|'t_0\rangle. \quad (18)$$

We can most easily apply this equation if  $\mathcal{H}'$  is diagonalized. This leads us to the next step.

(iii) Diagonalization of the transformed Hamiltonian is easily accomplished for the simple spin system by choosing a representation in which the axis of quantization is along  $\mathbf{H}_{\text{eff}}$ , i.e., by a rotation of  $Oz$  through the angle  $\beta$  about the  $x$ -axis from the direction of  $H$  to the direction of  $\mathbf{H}_{\text{eff}}$ .

$\beta = \tan^{-1} H_1 / (H - H_0)$ . The operator is the rotation matrix  $\mathcal{D}^{(j)}(0, \beta, 0)$ .

In a more complicated system where the fields are strong enough to introduce some decoupling of spins we suppose that the Hamiltonian is diagonalized by an operator  $S$ .<sup>(66)</sup>

In either case let us suppose that the eigenvalues of the diagonalized Hamiltonian are  $\lambda_i$ , that is to say the  $\lambda_i$  are the eigenvalues of  $S\mathcal{H}'S^{-1}$  or of  $\mathcal{D}(\beta)\mathcal{H}'\mathcal{D}(-\beta)$ .

We now make use of the relation

$$\exp -(i/\hbar)\mathcal{H}'(t-t_0) = S^{-1} \{ \exp -(i/\hbar)S\mathcal{H}'S^{-1}(t-t_0) \} S, \quad (19)$$

and notice that the time development of  $\mathcal{H}'$  has been replaced by the time development of  $S\mathcal{H}'S^{-1}$  whose eigenvalues will appear as the frequencies in the periodic motion. These eigenvalues are the nutational frequencies.

(iv) The final transformation is to apply  $\exp[-iJ_z\omega_0 t]$  which takes us back to the laboratory frame at time  $t$ .

By this sequence of operations we have found the form of the time-displacement operator  $U(t, t_0)$  defined by

$$|t\rangle = U(t, t_0)|t_0\rangle. \quad (20)$$

We have

$$U(t, t_0) = \{ \exp -(i/\hbar)J_z \omega_0 t \} S^{-1} \{ \exp -(i/\hbar)S\mathcal{H}'S^{-1}(t-t_0) \} \\ \times S \{ \exp (i/\hbar)J_z \omega_0 t_0 \}. \quad (21)$$

#### a. Example

A particle with spin- $\frac{1}{2}$ . In the field  $H$  alone, let the eigenstates be  $|+\rangle$ ,  $|-\rangle$ . The energy eigenvalues are  $\pm\frac{1}{2}\hbar\omega$ , with  $\omega = \gamma H$ . Probability amplitudes are  $a_+$ ,  $a_-$ . Suppose we are given  $a_+ = 1$ ,  $a_- = 0$  at time  $t_0$ . The problem is to find the values of  $a_+$  and  $a_-$  at later time  $t$ .

The state vector at time  $t_0$  is  $\begin{pmatrix} 1 \\ 0 \end{pmatrix}$ . Using (20) and (21) we can immediately write down

$$\begin{pmatrix} a_+(t) \\ a_-(t) \end{pmatrix} = \begin{pmatrix} \exp -\frac{1}{2}i\omega_0 t & 0 \\ 0 & \exp +\frac{1}{2}i\omega_0 t \end{pmatrix} \begin{pmatrix} S_{++}^{-1} & S_{+-}^{-1} \\ S_{-+}^{-1} & S_{--}^{-1} \end{pmatrix} \\ \times \begin{pmatrix} \exp -\frac{1}{2}ip(t-t_0) & 0 \\ 0 & \exp +\frac{1}{2}ip(t-t_0) \end{pmatrix} \\ \times \begin{pmatrix} S_{++} & S_{+-} \\ S_{-+} & S_{--} \end{pmatrix} \begin{pmatrix} \exp +\frac{1}{2}i\omega_0 t_0 & 0 \\ 0 & \exp -\frac{1}{2}i\omega_0 t_0 \end{pmatrix} \begin{pmatrix} 1 \\ 0 \end{pmatrix}. \quad (22)$$

We have used the values  $\pm\frac{1}{2}\hbar$  for the eigenvalues of  $J_z$  and  $\lambda_{\pm} = \pm\frac{1}{2}\hbar p$  for the eigenvalues of  $S\mathcal{H}'S^{-1}$ . If for this case, we identify  $S$  with  $\mathcal{D}^{(\frac{1}{2})}(\beta)$ , we have

$$\begin{pmatrix} S_{++} & S_{+-} \\ S_{-+} & S_{--} \end{pmatrix} \equiv \begin{pmatrix} \cos\beta/2 & \sin\beta/2 \\ -\sin\beta/2 & \cos\beta/2 \end{pmatrix} = \begin{pmatrix} c & s \\ -s & c \end{pmatrix}. \quad (23)$$



Performing the matrix multiplication we find

$$\begin{pmatrix} a_+(t) \\ a_-(t) \end{pmatrix} = \begin{pmatrix} \exp -\frac{1}{2}i\omega_0 t [c^2 \exp -\frac{1}{2}ip(t-t_0) + s^2 \exp +\frac{1}{2}ip(t-t_0)] \\ \exp +\frac{1}{2}i\omega_0 t [sc \exp -\frac{1}{2}ip(t-t_0) - sc \exp +\frac{1}{2}ip(t-t_0)] \end{pmatrix} \times \exp +\frac{1}{2}i\omega_0 t_0, \quad (24)$$

$$\text{whence} \quad |a_+(t)|^2 = 1 - \frac{1}{2} \sin^2 \beta [-\cos p(t-t_0)], \quad (25)$$

$$|a_-(t)|^2 = \frac{1}{2} \sin^2 \beta [1 - \cos p(t-t_0)], \quad (25a)$$

and

$$a_+ a_-^* = \frac{1}{2} \sin \beta \{ c^2 [1 - \exp -ip(t-t_0)] - s^2 [1 - \exp +ip(t-t_0)] \} \exp -i\omega_0 t. \quad (25b)$$

$$\tan \beta = H_1 / (H - H_0), \quad \text{where } H_0 = \omega_0 / \gamma.$$

Equations (25) and (25a) give the populations of the states. Notice the sinusoidal variation with frequency  $p$ . Notice also that the driving frequency  $\omega_0$  does not appear in these equations.

Equation (25b) gives the correlation between the states. The driving frequency appears in this equation as well as the nutational frequency,  $p$ . Notice that  $p$  occurs with the time interval  $(t-t_0)$ , whereas  $\omega_0$  occurs with the time  $t$ .

### b. Frequency diagram

Let us study the periodic terms which occur in equation (24). Firstly, the common factor  $\exp +\frac{1}{2}i\omega_0 t_0$  is irrelevant. It represents an arbitrary phase factor common to both states. Next, we see the factors  $\exp \pm \frac{1}{2}i\omega_0 t$ . These are periodic functions at frequencies  $m\omega_0$ , where  $m$  is the space quantum number with respect to the direction of the field  $H$ . But each of these terms is multiplied also by periodic terms with frequencies  $\pm \frac{1}{2}p$ . The  $\pm \frac{1}{2}$  in these factors is the space quantum number with reference to the direction of  $\mathbf{H}_{\text{eff}}$ .

These frequencies and the corresponding quantum labels can be given a convenient diagrammatic representation.

Figure 32a shows the energy levels of the states  $|+\rangle$ ,  $|-\rangle$  as a function of the magnetic field  $H$ . The levels are described by the equations  $\omega = \pm \frac{1}{2}\gamma H$ . (It is convenient to speak of the energy at this stage although the equation we have written is for the corresponding Bohr frequency).

Figure 32b shows the energy levels seen in the rotating frame, still plotted against the laboratory field  $H$  and supposing that the transverse field  $H_1$  has not yet been applied.

Figure 32c shows the energy levels for a finite value of  $H_1$ . These are the eigenvalues  $\lambda_{\pm}$  of  $\mathcal{D}(\beta)\mathcal{H}'\mathcal{D}(-\beta)$ . They are described by the equation

$$p = \pm \frac{1}{2}\gamma H_{\text{eff}} = \pm \frac{1}{2}\gamma [(H - H_0)^2 + H_1^2]^{\frac{1}{2}}. \quad (26)$$

But we must remember that the eigenstates are now described with reference to the rotated axis. In order to emphasise this the states have been labelled  $\oplus$   $\ominus$ . These states are superpositions of the original states as follows:

$$\begin{aligned} |\oplus\rangle &= \cos \beta/2 |+\rangle + \sin \beta/2 |-\rangle, \\ |\ominus\rangle &= -\sin \beta/2 |+\rangle + \cos \beta/2 |-\rangle. \end{aligned} \quad (27)$$

Figure 32d shows the energy levels after the transformation back to the laboratory frame. The level labelled  $\oplus$  gives rise to two levels displaced by  $\pm \frac{1}{2}\omega_0$ , corresponding to the eigenvalues  $\pm \frac{1}{2}$  of  $J_z$  for the states  $|+\rangle$ ,  $|-\rangle$ . Similarly the level labelled  $\ominus$  in Fig. 32c gives two levels in Fig. 32d. In Fig.

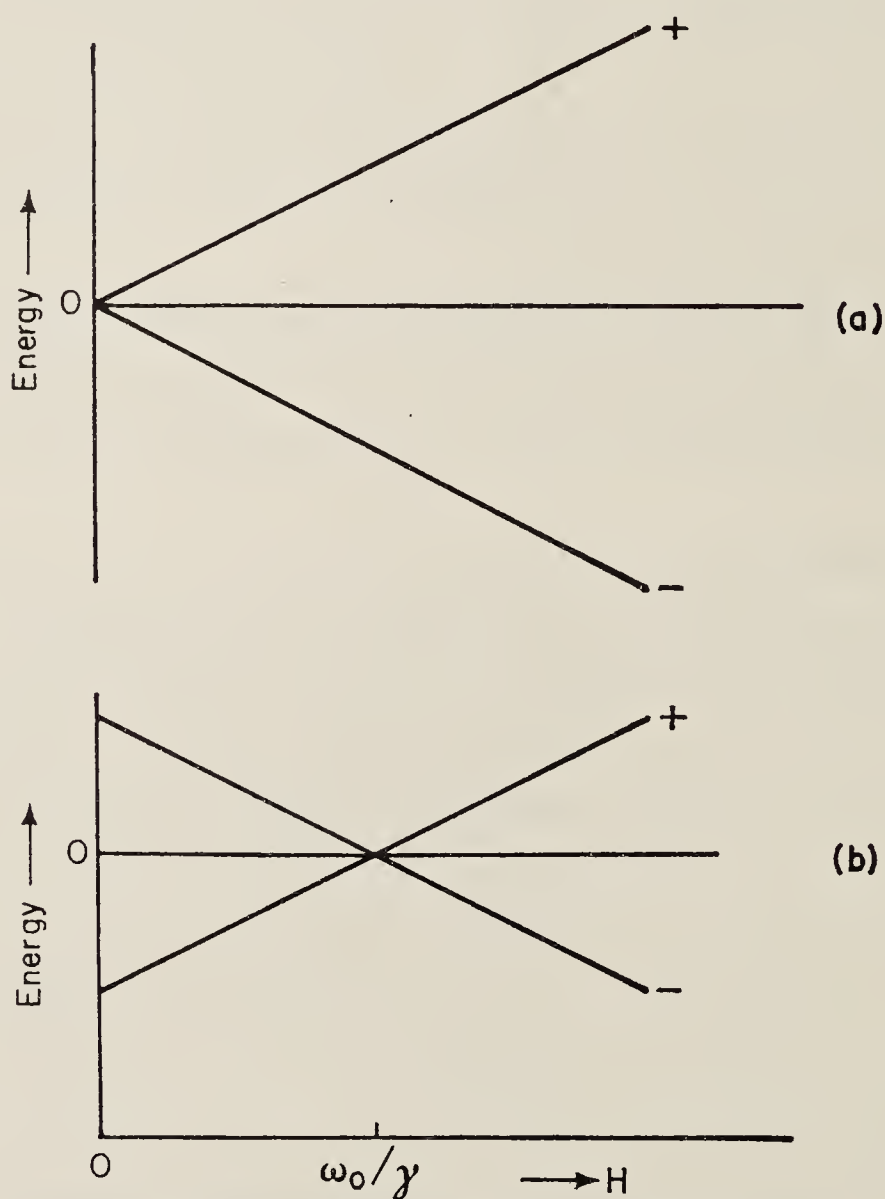


FIG. 32a. Energy of spin- $\frac{1}{2}$  system as function of magnetic field.

b. Energy of spin- $\frac{1}{2}$  system in rotating frame (angular frequency  $\omega_0$ : rotation parallel to  $H$ ).

32d the interval between the pairs of levels labelled  $+$ ,  $\oplus$  and  $-$ ,  $\oplus$  or  $+$ ,  $\ominus$  and  $-$ ,  $\ominus$  is  $\omega_0$ , whereas the interval between a pair labelled  $+$ ,  $\oplus$  and  $+$ ,  $\ominus$  or  $-$ ,  $\oplus$  and  $-$ ,  $\ominus$  is  $p$ .

Diagrams such as Fig. 32d are generalizations of ordinary term diagrams. An ordinary term diagram is a representation of the energies of different modes of a system where the Hamiltonian is time independent. The frequency



diagram shows the side bands which appear when a periodic perturbation is applied. The levels have the same physical reality as do the energy levels in an ordinary term diagram. They may be explored, as we shall see, by suitable monitoring of the system.

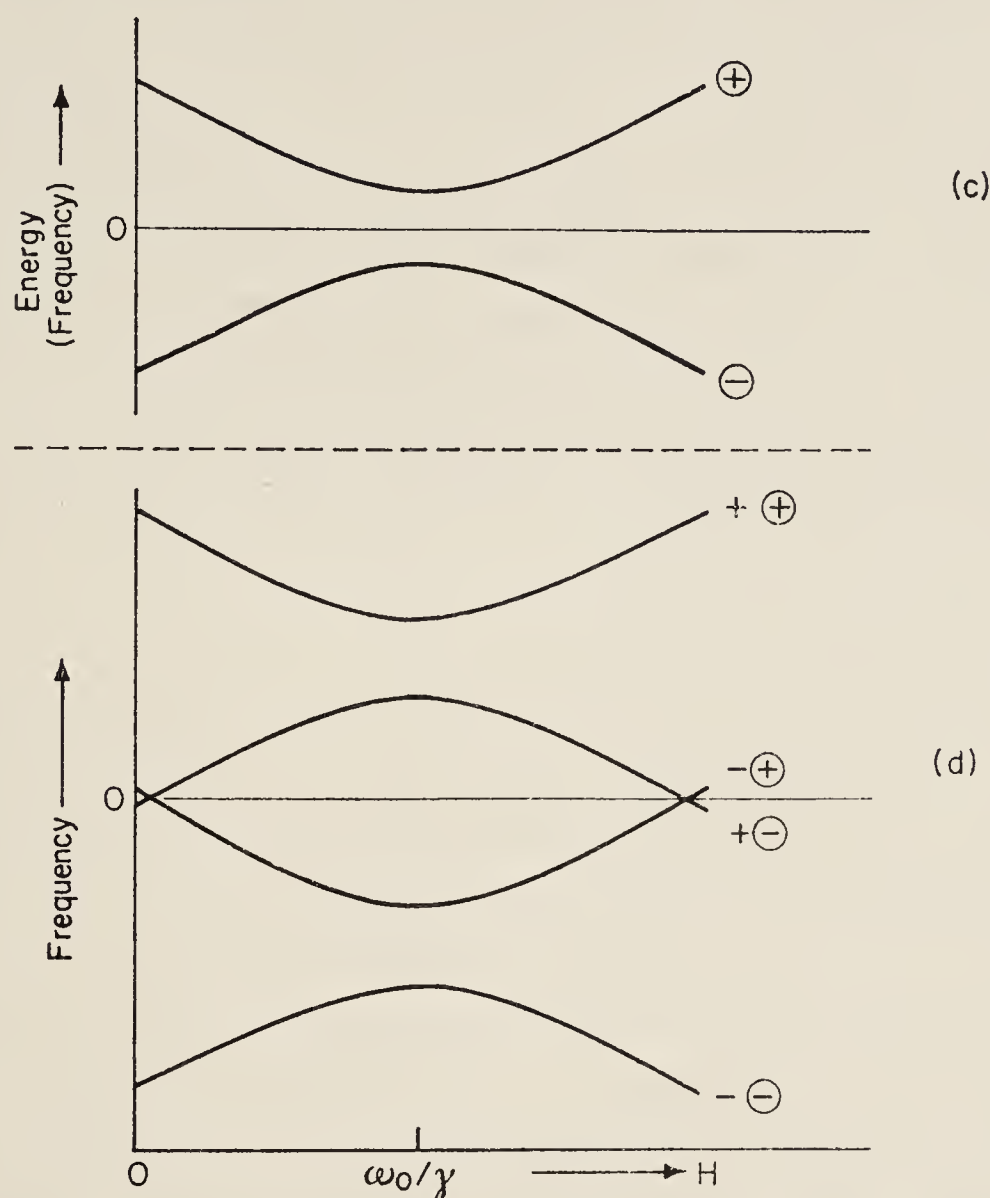


FIG. 32c. Energy in rotating frame: addition of transverse field  $H_1$ .

d. Frequency diagram in laboratory frame.

In general the nutational frequencies do not appear in steady state experiments but may be found in pulse or modulation experiments.

#### 4. APPLICATION TO DOUBLE RESONANCE EXPERIMENTS

In such experiments the considerations of the previous section apply to the excited states. Atoms are excited by broad band irradiation, experience the interaction with the magnetic fields, and decay by spontaneous emission of light. In a steady state experiment the irradiation with light is continuous and one needs to justify the separation of the interaction into the three parts: excitation, radio-frequency interaction, and spontaneous emission. The justification lies in a comparison of the coherence times of the optical and radio-frequency perturbations with the mean lifetime of the excited atoms. For broad band irradiation the coherence time of the light is typically  $10^{-10}$  sec,

whereas the mean lifetime is typically  $10^{-8}$  sec. Thus, phase continuity under irradiation is lost in a time short compared with the mean lifetime and it is a good approximation to consider the excitation as a random sequence of pulse processes. The coherence time of the radio-frequency interaction, on the other hand, is, for a continuous wave oscillator, the period for which the oscillator is switched on, so that continuity of phase of the radio-frequency perturbation is something that cannot be ignored. As for spontaneous emission, it is convenient to think of this as the result of a perturbation stimulated by random fluctuations having the spectrum of black body radiation at the absolute zero. For such a spectrum the coherence time needs careful definition, but it suffices here to think of the coherence time as the reciprocal of the frequency which is being stimulated. The time we have to consider therefore is of order  $10^{-15}$  sec which allows spontaneous emission also to be treated as a pulse process.

Our model is therefore as follows:

- (i) an atom is excited at time  $t_0$ ;
- (ii) its wave function evolves in the excited state under the influence of the magnetic fields. It is nearly always true in double resonance experiments that the wavelength of the radio-frequency field is large compared with the size of the experimental vessel, so that for different atoms we may ignore the dependence of the phase of the radio-frequency field on position and take account of the time variation only;
- (iii) it decays at time  $t$  later than  $t_0$ . We need make no distinction between the time of emission of light and the time of arrival at the photo-detector since the time of flight is negligibly small compared with the lifetime of the excited atoms and with the period of the radio-frequency field. However, since the atoms are distributed at random in the experimental cell, there can be no interference between light from different atoms. The net photo-electric signal is given by summing the effects of single atoms;
- (iv) to describe a steady state experiment the signal at time  $t$  is found by summing over random times of excitation  $t_0$ . That is, if the rate of excitation is constant,  $R$ , the number of atoms excited in the interval  $dt_0$  is  $Rdt_0$  and the net effect is found by integrating over  $t_0$ . (This approach neglects the statistical fluctuations).

The problem is reduced, therefore, to calculating the light emitted at time  $t$  by an atom known to have been excited to a particular state (or superposition-state) at time  $t_0$ . The calculation of the last section has enabled us to calculate the state function at time  $t$  and we need now to write an expression of the intensity of the emitted light. We shall see in a later section that it is of interest also to consider the state vector of the atom after the emission of light.



#### 4.1. EMISSION OF LIGHT

In the semi-classical theory applied to emission from atoms in energy eigenstates, the well-known procedure is to suppose that each excited atom will radiate like a set of independent oscillators whose dipole moments are given by the matrix elements of the electric dipole operator between a specified excited state and all lower states which connect with it. We need to generalize this procedure for the present situation where the atoms are being subjected to a time-dependent perturbation (the r-f field). We must now take dipole matrix elements between eigenstates of the perturbed system, and if we express these in terms of the energy eigenstates of the system without the radio-frequency field we shall find superposition-states and time-dependent phase factors both in the excited states and in the ground states. Moreover, the levels concerned are those of the frequency diagram rather than the time-independent term diagram. But we should notice that the transition amplitudes are very small if the system is far from resonance, (e.g. if the angle  $\beta$  is small in eqns (23, 24, 25) the amplitude  $a_+$  remains very close to unity and the amplitude  $a_-$  is always extremely small).

We generally meet one of the following two cases:

- (i) the ground state is single ( $J = 0$ ), in which case the question of radio-frequency mixing does not arise;

or (ii) if the ground state has structure the intervals are generally so different from the intervals between the excited states that when the radio-frequency field is near resonance for the latter, it is far from resonance for the former.

The conclusion is (so long as either (i) or (ii) above is true) that the required electric dipole matrix element is between a superposition-state for the excited states and an energy eigenstate of the unperturbed system for the lower state.

##### *a. Example*

Let the two-level system which we formerly discussed now represent the excited state of an atom. We shall use  $m$  or  $m'$  to label the two eigenstates. We may use the equations of Section III 3.1.a for this case, provided we take account of radiative damping. This we do by multiplying the amplitudes  $a_+$  and  $a_-$  of the eqn (24) by  $\exp -\frac{1}{2}\Gamma(t-t_0)$ , supposing that both states decay at the same rate.

Suppose that the atom in its ground state is also a two-level system labelled by  $\mu, \mu'$ . Then the electric dipole matrix elements which we need are  $\langle \mu | \mathbf{P} | t \rangle$ , where  $\mu$  can be  $+$  or  $-$ . The component of the radiation which passes an analyser parallel to the unit vector  $\mathbf{e}$  depends on  $\langle \mu | \mathbf{e} \cdot \mathbf{P} | t \rangle$ , and the intensity of light passing this analyser will be proportional to the modulus squared.

This will be the intensity at time  $t$  emitted by an atom excited at time  $t_0$ . We thus have

$$I(t, t_0) = K \sum_{\mu} |\langle \mu | \mathbf{e} \cdot \mathbf{P} | t \rangle|^2, \quad (28)$$

where  $K$  is an unimportant constant. (In the quantum field theory, this equation gives the probability of finding a photon at time  $t$ ).

Using the expansion

$$|t\rangle = a_+(t) |+\rangle + a_-(t) |-\rangle, \quad (29)$$

with  $a_+$ ,  $a_-$  given by (24) we have

$$I(t, t_0) = K \sum_{\substack{\mu \\ m, m'}} \langle \mu | \mathbf{e} \cdot \mathbf{P} | m \rangle \langle m' | \mathbf{e}^* \cdot \mathbf{P} | \mu \rangle a_m a_{m'}^* \quad (30)$$

The intensity at time  $t$  resulting from excitation at the uniform rate  $R$  is given by

$$I(t) = KRA_{mm'} \int_0^t a_m(t, t_0) a_{m'}^*(t, t_0) \exp -\Gamma(t-t_0) dt_0 \quad (31)$$

$$= KR \text{Tr}(A\sigma). \quad (31a)$$

In writing eqn (31a) we regard  $A$  as a matrix whose  $(m, m')$  element is given by

$$A_{mm'} = \sum_{\mu} \langle \mu | \mathbf{e} \cdot \mathbf{P} | m \rangle \langle m' | \mathbf{e}^* \cdot \mathbf{P} | \mu \rangle, \quad (31b)$$

and  $\sigma$ , whose  $(m, m')$  component is given by the integral in eqn (31), as the steady state density matrix for the excited atoms.

The elements of  $\sigma$  are:

$$\sigma_{++} = \frac{1}{\Gamma} \left[ 1 - \frac{1}{2} \frac{b^2}{\Gamma^2 + p^2} \right] \quad (32)$$

$$\sigma_{--} = \frac{1}{\Gamma} \left[ \frac{1}{2} \frac{b^2}{\Gamma^2 + p^2} \right] \quad (32a)$$

$$\sigma_{+-} = \sigma_{-+}^* = \frac{b}{2\Gamma} \frac{\delta + i\Gamma}{\Gamma^2 + p^2} \exp -i\omega_0 t, \quad (32b)$$

where  $b = \gamma H_1$ ,  $\delta = \gamma(H - H_0)$ ,  $p = \gamma[(H - H_0)^2 + H_1^2]^{\frac{1}{2}}$ .

By suitable choice of the type and orientation of the analyser which transmits the light, the elements of the matrix  $A$  can be given real or imaginary values or zero. Thus the intensity of the light will be represented by a sum of elements of the matrix  $\sigma$  weighted by factors which are under the control of the experimenter. The diagonal elements of  $\sigma$  will contribute time-independent terms, but for those configurations of analyser which yield non-vanishing



values for the off-diagonal elements of  $A$ , we shall find in the sum terms of the form

$$\left(\frac{b\delta}{\Gamma^2 + p^2}\right) \frac{\sin \omega_0 t}{\cos \omega_0 t} \quad \text{and} \quad \left(\frac{b\Gamma}{\Gamma^2 + p^2}\right) \frac{\sin \omega_0 t}{\cos \omega_0 t}. \quad (33)$$

The intensity of the light will therefore be given as a sum of resonance functions of the Lorentzian type with denominators  $(\Gamma^2 + p^2)$ . The width at half intensity is  $2[(\Gamma/\gamma)^2 + H_1^2]^{\frac{1}{2}}$ . Arising from the off-diagonal elements are terms modulated at the driving frequency. The amplitudes of modulation are resonance functions of the bell-shaped type,  $\Gamma/(\Gamma^2 + p^2)$ , or the dispersion-shaped type,  $\delta/(\Gamma^2 + p^2)$ . It is worth noticing that the terms which arise from the diagonal elements of  $\sigma$  are proportional to  $b^2$  whereas those arising from the off-diagonal element are proportional to  $b$ .

The resonance functions which we have found are precisely those which arise in the Bloch theory of magnetic resonance. Their occurrence here and in that theory may be traced to the fact that the signal which is being described is to be associated with a multipole of order 1 in the expansion of the density operator; in other words they are characteristic of the polarization of the system. If we were to look into the detail of the type of polarizer required to bring out the off-diagonal elements of  $\sigma$  we should find that of necessity we must use a circular or elliptical analyser; a linear analyser would not suffice. Similarly, in order to excite the system as we have supposed at time  $t_0$  into the state  $|+\rangle$ , that is to say, to excite a polarized system, we would have required a circular or elliptical polarizer.

Had we studied a spin-1 system it would have been possible to contemplate alignment as well as polarization. Alignment can be generated and monitored by linear polarizers and analysers. In this case the resonance functions are slightly more complicated. They are given by Dodd and Series.<sup>(67)</sup> The monitoring of the density matrix by various means has been discussed by Carver and Partridge.<sup>(68)</sup>

## 5. MODULATION IN DOUBLE RESONANCE AND OPTICAL PUMPING EXPERIMENTS

### 5.1 MODULATION IN FLUORESCENT LIGHT

We have shown how the effect of a radio-frequency field on a system near resonance is by no means completely described in terms of its effect on the populations of the states. The field injects coherence into the atomic system, which may formally be described in terms of the off-diagonal elements of a density matrix. We have shown how this coherence might be expected to give

rise to modulation in the fluorescent light in a double resonance experiment.

These expectations have been fully borne out by experiment. Figures 33a to d show resonance curves for the amplitude of modulation of light in the Brossel-Bitter experiment.<sup>(69)</sup> Here we are monitoring a spin-1 system, so the

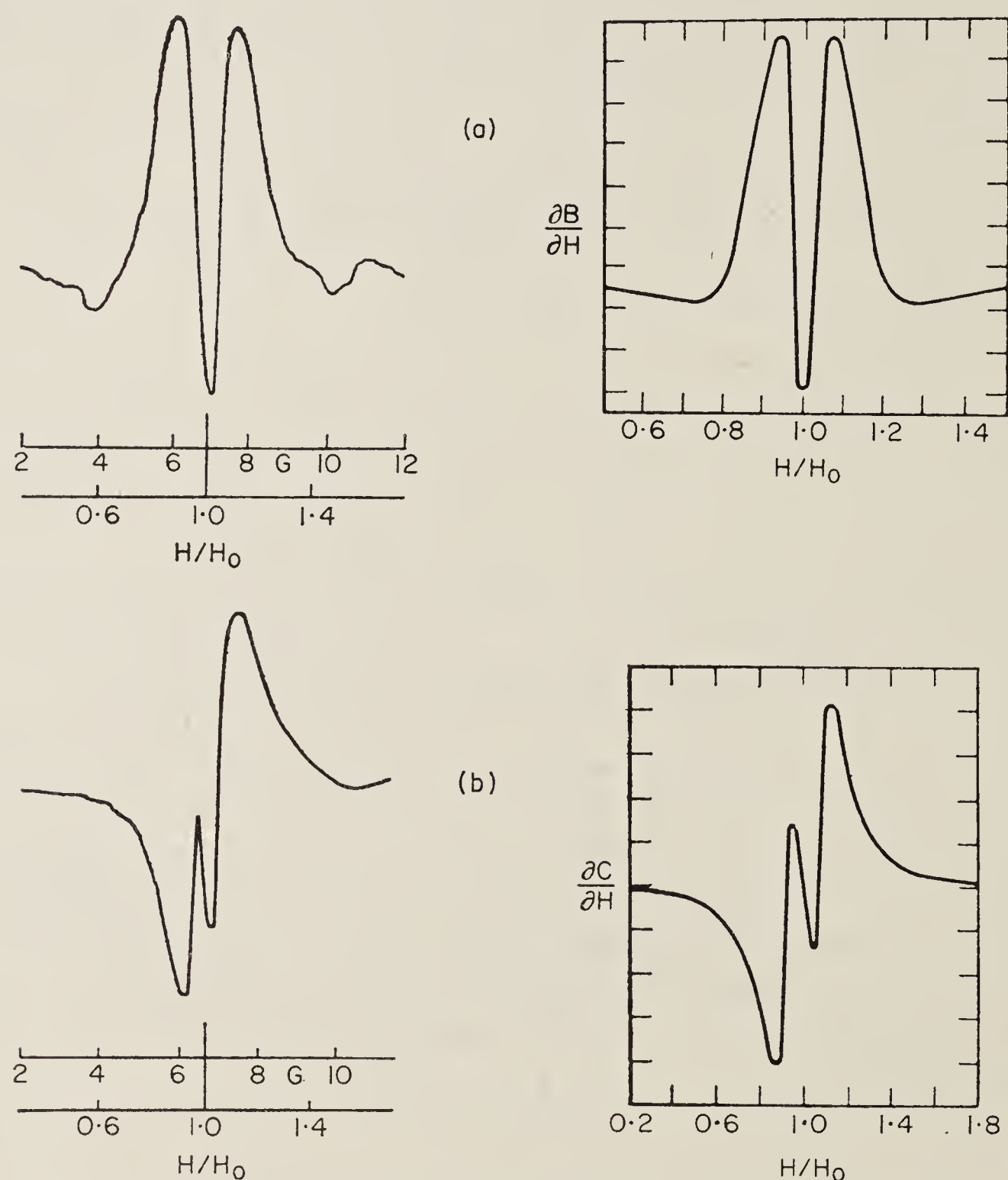


FIG. 33. Resonance functions for amplitude of modulation in the Brossel-Bitter experiment. a, b. In-phase and quadrature components at the fundamental frequency. The curves are derivatives with respect to magnetic field of the amplitude of modulation. Experimental curves on the left: theoretical curves on the right. (After Dodd, *et al.*<sup>(69)</sup>)

curves are not the simple Lorentzians but the more complicated functions referred to in the last section. In fact, the curves were taken by imposing on the system a low frequency modulation and by phase-sensitive detection so that the curves are, in fact, derivatives of the resonance functions.



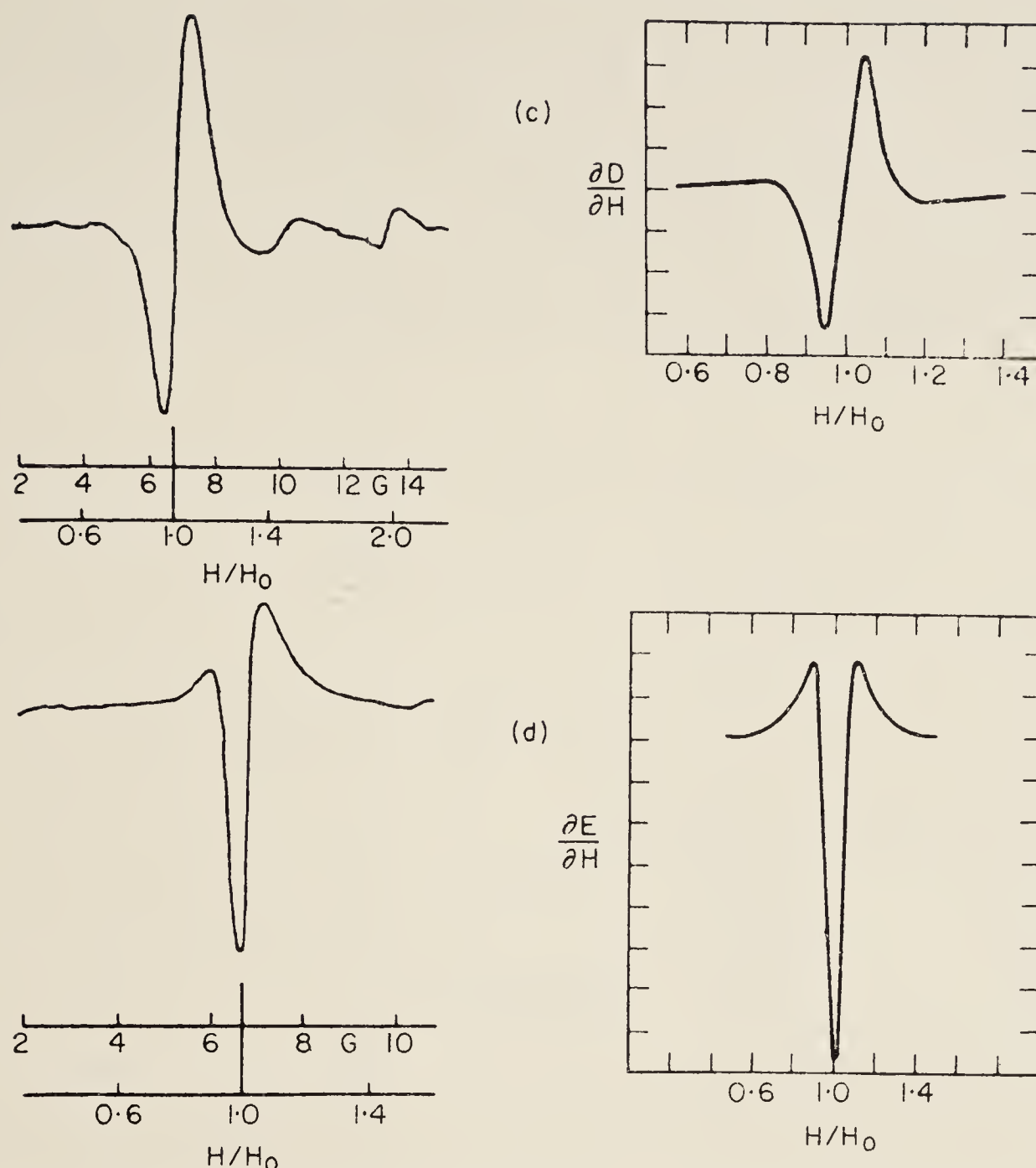


FIG. 33. c, d. In-phase and quadrature components at the second harmonic.  
(After Dodd *et al.*<sup>(69)</sup>)

## 5.2. MODULATION IN ABSORPTION

Our calculation of the radio-frequency interaction holds also for atoms in the ground states (provided an inequality of population has been achieved by optical pumping). Just as coherence between the excited states is shown by modulation in the fluorescent light, so also one might expect coherence between ground states to be shown by modulation in absorption. This too has been studied experimentally. Figure 34 shows modulation in absorption from the metastable state  $2^3S_1$  in helium.<sup>(70)</sup>

## 6. TRANSFER OF COHERENCE

### 6.1. TRANSFER OF COHERENCE BY EXCITATION

Consider now a system in which coherence has been generated by a radio-frequency field, for example, the ground states in an optical pumping experi-

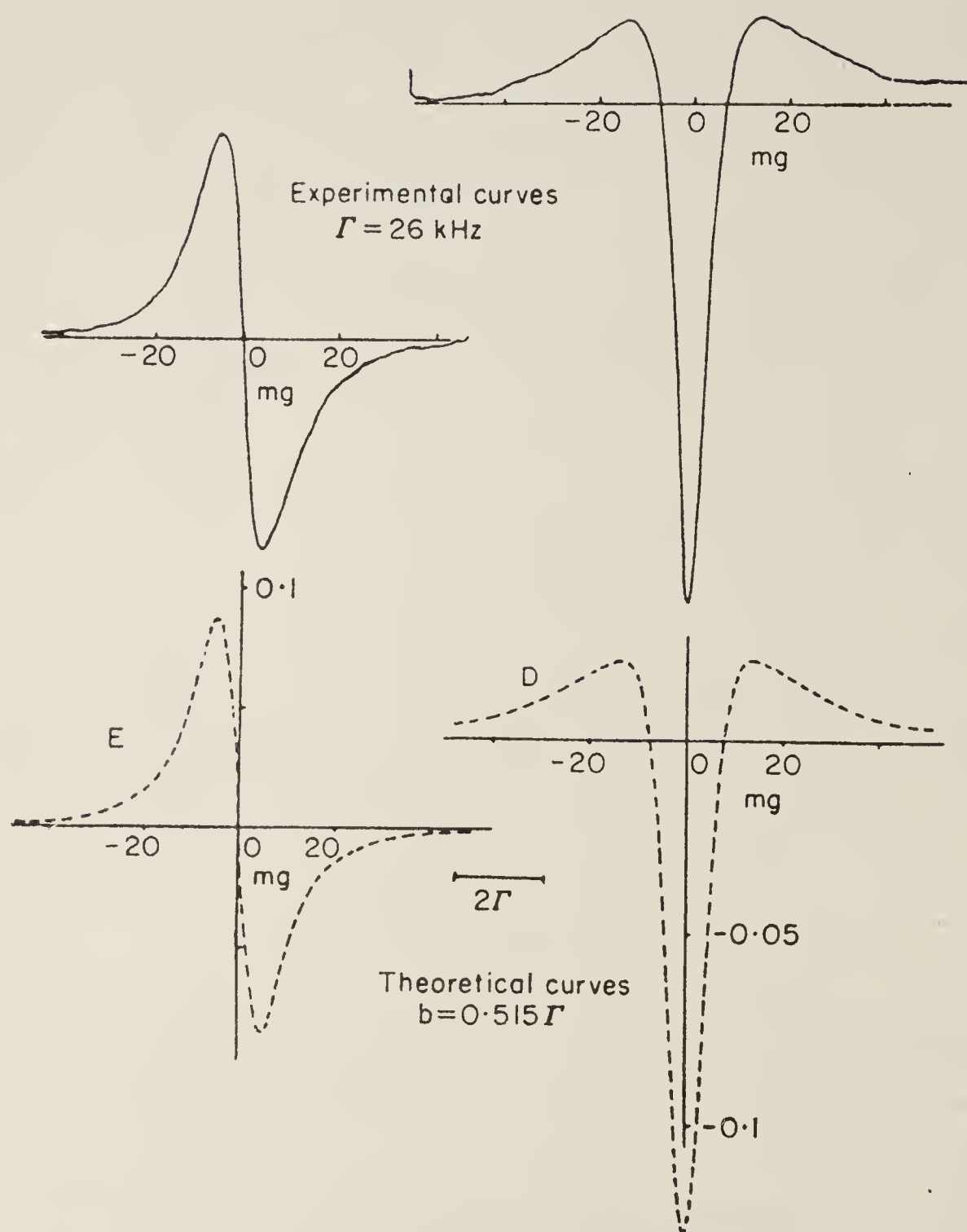


FIG. 34. Experimental and theoretical resonance curves for modulation in absorption from the metastable state  $2^3S_1$  in helium. In-phase and quadrature components at the second harmonic. These are to be compared with figures 33c and d. Experimental conditions: no polarizer, linear analyser,  $\omega_0/2\pi = 0.5$  kHz,  $\Gamma = 26$  kHz,  $b/\Gamma = 0.515$ . (After Partridge and Series.<sup>(70)</sup>)

ment as in the last section ( $2^3S_1$  helium). Suppose, for preciseness, we consider the coherence between the states  $|+1\rangle$  and  $|-1\rangle$  and ask what would be the effect of illuminating the atom with light polarized parallel to the magnetic field ( $\pi$ -light;  $\Delta m = 0$ ). There exist dipole matrix elements between  $2^3S_1$  and  $2^3P_1$ ; the states  $|\pm 1\rangle$  of  $2^3S_1$  connect with  $|\pm 1\rangle$  of  $2^3P_1$  respectively. Therefore, provided the spectrum of the light spans both these transitions in absorption, one might expect that the coherence between  $|\pm 1\rangle$  in  $2^3S_1$  would be transferred to  $|\pm 1\rangle$  in  $2^3P_1$ , and this indeed takes place. (See Fig. 35.)

We need however, to consider this possibility a little more carefully. While it is true that the coherence can be transferred by a single pulse process, it is not necessarily the case that such coherence will be transferred in a steady-state experiment. We can think out this question by analogy with the theory



of electric circuits. The coherence we are trying to inject into the upper state is represented by a periodic function at a specified frequency. The upper state (described by its density matrix) is to be thought of as a receiver through which the coherence is to pass. We know it will pass if the applied frequency matches the tuned frequency of the receiver to within its bandwidth. In our analogy the tuned frequency of the receiver is given by the interval between the eigenstates  $|\pm 1\rangle$  selected by the optical transitions. The bandwidth is given by the excited

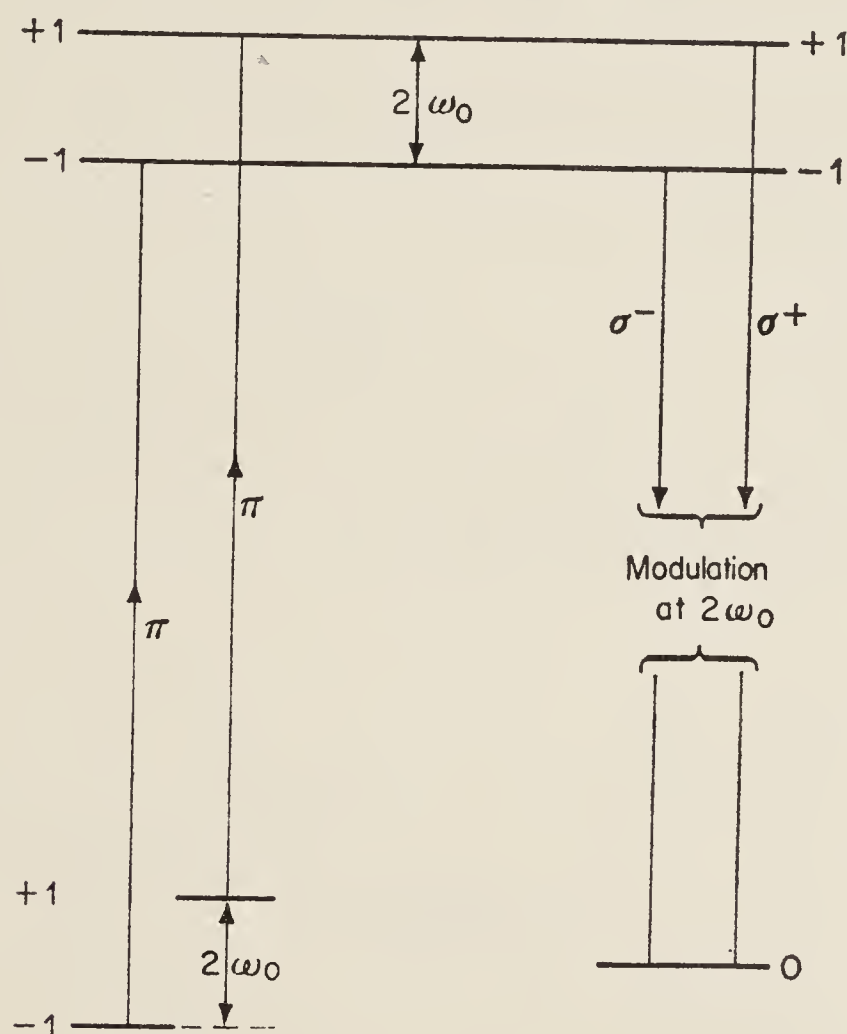


FIG. 35. Transfer of coherence from ground states to excited states and resulting modulation of the fluorescent light. The intervals between the levels are at the second harmonic of the driving frequency  $\omega_0$ . They are not the same as the intervals in a static magnetic field.

state damping constant. In a practical case we might be trying to inject a frequency of some kilohertz or megahertz into excited states separated by an interval of a few megahertz but with a damping constant of several hundred megahertz. Because the bandwidth is so large the frequency mis-match is irrelevant in many actual cases. It is very easy to transfer coherence from the ground states to excited states in optical pumping experiments.

The coherence thus transferred is, of course, shown up in the fluorescent light. For this reason it is possible to monitor optical pumping signals both for modulated as well as unmodulated components by studying the fluorescent light.

## 6.2. TRANSFER OF COHERENCE IN DECAY

The possibility of transferring coherence exists for spontaneous decay as well as for excitation by light. We must consider two significant differences:

- (i) spontaneous decay is an isotropic process whereas absorption can be anisotropic;
- (ii) the restrictions imposed by the bandwidth of the receiver are very severe in the case when the receiving states are ground states.

Let us consider the consequences.

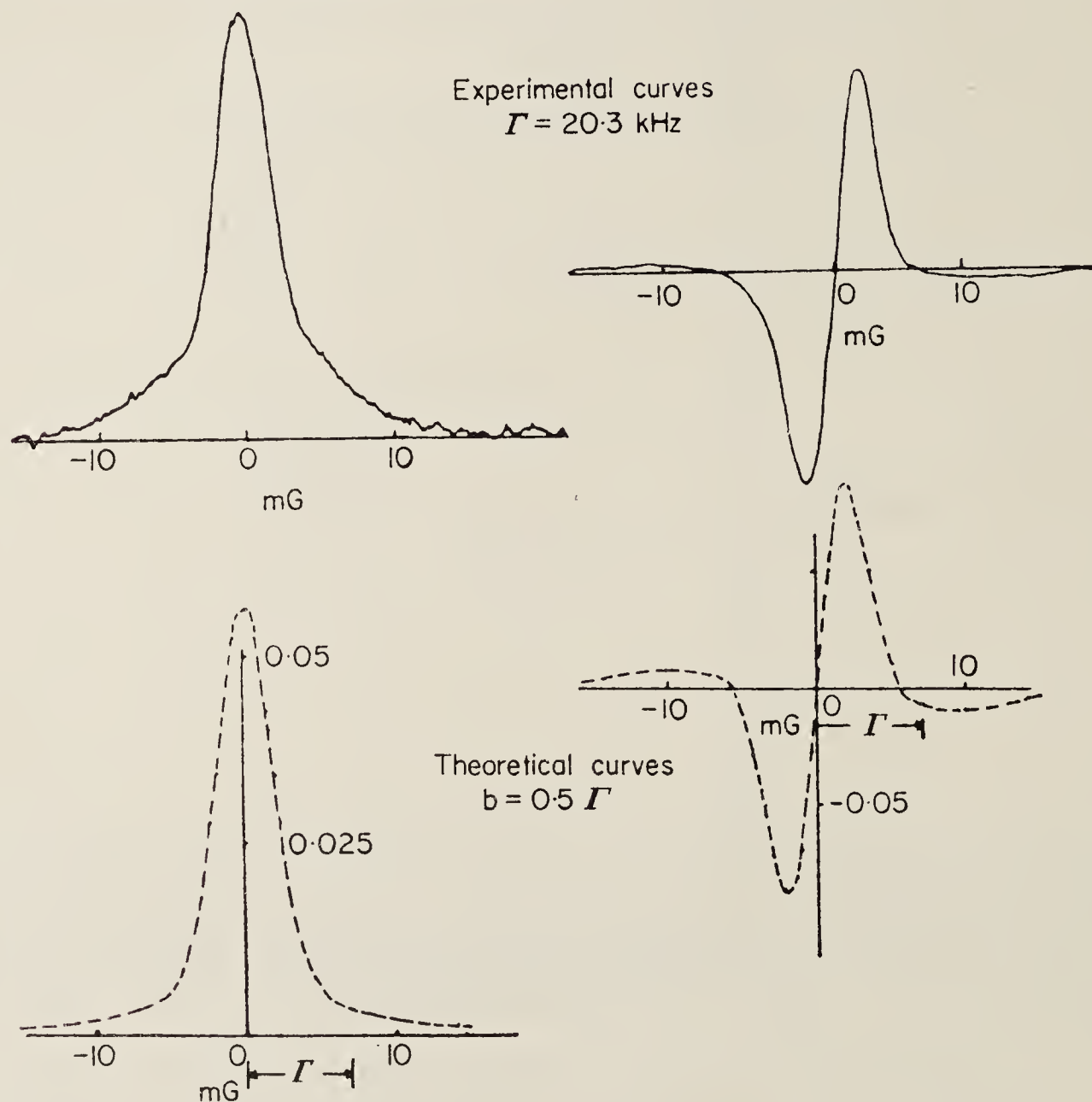


FIG. 36. Demonstration of circulation of coherence in optical pumping in helium. Experimental recordings compared with theoretical curves of the amplitude of modulation at  $4\omega_0$ . Experimental conditions: linear polarizer, no analyser,  $\omega_0/2\pi = 0.5 \text{ kHz}$ ,  $\Gamma = 20.3 \text{ kHz}$ .  $b/\Gamma = 0.5$ . (After Partridge and Series.<sup>(70)</sup>)

(i) Although spontaneous emission is isotropic we may still resolve the perturbation into modes of sharp frequency and specified polarization. The integration over frequencies gives the result for a steady-state broad-band process which we analysed in the last section. It remains to perform the addition over the three orthogonal modes of polarization. This eliminates the possibility of transfer of coherence through the agency of different modes, (e.g. a



$\pi$ -transition cannot couple with a  $\sigma^+$  transition), but there remains the possibility for transfer by the same mode acting in both transitions ( $\pi$  with  $\pi$ ,  $\sigma^+$  with  $\sigma^+$  and  $\sigma^-$  with  $\sigma^-$ ).

(ii) Turning now to the bandwidth of the receiving states, this may be of the order of a few kilohertz or even a few hertz. Therefore, the frequency to be injected must match the interval between the ground state energy levels to within that tolerance. The levels we are here concerned with are those appropriate to the system perturbed by the radio-frequency field, namely, those which appear in the frequency diagram, rather than the energy levels appropriate to the system in a static field alone. The condition of matching finds mathematical expression in factors such as  $\{\Gamma_\mu + i\omega_0[(\mu_1 - \mu_1') - (\mu_2 - \mu_2')]\}^{-1}$  which govern the probability for transfer of coherence from the  $(\mu_1, \mu_1')$  component of the density matrix to the  $(\mu_2, \mu_2')$  component via absorption followed by spontaneous decay<sup>(71)</sup>. For  $\omega_0 \geq \Gamma_\mu$ , the probability is very small unless  $[(\mu_1 - \mu_1') - (\mu_2 - \mu_2')]$  is zero.

In Fig. 36 are shown resonance curves for the amplitude of modulation at  $4\omega_0$  in the optical pumping experiment in  $2^3S_1$  of  $^4\text{He}$  we referred to earlier. Evidence from the line-shape proves that the signals are due to coherence which was injected into the ground state, carried into the excited state and

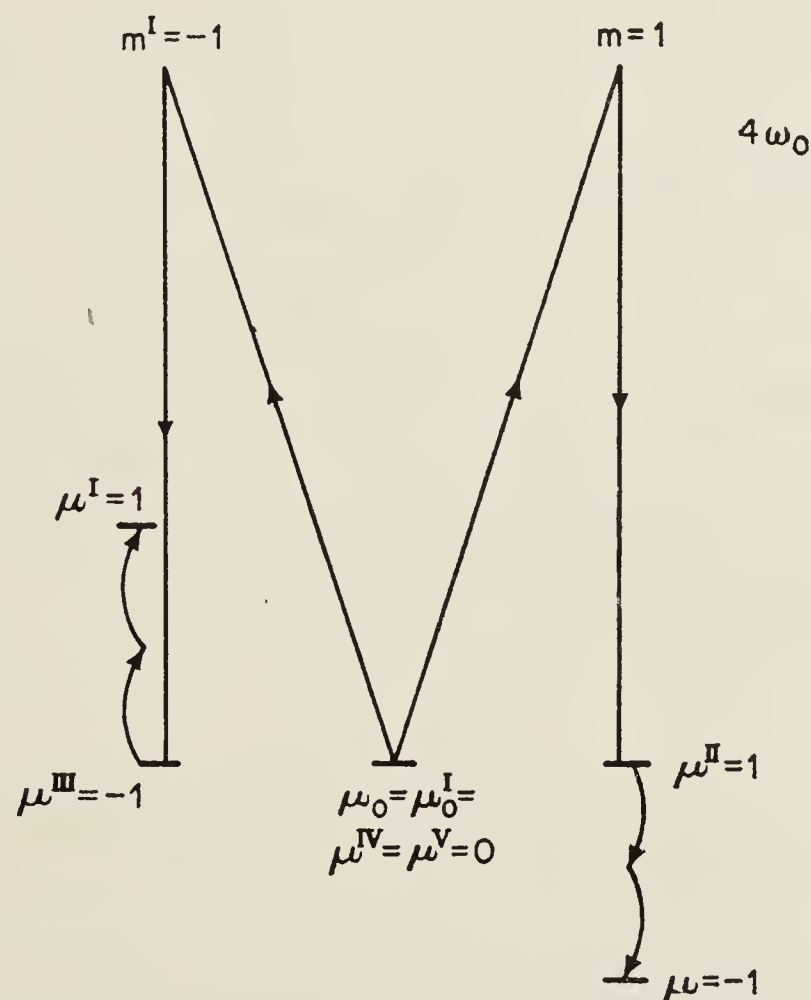


FIG. 37. Diagram showing the generation of coherence at  $4\omega_0$  by the following sequence of processes:

- (i) coherent absorption of  $\sigma^+$  and  $\sigma^-$  light,
- (ii) transfer of coherence by  $\pi$  mode of decay,
- (iii) radio-frequency mixing.

back to the ground state by absorption followed by spontaneous decay, and monitored in the ground state by another absorption process. One of the sequences of transitions which contributed to this signal is represented in Fig. 37. It was shown that the strength of the signal was indeed frequency-dependent as is predicted by denominators of the form indicated in the last paragraph.

### 6.3. TRANSFER OF COHERENCE BY COLLISION

We have hitherto been speaking of processes taking place in individual atoms. We now consider the possibility of transferring coherence from one atom to another in collisions.

The process of spin exchange which we mentioned in an earlier section (I 6.9) may be represented as a transfer of longitudinal polarization by collision. The transfer of transverse polarization may be described as the transfer of coherence. There is no objection of principle, therefore, to the notion of the transfer of coherence by collisions. In fact, it takes place subject to the general rule that the frequency mis-match between the driving and receiving systems be not greatly in excess of the damping constant of the receiver.

An example illustrates what, at first sight, might appear to be surprising features of the phenomenon.

In a previous section we discussed the polarization of  $^3\text{He}$  in the ground state  $1^1S_0$  by collisions with optically pumped  $^3\text{He}$  atoms in the metastable state  $2^3S_1$ . Magnetic resonance of the  $^3\text{He}$  nuclei is monitored by detecting changes in the light absorbed by the metastable atoms. If one studies the absorption with the appropriate geometrical arrangement one finds modulation at the frequency at which one is driving the nuclear resonance. This is evidence that coherence injected into ground states has been transferred to metastable states of the atoms by collisions. The resonance curve (Fig. 23a) has a line-width of the order of a few hertz. It is to be noticed that such curves are obtained by measuring the absorption of light from atoms whose lifetime is of the order of milliseconds.

## 7. APPENDIX

We now return to the second case mentioned in Section III 3.

### 7.1. FIELD OSCILLATING SINUSOIDALLY PARALLEL TO A STATIC FIELD

The interaction Hamiltonian is

$$\begin{aligned}\mathcal{H} &= -\boldsymbol{\mu} \cdot \mathbf{k}(H + H_1 \cos ft) \\ &= \gamma J_z(H + H_1 \cos ft).\end{aligned}\tag{34}$$

We assume that the field is not strong enough to break down the internal coupl-



ing (gyromagnetic ratio  $\gamma$  independent of the field).  $J_z$  is an operator. The Hamiltonian is readily diagonalized by choosing the  $z$ -axis for space quantization and it is possible to integrate the equation of motion directly, without first eliminating the time-dependence.

Thus:

$$i\hbar \frac{\partial}{\partial t} |t\rangle = \mathcal{H} |t\rangle \quad (35)$$

yields

$$|t\rangle = \left[ \exp(-i/\hbar) \int_{t_0}^t \mathcal{H}(t') dt' \right] |t_0\rangle = U(t, t_0) |t_0\rangle, \quad (36)$$

with

$$\int_{t_0}^t \mathcal{H}(t') dt' = J_z [\gamma H(t - t_0) + (\gamma H_1/f)(\sin ft - \sin ft_0)]. \quad (37)$$

$$\text{Use the expansion } \exp -iaJ_z \sin ft = \sum_{r=-\infty}^{\infty} J_r(aJ_z) \exp -irft \quad (38)$$

( $J_r$  is the Bessel function of order  $r$ ).

Then

$$\begin{aligned} |m, t\rangle = & \left\{ \exp -im\omega(t - t_0) \left[ \sum_{r=-\infty}^{\infty} J_r(am) \exp -irft \right] \right. \\ & \times \left. \left[ \sum_{s=-\infty}^{\infty} J_s(am) \exp -isft_0 \right] \right\} |m, t_0\rangle \quad (39) \\ & (\omega = \gamma H; \quad a = \gamma H_1/f). \end{aligned}$$

Rearranging, we have

$$|m, t\rangle = \left\{ \sum_{r,s} J_r(am) J_s(am) [\exp -i(r-s)ft] [\exp -i(m\omega + sf)(t - t_0)] \right\} |m, t_0\rangle. \quad (40)$$

The periodic terms in the expansion are:

- (i) the precessional term with frequency  $(r-s)f$ , phase-locked to the driving field, and
- (ii) the nutational term with frequency  $(m\omega + sf)$  associated with the time interval  $(t - t_0)$ .

For steady state excitation the phase of this nutational term, as before, is random. However, under certain conditions this random phase disappears from the density matrix, whose  $(m, m')$  component is:

$$\begin{aligned} \sigma_{mm'} = & \sum_{\substack{r,s \\ r',s'}} J_r(am) J_s(am) J_{r'}(am') J_{s'}(am') \exp -i(r-s-r'+s')ft \\ & \times \exp -i(m\omega + sf - m'\omega - s'f)(t - t_0). \quad (41) \end{aligned}$$

The condition for elimination of the random phase is:

$$(m - m')\omega = -(s - s')f,$$

$$\omega = (\text{integer}) \times f / (m - m'). \quad (42)$$

This is simply the condition for the degeneracy of certain levels in the frequency diagram. Degeneracy occurs when certain integral multiples of the driving frequency match multiples of the Larmor precessional frequency.

The frequency diagram for the case  $J = 1$  is illustrated in Fig. 38. At  $H = 0$  ( $\omega = 0$ ) the levels  $m = \pm 1$  are degenerate, but there exists a family of such degenerate pairs. The oscillating field splits each level into an infinite set labelled by integers  $r$ . Associated with each such level is a Bessel function whose order is the corresponding integer and whose argument is  $am = m\gamma H_1/f$ . The degeneracy at zero field is removed by the static field  $H$ .

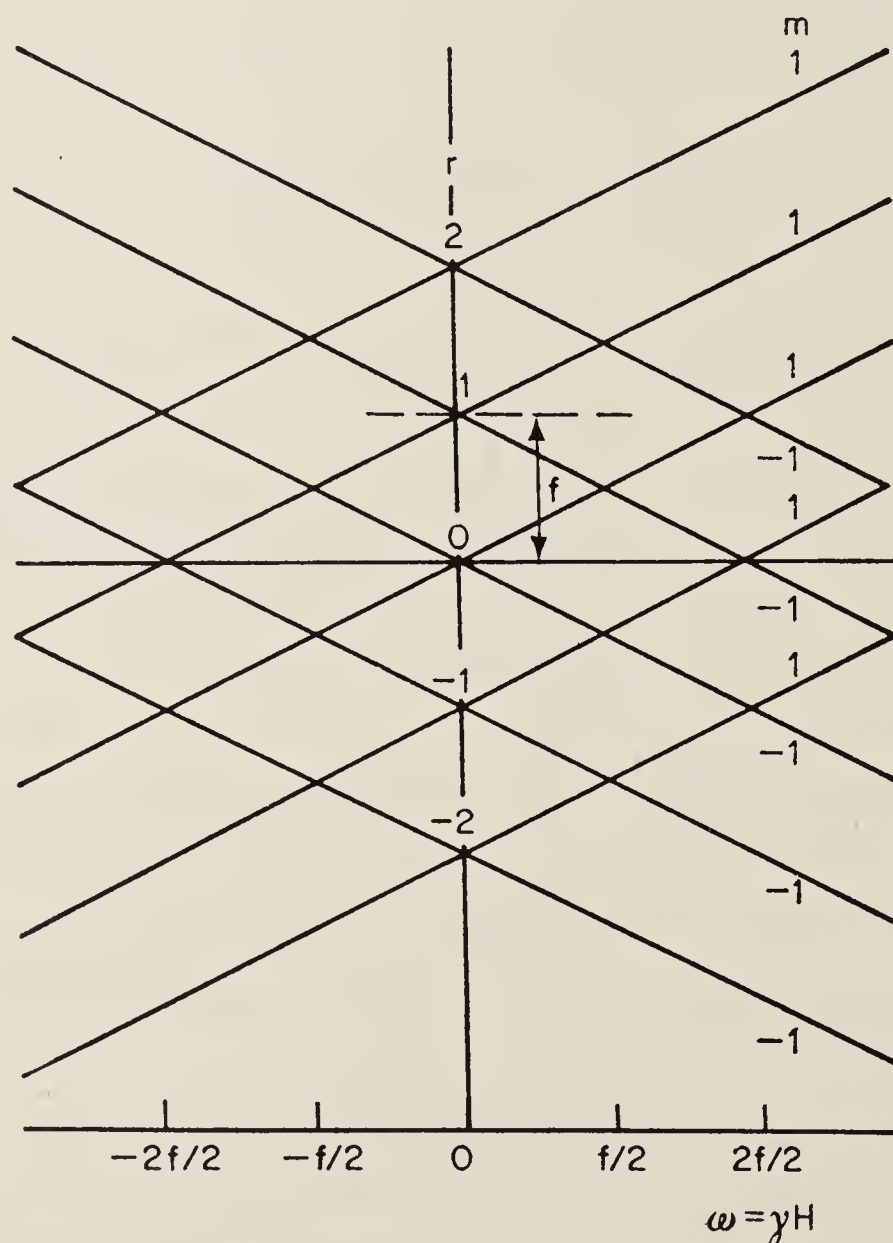


FIG. 38. Frequency diagram for system with  $J=1$ : magnetic field oscillating at frequency  $f$  parallel to static field  $H$ . Levels having  $m=0$  are not shown.

The degeneracies at zero and at non-zero fields given by eqn (42) are a type of level-crossing similar to that discussed in a previous section. If account is taken of the actual width of excited levels the degeneracy extends over a region  $\Gamma$ . If atoms are excited from some initial state by light of polarization such that two different states  $m, m'$  can be excited, we find in the fluorescent



light an interference effect which we may describe as a resonance between the driving frequency and the Larmor frequency. These resonances have width  $\Gamma$  and suffer no radio-frequency broadening. The relative intensity of different resonances is given by a product of Bessel functions. The radio-frequency field strength governs these relative intensities. Resonances of this sort have been studied by Geneux and Favre,<sup>(72)</sup> Aleksandrov *et al.*<sup>(73)</sup> and by Chapman and Series.<sup>(74)</sup> It will be appreciated that modulation phenomena are associated with the resonances. Figure 39 shows an example of resonances in the  $6^3P_1$  state of mercury. The curves show the amplitude of modulation of the fluorescent light at the second harmonic of the driving frequency which in this case was 5 MHz. This is the interval between resonances, and was chosen so that the resonances were resolved against their width (2 MHz). The occurrence of the outermost resonances indicates that the Bessel function  $J_5$  was significantly different from zero, which implies that  $\gamma H_1$  was a substantial fraction of 5 MHz.

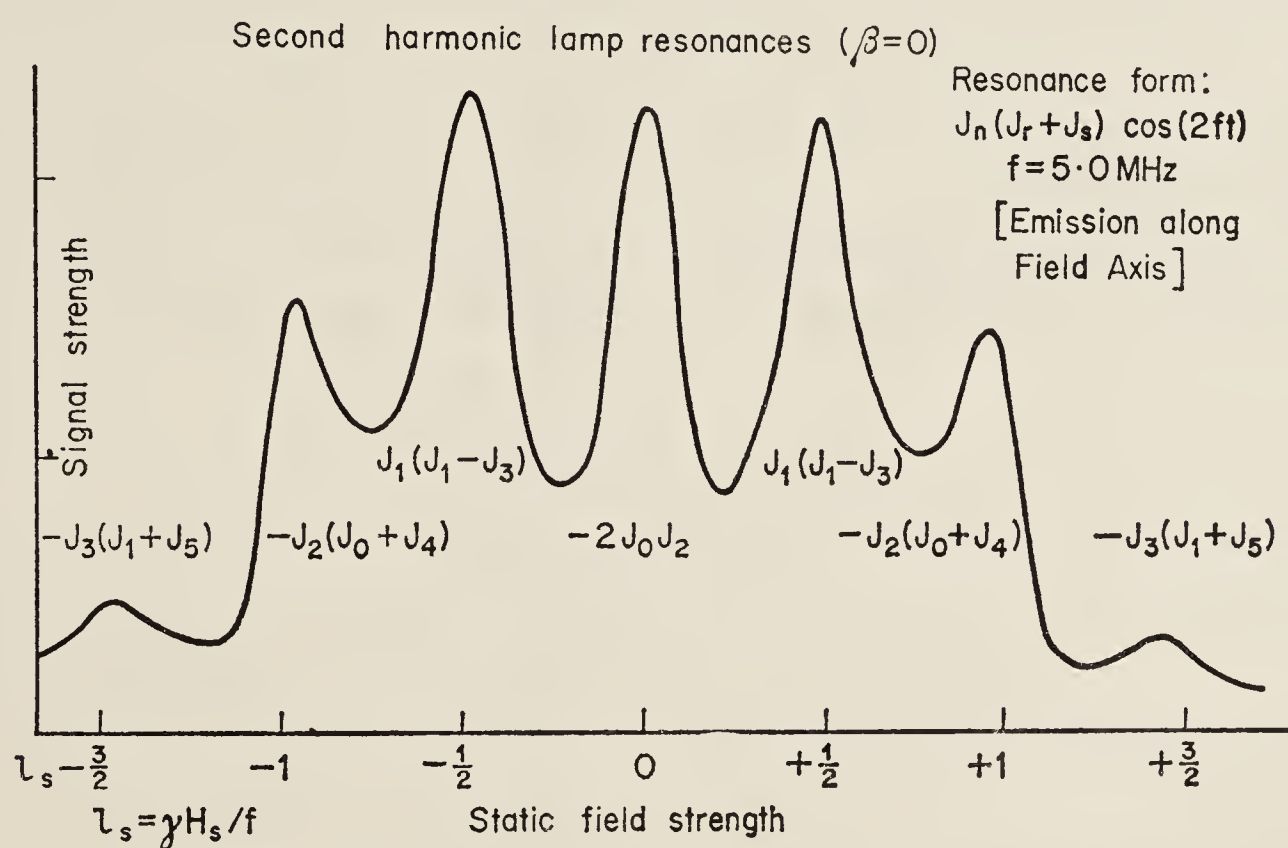


FIG. 39. Level-crossing in  $^3P_1$  state of mercury subjected to parallel static and oscillating magnetic fields. Excitation by light polarized perpendicular to the fields.

## IV RADIO-FREQUENCY INTERACTIONS

### (b) PERTURBATIONS

We took as an example in the last section the case of a two-level system interacting with a rotating field. The resonance functions were symmetrical or anti-symmetrical about the field  $H = H_0$ , which is the field where the applied frequency  $\omega_0$  exactly matches the interval between energy levels in Fig. 32a, i.e.,

the field where the levels cross in Fig. 32b. This is true also for multi-level systems where the levels are equally spaced as, for example, a spin-system having  $J > \frac{1}{2}$ , in a magnetic field. But it is not true for a rotating field interacting with a system where the levels are unequally spaced as, for example, in the case of a coupled-spin system which is being broken down by the magnetic field. In such a case the peaks of the resonances are displaced by an amount depending on  $H_1$  and the resonance functions are no longer symmetrical. Such displacements are found, not only for the three-level system interacting with a rotating field, but also for a two-level system interacting with an oscillating field applied perpendicular to the static field. We shall consider these two cases.

### 1. SYSTEM OF THREE UNEQUALLY SPACED LEVELS INTERACTING WITH ROTATING MAGNETIC FIELD

Let us first apply the transformation which removes the time dependence and consider the energy levels in the rotating frame as a function of  $\omega_0$ . Consider the example shown in Fig. 40a where the states are quantized with respect to the axis of rotation and the energy levels have been displaced from their positions in the laboratory frame by  $m\omega_0$ . The transverse field  $H_1$  is supposed zero.

In Fig. 40(b) is shown the effect of applying the transverse field. The energy

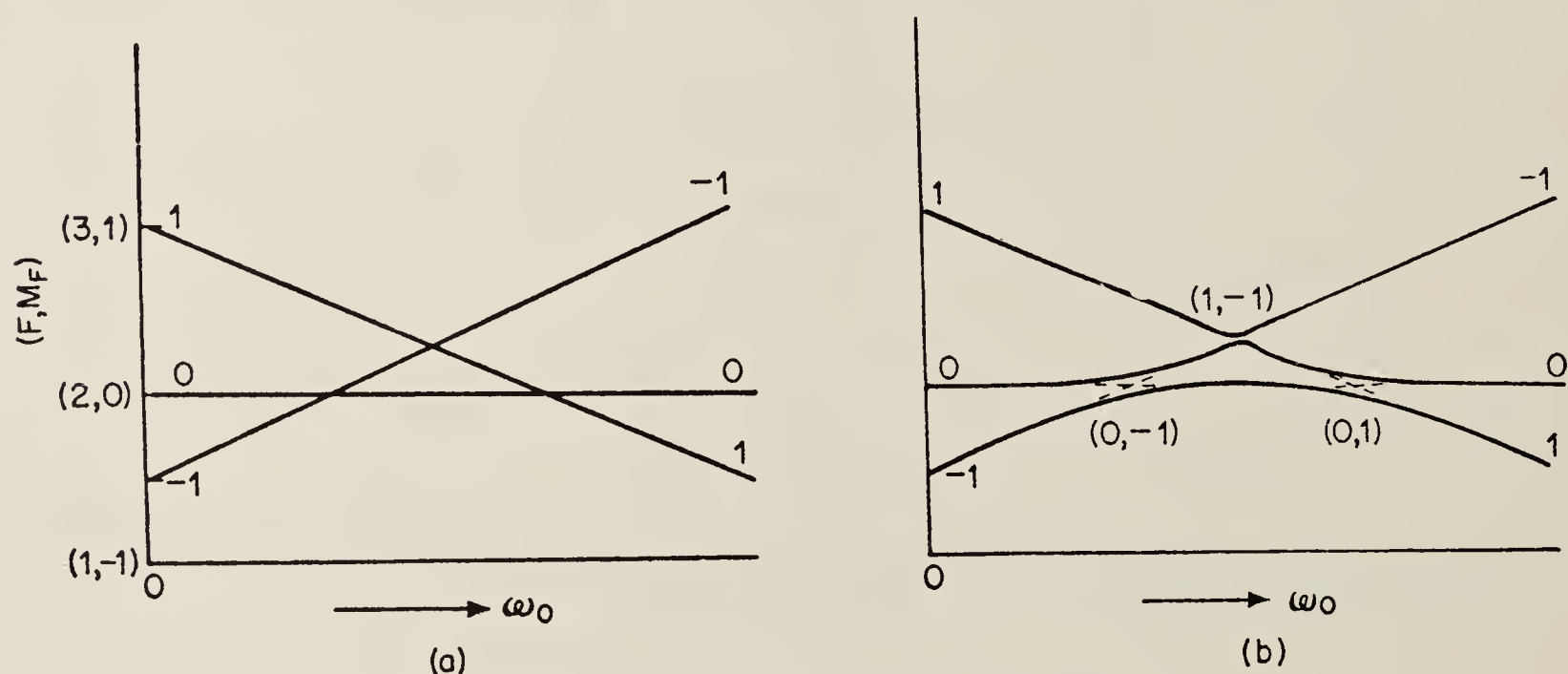


FIG. 40. System of three unequally spaced levels.  
a. Energy in rotating frame, as function of  $\omega_0$ .  
b. Perturbation introduced by transverse field  $H_1$ .

levels are perturbed, and we must recall that the original quantum numbers are no longer good quantum numbers. The levels in this diagram are the eigenvalues of the transformed Hamiltonian  $S\mathcal{H}'S^{-1}$  referred to in III 3.1 (iii).

#### 1.1. DISPLACEMENT OF THE RESONANCES

The centres of the resonances we shall take to be at the positions of closest



approach of the levels of the diagonalized Hamiltonian, though some argument is needed to justify this assumption.<sup>(75)</sup> These positions do not necessarily coincide with the intersections of levels in Fig. 40a. The intersection  $(0, -1)$  for example is displaced because matrix elements of the perturbation exist between  $|1\rangle$  and  $|0\rangle$  but not between  $|1\rangle$  and  $|-1\rangle$ .

As a first approximation to the correction we apply to the level 0 the perturbation it experiences from 1,  $\Delta_{10}$ . The resonance condition is then given in terms of  $\Delta_{10}$  and the Bohr frequencies  $\Omega$ , as follows:

$$\Omega_0 - \Delta_{10} = \Omega_{-1} + \omega_0. \quad (43)$$

Second order perturbation theory yields

$$\Delta_{10} = \frac{|b_{10}|^2}{(\Omega_1 - \omega_0) - \Omega_0} \quad (44)$$

$b_{10}$  is the matrix element of the perturbation. The denominator in (44) is the difference between the levels in Fig. 40a.

Since  $|b_{10}|^2$  is proportional to  $H_1^2$  the theory in this approximation predicts a displacement of the resonances proportional to  $H_1^2$ . This correction has been widely quoted in the literature (Salwen, for example).<sup>(76)</sup> It is customary to plot the position of the peak of the resonance against  $H_1^2$  and to make a linear extrapolation to zero to obtain the unperturbed position. However, the approximation on which this procedure is based breaks down if  $\Delta_{10}$  is comparable with the interval between the interacting levels. It is clear that a better solution is obtained by using for the energy denominator in eqn (44), the interval between the *perturbed* levels, Fig. 40b. An analytical solution has recently been given by Pegg who finds that in the case studied the displacement of the resonance was a function of  $|H_1|$ , not of  $H_1^2$ .

## 1.2. MULTIPLE QUANTUM TRANSITIONS

In the last section we concentrated on resonances corresponding to intersections of levels for which  $\Delta m = \pm 1$ , since the perturbation due to  $H_1$  was supposed to have non-vanishing matrix elements between such states and no others. But the perturbation in second order connects levels with  $\Delta m = \pm 2$ , so that weaker resonances are to be expected for such intersections also. Thus a weaker resonance will occur for the intersection  $(1, -1)$  in Fig. 40b. The characteristics of the resonance may be read from the figure:

- (i) the position at which it occurs (the position of closest approach of the levels of the diagonalized Hamiltonian) will be approximately half-way between the intersections of  $(0, -1)$  and  $(1, 0)$  in Fig. 40(a);
- (ii) the width of the resonance will be one-half that of the  $\Delta m = \pm 1$  resonances because the levels intersect twice as steeply.

Such resonances are called multiple-quantum resonances because they correspond to an exchange of two radio-frequency quanta. Their occurrence in double resonance experiments was described in Section I 3.1.

## 2. TWO LEVEL SYSTEM WITH OSCILLATING FIELD PERPENDICULAR TO STATIC FIELD

This case, though apparently quite different from the preceding case, nevertheless has much in common with it.

### 2.1. DISPLACEMENT OF THE RESONANCES

Figure 41a shows the energy levels as a function of  $H$  in the laboratory frame. Resonances at  $+H_0$  and  $-H_0$  are induced by the clockwise and counter-clockwise rotating fields into which the oscillating field may be resolved. Each of these resonances perturbs the other so that their peaks do not fall exactly at the field  $\pm H_0$ . The shifts are known as Bloch-Siegert shifts. They may be understood by reference to the frequency diagram. (See Fig. 41b).

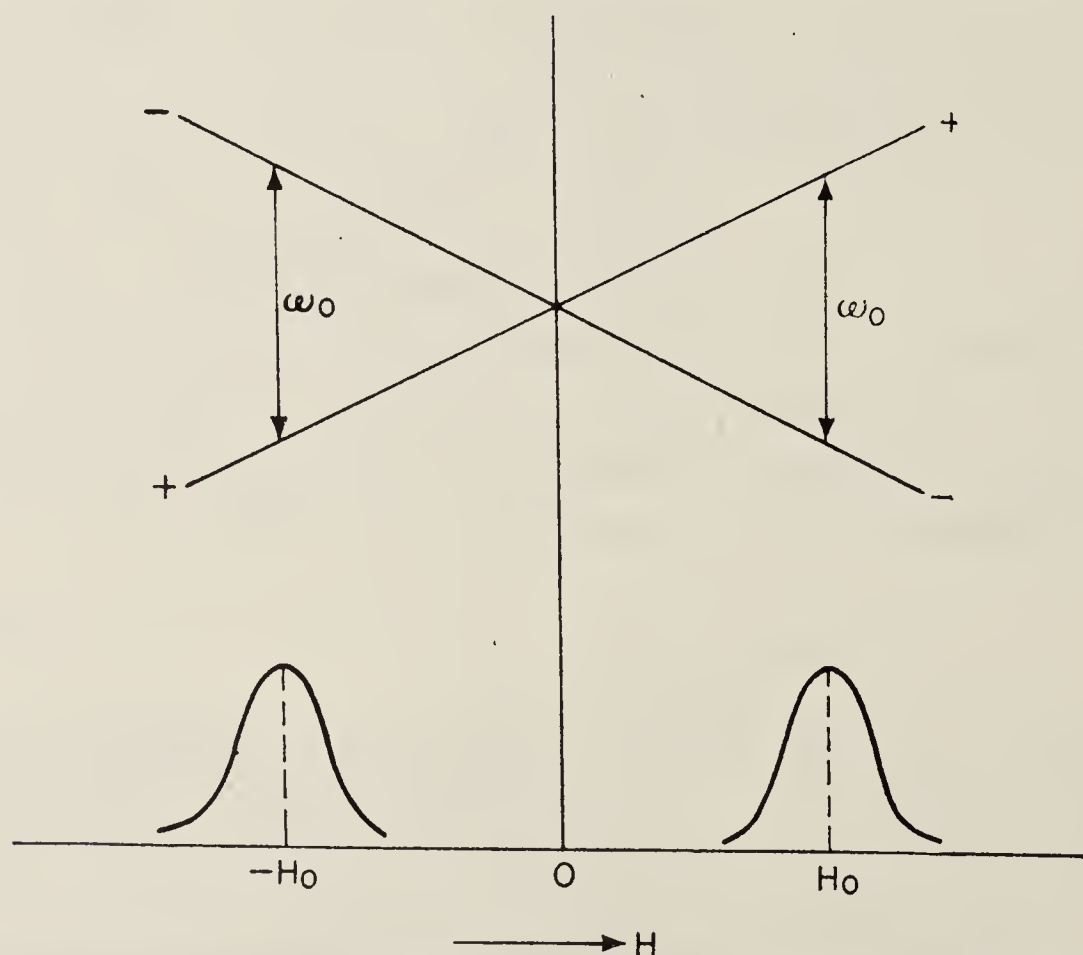


FIG. 41a. Resonances for spin- $\frac{1}{2}$  system at positive and negative values of the field.

Consider first that component of the field which gives rise to the resonance at  $-H_0$ . The frequency diagram, Fig. 41b, shows levels in the region of  $+H_0$  separated by approximately the interval  $\omega_0$ . The equations for the levels are:

$$\begin{aligned}\Omega_{mn} &= m(-\omega_0) + n[(\omega + \omega_0)^2 + |b_{+-}|^2]^{\frac{1}{2}} \\ &\approx -m\omega_0 + n(\omega + \omega_0) [1 + \frac{1}{2}|b_{+-}|^2/(\omega + \omega_0)^2],\end{aligned}\quad (45)$$



where  $m$ , the quantum number along the static field, takes the values  $\pm \frac{1}{2}$  as does  $n$ , the quantum number referred to  $H_{\text{eff}}$ .  $\omega = H$ , and  $b_{+-} = \frac{1}{2}\gamma H_1$  is the matrix element of the perturbation.

The resonance near  $H_0$  is stimulated by the other component of the rotating field. This resonance occurs at that value of the field for which the interval between  $\Omega_{++}$  and  $\Omega_{--}$  is equal to  $\omega_0$ , i.e. when

$$\omega_0 = \Omega_{++} - \Omega_{--} = -\omega_0 + (\omega_{\text{res}} + \omega_0) [1 + \frac{1}{2}|b_{+-}|^2/(\omega_{\text{res}} + \omega_0)^2],$$

where  $\omega_{\text{res}} = \omega_0 - \frac{1}{2}|b_{+-}|^2/(\omega_{\text{res}} + \omega_0) = \gamma H_0 - \delta.$  (46)

$\delta$  is the Bloch–Siegert shift.

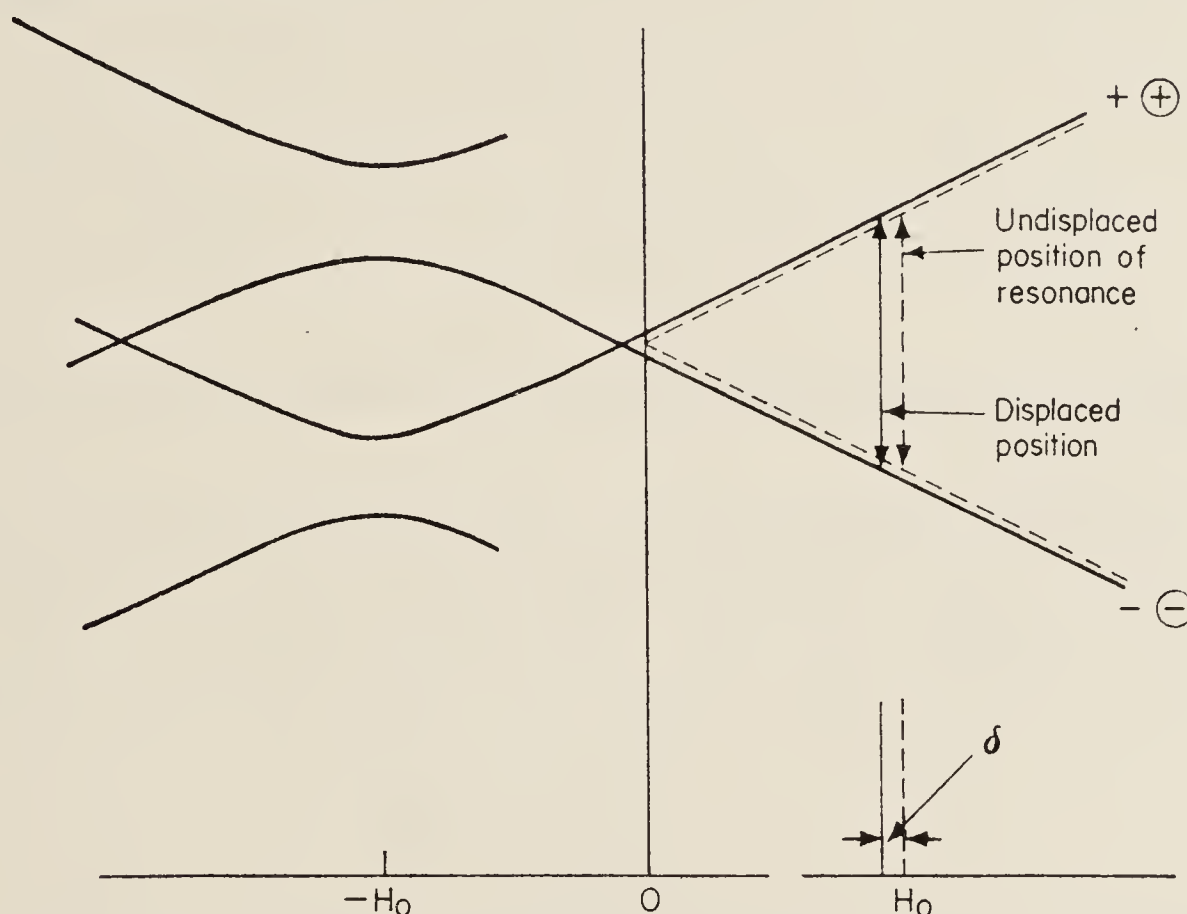


FIG. 41b. Bloch–Siegert shift illustrated by means of the frequency diagram.

## 2.2. MULTIPLE QUANTUM RESONANCES

Consider now the frequency diagram for the component of the field which stimulates the resonance at  $+H_0$  (Fig. 42). We see the possibility of a resonance near  $3H_0$ , since here the pair of levels  $-+$  and  $+-$  (upper and lower, respectively) are separated by  $\omega_0$ . Since the quantum numbers (laboratory frame) are inverted, this resonance needs the counter-rotating component of the field. The amplitudes of the interacting levels depend on the first rotating field, and are given by  $b_{+-}/p$  (eqn (24)). The transition matrix element is proportional to  $b_{+-}$ , so the amplitude of the resonance is proportional to  $|b_{+-}|^2 b_{+-}$ , and the transition probability to  $|b_{+-}|^6$ .

The position of the resonance is not exactly at  $3H_0$  but is displaced by an amount equal to the Bloch–Siegert shift.

From Fig. 42 we may construct a further frequency diagram corresponding to the resonance near  $3H_0$  by transforming to the counter-rotating frame

(Fig. 43a) and back to the laboratory frame (Fig. 43b). We now see the possibility of a resonance near  $5H_0$  induced by the first rotating component. The process may be continued indefinitely.

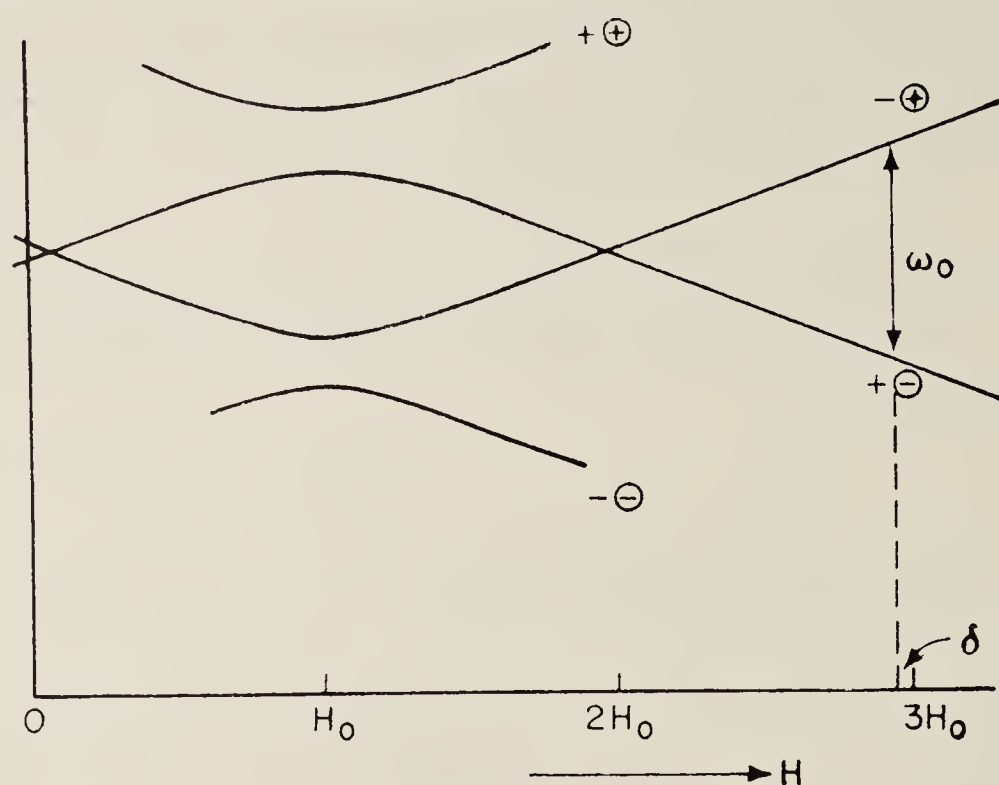


FIG. 42. Possibility of resonance near  $3H_0$  illustrated by means of the frequency diagram.

Each new diagram contains two new levels. For each successive resonance a new factor  $|b_{+-}|^4$  appears in the transition probability. If the resonances are studied with increasing values of  $b_{+-}$  (proportional to  $H_1$ ) successive resonances appear in turn. The diagrams represent a treatment by successive approximation.

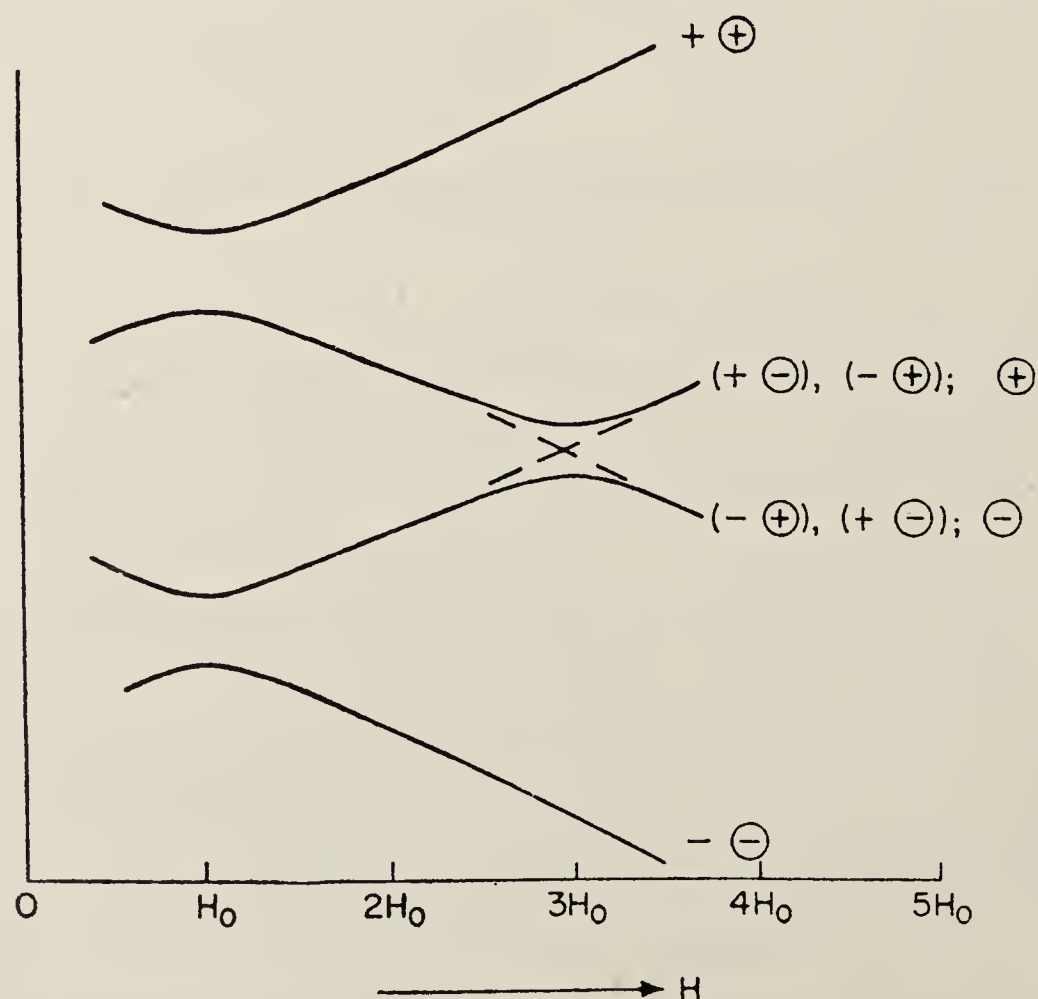


FIG. 43a. The frequency diagram of Fig. 42 transformed to the counter-rotating frame. The perturbation due to the transverse field  $H_1$  (counter-rotating component) is shown.



A formal treatment which is equivalent to the foregoing approach has been given by Shirley<sup>(77)</sup> and has been adapted by Pegg<sup>(75)</sup> in the work previously quoted.

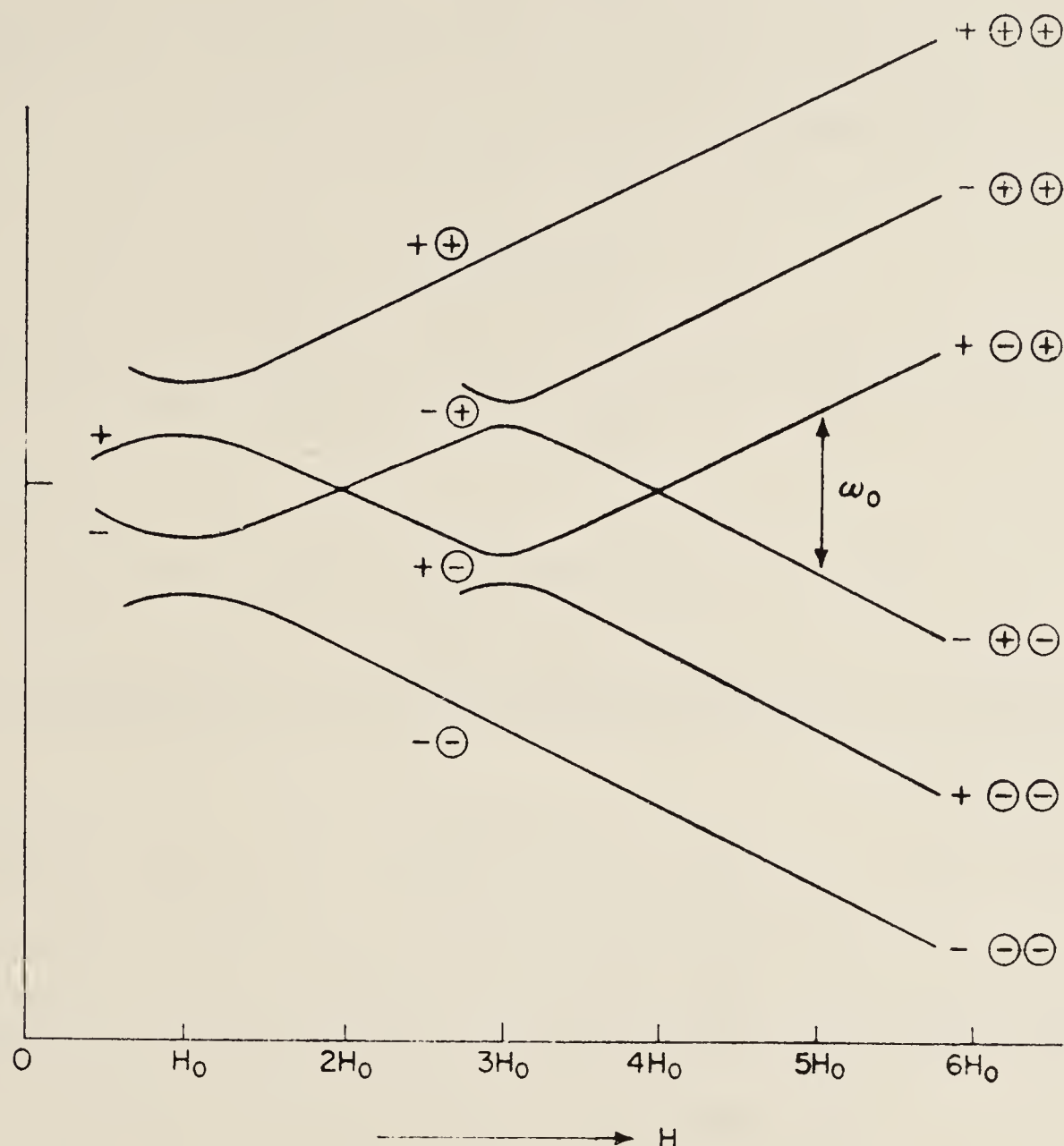


FIG. 43b. Frequency diagram in the laboratory frame representing the effects of rotating field and counter-rotating field in first approximation. The diagram shows the possibility of a resonance near  $5H_0$ .

### 3. TWO LEVEL SYSTEM WITH OSCILLATING FIELD: HANLE EFFECT

Figures 41b and 42 show frequency diagrams for the two rotating fields separately, and in each case they are valid in the region  $H = 0$ . In Fig. 43b, representing the case of both fields acting together, the levels near  $H = 0$  have not been drawn since, in this region, the perturbations due to both fields are comparable in strength and neither may be regarded as a perturbation on the other. The symmetry of the situation argues for a diagram which is symmetrical about  $H = 0$ , whereas both 41b and 42 are asymmetrical.

The situation near  $H = 0$  may be analysed by regarding the static field as a perturbation on the oscillating field, treating the latter by the method given in Section III 7.

Consider the oscillating field  $H_1 \cos ft$ , together with the small, static trans-

verse field  $H$  acting on our two-level atomic system (Fig. 44). Choose an axis of quantization parallel to the oscillating field ( $Oz$ ). Let  $Ox$  be the direction of the static field.

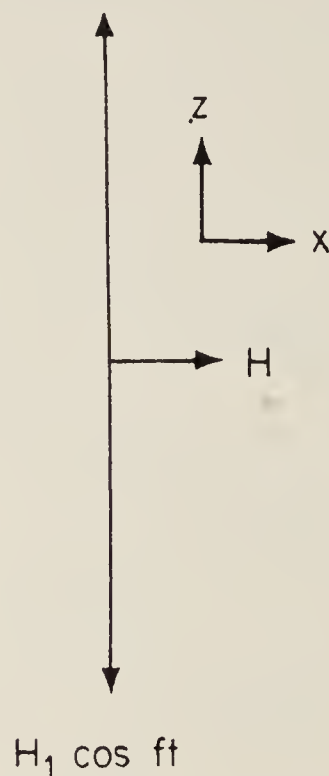


FIG. 44. Hanle effect with an oscillating field. The interaction with the transverse field  $H$  is regarded as a small perturbation on the interaction with the oscillating field  $H_1 \cos ft$ .

The Hamiltonian is

$$\begin{aligned}\mathcal{H} &= (\omega_1 \cos ft) J_z + \omega J_x \\ &= \mathcal{H}_0 + \mathcal{H}_1.\end{aligned}\quad (47)$$

The equation of motion under  $\mathcal{H}_0$  above may be solved exactly to find the states  $|t, t_0, \pm\rangle$  which develop at time  $t$  from the states  $|\pm\rangle$  at  $t_0$ . We have

$$|t, t_0, +\rangle = \sum_r J_r(\tfrac{1}{2}a) \exp -irft \sum_s J_s(\tfrac{1}{2}a) \exp isft_0 |+\rangle \quad (48)$$

$$|t, t_0, -\rangle = \sum_{r'} J_{r'}(\tfrac{1}{2}a) \exp ir'ft \sum_{s'} J_{s'}(\tfrac{1}{2}a) \exp -is'ft_0 |-\rangle. \quad (49)$$

The following is also a solution:

$$|t, t_0, -\rangle^* = \sum_{r'} J_{r'}(\tfrac{1}{2}a) \exp ir'ft \sum_{s'} J_{s'}(\tfrac{1}{2}a) \exp is'ft_0 |-\rangle. \quad (50)$$

This state, which develops from

$$|t_0, t_0, -\rangle^* = \sum_q J_q(a) \exp iqft_0 |-\rangle. \quad (51)$$

at time  $t_0$  differs from  $|t, t_0, -\rangle$  by an arbitrary phase factor. We shall find  $|t, t_0, -\rangle^*$  more convenient than  $|t, t_0, -\rangle$  because its phase is more conveniently related to that of  $|t, t_0, +\rangle$  than is the phase of  $|t, t_0, -\rangle$ .

Notice that linear superpositions of the states we have written down are also solutions of the equation of motion under  $\mathcal{H}_0$ .

The complete problem requires the addition of  $\mathcal{H}_1$  to  $\mathcal{H}_0$ , so we try to find linear superpositions which are also eigenstates of  $\mathcal{H}_1$ .



We notice that there are degeneracies in the  $t$ -dependence of  $|t, t_0, +\rangle$  and  $|t, t_0, -\rangle^*$ , namely, when  $r' = -r$ .

Now consider the superposition states:

$$\begin{aligned} |t, t_0, \pm\rangle^x &= (1/\sqrt{2}) [|t, t_0, +\rangle \pm |t, t_0, -\rangle^*] \\ &= (1/\sqrt{2}) \sum_s J_s(\tfrac{1}{2}a) \exp isft_0 \left[ \sum_r J_r(\tfrac{1}{2}a) \exp -irft |+\rangle \right. \\ &\quad \left. \pm \sum_{r'} J_{r'}(\tfrac{1}{2}a) \exp ir'ft |-\rangle \right]. \end{aligned} \quad (52)$$

For those terms for which  $r' = -r$  we can take out the common factor  $J_r(\tfrac{1}{2}a) \exp -irft$ , using  $J_r(\tfrac{1}{2}a) = (-1)^r J_{-r}(\tfrac{1}{2}a)$ .

We obtain

$$\begin{aligned} |t, t_0, +\rangle^x &= (1/\sqrt{2}) \sum_s J_s(\tfrac{1}{2}a) \exp isft_0 \left\{ \sum_{r \text{ even}} J_r(\tfrac{1}{2}a) \exp -irft \right. \\ &\quad \left. \times [|+\rangle + |-\rangle] + \sum_{r \text{ odd}} J_r(\tfrac{1}{2}a) \exp -irft [|+\rangle - |-\rangle] \right\} + \dots \end{aligned} \quad (53)$$

and similarly for  $|t, t_0, -\rangle^x$ .

The states  $(1/\sqrt{2}) [|+\rangle \pm |-\rangle]$  are eigenstates of  $\mathcal{H}_1$  with eigenvalues  $\pm \frac{1}{2}\hbar\omega$ . Thus the states  $|t, t_0, \pm\rangle^x$  have the following properties:

- (i) they satisfy the wave equation under  $\mathcal{H}_0$ ;
- (ii) with neglect of terms  $r' \neq -r$ , the even and odd parts of the wave function are separately eigenfunctions of  $\mathcal{H}_1$  for all  $t$ , since

$$\mathcal{H}_1[|+\rangle \pm |-\rangle]/\sqrt{2} = \pm \frac{1}{2}\hbar\omega [|+\rangle \pm |-\rangle]/\sqrt{2}.$$

Thus the states  $|t, t_0, \pm\rangle^x$  are convenient zero-order states on which to base a small perturbation  $\mathcal{H}_1$ .

Let us calculate the matrix of  $\mathcal{H}_1$  in this basis. For the diagonal elements we have:

$$\begin{aligned} {}^x\langle t, t_0, \pm | \mathcal{H}_1 | t, t_0, \pm \rangle^x &= \pm \frac{1}{4}\hbar\omega \left[ \sum_r J_r(\tfrac{1}{2}a) \exp -irft \sum_{r'} J_{r'}(\tfrac{1}{2}a) \exp -ir'ft \right] \\ &\quad \times \left[ \sum_s J_s(\tfrac{1}{2}a) \exp isft_0 \sum_{s'} J_{s'}(\tfrac{1}{2}a) \exp -is'ft_0 \right] + c.c. \\ &= \pm \frac{1}{4}\hbar\omega \sum_p J_p(a) \exp -ipft + c.c. \\ &= \pm \frac{1}{2}\hbar\omega \sum_p J_p(a) \cos pft \end{aligned} \quad (54)$$

(We have used a Bessel function contraction theorem, with  $p = r + r'$ ; by the same theorem the second square bracket is identically unity.)

$$= \pm \frac{1}{2} \hbar \omega \left[ J_0(a) + \sum_{\substack{p=2 \\ \text{even integers}}}^{\infty} 2J_p(a) \cos pft \right] \quad (54a)$$

For the off-diagonal elements,

$$\begin{aligned} {}^x\langle t, t_0, \mp | \mathcal{H}_1 | t, t_0, \pm \rangle^x &= \pm \frac{1}{4} \hbar \omega \sum_p J_p(a) \exp -ipft - c.c. \\ &= \pm \frac{1}{2} i \hbar \omega \sum_p J_p(a) \sin pft \\ &= \pm \frac{1}{2} i \hbar \omega \left[ \sum_{\substack{p=1 \\ \text{odd integers}}}^{\infty} 2J_p(a) \sin pft \right]. \end{aligned} \quad (54b)$$

Thus, for the time-independent component, and for the even harmonics, the matrix is diagonal. For the odd harmonics the matrix is diagonalized by a rotation of  $\pi/2$  about  $Oz$ . The diagonalization removes the factor  $i$  from (54b).

If the oscillating field were absent ( $H_1 = 0$ ), the matrix would be diagonal with elements  $E_0 = \pm \frac{1}{2} \hbar \omega$ . In the presence of the oscillating field we find diagonal elements,

$$E_0 \left[ J_0(a) + \sum_{\substack{\text{even} \\ \text{harmonics}}} 2J_p(a) \cos pft \right], \quad (55)$$

and off-diagonal elements

$$E_0 \left[ \sum_{\substack{\text{odd} \\ \text{harmonics}}} 2J_p(a) \sin pft \right]. \quad (56)$$

Thus the oscillating field has the effect of modifying the  $g$ -value of the spin system. Measured in the  $x$ -direction the  $g$ -value is predicted to be

$$g_x = g_0 \left[ J_0(a) + \sum_{\substack{\text{even} \\ \text{harmonics}}} 2J_p(a) \cos pft \right], \quad (57)$$

and in the  $y$ -direction,

$$g_y = g_0 \left[ \sum_{\substack{\text{odd} \\ \text{harmonics}}} 2J_p(a) \sin pft \right]. \quad (58)$$

In the  $z$ -direction the  $g$ -value remains unchanged.

The results have been obtained by finding the matrix of the perturbation  $\mathcal{H}_1$  in a representation based on the eigenstates of  $\mathcal{H}_0$ , and are valid only for  $\omega \ll f$ . A more elegant treatment has recently been given by Pegg and Series.<sup>(77a)</sup>

The time-independent part of this result was obtained by Cohen-Tannoudji and Haroche,<sup>(78)</sup> and has been verified experimentally by them. Their derivation was based on the notion of “dressed atoms”—they derived the stationary states of a closed system consisting of (atoms + radio-frequency field), and



used the coherent state formalism of Glauber<sup>(79)</sup> to form superposition-states representing the oscillating field. The experimental study was by means of a level-crossing experiment for ground states.

## V. REFRACTIVE INDEX AS A MONITOR OF OPTICAL PUMPING

### 1. INTERACTION OF LIGHT WITH INDIVIDUAL ATOMS

Our discussion of the interaction between light and atoms has been based on the interaction with individual atoms. Thus, in III, eqn (31a), we derive an expression for the intensity of fluorescent light:

$$I(t) \propto \text{Tr}(A\sigma), \quad (59)$$

where  $A$  is a matrix whose  $(m, m')$  element is

$$A_{mm'} = \sum_{\mu} \langle \mu | \mathbf{e} \cdot \mathbf{P} | m \rangle \langle m' | \mathbf{e}^* \cdot \mathbf{P} | \mu \rangle \quad (60)$$

and  $\sigma$  is the density matrix of the assembly.

Equation (59) is obtained by summing the intensities of light from the different atoms in the assembly.

Equations similar to (59) have been used also for absorption.

We should not lose sight of the fact that contributions to the intensity, either in emission or in absorption, may arise from the off-diagonal elements of the density matrix as well as from the diagonal elements.

### 2. COHERENCE BETWEEN RADIATION FROM DIFFERENT ATOMS

The basis of eqn (59) must be re-examined when there is a possibility of interference between the light from different atoms. Such a possibility arises in the case of forward-scattering. The classical theory of refractive index interprets the dispersion of velocity of light in a medium as due to interference in forward scattering. Moreover, absorption is intimately related to dispersion and we monitor optical pumping by measuring the amount of light absorbed when a beam of light traverses the gas. We need to consider therefore, whether a theory of absorption based on the propagation of light through a medium (theory of dispersion) would lead us back to eqn (59), and whether this approach might not disclose other topics of interest. We shall see that the notion of an optically pumped vapour as a macroscopic medium having an anisotropic, time-dependent, complex refractive index is indeed useful.

#### 2.1 ABSORPTION, REFRACTIVE INDEX, ELECTRIC POLARIZABILITY

The absorption coefficient of a medium is related to the imaginary part of the refractive index  $n^{(i)}$ . This may be obtained from the bulk polarization and this,

in turn, from the polarizability of individual atoms. We start from an expression for the polarizability tensor,  $\alpha_{rs}^{(j)}$  of the  $j$ th atom, where  $r$  and  $s$  refer to the base vectors.

$$\mathbf{e}_{\pm 1} = \mp (\mathbf{i} \pm i\mathbf{j})/2^{\frac{1}{2}}, \quad \mathbf{e}_0 = \mathbf{k}. \quad (61)$$

( $\mathbf{i}, \mathbf{j}, \mathbf{k}$ , are Cartesian unit vectors).

We have:

$$\alpha_{rs}^{(j)}(k, t) = \sum_{\substack{\mu \\ m=\mu+r \\ \mu'=m-s}} \frac{A_{rs}(\mu', \mu; m)}{\hbar(k_m - k_\mu - k - \frac{1}{2}i\Gamma_m)} a_\mu(t) a_{\mu'}^*(t) \dots \quad (62)$$

where  $A_{rs}(\mu', \mu; m) = \langle \mu' | \mathbf{e}_s^* \cdot \mathbf{P} | m \rangle \langle m | \mathbf{e}_r \cdot \mathbf{P} | \mu \rangle$ ,

$k$  is the frequency of the incident light,  $m, m' \dots$  are excited states  $\mu, \mu' \dots$  are ground states,  $k_m, k_\mu$  are Bohr frequencies,  $\Gamma_m$  is a damping constant. (Details of the calculation are to be found in Series.<sup>(80)</sup>)

The bulk polarizability tensor,  $\alpha_{rs}$ , is calculated by summing (62) over the  $N$  atoms per unit volume. These have a distribution of resonance frequencies  $k_{m\mu} = k_m - k_\mu$  given by

$$dN = (N/\Delta\pi^{\frac{1}{2}}) \exp[-\{(\delta k_{m\mu})^2/\Delta^2\}] dk_{m\mu},$$

where  $\Delta$  is a measure of the Doppler width of the distribution, and

$$\delta k_{m\mu} = k_{m\mu} - (k_{m\mu})_0, \text{ with } (k_{m\mu})_0 \text{ the peak.}$$

In making the sum we replace  $a_\mu(t) a_{\mu'}^*(t)$  by its value  $\sigma_{\mu\mu'}(t)$  averaged over atoms in ground states. The result is

$$\alpha_{rs}(k, t) = \sum_{\substack{\mu \\ m=\mu+r \\ \mu'=m-s}} \frac{N A_{rs}(\mu, \mu'; m)}{\hbar \Delta} \sigma_{\mu\mu'}(t) Z(x_{m\mu} + iy), \dots \quad (63)$$

where  $Z(x + iy)$  is the plasma dispersion function

$$Z(x + iy) = \pi^{-\frac{1}{2}} \int_{-\infty}^{\infty} \frac{\exp(-t^2)}{t - (x + iy)} dt; \quad x_{m\mu} = \frac{k - (k_{m\mu})_0}{\Delta}; \quad y = \frac{\Gamma_m}{2\Delta}. \quad (64)$$

(We have ignored the contribution to refractive index which arises from excited atoms since, in optical pumping experiments, the bulk of the population is in ground states.)

### a. Absorption

The absorption coefficient,  $\chi$ , is related to the bulk polarizability,  $\alpha$ , by

$$\chi_{rs} = (4\pi k/c) \alpha_{rs}^{(i)} \quad (65)$$

where  $\alpha^{(i)}$  is the imaginary part of  $\alpha$ . The imaginary part of  $\alpha$  arises from the imaginary part of  $Z$  (eqn (63)).

Now, in exploring a resonance between ground states we are concerned with changes in the density matrix  $\sigma_{\mu\mu'}$  which occur over relatively small varia-



tions of magnetic field, in the course of which  $Z$  remains practically constant. (The variation of  $Z$  is given by the variation of  $x_{m\mu}$  with magnetic field, so we have to compare changes in the Zeeman splitting of the ground states,  $\delta k_\mu$ , with the Doppler width,  $\Delta$ ).

If we can treat  $Z$  as constant, the absorption coefficient is proportional to

$$\sum_{\substack{\mu, \mu' \\ m}} A(\mu, \mu'; m) \sigma_{\mu\mu'}(t).$$

This is equivalent to eqns (59) and (60) (with  $m, m'$  and  $\mu, \mu'$  interchanged, because these equations refer to emission from excited states).

We have shown, therefore, that an analysis based on the classical theory of the propagation of light in dielectrics gives the same result for absorption, in optically thin vapours, as an analysis based on the interaction of light with individual particles.

### *b. Dispersion*

We may expect that this approach would be rewarding if we considered the region away from absorption. We should then study the real part of eqn (63). The equation predicts that manifestations of optical pumping in ground states (resonances, modulation effects, etc.) could be studied by any technique which measured refractive index, since the optical pumping effects are described analytically by the density matrix, which is linearly related to the refractive index. Many such studies have indeed been made. The Faraday effect and magnetic birefringence, which measure various combinations of the tensor components of the anisotropic refractive index, have proved particularly useful.

For these dispersion studies it is advantageous to use monitoring light whose spectrum is displaced in frequency from the absorption region of the medium. This light does not then contribute to the optical pumping, and the effect of the pumping beam itself can be studied free from perturbations due to the monitoring.

## 2.2. EMISSION: RESONANCES IN EXCITED STATES

Our discussion has been based on the constancy of the function  $Z$  over the region of magnetic resonance. While it is true that this is constant to a high degree of approximation for ground-state resonances,  $Z$  is not constant for excited state resonances. These resonances appear in eqn (63) as changes in the value of the function  $Z$  itself, since it is only through changes in  $(k_{m\mu})_0$  that the effect of the magnetic field on excited states shows itself. ( $(k_{m\mu})_0$  is simply the frequency of the  $(\mu, m)$  Zeeman component of the absorption line). Now, changes of  $(k_{m\mu})_0$  are significant only if they are comparable with the Doppler width. A detailed study of the consequences of this shows that curves of magnetic resonance in excited states, as explored by techniques which measure refractive index, are Doppler-broadened. This is in sharp contrast

with such curves as ordinarily studied (e.g. in the Brossel–Bitter experiment), where the great advantage of the technique is the elimination of Doppler broadening.

The difference between our present analysis and the earlier study of the Brossel–Bitter experiment is that we are now, for the first time, taking account of the possibility of coherence between light radiated by different atoms. In the Brossel–Bitter experiment, as in conventional experiments on resonance fluorescence, one studies the laterally-scattered light where there is no such coherence. In our present analysis of refractive index the coherence in forward-scattering makes itself felt by Doppler-broadening of the resonance curves.

There remains a further important point to be made in connection with forward-scattering. In optically thick vapours the transmitted light suffers multiple scattering and its intensity is not linearly related to the refractive index. A consequence of the multiple scattering is that the magnetic resonance curves experience coherence narrowing to a degree far in excess of coherence narrowing in the laterally scattered light. Indeed, zero-field level-crossing curves in sodium have been obtained by Hackett<sup>(81)</sup> which are actually narrower than curves obtained in lateral scattering. The analysis of this situation is complicated, and we shall not pursue it here.

The important points are:

- (i) the result for emission is very different from that for absorption; and
- (ii) coherence narrowing of excited state resonances is very marked in forward scattering.

#### ACKNOWLEDGEMENTS

In preparing these lectures and in submitting the figures for publication I have drawn freely on the work of colleagues, among whom are: G. Chapman, A. Corney, J. N. Dodd, W. N. Fox, W. Gough, B. P. Kibble, K. R. Lea, S. Pancharatnam, R. B. Partridge, D. Pegg, G. J. Ritter, M. J. Taylor and D. Warrington.

I have also used material published by Arditi and Carver<sup>(83)</sup> (Fig. 26), by Cohen–Tannoudji<sup>(82)</sup> (Fig. 27) and by Smith and Gallagher<sup>(31)</sup> (Fig. 31).

The Royal Society has kindly given permission to reproduce Figs. 3, 5 to 9 and 33, and the Institute of Physics and the Physical Society permission to reproduce Figs. 11, 12, 14, 23a, 34 and 36.

#### REFERENCES

1. Brossel, J. and Bitter, F. *Phys. Rev.* **86**, 308 (1952).
2. Ritter, G. J. and Series, G. W. *Proc. R. Soc. A.* **238**, 473 (1957).
3. Pegg, D. T. *J. Phys. B.* **2**, 1097, 1104 (1969).
4. Heydenburg, N. P., Larrick, L. and Ellett, A. *Phys. Rev.* **40**, 1041 (1932).
5. Schmieder, R. W., Lurio, A. and Happer, W. *Phys. Rev.* **173**, 76 (1968).
6. Gough, W. and Series, G. W. *Proc. phys. Soc.* **85**, 469 (1965).
7. Kibble, B. P. and Series, G. W. *Proc. phys. Soc.* **78**, 70 (1961).



8. Brog, K. C., Eck, T. G. and Wieder, H. *Phys. Rev.* **153**, 91 (1967).
9. Kusch, P. *Phys. Rev.* **101**, 627 (1956).
10. Winter, J. M. *Annls. Phys.* **19**, 746 (1959).
11. Colegrove, F. D., Schearer, L. D. and Walters, G. K. *Phys. Rev.* **132**, 2561 (1963).
12. Greenhow, R. C. *Phys. Rev.* **136**, A660 (1964). (Also: Thesis, University of Oxford.)
13. Cohen-Tannoudji, C., Dupont-Roc, J., Haroche, S. and Laloë, F. *Phys. Rev. Lett.* **22**, 758 (1969).
14. Franzen, W. *Phys. Rev.* **115**, 850 (1959).
15. Barrat, J. P. and Cohen-Tannoudji, C. *J. Phys. Radium, Paris.* **22**, 329, 443 (1961).
16. Pancharatnam, S. *J. opt. Soc. Am.* **56**, 1636 (1966).
17. Happer, W. and Saloman, E. B. *Phys. Rev.* **160**, 23 (Appendix) (1967).
18. Omont, A. and Meunier, J. *Phys. Rev.* **169**, 92 (1968).
19. Kretzan, H. and Walther, H. *Phys. Lett.* **27A**, 718 (1968).
20. Bouchiat, M. A. and Brossel, J. *Phys. Rev.* **147**, 41 (1966).
21. Minguzzi, P., Strumia, F. and Violino, P. *Optics Commun.* **1**, 1 (1969).
22. Ensberg, E. S. and zu Putlitz, G. *Phys. Rev. Lett.* **22**, 1349 (1969).
23. Bucka, H., Ney, J. and Heppke, G. *Zeit. angew. Phys.* **20**, 354 (1966).
24. Wood, R. W. "Physical Optics", Macmillan, London. (1934).
25. Budick, B., Novick, R. and Lurio, A. *Appl. Optics*, **4**, 229 (1965).
26. Bell, W. E., Bloom, A. L. and Lynch, J. *Rev. Scient. Instrum.* **32**, 688 (1961).
27. Atkinson, R. J., Chapman, G. D. and Krause, L. *J. opt. Soc. Am.* **55**, 1269 (1965).
28. Burling, D. H. and Czajkowski, M. *J. opt. Soc. Am.* **57**, 1162 (1967).
29. Berdowski, W., Shiner, T. and Krause, L. *Appl. Optics.* **6**, 1683 (1967).
30. Otten, E. W. and zu Putlitz, G. Private Communication (1969).
31. Smith, W. W. and Gallagher, A. *Phys. Rev.* **145**, 26 (1966).
32. Garrett, W. *J. Appl. Phys.* **22**, 9 (1951).
33. Franzen, W. *Rev. Scient. Instrum.* **33**, 933 (1962).
34. Dupont-Roc, J., Haroche, S. and Cohen-Tannoudji, C. *Phys. Lett.* **28A**, 638 (1969).
35. Gallagher, A. and Lurio, A. *Phys. Rev.* **136**, A87 (1964).
36. Series, G. W. *Proc. phys. Soc.* **89**, 1017 (1966).
37. Pebay-Peyroula, J. C. Proceedings of the Sommerfeld Memorial Meeting, Munich. North-Holland Publishing Co., Amsterdam (1969).
38. Pebay-Peyroula, J. C. Colloques Internationaux du CNRS, Publication No. 162. Editions due CNRS, Paris (1967).
39. Lombardi, M. and Pebay-Peyroula, J. C. *C.r. hebd. Seanc. Acad. Sci., Paris*, **261**, 1485 (1965).
40. Kaul, R. D. *J. opt. Soc. Am.* **57**, 1156 (1967).
41. Krause, D. and Soltysik, E. A. *Phys. Rev.* **175**, 142 (1968).
42. Barrat, J. P. *J. Phys. Radium, Paris.* **20**, 541, 633, 657, (1959).
43. Omont, A. *J. Phys. (Paris)* **26**, 576 (1965).
- 43a. D'Yakonov, M. I. and Perel', V. I. *Soviet Phys. J.E.T.P.* **20**, 997 (1965).
44. Huber, G. and Otten, E. W. *J. Phys. (Paris)*. Proceedings of Colloque de Spectroscopie Atomique (Caen) (1968).
45. Corney, A and Series, G. W. *Proc. phys. Soc.* **83**, 207 and 213 (1964).
46. Corney, A. and Series, G. W. *Proc. phys. Soc.* **83**, 331 (1964).
47. Corney, A. *J. phys. B (Proc. phys. Soc.)* **1**, 458 (1968).

48. zu Putlitz, G. *Ergebn. exakt. Naturw.* **37**, 105 (1964).
49. Budick, B. "Advances in Atomic and Molecular Physics", Vol. 3. Academic Press (1967).
50. Major, F. G. "Methods of Experimental Physics", Vol. 7B, Atomic Interactions. Academic Press (1968).
51. Pipkin, F. M. and Lambert, R. H. *Phys. Rev.* **127**, 787 and references given there (1962).
52. White, C. W., Hughes, W. M., Hayne, G. S. and Robinson, H. G. *Phys. Rev.* **174**, 23 (1968).
53. Besch, H. J., Köpf, U. and Otten, E. W. *Phys. Lett.* **25B**, 120 (1967).
54. Metcalf, H., Brandenberger, J. R. and Baird, J. C. *Phys. Rev. Lett.* **21**, 165 (1968).
55. Fontana, P. R. and Himmell, L. C. *Phys. Rev.* **162**, 23 (1967).
56. Fontana, P. R. and Wing, W. H. *Bull. Am. Phys. Soc.* **12**, 95 (1967).
57. Handrich, E., Steudel, A., Wallenstein, R. and Walther, H. Proceedings of the Sommerfeld Memorial Meeting, Munich. North-Holland Publishing Co., Amsterdam (1969).
58. Feiertag, D. and zu Putlitz, G. *Z. Phys.* **208**, 447 (1968).
59. Ma, I. J., Mertens, J., zu Putlitz, G. and Schütte, G. *Z. Phys.* **208**, 266 (1968).
60. Zare, R. N. *J. Chem. Phys.* **45**, 4510 (1966).
61. Crosley, D. R. and Zare, R. N. *Phys. Rev. Lett.* **18**, 942 (1967).
62. Crosley, D. R. and Zare, R. N. *J. Chem. Phys.* **49**, 4231 (1968).
63. Imbusch, G. F., Chinn, S. R. and Geschwind, S. *Phys. Rev.* **161**, 295 (1967).
64. Chase, L. L. *Phys. Rev. Lett.* **21**, 888 (1968).
65. Cohen-Tannoudji, C. and Haroche, S. *J. de Phys.* **30**, 125 (1969).
66. Franzen, W. and Alam, M. *Phys. Rev.* **133**, A460 (1964).
67. Dodd, J. N. and Series, G. W. *Proc. R. Soc. A* **263**, 353 (1961).
68. Carver, T. R. and Partridge, R. B. *Amer. J. Phys.* **34**, 339 (1966).
69. Dodd, J. N., Series, G. W. and Taylor, M. J. *Proc. R. Soc. A* **273**, 41 (1963).
70. Partridge, R. B. and Series, G. W. *Proc. phys. Soc.* **88**, 969 (1966).
71. Series, G. W. *Proc. phys. Soc.* **88**, 957 (1966).
72. Geneux, E. and Favre, C. J. *Phys. Letters*, **8**, 190 (1964).
73. Aleksandrov, E. B., Konstantinov, O. V., Perel', V. I. and Khodovoi, V. A. *Soviet Phys. JETP* **45**, 503 (original); **18**, 346 (English translation) (1964).
74. Chapman, G. D. and Series, G. W. *J. Phys. B* **3**, 72 (1970).
75. Pegg, D. T. *J. Phys. B* **2**, 1097, 1104 (1969).
76. Salwen, H. *Phys. Rev.* **99**, 1274 (1955).
77. Shirley, J. *Phys. Rev.* **138**, B979 (1965).
- 77a. Pegg, D. T. and Series, G. W. *J. Phys. B* **3**, L33 (1970).
78. Cohen-Tannoudji, C. and Haroche, S. *C.r. hebd. Seanc. Acad. Sci., Paris*, **262**, 268 (1966).
79. Glauber, R. J. "Les Houches Lectures, 1964". In "Quantum Optics and Electronics", (Eds. C. de Witt *et al.*), p. 65. Gordon and Breach, New York (1965).
80. Series, G. W. *Proc. phys Soc.* **88**, 995 (1966).
81. Hackett, R. Q. Thesis, University of Oxford. (1968).
82. Cohen-Tannoudji, C. *Annls. Phys.* **7**, 423, 469 (1962).
83. Arditi, M. and Carver, T. R. *Phys. Rev.* **112**, 449 (1958).



## Thirty Years of Optical Pumping†

G. W. SERIES

J. J. Thomson Physical Laboratory, Whiteknights,  
Reading RG6 2AF, England

**ABSTRACT.** This article traces the development of optical pumping from the ideas first elaborated by Kastler in 1950. It deals with the general characteristics of optical pumping, the optical 'magnetization' of gases and vapours, spin exchange, metastability exchange, orientation by collision, multiple quantum resonances, atomic coherences, quantum beats, and dressed atoms; and concludes with a note on laser spectroscopy.

### 1. Introduction

Spectroscopy is, shall we say, experimental Fourier analysis. We study the relative intensities, frequency by frequency, in a beam of light to discover the kind of motions in atoms or molecules responsible for emitting or absorbing the light at those particular frequencies.

Optical pumping is, to put it crudely, spectroscopy without a spectroscope. Optical pumpers are not very interested in the frequency of the light. They study the changes in *intensity* or *polarization* of light when they disturb atoms in some way—by applying magnetic fields, for example. The changes of intensity or polarization tell them about atomic motions in fine detail; Zeeman effects, hyperfine structures, and so on. In optical pumping the light is used as a handle with which to turn the atoms over. It is surprisingly efficient. This article surveys what has been done by its practitioners since 'pompage optique' was introduced into physics over thirty years ago. The story has been one of continual surprises. The sophisticated young physicist of today will see it as a disclosure of the obvious: that is a measure of the importance and success of the subject.

### 2. Light and atoms

It was in May 1950 that Kastler's paper to the Société Française de Physique was delivered and the term 'pompage optique' used for the first time in public. It may come as a shock to the reader to realize that when, nine years later, the first international conference on optical pumping was held at Ann Arbor, Michigan, no laser beam had ever carved its coherent path through ruby rod, nor was stimulated emission much talked about outside microwave laboratories. Nevertheless, optical pumping was well enough established at that time for the production of a bibliography of some 102 items. Lasers (known then as optical masers) were, indeed, under discussion at the conference, for the seminal paper by Schawlow and Townes had just been published. But a sensitive government had cast a security blanket over the formal communications, and our American colleagues at Ann Arbor were in

---

† This article contains the substance of a lecture delivered at the 12th annual conference of the European Group for Atomic Spectroscopy, held at Pisa in September 1980.



frantic dispute with Washington over the question whether such delicate topics as optical transitions in caesium vapour could properly be permitted to be talked about in an international scientific gathering.

Kastler himself tells us when the seeds of optical pumping were sown. In his Nobel Lecture (he was awarded the Prize in 1966) he takes us back to the early 1930s, to the observation that light scattered in studies of the Raman effect had been found to contain a depolarized as well as a polarized component: the depolarization had been ascribed to the effect on the scattered light of vibrational motions within the molecules. He refers also to the work of Rubinowicz on selection rules in atomic spectra—rules that were derived from considerations of conservation of angular momentum between atoms and light. And, finally, he refers to his own work of that period on the stepwise excitation of fluorescence from mercury vapour. In all this he saw how the polarization of light could control, and be controlled by, the angular momentum of atoms. Light was a handle with which one could take hold of atoms and turn them over (Kastler 1967).

This is all very obvious to physicists today, but we should recall the psychological barrier which Kastler had to overcome before he could create a whole new branch of physics out of this simple observation. We must remember that the interaction between light and atoms is very, very weak. Remember that, when we work out our theories of atomic structure, we write in our Coulomb forces and our Lorentz forces, we work out the energies of stationary states, and only *then* do we say—oh yes, of course, and there is a correction of a few parts per million arising from the fact that atoms are potential sources of electromagnetic radiation. Indeed, when we use light to turn atoms over, the handle is exceedingly flimsy.

### 3. Magnetic resonance

This was another ingredient in the development of optical pumping. In the years immediately following World War II there had been a great development in the application of magnetic resonance to atoms and molecules in beams, and the first coupling of these ideas with Kastler's notions concerning light and the orientation of atoms were expressed in relation to *excited* states. The pioneer experiment was carried out at MIT by Brossel (then a young colleague of Kastler) and Bitter (1952); the change in polarization of fluorescent light from an atomic vapour was to act as monitor for magnetic resonance in the excited state.

The material chosen was mercury vapour, enclosed in the cell shown in fig. 1. The vapour pressure of the element, at room temperature, is low enough so that the atoms, as they cross the cell, hardly ever collide with one another. They are irradiated with light from a mercury lamp whose emission lines exactly correspond with the absorption lines of the atoms in the cell. In particular, the atoms absorb the strong line at 254 nm which excites them from the ground state,  $^1S_0$ , to the excited state  $^3P_1$  (fig. 2). This excited state actually has three Zeeman levels  $m=0, \pm 1$ , separated by the application of the static magnetic field  $B$  indicated in fig. 1. Of these three levels, only  $m=0$  is populated because the light is linearly polarized, its electric vector being parallel to  $B$  ( $\pi$ -polarization). If the atoms were allowed to radiate without further perturbation, they would emit light of the same polarization, indicated by the broken line in fig. 2. A detector placed as shown in fig. 1 would not record this radiation since it is emitted in an American doughnut pattern, the axis of which lies along the magnetic field direction. But now, suppose that the atoms are



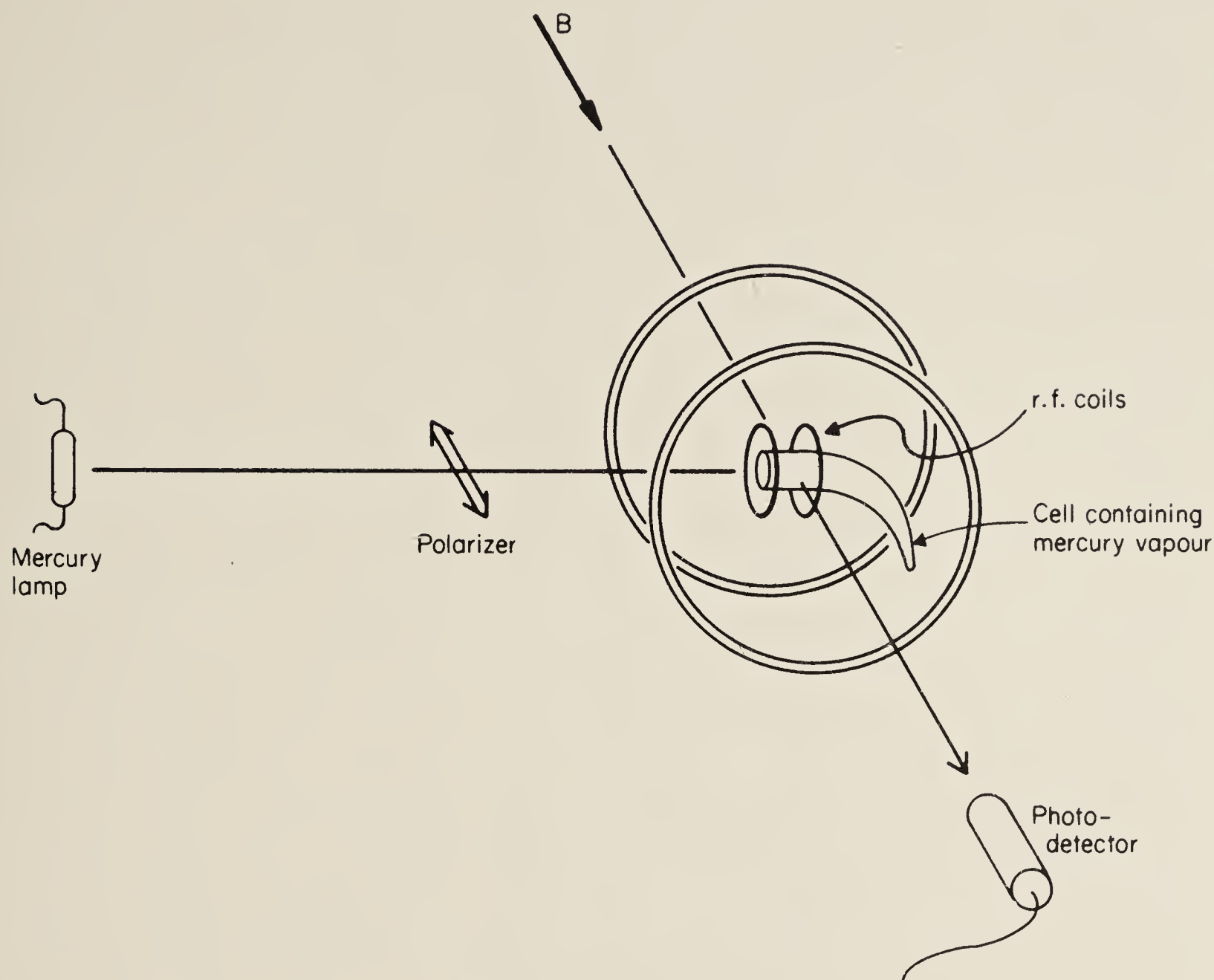


Fig. 1. Scheme of the Brossel-Bitter experiment. The large coils round the cell carry a current to generate the static magnetic field  $B$ .

perturbed before they radiate. This can be accomplished by a magnetic field oscillating at radio-frequencies, established by circulating an alternating current through the smaller coils, provided it is strong enough and of the right frequency. Such an oscillating field causes the atoms to be transferred to the Zeeman levels  $m \pm 1$ , as indicated in fig. 2. This is magnetic resonance, and occurs most strongly when the quantum energy of the oscillating field,  $\hbar\omega_0$ , exactly matches the Zeeman splitting,  $\Delta E$ . The process of spontaneous emission now results in radiation whose frequency is slightly different from what it was before (which is not important) and whose polarization has been changed (which is of the utmost importance). Emissions in which the  $m$ -quantum number changes by one unit (as in this case) are labelled  $\sigma^+$  or  $\sigma^-$ , and the intensity has a dumbbell-shaped distribution in space, the axis being along the direction of the magnetic field. In this direction the light is circularly polarized: seen perpendicularly to the field it is linearly polarized with its  $E$ -vector perpendicular to the magnetic field, and intermediately it is elliptically polarized. This contrasts with the polarization of the unperturbed emission,  $\pi$ , in which the change in the  $m$ -quantum number was zero. This is linearly polarized irrespective of the direction of emission. The fact that magnetic resonance has occurred is therefore easily detected by the use of polarizers or simply by relying on the changes in the spatial distribution of the intensity of the spontaneously emitted light. A typical resonance curve is shown in fig. 3.

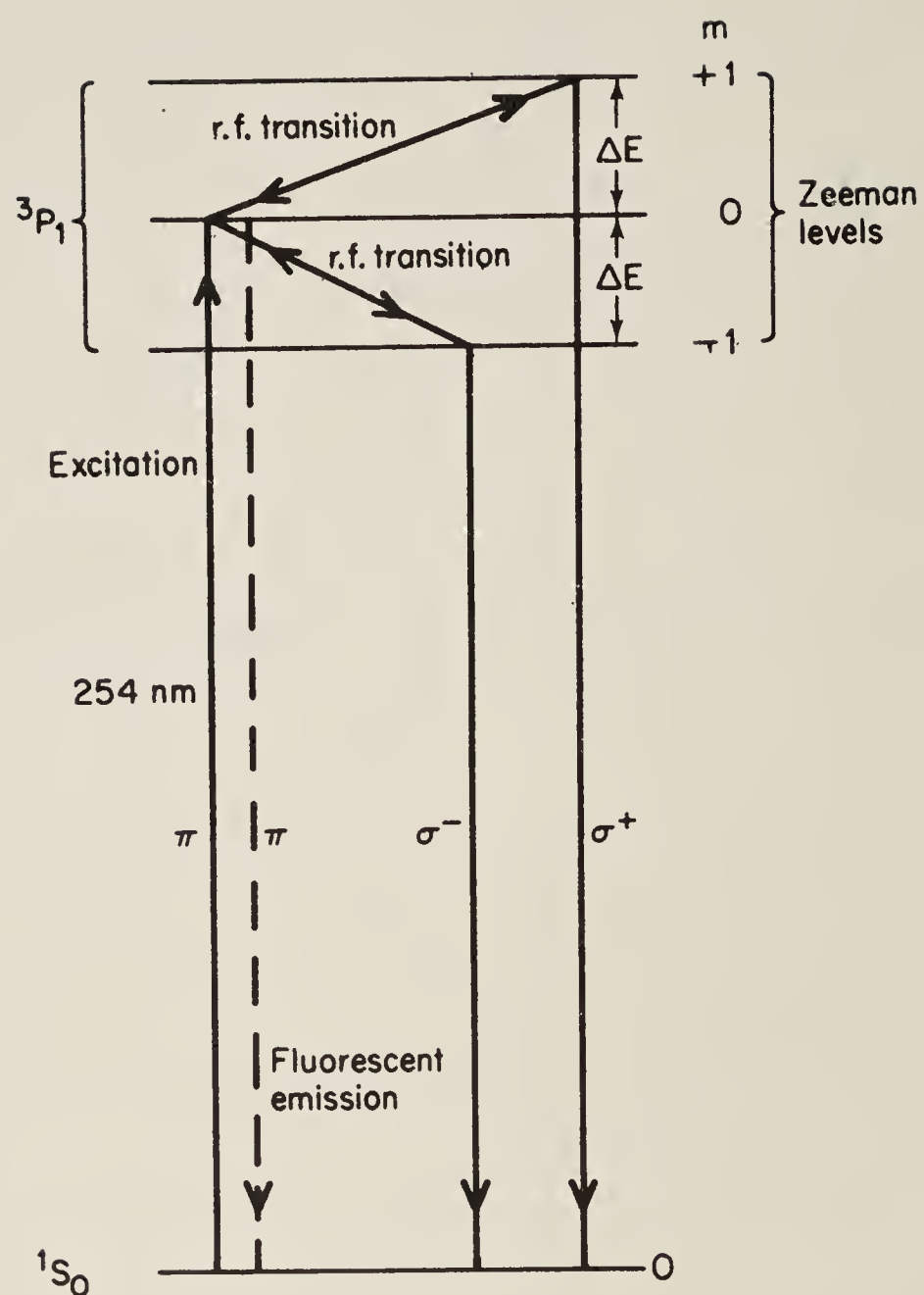


Fig. 2. The transitions in the Brossel-Bitter experiment.

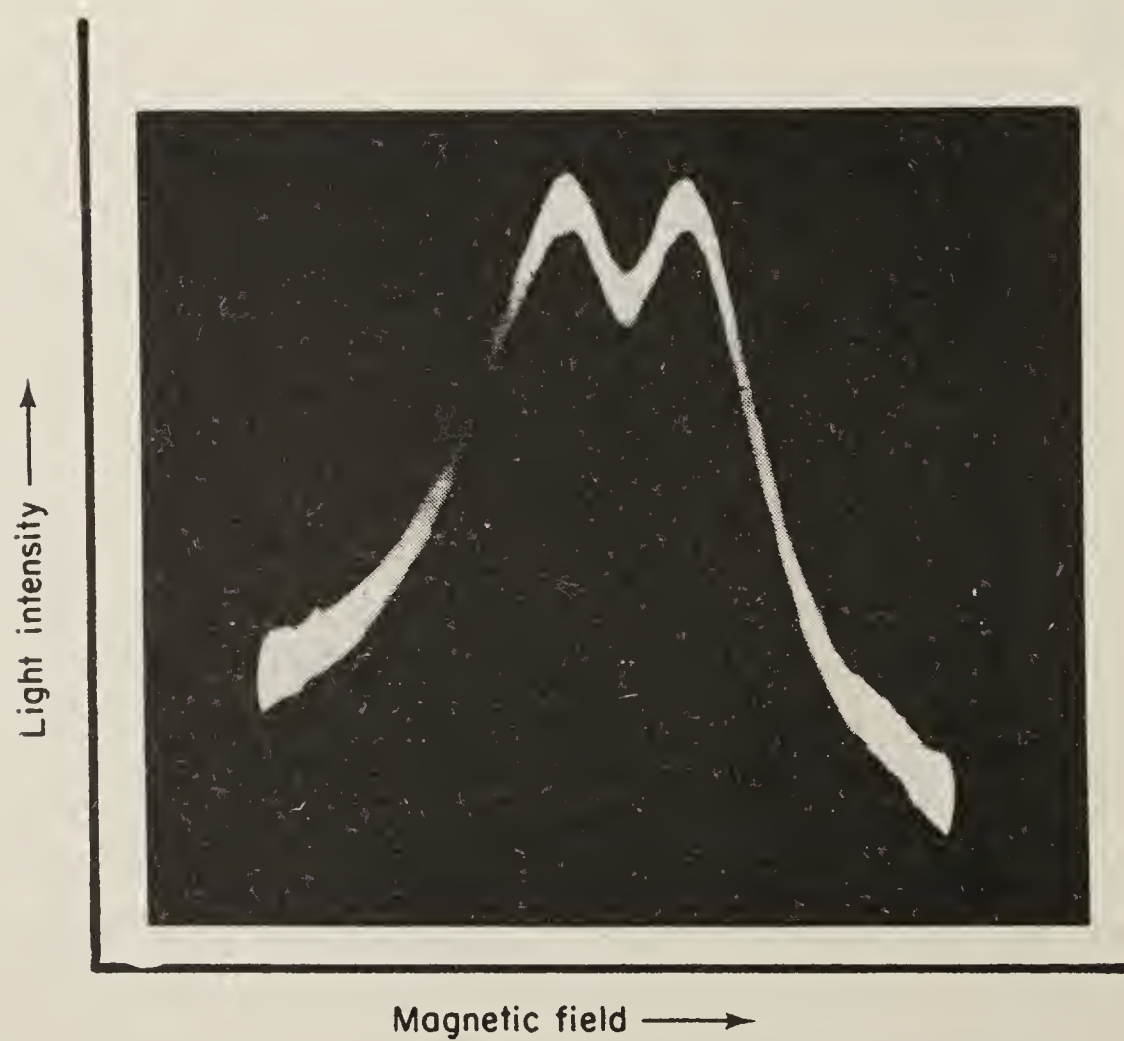


Fig. 3. Experimental magnetic resonance curve obtained in the Brossel-Bitter experiment. Intensity of light is plotted against magnetic field, the r.f. resonance frequency being held constant ( $\omega_0$ ). At the middle of the curve the Zeeman splitting  $\Delta E$  satisfies the equation  $\Delta E = \hbar\omega_0$ .



The outcome of the Brossel–Bitter experiment was—superficially—simply an accurate determination of the Zeeman structure of a particular excited state of mercury: not a very exciting piece of information. But its greater importance lay in its demonstration of the possibilities for the manipulation of atoms by means of light.

#### 4. Optical pumping: ground states

It was very soon realised that, if the ground states of the atoms possessed Zeeman or hyperfine structure, then the cycle of *resonance fluorescence*—excitation of atoms by light followed by spontaneous, radiative decay—would alter the relative numbers of atoms occupying each of these ground states. Now, inequality of population between Zeeman levels amounts to magnetization, so we arrive at the intriguing conclusion that *one can magnetize an atomic vapour simply by shining light into it*.

Figure 4 shows how this works out for the alkali atoms whose ground states have electronic spin  $\frac{1}{2}$ . (In fact, all the alkalis have hyperfine structure, which we ignore in this discussion. The hyperfine structure complicates the story but does not invalidate the principle.) In the figure we represent the two Zeeman components of the ground state,  $^2S_{1/2}$ , by spots separated horizontally and labelled  $\pm\frac{1}{2}$  (the  $m$ -quantum number) indicating the two possibilities for the orientation of the angular momentum. Likewise the excited state  $^2P_{1/2}$  is reached from the ground state by absorption of the yellow line  $D_1$ ,  $\lambda=589.6$  nm. Sodium vapour, in thermal equilibrium in a cell, consists of atoms equally distributed between the  $\pm\frac{1}{2}$  components of the ground state. The vapour is unmagnetized. Now suppose we irradiate it with circularly polarized  $D_1$  light to induce the  $\sigma^+$  transition. Only the atoms in the component state  $-\frac{1}{2}$  are able to absorb this light: those in  $+\frac{1}{2}$  are unable to absorb the angular momentum carried by  $\sigma^+$  light since there is no component  $+\frac{3}{2}$  in the excited state. When the excited atoms decay to the ground state, it may be to the component  $-\frac{1}{2}$ , which would restore the original situation, or it may be to the component  $+\frac{1}{2}$ . The latter possibility results in a net transfer of atoms from  $-\frac{1}{2}$  to  $+\frac{1}{2}$ , and this is magnetization. The direction of magnetization is that of the axis of

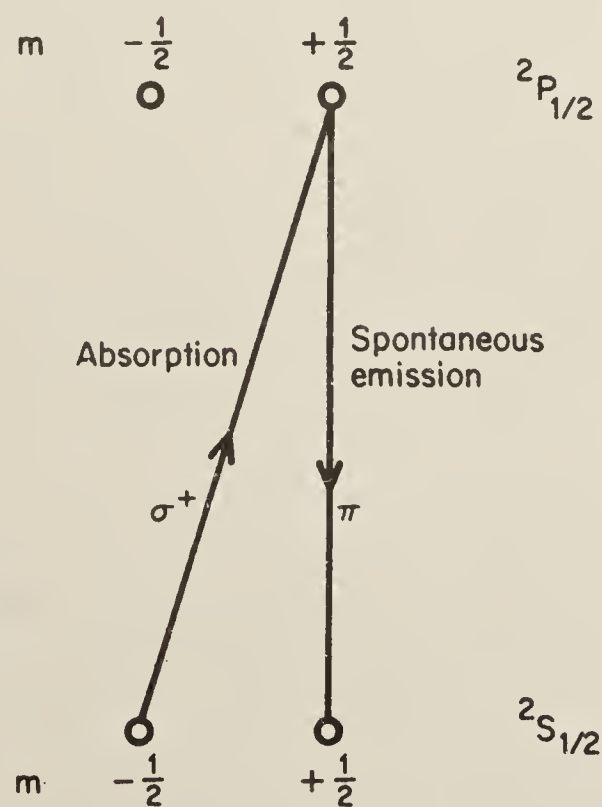


Fig. 4. A cycle of optical pumping.



circular polarization of the light, which is its direction of propagation. What we have described here is one cycle of optical pumping. The term 'polarization' which we have hitherto used only for the light is commonly used also for an assembly of atoms in which the angular momentum component states are unequally populated. 'Polarization' and 'magnetization' are often used indiscriminately, but for some purposes it is necessary to be more specific, and one speaks of 'orientation' (of a dipole) and 'alignment' (of a quadrupole).

## 5. Characteristics of optical pumping experiments

Following Kastler's paper in 1950 there was a great explosion of activity in optical pumping: in Paris, of course, but also particularly in North America. The great attractions of the work were (i) its conceptual simplicity, (ii) that the apparatus was simple, and (iii) that it offered the possibility of making spectroscopic measurements of enormously increased accuracy.

The conceptual simplicity was founded on the well-known selection rules and principles of conservation of energy and angular momentum governing the interaction of light, on the one hand, and radio-frequency fields, on the other, with free atoms. And, indeed, there was scope for much more sophisticated theoretical work which, as we shall see later, turned out to be richly rewarding, and was carried through with great subtlety.

The apparatus required for many experiments was table-top size (fig. 5). The excited state work was carried out from the first with atomic vapours in sealed cells. For the ground state work, it was not known in the early days whether the effects of optical pumping would be destroyed by collisions between the atoms and residual gases, so the first experiments were carried out in atomic beams. But it soon became clear that ground state experiments, too, could be carried out in sealed cells.

As to the accuracy of measurement, the most obvious attraction here was the promise for excited states, because the magnetic resonance curves that were obtained gave Zeeman and hyperfine intervals free of Doppler broadening, whereas these intervals as measured by conventional spectroscopic methods are subject to this nuisance, and are typically a hundred times broader than the magnetic resonance curves of free atoms, with consequential problems of unresolved structures and imprecise measurement. But this article is more concerned with ground-state work, and it was not at all obvious for such states that magnetic resonance based on optical pumping techniques offered any advantage at all over 'conventional' atomic beam studies. What we shall see is that the ground-state work prospered rather on account of the surprises it had in store than because of the possibilities that were foreseen at the outset. But some applications were rather straightforward, and these we shall appraise briefly. Later on we shall look more closely at the surprises.

Let us first recall the essentials of an optical pumping-magnetic resonance experiment. One may distinguish three processes: the pumping, the magnetic resonance, and the monitoring of the resonance. The essential feature of the pumping process is that the atoms are redistributed over the ground states (fig. 4). With an eye on the monitoring process we see (fig. 6) that this redistribution reduces the amount of light that the atoms are able to absorb. In the region of magnetic resonance, the oscillating radio-frequency field (applied by means of an oscillating current in the small coils round the bulb seen in fig. 5) is effective in restoring the equality of



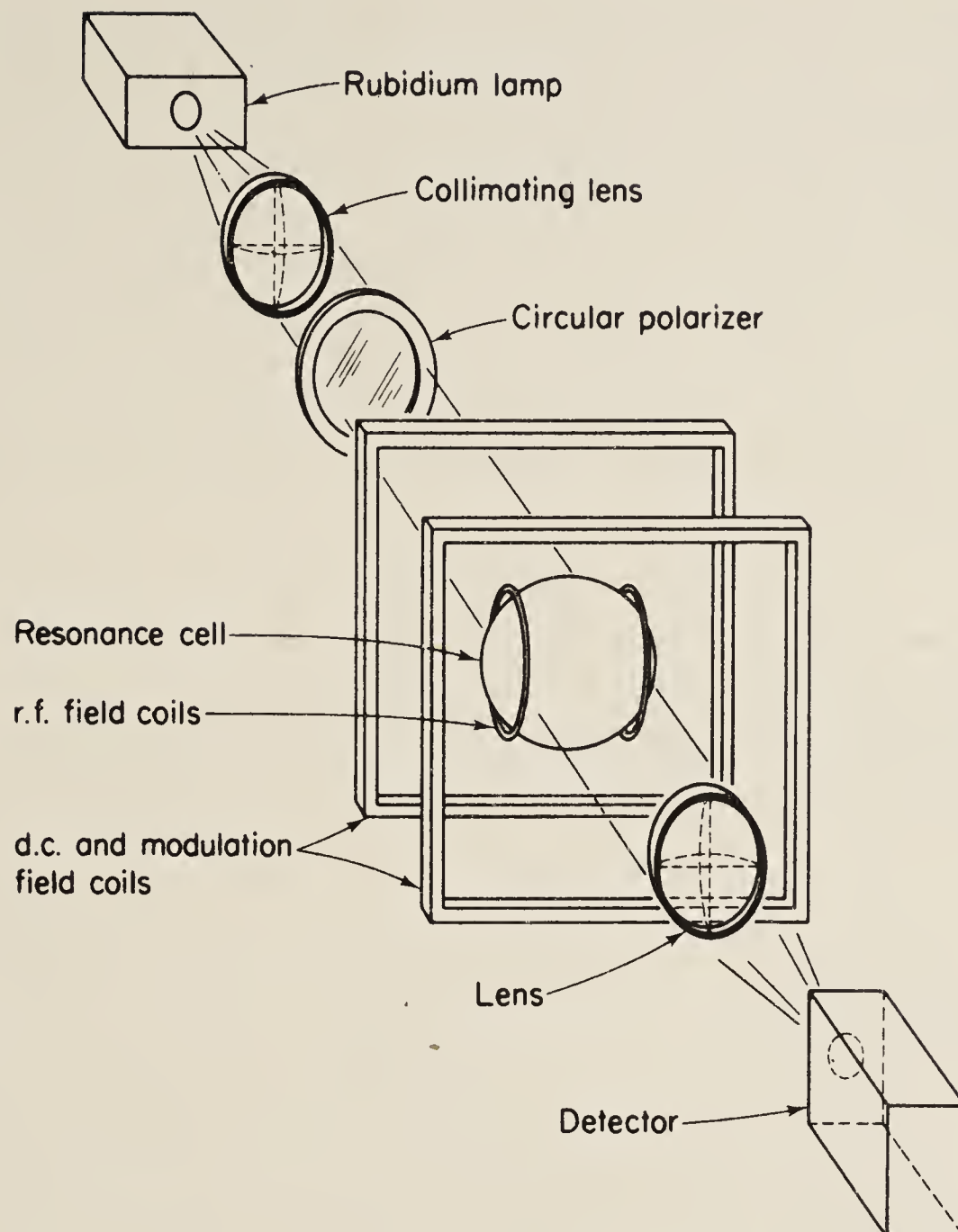


Fig. 5. Scheme of an optical pumping experiment. The function of the components described in the text. The physical processes are indicated in fig. 6.

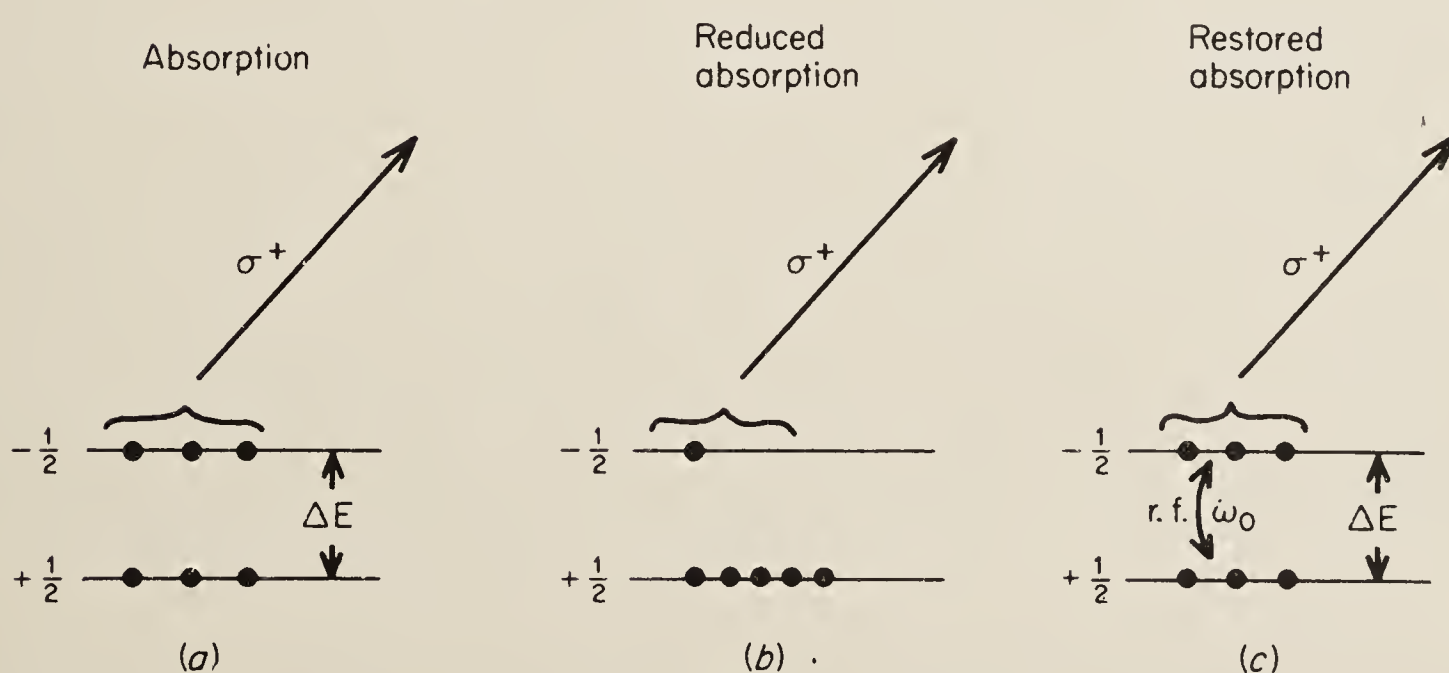


Fig. 6. The two functions of light: optical pumping and monitoring magnetic resonance. (a) The original distribution of atoms, three in each state. Circularly polarized light is absorbed by atoms in the upper state but not from those in the lower, leading to optical pumping. (b) After one cycle of optical pumping (transfer of two atoms) the vapour is more transparent. (c) The radio-frequency field restores atoms to the upper state, most efficiently at resonance, when  $\Delta E = \hbar\omega_0$ , and this results in a restoration of absorption.

population between the two levels: the absorption is then restored. The resonance may be monitored, therefore, by looking for changes in the absorption of light by atoms in the cell. The light beam may be the same as is used for the pumping, or it may be a beam set up separately. This latter arrangement gives more control. Under some circumstances the absorption from the monitoring beam is modulated at the same frequency as the applied r.f. field—the depth of modulation being a maximum at the peak of the resonance. If the modulated, transmitted light is used to generate a photocurrent, this may be amplified and used as the oscillator which drives the r.f. current through the coils. The apparatus is then self-adjusting. The frequency of the oscillator locks itself to the peak of the resonance whose angular frequency  $\omega_0$  is given by the equation

$$\hbar\omega_0 = \Delta E$$

where  $\Delta E$  is the energy gap between the levels.

If the energy gap  $\Delta E$  is a Zeeman interval it is under the experimenter's control by varying an external magnetic field. In this case  $\Delta E = g\beta B$ , where  $B$  is the magnetic flux density,  $\beta$  is the Bohr magneton ( $9.27 \times 10^{-24} \text{ J T}^{-1}$ ) and  $g$  is a numerical factor known as the Landé  $g$ -factor. Optical pumping experiments are frequently undertaken in order to determine these  $g$ -factors. With simple apparatus hardly more elaborate than is illustrated in fig. 5 it proved possible to accomplish this for many atoms: the alkalis and the odd isotopes of mercury were particularly favourable objects of study.

When  $\Delta E$  is a hyperfine interval no external field is necessary. Each hyperfine level, generally labelled  $F$ , consists of one or more Zeeman components, labelled  $m_F$ . These all have the same energy. Optical pumping transfers atoms between levels of different  $F$  and the r.f. field restores them. For a detailed analysis one needs to consider which of the  $m_F$  are involved, but this is unimportant if one is only concerned with the position of the peak of the resonance, which again is given by  $\hbar\omega_0 = \Delta E = E_F - E_{F'}$ , the energy difference between levels of different  $F$ . Hyperfine intervals also have been determined by optical pumping for many atoms.

Optical pumping experiments are quite suitable for undergraduates to perform, and allow fundamental quantities to be determined. For example, the nuclear spin  $I$  of alkali atoms may be deduced from even a 10% determination of the  $g$ -factor of the ground state hyperfine levels,  $g_F$ . In this case a small external field of the order of  $10^{-4} \text{ T}$  is applied to separate the Zeeman components  $m_F$  of the hyperfine levels. The required r.f. field may be provided by a signal generator operating below 1 MHz.  $I$  is determined from the relation  $g_F = g_J/(I + \frac{1}{2})$ , where  $g_J = 2$  (the Landé factor for the ground state,  $^2\text{S}_{1/2}$ ). Of course, stray laboratory fields need to be cancelled out; this is normally done with sets of Helmholtz coils about 40 cm radius. For measurements of high precision, special care has to be taken in the cancellation of stray fields and in the avoidance of inhomogeneities in the additional fields that are applied.

## 6. Resonance line-width: buffer gases and wall coatings

The precision of measurement depends on the resonance linewidth. The early ideas suggested that the linewidth would be limited by the time-of-flight of atoms across the cell, say  $10^{-4} \text{ s}$ , this being the time for which the atoms would interact, without interruption of phase, with the r.f. field. The resonance linewidth, the inverse of the interaction time, would then be about  $10/2\pi \text{ kHz}$  (fig. 7). But it was soon discovered that this interaction time could be lengthened by two devices,



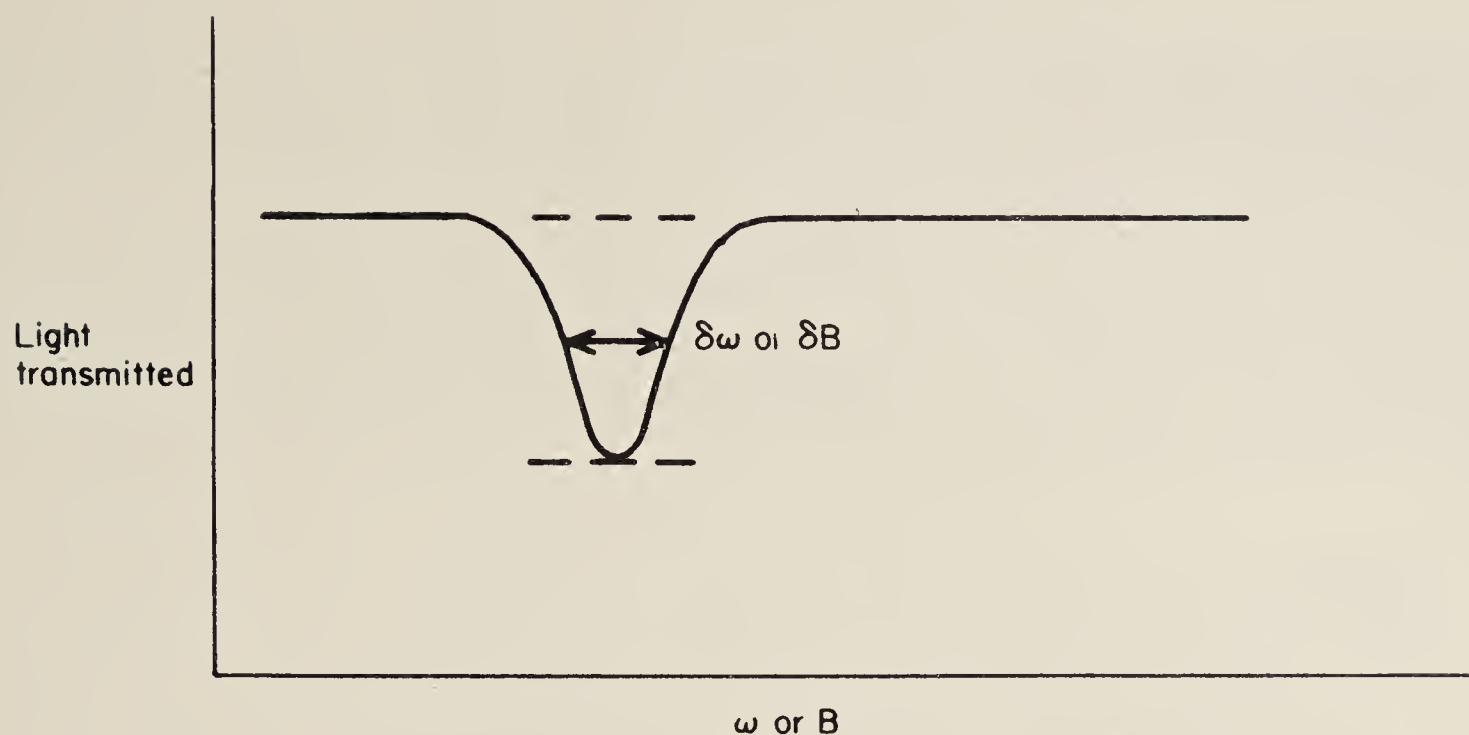


Fig. 7. Resonance curve. Either  $\omega$  or  $B$  may be varied, the other being held constant. The width at half-dip,  $\delta\omega$ , is equal to the reciprocal of the interaction time. Longer interaction times lead to narrower resonance curves and increased precision in the determination of line-centre. (If  $B$  is varied,  $\delta B = (\hbar/g\beta)\delta\omega$ .)

appropriate in varying degree to different kinds of atom: (a) the use of *buffer gases*, at pressures of the order of a few torr, and (b) the use of *wall coatings*.

### 6.1. Buffer gases

It was realized that oriented alkali atoms might undergo many thousands of collisions with inert gas atoms without losing their orientation, that is to say, without reverting to their equal distribution between the Zeeman states. This is at first sight surprising, but it is understandable when one recalls that, for alkali atoms in their ground states no less than for noble gas atoms, the electrons are distributed round their respective nuclei with spherical symmetry and zero orbital angular momentum. The orientation of the alkalis arises solely from the intrinsic spin of the valence electron, and this is perturbed hardly at all in the collisions, where the dominating forces are electrostatic and exert no magnetic torque.

Alkali atoms, then, mixed with a much greater proportion of buffer gas, find their progress to the wall of the cell impeded by collisions but do not lose their orientation. The interaction time with r.f. fields can be lengthened to the order of seconds, with corresponding reduction of resonance linewidth—provided the static fields can be made sufficiently homogeneous. A remark made in this context at the Ann Arbor Conference bears on this: ‘Surely at some point, you have to worry because of the nails in your shoes’. ‘O yes: we leave our shoes outside the laboratory: what really worries us are the hinge-pins in our spectacle-frames.’

### 6.2. Wall coatings

It was found that a number of wax-like materials—the saturated paraffins—applied to the walls would also allow thousands of collisions of oriented alkali atoms without loss of orientation. (Polish candles worked especially well but eicosane works well outside Poland.) Again, resonance line-widths could be drastically reduced and high precision gained.

The use of buffer gases and wall coatings brought their own particular difficulties and opportunities. On the one hand, it was not correct to suppose that collisions with these inert objects brought *no* change to the atoms. The cumulative effect of many collisions induces gradual phase changes in the precession of the atoms, which are equivalent to frequency shifts. Many studies were made of such pressure shifts, and wall shifts, both because it was necessary to apply corrections to the measured resonance frequencies, and also for the interest of studying the collisions themselves. Figure 8 shows some examples.

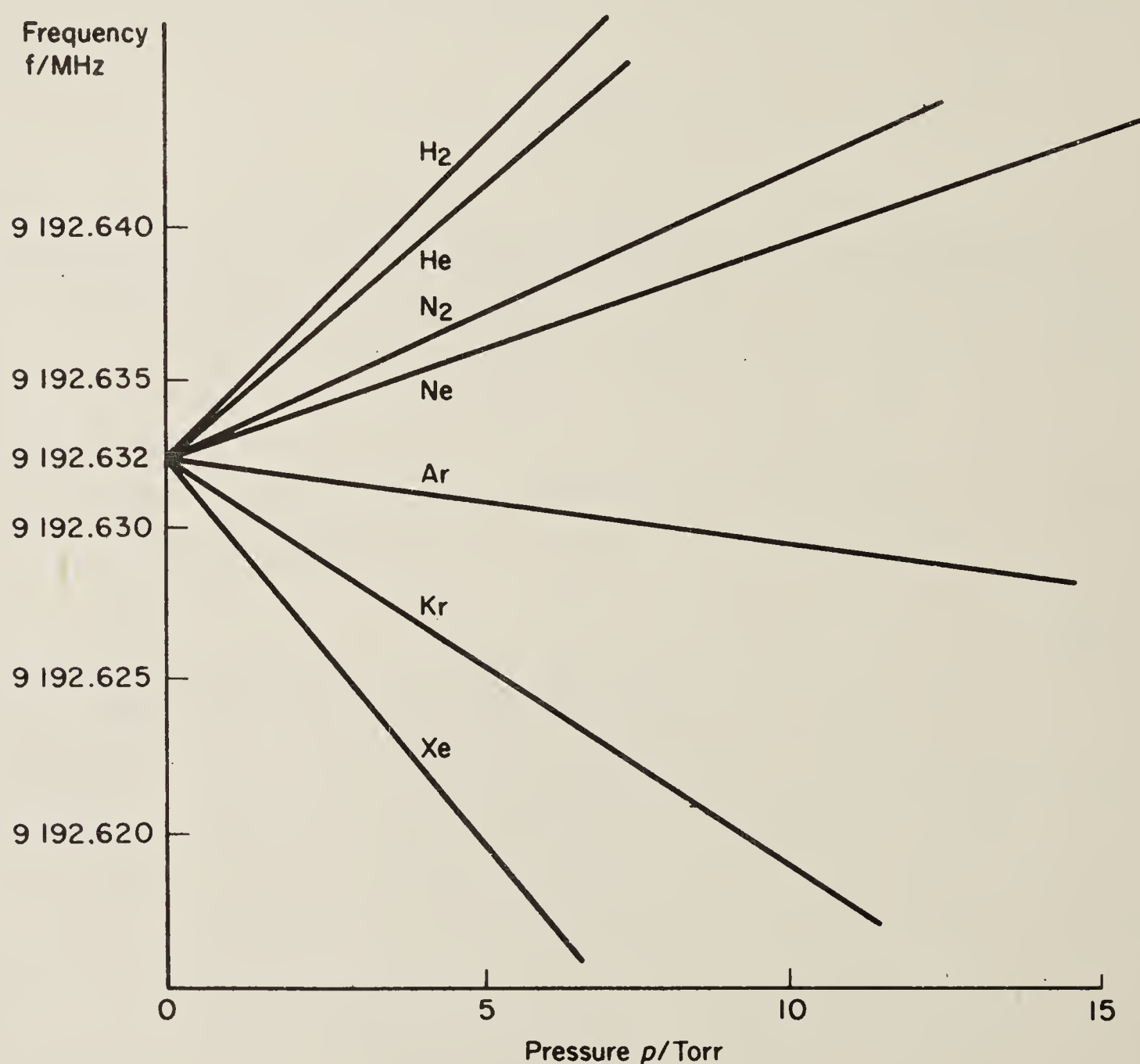


Fig. 8. Variation of resonance frequency with pressure for optically-pumped caesium atoms, for a variety of buffer gases. The resonance being studied here is the hyperfine interval in the ground state of caesium, which is used for the SI standard of frequency (that is, to define the second). (Arditi and Carver 1961.)

## 7. Relaxation

The determination of relaxation times—spin lifetimes—under various conditions provided a rich field of study. The relaxation time is simply related to the inverse of the measured linewidth. The lifetime was different, for example, for walls coated with ordinary paraffins and with deuterated paraffins. This emphasized the importance of the interaction between the alkali and the atomic nuclei in the wall coatings. Again, as a result of very detailed studies of relaxation times for alkalis in collision with inert gases, Mme Bouchiat was able to demonstrate the formation of alkali-rare-gas molecules having a substantial association time before the partners separated.



Chemists turned to this field to measure reaction rates between alkalis and reactive molecules. The linewidth now became a measure of chemical activity.

## 8. Magnetometers and frequency standards

In the context of magnetic resonance curves of very narrow linewidth, with the potentiality, therefore, of exploiting the resonance condition  $\hbar\omega_0 = \Delta E$  with very high accuracy, two cases of special interest have been developed commercially: one as a magnetometer, the other as a frequency standard.

For the magnetometer,  $\Delta E$  is the splitting of levels resulting from an ambient magnetic field. The energy difference is (to a first approximation) proportional to the field, so if the apparatus is made self-oscillating, and if the frequency of the oscillator is measured (and this can be done with exceedingly high accuracy), and if the constant of proportionality is known (as it is for the substances commonly used), we can determine the value of the field. Magnetometers using this principle have been flown in satellites, and are routinely used in geophysical observations.

The second commercial application of self-oscillating optically pumped cells is in the production of secondary standards of frequency. In this case  $\Delta E$  is an energy interval characteristic of the atom in zero fields: the interval between two hyperfine levels in the ground state of rubidium proves to be suitable. The electrical oscillator (which may be used to control a clock) is, by means of the optical pumping, magnetic resonance and photoelectric detection, actually locked to the precessional motions of electrons in rubidium atoms about their nuclei, the hyperfine interaction. The frequency is, of course, liable to be influenced by the pressure of buffer gas in the bulb, but a mixture of gases can be chosen to make this effect very small. The frequency is also influenced by the intensity of the pumping light, so the rubidium clock is not suitable for a primary standard. But it serves very well if one is content with timekeeping to an accuracy of 1 second in  $10^{11}$ .

## 9. Spin exchange

We now turn to a most important effect, spin exchange. It was introduced into optical pumping by Dehmelt, and was well known before the Ann Arbor conference. If you have a mixture of two different alkali metal vapours in a vessel, orientation in the atoms of one of them can be transferred to those of the other by collisions—so-called '*spin exchange*' collisions.

Thus, if you have sodium and rubidium, and pump with sodium light, you can magnetize the sodium directly, and the rubidium indirectly by collisions. Then you can carry out magnetic resonance on the *rubidium*, the effects of which will be reflected in the orientation of the sodium atoms, and the monitoring can be by *sodium* light. Thus, with sodium light, one can display a magnetic resonance signal from the ground states of *rubidium*.

Many substances were studied in this way—N, P, Cu, Ag, Eu, Li—but surely the most impressive studies were those of the free electron. The ingredients of the experiment were a gas discharge, to produce electrons, sodium vapour enclosed in the same cell, and a sodium resonance lamp. The free electron *g*-factor was determined by looking at changes in the absorption of sodium light. Unfortunately, other methods ultimately proved superior, but the spin-exchange method was ingenious and well worth the trial it was given. Dehmelt, Franken and their younger colleagues worked at it for many years.

A great story also attaches to optical pumping measurements of hyperfine structure in the ground states of hydrogen  $^1\text{H}$ , deuterium  $^2\text{H}$  and tritium  $^3\text{H}$  by Pipkin and his colleagues. Of course, it will be realized that hydrogen atoms cannot be pumped directly with their own resonance radiation because of the inconvenience of working with radiation in the far ultraviolet. Pipkin used the spin-exchange method to improve on the atomic beam and other direct studies, but the work was superseded by the invention of the hydrogen maser. It is fair to say that the use of wall coatings in the hydrogen maser was inspired by the use of wall coatings in optical pumping.

### 10. Metastability exchange

An important variant on the transfer of orientation by spin exchange was the discovery that one could orientate atoms in the ground states by collisions with optically-pumped atoms in metastable states; a technique introduced and explored by L. F. Schearer. The atomic species originally studied, and much studied since, was  $^3\text{He}$ . In a gas discharge the metastable state  $(1s2s)^3S_1$  is heavily populated. This can serve as a 'ground' state for optical pumping with light from a  $^3\text{He}$  lamp. But the nucleus of  $^3\text{He}$  spin  $\frac{1}{2}$ , and the orientation of the metastable state achieved by optical pumping with circularly polarized light implies that the atomic nuclei in this state, strongly coupled to the electrons, be themselves partially oriented.

Now consider collisions between oriented, metastable atoms and unoriented, ground state atoms (fig. 9). In the break-up of the unstable molecules that are formed there is a substantial probability that the oriented nuclei will be associated with the ground state electronic structures, while the non-oriented nuclei will be associated with the metastable structures. In the assembly, after averaging over many collisions, one finds a substantial orientation of nuclei in the atomic ground states.

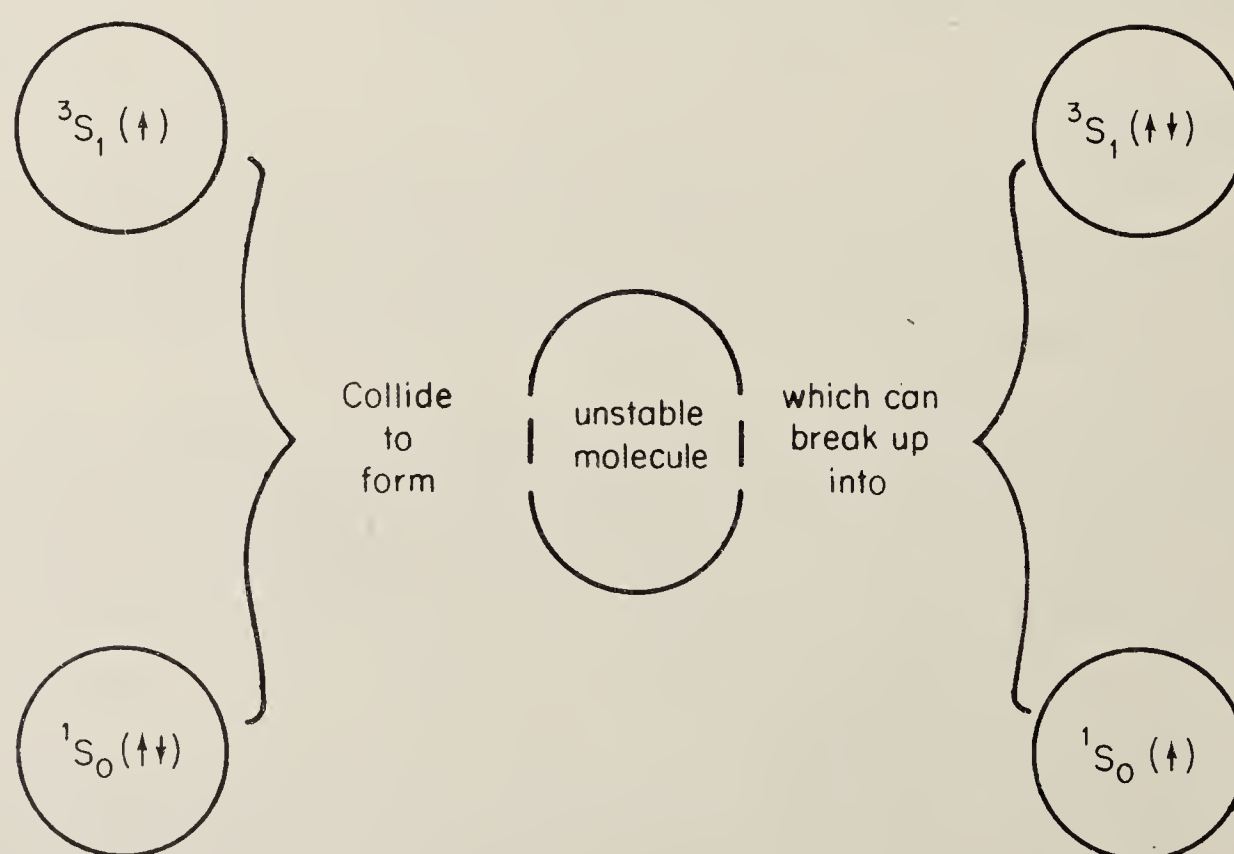


Fig. 9. Collision between an oriented metastable atom,  $^3S_1$ , and an unoriented ground state atom,  $^1S_0$ , leading to an exchange of nuclear orientation (transfer of nuclear angular momentum) between the two atoms. In ground state atoms the angular momentum resides entirely in the nuclei. Before the collisions the nuclear spins are in random directions (up and down equally probable, indicated by the small arrows). After the collisions there is a substantial probability that they are oriented (arrow up only).



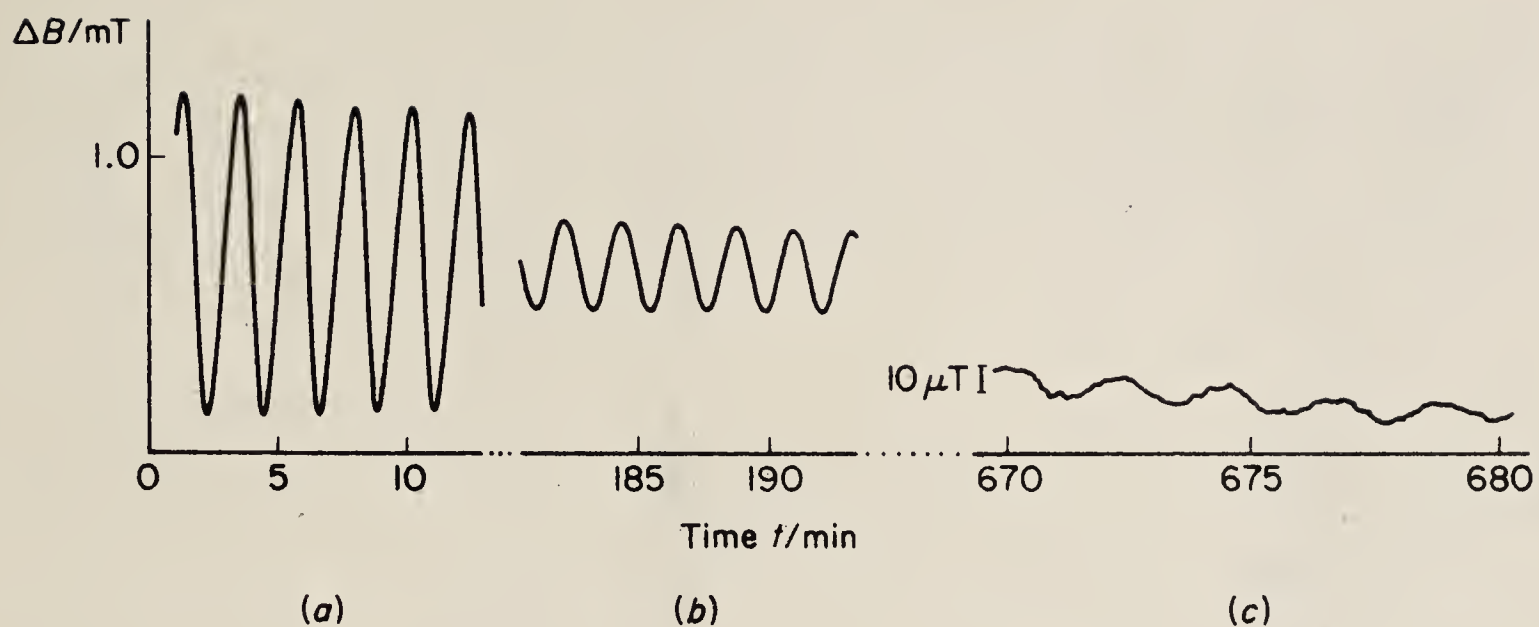


Fig. 10. Precession of oriented  $^3\text{He}$  nuclei in the gas at low pressure with continuity of phase over nearly 12 hours. (Cohen-Tannoudji and Haroche 1969.)

But this is very remarkable, because the ground state itself is  $^1\text{S}_0$ , that is to say, it has a tight, spherically symmetrical distribution of electric charge, and both the orbital and spin components of the electronic angular momentum are zero. Inside this protective structure lies the oriented nucleus. If the external magnetic fields (which could interact directly with the nucleus) are kept under control, external electric fields cannot penetrate the shielding electrons, and the nucleus can retain its orientation for very long periods. Figure 10, demonstrating a remarkable experiment by Cohen-Tannoudji and Haroche, shows the slow precession of  $^3\text{He}$  nuclei round a weak external magnetic field, continuous over a period of nearly 12 hours. The magnetometer used to record this very weak signal was a device based on optically-pumped rubidium vapour.

### 11. Orientation by collision: further experiments

This technique of transfer of orientation has been applied in many different contexts.

Laloë has shown how, in a gas discharge in  $^3\text{He}$ , oriented in the ground state, the orientation is transferred in the ordinary process of excitation to the whole range of excited states.

Scheerer has shown how the orientation may be transferred from metastable helium atoms in a gas discharge to a whole variety of other kinds of atoms, introduced as impurities and ionized by collision with helium metastables. These ionizing collisions are evidently very sensitive to spin-orientation.

### 12. Multiple quantum resonances

We now turn to one of the surprises of optical pumping discovered in the very early days by Brossel, Cagnac, Margerie and Winter working at Kastler's laboratory.

An atomic beam of sodium was under study, irradiated over the first part of its length with circularly polarized light to pump the atoms, and surrounded downstream by coils to induce magnetic resonance between the ground-state Zeeman levels. The expected resonances between adjacent levels were observed, but, for higher values of the r.f. field new, additional resonances appeared. These were of two types, illustrated in fig. 11.

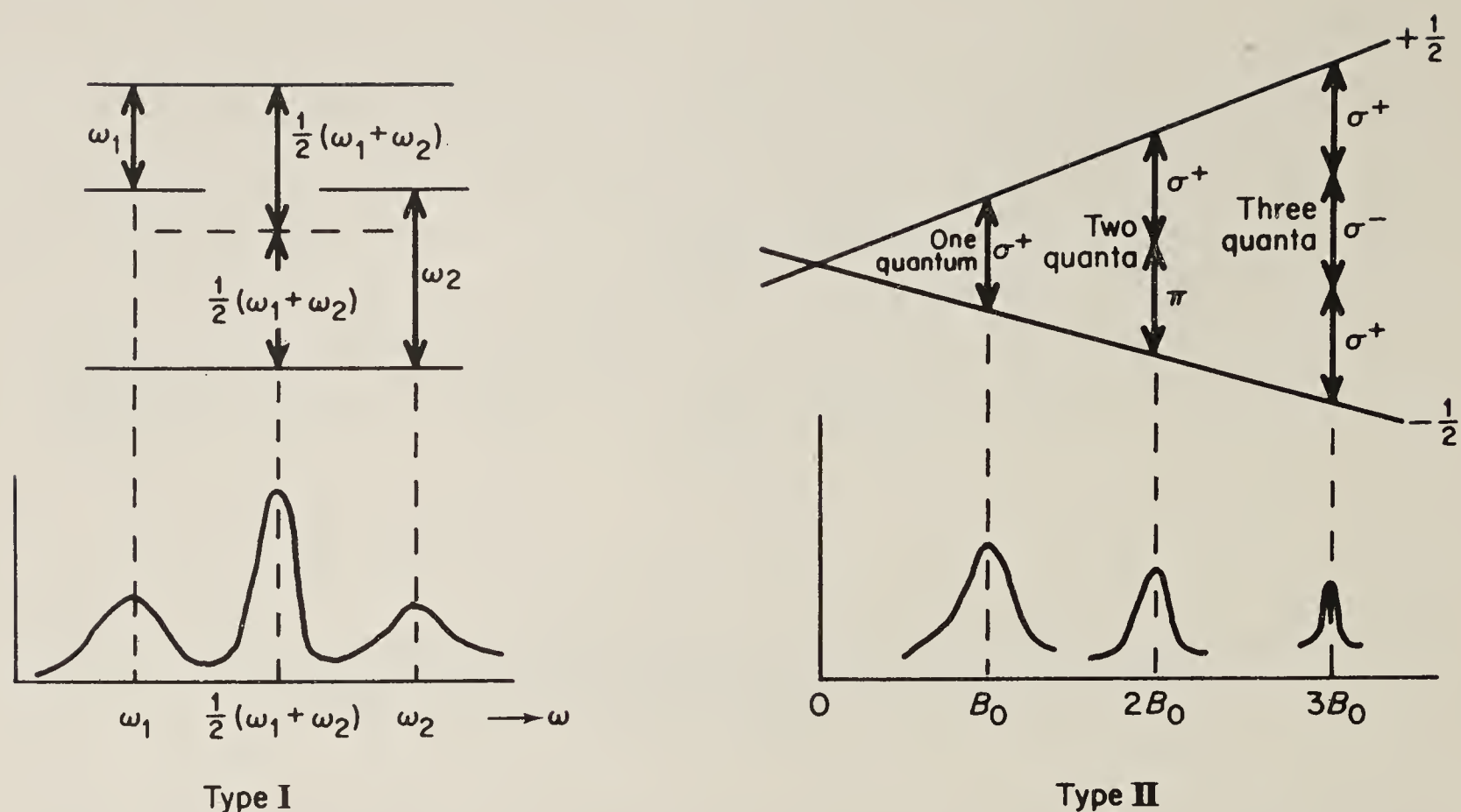


Fig. 11. Multiple quantum resonances. Type I. The resonance curves at  $\omega_1$  and  $\omega_2$  correspond to single-quantum transitions between levels. If the r.f. field strength is increased these resonance curves broaden. When they perceptibly overlap a new, narrow resonance appears half-way between them. Type II. The lines labelled  $\pm \frac{1}{2}$  represent the energy levels of a spin  $\frac{1}{2}$  atom in a steady magnetic field of flux density  $B$ . Circularly polarized radiation at frequency  $\omega$  gives a resonance at  $B_0$  where the energy difference is equal to  $\hbar\omega$ . The resonances at  $2B_0$ ,  $3B_0$ ... appear if radiation of other polarizations is present with sufficient intensity. (A linearly polarized field can be resolved into  $\sigma^+$  and  $\sigma^-$  circularly polarized components and can generate a three-quantum resonance, as shown.)

Type I resonances appeared half-way between resolved resonances when the strength of the r.f. field was increased. The frequency did not correspond to the interval between adjacent levels, but to one-half of the interval between non-adjacent levels. For this type of resonance a third, intermediate level is present and forms an important part of the interpretation, but it does not lie half-way between the outer levels. (This spacing of levels can easily be controlled by varying a magnetic field applied to the vapour: a small field produces equal spacings; a larger field produces inequalities as the level spacings become comparable in magnitude to the hyperfine structure.)

Type II resonances do not require the third, intermediate level. They are sometimes called 'sub-harmonic' resonances, in that the frequency of the radiation is a sub-multiple of the interval between the levels; thus, they satisfy the equation

$$\hbar\omega = (\Delta E)/n \quad \text{where } n \text{ is an integer}$$

Like resonances of Type I they require r.f. fields of much greater amplitude than are required for direct resonances. Their characteristic is that different polarizations of the r.f. field act together to induce the transition, but overall the conservation laws for energy and angular momentum are satisfied.

It need hardly be said that the observation of these resonances stimulated a great deal of theoretical study, and the examination of detailed features such as linewidth and shape still finds a place in research journals. Readers acquainted with recent developments in laser spectroscopy will know that resonances of Type I can be



generated with visible and ultraviolet light in such a way as to be free of Doppler broadening. In these applications the light which contributes the two steps of the transition travels in opposite directions; and the positive Doppler shift in one beam cancels the negative shift in the other. Resonances of Type II, however, appear not to have been explored with radiation at frequencies outside the radio bands.

### 13. Atomic coherences

Almost everything that has been mentioned so far can be understood in terms of the transfer of atoms between energy eigenstates. Atoms are either in state A, characterized by its energy  $E_A$ , and component of angular momentum  $m_A$  (in units of  $\hbar$ ), or they are in state B, characterized by  $E_B$  and  $m_B$ . The action of the light and r.f. fields is to transfer them from state A to state B, and so on. But it is not actually the case, in this kind of work, that atoms are *either* in state A *or* in state B. Under irradiation, in general, the *state* of the atoms (this word is being used in a technical, quantum-mechanical sense) is a coherent superposition of A and B: the atoms are in A with a certain probability and in B with a certain (usually, different) probability, and these probabilities are correlated. This correlation is called 'coherence'.

The correlation is perhaps most easily understood in the phenomenon known as 'free precession' which can occur, for example, for atoms that are left to evolve after an r.f. field which has been stimulating them for magnetic resonance is suddenly switched off. The atoms are left partly in state A, partly in state B. For the former state the time-dependent part of the wavefunction is  $\exp(-iE_A/\hbar)t$ , for the latter,  $\exp(-iE_B/\hbar)t$ . But the wavefunction for each atom in the assembly is the sum of the two wavefunctions, each with its appropriate time-factor. Now, in whatever way the atoms are monitored, the calculated signal will contain this two-part wavefunction multiplied by its complex conjugate, and we shall find in the answer a sum of direct terms, with time-factors  $|\exp(-iE_A/\hbar)t|^2$ ,  $|\exp(-iE_B/\hbar)t|^2$ , and cross-terms, with time-factors  $\exp[\pm i(E_A - E_B)/\hbar)t]$ . These latter, representing the correlation, will lead to the real functions  $\cos \Delta t$ ,  $\sin \Delta t$ , where  $\Delta = (E_A - E_B)/\hbar$ . That tells us that all the atoms in the assembly are precessing with the same phase, so that macroscopic modulation effects are exhibited by the assembly. Such effects are well known in nuclear magnetic resonance, for example: they represent a macroscopic, precessing magnetic moment which gives rise to an oscillating voltage in a coil, the observed signal. In optical pumping the monitoring operation is the absorption of light and the observed signal is generally a modulated photoelectric current.

The *free* precession we have taken for our example is invariably damped, so the time-dependence we have calculated will contain an additional factor, almost always of the form  $\exp(-\Gamma t)$ . But we find modulation also under steady-state *forced* precession, where there is no damping, but the field (frequency  $\omega/2\pi$ ) forces its time-dependence on to the atoms. The coherence then reveals itself as modulation at the same frequency, and sometimes at harmonic frequencies, depending on the particulars of the experiment. The modulated absorption of light which forms the basis of the self-acting magnetometer and frequency standard we described in Section 8 is an example of this forced coherence. It is generally referred to as 'Hertzian coherence'.

The first observation of modulated absorption in an optical pumping experiment was made by Bell and Bloom in 1957, following a suggestion by Dehmelt. Those experiments were interpreted using the model that the atoms undergoing magnetic



resonance constituted precessing magnets, and presented periodically-varying cross sections for absorption to a transverse beam of light. But the notion of coherence crystallized formally from very different experiments carried out in Paris and followed up, in a different direction, in Oxford. These we shall now describe

#### 14. Coherent scattering

We referred in Section 3 to the pioneer experiment of Brossel and Bitter on magnetic resonance in an excited state of mercury. The resonance was detected by measuring changes in the intensity of the *fluorescent* light as a magnetic field was varied through resonance.

Pursuing this experiment in Paris, Barrat investigated the shape and width of the resonance curves as the vapour pressure of the mercury was varied. Contrary to all expectations it was found that the width of the curves *decreased* as the pressure was increased. Of course, the usual consequence of increasing vapour pressure is to *increase* the width of resonance curves. For to increase the pressure is to increase the frequency of collisions and to decrease the time of phase-continuous interaction with radiation—hence, to increase the spectral width. The narrowed curves were interpreted as a consequence of the multiple scattering of the fluorescent radiation in the vapour; that is to say, if the density of atoms or the size of the containing vessel is sufficient, it is possible for radiation emitted by one atom to be absorbed by another, rather than to escape directly. It was supposed that the emitting atoms were in *coherent superpositions* of Zeeman states, and that the coherence was conveyed from atom to atom via fluorescent light. Thus, the correlation between states (which ultimately determines the resonance linewidth) survived longer than individual atoms, and the resonance curves were correspondingly reduced in width. This phenomenon was called ‘coherent scattering’.

Reflecting on these experiments while in Oxford, I concluded that, if coherence could be conveyed from atom to atom via the light, it should be present also in the light itself. If the decay of an atom results in the emission of a photon, then this photon must be characterized, not by one frequency, but by a coherent superposition of frequencies. For each atom in the assembly the phase relations in the time-dependent part of the wavefunction are the same, hence the phase relations between the different frequencies in the emitted photons must be the same, and the light from the assembly should behave like a coherent mixture of waves of different frequencies: the intensity should exhibit beats. (The term ‘quantum beat’ is now commonly used to describe this phenomenon.) Dodd, Fox and Taylor looked for these beats and found them easily. At resonance they are very strong. Detailed study of their resonance line shape proved to be very rewarding in that entirely new kinds of resonance curves were found (fig. 12). It turned out that these new line shapes were characteristic for resonances of *alignment* (for which a precessing ellipsoid is a representative model), in contrast to *orientation* (for which a precessing arrow is a representative model). The alignment, in these experiments, was imposed on the system by the linear polarizers used to excite the atoms. Circular polarizers impose orientation.

The modulation observed in the work at Oxford represents coherence in the light emitted in the *spontaneous* decay of atoms from a coherent superposition of energy eigenstates. The modulation observed by Bell and Bloom represents coherence in the light absorbed in the *stimulated* excitation of atoms from a coherent superposition of energy eigenstates. In a great variety of experiments carried out subsequently it was



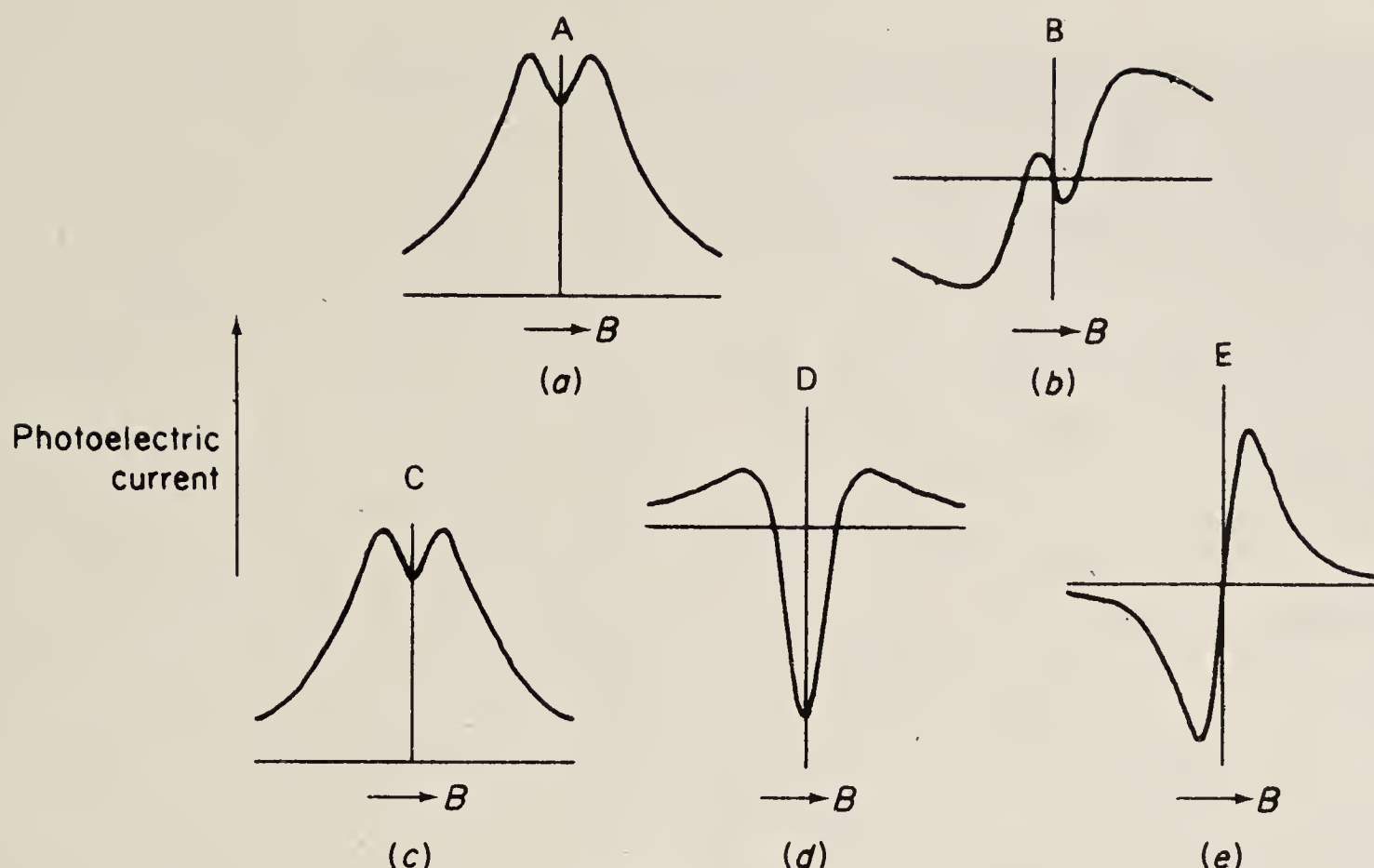


Fig. 12. Resonance line-shapes for alignment. Photoelectric current is plotted against magnetic field, in the vicinity of resonance. (a) (investigated by Brossel and Bitter) shows the variation of mean intensity of fluorescent light (cf. fig. 3). The remaining four curves show the variation of the strength of the light-beats. (b) and (c) are the amplitudes of sine and cosine components of modulation at the frequency of the r.f. field,  $\omega_0$ . (d) and (e) are the corresponding quantities at frequency  $2\omega_0$  (cf. fig. 15).

shown that this coherence is no fragile thing. It can be conveyed from one set of states  $(J, m_J)$  to another  $(J', m'_J)$  by violent pulse processes, like spontaneous decay, and even from one atom to another by collisions. Thus, spin-exchange and metastability exchange collisions can serve to transmit modulation, no less than magnetization.

### 15. The optical pumping cycle: light shifts

The climax of this phase of activity in optical pumping came with the publication, by Barrat and Cohen-Tannoudji (1961) of a differential equation governing the time-evolution of all the elements of the atomic density matrix in an optical pumping experiment. By integration of such an equation one obtains these matrix elements themselves, which form the basis for predicting the results of any experiment. (For any 'observable' one forms the appropriate 'monitoring operator' and applies it to the atomic density matrix.)

A most unexpected prediction of the theory was that the effect of a beam of light on an atomic vapour was not only to induce absorption, but also to bring about a shift of the atomic energy levels. Thus, if the interval between ground-state Zeeman levels was being explored by observation of a magnetic resonance, the position of the peak might be shifted by changes in the intensity of the beam of light used for pumping. To bring about such shifts the spectral distribution of the light has to be slightly off-resonance, so the phenomenon was conveniently studied by taking advantage of spectral isotope shifts: the light from one isotope was used to irradiate atoms of the other. In this way the predictions of the theory were brilliantly confirmed by Barrat and Cohen-Tannoudji. Of course, it is very important to

understand and to be able to control these shifts in, for example, optical-pumping magnetometers (section 8).

It was recognized that these so-called 'lamp shifts' were part and parcel of the same interactions which give rise to spectroscopic 'Lamb shifts'. The latter are generated by the fluctuating zero-point electromagnetic fields which are with us even in darkness; the former are under our control by the operation of switching a lamp.

A very simple interpretation of light shifts was subsequently given by Pancharatnam. An incident light field,  $E_\omega \exp(-i\omega t)$ , polarizes an atom. The polarizability is  $\alpha(\omega) = (e^2 f / 2m\omega_0) / (\omega_0 - \omega - \frac{1}{2}i\Gamma)$ ; ( $f$ : oscillator strength;  $\omega_0$ : atomic resonance frequency;  $\Gamma$ : upper-state damping constant). The energy of interaction,  $\Delta W$ , is equal to  $\int \alpha(\omega) |E_\omega|^2 d\omega$ , which is complex. This was interpreted by Pancharatnam as an addition to the energy  $E_A$  of the unperturbed atom in state A. Thus, the real part of  $\Delta W$  is the light shift. One may think of it as an a.c. Stark effect. Whether or not it vanishes depends on the relative position of the two factors in the integral, as illustrated in fig. 13. The imaginary part of  $\Delta W$  does not vanish. It represents a damping of the lower state arising from absorption of light. The absorption rate, per atom, is  $(-2/\hbar) \text{Im}(\Delta W)$ . Pancharatnam's analysis really brings out the point that the interaction energy should not be considered to be an attribute of the *atom*, but of the combined system, *atom plus light*. This view gained wide currency in the context of the experiments to be described in the next section.

## 16. Dressed atoms

One of the attractions of optical pumping experiments was that they provided a means for the study of interactions of atoms with *broad-band* light fields, on the one hand, and with *monochromatic* fields, on the other. The light shifts of the last section showed up with the broad-band fields characteristic of radiation from laboratory lamps. (The phenomenon was fully investigated in the pre-laser era.) More dramatic were the effects studied with strong monochromatic fields. It was discovered by Cohen-Tannoudji and Haroche that the properties of atoms in ground states can be profoundly altered by subjecting them to strong, off-resonance, radio-frequency

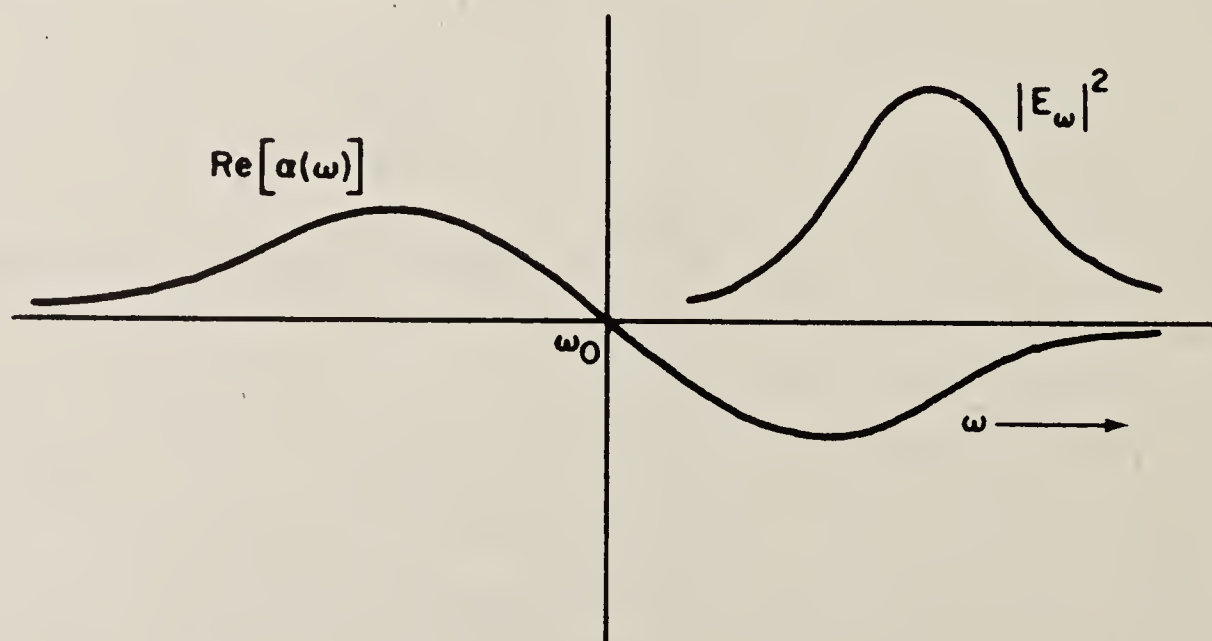


Fig. 13. The real part of the polarizability,  $\text{Re}[\alpha(\omega)]$ , plotted against  $\omega$ , is anti-symmetrical about the resonance frequency,  $\omega_0$ . The spectrum of the irradiating light,  $|E_\omega|^2$ , is plotted in the same figure, and is here shown as centred on a frequency different from  $\omega_0$ . In this case the light shift—given by the integral of the product of these two curves—does not vanish. But if  $|E_\omega|^2$  were centred on  $\omega_0$  the integral would vanish.



fields. Such atoms were called 'dressed atoms'. The term emphasizes the point that the systems under study are (atoms + field), not, simply, atoms. Their properties were investigated experimentally by variants of the methods we have discussed in preceding sections: the fields applied in these methods are to be regarded as probing fields: the dressing field is additional.

The problem of dressed atoms is to investigate the properties of atoms under irradiation by a strong, oscillating field  $B(t) = B_1 \cos \omega t$ . Cohen-Tannoudji and Haroche gave a fully quantum-mechanical analysis, but the same results are obtained by adopting the view that  $B_1 \cos \omega t$  is a classical field. The magnetic properties associated with the angular momentum imply a precession of the atoms about  $B(t)$ . Since this is varying with time, so also is the frequency of precession, that is to say, the atoms are undergoing frequency-modulated precession. A Fourier analysis of this motion reveals a time-independent component of amplitude  $J_0(\omega_1/\omega)$ , where  $J_0$  is a Bessel function of zero order, and the argument,  $\omega_1/\omega$ , is the ratio of the precessional frequency in the field  $B_1$  to the oscillatory frequency. If we make a steady-state measurement of the magnetic properties of such 'dressed atoms', we expect to find that these are multiplied by the factor  $J_0(\omega_1/\omega)$ . And so it turns out. Figure 14 illustrates the results of experiments carried out by Cohen-Tannoudji and Haroche on rubidium atoms in their ground state. The curve shows the observed and predicted values of the Landé  $g$ -factor. Notice that it proved possible, by sufficiently strong irradiation, to change the sign of the magnetic moment of these atoms—corresponding to negative values of the function  $J_0$ .

Observation of time-independent effects does not exhaust the subject. Chapman and I, by a study of modulated fluorescent light, showed how the free-atom properties are modified by Bessel functions  $J_r(\omega_1/\omega)$  when the  $r$ th harmonic of  $\omega$  is detected.

Particularly noteworthy in this work is that the analytical problem of the dressed atom can be solved in the semi-classical theory (atoms quantized, fields classical) without approximation. The calculation of light shifts, as outlined in the last section,

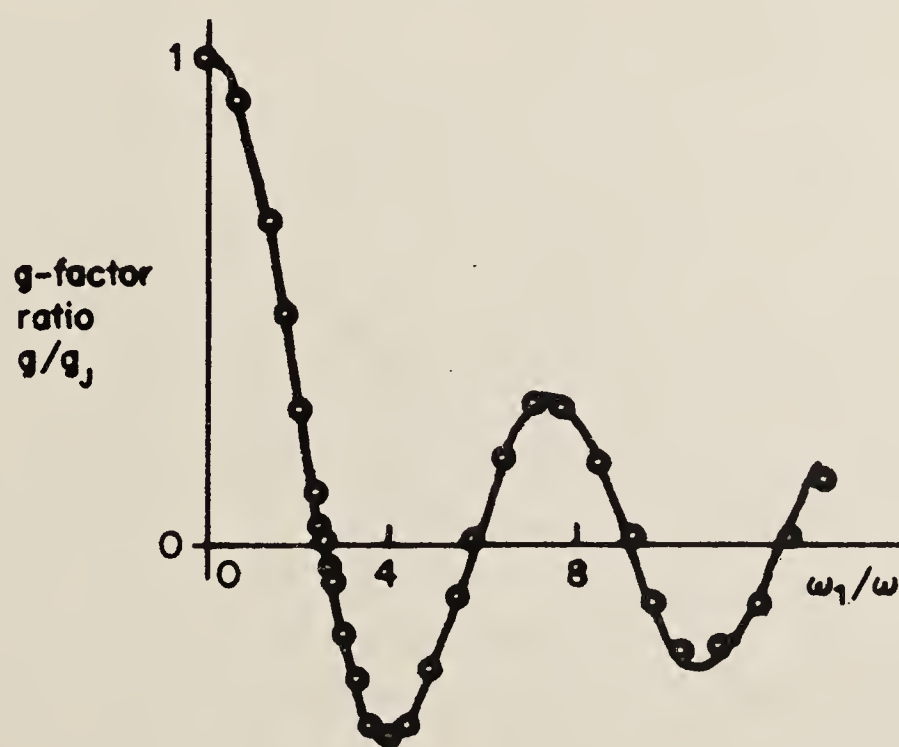


Fig. 14. Landé  $g$ -factors of dressed atoms. The curve is a plot of  $J_0(\omega_1/\omega)$ , where  $\omega_1$  is proportional to the amplitude of the dressing field and  $\omega$  is its frequency.  $g_j$  is the value of the  $g$ -factor for the free atom. The points represent experimental values. (Cohen-Tannoudji and Haroche 1966.)



represents an approximation to first order in the intensity of the field. Higher orders correspond to successive terms in the expansion of the Bessel function  $J_0$ .

### 17. Optical properties of the vapour

In the early work on optical pumping, attention was concentrated on the changes in the atoms by the action of the light, but it gradually came to be realized that it was profitable to change the emphasis: to ask how the light was modified by the presence of the vapour.

An assembly of atoms which have undergone optical pumping constitutes an *anisotropic medium* for the propagation of light. Moreover, if the atoms are subject to oscillatory fields, as in a magnetic resonance experiment, the anisotropy is *time-dependent*. The optical properties of the vapour can be described in terms of a *polarization tensor*, whose elements are time-dependent. The propagation of light through the medium can then be analysed by the methods of classical theory, applying Maxwell's equations to the medium, just as one had applied Schrödinger's equation to the atoms. In Paris, Laloe, Leduc and Minguzzi in particular have developed this point of view: in the U.S.A., Happer. Especially valuable contributions were made by Pancharatnam, who brought to optical pumping a profound knowledge of the interaction of light with anisotropic media which he had gained by the study of crystal optics in the Raman Research Institute in Bangalore. In this field also Italian physicists, notably Gozzini and his colleagues in Pisa, have been active. Gozzini very early pointed to the possibilities of using the Faraday rotation produced by a polarized medium as a sensitive probe for an optically pumped medium.

Faraday rotation is a manifestation of *dispersion* rather than *absorption*. There is a particular advantage in using phenomena based on *dispersion* to probe a vapour. While both absorption and dispersion undergo strong variations in the region of resonance, absorption (related to intensity) falls off as  $1/x^2$ , where  $x$  is the frequency offset from resonance, whereas dispersion (related to field) falls off only as  $1/x$ . Therefore dispersion effects are still considerable when the frequency of the *probe* light is sufficiently far off resonance for absorptive effects—changes of population—to be negligible. By way of example, fig. 15 shows some results obtained by Pancharatnam in the last experiment he carried out before his death in 1969. The resonance curves correspond to *modulated birefringence* in an optically pumped vapour of  $^4\text{He}$ , monitored by light from a  $^3\text{He}$  lamp—off-resonance by virtue of the spectroscopic isotope shift. In this experiment the optical pumping was carried out by linearly polarized light from a  $^4\text{He}$  lamp, so that the sample was *aligned*, having the properties of a uniaxial crystal transparent to light from the  $^3\text{He}$  lamp. The oscillatory field applied for magnetic resonance caused precession of the axis of alignment and modulation of the transmitted light. The resonance curves, representing the amplitude of modulation, were obtained by slowly changing a 'static' magnetic field.

In fig. 16 are shown the relative positions of the  $^4\text{He}$  and  $^3\text{He}$  lines used in this work. Though each line has a structure, the strong component of  $^3\text{He}$  is well separated from the components of  $^4\text{He}$ .

### 18. Optical pumping and laser spectroscopy: concluding remarks

Readers who have been close to the evolution of optical pumping will be aware of the superficialities of this account and of the many omissions. Younger readers, who



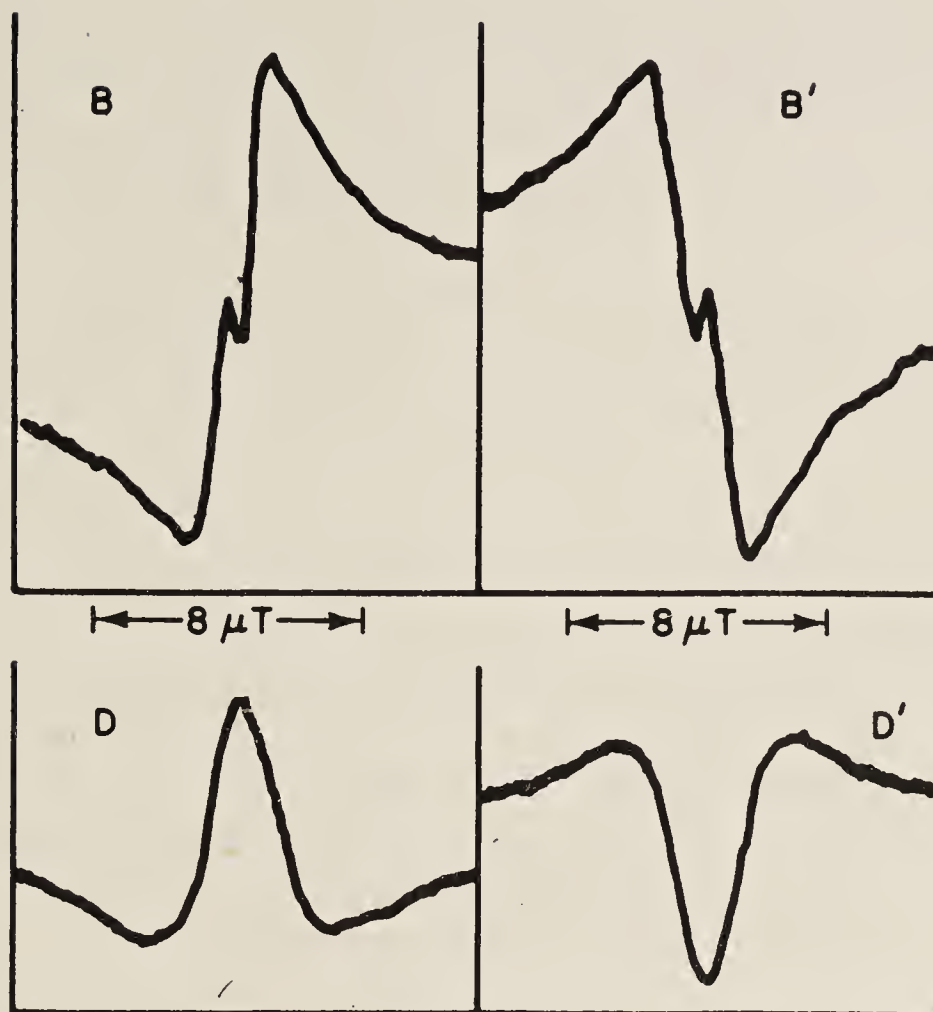


Fig. 15. Resonance curves in the excited state  $2^3S_1$  of  $^4\text{He}$ , obtained by measurements based on modulated birefringence. (Notice that the shapes of these curves are those of (b) and (d) in fig. 12.) (Pancharatnam 1968.)

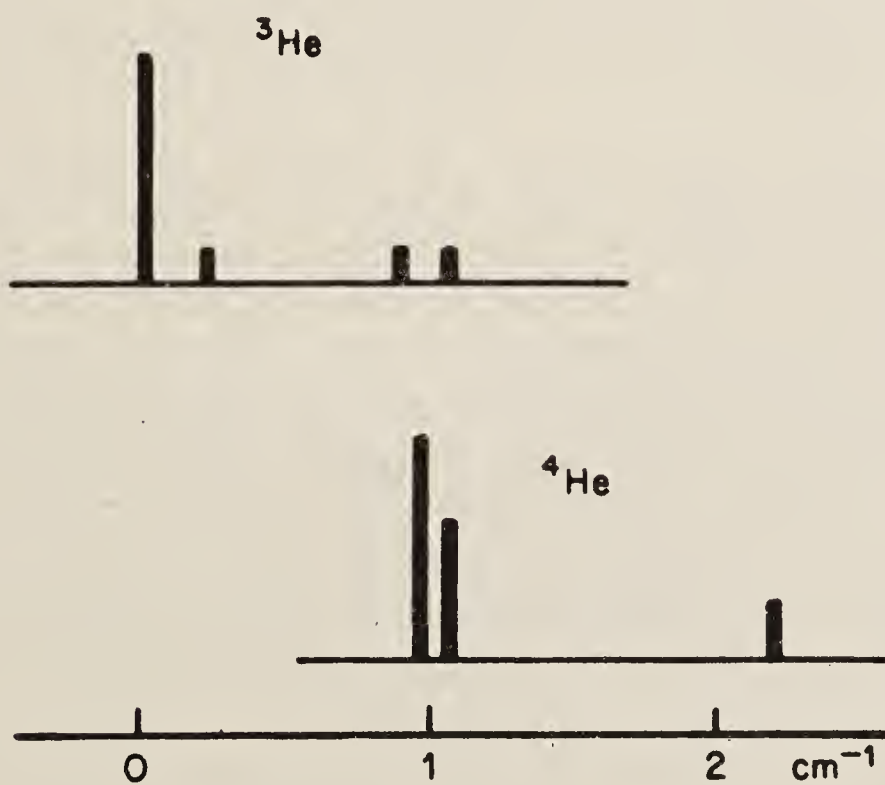


Fig. 16. Spectral components of  $1.08\mu\text{m}$  lines of  $^4\text{He}$  and  $^3\text{He}$ . The energy differences between the structures here expressed in  $\text{cm}^{-1}$  are attributable to the nuclear spin of  $^3\text{He}$  and to the difference in nuclear masses. The feature on which Pancharatnam's experiment was based is that the strong component of the  $^3\text{He}$  line is well separated from the components of the  $^4\text{He}$  line.

have grown up in the age of lasers, will recognize that many of the topics mentioned here are commonplace in laser spectroscopy. For them it may be worth while to underline some of the discoveries that optical pumpers made and made available for exploitation with the more powerful and sharper spectroscopic tools of the present age.

First, there was the recognition that, though the interaction between light and atoms is weak, nevertheless a light-beam that is *polarized*, or *directional*, or *limited in spectral range*—that is, different in some significant way from isotropic black-body radiation—can profoundly change the distribution of atoms over energy eigenstates.

Secondly, there was the discovery that this changed distribution could be transmitted to other species—atoms, ions, electrons—by spin-exchange and by other types of collision.

Thirdly, it was brought into the consciousness of atomic physicists that many atomic properties that could be measured were a consequence of atoms being brought into *coherent superpositions* of stationary states, and that analyses in terms of *occupation* of stationary states were inadequate. These coherences, though induced by phase-continuous interactions, could be transferred by collisions, radiative decay, or other pulse-like, random processes.

Fourthly, there was a very thorough study of the interaction of atoms with electromagnetic fields, strong and weak, broad-band and monochromatic. In this connection the relationship between fully quantum analysis and semi-classical analysis was intimately explored.

Fifthly, there was the recognition of the reciprocal interplay between the quantum-mechanical evolution of the assembly of atoms and the Maxwellian evolution of light-waves propagating through the assembly.

What, then, are the new features of atomic resonance spectroscopy with lasers as against atomic resonance spectroscopy with radio-frequency fields? There are, surely, three very significant new features, all deriving from the very large factor,  $10^6$  or  $10^7$ , between the frequencies of r.f. fields used in optical pumping and those of laser fields at optical frequencies.

- (i) For interactions at optical frequencies one *must* take account of spontaneous emission: the probability for this process is proportional to the cube of the frequency. For r.f. fields one could justifiably ignore spontaneous emission. That made possible the successes of the semi-classical analysis. Spontaneous emission is a process which physicists know how to deal with mathematically. That is not to say that they understand the mechanism.
- (ii) At optical frequencies, atoms present a very complicated structure of energy levels. At radio frequencies one could choose extremely simple, equally spaced Zeeman levels as the structure under investigation. Even hyperfine structures, though more complicated than Zeeman structures, are much simpler than the whole energy level structures of atoms. But there is to be seen, in current activity in laser spectroscopy, special attention being given to Rydberg states of atoms (Latimer 1979). The energy structure of these, again, is notable for its regularities.
- (iii) At optical frequencies the wavelength of the radiation is small compared with the size of the sample, so propagation effects assume a special importance—witness the current activity in the phenomenon of ‘superradiance’ (MacGillivray and Feld 1981). By way of contrast, it was nearly



always true of the radio frequencies used in optical pumping that the wavelength was large compared with the sample, so that the phase of the field was the same for all atoms in the assembly.

There are also, of course, significant advances which have been made in what may be called 'conventional optical pumping' through the use of lasers. These stem, not so much from the narrow-band aspect of laser light—although selectivity in spectral range is extremely valuable—as from its spectral brightness and directionality. To have a bright, tunable source of light has enormously extended the range of states accessible for study; notably, excited states. But narrow-band lasers have widened the scope for study of ground states also: stimulated emission brings a new mechanism into the optical pumping cycle, and phenomena have been reported in relation to ground states which are not yet understood. For laser spectroscopy in which optical pumping plays a significant role, precise measurement of the optical frequency is generally not important. The useful information is in the *intensity* of the observed signal, and in its variation with time, or magnetic field, or some other parameter. Kastler's original thought is still to the fore: light is a handle which the spectroscopist may use to grasp atoms and hold them up for inspection. Laser physics has much to contribute to optical pumping, and much to learn from it.

### Acknowledgements

Thanks are due to the Publishers of the Journals cited for permission to reproduce figs. 8, 10, 14 and 15.

### References

- ARDITI, M., and CARVER, T. R., 1961, *Phys. Rev.*, **124**, 800.  
 BARRAT, J.-P., and COHEN-TANNOUDJI, C., 1961, *J. Phys. et le Rad.*, **22**, 329, 433.  
 BROSSEL, J., and BITTER, F., 1952, *Phys. Rev.*, **86**, 308.  
 COHEN-TANNOUDJI, C., and HAROCHE, S., 1966, *Compt. Rend.*, **262**, 268.  
 COHEN-TANNOUDJI, C., and HAROCHE, S., 1969, *Phys. Rev. Lett.*, **22**, 759.  
 KASTLER, A., 1967, *Physics Today*, **20**, 34 (Nobel Prize Lecture).  
 LATIMER, C. J., 1979, *Contemp. Phys.*, **20**, 631.  
 MACGILLIVRAY, J. C., and FELD, M. S., 1981, *Contemp. Phys.*, **22**, 299.  
 PANCHARATNAM, S., 1968, *Phys. Lett. A*, **27**, 509.

### General references

- BERNHEIM, R. A., 1965, *Optical Pumping: an Introduction* (Benjamin).  
 BROSSEL, J., 1965, *Quantum Optics and Electronics*. Proceedings of the Les Houches Summer School 1964. Edited by C. De Witt, A. Blandin and C. Cohen-Tannoudji (Gordon & Breach), pp. 187–327.  
 COHEN-TANNOUDJI, C., and KASTLER, A., 1966, *Progress in Optics* (North Holland), pp. 1–81.  
 SERIES, G. W., 1970, *Quantum Optics*: Proceedings of the Scottish Universities Summer School, 1969. Edited by S. M. Kay and A. Maitland (Academic Press), pp. 395–482.





## Light Beats as Indicators of Structure in Atomic Energy Levels

Light emitted in the decay of atoms from different energy levels is incoherent. Suppose, however, that the atoms are subject to an oscillatory field capable of inducing transitions between a pair of excited energy eigenstates. The state of atoms initially excited to one or other of these eigenstates will become a coherent mixture of both. One might expect that this coherence would be reflected in coherence between radiations of different frequencies emitted when the excited atoms decay spontaneously. This would manifest itself as a modulation of the optical radiation (i.e. light beats) at the frequency of the oscillatory field.

We have observed this modulation in the resonance radiation 2537 Å emitted in the decay of level  $6^3P_1$  in mercury. In a magnetic field  $H$  the three eigenstates  $|m_J\rangle = |1\rangle, |0\rangle, |-1\rangle$  are separated in energy by two equal intervals,  $g_J\beta H = \hbar\omega$ . We refer to the even isotopes only, although natural mercury was used in the experiments. Under the simultaneous influence of  $H$  and a magnetic field  $H_1$  oscillating in a plane perpendicular to  $H$  at a radio frequency  $\omega_0$  near  $\omega$ , modulation frequencies  $\omega_0$  and  $2\omega_0$  are to be expected if the direction of observation is suitably chosen.

The apparatus is similar to that used by Brossel and Bitter (1952) for observing 'double resonance' in the level  $6^3P_1$ , except that the photoelectric current which records the intensity of the fluorescent radiation is applied to a narrow-band amplifier tuned to one of the harmonics of the oscillator frequency. Audio-frequency modulation of the magnetic field, and phase-sensitive detection are employed. Oscillators at a fixed frequency about 14 Mc/s are used, and the magnetic field varied through the various resonances.

The components of the photoelectric current which are detected are those which arise from the light beats and those which form part of the noise spectrum. The former are proportional to the depth of modulation of the fluorescent radiation: the latter depend on its intensity, which varies with magnetic field to produce the double resonance intensity signal as observed by Brossel and Bitter. The two effects are distinguishable in the following ways: (i) the shapes of the resonance curves are different, (ii) the intensities of the two types of signal depend in different ways on the polarization of the exciting radiation and the direction of observation. When the two signals occur together, the modulation signal alone is obtained by normalization and subtraction.

Resonance curves are obtained which are symmetrical (or anti-symmetrical) about  $H = H_0 = \hbar\omega_0/g_J\beta$ , and about  $H = H_0/2$ , where  $\omega_0$  is the frequency of the oscillatory field. The observations, which to date are exploratory only, are summarized in the following table.

If the light beats are a consequence of coherence between the original eigenstates, one might expect the amplitude of the beats to be related to the cross products  $(a_1^*a_0 + a_1a_0^*)$ , etc., where the coefficients  $a$  are defined in the expansion of the excited state,  $|j\rangle = a_1(t)|1\rangle + a_0(t)|0\rangle + a_{-1}(t)|-1\rangle$ . These cross products have been evaluated, assuming that the states are subject to no perturbation other than the radio-frequency interaction, for initial conditions appropriate



(1)	(2)	(3)	(4)	(5)
Perpendicular to $H$	$\left\{ \begin{array}{l} \omega_0 \\ \omega_0 \\ 2\omega_0 \end{array} \right.$	$\begin{array}{l} H_0/2 \\ \dagger \text{No resonance detected at } H_0 \\ H_0 \end{array}$	$\begin{array}{l} L \\ \\ L \end{array}$	See footnote ‡ $ 1\rangle$ and $ -1\rangle$
Approximately $\tan^{-1}\sqrt{2}$ to $H$	$\left\{ \begin{array}{l} \omega_0 \\ \omega_0 \\ 2\omega_0 \end{array} \right.$	$\begin{array}{l} H_0/2 \\ H_0 \\ H_0 \end{array}$	$\begin{array}{l} L \\ D \\ L \end{array}$	See footnote ‡ $ 1\rangle$ and $ 0\rangle$ ; $ 0\rangle$ and $ -1\rangle$ $ 1\rangle$ and $ -1\rangle$
Parallel to $H$	$\left\{ \begin{array}{l} \omega_0 \\ 2\omega_0 \end{array} \right.$	$\begin{array}{l} \dagger \text{No beats detected} \\ \dagger \text{No beats detected} \end{array}$		

(1) Direction of observation; (2) detector tuning; (3) value of field at resonance; (4) line shape, the phase-sensitive method of detection displayed the derivative of L (Lorentz-type) and of D (dispersion-type) curves; (5) interpretation: coherent decay from the states.

to the method of excitation of the atoms. The cross products contain terms which oscillate at frequencies  $\omega_0$ ,  $2\omega_0$ , whose amplitudes, as functions of magnetic field, are broadly in agreement with the observations. In particular, the dispersion-type curve recorded in line 5 of the table is predicted. The absence of signal in those cases marked † is to be expected as a consequence of the orthogonality of the polarization vectors.

Unexpected resonances occur at fields  $H_0/2$  both in the unmodulated component of the fluorescent light, and in the component modulated at frequency  $\omega_0$  (see footnote ‡).

We wish to distinguish the light beats observed here from those observed by Forrester, Gudmundsen and Johnson (1955). In that experiment, each atom was radiating a sharp frequency (to the extent that we can assume incoherent excitation in the light source, and also, very long lifetimes), and the beat frequency between pairs of atoms could range over the combined Doppler widths of two spectral lines. In our experiments, sharp beat frequencies are present in the radiation from each atom, and these appear in the ensemble with a much more favourable ratio of signal to noise.

Modulation of light has also been observed by Bell and Bloom (1957). The phenomenon depended on radio-frequency mixing in the ground states. The modulation was observed in absorption.

The coherence exhibited in our experiments is that which is exhibited in an entirely different way in the experiments of Guiochon, Blamont and Brossel (1957) and of Barrat and Brossel (1958) on the multiple diffusion of resonance radiation.

Clarendon Laboratory,  
Oxford.  
8th June 1959.

J. N. DODD§.  
W. N. FOX.  
G. W. SERIES.  
M. J. TAYLOR.

‡ *Note added in proof.*—Since the manuscript was submitted it has been confirmed that the resonances at  $H_0/2$  occur only when the atoms are excited by a coherent mixture of  $\sigma$  and  $\pi$  radiation, produced by setting a polarizer at  $45^\circ$  to the magnetic field. The occurrence of these resonances, together with that of the others, can now be understood in terms of a theory of the light beats which is being prepared for publication.

§ On leave of absence from the University of Otago, New Zealand.



BARRAT, J. P., and BROSSEL, J., 1958, *C.R. Acad. Sci., Paris*, **246**, 2744.

BELL, W. E., and BLOOM, A. L., 1957, *Phys. Rev.*, **107**, 1559.

BROSSEL, J., and BITTER, F., 1952, *Phys. Rev.*, **86**, 308.

FORRESTER, A. J., GUDMUNDSEN, R. A., and JOHNSON, P. O., 1955, *Phys. Rev.*, **99**, 1691.

GUIOCHON, M. A., BLAMONT, J. E., and BROSSEL, J., 1957, *J. Phys. Radium*, **18**, 99.





## Line Shapes in the Method of Intersecting Energy Levels

By B. P. KIBBLE AND G. W. SERIES

Clarendon Laboratory, Oxford

*MS. received 22nd February 1961*

**Abstract.** The first part of this work is a study of the changes of intensity of the resonance fluorescence from mercury vapour as a small magnetic field  $H$  is applied either parallel or anti-parallel to the direction of the incident light. The changes follow either a Lorentzian or a dispersion-type function of the Zeeman splitting of the excited state, according to the orientations of polarizer and analyser in the beams of light.

In an experiment with an additional oscillatory field at a frequency  $\omega_0$ , similar curves are observed in the region  $H = H_0/2$ . ( $H_0$  is the field for which  $\omega_0$  is the Larmor frequency.)

The observations are relevant to a recently developed technique in which intensity changes of this sort are used to make precision measurements in spectroscopy. The Lorentzian line shape is usually observed. The possibility of obtaining line profiles of other shapes was pointed out by Franken.

---

### § 1. INTRODUCTION

WE wish to report some observations concerning the shape of the resonance curves which are found in the spectroscopic technique known as 'level-crossing', or, alternatively, as "the method of intersecting energy levels" (Colegrove, Franken, Lewis and Sands 1959, Hirsch 1960, Hirsch and Stager 1960, Thaddeus and Novick 1960, Dodd 1961). The method has been applied by the above authors to the precise determination of  $g$ -values and hyperfine structure intervals and can be used also for the measurement of lifetimes of excited states, so that a study of the resonance line-shape is of practical, as well as of academic interest. The basis of the method is the change in intensity of the resonance radiation, observed either in transmission or in fluorescence, in circumstances in which a pair of excited levels intersect. Thus, suppose that the energies of the states  $|b\rangle$  and  $|c\rangle$  are functions of an applied magnetic field  $H$  (Fig. 1). At either side of the intersection the intensity  $I$  of the resonant fluorescent light is the sum of the intensities  $I_{ab}$  and  $I_{ac}$ . In the region of the intersection there is an additional contribution to  $I$  which arises from interference between the time-dependent wave-functions of the degenerate states.

A particular case of intersecting levels is realized in the coalescence at  $H = 0$  of a set of Zeeman levels. The polarization of the fluorescent light in a case of this sort (Hg,  $\lambda 2537 \text{ \AA}$ ,  $6^3P_1 - 6^1S_0$ ) was studied in detail by Hanle (1924, 1925). Since the Zeeman structure of the line  $2537 \text{ \AA}$  is normal, the changes of intensity, as well as the changes of polarization, are easily understood in terms of the classical theory of scattering. When there is no applied field, the spatial

distribution of the fluorescent light corresponds to radiation from a dipole which oscillates parallel to the electric vector of the incident light. In the presence of a strong magnetic field the radiation pattern is that of a precessing, oscillating dipole. In the transitional region between weak and strong fields the radiation pattern is governed by the angle through which the dipole precesses during the lifetime of the excited atoms.

Quantum-mechanical analysis of experiments of this type predicts that, for the geometrical arrangements which are normally used, and for single scattering processes, the intensity should be a Lorentzian function of the interval  $E_{bc}$  with half-intensity width  $2\Gamma$ , where the states  $|b\rangle$  and  $|c\rangle$  are taken to have the same decay constant  $\Gamma$ . This type of curve was observed in the work referred to above, and is seen in Figs 3(a) and (c). However, it was pointed out by Franken (1961), that, for certain geometrical arrangements the intensity should follow a dispersion type of curve.

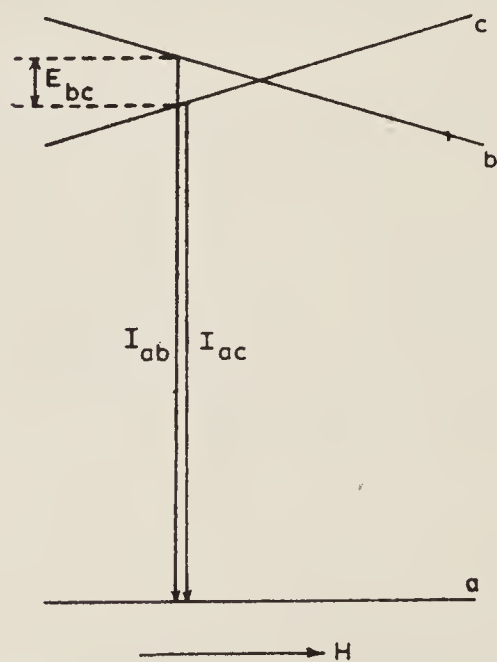


Fig. 1. Intersecting levels.

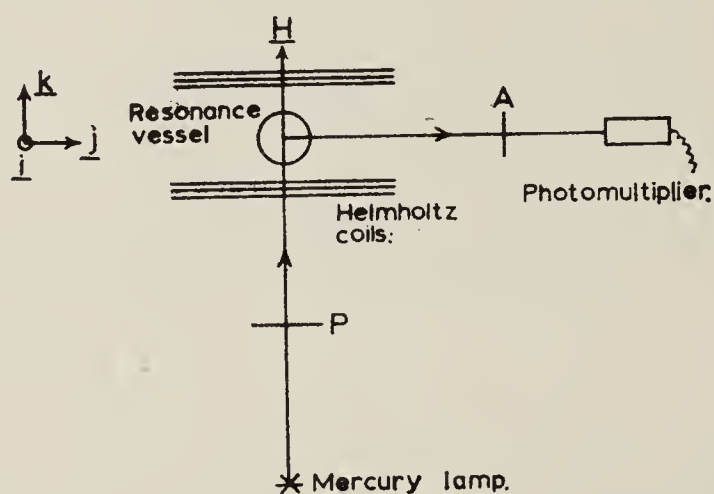


Fig. 2. Disposition of apparatus.

We report here that the dispersion type of line shape has now been observed in the region of  $H=0$  in the resonance fluorescence from mercury vapour.  $|b\rangle$  and  $|c\rangle$  in this case are the states  $|m = \pm 1\rangle$  which belong to  $^3P_1$  in the even isotopes. The dispersion shape has also been observed in non-zero fields in a more complicated radio-frequency experiment in which hitherto only the Lorentzian shape had been observed.

## § 2. THE BASIC EXPERIMENT

The disposition of apparatus is indicated in Fig. 2. The analyser A passes fluorescent light whose electric vector is in the direction  $\mathbf{i}$  (normal to the paper; right-handed axes are used). The magnetic field  $\mathbf{H}$ , applied by Helmholtz coils in the direction  $\pm \mathbf{k}$  alternates sinusoidally at 30 c/s a few gauss on either side of zero. The changes of light intensity, measured photoelectrically, are displayed as functions of the magnetic field on an oscilloscope. The four traces shown in Figs 3(a), (b), (c) and (d) correspond to orientations of the polarizer in the directions  $\mathbf{i}$ ,  $\mathbf{j} - \mathbf{i}$ ,  $\mathbf{j}$ ,  $\mathbf{j} + \mathbf{i}$ , respectively. No changes in the fluorescent light are observed when the analyser is in the direction  $\mathbf{k}$ . When the analyser is removed, traces are obtained similar to those in Figs 3(a), (b), (c) and (d).



The changes of intensity illustrated in Fig. 3 correspond to about 50% of the fluorescent light when the field is 'strong'. In the ideal case one would expect changes of 100% in 3 (a) and 3 (c); but in practice this figure is reduced by the effects of multiple scattering in the mercury vapour, by the presence of foreign gas, and of isotopes with nuclear spin, and by small departures from the ideal geometrical conditions.

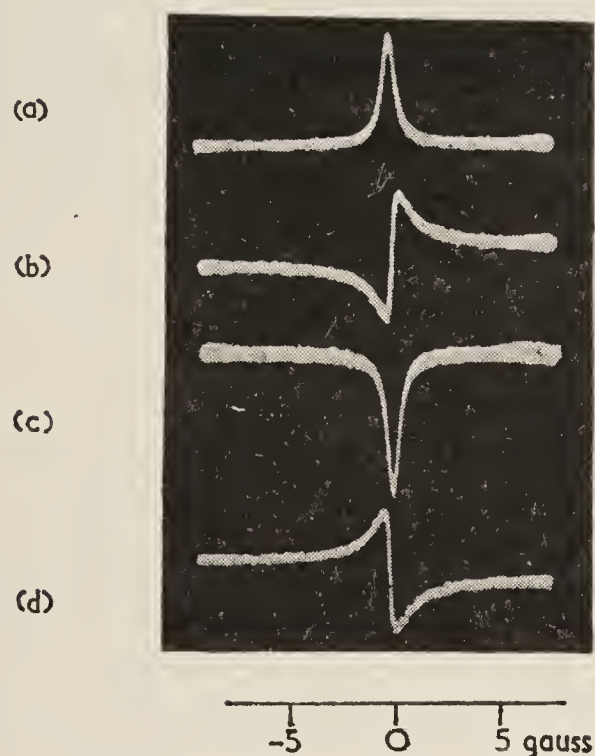


Fig. 3. Intensity of light as a function of magnetic field in the region  $H=0$ , for different directions of polarization of the exciting light.

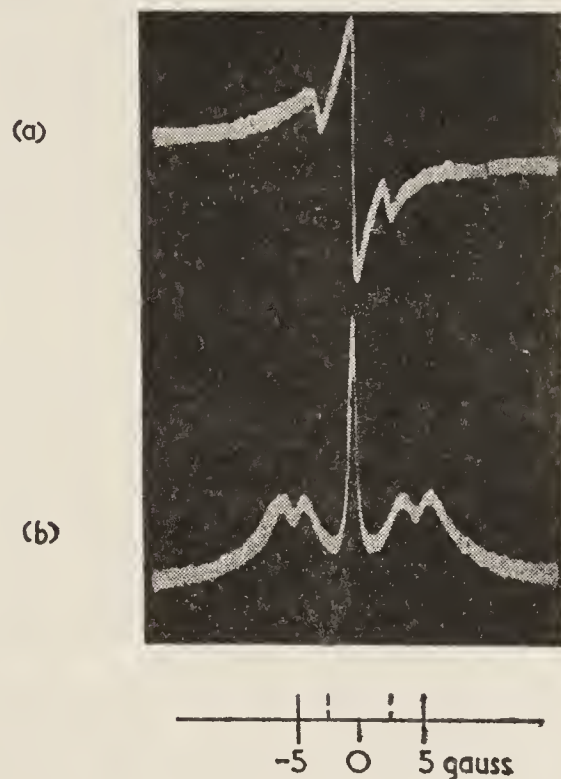


Fig. 4. Effect of an additional field at radio frequencies. (a) Resonances of the dispersion type in the region of  $\frac{1}{2}H_0$ . (b) Double-peaked resonances in the region of  $H_0$ .  $H_0 = \pm 5.0$  gauss.

The shapes of the resonance curves are qualitatively as one would anticipate, either by the classical theory or by the quantum-mechanical analysis. The widths at half-intensity in 3 (a) and 3 (c), and the distances between the maxima and minima in 3 (b) and 3 (d) are approximately in agreement with the known lifetime of the level  $^3P_1$  ( $1.18 \times 10^{-7}$  sec). No attempt was made to distinguish between the true lifetime and the coherence time (Barrat 1959), but simply to investigate whether dispersion-type curves did in fact appear under the postulated circumstances. The analytical condition for obtaining curves of the dispersion type is that the product  $f_{ba}g_{ab}f_{ac}g_{ca}$  be pure imaginary, where  $f$  and  $g$  are the matrix elements of the interaction energy for the processes of absorption and emission of light, respectively.

A certain difficulty in applying the theory arises when the intersection takes place at  $H=0$ , since, owing to the presence of stray fields, the actual field does not remain in the direction  $\pm \mathbf{k}$  when the applied field is small, so that it would appear that the states should be defined with respect to a rotated axis of quantization. However, the positive direction of the applied field may at all times be used as axis, notwithstanding the stray fields, provided that  $\gamma H_{\text{stray}} \ll \Gamma$  ( $\gamma$  is the gyromagnetic ratio). The essence of the proof lies in showing that the



expression  $(f_{ab}g_{ba} + f_{ac}g_{ca})$  is invariant to the axis of quantization, where the states are eigenstates of  $J_z$  with respect to the particular  $z$  axis chosen. If, in the group which comprises  $|b\rangle$  and  $|c\rangle$ , there are other eigenstates of  $J_z$ , then  $f_{am}g_{ma}$  must be summed over all the eigenstates  $|m\rangle$ . It is assumed that there are no eigenstates of  $J_z$  other than  $|a\rangle$  in the group to which  $|a\rangle$  belongs.

It is easy to appreciate classically that small, stray fields are immaterial, since a field which produces only a small angle of precession during the lifetime of the atoms has a correspondingly small effect on the fluorescent light. The direction of such a small field, is, therefore, of no significance.

The energy of the state  $|m_J\rangle$  in the field  $\mathbf{H}$  is  $g_J\beta m_J|H|$ . When the direction of the field is reversed, but the axis of quantization left unchanged, the states  $|m_J\rangle$  are still eigenstates of the Hamiltonian, but the energies are  $-g_J\beta m_J|H|$ . Hence levels of different  $m_J$  cross in zero field just as indicated in Fig. 1.

### § 3. THE RADIO-FREQUENCY EXPERIMENT

The radio-frequency experiment to which we referred above represents a more subtle case of intersecting levels. An oscillatory magnetic field at frequency  $\omega_0$  is applied to the scattering vapour in the plane normal to  $\mathbf{H}$ . Under these conditions the intensity of the fluorescent light changes in a resonant manner, not only in the region  $H = H_0 = \omega_0/\gamma$  (Brossel and Bitter 1952), but also, if the polarization of the exciting light is suitable, in the region  $H = \frac{1}{2}H_0$  (Dodd, Fox, Series and Taylor 1959, Dodd, Series and Taylor 1961, to be published). These latter changes may be associated with intersections between levels belonging to  $|m=0\rangle$  and  $|m=\pm 1\rangle$  in a diagram which represents the frequencies of the atomic wave functions under the time-dependent perturbation (Dodd and Series 1961). (In a normal term diagram, the levels intersect only at  $H=0$ .)

Lorentzian line shapes in the region  $H_0/2$  were observed in the work reported above. Line shapes of the dispersion type are again to be expected if the same product of matrix elements as before is pure imaginary. This condition is fulfilled for matrix elements which connect the ground state with the excited states  $|0\rangle$ ,  $|1\rangle$  and  $|0\rangle$ ,  $|-1\rangle$  when the apparatus is arranged as follows: the incident and scattered light beams in the directions  $\mathbf{k}$  and  $\mathbf{j}$ , as in Fig 2; the field  $\mathbf{H}$  in the direction  $(\mathbf{k} - \mathbf{j})$ , and the radio-frequency field in the direction  $\mathbf{i}$ ; the incident light plane polarized in the direction  $(\mathbf{i} - \sqrt{2}\mathbf{j})$  and the scattered light analysed in the direction  $(\mathbf{i} + \sqrt{2}\mathbf{k})$ .

Fig. 4 (a) shows an oscilloscope trace observed under these conditions. Lines of the expected shape are seen in the region of magnetic fields  $\pm 2.5$  gauss, together with a similar, more prominent line in the region of  $H=0$  as before. Fig. 4 (b), for comparison, shows the double-peaked resonances in the region  $H = H_0 = \pm 5.0$  gauss, as observed by Brossel and Bitter. The amplitude of  $\mathbf{H}$ , and of the oscillatory field at 10.5 Mc/s, were unchanged between Figs 4 (a) and 4 (b), but  $\mathbf{H}$  was applied to the direction  $\mathbf{j}$  in 4 (b), the polarizer was set parallel to  $\mathbf{i}$  and the analyser to  $\mathbf{k}$ . Under these conditions, resonances at  $H_0/2$  are not to be expected.

In the light of these observations, it is clear that care must be taken with the disposition and alignment of apparatus when the method of intersecting levels is applied to precision measurements.



## REFERENCES

- BARRAT, J. P., 1959, *J. Phys. Radium*, **20**, 541, 633, 657.  
BROSSEL, J., and BITTER, F., 1952, *Phys. Rev.*, **86**, 308.  
COLEGROVE, F. D., FRANKEN, P. A., LEWIS, R. R., and SANDS, R. H., 1959, *Phys. Rev. Letters*, **3**, 420.  
DODD, J. N., 1961, *Proc. Phys. Soc.*, **77**, 669.  
DODD, J. N., FOX, W. N., SERIES, G. W., and TAYLOR, M. J., 1959, *Proc. Phys. Soc.*, **74**, 789.  
DODD, J. N., and SERIES, G. W., 1961, *Proc. Roy. Soc.*, in the press.  
FRANKEN, P. A., 1961, *Phys. Rev.*, **121**, 508.  
HANLE, W., 1924, *Z. Phys.*, **30**, 93.  
——— 1925, *Ergebn. exakt. Naturw.*, **4**, 214.  
HIRSCH, H. R., 1960, *Bull. Amer. Phys. Soc.*, [II], **5**, 274.  
HIRSCH, H. R., and STAGER, C. V., 1960, *J. Opt. Soc. Amer.*, **50**, 1052.  
THADDEUS, P., and NOVICK, R., 1961, *Bull. Amer. Phys. Soc.*, [II], **6**, 74.





# Theory of modulation of light in a double resonance experiment

BY J. N. DODD†

*Department of Physics, University of Otago, Dunedin, New Zealand,*

AND G. W. SERIES

*Clarendon Laboratory, University of Oxford*

*(Communicated by H. G. Kuhn, F.R.S.—Received 3 December 1960—*

*Revised 8 May 1961)*

A theory is formulated to describe the modulation which has been observed in fluorescent light from atoms subjected simultaneously to optical and radio-frequency radiation. The optical field stimulates one or more of a set of excited states of the atom, between which the radio-frequency field establishes coherence. This coherence is manifest in the fluorescent radiation. Interference between radiations of different frequency leads to modulation. General expressions are given for the intensity of the fluorescent light as a function of time. The Zeeman structure of the transition ( $6^3P_1 - 6^1S_0$ ),  $\lambda 2537 \text{ \AA}$ , in mercury is studied in detail. Modulation at frequencies, 1, 2, 3 and 4 times that of the radio-frequency field,  $\omega_0$ , is predicted, and resonant effects at static magnetic fields, 0,  $\frac{1}{2}$ , 1,  $\frac{3}{2}$ , 2 and 3 times  $H_0$ , the field for which  $\omega_0$  is the Larmor frequency. Resonances at fields other than  $H_0$  are due to excitation with light of mixed polarization. Most of the predicted effects have been found experimentally.

A 'frequency diagram' is introduced and discussed, to represent the combined effects of static and radio-frequency magnetic fields. To each excited state belong a set of  $r$  frequencies, where  $r$  is the number of states linked by the radio-frequency perturbation. The 9 levels are drawn, as functions of  $H$ , for the states  $m_J = 0, \pm 1$ , of  $^3P_1$ . The resonances at fields other than  $H_0$  may be associated with intersections of frequency levels belonging to different  $m_J$ .

## 1. INTRODUCTION

It has been shown experimentally that the fluorescent light in a double resonance experiment is strongly modulated (Dodd, Fox, Series & Taylor 1959). A theory of the phenomenon is presented in this paper.

In a double resonance experiment, free atoms are subjected simultaneously to optical and radio-frequency radiations, both of which are near to resonant frequencies of the atoms. The first experiment of this type (Brossel & Bitter 1952) was performed with mercury vapour situated in a uniform magnetic field. Optical radiation at  $2537 \text{ \AA}$  excited the atoms from the ground state,  $^1S_0$ , to the state  $m = 0$  of the level  $^3P_1$ , from which transitions to  $m = \pm 1$  were induced by a radio-frequency field at the Larmor frequency. The transitions were detected by the changes which they brought about in the polarization and spatial distribution of the fluorescent light.

A complete description of the response of the atoms to the electromagnetic fields cannot, however, be given simply in terms of populations of states, but must take account of the fact that the occupation probabilities are not independent. The phases of the probability amplitudes are related to the phase of the radio-frequency field.

† On leave at the Clarendon Laboratory, Oxford, 1959.



and hence to one another. In the fluorescent light, the coherence between the excited states is manifest as interference between optical radiations of different frequencies. It is this interference, giving rise to modulation, which was detected in the experiments of Dodd *et al.*

In this paper, and in that of Barrat which follows, the problem is formulated in terms of probability amplitudes. Related phenomena have been interpreted in other ways. Under similar conditions of irradiation of an atomic vapour with optical and radio-frequency fields, Bell & Bloom (1957) detected modulation in the absorbed light. Following Dehmelt's suggestion (1957) they used a phenomenological model, based on the Bloch equations, to interpret their experiments. We believe that the two sets of experiments are the emission and absorption counterparts of each other, and that both can be legitimately described either by the quantum-mechanical or by the phenomenological model.

In the following sections we calculate the intensity of light scattered by a single atom, and assume that there is no coherence between light scattered by different atoms. This is justifiable only to the extent that we are concerned with laterally scattered radiation whose wavelength is very much smaller than the mean distance between neighbouring atoms. We assume also that there is no multiple scattering. The assumption that different atoms radiate incoherently allows us to ignore the dependence of phase on the position of the scattering centre. The size of the sample is small compared with the wavelength at radio-frequencies.

The calculations in this paper have been carried through with particular reference to the transition ( $6^3P_1 - 6^1S_0$ ),  $\lambda 2537 \text{ \AA}$  in mercury, where the radio-frequency mixing is taking place between the Zeeman states of the upper level. This is a particularly simple case in that the three excited states are equally spaced in energy and are damped at the same rate, and in that there is only one ground state. The principles of the calculation could be applied to other situations: for example, the radio-frequency transitions could be between multiplet or hyperfine states. When radio-frequency mixing in the ground states is to be studied, some assumption concerning phase memory would have to be made, equivalent to that of introducing radiative damping into the excited state.

## 2. FORMULATION OF THE PROBLEM

Consider an atom in a uniform magnetic field  $H$ . Of the possible eigenstates we shall be concerned only with a non-degenerate ground state  $|g\rangle$  and a set of excited states  $|m\rangle$  which belong to a particular level of angular momentum  $J$ . It is supposed that the states  $|m\rangle$ , and no others, are accessible from  $|g\rangle$  by optical excitation, owing to the limited spectral range of the light. The  $|m\rangle$  are connected with one another by the radio-frequency perturbation.

In order to avoid unnecessary complication, the particular value  $J = 0$  is chosen for  $|g\rangle$ . Since this restriction may readily be lifted, we prefer not to impose on the excited states the restrictions on  $J$  which electric dipole transitions from  $|g\rangle$  would require.



(i) *The states and the Hamiltonians*

The state of the atom,  $|t\rangle$ , at any time  $t$  satisfies the equation

$$i\hbar d|t\rangle/dt = \mathcal{H}|t\rangle, \quad (1)$$

where the Hamiltonian  $\mathcal{H}$  may be written, to describe the type of experiment we are considering,

$$\mathcal{H} = \mathcal{H}_0 + \gamma \mathbf{J} \cdot \mathbf{H} + \mathcal{H}_D + \mathcal{H}_{\text{r.f.}} + \mathcal{H}_{\text{opt.}} \quad (2)$$

The first two terms on the right describe the interactions within the atom and the effect of the field  $\mathbf{H}$ ;  $\gamma$  is the gyromagnetic ratio.

The third term describes the radiative damping of the excited states. We assume that the matrix of  $\mathcal{H}_D$  is diagonal, with elements  $-\frac{1}{2}i\hbar\Gamma$  for the states  $|m\rangle$ , and zero for  $|g\rangle$ .

The fourth and fifth terms describe the radio-frequency and optical perturbations, respectively. These are formulated semi-classically, and discussed in detail below.

The state of the atom may be expressed as a superposition of states independent of time by the expansion

$$|t\rangle = \sum_m a_m(t) |m\rangle + a_g(t) |g\rangle. \quad (3)$$

Explicit forms for the  $a_m$  and  $a_g$  are found by solving the equation of motion, given that the atom is initially in the state  $|g\rangle$ .

 (ii) *Method of solution*

Since the optical excitation is weak ( $a_g \approx 1$  at all times), we can treat  $\mathcal{H}_{\text{opt.}}$  as a small perturbation and write  $\mathcal{H} = \mathcal{H}^* + \mathcal{H}_{\text{opt.}}$ , where

$$\mathcal{H}^* = \mathcal{H}_0 + \gamma \mathbf{J} \cdot \mathbf{H} + \mathcal{H}_D + \mathcal{H}_{\text{r.f.}}$$

Let  $|\rangle$  symbolize a state of the system at time  $t$  which would evolve from the state  $|t_0\rangle$  under the influence of  $\mathcal{H}^*$  only. The equation of motion of this state is

$$i\hbar d|\rangle/dt = \mathcal{H}^*|\rangle, \quad (4)$$

with the condition  $|\rangle = |t_0\rangle$  when  $t = t_0$ . The transformation from  $|t_0\rangle$  to  $|\rangle$  may conveniently be expressed by defining an operator  $U(t, t_0)$  as follows:

$$U(t, t_0) |t_0\rangle = |\rangle. \quad (5)$$

It is then readily verified that  $|t\rangle$ , the solution of (1) may be written

$$\begin{aligned} |t\rangle = & U(t, 0)|0\rangle + \frac{1}{i\hbar} \int_0^t dt_0 U(t, t_0) \mathcal{H}_{\text{opt.}}(t_0) U(t_0, 0) |0\rangle \\ & + \text{terms of second order in } \mathcal{H}_{\text{opt.}}. \end{aligned} \quad (6)$$

With the use of explicit expressions for  $\mathcal{H}_{\text{opt.}}$  and  $U$  which are to be obtained in section (3), equation (6) may be expanded in the form of equation (3), thereby obtaining the coefficients  $a_m(t) \equiv \langle m|t\rangle$ . The precise value of  $a_g(t)$  is not of particular interest, provided it does not depart greatly from unity.

It remains to calculate the intensity of the fluorescent light as a function of time. This is proportional to the modulus squared of the matrix element of the electric dipole operator  $\mathbf{P}$  between the states  $|t\rangle$  and  $|g\rangle$ . The result, and its justification by a Correspondence argument, is given in §4.

### 3. SOLUTION OF THE EQUATION OF MOTION

#### (i) The operator $\mathcal{H}_{\text{opt.}}$

Let the electric field of the incident light at time  $t$  be  $\mathbf{E}_i(t) = E_i(t) \mathbf{e}_i^0$ , where  $\mathbf{e}_i^0$  is a unit vector representing the direction of polarization. We shall see in due course that  $E_i(t)$  need not be completely specified: the significant quantity is the real correlation function  $\langle E_i(t) E_i(t+\tau) \rangle$ . This will ultimately be chosen to represent a steady beam of light of spectral width greater than any of the frequency differences with which we are concerned, in the neighbourhood of the excitation frequencies of the states  $|m\rangle$ .

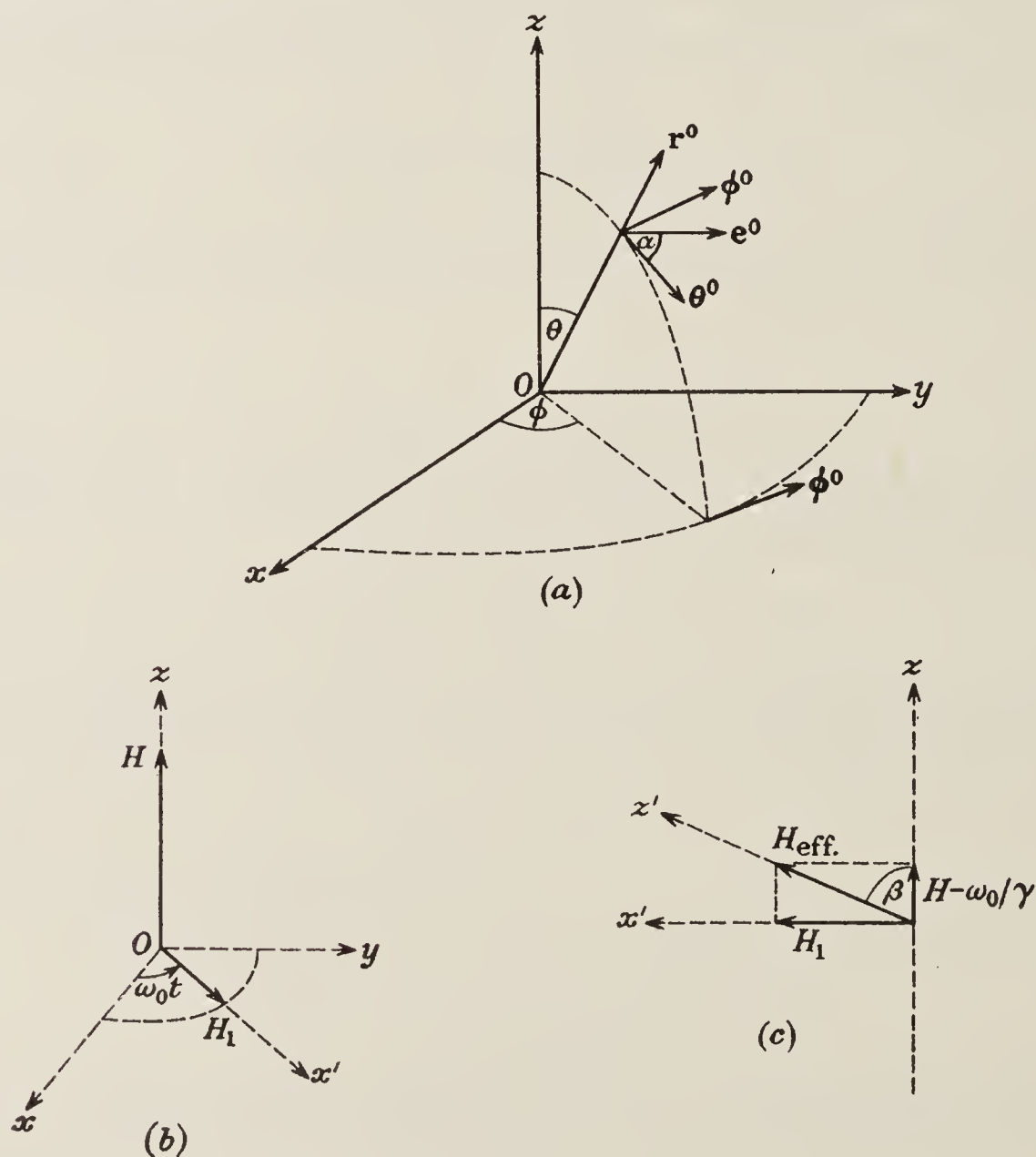


FIGURE 1. The notation.

The operator  $\mathcal{H}_{\text{opt.}}$  we consider only in the first approximation, in which it is the scalar product  $\mathbf{E}_i \cdot \mathbf{P}$ , where  $\mathbf{P}$  is the electric dipole operator. We shall write

$$\mathcal{H}_{\text{opt.}} = -E_i(t) \mathbf{e}_i^0 \cdot \mathbf{P} \equiv -E_i(t) F. \quad (7)$$

The only matrix elements of  $F$  which do not vanish are those between the excited states  $|m\rangle$  and the ground state  $|g\rangle$ ; we write them as  $F_m \equiv \langle m | F | g \rangle$ .



For later reference we expand  $\mathbf{e}^0$ . Let the direction of the light be specified by  $\theta, \phi$  (figure 1(a)), and let the electric vector make an angle  $\alpha$  with the unit vector associated with  $\theta$ . Then

$$\begin{aligned}\mathbf{e}^0 = & \mathbf{i}(\cos \theta \cos \phi \cos \alpha - \sin \phi \sin \alpha) \\ & + \mathbf{j}(\cos \theta \sin \phi \cos \alpha + \cos \phi \sin \alpha) \\ & + \mathbf{k}(-\sin \theta \cos \alpha).\end{aligned}\quad (8)$$

(ii) *The operator  $U$*

Through equations (4) and (5),  $U$  is related to

$$\mathcal{H}^* = \mathcal{H}_0 + \gamma \mathbf{J} \cdot \mathbf{H} + \mathcal{H}_D + \mathcal{H}_{\text{r.f.}}$$

We are interested in the effect of a radio-frequency field of amplitude  $H_1$  rotating with angular velocity  $\omega_0$  in a plane perpendicular to  $\mathbf{H}$ , the  $z$ -direction (figure 1(b)). The perturbation operator is

$$\mathcal{H}_{\text{r.f.}} = \gamma \mathbf{J} \cdot \{(H_1 \cos \omega_0 t) \mathbf{i} + (H_1 \sin \omega_0 t) \mathbf{j}\}. \quad (9)$$

With this form for  $\mathcal{H}_{\text{r.f.}}$ , the Hamiltonian  $\mathcal{H}^*$  may be written (Salwen 1955, for example)

$$\mathcal{H}^* = \exp \{(-iJ_z \omega_0 t/\hbar)\} \mathcal{H}_1 \{\exp (iJ_z \omega_0 t/\hbar)\}, \quad (10)$$

where

$$\mathcal{H}_1 = \mathcal{H}_0 + \mathcal{H}_D + \gamma H J_z + \gamma H_1 J_x. \quad (11)$$

It is convenient to make a unitary transformation  $T$  to a co-ordinate system  $Ox'y'z$  rotating about  $Oz$  with angular velocity  $\omega_0$ . This transforms  $\mathcal{H}^*$  to  $\mathcal{H}_1$ , and  $|\rangle$  into  $|\rangle' = \exp (iJ_z \omega_0 t/\hbar)|\rangle$ . The equation of motion (4) now becomes (Rabi, Ramsey & Schwinger 1954)

$$i\hbar d|\rangle'/dt = (\mathcal{H}_1 - \omega_0 J_z) |\rangle' = \mathcal{H}' |\rangle', \quad (12)$$

where

$$\mathcal{H}' = \mathcal{H}_0 + \mathcal{H}_D + \delta J_z + b J_x, \quad (13)$$

in which

$$\delta = \omega - \omega_0, \quad \omega = \gamma H \quad \text{and} \quad b = \gamma H_1.$$

The Hamiltonian  $\mathcal{H}'$  is now independent of time, and the equation of motion (12) may readily be solved giving

$$|\rangle' = \exp \{(\mathcal{H}'/i\hbar)(t - t_0)\} |\rangle'_{t_0}, \quad (14)$$

where the state  $|\rangle$  at  $t = t_0$  is written  $|\rangle'_{t_0}$ .

By applying the inverse transformation,  $T^{-1}$ , to  $|\rangle'$  and  $|\rangle'_{t_0}$ , we find the relation between  $|\rangle$  and  $|\rangle_{t_0}$ , which, by comparison with equation (5), yields

$$U(t, t_0) = \exp (-iJ_z \omega_0 t/\hbar) \exp \{(\mathcal{H}'/i\hbar)(t - t_0)\} \exp (iJ_z \omega_0 t_0/\hbar). \quad (15)$$

In the evaluation of the intensity of fluorescent radiation, we shall need the matrix elements  $U_{mn} \equiv \langle m|U|n\rangle$  taken between any two of the excited states  $|m\rangle$  and  $|n\rangle$  (the letter  $n$  is used for possible values of  $m$  to avoid difficulties in notation created by the use of subscripts and primes). The  $U_{mn}$  are obtained from the eigenstates and eigenvalues of  $J_z$  and  $\mathcal{H}'$ .

The eigenstates of  $J_z$  are  $|g\rangle$  and  $|m\rangle$ , with eigenvalues 0 and  $m\hbar$ , respectively.

The eigenstates of  $\mathcal{H}'$  are most easily expressed in terms of a co-ordinate system produced by a rotation of  $Oz$  about  $Oy'$  by an angle  $\beta = \tan^{-1}(b/\delta)$  (figure 1(c)).  $\mathcal{H}'$  may then be written  $\mathcal{H}_0 + \mathcal{H}_D + pJ_z$ , where  $p = (\delta^2 + b^2)^{1/2}$ . As the field  $H$  increases from zero, through the resonant field  $H_0 = \omega_0/\gamma$ , to infinity, the angle  $\beta$  passes from the value  $\pi$ , through  $\frac{1}{2}\pi$  to zero. The eigenvalues of  $\mathcal{H}'$  are

$$0 \quad \text{and} \quad \hbar\lambda_\mu = \hbar(k_0 - \frac{1}{2}i\Gamma + \mu p),$$

corresponding respectively to the eigenstates  $|\gamma\rangle$  and  $|\mu\rangle$  of the atom in  $H_{\text{eff}}$ , the effective field in the rotating co-ordinate system. The states  $|m\rangle$  and  $|\mu\rangle$ ,  $|g\rangle$  and  $|\gamma\rangle$  are related by the linear transformations

$$|\mu\rangle = \sum_m \langle m|\mu\rangle |m\rangle = \sum_m \mathcal{D}^J(0, \beta, 0)_{m\mu} |m\rangle; \quad |\gamma\rangle = |g\rangle, \quad (16)$$

where the  $\mathcal{D}^J(0, \beta, 0)_{m\mu}$  are elements of the rotation matrix (Rose 1957, for example).

Using these results we obtain

$$\begin{aligned} U_{mn}(t, t_0) &= \langle m | \exp(-iJ_z\omega_0 t/\hbar) \exp(\mathcal{H}'/i\hbar)(t-t_0) \exp(iJ_z\omega_0 t_0/\hbar) | n \rangle \\ &= \exp(-im\omega_0 t) \exp(in\omega_0 t_0) \sum_\mu \langle m|\mu\rangle \langle \mu | \exp(\mathcal{H}'/i\hbar)(t-t_0) | n \rangle \\ &= \exp(-im\omega_0 t) \exp(in\omega_0 t_0) \sum_{\mu, \nu} \langle m|\mu\rangle \langle \mu | \exp(\mathcal{H}'/i\hbar)(t-t_0) | \nu \rangle \langle \nu | n \rangle \\ &= \exp(-im\omega_0 t) \exp(in\omega_0 t_0) \sum_\mu \langle m|\mu\rangle \langle \mu | n \rangle \exp\{-i\lambda_\mu(t-t_0)\}, \end{aligned} \quad (17)$$

since the  $|\mu\rangle$  are eigenstates of  $\mathcal{H}'$ .

### (iii) Expansion of the state $|t\rangle$

We are now in a position to find the coefficients  $a_m(t)$  of equation (3). From equation (6) we find, by forming the bracket product with  $|m\rangle$ ,

$$a_m(t) \equiv \langle m | t \rangle = \langle m | U(t, 0) | 0 \rangle + (1/i\hbar) \int_0^t dt_0 \langle m | U(t, t_0) \mathcal{H}_{\text{opt.}}(t_0) U(t_0, 0) | 0 \rangle, \quad (18)$$

in which  $|0\rangle$ , the state at  $t = 0$ , is simply  $|g\rangle$ . Since  $|g\rangle$  is an eigenstate of  $J_z$  with eigenvalue 0, and since  $|\gamma\rangle = |g\rangle$  is an eigenstate of  $\mathcal{H}'$  with eigenvalue 0,  $|g\rangle$  is also an eigenstate of  $U$  with eigenvalue 1 for all  $t$ . Hence the first term on the right of equation (18) is  $\langle m | g \rangle = 0$ , and the second term reduces to

$$(1/i\hbar) \int_0^t dt_0 \langle m | U(t, t_0) \mathcal{H}_{\text{opt.}}(t_0) | g \rangle.$$

With the use of equation (7) this becomes

$$(1/i\hbar) \int_0^t dt_0 E_i(t_0) \sum_n F_n \langle m | U(t, t_0) | n \rangle. \quad (19)$$

Finally, from (17), (19) and (3) we have

$$\begin{aligned} |t\rangle &= a_g |g\rangle + (1/i\hbar) \int_0^t dt_0 E_i(t_0) \sum_{m\mu n} \langle m|\mu\rangle \langle \mu | n \rangle F_n \\ &\quad \times \exp(-im\omega_0 t) \exp\{-i\lambda_\mu(t-t_0)\} \exp(in\omega_0 t_0) |m\rangle. \end{aligned} \quad (20)$$



The physical meaning of the second term on the right is simply the following: the coefficient  $(1/i\hbar) E_i(t_0) F_n dt_0$  represents the probability amplitude of the state  $|n\rangle$  when the optical perturbation acts on an atom in state  $|g\rangle$  (which is approximately the state  $|t_0\rangle$ ) for a time  $dt_0$  at  $t_0$ ; the coefficient

$$\sum_{\mu} \langle m|\mu\rangle \langle \mu|n\rangle \exp(-im\omega_0 t) \exp\{-i\lambda_{\mu}(t-t_0)\} \exp(in\omega_0 t_0)$$

represents the probability amplitude of the state  $|m\rangle$  at time  $t$  when the radio-frequency and damping perturbations have acted for a time  $(t-t_0)$  on an atom which, at time  $t_0$ , was in the state  $|n\rangle$ ; (this coefficient, in a different form, and without the radiative damping, was derived by Majorana (1932) (see also Ramsey 1956, appendix E); the combined coefficients, summed over the  $m$ ,  $\mu$  and  $n$ , and integrated over  $t_0$ , represent the net effect of optical, radio-frequency and damping perturbations in an approximation in which the excitation rate is weak compared with the rate of spontaneous decay, that is to say, the probability of finding the atom in the ground state is always very much greater than the probability of finding it excited ( $a_g \approx 1$ ).

#### 4. THE FLUORESCENT RADIATION

##### (i) Calculation of the intensity $I$

The energy flux per unit area of radiation in an electromagnetic field specified by the complex vectors  $\mathbf{E}$ ,  $\mathbf{H}$ , is given by

$$\mathbf{S}_{\text{av.}} = c(\mathbf{E} \wedge \mathbf{H}^* + \mathbf{E}^* \wedge \mathbf{H})/16\pi.$$

Using  $\mathbf{H} = \mathbf{r}^0 \wedge \mathbf{E}$  for electromagnetic waves propagated in the direction of the unit vector  $\mathbf{r}^0$ , one obtains

$$\mathbf{S}_{\text{av.}} = I\mathbf{r}^0 = c(\mathbf{E}^* \cdot \mathbf{E}/8\pi) \mathbf{r}^0. \quad (21)$$

The radiation field  $\mathbf{E}(r, \theta, \phi, t)$ , to first approximation, is related to the matrix element  $\langle g|P|t\rangle$  by

$$\mathbf{E} = (2k^2/rc^2) \langle g|\mathbf{P} - (\mathbf{r}^0 \cdot \mathbf{P}) \mathbf{r}^0|t\rangle. \quad (22)$$

Its component in the direction  $\mathbf{e}^0$ , which lies in the plane normal to  $\mathbf{r}^0$  (see figure 1(a)) is

$$\mathbf{e}^0 \cdot \mathbf{E} = (2k^2/rc^2) \langle g|\mathbf{e}^0 \cdot \mathbf{P}|t\rangle. \quad (23)$$

Equation (22) may be derived by a Correspondence argument (see, for example, Condon & Shortley 1951, pp. 89, 90) when the states concerned are pure states of a time-independent Hamiltonian. Its application when  $|t\rangle$  is expressed as a linear superposition of such states may be justified from the superposition theorem for electric fields.

The expression for  $I$  thus depends on the form of the matrix elements  $\langle g|\mathbf{e}^0 \cdot \mathbf{P}|t\rangle$ , which, are, by equation (20)

$$\begin{aligned} \langle g|\mathbf{e}^0 \cdot \mathbf{P}|t\rangle &= (1/i\hbar) \int_0^t dt_0 E_i(t_0) \sum_{m\mu n} G_m^* \langle m|\mu\rangle \langle \mu|n\rangle F_n \\ &\quad \times \exp(-im\omega_0 t) \exp\{-i\lambda_{\mu}(t-t_0)\} \exp(in\omega_0 t_0), \end{aligned} \quad (24)$$

in which we have introduced  $G_m^* = \langle g|\mathbf{e}^0 \cdot \mathbf{P}|m\rangle$ . By this definition  $F_m$  and  $G_m$  are defined identically except for the direction of the polarization vector.

Combining equations (21), (23) and (24) we arrive at the following expression for the intensity of light at time  $t$ , plane polarized in the direction  $\mathbf{e}^0$ , due to the scattering from one atom:

$$I = \frac{k_0^4}{2\pi c^3 \hbar^2 r^2} \int_0^t dt_0 E_i(t_0) \sum_{m\mu n} G_m^* \langle m|\mu\rangle \langle \mu|n\rangle F_n \exp(-im\omega_0 t) \\ \times \exp\{-i\lambda_\mu(t-t_0)\} \exp(in\omega_0 t_0) \\ \times \int_0^t dt'_0 E_i(t'_0) \sum_{m'\mu' n'} F_n^* \langle n'|\mu'\rangle \langle \mu'|m'\rangle G_{m'} \exp(im'\omega_0 t) \exp\{i\lambda_{\mu'}^*(t-t'_0)\} \\ \times \exp(-in'\omega_0 t'_0), \quad (25)$$

in which  $k_0$  is an average optical frequency. For laterally scattered radiation from  $N$  atoms the expression is to be multiplied by  $N$  and  $(1/r^2)$  replaced by a mean value,  $(1/r_0^2)$ .

The dependence on  $t, t_0$  and  $t'_0$  of the terms in equation (25) is of the form

$$\exp\{-i(m-m'-n+n')\omega_0 t\} \int_0^t dt_0 \exp\{-(\Gamma+ix)(t-t_0)\} \int_0^t dt'_0 E_i(t_0) E_i(t'_0) \\ \times \exp\{-(\frac{1}{2}\Gamma-ik')(t_0-t'_0)\} \quad (26)$$

$$\text{in which} \quad k' = k_0 + \mu'p + n'\omega_0 \quad \text{and} \quad x = (\mu-\mu')p + (n-n')\omega_0. \quad (27)$$

In order to evaluate the double integral it is not necessary to specify the field  $E_i(t_0)$  itself, nor even the product  $\Phi(t_0, \tau) = E_i(t_0) E_i(t_0 + \tau)$ , where  $\tau = (t_0 - t'_0)$ . It is sufficient to know the average value  $\langle \Phi(t_0, \tau) \rangle$ , taken with fixed  $\tau$  over a time, centred on  $t_0$ , which covers many periods of the optical frequency  $k'$ . To see this, notice that the only term in (26), apart from  $\Phi$ , which oscillates rapidly, is  $\exp -(\frac{1}{2}\Gamma - ik')\tau$ . Now fix  $\tau$ , and integrate over a range of  $t_0$  large compared with  $1/k'$  but small compared with  $(\Gamma^2 + x^2)^{\frac{1}{2}}$ . The only quantity which changes appreciably during this time is  $\Phi$ . The value of (26) is therefore unchanged if we substitute for  $\Phi$  the mean value

$$\langle \Phi(t_0, \tau) \rangle = \frac{1}{2T_0} \int_{t_0-T_0}^{t_0+T_0} \Phi(t, \tau) dt.$$

The advantage of introducing  $\langle \Phi \rangle$  is that it is closely related to a quantity which can actually be measured, the power spectrum of the incident light.

Several cases now can be distinguished:

(i) The intensity of the exciting light is independent of time, as in the ordinary double resonance experiment. In this case  $\langle \Phi \rangle$  is the auto-correlation function for stationary fields. It is a function of  $\tau$  only, not of  $t_0$ , and is related to the power spectrum  $\rho(k)$ :

$$\langle E_i(t_0) E_i(t'_0) \rangle = \langle \Phi(\tau) \rangle = \frac{8\pi}{c} \int_{-\infty}^{+\infty} dk \rho(k) \exp(-ik\tau), \quad (28)$$

(see, for example, Born & Wolf 1959, p. 501; the factor  $\exp(-2\pi i\nu t)$  in their equation (27) should read  $\exp -2\pi i\nu\tau$ ).

(ii) The exciting light is modulated or pulsed. In this case  $\langle \Phi \rangle$  is a function of  $t_0$  as well as of  $\tau$ . We shall not pursue the analysis of this case, but refer to it again at the end of § 6.



Returning to case (i) and inserting (28) into (26), we find that the integral over  $t'_0$  may be expressed

$$\frac{8\pi}{c} \int_{t_0-t}^{t_0} d\tau \exp(-\frac{1}{2}\Gamma\tau) \int_{-\infty}^{+\infty} dk \rho(k) \exp\{-i(k-k')\tau\}. \quad (29)$$

Again, we distinguish cases for which  $\rho(k)$  has different forms:

(a) Monochromatic light of angular frequency  $k'$ . In this case the form of  $\rho(k)$  is  $R\delta(k-k')$ , the double integral (29) becomes  $(16\pi R/c\Gamma) \exp \frac{1}{2}\Gamma(t-t_0)$  for  $t_0 \gg 1/\Gamma$ , and (26) reduces to

$$\frac{16\pi R}{c\Gamma} \frac{1}{(\frac{1}{2}\Gamma + ix)} \exp\{-i(m-m'-n+n')\omega_0 t\}. \quad (30)$$

(b) White light. In this case  $\rho(k) = \rho_0$ , independent of  $k$ , the integral over  $k$  in (29) becomes  $\rho_0 \delta(\tau)$ , the value of (29),  $8\pi\rho_0/c$ , and (26) reduces to

$$\frac{8\pi\rho_0}{c} \frac{1}{(\Gamma + ix)} \exp\{-i(m-m'-n+n')\omega_0 t\}. \quad (31)$$

(c) Quasi-monochromatic light of mean angular frequency  $k'$  and spectral width  $\Delta \gg \Gamma$ , such as was used in the experiments. In this case  $\rho(k)$  might take the form, for example,  $\rho_0 \exp\{-(k-k')^2/\Delta^2\}$ . More important than the exact form of  $\rho(k)$ , provided it is a slowly varying function, is the time  $\tau_\Delta \approx 1/\Delta$  over which coherence persists in the optical field, for if  $\tau_\Delta$  is much less than the lifetime of the atoms, then we find the same result as for white light, as may readily be shown:

Choose a time  $\tau_0$  such that  $1/\Delta \ll \tau_0 \ll 1/\Gamma$ . Now the integral over  $k$  in (29) behaves like  $\rho_0 \delta(k-k')$  except in the region  $|\tau| < \tau_0$ . Inside this region we may, to a good approximation, replace  $\exp -\frac{1}{2}\Gamma\tau$  by unity. The expression (29) thus has the value, in this case,

$$\begin{aligned} \frac{8\pi}{c} \int_{t_0-t}^{t_0} d\tau \int_{-\infty}^{+\infty} dk \rho(k) \exp\{-i(k-k')\tau\} &= \frac{8\pi}{c} \int_{-\infty}^{+\infty} dk \rho(k) \int_{t_0-t}^{t_0} d\tau \exp\{-i(k-k')\tau\} \\ &= \frac{8\pi}{c} \int_{-\infty}^{+\infty} dk \rho(k) \delta(k-k') = \frac{8\pi}{c} \rho(k') \end{aligned}$$

from which the expression (26) again reduces to (31), the result obtained for white light.

If the spectral range of the light not only greatly exceeds  $\Gamma$ , but also spans all possible values of  $k'$  in equation (27), equation (25) becomes, for  $N$  atoms,

$$\left\| I = \frac{4Nk_0^4}{\Gamma c^4 \hbar^2 r_0^2} \rho(k_0) \sum_{\substack{m\mu n \\ m'\mu' n'}} \mathcal{F}_{nn'} \langle m|\mu \rangle \langle \mu|n \rangle \langle n'|\mu' \rangle \langle \mu'|m' \rangle \mathcal{G}_{mm'} \frac{\Gamma}{\Gamma + ix} \right\| \times \exp\{-i(m-m'-n+n')\omega_0 t\}, \quad (32)$$

where  $m, \mu, n, m', \mu', n'$  take the values  $-J, -J+1, \dots, J$ . We have introduced the notation  $\mathcal{F}_{nn'} = F_n F_{n'}^*$ ,  $\mathcal{G}_{mm'} = G_m^* G_{m'}$ , where  $F$  and  $G$ , it will be recalled, refer to excitation by, and the observation of, plane polarized light

$$F_n = \langle n | \mathbf{e}_i^0 \cdot \mathbf{P} | g \rangle, \quad G_m = \langle m | \mathbf{e}^0 \cdot \mathbf{P} | g \rangle.$$

For convenience, we here repeat the definitions of the other symbols

$$\langle m|\mu\rangle = \mathcal{D}^J(0, \beta, 0)_{m\mu}; \quad x = (\mu - \mu')p + (n - n')\omega_0; \quad p = (\delta^2 + b^2)^{\frac{1}{2}};$$

$$b = \gamma H_1; \quad \delta = \omega - \omega_0; \quad \omega = \gamma H; \quad \beta = \tan^{-1}(b/\delta);$$

and  $\rho(k_0)$  is the energy flux of the incident light per unit area, per unit spectral range.

The elements  $\mathcal{F}_{nn'}$ , and  $\mathcal{G}_{mm'}$  form what may be termed the excitation and emission matrices, respectively. They may be generalized to unpolarized light, and to polarized light other than plane. Thus, for unpolarized light, the matrix element  $\mathcal{F}_{nn'}^u$  may be formed by adding to  $(F_n F_n^*)$  the element formed by using the polarization vector perpendicular to  $\mathbf{e}_i^0$ . Introducing the unit vectors  $\mathbf{r}^0$ ,  $\boldsymbol{\theta}^0$  and  $\boldsymbol{\phi}^0$  (figure 1(a)), we define

$$\mathbf{F}_n = \langle n | \mathbf{P} - (\mathbf{r}^0 \cdot \mathbf{P}) \mathbf{r}^0 | g \rangle = \langle n | (\boldsymbol{\theta}^0 \cdot \mathbf{P}) \boldsymbol{\theta}^0 + (\boldsymbol{\phi}^0 \cdot \mathbf{P}) \boldsymbol{\phi}^0 | g \rangle. \quad (33a)$$

Then we have for unpolarized light,

$$\mathcal{F}_{nn'}^u = \mathbf{F}_n \cdot \mathbf{F}_{n'}^*, \quad (33b)$$

and for circularly polarized light

$$\mathcal{F}_{nn'}^c = F_n^c F_{n'}^{*c}, \quad (33c)$$

in which  $F_n^c = \frac{1}{2}(\boldsymbol{\theta}^0 \pm i\boldsymbol{\phi}^0) \cdot \mathbf{F}_n$ .

Explicit forms for  $\mathcal{F}_{nn'}$  and  $\mathcal{G}_{mm'}$  in a particular case are given in §5.

## (ii) Discussion of the result, equation (32)

Consider first the case when the polarization of the exciting light allows excitation to only one state  $|n\rangle$  of the excited level, so that  $n' = n$ . The result (32) shows that the light intensity is modulated at frequencies  $|m - m'| \omega_0$ . The angular dependence of the emitted light is contained in the elements  $\mathcal{G}_{mm'}$  of the emission matrix. The rotation matrix elements give the variation of intensity with field and frequency. They all show some type of resonant behaviour near  $\delta = 0$ , i.e. when  $H = H_0 = \omega_0/\gamma$ . The term  $\Gamma/(\Gamma + ix)$ , which reduces to  $\Gamma/\{\Gamma + i(\mu - \mu')p\}$ , also shows resonant behaviour near  $\delta = 0$  unless  $\mu = \mu'$ , in which case it is independent of  $H$ . The terms of zero-frequency ( $m = m'$ ) sum to give the well known Brossel-Bitter resonance (Brossel & Bitter 1952).

The more general case when more than one of the  $|n\rangle$  are simultaneously excited shows additional features which have been observed in the experiments, namely, modulation at frequencies higher than the maximum value of  $|m - m'| \omega_0$ , and resonance effects at frequencies other than  $H_0$ . The possible modulation frequencies are now  $|m - m' - n + n'| \omega_0$ . The extra resonance effects are seen in the behaviour of the term  $\Gamma/(\Gamma + ix)$  when  $x = 0$ , i.e. when  $(\mu - \mu')p = (n' - n)\omega_0$ . In the case of the  $^3P_1 - ^1S_0$  transition, modulation up to the fourth harmonic is present, and resonances occur when  $H = 0, \frac{1}{2}H_0, \frac{3}{2}H_0, 2H_0$  and  $3H_0$ . Not all of these may be strong enough to be easily observable.



5. APPLICATION TO THE TRANSITION  $6^3P_1 - 6^1S_0$  IN MERCURY

Atoms in the ground level  $6^1S_0$  are excited by light of wavelength 2537 Å to the level  $6^3P_1$ , whose states  $|m_J = 0, \pm 1\rangle$  are connected by the radio-frequency field. The expression (32) for the intensity of the fluorescent light is most readily understood by separate attention to the three parts of the process.

## (ia) Excitation

The coefficients  $F_n$  for the case of incident light passing through a linear polarizer specified by the unit vector  $\mathbf{e}_i^0$  are given by  $F_n = \mathbf{e}_i^0 \cdot \langle n | \mathbf{P} | g \rangle$ . Using the matrix elements for  $\langle n | \mathbf{P} | g \rangle$  given by Condon & Shortley (1951, p. 53), and equation (8) we obtain

$$\left. \begin{aligned} F_{\pm 1} &= 2^{-\frac{1}{2}} P (\cos \alpha_i \cos \theta_i \mp i \sin \alpha_i) \exp(\mp i \phi_i), \\ F_0 &= -P (\cos \alpha_i \sin \theta_i), \end{aligned} \right\} \quad (34)$$

where  $P = \langle 1 | P | 0 \rangle$ .

For the particular case of light incident along the  $x$ -axis, polarized so that the electric vector makes an angle  $\alpha_i$  with the direction of the field, the excitation matrix becomes

$$\mathcal{F}_{nn'} = |P|^2 \begin{pmatrix} \frac{1}{2} \sin^2 \alpha_i & -2^{-\frac{1}{2}} i \sin \alpha_i \cos \alpha_i & \frac{1}{2} \sin^2 \alpha_i \\ 2^{-\frac{1}{2}} i \sin \alpha_i \cos \alpha_i & \cos^2 \alpha_i & 2^{-\frac{1}{2}} i \sin \alpha_i \cos \alpha_i \\ \frac{1}{2} \sin^2 \alpha_i & -2^{-\frac{1}{2}} i \sin \alpha_i \cos \alpha_i & \frac{1}{2} \sin^2 \alpha_i \end{pmatrix} \quad (35a)$$

For the case of unpolarized light, a matrix obtained by replacing  $\alpha_i$  by  $\alpha_i + \frac{1}{2}\pi$  must be added to the above. The excitation matrix is then

$$\mathcal{F}_{nn'}^u = |P|^2 \begin{pmatrix} \frac{1}{2} & 0 & \frac{1}{2} \\ 0 & 1 & 0 \\ \frac{1}{2} & 0 & \frac{1}{2} \end{pmatrix}. \quad (35b)$$

## (ib) The mixing of states

The effect of the radio-frequency magnetic field in producing a coherent mixture of the states  $|m\rangle$  is contained in the products

$$\langle m | \mu \rangle \langle \mu | n \rangle \langle n' | \mu' \rangle \langle \mu' | m' \rangle.$$

The rotation matrix elements, for  $J = 1$ , are

$$\langle m | \mu \rangle = \begin{pmatrix} \cos^2 \frac{1}{2} \beta & -\sqrt{2} \sin \frac{1}{2} \beta \cos \frac{1}{2} \beta & \sin^2 \frac{1}{2} \beta \\ \sqrt{2} \sin \frac{1}{2} \beta \cos \frac{1}{2} \beta & \cos^2 \frac{1}{2} \beta - \sin^2 \frac{1}{2} \beta & -\sqrt{2} \sin \frac{1}{2} \beta \cos \frac{1}{2} \beta \\ \sin^2 \frac{1}{2} \beta & \sqrt{2} \sin \frac{1}{2} \beta \cos \frac{1}{2} \beta & \cos^2 \frac{1}{2} \beta \end{pmatrix} \quad (36)$$

in which  $\beta$  is defined in §3 (figure 1(c)). The elements  $\langle \mu | m \rangle$  are obtained by transposition of rows and columns.

The variation of these matrix elements, and of the factor  $\Gamma/(\Gamma + ix)$ , with  $H$ , gives rise to resonances in the steady and modulated components of the fluorescent radiation.

(ic) *Emission*

The angular distribution of the fluorescent light is determined by the emission matrix  $\mathcal{G}_{mm'}$ . If no analyzer is used,  $\mathcal{G}_{mm'}^u = \mathbf{G}_m^* \cdot \mathbf{G}_{m'}$  with

$$\left. \begin{aligned} \mathbf{G}_{\pm 1} &= \mp 2^{-\frac{1}{2}} P(\theta^0 \cos \theta \mp i\phi^0) e^{\mp i\phi}, \\ \mathbf{G}_0 &= -P\theta^0 \sin \theta. \end{aligned} \right\} \quad (37)$$

For observation in the direction  $\theta, \phi$  the emission matrix becomes

$$\mathcal{G}_{mm'}^u = |P|^2 \begin{pmatrix} \frac{1}{2}(\cos^2 \theta + 1) & 2^{-\frac{1}{2}} \sin \theta \cos \theta e^{i\phi} & \frac{1}{2} \sin^2 \theta e^{i2\phi} \\ 2^{-\frac{1}{2}} \sin \theta \cos \theta e^{-i\phi} & \sin^2 \theta & -2^{-\frac{1}{2}} \sin \theta \cos \theta e^{i\phi} \\ \frac{1}{2} \sin^2 \theta e^{-i2\phi} & -2^{-\frac{1}{2}} \sin \theta \cos \theta e^{-i\phi} & \frac{1}{2}(\cos^2 \theta + 1) \end{pmatrix}. \quad (38)$$

If an analyzer is used to select the electric vector at angle  $\alpha$ , the elements of the emission matrix are  $\mathcal{G}_{mm'} = G_m^* G_{m'}$ , where the  $G_m = \mathbf{e}^0 \cdot \mathbf{G}_m$  are given by equations like (34).

(ii) *Excitation to a single state*

The terms of equation (32) will be evaluated for the particular case of excitation to the state  $|0\rangle$  exclusively (light incident along the  $x$ -axis,  $\alpha_i = 0$ ). Writing  $I_0$  for the accumulation of constants, we find

$$\begin{aligned} I = I_0 \frac{N}{\Gamma} & [\sin^2 \theta + (\cos^2 \theta - \frac{1}{2} \sin^2 \theta) 2A \\ & - \sin \theta \cos \theta \{B \cos(\omega_0 t - \phi) + C \sin(\omega_0 t - \phi)\} \\ & - \sin^2 \theta \{D \cos(2\omega_0 t - 2\phi) + E \sin(2\omega_0 t - 2\phi)\}] \end{aligned} \quad (39)$$

in which

$$\begin{aligned} A &= \frac{b^2(4\delta^2 + b^2 + \Gamma^2)}{(\delta^2 + b^2 + \Gamma^2)(4\delta^2 + 4b^2 + \Gamma^2)}, \\ B &= \frac{2b\delta(4\delta^2 - 2b^2 + \Gamma^2)}{(\delta^2 + b^2 + \Gamma^2)(4\delta^2 + 4b^2 + \Gamma^2)}, \\ C &= \frac{2b\Gamma(4\delta^2 + b^2 + \Gamma^2)}{(\delta^2 + b^2 + \Gamma^2)(4\delta^2 + 4b^2 + \Gamma^2)}, \\ D &= \frac{b^2(2\delta^2 - b^2 - \Gamma^2)}{(\delta^2 + b^2 + \Gamma^2)(4\delta^2 + 4b^2 + \Gamma^2)}, \\ E &= \frac{3b^2\Gamma\delta}{(\delta^2 + b^2 + \Gamma^2)(4\delta^2 + 4b^2 + \Gamma^2)}. \end{aligned}$$

The quantity  $A$  determines the variation of the unmodulated component of the fluorescent light as one alters  $H$  (or  $\omega_0$ ); this displays a resonance when

$$\delta = \omega - \omega_0 = 0,$$

i.e. at  $H = H_0$ . The variation is exactly that described by Brossel & Bitter (1952).

The intensity is also modulated at the first and second harmonics of the applied radio-frequency, the variation of amplitude and phase of the modulations being



described by the quantities  $B$ ,  $C$  and  $D$ ,  $E$ , respectively. The quantities  $B$  and  $C$  bear a striking resemblance to the solutions of the Bloch equations, which lends support to the belief that the modulation may also be described by the phenomenological approach of Bell & Bloom (1957). It is to be noticed that the phase of the modulations (with respect to that of the oscillating field) varies as one goes through resonance, and is a function of the azimuth angle  $\phi$ .

The variations have received experimental confirmation in work which has been briefly reported (Dodd *et al.* 1959) and which is to be more fully described in a later paper. In particular, the variations with angle of observation, and of polarizer and analyzer have been confirmed.

### (iii) *Excitation to a mixture of states*

As a further example we show how, and under what conditions, resonances can occur near the fields  $H = \frac{1}{2}H_0$  and  $\frac{3}{2}H_0$ .

The general expression for the intensity (equation (32)) is a formidable one, but it is possible to extract from the summations those terms which have a resonance in a certain region of magnetic field. Resonances occur when the quantity  $x = (\mu - \mu')p + (n - n')\omega_0$  in the equation passes through zero. For the particular terms in which  $n - n' = +1$ ,  $\mu - \mu' = -2$ , and  $n - n' = -1$ ,  $\mu - \mu' = +2$ , this leads to the condition  $2p = \omega_0$  for resonance. Expressed in terms of fields the condition is

$$H = H_0 \pm \frac{1}{2}H_0(1 - 4H_1^2/H_0^2)^{\frac{1}{2}}. \quad (40)$$

If  $H_1$  is not too large this gives  $H \approx \frac{1}{2}H_0$  and  $H \approx \frac{3}{2}H_0$  for the resonances. As  $H_1$  approaches the value  $\frac{1}{2}H_0$ , both resonances move towards  $H_0$ .

The frequencies of modulation of the intensity at these resonances are the possible values of  $|m - m' - n + n'|\omega_0$ . Since  $m - m'$  can take all values from zero to  $\pm 2$  (and recalling that we have selected those terms for which  $n - n' = \pm 1$ ) we find terms in unmodulated, fundamental, second- and third-harmonic components of the intensity. The strengths of the resonances of these various components are not all the same; they depend on some power of  $H_1/H_0$ . The strongest resonances predicted (for small  $H_1$ ) are those of the unmodulated and fundamental components which occur near  $\frac{1}{2}H_0$ . These have been observed. Resonances near  $\frac{1}{2}H_0$  and  $\frac{3}{2}H_0$  have also been observed in the light modulated at the second and third harmonics. The third harmonic resonance at  $\frac{3}{2}H_0$  is stronger than that at  $\frac{1}{2}H_0$  as predicted by the theory.

A necessary condition for the production of these resonances at  $\frac{1}{2}H_0$  and  $\frac{3}{2}H_0$  is the excitation of a mixture of states  $|n\rangle$  between which  $n$  differs by unity. For light incident along the  $x$ -axis, this implies that plane polarized light must be polarized obliquely to the magnetic field. This accords with the appearance of the factor  $\sin \alpha_i \cos \alpha_i$  which is common to all the terms at present under consideration. The necessity of oblique polarization has been confirmed by experiment.

Among the other terms in equation (32) are some which give rise to resonances at zero field, at  $2H_0$  and at  $3H_0$ . Modulations up to the fourth harmonic are found at these fields. Systematic experimental study of the higher modulations has not yet been undertaken.

## 6. FREQUENCY DIAGRAM

In the course of these studies we have found it useful to develop a frequency diagram for the excited state  $J = 1$  to represent its structure under the simultaneous application of a steady field along  $Oz$  and rotating field in the  $xy$  plane. A diagram of this type for  $J = \frac{1}{2}$  was drawn by Pryce (1950). The frequency diagram is simply a generalization, for the case when the Hamiltonian function is time-dependent, of the normal term diagram. To each state, in the normal case, there corresponds one and only one frequency. When the Hamiltonian is periodic in time there may be more than one. The representation of radiation damping by broadened energy levels is a familiar example of this generalized term diagram.

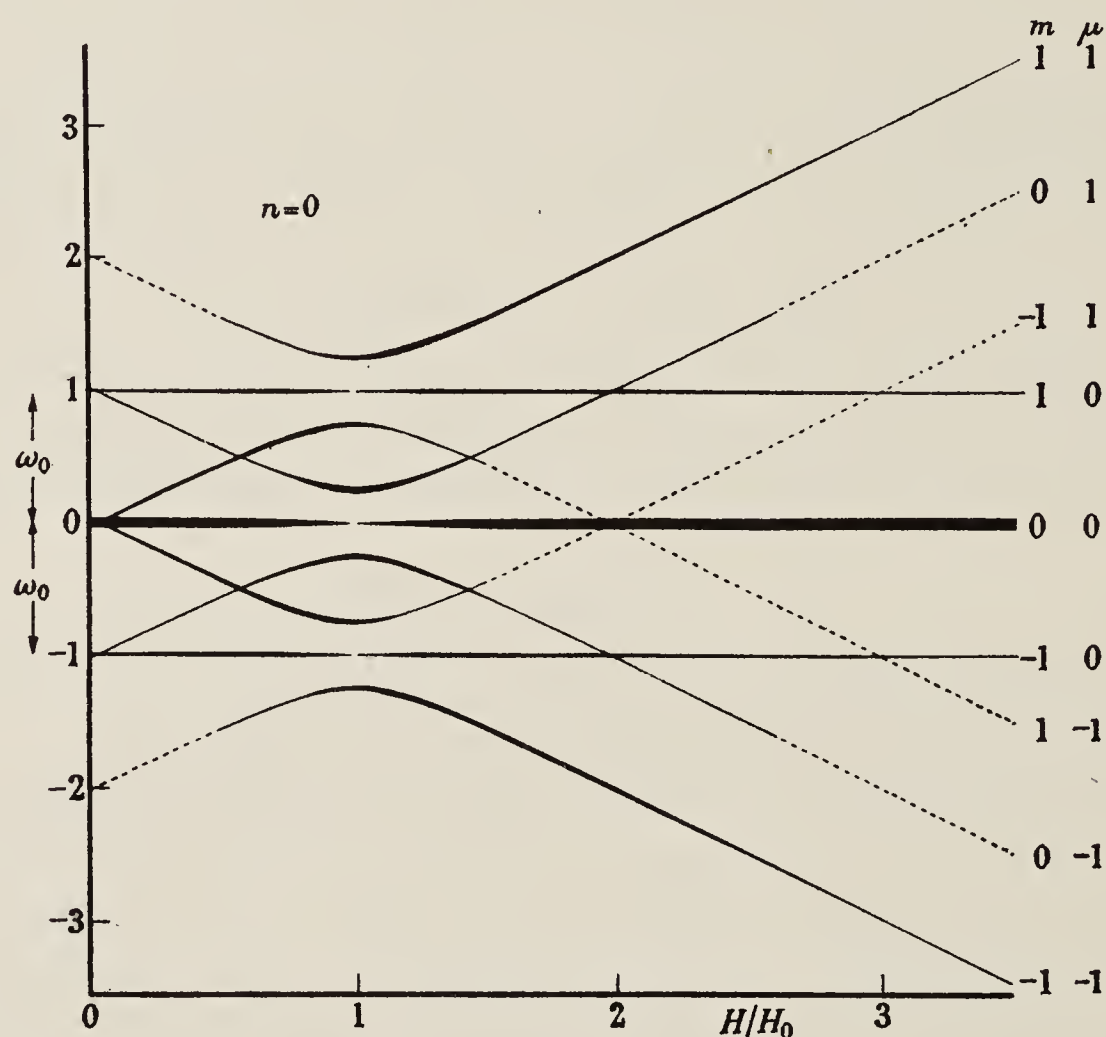


FIGURE 2. The frequency diagram.

The terms in equation (20) which represent the excited state contain, after separating the factor  $\exp\{-i(k_0 - \frac{1}{2}i\Gamma)\}$ , oscillating terms of frequency  $(m\omega_0 \pm \mu p)$ . For example, when  $n = 0$  the probability amplitudes of the states  $|1\rangle$ ,  $|0\rangle$ , and  $|-1\rangle$  are in the ratio

$$\begin{aligned}
 & [2sc^3 \exp\{-i(\omega_0 + p)t'\} - 2sc(c^2 - s^2) \exp(-i\omega_0 t') \\
 & \quad - 2s^3c \exp\{-i(\omega_0 - p)t'\}] \exp(-i\omega_0 t_0) \\
 & : [2s^2c^2 \exp(-ipt') + (c^2 - s^2)^2 \\
 & \quad + 2s^2c^2 \exp\{-i(-p)t'\}] \\
 & : [2s^3c \exp\{-i(-\omega_0 + p)t'\} + 2sc(c^2 - s^2) \exp\{-i(-\omega_0)t'\} \\
 & \quad - 2sc^3 \exp\{-i(-\omega_0 - p)t'\}] \exp\{-i(-\omega_0)t_0\}
 \end{aligned}$$

in which  $s = \sin \frac{1}{2}\beta$ ,  $c = \cos \frac{1}{2}\beta$  and  $t' = t - t_0$ . The frequency diagram associated with the excited level is shown in figure 2.



The interpretation of the diagram is facilitated by recalling how the expansion was obtained. The states  $|m\rangle$  were defined with reference to a laboratory co-ordinate system in which a steady magnetic field  $\mathbf{H}$  is applied along  $Oz$ . The frequencies of the  $|m\rangle$ ,  $(k_0 + m)\gamma H$ , are shown in figure 3 (a) as functions of  $H$ .

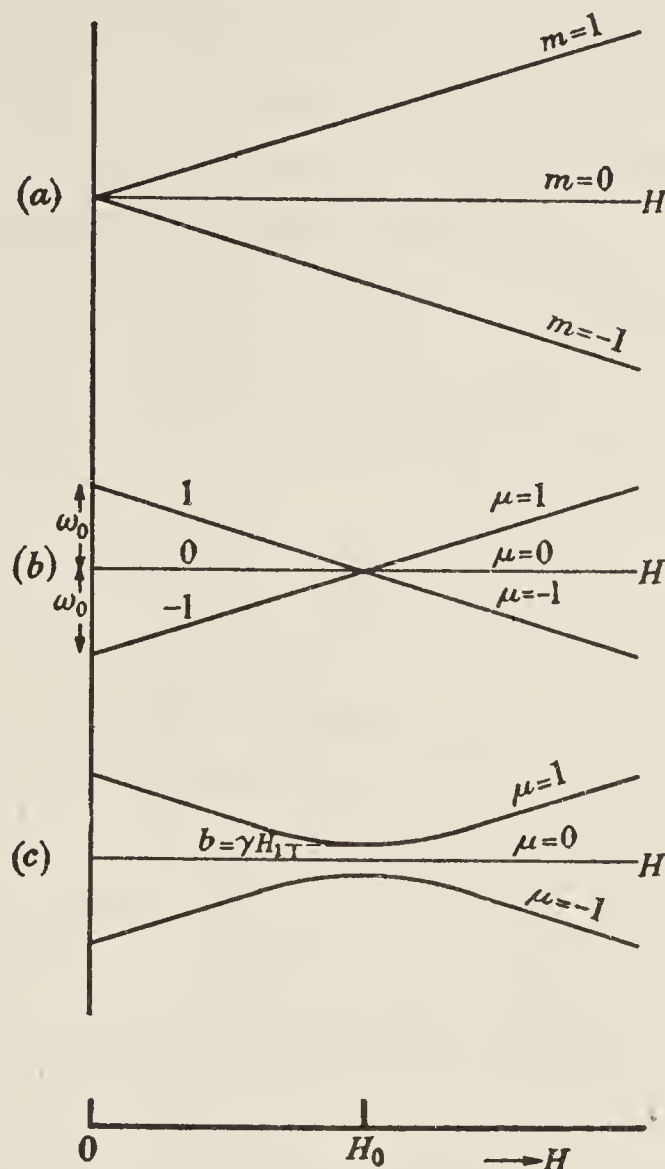


FIGURE 3. Precessional frequencies,  $f$ , as functions of  $H$ . (a) Laboratory co-ordinate system.  $f = m\gamma H$  about  $\mathbf{H}$ . (b) Rotating co-ordinate system. No radio-frequency field.  $f = \mu\gamma |H - H_0|$  about  $\mathbf{H}_{\text{eff}}$ . (c) Rotating co-ordinate system. Radio-frequency field applied.  $f = \mu\gamma [(H - H_0)^2 + H_1^2]^{\frac{1}{2}}$  about  $\mathbf{H}_{\text{eff}}$ .

The transformation was then made to a co-ordinate system rotating about  $Oz$  with angular velocity  $\omega_0$ , in which system the frequencies of the  $|m\rangle$  are decreased by  $m\omega_0$ . In anticipation of the subsequent addition of the field  $\mathbf{H}_1$ , it was found convenient to quantize with reference to an axis  $Oz'$ , parallel to the effective field in the rotating system. The quantum numbers  $\mu$  label the states with reference to  $Oz'$ . Before  $\mathbf{H}_1$  is added the effective field is always either parallel or anti-parallel to  $Oz$ , according as  $H$  is greater or less than  $\omega_0/\gamma$ . The state  $|\mu = 1\rangle$  always has a higher frequency than  $|\mu = 0\rangle$  or  $|\mu = -1\rangle$  and lies above them in figure 3 (b) for all values of  $H$ .

The field  $\mathbf{H}_1$  was then added. In the rotating system  $\mathbf{H}_1$  is steady, along  $Ox'$ . The effective field,  $[(\mathbf{H} - \omega_0/\gamma) + \mathbf{H}_1]$  now makes an angle  $\beta$  with  $Oz$ . The Larmor precessional frequencies,  $\mu p$ , about  $\mathbf{H}_{\text{eff}}$ , are shown in figure 3 (c).  $p$  is often termed the 'flipping frequency'.

Since the  $|\mu\rangle$  are linear superpositions of the  $|m\rangle$  each of the  $|m\rangle$  is fractionally associated with each level in figure 3 (c). Thus, in the return to the laboratory system,

when the frequency of each state  $|m\rangle$  is increased by  $m\omega_0$ , the diagram of figure 2 is obtained, in which the number of frequency levels is  $(2J+1)^2$ .

The thicknesses of the levels in figure 2 indicate the relative magnitudes of the coefficients of each frequency term in the expansion. The magnitudes used are those appropriate to  $n=0$ . While they give some representation of relative probabilities, they are neither probability amplitudes nor true probabilities. Within a given  $|m\rangle$ , the coefficients give relative probabilities for the three frequencies  $\mu p$ . The sum of these probabilities is the relative probability amplitude of the state  $|m\rangle$ .

Transitions induced by the rotating magnetic field must be interpreted on the diagram in the following manner: absorption or emission of a radio-frequency photon corresponds to a change of frequency by  $\omega_0$ , i.e. a jump between two parallel curves. In this transition  $m$  changes by  $\pm 1$ , but  $\mu$  remains unchanged (as it must, since it labels the eigenstates in the rotating co-ordinate system, in which the Hamiltonian is independent of time).

#### *Use of the diagram*

One can see immediately from the diagram that the Brossel-Bitter 'double resonance' curve is double-peaked. The thicknesses of the levels which represent the states  $|m = \pm 1\rangle$  are greatest in the region of  $H_0$ , but have their maxima, at two values of the field slightly higher and lower than  $H_0$ . As  $H_1$  is reduced the curves for  $\mu = \pm 1$  approach their asymptotes as in figure 3(b), and the positions of maximum thickness move closer to the centre. Not indicated in figure 2 is the natural width of the levels due to radiative decay. Thus, when  $H_1$  becomes small, the resolution of the double peak is lost in the natural width of the resonance. Figure 2 is drawn for a ratio  $H_1/H_0 = \frac{1}{4}$ , which is higher than is used for most experiments of the double resonance type, but corresponds to the conditions used in the experiments of Dodd *et al.* (1959).

Questions concerning the coherence between different states, and possibilities of light modulation, may also be answered by reference to the diagram. Let us suppose that the exciting light is steady, and of wide spectral range. In a Fourier expansion of the amplitude of the light vector, the phases of the components  $\mathbf{E}(k)$  will be random, corresponding to the random positions and motion of the radiating atoms in the source. Hence the optical perturbation will excite incoherently states which are at different levels in the frequency diagram (the word 'state' here is not used in its ordinary sense). The radio-frequency perturbation, however, links states of different  $m$  but the same  $\mu$ . Thus, if the optical perturbation excites  $(m, \mu) = (0, 0)$ , then the radio-frequency perturbation will establish coherence between  $(1, 0)$ ,  $(0, 0)$  and  $(-1, 0)$ , whatever the value of the field  $H$ . The frequency differences which are found between the coherent levels ( $\omega_0$  and  $2\omega_0$  in this case) are found as modulation frequencies in the fluorescent radiation. The depth of modulation will depend on those parameters ( $H$ ,  $H_1$ , etc.) which govern the relative 'weights' of the coherent states.

Light of the particular polarization which excited  $(0, 0)$  will excite  $(0, 1)$  and  $(0, -1)$  also, but since the frequencies associated with these states are different, they are excited by different components of the optical field, and therefore incoherent with



respect to the states  $\mu = 0$ . Frequency differences between incoherent levels do not appear in the modulation of the fluorescent radiation.

An important exception to the rule that levels of different  $\mu$  are incoherent occurs when such levels intersect, for then they may be excited by the same component of the optical field. In this case, provided the excitation has taken place from some common initial level, coherence obtains between the intersecting levels and all others of the same values of  $\mu$ . The consequences of this coherence were examined analytically in §5(iii). The diagram allows similar conclusions to be drawn more directly. Consider, for example, the relative positions of the levels when  $H \approx \frac{1}{2}H_0$ . Coherence obtains between  $(0, 1)$  and  $(1, -1)$  because of the intersection when they are both excited from the same ground level. Further, by virtue of the radio-frequency perturbation, all other levels which have  $\mu = 1$  or  $-1$  are coherent with the intersecting pair. Only the levels  $\mu = 0$  remain incoherent. The possible frequency differences between the coherent levels are  $0, \omega_0, 2\omega_0, 3\omega_0$ ; consequently the fluorescent light is modulated at these frequencies. The phenomenon is confined to the region of intersection since the coherence between  $(0, 1)$  and  $(1, -1)$  is lost as one moves away.

One can immediately see, from a study of figure 2, at what fields are to be found the resonances associated with intersections, and at what frequencies the light will be modulated. In addition to the intersections near  $\frac{1}{2}H_0$  which we have discussed, there exist intersections near  $\frac{3}{2}H_0$  with possibilities for modulation up to, but not exceeding the third harmonic, and further intersections near the fields  $0, 2H_0$  and  $3H_0$ . The possibilities for modulation here include the fourth harmonic.

The association of intersections in the frequency diagram with abnormal intensities in the fluorescent light relates this work with that of Hanle (1924, 1925) on the polarization of resonance radiation in low fields, and with that of Colegrove, Franken, Lewis & Sands (1959) on intensity changes in the region of intersecting energy levels. All these phenomena are completely described by equation (32), with  $\omega$  (i.e.  $H$ ) taking small positive and negative values in the neighbourhood of  $\omega = 0$ , and with  $H_1$  and  $\omega_0 = 0$ . It is to be noticed that the half-intensity widths of the resonances which are associated with intersecting levels both in modulated and in unmodulated light, are determined by the natural widths of the levels. This contrasts with the resonances which occur at  $H_0$  for which the half-intensity widths are determined by the magnitude of the radio-frequency field if that is sufficiently strong. These predictions are borne out by the experiments.

Finally, it is to be noticed that further possibilities for coherence arise if the exciting radiation is modulated or pulsed, for coherence then resides in the optical perturbation itself. The consequences of this can be deduced qualitatively from a frequency diagram such as figure 2 if a radio-frequency field (or other periodic perturbation of sharp frequency) is acting on the scattering material, or from an ordinary term diagram if there is no such field.

We have been stimulated in the development of these calculations by daily contact with the experimental work, most of which has been carried out by Dr M. J. Taylor. On the theoretical side, we are deeply grateful to Professor J. P. Barrat for allowing

us to study his work before publication, to Professor W. E. Lamb and Dr R. J. Blin-Stoyle for criticism of early drafts of this paper, and to a referee for his constructive suggestions, in particular for his suggestion of the use of the operator  $U$ . We owe to Professor Barrat the suggestion that resonances at fields other than  $H_0$  may be due to coherent excitation into states of different polarization.

## REFERENCES

- Bell, W. & Bloom, A. 1957 *Phys. Rev.* **107**, 1559.  
 Born, M. & Wolf, E. 1959 *Principles of optics*. London: Pergamon Press.  
 Brossel, J. & Bitter, F. 1952 *Phys. Rev.* **86**, 308.  
 Colegrove, F. D., Franken, P. A., Lewis, R. R. & Sands, R. H. 1959 *Phys. Rev. Lett.* **3**, 420.  
 Condon, E. U. & Shortley, G. H. 1951 *The theory of atomic spectra*. Cambridge University Press.  
 Dehmelt, H. G. 1957 *Phys. Rev.* **105**, 1924.  
 Dodd, J. N., Fox, W. N., Series, G. W. & Taylor, M. J. 1959 *Proc. Phys. Soc.* **74**, 789.  
 Hanle, W. 1924 *Z. Phys.* **30**, 93.  
 Hanle, W. 1925 *Egebn. exakt. Naturw.* **4**, 214.  
 Majorana, E. 1932 *Nuovo Cim.* **9**, 43.  
 Pryce, M. H. L. 1956 *Phys. Rev.* **77**, 136.  
 Rabi, I. I., Ramsey, N. F. & Schwinger, J. 1954 *Rev. Mod. Phys.* **26**, 167.  
 Ramsey, N. F. 1956 *Molecular beams*. Oxford University Press.  
 Rose, M. E. 1957 *Elementary theory of angular momentum*. New York: John Wiley and Sons, Inc.  
 Salwen, H. 1955 *Phys. Rev.* **99**, 1274.



Theory of modulation of light in a double resonance experiment

J.N. Dodd and G.W. Series. Proc.Roy.Soc. A 263, 353 (1961)

Errata

- pages 356, equations (7), (19) and (20). Insert minus sign  
358. before  $E_i(t)$ .
- page 360. line 16. Replace  $(t_0 + \tau)$  by  $(t_0 - \tau)$ .  
line 21. Replace  $(\Gamma^2 + x^2)^{\frac{1}{2}}$  by  $1/(\Gamma^2 + x^2)^{\frac{1}{2}}$ .
- page 361. line 10. Multiply by  $2\pi$  the two expressions in  
this line, and the expression (31) below.  
line 21. Replace  $8\pi$  by  $16\pi^2$  twice.  
equation (32). Replace 4 by  $8\pi$ .  
line 19. Replace  $\delta(k-k')$  by  $\delta(\tau)$ .
- page 363. line 9. Replace (1951, p.53) by (1951, p.63).  
equation (34). Insert  $\bar{+}$  on the right-hand side of  
the top equation.
- page 367. line 4. Replace  $(k_0 +)m\gamma H$  by  $(k_c + m\gamma H)$ .

Supplementary notes (May, 1965)

A. The argument which follows equation (27) on page 360 is not strictly valid. It purports to relate the 'instantaneous intensity,  $I(t)$  (equation (25), derived from (21)), to  $\langle \Phi(t_0, \tau) \rangle$  the average of the quadratic function  $E_i(t_0)E_i(t_0 - \tau)$  of the incident light. The conclusion, while not valid for  $I(t)$  itself, is nevertheless valid for  $\langle I(t) \rangle = \frac{1}{2T_0} \int_{t-T_0}^{t+T_0} I(s)ds$ , provided that  $\langle \Phi(t_0, \tau) \rangle$  is constant over time intervals of the order of  $T_0$ .  $\langle I(t) \rangle$  should replace  $I$  in equation (32).

B. Case (ii) at the bottom of page 360 has now been studied:  
 Aleksandrov, E.B. 1963, 64. *Optik i Spektrosk.* 14, 436; 17, 957.  
 Corney, A. and Series, G.W. 1964. *Proc.Phys.Soc.* 83, 207, 213, 331.  
 Dodd, J.N., Kaul, R.D. and Warrington, D.M. 1964. *Proc.Phys.Soc.* 84, 176.  
 Konstantinov, O.V. and Perel', V.I. 1963. *J.E.T.P.(USSR)* 45, 279.  
 Skalinski, T. and Rosinski, K. 1965. *Journ.App.Math.and Phys.* 16, 15.

C. For monochromatic light of frequency  $k \neq k'$ , equation (30) on page 361 becomes

$$\frac{8\pi R}{c} \left( \frac{1}{\Gamma + ix} \right) \left[ \frac{1}{\frac{1}{2}\Gamma + i(k-k')} + \frac{1}{\frac{1}{2}\Gamma - i(k-k'-x)} \right] \exp\{-i(m-m'-n+n')\omega_0 t\}$$



# The modulation of light in a double resonance experiment

BY J. N. DODD\*

*Department of Physics, University of Otago, Dunedin, New Zealand*

G. W. SERIES AND M. J. TAYLOR

*Clarendon Laboratory, University of Oxford*

*(Communicated by H. G. Kuhn, F.R.S.—Received 5 April 1962—*

*Revised 10 October 1962—Read 1 November 1962)*

This work is an experimental study of the modulation which has been found in resonance radiation when the fluorescing vapour is subjected to static and radio-frequency magnetic fields, as in the double resonance experiment of Brossel & Bitter. The particular example chosen for study in this work also was the resonance line  $\lambda 2537 \text{ \AA}$  of mercury. The experimental observations are compared with the predictions of a theoretical treatment which has already been published.

The phenomenon was studied under a variety of geometrical configurations. When the polarization of the exciting light allowed excitation to only one excited state (a component of a Zeeman multiplet), the depth of modulation was found to depend on the closeness to resonance of the frequency,  $\omega_0$ , of the radio-frequency field to the Larmor precessional frequency,  $\omega = \gamma H$ , in the static field  $H$ .

When the polarization of the exciting light allowed excitation to more than one component of the multiplet, resonance effects were found in the depth of modulation and in the mean intensity of the fluorescent light at fields where the applied frequency was equal, not to the Larmor frequency alone, but to combinations of the Larmor frequency with the nutational frequency. From a quantum-mechanical point of view, these new phenomena are related to the interference effects which are found in resonance fluorescence when there is degeneracy between excited states: in the present case the degeneracy is induced by the radio-frequency field.

The ease with which the geometrical conditions could be altered allowed the theory to be tested in considerable detail without quantitative assessment of the resonance line contours: nevertheless, a quantitative study was made of one particular feature. The predictions of the theory were confirmed at all points where they were tested.

## 1. INTRODUCTION

This experimental study of resonance fluorescence in mercury is a contribution to an understanding of the emission of light by free atoms. Unsophisticated descriptions of spontaneous emission are usually given in terms of transitions between stationary states of energy: the light emitted when an atom decays from the stationary state  $|j\rangle$  to the stationary state  $|i\rangle$  is supposed to be a quantum of electromagnetic field of frequency  $\nu_{ij} = (\epsilon_j - \epsilon_i)/h$ , where  $\epsilon_i$  and  $\epsilon_j$  are the energies of  $|i\rangle$  and  $|j\rangle$ . The probability of emission is found through correspondence with the classical theory of radiation by associating with the transition from  $|j\rangle$  to  $|i\rangle$  a virtual oscillator of moment  $\langle i | \mathbf{P} | j \rangle$ , where  $\mathbf{P}$  is an operator chosen to represent the particular type of radiation—usually electric dipole. In this simple model, all the virtual oscillators are independent because the stationary states are independent. Thus, the state  $|i\rangle$  may be reached from an initial state  $|k\rangle$  different from  $|j\rangle$ , but the phases of the radiations  $\nu_{ij}$  and  $\nu_{ik}$  are random. In an assembly of atoms radiating spontaneously, the phases of all such radiations are uncorrelated, as was

\* On leave at the Clarendon Laboratory, Oxford, 1959.



demonstrated in the experiments of Forrester, Gudmundsen & Johnson (1955). The exceedingly weak modulation which these authors detected in the radiation from a mercury lamp was just that which was to be expected from an assembly of independent oscillators.

We shall describe experiments in which the light from an assembly of radiating atoms is strongly modulated. The process of spontaneous emission may still be understood in terms of the foregoing model, except that the requirement of independence of the virtual oscillators must be abandoned, and the concept of 'superposition-state' invoked. For each atom, the 'initial state' of the process of radiation is no longer a stationary state of energy, but a superposition of such states. The time-dependent coefficients (probability amplitudes) of each constituent of the superposition state are periodic functions. These may differ in frequency, but the relative phases are perfectly definite, and depend on the experimental conditions—that is, on the way in which the 'initial state' is prepared. Hence the quantum of electromagnetic field—if the word 'quantum' is retained to describe the field emitted by one atom—is no longer characterized by a single frequency, but by a superposition of discrete frequencies in which the relative phases are determined by the experimental conditions, and are the same for all atoms in the assembly. The modulation of the light from the assembly is the manifestation of coherence between radiations from different stationary states of the atoms.

The experiments were carried out with the mercury resonance radiation  $\lambda 2537 \text{ \AA}$  ( $6^1S_0 - 6^3P_1$ ), a case chosen for its simplicity. The scattering atoms were subjected to a steady magnetic field  $\mathbf{H}$  and an oscillatory field  $\mathbf{H}_1$  at the radio-frequency  $\omega_0/2\pi$ , in the perpendicular plane. The only stationary states which one need consider in this case are the eigenstates  $|^1S_0; m = 0\rangle$  and  $|^3P_1; m = 0, \pm 1\rangle$  of the Hamiltonian function which represents the atom in the field  $\mathbf{H}$  alone. When  $\omega_0$  is in the neighbourhood of the Larmor precessional velocity of the atoms in the field  $\mathbf{H}$ , the oscillatory field constitutes a strong time-dependent perturbation, under which the state of the atom at any time (that which satisfies the Schrödinger equation of motion) may be written as a superposition of the four eigenstates. In this superposition state the relative phases of the probability amplitudes are related to the phase of the radio-frequency field. These relative phases determine the phase of modulation of the fluorescent light. Figure 1 illustrates the processes for the case when the exciting light is polarized so that the only allowed transition from the ground state is to the state  $|^3P_1; m = 0\rangle$ . The structure of the excited state is here oversimplified. A more complete representation is given in figure 2 of the theoretical paper by Dodd & Series (1961).

In support of the contention that correlation between radiations of different frequency resides in the light from each atom, it is particularly significant that modulation was easily detected at a frequency (about 10 Mc/s) orders of magnitude smaller than the spectral width of the fluorescent light (the completely unresolved superposition of the Doppler-broadened Zeeman components, individually of width about 1000 Mc/s, and collectively, inappreciably greater). For no modulation can exist in radiation which forms a spectral continuum unless the components are correlated: the modulation we have observed implies correlation between each



arbitrarily chosen spectral component and the components removed from it by the modulation frequencies. This correlation could not have existed between the radiations from different atoms since, in the attenuated vapour, the atoms were radiating independently. We must therefore seek the correlation within the radiation from each individual atom; that is to say, for each atom, the probability for the emission of light in a particular direction must have been time-dependent.

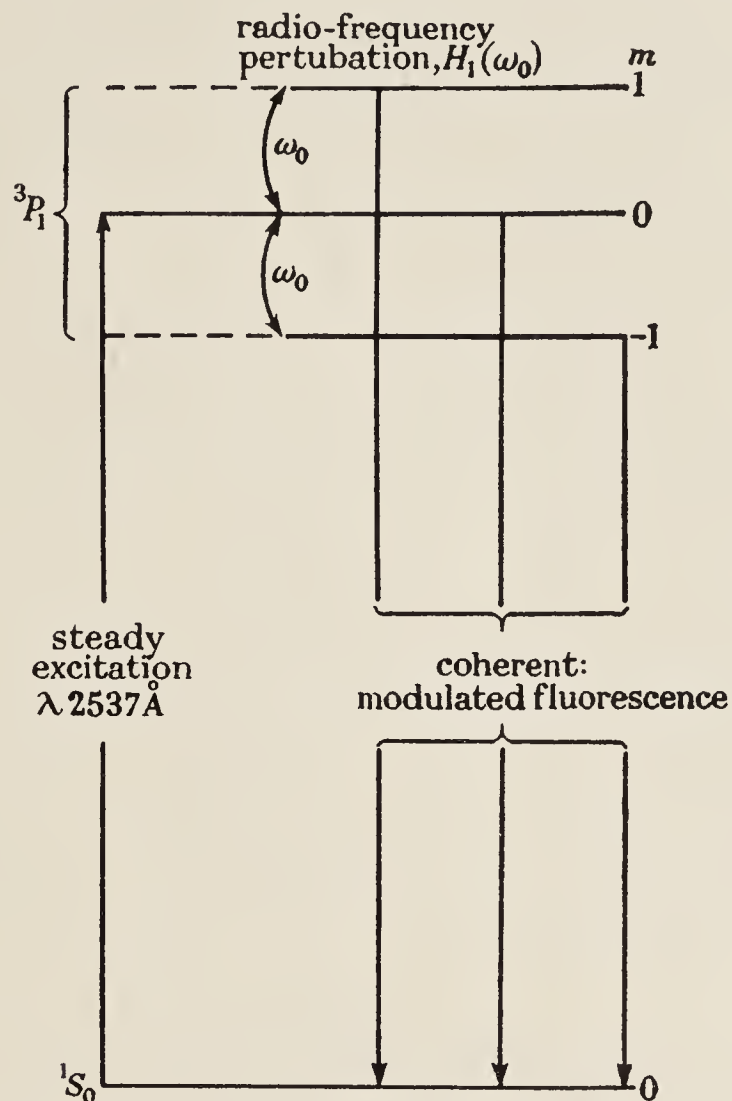


FIGURE 1. The stationary states and the perturbations.

It is convenient at this point to remark that the usual description of resonance fluorescence as the excitation of an atom from one stationary state of energy to another, followed at a later time by spontaneous decay, is an oversimplification. From the point of view adopted in this paper, it is, at first sight, untenable; for the irradiation of atoms with resonance radiation also constitutes a time-dependent perturbation under which the state of the atom is not one or other of a pair of mutually exclusive stationary states, but a superposition of them. The reason why it is legitimate to treat the optical perturbation differently from the radio-frequency perturbation is simply that the coherence time of the optical field is very much shorter than the lifetime of the excited states, and that of the radio-frequency field very much longer. The spectrum of the exciting field is that of a Doppler- or pressure-broadened spectral line, of half-intensity width of the order of 1000 Mc/s, and coherence time  $\tau_\Delta \sim 1/\Delta \sim 10^{-10}$  s. The lifetime of the excited state is  $\sim 10^{-7}$  s. Hence, in the atomic wave function, continuity of phase due to the irradiation is lost in a small fraction of a lifetime, and it is a good approximation to regard the optical excitation as instantaneous. The effect of a steady beam of radiation from

an ordinary light source is to induce uncorrelated excitations at a uniform rate. We have already made use of this approximation, and shall do so throughout the paper. On the other hand, the coherence time of the radio-frequency field is as long as the duration of the experiment, since the field is provided by a continuous wave oscillator. The phase of this field is a well-defined function of time which must be taken into account when the time-dependence of the fluorescent light is studied.

It will have been noticed that the system studied is exactly that studied by Brossel & Bitter in their 'double resonance' experiment (1952). It was, in fact, by reflecting on that experiment that we were led to look for modulation in the fluorescent light. Brossel and his colleagues (Guiochon, Blamont & Brossel 1956, 1957; Boutron, Barrat & Brossel 1957; Barrat 1959) had observed a narrowing of the double resonance line with increase of density of the scattering vapour. This they interpreted with the concept of 'coherent scattering'—a form of multiple scattering of resonance radiation in which phase information is passed from atom to atom via the light. This suggested to us that it might be possible to find phase information in the fluorescent light itself and not only in the secondary phenomena.

In § 2 we describe the apparatus. In § 3 we apply the theoretical results of Dodd & Series (1961) to the experimental situations explored in the present work. In § 4 we report the observations and compare them with the predictions of § 3. A brief account of a classical model is given in an appendix. In the actual course of events the theoretical and experimental work were undertaken together: sometimes one was in advance, sometimes the other. A preliminary publication was made when the main features of the phenomenon had been established (Dodd, Fox, Series & Taylor 1959).

## 2. THE EXPERIMENTAL ARRANGEMENT

### (i) *Disposition of apparatus*

Figure 2 (i) illustrates the arrangement which was usually used.

The resonance vessel was of strain-free silica in the shape of a Wood's horn; the diameter of the end-face was about 2 cm, and the length of the straight portion about 5 cm. The vessel contained natural mercury whose vapour pressure was stabilized by immersing the tip of the horn in ice.

The exciting radiation, 2537 Å, was provided by a commercial 'high-pressure' mercury lamp (125 W Osram from which the glass envelope had been cut off); run at about 250 mA d.c., and cooled by a gentle stream of air to reduce self-reversal. Rochon prisms of calcite, about 2 cm square end-face, were used as polarizers and, where necessary, as analyzers. These prisms allow a greater flux of light than Glazebrook prisms of the same aperture. (The second image produced by a calcite Rochon is strongly deviated and readily screened off.) A column of vapour about 1½ cm long near the end-face of the resonance vessel was illuminated. The fluorescent light was focused on to a photomultiplier; an E.M.I. 6255 with the four last stages connected together, for most of the work, and an RCA IP 28 when the modulation frequency was in excess of 40 Mc/s. The circuits for analysis of the photoelectric current will be described below.



The static magnetic field  $\mathbf{H}$  was provided by a Helmholtz pair of diameter about 24 cm. A range of field strength from 0 to 20 G was adequate. No great precision in the determination of its magnitude was aimed at, but since it was necessary to be certain of its direction at the lower end of the range, it was found desirable to compensate for the stray field, by means of auxiliary coils, to about 0.05 G.

It was desired to study the fluorescent light emitted in various directions relative to  $\mathbf{H}$ . A convenient arrangement was to fix the positions of light source, scattering vessel and photomultiplier so that the fluorescent and exciting beams were at right angles, and to provide for movement of the Helmholtz coils so that their axis always lay in the plane normal to the exciting beam.

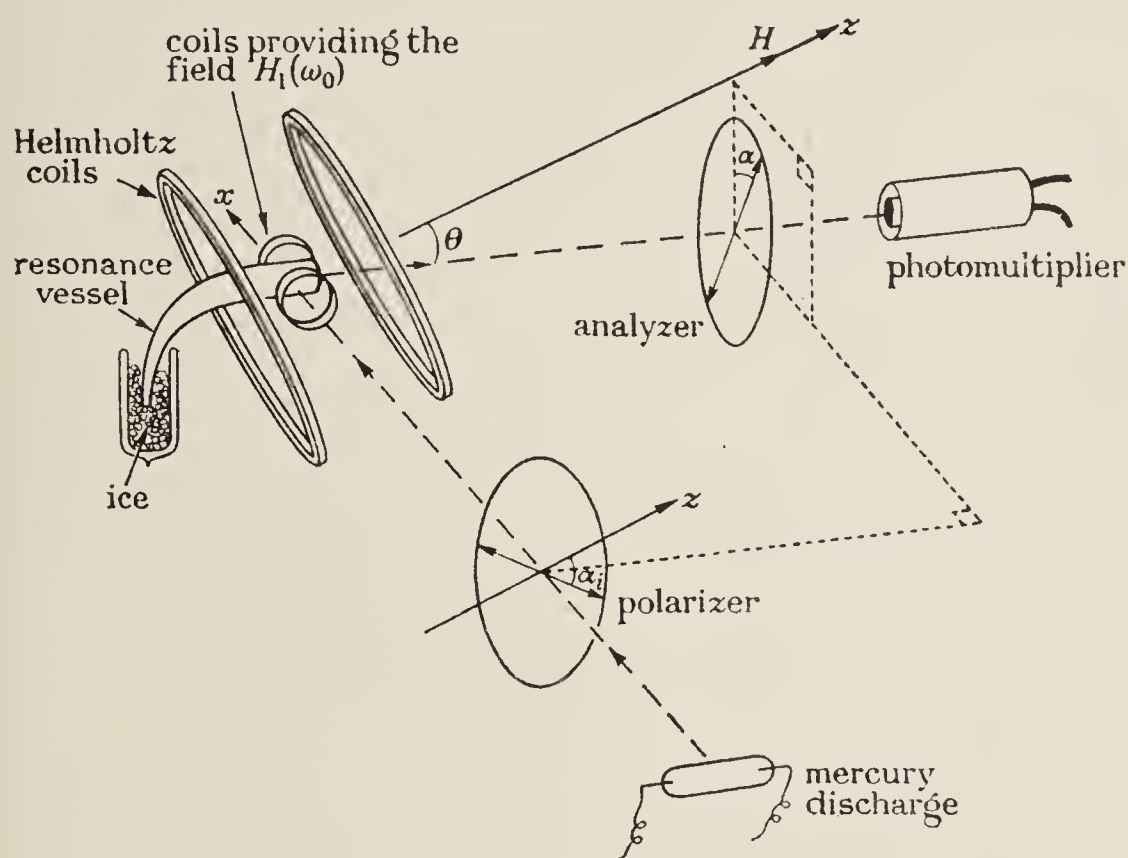


FIGURE 2(i)

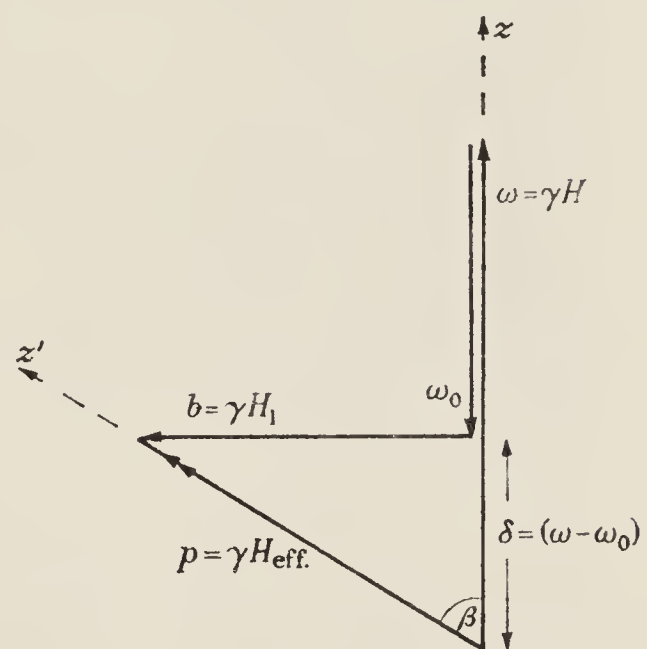


FIGURE 2(ii)

FIGURE 2. (i) Disposition of apparatus. (ii) The notation.

The co-ordinate system chosen to represent this arrangement is indicated in figure 2(i): the  $z$  axis is parallel to  $\mathbf{H}$  and the  $x$  axis parallel to the exciting beam. The fluorescent beam lies in the  $y$ - $z$  plane, making with the  $z$  axis an angle  $\theta$ . Of particular interest were the configurations  $\theta = 0, 55$  and  $90^\circ$ . The state of (linear) polarization of the beams incident on the mercury vapour and on the detector, respectively, is specified by the angles  $\alpha_i$  and  $\alpha$  which the electric vectors make with the  $x$ - $z$  and  $y$ - $z$  planes.

The radio-frequency was chosen to be considerably greater than the natural width of the energy levels ( $\sim 1$  Mc/s), yet not too high to make detection of the modulation difficult: the response of the photomultiplier set this upper limit. A frequency of 13.8 Mc/s was convenient, corresponding to a field  $H_0$  of about 6.65 G. A power oscillator at this frequency, driving a tuned circuit via a coupling loop, provided a field of amplitude up to 6 G in the coil which surrounded the scattering vessel. The requirement that the direction of this oscillatory field be always perpendicular to  $\mathbf{H}$  was met by fixing the coil with its axis parallel to the

incident light. This arrangement facilitated the enclosure of the tuned circuit in a metal shield to prevent excessive radiation of radio-frequency power, a point to which it was necessary to pay particular attention for reasons detailed below.

It is well known that when an oscillatory field is used to induce magnetic dipole transitions  $\Delta m = \pm 1$ , only one of the two rotating components is effective. We used an oscillatory field only for reasons of convenience. The effect of the counter-rotating component was taken into account in the quantitative work.

### (ii) *The experiments*

It was convenient, as in most paramagnetic resonance work, to maintain the radio-frequency constant, and to study the depth of modulation as a function of the steady field,  $H$ . It was anticipated that the amplitude of modulation of the fluorescent light would be greatest when the Larmor precessional frequency,  $\omega$  ( $= \gamma H$ ), of the excited state was equal to the applied radio-frequency,  $\omega_0$ . (When the word 'frequency' is used, we shall generally mean angular frequency.) In fact, the phenomenon turned out to be more complicated than this: resonance effects were discovered centred not only upon the field  $H_0 = \omega_0/\gamma$ , but also upon the fields  $0$ ,  $\frac{1}{2}H_0$ ,  $\frac{3}{2}H_0$  and  $2H_0$ . The resonance line shapes were not simple Lorentzians.

It was arranged to vary  $H$  at a uniform rate. A low-frequency modulation (about 220 c/s), of amplitude small compared with the resonance line-width, was applied to  $H$  in order to allow phase-sensitive detection. The photoelectric current was therefore doubly modulated: at a radio-frequency, and at a low audio-frequency. This signal was applied to a carefully screened unit comprising an amplifier tuned to the radio frequency, a detector, and a cathode follower. From this unit the output, now modulated only at the audio-frequency, was taken to the amplifying and rectifying system which constituted the phase-sensitive detector, the last stage of which drove a pen recorder.

The complete equipment recorded a plot of  $(\partial S/\partial H)$  against  $H$ , where  $S$  signifies the amplitudes of the radio-frequency signal. Typical records are seen in figures 5 to 7.

### (iii) *Phase control of the photoelectric signal: the effect of stray radiation*

The tuned detector was sensitive, not only to the photoelectric signal, but also to radiation from the radio-frequency oscillator and coupling loop. It was found useful to allow some of this radiation to penetrate the screening, and hence to provide a reference signal against which the phase of the photoelectric signal could be ascertained. Variation of phase of the latter relative to that of the oscillator could be achieved by slight mis-tuning of the resonant circuit round the absorption cell.

Let the photoelectric signal at frequency  $\omega_0$  be written (see equation (2) § 3)

$$V_B \cos \omega_0 t + V_C \sin \omega_0 t,$$

and the signal induced by the radiation

$$V_R \cos (\omega_0 t - \epsilon),$$



where the phase difference  $\epsilon$  is at our disposal. Clearly, if  $\epsilon = 0$ , and if  $V_R \gg V_B$  and  $V_C$ , the net amplitude is very nearly  $(V_R + V_B)$ . Only the changes

$$\partial(V_R + V_B)/\partial H = \partial(V_B)/\partial H$$

are recorded. The equipment is now sensitive to  $V_B$  both in magnitude and sign, but not to  $V_C$ . Similarly, by choosing  $\epsilon = \frac{1}{2}\pi$ ,  $V_C$  may be studied independently of  $V_B$ .

This rather primitive procedure for control of the phase was in the early work accidental rather than deliberate. It was not obvious at the outset of the experiments that the frequency of the photoelectric signal would be identical with that of the oscillator. When the early tracings had been interpreted, it was decided that this simple technique was adequate for qualitative display.

#### (iv) *Spurious signals: the effect of noise*

The mean intensity of the fluorescent light was shown by Brossel & Bitter to be a resonance function of  $H$ , as represented by the term  $A$  in equation (2), and in figure 3. The photoelectric shot noise is therefore a function of  $H$ , and contributes to the recorded signal to an extent determined by the bandwidth of the radio-frequency amplifier. The effect was minimized, not only by improving the amplifier, but also by choosing a geometrical configuration in which the mean intensity of the light is independent of the field, namely, when the direction of the fluorescent light makes an angle  $\theta = \tan^{-1} \sqrt{2}$  with  $\mathbf{H}$ . The modulation is not independent of field in this direction: on the contrary, the arrangement is a particularly favourable one, and was generally used except when the object of study was the dependence of the modulation on the angle of emission.

#### (v) *Observation of the mean intensity of the light*

It was clearly a matter of interest to observe the mean intensity under various conditions. For purposes of display it was sufficient to develop a voltage from the photoelectric current through a megohm resistor, and to apply this signal directly to an oscilloscope with broad-band, low-frequency amplification. Typical displays are seen in figure 8, where, in all cases, the abscissa is proportional to the field  $H$ .

The changes of intensity in the region  $H = H_0$  found by Brossel & Bitter were observed, but not closely studied. In the region near  $H = \frac{1}{2}H_0$ , however, both the mean intensity of the light and the amplitude of modulation showed an unexpected and particularly interesting dependence on magnetic field when the exciting light was obliquely polarized. A quantitative study was made of these effects in the mean intensity. For this investigation, the method of low-frequency modulation, followed by phase-sensitive detection and recording, was used.

### 3. THEORETICAL PREDICTIONS

Quantum-mechanical calculations leading to explicit expressions for  $I(t)$ , the intensity of the fluorescent light, as a function of time, have been made by Dodd & Series (1961) in a paper we shall refer to as D. & S. and independently by Barrat (1961), with results which are in complete agreement. We shall use the notation and formulae of D. & S.

The calculations are for a single scattering process, but for reasons which are explained later (§ 4, case 1 (a)), it is believed that they should correspond closely to the results of the present experiments, in which some multiple scattering was certainly taking place. The expression for the intensity of the fluorescent light is, in its most general form (D. & S., equation (32)).

$$I = I_0 \sum_{\substack{m, \mu, n \\ m', \mu', n'}} \mathcal{F}_{nn'} \langle m | \mu \rangle \langle \mu | n \rangle \langle n' | \mu' \rangle \langle \mu' | m' \rangle \mathcal{G}_{mm'} \frac{\Gamma}{\Gamma + ix} \exp\{-i(m - m' - n + n') \omega_0 t\} \quad (1)$$

in which  $m, \mu, n, m', \mu', n'$  take the values  $-J, -J + 1, \dots, +J$ .

$$\mathcal{F}_{nn'} = F_n F_{n'}^* = \langle n | \mathbf{e}_i^0 \cdot \mathbf{P} | g \rangle \langle g | \mathbf{e}_i^0 \cdot \mathbf{P} | n' \rangle$$

and

$$\mathcal{G}_{mm'} = G_m^* G_{m'} = \langle g | \mathbf{e}^0 \cdot \mathbf{P} | m \rangle \langle m' | \mathbf{e}^0 \cdot \mathbf{P} | g \rangle$$

refer to excitation by, and the emission of, light polarized with the electric vector parallel to the unit vectors  $\mathbf{e}_i^0$  and  $\mathbf{e}^0$ , respectively.  $\mathbf{P}$  is the electric dipole operator;  $|g\rangle$  is the ground state.  $\mathcal{F}$  and  $\mathcal{G}$  may be generalized to light of other polarizations (D. & S., p. 362).  $\langle m | \mu \rangle = \mathcal{D}^J(0, \beta, 0)_{m, \mu}$ , etc., are matrix elements which correspond to a rotation of the  $z$  axis about  $Oy$  by an angle  $\beta$ .  $\Gamma$  is the decay constant of the excited state.

$$x \text{ is the frequency } (n - n') \omega_0 + (\mu - \mu') p,$$

where  $p = (\delta^2 + b^2)^{\frac{1}{2}}$ ,  $b = \gamma H$ ,  $\delta = (\omega - \omega_0)$  and  $\omega = \gamma H$ .

The relations between  $p, b, \delta, \omega, \omega_0$  and  $\beta$  are shown geometrically in figure 2 (ii).

#### (i) Conditions for coherence

The right-hand side of equation (1) is obtained by taking the modulus squared of an expression which represents the (complex) field of the emitted light,  $\mathbf{E}$ . This expression is the sum of a number of periodic terms for each of which the frequency depends not only on the quantum number  $m$ , which labels the energy eigenstates for the process of emission of light, but also on  $n$ , which labels them for the process of excitation, and on  $\mu$ , which labels them with respect to the axis  $z'$  in the rotating co-ordinate system (figure 2 (ii); see also D. & S., p. 358). These different labels are introduced because it is necessary to take products of different combinations of the states. For the same reason,  $m', \mu'$ , and  $n'$  are introduced in calculating the conjugate complex field. In taking the modulus squared of  $\mathbf{E}$  to find the intensity of the light, terms for which  $m, \mu$  and  $n$  are identical with  $m', \mu'$  and  $n'$ , respectively, give the contribution of the separate components of  $\mathbf{E}$ , whereas the cross-terms represent the possibilities for interference. The factors  $\Gamma/(\Gamma + ix)$  are quantitative measures of the degree of coherence: a particular term in (1) is significant or negligible according as  $x$  (defined above) is much smaller than, or much greater than  $\Gamma$ .

#### (ii) The factors of equation (1)

Apart from the factors  $\Gamma/(\Gamma + ix)$ , equation (1) contains the essential elements of a double resonance experiment in an easily recognizable form:

(a) The factors  $\mathcal{F}_{nn'}$  are determined by the direction and polarization of the exciting light beam. They form an 'excitation matrix'.



(b) The products  $\langle m|\mu\rangle\langle\mu|n\rangle$  and  $\langle n'|\mu'\rangle\langle\mu'|m'\rangle$  describe the effectiveness of the perturbing field  $H_1$  in mixing the states. The  $\langle m|\mu\rangle$ , etc., are functions of  $H_1$  and  $H$ , and show resonance behaviour in the region  $H = H_0$ . Together with the  $\mathcal{F}_{nn'}$ , they determine the probability amplitudes of the states  $|m\rangle$  and their conjugates at the moment of emission.

(c) The factors  $\mathcal{G}_{mm'}$  are determined by the direction in which the fluorescent light is observed, and by the orientation of an analyzer, if one is used. They form an 'emission matrix'.

(d) Finally, the exponential factors describe the modulation of the fluorescent light. The terms occur in conjugate pairs, leading to real sine or cosine functions of time. As expected, modulation is predicted at the frequency  $\omega_0$  and at certain integral multiples.

### (iii) Distinguishable cases

As we have mentioned, a quantitative measure of the degree of coherence is contained in the factors  $\Gamma/(\Gamma + ix)$ . Coherence between the components  $(n, \mu, m)$  and  $(n', \mu', m')$  of the field is significant if  $x = (n - n')\omega_0 + (\mu - \mu')p \leq \Gamma$ . This condition may be realized in a number of ways which are distinguishable, both in principle, and by the different geometrical configurations suitable for their study.

*Case 1.* In this case, the direction and polarization of the incident light are so chosen that the atoms are excited to a pure eigenstate rather than to a superposition-state. The analytical expression of this is  $n = n'$ , i.e. we are dealing with the diagonal elements only of the excitation matrix. We must, however, allow all combinations of  $m$  and  $m'$  in the rotation matrices, and hence also in the emission matrix, to describe the superposition state formed by the radio-frequency perturbation. Among the terms so specified are those in which  $\mu = \mu'$ . These represent complete coherence between the components  $(n, \mu, m)$  and  $(n', \mu', m')$ , since a consequence of  $n = n'$  and  $\mu = \mu'$  is  $x = 0$ . We notice that the factor  $\Gamma/(\Gamma + ix)$  is now independent of  $H$ . The resonances observed under the conditions of case 1 correspond to the resonance behaviour of the rotation matrix elements  $\langle m|\mu\rangle$ ,  $\langle\mu|n\rangle$ , etc. This occurs only at  $H = H_0$ , the field at which the Larmor precessional frequency matches the applied frequency.

The condition  $\mu = \mu'$  is simply the analytical expression of the coherence induced by the radio-frequency field, and corresponds to the fact that states labelled  $|\mu\rangle$  are eigenstates of the *complete* Hamiltonian (that is, including the radio-frequency perturbation) in the rotating co-ordinate system (D. & S., pp. 358, 367).

The phenomena studied under case 1 are the simplest of those we have investigated. They allow a particularly straightforward interpretation in terms of the classical model (see appendix).

*Case 2.* The direction and polarization of the incident light are so chosen in this case that the process of excitation itself raises atoms to a superposition state, that is, we have to consider terms in the excitation matrix for which  $n \neq n'$ . As before, so now also we must allow all combinations of  $m$  and  $m'$ . Although  $n \neq n'$ , it is still possible to satisfy  $x \leq \Gamma$ , but only if  $\mu \neq \mu'$ , and then only for particular values of  $p$ . The condition  $\mu \neq \mu'$  indicates that these terms do not represent coherence in the sense of case 1. Rather, we have now a consequence of degeneracy between the

frequencies of different components of the atomic wave function. This occurs only in the neighbourhood of particular values of  $H$  (since  $p$  is a function of  $H$ ). The coherence factor passes through resonance as  $H$  is varied, while the rotation matrix elements are changing monotonically. In the frequency diagram (D. & S., p. 366) the conditions are met where different levels intersect. It is worth noticing in particular that resonance phenomena under this heading occur at fields *other* than that which corresponds to the Larmor precessional frequency.

*Case 3.* In what has gone before we have supposed that  $\omega_0 \gg \Gamma$ , which was indeed true for the experiments described in this paper. We mention, for completeness, the case  $\omega_0 \ll \Gamma$ , for this condition, together with the condition  $\mu = \mu'$ , is sufficient to ensure that  $x \ll \Gamma$  for all  $m, m', n$  and  $n'$ . This means that if  $\omega_0$  is sufficiently small, new interference phenomena may appear in experimental arrangements which exclude the phenomena of cases 1 and 2. Experiments to demonstrate this condition have been carried out by Mr B. P. Kibble, and will be reported in a future communication (Kibble & Series 1963).

(iv) *Detailed calculations for particular cases*

*Case 1. Excitation to a pure state*

We must refer back to the analytical expression (1) to obtain the details of the amplitude of modulation. We treat the case when all elements of the excitation matrix vanish except  $\mathcal{F}_{00}$ . This condition is realized experimentally by using light plane polarized with the electric vector parallel to  $\mathbf{H}$ . Of the terms in (1) which do not vanish, those for which  $m = m'$  sum to give the expression obtained by Brossel & Bitter (1952) for the mean intensity of the light. The only possibilities for modulation are  $|m - m'| = 1$  or 2. There are 27 terms which represent the mean intensity, 36 which represent modulation at  $\omega_0$ , and 18 at  $2\omega_0$ . The following expression is obtained for the intensity of fluorescent light in the direction  $(\theta, \phi)$ :

$$\begin{aligned} I_{00} = I^0 & [\sin^2 \theta + (\cos^2 \theta - \tfrac{1}{2} \sin^2 \theta) 2A \\ & - \sin \theta \cos \theta \{B \cos (\omega_0 t - \phi) + C \sin (\omega_0 t - \phi)\} \\ & - \sin^2 \theta \{D \cos (2\omega_0 t - 2\phi) + E \sin (2\omega_0 t - 2\phi)\}], \end{aligned} \quad (2)$$

in which

$$A = \frac{b^2(4\delta^2 + b^2 + \Gamma^2)}{(\delta^2 + b^2 + \Gamma^2)(4\delta^2 + 4b^2 + \Gamma^2)},$$

$$B = \frac{2b\delta(4\delta^2 - 2b^2 + \Gamma^2)}{(\delta^2 + b^2 + \Gamma^2)(4\delta^2 + 4b^2 + \Gamma^2)},$$

$$C = \frac{2b\Gamma(4\delta^2 + b^2 + \Gamma^2)}{(\delta^2 + b^2 + \Gamma^2)(4\delta^2 + 4b^2 + \Gamma^2)},$$

$$D = \frac{b^2(2\delta^2 - b^2 - \Gamma^2)}{(\delta^2 + b^2 + \Gamma^2)(4\delta^2 + 4b^2 + \Gamma^2)},$$

$$E = \frac{3b^2\Gamma\delta}{(\delta^2 + b^2 + \Gamma^2)(4\delta^2 + 4b^2 + \Gamma^2)}.$$



$I^0$  is a constant.  $A, B, C, D$  and  $E$ , are functions of  $\delta$  (and therefore of  $H$ ), which are plotted for particular values of  $b/\Gamma$ , in figure 3. They all show resonance behaviour about  $\delta = 0$  ( $H = H_0$ ).

When the fluorescent light has passed through an analyzer which passes the electric vector at angle  $\alpha$  (figure 2), the expression becomes

$$I_{00}^\alpha = I^0[(\cos^2 \alpha \cos^2 \theta + \sin^2 \alpha) A + (\cos^2 \alpha \sin^2 \theta) (1 - 2A) - \cos \alpha \sin \theta (\cos^2 \alpha \cos^2 \theta + \sin^2 \alpha)^{\frac{1}{2}} \{B \cos(\omega_0 t - \phi - \psi) + C \sin(\omega_0 t - \phi - \psi)\} + (\cos^2 \alpha \cos^2 \theta + \sin^2 \alpha) \{D \cos(2\omega_0 t - 2\phi - \chi) + E \sin(2\omega_0 t - 2\phi - \chi)\}], \quad (3)$$

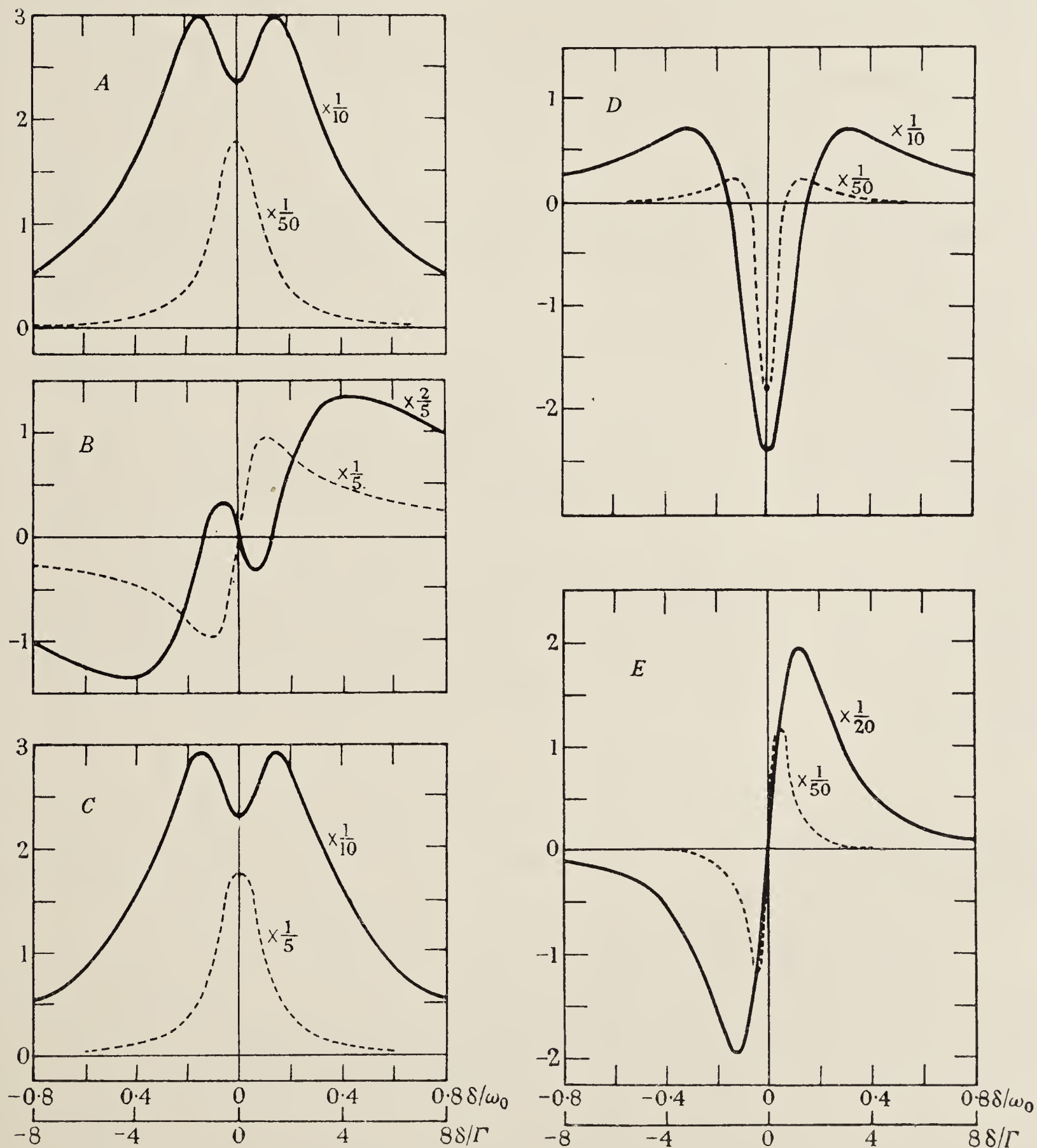


FIGURE 3. The functions  $A, B, C, D$  and  $E$  plotted for  $b/\Gamma = 2.0$  (full lines) and  $0.2$  (broken lines). The values  $\omega_0/2\pi = 13.8$  Mc/s;  $b/\omega_0 = 0.2$  and  $0.02$ ;  $\Gamma = 1.35$  Mc/s ( $\tau = 1.18 \times 10^{-7}$  s) were used on a computer.

where 
$$\tan \psi = \frac{\tan \alpha}{\cos \theta}; \quad \tan \chi = \frac{2 \sin \alpha \cos \alpha \cos \theta}{\cos^2 \alpha \cos^2 \theta - \sin^2 \alpha}$$

Modulation is now predicted for certain values of  $\theta$  where before there was none, but the dependence on  $H$  is exactly as before.

The following features of the above expressions were tested by experiment (§ 4, case 1):

- (i) The form of the curves  $A, B, C, D$  and  $E$  as functions of  $H$ .
- (ii) The dependence on  $\theta$ .
- (iii) The dependence on  $\alpha$ .
- (iv) The ratio  $B/A$ .

### Case 2. Mixed excitation

*General remarks.* The more general case, that some of the off-diagonal elements of the excitation matrix do not vanish, is realized by polarizing the incident light in any direction other than parallel to  $\mathbf{H}$ . To describe this situation we use the term 'mixed excitation'.

With the restriction  $n = n'$  lifted, we find in equation (1) non-vanishing terms with modulation up to  $4\omega_0$ , having resonances in those regions of  $H$  which satisfy the condition  $x = 0$ .  $H = H_0$  does not satisfy this condition.

*Particular examples:* (a) *Resonances at  $\frac{1}{2}H_0$  and  $\frac{3}{2}H_0$ .* The effects at  $H \approx \frac{1}{2}H_0$  and  $\frac{3}{2}H_0$  were studied experimentally in considerable detail. Accordingly, we work out the relevant terms of equation (1). In order to select these terms we could use the analytical condition  $x_{\text{res.}} = (\mu - \mu') p_{\text{res.}} + (n - n') \omega_0 = 0$ , where  $p_{\text{res.}}$  is a value of  $p$  near  $\frac{1}{2}H_0$  or  $\frac{3}{2}H_0$ , to determine which values of  $\mu, \mu', n, n'$  need be considered, but it is easier to make use of the frequency diagram (D. & S., p. 366: the labels  $m, \mu$ , on the right of figure 2 are to be replaced by  $n, \mu$ , when the process of excitation is under discussion). The levels which intersect at the fields we are interested in are described by

$$(n, \mu), (n', \mu') = (0, 1), (1, -1) \quad \text{and} \quad (0, -1), (-1, 1),$$

respectively. These levels are coherent with all others of the same values of  $\mu$  and  $\mu'$ . We thus pick out the terms

$n$	$n'$	$\mu$	$\mu'$	}	
0	1	1	-1		
1	0	-1	1		
0	-1	-1	1		
-1	0	1	-1		

taken with all possible combinations of  $m$  and  $m'$ .

In this way we select 36 terms from the total of 729. For these 36, the condition  $x_{\text{res.}} = 2p_{\text{res.}} - \omega_0 = 0$  is satisfied near  $H = \frac{1}{2}H_0$  and  $\frac{3}{2}H_0$ . These terms reduce to the



following expressions in the particular case when the light is incident along the  $x$  axis; it is supposed that no analyzer is used:

$$I(\alpha; \theta, \phi) = \frac{I^0 \sin \alpha_i \cos \alpha_i}{2p^4 \Omega^2} \left[ \begin{aligned} & -\sin \theta \cos \theta \Gamma b^2 (p - \delta)^2 \{ \Gamma \sin \phi + (2p - \omega_0) \cos \phi \} \quad (a) \\ & - (\cos^2 \theta - \tfrac{1}{2} \sin^2 \theta) \Gamma b^3 (p - \delta) \{ \Gamma \sin \omega_0 t + (2p - \omega_0) \cos \omega_0 t \} \quad (b) \\ & + \tfrac{1}{4} \sin^2 \theta \Gamma b (p - \delta)^3 \{ \Gamma \sin (\omega_0 t + 2\phi) - (2p - \omega_0) \cos (\omega_0 t + 2\phi) \} \quad (c) \\ & + \sin \theta \cos \theta \Gamma b^4 \{ \Gamma \sin (2\omega_0 t - \phi) + (2p - \omega_0) \cos (2\omega_0 t - \phi) \} \quad (d) \\ & - \tfrac{1}{4} \sin^2 \theta \Gamma b^3 (p + \delta) \{ \Gamma \sin (3\omega_0 t - 2\phi) + (2p - \omega_0) \cos (3\omega_0 t - 2\phi) \} \quad (e) \end{aligned} \right] \quad (4)$$

where  $\Omega^2 = \Gamma^2 + (2p - \omega_0)^2$ .

We notice the following features of these expressions:

(i) The occurrence of the denominator  $\Omega^2$  in each of them, as a consequence of the criterion for the selection of terms. By virtue of this denominator, each term shows resonance behaviour when  $2p = \omega_0$ . The value of  $p = p_{\text{res.}}$  so determined yields the condition for resonance  $H_{\text{res.}} = H_0 \pm \frac{1}{2} H_0 (1 - 4H_1^2/H_0^2)^{\frac{1}{2}}$ . As expected,  $H_{\text{res.}}$  tends to  $\frac{1}{2} H_0$  or  $\frac{3}{2} H_0$  when  $H_1/H_0$  is small, but as  $H_1$  increases the resonance values of  $H$  move towards  $H_0$  until, when  $H_1$  exceeds  $\frac{1}{2} H_0$ , no real solution of  $2p = \omega_0$  exists. The two resonances merge into one whose intensity thereafter decreases. These results may be obtained from a study of the movement of levels in the frequency diagram. As  $H_1$  increases, the curves  $\mu = \pm 1$  become flatter, and the points of intersection move towards  $H = H_0$  until, when  $H_1 = \frac{1}{2} H_0$ , the levels  $(0, 1)$ ,  $(1, -1)$  and  $(0, -1)$ ,  $(-1, 1)$  are tangential to one another at the field  $H_0$ . Thereafter they draw apart, and the intensity of the single resonance that remains, being determined by the amount of overlap of the radiation-broadened levels, rapidly decreases.

(ii) The further role of the denominator  $\Omega^2$  in determining, subject to a small distortion mentioned below, the half-intensity widths of the resonances,  $2\Gamma$  in terms of frequency. Because of the curvature of the levels, however, the widths, in units of magnetic field, increase with  $H_1$ .

(iii) The frequencies of modulation. These are 0,  $\omega_0$ ,  $2\omega_0$  and  $3\omega_0$ , as expected.

(iv) The dependence on  $\alpha_i$ , the angle of polarization of the incident light. All the terms are zero if  $\alpha_i = 0$  or  $\pm 90^\circ$ , and are greatest when  $\alpha_i = \pm 45^\circ$ .

(v) The occurrence of a term proportional to  $\Gamma$  (Lorentz-type function) and a term proportional to  $(2p - \omega_0)$  (dispersion-type function) for each frequency of modulation (including 0).

(vi) The effect of the factors  $p^{-4}$  and some power of  $(p \pm \delta)$  in distorting the profiles of the resonance curves, in so far as both  $p$  and  $\delta$  are functions of  $H$ .

(vii) The effect of  $(p \pm \delta)$  to some power on the relative intensities of the two resonances within a given term. For  $p$  is, by definition, always a positive quantity, and  $\delta$  changes sign between  $\frac{1}{2} H_0$  and  $\frac{3}{2} H_0$ , so that  $(p \pm \delta)$  has different values in these two regions.

The relative intensities of the resonances when  $b \ll \omega_0$  are seen in the table below which shows the maxima of the Lorentzian terms (a) to (e) at the two fields.  $p_{\text{res.}}$  has been expressed in terms of  $\omega_0$  and  $b$ . Geometrical factors, and a common factor 8

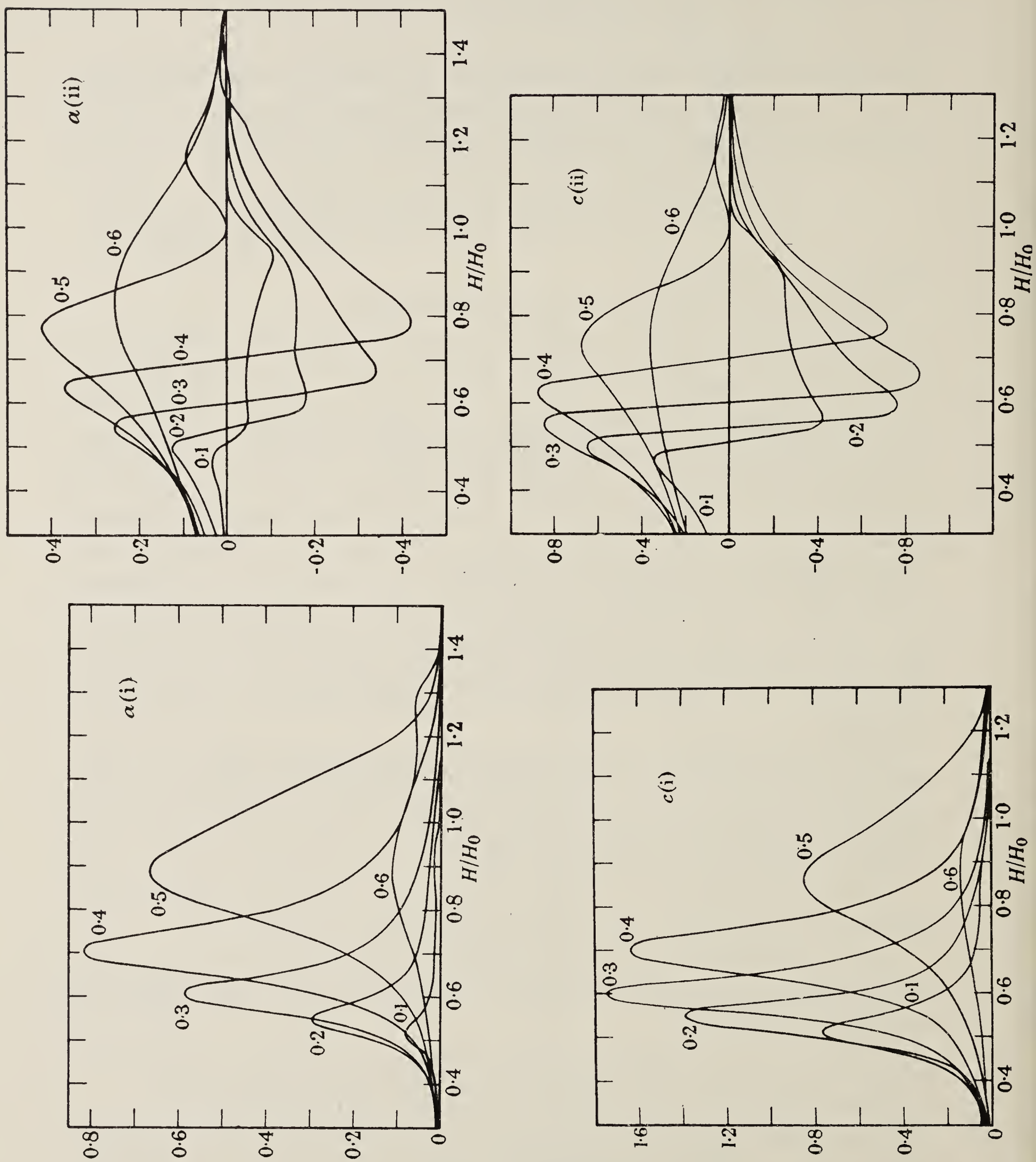


FIGURE 4. For legend see foot of facing page.



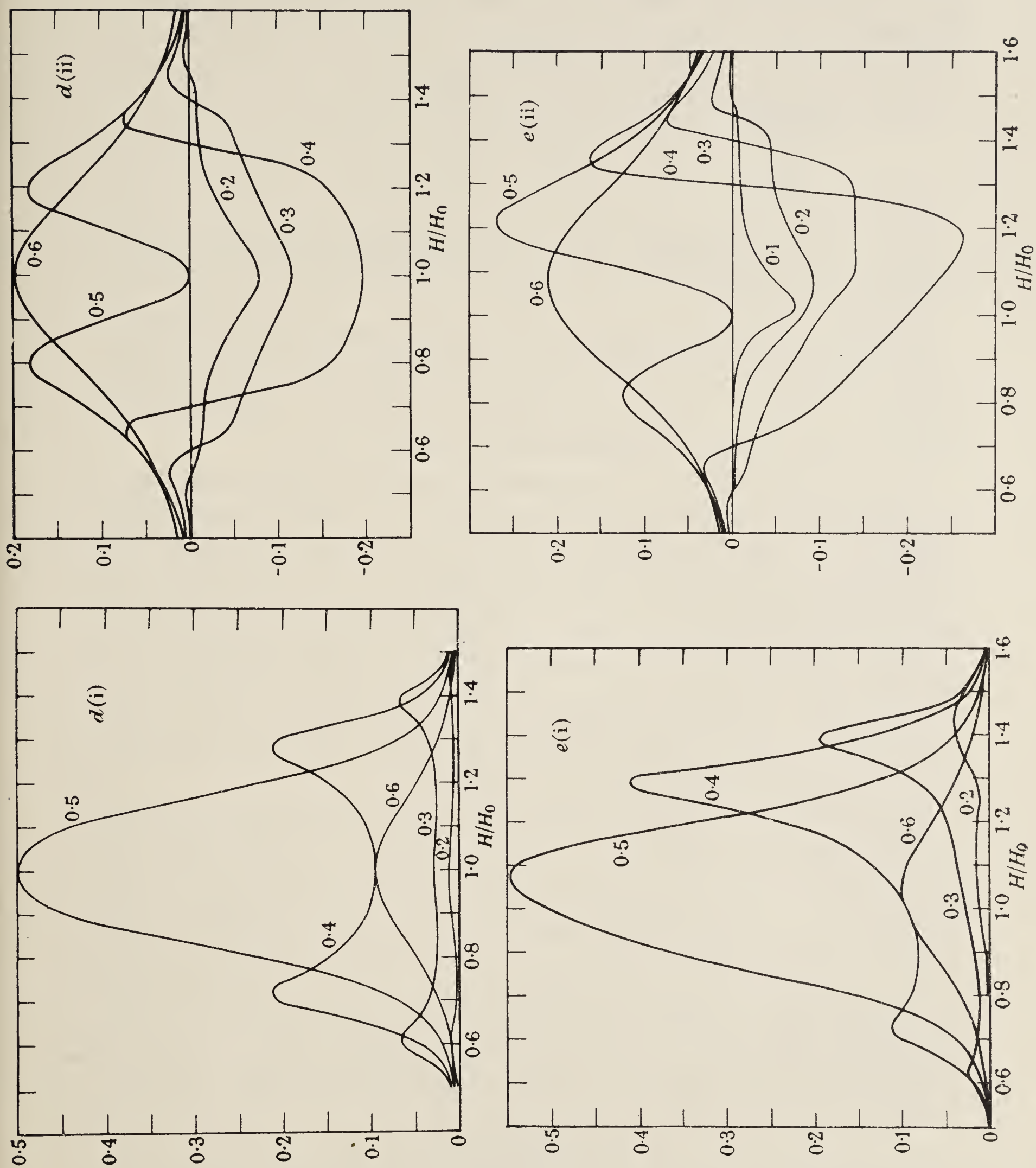


FIGURE 4. Mixed excitation: the coefficients of the sine terms ( $a(i)$  to  $e(i)$ ) and of the cosine terms ( $a(ii)$  to  $e(ii)$ ) of equation (4). (Curves for  $b(i)$  and  $(ii)$  are obtained by reflecting  $e(i)$  and  $(ii)$  in the line  $H = H_0$ .) In each case the product of the angular factors has been set equal to unity. Ordinates are in units of  $I/I_0$ . The parameter which labels the curves is the value of  $b/\omega_0$ .

have been omitted. The maximum values are all proportional to some power of  $(b/\omega_0) = z$ .

TABLE 1

position of resonance	term				
	(a)	(b)	(c)	(d)	(e)
$\frac{1}{2}H_0$	$z^2$	$z^3$	$z$	$z^4$	$z^5$
$\frac{3}{2}H_0$	$z^6$	$z^5$	$z^7$	$z^4$	$z^3$

Most of the features to which we have drawn attention are exemplified in figure 4, which represents the terms of equation (4), and are vindicated by the experimental work reported in § 4(ii).

*Particular examples:* (b) *Resonances near  $H = 0$ .* By using the frequency diagram, or by using the analytical condition  $x_{\text{res.}} = (\mu - \mu')p_{\text{res.}} + (n - n')\omega_0 = 0$ , we discover that resonances are also to be expected in the regions  $H = -H_0, 0, 2H_0, 3H_0$ . Of these, we concern ourselves for the moment only with the region  $H = 0$ . Coherence effects at the other fields are expected to be very weak.

The properties of mercury resonance fluorescence in the region  $H = 0$  but without the radio-frequency field, were studied by Hanle (1924, 1925), who found strong changes in the degree of polarization as  $H$  was increased from zero to the field at which the Zeeman splitting became comparable with the natural width of the energy levels. Fermi & Rasetti (1925), using an oscillatory field of variable amplitude, but no steady field, found that the polarization depended strongly on the relative magnitudes of the precessional frequency,  $\gamma H_1$ , and the frequency of oscillation,  $\omega_0$ . Our equations should quantitatively describe the first effect, but not the second. For Hanle's experiment, the frequency diagram reduces to the normal term diagram, and the Hanle effect appears as a result of the coalescence at  $H = 0$  of the three energy levels  $m = 1, 0$ , and  $-1$ .

With the addition of the radio-frequency field and the generalization of the term diagram into the frequency diagram, levels  $m = 1, 0$  and  $-1$  still coalesce at  $H = 0$ , and we should expect still to observe the Hanle effect. In fact, we do (§ 4). The situation is now richer, however, for there exist possibilities of modulation up to  $4\omega_0$ . In many of the experimental records (e.g. figure 6) strong modulation is found near  $H = 0$ . But it is important to remember that an oscillatory magnetic field was used in our experiments, as in those of Fermi & Rasetti, whereas our equations refer to a rotating field. The effects of a counter-rotating component are likely to be particularly strong near  $H = 0$ , and not simply additive. For this reason, no detailed comparison is made in § 4 between the observations near  $H = 0$  and the predictions of the theory.

#### 4. OBSERVATIONS

We now describe the results of the experiments, comparing them with the predictions of the last section. Unless otherwise stated the frequency  $\omega_0/2\pi$  is 13.8 Mc/s, corresponding to  $H_0 = 6.65$  G. It is to be understood:

(a) that the studies of resonance line profiles, although pursued in considerable detail, were generally qualitative. The feature which most readily lent itself to quantitative study is described in § 4, case 2(c).



(b) that in order to detect modulation, it was necessary to tune the radio-frequency amplifiers to harmonics of the driving frequency,  $\omega_0$ . Modulation was not detected when the amplifiers were mis-tuned. That the frequencies of modulation were exactly  $\omega_0$  and its harmonics is proved by the success with which the effects of stray radiation were interpreted (§ 2(iii)).

It is to be borne in mind that the experimental conditions did not completely correspond with the assumptions of the theory. We shall, in due course, point out the effects of the following departures from the ideal conditions:

(a) The material studied was not a single nuclear species, but the natural mixture of isotopes in mercury.

(b) The resonance radiation was to some extent multiply, not singly scattered.

(c) The radio-frequency field was not uniform over the sample, either in magnitude or direction.

(i) Case 1. *Pure excitation*

(a) *The form of the functions  $A$ ,  $B$ ,  $C$ ,  $D$  and  $E$*

The function  $A$  describes the mean intensity of the light. This was studied in detail by Brossel & Bitter (1952), and found to correspond closely to the analytical form of the function. It now appears, in the light of the discovery by Brossel and his colleagues of the coherent diffusion of resonance radiation (Guiochon *et al.* 1956, 1957; Barrat 1959) that the phenomenon is rather more subtle than was at first understood. When multiple diffusion takes place, as it was taking place in their work and in ours, the function  $A$  still describes the form of the magnetic resonance curve, but the parameter  $1/\Gamma$  is no longer the mean lifetime of the excited state of the atom, but a 'coherence time' which depends on the geometrical conditions, and on the atomic concentration. In experiments using natural mercury, each isotope in the resonance vessel contributes to the resonance curves independently of the others. Curves representing the even isotopes (which dominate the natural mixture) are all centred at the same value of magnetic field, and sum to yield a resultant curve which is experimentally indistinguishable from the function  $A$ , although the parameter is some mean of the values appropriate to the individual constituents.

It was observed qualitatively in our experiments that the changes in mean intensity as  $H$  was varied through the resonance region followed the function  $A$ . The changes were approximately twice as great for  $\theta = 0^\circ$  as for  $\theta = 90^\circ$ , and of opposite sign, while in the direction  $\theta = 55^\circ$  ( $\tan^{-1}\sqrt{2}$ ) the effect was almost zero. This observed dependence on  $\theta$  is predicted in equation (2).

Because the function  $A$  describes so well the observed mean intensity of the light for the natural mixture of isotopes, even when multiple scattering is taking place, we would expect that the functions  $B$ ,  $C$ ,  $D$  and  $E$ , and the functions studied under case 2, all of which have been calculated for single scattering, would be applicable to our experimental conditions, except that  $\Gamma$  would not be the reciprocal lifetime of  $^3P_1$ , but a parameter to be determined experimentally.

In figure 5, the observed resonance curves  $\partial S/\partial H$  (where  $S$  is the amplitude of modulation) are compared with theoretical curves  $\partial B/\partial H$ , etc., plotted for the values

$H_1/H_0 = 0.08$ ,  $\Gamma/\gamma H_0 = 0.075$ . The experimental conditions were: polarizing angle  $\alpha_i = 0^\circ$ ; no analyzer; direction of observation,  $\theta = 55^\circ$ ;  $H_0 = 6.65$  G;  $H_1 \approx 0.6$  G; ( $H_1/H_0 \approx 0.09$ ). The phase  $\epsilon$  (§ 2(iii)) was arbitrarily adjusted until curves of the desired symmetry were obtained.

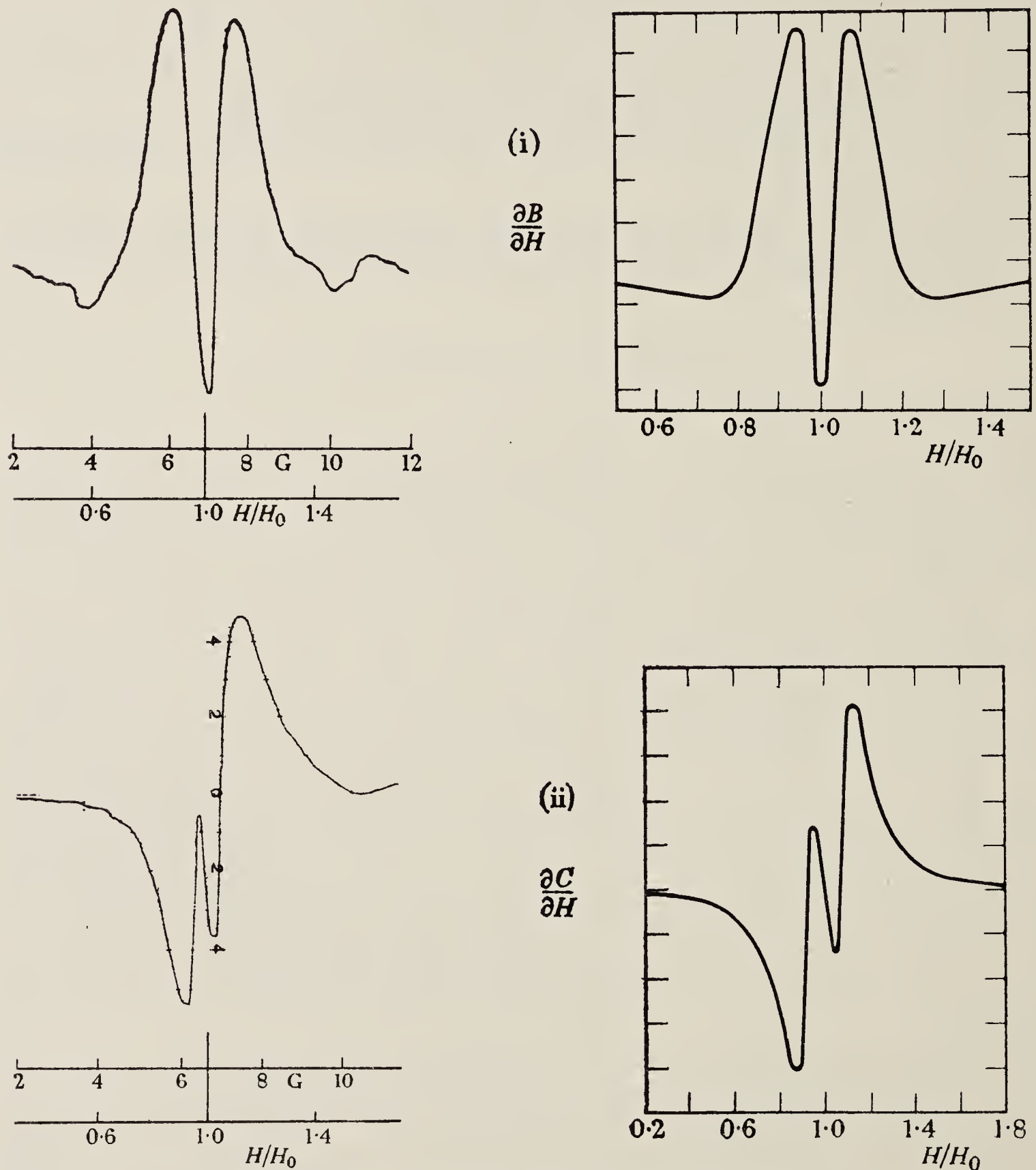


FIGURE 5 (i and ii). For legend see p. 59.

The resemblance between the experimental and theoretical curves is remarkably close, though the experimental curves are wider. Had fitting been seriously attempted, greater care would have been taken with the uniformity of the radio-frequency field. The small asymmetries, which are more pronounced in (ii) and (iv) than in (i) and (iii) reflect admixtures of the components in quadrature.

When  $H_1$  was reduced the curves narrowed, and the central feature in (i) and (ii) was eliminated. Thus, 4(i) came to resemble an inverted  $V$  rather than an  $M$ , and



(ii) became more like a conventional dispersion curve. This is in agreement with the theory, and represents the diminished effect of the radio-frequency perturbation in comparison with the radiation damping when  $\gamma H_1$  falls significantly below  $\Gamma$ .

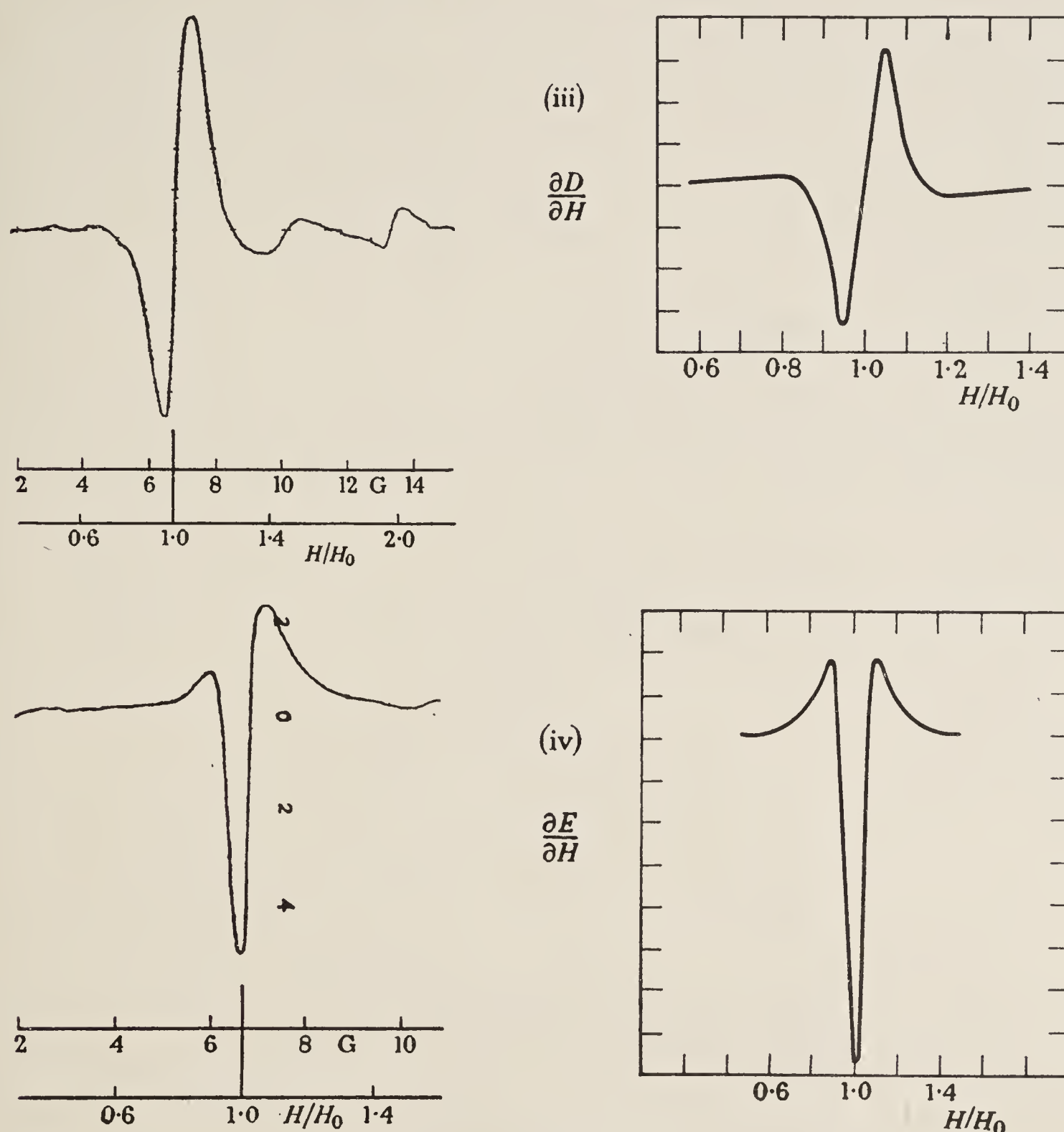


FIGURE 5 (iii and iv)

FIGURE 5. Experimental recordings compared with theoretical curves. (i) and (ii) modulation at  $\omega_0$ ; (iii) and (iv) modulation at  $2\omega_0$ . Experimental conditions:  $\omega_0/2\pi = 13.8$  Mc/s ( $H_0 = 6.65$  G)  $H_1 \approx 0.6$  G. Parameters for theoretical curves:  $b/\omega_0 = 0.08$ ,  $\Gamma/\omega_0 = 0.075$  ( $\tau = 1.53 \times 10^{-7}$  s).

In figure 5 (iii) the experimental record has been extended along the axis of  $H$  in order to show the feature near  $2H_0$ . This was a reproducible effect not predicted by the theory, and finds its explanation in the non-uniformity of the radio-frequency field. It is to be associated with double-quantum transitions of the type investigated by Winter (1959). If there is a component of the radio-frequency field along  $H$  as well as in the perpendicular direction, transitions are allowed in which  $\Delta m = \pm 1$ ,  $\Delta(\text{energy}) = \pm 2\hbar\omega_0$ . Such transitions are known to give rise to resonance

effects in the mean intensity of the light at fields near  $2H_0$ . Their intensity depends on the product of the transverse and longitudinal components of the radio-frequency field. Similar effects are to be expected near  $2H_0$  in light modulated at  $2\omega_0$ . We have not attempted a theoretical analysis of these effects, but we obtained experimental evidence to justify this interpretation. First, the geometry of the radio-frequency coil was such that a small longitudinal component was always present even when the axis of the coil was perpendicular to  $H$ . This would account for the presence of the feature under normal conditions. Secondly, when an adjustment was made deliberately to increase the longitudinal component, the feature at  $2H_0$  rapidly increased in intensity relative to the main resonance at  $H_0$ . Systematic analysis was not undertaken.

In addition to the feature we have just discussed, certain irregularities, which could not certainly be distinguished from noise, were to be seen in some of the recordings in the region 9 to 10 G. An effect here due to the isotopes with nuclear spin is not unexpected, for the field corresponds to a  $g$ -value of 1, which is the  $g_F$ -value of two of the hyperfine components. No other effects of the odd isotopes were observed.

(b) *The dependence on the direction of observation,  $\theta$ , and the use of an analyzer*

The observations are summed up in table 2.

TABLE 2

$\theta$	analyzer	modulation
0°	no	none
	yes	$2\omega_0^*$
55°	no	$\omega_0, 2\omega_0$
	yes	$\omega_0^{*\dagger}, 2\omega_0^{*\dagger}$
90°	no	$2\omega_0$
	yes	$\omega_0^{*\dagger}, 2\omega_0^\dagger$

\* Phase dependent on orientation of analyzer.

† Amplitude dependent on orientation of analyzer.

These observations are in agreement with the theory (cf. in particular the discussion of the classical model in the appendix).

(c) *Depth of modulation*

A measurement was made of the depth of modulation of the fluorescent light in a convenient direction,  $\theta = 55^\circ$ . The particular component chosen for study was the function  $B(\omega_0)$ . The depth of modulation is greatest at  $H \approx H_0 \pm \sqrt{2} H_1$ , and approaches its maximum value asymptotically as  $H_1$  is increased. The observed ratio: (maximum amplitude of the current modulated at  $\omega_0$ )/(mean current) was about 6 %. The ratio calculated from equation (2) is about 40 %.

The significant feature of the measurement is that it confirms that the modulation is a large effect: sophisticated instrumentation is not required to detect it. We attach no importance to the discrepancy with the theoretical figure, for the ratio may be degraded in a number of ways. On the one hand, the straggling of transit



times in the photomultiplier would begin to be troublesome at this frequency; on the other, the mean intensity of the light would be augmented, absolutely, by light scattered from the resonance vessel, and relatively, by the depolarization of resonance radiation through collisions with foreign gas and through multiple scattering. The latter is a large effect (Rollet, Brossel & Kastler 1956).

A further measurement, imprecise, but nevertheless significant was made, namely, the comparison of the amplitude of modulation with the *change* in the mean intensity at resonance. In this comparison the effects of scattered light and of depolarization of the resonance radiation are eliminated. With the use of an analyzer (otherwise there are no changes in the mean intensity when  $\theta = 55^\circ$ , the ratio (maximum amplitude of modulated current)/(change in mean current at resonance) was measured, and found to be  $3.8 \pm 2.0$ . The ratio calculated from equation (2) is 2.3.

### (ii) *Case 2. Mixed excitation*

We have remarked that new features appear in the modulated light, and in the mean intensity, particularly in the regions  $H \approx \frac{1}{2}H_0$  and  $\frac{3}{2}H_0$ , when the incident light is plane polarized obliquely to the field. The features have the form of resonance curves whose profiles approximate to the Lorentzian or the dispersion type of function. For the modulated light, we have investigated qualitatively the intensity of these resonances, their dependence upon radio-frequency field strength, angle of observation, etc. We have found nothing which does not support the theoretical expression, equation (4), illustrated in figure 4, except that, for the modulation at  $2\omega_0$ , the resonances near  $\frac{1}{2}H_0$  and  $\frac{3}{2}H_0$  were not of equal strength, which the theory requires them to be. We do not regard this discrepancy as important, since the signals were weak, and isolated from others only by judicious choice of angle of observation, angle of polarizer, and phase adjustment.

A quantitative study was made of the effects in the mean intensity of the light. This is described in (c) below.

In all this work the disposition of apparatus was as in figure 2, and  $\omega_0/2\pi$ , unless otherwise stated, 13.8 Mc/s. The fluorescent light was generally observed in the direction  $\theta = 55^\circ$ , without an analyzer. The incident light was plane polarized with the electric vector making an angle  $\alpha_i$  with the direction of **H**. Unless otherwise stated,  $\alpha_i = 45^\circ$ , corresponding to mixed ( $\sigma^+ + \sigma^- + \pi$ ) excitation.

Some of the experimental curves show features near  $H = 0$  and  $2H_0$ . We pay no particular attention to these for reasons given in § 3, case 2 (b), and in § 4, case 1 (a).

#### (a) *Comparison of pure and mixed excitation (modulation at $\omega_0$ )*

Figure 6 shows experimental curves for the component of fluorescent light modulated at  $\omega_0$ , under various conditions of excitation. The frequency  $\omega_0/2\pi$  was, for these curves, 27.6 Mc/s instead of the usual 13.8 Mc/s, in order that overlapping of the various features might be avoided. The parameter  $b/\omega_0$  was about 0.2 (cf. figure 4c (i)).

The following points are illustrated in figure 6:

(i) Under pure excitation, the resonance near  $H_0$  is strong. A weaker feature is present near  $H = 0$ .

(ii) Under mixed ( $\sigma^+ + \sigma^-$ ) excitation, the amplitude of modulation is halved, its phase reversed, and the additional feature near  $H = 0$  is relatively much stronger.

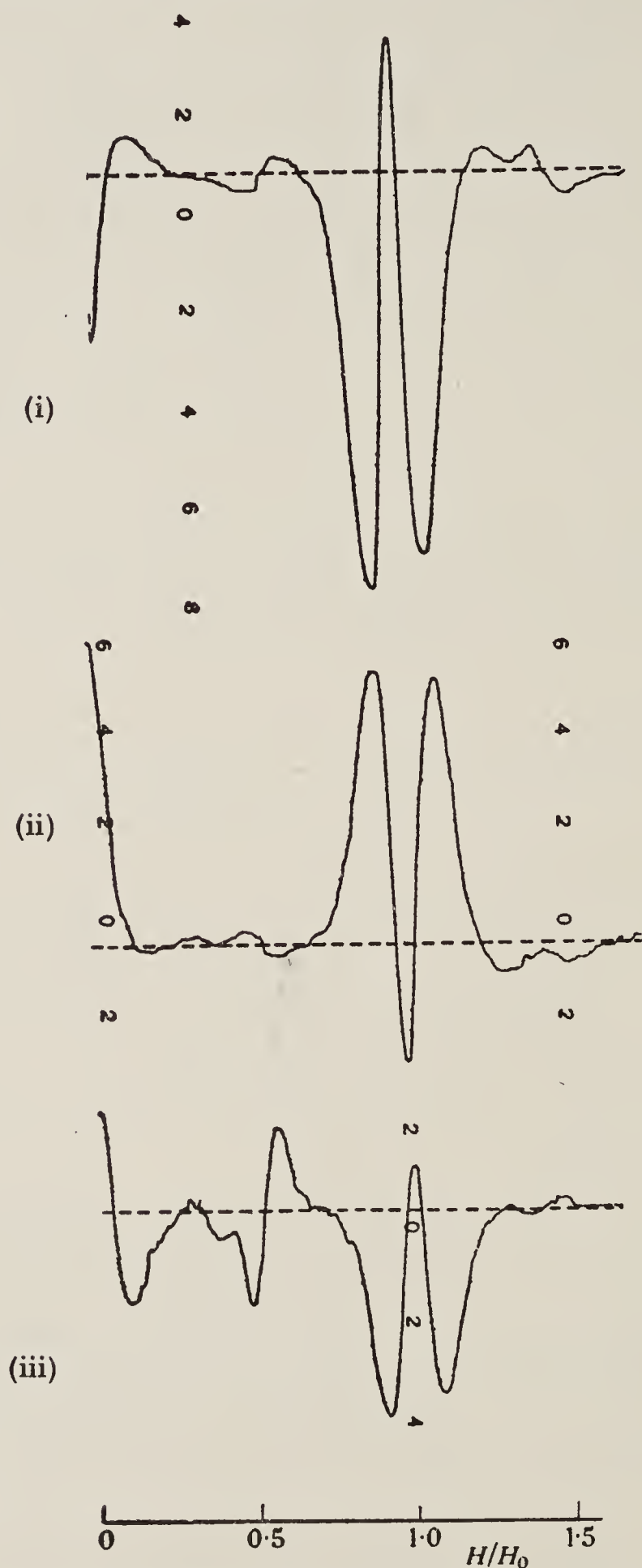


FIGURE 6. Modulation at  $\omega_0$  induced by light of different polarizations. (i)  $\alpha_i = 0^\circ$ . Pur excitation ( $\pi$ ). (ii)  $\alpha_i = 90^\circ$ . Mixed excitation ( $\sigma^+ + \sigma^-$ ). (iii)  $\alpha_i = 45^\circ$ . Mixed excitation ( $\sigma^+ + \sigma^- + \pi$ ).

(iii) Under mixed ( $\sigma^+ + \sigma^- + \pi$ ) excitation, the feature near  $H_0$  becomes the algebraic sum of the  $\sigma$  and  $\pi$  signals (incoherent superposition), the feature near  $H = 0$  is still present, and a new resonance appears near  $\frac{1}{2}H_0$ . Since this represents something other than the algebraic addition of the other two curves, it is proper to describe it by the term 'coherent superposition'.



The (integrated) profile of the new resonance corresponds to the Lorentzian term of expression (c) on the right-hand side of equation (4), and to figure 4c(i). (Expression (c) of equation (4) is much stronger than expression (b), which also represents modulation at  $\omega_0$ .) It was verified that the peak of the new resonance moved with increasing  $H_1$ , and that its profile changed, qualitatively, as predicted by the theory. A significant difference between this resonance and the resonance of the first type, near  $H_0$ , is that the width of this resonance is determined principally by  $\Gamma$ , and only in a secondary way by  $\gamma H_1$ , whereas the width of the first type of resonance depends on functions like  $[\Gamma^2 + (\gamma H_1)^2]^{\frac{1}{2}}$ .

The predicted dependence on  $\theta$  was verified.

No trace was found of a resonance near  $\frac{3}{2}H_0$ , in agreement with the theoretical prediction that the relative intensity of such a resonance would be very small.

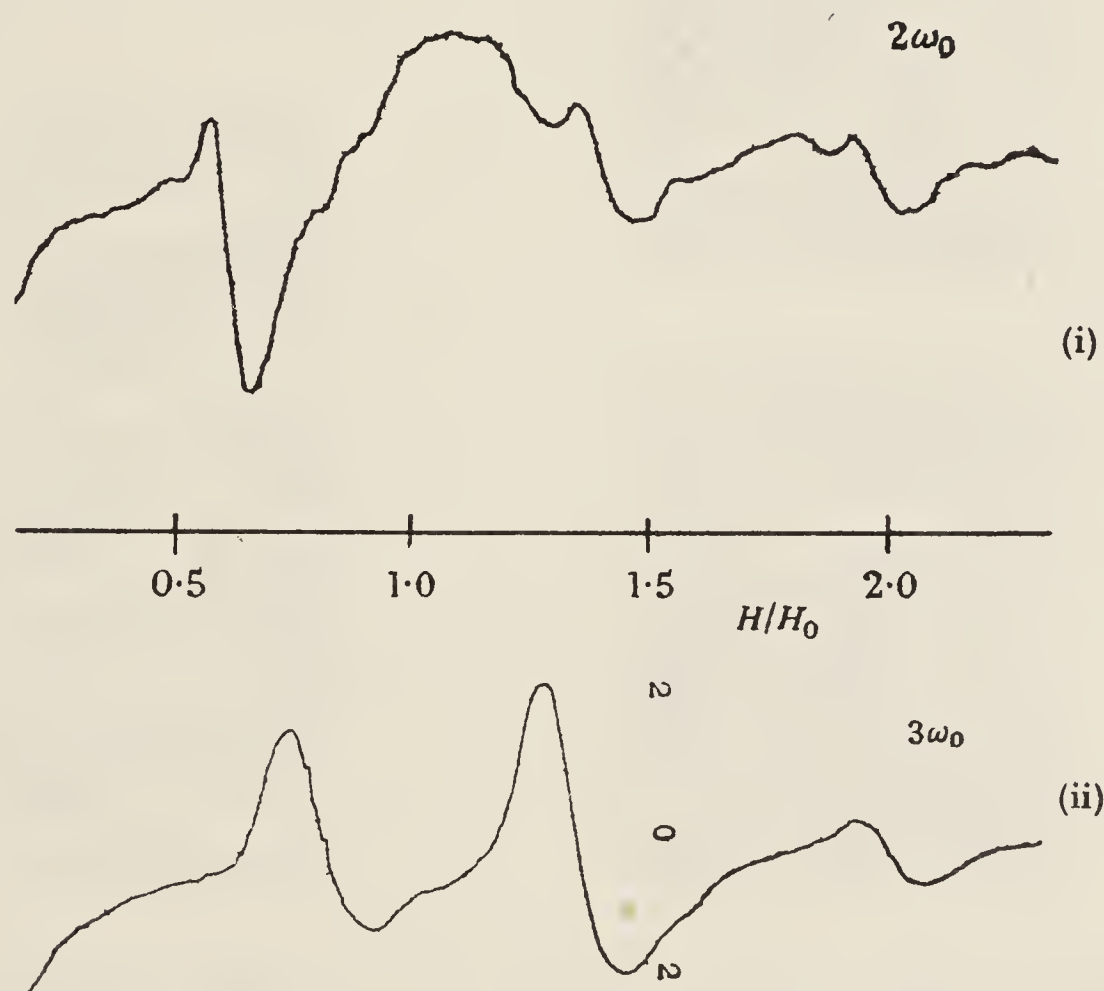


FIGURE 7. Modulation induced by mixed ( $\sigma + \pi$ ) excitation (i) at  $2\omega_0$ , (ii) at  $3\omega_0$ .

(b) Modulation at  $2\omega_0$  and  $3\omega_0$

Figure 7(i) shows the modulation at  $2\omega_0$  under mixed excitation. The new resonances were weak, and followed expression (d) of equation (4) in their dependence on  $\theta$ . We have already commented on the relative intensities of the two new resonances. The feature near  $2H_0$  appeared much more strongly with pure excitation, and is confidently interpreted as a double-quantum phenomenon of the type discussed under case 1(a) of this section.

Figure 7(ii) demonstrates modulation at  $3\omega_0$ , a frequency at which no signal at all appears under pure excitation. A strong radio-frequency field was needed to study these resonances ( $b/\omega_0 \approx 0.47$ ). It will be noticed in passing that a resonance is to be seen at  $2H_0$ , for the same reason as before. We are primarily interested,

however, in the strong resonances which appear on either side of  $H_0$ , displaced towards it from  $\frac{1}{2}H_0$  and  $\frac{3}{2}H_0$ , respectively. The stronger resonance is that at the higher field. These observations reflect very satisfactorily the general behaviour of the theoretical curves, figure 4 (e). (It will be recalled that the experimental curves are the derivatives of the amplitude of modulation.)

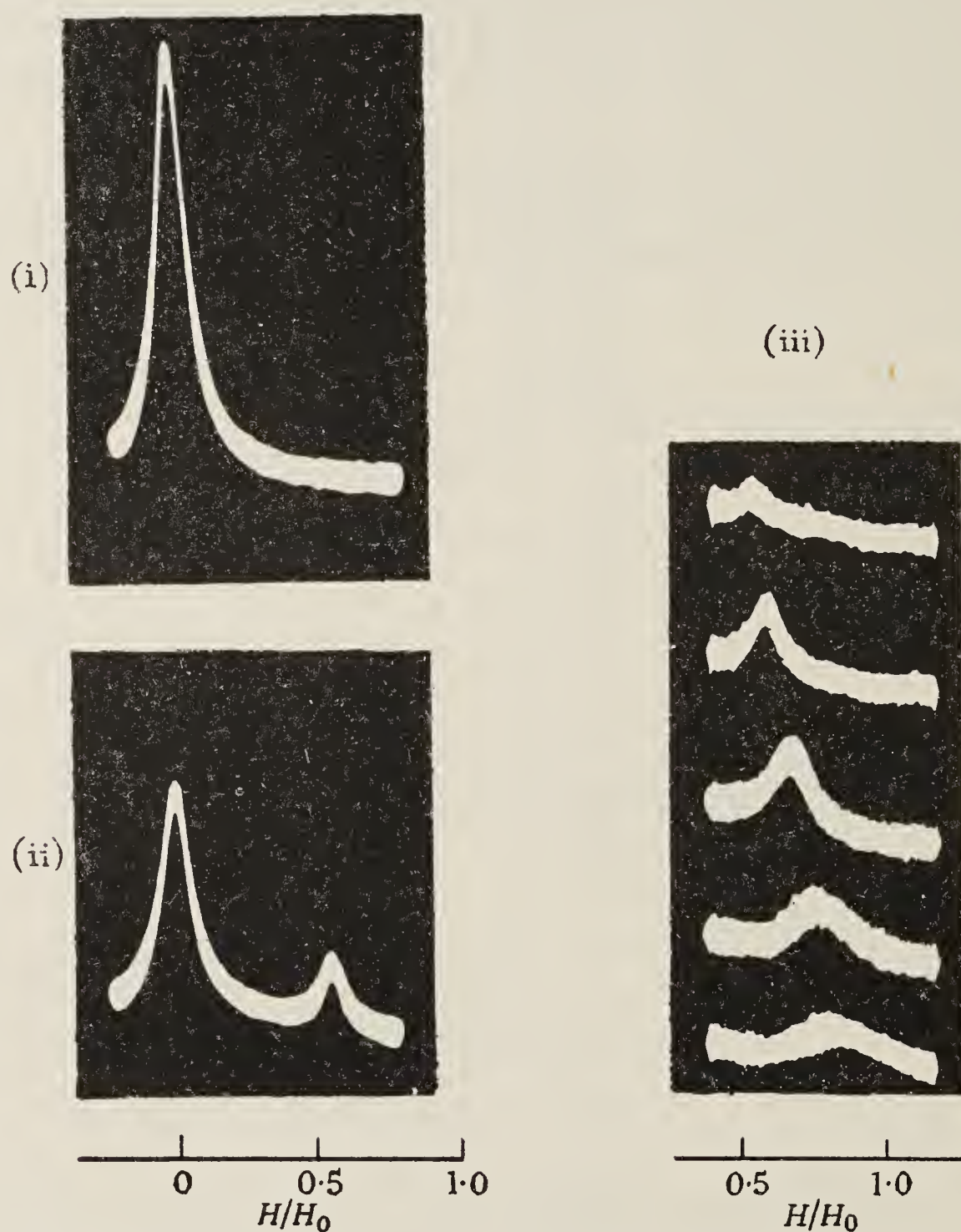


FIGURE 8. Oscillograms showing changes in the mean intensity of the light as a function of  $H$ . (i) Radio-frequency field off; (ii) radio-frequency field on; (iii) the effects of increasing radio-frequency field strength on the feature near  $\frac{1}{2}H_0$  (the sequence reads from the top downwards).

(c) *The mean intensity of the light*

Figure 8(ii) shows the new resonance in the mean intensity near  $\frac{1}{2}H_0$ , together with the similar feature near  $H = 0$  which is associated with the Hanle effect. Figure 8(iii) shows the dependence on  $H_1$  of the new resonance. Observation in the direction  $\theta = 55^\circ$  allows its isolation from the Brossel-Bitter resonance, since the two phenomena depend in different ways on  $\theta$ .

A quantitative study was made of the position of the peak as a function of  $(b/\omega_0)$ , and the profile was examined for a selected value of  $(b/\omega_0)$ . The measurements of



$H$  and  $\omega_0$  which this entailed were straightforward: more difficult was the measurement of  $b$ . Relative measurements of  $b$  were made by measuring the induced voltage across a probe consisting of a couple of turns of 20 gauge wire, one on either side of the resonance vessel. Absolute values were deduced from these measurements by a method based on that used by Brossel & Bitter (1952). The uncertainty in  $b$ , so determined, was about 12 %, though relative values were reliable to 1 or 2 %. The method yielded incidentally a value for the mean coherence time,  $1/\Gamma$ , appropriate to the conditions of our experiment, of  $(1.53 \pm 0.07) \times 10^{-7}$  s.

For this quantitative work the signals were obtained by low frequency modulation, phase-sensitive detection and recording, not by oscilloscope display as in figure 8.

The measurements of the position of the peak are shown in figure 9(i), together with the corresponding theoretical curve (solid line). The broken line represents the addition to the theoretical curve of a first-order correction to take account of the counter-rotating component of the radio-frequency field.

In figure 9(ii), the crosses show the profile determined by integrating the mean of a number of experimental curves taken with  $b/\omega_0$  covering a range  $\pm 12$  % on either side of the nominal value 0.34. Before taking the mean, the curves were brought into coincidence at the point of zero gradient—the peak in figure 9(ii). The solid lines show the calculated profiles for the two values of  $b/\omega_0$  at the ends of the range, 0.30 and 0.38. These theoretical curves have been displaced along the axis of  $H/H_0$ , and their ordinates have been scaled, so as to bring their peaks into coincidence at the point where the peak of the curve,  $b/\omega_0 = 0.34$ , would fall. The ringed cross which represents the peak of the experimental curve has been brought to the same point. In order to establish the base-line for the experimental curve, one further point, marked with a ringed cross, was used for fitting.

Bearing in mind the uncertainty in the measured values of  $b$  and in the experimentally determined value of  $\Gamma$ , and the non-uniformity of  $H_1$  over the sample, we regard the agreement between theory and experiment as very satisfactory.

### (iii) *Further observations*

These studies are being continued by Mr. B. P. Kibble who has kindly allowed us to report briefly his observations:

#### (a) *The mean intensity of the light*

By a geometrical arrangement chosen so that the product  $\mathcal{F}_{10} \mathcal{G}_{10}$  was pure imaginary, the profile of the resonance near  $\frac{1}{2}H_0$  was converted to a dispersion-shaped curve (Kibble & Series 1961). This is in agreement with the theory.

#### (b) *Resonances at low frequencies (case 3)*

It has been found that modulation is still to be observed when the frequency of the perturbation is much smaller than the natural width of the levels. The value  $\omega_0/2\pi \approx 1$  kc/s was used ( $\Gamma \approx 1$  Mc/s). Resonance curves have been obtained centred on a field indistinguishable from zero. In order to avoid the complication of the anti-resonant component, a rotating rather than an oscillatory field was used.

Modulation at the frequencies  $\omega_0$ ,  $2\omega_0$ ,  $3\omega_0$  and  $4\omega_0$  has been demonstrated without difficulty. With suitably chosen conditions, the curves at  $\omega_0$  and  $2\omega_0$  are represented by the functions  $B$ ,  $C$  and  $D$ ,  $E$ , respectively. The resonance curve at  $4\omega_0$  is represented by a new function, as predicted by the theory when  $\omega_0 \ll \Gamma$ . Details of this work will be published shortly (Kibble & Series 1963).

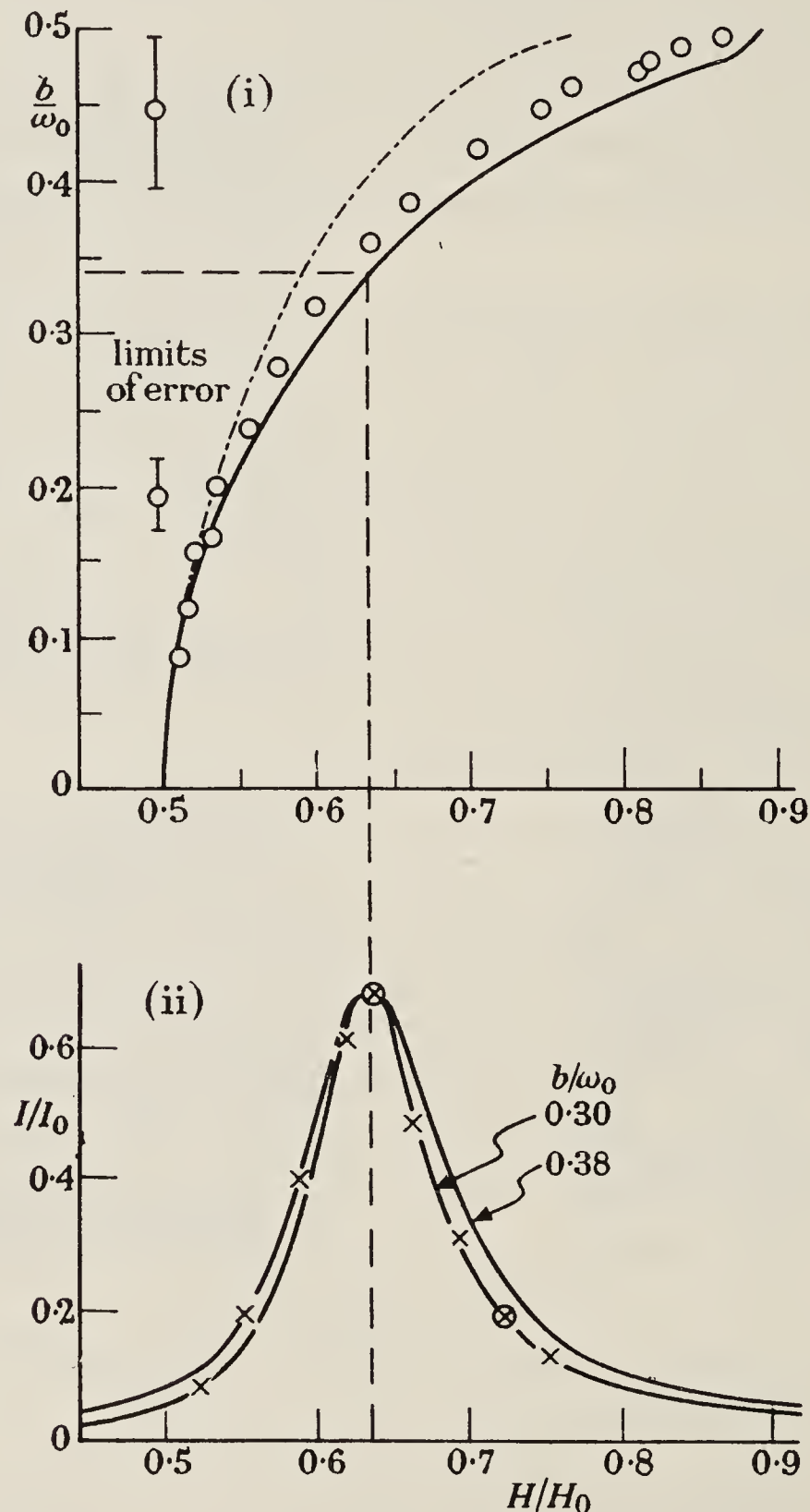


FIGURE 9. The feature near  $\frac{1}{2}H_0$ . (i) Position of the peak as a function of  $(b/\omega_0)$ . The points are experimental; the solid line represents the theory; and the broken line, the theory corrected to a first approximation for the effect of the counter-rotating component of the radio-frequency field. (ii) The profile. The crosses are experimental points taken for  $b/\omega_0$  nominally 0.34. The solid lines are theoretical curves for  $\omega_0/2\pi = 13.8$  Mc/s,  $\tau = 1/2\pi\Gamma = 1.53 \times 10^{-7}$  s. The two ringed points have been used for fitting.

### 5. CONCLUDING REMARKS

We have already mentioned the connexion between this work and the studies by Brossel, Barrat and their colleagues on the coherent scattering of resonance radiation. We wish to emphasize also its close connexion with the work of Colegrove,



Franken, Lewis & Sands (1960; see also Franken 1961) on the anomalous absorption and scattering of resonance radiation, for these experiments again demonstrate coherence between radiation scattered from different stationary states of energy, which is indeed the quantum-mechanical explanation of the Hanle effect. There is a close connexion, too, with the work of Bell & Bloom (1957, 1961*a, b*) on the modulation of absorbed resonance radiation, for here the coherence was established, in the earlier work, by radio-frequency mixing of the ground states, and in the later, by modulation of the exciting radiation at a frequency corresponding to the splitting of the ground states.

We wish to acknowledge the encouragement of Professor B. Bleaney, F.R.S., and of our colleagues, in the Clarendon Laboratory, and in particular, the help of Dr W. N. Fox in the early stages of the work. One of us (M. J. T.) acknowledges gratefully the award of a maintenance grant by the Department of Scientific and Industrial Research.

#### APPENDIX. THE CLASSICAL MODEL

The mercury resonance line  $\lambda 2537 \text{ \AA}$  exhibits the normal Zeeman effect (except that the Landé  $g$ -factor is approximately 1.5 instead of 1), so that its behaviour in resonance fluorescence is susceptible of a simple explanation in classical terms. The classical model is particularly useful in making qualitative predictions about the directional properties of the fluorescent light, whether or not it is modulated, and at what frequencies, etc. It is also capable of quantitative analysis, but this we shall not attempt. We shall merely indicate how, in a simple case, the modulation may be understood.

Let us introduce the rotating co-ordinate system used by Larmor, and now so commonly used in problems of magnetic resonance. Let  $S(\mathbf{i}, \mathbf{j}, \mathbf{k})$  be a Cartesian co-ordinate frame in the laboratory, and let  $S'(\mathbf{i}', \mathbf{j}', \mathbf{k})$  be a frame rotating about  $\mathbf{H} = H\mathbf{k}$  with angular velocity  $\omega_0$ . The field in  $S'$  is the static field

$$\mathbf{H}_{\text{eff.}} = (\mathbf{H} - \omega_0/\gamma) + \mathbf{H}_1$$

(figure 2ii). Consider now the consequences of exciting atoms with light whose electric vector is parallel to  $\mathbf{H}$  (pure, or  $\pi$ -excitation). The electric oscillators of the classical atoms will precess with random phase round  $\mathbf{H}_{\text{eff.}}$ , forming a double cone of semi-angle  $\beta = \tan^{-1}(H_1/(H - H_0))$ . The properties of the fluorescent light may now be deduced in terms of the radiation from these oscillators.

Consider in particular the situation at resonance ( $\beta = \frac{1}{2}\pi$ ). The cone becomes a disk, normal to  $\mathbf{H}_1$ , with the oscillations taking place along diameters which rotate in their own plane with frequency  $\gamma H_1$  and random phase. Seen along  $\mathbf{H}_1$  in  $S'$ , the radiation will be circularly polarized and uniform in intensity. But from any particular direction in the  $\mathbf{i}$ - $\mathbf{j}$  plane in  $S$  the disk will be seen face-on, then edge-on, alternating at the frequency  $2\omega_0$ . The radiation will thus consist of an unmodulated component polarized parallel to  $\mathbf{H}$  (the  $\pi$ -radiation) and a component modulated at the frequency  $2\omega_0$  polarized perpendicular to  $\mathbf{H}$  (the  $\sigma$ -radiation). The modulation may be simply interpreted as the interference between  $\sigma^+$  light at the frequency  $(k_0 + \omega_0)$  and  $\sigma^-$  light at  $(k_0 - \omega_0)$ .

Again, at resonance, the light emitted in the direction  $\mathbf{k}$  in  $S'$  will be linearly polarized and unmodulated, but in  $S$  the direction of linear polarization will rotate at the frequency  $2\omega_0$ . The light, seen in  $S$ , will be unmodulated, unless viewed through a plane analyzer, in which case there will be modulation at the frequency  $2\omega_0$ . As before, this corresponds to interference between the components, in the plane of the analyzer, of the  $\sigma^+$  and  $\sigma^-$  radiations.

Modulation at the frequency  $\omega_0$  might be expected under conditions in which ( $\sigma^+$  and  $\pi$ ) or ( $\sigma^-$  and  $\pi$ ) radiations can interfere. Clearly, this cannot be expected for emission in the  $\mathbf{k}$ -direction where there is no  $\pi$ -radiation, but in the  $\mathbf{i}$ - $\mathbf{j}$  plane it is possible to find suitable conditions. A study of the model allows the conclusion that a plane analyzer, oblique to the  $\mathbf{k}$ -direction ( $\alpha \neq 0$  or  $\frac{1}{2}\pi$ ) will transmit light modulated at  $\omega_0$  as well as at  $2\omega_0$ . In the same way, one finds that radiation oblique to the  $\mathbf{i}$ - $\mathbf{j}$  plane ( $\theta \neq 0$  or  $\frac{1}{2}\pi$ ) is modulated at  $\omega_0$  and at  $2\omega_0$ , even when no analyzer is used.

These conclusions, established under the restriction of case 1, are the same as those predicted by equations (2) and (3). It is possible also to apply the model to case 2, but this we shall not here attempt.

#### REFERENCES

- Barrat, J. P. 1959 *J. Phys. Rad.* **20**, 541, 633, 657.  
 Barrat, J. P. 1961 *Proc. Roy. Soc. A*, **263**, 371.  
 Bell, W. & Bloom, A. 1957 *Phys. Rev.* **107**, 1559.  
 Bell, W. & Bloom, A. 1961a *Phys. Rev. Lett.* **6**, 280.  
 Bell, W. & Bloom, A. 1961b *Phys. Rev. Lett.* **6**, 623.  
 Boutron, F., Barrat, J. P. & Brossel, J. 1957 *C.R. Acad. Sci., Paris*, **245**, 2250.  
 Brossel, J. & Bitter, F. 1952 *Phys. Rev.* **86**, 308.  
 Colegrove, F. D., Franken, P. A., Lewis, R. R. & Sands, R. H. 1959 *Phys. Rev. Lett.* **3**, 420.  
 Dodd, J. N., Fox, W. N., Series, G. W. & Taylor, M. J. 1959 *Proc. Phys. Soc.* **74**, 789.  
 Dodd, J. N. & Series, G. W. 1961 *Proc. Roy. Soc. A*, **263**, 353.  
 Fermi, E. & Rasetti, F. 1925 *Z. Phys.* **33**, 246.  
 Forrester, A. J., Gudmundsen, R. A. & Johnson, P. O. 1955 *Phys. Rev.* **99**, 1691.  
 Franken, P. A. 1961 *Phys. Rev.* **121**, 508.  
 Guiochon, M. A., Blamont, E. & Brossel, J. 1956 *C.R. Acad. Sci., Paris*, **243**, 1859.  
 Guiochon, M. A., Blamont, E. & Brossel, J. 1957 *J. Phys. Rad.* **18**, 99.  
 Hanle, W. 1924 *Z. Phys.* **30**, 93.  
 Hanle, W. 1925 *Ergebn. exakt. Naturw.* **4**, 214.  
 Kibble, B. P. & Series, G. W. 1961 *Proc. Phys. Soc.* **78**, 70.  
 Kibble, B. P. & Series, G. W. 1963 (in course of publication).  
 Rollet, N., Brossel, J. & Kastler, A. 1956 *C.R. Acad. Sci., Paris*, **242**, 240.  
 Winter, J. M. 1959 *Ann. Phys., Paris*, **4**, 745.



# Theory of resonance fluorescence excited by modulated or pulsed light

A. CORNEY and G. W. SERIES

Clarendon Laboratory, Oxford

*MS. received 23rd September 1963*

**Abstract.** When resonance fluorescence is excited in atoms whose excited states have Zeeman or hyperfine structure, it is to be expected that the character of the fluorescent light will be affected if the intensity of the exciting light is modulated or pulsed. An earlier theory of resonance fluorescence is developed to take account of such variations of the intensity of the exciting light. Resonance effects are predicted if the light is modulated at a frequency which coincides with a characteristic frequency of the atoms. A particular case, which has been studied experimentally, is worked out in detail. If the exciting light is pulsed, the prediction is that the fluorescent light will be modulated, in addition to being damped at the ordinary rate for spontaneous emission.

## 1. Introduction

Interest in resonance fluorescence has revived in recent years, partly because of the spectroscopic applications of 'double resonance' and 'level-crossing' experiments, and partly because of the illustrations which such experiments afford of the interactions between electromagnetic fields and free atoms.

As a natural development from earlier work, we have considered the consequences of exciting resonance fluorescence by light whose intensity is not constant in time; in particular, by modulated or pulsed light. By virtue of the time dependence of the intensity, a certain coherence is established between different spectral components of the light, so that when it is used to excite fluorescence in atoms whose excited states have Zeeman or hyperfine structure, the character of the fluorescent light is not the same as when the exciting light is uniform in time. If the exciting light is modulated, for example, the fluorescent light is itself modulated at the same frequency, but the amplitude of modulation undergoes changes which indicate an atomic resonance when the frequency of modulation coincides with the interval between two atomic energy levels.

Experiments using modulated light for the excitation of resonance fluorescence have been carried out, and are described in the accompanying paper (Corney and Series 1964). The excited states in question were the Zeeman components of the  $5^3P_1$  level of cadmium. Resonance phenomena were found when the frequency of modulation of the light coincided with the intervals between the Zeeman levels.

The object of this paper is primarily to derive detailed theoretical expressions for comparison with the experiments. For this purpose, it was convenient to extend a theoretical treatment of resonance fluorescence (Dodd and Series 1961, to be referred to as DS) which was developed to describe a double-resonance experiment of the type introduced by Brossel and Bitter (1952). The general expressions derived in § 2 of this paper, therefore, apply to experiments in which the atoms experience not only a static magnetic field and light whose intensity varies with time, but also a rotating magnetic

field. It is easy to separate the effects of the two time-dependent perturbations, so that the complication is not serious, but rather reveals interesting possibilities for further experiments. The simplification in which the rotating magnetic field is eliminated is made in § 3. In § 4 we show how the same results may be derived by the use of a classical model.

Since the earlier theoretical work was concerned with the Zeeman structure of the excited state, the formulae derived here do not apply explicitly to hyperfine or other types of structure. The case of a 2-level structure of unspecified origin would present no new difficulties, and more complicated cases could then be treated by methods of approximation. One would expect the general features of the results to be similar to the case of Zeeman structure treated here.

## 2. Extension of the theory of DS

The theory describes the behaviour of an atom in a uniform magnetic field  $\mathbf{H}$ , irradiated by light whose electric field at the atom at time  $t$  is  $E(t)\mathbf{e}_1^0$ , where  $\mathbf{e}_1^0$  is a unit vector. The light is resonance radiation connecting the ground state  $|g\rangle$  with a set of excited states  $|m\rangle$  which belong to a given level of angular momentum  $\mathbf{J}$ . For simplicity, it is supposed that the value of  $J$  for the ground state is zero. (Particular examples are the resonance lines of zinc, cadmium and mercury,  $^1P_1$  or  $^3P_1-^1S_0$ .) It was supposed in DS that the atoms were subjected also to a magnetic field  $\mathbf{H}_1(t)$  rotating with angular frequency  $\omega_0$  in a plane perpendicular to  $\mathbf{H}$ . Although we are not now primarily concerned with the effects of  $\mathbf{H}_1(t)$ , we shall, for the time being, suppose that this field is present.

As in DS, we treat the process of excitation in detail and justify the approximations which are made. The resulting equation (6) could have been obtained more directly by use of the pulse approximation (Franken 1961) at the expense of insight into the nature of the problem.

We take up the argument of DS on p.360 in connection with the correlation integral

$$\langle \Phi(t_0, \tau) \rangle = \frac{1}{2T_0} \int_{t_0-T_0}^{t_0+T_0} E(t)E(t-\tau) dt \quad (1)$$

which we shall evaluate now explicitly as a function of  $t_0$ . We shall show that, for broad-band excitation,  $\langle \Phi(t_0, \tau) \rangle$  has the same dependence on  $t_0$  as  $\langle \Phi(t_0, 0) \rangle$ , which itself is proportional to the intensity of the light at time  $t_0$ . After the dependence on  $t_0$  has been factorized out, the correlation integral may be treated as in DS. The rest of the work is straightforward. We take the opportunity of correcting two misprints in DS: on p.360, line 16,  $E_i(t_0+\tau)$  should read  $E_i(t_0-\tau)$ ; and on p.361, line 19,  $\delta(k-k')$  should read  $\delta(\tau)$ .

The formal reduction of the correlation integral may be treated as follows. Define functions

$$\left. \begin{aligned} E(t_0, t) &= E(t) & \text{for } t_0 + T_0 > t > t_0 - T_0 \\ E(t_0, t-\tau) &= E(t-\tau) & \text{and zero for all other values of } t. \end{aligned} \right\}$$

The value of  $\langle \Phi(t_0, \tau) \rangle$  is unaltered if these new functions are used in the integrand instead of  $E(t)$  and  $E(t-\tau)$ . The new functions are introduced in order to allow the extension of the limits of integration from  $t_0 \pm T_0$  to  $\pm \infty$  without altering the value of the integral, thereby enabling it to be expressed in terms of the Fourier transform coefficients of  $E(t_0, t)$  and  $E(t_0, t-\tau)$ . The two sets of Fourier coefficients are not, in fact, identical, but differ from each other by an amount which tends to zero as  $\tau/T_0$  tends to



zero. But, for quasi-monochromatic light of spectral width  $\Delta$ , the correlation integral itself vanishes for values of  $\tau \gg 1/\Delta$ . If, therefore, we can ensure that  $T_0 \gg 1/\Delta$ , we may treat  $E(t_0, t)$  and  $E(t_0, t - \tau)$  as identical functions of the variable  $t$ , and we need not distinguish between the two sets of Fourier coefficients. Now, the upper limit for  $T_0$  is set by the requirement  $T_0 \ll 1/(\Gamma^2 + x^2)^{1/2}$ , so that the functions may be treated as identical provided  $\Delta \gg (\Gamma^2 + x^2)^{1/2}$ . This condition is satisfied in the experiments with which we are concerned.

The Fourier coefficients  $E(t_0, k)$  are defined through the equation

$$E(t_0, t) = \frac{1}{\sqrt{(2\pi)}} \int_{-\infty}^{+\infty} E(t_0, k) \exp(-ikt) dk. \quad (2)$$

Making use of the fact that  $E(t_0, t - \tau)$  has the same Fourier coefficients as  $E(t_0, t)$ , we obtain

$$\langle \Phi(t_0, \tau) \rangle = \frac{1}{2T_0} \int_{-\infty}^{+\infty} |E(t_0, k)|^2 \exp(-ik\tau) dk. \quad (3)$$

We wish to relate this correlation function to the intensity of the incident light, i.e. to the mean value of  $E^2(t_0)$ , which is simply  $\langle \Phi(t_0, 0) \rangle$ . In the experiments which we wish to consider, the modulation was performed without altering the spectral distribution of the intensity, i.e.  $\langle \Phi(t_0, 0) \rangle$  is independent of  $k$ .  $|E(t_0, k)|^2$  may therefore be written  $\sigma(t_0)\rho(k)$ . It follows that

$$\langle \Phi(t_0, \tau) \rangle = \sigma(t_0) \int_{-\infty}^{+\infty} \rho(k) \exp(-ik\tau) dk. \quad (4)$$

We are not interested in the form of  $\rho(k)$ , though we have assumed that it extends smoothly over a sufficiently wide range of  $k$ .

We may now proceed as in DS to evaluate the integrals over  $\tau$  for white light and for quasi-monochromatic light. The result is simply  $\rho(k')$ . (The case of monochromatic light may be treated by direct integration at an earlier stage.)

Returning to expression (26) of DS, we are left with the integral over  $t_0$ , which reduces to

$$\int_0^t dt_0 \sigma(t_0) \exp[-(\Gamma + ix)(t - t_0)]. \quad (5)$$

The general expression for the intensity corresponding to equation (32) of DS is now

$$I = \frac{4Nk_0^4}{\Gamma c^4 \hbar^2 r_0^2} \rho(k_0) \sum_{\substack{m, \mu, n \\ m', \mu', n'}} \mathcal{F}_{nn'} \langle m | \mu \rangle \langle \mu | n \rangle \langle n' | \mu' \rangle \langle \mu' | m' \rangle \mathcal{G}_{mm'} \Gamma \\ \times \exp[-i(m - m' - n + n')\omega_0 t] \int_0^t dt_0 \sigma(t_0) \exp[-(\Gamma + ix)(t - t_0)]. \quad (6)$$

### 2.1. Modulated excitation

We write  $\sigma(t_0) = 1 + \cos ft_0$ . Provided  $t \gg 1/\Gamma$ , the integral over  $t_0$  has the value

$$\frac{1}{\Gamma + ix} + \frac{\frac{(\Gamma + ix)}{2} \cos ft}{(\Gamma + ix)^2 + f^2} + \frac{f \sin ft}{(\Gamma + ix)^2 + f^2}. \quad (7)$$

This result predicts that the fluorescent light will be modulated at the same frequency as the exciting radiation, as was to be expected. A more important prediction is that the amplitude of the modulation will show resonance phenomena when the applied frequency  $f$  is in the neighbourhood of any one of the frequencies  $x$ . These are the frequencies which are represented as differences between levels in the 'frequency diagram' (DS, p.366).

### 2.2. Pulsed excitation

We take  $\sigma(t_0)$  equal to unity for a period of duration  $\Theta$  centred on  $t_0$ , and zero elsewhere. The interesting phenomena are those which arise when  $\Theta$  is much smaller than the lifetime of the atoms or the period of the frequencies  $x$ , whichever is the least. In such a case, the integral over  $t_0$  has the value

$$\Theta \exp[-(\Gamma + ix)(t - t_0)]. \quad (8)$$

It is predicted that the fluorescent light will be modulated at the frequencies  $x$ , damped at the rate of spontaneous radiation from the atom. When  $x = \Gamma$ , the modulation will be critically damped.

### 3. Application to particular cases: static magnetic field

It has been convenient up to this point to retain the generality of a time-dependent magnetic field as well as time-dependent incident light. We now wish to isolate the effects which stem from the time dependence of the light. Removal of the rotating magnetic field is described by setting  $H_1 = \omega_0 = 0$  in equation (25) of DS. (The static field  $\mathbf{H}$  remains as before.) In this case,  $\mu = n = m$ ,  $\mu' = n' = m'$ , and equation (6) reduces to

$$I = I_0 \sum_{m, m'} \mathcal{F}_{m, m'} \mathcal{G}_{m, m'} \Gamma \int_0^t dt_0 \sigma(t_0) \exp[-(\Gamma + ix)(t - t_0)] \quad (9)$$

where  $x = (m - m')\omega$ ,  $\omega = \gamma H$ .

#### 3.1. The directions of the beams of light

It is convenient to study the case in which the fluorescent light is taken at right angles to the direction of the incident light (unit vectors  $\mathbf{j}$  and  $\mathbf{i}$  respectively), and the field  $\mathbf{H}$  is at right angles to both (unit vector  $\mathbf{k}$ ). The electric vector of the incident light makes an angle  $\alpha_i$  with the direction of  $\mathbf{H}$ ; the fluorescent light is taken through an analyser which passes the electric vector inclined at the angle  $\alpha$  to  $\mathbf{H}$ . In this case the excitation and emission matrices for  $J = 1$  are

$$\mathcal{F}_{m, m'} = |P|^2 \begin{pmatrix} \frac{1}{2}s_i^2 & \frac{-i}{\sqrt{2}}s_i c_i & \frac{1}{2}s_i^2 \\ \frac{i}{\sqrt{2}}s_i c_i & c_i^2 & \frac{i}{\sqrt{2}}s_i c_i \\ \frac{1}{2}s_i^2 & \frac{-i}{\sqrt{2}}s_i c_i & \frac{1}{2}s_i^2 \end{pmatrix} \quad \begin{matrix} \text{in which } s_i = \sin \alpha_i \\ \text{and } c_i = \cos \alpha_i \end{matrix} \quad (10)$$

and

$$\mathcal{G}_{m, m'} = |P|^2 \begin{pmatrix} \frac{1}{2}s^2 & \frac{-1}{\sqrt{2}}sc & -\frac{1}{2}s^2 \\ \frac{-1}{\sqrt{2}}sc & c^2 & \frac{1}{\sqrt{2}}sc \\ -\frac{1}{2}s^2 & \frac{1}{\sqrt{2}}sc & \frac{1}{2}s^2 \end{pmatrix} \quad \begin{matrix} \text{in which } s = \sin \alpha \\ \text{and } c = \cos \alpha \end{matrix}$$



3.1.1. *Modulated incident light.* Combining the expressions (7), (9) and (10), we have

$$\begin{aligned} \frac{I}{I_0\Gamma} = & \cos^2\alpha_i \cos^2\alpha \left\{ \frac{1}{\Gamma} + \cos ft \left( \frac{\Gamma}{\Gamma^2 + f^2} \right) + \sin ft \left( \frac{f}{\Gamma^2 + f^2} \right) \right\} \\ & + \frac{1}{2} \sin 2\alpha_i \sin 2\alpha \left\{ \left( \frac{\omega}{\Gamma^2 + \omega^2} \right) + \frac{1}{2} \cos ft \left[ \frac{\omega - f}{(\omega - f)^2 + \Gamma^2} + \frac{\omega + f}{(\omega + f)^2 + \Gamma^2} \right] \right. \\ & \quad \left. + \frac{1}{2} \sin ft \left[ \frac{\Gamma}{(\omega - f)^2 + \Gamma^2} - \frac{\Gamma}{(\omega + f)^2 + \Gamma^2} \right] \right\} \\ & + \frac{1}{2} \sin^2\alpha_i \sin^2\alpha \left\{ \left[ \frac{1}{\Gamma} - \frac{\Gamma}{\Gamma^2 + 4\omega^2} \right] + \frac{1}{2} \cos ft \left[ \frac{2\Gamma}{f^2 + \Gamma^2} - \frac{\Gamma}{(f + 2\omega)^2 + \Gamma^2} - \frac{\Gamma}{(f - 2\omega)^2 + \Gamma^2} \right] \right. \\ & \quad \left. + \frac{1}{2} \sin ft \left[ \frac{2f}{f^2 + \Gamma^2} - \frac{f + 2\omega}{(f + 2\omega)^2 + \Gamma^2} - \frac{f - 2\omega}{(f - 2\omega)^2 + \Gamma^2} \right] \right\}. \end{aligned} \quad (11)$$

The result demonstrates that, with suitable orientations of polarizer and analyser, one may expect to find resonance effects in the amplitude of modulation, centred on the fields  $H = f/\gamma$  and  $f/2\gamma$ , that is, when the applied frequency is equal, either to the Larmor precessional frequency of the excited atoms in the field  $H$ , or to twice that frequency. The effects may be interpreted as interferences between the  $\sigma$  and  $\pi$ , and between the  $\sigma^+$  and  $\sigma^-$  Zeeman components of the fluorescent radiation. The coherence upon which the interference is based is generated by the coherence which the modulation imparts to the spectral components of the incident light.

Equation (11) is in good agreement with the experimental observations.†

3.1.2. *Pulsed incident light.* In this case, the expressions (8), (9) and (10) combine to give

$$\begin{aligned} \frac{I}{I_0\Gamma} = & \Theta \exp[-\Gamma(t - t_0)] \left\{ \cos^2\alpha_i \cos^2\alpha + \frac{1}{2} \sin 2\alpha_i \sin 2\alpha \sin \omega(t - t_0) \right. \\ & \quad \left. + \frac{1}{2} \sin^2\alpha_i \sin^2\alpha [1 - \cos 2\omega(t - t_0)] \right\} \end{aligned} \quad (12)$$

where  $\Theta$  is the duration of the pulse applied at the time  $t_0$ .

In this case, the coherence which the pulsing imparts to the spectral components of the incident light is reflected in the modulation, which is a manifestation of interference between different Zeeman components of the fluorescent light.

Equation (12) has not yet been tested by experiment.

## 4. Classical model

In earlier papers (Dodd, Series and Taylor 1963, Kibble and Series 1963) it was shown that the results of certain modulation experiments could be interpreted by using a classical model of the fluorescing atoms. The present case may be treated similarly. The atoms are supposed to behave as isotropic oscillators which the exciting light sets into damped oscillation at their natural frequency. (This is the 'pulse approximation' which is based upon the assumption that the coherence time of the incident light is much smaller than the half-life of the oscillators.) The creation of dipoles is treated as a sequence of uncorrelated processes at a rate proportional to the intensity of the light.

† See note added in proof at end of article.

We treat the case when the geometrical arrangement is as specified in the last section. Consider the behaviour of one such dipole excited at time  $t_0$ . The component  $P \cos \alpha_i$  of the amplitude  $\mathbf{P}$ , parallel to the field  $\mathbf{H}$ , will be unaffected by it. The component  $P \sin \alpha_i$ , perpendicular to the field, will, at time  $t$ , have precessed about it by the angle  $\omega(t-t_0)$ , where  $\omega = \gamma H$ . Both components will decay at the same rate,  $\Gamma/2$ . At time  $t$ , the component parallel to the analyser will be

$$P(t) = P[\cos \alpha_i \cos \alpha + \sin \alpha_i \sin \alpha \sin \omega(t-t_0)] \exp[-\frac{1}{2}\Gamma(t-t_0)].$$

To find the intensity of fluorescent light at time  $t$ , we multiply  $|P(t)|^2$  by the number of dipoles excited in the interval  $dt_0$ , that is  $\sigma(t_0) dt_0$ , and integrate over  $t_0$  from 0 to  $t$ .

The results are identical with those of the preceding sections.

### Acknowledgments

The work was done during the tenure by one of us (A.C.) of a Research Studentship from the Department of Scientific and Industrial Research.

### References

- BROSSEL, J., and BITTER, F., 1952, *Phys. Rev.*, **86**, 308.  
 CORNEY, A., and SERIES, G. W., 1964, *Proc. Phys. Soc.*, **83**, 213.  
 DODD, J. N., and SERIES, G. W., 1961, *Proc. Roy. Soc. A*, **263**, 353.  
 DODD, J. N., SERIES, G. W., and TAYLOR, M. J., 1963, *Proc. Roy. Soc. A*, **273**, 41.  
 FRANKEN, P. A., 1961, *Phys. Rev.*, **121**, 508.  
 KIBBLE, B. P., and SERIES, G. W., 1963, *Proc. Roy. Soc. A*, **274**, 213.

*Note added in proof.* Experiments have now been carried out in which atoms subjected to an oscillatory magnetic field as well as a static field were irradiated by modulated light. The results are in good agreement with expressions which are derived from equations (6), (7) and (10).



# Double resonance excited by modulated light

A. CORNEY and G. W. SERIES

Clarendon Laboratory, Oxford

*MS. received 23rd September 1963*

**Abstract.** A type of double resonance experiment is reported in which resonance fluorescence from an atomic vapour is excited by modulated light. The amplitude of modulation of the fluorescent light undergoes changes which indicate an atomic resonance when the frequency of modulation is equal to the Larmor frequency of the atoms in an applied magnetic field, or equal to twice that frequency. The effects have been studied in the intercombination line,  $\lambda$  3261 Å, of cadmium. They are in good agreement with theoretical predictions.

The method could be applied to the spectroscopy of excited atoms.

## 1. Introduction

The resonance fluorescence of atomic vapours has been studied extensively in recent years, partly on account of its intrinsic interest, and partly because of its application to the spectroscopy of excited atoms. Following the double-resonance experiment of Brossel and Bitter (1952), a number of detailed studies have been made of the properties of the fluorescent radiation when the atoms are subjected to time-dependent magnetic fields (Barrat 1959, 1961, Barrat *et al.* 1963, Dodd and Series 1961, Dodd, Series and Taylor 1963, Kibble and Series 1963). It was natural to expect that double-resonance phenomena of a rather different sort would arise if atoms in a static magnetic field were excited by light modulated at a frequency which corresponded to one of the precessional frequencies of the atoms in the field. Bell and Bloom (1961) have studied resonance effects in the absorbed light which occur at the precessional frequencies in the ground state. Resonance effects in the fluorescent light at the excited state precessional frequencies are reported in this paper.

A suitable case for study was the intercombination resonance line of cadmium,  $\lambda$ 3261 Å, ( $5^3P_1 - 5^1S_0$ ). The irradiated vapour was subjected to a steady magnetic field. When the incident light was modulated, so also was the fluorescent light, at the same frequency. The new resonance phenomena were indicated by changes in the amplitude of modulation of the fluorescent light when the frequency of modulation was equal to the Larmor frequency of the excited atoms in the applied field, or to half the Larmor frequency. (Since the even isotopes dominate the mixture in naturally occurring cadmium, the frequency in question is that of the  $^3P_1$  level without hyperfine structure.)

*Note added in proof.* A similar experiment has been performed by Aleksandrov (1963).

## 2. Experimental arrangement

Modulation of the incident light was achieved at the source by using a radiofrequency field to excite a discharge in a tube containing neon and cadmium vapour, a method chosen for simplicity rather than high efficiency. It proved possible by this means to obtain in the radiation  $\lambda$ 3261 Å a depth of modulation of about 1% at 462 kc/s. A higher

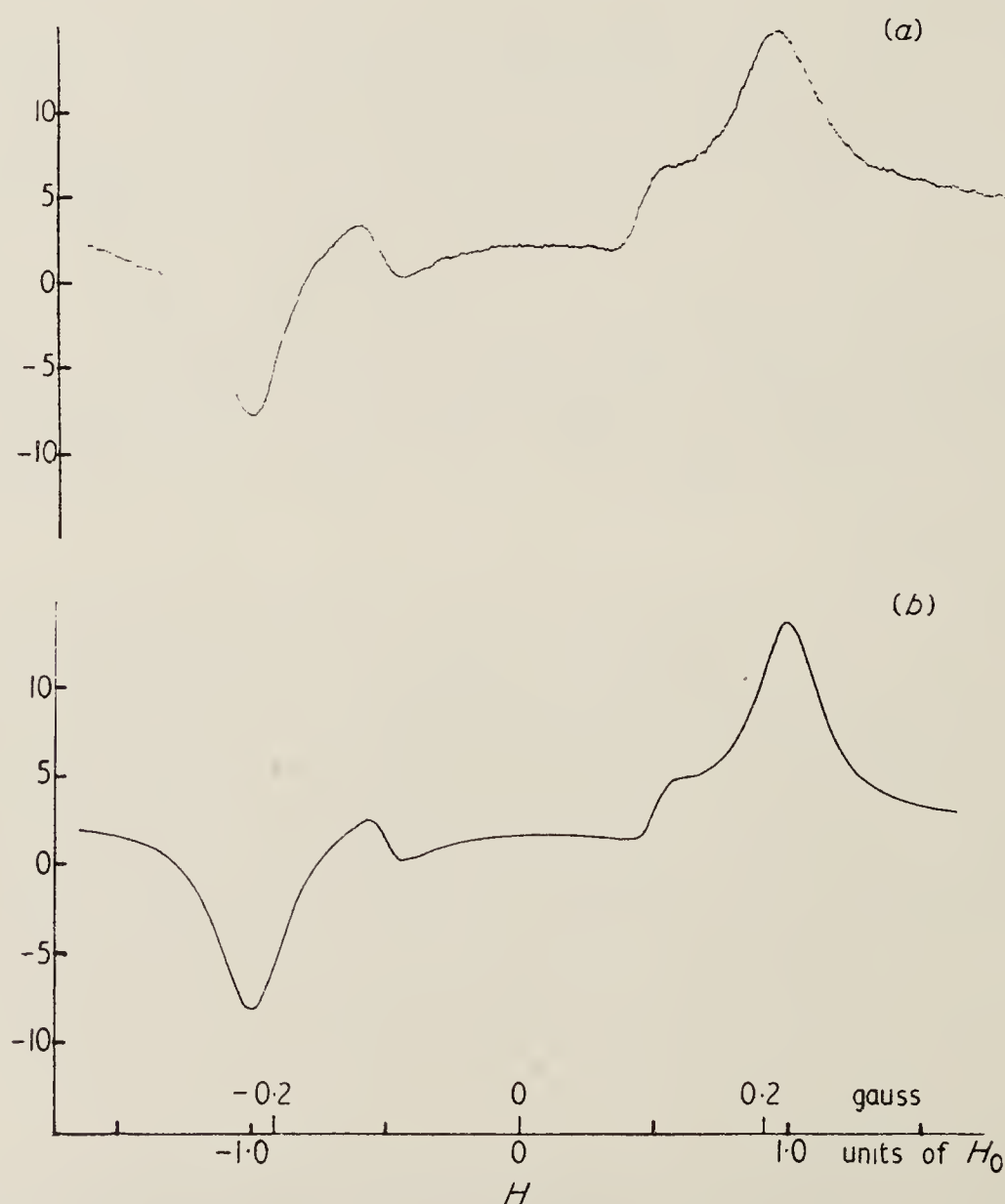
frequency would have been desirable, but could not be obtained by this technique without deterioration of the depth of modulation.

The resonance vessel was enclosed in an oven at about 200 °C. Stray magnetic fields (a.c. and d.c.) were reduced to about  $5 \times 10^{-4}$  G, a figure about one-eightieth of the half-intensity width of the Hanle depolarization curves. A magnetic field  $H$  was applied in a direction at right angles to the incident and fluorescent light, and slowly varied from about  $-0.4$  to  $+0.4$  G. A linear polarizer and a linear analyser were used, though these are not essential for the study of some of the phenomena.

The fluorescent light in a direction at right angles to the incident light was focused on a photomultiplier. The photoelectric signal was passed through an amplifier tuned to 462 kc/s, and then applied to a phase-sensitive detector, the output from which was recorded using a time constant of about one second. The recorded signals are plots, in arbitrary units, of the amplitude of the sine or cosine components of modulation of the fluorescent light, or some linear combination of these, as functions of magnetic field. The phases are relative to the phase of the modulation of the incident light.

### 3. Results

To illustrate the phenomenon (see figure (a)), we have chosen a situation in which resonance effects are to be seen centred on the fields  $\pm H_0$  and  $\pm H_0/2$ , where  $H_0 = f/\gamma$ ,



Amplitude of the sine component of modulation of the fluorescent light (arbitrary units), as a function of magnetic field. Polarizer and analyser have both been set at  $45^\circ$  to the field. Resonance effects are to be seen near  $\pm H_0$  and  $\pm H_0/2$ . (a) Experimental, (b) theoretical.



$f$  being the applied frequency and  $\gamma$  the gyromagnetic ratio. Curves of this type are obtained, for a particular setting of the phase control, when the polarizer and analyser are both at  $45^\circ$  to the field. It will be noticed that the effects near  $\pm H_0$  have the general shape of Lorentzian curves, while the curves near  $\pm H_0/2$ , on the other hand, are dispersion type. For equal magnitudes of the field the effects near  $\pm H_0$  are in anti-phase while those near  $\pm H_0/2$  are in phase.

In the figure (b) is plotted a curve based on a theory of the effect worked out in the preceding paper (Corney and Series 1964; the particular case illustrated is described by the coefficient of  $\sin ft$  in equation (11)). The value of the decay constant  $\Gamma$  needed in the evaluation of the formulae was based on the lifetime  $2.25 \times 10^{-6}$  sec measured by Barrat and Butaux (1961). The value of the coherence time deduced from Hanle depolarization curves taken under the conditions of our experiments differs by about 4% from the above value, a difference which would be barely perceptible in the figure (b) if the coherence time had been used instead of the lifetime. The agreement between the experimental and theoretical curves is very satisfactory. The theory predicts that the modulation represented in the figure should be accompanied by modulation in quadrature. The amplitude should follow a dispersion-type profile at  $\pm H_0$ , and Lorentzian-type profiles at  $\pm H_0/2$ . For equal magnitudes of the field near  $\pm H_0$  the modulation should be in anti-phase, while near  $\pm H_0/2$  they should be in phase. All these details have been verified by experiment.

The effects correspond to a redistribution in space of the fluorescent light when the applied frequency of modulation is in resonance with the atomic precessional frequency. They are manifestations of interference between the Zeeman components of the fluorescent light; those at  $H_0$ , between the  $\sigma$  and  $\pi$  components, and those at  $H_0/2$ , between the  $\sigma^+$  and  $\sigma^-$  components. This is convincingly demonstrated by the dependence of the effects on the angles of polarizer and analyser: the effects at  $H_0$ , for example, are eliminated when the polarizer is crossed with the magnetic field, thus allowing only  $\sigma^+ + \sigma^-$  excitation.

#### 4. Conclusion

Our aim in this work has been the study of the phenomenon itself. Nevertheless, it is clear that the method could be applied to the spectroscopy of excited atoms in the same way as the double-resonance technique of Brossel and Bitter. An advantage to be gained by the present method is that the sharpness of resonance is believed to be determined by the radiation width of the levels only (within the approximation that the probability for excitation is very much smaller than the probability for spontaneous decay), whereas in the other method the oscillatory field which induces the transitions makes a definite contribution to the width of the resonance curves.

The rather complicated contours of the figure, which might lead one to avoid the method as a technique for quantitative spectroscopy, arise simply because of the incomplete resolution of four distinct resonance curves. Two of these, those which are found on the same side of zero field (positive or negative), arise because there are two different intervals in the three-level system with which we are working. A two-level system would display only one resonance in positive fields and one in negative fields. The resonance in negative fields could be removed (in principle) by using a rotating beam of light to excite the fluorescence instead of a modulated beam. When a modulated beam is used, the tail of this resonance overlaps the resonance in the corresponding positive field, and slightly distorts it in a manner akin to the Bloch-Siegert effect. The

distortion can be reduced by working at a higher frequency. The use of electro-optical shutters to modulate the light would allow the resonances to be shifted to fields large compared with their widths. Under these conditions, the shapes of the curves are predicted to be simple Lorentzian or dispersion functions, or some combination of these, depending on the choice of phase.

### Acknowledgments

The work was done during the tenure by one of us (A.C.) of a Research Studentship from the Department of Scientific and Industrial Research.

### References

- ALEKSANDROV, E. B., 1963, *Optik i Spektrosk.*, **14**, 436 (*Optics and Spectrosc.*, **15**, 232).  
BARRAT, J. P., 1959, *J. Phys. Radium*, **20**, 541, 633, 657.  
——— 1961, *Proc. Roy. Soc. A*, **263**, 371.  
BARRAT, J. P., and BUTAUX, J., 1961, *C.R. Acad. Sci., Paris*, **253**, 2668.  
BARRAT, J. P., LEDER, D., and RIBAUT, M., 1963, *J. Phys. Radium*, **24**, 221.  
BELL, W. E., and BLOOM, A., 1961, *Phys. Rev. Letters*, **6**, 280, 623.  
BROSSEL, J., and BITTER, F., 1952, *Phys. Rev.*, **86**, 308.  
CORNEY, A., and SERIES, G. W., 1964, *Proc. Phys. Soc.*, **83**, 207.  
DODD, J. N., and SERIES, G. W., 1961, *Proc. Roy. Soc. A*, **263**, 353.  
DODD, J. N., SERIES, G. W., and TAYLOR, M. J., 1963, *Proc. Roy. Soc. A*, **273**, 41.  
KIBBLE, B. P., and SERIES, G. W., 1963, *Proc. Roy. Soc. A*, **274**, 213.



# Proposal for Measuring Lamb Shifts by the Study of Modulated, Fluorescent Light

G. W. SERIES

Clarendon Laboratory, University of Oxford, Oxford, England

(Received 15 June 1964)

A method is proposed for measuring the interval between two atomic energy levels of different parity. The method is related to optical radio-frequency double resonance and level-crossing experiments in that the behavior of atoms in excited states is deduced from observations of the fluorescent light. In contrast with the oscillating electric field ordinarily used to stimulate transitions between states of opposite parity, a small, static electric field is required. The rate at which atoms are excited is required to be modulated; consequently, the fluorescent light will be modulated. The amplitude of modulation will depend on the parameters. A general expression is derived. Two cases are of particular interest: (1) A resonance effect is predicted if the frequency of modulation matches the interval between the perturbed levels. This effect could best be studied for frequencies much greater than the combined natural widths of the levels. (2) For frequencies smaller than the natural width, a level-crossing effect is predicted whose peak occurs at the point of intersection of the unperturbed levels. The method might be applied to measure intervals between the  $2s$  and  $2p$  levels in hydrogen. Estimates are given of the required fields and frequencies.

## 1. INTRODUCTION

IN recent years a number of new techniques have been developed for studying the intervals between close-lying energy levels in excited atoms.<sup>1</sup> The techniques have in common the measurement of the intensity of the radiation emitted when the atoms decay, but the fundamental basis of the experiments is different according to whether the states concerned are members of a Zeeman or hyperfine multiplet, in which case they are of the same parity and decay at the same rate, or whether they are of different parity, and decay at different rates, as, for example, the  $2^2S_{1/2}$  and  $2^2P_{1/2}$  states in hydrogen. In both cases the application of oscillating fields, capable of inducing transitions between the states of interest, causes changes in the emitted radiation. In the former case the character of the transitions is magnetic dipole. The effect of these transitions is primarily to alter the spatial distribution of the radiation; the spectral distribution changes very little. In the latter case the transitions are electric dipole. The change of parity which this implies requires that the atom must decay to an entirely different term, so that the spectral distribution of the radiation changes profoundly.

In the case when the states are members of a multiplet, changes in the spatial distribution of the light occur also when the energy levels are degenerate, a situation which is frequently found in the intermediate-field region of the Zeeman effect in hyperfine structure. (In fact, the effect was discovered in connection with the ordinary triplet structure in helium.<sup>2</sup>) The method of locating these level crossings by measuring the intensity of the fluorescent radiation in some particular direction, as a function of magnetic field, is a very elegant method of studying hyperfine or multiplet structure, partly on account of its simplicity, and

partly because the precision with which the points of intersection may be determined is limited only by the natural width of the energy levels.

The level-crossing technique cannot be applied when the degenerate levels are an isolated pair of different parity, since the states concerned cannot then be transformed into one another by rotations. A superficial analysis might suggest that the mixing of states provided by a static electric field would allow level-crossing effects to be detected, but on examination it becomes clear that the intensity of the fluorescent radiation must be independent of the degree of mixing (cf. Sec. 5).

Rose and Carovillano<sup>3</sup> considered the possibilities of detecting level crossings in the  $n=2$  states of hydrogen, with a view to determining the Lamb shift. The  $p$ - $p$  intersections, which can in principle be located by the technique we have mentioned, give no information about the Lamb shift. The  $s$ - $p$  intersections can in this case be located by the level-crossing technique by taking advantage of the proximity of other  $p$  states, for a strong electric field can mix into the  $s$  state some fraction of a nearby  $p$  state and endow it with sufficient  $p$  character to make the experiment feasible. However, if the field is to be sufficiently strong to achieve this mixing, the perturbation of energy levels will be such that the position of the level crossing becomes quite insensitive to the value of the Lamb shift.

The purpose of this paper is to propose a type of experiment which would allow the location of crossing points between energy levels of different parity, and thus provide an alternative method for measuring the Lamb shift. The basis of the method is to exploit the possibility of temporal, rather than spatial, redistribution of resonance fluorescence. We propose to consider changes in the amplitude of modulation of the fluorescent light when the rate of excitation of the atoms (either by light or by electron impact) is modulated.

A small, static electric field is required to mix the

<sup>1</sup> J. Brossel and F. Bitter, Phys. Rev. 86, 308 (1952); W. E. Lamb and M. Skinner, *ibid.* 78, 539 (1950). For a review of later developments, see G. W. Series, Rept. Progr. Phys. 22, 280 (1959).

<sup>2</sup> F. D. Colegrove, P. A. Franken, R. R. Lewis, and R. H. Sands, Phys. Rev. Letters 3, 420 (1959).

<sup>3</sup> M. E. Rose and R. L. Carovillano, Phys. Rev. 122, 1185 (1961).



states, but the requirement of Rose and Carovillano for an optimum effect, that the field should be parallel to the axis of quantization, does not concern us here. The argument will hold for any pair of states between which a perturbation can be established by a suitably oriented electric field. One variant of the experiment makes use of the fact that the degree of mixing provided by a field of constant magnitude depends on the separation of the energy levels; another makes use of the resonance effects which are to be expected when the frequency of modulation matches the interval between the perturbed levels. Resonances of this sort have been studied when the states concerned were members of a Zeeman multiplet.<sup>4</sup>

We shall analyze the case of an isolated pair of excited energy levels belonging to states of opposite parity, having in mind any pair of intersecting  $s$  and  $p$  levels in hydrogen-like atoms. The presence of other fine structure levels will not substantially affect the argument. We shall consider first the effect of an electric field on the excited states and energy levels, and calculate the intensity of the light which would be emitted from an atom instantaneously excited into the  $p$  state. We shall show that this should be modulated. We shall then show that the intensity of the fluorescence from atoms excited to the  $p$  state at a uniform rate is unmodulated, independent of the electric field, and independent of the proximity of the  $s$  state. Finally, we shall show that, when the rate of excitation is modulated, the amplitude of modulation of the fluorescent light *does* depend on the interval between the  $s$  and  $p$  levels.

## 2. TIME-DEPENDENT WAVE FUNCTION OF THE EXCITED ATOM

Consider the effect of a perturbing electric field on an atom whose eigenstates  $|a\rangle$ ,  $|b\rangle$  of the Hamiltonian  $\mathcal{H}_0$  have eigenvalues  $\hbar k_a$ ,  $\hbar k_b$ . Let  $\hbar V$  be the perturbation Hamiltonian. We shall treat radiative decay by introducing a damping Hamiltonian  $\mathcal{H}_D$  whose matrix is diagonal, with elements 0 for  $|a\rangle$  and  $-i\hbar\gamma/2$  for  $|b\rangle$ , that is to say, the state  $|a\rangle$  is supposed to be non-radiative.  $V$  is independent of time, as are  $\mathcal{H}_0$  and  $\mathcal{H}_D$ . (See Fig. 1.)

Let  $|t\rangle$  be the state of the atom at time  $t$ . We need to solve the equation of motion

$$i\hbar(d|t\rangle/dt) = (\mathcal{H}_0 + \mathcal{H}_D + \hbar V)|t\rangle. \quad (1)$$

Expanding  $|t\rangle$  in eigenstates of  $\mathcal{H}_0$  in the interaction representation:

$$|t\rangle = a(t) \exp(-ik_a t) |a\rangle + b(t) \exp(-ik_b t) |b\rangle, \quad (2)$$

substituting (2) in (1), and using the orthogonal

<sup>4</sup> E. B. Aleksandrov, Opt. i Spektroskopiya 14, 436 (1963) [English transl.: Opt. Spectry. (USSR) 14, 232 (1963)]. A. Corney and G. W. Series, Proc. Phys. Soc. (London) 83, 207, 213, and 331 (1964). O. Nedelec and J. C. Pebay-Peyroula, Compt. Rend. 254, 1951 (1962).

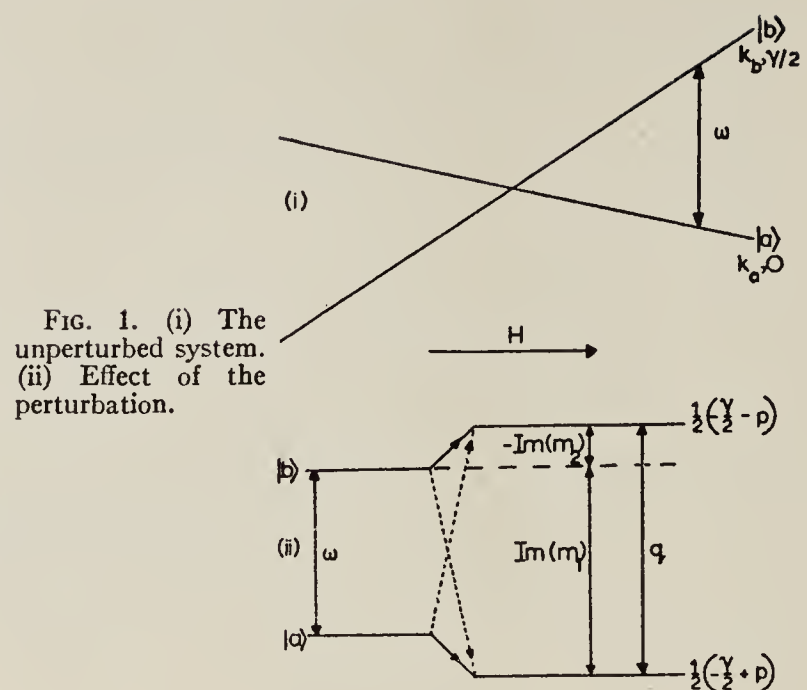


FIG. 1. (i) The unperturbed system. (ii) Effect of the perturbation.

property of  $|a\rangle$  and  $|b\rangle$ , we obtain two equations from which the differential equation for  $b(t)$  may be obtained:

$$\ddot{b} + \dot{b}(\gamma/2 - i\omega) + b(|V|^2 - i\omega\gamma/2) = 0, \quad (3)$$

where  $\omega = k_b - k_a$ .

The general solution

$$b = B_1 \exp(m_1 t) + B_2 \exp(m_2 t) \quad (4)$$

satisfies (3) with

$$m_1 = \frac{1}{2}\{(-\gamma/2 + p) + i(\omega + q)\}$$

and

$$m_2 = \frac{1}{2}\{(-\gamma/2 - p) + i(\omega - q)\}, \quad (5)$$

where

$$p = \frac{1}{2}\{(\gamma^2/4 - \omega^2 - 4|V|^2) + [(\gamma^2/4 + \omega^2 + 4|V|^2)^2 - 4|V|^2\gamma^2]^{1/2}\}^{1/2},$$

$$q = \frac{1}{2}\{-(\gamma^2/4 - \omega^2 - 4|V|^2) + [(\gamma^2/4 + \omega^2 + 4|V|^2)^2 - 4|V|^2\gamma^2]^{1/2}\}^{1/2},$$

and

$$pq = \gamma\omega/2. \quad (6)$$

The two terms in the probability amplitude of  $|b\rangle$ ,

$$\{B_1 \exp(m_1 t) + B_2 \exp(m_2 t)\} \exp(-ik_b t),$$

indicate that the atom can exist in state  $|b\rangle$  at either of two levels which differ in frequency by  $\text{Im}(m_1 - m_2) = q$ , and with decay constants  $\text{Re}(m_1) = \frac{1}{2}(-\gamma/2 + p)$  and  $\text{Re}(m_2) = \frac{1}{2}(-\gamma/2 - p)$ , respectively. Similarly, the solution for  $a(t)$  expressed in the form  $a(t) = A_1 \exp(n_1 t) + A_2 \exp(n_2 t)$  yields

$$n_1 = \frac{1}{2}\{(-\gamma/2 + p) - i(\omega - q)\}$$

and

$$n_2 = \frac{1}{2}\{(-\gamma/2 - p) - i(\omega + q)\}.$$

The exponents  $(n_1 - ik_a)t$ ,  $(n_2 - ik_a)t$  in the probability amplitude of  $|a\rangle$  are identical with those in the probability amplitude of  $|b\rangle$ . In deriving this familiar



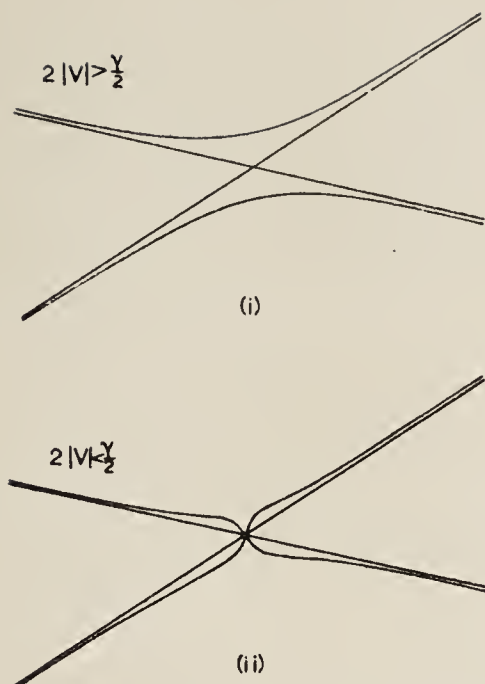


FIG. 2. Effect of the perturbation in the region of the level crossing.

(i)  $2|V| > \gamma/2$ ;  
(ii)  $2|V| < \gamma/2$ .

result, we wish to emphasize that if an atom is either in state  $|a\rangle$  or in state  $|b\rangle$ , its wave function contains two frequencies. States  $|a\rangle$  and  $|b\rangle$  share the same energy levels and the same decay constants, but the probability amplitudes depend on the initial conditions and on the time.

Solutions corresponding to (5) were obtained by Lamb<sup>5</sup> who pointed out an interesting feature of the result in the region of the level crossing. When  $2|V| > \gamma/2$ , the energy levels repel one another, as in Fig. 2(i), but when  $2|V| < \gamma/2$ , the levels continue to cross at the same point where they would have crossed in the absence of the perturbation, as in Fig. 2(ii). In case (i), the states are completely mixed at the crossing point, but in case (ii) the mixing is only partial. The variation of the mixing in the region of the crossing point is the basis of one form of the experiment we are proposing.

The solution (4) is completed by finding  $B_1$  and  $B_2$  for given initial conditions. The conditions  $b=1$  and  $a=0$  at  $t=0$  lead to

$$\begin{aligned} B_1 &= (\gamma/2 + m_2)/(m_2 - m_1), \\ B_2 &= (\gamma/2 + m_1)/(m_1 - m_2), \end{aligned} \quad (7)$$

and

$$A_1 = -A_2 = iV_{ab}/(m_2 - m_1).$$

We are now in a position to consider the emission of light by an excited atom.

### 3. THE EMISSION LIGHT

We consider the decay from the excited state to a lower state  $|g\rangle$ . We suppose that matrix elements of the electric dipole exist between  $|b\rangle$  and  $|g\rangle$ , but not between  $|a\rangle$  and  $|g\rangle$ . The intensity of the component of radiation whose electric vector is parallel to the unit vector  $\mathbf{e}^0$  is proportional to

$$|\langle g | \mathbf{e}^0 \cdot \mathbf{P} | t \rangle|^2.$$

<sup>5</sup> W. E. Lamb, Phys. Rev. 85, 259 (1952).

Expanding  $|t\rangle$ , we find that  $I(t,0)$ , the intensity at time  $t$  from atoms excited at  $t=0$ , is proportional to  $|b(t)|^2$ , where the constant of proportionality depends on the matrix element  $|\langle g | \mathbf{e}^0 \cdot \mathbf{P} | b \rangle|^2$ , the direction in which the light is observed, and other constants which need not concern us.

Using Eq. (4), with  $m_1$  and  $m_2$  given by (5) and  $B_1$  and  $B_2$  by (7), we find

$$I(t,0) \propto c_1 \exp(-\gamma/2 + p)t + c_2 \exp(-\gamma/2 - p)t + 2(\alpha \cos qt - \beta \sin qt) \exp(-\gamma/2)t, \quad (8)$$

where

$$\begin{aligned} c_1 &= |B_1|^2 = \{(\gamma/2 - p)^2 + (\omega - q)^2\}/4(p^2 + q^2), \\ c_2 &= |B_2|^2 = \{(\gamma/2 + p)^2 + (\omega + q)^2\}/4(p^2 + q^2), \end{aligned} \quad (9)$$

and

$$\begin{aligned} (\alpha + i\beta) &= B_1 B_2^* = \{(p^2 - \gamma^2/4 + q^2 - \omega^2) \\ &\quad + i(q\gamma - 2p\omega)\}/4(p^2 + q^2). \end{aligned}$$

Equation (8) predicts that the radiation from an assembly of atoms excited simultaneously and instantaneously to the state  $|b\rangle$  should consist of two components exponentially damped at different rates, and a component modulated at the frequency  $q$  damped at half the unperturbed rate of radiation from  $|b\rangle$ . The modulation arises from the fact that the atom can exist in the state  $|b\rangle$  at two different levels of frequency. It is to be noticed that  $q$  is the interval between the perturbed, not the unperturbed levels.

### 4. THE PROCESS OF EXCITATION

We suppose that the atoms are excited to  $|b\rangle$  either by light of spectral range  $\Delta$  much greater than  $q$ , or by electron impact. Coherence of phase in the process of excitation is lost in a time  $\sim 1/\Delta$  in the first case, or within the interaction time in the second. Provided these times are much smaller than the mean lifetime of the excited atom, we may treat the process of excitation as a rate process. The rate of excitation may be uniform or time-dependent: In either case, we may write that the probability of excitation in the interval  $dt_0$  is  $\sigma(t_0)dt_0$ .

The effect of a perturbation on a rate process is determined by its effect on the initial state. If, therefore, the state from which the atoms are excited is not perturbed by the electric field (which will be true for the  $1^2S_{1/2}$  state in hydrogen), the rate at which atoms are introduced into state  $|b\rangle$  will be independent of  $V$ .

### 5. STEADY-STATE SITUATION

Before we take up the question of modulated excitation, it is worth while verifying that the analysis of Secs. 2 and 3 yields a sensible result for the case of excitation at a uniform rate. Using Eq. (8) with  $(t-t_0)$  for  $t$ , and setting  $\sigma(t_0)=r$ , a constant, we find that the intensity of radiation at time  $t$  from an assembly of

atoms excited to state  $|b\rangle$  at a uniform rate is

$$I(t) = r \int_0^t I(t, t_0) dt_0$$

$$= K \left\{ \frac{c_1}{\gamma/2 - p} + \frac{c_2}{(\gamma/2 + p)} + \frac{(\alpha\gamma - 2\beta q)}{(\gamma^2/4 + q^2)} \right\}, \quad (10)$$

where  $K$  is a constant. The steady-state intensity is independent of time, as one would require.

With the help of Eqs. (6) and (9), the sum of the three terms in square brackets may be reduced to  $1/\gamma$ . This result is the analytical justification of the remark that the intensity of the fluorescent light is independent of  $\omega$  and  $|V|$ , that is, independent of the degree of mixing of states  $|a\rangle$  and  $|b\rangle$ . To interpret this result, it is not sufficient to think merely in terms of populations and decay rates. It is tempting to argue that the modified decay constants of state  $|b\rangle$  just compensate the fact that some of the excited atoms are transferred by the perturbation to the nonradiating state  $|a\rangle$ . This is to overlook the cross term (the third term) in Eq. (10), which expresses the correlation between the partial probability amplitudes  $B_1$  and  $B_2$ . The contribution of the cross term is not negligible: Its value, to first order in  $|V|^2$ , is  $-|V|^2\gamma/(\gamma^2/4 + \omega^2 + 4|V|^2)^2$ . Nevertheless, the conclusion is entirely acceptable that if atoms are excited to the state  $|b\rangle$  at a uniform rate, then the intensity of the fluorescent light from state  $|b\rangle$  should be independent of the perturbation.

## 6. MODULATED EXCITATION

Suppose that the rate of excitation is modulated at the angular frequency  $f$ . We write  $\sigma(t_0) = r(1 + \cos ft_0)$ , and proceed as in the last section.

We have

$$I(t) = r \int_0^t (1 + \cos ft_0) I(t, t_0) dt_0$$

$$= K \{ A + B \cos ft + C \sin ft \}, \quad (11)$$

where

$$A = \frac{c_1}{\gamma/2 - p} + \frac{c_2}{\gamma/2 + p} + \frac{(\alpha\gamma - 2\beta q)}{\gamma^2/4 + q^2} = \frac{1}{\gamma},$$

$$B = \frac{c_1(\gamma/2 - p)}{(\gamma/2 - p)^2 + f^2} + \frac{c_2(\gamma/2 + p)}{(\gamma/2 + p)^2 + f^2}$$

$$+ \frac{\frac{1}{2}[\alpha\gamma - 2\beta(q + f)]}{\gamma^2/4 + (q + f)^2} + \frac{\frac{1}{2}[\alpha\gamma - 2\beta(q - f)]}{\gamma^2/4 + (q - f)^2},$$

and

$$C = \frac{c_1 f}{(\gamma/2 - p)^2 + f^2} + \frac{c_2 f}{(\gamma/2 + p)^2 + f^2}$$

$$+ \frac{\frac{1}{2}[2\alpha(q + f) + \beta\gamma]}{\gamma^2/4 + (q + f)^2} - \frac{\frac{1}{2}[2\alpha(q - f) + \beta\gamma]}{\gamma^2/4 + (q - f)^2}.$$

It is predicted that the fluorescent light should be modulated, and that the amplitude and phase of the

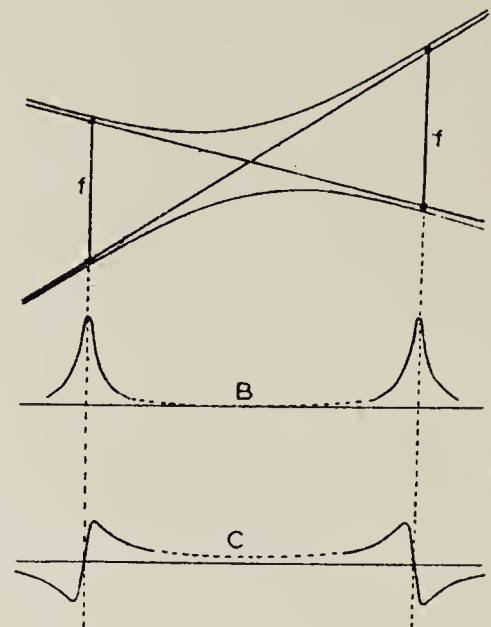


FIG. 3. Resonance effects in the amplitude of the cosine component of the modulation (B) and the sine component (C) when  $f \gg \gamma$ .

modulation should depend on  $\omega$ ,  $\gamma$ ,  $|V|$ , and  $f$ . We shall consider the variations with  $\omega$ , regarding the other quantities as parameters. It is convenient to consider the functions  $B$  and  $C$  separately. Experimentally, they can be isolated by phase-sensitive detection of the modulated component of a photoelectric signal.

The variations of  $B$  and  $C$  are of two types. The cross terms (those containing  $\alpha$  and  $\beta$ ) exhibit resonance phenomena when  $\pm q$  (the separation of the perturbed levels) is in the neighborhood of  $f$ . These we shall study under the condition  $\omega$  (and therefore  $q$ , and therefore  $f$ )  $\gg \gamma/2$ . On the other hand, when  $f \ll \gamma/2$ , the direct terms in  $B$  and  $C$  which have the coefficient  $c_1$  are sensitive to the relative magnitudes of  $f$  and  $|V|$ . This will yield changes in the magnitudes of  $B$  and  $C$  in the region of the level crossing. We shall study this effect under the condition  $|V| \ll \gamma/2$ , which simplifies the analysis and leads to the greatest precision in the location of the level crossing, though it is not a necessary restriction.

### A. Resonance Effects

By choosing  $f$  sufficiently large, the resonance terms in  $B$  and  $C$ , those with the denominators  $\{\gamma^2/4 + (q \pm f)^2\}$ , dominate the others. These terms are combinations of slightly distorted Lorentzian and dispersion-type functions, both of which go through resonance when  $\pm q = f$ . Sufficiently far away from the region of the intersection the value of  $q$  will be only slightly different from  $\omega$ , the unperturbed separation of the levels. Although we are regarding  $\omega$  as the primary variable, it is analytically simpler to regard the resonances as functions of  $q$ .

The distortion is due to the slow variation of  $\alpha$  and  $\beta$  with  $\omega$ . The width at half intensity of the Lorentzian component (as a function of  $q$ ) is  $\gamma$ , so that the condition for separation of the resonance terms from the background is  $f \gg \gamma$ . The relative contributions of the Lorentzian and dispersion components in the region of



resonance is  $\alpha/\beta$  in the case of  $B$  and  $\beta/\alpha$  in the case of  $C$ . In the approximations  $|V|^2 \ll (\gamma^2/4 + \omega^2 + 4|V|^2)$ ,  $\omega \gg \gamma/2$ , we find  $\alpha/\beta \rightarrow \omega/\gamma$ . These approximations are valid sufficiently far away from the region of intersection, so that the Lorentzian component will be dominant in the cosine component of the modulation ( $B$ ) and the dispersion shape in the sine component ( $C$ ). (See Fig. 3.)

### B. Level-Crossing Effects

As  $f$  is reduced below  $\gamma$ , the resonance curves on either side of the intersection draw together, while the background terms assume a relatively greater importance. The sum of the terms  $C$  is smaller than the sum  $B$  in the ratio  $f/(\gamma/2)$ , that is to say, the phase of the modulation remains almost constant as the intersection is traversed. We shall consider the variation of the only significant contribution to the amplitude  $B$ .

Under the approximations  $|V| \ll \gamma/2$ ,  $f \ll \gamma/2$ , the last three terms in  $B$  sum to  $(1-x^2)/\gamma$ , where  $x^2 = |V|^2/(\gamma^2/4 + \omega^2)$ . The first term,  $c_1(\gamma/2 - p)/\{(\gamma/2 - p)^2 + f^2\}$ , reduces to 0 if  $(f/\gamma) \gg x^2$  and  $x^2/\gamma$  if  $(f/\gamma) \ll x^2$ . Hence, as  $f \rightarrow 0$ , the amplitude of modulation of the fluorescent light becomes independent of  $\omega$  and  $|V|$ , which is in satisfactory agreement with the result obtained for the limiting case when the rate of excitation is constant. On the other hand, if  $f \gg |V|^2\gamma/(\gamma^2/4 + \omega^2)$ , one will expect to find changes in the amplitude of modulation given by

$$B = \{1 - |V|^2/(\gamma^2/4 + \omega^2)\}/\gamma, \quad (12)$$

namely, a resonance curve of width  $\gamma$  at half-intensity, centered on  $\omega=0$ . It will be noticed that if the condition  $f \gg |V|^2\gamma/(\gamma^2/4 + \omega^2)$  is satisfied at  $\omega=0$ , it will be satisfied also for nonzero values of  $\omega$ .

### 7. DISCUSSION

The resonance effects predicted in Sec. 6.A bear an interesting relation to the conventional type of double resonance experiment. In such experiments an *oscillating* electric field is used to induce transitions from  $|b\rangle$  to  $|a\rangle$  in an assembly of atoms excited at a uniform rate. The peak of the resonance curve is found when the applied frequency is equal to  $\omega$ , the interval between the unperturbed levels. In the present case a *static* electric field induces transitions for which the frequency of resonance is zero. The frequency  $q$  is that at which the probability amplitudes oscillate between

$|b\rangle$  and  $|a\rangle$ . The phase of this nutational motion is not synchronous for different atoms when the rate of excitation is uniform, but it becomes so if the process of excitation is modulated at the nutational frequency. One finds a resonance in the amplitude of modulation of the fluorescent light at the frequency  $q$ , not  $\omega$ . The difference between  $q$  and  $\omega$  is small and could be estimated in any particular case, but it might be possible to find the position of the crossing point without applying this correction by studying the resonances on either side of the intersection, since the displacements of the two peaks are equal and in opposite directions.

The level-crossing experiment suggested in Sec. 6.B should yield a symmetrical curve whose peak corresponds to the point of intersection of the unperturbed levels. The fields and frequencies for studying such curves in the  $n=2$  states of hydrogen are easily within reach. Crossing points for which  $\Delta m = \pm 1$  (in the notation of Lamb,<sup>6</sup> these are  $\beta e$ ,  $\alpha c$  and  $\beta d$ ) are found at approximately 500, 4500, and 7000 G, respectively. For the first of these the perturbation  $|V|$  introduced by thermal motion at right angles to the field  $\mathbf{H}$  allows the conditions under which Eq. (12) was derived to be satisfied. The conditions were  $4|V|^2/\gamma^2 \ll f/\gamma \ll \frac{1}{2}$ . The value of  $\gamma/2\pi$  for the states  $2^2P_{1/2}$  is close to 100 Mc/sec. Taking  $v = 2.4 \times 10^5$  cm/sec, the mean thermal velocity at 0°C,  $\mathbf{E} = (v/c) \times \mathbf{H}$  is approximately 1.3 V/cm and  $|V|/2\pi$  approximately 2.4 Mc/sec. The choice  $f/2\pi = 3$  Mc/sec then yields  $f/\gamma = 3 \times 10^{-2}$ , which lies conveniently between  $\frac{1}{2}$  and  $4|V|^2/\gamma^2 = 2.3 \times 10^{-3}$ .

The larger fields at the crossing points  $\alpha c$  and  $\beta d$  increase the electric field due to thermal motion to the point where the approximations are not justified, but if  $f$  is increased to be at least comparable with  $4|V|^2/\gamma$ , the predicted effects should still be observable. The approximation  $|V| \ll \gamma/2$  was introduced merely to simplify the analysis. As  $f$  is increased the resonance curves will widen, but should still remain symmetrical.

The crossing  $\beta f$ , which occurs at about 1000 G requires a component of  $\mathbf{E}$  parallel to  $\mathbf{H}$  which the motional electric field cannot provide. For this crossing, an applied electric field of a few volts per cm would be necessary.

### ACKNOWLEDGMENTS

I wish to thank Dr. A. Corney and Dr. B. P. Kibble for their critical reading of the manuscript and for checking some of the calculations.

<sup>6</sup> W. E. Lamb and R. C. Retherford, Phys. Rev. 79, 549 (1950).





# The forward scattering of resonance radiation, with special reference to double resonance and level-crossing experiments

BY A. CORNEY, B. P. KIBBLE† AND G. W. SERIES

*Clarendon Laboratory, University of Oxford*

*(Communicated by B. Bleaney, F.R.S.—Received 21 September 1965)*

A theoretical and experimental study has been made of the intensity of forward scattered light in conditions of radio-frequency double resonance and level-crossing. The main conclusions are (i) that the magnetic resonance and level-crossing effects which are familiar in the laterally scattered light are to be found also in the forward scattered light, but (ii) that the resonance curves are Doppler-broadened, and the strength of the oscillatory field necessary to generate them is correspondingly increased, and (iii) that coherence narrowing is much more pronounced in forward than in lateral scattering.

The differences derive from the coherence between the radiation from different atoms which is present in forward, but not in lateral scattering, and which is implicitly recognized in the classical theory of the propagation of light in polarizable media. The equations of electromagnetism form the basis of the present analysis. In the presence of the oscillatory magnetic field the polarization tensor is complex and time-dependent. The time dependence leads to the result that the number of eigenwaves necessary to describe propagated waves in the medium is four, as against the usual two. An arbitrary wave is resolved into a superposition of the four eigenwaves, all of which have different propagation constants. The analysis is very general, and is applicable to experiments with lasers. The components of the polarization tensor are derived by finding first the polarizability of individual atoms from a semi-classical theory of their interaction with light and magnetic fields. The macroscopic polarization, obtained by summing over individual atoms, is then given by folding the individual polarizabilities with the Doppler distribution of resonance frequencies.

In the particular case studied in detail (the inter-combination resonance line, 2537 Å, in mercury), the Doppler width is much greater than the radiation width, and the imaginary (absorptive) part of the polarizability is Gaussian.

Expressions are derived in a 'weak scattering' approximation for the intensity of the forward scattered light. They are magnetic resonance functions which are found to be the Doppler-broadened equivalents of the familiar functions, based on Lorentzians, characteristic of scattering by a single atom. In the case of double resonance the forward scattered light is strongly modulated, as is the laterally scattered light.

To investigate coherence narrowing, the zero-field level-crossing has been studied with the restriction of 'weak scattering' removed. The result is obtained that the width of level-crossing curves is inversely proportional to the vapour density for magnetic fields such that the Zeeman splitting is small in relation to the Doppler width. This analytical result has been verified experimentally.

## 1. INTRODUCTION

This work continues a study of the properties of the fluorescent radiation in optical radio-frequency double resonance and level-crossing experiments (Brossel & Bitter 1952; Colegrove, Franken, Lewis & Sands 1959). In experiments of this type, observation of resonance radiation scattered laterally from an atomic vapour subjected to static and oscillatory magnetic fields provides a means of monitoring the behaviour of atoms in excited states, and has led to numerous measurements of hyperfine structures,  $g$ -values and lifetimes. Studies of the interaction processes themselves have brought to light the phenomena of coherence narrowing (Guiochon,

† Now at Department of Physics, University of Windsor, Windsor, Ontario.



Blamont & Brossel 1956; Barrat 1959) and of modulation of the fluorescent light (Dodd & Series 1961; Dodd, Series & Taylor 1963; Kibble & Series 1963).

It appeared to us plausible that observation of the forward scattered radiation might lead to a great increase in sensitivity of these methods, since the radiation scattered in the forward direction from different atoms is coherent, whereas the radiation scattered laterally is incoherent. We shall show in this paper that the expected increase in the intensity of the light is to be set against a broadening of the resonance curves which arises from the wide Doppler distribution of the resonance frequencies of the atoms. The need to introduce the Doppler distribution is evident when the problem is studied in terms of the progression of electromagnetic waves through the vapour. As is well known, the wave which actually progresses through a medium may be interpreted as the result of the interference of the forward scattered wave with the primary wave. The latter may be removed by suitable experimental technique, so that we are left solely with the forward scattered component. The fact that we are dealing with an attenuated vapour does not invalidate a treatment on the lines of the classical theory of dispersion (see Kronig 1926). Hence one is led to introduce the bulk polarizability of the medium, which requires a summation over the Doppler distribution of the resonance frequencies. In so far as the spectral width of this distribution is normally much greater than the damping constant of individual atoms, the result is that the assembly of atoms behaves, in respect of the forward scattered light, like a set of identical, static oscillators whose damping constant has been greatly increased. The argument does not hold for the laterally scattered light since, in the attenuated vapours we are considering, there is no constructive interference in the light from different atoms. Each contributes independently to the total intensity. Since it is the damping constant which determines the width of magnetic resonance curves and the strength of the oscillating field necessary to generate them, it would appear that the width, and the required field strength, would need to be greatly increased if the resonances are to be studied by detecting forward scattered light.

There is, however, a further difference between forward and lateral scattering, namely that the coherence narrowing which is brought about by multiple scattering when the vapour density is increased is much stronger in the former case than in the latter. In an experiment in which no special attempt was made to achieve the greatest possible narrowing, a curve 100 times narrower than the Doppler width was obtained.

#### (i) *Isolation of the forward scattered light*

In studying the forward scattered light, the problem arises of the necessity of separating it from the much stronger primary radiation. Dicke & Griffiths (1957) contrived a physical separation of the primary and scattered beams by preparing the scattering medium (sodium vapour) in the form of a coarse diffraction grating. The light in orders other than the zero order is predominantly scattered light, yet retains the coherence properties characteristic of forward scattering. Bradley & Fork (1964) suppressed the primary beam by using an interference technique. The scattering vapour was placed in one arm of a Mach-Zehnder interferometer,



and changes in the refractive index in the neighbourhood of the resonance line were studied when the vapour was subjected to magnetic fields.

The method envisaged in the present work is to place the scattering vapour between crossed polarizer and analyser, and to measure the transmission of the system to collimated resonance radiation (figure 1). Any light which passes the analyser under these conditions must be scattered light. By applying various magnetic fields to the vapour, both level-crossing and double resonance phenomena could be explored. The system chosen for detailed study was the resonance radiation of mercury,  $2537 \text{ \AA}$  ( $6^3P_1-6^1S_0$ ). The following discussion refers to the even isotopes.

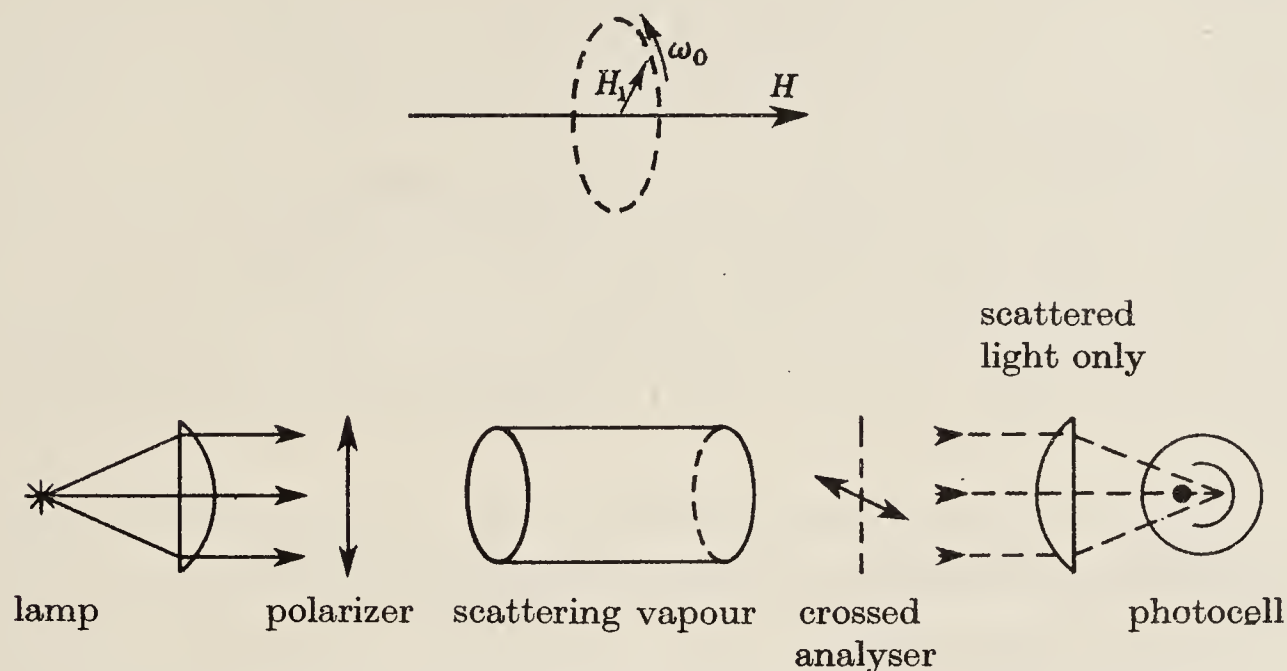


FIGURE 1. Idealized experiment for studying forward scattered light.

### (ii) *Level-crossing experiment*

The Zeeman levels  $m = \pm 1$  of the excited state  $^3P_1$  cross at zero magnetic field. The level-crossing can be explored by varying a magnetic field applied to the vapour in the direction of propagation of the light, from negative, through zero, to positive values. It is easily seen that this geometrical arrangement is suitable for studying the level-crossing phenomena if the incident light is linearly polarized, for in this case both the exciting and scattered beams are coherent superpositions of  $\sigma^+$  and  $\sigma^-$  radiations.

From a more conventional point of view, the experiment we are here contemplating might be described as a study of the Faraday effect in the neighbourhood of an optical resonance line, such as was made many years ago by Macaluso & Corbino (1898). Using a spectrograph, these authors measured the Faraday rotation in sodium vapour as a function of wavelength. However, since our intention was that the present experiments should resemble as closely as possible those on the lateral scattering of resonance radiation, we were not concerned to measure the rotation, or to introduce spectral resolution. A photoelectric cell was used to measure the total intensity of the light which passed the analyser. Plots of the photocurrent as a function of magnetic field do indeed resemble level-crossing curves, and exhibit the phenomenon of coherence narrowing.

*(iii) Double resonance experiment .*

If a transverse magnetic field is applied to the vapour in addition to the fields described in the last section, we have an arrangement for studying double resonance phenomena. While it is true that magnetic resonances are normally studied at high radio-frequencies, the phenomenon itself can be studied much more conveniently at low frequencies (Kibble & Series 1963), even at frequencies well below the radiation width of the energy levels. In the limit of zero frequency, the experiment reduces to a study of the interaction of resonance radiation with atoms in static fields. The resonance is explored by variation of the longitudinal field through the value zero, which corresponds to the peak of the resonance. The double resonance signal is the difference between the intensities of the transmitted light with and without the transverse field.

At the peak of the resonance the vapour experiences simply the transverse field. From a macroscopic point of view we are studying magnetic double refraction. The light which passes the analyser will depend on the orientation of the polarizer with respect to  $H_1$ . The most interesting case is when the electric vector of the incident light is at  $45^\circ$  to  $H_1$ . This orientation was chosen for some of the experiments.

If the transverse field is in fact rotated, but at a frequency much smaller than the Doppler width, it is predicted that the transmitted light should be modulated at four times the frequency of revolution. It is easy to understand this modulation when the experiment is interpreted as magnetic double refraction, for whereas in general the birefringence generates elliptically polarized light, some component of which passes the analyser, no light will pass when the transverse field is either parallel or perpendicular to the axis of the polarizer, that is, four times per revolution.

This description of the modulation is incomplete if the longitudinal field is different from the resonance value,  $H_0 = \omega_0/\gamma$  ( $\omega_0$  is the angular frequency of rotation), for in this case there is a difference in strength between the  $\sigma^+$  and  $\sigma^-$  interactions which generates a modulation at  $2\omega_0$  in addition to the modulation at  $4\omega_0$ .

The situation is different again when  $\omega_0$  greatly exceeds the Doppler width, for in this case the resonance field  $H_0$  separates the levels  $m = \pm 1$  by much more than the Doppler width, and the  $\sigma^+$  and  $\sigma^-$  resonances are stimulated by different Fourier components of the incident light, that is to say, incoherently. Each circular component generates elliptically polarized light independently of the other, and the transmitted light is modulated at  $2\omega_0$ . There is no modulation at  $4\omega_0$ .

A qualitative interpretation of these effects in terms of radiation from superposition states of the  $|m\rangle$  would follow the arguments in the earlier papers relating to lateral scattering. A detailed analysis in terms of the propagation of light in an anisotropic medium, which therefore takes account of the coherence between light scattered from different atoms, is given in the next section. The expressions for the transmitted intensity reduce, in the limit of low vapour density, to easily recognizable forms, for they are the Doppler-broadened equivalents of the



combinations of Lorentzian functions which are found for lateral scattering. The Lorentzian functions are characteristic of single atoms and of incoherent assemblies; the Doppler-broadened forms, of assemblies radiating coherently.

## 2. THEORETICAL ANALYSIS

The problem to be treated is the propagation of resonance radiation through an attenuated vapour subjected to time-dependent magnetic fields. As in the conventional study of anisotropic media, we seek plane wave solutions of Maxwell's equations, assuming the existence of a macroscopic polarizability. This assumption may readily be justified, notwithstanding the fact that the granular structure of the medium is emphasized in discussing the lateral scattering (Kronig 1926).

An analysis by Kramers (1930), applicable to the case of static fields, shows that when the polarizability of the medium is small, the electric vector of the wave is transverse to the direction of propagation, for arbitrary direction of the magnetic field. This result is applicable to our case. However, since with time-dependent fields the polarizability is also time dependent, the equations from which the eigenwaves are derived are now more complicated.

### (i) *The eigenwaves*

For transverse, plane waves propagated in the  $z$  direction, Maxwell's equations for the electric vector  $\mathbf{E}(z, t)$  reduce to

$$\nabla^2 \mathbf{E} = \frac{1}{c^2} \frac{\partial^2}{\partial t^2} [\boldsymbol{\epsilon}(t) \mathbf{E}], \quad (1)$$

where  $\boldsymbol{\epsilon}(t)$  is the dielectric tensor, related to the polarizability tensor  $\boldsymbol{\alpha}(t)$  by

$$\boldsymbol{\epsilon}(t) = \mathbf{1} + 4\pi\boldsymbol{\alpha}(t). \quad (1a)$$

The form of  $\boldsymbol{\alpha}(t)$  appropriate to our problem (see equation (2) below) leads to solutions of (1) in the form of pairs of harmonic waves,  $\sigma_1^{(l)}$  and  $\sigma_{-1}^{(l)}$ . The members of a pair are coupled by components of  $\boldsymbol{\alpha}^{(l)}(t)$ , which are therefore given the same index,  $(l)$ , which labels the pair. The members of the pair  $(l)$  do not have the same frequency. This has been taken into account in deriving explicit expressions for the components of  $\boldsymbol{\alpha}^{(l)}(t)$  (equations (13)).

With a static magnetic field  $\mathbf{H}$  applied to the medium in the  $z$  direction, and with a field  $\mathbf{H}_1$  rotating with angular velocity  $\omega_0$  in the  $x$ - $y$  plane, the form of  $\boldsymbol{\alpha}^{(l)}(t)$  is

$$\begin{pmatrix} \alpha_{11}^{(l)} & \alpha_{10}^{(l)} e^{-i\omega_0 t} & \alpha_{1-1}^{(l)} e^{-2i\omega_0 t} \\ \alpha_{01}^{(l)} e^{i\omega_0 t} & \alpha_{00}^{(l)} & \alpha_{0-1}^{(l)} e^{-i\omega_0 t} \\ \alpha_{-11}^{(l)} e^{2i\omega_0 t} & \alpha_{-10}^{(l)} e^{i\omega_0 t} & \alpha_{-1-1}^{(l)} \end{pmatrix}. \quad (2)$$

The indices 1, 0,  $-1$ , refer to the basic vectors

$$\mathbf{e}_1^0 = -(\mathbf{i} + i\mathbf{j})/\sqrt{2}, \quad \mathbf{e}_0^0 = \mathbf{k}, \quad \mathbf{e}_{-1}^0 = (\mathbf{i} - i\mathbf{j})/\sqrt{2}$$

(in conformity with the notation of Condon & Shortley (1951) and of Rose (1957)).

With  $\alpha^{(l)}(t)$  given by (2), the solution of (1) is found to be of the form

$$\mathbf{E} = \sum_l \{ E_1^{(l)} \exp i[K^{(l)}z - kt + (l-1)\omega_0 t] \mathbf{e}_1^0 + E_{-1}^{(l)} \exp i[K^{(l)}z - kt + (l+1)\omega_0 t] \mathbf{e}_{-1}^0 \}, \quad (3)$$

where

$$E_{\pm 1}^{(l)} = \mp (E_x^{(l)} \mp i E_y^{(l)})/\sqrt{2}$$

and

$$l = 0, \pm 1, \pm 2, \dots$$

An arbitrary wave in the medium may be expressed as a superposition of the eigenwaves of (1). The eigenwaves are those combinations of the components of (3) which share the same  $K^{(l)}$ . The value of  $K^{(l)}$  for each eigenwave, and the corresponding ratio  $E_1^{(l)}/E_{-1}^{(l)}$  are found by substituting (3) in (1). The resulting vector equation is then separated into its vector components, and into terms of the same time dependence. This yields an infinite set of equations, coupled in pairs as follows:

$$\left. \begin{aligned} E_1^{(l)} \{ \epsilon_{11}^{(l)} - K^{(l)2} c^2 / [k - (l-1)\omega_0]^2 \} + E_{-1}^{(l)} \epsilon_{1-1}^{(l)} &= 0, \\ E_1^{(l)} \epsilon_{-11}^{(l)} + E_{-1}^{(l)} \{ \epsilon_{-1-1}^{(l)} - K^{(l)2} c^2 / [k - (l+1)\omega_0]^2 \} &= 0, \end{aligned} \right\} \quad (4)$$

in which  $\epsilon_{1-1}^{(l)}$  and  $\epsilon_{-11}^{(l)}$  are the amplitudes of  $\epsilon_{1-1}^{(l)}(t)$  and  $\epsilon_{-11}^{(l)}(t)$ .

From each such pair we may derive two values of  $(\pm) K^{(l)}$ , and the corresponding ratios  $E_1^{(l)}/E_{-1}^{(l)}$ , that is to say, two eigenwaves. The equation for  $K^{(l)}$ , obtained by eliminating  $E_1^{(l)}/E_{-1}^{(l)}$ , is

$$\{ \epsilon_{11}^{(l)} - K^{(l)2} c^2 / [k - (l-1)\omega_0]^2 \} \{ \epsilon_{-1-1}^{(l)} - K^{(l)2} c^2 / [k - (l+1)\omega_0]^2 \} - \epsilon_{1-1}^{(l)} \epsilon_{-11}^{(l)} = 0. \quad (5)$$

This equation may be solved rigorously, but the solution is complicated by the occurrence of the terms  $(l \pm 1)\omega_0$  which appear with  $k$  in the denominators. The latter is of order  $10^9$  Mc/s, while the former (in the applications we are concerned with) varies from 0 to, say, 10 or  $10^3$  Mc/s. It is, for our purposes, a very good approximation to neglect  $(l \pm 1)\omega_0$  in the denominators in comparison with  $k$ , though it may not be so for all applications.

With this approximation we have

$$K_{\alpha,\beta}^{(l)2} c^2 / k^2 = \frac{1}{2} (\epsilon_{11}^{(l)} + \epsilon_{-1-1}^{(l)}) \pm r^{(l)},$$

where

$$r^{(l)} = [\frac{1}{4} (\epsilon_{11}^{(l)} - \epsilon_{-1-1}^{(l)})^2 + \epsilon_{1-1}^{(l)} \epsilon_{-11}^{(l)}]^{\frac{1}{2}}, \quad (6)$$

and the suffixes  $\alpha, \beta$  correspond with  $+, -$ , respectively.

Using (6) in (4), and making use of the fact that  $\epsilon_{-11}^{(l)} = \epsilon_{1-1}^{(l)}$ , we obtain

$$(E_1^{(l)}/E_{-1}^{(l)})_{\alpha,\beta} = [\frac{1}{2} (\epsilon_{11}^{(l)} - \epsilon_{-1-1}^{(l)}) \pm r^{(l)}] / \epsilon_{-11}^{(l)}. \quad (7)$$

The final expressions are simplified by the substitution

$$2\epsilon_{-11}^{(l)} / (\epsilon_{-1-1}^{(l)} - \epsilon_{11}^{(l)}) = \tan \theta^{(l)}, \quad (\theta^{(l)} \text{ complex}), \quad (8)$$

in terms of which the eigenwaves may be written

$$\mathbf{A}_r^{(l)}(t) \exp i[K_r^{(l)}z - (k - l\omega_0)t] \quad (r = \alpha, \beta),$$

with

$$\left. \begin{aligned} \mathbf{A}_\alpha^{(l)} &= -s^{(l)} \mathbf{e}_1^0 e^{-i\omega_0 t} + c^{(l)} \mathbf{e}_{-1}^0 e^{i\omega_0 t}, \\ \mathbf{A}_\beta^{(l)} &= c^{(l)} \mathbf{e}_1^0 e^{-i\omega_0 t} + s^{(l)} \mathbf{e}_{-1}^0 e^{i\omega_0 t}, \end{aligned} \right\} \quad (9)$$

where

$$s^{(l)} = \sin \frac{1}{2} \theta^{(l)}; \quad c^{(l)} = \cos \frac{1}{2} \theta^{(l)}.$$

These results might alternatively have been obtained by a treatment using a rotating coordinate system.

By superposition of the eigenwaves  $\mathbf{A}_\alpha^{(l)}$  and  $\mathbf{A}_\beta^{(l)}$  we can represent a wave of arbitrary polarization, but it is to be realized that the intensity of such a wave will



necessarily be modulated at the frequency  $2\omega_0$ . In order to represent an unmodulated wave (which is required to satisfy a boundary condition when the incident light is unmodulated), it is necessary to include at least two different values of  $l$ , that is to say, four eigenwaves and four different values of the velocity (figure 2). This result should be contrasted with the case when the polarizability is independent of time, in which case there are only two eigenwaves.

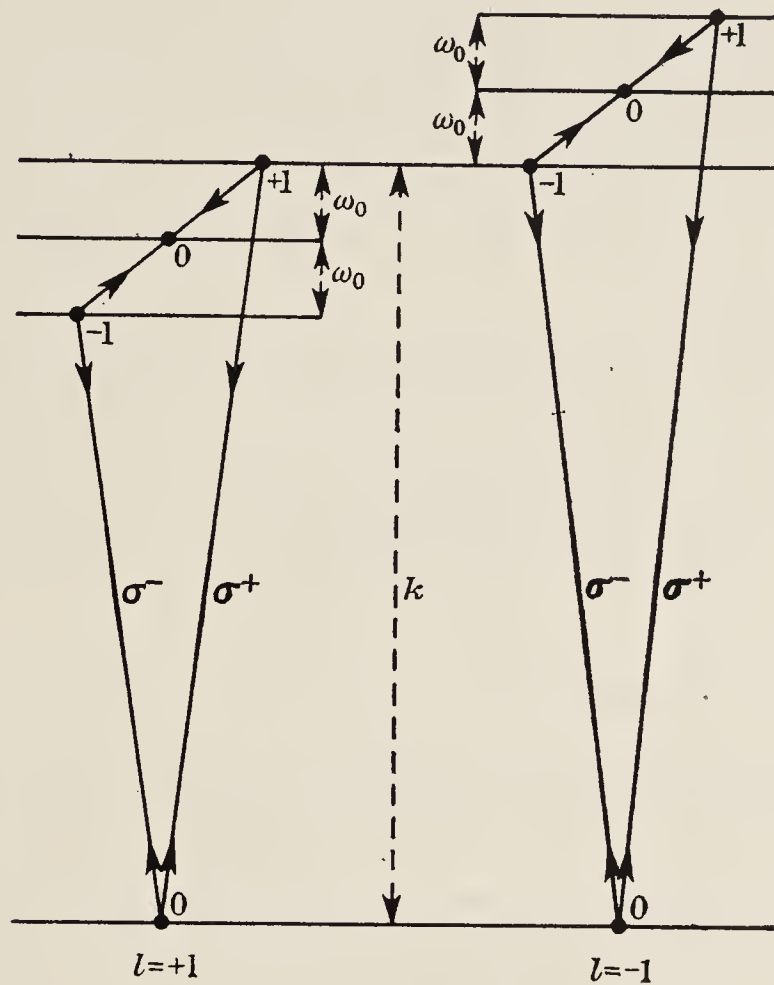


FIGURE 2. The eigenwaves.

$$l = 1 \quad \begin{cases} A_\alpha = -s\sigma^+(k) + c\sigma^-(k - 2\omega_0), \\ A_\beta = c\sigma^+(k) + s\sigma^-(k - 2\omega_0), \end{cases}$$

$$l = -1 \quad \begin{cases} A'_\alpha = -s'\sigma^+(k + 2\omega_0) + c'\sigma^-(k), \\ A'_\beta = c\sigma^+(k + 2\omega_0) + s'\sigma^-(k). \end{cases}$$

(ii) *The polarizability tensor*

We shall calculate this for the even isotopes of mercury, taking account only of the transition  $6^3P_1 - 6^1S_0$ , the intercombination resonance line. The system is typical of those which show a classical Zeeman effect. A semi-classical calculation of the response of stationary mercury atoms in the ground state  $|g\rangle$  to the combination of magnetic fields we have described, and to an electric field  $\mathbf{E}(t)$ , representing irradiation by light, has been given by Dodd & Series (1961). If  $\mathbf{E}(t)$  is particularized as  $\mathbf{E}e^{-ikt}$ , their equation (20) may be integrated directly to give an expression for  $|t\rangle$ , the state vector of an atom at time  $t$ . The matrix element  $\langle g|\mathbf{P}|t\rangle$  then gives the induced electric dipole moment, and yields the polarizability tensor per atom:

$$\langle g|\mathbf{P}|t\rangle = \boldsymbol{\alpha}^{(i)}\mathbf{E}e^{-ikt}, \quad (10)$$

where the index  $(i)$  labels one atom. (The calculation of the induced dipole moment when there is a multiplicity of states in the ground level is considered elsewhere (Series 1966).)

From (10) we have (after the correction of equations (7), (19), (20), and (24) of Dodd & Series by introducing a minus sign in the equation for  $\mathcal{H}_{\text{opt.}}$ ),

$$\alpha_{mn}^{(i)}(t) = \frac{1}{\hbar} \mathcal{F}_{mn} \sum_{\mu} \frac{\langle m|\mu\rangle \langle \mu|n\rangle \exp[-i(m-n)\omega_0 t]}{(k_{n,\mu} - k - \frac{1}{2}i\Gamma)}, \quad (11)$$

where

$$\mathcal{F}_{mn} = \langle g|\mathbf{e}_m^* \cdot \mathbf{P}|m\rangle \langle n|\mathbf{e}_n \cdot \mathbf{P}|g\rangle,$$

$\langle m|\mu\rangle$  and  $\langle \mu|n\rangle$  are rotation matrix elements, and  $m, n$  and  $\mu$  take the values 0,  $\pm 1$ . (We are not interested in  $\mathcal{F}_{mn}$  when either  $m$  or  $n = 0$ .) The frequencies  $k_{n,\mu} = k_i + n\omega_0 + \mu p$  are the resonance frequencies of the atom under the influence of the magnetic fields.  $k_i$  is the resonance frequency in the absence of fields, and  $p$  the Larmor frequency in the 'effective' field  $[(H - H_0)^2 + H_1^2]^{\frac{1}{2}}$ .  $\Gamma$  is the damping constant of the excited state.

The bulk polarizability is obtained by summing (11) over the  $N$  atoms per unit volume. Introducing the Doppler distribution of the resonance frequencies  $k_i$ , we have,

$$dN = N(k_i) dk_i = (N/\Delta\pi^{\frac{1}{2}}) \exp[-(k_0 - k_i)^2/\Delta^2] dk_i,$$

where  $2\Delta(\ln 2)^{\frac{1}{2}}$  is the width at half maximum, and  $k_0$  is the frequency of the peak. Thus

$$\begin{aligned} \alpha_{mn}(t) &= \sum_i \alpha_{mn}^{(i)}(t) = \int \alpha_{mn}^{(i)}(t) dN \\ &= (N/\Delta\pi^{\frac{1}{2}}) (\mathcal{F}_{mn}/\hbar) \sum_{\mu} \langle m|\mu\rangle \langle \mu|n\rangle \exp[-i(m-n)\omega_0 t] \int_{-\infty}^{\infty} \frac{e^{-t^2}}{t - (x_{n,\mu} + iy)} dt \\ &= N(\mathcal{F}_{mn}/\hbar\Delta) \sum_{\mu} \langle m|\mu\rangle \langle \mu|n\rangle \exp[-i(m-n)\omega_0 t] Z(x_{n,\mu} + iy), \end{aligned} \quad (12)$$

where

$$\begin{aligned} t &= (k_i - k_0)/\Delta, \\ x_{n,\mu} &= [k - (k_0 + n\omega_0 + \mu p)]/\Delta, \\ y &= \Gamma/2\Delta, \end{aligned}$$

and  $Z(x + iy)$  is the plasma dispersion function,

$$\pi^{-\frac{1}{2}} \int_{-\infty}^{\infty} \frac{e^{-t^2}}{t - (x + iy)} dt.$$

The real and imaginary parts of  $Z(x + iy)$  have been tabulated (Fried & Conte 1961). In our particular case,  $y$  is of order  $10^{-3}$ , and the imaginary part of  $Z$ , which determines the absorption of the medium, is almost Gaussian. The real part is antisymmetrical about  $x = 0$ , with turning points at  $x \approx \pm 1$ . The function is plotted in figure 1a. Some properties of  $Z$  are discussed in the appendix.

The matrix elements  $\alpha_{mn}^{(l)}$  which describe the response of the medium to the components ( $l$ ) of the field  $\mathbf{E}^{(l)}$  (equation (3)) are

$$\left. \begin{aligned} \alpha_{11}^{(l)} &= (NP^2/\hbar\Delta) \{c^4 Z[(a^{(l)} - p)/\Delta] + 2s^2 c^2 Z(a^{(l)}/\Delta) + s^4 Z[(a^{(l)} + p)/\Delta]\}, \\ \alpha_{-1-1}^{(l)} &= (NP^2/\hbar\Delta) \{s^4 Z[(a^{(l)} - p)/\Delta] + 2s^2 c^2 Z(a^{(l)}/\Delta) + c^4 Z[(a^{(l)} + p)/\Delta]\}, \\ \alpha_{-11}^{(l)}(t) &= (NP^2/\hbar\Delta) \{s^2 c^2 Z[(a^{(l)} - p)/\Delta] - 2s^2 c^2 Z(a^{(l)}/\Delta) \\ &\quad + s^2 c^2 Z[(a^{(l)} + p)/\Delta]\} \exp(2i\omega_0 t), \\ \alpha_{1-1}^{(l)}(t) &= (NP^2/\hbar\Delta) \{s^2 c^2 Z[(a^{(l)} - p)/\Delta] - 2s^2 c^2 Z(a^{(l)}/\Delta) \\ &\quad + s^2 c^2 Z[(a^{(l)} + p)/\Delta]\} \exp(-2i\omega_0 t), \end{aligned} \right\} \quad (13)$$



where  $a^{(l)} = (k - l\omega_0 - k_0 + \frac{1}{2}i\Gamma)$ ,  $s = \sin \frac{1}{2}\beta$ ,  $c = \cos \frac{1}{2}\beta$ , and  $\beta$  is the angle  $\tan^{-1} H_1/(H - H_0)$ .  $P$  is the reduced matrix element  $\langle 1; P; 0 \rangle$ .

The refractive indices  $n_{\alpha, \beta} = K_{\alpha, \beta} c/k$  may be expressed in terms of the  $\alpha_{mn}$ , and hence in terms of the  $Z$ , through equations (6) and (1a). The following combinations of the  $Z$  are of frequent occurrence:

$$\left. \begin{aligned} F^{(l)} &= Z[(a^{(l)} - p)/\Delta] - Z[(a^{(l)} + p)/\Delta] && \text{(the Faraday function),} \\ D^{(l)} &= Z[(a^{(l)} - p)/\Delta] + Z[(a^{(l)} + p)/\Delta] && \text{(the mean dispersion function),} \\ B^{(l)} &= Z(a^{(l)}/\Delta) - \frac{1}{2}D^{(l)}, && \text{(the birefringence function).} \end{aligned} \right\} \quad (14)$$

In terms of these functions we have:

$$\left. \begin{aligned} \alpha_{11}^{(l)} - \alpha_{-1-1}^{(l)} &= (NP^2/\hbar\Delta) F^{(l)} \cos \beta, \\ \alpha_{11}^{(l)} + \alpha_{-1-1}^{(l)} &= (NP^2/\hbar\Delta) (D^{(l)} + B^{(l)} \sin^2 \beta), \\ \alpha_{-11}^{(l)}(t) &= -\frac{1}{2}(NP^2/\hbar\Delta) B^{(l)} \sin^2 \beta e^{2i\omega_0 t}, \\ \alpha_{1-1}^{(l)}(t) &= -\frac{1}{2}(NP^2/\hbar\Delta) B^{(l)} \sin^2 \beta e^{-2i\omega_0 t}. \end{aligned} \right\} \quad (13a)$$

We then obtain

$$n_{\alpha, \beta}^{(l)} = 1 + (\pi NP^2/\hbar\Delta) [D^{(l)} + B^{(l)} \sin^2 \beta \pm (F^{(l)2} \cos^2 \beta + B^{(l)2} \sin^4 \beta)^{\frac{1}{2}}]. \quad (15)$$

$F$ ,  $B$  and  $D$  will be recognized as familiar functions when the following special cases are examined:

With a longitudinal field only ( $\beta = 0$ ), the eigenwaves are the circularly polarized waves  $\sigma^+$  and  $\sigma^-$ . The mean refractive index of these waves is given by

$$\frac{1}{2}(n_{\sigma^+} + n_{\sigma^-}) = 1 + (\pi NP^2/\hbar\Delta) D, \quad (15a)$$

and the difference in the refractive indices by

$$(n_{\sigma^+} - n_{\sigma^-}) = (2\pi NP^2/\hbar\Delta) F. \quad (15b)$$

When the field is transverse and static ( $\omega_0 = 0$ ,  $\beta = \frac{1}{2}\pi$ ), the eigenwaves are the linearly polarized waves  $\pi$  and  $\sigma$ . In this case the mean refractive index is

$$\frac{1}{2}(n_{\pi} + n_{\sigma}) = 1 + (\pi NP^2/\hbar\Delta) (B + D), \quad (15c)$$

and the difference

$$(n_{\pi} - n_{\sigma}) = (2\pi NP^2/\hbar\Delta) B. \quad (15d)$$

The functions  $F$ ,  $B$  and  $D$  are plotted in figure 3 to illustrate the role of  $p$  and  $\omega_0$ .

### (iii) The transmitted intensity

The general expression for a wave in the medium is

$$\mathbf{E}(k) = \sum_{\substack{l \\ r=\alpha, \beta}} a_r^{(l)} \mathbf{A}_r^{(l)}(t) \exp i[K_r^{(l)} z - (k - l\omega_0) t], \quad (16)$$

where the  $\mathbf{A}_r^{(l)}(t)$  are given by equations (9) and the  $a_r^{(l)}$  are determined from boundary conditions.

For an unmodulated, linearly polarized incident wave,  $E_0(k) [(\mathbf{i} - \mathbf{j})/\sqrt{2}] e^{-ik(t-z/c)}$ , which strikes the medium in the plane  $z = 0$ , the boundary condition requires the inclusion of two pairs of eigenwaves,  $l = \pm 1$  (figure 2). The condition is satisfied by

$$\left. \begin{aligned} a_\alpha &= \frac{1}{2} E_0(k) s(1+i); & a'_\alpha &= \frac{1}{2} E_0(k) c'(1-i), \\ a_\beta &= -\frac{1}{2} E_0(k) c(1+i); & a'_\beta &= \frac{1}{2} E_0(k) s'(1-i), \end{aligned} \right\} \quad (17)$$

where the primed and unprimed quantities refer to  $l = +1$  and  $l = -1$  respectively, and  $s$  and  $c$  are defined in equations (8) and (9).

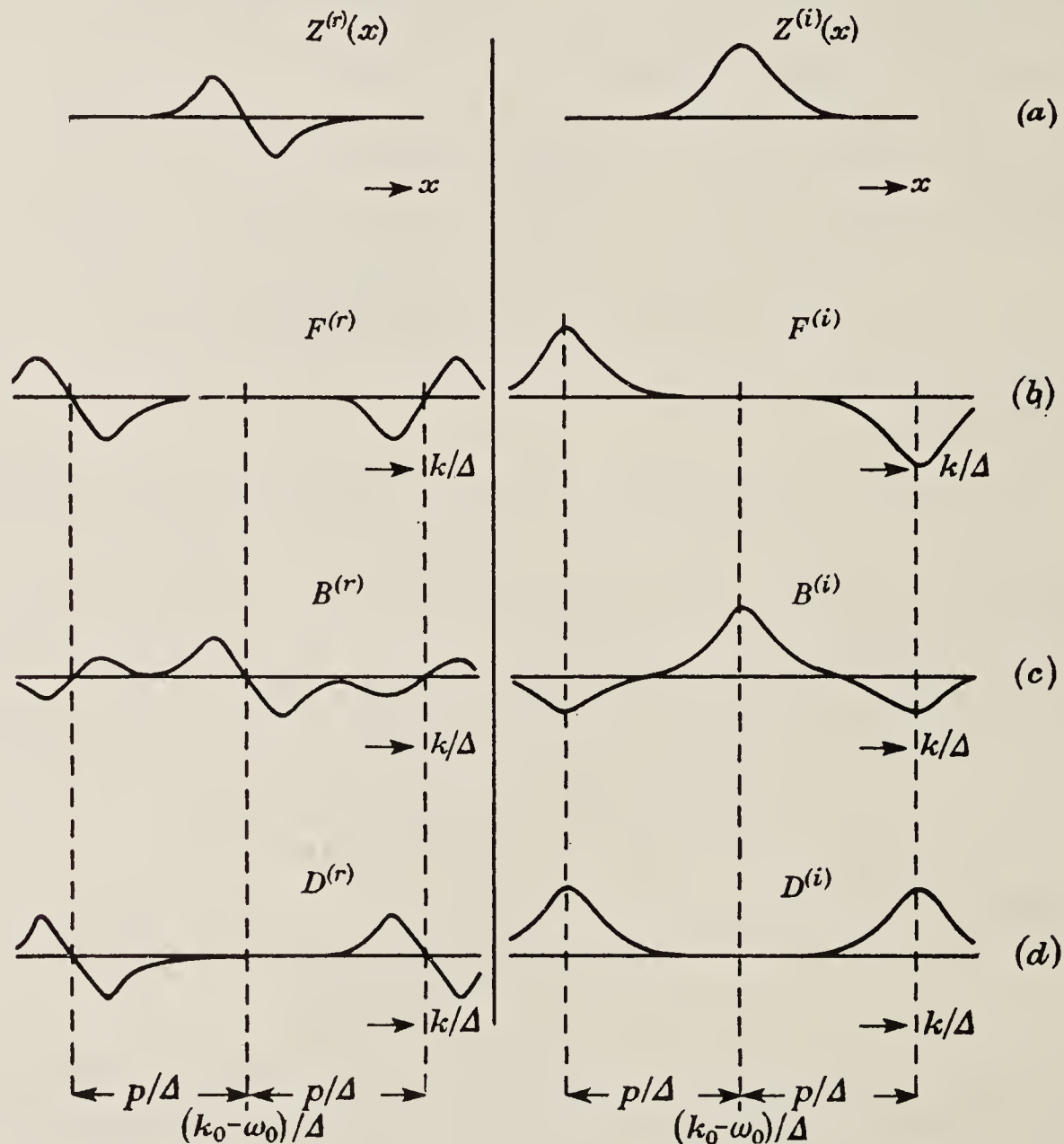


FIGURE 3. Real and imaginary parts of the dispersion functions, plotted for  $y \ll 1$  ( $\Delta \gg \Gamma$ ). (a)  $Z(x) = Z^{(r)}(x) + iZ^{(i)}(x)$ . The curves are centred at  $x = 0$ . The turning points of  $Z^{(r)}(x)$ , and the half-value points of  $Z^{(i)}(x)$ , occur near  $x = 1$ . (b), (c), (d).  $F$ ,  $B$  and  $D$  as functions of  $(k/\Delta)$ , with  $l = 1$ . The central frequency is  $(k_0 - \omega_0)/\Delta$ . For  $l = -1$  the functions are displaced by  $2\omega_0/\Delta$  along the axis of  $(k/\Delta)$ . A particular value of  $p$  greater than  $\Delta$  has been chosen.

With the use of these coefficients and the expressions for the  $\mathbf{A}$  given by (9), the wave at  $z = L$  is found to be

$$\mathbf{E}(k, L) = E_0(k) e^{-ikt} \mathbf{\Omega}, \quad (18)$$

where

$$\begin{aligned} \mathbf{\Omega} = & -\frac{1}{2} \{ [s^2(1+i) \mathbf{e}_1^0 - sc(1+i) \mathbf{e}_{-1}^0 e^{2i\omega_0 t}] \exp[iK_\alpha L] \\ & + [c^2(1+i) \mathbf{e}_1^0 + sc(1+i) \mathbf{e}_{-1}^0 e^{2i\omega_0 t}] \exp[iK_\beta L] \\ & + [s'c'(1-i) \mathbf{e}_1^0 e^{-2i\omega_0 t} - c'^2(1-i) \mathbf{e}_{-1}^0] \exp[iK'_\alpha L] \\ & + [-s'c'(1-i) \mathbf{e}_1^0 e^{-2i\omega_0 t} - s'^2(1-i) \mathbf{e}_{-1}^0] \exp[iK'_\beta L] \}. \end{aligned}$$



The component which passes an analyser parallel to the unit vector  $\mathbf{e}^0$  (which we shall take to be  $(\mathbf{i} + \mathbf{j})/\sqrt{2}$ ) is  $\mathbf{e}^0 \cdot \mathbf{E}(k, L)$ , and the intensity of the Fourier component  $k$  is the modulus squared of this quantity. The total transmitted intensity is

$$I = \int_{-\infty}^{\infty} \rho(k) |\mathbf{e}^0 \cdot \boldsymbol{\Omega}|^2 dk, \quad (19)$$

where  $\rho(k) = E_0^2(k)$  is the spectral density of the incident radiation.

(iv) *The weak scattering approximation*

The only important approximation we have made so far is that the polarization of the medium be small, i.e.  $(n-1) \ll 1$ . This secures that the waves be transverse, and is equivalent to ignoring the  $\pi$  radiation.

A more stringent approximation, namely  $(n-1)kL/c \ll 1$ , enables us to reduce equation (19) to simple and recognizable forms, and to make a close comparison with lateral scattering. This we shall call the 'weak scattering' approximation, since the results correspond to single scattering, as opposed to multiple scattering, in the lateral case.

To assess the validity of the weak scattering approximation in any particular case, we need to evaluate the expression for the refractive index, (15). We have

$$(n_{\alpha, \beta} - 1) = (\pi NP^2/\hbar\Delta) [D + B \sin^2 \beta \pm (F^2 \cos^2 \beta + B^2 \sin^4 \beta)^{\frac{1}{2}}]. \quad (20)$$

The maximum value of the expression in square brackets is of the order of the maximum value of  $Z$ , which tends to 1 when  $\Delta \gg \Gamma$ , and to  $2\Delta/\Gamma$  when  $\Delta \ll \Gamma$ . It will nearly always be true that  $\Delta \gg \Gamma$ , so that the important factor on the right hand side is the first. For the resonance line of mercury, 2537 Å, in the vapour at 0 °C,  $\Delta \gg \Gamma$ , and the value of  $(\pi NP^2/\hbar\Delta)$  is of order  $10^{-7}$ . Hence, for a path length of 1 cm,  $(n-1)kL/c$  is of order  $10^{-2}$ , which satisfies the condition.

The approximation  $(n-1)kL/c \ll 1$  enables us to simplify the expressions  $e^{iKL} = e^{inkL/c}$  in equation (18). We have

$$\begin{aligned} e^{iKL} &= e^{ikL/c} e^{i(n-1)kL/c} \\ &\approx e^{ikL/c} [1 + i(n-1)kL/c], \end{aligned} \quad (21)$$

with  $(n-1)$  given by equation (20) above.

It is particularly to be noticed that this approximation takes account of absorption, no less than dispersion.  $D$ ,  $B$  and  $F$  are complex functions of  $k$ . Hence  $n$  is also complex. The results we shall derive arise from differential absorption of the eigenwaves as well as from differential dispersion.

Using equations (20) and (21) in (18), and taking the scalar product of  $\mathbf{E}(k, L)$  with the unit vector  $(\mathbf{i} + \mathbf{j})/\sqrt{2}$  (chosen to be perpendicular to the polarization of the incident light), we find the component  $E_{\perp}$  which passes a crossed analyser:

$$E_{\perp} = E_0(k) e^{-ik(t-L/c)} (kL/c) (\pi NP^2/\hbar\Delta) \Omega_{\perp}, \quad (22)$$

where

$$\begin{aligned} \Omega_{\perp} &= -\frac{1}{2} \{ D + B \sin^2 \beta + F \cos \beta + B \sin^2 \beta \sin 2\omega_0 t - iB \sin^2 \beta \cos 2\omega_0 t \\ &\quad - D' - B' \sin^2 \beta + F' \cos \beta - B' \sin^2 \beta \sin 2\omega_0 t - iB' \sin^2 \beta \cos 2\omega_0 t \}. \end{aligned}$$

(It will be recalled that the unprimed and primed quantities refer to  $l = +1$  and  $-1$ , respectively.)

We notice in (22) the factor  $(NL)$ , which is independent of frequency, and which appears as  $(NL)^2$  when the intensity is calculated by (19). Now,  $(NL)$  is the number of atoms per unit cross section of the beam, so that the appearance of this factor squared demonstrates explicitly the coherence between different atoms.

(v) *Magnetic resonance in the weak scattering approximation*

Calculation of the intensity of the transmitted light requires the evaluation of  $|E_{\perp}|^2$ , and hence, among other things, a consideration of simple cross products such as  $D^* B \sin^2 \beta$ , in which the dispersion functions have the same value of  $l$ , and mixed cross products such as  $D^* B' \sin^2 \beta$ , in which the functions have different  $l$ . The relative magnitudes of terms of these two types depends on  $\omega_0$ , since  $F$ ,  $B$  and  $D$  are centred at  $(k_0 - \omega_0)/\Delta$  (see figure 3), whereas  $F'$ ,  $B'$ , and  $D'$  are centred at  $(k_0 + \omega_0)/\Delta$ . Thus, for sufficiently large values of  $\omega_0$ , the functions belonging to different  $l$  no longer overlap, and the mixed cross products become negligibly small. The condition under which the mixed cross products may be neglected is that  $2\omega_0$  should greatly exceed the resonance line width, the minimum value of which (in units of  $\Delta$ ) will be of the order of the width of the  $Z$  function,  $\delta_z = \Delta_z/\Delta$ . We shall think of  $\Delta_z/\Delta$  as loosely defined, though it could be defined precisely, as, for example, the width at half-intensity of the imaginary part of  $Z$ .

We are led to consider separately, therefore, the two situations, (a)  $\omega_0 \gg \Delta_z$ , in which the mixed cross terms may be neglected, and (b)  $\omega_0 \ll \Delta_z$ , in which the two sets of functions are indistinguishable. In these situations we have

$$(a) \quad \omega_0 \gg \Delta_z,$$

$$\Omega_{\perp} \approx -\frac{1}{2}(D + B \sin^2 \beta + F \cos \beta + B' \sin^2 \beta \sin 2\omega_0 t - iB \sin^2 \beta \cos 2\omega_0 t) \quad (23a)$$

in the region  $k = k_0 + \omega_0$ , and an identical expression in the primed quantities in the region  $k = k_0 - \omega_0$ , and

$$(b) \quad \omega_0 \ll \Delta_z,$$

$$\Omega_{\perp} \approx -(F \cos \beta - iB \sin^2 \beta \cos 2\omega_0 t). \quad (23b)$$

Using equations (19), (22) and (23), and treating  $\rho(k)$  as constant over the regions where the dispersion functions have appreciable values, we obtain expressions for the intensity in terms of integrals over  $k$  of quadratic forms of the dispersion function.

These integrals are of the form

$$\int_{-\infty}^{\infty} |F|^2 dk, \int_{-\infty}^{\infty} |B|^2 dk, \int_{-\infty}^{\infty} |D|^2 dk, \int_{-\infty}^{\infty} FB^* dk, \int_{-\infty}^{\infty} BD^* dk, \text{ and } \int_{-\infty}^{\infty} DF^* dk,$$

and may be performed analytically. The results are given in the appendix. They are all based on the result

$$\int_{-\infty}^{\infty} Z(x - a - iy) Z(x + b + iy) dx = -i2^{\frac{1}{2}}\pi Z\left\{\frac{1}{2^{\frac{1}{2}}}(a + b) + i2^{\frac{1}{2}}y\right\}, \quad (24)$$

which is derived in the appendix.



The form of the variables in this result is particularly to be noticed.  $a$  and  $b$  take the values  $(0, \pm 1)p/\Delta$ , and  $y = \Gamma/2\Delta$ , so that the variables on the right hand side of (24) are  $(0, 1, 2)p/2^{\frac{1}{2}}\Delta$  and  $y = \Gamma/2^{\frac{1}{2}}\Delta$ . We shall shortly be making a comparison between the general form of the dispersion function as it occurs in this result and the Lorentzian form to which it reduces, namely  $-2^{\frac{1}{2}}\Delta/[(0, 1, 2)p + i\Gamma]$  (see appendix, § IV).

The final expressions for the intensity may be expressed in terms of linear combinations of the components of  $Z$ , that is,

$$\left. \begin{aligned} Z(rp' + i\Gamma') &= X(rp', \Gamma') + iY(rp', \Gamma'), \\ r &= 0, 1, 2; \quad p' = p/2^{\frac{1}{2}}\Delta; \quad \Gamma' = \Gamma/2^{\frac{1}{2}}\Delta. \end{aligned} \right\} \quad (25)$$

The combinations we need are:

$$\left. \begin{aligned} V_{12}(p') &= X(2p', \Gamma') - 2X(p', \Gamma'), \\ W_0(p') &= Y(0, \Gamma'), \\ W_{01}(p') &= Y(0, \Gamma') - Y(p', \Gamma'), \\ W_{02}(p') &= Y(0, \Gamma') - Y(2p', \Gamma'), \\ W_{012}(p') &= W_{01}(p') - \frac{1}{4}W_{02}(p'). \end{aligned} \right\} \quad (26)$$

(a) *The case  $\omega_0 \gg \Delta_z$*

In this case, the intensity of the transmitted light is found to be

$$I_a = I_0[W_0 - A_Z - D_Z \sin 2\omega_0 t - E_Z \cos 2\omega_0 t], \quad (27)$$

with  $I_0 = \rho(k_0)(kL/c)^2(\pi NP^2/\hbar\Delta)^2(2^{\frac{3}{2}}\pi\Delta)$ , and

$$\left. \begin{aligned} A_Z &= \sin^2 \beta W_{01} - \sin^4 \beta W_{012}, \\ D_Z &= \sin^2 \beta [W_{01} - \frac{1}{2}W_{02}] - \sin^4 \beta W_{012}, \\ E_Z &= -\frac{1}{2} \cos \beta \sin^2 \beta V_{12}. \end{aligned} \right\} \quad (28)$$

$I_0 W_0$  is the intensity when  $H_1$  is zero.

$A_Z$ ,  $D_Z$  and  $E_Z$  are resonance functions of the variable  $\delta/\Delta = \gamma(H - H_0)/\Delta$ , which occurs in  $\beta = \tan^{-1}(b/\delta)$ , ( $b = \gamma H_1$ ), and also in  $p/\Delta = (\delta^2 + b^2)^{\frac{1}{2}}/\Delta$ .  $A_Z$  and  $D_Z$  are plotted in figure 4 for various values of  $b/\Delta$ . The plot of  $A_Z$  immediately calls to mind the double-resonance curves of Brossel & Bitter (1952).  $D_Z$  is similar to the resonance curve  $D$  for modulated light found by Dodd *et al.* (1963; figure 3), and  $E_Z$  (not shown in figure 4) is similar to the quadrature resonance curve  $E$ . Clearly, the functions  $A_Z$ ,  $D_Z$  and  $E_Z$  must be intimately related to the functions which describe the intensity of the laterally scattered light. They are, indeed, the generalized forms of these functions, and reduce identically to the expressions in the earlier papers if the generalized form of the dispersion function,  $Z(p/2^{\frac{1}{2}}\Delta)$ , is replaced by its Lorentzian equivalent  $-2^{\frac{1}{2}}\Delta/(p + i\Gamma)$ . Notice that if the dimensionless form  $-1/(x + i)$  is used for the Lorentz function, the scale constant for the frequency,  $2^{\frac{1}{2}}\Delta$ , is to be replaced by  $\Gamma$ .

Moreover, if equation (32) of Dodd & Series (1961) is applied to forward scattering with the geometrical arrangement we are here contemplating, the resulting expression has exactly the form of equation (27) with  $A_Z$ ,  $D_Z$  and  $E_Z$  replaced

by  $A$ ,  $D$  and  $E$ . This expression gives the intensity of the forward scattered light with neglect of coherence between the radiation scattered from different atoms.

More important than the change which this coherence brings about in the shape of the resonance functions is the change of width on the frequency scale, as expressed by the change of scale constant from  $\Gamma$  to  $\Delta\sqrt{2}$ , that is, in the case of the mercury resonance line, from the order of 1 Mc/s to the order of 1000 Mc/s. The change of

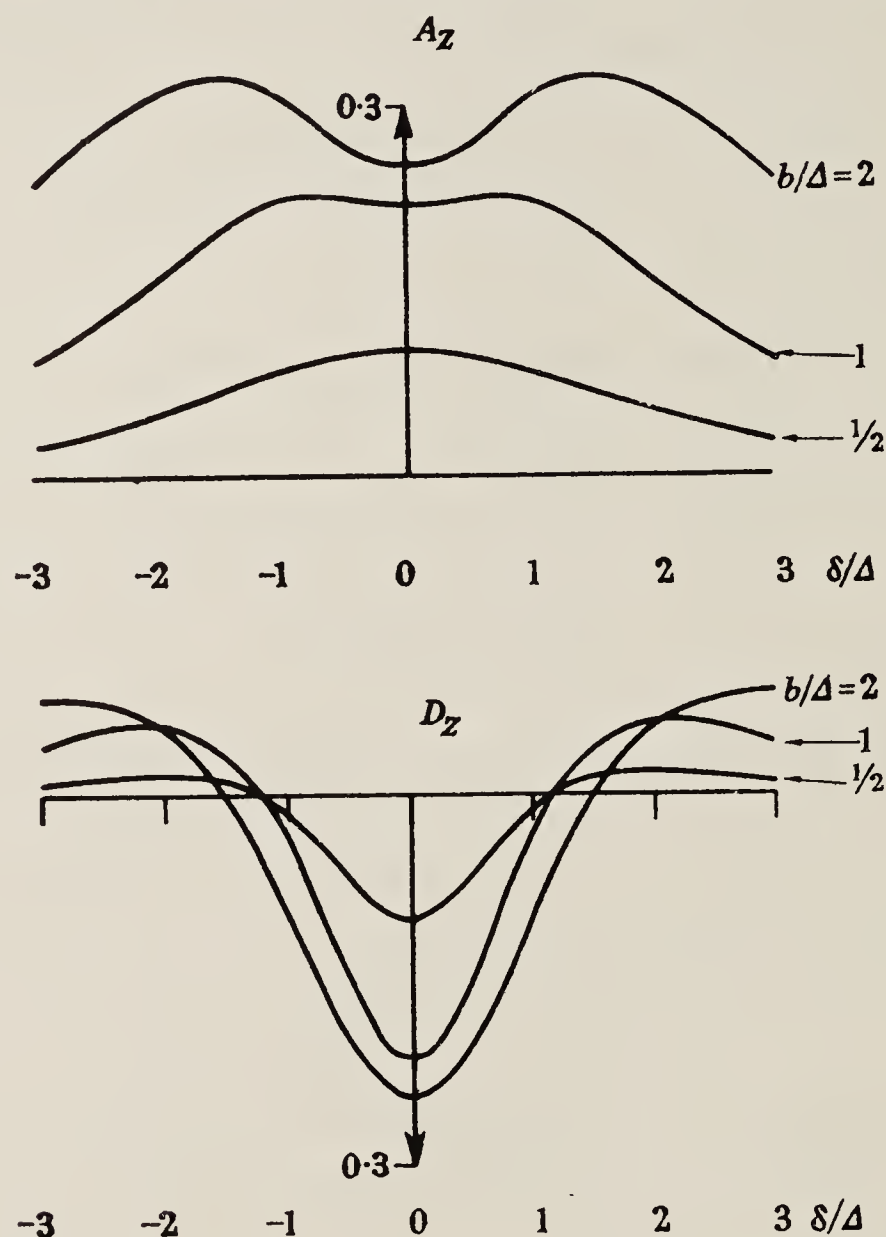


FIGURE 4. The resonance functions  $A_Z$  and  $D_Z$ , plotted for  $\Delta \gg \Gamma$ .  
(a)  $b/\Delta = 2$ ; (b)  $b/\Delta = 1$ ; (c)  $b/\Delta = \frac{1}{2}$ .

scale constant affects not only the width of the resonance curves, but also the strength of the transverse field required to produce a measurable effect. Whereas one can detect resonances in the laterally scattered light with radio-frequency fields of order 0.05 G, one would require about 50 G to produce effects in the forward scattered light.

(b) *The case  $\omega_0 \ll \Delta_z$*

In this case, the intensity of the transmitted light calculated from (19) and (23) is

$$\begin{aligned} I_b &= I_0[P_Z + Q_Z \cos 2\omega_0 t + R_Z \cos 4\omega_0 t] \\ &= I_0[\tfrac{1}{2}K_Z + \tfrac{1}{2}F_Z(1 + \cos 4\omega_0 t) + 2E_Z \cos 2\omega_0 t], \end{aligned} \quad (29)$$

where  $I_0$  and  $E_Z$  are the expressions defined in equations (27) and (28),

$$K_Z = 2 \cos^2 \beta W_{02} \quad \text{and} \quad F_Z = \sin^4 \beta W_{012}. \quad (30)$$



The second form of equation (29) is written so as to correspond with equation (1) of Kibble & Series (1963), where functions  $K$  and  $F$  are introduced to describe the intensity of laterally scattered light when  $\omega_0 \ll \Gamma$ . As in case (a), the application of equation (32) of Dodd & Series (1961) to the conditions of the present section yields an expression similar to (29), with  $K_Z$ ,  $F_Z$  and  $E_Z$  replaced by  $K$ ,  $F$  and  $E$  respectively.

(vi) *Level-crossing in the weak scattering approximation*

The foregoing analysis is unnecessarily complicated when the applied magnetic fields are static, particularly if they are transverse or longitudinal. Nevertheless, it is easy to treat these situations as special cases of equation (29).

(a) *Static, transverse fields*

The result is obtained by setting  $\omega_0 = 0$  and  $\beta = \frac{1}{2}\pi$ . The phases in (29) have been chosen so that at time  $t = 0$  the transverse field  $H_1 = b/\gamma$  is in the direction  $\mathbf{i}$ , that is, at  $45^\circ$  to the electric vector of the light. Equation (29) reduces to

$$I_{\text{tr.}} = I_0[W_{012}(p = b)], \quad \text{which, for } \Delta \gg \Gamma,$$

$$\text{becomes} \quad I_0 \pi^{\frac{1}{2}} \{ [1 - \exp(-b^2/2\Delta^2)] - \frac{1}{4}[1 - \exp(-2b^2/\Delta^2)] \}. \quad (31)$$

$I_{\text{tr.}}$  is plotted against  $b/\Delta$  in figure 9(b).

The result (31) expresses the case of resonance at frequency zero, but, from another point of view, we may regard it as a case of multiple level-crossing. For, if we choose the direction of the transverse field as axis of quantization, the exciting light, linearly polarized at  $45^\circ$  to this axis, will excite the states  $|m = 0, \pm 1\rangle$ . The three Zeeman levels cross as the transverse field is reduced through zero.

The simpler case of the crossing of two levels is discussed in the next section.

(b) *Static, longitudinal fields*

The states  $|m = \pm 1\rangle$ , referred to the longitudinal axis, are excited by the linearly polarized light. With the transverse field equal to zero ( $b = 0$ ), the two levels cross as the longitudinal field  $H$  is reduced through zero. The intensity is obtained from (29) by setting  $\beta = 0$ . We obtain

$$I_{1c} = I_0[W_{02}(p = h)] = I_0 \pi^{\frac{1}{2}} [1 - \exp(-2h^2/\Delta^2)] \quad \text{when } \Delta \gg \Gamma, \quad (h = \gamma H). \quad (32)$$

$I_{1c}$  is plotted against  $h/\Delta$  in figure 5. Its resemblance to a zero-field level-crossing curve studied in laterally scattered light is obvious (see, for example, Kibble & Series 1961), but whereas the corresponding curve for laterally scattered light is an inverted Lorentzian of width at half-height equal to  $\Gamma$ , the curve of figure 5 is an inverted Gaussian of width  $h_{\frac{1}{2}} = \Delta(2 \ln 2)^{\frac{1}{2}} = 2^{-\frac{1}{2}}\Delta_D$ , where  $\Delta_D$  is the width at half-height of the Doppler distribution. The change of shape and change of scale constant appear in the level-crossing curve, just as in the magnetic resonance curves.

(vii) *Multiple scattering: coherence narrowing*

The condition  $(n-1)kL/c \ll 1$  can be secured in any given case by making  $N$ , the vapour density, or  $L$ , the length of the resonance vessel, sufficiently small. If we relax this condition by allowing  $(NL)$  to increase, we encounter the effects

of multiple scattering which, in laterally scattered light, give rise to 'coherence narrowing' (Barrat 1959). This is a narrowing of magnetic resonance curves which accompanies an increase of vapour density, and is explained as a transfer of coherence from atom to atom through the agency of the resonance radiation. In lateral scattering, the efficiency of the process is degraded by the element of randomness in the direction of scattering, but in forward scattering the direction is no longer random, and we might expect to find an enhancement of coherence narrowing. This is, in fact, what equations (18) and (19) predict.

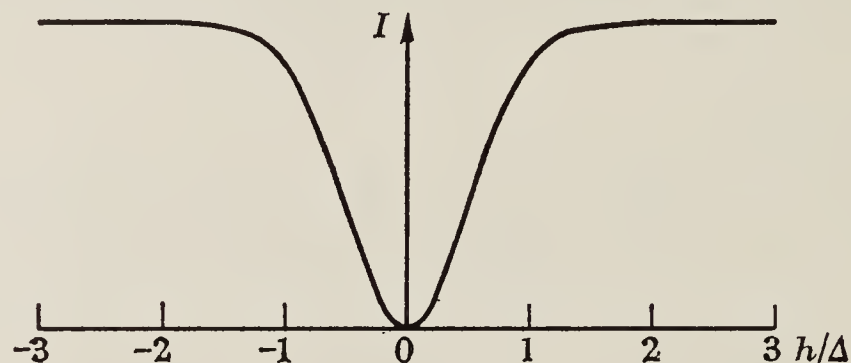


FIGURE 5. Theoretical zero-field level-crossing curve in the weak scattering approximation.

We shall study the coherence narrowing of the zero-field level-crossing, partly on grounds of simplicity, and partly because, in this case, we may remove also the other restriction under which we were working, namely  $(n-1) \ll 1$ . This restriction enabled us to use a transverse-wave solution for the eigenwaves in the general case when the field was oblique to the direction of propagation. When the field is in the direction of propagation, the polarizability tensor is diagonal, the eigenwaves are  $\sigma^+$  and  $\sigma^-$ , and the propagation constants may be found without approximation.

The component of the field which passes the crossed analyser,  $E_{\perp}$ , is given by equation (18) with

$$\left. \begin{aligned} s^2 &= \sin^2 \frac{1}{2}\theta = 1, \quad c^2 = \cos^2 \frac{1}{2}\theta = 0; \\ \text{whence} \quad E_{\perp} &= \frac{1}{2}iE_0(k)e^{-ikt}[\exp(iK_{\alpha}L) - \exp(iK_{\beta}L)], \\ \text{with} \quad K_{\alpha,\beta} &= (k/c)[1 + (\pi NP^2/\hbar\Delta)(D \pm F)]. \end{aligned} \right\} \quad (33)$$

(Primed and unprimed quantities are now identical.)

The transmitted intensity is

$$I_{\text{cn}} = \int \rho(k) |\sin \Phi|^2 \exp(-2K^{(i)}L) dk, \quad (34)$$

where  $\Phi = (kL/c)(\pi NP^2/\hbar\Delta)F(h/\Delta) = (kL/2c)(n_{\alpha} - n_{\beta})$ ,

and  $K^{(i)}L = (kL/c)(\pi NP^2/\hbar\Delta)D^{(i)}(h/\Delta) = (kL/2c)(n_{\alpha}^{(i)} + n_{\beta}^{(i)} - 2)$ ,

with  $h = \gamma H$ .  $K^{(i)}$ ,  $D^{(i)}$  and  $n^{(i)}$  are the imaginary parts of these complex functions.

The limiting value of equation (34) when  $(NL)$  is small (i.e. when  $\Phi$  and  $K^{(i)}L$  are  $\ll 1$ ) is given by (32), as one can easily verify. The integral is not readily evaluated when  $\Phi$  and  $K^{(i)}L$  are not small, but interesting conclusions, valid for all values of  $(NL)$ , can be drawn for the range of  $H \ll \Delta/\gamma$ . In this region,  $F$  is linearly proportional



to  $\gamma H/\Delta$  and  $D^{(i)}$  is independent of  $H$  (see appendix). The intensity then depends on  $H$  only through the factor  $|\sin \Phi|^2$  in (34), in which  $H$  occurs with  $N$  and  $L$  in the form  $(NLH)$ . Hence the intensity would be a function of  $(NLH)$ , and not of  $(NL)$ , were it not for the attenuation, which depends strongly on  $(NL)$ . We therefore consider the reduced intensity

$$I^0 = \frac{\int \rho(k) |\sin \Phi|^2 \exp(-2K^{(i)}L) dk}{\int \rho(k) \exp(-2K^{(i)}L) dk}, \quad (35)$$

in which the normalization factor

$$\int \rho(k) \exp(-2K^{(i)}L) dk$$

is the intensity of light in front of the analyser, with zero field applied to the vapour. The effect of attenuation on the intensity has now been largely removed, since

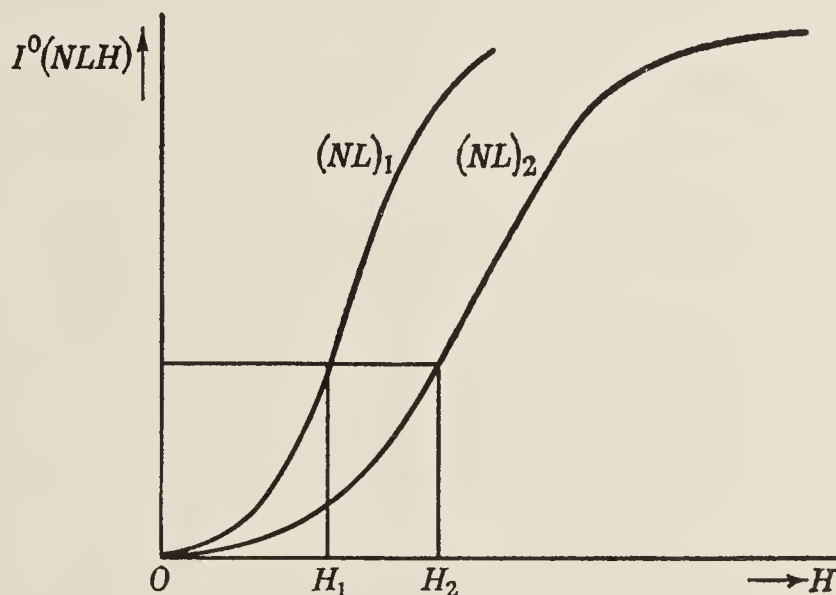


FIGURE 6. Coherence narrowing. Schematic curve, with disregard of distortion caused by attenuation.  $H_1/H_2 = (NL)_2/(NL)_1$ , ( $\gamma H \ll \Delta$ ).

the variations of  $|\sin \Phi|^2$  with  $k$  occur over a range in which  $\exp(-2K^{(i)}L)$  is changing slowly. (This is a consequence of the factor  $\gamma H/\Delta$  in  $\Phi$ , but not in  $K^{(i)}$ .)  $I^0$  is therefore a function of  $(NLH)$ , not of  $(NL)$ , and we may write

$$I^0 = I^0(NLH), \quad (36)$$

subject to a small distortion caused by changes in the weighting function when  $(NL)$  changes.

Equation (36) implies coherence narrowing, for whatever be the form of  $I^0$  as a function of  $H$  for a given  $(NL)$ , the curve must shrink towards the  $I^0$  axis as  $(NL)$  is increased. Moreover, the shrinking is linearly proportional to  $(NL)$  even for large values of  $(NL)$ . This, as we predicted from general considerations, is a far stronger dependence on density than in lateral scattering. (Pressure-broadening has been neglected in this analysis, but it is believed that the results are insensitive to this effect).

While the linear relation has been deduced only for the region  $H \ll \Delta/\gamma$ , coherence narrowing takes place also in stronger fields. As the vapour density is increased, the level-crossing curve as a whole contracts towards the axis of  $I$  until the whole of the significant variation is found in the region  $H \ll \Delta/\gamma$ .

Finally, it is to be noticed that the linear relation deduced for longitudinal fields is not to be expected to hold for fields in arbitrary directions. Consider, for example, a static transverse field. The function  $B(\gamma H_1/\Delta)$  takes the place of  $F(\gamma H/\Delta)$  in equation (34). In the approximation  $H_1 \ll \Delta/\gamma$ ,  $B$  is proportional to  $H_1^2$ . Hence the reduced intensity is a function of  $(NLH_1^2)$ , subject to the distortion introduced by attenuation. This again implies coherence narrowing, but the dependence on density is weaker than in the case of longitudinal fields.

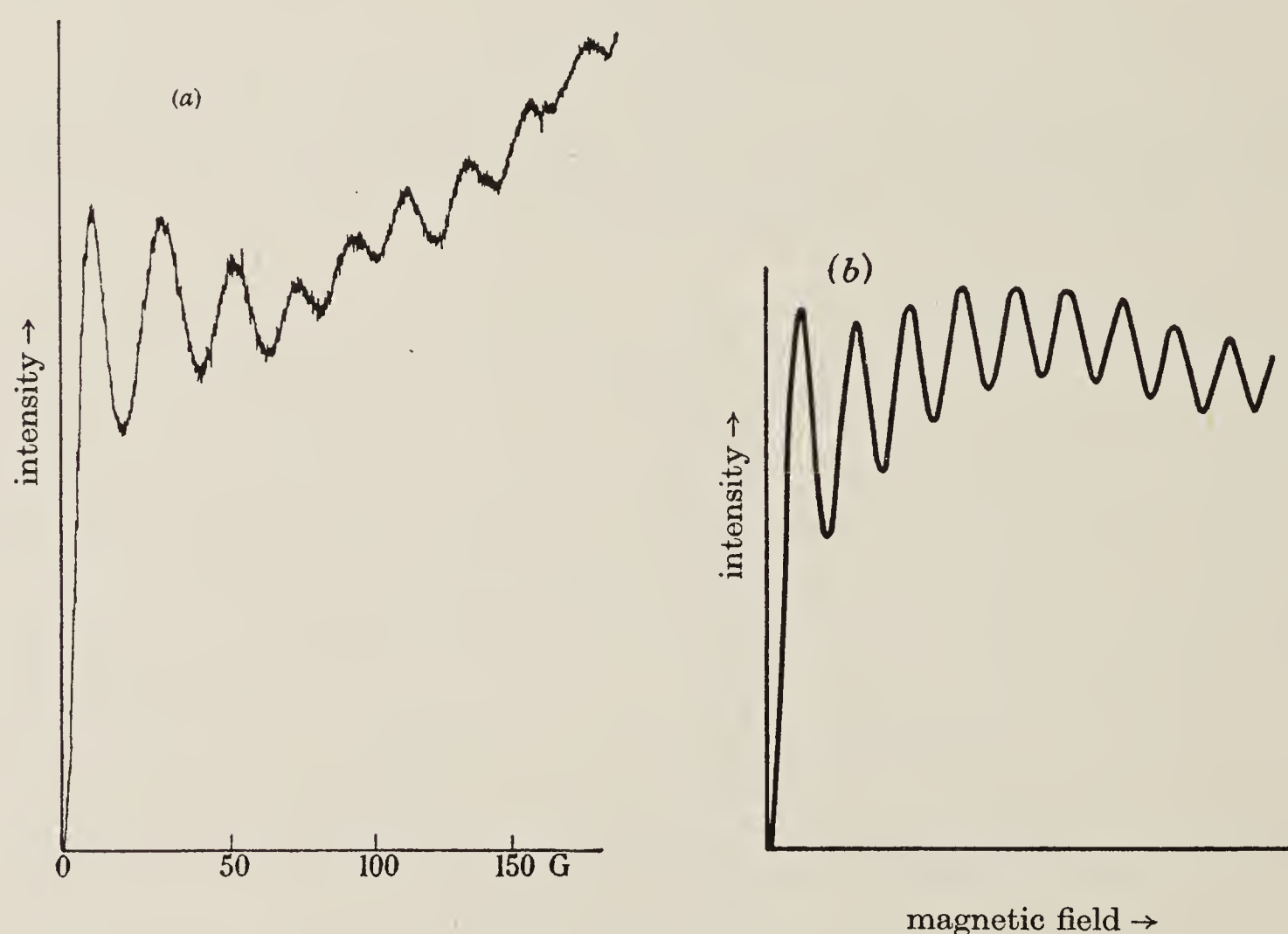


FIGURE 7. Zero-field level-crossing illustrating coherence narrowing and the effect of a light source of limited spectral range. (a) Experimental. (b) Theoretical.

(a) *Limitation of the spectral range of the light*

Returning to equation (34), we notice that the integrand oscillates as  $H$  is increased, owing to the factor  $|\sin \Phi|^2$ . These oscillations are smoothed out when the integration over  $k$  is performed, provided that the spectral density of the light is uniform over a sufficiently wide range. If the range of  $\rho(k)$  is restricted, the oscillations may not be entirely lost. This is illustrated in figure 7 (b), where a Gaussian form of width  $\Delta$  has been chosen for  $\rho(k)$ . Certain approximations which do not affect the features of the curve have been made in evaluating the integral.

The oscillations may be likened to the white-light fringes in interferometry which occur, as in the present analysis, when a limited portion of a spectral continuum is used as a light source.



## 3. EXPERIMENTAL STUDY

The experiments were not designed to verify the predictions of the last chapter, but rather to look for effects in the transmitted light when the magnitude of the applied fields was such that effects would certainly have been detected in the laterally scattered light. These experiments gave negative results. Positive results were obtained only when the fields were increased to larger values, as the analysis predicts. The orders of magnitude we have in mind in the following discussion are:

Doppler width at room temperature,  $\Delta \sim 10^9 \text{ c/s} \sim 500 \text{ G}$ .

Radiation width of  $^3P_1$  energy levels,  $\Gamma \sim 10^6 \text{ c/s} \sim 0.5 \text{ G}$ .

Width of zero-field level crossing ( $m = \pm 1$ ) studied in laterally scattered light  $\sim 0.5 \text{ G}$ . (Magnetic resonance signals can be detected with values of the transverse field as small as one-tenth of this.)

Range of magnetic fields used in the present experiments, 0 to 150 G.

The apparatus consisted of a mercury lamp, an absorption cell between crossed Rochon prisms, and lenses to collimate the light and focus it on to a photocell (figure 1). The lamp was a silica capsule, about the size of a half-watt resistor, filled with a few milligrams of natural mercury (or, for some experiments, separated isotopes), placed inside a cavity, and excited by a magnetron working at microwave frequencies. The absorption cell was cylindrical, about 5 cm long, and furnished with good quality end windows strong enough to support evacuation with negligible strain-induced birefringence. It was mounted in a box with provision for varying the temperature between 20 and 100 °C, and surrounded with Helmholtz coils to provide longitudinal and transverse fields.

Ideally, it would have been desirable to use a pinhole as the light source, and at the detector, in order to exclude light scattered near, but not in, the forward direction. (In this context, the forward direction means the range of directions comprised within the main cone of the Fraunhofer diffraction.) Since the more significant experiments yielded negative results, this refinement was considered unnecessary.

The experiments which yielded positive results are described below.

(i) *Longitudinal fields: the level-crossing curve, and coherence narrowing*

In figure 7(a) is shown a plot of the transmitted intensity as a function of longitudinal field, with the cell containing natural mercury at 75 °C. Its resemblance to the theoretical curve in figure 7(b) is striking. Identity of the curves is not to be expected because of the approximations made in computing the theoretical curve.

If figure 7(a) is combined with its image in negative fields, the zero-field level-crossing curve is obtained. Its shape is not Lorentzian, as are level-crossing curves obtained in laterally scattered light, and its width is determined by the vapour density and by the length of the absorption cell. Most striking is the fact that the width of the curve shown, while greater than the radiation width, is nevertheless only a small fraction of the Doppler width.

The peaks and troughs of figure 7(a) were reproduced almost identically when the vapour density was increased, but at lower values of the magnetic field. Such curves,

normalized to the same intensity in corresponding peaks, are identified as the reduced intensity  $I^0$  of equations (35) and (36). For particular features, the product of field strength and particle density,  $N$ , was constant until the field exceeded about 50 G. This behaviour is illustrated in figure 8, where  $H_f$ , the field at which a particular feature is found, is plotted against  $1/N$ . The four curves  $I_1, I_2, I_3, I_4$  correspond to the first peak, first trough, second peak and second trough, respectively. The linear behaviour is predicted by the theory (§2(vii)) in the approximation  $\gamma H/\Delta \ll 1$ . In the experiments, the linear region extends up to values of  $H$  given by  $\gamma H/\Delta \sim 0.1$ .

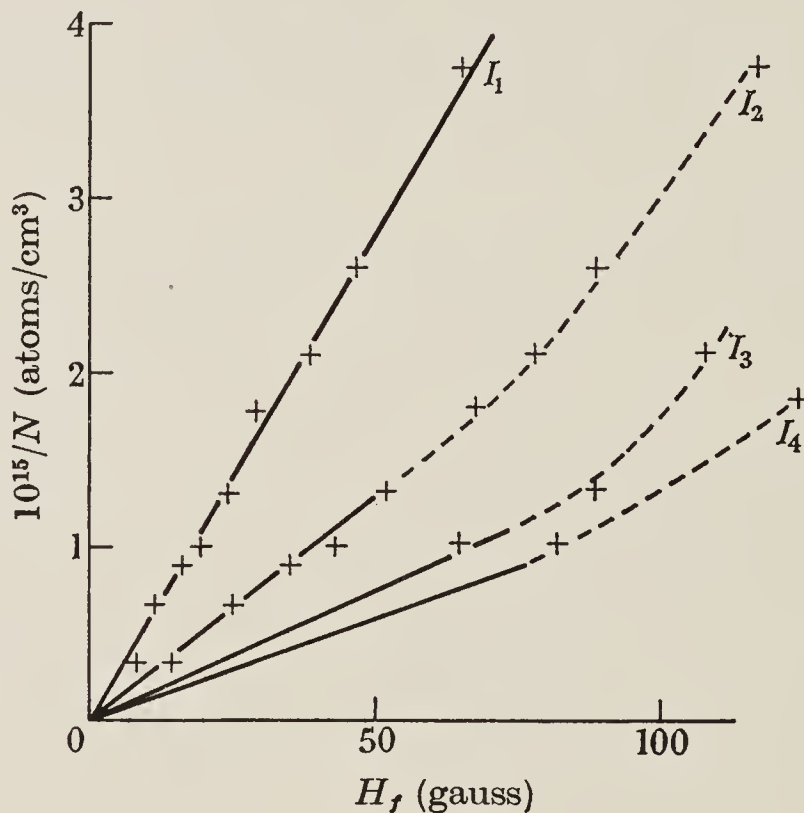


FIGURE 8. Coherence narrowing.  $1/N$  plotted against  $H_f$ .  $H_f$  is the field at which a particular feature occurs for a given value of  $N$ . The different curves refer to the peaks and troughs of figure 7.

An interesting detail was the observation that, when working with natural mercury, every 12th undulation of the sort seen in figure 7(a) was missing. With single isotopes, the effect was no longer present. This supports the interpretation, given in §2(vii)(a), that the undulations are analogous to 'white light' fringes in interferometry, in which the pattern changes according to the spectral composition of the light.

#### (ii) *Transverse fields*

Transverse fields up to 125 G were applied in a direction at  $45^\circ$  to the electric vector of the light. The change in intensity brought about by the transverse field was observed for different values of the longitudinal field.

In figure 9(a) is a plot of the intensity as a function of the transverse field for zero longitudinal field. This corresponds to the case of resonance at zero frequency studied in §2(vi)(a), except that the theoretical result, equation (31) and figure 9(b), was derived in the weak scattering approximation. For the experimental curve this approximation is invalid since the vapour density ( $\sim 10^{15}$  atoms/cm<sup>3</sup>) was too high. Comparison of the experimental and theoretical curves gives an indication of the extent of coherence narrowing. ( $b/\Delta = 1$  corresponds to a field of about 500 G)



It will be noticed that the curves rise less steeply when the field is transverse than when it is longitudinal. This is a consequence of the weakness of magnetic birefringence compared with Faraday rotation, and is expressed analytically by the quadratic dependence of  $B$  on  $H$ , and the linear dependence of  $F$ , for  $(\gamma H/\Delta) \ll 1$ .

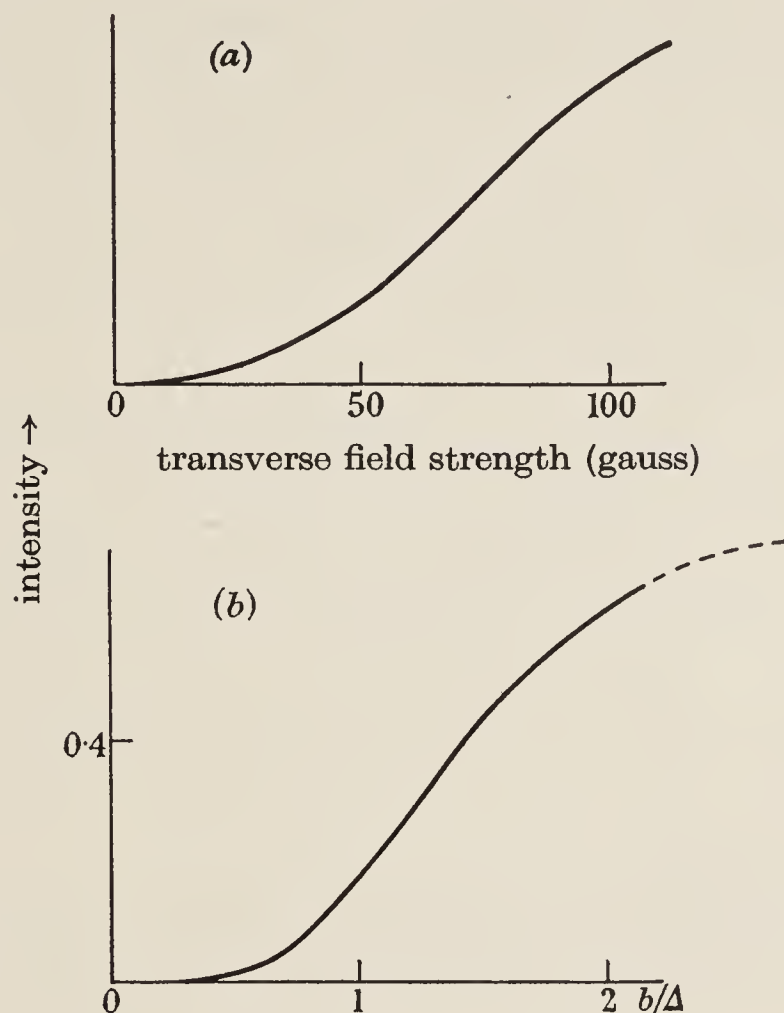


FIGURE 9. Magnetic resonance at zero frequency: intensity as a function of transverse field strength. (a) Experimental, under conditions of multiple scattering ( $N \sim 10^{15}$  atoms/cm<sup>3</sup>). (b) Theoretical, in the weak scattering approximation: the function  $W_{012}(b/\Delta)$ .

#### 4. CONCLUSIONS

The experiments support the analytical result that magnetic resonance and level-crossing phenomena do appear in the forward scattered light, but that the resonance line-shapes and widths are different from those which are found in laterally scattered light. The analysis yields the result that in forward scattering the plasma dispersion function plays the part which the Lorentzian plays in lateral scattering. When the Doppler width is much greater than the radiation width the calculated resonance line shapes are the Gaussian equivalents of the expressions found for lateral scattering. The Doppler width, rather than the radiation width, is the parameter in terms of which the effectiveness of magnetic fields is to be measured. Coherence narrowing is more pronounced in forward than in lateral scattering. For level crossing, the coherence narrowing is linearly proportional to the vapour density when the field is sufficiently small.

We are grateful to Dr S. Pancharatnam for his constructive suggestions concerning the presentation of the material, and for his help with some of the calculations. Two of us (A. C. and B. P. K.) are grateful for financial support from the Science Research Council.

## APPENDIX

(I) The function  $Z$ 

The evaluation of the integrals in § 2(v) is based on the results

$$\int_{-\infty}^{\infty} Z^*[(x-a), y] Z[(x+b), y] dx = -i2^{\frac{1}{2}}\pi Z[2^{-\frac{1}{2}}(a+b), 2^{\frac{1}{2}}y], \quad (\text{A } 1a)$$

and 
$$\int_{-\infty}^{\infty} Z[(x-a), y] Z[(x+b), y] dx = 0, \quad (\text{A } 1b)$$

where  $x, y, a$ , and  $b$  are real, and  $Z(x, y)$  is defined:

$$Z(x, y) = \pi^{-\frac{1}{2}} \int_{-\infty}^{\infty} \frac{e^{-t^2}}{t - (x + iy)} dt. \quad (\text{A } 2)$$

These results may be obtained by substituting (A 2) into the left hand side of (A 1) and changing the order of integration, as follows:

$$\begin{aligned} \text{left hand side} &= \pi^{-1} \int_{-\infty}^{\infty} dx \int_{-\infty}^{\infty} \frac{e^{-t^2} dt}{t - (x - a \mp iy)} \int_{-\infty}^{\infty} \frac{e^{-s^2} ds}{s - (x + b + iy)} \\ &= \pi^{-1} \int_{-\infty}^{\infty} e^{-t^2} dt \int_{-\infty}^{\infty} e^{-s^2} ds \int_{-\infty}^{\infty} \frac{dx}{[t - (x - a \mp iy)][s - (x + b + iy)]}, \end{aligned} \quad (\text{A } 3)$$

where the upper and lower signs in front of  $iy$  in the integrals over  $t$  and  $x$  correspond to (A 1a) and (A 1b) respectively.

The integral over  $x$  is easily evaluated by breaking the integrand into partial fractions and integrating the two parts separately. The result is

$$\frac{1}{(s-t) - (a+b) - iy(1 \pm 1)} [\mp \pi i - \pi i], \quad (\text{A } 4)$$

which immediately leads to (A 1b).

To establish (A 1a), we return to (A 3) with the result (A 4), and introduce the new variables  $u = (s-t)/\sqrt{2}$ ,  $v = (s+t)/\sqrt{2}$ . (A 3) then becomes

$$-i\sqrt{2} \int_{-\infty}^{\infty} e^{-v^2} dv \int_{-\infty}^{\infty} \frac{e^{-u^2} du}{u - \sqrt{2}[\frac{1}{2}(a+b) + iy]}, \quad (\text{A } 5)$$

which is equal to the right hand side of (A 1a).

(II) The functions  $F, D$  and  $B$ 

These are defined:

$$\left. \begin{aligned} F(x, c, y) &= Z[(x-c), y] - Z[(x+c), y], \\ D(x, c, y) &= Z[(x-c), y] + Z[(x+c), y], \\ B(x, c, y) &= Z(x, y) - \frac{1}{2}D(x, c, y). \end{aligned} \right\} \quad (\text{A } 6)$$

We are interested in integrals such as  $\int_{-\infty}^{\infty} |F|^2 dx$ . It is clear that use of (A 1) will enable these integrals to be expressed in terms of the real and imaginary parts of  $Z[2^{-\frac{1}{2}}rc, 2^{\frac{1}{2}}y]$ , ( $r = 0, 1, 2$ ), which we shall write as

$$Z(rc') = X(rc') + iY(rc'), \quad (\text{A } 7)$$

omitting the parameter  $2^{\frac{1}{2}}y$ , and using  $c' = 2^{-\frac{1}{2}}c$ .



(III) *Integrals used in §2(v)*

The required results are:

$$\int_{-\infty}^{\infty} |F|^2 dx = 2^{\frac{3}{2}}\pi[Y(0) - Y(2c')]. \quad (\text{A } 8a)$$

$$\int_{-\infty}^{\infty} |D|^2 dx = 2^{\frac{3}{2}}\pi[Y(0) + Y(2c')]. \quad (\text{A } 8b)$$

$$\int_{-\infty}^{\infty} |B|^2 dx = 2^{\frac{3}{2}}\pi\{[Y(0) - Y(c')] - \frac{1}{4}[Y(0) - Y(2c')]\}. \quad (\text{A } 8c)$$

$$\int_{-\infty}^{\infty} F^* D dx = -i2^{\frac{3}{2}}\pi X(2c'). \quad (\text{A } 8d)$$

$$\int_{-\infty}^{\infty} F^* B dx = -i2^{\frac{3}{2}}\pi[X(c') - \frac{1}{2}X(2c')]. \quad (\text{A } 8e)$$

$$\int_{-\infty}^{\infty} D^* B dx = -2^{\frac{3}{2}}\pi\{[Y(0) - Y(c')] - \frac{1}{2}[Y(0) - Y(2c')]\}. \quad (\text{A } 8f)$$

(IV) *Limiting cases*

Of particular interest is the form of  $Z(x, y)$  in the limiting cases  $y \gg 1$  and  $y \ll 1$ , for, with  $y = \Gamma/2\Delta$ , these represent the Lorentzian form ( $\Gamma \gg \Delta$ ) and the Gaussian form ( $\Delta \gg \Gamma$ ), respectively.

(a) *Lorentzian form*

The approximation  $y \gg 1$  must lead to the function  $Z(x, y) = 1/(x + iy)$ , but it is instructive to see formally how this comes about.

In the definition of  $Z$  (equation (A 2)), write  $t = s/\Delta$ ,  $x = k/\Delta$ ,  $y = \Gamma/2\Delta$ . Then, since  $(1/\Delta\pi^{\frac{1}{2}})e^{-(s/\Delta)^2}$  will behave like  $\delta(s)$  as  $\Delta \rightarrow 0$ , we have

$$\begin{aligned} Z(x, y) \equiv Z_L(x, y) &= \Delta \int_{-\infty}^{\infty} \frac{\delta(s)}{(s/\Delta) - (x + iy)} d(s/\Delta) = \int_{-\infty}^{\infty} \frac{\delta(s)}{(s/\Delta) - (k + i\Gamma/2)/\Delta} ds \\ &= \frac{-\Delta}{k + \frac{1}{2}i\Gamma}. \end{aligned} \quad (\text{A } 9)$$

This is of Lorentzian form, and of the correct normalization for use in the expression for the polarizability (equation (12)).

(b) *Gaussian form*

$$\text{We have} \quad Z(x, y) \equiv Z_G(x) = \pi^{-\frac{1}{2}} \int_{-\infty}^{\infty} \frac{e^{-t^2}}{t - (x + iy)} dt. \quad (\text{A } 10)$$

Regarding  $t$  as a variable in the complex plane, we obtain

$$Z_G(x) = X_G(x) + iY_G(x) = \pi^{-\frac{1}{2}}P \int_{-\infty}^{\infty} \frac{e^{-t^2}}{t - x} dt + i\pi^{\frac{1}{2}}e^{-x^2}. \quad (\text{A } 11)$$

The first term on the right-hand side is real, and may be developed by the expansion (Heitler 1954, p. 69)

$$\frac{P}{x} = \int_0^\infty \sin kx \, dk \quad (\text{A } 12)$$

to yield 
$$X_G(x) = -2 \int_0^\infty e^{-t^2} \sin 2xt \, dt \quad (\text{A } 13a)$$

$$= -2 e^{-x^2} \int_0^x e^{t^2} \, dt. \quad (\text{A } 13b)$$

These alternative forms of  $X_G$  are conjugate to

$$Y_G(x) = \pi^{\frac{1}{2}} e^{-x^2}. \quad (\text{A } 14)$$

(V) *Expansion of the functions for small values of  $h/\Delta$*

The expansions of  $F(h/\Delta)$ ,  $D^{(i)}(h/\Delta)$  and  $B(h/\Delta)$  for  $h/\Delta \ll 1$ , referred to in §2(vii), are

$$F(x + h/\Delta) = 4(h/\Delta) [xZ(x) + 1] + \dots, \quad (\text{A } 15a)$$

$$D^{(i)}(x + h/\Delta) = 2Y(x) [1 - (h/\Delta)^2 (1 - 2x^2)] + \dots, \quad (\text{A } 15b)$$

$$B(x + h/\Delta) = (h/\Delta)^2 \{Z(x) + 2x[1 - xZ(x)]\} + \dots \quad (\text{A } 15c)$$

The coefficients of  $h/\Delta$  and  $(h/\Delta)^2$  do not exceed order unity.

#### REFERENCES

- Barrat, J. P. 1959 *J. Phys. Rad.* **20**, 541, 633, 657.  
 Bradley, L. C. & Fork, R. L. 1964 *Appl. Optics*, **3**, 137.  
 Brossel, J. & Bitter, F. 1952 *Phys. Rev.* **86**, 308.  
 Colegrove, F. D., Franken, P. A., Lewis, R. R. & Sands, R. H. 1959 *Phys. Rev. Lett.* **3**, 420.  
 Condon, E. U. & Shortley, G. H. 1951 *The theory of atomic spectra*. Cambridge University Press.  
 Dicke, R. H. & Griffiths, R. B. 1957 *Rev. Sci. Instrum.* **28**, 646.  
 Dodd, J. N. & Series, G. W. 1961 *Proc. Roy. Soc. A*, **263**, 353.  
 Dodd, J. N., Series, G. W. & Taylor, M. J. 1963 *Proc. Roy. Soc. A*, **273**, 41.  
 Fried, B. D. & Conte, S. D. 1961 *The plasma dispersion function*. London: Academic Press Ltd.  
 Guiochon, M. A., Blamont, E. & Brossel, J. 1956 *C. R. Acad. Sci., Paris*, **243**, 1859.  
 Heitler, W. 1954 *The quantum theory of radiation* (3rd ed.) Oxford University Press.  
 Kibble, B. P. & Series, G. W. 1963 *Proc. Roy. Soc. A*, **274**, 213.  
 Kramers, H. A. 1930 *Proc. Acad. Amst.* **33**, 959; 1956 *Collected Sci. Papers*, 522. Amsterdam: North-Holland.  
 Kronig, R. de L. 1926 *J. Opt. Soc. Amer.* **12**, 547.  
 Macaluso, D. & Corbino, O. M. 1898 *C.R. Acad. Sci., Paris*, **127**, 548.  
 Rose, M. E. 1957 *Elementary theory of angular momenta*. New York: John Wiley and Sons, Inc.  
 Series, G. W. 1966 (submitted for publication in *Proc. Phys. Soc.*).



# Theory of the modulation of light in optical pumping experiments

G. W. SERIES

Clarendon Laboratory, Oxford

*MS. received 1st March 1966*

**Abstract.** The absorption of light by optically pumped atoms undergoing magnetic resonance is calculated from expressions based on a simplification of Barrat and Cohen-Tannoudji's theory of optical pumping. The density matrix for the system is first derived in orders of approximation which correspond to successive cycles of pumping. The off-diagonal elements of the matrix, and consequently the absorption of light, are modulated. The amplitudes of modulation are resonance functions which are, in general, more complicated than solutions of the Bloch equations. The selection rules for electric dipole radiation limit the possible frequencies of modulation to  $\omega_0$  and  $2\omega_0$  for primary interactions ( $\omega_0$  is the applied frequency), but modulation at higher frequencies can arise through the circulation of coherence in optical pumping cycles. The functions which represent the amplitude of modulation at  $4\omega_0$  are derived in first and second order, for comparison with experiment.

## 1. Introduction

This work, and the experimental papers which follow, developed from studies of the modulation of fluorescent light in optical radio-frequency double-resonance experiments (Dodd and Series 1961, Dodd *et al.* 1963, Kibble and Series 1963). Those papers were concerned with the light emitted by atoms subjected to magnetic resonance in excited states. Here we are concerned with the corresponding problem in absorption: how does magnetic resonance in the ground states of an atom affect the amount of light it absorbs?

The problem was broached ten years ago by Dehmelt (1957) in connection with magnetic resonance in optical pumping, and studied by Bell and Bloom (1957). Their analysis followed Bloch's phenomenological approach to magnetic resonance: they argued that precessing macroscopic magnetization in an atomic vapour should, under appropriate geometrical conditions, give rise to modulation in absorption. Moreover, the amplitude of the modulation should be a resonance function of the same form as the well-known solution of Bloch's equations, namely

$$\frac{\Gamma^2}{(\omega - \omega_0)^2 + (\gamma H_1)^2 + \Gamma^2} \cos \omega_0 t + \frac{\omega \Gamma}{(\omega - \omega_0)^2 + (\gamma H_1)^2 + \Gamma^2} \sin \omega_0 t \quad (1)$$

using the notation of this paper.

The work on the emission of light from excited states had revealed that modulation of the type described by equation (1) arises only in special cases. More detailed attention to the interactions between the light and the atoms would seem to be necessary to describe absorption properly.

The theory of optical pumping proposed by Barrat and Cohen-Tannoudji (1961, to be referred to as BC-T) provides a very convenient framework for working out the

details. The theory is developed in terms of the quantized electromagnetic field. The theory of Dodd and Series (to be referred to as DS) for double-resonance experiments was semi-classical; that is, the fields were treated classically, but the atoms quantized. The treatment can be extended to include spontaneous emission, and hence complete cycles of optical pumping, if the existence of an additional field is postulated, having properties which correspond to 'vacuum fluctuations'. The same results are obtained as those of BC-T. In the present work we shall use the results of BC-T, slightly modified to suit our purpose, for the response of an atom to a cycle of optical pumping, and those of DS for its response to a radio-frequency field.

The results we shall obtain for modulation in absorption are very similar to those for modulation in emission, but they go further. Most noteworthy is the prediction that the coherence between atomic ground states which is generated by the radio-frequency field should survive not only excitation, but also the random, isotropic perturbation which is responsible for spontaneous decay. That coherence can survive spontaneous decay has been proved by the light-shift work of Cohen-Tannoudji (1962). It is manifested here in a less subtle way, namely, by higher-order modulation effects in the absorbed light. These effects have been found experimentally, and are reported in the following paper (Partridge and Series 1966).

## 2. Formulation of the problem

The model we use is the simplest that will bring out the essentials of the problem. We consider an atom whose accessible states are a set of space-quantized ground states  $|\mu\rangle$  and a similar set of excited states  $|m\rangle$ . The  $|\mu\rangle$  and the  $|m\rangle$ , respectively, are the rotation components of levels of definite angular momentum  $J$  and  $J_e$ , and are connected with one another by electric dipole radiation.

An assembly of atoms of this type is in a magnetic field  $\mathbf{H}$ , the direction of which Oz we choose as the axis of quantization. A field  $\mathbf{H}_1$  rotates in the  $xy$  plane with angular velocity  $\omega_0$ . The atoms are illuminated by polarized resonance radiation represented by the electric field  $\mathbf{E}_1(t)$  whose intensity  $\langle E_1^2 \rangle$  is uniform in time, and whose spectral distribution  $\rho(k)$  is wide compared with the radiation width  $\Gamma_e$  of the excited states. The field  $\mathbf{E}_1(t)$  is the 'pumping' light.

To find the absorption of light by the atoms, we may measure the intensity of the 'pumping' light after it has passed through the assembly or we may use an independent beam to monitor the atoms, in which case this beam must be weak compared with the pumping beam. There may or may not be an analyser in the monitoring beam.

The analysis proceeds by calculating the density matrix for the assembly of atoms under the optical and radio-frequency perturbations. It is then a straightforward matter to calculate the rate of absorption of light.

### 2.1. Simplifying assumptions and basic equation

To obtain their results, Barrat and Cohen-Tannoudji take advantage of the short coherence times of the perturbations which bring about excitation and decay. This enables them to treat both parts of the optical pumping cycle as rate processes, for which the formalism of the density matrix is especially suited. The radio-frequency interaction is not, however, a rate process and must be treated differently. These perturbations taken together lead to the differential equation (V-12) of BC-T.

The solution outlined in BC-T is unsuitable for our purpose since it imposes the restriction  $\gamma H_1 \ll \omega_0$ . To obtain a relatively straightforward solution which approximates to the conditions of the experiments we wish to interpret, we relax the condition



on  $H_1$ , and make instead the two following assumptions:

- (i) The 'light shifts' are negligible.
- (ii) The relaxation rates are independent of  $\mu$ .

Assumption (i) will be valid if the spectral distribution of the light is uniform or symmetrical over the region of absorption, or if relaxation processes other than excitation by light are dominant.

Assumption (ii) is not generally true, but it will be valid if the relaxation by light is subsidiary to other, random, relaxation processes. In the experiments we wish to interpret, relaxation by light was noticeable but was not the dominant cause of relaxation. In these circumstances it is a reasonable assumption. With these assumptions, we can replace the middle set of terms in (V-12) by  $-\Gamma\rho_{\mu\mu'} + R\delta_{\mu\mu'}$ .  $\Gamma$  and  $R$  are independent of  $\mu$ .  $R\delta_{\mu\mu'}$  represents regeneration from the various relaxing mechanisms at the rate  $R/s$  into a statistical ensemble of  $s$  equally populated, uncorrelated states. Elimination from (V-12) of the terms describing  $\mu$ -dependent relaxation allows us to work in the laboratory representation for the density matrix, and to remove the restriction

$$\mu - \mu' = \mu'' - \mu'''$$

of BC-T. We also assume that  $\Gamma_e$  is much greater than  $\omega_0$ ,  $\omega_e$  or  $\gamma H_1$ , which is usually valid. This simplifies the last term of (V-12), and makes the equations less cumbersome. In cases where this approximation is not legitimate, the analysis is not altered in any important way. The basic differential equation now becomes

$$\frac{d}{dt}\sigma_{\mu\mu'} = -\frac{i}{\hbar}[\mathcal{H}^*, \sigma]_{\mu\mu'} + R\delta_{\mu\mu'} + \sum_{\mu''\mu'''} B_{\mu''\mu'''}^{\mu\mu'} \sigma_{\mu''\mu'''} \quad (2)$$

$\sigma$  is the density matrix in the laboratory representation.

$$\mathcal{H}^* = \mathcal{H}_0 + \mathcal{H}_{\text{stat}} + \mathcal{H}_{\text{rf}} + \mathcal{H}_D$$

is a Hamiltonian whose first term represents the Hamiltonian in the absence of fields, and subsequent terms the effects of the static field, of the radio-frequency field and of damping, respectively. It is identical with the  $\mathcal{H}^*$  used in DS. The term in  $B_{\mu''\mu'''}^{\mu\mu'}$  represents the effect of one cycle of optical pumping. The coefficient may be written

$$B_{\mu''\mu'''}^{\mu\mu'} = \frac{\rho(k_0)}{\hbar^2} \sum_{m, m'} \langle \mu'' | \mathbf{e}_1^{0*} \cdot \mathbf{P} | m \rangle \langle m' | \mathbf{e}_1^0 \cdot \mathbf{P} | \mu''' \rangle \\ \times C(J_e, m; J, \mu) C(J_e, m'; J, \mu') \quad (3)$$

subject to  $m - \mu = m' - \mu' = 0, \pm 1$ .  $\rho(k_0)$  is the spectral density of the exciting light, assumed constant over the resonance region  $k_0$ , and  $\mathbf{e}_1^0$  is a unit vector specifying its direction of polarization. The  $C$  are Clebsch-Gordan coefficients that give the relative magnitudes of the electric dipole matrix elements between the  $|J_e, m\rangle$  and the  $|J, \mu\rangle$ . The expression (3) is equivalent to that given in BC-T.  $B_{\mu''\mu'''}^{\mu\mu'}$  is a rate constant for excitation whose magnitude, under our assumption (ii), is certainly less than  $\Gamma$ , the damping constant for the  $|\mu\rangle$ .

## 2.2. Method of solution

A solution of equation (2) may be obtained by iteration as a power series in  $B/\Gamma$ . The zero-order equation, which may be solved exactly, is

$$\frac{d}{dt}\sigma_{\mu\mu'}^{(0)} = -\frac{i}{\hbar}[\mathcal{H}^*, \sigma^{(0)}]_{\mu\mu'} + R\delta_{\mu\mu'}. \quad (4)$$

The solution of this equation depends in turn on the solution of

$$\frac{d}{dt}\sigma_{\mu\mu'}^* = -\frac{i}{\hbar}[\mathcal{H}^*, \sigma^*]_{\mu\mu'} \quad (5)$$

which can be found from DS, equations (4), (5) and (17). (We are here applying  $\mathcal{H}^*$  to the ground states.) The solution in DS is given in terms of the time-displacement operator  $U(t, t_0)$  applied to the state vectors. Applying this to the density matrix, we have

$$\begin{aligned} \sigma_{\mu\mu'}^*(t) &= \sum_{\mu''\mu'''} U_{\mu\mu''}(t, t_0) U_{\mu''\mu'}^+(t, t_0) \sigma_{\mu''\mu'''}^*(t_0) \\ &= \sum_{\mu''\mu'''} U_{\mu''\mu'}^{\mu\mu'}(t, t_0) \sigma_{\mu''\mu'''}^*(t_0) \end{aligned} \quad (6)$$

which defines the coefficient  $U_{\mu''\mu'}^{\mu\mu'}$ . From DS, equation (17), we find

$$\begin{aligned} U_{\mu''\mu'}^{\mu\mu'}(t, t_0) &= \exp\{-i(\mu - \mu' - \mu'' + \mu''')\omega_0 t\} \sum_{ll'} \langle \mu | l \rangle \langle l | \mu'' \rangle \langle \mu''' | l' \rangle \langle l' | \mu' \rangle \\ &\quad \times \exp[-i\{(\mu'' - \mu''')\omega_0 + (l - l')p - i\Gamma\}(t - t_0)]. \end{aligned} \quad (7)$$

Notice that  $\mu, \mu', \mu''$  and  $\mu'''$  here take the place of the  $m, m', n$  and  $n'$  of DS. The  $\mu$  and  $\mu'$  of DS are replaced by  $l$  and  $l'$ .  $p$  is the nutational frequency

$$p = \gamma\{(H - H_0)^2 + H_1^2\}^{1/2}.$$

### 2.3. Zero-order solution

The exact solution of equation (4) is

$$\sigma_{\mu\mu'}^{(0)}(t) = \sigma_{\mu\mu'}^*(t) + \sum_{\mu_0\mu_0'} R \int_0^t U_{\mu_0\mu_0'}^{\mu\mu'}(t, t_0) \delta(\mu_0, \mu_0') dt_0 \quad (8)$$

which may be checked by direct substitution.  $\sigma^*(t)$  rapidly damps out, owing to the factor  $e^{-\Gamma t}$  in  $U$ . The summation and integration in the second term may readily be performed to leave the steady-state solution

$$\sigma^{(0)}(\mu_1, \mu_1', t) = \frac{R}{\Gamma} \delta(\mu_1, \mu_1'). \quad (9)$$

Equation (9) tells us that the radio-frequency perturbation does not alter the statistical equilibrium. The regeneration rate  $R/s$  is, of course, equal to  $\Gamma$  in the approximation in which relaxation by the light is neglected.

### 2.4. First-order solution

We now return to equation (2) to include the term  $\sum_{\mu''\mu'''} B_{\mu''\mu'''}^{\mu\mu'} \sigma_{\mu''\mu'''}^*$ . The approximation methods of time-dependent perturbation theory allow us to take account of this by expanding  $\sigma(t)$  in the form

$$\sigma(t) = \sigma^{(0)}(t) + \sigma^{(1)}(t) + \sigma^{(2)}(t) + \dots \quad (10)$$

with  $\sigma^{(1)}, \sigma^{(2)}, \dots$  expressed formally as

$$\sigma^{(1)}(t) = \int_0^t U(t, t_1) B \sigma^{(0)}(t_1) B^+ U^+(t, t_1) dt_1 \quad (11a)$$

$$\sigma^{(2)}(t) = \int_0^t U(t, t_2) B \sigma^{(1)}(t_2) B^+ U^+(t, t_2) dt_2. \quad (11b)$$



The solution of these equations will lead us to multiple products of functions of the quantum numbers; so we introduce subscripts to distinguish the states after successive perturbations. Unprimed labels will refer to ket vectors; primes will be used for the corresponding set of bras. Thus the  $|\mu_0\rangle$  are the states regenerated from the random relaxing processes (equation (2)), and the  $\langle\mu_0'|$  are a similar set of bras. The numbers  $\mu_1, \mu_1'$  label the states for the zero-order solution (equation (9)), the numbers  $\mu_2, \mu_2'$  label the states for the solution after one cycle of optical pumping, and so on, as required. The notation and the perturbations are illustrated in figure 1.

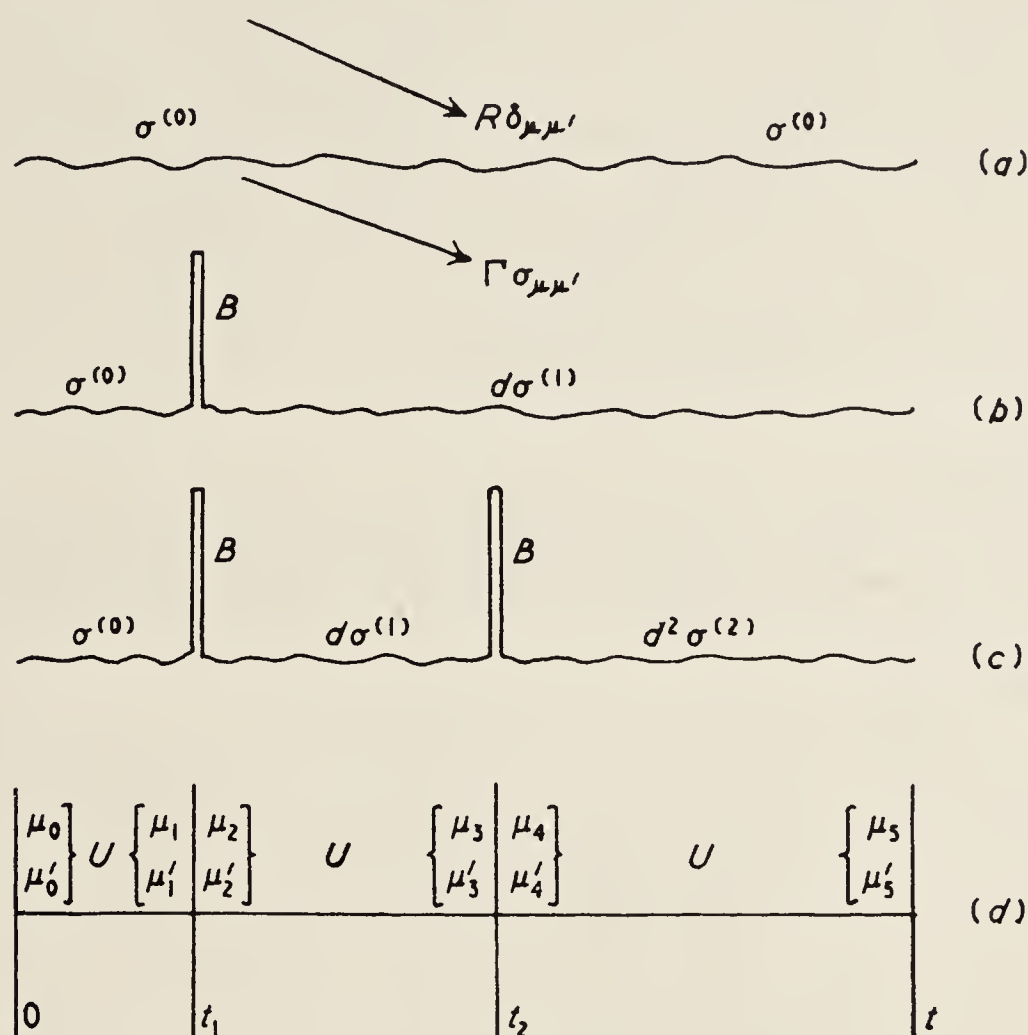


Figure 1. Representation of the time development of the density matrix under the given perturbations. (a) Zero-order solution: equilibrium between damping  $\Gamma$  and regeneration  $R$ . (b) Element of first-order solution produced by one cycle of optical pumping (operator  $B$ ), infinitesimal of first order. (c) Element of second-order solution produced by two cycles of optical pumping, infinitesimal of second order. (d) The time-development operator  $U$  and the labels given to the state vectors at different times.

With this notation, equation (11a) yields, for the elements of the first-order solution,

$$\begin{aligned}
 \sigma^{(1)}(\mu_3, \mu_3', t) &= \int_0^t dt_1 \sum_{\mu_2 \mu_2'} U_{\mu_2 \mu_2'}^{\mu_3 \mu_3'}(t, t_1) \sum_{\mu_1 \mu_1'} B_{\mu_1 \mu_1'}^{\mu_2 \mu_2'} \sigma^{(0)}(\mu_1, \mu_1', t_1) \\
 &= \sum_{\mu_2 \mu_2'} \exp\{-i(\mu_3 - \mu_3' - \mu_2 + \mu_2')\omega_0 t\} \\
 &\quad \times \sum_{l_1 l_1'} \frac{\langle \mu_3 | l_1 \rangle \langle l_1 | \mu_2 \rangle \langle \mu_2' | l_1' \rangle \langle l_1' | \mu_3' \rangle}{\Gamma + i\{(\mu_2 - \mu_2')\omega_0 + (l_1 - l_1')p\}} \\
 &\quad \times \sum_{\mu_1 \mu_1'} B_{\mu_1 \mu_1'}^{\mu_2 \mu_2'} \frac{R}{\Gamma} \delta(\mu_1, \mu_1').
 \end{aligned} \tag{12}$$

### 2.5. Second-order solution

The second-order solution is obtained similarly by using  $\sigma^{(1)}$  to obtain  $\sigma^{(2)}$ :

$$\begin{aligned}\sigma^{(2)}(\mu_5, \mu_5', t) &= \int_0^t dt_2 \sum_{\mu_4 \mu_4'} U_{\mu_4 \mu_4'}^{\mu_5 \mu_5'}(t, t_2) \sum_{\mu_3 \mu_3'} B_{\mu_3 \mu_3'}^{\mu_4 \mu_4'} \sigma^{(1)}(\mu_3, \mu_3', t_2) \\ &= \sum_{\substack{\mu_4 \mu_4' \\ \mu_3 \mu_3' \\ \mu_2 \mu_2' \\ \mu_1 \mu_1'}} \exp\{-i(\mu_5 - \mu_5' - \mu_4 + \mu_4' + \mu_3 - \mu_3' - \mu_2 + \mu_2')\omega_0 t\} \\ &\quad \times \sum_{l_2 l_2'} \frac{\langle \mu_5 | l_2 \rangle \langle l_2 | \mu_4 \rangle \langle \mu_4' | l_2' \rangle \langle l_2' | \mu_5' \rangle}{\Gamma + i\{(\mu_4 - \mu_4' - \mu_3 + \mu_3' + \mu_2 - \mu_2')\omega_0 + (l_2 - l_2')p\}} \\ &\quad \times \sum_{l_1 l_1'} \frac{\langle \mu_3 | l_1 \rangle \langle l_1 | \mu_2 \rangle \langle \mu_2' | l_1' \rangle \langle l_1' | \mu_3' \rangle}{\Gamma + i\{(\mu_2 - \mu_2')\omega_0 + (l_1 - l_1')p\}} \\ &\quad \times B_{\mu_3 \mu_3'}^{\mu_4 \mu_4'} B_{\mu_1 \mu_1'}^{\mu_2 \mu_2'} \left(\frac{R}{\Gamma}\right)^2 \delta(\mu_1, \mu_1').\end{aligned}\quad (13)$$

### 2.6. Complete solution

Successive terms of the complete solution (10) are of relative magnitude  $(B/\Gamma)(R/\Gamma)$ . In so far as  $B$  is small compared with  $\Gamma$ , the higher terms become rapidly less important.

### 2.7. Absorption of light

It is shown in BC-T that the rate of absorption of light is given by an expression equivalent to

$$L_A = \frac{k_0}{\hbar} \rho_s(k_0) \sum_{\mu \mu'} \mathcal{F}_{\mu' \mu} \sigma_{\mu \mu'} \quad (14)$$

where

$$\mathcal{F}_{\mu' \mu} = \sum_m \langle \mu' | \mathbf{e}_s^{0*} \cdot \mathbf{P} | m \rangle \langle m | \mathbf{e}_s^0 \cdot \mathbf{P} | \mu \rangle. \quad (15)$$

The subscript  $s$  is used to indicate that we are here concerned with the sampling (or monitoring) beam which may or may not be the same as the pumping beam. It is assumed in (14) that the spectral density  $\rho_s(k_0)$  is uniform over the region of absorption  $k_0$ .

It is to be noticed that, since we are concerned with electric dipole radiation,  $|\mu - \mu'| \leq 2$ .

We may need to generalize (14) in a number of ways:

(i) If the incident light is unpolarized, we must calculate the right-hand side of (14) separately for each of the orthogonal states of polarization.

(ii) If the atoms are being excited to several sets of states  $|m\rangle$  whose separations are large compared with  $\Gamma_e$ , though possibly not large compared with the Doppler width (as, for example, from  $^3S_1$  in helium to  $^3P_0$ ,  $^3P_1$  and  $^3P_2$ ), the summation is to be taken for each set separately, using the values of  $\rho(k_0)$  appropriate to the particular set.

(iii) If an analyser ( $\mathbf{e}_a^0$ ) is interposed between the sample and the detector, equation (14) is to be multiplied by  $(\mathbf{e}_s^0 \cdot \mathbf{e}_a^{0*})(\mathbf{e}_s^{0*} \cdot \mathbf{e}_a^0)$ .

## 3. Discussion of the results

We consider the application of equation (14) to successive orders of the solution for  $\sigma(t)$ .



### 3.1. Zero-order solution

The result gives us the rate of absorption from a sample in which the atoms are uniformly distributed between uncorrelated states. There is no effect whatever of the radio-frequency perturbation.

### 3.2. First-order solution

Apart from trivial factors, the result is identical with that obtained in DS (equation (32)) for the fluorescent light in a double-resonance experiment. One cycle of optical pumping produces polarization, or alignment, or leaves the atoms in superposition states, just as in the process of excitation in the double-resonance experiment. The radio-frequency mixing takes place in the same way, and the effects to be found in absorption are identical with those found in emission.

The light will be modulated by virtue of the factor  $\exp\{-i(\mu_3 - \mu_3' - \mu_2 + \mu_2')\omega_0 t\}$ , and the amplitudes of modulation will be resonance functions. The possible values of  $\mu_3 - \mu_3' - \mu_2 + \mu_2'$  are limited to 0,  $\pm 1$ ,  $\pm 2$ ,  $\pm 3$ ,  $\pm 4$  because of the limitations imposed by electric dipole radiation.

An important distinction is to be made between terms for which  $\mu_2 = \mu_2'$  and those for which  $\mu_2 \neq \mu_2'$ . The latter represent interference effects arising from atoms left in superposition states after one cycle of optical pumping. Such terms are negligible when  $\omega_0 \gg \Gamma$  (except in a special case to be discussed below) because of the factor

$$[\Gamma + i\{(\mu_2 - \mu_2')\omega_0 + (l_1 - l_1')p\}]^{-1}.$$

The vanishing of these terms expresses the fact that coherence cannot be transferred in spontaneous decay if the interval between levels is large compared with their width. The modulation at  $3\omega_0$  and  $4\omega_0$  can arise only through these cross terms, and therefore only when  $\omega_0 \gg \Gamma$ .

The direct terms  $\mu_2 = \mu_2'$  are not affected by the magnitude of  $\omega_0$  in relation to  $\Gamma$ , but the modulation frequencies for these terms are limited to  $(0, \pm 1, \pm 2)\omega_0$ . Such terms describe the action of the radio-frequency field on atoms left in eigenstates after the pumping cycle. The term ' $\alpha$  processes' is used in the next paper (Partridge and Series 1966) to describe these interactions.

The exception to which we referred is the case in which

$$(\mu_2 - \mu_2')\omega_0 + (l_1 - l_1')p \ll \Gamma. \quad (16)$$

Terms whose quantum numbers satisfy this relation may have appreciable values when  $\mu_2 \neq \mu_2'$ , even if  $\omega_0 \gg \Gamma$ . The condition (16) points to a 'level crossing' between the precessional frequency  $(\mu_2 - \mu_2')\omega_0$  and the nutational frequency  $(l_1 - l_1')p$ ; in classical terms, the precessional and nutational motions remain in phase for times long compared with the mean lifetime. The phenomenon was analysed and received experimental confirmation in the studies on fluorescent light (DS, p. 365, Dodd *et al.* 1963, pp. 52, 61). Although it is a magnetic resonance phenomenon, the resonances are found at fields other than those where the Larmor frequency is equal to  $\omega_0$ . We shall not pursue these resonances here. Further discussion will be limited to resonances centred on fields where the Larmor frequency is equal to  $\omega_0$ .

If the atoms are excited and monitored by light parallel to the magnetic field, as will frequently be the case, only the  $\sigma^\pm$  components take part in the optical processes with the result that the odd harmonics of the modulation will be absent. With this geometrical arrangement modulation in first order is found only at the frequencies  $2\omega_0$  and  $4\omega_0$ .

### 3.3. Second-order solution

In this order modulation arises at higher frequencies. Such effects were not studied in the double-resonance experiments. In principle they are to be expected in such experiments, but only in their full generality if the ground state is of sufficiently high multiplicity. (In the case studied the ground state was single.)

As in the first-order solution modulation at frequencies greater than  $2\omega_0$  can arise only when  $\omega_0 \ll \Gamma$ . If this condition is satisfied, modulation frequencies up to  $8\omega_0$  are to be expected under appropriate geometrical conditions. Each cycle of optical pumping allows an additional  $4\omega_0$  in the range of possible modulation frequencies.

### 3.4. Resonance functions when $\omega_0 \ll \Gamma$

The mean intensity of the light, and the amplitudes of modulation at the various frequencies, are resonance functions determined by the values of the rotation matrix elements  $\langle \mu | l \rangle$  etc., and by the resonance denominators, which reduce to  $\Gamma + i(l-l')p$  when  $\omega_0 \ll \Gamma$ . The optical processes impose certain conditions on the  $|l-l'|$  just as they do on the  $|\mu-\mu'|$ , for the  $l, l'$  are quantum numbers referred to an axis along the effective field in the rotating frame. In the first-order solution the final absorption requires  $|l_1-l_1'| \leq 2$  for two reasons: first, because of the first cycle of optical pumping which requires  $|\mu_2-\mu_2'| \leq 2$ , and, second, because the final absorption requires  $|\mu_3-\mu_3'| \leq 2$ . In the second-order solution we must have  $|l_1-l_1'| \leq 2$  because of the primary pumping cycle, and  $|l_2-l_2'| \leq 2$  because of the final absorption. In higher orders, values of  $|l-l'|$  in excess of 2 are permitted for the  $l, l'$  which are not directly associated with the first and last absorptions.

Considerations such as these were developed by Carver and Partridge (1966). It is concluded that the resonance functions in first and second order will be combinations of terms having denominators  $\Gamma^2$ ,  $\Gamma^2+p^2$ ,  $\Gamma^2+4p^2$ . Most of these functions were calculated in DS for  $J = 1$ , in a situation which corresponded to our first-order solution. We already know that our first-order solution (12) is identical with that of DS, and for  $J = 1$  will yield the same resonance functions,  $A, B, C, D, E, F, G$ . In the first-order solution for  $J > 1$  we shall find linear combinations of these functions. In the second-order solution we shall find products and linear combinations of products of these and similar functions based on the denominators  $\Gamma^2$ ,  $\Gamma^2+p$ ,  $\Gamma^2+4p^2$ .

## 4. Application to the case $J = 1$

By way of example we shall work out the form of the resonance functions for the modulation at  $4\omega_0$  in the case  $J = 1$ . The results are needed for comparison with experiment. The reason for studying this modulation is that its existence provides proof of the circulation of coherence in cycles of optical pumping. The modulation arises in both the first- and second-order solutions.

We limit the possibilities to the case of excitation by linearly polarized light travelling parallel to the magnetic field ( $\sigma^+$  and  $\sigma^-$  excitation only).

### 4.1. Modulation at $4\omega_0$ : first-order solution

The possible values of the  $\mu$  which together yield the required modulation are first found. These values enable us to pick out the required values of  $m$ , and hence to determine the geometrical arrangement which makes the coefficients  $B$  and  $\mathcal{F}$  non-vanishing. In the present case we must have  $\mu_3-\mu_3'-\mu_2+\mu_2' = \pm 4$ . Moreover, the system must begin and end in an eigenstate:  $\mu_1 = \mu_1'$  and  ${}_3m = {}_3m'$ . We have in mind the normal



optical pumping arrangement, in which the direction of the pumping beam is along the direction of the magnetic field, so that the only excitation processes we can allow are subject to the selection rule  $m - \mu = \pm 1$ . The only values which satisfy these conditions are shown in the table. A linear polarizer will be necessary to establish coherence between the  $\sigma^\pm$  excitation processes.

Possible values of the $\mu$ and the $m$										Terms yielded
$\mu_1$	$\mu_1'$	${}_1m_2$	${}_1m_2'$	$\mu_2$	$\mu_2'$	$\mu_3$	$\mu_3'$	${}_3m$	${}_3m'$	
0	0	-1	1	-1	1	1	-1	0	0	$\exp\{-i(4\omega_0)t\}$
0	0	1	-1	1	-1	-1	1	0	0	$\exp\{i(4\omega_0)t\}$

The resonance functions depend on the  $\mu$  only and are found by evaluating the sum over  $l$  and  $l'$  in equation (12), incorporating the condition  $\omega_0 \ll \Gamma$ . (The rotation matrix elements are given in DS, p. 363.)

The result, in so far as the modulation terms are concerned, is identical with that given in Kibble and Series (1963), namely

$$\Gamma^{-1}(F + iG) \exp\{-i(4\omega_0 t)\} + \text{complex conjugate} \simeq 2\Gamma^{-1}F \cos 4\omega_0 t \quad (17)$$

where  $F = 3b^4/(\Gamma^2 + p^2)(\Gamma^2 + 4p^2)$ ,  $G = (2\omega_0/\Gamma)F$ ,  $b = \gamma H_1$ .

#### 4.2. Modulation at $4\omega_0$ : second-order solution

The procedure for picking out the relevant terms is in principle the same as before, but the possibilities now are very much more numerous, since the modulation term is

$$\exp\{-i(\mu_5 - \mu_5' - \mu_4 + \mu_4' + \mu_3 - \mu_3' - \mu_2 + \mu_2')\omega_0 t\}.$$

At least twelve different combinations of the  $\mu$  yield  $\exp\{-i(4\omega_0)t\}$ , and these may be coupled to the  $m$  in a diversity of ways such that the number of different possibilities is of the order of fifty. However, many of these yield identical resonance functions. The following new resonance functions are encountered:

$$\begin{aligned} & \text{(i) } (1 - 2A)F \\ & \text{(ii) } (D + iE)^2 \\ & \text{(iii) } F\{A - 2D - \tfrac{1}{2}F + H - i(E + J)\} \\ & \text{(iv) } (X + iY)(X' + iY') \\ & \text{(v) } (B + iC)(X' + iY'). \end{aligned} \quad (18)$$

$A$ ,  $B$ ,  $C$ ,  $D$  and  $E$  are the functions studied in the earlier papers.  $F$  is given above (equation (17)).

$$\begin{aligned} H &= \frac{\Gamma^2}{\Gamma^2 + 4p^2} & J &= \frac{2\delta\Gamma}{\Gamma^2 + 4p^2} \\ X &= \frac{b\delta(4\delta^2 + b^2 + \Gamma^2)}{\Delta_2} & X' &= \frac{3b^3\delta}{\Delta_2} \\ Y &= \frac{b\Gamma(4\delta^2 + 5b^2/2 + \Gamma^2)}{\Delta_2} & Y' &= \frac{3b^3\Gamma}{\Delta_2} \end{aligned}$$

where  $\Delta_2 = (\Gamma^2 + p^2)(\Gamma^2 + 4p^2)$ ,  $b = \gamma H_1$  and  $\delta = \gamma(H - H_0)$ .

Some of the combinations which give rise to these functions are shown diagrammatically in figure 2.

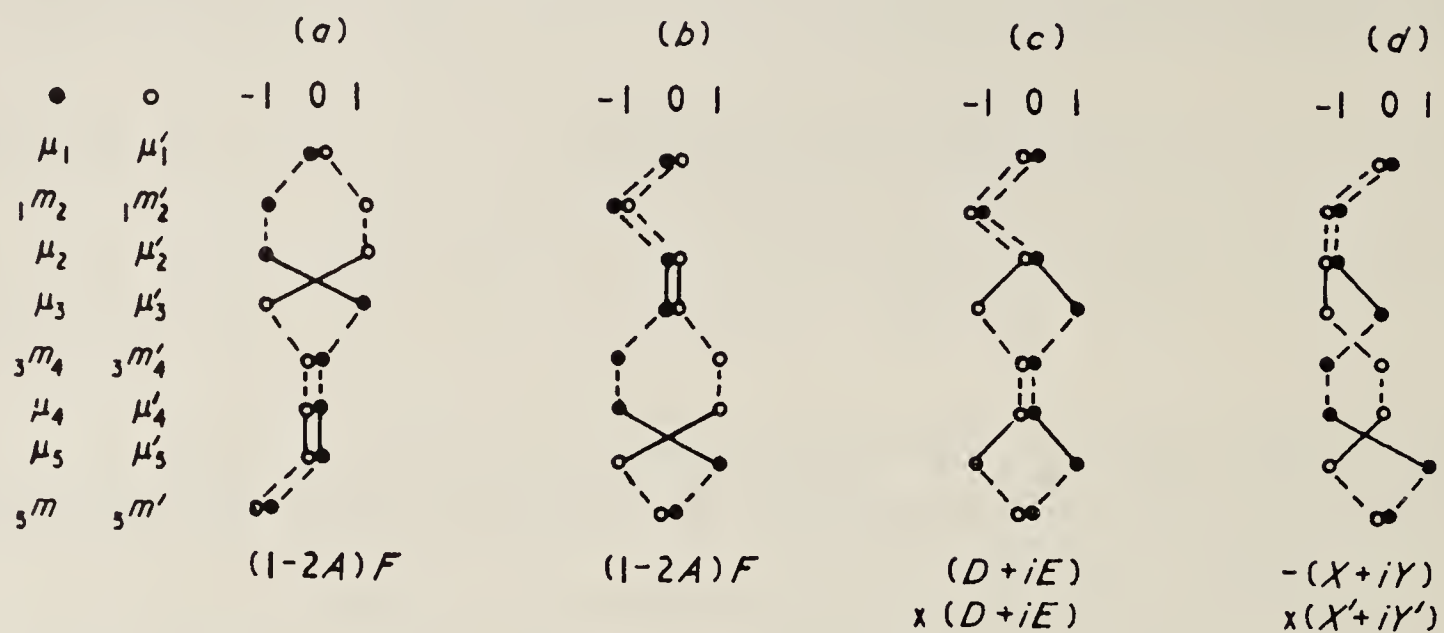


Figure 2. Generation of modulation at  $4\omega_0$  in the second-order solution. The diagrams show sequences of quantum numbers which yield the time-dependent factor  $\exp\{-i(4\omega_0 t)\}$ . Closed and open circles represent ket and bra labels, respectively. Full and broken lines represent radio-frequency and optical links, respectively.

Pairs of links representing spontaneous emission are always parallel.

The relative weights of these resonance functions will depend on the spectral distributions of the pumping light and the monitoring light, and the relative strengths of the optical transitions. The resulting expressions will clearly be cumbersome, but a study of the functions themselves reveals some useful characteristics.

The functions  $A$ ,  $C$ ,  $D$ ,  $F$ ,  $H$ ,  $Y$  and  $Y'$  are symmetrical functions of  $\delta$ , while  $B$ ,  $E$ ,  $J$ ,  $X$  and  $X'$  are anti-symmetrical. The resultant expression, formed by adding the above products with appropriate weights, will be of the form  $P+iQ$ , where  $P$  is symmetrical and  $Q$  anti-symmetrical. Hence the net second-order signal should consist of a symmetrical signal with an anti-symmetrical signal in quadrature.

#### 4.3. Net modulation at $4\omega_0$

The net signal at  $4\omega_0$  is obtained by adding the first- and second-order contributions (17) and (18), each multiplied by the appropriate  $B$  and  $\mathcal{F}$  coefficients and the time-dependent factor. We notice an important difference between the first- and second-order contributions, namely that the  $B$  coefficient occurs once in the first order and twice in the second. The  $B$  coefficient is a rate constant for excitation. We may remove the  $m$  and  $\mu$  dependence, and extract a common factor  $\Gamma_p$  (the reciprocal of the pumping time  $T_p$  of BC-T). The final expression may then be written in the form

$$I(4\omega_0) \propto \left(F + \frac{\Gamma_p}{\Gamma} P\right) \cos 4\omega_0 t + \frac{\Gamma_p}{\Gamma} O \sin 4\omega_0 t. \quad (20)$$

It is to be noticed that the term in  $\cos 4\omega_0 t$  represents a symmetrical resonance signal which arises partly from the first-order solution and partly from the second. The general form of this signal is bell shaped. On the other hand, the term in quadrature represents



an anti-symmetrical signal which arises only in second order. The general form of this is dispersion shaped. It will be recalled, however, that we have neglected a first-order bell-shaped term  $(2\omega_0/\Gamma)F \sin 4\omega_0 t$  (equation (17)). The relative magnitudes  $\omega_0/\Gamma$  and  $\Gamma_p/\Gamma$  are independent of one another, so that it is possible to choose experimental conditions which justify the neglect of this term, and leave the quadrature signal entirely composed of anti-symmetrical components. Detection of such a signal will constitute strong evidence of second- (or higher-) order processes.

#### 4.4. Dependence of signal strengths on $\omega_0/\Gamma$

A condition for the occurrence at full strength of the modulation at  $4\omega_0$  is  $\omega_0/\Gamma \ll 1$ . However, if this ratio is allowed to increase, the various components of the signal decrease at different rates, and may thereby be distinguished.

When the radio-frequency field is large, the first-order terms decrease as  $1/(\Gamma + 2i\omega_0)$  (equation (12) and the table in § 4.1; when  $p$  is large only the terms  $l_1 = l_1'$  need be considered). Under the same condition, the second-order contributions generally decrease more rapidly. Some terms, represented by route (a) in figure 2, for example, decrease as  $1/(\Gamma + 4i\omega_0)(\Gamma + 2i\omega_0)$ . On the other hand, terms represented by route (b) decrease at the same rate as the first-order solution.

#### 4.5. Comparison with experiment

The signals found experimentally consisted of a strong symmetrical signal together with a weak anti-symmetrical signal in quadrature. The symmetrical signal was compared with plots of the function  $F$ , but appeared to fall more steeply. A better representation was given by the expression  $(1 - 2A)F$ . The anti-symmetrical signal could be approximately represented by the expression  $DE$ .

The strength of the symmetrical signal was studied as a function of frequency, and compared with the expression  $1/(\Gamma^2 + 4\omega_0^2)$ , which represents the frequency dependence of the first-order solution. The strength decreased more than twice as rapidly as predicted by this expression. This behaviour is typified by the functions (i) and (iii) in the second-order solution (18).

The experiments provide strong evidence for the reality of the second-order processes; indeed, they appear to be dominant. The reason for this has not been explained quantitatively.

### 5. Conclusion

It is predicted that the absorption of light by optically pumped atoms undergoing magnetic resonance will be modulated at integral multiples of the applied frequency, and that the amplitudes of modulation will be resonance functions. These functions are combinations of functions already familiar from double-resonance experiments. They are more complicated than the well-known solutions of Bloch's magnetic resonance equations.

The modulation at frequencies higher than twice the applied frequency corresponds to coherence which has survived spontaneous decay. The coherence does not survive if the frequency greatly exceeds the damping constants of the ground states.

Signals have been observed experimentally which correspond to the circulation of coherence through at least two complete cycles of optical pumping.

## Acknowledgments

The development of the theory has been greatly stimulated by experimental observations originally made by Drs. K. R. Lea and R. C. Greenhow, and continued by Dr. R. B. Partridge. I am grateful to Dr. Partridge and to Dr. S. Pancharatnam for their comments on early drafts of this paper.

## References

- BARRAT, J. P., and COHEN-TANNOUDJI, C., 1961, *J. Phys. Radium*, **22**, 329–36, 443–50.  
BELL, W., and BLOOM, A., 1957, *Phys. Rev.*, **107**, 1559–65.  
CARVER, T. R., and PARTRIDGE, R. B., 1966, *Amer. J. Phys.*, **34**, 339–50.  
COHEN-TANNOUDJI, C., 1962, *Ann. Phys., Paris*, **7**, 423–61, 469–504.  
DEHMELT, H. J., 1957, *Phys. Rev.*, **105**, 1924–5.  
DODD, J. N., and SERIES, G. W., 1961, *Proc. Roy. Soc. A*, **263**, 353–70.  
DODD, J. N., SERIES, G. W., and TAYLOR, M. J., 1963, *Proc. Roy. Soc. A*, **273**, 41–68.  
KIBBLE, B. P., and SERIES, G. W., 1963, *Proc. Roy. Soc. A*, **274**, 213–24.  
PARTRIDGE, R. B., and SERIES, G. W., 1966, *Proc. Phys. Soc.*, **88**, 969–82.



# The transfer of coherence by collisions of $^3\text{He}$ atoms

R. B. PARTRIDGE† and G. W. SERIES

Clarendon Laboratory, Oxford

MS. received 1st March 1966

**Abstract.** Magnetic resonance in the ground states of  $^3\text{He}$  has been studied through the interaction with metastable atoms in a gas discharge. Modulation showing the characteristics of the ground-state resonances is observed in a transverse beam of light absorbed by the metastable atoms. This is evidence of the transfer of transverse magnetization (coherence between eigenstates) by collision. A theory is developed which explains the observations in detail.

The fact that coherence can be transferred by spin exchange in collision offers the possibility of exploitation in level-crossing or modulation experiments on spectroscopically inaccessible systems.

## 1. Introduction

In a type of optical pumping experiment first performed by Dehmelt (1957) a mixture of vapours is illuminated by the polarized resonance radiation of one of them, and polarization so generated in this system is communicated to the other by collisions. Magnetic resonance experiments in the second system may be monitored by changes in transparency of the first.

By an extension of the method nuclear resonances in the ground state of  $^3\text{He}$  have been studied (Colegrove *et al.* 1963, Greenhow 1964). The interacting systems in this case are metastable  $^3\text{He}$  atoms ( $1s2s\ ^3S_1$ ) polarized by optical pumping as described in the preceding paper (Partridge and Series 1966), and  $^3\text{He}$  atoms in ground states ( $1s^2\ ^1S_0$ ). Since, in the ground states, the electronic angular momentum is zero, the polarization which the atoms acquire by collision is entirely nuclear. Magnetic resonance at the nuclear precession frequency can be monitored by studying the absorption of radiation ( $2\ ^3S-2\ ^3P:10\ 830\ \text{\AA}$ ) by the metastable atoms.

In experiments of this type attention has usually been directed to the longitudinal polarization. It is known that the transfer of longitudinal polarization is very efficient. The cross section for this process in  $^3\text{He}$  is of the order of  $4 \times 10^{-16}\text{ cm}^2$ . Less attention has been paid to the transfer of transverse polarization, although Colegrove *et al.*, and also Greenhow, monitored the transverse relaxation of  $^3\text{He}$  nuclei with a transverse beam of light. Schearer *et al.* (1963) also observed modulation at the nuclear resonance frequency in the transverse beam and constructed a magnetometer based on their observations. The experiments reported here were designed to extend the observations and interpret the phenomenon.

Ruff and Carver (1965) have recently performed similar experiments with the Na-H system, both types of atom being in the ground states. Modulation at the hydrogen resonance frequency was observed in a transverse beam of sodium light.

We wish to underline the point which Ruff and Carver make concerning the significance of experiments of this type. Observation of modulation is interpreted as

† Now at Palmer Physical Laboratory, Princeton University, Princeton, N.J., U.S.A.

evidence of coherence between the eigenstates (that is, transverse polarization) of the absorbing system. This coherence, the characteristics of which are those of the system undergoing resonance, must have been transferred to the absorbing system in the process of collision. If coherence can be transferred in this way, then it should be possible to apply the recently developed spectroscopic techniques which depend on coherence between eigenstates to systems which themselves are spectroscopically inaccessible. The point should not be overlooked, however, that the success of Ruff and Carver's experiment and of our own depends on the strength of the electron exchange in relation to other interactions.

In §§ 2 and 3 of this paper we shall describe the experiments and the observations, and in § 4 develop a theory in terms of which the observations may be interpreted. The theory is based on earlier theories of spin exchange (Wittke and Dicke 1956, Purcell and Field 1956, Balling *et al.* 1964), and incorporates the concept of metastability exchange (Colegrove *et al.* 1963). A 'strong' collision between one atom in the ground state and one in the metastable state results in an exchange of electron spins and excitation energy, so that a nucleus which enters the collision in a ground-state atom may leave it in a metastable atom. It is assumed here that the transverse, as well as the longitudinal, components of the spins are conserved in the collision. Owing to the shortness of duration of the collision in relation to the hyperfine interaction the nuclear and electron spins in the newly formed metastable atom are entirely uncorrelated. However, because the spin orientations of the nuclei which enter the metastable atoms are conserved, a precessional motion at the driving frequency of the nuclear resonance is transmitted to these atoms. This frequency is very different from their Larmor frequency. The amplitude of the response is determined by the difference between the two frequencies in relation to the damping constant.

The principles of the theory could be applied to other colliding spin systems, but the details in § 4 are worked out for the particular system under discussion.

## 2. The experimental arrangement

This closely resembled the arrangement described in the preceding paper (Partridge and Series 1966). It is shown diagrammatically in figure 1.

The sample cell in this experiment contained  $^3\text{He}$  gas at a pressure of 1 mmHg. The same cell was used by Greenhow (1964) for his experiments on nuclear nutation in  $^3\text{He}$ .

The sample was pumped by circularly polarized  $1\ \mu\text{m}$  radiation from a  $^4\text{He}$  lamp. The cell was placed in a weak static field  $H$ , of order 0.2–0.4 G. The radio-frequency field for magnetic resonance ( $H_1$ ) was of amplitude less than 1 mG, at a frequency 1.07 kc/s ( $\omega_0/2\pi$ ) in the perpendicular plane. Since this frequency is three orders of magnitude larger than the resonance linewidths, an oscillating field was used, and the perturbation due to the counter-rotating component ignored.

The monitoring lamp used in the cross beam contained  $^3\text{He}$  at a pressure of 1.5 mmHg. It was constructed with a re-entrant window to reduce self-reversal of the  $1\ \mu\text{m}$  radiation.

The detecting equipment allowed phase-sensitive detection of the modulated photoelectric signal, rectification, and direct recording.

## 3. Experimental results

The experiments reported by Schearer *et al.* (1963) were first repeated. It was confirmed that modulated absorption was present in the cross beam at those values of



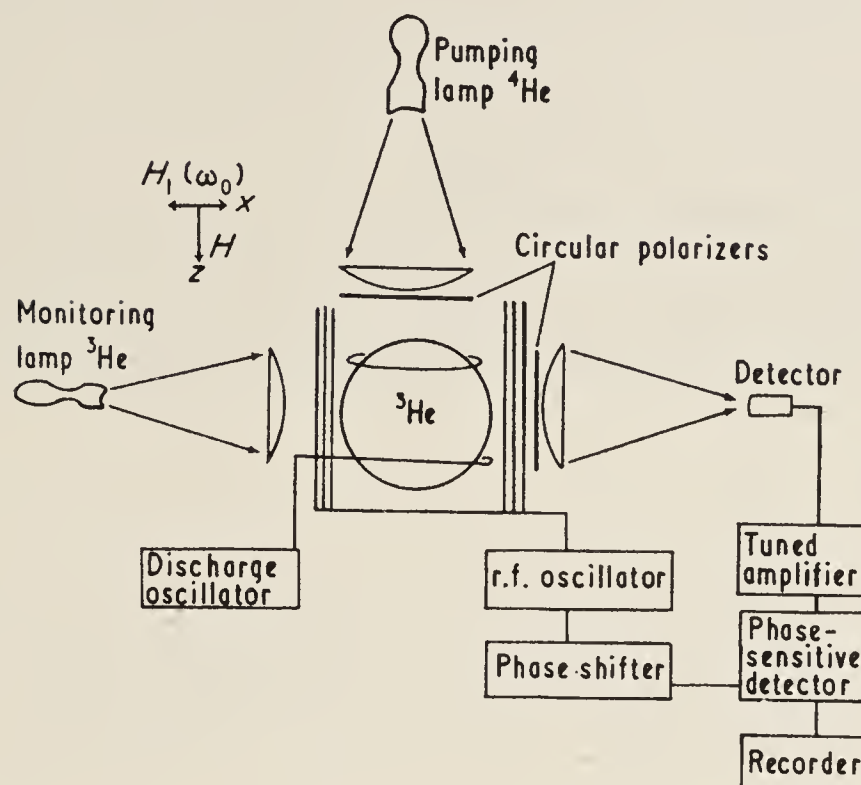


Figure 1. Disposition of apparatus. The static magnetic field  $H$  was in the direction of the pumping beam. The radio-frequency field  $H_1$  was in the direction of the monitoring beam.

the magnetic field which satisfied the condition for *nuclear* resonance at the applied frequency. The experiments were then extended in an attempt to confirm some of the predictions arising from the theory presented in § 4.

### 3.1. Resonance functions

The modulation was present when the sample was monitored by circularly polarized light, as in the experiments of Bell and Bloom (1957). The symmetrical resonance signal found by Schearer *et al.* was accompanied by an antisymmetrical signal in quadrature as predicted by the theory (equation (19b)). Representing the modulated part of the signal by

$$I_A = \chi''_{\text{exp}} \cos \omega_0 t - \chi'_{\text{exp}} \sin \omega_0 t$$

we may compare  $\chi''_{\text{exp}}$  and  $\chi'_{\text{exp}}$  with the corresponding functions derived from the theory. These are the familiar Bloch (1946) functions:

$$\chi' = \frac{b\delta}{\delta^2 + b^2 + \Gamma_g^2}, \quad \chi'' = \frac{b\Gamma_g}{\delta^2 + b^2 + \Gamma_g^2} \quad (1)$$

with  $b = \gamma_g H_1$ ,  $\delta = \gamma_g (H - H_0)$ , and  $H_0 = \omega_0 / \gamma_g$ .  $\Gamma_g$  is the damping constant and  $\gamma_g$  the gyromagnetic ratio. The subscript  $g$  indicates that  $\Gamma_g$  and  $\gamma_g$  refer to the ground states, not the metastable states.

The experimental and theoretical functions are compared in figure 2 (see p. 986). The qualitative agreement is entirely satisfactory.

The dependence of  $\chi''$  and  $\chi'$  on  $b$  was tested. The linewidth proved to be sensitive to spatial inhomogeneities in  $b$ , but with a sufficiently homogeneous field, the dependence predicted by (1) was verified.

### 3.2. Damping constant

Measurement of  $\Delta_{1/2}$ , the half-width of the  $\chi''$  curves at half-height, allowed an

experimental determination of the damping constant by use of the relation

$$\Gamma_g^2 = \Delta_{1/2}^2 - (\gamma_g H_1)^2 \quad (2)$$

with  $\gamma_g = 3.245 \text{ kc/s G}^{-1}$  (Anderson 1949).

The value of  $\Gamma_g$  so obtained depended on the discharge conditions in the cell: values ranging from 1.0 to 3.0 c/s were found. These values agree well with those obtained by Greenhow (1964) using the same sample cell, but a different experimental method. They are larger than the values reported by Schearer *et al.* (1963).

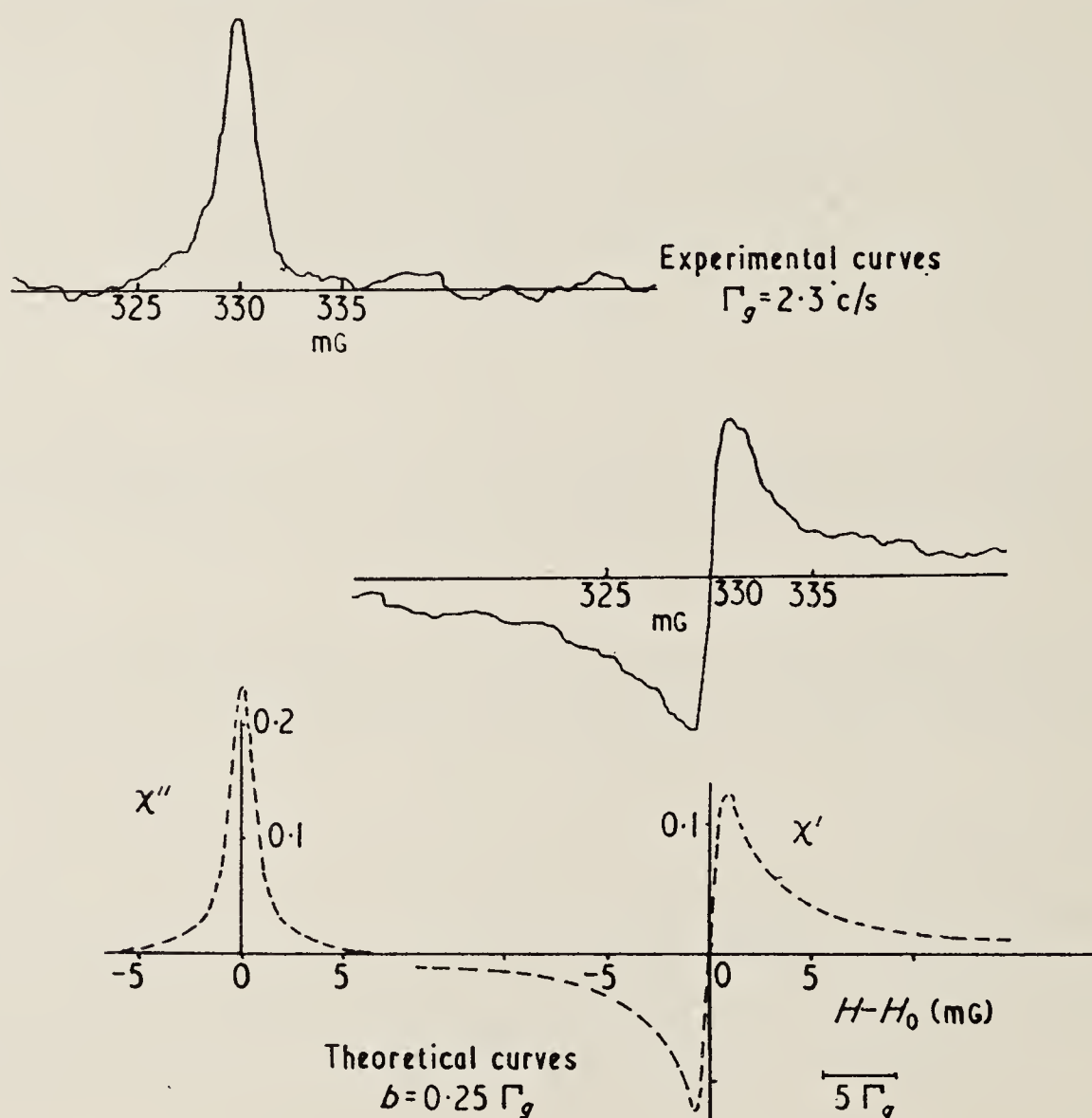


Figure 2. The amplitudes of modulation,  $\chi'$  and  $\chi''$ , as functions of magnetic field  $H$ . For the experimental curves,  $H_1 = 0.18 \text{ mG}$ ,  $\omega_0/2\pi = 1.07 \text{ kc/s}$ ,  $\Gamma_g = 2.3 \text{ c/s}$ . The integrating time constant was 1 sec. The theoretical curves were plotted for  $b/\Gamma_g = 0.25$ , corresponding to the experimental conditions.

It is particularly to be noticed that these resonance curves, of widths a few cycles per sec, were studied by monitoring atoms, the lifetimes of which are of the order of  $10^{-4} \text{ sec}$ .

### 3.3. Polarization of the light

The results quoted above were obtained by the use of a circular polarizer in the cross beam, either before or after the sample cell. With a linear polarizer the signals disappeared almost entirely. For no orientation of the polarizer, placed before or after the cell, was modulation found in excess of 1% of the effect with a circular polarizer.

The theory predicts that no modulation should be generated with a linear polarizer. We interpret the small signals as arising from small departures from the ideal geometrical conditions, and regard the experimental test as a confirmation of the theory.



We attach as much importance to this null result as to the positive results obtained with a circular polarizer. For it is predicted that any system having spin greater than  $\frac{1}{2}$  should yield, with this geometrical arrangement, modulation signals represented by the  $B$  and  $C$  functions mentioned in the preceding paper, or some linear combination of them (Carver and Partridge 1966). The hyperfine structure of the  $2^3S_1$  states has  $F = \frac{1}{2}$  and  $\frac{3}{2}$ . The fact that strong modulation was not found in the cross beam using a linear polarizer is further evidence that the modulation effects are being generated in a spin  $\frac{1}{2}$  system, rather than in the metastable atoms themselves.

#### 4. Theoretical analysis

Our aim will be to determine the effect of collisions on the density matrix for atoms in metastable states when the colliding atoms are in ground states undergoing magnetic resonance. With knowledge of this density matrix it is a straightforward, though tedious, matter to calculate the absorption of light.

##### 4.1. The notation

Let  $\sigma(g)$  denote the partial density matrix for atoms in the ground states  $1s^2^1S_0$ . In these states there is no hyperfine interaction, and the conventional labels  $(F, m_F)$  are identical with  $(I, m_I)$ .  $g$  will be used to label the states, and to represent the value of  $m_I$ . The axis of quantization is in the direction of the static field  $H_z$ .

Let  $\sigma(\mu)$  denote the partial density matrix for atoms in the metastable states  $1s2s^3S_1$ .  $\mu$  will be used to label the hyperfine states  $(F, m_F)$ , and to represent the value of  $m_F$ . We shall need to express  $\sigma(\mu)$  also in the decoupled representation  $\sigma^*(m_I, m_J)$ . (The asterisk serves to identify the matrix as describing the metastable atoms.) Let  $T$  be the transformation matrix, so that

$$\sigma(\mu) = T\sigma^*(m_I, m_J)T^{-1}. \quad (3)$$

The electronic properties of the metastable atoms are described by the density matrix  $\sigma^*(e)$ , the elements of which are

$$\sigma^*(m_J, m_J') = \sum_{m_I} \sigma^*(m_I, m_J; m_I', m_J')\delta(m_I, m_I'). \quad (4a)$$

The nuclear properties are described by the matrix  $\sigma^*(n)$ , the elements of which are

$$\sigma^*(m_I, m_I') = \sum_{m_J} \sigma^*(m_I, m_J; m_I', m_J')\delta(m_J, m_J'): \quad (4b)$$

##### 4.2. The collisions

$\sigma(g)$  and  $\sigma(\mu)$  and its contracted forms describe the steady-state properties of the assembly. The collisions introduce, on the one hand, loss, and on the other hand, regeneration, for both ground and metastable atoms. If we represent the collisions as a sequence of uncorrelated processes occurring at a uniform rate, we may describe the loss and regeneration by introducing rate constants.

Each collision will yield a pair of atoms, of which one is in the ground state and one in the metastable state. There will be two types of collision, one in which the atoms (labelled by the nuclei) exchange metastability, and one in which they do not. The former case is our main interest. The latter case should, strictly, be written into the equations, but since we shall solve them by successive approximation, and since the uninteresting case does not yield a major term in the equations, we shall ignore it.

In the case where the atoms exchange metastability, the density matrices which we use to represent the products of the collision are based on the assumptions (i) that the nuclear and electronic parts separately of the density matrices are unaltered by the collisions, and (ii) that the nuclear and electronic parts of the newly formed metastable atoms are entirely uncorrelated. Accordingly, the density matrices for the ground-state and metastable atoms immediately after the collision are written  $\sigma^*(n)$  and  $[\sigma^*(e) \times \sigma(g)]$ , respectively.

Introducing now the damping constants  $\Gamma_g'$  and  $\Gamma_\mu'$  to represent loss from the ground and metastable states, respectively, and the rate constants  $R_g$  and  $R_m$  to represent regeneration, we may write differential equations for the effect of collisions. The equations are

$$\left[ \frac{d}{dt} \sigma(g) \right]_{\text{coll}} = -\Gamma_g' \sigma(g) + R_g \sigma^*(n) \quad (5a)$$

$$\left[ \frac{d}{dt} \sigma(\mu) \right]_{\text{coll}} = -\Gamma_\mu' \sigma(\mu) + R_m [T \sigma^*(e) \times \sigma(g) T^{-1}]. \quad (5b)$$

We shall later make use of a selection rule which can be derived from the last term of (5b). Since  $\mu = g + m_J$ , we have

$$(\mu - \mu') = (g - g') + (m_J - m_J'). \quad (6)$$

While this rule must hold in general, we wish to apply it when the matrix  $\sigma^*(e)$  corresponds to a random, isotropic distribution of electron spins (the zero-order solution  $\sigma^{*(0)}(e)$ , § 4.4.1). In this case, the off-diagonal components of  $\sigma^*(e)$  are zero, and all components of  $\sigma(\mu)$  vanish unless  $m_J = m_J'$ . We have, therefore,

$$\mu - \mu' = g - g' \quad (6a)$$

which must be satisfied for all collisions in which the newly formed metastable atoms are described by  $\sigma^{*(0)}(e) \times \sigma(g)$ .

It is worth noticing that (6a) holds also if the electron spins are polarized but uncorrelated, for it depends, not on the equality of the diagonal elements of  $\sigma^*(e)$ , but on the absence of off-diagonal elements. (6) and (6a) are analogous to the rules which govern the transfer of coherence in the interaction of atoms with light (see Series 1966, to be referred to as I, and references quoted there).

#### 4.3. The equations of motion

The complete equations for the time derivatives are obtained by including the other perturbations (static field, radio-frequency field, optical pumping, other causes of damping). The equations are

$$\frac{d}{dt} \sigma(g) = -\frac{i}{\hbar} [(\mathcal{H}_0 + \mathcal{H}_{\text{stat}} + \mathcal{H}_{\text{rf}}), \sigma(g)] - \Gamma_g \sigma(g) + R_g \sigma^*(n) \quad (7a)$$

$$\begin{aligned} \frac{d}{dt} \sigma(\mu) = & -\frac{i}{\hbar} [(\mathcal{H}_0 + \mathcal{H}_{\text{stat}}), \sigma(\mu)] - \Gamma_\mu \sigma(\mu) + R\mathbf{1} + B\sigma(\mu)B^+ \\ & + R_m [T \sigma^*(e) \times \sigma(g) T^{-1}]. \end{aligned} \quad (7b)$$

The notation is similar to that used in I, the first paper of this series.  $B$  is the operator which represents one cycle of optical pumping, and  $\Gamma_\mu$  is taken to include all forms of damping of metastable atoms. The term  $R\mathbf{1}$  represents the regeneration of atoms by



the discharge at the rate  $R/s$  into a statistical ensemble of  $s$  equally populated, uncorrelated, metastable states. No regeneration term other than  $R_g\sigma^*(n)$  is written for  $\sigma(g)$ , and  $\Gamma_g$  is identified with  $\Gamma_g'$ , since the collisions constitute the major source of regeneration and damping for atoms in ground states.  $\mathcal{H}_{\text{rf}}$  does not appear in the equation for the  $|\mu\rangle$  since the oscillating field is too weak, and too far from resonance to have any direct effect on atoms in the metastable states.

These equations can be solved by successive approximation. A zero-order solution  $\sigma^{(0)}(\mu)$  may be obtained by taking the right-hand side of (7b) as far as the term in  $R$ . Including next the term in  $B$ , one may obtain  $\sigma^{(1)}(\mu)$ , a first-order increment to  $\sigma^{(0)}(\mu)$ . Using this in (7a) a solution  $\sigma(g)$  may be found which, when used in the final term of (7b) will yield a second-order solution  $\sigma^{(2)}(\mu)$ . This is the contribution to  $\sigma(\mu)$  which we are seeking.

#### 4.4. Solution of the equations

4.4.1.  $\sigma^{(0)}(\mu)$ . The commutator bracket in equation (7b) is easily reduced to

$$-i(k_\mu - k_{\mu'})\sigma_{\mu\mu'}$$

where  $k_\mu$  is the Bohr frequency of the state  $|\mu\rangle$ . Taking the terms in  $\Gamma_\mu$  and  $R$ , together with the commutator bracket, the solution is

$$\sigma_{\mu\mu'}^{(0)}(t) = \sigma_{\mu\mu'}^{(0)}(0) \exp[-\{\Gamma_\mu + i(k_\mu - k_{\mu'})\}t] + \frac{R}{\Gamma_\mu} \delta_{\mu\mu'}. \quad (8)$$

The transient, as well as the steady-state, solution has been written here, since we need to know the time-development operator for the solutions below.

4.4.2.  $\sigma^{(1)}(\mu)$ . Proceeding as in I, § 2.4, the first-order increment, which represents the result of one cycle of optical pumping, is

$$\sigma_{\mu\mu'}^{(1)}(t) = \sum_{\mu_1\mu_1'} B_{\mu_1\mu_1'}^{\mu\mu'} \frac{(R/\Gamma_\mu)\delta(\mu_1, \mu_1')}{\Gamma_\mu + i(k_\mu - k_{\mu'})}. \quad (9)$$

This is the steady-state solution.

The magnitude of the off-diagonal, relative to the diagonal components of  $\sigma^{(1)}(\mu)$  depends on the  $B$  coefficient, and on the magnitude of  $k_\mu - k_{\mu'}$ , relative to  $\Gamma_\mu$ .

For the particular states  $|\mu\rangle$  with which we are concerned, the hyperfine structure is much larger than the natural width, and the off-diagonal elements connecting states of different  $F$  will be negligibly small. Matrix elements of this sort will be discarded. On the other hand, off-diagonal elements which connect states of the same  $F$  but different  $m_F$  will not necessarily be small. For such elements, we shall write

$$k_\mu - k_{\mu'} = (\mu - \mu')g_F\omega_L$$

where  $g_F\omega_L$  is the Larmor frequency of the level  $F$ , and  $\mu, \mu'$  are the values of  $m_F, m_F'$ .

Although we shall need these matrix elements later, we shall discard them at this stage because, if the pumping light is polarized so as to generate maximum polarization in the metastable states, the coefficient  $B$  will be zero for these off-diagonal elements. It is nevertheless worth noticing that, if  $B$  does not vanish, then the condition  $\omega_L \gg \Gamma_\mu$  (see equation (12) below), which allows the coherence in collisions to survive in the steady state, would also allow off-diagonal components of  $\sigma(\mu)$  to be generated in the optical pumping cycle. These in turn would generate an initial coherence in  $\sigma(g)$ , and lead to modulation terms additional to those calculated below. Of these terms, those at the frequency  $\omega_0$  would be of comparable strength with those calculated; terms at harmonic frequencies would also be found, the amplitudes of which would depend on the ratio  $\omega_L/\Gamma_\mu$ .

4.4.3.  $\sigma(g)$ . With the exclusion of the off-diagonal elements of  $\sigma^{(1)}(\mu)$ , equation (9) represents a polarized incoherent assembly of metastable atoms, and  $\sigma^*(n)$  is proportional to  $\begin{pmatrix} 1 & 0 \\ 0 & 0 \end{pmatrix}$ . We need not write down the coefficient. The solution of (7a) is now straightforward (equation (8) of I, for example, without the summation over  $\mu_0$ ), and yields

$$\sigma_{gg'}(t) \propto \exp\{-i(g-g')\omega_0 t\} \sum_{l,l'} \frac{\langle g_0|l\rangle \langle l|g\rangle \langle g'|l'\rangle \langle l'|g_0\rangle}{\Gamma_g + i(l-l')p} \quad (10)$$

where  $\langle g|l\rangle$  etc. are elements of the rotation matrix, and  $p = \gamma_g\{(H-H_0)^2 + H_1^2\}^{1/2}$ .

4.4.4.  $\sigma^{(2)}(\mu)$ . Returning to (7b) with the expression for  $\sigma(g, t)$ , and using for  $\sigma^*(e)$  the steady-state zero-order solution  $\sigma^{*(0)}(e)$ , we may integrate the equation by the methods used before. It is found that the  $(\mu, \mu', g, g')$  component has the denominator

$$\Gamma_\mu + i(\mu - \mu')g_F\omega_L - i(g - g')\omega_0. \quad (11)$$

The selection rule  $\mu - \mu' = g - g'$ , equation (6a), is applicable to this case. Hence,  $g - g'$  may be eliminated from (11) in favour of  $\mu - \mu'$ , and the solution of equation (7b) written in the simple form

$$\sigma_{\mu\mu'}^{(2)}(t) \propto [T\sigma^{(0)}(e) \times \sigma(g, t)T^{-1}]_{\mu\mu'} \frac{R_m}{\Gamma_\mu + i(\mu - \mu')(g_F\omega_L - \omega_0)}. \quad (12)$$

This result shows how the time dependence of  $\sigma(g, t)$  is incorporated into  $\sigma^{(2)}(\mu, t)$ . It goes beyond the assumptions concerning the collisions in that it describes the steady-state situation, rather than the effect of a single pulse. Assumption (i) was that all the components of  $\sigma(n)$  are transferred in the collision, whereas (12) shows that, in the steady state which results from a sequence of uncorrelated pulses at a uniform rate, the off-diagonal components of the density matrix do not survive if  $g_F\omega_L - \omega_0 \gg \Gamma_\mu$ . A condition of this sort is not peculiar to the collision interaction: it is a feature of rate processes in general, and in particular of the optical pumping cycle (cf. § 4.4.2).

A diagrammatic representation of the condition for the survival of coherence is illustrated in figure 3.  $k$  is proportional to the energy exchanged in the collision. An

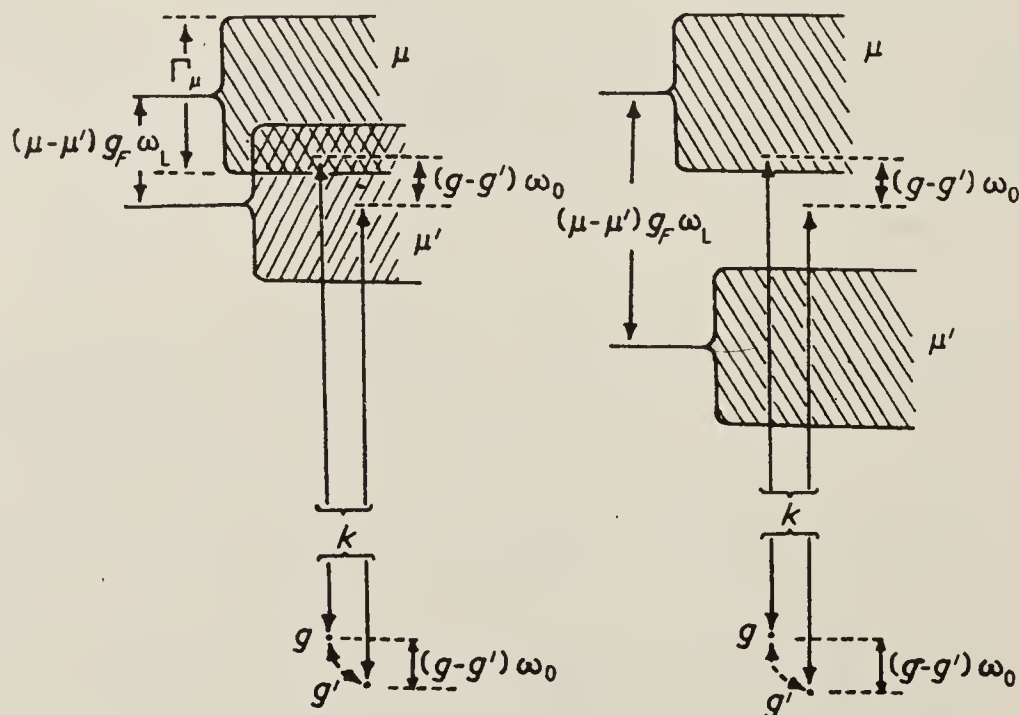


Figure 3. Condition for the survival of coherence in collisions.  $k$  is proportional to the energy exchanged in the collision. Case (a),  $(\mu - \mu')g_F\omega_L - (g - g')\omega_0 < \Gamma_\mu$ ,  $k$  falls within the region of resonance for  $\mu$  and  $\mu'$  and coherence survives; case (b),  $(\mu - \mu')g_F\omega_L - (g - g')\omega_0 > \Gamma_\mu$ ,  $k$  falls within the region of resonance for  $\mu$ , but not for  $\mu'$ , and coherence does not survive.



arrow labelled  $k$  links the states  $|g\rangle$  and  $|\mu\rangle$  of the atom which is to be excited. An arrow of the same length links  $|g'\rangle$  and  $|\mu'\rangle$  also. The diagram shows that if  $k$  occurs within the resonance region for one transition, and if

$$(\mu - \mu')g_F\omega_L - (g - g')\omega_0 < \Gamma_\mu$$

then both transitions may be stimulated, whereas if  $(\mu - \mu')g_F\omega_L - (g - g')\omega_0 > \Gamma_\mu$ , one transition or the other, but not both, may be stimulated. Coherence which may have existed between  $|g\rangle$  and  $|g'\rangle$  will be transferred to  $|\mu\rangle$  and  $|\mu'\rangle$  in the first case, but not in the second. The condition simplifies to the form given above by use of the selection rule  $\mu - \mu' = g - g'$ , with  $g, g' = \pm \frac{1}{2}$ .

#### 4.5. Explicit form of $\sigma^{(2)}(\mu, t)$

The transformation matrix  $T$  consists of the array of Wigner coupling coefficients as shown in the table.

$m_J, m_I$	$1, \frac{1}{2}$	$1, -\frac{1}{2}$	$0, \frac{1}{2}$	$0, -\frac{1}{2}$	$-1, \frac{1}{2}$	$-1, -\frac{1}{2}$
$F, m_F$						
$\frac{3}{2}, \frac{3}{2}$	1	0	0	0	0	0
$\frac{3}{2}, \frac{1}{2}$	0	$(\frac{1}{3})^{1/2}$	$(\frac{2}{3})^{1/2}$	0	0	0
$\frac{3}{2}, -\frac{1}{2}$	0	0	0	$(\frac{2}{3})^{1/2}$	$(\frac{1}{3})^{1/2}$	0
$\frac{3}{2}, -\frac{3}{2}$	0	0	0	0	0	1
$\frac{1}{2}, \frac{1}{2}$	0	$(\frac{2}{3})^{1/2}$	$-(\frac{1}{3})^{1/2}$	0	0	0
$\frac{1}{2}, -\frac{1}{2}$	0	0	0	$(\frac{1}{3})^{1/2}$	$-(\frac{2}{3})^{1/2}$	0

We have also

$$\sigma^{*(0)}(e) \equiv \sigma^{*(0)}(m_J, m_J') = \frac{1}{3} \begin{pmatrix} 1 & 0 & 0 \\ 0 & 1 & 0 \\ 0 & 0 & 1 \end{pmatrix} \quad (13)$$

and we shall write

$$\sigma(g, t) = \begin{pmatrix} \sigma_{++} & \sigma_{+-} \\ \sigma_{-+} & \sigma_{--} \end{pmatrix}. \quad (14)$$

The matrix elements are given by equation (10), in which  $g, g', l, l'$ , take the values  $\pm \frac{1}{2}$ . In writing the denominators  $\Gamma_\mu + i(\mu - \mu')(g_F\omega_L - \omega_0)$ , we shall suppress the subscript on  $\Gamma_\mu$ , and write  $g_F\omega_L - \omega_0$  as  $\omega_a, \omega_b$  for  $F = \frac{3}{2}$  and  $F = \frac{1}{2}$  respectively.

Using these expressions in equation (12) we find

$$[\sigma^{(2)}(\mu, t)]_{F=3/2} = A \begin{pmatrix} \frac{3\sigma_{++}}{\Gamma} & \frac{3^{1/2}\sigma_{+-}}{\Gamma + i\omega_a} & 0 & 0 \\ \frac{3^{1/2}\sigma_{-+}}{\Gamma - i\omega_a} & \frac{2\sigma_{++} + \sigma_{--}}{\Gamma} & \frac{2\sigma_{+-}}{\Gamma + i\omega_a} & 0 \\ 0 & \frac{2\sigma_{-+}}{\Gamma - i\omega_a} & \frac{\sigma_{++} + 2\sigma_{--}}{\Gamma} & \frac{3^{1/2}\sigma_{+-}}{\Gamma + i\omega_a} \\ 0 & 0 & \frac{3^{1/2}\sigma_{-+}}{\Gamma - i\omega_a} & \frac{3\sigma_{--}}{\Gamma} \end{pmatrix} \quad (15a)$$

and

$$[\sigma^{(2)}(\mu, t)]_{F=1/2} = A \begin{pmatrix} \frac{\sigma_{++} + 2\sigma_{--}}{\Gamma} & \frac{-\sigma_{+-}}{\Gamma + i\omega_b} \\ \frac{-\sigma_{-+}}{\Gamma - i\omega_b} & \frac{2\sigma_{++} + \sigma_{--}}{\Gamma} \end{pmatrix} \quad (15b)$$

where  $A$  is a constant.

#### 4.6. Cross beam modulation signals

4.6.1. *Spectral density of the light.* The rate of absorption of radiation by the metastable atoms is given by the generalized form of I, equation (14):

$$L_A = \text{Tr}[\mathcal{A}\sigma(\mu, t)] \quad (16)$$

where  $\mathcal{A}_{\mu\mu'} = \sum_m (k_m/\hbar) \rho(k_m) \langle \mu' | \mathbf{e}_i^{0*} \cdot \mathbf{P} | m \rangle \langle m | \mathbf{e}_i^0 \cdot \mathbf{P} | \mu \rangle$ ,  $\mathbf{e}_i^0$  is the unit vector specifying the polarization of the light,  $\mathbf{P}$  is the electric dipole operator, and the  $|m\rangle$  are the states belonging to  $2^3P_{0,1,2}$ .  $\rho(k_m)$  is the spectral density of the light in the region of absorption,  $k_m$ .

If  $\rho(k_m)$  were constant for all transitions in the sum over  $m$ , the net absorption would be constant. This is because of the orbital spherical symmetry of the metastable level. For the lamps used in the investigation (both  $^3\text{He}$  and  $^4\text{He}$ ) the spectral density was not constant over the  $m$ .

4.6.2. *Character of the polarizer.* A significant difference between the results to be expected in monitoring magnetic resonance experiments with a linear and with a circular polarizer was pointed out by Carver and Partridge (1966). The present case affords an example.

Evaluation of the monitoring operator  $\mathcal{A}$  for the linear polarizer specified by the vector  $\mathbf{e}^0 = \mathbf{k} \sin \theta + \mathbf{j} \cos \theta$  yields, for the states  $F = \frac{1}{2}$ ,

$$\mathcal{A}_{F=1/2}^{\text{lin}} = K \begin{pmatrix} 1 + K' \cos^2 \theta & 0 \\ 0 & 1 + K' \cos^2 \theta \end{pmatrix} \quad (17)$$

where  $K$  and  $K'$  are constants which depend on the spectral density of the light. Formation of the trace specified in equation (16) shows that only the diagonal components of  $\sigma(g, t)$  appear in the result; that is to say, the  $F = \frac{1}{2}$  components will contribute no modulated absorption to the cross beam. Similarly it may be shown that no modulation is contributed by the  $F = \frac{3}{2}$  components. It is predicted that the absorption from a linearly polarized beam should be unmodulated.

This result is characteristic of systems having spin  $\frac{1}{2}$ , and derives from the spin  $\frac{1}{2}$  system out of which  $\sigma(\mu, t)$  was built. The result does not apply to systems having spin greater than  $\frac{1}{2}$ . Modulation would have been found for a linearly polarized cross beam monitoring magnetic resonance within the states of  $F = \frac{3}{2}$  themselves.

On the other hand, the monitoring operator which corresponds to the circular polarizer specified by  $\mathbf{e}^0 = 2^{-1/2}(\mathbf{k} + i\mathbf{j})$  is, for the states  $F = \frac{1}{2}$ ,

$$\mathcal{A}_{F=1/2}^{\text{circ}} = \begin{pmatrix} K'' & K''' \\ K''' & K'' \end{pmatrix} \quad (18)$$

where  $K''$  and  $K'''$  again are constants. Formation of the trace in (16) now leads to the result

$$(L_A)_{F=1/2} = \frac{\text{const.}}{\Gamma^2 + \omega_b^2} \left\{ \text{const.} + \frac{b(\Gamma\delta + \Gamma_g\omega_b)}{\Gamma_g(\delta^2 + b^2 + \Gamma_g^2)} \cos \omega_0 t + \frac{b(\Gamma\Gamma_g - \omega_b\delta)}{\Gamma_g(\delta^2 + b^2 + \Gamma_g^2)} \sin \omega_0 t \right\} \quad (19)$$

and a similar expression for  $(L_A)_{F=3/2}$ .

This is the modulation in which we are interested. The amplitudes of modulation are resonance functions of the variable  $\delta$  with the characteristics of magnetic resonance in the ground states.

It is instructive to study equation (19) in the limiting cases  $\omega_b \ll \Gamma$  and  $\omega_b \gg \Gamma$ . Although we are thinking of  $\delta$  as the variable, its value in the region of resonance will be of the order of  $\Gamma_g$ . We have, therefore, the following cases:



case (a)  $\omega_b \ll \Gamma$

$$(L_A)_a \rightarrow \frac{\text{const.}}{\Gamma \Gamma_g} \left( \text{const.} + \frac{b\delta}{\delta^2 + b^2 + \Gamma_g^2} \cos \omega_0 t + \frac{b\Gamma_g}{\delta^2 + b^2 + \Gamma_g^2} \sin \omega_0 t \right); \quad (19a)$$

case (b)  $\omega_b \gg \Gamma$

$$(L_A)_b \rightarrow \frac{\text{const.}}{\omega_b \Gamma_g} \left( \text{const.} + \frac{b\Gamma_g}{\delta^2 + b^2 + \Gamma_g^2} \cos \omega_0 t - \frac{b\delta}{\delta^2 + b^2 + \Gamma_g^2} \sin \omega_0 t \right). \quad (19b)$$

In case (b) the signal is smaller than in case (a) by the factor  $\omega_b/\Gamma$ . This exemplifies the condition for the survival of coherence,  $\omega_b \ll \Gamma$ .

For reasons of practical convenience this condition was not satisfied in the experiments. Numerical values were:  $\Gamma \sim 75$  kc/s;  $\omega_b \sim 600$  kc/s. The fact that signals were detected under these unfavourable conditions demonstrates the efficiency of the postulated mechanism for the transfer of coherence in collisions.

## 5. Conclusion

It has been confirmed that transverse magnetization in the ground states of  $^3\text{He}$  leads to modulation in light absorbed by metastable atoms. Earlier studies (Schearer *et al.* 1963) emphasized the application to magnetometry. The present interpretation of these experiments in terms of the transfer of coherence between eigenstates suggests that the spectroscopic techniques which rely on such coherence (modulation and level-crossing phenomena) might be applicable to systems which are themselves spectroscopically inaccessible. It is unlikely, however, that the transfer of coherence would be efficient if interactions other than electron exchange dominated the collisions, or if the frequency mismatch of the systems were greatly in excess of the damping constant of the receiving system.

## Acknowledgments

We wish to acknowledge many helpful discussions with Professor T. R. Carver, who made substantial contributions to the analysis in § 4 of this paper.

## References

- ANDERSON, H. L., 1949, *Phys. Rev.*, **76**, 1460–70.
- BALLING, L. C., HANSON, R. J., and PIPKIN, F. M., 1964, *Phys. Rev.*, **133**, A607–26.
- BELL, W. E., and BLOOM, A. L., 1957, *Phys. Rev.*, **107**, 1559–65.
- BLOCH, F., 1946, *Phys. Rev.*, **70**, 460–85.
- CARVER, T. R., and PARTRIDGE, R. B., 1966, *Amer. J. Phys.*, **34**, 339–50.
- COLEGROVE, F. D., SCHEARER, L. D., and WALTERS, G. K., 1963, *Phys. Rev.*, **132**, 2561–72.
- DEHMELT, H. G., 1957, *Phys. Rev.*, **105**, 1924–5.
- GREENHOW, R. C., 1964, *Phys. Rev.*, **136**, A660–2.
- PARTRIDGE, R. B., and SERIES, G. W., 1966, *Proc. Phys. Soc.*, **88**, 969–82.
- PURCELL, E. M., and FIELD, G. B., 1956, *Astrophys. J.*, **124**, 542–9.
- RUFF, G. A., and CARVER, T. R., 1965, *Phys. Rev. Letters*, **15**, 282–4.
- SCHEARER, L. D., COLEGROVE, F. D., and WALTERS, G. K., 1963, *Rev. Sci. Instrum.*, **34**, 1363–6.
- SERIES, G. W., 1966, *Proc. Phys. Soc.*, **88**, 957–68.
- WITTKE, J. P., and DICKE, R. H., 1956, *Phys. Rev.*, **103**, 620–31.





# Should resonance curves in optical pumping be Doppler-broadened?

G. W. SERIES

Clarendon Laboratory, Oxford

*MS. received 1st March 1966*

**Abstract.** Existing theories of optical pumping do not take into account the relative phase of the optical field which monitors the resonances. In experiments on excited atoms the optical phase relations have a profound effect on magnetic resonance curves. Signals in the forward-scattered light show Doppler broadening, modified by strong coherence narrowing; a result quite different from that for the laterally scattered light. The question is raised as to whether similar effects are to be expected for resonances in the ground states.

The problem is analysed in terms of the classical theory of the propagation of light in polarizable media. The (complex) polarizability of the sample under conditions of optical pumping and magnetic resonance is calculated to first order in perturbation theory. An expression is obtained similar to that found for resonance in the excited states, but different in so far as the factor which describes the magnetic resonance (the density matrix for the ground states) is independent of the factor which describes the Doppler effect (the plasma dispersion function). Since the intensity of the transmitted light is a function of the imaginary part of the polarizability, the conclusion is that the ground-state resonance curves should not be Doppler-broadened, which is in agreement with the known facts.

## 1. Introduction

Theories of optical pumping are usually formulated by studying the response of an atom, or a statistical assembly of atoms, to a bath of radiation for which the phase in the optical field is not specified, whereas experiments are normally performed by subjecting the atoms to a beam of light which propagates through the sample. The phase of the radiation is therefore a function of the position of the atoms, and the question arises as to whether this has any bearing on the optical pumping signal.

In a recent study of this question in relation to double-resonance and level-crossing experiments in excited states (Corney, Kibble and Series 1966, to be referred to as CKS) it was predicted that profound differences are to be expected in the magnetic resonance curves found in forward-propagated, as against laterally scattered, light. The differences arise from the coherence of phase in the light wave scattered by different atoms in the forward, as compared with the oblique, directions. The consequences of this coherence were predicted to be (i) that magnetic resonance curves taken at low vapour densities should be Doppler-broadened by an amount proportional to the frequency of the optical transition, and (ii) that the coherence narrowing which occurs with increase of vapour density should be much more pronounced in forward than in lateral scattering.

It is to be understood that the Doppler effect we are here concerned with is the effect in relation to the optical frequencies. The effect at the magnetic resonance frequency,

for which questions of motional narrowing would have to be taken into account, is a different problem which we shall not consider. It is, in any case, an effect which differs by many orders of magnitude from the Doppler effect at optical frequencies.

In so far as they were tested by experiment, the predictions of Doppler broadening and coherence narrowing in double-resonance and level-crossing curves were fulfilled. On the other hand, it is well known that optical pumping experiments yield exceedingly narrow resonance curves, showing no evidence that the Doppler effect at optical frequencies has any effect whatever on their width. The object of this paper is to show how the results for optical pumping on the one hand, and double resonance on the other, can be reconciled.

The method of analysis used in CKS was to describe the fields classically, and to seek solutions of Maxwell's equations. The interaction between the fields and the atoms was taken into account by calculating the bulk polarizability of the medium, obtained by summing the polarizabilities of individual atoms. In this way proper account is taken of the phase of the scattered radiation. By virtue of the complementary nature of absorption and scattering, this method of analysis should suffice for optical pumping signals (absorption) no less than for double resonance (emission).

The problem is approached in this paper in the same way as in CKS. The polarizability of the atoms under conditions of optical pumping is calculated to the first order of approximation in time-dependent perturbation theory. It is immediately obvious from the result that Doppler broadening is not to be expected for ground-state resonances. The experimental results for double resonance and level crossing on the one hand, and optical pumping on the other, can therefore be reconciled by the same method of analysis.

## 2. Formulation of the problem

The case chosen by Corney, Kibble and Series for calculation of the polarizability tensor was the intercombination resonance transition ( $6^1S_0-6^3P_1$ ) in the even isotopes of mercury. Since, in that case, the ground level is single, the results of the calculation cannot be used to interpret optical pumping experiments. The model and the notation used here for calculating the interaction between the radiation and individual atoms will be similar to that used by Barrat and Cohen-Tannoudji (1961) and by Series (1966, to be referred to as I). In the latter paper the notation was adapted to a semi-classical calculation.

The light which is used for pumping and for monitoring excites atoms from a set of ground states  $|\mu\rangle$  to a set of excited states  $|m\rangle$ . It is supposed that magnetic resonance is confined to the ground states—a perfectly realistic situation, since either the  $g$  values, or the lifetimes, or both, will generally be entirely different for the  $|\mu\rangle$  and the  $|m\rangle$ .

### 2.1. The optical field

To find the polarizability as a function of frequency, we need the response of the atoms to a Fourier component of the monitoring field. This represents only an infinitesimal part of the total perturbation due to the light. We treat this infinitesimal part as a small perturbation superimposed on the interaction due to the total pumping field  $\mathbf{E}_1(t)$ . It is supposed that the density matrix is known for atoms irradiated by the field  $\mathbf{E}_1(t)$  and undergoing magnetic resonance. The perturbation due to the Fourier component  $\mathbf{E}(k)dk e^{-ikt}$  is calculated.  $\mathbf{E}(k)dk e^{-ikt}$  may be a Fourier component of  $\mathbf{E}_1(t)$  itself, or of a separate monitoring beam, provided this is weak.



## 2.2. The complete Hamiltonian

The problem may be solved in general terms without specifying the other perturbations in detail, but for the sake of definiteness we shall suppose that the atoms are subjected to the perturbations detailed in I, namely, a static magnetic field  $\mathbf{H}$ , a rotating magnetic field  $\mathbf{H}_1$  which is driving the  $|\mu\rangle$  in forced precession, together with the optical field  $\mathbf{E}_i(t)$ , and radiative decay. All these perturbations are described by a Hamiltonian  $\mathcal{H}_I$ . Adding the perturbation due to  $\mathbf{E}(k)dk e^{-ikt}$ , we write the complete Hamiltonian

$$\mathcal{H} = \mathcal{H}_I + \mathcal{H}'. \quad (1)$$

In the electric dipole approximation we have

$$\mathcal{H}' = -\{\mathbf{E}(k)dk e^{-ikt}\} \cdot \mathbf{P} = -FE(k)dk e^{-ikt} \quad (1a)$$

where  $F$  is the operator  $(\mathbf{e}^0 \cdot \mathbf{P})$ .  $\mathbf{e}^0$  is a unit vector in the direction of  $\mathbf{E}(k)$ .

## 2.3. Method of solution

A quantized field calculation of the effect on an atom of an incident radiation field yields the so-called coherent and incoherent contributions to the scattering cross section (Breit 1933, especially pp. 106, 107, Heitler 1954). Only the coherent scattering contributes to the refractive index, which is our present concern. In a semi-classical calculation of the induced dipole moment the same distinction is found. One calculates the perturbation of the atom by the incident field, postulating also the presence of an incoherent field to take account of spontaneous decay. The effect of this field on the excited states may be represented by a damping constant. Its effect on the ground states is to introduce terms which are incoherent with the incident radiation. In the following calculation only terms coherent with the incident field are kept.

The effect of the perturbation is calculated to first order, and the expectation value of the induced electric dipole moment is obtained. Hence the polarizability for the atom in question may be calculated, and averaged over an assembly. This yields the bulk polarization in terms of  $\sigma_{\mu\mu'}(t)$ , the density matrix of the assembly under the Hamiltonian  $\mathcal{H}_I$ , which is supposed to be known.

## 2.4. The perturbation calculation

Let

$$|t\rangle = \sum_{\mu} a_{\mu}(t)|\mu\rangle + \sum_m a_m(t)|m\rangle \quad (2)$$

represent the state of an atom at time  $t$  under the Hamiltonian  $\mathcal{H}_I$ . The perturbation  $\mathcal{H}'$  introduces into the equations of motion terms  $\sum_{\mu} \mathcal{H}'_{m\mu}(t)a_{\mu}(t)$  and  $\sum_m \mathcal{H}'_{\mu m}(t)a_m(t)$ . The former represent stimulated absorption, the latter stimulated emission. We shall discard the latter since the  $a_m(t)$  are much smaller than the  $a_{\mu}(t)$ . In this approximation the  $a_{\mu}(t)$  are unaffected by the perturbation, and we need only calculate the increments to the  $a_m(t)$ .

Let  $a_m^{(1)}(k, t)$  be the (infinitesimal) increment to  $a_m(t)$  generated by the perturbation. From the Schrödinger equation of motion we have

$$\dot{a}_m^{(1)}(k, t) = -i(k_m - \frac{1}{2}i\Gamma_m)a_m^{(1)}(k, t) - \frac{i}{\hbar} \sum_{\mu} \mathcal{H}'_{m\mu}(t)a_{\mu}(t). \quad (3)$$

$\hbar k_m$  is the energy of  $|m\rangle$  in the static field, and the term  $\frac{1}{2}i\Gamma_m$  represents the effect of spontaneous emission. (The radio-frequency field is supposed to be ineffective for the excited states.)

In order to integrate equation (3) we need to know the time dependence of  $a_\mu(t)$ . The form of this was found in earlier studies of atoms undergoing magnetic resonance, with damping and regeneration (see I, and references given there). It is

$$a_\mu(t) = \sum_l a_{\mu l}^0 \exp(-ik_{\mu l}t). \quad (4)$$

The frequencies  $k_{\mu l}$  are combinations of integral multiples of the precessional and nutational frequencies.

With  $\mathcal{H}'$  given by equation (1a) and  $a_\mu(t)$  by (4), we find

$$a_m^{(1)}(k, t) = E(k)dk e^{-ikt} \sum_{\mu, l} \frac{F_{m\mu} a_{\mu l}^0 \exp(-ik_{\mu l}t)}{\hbar(k_m - k_{\mu l} - k - \frac{1}{2}i\Gamma_m)}. \quad (5a)$$

In ordinary circumstances the nutational frequencies  $k_{\mu l} - k_{\mu l'}$  are very much smaller than  $\Gamma_m$ , so that we can ignore the  $l$  dependence of the denominator, which then becomes  $\hbar(k_m - k_\mu - k - \frac{1}{2}i\Gamma_m)$ . The summation over  $l$  may be carried out by (4), and (5a) reduces to

$$a_m^{(1)}(k, t) = E(k)dk \exp(-ikt) \sum_\mu \frac{F_{m\mu} a_\mu(t)}{\hbar(k_m - k_\mu - k - \frac{1}{2}i\Gamma_m)}. \quad (5b)$$

The addition of the  $a_m^{(1)}(k, t)$  to the coefficients  $a_m(t)$  in equation (2) yields the state  $|t'\rangle$ , which represents the effect of the perturbation in first order.

### 2.5. The polarizability tensor

The expectation value of the electric dipole moment is given by  $\langle t'|\mathbf{P}|t'\rangle$ . The dipole induced by the perturbation is the difference between this and  $\langle t|\mathbf{P}|t\rangle$ . We find terms in  $e^{ikt}$  as well as in  $e^{-ikt}$ . We retain only the latter, since the former couple with the complex conjugate wave in the medium.

The induced dipole is then given by

$$\mathbf{P}^{(1)} = \sum_{\mu', m} \langle \mu'|\mathbf{P}|m\rangle a_{\mu'}^*(t) a_m^{(1)}(k, t) \quad (6)$$

and the polarizability  $\alpha^{(i)}(k, t)$  of the  $i$ th atom is obtained from the defining equation

$$\mathbf{P}^{(1)} = \alpha^{(i)}(k, t) \mathbf{E}(k)dk e^{-ikt}. \quad (7)$$

Introducing unit vectors  $\mathbf{e}_r^0$ ,  $\mathbf{e}_s^0$ , members of the set  $\mathbf{e}_1^0 = -(\mathbf{i} + i\mathbf{j})/2^{1/2}$ ,  $\mathbf{e}_0^0 = \mathbf{k}$ ,  $\mathbf{e}_{-1}^0 = (\mathbf{i} - i\mathbf{j})/2^{1/2}$ , and using (5b) and (6) in (7), we obtain the following expression for the components of  $\alpha^{(i)}$ :

$$\alpha_{rs}^{(i)}(k, t) = \sum_{\substack{\mu \\ m = \mu + r \\ \mu' = m - s}} \frac{\mathcal{F}_{rs}}{\hbar(k_m - k_\mu - k - \frac{1}{2}i\Gamma_m)} a_\mu(t) a_{\mu'}^*(t) \quad (8)$$

where

$$\mathcal{F}_{rs} = \langle \mu'|\mathbf{e}_s^{0*} \cdot \mathbf{P}|m\rangle \langle m|\mathbf{e}_r^0 \cdot \mathbf{P}|\mu\rangle.$$

The bulk polarizability is calculated from (8) by summing over the  $N$  atoms per unit volume. These have a Doppler distribution of resonance frequencies,  $k_{m\mu} = k_m - k_\mu$ . The distribution function is  $dN = (N/\Delta\pi^{1/2}) \exp[-\{(\delta k_{m\mu})^2/\Delta^2\}] dk_{m\mu}$ , where

$$\delta k_{m\mu} = k_{m\mu} - (k_{m\mu})_0$$

and  $(k_{m\mu})_0$  is the peak of the distribution. In making the sum we must replace  $a_\mu(t) a_{\mu'}^*(t)$



by its average value  $\sigma_{\mu\mu'}(t)$ . The result is

$$\alpha_{rs}(k, t) = \sum_{\substack{\mu \\ m=\mu+r \\ \mu'=m-s}} \frac{N\mathcal{F}_{rs}}{\hbar\Delta} \sigma_{\mu\mu'}(t) Z(x_{m\mu} + iy) \quad (9)$$

where  $Z(x+iy)$  is the plasma dispersion function

$$Z(x+iy) = \pi^{-1/2} \int_{-\infty}^{\infty} \frac{\exp(-t^2)}{t - (x+iy)} dt, \quad x_{m\mu} = \frac{k - (k_{m\mu})_0}{\Delta} \text{ and } y = \frac{\Gamma_m}{2\Delta}.$$

Equation (9) is to be compared with equation (12) of CKS, but it is to be recalled that the notation there is different. The  $|\mu\rangle$  in CKS(12) are the states into which the  $|m\rangle$  transform under rotations, and are not ground states of the atom, as in this paper.

## 2.6. Interpretation of the result

It is easy to deduce from equation (9) that the optical pumping resonances will not be Doppler-broadened. The signal, that is the variation of light intensity with magnetic field, is determined by the variation of the polarizability with the field. The variations we are interested in are those described by the terms  $\sigma_{\mu\mu'}(t)$  (see I, equations (12) and (13), for example). A resonance in  $\sigma_{\mu\mu'}(t)$  is traversed in a range of magnetic field of the order of  $\Gamma_\mu$ , and over this range the changes in the functions  $Z$  are completely negligible. Hence the signal is determined solely by the behaviour of  $\sigma_{\mu\mu'}(t)$  with field: the Doppler effect, which is contained within the  $Z$ , is completely irrelevant.

The situation is entirely different for magnetic resonance in the excited states. The only terms in the polarizability (CKS, equation (12)) which go through a resonance are the  $Z$  functions themselves, by virtue of the terms  $\mu p/\Delta$  in the denominators where

$$p = \gamma\{(H - H_0)^2 + H_1^2\}^{1/2}.$$

Doppler broadening arises since these changes are scaled in relation to  $\Delta$  rather than to  $\Gamma_m$ .

## 2.7. Intensity of the transmitted light

Knowledge of the polarizability enables us to calculate the eigenwaves and propagation constants as in CKS, and hence to determine the intensity of the transmitted light. The result will be approximate in that it is based on perturbation theory in first order, but if the monitoring beam is different from the pumping beam, and relatively weak, the approximation will be very good. We shall not carry out the calculations here, but will draw attention to some features of the result.

(i) If no analyser is used, or if the analyser passes some component of the incident light, and if the vapour density and path length are small, then the signal is a linear function of the imaginary part of the polarizability. This represents absorption from the monitoring beam, and corresponds to the solution

$$I_A = \sum_{\mu, \mu'} [\rho(k)\mathcal{F}]_{\mu'\mu} \sigma_{\mu\mu'}$$

which is usually given (Barrat and Cohen-Tannoudji 1961).

(ii) At higher vapour densities the optical thickness of the sample would lead to exponential attenuation at a rate proportional to the imaginary part of the polarizability. Thus, multiple products of the form  $\sigma_{\mu\mu'}\sigma_{\mu''\mu'''} \dots$  could arise in the solution. If, for example, one were studying a modulated signal at the frequency  $(\mu - \mu')\omega_0$ , one might

find also, in higher order, frequencies  $(\mu - \mu' + \mu'' - \mu''')\omega_0$ , etc. Moreover, one might expect broadening and distortion of the resonance curves just as spectral profiles obtained in absorption are broadened and distorted when the samples are optically thick.

(iii) If the analyser is crossed with the polarizer, the term linear in the polarizability is suppressed. The first non-vanishing terms are quadratic. These terms correspond to the forward-scattered radiation which was analysed in considerable detail in CKS. For such terms the relative phase of the eigenwaves is more important than the attenuation. This is the underlying reason why the Doppler distribution is important in the one case, but not in the other.

### 3. Conclusion

A study of the polarizability tensor for an assembly of atoms undergoing optical pumping reveals that Doppler broadening is not to be expected when magnetic resonance in the ground states is detected by measuring the absorption of light. This result is to be contrasted with the Doppler broadening of excited-state resonance curves obtained by measuring the forward-scattered light. Doppler broadening arises in the latter case because the coherence between waves scattered from different atoms is partially destroyed by the spread of resonance frequencies due to their random motion. The assembly of moving atoms behaves approximately like an assembly of static atoms, the damping constant of which has been greatly increased. In the case of absorption the important phase relations are those between the induced dipoles and the driving field: the relative phases of different atomic dipoles are irrelevant.

### Acknowledgments

I wish to acknowledge stimulating discussions with Dr. S. Pancharatnam.

### References

- BARRAT, J., and COHEN-TANNOUDJI, C., 1961, *J. Phys. Radium*, **22**, 329–36, 443–50.
- BREIT, G., 1933, *Rev. Mod. Phys.*, **5**, 91–140.
- CORNEY, A., KIBBLE, B. P., and SERIES, G. W., 1966, *Proc. Roy. Soc. A*, in the press.
- HEITLER, W., 1954, *The Quantum Theory of Radiation* (Oxford: Clarendon Press).
- SERIES, G. W., 1966, *Proc. Phys. Soc.*, **88**, 957–68.



# The level-crossing effect in resonance fluorescence stimulated by monochromatic light

G. W. SERIES

Clarendon Laboratory, Oxford

*MS. received 31st May 1966, in revised form 1st August 1966*

**Abstract.** Analyses of the level-crossing effect have usually been given for broad-band excitation of resonance fluorescence. The fluorescence excited by monochromatic light from an assembly of static atoms would be expected to show a modified form of level-crossing effect, but, when motion of the atoms is taken into account, the same result is obtained as for broad-band excitation.

## 1. Introduction

'Level-crossing' phenomena in the resonance fluorescence of atomic vapours are anomalies in the spatial distribution of fluorescent light which occur when a pair of excited levels in the atomic term diagram is degenerate (Colegrove *et al.* 1959, Franken 1961). The effects are usually studied by measuring the changes in intensity of the fluorescent light recorded by a detector in a fixed position as a magnetic field is varied through the region where the levels intersect. With a suitable geometrical arrangement the changes in intensity, as a function of magnetic field, may be represented by Lorentzian curves whose widths are simply the sum of the natural widths of the intersecting levels.

Experiments of this sort are normally carried out with 'broad-band' excitation that is, the spectral width of the exciting light is large compared with the natural width of the levels concerned. The purpose of this paper is to draw attention to the form of level-crossing curves to be expected for sharp-line excitation, that is when the spectral width is small compared with the natural width. Experiments using this type of excitation are clearly feasible using laser light sources, but have not yet been reported so far as we are aware.

A first glance at the problem might lead one to expect that level-crossing curves excited in this way should be exceedingly narrow. It is recalled (Heitler 1954) that the spectral profile of resonance fluorescence excited by broad-band excitation from a two-level atom should be a Lorentzian of width equal to the natural width of the excited level, but that when the exciting radiation is monochromatic, the fluorescent light should also be monochromatic. It might be supposed that the level-crossing curves should be correspondingly narrow.

We believe this result to be wrong because it neglects both the perturbation which gives rise to spontaneous emission and the random motion of the atoms in the vapour. The result predicted by the following analysis is that level-crossing curves excited by monochromatic light should be identical with those obtained by broad-band excitation, provided that the Doppler width for absorption in the vapour is large compared with the natural width, which is generally the case.

## 2. Theory

The treatment of resonance fluorescence by Heitler (1954) forms a convenient

starting point. Consider the absorption of light of frequency  $k$ , and specified wave vector and polarization, by an atom originally in state  $|i\rangle$ , and the emission of light of frequency  $k'$ , and specified wave vector and polarization, which leaves the atom in state  $|j\rangle$ .  $|j\rangle$  may be, but need not be, identical with  $|i\rangle$ . The probability amplitude for this two-stage process proceeding via the intermediate state  $|p\rangle$  is proportional to

$$\frac{f_{pi}g_{jp}}{(k - k_p + \frac{1}{2}i\Gamma_p)(k - k' - k_j + \frac{1}{2}i\Gamma_j)} \quad (1)$$

(Heitler 1954, p. 199, equation (10)). The notation here is different from that of Heitler.  $f_{pi}$  and  $g_{jp}$  are matrix elements for absorption and emission, respectively. They take the form  $\langle p|\mathbf{e}_i^0 \cdot \mathbf{P}|i\rangle$ ,  $\langle j|\mathbf{e}_s^{0*} \cdot \mathbf{P}|p\rangle$ , where  $\mathbf{P}$  is the electric dipole operator, and  $\mathbf{e}_i^0$  and  $\mathbf{e}_s^0$  are unit vectors in the direction of the electric vectors of the incident and scattered light.  $k_p$  and  $\Gamma_p$ ,  $k_j$  and  $\Gamma_j$  are the resonance frequencies and damping constants of  $|p\rangle$  and  $|j\rangle$  respectively, where  $k_p$  and  $k_j$  are measured relative to the energy of  $|i\rangle$ . A result substantially identical with (1) was obtained by Kibble and Pancharatnam (1965) in a semi-classical calculation of the step-wise excitation of an atom by two monochromatic radiation fields.

It is to be understood that equation (1) is the result of a first-order calculation whose validity rests on the assumption that the probability for absorption is very much smaller than the probability for spontaneous emission. This is a very realistic assumption for light fields of ordinary intensity and we shall proceed on this basis.

An expression similar to (1), with  $k_p$  and  $\Gamma_p$  replaced by  $k_q$  and  $\Gamma_q$ , obtains for scattering via the intermediate state  $|q\rangle$ . (In cases which are generally studied,  $\Gamma_q$  is equal to  $\Gamma_p$  since the states are members of the same hyperfine or Zeeman set. It is convenient, however, to retain the generality and to introduce  $\Gamma = \frac{1}{2}(\Gamma_p + \Gamma_q)$  in equation (3b) below.)

When the scattering may take place via either  $|p\rangle$  or  $|q\rangle$ , the probability amplitude is the sum of the two expressions. The intensity of fluorescent light of frequency  $k'$  is proportional to the squared modulus of the sum, and the level-crossing phenomena are represented by cross terms such as

$$\frac{f_{pi}g_{jp}f_{qi}^*g_{jq}^*}{(k - k_p + \frac{1}{2}i\Gamma_p)(k - k_q - \frac{1}{2}i\Gamma_q)\{(k - k' - k_j)^2 + (\frac{1}{2}\Gamma_j)^2\}} \quad (2)$$

The total emission, irrespective of frequency, is obtained by integrating (2) over  $k'$  from 0 to  $\infty$ . The result is

$$\frac{(2\pi/\Gamma_j)f_{pi}g_{jp}f_{qi}^*g_{jq}^*}{(k - k_p + \frac{1}{2}i\Gamma_p)(k - k_q - \frac{1}{2}i\Gamma_q)} \quad (3a)$$

which is more conveniently written

$$\frac{A + iB}{\delta - i\Gamma} \left( \frac{1}{k - k_p + \frac{1}{2}i\Gamma_p} - \frac{1}{k - k_q - \frac{1}{2}i\Gamma_q} \right) \quad (3b)$$

where  $\delta = k_p - k_q$  and  $\Gamma = \frac{1}{2}(\Gamma_p + \Gamma_q)$ . Gallagher and Lurio (1964, appendix, equation (19)) give this result in substantially the same form.

### 2.1. Broad-band excitation

Since the spectral components of the exciting light contribute independently to the fluorescent intensity, the terms which represent the level-crossing effect in this case are



obtained by integrating (3b) over  $k$ . If the range of integration spans  $k_p$  and  $k_q$ , and is much greater than  $\Gamma_p$  and  $\Gamma_q$ , the terms inside the brackets integrate to  $\mp \pi i$  respectively, and the result is

$$\frac{2\pi(A + iB)}{\Gamma + i\delta} \quad (4)$$

which is the well-known result (Franken 1961).

## 2.2. The Doppler effect

The equations we have so far obtained refer to a static atom. If the atom is in motion with velocity  $\mathbf{v}$ , we need to distinguish between frequencies measured in the laboratory frame and in the rest frame of the atom. In the laboratory frame  $k$  is unaltered, but the resonance frequencies of the atom to light of wave vector  $\mathbf{k}$  need to be corrected by the factor  $(1 + \mathbf{v} \cdot \mathbf{k}/k)$ . Similarly, the frequency of the fluorescent light ( $k'$  in the rest frame of the atom) needs to be corrected by a factor which takes account of its direction relative to  $\mathbf{v}$  and  $\mathbf{k}$ . Details of this frequency distribution have been studied, for example, by Hummer (1962). However, the frequency of the fluorescent light is of no interest in the experiments with which we are concerned, since the detector measures the total intensity of the fluorescent light without spectral discrimination. The effect of atomic motions on the intensity of the light is adequately described by correcting  $k_p$ ,  $k_q$  and  $\delta$  in equations such as (3b) with the factor written above, and integrating over the corresponding distributions of  $k_p'$ ,  $k_q'$  and  $\delta'$ , where  $k_p' = k_p(1 + \mathbf{v} \cdot \mathbf{k}/k)$ , etc. The distributions of  $k_p'$  and  $k_q'$  represent the Doppler broadening of the absorption profile of the assembly and are generally much wider than  $\Gamma_p$  or  $\Gamma_q$ . On the other hand, the values of  $\delta$  in which we are interested are of the order of magnitude of  $\Gamma$ , and the Doppler broadening of  $\delta$  is negligibly small. The factor  $\delta - i\Gamma$  may therefore be treated as constant, and the integration over the velocity distribution reduces to integration of the two terms inside the brackets over ranges of  $k_p'$  and  $k_q'$  large compared with  $\Gamma_p$  and  $\Gamma_q$ . These integrations, with fixed  $k$ , give exactly the same result as the integration over a wide range of  $k$  with fixed  $k_p$  and  $k_q$ . The relevant variables are not  $k$  or  $k_p'$  or  $k_q'$  considered in isolation, but  $k - k_p'$  and  $k - k_q'$ . The predicted result for the level-crossing effect stimulated by monochromatic light in the region of absorption is therefore the same as that for broad-band excitation, provided that the Doppler broadening of the absorption line is large compared with the natural width.

## 3. Conclusion

The well-known result for the level-crossing effect in resonance fluorescence was obtained for excitation of the atoms by broad-band excitation, without consideration of the motion of the atoms in the sample. If the exciting light is monochromatic, a different result is obtained so long as the atoms are considered to be static, but when their random motion is taken into account, the same result is obtained as for broad-band excitation. The important variable is the spectral distribution of the exciting light *as seen by the atoms* in relation to the natural width of the excited levels. If this distribution is broad compared with the natural width, either because of the character of the light source or because of the Doppler effect of the moving atoms, the level-crossing curves will be represented by some superposition of the functions  $\Gamma^2/(\Gamma^2 + \delta^2)$  and  $\delta\Gamma/(\Gamma^2 + \delta^2)$  as calculated by Franken (1961).

These predictions are related to the well-known fact that when monochromatic

light is scattered by moving atoms, the scattered light is not monochromatic, but is subject to a spectral distribution which reflects the velocity distribution of the atoms. The details of the spectral distribution are not relevant in level-crossing experiments since the quantity which is measured is the intensity integrated over frequency.

### Acknowledgments

I wish to acknowledge the benefit of discussions with Dr. S. Pancharatnam, particularly in regard to the validity of equation (1).

### References

- COLEGROVE, F. D., FRANKEN, P. A., LEWIS, R. R., and SANDS, R. H., 1959, *Phys. Rev. Letters*, **3**, 420-2.
- FRANKEN, P. A., 1961, *Phys. Rev.*, **121**, 508-12.
- GALLAGHER, A., and LURIO, A., 1964, *Phys. Rev.*, **136**, A87-105.
- HEITLER, W., 1954, *The Quantum Theory of Radiation*, 3rd edn (London: Oxford University Press).
- HUMMER, D. G., 1962, *Mon. Not. R. Astr. Soc.*, **125**, 21-37.
- KIBBLE, B. P., and PANCHARATNAM, S., 1965, *Proc. Phys. Soc.*, **86**, 1351-63.



# Theory of frequency and polarization modulation in resonance fluorescence†

G. W. SERIES

J. J. Thomson Physical Laboratory, University of Reading, Berks.

*MS. received 7th August 1969*

**Abstract.** A treatment of resonance fluorescence is given in which the properties of the incident and scattered light are expressed in terms of coherency matrices. Calculations are made for two successive scattering processes corresponding to the experiments described in an accompanying paper. For the first process the scattering atoms are subjected to a magnetic field consisting of parallel static and oscillating components. The fluorescent light is frequency-modulated and may also be polarization-modulated. This light excites fluorescence in a second cell in which the atoms are subjected to a static magnetic field. The equations show under what conditions the second fluorescence is intensity-modulated and describe the resonances in the amplitude of modulation which occur when the modulation frequency matches a Zeeman interval of the excited atoms.

## 1. Introduction

An accompanying paper (Chapman and Series 1970) gives an account of a variety of double-scattering experiments for light interacting with atomic vapours subject to static and time-dependent magnetic fields. An analysis of the scattering processes is given here.

The work forms part of a continuing programme of studies of modulation effects in resonance fluorescence. The present set of experiments was designed to look for resonances associated with frequency modulation of the exciting light. The source of frequency-modulated light was itself a scattering cell, so that analysis of the experiment requires the analysis of two consecutive processes of resonance fluorescence: first, the excitation of fluorescence in a vapour under conditions such that the fluorescent light is frequency-modulated, and, secondly, the fluorescence of a similar vapour when illuminated by fluorescent light from the first.

The outcome of the experiments was that under certain conditions the fluorescent light from the second cell was intensity-modulated (and hence gave rise to a modulated photoelectric current), and that the amplitude of modulation showed resonances when the modulation frequency matched a Zeeman interval between the excited states of the scattering atoms. An important condition for generating this intensity modulation was that two orthogonally polarized modes of the frequency-modulated light should be coherent, that is to say, the exciting light should be polarization-modulated. From this point of view the experiments have much in common with the work of Aleksandrov (1965). The two sets of experiments differ in the way in which the light used for the excitation of fluorescence was prepared. Aleksandrov used an arrangement based on the Faraday effect to bring about sinusoidal oscillation of the plane of polarization of light from a conventional light source. His analysis is based directly on the concept of polarization modulation. The arrangement used by Chapman and Series sprang from a desire to study frequency modulation, and the present analysis reflects this point of view. In Aleksandrov's case the description of the polarization-modulated light does not call for an analysis of the emission of light from a source and his analysis relates to one scattering process only.

† This work was carried out at the Clarendon Laboratory, Oxford



## 2. Statement of the problem

We distinguish the two scattering processes in the experiments of Cha Series as taking place in the 'source cell' and 'experimental cell', respectively.

Atoms in the source cell are subjected to magnetic fields  $(H_s + H_1 \cos ft)$  where  $\mathbf{k}$  is a unit vector. We shall take the direction of  $\mathbf{k}$  to be the axis of quantization for atoms in the source cell.

Atoms in the experimental cell are subjected to a static magnetic field  $\mathbf{h}$  where  $\mathbf{h}$  is a unit vector in an arbitrary direction. We shall take this direction to be the axis of quantization for atoms in the experimental cell.

We shall specify the light by the elements of coherency matrices defined in three-dimensional physical space. These matrices represent the measurable properties of the light. For each of the two scattering processes we shall show how the matrix representing the scattered light may be obtained from the matrix representing the incident light. Fields representing the light will be used in the course of the calculation, but will not appear in the final results. The calculation itself will be classical, similar to that given in an earlier paper (Dodd and Series 1961).

The essential features of the analysis are brought out by studying as an example the case of an even isotope of mercury (transition  $^3P_1 - ^1S_0$ ; 2537 Å). This work could be generalized as was the earlier work (Franzen and Alam 1964; *et al.* 1968).

The significant difference between the situation analysed in the earlier paper and the situation considered here is that here, for the source cell, we are concerned with a time-dependent field oscillating *parallel* to a steady field, whereas in the earlier work the time-dependent field was *rotating round* the steady field. In both cases the time development of the excited state can be solved exactly. A further difference is that, in this paper, the fields representing the light are treated more completely.

## 3. Scattering in the source cell

The Hamiltonian for atoms in the source cell may be written

$$\mathcal{H}_s = \mathcal{H}_0 + \gamma \mathbf{J} \cdot \mathbf{k}(H_s + H_1 \cos ft) + \mathcal{H}_D - \mathbf{E}^{(0)}(t) \cdot \mathbf{P}$$

where  $\mathcal{H}_0$  is the Hamiltonian in the absence of fields,  $\mathbf{J}$  is the angular momentum operator,  $\gamma$  is the gyromagnetic ratio,  $\mathcal{H}_D$  describes radiative damping of the states,  $\mathbf{E}^{(0)}(t)$  is the field of the incident light, regarded as independent of position over the volume of any particular atom, and  $\mathbf{P}$  is the electric dipole operator.

The only states with which we need to be concerned are the ground state  $|^1S_0; 0\rangle$ , which we shall call  $|g\rangle$ , and the space-quantized states  $|^3P_1; 0\rangle$  of the excited level, which we shall call  $|n\rangle$ . (We use  $n$ , which takes the values 1, 2, 3, 4, 5, 6, 7, 8, 9, 10, 11, 12, 13, 14, 15, 16, 17, 18, 19, 20, 21, 22, 23, 24, 25, 26, 27, 28, 29, 30, 31, 32, 33, 34, 35, 36, 37, 38, 39, 40, 41, 42, 43, 44, 45, 46, 47, 48, 49, 50, 51, 52, 53, 54, 55, 56, 57, 58, 59, 60, 61, 62, 63, 64, 65, 66, 67, 68, 69, 70, 71, 72, 73, 74, 75, 76, 77, 78, 79, 80, 81, 82, 83, 84, 85, 86, 87, 88, 89, 90, 91, 92, 93, 94, 95, 96, 97, 98, 99, 100, as the space quantum number for excited atoms in the source cell and  $m$ , which takes the same values, for excited atoms in the experimental cell.)

We shall treat the interaction with the light as a small perturbation, and write

$$\mathcal{H}_s = \mathcal{H}_s' - \mathbf{E}^{(0)}(t) \cdot \mathbf{P}.$$

The equation of motion under  $\mathcal{H}_s'$  will be solved first. Expressed in terms of the time-displacement operator  $U'(t, t_0)$ , the equation is

$$i\hbar \frac{d}{dt} U'(t, t_0) = \mathcal{H}_s' U'(t, t_0)$$



The solution of (3) is

$$U'(t, t_0) = \exp \left( -\frac{i}{\hbar} \left[ (\mathcal{H}_0 + \mathcal{H}_D)(t - t_0) + \gamma(\mathbf{J} \cdot \mathbf{k}) \left\{ H_s(t - t_0) + \left( \frac{H_1}{f} \right) (\sin ft - \sin ft_0) \right\} \right] \right). \quad (5)$$

$U'(t, t_0)$  is diagonal in the  $|g\rangle, |n\rangle$  representation. Its eigenvalues are

$$U_{gg}'(t, t_0) = 1 \quad (6a)$$

and

$$\begin{aligned} U_{nn}'(t, t_0) &= \exp \left( -i \left[ (k_s - \frac{1}{2}i\Gamma)(t - t_0) + n \left\{ \omega_s(t - t_0) + \left( \frac{\omega_1}{f} \right) (\sin ft - \sin ft_0) \right\} \right] \right) \\ &= \exp \left\{ -i(k_s + n\omega_s - \frac{1}{2}i\Gamma)(t - t_0) \right\} \sum_{r,s=-\infty}^{\infty} J_r(an) J_s(an) \exp \{ -if(rt - st_0) \} \end{aligned} \quad (6b)$$

where the energy of the ground state is taken as zero. We have introduced  $k_s$  for the Bohr frequency of the excited states in the absence of magnetic fields, and  $\Gamma$  for their damping constant.  $\omega_s = \gamma H_s$ ,  $\omega_1 = \gamma H_1$ .

In equation (6b) we have used the expansion in Bessel functions

$$\exp(-ian \sin ft) = \sum_{r=-\infty}^{\infty} J_r(an) \exp(-irft) \quad (7)$$

in which  $a = \omega_1/f$ .

The complete equation of motion

$$i\hbar \frac{d}{dt} |t\rangle = [\mathcal{H}_s' - \mathbf{E}^{(0)}(t) \cdot \mathbf{P}] |t\rangle \quad (8)$$

may now be solved by methods of approximation. The solution, to first order in  $\mathbf{E}^{(0)}(t)$ , is

$$|t\rangle = |g\rangle + \frac{i}{\hbar} \int_0^t dt_0 U'(t, t_0) [\mathbf{E}^{(0)}(t_0) \cdot \mathbf{P}] U'(t_0, 0) |g\rangle \quad (9)$$

where the atoms are taken to be initially in the state  $|g\rangle$ .

If the field  $\mathbf{E}^{(0)}(t)$  were linearly polarized we could write it in the form  $\mathbf{E}^{(0)}(t) \mathbf{e}^{(0)}$ , where  $\mathbf{e}^{(0)}$  is a unit vector. We need not work under this restriction. Retaining generality, we write

$$\mathbf{E}^{(0)}(t) = \sum_{v=i,j,k} E_v^{(0)}(t) \mathbf{e}_v^{(0)} \quad (10)$$

where the unit vectors  $\mathbf{e}^{(0)}$  form an orthogonal set. Equation (9) may then be expanded:

$$|t\rangle = |g\rangle + \frac{i}{\hbar} \sum_{n,v} \int_0^t dt_0 E_v^{(0)}(t_0) U_{nn}'(t, t_0) \langle n | \mathbf{e}_v^{(0)} \cdot \mathbf{P} | g \rangle |n\rangle. \quad (11)$$

The field of the light radiated by atoms represented by this state vector is obtained semi-classically in terms of the matrix element  $\langle g | \mathbf{P} | t \rangle$ . With the help of equations (11) and (6), and with some rearrangement of the time dependencies, this matrix

element is proportional to

$$\begin{aligned} D_s^{(1)}(k_s, t) = & - \sum_{n, \nu} (e_\nu^{(0)} \cdot D_{ng}) D_{gn} \sum_{r, s = -\infty}^{\infty} J_r(an) J_s(an) \exp\{-if(r-s)t\} \\ & \times \int_0^t d\tau_0 E_\nu^{(0)}(t-\tau_0) \exp\{-i(k_s + n\omega_s + fs - \tfrac{1}{2}i\Gamma)\tau_0\}. \end{aligned} \quad (12)$$

We have retained only the angular parts  $D_{ng} \equiv \langle n | D | g \rangle$  of matrix elements such as  $\langle n | P | g \rangle$ , and replaced the variable  $t_0$  by  $\tau_0 = t - t_0$ .

The radiation field  $E(r, t)$  at a point P displaced  $r$  from the oscillating dipole  $D$  is proportional to the projection of the retarded value of  $D$  on to the plane perpendicular to  $r$ :

$$E_s^{(1)}(r, t) \propto P(r_0) \cdot D_s^{(1)}\left(t - \frac{r}{c}\right) \quad (13)$$

where  $P(r_0)$  is the dyadic  $(\mathcal{J} - r_0 r_0)$ .  $\mathcal{J} = ii + jj + kk$  and  $r_0$  is a unit vector along  $r$ . The action of a linear polarizer in the direction of the unit vector  $e^{(1)}$  perpendicular to  $r$  is given by replacing  $P(r_0)$  by the dyadic  $e^{(1)} e^{(1)}$ . Similarly, a general dyadic  $T^{(1)}$  would represent the action of a birefringent plate or other polarizing device.

The field at P due to all the atoms in the cell will be a sum of expressions similar to equation (13), in which, if P is well outside the source, the geometrical factors will be approximately the same for all atoms. However, the distances  $r$  will be random, resulting in random phases between the contributions from different atoms. There will also be random-phase factors arising from the random phase of the primary light at the sites of different atoms in the cell. In forming quadratic functions of the field we may therefore ignore cross terms between the fields of different atoms.

For the moment we may ignore also the random motion of the atoms. This will be taken into account in due course by introducing a Doppler distribution of the frequency.

#### 4. Matrix representation of light fields

We have derived an expression for the scattered field  $E^{(1)}(t)$  in terms of the vector components of the primary field  $E^{(0)}(t)$ , but these fields are not measurable. We shall now define coherency matrices whose elements are measurable quantities. The definitions are very close to those which have been used elsewhere (see, for example, the textbook by O'Neill (1963), where references to the original work are given).

For the field given by

$$E(t) = \sum_{\nu=i,j,k} E_\nu(t) e_\nu \quad (14)$$

where the  $e_\nu$  form a set of orthogonal unit vectors, the coherency matrix  $\sigma(t, \tau)$  is defined by its elements

$$\sigma_{ij}(t, \tau) = \frac{1}{2T} \int_{t-T}^{t+T} dt' E_i(t') E_j^*(t' - \tau) \quad (15)$$

where the asterisk denotes complex conjugation.

In forming these cross-correlation functions of the field, the averaging time  $T$  is to be long compared with optical periods but short compared with the period of any modulation in which we may be interested.

We take  $\text{Tr } \sigma(t, \tau = 0)$  as proportional to the intensity of the light at time  $t$ . The intensity as usually defined would be the value of  $\text{Tr } \sigma(t, \tau = 0)$  as  $T$  tends to infinity. By averaging over a finite rather than an infinite time we retain the freedom to study time-varying fields. Fluctuations of the intensity are not considered.



### 5. Matrix of the primary light

We have supposed the field of the primary light to be given by equation (10). Its coherency matrix  $\sigma^{(0)}(t, \tau)$  is constructed as in equation (15). We shall suppose that  $\sigma^{(0)}(t, \tau)$  is independent of  $t$ . It may then be expressed in terms of the spectral cross-correlation coefficients  $\hat{\rho}_{ij}^{(0)}(k)$ :

$$\sigma_{ij}^{(0)}(\tau) = (2\pi)^{-1} \int_{-\infty}^{\infty} dk \hat{\rho}_{ij}^{(0)}(k) \exp(-ik\tau) \quad (16)$$

where  $\hat{\rho}_{ij}^{(0)}(k)$  are the cross products  $E_i^{(0)}(k)E_j^{(0)*}(k)$  of the Fourier components of the field.

### 6. Matrix of the light from the source

The field at P of the light scattered by one atom of the source (labelled by  $k_s$ ) is given by equations (12) and (13), with  $\mathbf{T}^{(1)}$  written as the generalization of  $\mathbf{P}(r_0)$  in equation (13). The coherency matrix is

$$\begin{aligned} \sigma_{kl}^{(1)}(k_s, t, \tau) = & \sum_{\substack{n, n' \\ i, j}} \left( \sum_{\substack{r, r' \\ s, s'}} J_r(an) J_s(an) J_{r'}(an') J_{s'}(an') \exp\{-if(r' - s')\tau\} \right. \\ & \times \left[ \frac{1}{2T} \int_{t-T}^{t+T} dt' \exp\{-if(r - s - r' + s')t'\} \right. \\ & \times \int_0^{t'} d\tau_0 E_i^{(0)}(t' - \tau_0) \exp(-i\alpha_s \tau_0) \int_0^{t' - \tau} d\tau_0' E_j^{(0)*}(t' - \tau - \tau_0') \\ & \left. \left. \times \exp(i\alpha_s \tau_0') \right] \right) (\mathbf{T}^{(1)} \cdot \mathbf{D}_{gn})_k (\mathbf{D}_{ng} \cdot \mathbf{e}_i^{(0)}) (\mathbf{e}_j^{(0)*} \cdot \mathbf{D}_{gn'}) (\mathbf{D}_{n'g} \cdot \mathbf{T}^{(1)*})_l \end{aligned} \quad (17)$$

in which

$$\alpha_s = k_s + n\omega_s + fs - \frac{1}{2}i\Gamma$$

and

$$\alpha_s' = k_s + n'\omega_s + fs' + \frac{1}{2}i\Gamma.$$

#### 6.1. The time integrals

The time-dependent factors of equation (17), namely  $\exp\{-if(r' - s')\tau\}$  multiplied by the triple time integral, we denote by  $\phi_{ij}^{(1)}(t, \tau)$ . With some manipulation (see appendix 2), this may be expressed in terms of  $\sigma_{ij}^{(0)}(\tau)$  and hence, with the help of equation (16), in terms of  $\hat{\rho}_{ij}^{(0)}(k)$ . For broad-band excitation these latter quantities are independent of  $k$  and may be treated as constants  $\hat{\rho}_{ij}^{(0)}(k_0)$  in the region of interest. The integrals may then be evaluated to yield

$$\phi_{ij}^{(1)}(t, \tau) = \frac{\hat{\rho}_{ij}^{(0)}(k_0) \exp\{-if(r - s - r' + s')t\}}{\Gamma + i\{(n - n')\omega_s + (s - s')f\}} \exp\{-i(k_s + n'\omega_s + fr' + \frac{1}{2}i\Gamma)\tau\}. \quad (18)$$

The  $t$ -dependent modulation appears explicitly. There is a Lorentzian denominator describing the possibility of resonances between the driving frequency  $f$  and the Larmor frequency  $\omega_s$ .

#### 6.2. Assembly of atoms: Doppler distribution

The above result has been obtained for a static atom interacting with the fields. For atoms moving with velocity  $\mathbf{v}$  the interaction with a field with wave vector  $\mathbf{k}$  may be represented by scaling the atomic frequencies with the factor  $(1 \pm \mathbf{v} \cdot \mathbf{k}/k)$  (Series 1966). The generalization of  $\phi_{ij}^{(1)}$  for the assembly of atoms  $\Phi_{ij}^{(1)}$  is then given by the integral of equation (18) so modified, weighted by the distribution function over  $\mathbf{v}$ .

Let  $k$  be the wave vector of the emitted light of frequency  $k_1$  (measured in the rest frame of the atom), and let  $v_{\parallel}$  and  $v_{\perp}$  be the components of  $v$  parallel and perpendicular to  $k$ . The Doppler shift  $\delta k$  of the emitted light is  $k_1(v_{\parallel}/c)$ . The Doppler shift  $\delta k_0$  in excitation is  $-(k_1/c)(v_{\parallel} \cos \theta + v_{\perp} \sin \theta)$ , where  $\theta$  is the direction between the incoming and the outgoing beams. The distribution function for  $v_{\parallel}$  and  $v_{\perp}$  is  $\exp\{-\alpha(v_{\parallel}^2 + v_{\perp}^2)\}$ , where  $\alpha$  is a constant.

Of the frequencies appearing in equation (18), only the optical frequencies are significantly affected, that is, we must write  $\hat{\rho}_{ij}^{(0)}(k_0 + \delta k_0)$  for  $\hat{\rho}_{ij}^{(0)}(k_0)$ , and

$$k_s + n'\omega_s + fr' + \delta k$$

in the last exponential factor. The frequencies  $n'\omega_s$  and  $fr'$  are small compared with the Doppler width in the experiments we wish to describe, so that we may ignore these terms and write  $k_1 + \delta k$  for the Doppler-shifted frequency. Moreover, the value of  $\Phi_{ij}^{(1)}$  will be vanishingly small for values of  $\tau$  much greater than the reciprocal of the spectral width of the distribution function, and, since this is much greater than  $\Gamma$ , we may replace  $\exp(\frac{1}{2}\Gamma\tau)$  by unity.

The net result for the assembly of atoms is that  $\phi_{ij}^{(1)}$ , given by equation (18), is to be replaced by

$$\begin{aligned} \Phi_{ij}^{(1)}(t, \tau) = & \frac{\exp\{-if(r-s-r'+s')t\}}{\Gamma + i\{(n-n')\omega_s + (s-s')f\}} \\ & \times K \int \int_{-\infty}^{\infty} \hat{\rho}_{ij}^{(0)}(k_0 + \delta k_0) \exp\{-\alpha(v_{\parallel}^2 + v_{\perp}^2)\} \exp\{-i(k_1 + \delta k)\tau\} dv_{\parallel} dv_{\perp} \end{aligned} \quad (19)$$

where  $K$  is a normalizing constant. The integrals assume convenient forms in two special cases:

(i)  $\hat{\rho}(k_0)$  is wide in comparison with the *Doppler* distribution and may be treated as constant in both integrations. (We have previously assumed only that it is wide in comparison with  $\Gamma, f$  and  $\omega_s$ .) In this case the integration over  $v_{\perp}$  is simply the integral over its distribution, since  $\delta k$  is independent of  $v_{\perp}$ . Changing the variable  $v_{\parallel}$  to  $k = k_1(1 + v_{\parallel}/c)$ , we are left with

$$K' \hat{\rho}_{ij}^{(0)}(k_0) \int_{-\infty}^{\infty} \exp\left\{-\frac{(k-k_1)^2}{\Delta_1^2}\right\} \exp(-ik\tau) dk \quad (20)$$

where  $\Delta_1$  is a measure of the width of the Doppler distribution.

(ii) The scattered light is taken at right angles to the incident light ( $\theta = \frac{1}{2}\pi$ ). In this case the integrand breaks into two parts and the result may conveniently be written

$$K'' \int_{-\infty}^{\infty} \hat{\rho}_{ij}^{(0)}(k') \exp\left\{-\frac{(k'-k_1)^2}{\Delta_1^2}\right\} dk' \int_{-\infty}^{\infty} \exp\left\{-\frac{(k-k_1)^2}{\Delta_1^2}\right\} \exp(-ik\tau) dk. \quad (21)$$

We shall use this second result, replacing the Gaussians by the normalized function  $\rho^{(1)}(k, k_1, \Delta_1)$ . The final form is

$$\begin{aligned} \Phi_{ij}^{(1)}(t, \tau) = & \left[ \frac{\exp\{-if(r-s-r'+s')t\}}{\Gamma + i\{(n-n')\omega_s + (s-s')f\}} \int_{-\infty}^{\infty} \rho^{(1)}(k, k_1, \Delta_1) \exp(-ik\tau) dk \right] \\ & \times \int_{-\infty}^{\infty} \hat{\rho}_{ij}^{(0)}(k') \rho^{(1)}(k', k_1, \Delta_1) dk'. \end{aligned} \quad (22)$$

### 6.3. Final form of the matrix

Returning to equation (17) with the result (22), we notice that the indices  $r, r', s, s'$  occur only in the combinations  $s-s'$  and  $r-r'-s+s'$ , and in no other terms apart from



the Bessel functions. It is therefore useful to contract the summations over these indices as follows:

$$\sum_{\substack{r, r' \\ s, s'}} J_r(an) J_s(an) J_{r'}(an') J_{s'}(an') = \sum_{q, (p+q)} J_q(an - an') J_{p+q}(an - an') \quad (23)$$

with  $q = s - s'$  and  $p = r - r' - s + s'$ .

The last four sets of parentheses of equation (17) may be taken with the factor

$$\int_{-\infty}^{\infty} dk' \hat{\rho}_{ij}^{(0)}(k') \rho^{(1)}(k', k_1, \Delta_1)$$

of equation (22) to form a matrix with elements  $G_{kl}^{(1)}(n, n')$ , which by virtue of the summation over  $i$  and  $j$  may be regarded as formed by a succession of transformations on the matrix  $\hat{\rho}^{(0)}(k')$ :

$$G_{kl}^{(1)}(n, n') = \int_{-\infty}^{\infty} dk' \rho^{(1)}(k', k_1, \Delta_1) \{ \mathbf{T}^{(1)} \mathbf{D}_{gn} \mathbf{D}_{gn}^\dagger \mathbf{R}^{(1)} \hat{\rho}^{(0)}(k') \mathbf{R}^{(1)-1} \\ \times \mathbf{D}_{gn'} \mathbf{D}_{gn'}^\dagger \mathbf{T}^{(1)\dagger} \}_{kl}. \quad (24)$$

In this expression the matrices  $\mathbf{R}^{(1)}$  are introduced to rotate the basis vectors  $e^{(0)}$  from the frame  $S^{(0)}$  used to specify the primary light (§§ 4 and 5) to the frame  $S^{(1)}$  used for quantization of the atoms (§ 3). The matrices  $\mathbf{D}_{gn} (\mathbf{D}_{gn}^\dagger)$  are three-by-one column (row) matrices representing the vectors  $D_{gn} (D_{ng} = D_{gn}^*)$ .

We have now reduced the elements of the coherency matrix of the light scattered from the assembly to the form

$$\sigma_{kl}^{(1)}(t, \tau) = \sum_{n, n'} \mathcal{G}^{(1)}(n, n'; t, \tau) G_{kl}^{(1)}(n, n') \quad (25)$$

with

$$\mathcal{G}^{(1)}(n, n'; t, \tau) = \int_{-\infty}^{\infty} dk \rho^{(1)}(k, k_1, \Delta_1) \exp(-ik\tau) \\ \times \sum_{p, q} \frac{J_q(an - an') J_{p+q}(an - an') \exp(-ipft)}{\Gamma + i\{(n - n')\omega_s + qf\}} \quad (26)$$

and  $G_{kl}^{(1)}(n, n')$  given by (24). It should be noted that all the time dependence of  $\sigma^{(1)}$  is contained in the factors  $\mathcal{G}^{(1)}$ .

The intensity of the light passing the device represented by  $\mathbf{T}^{(1)}$  is proportional to

$$I^{(1)}(t) = \text{Tr} \sigma^{(1)}(t, \tau = 0) = \sum_{n, n'} \mathcal{G}^{(1)}(n, n'; t, \tau = 0) \text{Tr} \mathbf{G}^{(1)}(n, n'). \quad (27)$$

## 7. Scattering in the experimental cell

The Hamiltonian in this case is

$$\mathcal{H}_e = \mathcal{H}_0 + \gamma \mathbf{J} \cdot \mathbf{h}(H_e) + \mathcal{H}_D - E^{(1)}(t) \cdot \mathbf{P}. \quad (28)$$

Proceeding as in § 3, with  $\mathbf{h}$  as the axis of quantization and  $|m\rangle$  as the excited eigenstates, we find the time-displacement operator corresponding to the first three terms of equation (28). Its eigenvalues are

$$U_{mm}'(t, t_0) = \exp\{-i(k_e + m\omega_e - \frac{1}{2}i\Gamma)(t - t_0)\}. \quad (29)$$

As before, we obtain an approximate solution for the state vector under the complete Hamiltonian  $\mathcal{H}_e$  and thence derive the radiated field and its coherency matrix  $\sigma^{(2)}(t, \tau)$ . The time-dependent parts of the elements of this matrix are reduced to integrals

involving  $\sigma_{kl}^{(1)}(t, \tau)$ . These may be evaluated to yield

$$\phi^{(2)}(t, \tau) = \frac{2\pi\rho^{(1)}(k_1) \exp(-ipft)}{\Gamma + i\{(m-m')\omega_e - pf\}} \exp\{-i(k_e + m'\omega_e + \frac{1}{2}i\Gamma)\tau\} \quad (30)$$

which is to be compared with equation (18). The matrix suffixes  $k, l$  are in this case attached to time-independent factors which have been omitted from equation (30).

Incorporating the Doppler distribution  $\rho^{(2)}(k, k_2, \Delta_2)$  as before, we finally obtain the following expression for the coherency matrix of the light scattered from the experimental cell and passing through an analysing plate  $\mathbf{T}^{(2)}$ :

$$\sigma^{(2)}(t, \tau) = \sum_{\substack{n, n' \\ m, m'}} \mathcal{G}^{(2)}(m, m', n, n'; t, \tau) \mathbf{G}^{(2)}(m, m', n, n') \quad (31)$$

with

$$\mathbf{G}^{(2)}(m, m', n, n') = \mathbf{T}^{(2)} \mathbf{D}_{gm} \mathbf{D}_{gm'}^\dagger \mathbf{R}^{(2)} \mathbf{G}^{(1)}(n, n') \mathbf{R}^{(2)-1} \mathbf{D}_{gm'} \mathbf{D}_{gm'}^\dagger \mathbf{T}^{(2)\dagger} \quad (32)$$

and

$$\begin{aligned} \mathcal{G}^{(2)}(m, m', n, n'; t, \tau) &= 2\pi \int_{-\infty}^{\infty} dk' \rho^{(1)}(k', k_1, \Delta_1) \rho^{(2)}(k', k_2, \Delta_2) \\ &\times \int_{-\infty}^{\infty} dk \rho^{(2)}(k, k_2, \Delta_2) \exp(-ik\tau) \\ &\times \sum_{p, q} \frac{J_q(an - an') J_{p+q}(an - an') \exp(-ipft)}{[\Gamma + if\{(n - n')l_s + q\}][\Gamma + if\{(m - m')l_e - p\}]} \end{aligned} \quad (33)$$

In equation (32)  $\mathbf{R}^{(2)}$  is the matrix which rotates the axis from  $|n\rangle$  to  $|m\rangle$  quantization.  $\mathbf{G}^{(1)}(n, n')$  is given by equation (24). In equation (33) we have introduced the dimensionless symbols  $l_s = \omega_s/f = \gamma H_s/f$  and  $l_e = \omega_e/f = \gamma H_e/f$ . Similarly,  $a = \gamma H_1/f$ . The quantum numbers  $n, n', m$  and  $m'$  take the values 0,  $\pm 1$ . The integers  $p, q$  take all integral values and zero.

The intensity of light reaching the photodetector is proportional to

$$\begin{aligned} I^{(2)}(t) &= \text{Tr } \sigma^{(2)}(t, \tau = 0) \\ &= \sum_{\substack{n, n' \\ m, m'}} \mathcal{G}^{(2)}(m, m', n, n'; t, \tau = 0) \text{Tr } \mathbf{G}^{(2)}(m, m', n, n'). \end{aligned} \quad (34)$$

## 8. Discussion of the results

### 8.1. Light scattered from the source cell

Let us consider first the properties of the light scattered from the source cell, given by equations (24) to (27). Modulation is expressed by the factor  $\exp(-ipft)$  in  $\sigma^{(1)}(t, \tau)$ , but this modulation is not realized under all experimental conditions. Let us restrict the discussion to the cases studied in the experiments, where the light in which we are interested is that scattered in the direction of the magnetic fields, which is the axis of quantization. Suppose that  $\mathbf{T}^{(1)}$  represents a circular polarizer. Then only one value of  $n$  survives in the product  $\mathbf{T}^{(1)} \mathbf{D}_{gn}$ , and the same value in  $\mathbf{D}_{gn'}^\dagger \mathbf{T}^{(1)\dagger}$ , so we may put  $n = n' = n_0$ . The Bessel functions then have the value zero unless  $p = q = 0$ , in which case the factor  $\exp(-ipft)$  reduces to unity, and the denominator in equation (26) to  $\Gamma$ . To realize the modulation therefore, it is essential to use an experimental arrangement which transmits light of both circular polarizations. This is because the modulation is associated with terms  $n \neq n'$  in equation (26).



This condition is necessary, but not sufficient. Let us consider  $\mathbf{R}^{(1)}\hat{\rho}^{(0)}\mathbf{R}^{(1)-1}$ , the coherency matrix of the primary light represented in the frame  $S^{(1)}$  ( $z$  axis parallel to the axis of quantization). If the  $x$  and  $y$  diagonal components are equal, the real parts of the scalar quantities  $\mathbf{D}_{ng}^\dagger \mathbf{R}^{(1)}\hat{\rho}^{(0)}\mathbf{R}^{(1)-1}\mathbf{D}_{gn'}$  vanish. From this it follows that a second necessary condition for modulation is that the primary illumination be anisotropic in the plane perpendicular to the magnetic fields. If this condition is fulfilled, the light scattered in the direction of the magnetic field will be at least partially plane polarized.

Suppose this is the case, and that the light is transmitted through a linear polarizer (represented by  $\mathbf{T}^{(1)}$ ). The intensity will be modulated as described by the factors  $\exp(-ipft)$  in  $\sigma^{(1)}(t, \tau = 0)$ . The amplitudes of the modulation depend on the values of the Bessel functions and vary with the static magnetic field on the cell according to the values of  $[\Gamma + i\{(n - n')\omega_s + qf\}]^{-1}$ .

If the linear polarizer is rotated by  $\frac{1}{2}\pi$ , the effect is the same as if the primary lamp were rotated by  $\frac{1}{2}\pi$  about the magnetic field, that is, the amplitude of the modulation changes sign. When no polarizer is present, therefore, the net intensity modulation vanishes. A photodetector would register a steady current, and spectral analysis of the light would reveal the distribution function  $\rho(k, k_1, \Delta_1)$ , which is the same as that of fluorescent light from the cell in the absence of magnetic fields. Nevertheless, the light is frequency-modulated. The frequency-modulation sidebands do not appear in  $\rho(k, k_1, \Delta_1)$  because we have assumed that  $\Delta_1$  is large compared with the applied frequency  $f$  and with the Larmor splittings  $\omega_s$ .

### 8.2. Light scattered from the experimental cell

The result is given by equations (31) and (34). We are interested only in the cases in which the light falling on the cell is not intensity-modulated.  $\mathbf{T}^{(1)}$  may represent, therefore, an unobstructed light path or it may represent a birefringent plate. The important condition is that it should not selectively absorb any component of the light incident upon it, though it may introduce phase differences.

The light scattered from the experimental cell is represented by the transformation of the coherency matrix  $\sigma^{(1)}(t, \tau)$  into a sum of matrices of the form

$$\mathbf{T}^{(2)}(\mathbf{D}_{gm}\mathbf{D}_{gm'}^\dagger)\sigma^{(1)}(t, \tau)(\mathbf{D}_{gm'}\mathbf{D}_{gm}^\dagger)\mathbf{T}^{(2)-1}.$$

For the terms having  $m = m'$ , the matrices  $\mathbf{T}^{(2)}(\mathbf{D}_{gm}\mathbf{D}_{gm'}^\dagger)$  act like the matrices  $\mathbf{T}^{(1)}$  representing a linear polarizer, and the scattered light is intensity-modulated. This is true even when  $\mathbf{T}^{(2)}$  represents the unit dyadic (apart from some special directions). However, for terms in which  $m \neq m'$  the analogy with a linear polarizer is not exact. In this case an important factor is the denominator,  $\Gamma + i\{(m - m')\omega_e - pf\}$  in (33). Such terms contribute strongly to the result only if the resonance condition  $(m - m')\omega_e = pf$  is satisfied.

Two types of resonance in the amplitudes of modulation are therefore predicted by the equations, one a function of the field  $H_s$  on the source cell, the other a function of the field  $H_e$  on the experimental cell. The resonance conditions are, in the first case,

$$H_s = \frac{-qf}{\gamma(n - n')} \quad (35)$$

and, in the second,

$$H_e = \frac{pf}{\gamma(m - m')}. \quad (36)$$

The resonance curves are Lorentzian- or dispersion-shaped, or some combination of these. Their width is determined by the damping constant of the excited states. The oscillating field makes no contribution to the width of the curves.



### 8.3. Relationship with other phenomena

The expressions we have derived for the scattered light also represent the results of other types of experiment including the Fermi–Rasetti effect, the Hanle effect and the excitation of resonances by intensity-modulated light.

The experiment performed by Fermi and Rasetti (1925) was to study changes in the polarization of fluorescent light from an arrangement similar to our ‘source cell’ as a function of the quantity  $a = \gamma H_1/f$ . The result is described by equations (24) to (27), and in particular by the dependence of the Bessel functions on  $a$ . In the experiments of Chapman and Series  $a$  was regarded as a parameter, not a variable.

The Hanle effect is given in equations (24) to (27) by putting  $f = 0$ . The sums over  $p$  and  $q$  may then be evaluated, and the product of Bessel functions reduces to  $J_0(0) = 1$ . The remaining factors are equivalent to the results of Breit (1933) and Franken (1961). In a similar way equations (31) to (34) describe the Hanle effect in the experimental cell.

Equations (24) to (27) are equivalent to the results of Geneux and Favre (1964) and of Aleksandrov *et al.* (1964).

We have shown how equations (24) to (27) describe intensity-modulated light for matrices  $\mathbf{T}^{(1)}$  representing, for example, linear polarizers. With  $\mathbf{T}^{(1)}$  chosen in this way, equations (31) to (34) represent the excitation of fluorescence in the experimental cell by intensity-modulated light. The factors  $\exp(-ipft)[\Gamma + if\{(m - m')l_e - p\}]^{-1}$  typically describe resonance effects in experiments of this type (Corney and Series 1964).

## 9. Diagrammatic representation of the analysis

### 9.1. Scattering in the source cell

Figure 1 is a ‘frequency diagram’ representing the atoms in the source cell. A ‘frequency diagram’ is a generalization of the normal term diagram for the case when the Hamiltonian function is time-dependent (Dodd and Series 1961). Each level represents the frequency of a periodic term in the wave function.

In the middle of the diagram is shown the splitting of the term  $^3P_1$  into its Zeeman components by the static field  $H_s = \omega_s/\gamma$ . The effect of the oscillating field is to split the levels  $n, n' = \pm 1$  into an infinite sequence of levels separated by the frequency  $f$ , the frequency-modulation sidebands, labelled by the integers  $s, s'$  or  $r, r'$ . Associated with each level is an amplitude  $J_s(n\gamma H_1/f)$ . A particular level  $(n, s)$  may or may not coincide with a level  $(n', s')$ . However, as  $H$  is varied, the whole structure belonging to  $n = -1$  moves relative to the structure belonging to  $n' = 1$ , so that for particular values of  $H_e$  the one set of levels is in coincidence with the other set, though displaced from it. Resonance effects are to be expected whenever there is a coincidence of levels. Figure 1 is drawn for such a coincidence, the relative displacement being  $4f$ .

The figure indicates also the interaction of the atoms with light. Although in the analysis we have not made a Fourier representation of the incident light, it is convenient to use this representation in the diagram. Thus the excitation of an atom by one Fourier component of the light is represented by the arrow  $k$ , which is shown in resonance with the levels  $(n = -1, s = 1)$ ,  $(n' = 1, s' = -3)$ . By the action of the oscillating field along the axis of quantization, transitions  $\Delta n = 0$  may be stimulated, that is, terms in the wave function may be generated in which the frequency changes by multiples of  $f$  while the quantum number  $n$  does not change. These transitions are represented by the arrows labelled  $f$ . The labels  $r, r'$  are used for these new levels. The wave function of the excited atom now contains terms represented by  $(n = -1, r = 0)$  and  $(n' = 1, r' = -1)$ . These terms, having been generated by the same Fourier component of the light, together with an oscillating magnetic field of well-determined



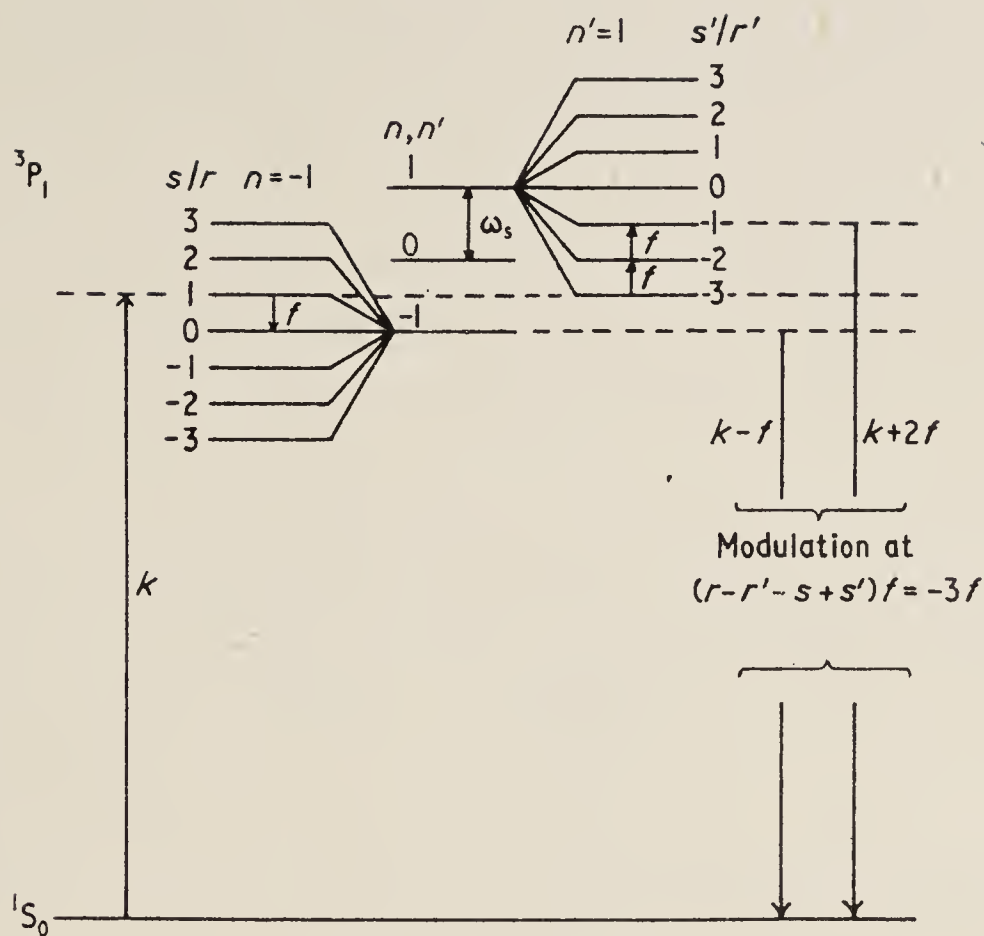


Figure 1. Frequency diagram, showing optical and radio-frequency transitions for the source cell.  $\omega_s = \gamma H_s$  is the splitting of Zeeman levels in the field  $H_s$ . The structures labelled  $s, s'$  or  $r, r'$  are sidebands generated by the oscillating field. The arrow  $k$  upwards represents optical excitation, the arrows  $f$  represent radio-frequency transitions and the arrows  $k+2f, k-f$  downwards represent coherent emission of light leading to modulation.

phase, are coherent. The light emitted by the atom in its decay therefore contains a component modulated in intensity at the frequency

$$\{k + (r-s)f\} - \{k + (r'-s')f\} = (r-r' + s-s')f = pf.$$

The net modulation of the light contains components at frequencies corresponding to all possible combinations of the type considered above, each combination being weighted with products of Bessel functions. The net effect of all combinations for which  $n = n'$  is that the intensity modulation is zero, though the light is frequency-modulated. By devising experiments in which one obtains interference between components of different  $n$  (for example, by taking light obliquely to the direction of the fields, or by using polarizers or by using a second scattering cell as in the experiment under consideration) the frequency modulation may be converted to intensity modulation.

## 9.2. Scattering in the experimental cell

The frequency diagram in this case is identical with the normal term diagram, since the only field on the cell is the static field  $H_e$ . Figure 2 shows the splittings  $\omega_e$  in the field  $H_e$ .

The Fourier component  $k$  of the incident light is coherent with a component  $k+pf$ , owing to the modulation. The same coherence exists in the scattered light. Resonance effects are found when  $pf$  is equal to  $(m-m')\omega_e$ , that is, at values of  $H_e$  equal to  $\frac{1}{2}pf/\gamma$  and  $pf/\gamma$ . These resonance effects are variations in the amplitude of modulation of the scattered light. The demonstration of any particular resonance demands a geometrical arrangement which allows the appropriate optical transitions.

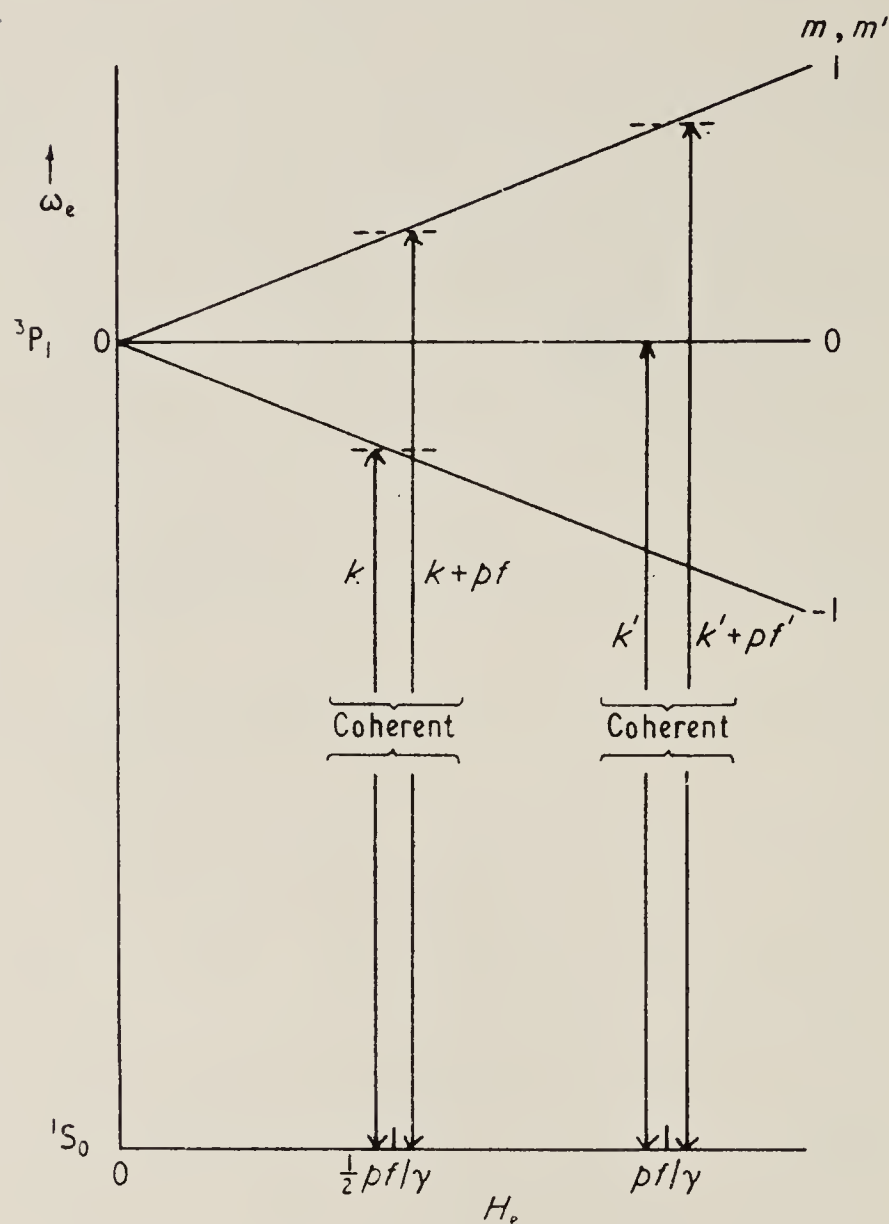


Figure 2. Frequency diagram for the experimental cell. The modulated excitation is represented by the arrows  $k$ ,  $k+pf$  upwards. A resonance condition is satisfied when  $H_e = \frac{1}{2}pf/\gamma$  or  $pf/\gamma$ . The emitted light, represented by the arrows downwards, is also modulated. Resonances are detected by measuring the amplitude of modulation.

### Acknowledgments

It is a pleasure to acknowledge numerous discussions with Dr. G. D. Chapman on the advantages of using a matrix notation for the light fields, and on the validity of the results obtained. I am indebted to Dr. A. Corney for contributions to this work in its early stages. I am most grateful also to the late Dr. S. Pancharatnam for his careful reading of various drafts of this manuscript and for his constructive criticisms.

### Appendix 1. Classical model

A simple classical model can be used to find the intensity of light emitted from the source. Suppose an oscillating dipole is excited in the  $x$  direction at time  $t_0$ . It precesses in the  $xy$  plane under the fields  $H_s + H_1 \cos ft$  applied along the  $z$  axis. The precessional velocity at time  $t$  is

$$\omega(t) = \gamma(H_s + H_1 \cos ft) = \omega_s + \omega_1 \cos ft.$$

The angle of precession executed in time  $t - t_0$  is

$$\chi = \int_{t_0}^t \omega(t) dt = \omega_s(t - t_0) + a(\sin ft - \sin ft_0)$$



and the damping factor for the amplitude is  $\exp\{-\frac{1}{2}i\Gamma(t-t_0)\}$ . The component of the radiated field which passes an analyser parallel to the  $x$  axis is proportional to  $\exp\{-\frac{1}{2}i\Gamma(t-t_0)\cos\chi\}$ , and the intensity  $I(t, t_0)$  is given by

$$I(t, t_0) \propto \exp[-\Gamma(t-t_0)\cos^2\{\omega_s(t-t_0)+a(\sin ft-\sin ft_0)\}].$$

Writing the cosine in complex exponential functions and using the expansion in Bessel functions given in the text, we arrive at

$$\begin{aligned} I(t, t_0) &= \sum_{\substack{r, r' \\ s, s' \\ \epsilon, \epsilon'}} J_r(a\epsilon)J_s(a\epsilon)J_{r'}(a\epsilon')J_{s'}(a\epsilon') \exp\{i(r+r'-s-s')ft\} \\ &\quad \times \exp\{i(s+s')f(t-t_0)\} \exp[-\{\Gamma-i(\epsilon+\epsilon')\omega_s\}(t-t_0)] \\ &= \sum_{\substack{p, q \\ \epsilon, \epsilon'}} J_{p+q}(-a\epsilon-a\epsilon')J_q(-a\epsilon-a\epsilon') \exp(-ipft) \exp(-[\Gamma+i\{qf-(\epsilon+\epsilon')\omega_s\}]) \\ &\quad \times (t-t_0) \end{aligned}$$

where  $\epsilon, \epsilon'$  take the values  $\pm 1$ .

If dipoles are excited at a constant rate  $R$ , the steady-state intensity at time  $t$  is given by

$$\begin{aligned} I(t) &= R \int_0^t I(t, t_0) dt_0 \\ &= R \sum_{\substack{p, q \\ \epsilon, \epsilon'}} J_{p+q}(-a\epsilon-a\epsilon')J_q(-a\epsilon-a\epsilon') \frac{\exp(-ipft)}{\Gamma+i\{qf-(\epsilon+\epsilon')\omega_s\}} \end{aligned}$$

which is a particular case of the trace of the matrix  $\sigma^{(1)}(t, \tau=0)$  in the text (equation (26)).  $\epsilon$  and  $\epsilon'$  are not to be identified with  $n$  and  $n'$  since in this analysis the motion is not resolved into its circularly polarized components.

## Appendix 2. Evaluation of the time integrals

We evaluate here the quantity  $\phi^{(1)}(t, \tau)$  introduced in § 6.1:

$$\begin{aligned} \phi^{(1)}(t, \tau) &= \exp\{-if(r'-s')\tau\} \left[ \frac{1}{2T} \int_{t-T}^{t+T} dt' \exp\{-if(r-s-r'+s')t'\} \right. \\ &\quad \times \int_0^{t'} d\tau_0 E_i^{(0)}(t'-\tau_0) \exp(-i\alpha_s\tau_0) \int_0^{t'-\tau} d\tau_0' E_j^{(0)*}(t'-\tau-\tau_0') \\ &\quad \left. \times \exp(i\alpha_s\tau_0') \right]. \end{aligned} \tag{A1}$$

Our aim is to manipulate the order of integration so that, in the integral over  $t'$ , the integrand is simply  $E_i^{(0)}(t'-\tau_0)E_j^{(0)*}(t'-\tau-\tau_0')$ .

(i) If  $2T$  is chosen to be much smaller than  $\{f(r-s-r'+s')\}^{-1}$ ,

$$\exp\{-if(r-s-r'+s')t'\}$$

can be taken outside the integral over  $t'$ , with  $t$  substituted for  $t'$ . (ii) The integrals over  $\tau_0$  and  $\tau_0'$  are insensitive to the upper limits since we are dealing with fields of short coherence time. We therefore have to evaluate

$$\int_0^\eta d\tau_0 \exp\{-i(\alpha_s - \alpha_s')\tau_0\} \int_0^\zeta d\tau_0' \exp\{-i\alpha_s'(\tau_0 - \tau_0')\} \\ \times \left[ \frac{1}{2T} \int_{t-T}^{t+T} dt' E_i^{(0)}(t' - \tau_0) E_j^{(0)*}(t' - \tau - \tau_0') \right] \quad (A2)$$

where  $\eta$  and  $\zeta$  are independent of  $t'$ . The quantity in square brackets is simply  $\sigma_{ij}^{(0)}(\tau + \tau_0' - \tau_0)$ , which we express in terms of its spectral density by equation (16). The broad-band approximation allows us to treat this as constant  $\hat{\rho}_{ij}^{(0)}(k_0)$ , so that we have

$$\sigma_{ij}^{(0)}(\tau + \tau_0' - \tau_0) = \hat{\rho}_{ij}^{(0)}(k_0) \delta(\tau_0 - \tau_0' - \tau). \quad (A3)$$

The integration over  $\tau_0'$  may then be performed, leaving  $\hat{\rho}_{ij}^{(0)}(k_0) \exp(-i\alpha_s'\tau)$ . There remains the integral over  $\tau_0$  which is readily evaluated to yield

$$i(\alpha_s - \alpha_s')^{-1} = [\Gamma + i\{(n - n')\omega_s + (s - s')f\}]^{-1}. \quad (A4)$$

(The integral vanishes at the upper limit since we are concerned with times  $\eta \gg \Gamma^{-1}$ .) The final result is

$$\phi^{(1)}(t, \tau) = \frac{\hat{\rho}_{ij}^{(0)}(k_0) \exp\{-if(r - s - r' + s')t\}}{\Gamma + i\{(n - n')\omega_s + (s - s')f\}} \exp\{-i(k_s + n'\omega_s + fr' + \frac{1}{2}i\Gamma)\tau\}. \quad (A5)$$

## References

- ALEKSANDROV, E. B., 1965, *Opt. Spektrosk.*, **19**, 452-5 (*Opt. Spectrosc.*, **19**, 252-3).  
 ALEKSANDROV, E. B., KONSTANTINOV, O. V., PEREL', V. I., and KHODOVOI, V. A., 1964, *Zh. Eksp. Teor. Fiz.*, **45**, 503-10 (*Sov. Phys.-JETP*, **18**, 346-50).  
 BREIT, G., 1933, *Rev. Mod. Phys.*, **5**, 91-140.  
 CHAPMAN, G. D., and SERIES, G. W., 1970, *J. Phys. B: Atom Molec. Phys.*, **3**, 72-83.  
 CORNEY, A., and SERIES, G. W., 1964, *Proc. Phys. Soc.*, **83**, 207-12, 213-6.  
 DODD, J. N., and SERIES, G. W., 1961, *Proc. R. Soc. A*, **263**, 353-70.  
 FERMI, E., and ROSSETTI, F., 1925, *Z. Phys.*, **33**, 246-50.  
 FRANKEN, P. A., 1961, *Phys. Rev.*, **121**, 508.  
 FRANZEN, W., and ALAM, M., 1964, *Phys. Rev.*, **133**, A460-7.  
 FRANZEN, W., NEWELL, P. B., and EDMONDS, D. S., 1968, *Phys. Rev.*, **170**, 17-27.  
 GENEUX, E., and FAVRE, C. J., 1964, *Phys. Lett.*, **8**, 190-2.  
 O'NEILL, E. L., 1963, *Introduction to Statistical Optics* (Reading, Mass.: Addison-Wesley).  
 SERIES, G. W., 1966, *Proc. Phys. Soc.*, **89**, 1017-20.



# 'LINE-CROSSINGS' IN THE FORWARD-SCATTERING OF RESONANCE RADIATION

R. Q. HACKETT  
Tonbridge School, Tonbridge, UK

and

G. W. SERIES  
J. J. Thomson Physical Laboratory, Whiteknights Park, Reading, UK

Received 10 July 1970

Phenomena similar to the well-known 'level-crossing' effects are to be expected in forward-scattering when there are coincidences in the resonance frequencies of *different* atoms. Such coincidences can be established between different isotopes by introducing Zeeman splittings to compensate spectroscopic isotope shifts. The phenomena have been demonstrated experimentally.

## 1. INTRODUCTION

'Level-crossing' effects in the resonance fluorescence of atomic vapours are normally studied in laterally scattered light, in which case there can be no interference in the light from different atoms. The effects are due to interferences between different polarization components of the light scattered from *single-atoms*.

In forward-scattering there are additional possibilities for interference since the light from different atoms is coherent. Some consequences of this - the Doppler broadening and enhanced coherence narrowing of level-crossing curves - are already known [1]. It is the purpose of this note to point out further consequences: that effects similar to those at 'level-crossings' are to be expected also at the crossings of absorption lines of *different atoms*. It is therefore possible to find these effects between different isotopes,

or between different hyperfine transitions in different atoms of the same isotope. We propose the name 'line-crossings' to describe these situations.

The essentials of an apparatus which we have used to study these effects are shown in fig. 1. The crossed polarizers would, in the absence of the vapour, prevent light from reaching the detector. If a photocurrent is recorded, it must arise from forward-scattered light. (As an alternative arrangement for studying the forward-scattered light one might use, for example, a Mach-Zehnder interferometer [2].) The current is measured as a function of the longitudinal magnetic field  $H$  whose function is to tune the Zeeman components of different absorption lines in coincidence.

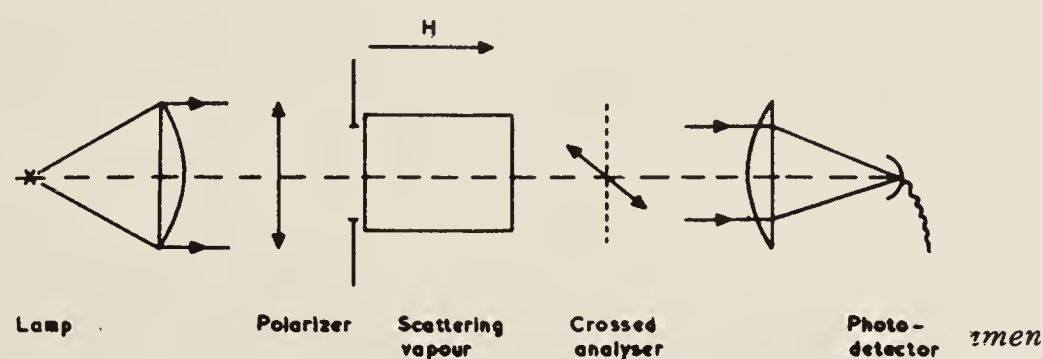


Fig. 1. Essentials of the arrangement for studying forward-scattered light.

## 2. ANALYSIS

The signal may be calculated by treating the interaction of the light with the vapour as propagation through an absorbing dielectric [1]. An analysis of the arrangement shown in fig. 1 leads to the result

$$I \propto \int_0^\infty \rho(k) |\sin \Phi_k|^2 \exp(-\alpha_k L) dk \quad (1)$$

where  $\rho(k)$  is the spectral density of the light at the front face of the cell and  $\Phi_k = (kL/2c)(n_+ - n_-)$ .  $n_+$  and  $n_-$  are the complex refractive indices for the circularly polarized components of the incident light of angular frequency  $k$ ,  $\alpha_k$  is their mean absorption coefficient, and  $L$  is the length of the cell. In the case where  $n_\pm$  are real,  $\Phi_k$  will be recognised as the angle of Faraday rotation and  $\rho(k) \sin^2 \Phi_k$  as the intensity passing the analyser for the spectral component  $k$ . Eq. (1) holds also when  $n_+, n_-$  and  $\Phi_k$  are complex.

For optically thin vapours (negligible absorption, small rotation) eq. (1) simplifies to

$$I \propto \int_0^\infty \rho(k) |\Phi_k|^2 dk \quad (2)$$

In evaluating this expression we use  $n = 1 + (2\pi NP^2/\hbar\Delta)Z$  for the refractive index.  $N$  is the number density of the atoms,  $P$  the reduced matrix element of the electric dipole operator,  $Z$  the 'plasma dispersion function' [3] which represents the Doppler-broadened polarizability through the resonance region, and  $2\Delta(\ln 2)^{1/2}$  is the Doppler half-intensity width.  $Z$  is a function of  $k$ , the resonance frequency  $k_0$ , the damping constant  $\Gamma$ , and  $\Delta$ .

We first give the result for the case when the vapour is a single atomic species with a single resonance line which shows the normal Zeeman effect. We have

$$n_+ - n_- = (2\pi NP^2/\hbar\Delta) [Z(k, k_0 - \omega, \Gamma, \Delta) - Z(k, k_0 + \omega, \Gamma, \Delta)] \quad (3)$$

The expression in square brackets is called the Faraday function  $F$ . It is the difference between two  $Z$  functions centered at  $(k_0 - \omega), (k_0 + \omega)$ , where  $\omega = \gamma H$ .

In terms of  $F$  eq. (2) becomes

$$I \propto \int_0^\infty \rho(k) |F|^2 dk \quad (4)$$

If  $\rho(k)$  is assumed constant, and if we take the case  $\Delta \gg \Gamma$ , the result of the integration is

$$I \propto 1 - \exp(-2\omega^2/\Delta^2) \quad (5)$$

(Integrals of the type (4) are evaluated in ref. [1] without the restriction  $\Delta \gg \Gamma$ .) The inverted gaussian (5) is the Doppler-broadened level-crossing curve centered on  $\omega = 0$ .

Now suppose we have two isotopes whose absorption lines occur at  $k_0 - s, k_0 + s$  respectively (isotope shift:  $2s$ ). The vapours may be mixed in the same cell or placed in separate cells so that the light passes through each in turn. For simplicity, suppose the Zeeman splittings are identical, and that we have the same number density and same path length for each. The contributions to the dispersion will be additive, so that eq. (4) becomes

$$I \propto \int_0^\infty \rho(k) |F_1 + F_2|^2 dk \quad (6)$$

where  $F_1$  and  $F_2$  are calculated from the two functions,  $Z(k, k_0 \pm s, \Gamma, \Delta)$ . Evaluating (6) with  $\rho(k)$  constant and  $\Delta \gg \Gamma$  we find

$$I \propto 1 - \exp(-2\omega^2/\Delta^2) - \frac{1}{2} \exp[-2(s-\omega)^2/\Delta^2] + \exp(-2s^2/\Delta^2) - \frac{1}{2} \exp[-2(s+\omega)^2/\Delta^2] \quad (7)$$

If the isotope structure is resolved against the Doppler width the last two terms will always be small. The first three terms describe *two* inverted gaussians: that centered on  $\omega = 0$  is the zero-field level-crossing common to both isotopes and that centered on  $\omega = s$  is the 'line-crossing' which occurs when the  $\sigma^+$  resonance line of one isotope coincides with the  $\sigma^-$  line of the other.

The simple results (5) and (7) depend on the assumption  $\rho(k) = \text{constant}$  which is an unrealistic assumption for many experiments one might wish to describe. However, the fact that the intensity goes through a minimum for a line-crossing does not depend on this assumption as we have verified by obtaining computer solutions of the equations using a variety of particular forms for  $\rho(k)$ .

An analytical proof may be given for the case when the spectrum of the incident light is confined to the wings of the crossing absorption lines. Here we may use a simple lorentzian form for the dispersion function and eq. (3) is replaced by

$$(n_+ - n_-)_{1+;2-} = \left( \frac{2\pi NP^2}{\hbar} \right) \left[ \frac{1}{(k_0 - s + \omega) - k} - \frac{1}{(k_0 + s - \omega) - k} \right] = \left( \frac{2\pi NP^2}{\hbar} \right) \frac{2\delta}{[(k_0 - k)^2 - \delta^2]} ,$$

where  $\delta = s - \omega$  is equal to zero at the crossing.



Using (8) in the expression for  $\Phi_k$ , neglecting  $\delta$  in the denominator in comparison with  $(k_0 - k)$  and integrating  $\Phi_k^2$  over the spectrum of the incident light, one finds that the variation of intensity in the region of the crossing is proportional to  $\delta^2$ , which gives a dip at the crossing point, as before.

### 3. EXPERIMENTAL TEST

#### (a) Single isotope

The phenomenon was tested with mercury isotopes, using an air-cooled microwave  $^{198}\text{Hg}$  lamp. A preliminary interferometric study of the spectral profile of the 2537 Å line showed this to be a bell-shaped curve of width about twice the Doppler width at room temperature. With this light source and a cell 1.5 cm in length containing  $^{198}\text{Hg}$  vapour at 0°C, curves of photo-current against magnetic field were obtained as shown in fig. 2a. These curves are well represented by a computer solution of eq. (1) taking  $\rho(k)$  to be a gaussian of the appropriate width. The change in intensity between zero-field and 1 kG is interpreted as the Doppler-broadened zero-field level-crossing: the fall at higher fields comes about because the Zeeman components of  $^{198}\text{Hg}$  are moving away from the source spectrum and the Faraday rotation in this region becomes negligibly small.

#### (b) Mixture of isotopes

Fig. 2b was obtained by using a cell containing the natural isotopic mixture at 0°C instead of the  $^{198}\text{Hg}$  cell. Comparison with fig. 2a shows (i) that the system transmits light at fields where formerly the intensity had fallen away, and (ii) that there is structure, notably dips at about 1.1 and 2.4 kG.

To interpret the experiments we refer to fig. 3 which shows the isotope and Zeeman structure of the 2537 Å line, representing the absorption spectrum of the vapour in the cell in relation to the spectrum of the  $^{198}\text{Hg}$  lamp used for illumination. Only the major absorption lines are shown.

The isotope 198 in the cell is responsible for the rise in intensity at small values of the field. The finite intensity at higher fields arises mainly from the strong dispersion of the  $200\sigma^+$  component as it enters the region of the source spectrum between 1.5 and 3 kG. (It will be realised that although spectral components on either side of the  $\sigma^+$  absorption line undergo Faraday rotations of opposite sign - the  $\sigma^-$  lines being relatively far away - these do not cancel one another

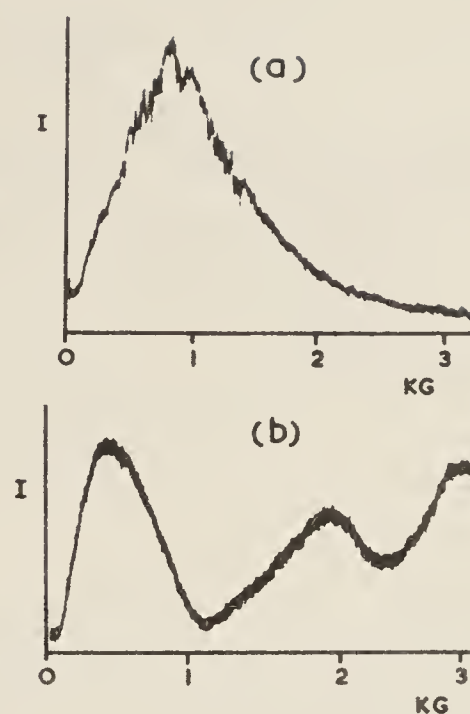


Fig. 2. Transmitted intensity against magnetic field. The light source, a microwave  $^{198}\text{Hg}$  lamp, was the same for both curves.

a) cell containing vapour of  $^{198}\text{Hg}$  at 0°C.

b) cell containing natural mixture of isotopes at 0°C.

but contribute independently to the observed signal.)

The dip at about 1.1 kG must be attributed to the crossing of  $200\sigma^+$  and  $198\sigma^-$ , where the dispersion associated with the former is compensated by the latter so that the Faraday rotation is greatly reduced. Likewise the dip at about 2.4 kG is attributed mainly to the crossing of  $202\sigma^+$  and  $198\sigma^-$ . Minor components of the 2537 Å line, not shown in fig. 3, contribute to the intensity, and some of these exhibit crossings. Close comparison with theoretical curves is not possible without more certain knowledge of the spectral profile of the source.

### 4. CONCLUSIONS

Notwithstanding these uncertainties it is claimed that the observations constitute evidence of anomalies in the intensity of forward-scattered light which arise from degeneracies of resonance frequencies of different atoms. It is tempting to offer this technique, in conjunction with the enhanced coherence narrowing which is available by increasing the optical density, as a method for measuring isotope shifts with high precision. Although it seems to us feasible to apply the method in some simple cases its general application would appear to be impracticable. The diffi-

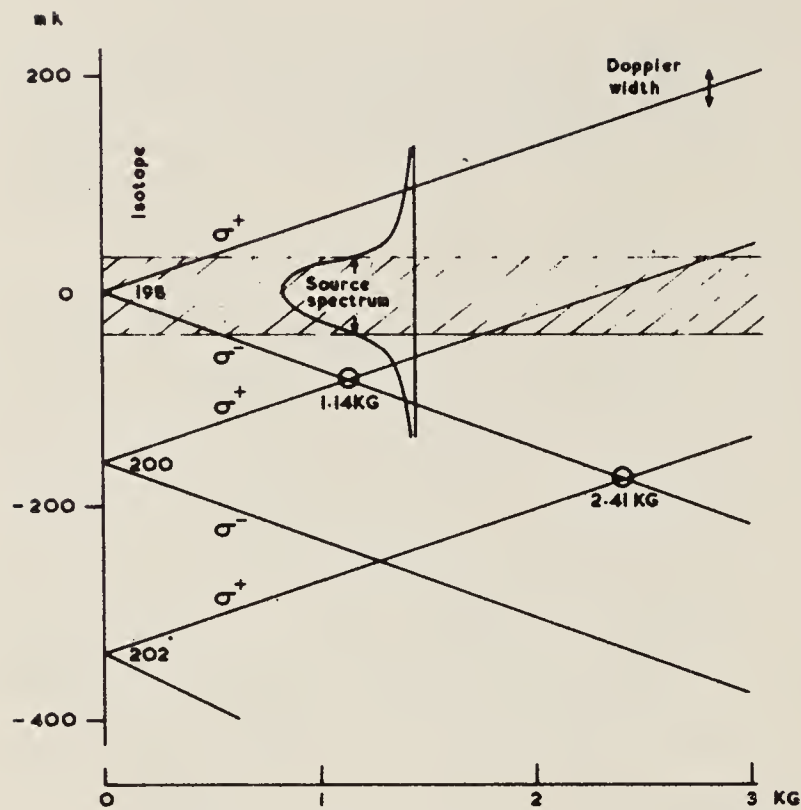


Fig. 3. Isotope and Zeeman structure of the 2537 Å line in relation to the emission line of the  $^{198}\text{Hg}$  source [4]. Only the strongest lines are shown. Relative abundances of the three isotopes are; 198: 10%, 200: 23%, 202: 33%. The significant crossings are encircled.

culties are: first, one needs accurate knowledge of the spectral profile of the source. Secondly, it is to be realised that different degrees of

coherence narrowing would result if the isotopes were present with different abundances. Further, it is incorrect to assume that the dispersion function is independent of the vapour density. One effect of pressure broadening is to change the damping constant and hence the dispersion function. We have found that changes of this sort distort the zero-field level-crossing curves so that the effect of increasing the vapour density can no longer be described as a narrowing of the curves. In the cases we have studied (sodium and mercury) it appears that this distortion sets a limit to what can be achieved by coherence-narrowing in forward scattering.

#### ACKNOWLEDGEMENT

This work was done at the Clarendon Laboratory, Oxford, during the tenure by one of us (RQH) of a Research Studentship from the Science Research Council.

#### REFERENCES

- [1] A. Corney, B. P. Kibble and G. W. Series Proc. Roy. Soc. A293 (1966) 70.
- [2] L. C. Bradley and R. L. Fork, Appl. Optics 3 (1964) 137.
- [3] B. D. Fried and S. D. Conte, The plasma dispersion function (Academic Press, London, 1961).
- [4] W. G. Schweitzer Jr., Journ. Opt. Soc. Amer. 53 (1963) 1055.



## Determination of the hyperfine structure of the level $3^2P_{3/2}$ of $^{23}\text{Na}$ by time-resolved level-crossing spectroscopy

JS Deech, P Hannaford† and G W Series

J J Thomson Physical Laboratory, University of Reading, UK

Received 10 December 1973

**Abstract.** Fluorescence from the  $3^2P$  states of sodium was studied as a function of time and magnetic field. The signals were recorded digitally and stored. By the use of a computer the signals were biased in favour of the longer-lived atoms and integrated over time. The improved resolution of the resulting level-crossing curves allowed the positions of level crossings to be determined with improved accuracy. A variety of biasing functions was studied and the advantages of the gaussian demonstrated.

Satisfactory agreement between theory of the line shape and experimental profiles was obtained after allowance had been made for the non-uniform spectral distribution of the exciting radiation; it was also necessary to allow for a small temperature-dependent component of the signal.

An iterative analysis of the level-crossing curves leads to the values  $a = 18.7 \pm 0.1$  MHz,  $b = 3.0 \pm 0.2$  MHz for the hyperfine interaction constants of the level  $3^2P_{3/2}$ . These results are compared with those of other authors for the same level and for the level  $4^2P_{3/2}$ .

### 1. Introduction

Level-crossing spectroscopy has been widely used over the past decade as a method for investigating fine or hyperfine structures of the excited states of free atoms. In some cases—the  $3^2P_{3/2}$  level of sodium is a case in point—the accuracy attained has been limited by incomplete resolution of the level-crossing signals. Recently attempts have been made to improve this situation by modifying the line profile which, in a conventional experiment, is governed by the sum of the natural widths of the crossing levels. We report further progress in this direction.

We have refined an experiment reported in 1968 by Copley *et al* in which level-crossing curves were narrowed by the device of taking fluorescent light from a sample of excited atoms biased in favour of those which had survived longer than average. The substance investigated in their experiment was sodium vapour, the atoms being excited to the level  $3^2P_{3/2}$  by resonance radiation from a sodium lamp. A Kerr cell interposed between the lamp and the vapour allowed atoms to be excited at a well-defined time by a pulse of light and the fluorescence light was detected photoelectrically after a predetermined delay. In this way the detector recorded the fluorescence from a biased sample. The experiment was set up using the normal geometrical arrangement for level-crossing experiments and was repeated for different values of magnetic field applied to the vapour.

The level-crossing curves obtained by Copley *et al* indeed showed improved resolution over level-crossing curves obtained in steady-state experiments, but the analysis

† On leave from the Division of Chemical Physics, CSIRO, PO Box 160, Clayton, Victoria, Australia 3168.

showed that spurious effects might be present owing to the sudden switching on of the detector. The spurious effects—oscillatory structure in the wings of the level-crossing curves—have their origin in the precession of the excited atoms in the magnetic field. Since the dipole radiation pattern rotates with the atoms, a detector in a fixed position will record a modulated, exponentially decaying signal following the excitation pulse. The modulation will appear as a function of time for a given field or as a function of the field for a given time. In the experiment just described, the dominant contribution to the signal will be for times immediately following the switching on of the detector: hence, for a given delay, oscillatory structure will appear as a function of the field. Such structure has been observed recently by Schenck *et al* (1973) and by Figger and Walther (1973).

This additional structure complicates the level-crossing curves. It may be eliminated, in principle, by biasing the signal in a different way. The present experiment was designed to allow different forms of biasing to be investigated systematically. The decay of the excited atoms was recorded by standard techniques as a function of time following the exciting pulse and the biasing introduced subsequently by performing an integration over time, incorporating any desired function of time into the integrand. The actual integrations were carried out in a computer, so that a whole family of biasing functions could be studied with the same experimental data.

The level  $3^2P_{3/2}$  of sodium was chosen for this case study because the level-crossing curves obtained by conventional methods contain barely resolved structures. We have improved the resolution and obtained values for the hyperfine interaction constants which we believe to be more reliable than those obtained by steady-state methods.

## 2. Description of the experiment

The most significant differences between this experiment and that of Copley *et al* are to be found in the techniques used for recording the signal and analysing the data. In addition, the magnetic field in this experiment was calibrated more accurately.

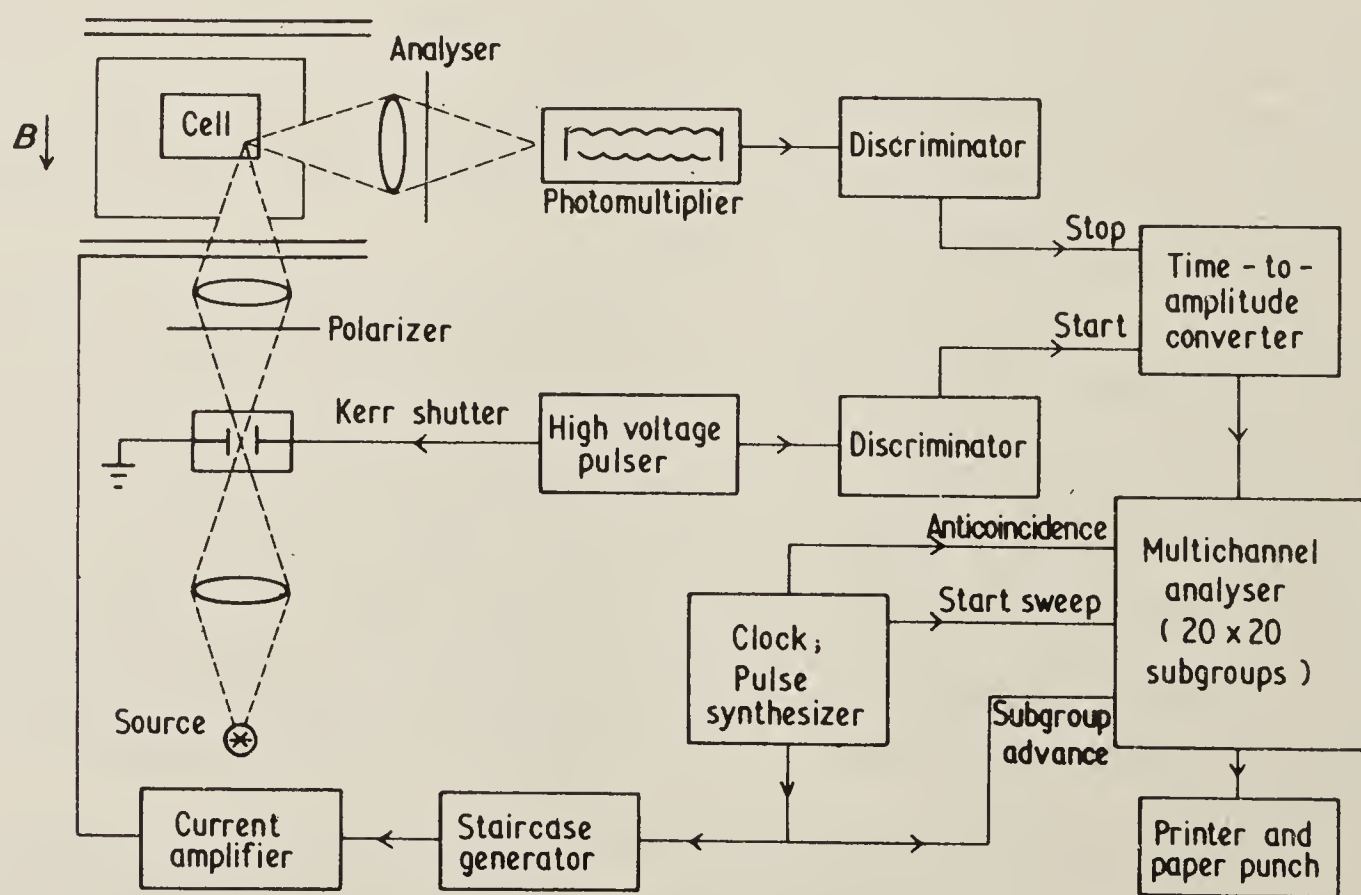


Figure 1. The apparatus.



Resonance radiation from a sodium lamp was pulsed by means of a Kerr shutter. Both the  $D_1$  and  $D_2$  lines were transmitted. The width of the optical pulse was approximately 20 ns with rise and fall times of about 8 ns. Its repetition rate was approximately 500 Hz. This optical pulse was focused into a cell containing sodium vapour at a pressure of about  $4 \times 10^{-6}$  Torr, corresponding to a temperature of 140 °C. Helmholtz coils surrounding the cell allowed the earth's field to be compensated and an additional field  $B$  to be applied in the direction of the incident light. The field  $B$  was calibrated in terms of the current in the coil by means of a rubidium magnetometer. The coil constant was measured to be  $(34.68 \pm 0.03)$  G/A.

The geometrical parameters of the experiment were as follows:

- (i) magnetic field: 0z
- (ii) incident light: direction, 0z; polarization (linear), 0y
- (iii) detected light: direction, 0y; polarization (linear), 0x.

With this arrangement, only level-crossing signals due to  $\Delta m = \pm 2$  crossings are detectable (see figure 3). Moreover, the intensity of the fluorescent light from  $3^2P_{1/2}$  should be independent of  $B$  provided that the spectrum of the incident light is uniform over the  $D_1$  line.

The commonly-used technique of delayed coincidences was used to measure the decay of the excited atoms as a function of time following their excitation by a pulse of resonance radiation. A reference pulse was derived from the high voltage pulse used to operate the Kerr shutter. The reference pulse was delayed and applied to the 'start' input of a time-to-amplitude converter. The photoelectron pulses from the photomultiplier (EMI 9816QB), after discrimination to eliminate spurious pulses not originating from the photocathode and to standardize those that were acceptable, were applied to the 'stop' input of the time-to-amplitude converter. The output from the converter has the form of a pulse of standard width whose amplitude is proportional to the time delay between a 'start' pulse and a 'stop' pulse. No output is produced if this delay is greater than the maximum conversion time which was set to be 200 ns. In addition, once a conversion has taken place, or if the maximum conversion time is exceeded, the converter is dead until the next 'start' pulse arrives. The spectrum of pulse heights from the output of the converter represents the probability of an atom spontaneously emitting a photon in the direction of the detector at a particular time following its excitation. These pulses are stored according to their amplitude in twenty channels of a 400 channel analyser. A channel width of about 9 ns was chosen in order to allow each decay spectrum to be studied over 180 ns, that is, for more than ten mean lifetimes of the excited state.

The emission of light as a function of time was investigated in this way at twenty different values of the magnetic field (this number was limited by the total availability of 400 channels in the analyser). The size of the field step could be set to any desired value, allowing either a 'panoramic' field scan over the entire range of interest (0–30 G) or a scan over any smaller region within this; the latter was useful when investigating the position of a particular level-crossing.

The procedure in carrying out an experiment was to start at the lowest field required and to collect a decay spectrum in the first twenty channel subgroup of the analyser for about two seconds. The field was then stepped to the next value and a decay spectrum accumulated in the second twenty channel subgroup for a further two seconds. After twenty values of the magnetic field in an increasing sequence, the field sweep was repeated. In practice about 4000 sweeps were carried out, each sweep requiring a time of about 40 seconds, so that an experimental run lasted for approximately 50 hours.



In order to sweep the magnetic field, a current generator was designed that could step from one current to another on a command pulse. The steps could be reproduced to within one part in a thousand over a period of 50 hours. The pulse that stepped the magnetic field was also used to switch the multichannel analyser from one twenty channel subgroup to the next. Another pulse, which started a few microseconds before the stepping pulse, was applied to the anticoincidence input of the multichannel analyser and remained there for two milliseconds. This ensured that data could not be accumulated while the magnetic field was changing from one value to another. Finally, a pulse was required every twenty steps to initiate a new sweep. The sequence of pulses needed to control the experiment (other than those needed to operate the Kerr shutter) was generated from logic circuits designed by Besch *et al* (1970).



**Figure 2.** Oscilloscope display of experimental data accumulated in the multichannel analyser. Decay spectra are shown for twenty values of the magnetic field, increasing from left to right.

Figure 2 shows an oscilloscope display of the contents of the memory of the multichannel analyser after an experiment such as that described above. The twenty decay spectra are easily identifiable, though it is difficult to distinguish visually the small differences between them. Before analysing data such as shown in figure 2, the spectra were corrected for 'pile-up' using a mathematical procedure similar to that described by Coates (1968). The correction is necessary because of the long dead time of the time-to-amplitude converter: only the first photoelectric 'stop' pulse following activation of the converter by a 'start' pulse can lead to an output. The converter then remains inoperable until the next 'start' pulse, and these arrive with a frequency of about 500 Hz.



By employing a count-rate of about 100 pulses per second at the output of the time-to-amplitude converter, the pile-up correction was kept small. The corrected data were analysed in the manner to be described in § 4.

### 3. Theory of the experiment

A theory of the shape of level-crossing curves to be expected for a variety of biasing functions applied to the fluorescence from a simple two-level system was given by Copley *et al.* It was assumed that the interval between the levels was linearly proportional to the magnetic field, and that the electric dipole matrix elements were independent of the field. Neither of these assumptions is valid in the present case. The analysis of the simple system did, however, bring out the following important points: (i) the use of step biasing functions introduces an oscillatory structure on the wings of the level-crossing curves and (ii) this structure may be eliminated by the use of a suitably chosen biasing function; it was shown that a gaussian function of a particular width in relation to the position of the peak has this desirable property, and it was further pointed out that the resultant modified level-crossing curves, being themselves gaussians, would have the advantage of improving the resolution of overlapping lines on account of the more sharply falling wings of gaussians compared with lorentzians.

These considerations guided the choice of biasing functions used in the present analysis. Step functions and gaussians of various widths were used, the oscillatory structure was observed, and its effect in 'pulling' the true level-crossing curve was examined systematically.

The analysis that follows takes account of the hyperfine and Zeeman interactions in the actual system, as distinct from the purely Zeeman interaction in the simple two-level system; it takes account also of the finite duration of the exciting pulse and allows for an arbitrary biasing function  $f(t)$ . The existence of the hyperfine interaction brings about a field-dependence of the electric dipole matrix elements. This also affects the shape of the level-crossing curves.

#### 3.1. The hamiltonian

The experiment is concerned ultimately with the determination of the hyperfine interaction constants  $a$  and  $b$  in the following hamiltonian, applied to the  $3^2P_{3/2}$  level of sodium:

$$\mathcal{H} = \mathcal{H}_0 + a\mathbf{I} \cdot \mathbf{J} + b \left[ \frac{3(\mathbf{I} \cdot \mathbf{J})^2 + \frac{3}{2}(\mathbf{I} \cdot \mathbf{J}) - I^2 J^2}{2I(2I-1)J(2J-1)} \right] + \mu_B \mathbf{B} \cdot (g_J \mathbf{J} - g_I \mathbf{I}) \quad (1)$$

(see eg Ramsey 1956).  $\mathcal{H}_0$  includes all interactions other than the hyperfine and Zeeman interactions.  $g_J$  and  $g_I$  are the electronic and nuclear Landé factors.  $a$  and  $b$  are proportional to the nuclear magnetic moment and the nuclear quadrupole moment respectively.  $\mu_B$  is the Bohr magneton.  $\mathbf{B}$  is the external field.

This hamiltonian was diagonalized from the representation  $\{\mathbf{F}^2, F_z\}$  where  $\mathbf{F} = \mathbf{I} + \mathbf{J}$  and its eigenfunctions  $|m\rangle$  and eigenvalues  $E_m$  were determined. A plot of these eigenvalues as a function of  $B$  (relative to the unperturbed energy of  $3^2P_{3/2}$ ) is shown in figure 3. The values of  $a$  and  $b$  used here are those obtained as a result of this work. The level crossings detectable in the present experiment, those having  $\Delta m = \pm 2$ , are marked A, B, C in the figure.

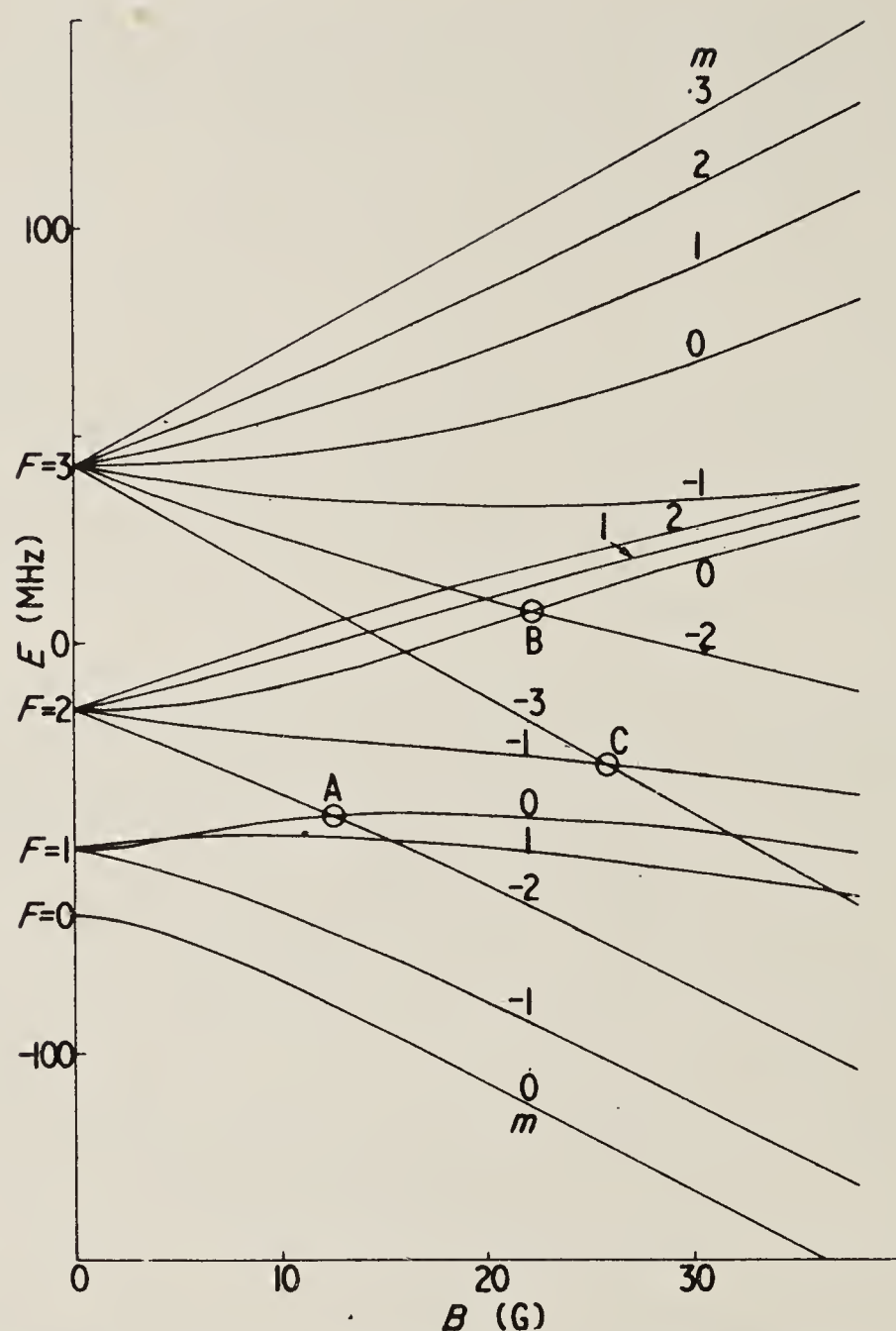


Figure 3. Energy eigenvalues for  $I = \frac{3}{2}$ ,  $J = \frac{3}{2}$ , plotted against magnetic field, with  $a = 18.7$  MHz,  $b = 3.0$  MHz.

A similar hamiltonian was used to find the eigenvalues and eigenfunctions  $|\mu\rangle$  for the ground state hyperfine Zeeman components. The interaction constants were taken to be  $a = 885.8$  MHz,  $b = 0$ .

### 3.2. The intensity of the resonance fluorescence

To calculate the intensity we used a formula given by Franken (1961). If atoms are excited instantaneously from their ground states at time  $t_0$ , then the intensity of fluorescent light at time  $t$  may be written in the form†

$$R(e_i, e_f, t-t_0) = \text{constant} \sum_{\substack{m, m' \\ \mu, \mu'}} f_{m\mu} f_{\mu m'} g_{m'\mu'} g_{\mu' m} \exp \left[ -\frac{i}{\hbar} (E_m - E_{m'}) (t - t_0) \right] \\ \times \exp[-\Gamma(t - t_0)]. \quad (2)$$

$R(e_i, e_f, t-t_0)$  is the rate of emission of photons of polarization  $e_f$  after excitation with light of polarization  $e_i$ . The  $f_{ij}$  and  $g_{ij}$  are matrix elements of vector components of the electric dipole operator for absorption and emission respectively: they are functions of  $B$ .  $\Gamma^{-1}$  is the mean lifetime for decay of alignment.

† The sign of the argument of the complex exponential given by Franken is incorrect, as pointed out by Stoke et al (1968).



Implicit in equation (2) is the assumption that the spectrum of the exciting light is uniform over the absorption spectrum in the neighbourhood of the resonance line. To allow for non-uniformity of the spectrum we introduce a weighting factor,  $Z_\mu(F)$ , for the terms in (2) representing excitation from the states belonging to the different ( $F$ ) of the ground level. The ratio  $r = Z_\mu(F = 1)/Z_\mu(F = 2)$  was treated as a parameter in fitting calculated to experimental level-crossing curves.

In our experiment, the excitation pulse has a finite duration. The intensity of fluorescent light must be calculated by summing the intensities from atoms excited at all previous times  $t_0$ . If we disregard the statistical nature of the excitation process we may write

$$I(t) = \int E(t_0)R(t-t_0) dt_0 \quad (3)$$

where  $E(t_0)$  is proportional to the rate of excitation at time  $t_0$  and  $R(t-t_0)$  is given by equation (2) supplemented by the factors  $Z_\mu$ . For simplicity we shall assume that  $E(t_0)$  is a rectangular function of time; Hilborn and DeZafra (1972) have shown that the exact shape of the pulse is not critical provided that the rise and fall times are shorter than the natural lifetime of the state being excited. We therefore write

$$\begin{aligned} E(t_0) &= \text{constant for } t_i < t_0 < t_f \\ &= 0 \text{ for } t_0 < t_i \text{ and } t_0 > t_f. \end{aligned} \quad (4)$$

The result of evaluating the integral in equation (3) is

$$I(B, t) = K \sum_{\substack{m, m' \\ \mu, \mu'}} \left( \frac{\Phi(m, m', \mu, \mu')}{\Gamma - i\omega_{mm'}} Z_\mu \exp(i\omega_{mm'} - \Gamma)(t - t_f) [1 - \exp(i\omega_{mm'} - \Gamma)(t_f - t_i)] \right) \quad (5)$$

where  $\omega_{mm'} = (E_m - E_{m'})/\hbar$ ;  $\Phi(m, m', \mu, \mu') = f_{m\mu} f_{\mu m'} g_{m'\mu'} g_{\mu'm}$ .  $I$  is a function of  $B$  through  $\Phi$ , as well as through the  $\omega_{mm'}$ .  $K$  is a constant of proportionality.

Equation (5) applies for times  $t > t_f$ , but if the time of observation occurs before the end of the excitation pulse, then  $t$  must replace  $t_f$  in the equation. In that case the first exponential factor reduces to 1 and the time dependence appears in the second exponential in the factor  $(t - t_i)$ . Furthermore,  $I(B, t) = 0$  for  $t < t_i$ . It should be noticed that, for  $t > t_i$ , the intensity is modulated at the frequencies  $\omega_{mm'}$  which are functions of  $B$ .

### 3.3. Use of a biasing function

The level-crossing signal is given by integration of  $I(B, t)$  over all observation times. The biasing function is incorporated at this stage:

$$S(B) = \int_0^\infty I(B, t) f(t) dt. \quad (6)$$

The calculated signal was in fact obtained by using a summation instead of the integration in (6), to correspond with the conditions of the experiment, namely, the accumulation of counts over finite intervals of time. Nevertheless, important conclusions concerning the effect of  $f(t)$  on  $S(B)$  can be drawn by evaluating the integral for special cases, and this we shall now do.

3.3.1.  $f(t) = \text{immediate step function}$ . If  $f(t) = 0$  for  $t < t_f$  and is a constant for  $t > t_f$ , we find

$$S_1(B) = K' \sum_{\substack{m, m' \\ \mu, \mu'}} \frac{\Phi(m, m', \mu, \mu')}{(\Gamma - i\omega_{mm'})^2} Z_\mu [1 - \exp(i\omega_{mm'} - \Gamma)W] \quad (7)$$

where we have used  $W$  for the pulse width ( $t_f - t_i$ ). For very small values of  $W$  we obtain the expression for steady-state level-crossing experiments, with denominators  $(\Gamma - i\omega_{mm'})$ . For long pulse widths,  $W \gg \Gamma^{-1}$ , the expression in square brackets is 1 and the expressions  $(\Gamma - i\omega_{mm'})$  are squared in the denominators. This modification to the steady-state expression has come about by supposing that a detector has been suddenly switched on immediately after a long period of irradiation.

3.3.2.  $f(t) = \text{delayed step function}$ . Let

$$\begin{aligned} f(t) &= 0 \text{ for } t < t_d \\ &= \text{constant for } t > t_d \text{ with } t_d > t_f. \end{aligned}$$

This corresponds to introducing a delay  $D_s = (t_d - t_f)$  between the end of the irradiation and the switching on of a detector. We find

$$S_2(B) = K'' \sum_{\substack{m, m' \\ \mu, \mu'}} \frac{\Phi(m, m', \mu, \mu')}{(\Gamma - i\omega_{mm'})^2} Z_\mu [1 - \exp(i\omega_{mm'} - \Gamma)W] \exp(i\omega_{mm'} - \Gamma)D_s. \quad (8)$$

The important point to notice about this expression is that modulation at the frequencies  $\omega_{mm'}$  is to be found for all values of  $W$  and  $D_s$ , and the signal is exponentially attenuated by the factor  $\exp(-\Gamma D_s)$ . Oscillatory structure is always present with this type of biasing function.

3.3.3.  $f(t) = \text{delayed gaussian function}$ . Let

$$f(t) = \exp \left[ - \left( \frac{t - t_{\max}}{T} \right)^2 4 \ln 2 \right]. \quad (9)$$

An example of such a gaussian is shown in figure 4 where the times  $t_{\max}$ ,  $t_i$  and  $t_f$  are indicated, together with various time intervals which are used in the analysis.

A particularly simple result emerges if the gaussian function, equation (9), is chosen so that its half-value width  $T$  is related to the delay at the peak,  $D_g = t_{\max} - t_f$ , by

$$D_g = \Gamma T^2 / 8 \ln 2. \quad (10)$$

We use (9) and (10) with (5) in equation (6) and make the further assumption that the contribution to the integral for values of  $t < t_f$  is negligible. This allows us to use (5) as it stands and to take the lower limit of the integral in (6) as  $-\infty$ .

$$\begin{aligned} S_3(B) &= K''' \sum_{\substack{m, m' \\ \mu, \mu'}} \frac{\Phi(m, m', \mu, \mu')}{\Gamma - i\omega_{mm'}} Z_\mu [1 - \exp(i\omega_{mm'} - \Gamma)W] \\ &\quad \times \left\{ T \exp \left[ - \frac{(\Gamma T)^2}{16 \ln 2} \right] \exp \left[ - \frac{(\omega_{mm'} T)^2}{16 \ln 2} \right] \right\}. \end{aligned} \quad (11)$$

If  $W$  is sufficiently small, the sole dependence of the result on  $\omega_{mm'}$  is in the gaussian factor in the last bracket, that is to say, the oscillatory structure has been eliminated and



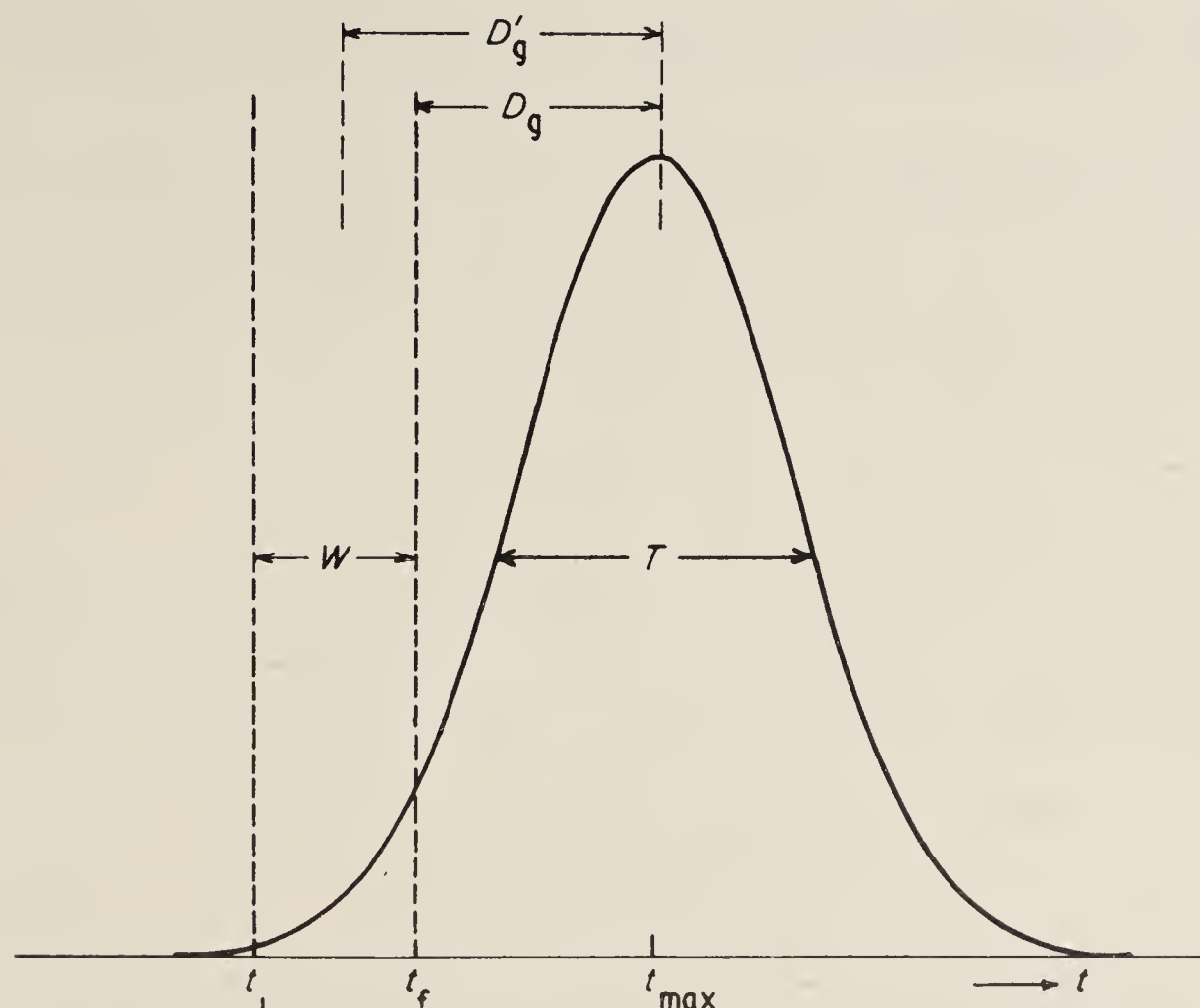


Figure 4. Gaussian biasing function showing parameters used in the analysis.

the normal lorentzian level-crossing function of width  $2\Gamma$  has been replaced by a gaussian of width  $(8 \ln 2)T^{-1}$ , which is under our control. Though the curves can be narrowed by increasing  $T$  (and also  $D$ , to preserve the relation (10)), it is undesirable to make  $T$  too large on account of the factor  $\exp[-(\Gamma T)^2/16 \ln 2]$ .

It should be emphasized that the curves are no longer gaussian functions of  $B$  as they are in the simple case treated by Copley *et al*, since, on the one hand, the  $\omega_{mm'}$  are not linear functions of  $B$  and, on the other hand,  $\Phi$  is a function of  $B$ .

To find a realistic condition under which it is a good approximation to neglect the contribution to the integral from values of  $t < t_f$ , we might require, say,  $D_g > T$ . With the help of (10) we find, in this case,

$$D_g > 8 \ln 2 / \Gamma = 5.5\tau \quad (12)$$

where  $\tau$  is the mean lifetime of the excited atoms. Using  $\tau = 16$  ns, we obtain  $D_g > T > 88$  ns as the required condition. This value should be compared with the values quoted in table 1.

In the reduction of the experimental data, it was not possible to ensure that the conditions of validity of equation (11) were satisfied, partly on account of the finite duration of the exciting pulse and partly on account of the finite time resolution of the equipment. For gross departures from the condition (10), the oscillatory structure was clearly seen (figure 5). When the condition was approximately satisfied this structure was suppressed.

#### 4. Treatment of experimental data

In this section we first describe the way in which experimental level-crossing curves were derived from experimental decay spectra. We go on to explain the procedure used

to obtain the best values for the magnetic dipole and electric quadrupole interaction constants.

Decay spectra were obtained in both positive and negative field directions over two regions of magnetic field. The first, in the range 0–30 gauss, spanned the complete region of interest which included the regions of the level crossings A, B, and C; we shall refer to these experiments as panoramic scans. The second, in the range 9–15 gauss, provided detailed scans in the region of crossing A.

#### 4.1. Construction of the experimental level-crossing curves

Let  $n(t_k, B)$  represent the experimental decay spectra after correction for pile-up and subtraction of background counts.  $t_k$  is the time at the start of the  $k$ th channel of the multichannel analyser and  $B$  is the value of the magnetic field. Level-crossing curves, represented by  $N(B)$ , were obtained by evaluating the weighted sum of the  $n(t_k, B)$  for fixed  $B$ :

$$N(B) = \sum_k n(t_k, B) f(t_k). \quad (13)$$

The summation was carried out for a variety of biasing functions  $f(t_k)$ . The level-crossing curves so obtained were scaled to make  $N(B) = 1$  when  $B = 0$ . An average was then taken of the curves obtained in both positive and negative field directions in order to eliminate effects due to slight misalignment of the field:

$$S_{\text{exp}} = \frac{1}{2}[N(B) + N(-B)]. \quad (14)$$

We shall refer to the symmetrical functions  $S_{\text{exp}}(B)$  as ‘experimental level-crossing curves’. Examples of these curves for the panoramic scans are shown in figure 5 and for the detailed scans in figure 6.

#### 4.2. Interpretation of the experimental curves

It is possible, in principle, to obtain values of  $a$  and  $b$  by making these constants adjustable parameters in seeking the best fit between the experimental curves and those calculated from the theory of § 3. Some previous investigators have chosen this approach, but we have preferred to rely less heavily on the theory of the line profile. We determined from the detailed scans the value of the magnetic field corresponding to the minimum in  $S_{\text{exp}}(B)$ ; this gives an approximate value for level-crossing A. The theory is used to calculate small corrections to this value. Rather more reliance on the theory is needed to interpret  $S_{\text{exp}}(B)$  in the neighbourhood of the crossings B and C.

The theory itself is tested on the panoramic scans which are sensitive not only to the positions of the level crossings, but also to the relative strengths of the various components of the signal over a wide range of magnetic field.

**4.2.1. The panoramic scans: test of the theory.** Comparison of  $S(B)$  (equation (6)) with  $S_{\text{exp}}(B)$  (equation (14)) for a particular biasing function  $f(t)$  requires

- (i) a value of  $\Gamma$ : this was always taken to be  $(1.61 \times 10^{-8})^{-1} \text{ rad s}^{-1}$ ;
- (ii) trial values of  $a$  and  $b$ : initial values were available from earlier work and these were improved iteratively;
- (iii) the constant  $K$  in  $S(B)$ : the field-dependent signal  $S(B_1 \neq 0) - S(B = 0)$  at some convenient field  $B_1$  was scaled to coincide with the corresponding experimental quantity



at that point. At the same time an allowance was made for the field-independent fluorescence from  $3^2P_{1/2}$ , which is included in  $S_{\text{exp}}(B)$  but not in  $S(B)$ , by adding a constant to  $S(B)$  to make  $S(B = 0) = S_{\text{exp}}(B = 0) = 1$ ;

(iv) a value of the parameter  $r = Z_u(F = 1)/Z_u(F = 2)$ : this was determined by least-squares adjustment.

Comparisons for the panoramic scans made on this basis showed fair agreement between theory and experiment, but a small systematic difference remained which could not be eliminated by variation of the parameters. It was found empirically that the difference could be taken up by subtracting from  $S_{\text{exp}}(B)$  a term proportional to  $B^2$ :

$$S'_{\text{exp}}(B) = S_{\text{exp}}(B) - kB^2. \quad (15)$$

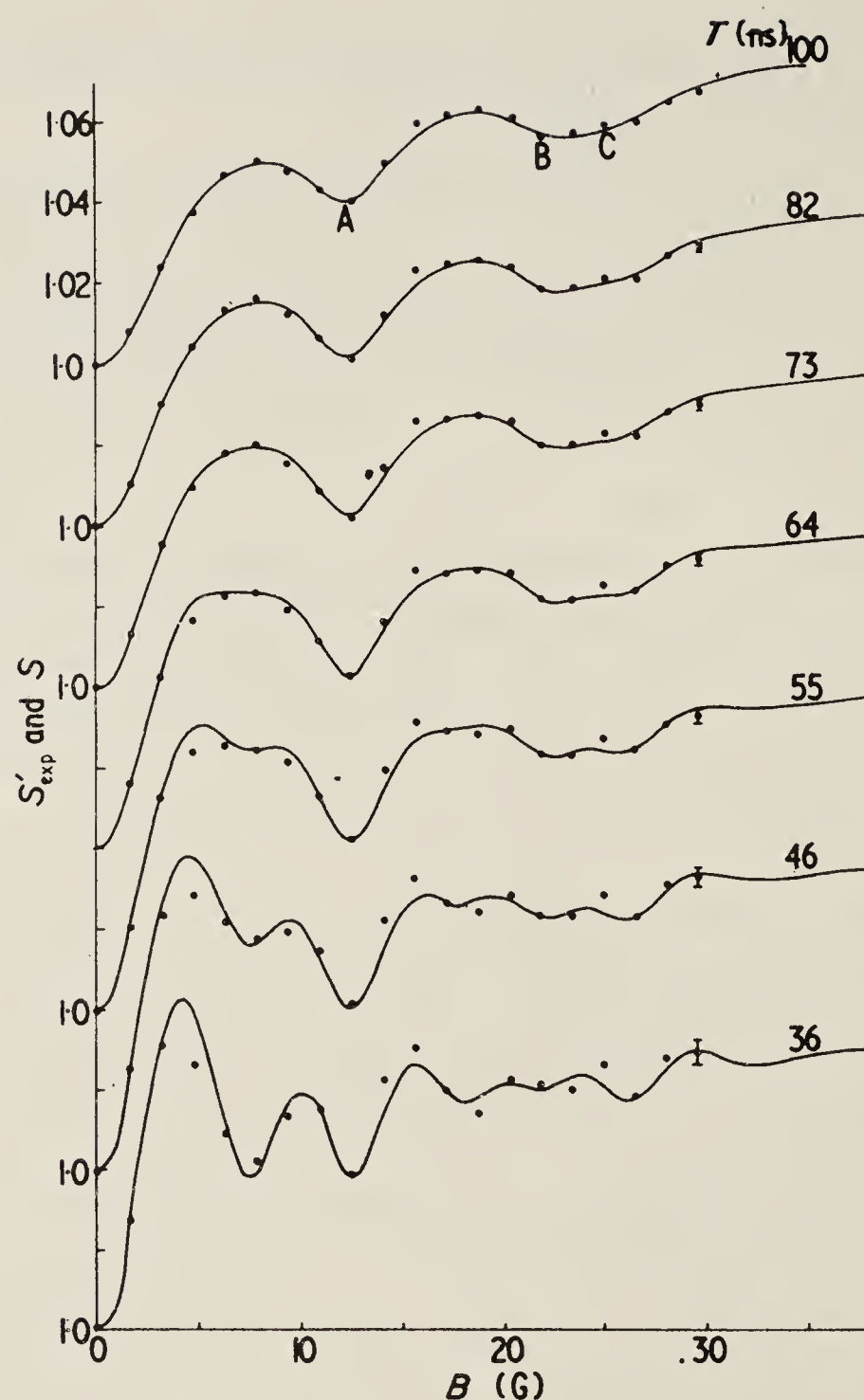
The same value of  $k$  secured agreement between theory and experiment whatever biasing function was chosen. It is to be emphasized that this was a small correction: its magnitude was about 1% of the signal at the highest fields used (30 G). By studying steady-state level-crossing curves, it was found that the effect depended on vapour density: it was present when the vapour density was maintained at the value used for the pulsed experiments, but disappeared when the density was reduced to  $\frac{1}{10}$  of that value: (temperature: 105°C). We believe the effect to be associated with the trapping of resonance radiation, and note that a similar effect has been reported by Feichtner *et al* (1967). These authors also used a correction proportional to  $B^2$ .

Figure 5 shows a series of comparisons between  $S'_{\text{exp}}(B)$  and the corresponding  $S(B)$ . The same experimental data were used with different biasing functions. All these were gaussians of various widths, the position of the peak relative to the exciting pulse being fixed. The values of the parameters are  $r = 1.3$  (a similar value was used by Baumann (1968) though the actual value depends on the particular lamp and optical depths used in the experiment) and  $k = 1.6 \times 10^{-5} \text{ G}^{-2}$ . There is satisfactory agreement between  $S'_{\text{exp}}(B)$  (circles) and  $S(B)$  (solid lines). In addition to the minima at about 12, 22 and 25 G, arising from the level-crossings A, B, and C respectively, oscillatory features will be noticed which become more conspicuous as the width of the biasing function is reduced. The matching condition (10) is approximately satisfied for  $T = 78 \text{ ns}$  with  $D'_g = 82 \text{ ns}$  as in the figure.

The values of  $a$  and  $b$  which ultimately emerge from the analysis depend on the values of  $r$  and  $k$ .  $r$  affects the relative strengths of the level-crossing signals at A, B and C and  $k$  adds a slight curve to the baseline. The simplest theory would have  $r = 1$  and  $k = 0$ . The values of  $r$  and  $k$  that were actually used change the values of  $a$  and  $b$  systematically by amounts comparable with the random errors.

**4.2.2. The crossing A.** Data from the detailed scans covering the region of the crossing A were treated as before to obtain  $S'_{\text{exp}}(B)$ , except that the correction term in equation (15) was taken as linear in  $B$ . (At the time when this calculation was carried out the linear correction appeared to be adequate: when the quadratic correction was adopted for the panoramic scans it was established that the linear correction actually used over the limited range gave results indistinguishable from those obtained with the quadratic correction.) The reduced data were fitted by least-squares analysis to a polynomial of sixth degree and the value of the magnetic field at the minimum was found. This procedure was carried out for a variety of biasing functions. Such a polynomial and the points from which it was derived are shown in figure 6.

To obtain values for the magnetic field corresponding to level-crossing A, the positions of the minima in the experimental curves need to be corrected for 'pulling' by the



**Figure 5.** Comparisons between  $S'_{\text{exp}}$  (points) and  $S$  (solid lines) for gaussian biasing functions having  $D'_g = 82$  ns and values of  $T$  marked in the figure. Values of other parameters are:  $a = 18.7$  MHz,  $b = 3.0$  MHz,  $\Gamma^{-1} = 16.1$  ns,  $r = 1.3$ ,  $k = 1.6 \times 10^{-5} \text{ G}^{-2}$ .

overlap of other level-crossing signals (in particular, those centred on zero field), by the distortion of the level-crossing signal arising from curvature of the energy levels and from variation of matrix elements with magnetic field, and by oscillatory structure which may have been introduced by the biasing function. The theory of the line profile was used to calculate these corrections. For assumed values of  $a$  and  $b$ , the position of the level-crossing could be calculated exactly.  $S(B)$  and the positions of its minima were then calculated using the values of  $a$  and  $b$  assumed for the calculation of the level-crossing and the set of biasing functions that were used for  $S'_{\text{exp}}(B)$ . The differences between the position of the level-crossing and the positions of the minima constituted a set of corrections which could be applied to the positions of the minima in  $S'_{\text{exp}}(B)$  to obtain *experimental* values for the level-crossing A. The corrections were insensitive to variations of  $a$  and  $b$  over the range of uncertainty of these quantities.

Table 1 summarizes the results obtained for the position of the level-crossing A using a family of gaussian biasing functions. In each entry the upper figures give the positions of the minima of the experimental level-crossing signals and the lower figures (in italics) show these positions corrected for 'pulling'. The figures in italics therefore



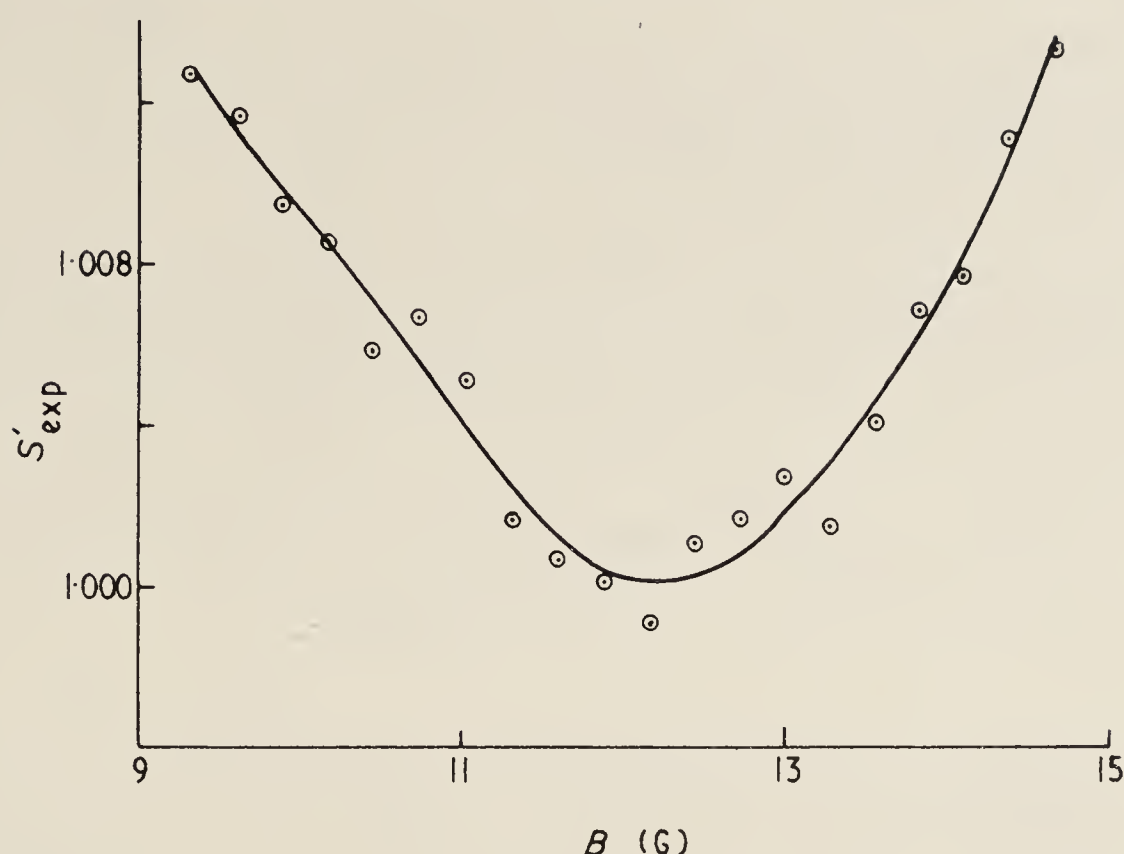


**Figure 6.** Experimental curve in the region of level crossing A. Parameters of the gaussian biasing function were  $D'_g = 82$  ns,  $T = 73$  ns.

**Table 1.** Positions of the level-crossing A obtained with a family of gaussian biasing functions.

(In each entry the upper figure is the experimentally-determined position of the minimum in  $S'_{\text{exp}}(B)$  and the lower figure (in italics) is the corrected position corresponding to the level-crossing. The errors shown are RMS statistical errors.)

$T(\text{ns})$	$D'_g(\text{ns})$			
	73	82	91	100
36	$12.28 \pm 0.12\text{G}$ <i>12.54</i>	$12.47 \pm 0.15$ <i>12.58</i>	$12.60 \pm 0.17$ <i>12.63</i>	$12.67 \pm 0.19$ <i>12.72</i>
55	$12.28 \pm 0.11$ <i>12.50</i>	$12.36 \pm 0.13$ <i>12.54</i>	$12.44 \pm 0.14$ <i>12.58</i>	$12.51 \pm 0.16$ <i>12.62</i>
73	$12.18 \pm 0.08$ <i>12.52</i>	$12.26 \pm 0.11$ <i>12.52</i>	$12.33 \pm 0.12$ <i>12.54</i>	$12.38 \pm 0.14$ <i>12.55</i>
91	$12.07 \pm 0.07$ <i>12.56</i>	$12.15 \pm 0.09$ <i>12.54</i>	$12.21 \pm 0.11$ <i>12.55</i>	$12.26 \pm 0.13$ <i>12.53</i>

represent the experimentally-determined positions of the level-crossing. The error limits shown in the table represent RMS statistical errors.

The delay of the peak of the gaussian is represented in the table by  $D'_g$ , measured from the peak of the excitation pulse (not from the end of the pulse as in § 3).  $T$  is the width at half intensity. The values of  $D'_g$  and  $T$  represent a useful working range for this particular level-crossing signal: at smaller values of  $T$  the oscillations are large and errors due to timing uncertainties in the experimental data become important; at larger values of  $T$  and smaller values of  $D'_g$  there is a significant loss of resolution and the corrections become large; at larger values of  $D'_g$  the statistical errors become large. The results in table 1 indicate that the corrected position of the level-crossing minimum is almost independent of  $D'_g$  and  $T$ , except for the  $T = 36$  ns row where the corrections

are the least reliable. If we discard this row of values, we find the position of the A crossing to be  $12.55 \pm 0.10$  G. The quoted error includes the estimated systematic errors as well as the statistical error.

**4.2.3. Evaluation of the interaction constants  $a$  and  $b$ .** Owing to the difficulty of resolving the level-crossing signals at B and C (see figure 5) no attempt was made to determine the positions of these minima directly. Instead, experimental data from the region from 19 to 30 G, which includes the level-crossings B and C, were fitted by least-squares analysis to the functions  $S(B)$ . For this purpose the position of level-crossing A was constrained to  $12.55 \pm 0.1$  G. The values of the constants  $a$  and  $b$  obtained in this way were

$$a = 18.7 \pm 0.1 \text{ MHz} \quad b = 3.0 \pm 0.2 \text{ MHz}.$$

**4.2.4. Assessment of the biasing functions.** In figure 7 are shown the corrections of § 4.2.2 evaluated for two families of biasing functions: step functions (7(a)) and gaussian functions (7(b)). In 7(a) the correction is plotted against the delay,  $D'_s$ . In 7(b) the correction is plotted against  $D'_g$  for a range of widths of the gaussian. It is clear from the figure that the correction is less sensitive to delay in 7(b) than in 7(a), provided that the parameters of the gaussian are chosen so as to suppress the oscillatory structure. This advantage of the gaussian is important experimentally, since  $t_f$ , the cut-off time of the excitation pulse is difficult to establish. The peak of the pulse may be located more accurately and was used as a time reference in the present experiments, but whatever reference point is used it is an advantage to work with functions where time delays need not be known accurately.

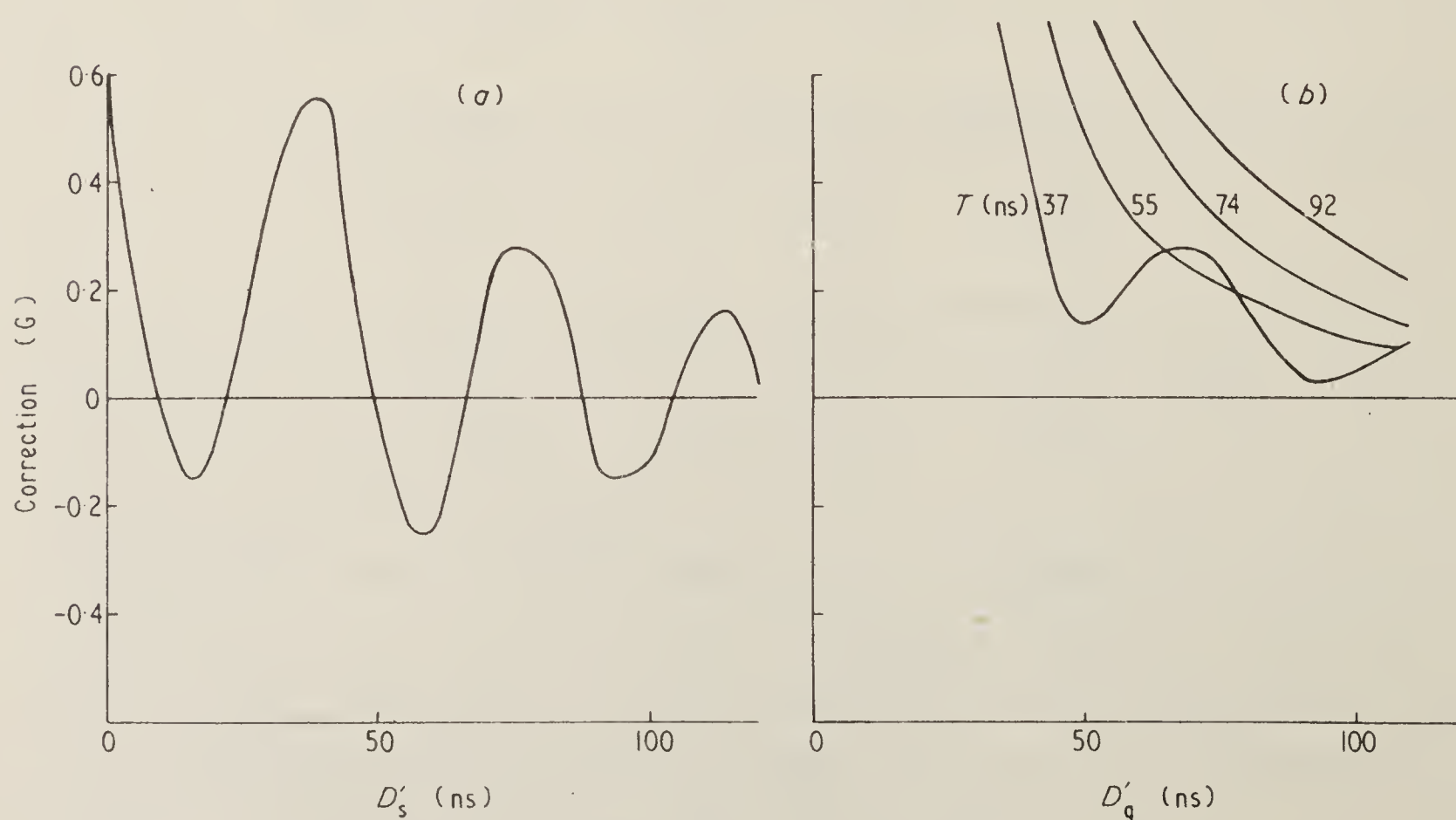


**Figure 7.** Corrections  $[B(\text{level-crossing}) - B(\text{minimum in } S)]$  for level-crossing A evaluated from the theory of the line profile for two families of biasing functions: (a) step functions. The delay  $D'_s$  is measured from the middle of the exciting pulse ( $D'_s = D_s + \frac{1}{2}W$ ); (b) gaussian functions with delay  $D'_g (= D_g + \frac{1}{2}W)$ . The behaviour of the curve  $T = 37$  ns reflects the oscillatory structure which develops in the level-crossing curves as  $T$  is reduced.



5. Discussion of results

In table 2(a) we compare the values of the magnetic dipole and electric quadrupole interaction constants of the level  $3^2P_{3/2}$  of sodium found in the present investigation with those obtained by previous workers using various techniques. Also included in table 2(a) are the computed values for the position of the level-crossing A corresponding to the  $a$  and  $b$  values quoted by various authors. Table 2(b) shows magnetic dipole and electric quadrupole interaction constants for the level  $4^2P_{3/2}$ .

Table 2.

Reference	Technique (1)	$a$ (MHz)	$b$ (MHz)	A (Gauss) (2)	$Q_{\text{hfs}}$ (barn) (3)
(a) The level $3^2P_{3/2}$					
Sagalyn (1954)	ODR	$19.5 \pm 0.6$	$2.4 \pm 1.4$	$(13.3 \pm 0.9)$	$0.098 \pm 0.060$
Perl <i>et al</i> (1955)	ABMR	$19.06 \pm 0.36$	$2.58 \pm 0.3$	$(13.0 \pm 0.3)$	$0.108 \pm 0.015$
Dodd and Kinnear (1960)	ODR	$18.5 \pm 0.6$	$2.25 \pm 0.4$	$(12.7 \pm 0.5)$	$0.097 \pm 0.021$
Baumann <i>et al</i> (1966)	ODR	$18.5^{+0.6}_{-0.2}$	$3.2 \pm 0.5$	$(12.4^{+0.2}_{-0.3})$	$0.138 \pm 0.025$
Ackermann (1966)	ODR	$18.7 \pm 0.4$	$3.4 \pm 0.4$	$(12.4 \pm 0.5)$	$0.145 \pm 0.021$
Schönberner and Zimmerman (1966)	LC	$18.65 \pm 0.10$	$2.82 \pm 0.30$	$(12.6 \pm 0.2)$	$0.121 \pm 0.014$
Baylis (1967)	LC	$19.1 \pm 0.4$	$2.5 \pm 0.4$	$(13.0 \pm 0.4)$	$0.104 \pm 0.019$
Baumann (1968)	LC	$18.8 \pm 0.3$	$2.9 \pm 0.4$	$(12.7 \pm 0.3)$	$0.123 \pm 0.020$
Copley <i>et al</i> (1968)	TRL C	$18.5 \pm 0.4$	$3.0 \pm 0.6$	$12.4 \pm 0.2$	$0.129 \pm 0.029$
Schmieder <i>et al</i> (1970)	LC	$18.9 \pm 0.3$	$2.4 \pm 0.3$	$(12.9 \pm 0.3)$	$0.101 \pm 0.014$
Mashinskii (1970a)	LC	$19.74 \pm 0.05$	$3.34 \pm 0.04$	$(13.10 \pm 0.03)$	$0.135 \pm 0.002$
Mashinskii (1970b)	LC			$12.65 \pm 0.05$	
Lange <i>et al</i> (1973)	LAB	$18.69 \pm 0.22$	$3.08 \pm 0.39$	$(12.6 \pm 0.3)$	$0.131 \pm 0.018$
Figger and Walther (1973)	TRL C	$18.62 \pm 0.08$	$3.04 \pm 0.19$	$12.46 \pm 0.05$	$0.130 \pm 0.009$
Present work	TRL C	$18.7 \pm 0.1$	$3.0 \pm 0.2$	$12.55 \pm 0.10$	$0.128 \pm 0.009$
(b) The level $4^2P_{3/2}$					
Krüger and Schleffler (1958)	ODR	$6.20 \pm 0.12$	$1.0 \pm 0.3$		$0.129 \pm 0.042$
Schönberner and Zimmermann (1966)	LC	$6.0006 \pm 0.030$	$0.86 \pm 0.09$		$0.114 \pm 0.013$
Schmieder <i>et al</i> (1970)	LC	$6.2 \pm 0.2$	$1.0 \pm 0.1$		$0.129 \pm 0.017$

(1) ODR—optical double resonance  
ABMR—atomic beam magnetic resonance  
LC—level-crossing  
TRL C—time-resolved level-crossing  
LAB—tunable laser/atomic beam  
(2) Position of the level-crossing A. Values in parentheses are calculated from quoted  $a$ ,  $b$  values. In other cases measured values are given.  
(3)  $Q_{\text{hfs}}$  (uncorrected for core polarization) obtained from quoted  $a$ ,  $b$  values using equation (17).

5.1. The level  $3^2P_{3/2}$

Our results for the level  $3^2P_{3/2}$  are in good agreement with those of most other recent determinations, with the notable exception of the level-crossing results of Baylis, Schmieder *et al* (1970) and Mashinskii (1970a); in particular they are in very good agreement with the preliminary results of Lange and his colleagues (1973) which were obtained by scanning the hyperfine structure of the sodium  $D_2$  line directly by means of a narrow bandwidth CW tunable dye laser and with those of Figger and Walther (1973) obtained

by a delayed detection method. The good agreement with the results of Copley *et al* (1968) should be regarded as rather fortuitous as in that investigation no allowance was made for the perturbing effect of (unresolved) oscillatory structure on the positions of the level-crossing minima. The precision claimed in the present investigation represents a significant improvement over that claimed in other investigations, with the exception of those on Mashinskii and of Figger and Walther.

The general lack of consistency between the various steady-state level-crossing results for the level  $3^2P_{3/2}$  of sodium seems to arise, at least in part, from the poor resolution exhibited by the level-crossing signals for this level: for the resolution available the accuracy of the method would be expected to rely rather heavily on the details of the theory used in fitting the data. It is interesting to note that the results of Baumann *et al* (1968), which are in good agreement with our results, were derived from level-crossing curves in which the A and B level-crossing signals appear to be better resolved than in other steady-state level-crossing experiments. The improvement in resolution was apparently due to the use of a strongly self-absorbed excitation line, resulting in preferential excitation from the  $F = 1$  states of the ground level. A weighting factor  $Z_\mu(F = 1)/Z_\mu(F = 2) = 1.44$  was required to fit Baumann's data, whereas Schmieder *et al* (1970) found the white light approximation satisfactory for the interpretation of their measurements. The technique of enhancing the relative intensity of a chosen level-crossing signal by deliberately biasing the spectral profile of the exciting radiation was later employed by Mashinskii (1970b) to obtain a direct measurement of crossing A; the value obtained ( $12.65 \pm 0.05$ ) is also in good agreement with our value, but it is in very poor agreement with the value corresponding to the  $a, b$  values found by the same author when the relative intensity of the A crossing signal is not enhanced (Mashinskii 1970a).

The values of  $a$  and  $b$  quoted in table 2(a) were used to derive values for the quadrupole moment of  $^{23}\text{Na}$ . Using the expression given by Kopfermann (1958)

$$Q_{\text{hfs}} = \left[ \frac{1}{c^2} \left( \frac{\mu_B}{e} \right)^2 \frac{4l(l+1)}{J(2J-1)} \frac{\mu_I}{\mu_N} \frac{1}{I} \frac{m_e}{m_p} \frac{F_r}{R_r} \right] \frac{b}{a} \quad (16)$$

together with the values  $\mu_I/\mu_N = 2.217 \pm 0.001$  (Sherriff and Williams 1951),  $\mu_B/e = 5.783 \times 10^{-5}$  (SI),  $F_r = 1.0025$  and  $R_r = 1.0051$  (Kopfermann 1958), we obtain

$$Q_{\text{hfs}}(^{23}\text{Na}) = 0.7983 b/a \text{ barn.} \quad (17)$$

Using our measured values we have  $b/a = 0.160 \pm 0.012$ , whence

$$Q_{\text{hfs}}(^{23}\text{Na}) = 0.128 \pm 0.009 \text{ barn.}$$

Correction for core polarization (Sternheimer 1957) yields

$$Q(^{23}\text{Na}) = 0.128 \times 0.805 = 0.103 \text{ barn.}$$

The last column of table 2(a) shows our uncorrected result, together with the values obtained by using in equation (17) the  $a, b$  values of other authors.†

† The  $Q_{\text{hfs}}$  value we obtained from equation (17) using  $a, b$  values reported by Schmieder *et al* (1970) differs significantly from the value they obtained. The discrepancy apparently arises from an error in their evaluation of equation (16). A similar error is also present in the values they obtained for the level  $4^2P_{3/2}$  of sodium and for the levels  $4^2P_{3/2}$  and  $5^2P_{3/2}$  of potassium.



### 5.2. The level $4^2P_{3/2}$

The level-crossing curves for the level  $4^2P_{3/2}$  are considerably better resolved than those for the level  $3^2P_{3/2}$  ( $a\tau \sim 590$ , compared with  $a\tau \sim 300$  for  $3^2P_{3/2}$ ). The results are assembled in table 2(b). The level-crossing results—particularly the  $b$  values—are in good agreement with each other and with the results of the optical double resonance investigation. Furthermore, the  $Q_{\text{hfs}}$  values corresponding to the reported  $a$  and  $b$  values are in good agreement with the value obtained from the  $3^2P_{3/2}$  data in the present investigation. (The difference between the core polarization correction factors for the two levels is expected to be small: inspection of the values reported for the levels  $n^2P_{3/2}$  and  $(n+1)^2P_{3/2}$  of potassium, rubidium and caesium (Sternheimer 1957) suggests that the factor for the level  $4^2P_{3/2}$  of sodium should be greater than that for the level  $3^2P_{3/2}$  by an amount not exceeding 5 %.) The improved agreement where the resolution is better supports our contention that improvements in resolution of level-crossing signals, even at the cost of poorer signal-to-noise ratios in the experimental curves, can lead to more reliable values of hyperfine interaction constants.

### 5.3. Ratios of the interaction constants and doublet intervals for $n = 3$ and $n = 4$

A check on the reliability of our results for the level  $3^2P_{3/2}$  may be made by comparing the values of the ratios  $a(3^2P_{3/2})/a(4^2P_{3/2})$ ,  $b(3^2P_{3/2})/b(4^2P_{3/2})$  with the value of the ratio of the fine structure intervals  $\Delta\nu(3^2P)/\Delta\nu(4^2P)$ , using  $a, b$  values for the level  $4^2P_{3/2}$  reported by other authors. (It is predicted theoretically that the values of these ratios should be the same (Kopfermann 1958).)

**Table 3.** Ratios of hyperfine interaction constants and doublet intervals

$a(3^2P_{3/2})/a(4^2P_{3/2})$	$b(3^2P_{3/2})/b(4^2P_{3/2})$	$\Delta\nu(3^2P)/\Delta\nu(4^2P)$
$3.0 \pm 0.1$ (i, ii)	$3.0 \pm 0.5$ (i, ii)	3.05 (iii)
$3.1 \pm 0.1$ (ii, ii)	$2.4 \pm 0.5$ (ii, ii)	

(i)—This work

(ii)—Schmieder *et al* (1970)

(iii)—Moore (1949)

Table 3 shows the values obtained for these ratios, using the  $4^2P_{3/2}$  results of Schmieder *et al*. The latter values are expected to be reliable because the  $4^2P_{3/2}$  level-crossing curves have good resolution. The very good agreement between the three ratios indicates that our  $a, b$  values for the level  $3^2P_{3/2}$  are consistent with the values obtained for the level  $4^2P_{3/2}$  by these authors. The rather poor agreement of the ratio  $b(3^2P_{3/2})/b(4^2P_{3/2})$  obtained using the  $3^2P_{3/2}$  value reported by Schmieder *et al* suggests that their  $b(3^2P_{3/2})$  value is too small.

## 6. Conclusion

Improved resolution in level-crossing curves has been obtained by biasing the signal in favour of longer-lived atoms. This technique is prone to introduce oscillatory structure

into the level-crossing curves. It proved advantageous to suppress this structure by the use of gaussian biasing functions with appropriate parameters.

The improved resolution allowed the determination of the positions of the level-crossings with less reliance on the theory of the line profile than is required for unresolved curves. Differences between results of some earlier investigators are attributed to errors introduced by profile analysis. The hyperfine interaction constants,  $a = 18.7 \pm 0.1$  MHz,  $b = 3.0 \pm 0.2$  MHz, which were obtained as a result of this work are believed to be more accurate than values obtained from unresolved curves.

### Acknowledgments

We wish to express our gratitude to Dr G H Copley who constructed a first version of the apparatus, to Dr M Krainska-Miszczak who made a substantial contribution at a later stage and to Mr C H Smith and Mr C Balague for valuable technical assistance. In addition we would like to thank Professor W J Sandle for many helpful discussions. The work was supported by the Science Research Council.

### References

- Ackermann H 1966 *Z. Phys.* **194** 253–69  
 Baumann M, Hartmann W, Krüger H and Oed A 1966 *Z. Phys.* **194** 270–9  
 Baumann M 1968 *Z. Naturf* **23A** 620–2  
 Baylis W E 1967 *Thesis* MPI–PAE Extraterr. 9/67 Munich (unpublished)  
 Besch H J, Farr W and Otten E W 1970 *Nucl. Instrum. Methods* **80** 277–83  
 Coates P B 1968 *J. Phys. E: Sci. Instrum.* **1** 878–9  
 Copley G, Kibble B P and Series G W 1968 *J. Phys. B: Atom. molec. Phys.* **1** 724–35  
 Dodd J N and Kinnear R W N 1960 *Proc. Phys. Soc.* **75** 51–60  
 Feichtner J D, Gallagher J H and Mizushima M 1967 *Phys. Rev.* **164** 44–8  
 Figger H and Walther H 1973 submitted to *Z. Phys.*  
 Franken P A 1961 *Phys. Rev.* **121** 508–12  
 Hilborn R C and DeZafra R L 1972 *J. Opt. Soc. Am.* **62** 1492–7  
 Kopfermann H 1958 *Nuclear Moments* (New York: Academic Press)  
 Kruger H and Scheffler K 1958 *J. Phys. Radium* **19** 854–7  
 Lange W, Luther J and Nottbeck B private communication.  
 Mashinskii A L 1970a *Optics and Spectroscopy* **28** 1–6  
 — 1970b *Optics and Spectroscopy* **28** 108–10  
 Moore C E 1949 *Atomic Energy Levels, Natl. Bur. Stds (U.S.) Circ. No 467* Vols I–III  
 Perl M L, Rabi I I and Senitzky B 1955 *Phys. Rev.* **98** 611–26  
 Ramsey N F 1956 *Molecular Beams* (Oxford: Clarendon Press)  
 Sagalyn P L 1954 *Phys. Rev.* **94** 885–92  
 Schenk P, Hilborn R C and Metcalf H 1973 *Phys. Rev. Lett.* **31** 189–92  
 Schmieder R W, Lurio A, Happer W and Khadjavi A 1970 *Phys. Rev.* **2A** 1216–28  
 Schonberger D and Zimmermann D 1968 *Z. Phys.* **216** 172–82  
 Sherriff R and Williams D 1951 *Phys. Rev.* **82** 651–5  
 Sternheimer R M 1957 *Phys. Rev.* **105** 158–69  
 Stoke H H, Fulop G, Klepner S and Reti O 1968 *Phys. Rev. Lett.* **21** 61–4



# *Time-Resolved Fluorescence Spectroscopy\**

J. N. DODD AND G. W. SERIES

## *1. Introduction: Coherence and Superposition States*

We may learn about the force fields that drive dynamical systems by studying their evolution in time from nonequilibrium configurations. What is to be discussed in this article is the kind of information that can be obtained about atoms from measurements of time variations with micro- or nanosecond resolution of the intensity of fluorescent light from an ensemble. All the atoms whose fluorescence is to be observed must have been prepared in the same way at the same time, to within the desired time resolution of the experiment.

Equivalent information may, of course, be obtained by direct spectral analysis, in the radio- or microwave regimes, of the variations in the fluorescent intensity. Again, a steady-state version of such experiments is provided by the level-crossing technique, which exploits the spatial interferences between radiations from different states when these are tuned

\* *Preliminary Remark.* Shortly after the authors had agreed to write this article, but before it was actually written, they were privileged to see a copy of the excellent review of the same subject written by S. Haroche for *High Resolution Laser Spectroscopy*, Ed. K. Shimoda, Springer, Berlin (1976). While the two articles share a great deal of common ground, that of Haroche is more detailed, reports more applications, and gives more technical information. Our article has more to say about the relation between “quantum beats” and other phenomena of coherence, about the geometrical features of the experiments, and about the effects of pulsed magnetic and electric fields.

---

J. N. DODD • Department of Physics, University of Otago, New Zealand.

G. W. SERIES • J. J. Thomson Physical Laboratory, University of Reading, Reading, U.K.

through degeneracy by the application of magnetic fields (see the article by Happer and Gupta, Chapter 9 of this work). Fundamentally, the characteristics of time-resolved measurements of intensity, of the spectral analysis of intensity variations, and of level-crossing experiments, are the same.

These studies of *intensity* variations are to be carefully distinguished from conventional spectral analyses where one studies (by way of the Fourier transform) the evolution in time of the amplitude of the field, that is to say, of the electric dipole moments of atoms oscillating at optical frequencies. The variations in *intensity* recorded by a detector at some position fixed in relation to the source arise partly on account of variations in the number of excited atoms (as, for instance, by radiative decay) and partly because of variations in the spatial orientation of the radiating dipoles. It is these variations in orientation that we shall be mainly concerned with. The detector registers variations of intensity as the dipoles in different atoms of the ensemble precess and nutate in synchronism. It is not a question of coherence between the fields oscillating at optical frequencies, but of the superposition of the anisotropic radiation patterns of the individual atomic dipoles. The synchronous precession may be brought about, for example, by the sudden application of an external field to an assembly of atoms fluorescing under steady excitation, so that the resulting modulation of the light recorded by the detector is a direct demonstration of Larmor precession, a “searchlight” effect. Less obviously, the precession may result from internal coupling of the orbital motion of the electron to its spin or to the nucleus. While under steady excitation these motions are randomly phased, they can be made synchronous in different atoms if these latter are excited simultaneously by a short pulse of polarized light. The intensity of the fluorescence is then modulated at fine or hyperfine frequencies.

The precessional motions can, of course, be determined by measuring the splittings of lines in the optical spectra, but we gain a very important advantage by studying the modulation of the intensity directly, which is that, to all intents and purposes, the Doppler effect is eliminated. The Doppler broadening of spectral lines in the optical region, being proportional to the frequency of the radiation, is of the order of 1 GHz. The Doppler broadening of the intensity variations, on the other hand, is smaller by the ratio of optical to radio or microwave frequencies—a factor of  $10^6$  or  $10^8$ —and is negligibly small in the present context.

### 1.1. Simple Theory of Quantum Beats

For a quantum-mechanical understanding of the modulation of the intensity of fluorescent light, the elementary notion of the decay of excited atoms from energy eigenstates is inadequate. An essential notion is the



preparation of atoms into superpositions of energy eigenstates and their decay from such superposition states. The preparation is easy to achieve. One aims to apply a sudden perturbation which breaks the symmetry of the preexisting environment. The atoms will evolve into equilibrium with the new environment—usually an exponential change characterized by a rate constant—but during the transient period there will exist atoms that were prepared in eigenstates of the old environment and that have evolved coherently from these states. In terms of eigenstates of the new environment, they are in a coherent superposition and will remain so for the duration of the transient.

The superposition state is the formal mathematical entity from which may be deduced the synchronous precession we spoke of in the last section.

To calculate the intensity of fluorescent light from an ensemble of atoms in superposition states it is plausible to use the ordinary formula for spontaneous emission from energy eigenstates with the superposition state taking the place of the initial eigenstate.

The ordinary formula reads

$$I \propto \sum_f |\langle f | \hat{D}_\alpha | e \rangle|^2 \quad (1)$$

where  $\hat{D}_\alpha$  is a component of the electric dipole operator,  $|e\rangle$  is the initial (excited) state of the transition, and  $\{|f\rangle\}$  is the set of final states that may connect with  $|e\rangle$  (for example, hyperfine states of the ground level)—it being understood that  $|e\rangle$  and the  $|f\rangle$  are eigenstates of whatever Hamiltonian describes the system.

In place of (1) we now write

$$I(t, t_0) \propto \sum_f |\langle f | \hat{D}_\alpha | t, t_0 \rangle|^2 \quad (2)$$

with

$$|t, t_0\rangle = \sum_e a_e(t, t_0) |e\rangle \quad (3)$$

The  $|e\rangle$  and the  $|f\rangle$  are eigenstates of the Hamiltonian under the *new* environment. Equation (3) shows the superposition state at time  $t$  generated by a sudden perturbation at time  $t_0$ . The coefficients  $a_e(t, t_0)$  may be calculated with knowledge of the previous Hamiltonian, of the nature of the perturbation, and also of the Hamiltonian under the new environment. This latter yields time-evolution factors  $\exp [(-i\omega_e - \frac{1}{2}\Gamma_e)(t - t_0)]$ , where  $\hbar\omega_e$  is the energy and  $\Gamma_e$  the damping constant of the state  $|e\rangle$ . In many cases the states  $|e\rangle$  will belong to the same hyperfine or Zeeman

structure and will have the same damping constant. Accordingly, we shall drop the subscript on  $\Gamma$ .

Insertion of (3) into (2) yields a sum of terms of the type

$$I_f(t, t_0) \propto \sum_{e, e'} [A + B \cos \omega_{ee'}(t - t_0) + C \sin \omega_{ee'}(t - t_0)] \exp [-\Gamma(t - t_0)] \quad (4)$$

where (here, as later) we write  $\omega_{ee'} = \omega_e - \omega_{e'}$ . It is often possible to choose the method of preparation so that either  $B$  or  $C$  is equal to zero. Equation (4) shows how the Bohr frequencies between levels of the excited superposition state appear as frequencies of modulation of the fluorescent light. Notwithstanding the very simple derivation offered here, the equation is indeed sufficient to describe the fluorescent light from free atoms in an optically thin vapor. It is implicit in many detailed studies of the interaction of light and atoms, for example, in the work of Breit<sup>(1)</sup> and of Barrat and Cohen-Tannoudji.<sup>(2,3)</sup> It disregards the differences in the time taken by light from different atoms to reach the detector, but these differences are negligibly small on the nanosecond scale for samples a few millimeters in extent.

When Eq. (4) is derived from first principles by means of the quantum theory of radiation the quantity we have called  $I_f(t, t_0)$  appears as the probability of occurrence of a process after which the atom is left in a state  $|f\rangle$  and the field is left as a coherent superposition of energy eigenstates for each of which the photon occupation number has increased by one unit. It is legitimate, therefore, to speak of one photon in the emitted field, but it is a mistake to suppose that the quantum energy of this photon is uniquely specified. Coherence between different energy eigenstates of the field implies coherence between time-dependent wave functions oscillating at different frequencies. A consequence of this coherence is that the probability that such a field will liberate a photoelectron at a detector is modulated. The modulation may be displayed by recording a large number of photoelectrons accumulated in a sequence of repetitions of the experiment, or as a transient current in a single-shot experiment. Since the modulation arises from coherence in the wave functions that enter into single quantum events, the term "quantum beat spectroscopy" has come into use to describe this kind of experiment.

Before leaving Eq. (4) it is to be noted that the coefficients  $A$ ,  $B$ , and  $C$  are not necessarily time independent. Whether they are or are not time-varying depends on the state of affairs before the sudden perturbation—the Hamiltonian might contain an oscillatory term—but in most spectroscopic applications these coefficients do not depend on time: The sole time dependence arises from the evolution of the system *after* the application of the perturbation.



## 1.2. *Methods of Preparation into Superposition States: Sudden Perturbations*

The “suddenness” of the symmetry-breaking perturbation is of the essence of the preparation of the system into a superposition state. (The preparation of the excited superposition state in a level-crossing experiment might appear to be an exception to this statement, but it is not, since the states that are coherently excited are eigenstates of the Hamiltonian exclusive of the interaction with the exciting light, that is, they are not eigenstates of the total Hamiltonian.) Among the common methods of preparation are excitation by pulses of light, of electrons, of ions, or by the sudden change of some parameter such as the electric or magnetic field. An important class of “sudden” preparations arises when an atom is formed from an ion by the capture of an electron, as in “beam-foil” experiments. Coherence effects generated in this and other ways are discussed in J. Andr  ’s article, Chapter 20 of this work.

Excitation by pulses is distinguishable from excitation by changes in some parameter since in the former case the environment before and after the pulse is the same, whereas in the latter this is not so. The former case takes on the characteristics of the latter if the pulse duration is long compared with the relaxation time of the atoms: the *essential* requirement is that the cutoff of the pulse be sudden, though it is *usually* desirable also that the duration of the pulse be short compared with the period of any modulation that is to be studied. Section 2 is mainly concerned with pulsed excitation, and Section 3 with sudden changes in magnetic and electric fields.

## 1.3. *Steady-State Excitation and Modulated Excitation: Applications*

It is instructive and useful to study the connection between pulsed excitation and steady-state excitation, on the one hand, and between pulsed excitation and modulated excitation on the other. Steady-state excitation, as, for example, by a resonance lamp emitting light at a constant rate, or by a uniform current of electrons, may be analyzed as a sequence of excitation pulses at random times, each pulse producing modulated fluorescence according to Eq. (4). In the case of the resonance lamp the pulses are constituted by wave packets of light whose coherence time is given roughly by the reciprocal of the spectral width. (Pulses of nanosecond duration, such as we have been considering until now, would contain many such wave packets). The interaction of the atoms with a succession of randomly phased wave packets is an incoherent set of processes so that the result of irradiation producing on average  $N$  excitations per second is given

by

$$I(t) \propto \int_0^t NI(t, t_0) dt_0 \quad (5)$$

with

$$I(t, t_0) \propto \sum_{e, e'} [A + B \cos \omega_{ee'}(t - t_0)] \exp [-\Gamma(t - t_0)] \quad (6)$$

a simplified version of Eq. (4). We have supposed the irradiation to have started at  $t_0 = 0$  and, by using the average rate of excitation, we have smoothed out the fluctuations. (A profound discussion of the phase problem and of the fluctuations of intensity in this type of calculation has been given by Durrant.<sup>(4)</sup>)

Carrying out the integration in (5) we have, for  $(t - t_0) \gg \Gamma^{-1}$ ,

$$I \propto N \left( \frac{A}{\Gamma} + \sum_{e, e'} \frac{B\Gamma}{\Gamma^2 + \omega_{ee'}^2} \right) \quad (7)$$

This expression is characteristic of level-crossing experiments. The interference terms (those with coefficient  $B$ ) vanish when the  $\omega_{ee'} \gg \Gamma$ .

Suppose now that the sequence of pulses is not random but that the rate of excitation is modulated according to  $N(t_0) = N_0(1 + m \cos \omega t_0)$ . Using this expression instead of  $N$  in Eq. (5) we obtain

$$\begin{aligned} I(t) \propto N_0 & \left( \frac{A}{\Gamma} + \sum_{ee'} \frac{B\Gamma}{\Gamma^2 + \omega_{ee'}^2} \right) \\ & + mN_0 \left[ \frac{A\Gamma}{\Gamma^2 + \omega^2} + \sum_{ee'} \frac{B\Gamma/2}{\Gamma^2 + (\omega - \omega_{ee'})^2} + \sum_{ee'} \frac{B\Gamma/2}{\Gamma^2 + (\omega + \omega_{ee'})^2} \right] \cos \omega t \\ & + mN_0 \left[ \frac{A\omega}{\Gamma^2 + \omega^2} + \sum_{ee'} \frac{B(\omega - \omega_{ee'})/2}{\Gamma^2 + (\omega - \omega_{ee'})^2} + \sum_{ee'} \frac{B(\omega + \omega_{ee'})/2}{\Gamma^2 + (\omega + \omega_{ee'})^2} \right] \sin \omega t \end{aligned} \quad (8)$$

It is seen that modulation of the rate of excitation has the consequences (a) that the intensity of fluorescent light is modulated at the same rate—this, of course, is to be expected, and (b) that resonances occur when  $\omega \approx \pm \omega_{ee'}$ . The resonance is to be seen in changes in the amplitude of modulation of the intensity variations. We notice that, if we are exploring a resonance with  $\omega \approx \omega_{ee'} \gg \Gamma$ , the expression for the intensity reduces to

$$I(t) \propto \frac{N_0 A}{\Gamma} + \frac{1}{2} \sum_{e, e'} \frac{mN_0 B}{[\Gamma^2 + (\omega - \omega_{ee'})^2]^{1/2}} \cos(\omega t - \phi)$$

where

$$\tan \phi = (\omega - \omega_{ee'})/\Gamma$$



The interference that is responsible for the resonance terms derives from a coherent superposition of the nondegenerate states  $|e\rangle$ ,  $|e'\rangle$ . The coherence results from the periodicity of the exciting pulses, not, as formerly, from the sudden application of a single pulse or short group of pulses.

Consider now the practical application of Eq. (7) (steady-state excitation), which is elaborated in the article on the level-crossing technique by Happer and Gupta (Chapter 9 of this work). "Resonances" are found at values of an applied magnetic field such that any of the  $\omega_{ee'}$  are zero. But to determine a fine or hyperfine interaction constant one needs to know a  $g$  factor, in addition to the experimentally determined magnetic field value, and this is normally done by carrying out a double-resonance experiment. However, this brings complications that are sometimes serious. It is necessary to provide a strong oscillating magnetic field in the MHz or GHz range. At best, this perturbs the atoms; at worst, it can set up a discharge in the cell that is difficult to control. However, the modulated-excitation technique can provide an elegant solution to this problem. The "resonance" may be shifted, according to Eq. (8), without the application of a strong, additional field on the sample. All that is necessary is to modulate the exciting light and to study the relationship between the frequency of the modulation and the shift of the resonance in the applied, static field. The validity of Eq. (8) has been established experimentally by Corney and Series<sup>(5,6)</sup> and by Skalinski *et al.*<sup>(7)</sup>

The technique of modulated excitation can be particularly useful in molecular spectroscopy, where one may be interested in measuring some small interval that responds only feebly to magnetic tuning. This situation arises, for example, where there is no electronic contribution to the magnetic moment but where, nevertheless, there may be paramagnetism on account of the rotation of the molecule. Magnetic moments arising in this way are of the order of nuclear magnetons. To explore the interval by double resonance would require an oscillating magnetic field of extremely high amplitude. The difficulty may be avoided by using modulated excitation, using an arrangement that generates a coherent superposition of the states whose separation is to be found. A recent application of this technique to  $I_2$  has been made by Broyer, Lehmann, and Vigué.<sup>(8)</sup>

## 1.4. Coherences between Different Atoms

### 1.4.1. Forward Scattering

In all that has gone before we have calculated the fluorescent intensity from many atoms in an ensemble by adding the intensities from individual atoms. This is a correct procedure for lateral scattering since the optical



paths to a point on the detector are random, but it is not correct for forward scattering in collimated light. Here, the paths from a plane-wave front in the incident beam to a parallel wave front in the scattered beam are independent of the position of the scattering atom, so that the fields scattered by all the atoms are coherent. This is the basis of the classical, atomic theory of dispersion. Because of this coherence it is possible to explore, by means of modulation techniques, classes of structures of greater generality than we have hitherto supposed.

The structures we have so far been concerned with are structures in the excited states of single atoms. In forward scattering we may expect to find evidence of structures in the lower states of atoms of the same kind, or, indeed, structures arising from differences between atoms of different kinds. As an example of this last class of structure, consider spectroscopic isotope shifts. Imagine a vapor consisting of a mixture of two isotopes excited by a plane wave front of light, pulsed, and of sufficient spectral width to excite corresponding transitions in the two kinds of atom. The atoms would respond resonantly at different frequencies, and the forward-scattered light from the two kinds of atom, being coherent, would beat at the difference frequency, that is, one would expect to find modulation at the frequency of the isotope shift. Since the individual resonances would be Doppler-broadened (and possibly pressure broadened), one would expect the modulation to damp out in a time given roughly by the reciprocal of the Doppler width.

An experiment of this kind has not, so far as we are aware, been performed, but a detailed analysis of forward scattering carried out by Corney *et al.*<sup>(9)</sup> showed that the level-crossing effects and the resonances in modulated light which are to be expected in double-resonance experiments should, indeed, be Doppler broadened for optically thin vapors, but that for optically thick vapors "coherence narrowing" should supervene (see Section 2.2). This was demonstrated experimentally for the zero-field level crossings in excited states of mercury and sodium. A very thorough study of level-crossing effects in forward scattering was carried out by Durrant and Landheer.<sup>(10)</sup>

That spectroscopic intervals between atoms of different kinds could be exhibited in forward scattering was shown by Hackett and Series,<sup>11</sup> who carried out the "level-crossing" equivalent of the modulation experiment described above. Changes in the intensity of forward-scattered light from a mixture of isotopes were observed when the Zeeman splitting of a particular transition was tuned into coincidence with the isotope shift. Since the interpretation is based on degeneracies in the transition frequencies rather than in the energy levels of single atoms, this kind of experiment was described as "line crossing" rather than "level crossing."



The possibility of observing coherence effects arising from structure in lower levels has recently been discussed by Chow *et al.*<sup>(12)</sup> The conditions that these authors derive are those that are valid in forward scattering, namely, that it should in principle be impossible to determine which atom of the assembly was responsible for the scattering, and also that any modulation effects should be damped through dephasing on account of Doppler broadening.

#### 1.4.2. Selective Reflection

Closely related to forward scattering is the phenomenon of selective reflection: the boundary of a vapor confined in a vessel behaves like a mirror if the vapor density is sufficiently high. The reflection coefficient is appreciable only in the region of an atomic absorption line, where a significant amount of light is scattered by the atoms. The light scattered from different atoms is coherent when the mean distance between neighboring atoms is substantially smaller than one wavelength, and when the ordinary geometrical conditions governing incident and scattered wavefronts are satisfied. Of course, the back-scattered light contains an incoherent component also: the relative intensity of the coherent and incoherent components depends on the vapor density.

The phenomenon of selective reflection is usually analyzed by treating the vapor as a homogeneous medium characterized by a (complex) refractive index derived from the polarizability of individual atoms. The reflection coefficient at the boundary can then be calculated by using classical electromagnetic theory. This treatment has been adequate for many investigations, though there are complications on account of the fact that the behavior of atoms near the wall of the vessel is not properly characterized by the bulk polarization of the medium (Cojan,<sup>(13)</sup> Schuurmans<sup>(14)</sup>).

All those classes of structure that were mentioned in the last section as capable of being studied in forward scattering, namely, structures in excited states and ground states of single atoms, and between atoms of different kinds—as, for example, spectroscopic isotope shifts—should also manifest themselves in specular reflection. Very little work has been done in this field, though the detailed analysis for level crossing and double resonance in excited states was carried out by Series<sup>(15)</sup> on the basis of the conventional theory, and the corresponding level-crossing experiment was done by Hanle and Stanzel.<sup>(16)</sup> The theory predicted that the level-crossing curve in reflected light under steady-state illumination of the vapor with white light should be similar to the ordinary (Lorentzian) level-crossing curve, except that it should be Doppler and pressure broadened. Explicit equations were given for the case of Doppler broadening. In the experiment, pressure



broadening predominated. Reflection from mercury vapor was studied under illumination with a mercury lamp. Zero-field level-crossing curves were obtained, several kG in width. The pressure-broadened damping constant under the conditions of the experiment (460 Torr) was 6.6 GHz, corresponding to a linewidth of 3.2 kG.

The more recent studies of Stanzel<sup>(17)</sup> and of Siegmund and Scharmann<sup>(18)</sup> show that the level-crossing curves are actually narrower than Series' theory predicts. The theory of Schuurmans is able to explain this narrowing in terms of the wall effect. (The coherence narrowing of level-crossing curves found in forward-scattered light is a different phenomenon. Its explanation lies in multiple scattering in the forward direction, not in a wall effect.)

There is little doubt that modulation phenomena could, in principle, be observed in light reflected from the boundary of a vapor under pulsed or modulated excitation. Study of such effects might at first sight seem impracticable on account of the very rapid loss of coherence arising from Doppler or pressure broadening. As to the latter, the vapor pressure need not be so high as in the example quoted (see, for example, Hansen and Webb<sup>(19)</sup>); as to the former, the Doppler effect could be eliminated by the techniques of saturated absorption and dispersion. The prospect is not so unattractive as would appear at first sight.

## 2. Pulsed Excitation: Lifetimes and Quantum Beats\*

Modulation of the light emitted from hydrogen atoms leaving a gas discharge through a channel in the cathode (canal rays) was observed about 50 years ago by van Traubenberg and Levy,<sup>(20)</sup> by Hertel,<sup>(21)</sup> and by Walerstein.<sup>(22)</sup> The modulation depended on the application of magnetic or electric fields to the canal rays and is an example of the effects we have been discussing. The phenomenon was interpreted in general terms on the basis of the known polarization properties of the Zeeman and Stark effects and on the classical model which Hanle<sup>(23,24)</sup> and others had used to describe the depolarization of resonance fluorescence by external fields, but the actual situation in hydrogen is, in fact, quite complicated and a detailed explanation could not be given.

With the revival of interest in resonance fluorescence in the late 1950s the phenomenon of modulation following pulsed excitation was discovered and studied in systems chosen for their simplicity. These we shall briefly describe below.

Since the early nineteen seventies, with the advantages offered by fast-pulse technology and tunable, pulsed lasers, the method of quantum

\* See also Chapter 20 of this work (J. Andr ).



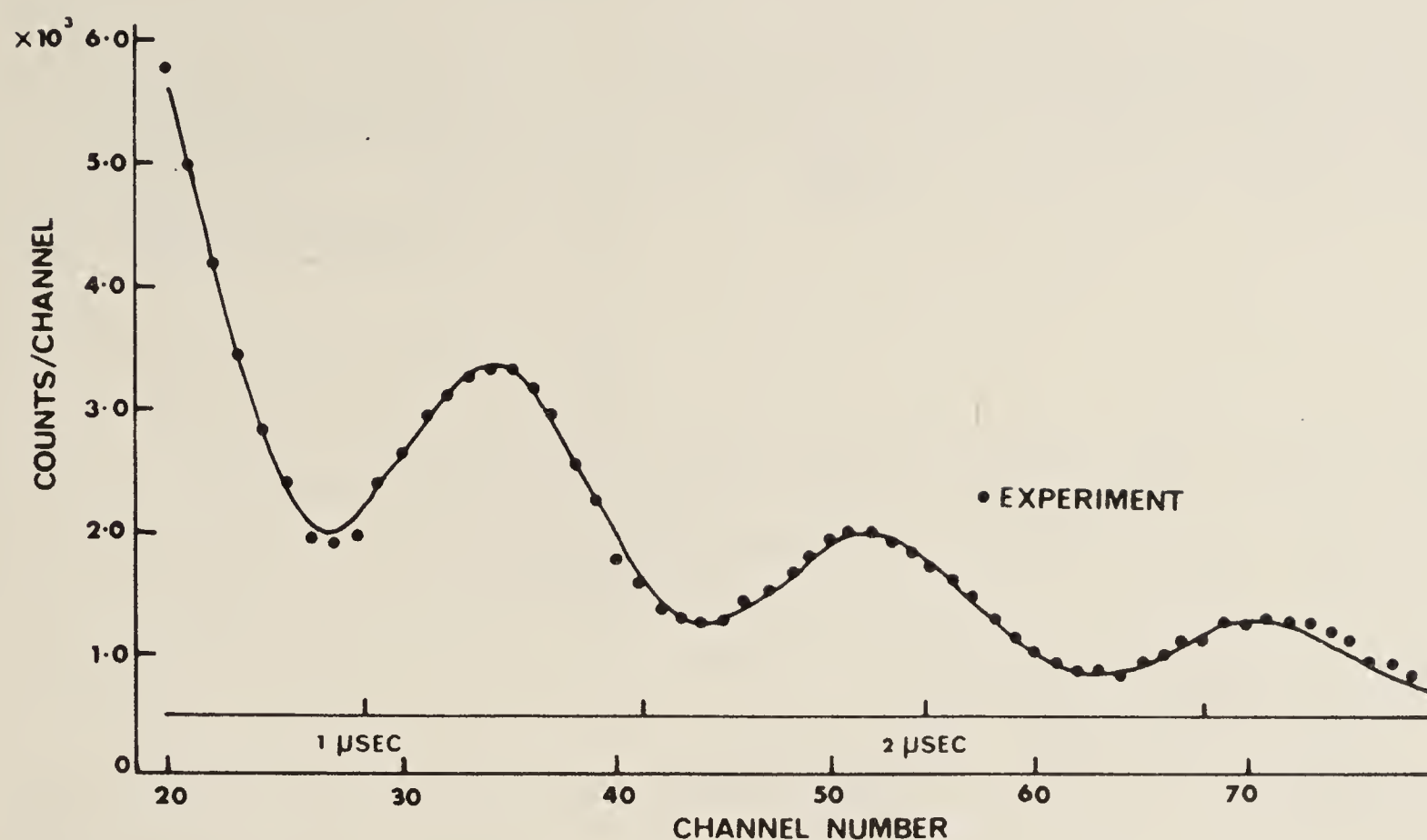


**Figure 1.** Modulation of fluorescence from the  $5^3P_1$  state of Cd. The points give the observed counts following a 200-ns pulse of optical excitation in a steady magnetic field of  $34.5 \mu\text{T}$  (from Dodd *et al.*<sup>(28)</sup>).

beats has been increasingly applied to the determination of fine and hyperfine structures and Stark splittings. We refer the reader to Haroche's review<sup>(25)</sup> for an account of this work. In the main part of this section we shall discuss the theory of quantum beat signals and shall single out for attention certain geometrical factors which arise also in steady-state and in modulated-fluorescence experiments. These geometrical factors are especially important in relation to the measurement of lifetimes.

## 2.1. Early Observations of Quantum Beats

### 2.1.1. Excitation by Resonance Radiation

Observation of modulation in fluorescent light from atoms excited by a pulse of resonance radiation was first reported by Aleksandrov<sup>(26)</sup> and, independently, by Dodd, Kaul, and Warrington.<sup>(27)</sup> The technique was improved by Dodd, Sandle, and Zissèrman,<sup>(28)</sup> whose experimental results are shown in Figure 1. The system studied was the vapor of Cd. The sinusoidal modulation at twice the Larmor frequency corresponds to the interval  $2g\mu_B B/\hbar$  between the levels  $M_J = \pm 1$  of the excited state  $5^3P_1$ . Figure 2 shows the levels and the transitions involved in excitation and in fluorescence.

The transition  $J = 0$  to  $J = 1$  lends itself particularly well to a classical interpretation. To achieve coherent excitation of the levels  $M_J = \pm 1$  the incident light is polarized at right angles to the magnetic field as shown in

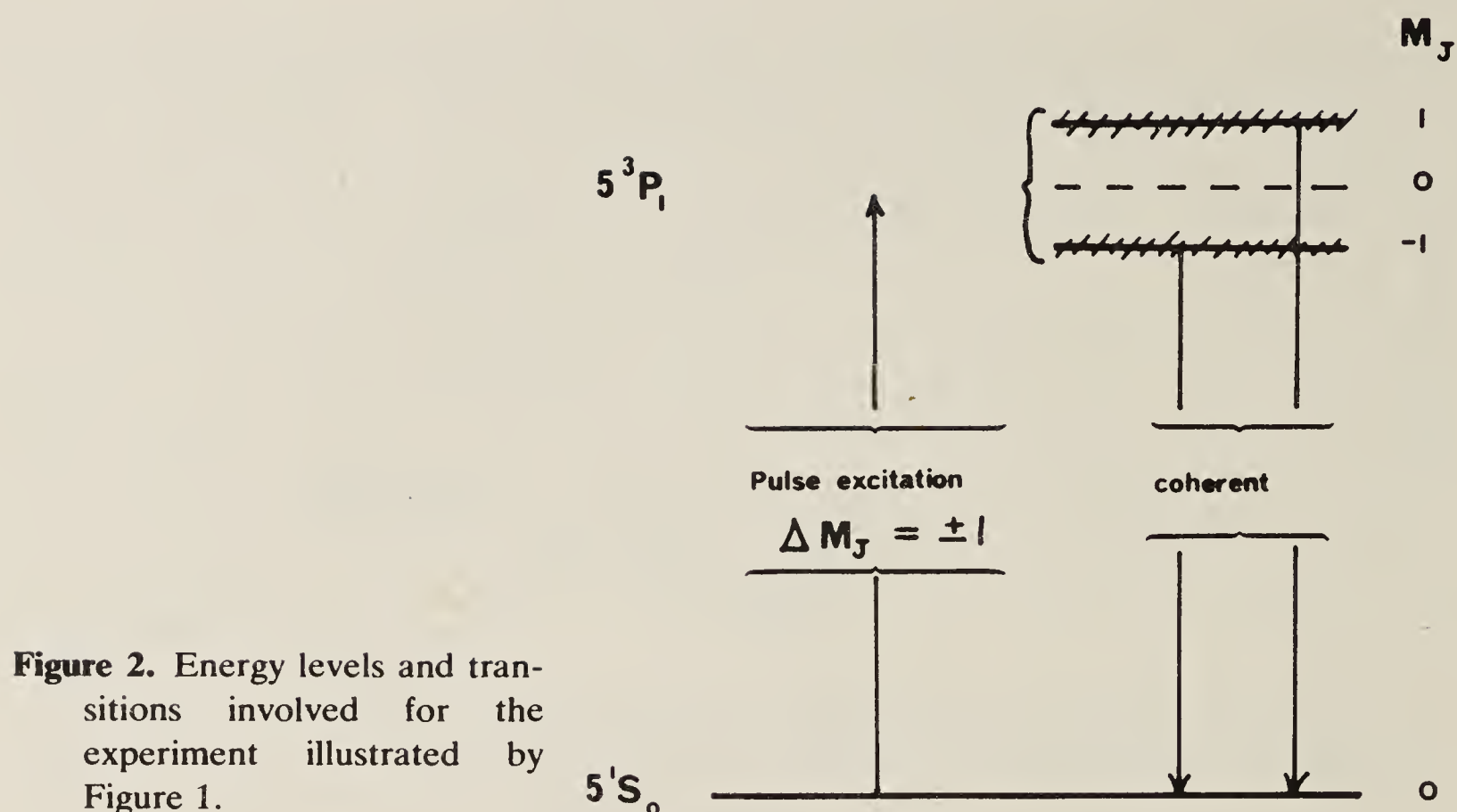


**Figure 2.** Energy levels and transitions involved for the experiment illustrated by Figure 1.

Figure 3a. Oscillating electric dipoles excited by light of this polarization experience a torque under the field and precess round it (Figure 3b). The anisotropy of the radiation pattern from a group of dipoles excited by a pulse of light results in a modulated response of the detector at twice the frequency of precession (twice the Larmor frequency). A field strength is chosen so that several such periods occur within the mean lifetime of the excited atoms. Clearly, the depth of modulation is dependent on the ratio of the duration of the exciting pulse to the period of precession. It will be noticed from the caption of Figure 1 that the duration of the pulse, about 200 ns, was substantially smaller than the period of the precession, about 700 ns, but not

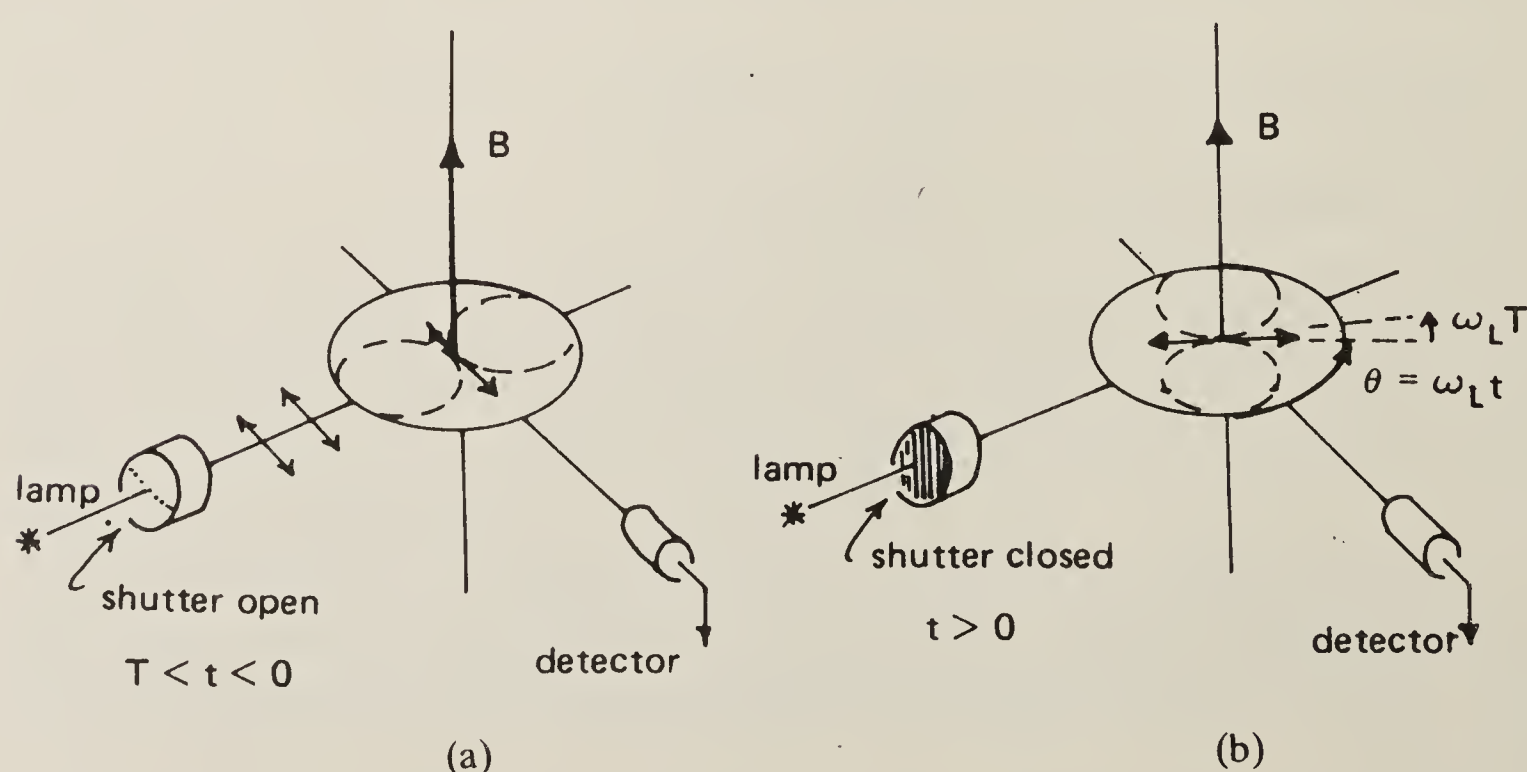


**Figure 3.** Classical model to illustrate modulated fluorescence. (a) Creation of dipoles by a short pulse of light. (b) Precession of bunched dipoles.



negligibly so. The depth of modulation is seen to be less than 100%. A measurement of the frequency of modulation gave the Landé factor of the excited state and the mean lifetime could be ascertained from the envelope of the modulation.

### 2.1.2. Excitation by Electrons

It was first demonstrated by Hadeishi and Nierenberg<sup>(29)</sup> that quantum beats could be produced by excitation of atoms with a short pulse of electrons. Again, the system studied was cadmium vapor. The states  $M_J = \pm 1$  of  $5^3P_1$  were excited coherently and the modulation observed in the fluorescent light corresponded to the Bohr frequency between them.

A more recent exploratory study of beats excited by electron impact has been reported by Bagaev *et al.*<sup>(30)</sup> The Zeeman components of  $n^1D_2$  ( $n = 4, 5, 6$ ) of He I were excited coherently in the gas by pulses of about 10 ns duration. The modulated fluorescence was studied for a range of magnetic fields of the order of tens of gauss, and it was concluded that, in experiments of this kind, unknown  $g$  factors could be determined to an accuracy of about 1 in  $10^4$ . This figure indicates the kind of accuracy one might hope to attain in a set of carefully executed experiments, but it should not be taken as indicating the best that could be achieved if the method were pushed to its limit.

The method of excitation by electron impact with the object of measuring lifetimes was applied to helium in the early nineteen fifties by Heron *et al.*<sup>(31)</sup> Since then it has been used extensively. Recent examples are to be found in the series of elegant experiments by King, Adams, and their co-workers.<sup>(32-34)</sup> A highly monoenergetic beam of electrons impinges on a jet of atoms to be studied. The energy of an inelastically forward-scattered electron is recorded. This defines the state of excitation of the target atom and the instant of excitation. The intensity of the fluorescent light as a function of time is studied by recording delayed coincidences between exciting electrons and fluorescent photons. Impressive accuracy has been achieved in the determination of the mean lifetime of a number of excited states in Hg I and Cd II.

For further examples the reader is referred to the article by R. G. Fowler, Chapter 26 of this work.

## 2.2. Excitation by Light, Theory: Geometrical Characteristics

In this section we amplify the simple expressions given in Section 1 and give an equation for the intensity of fluorescent light in terms of sums over

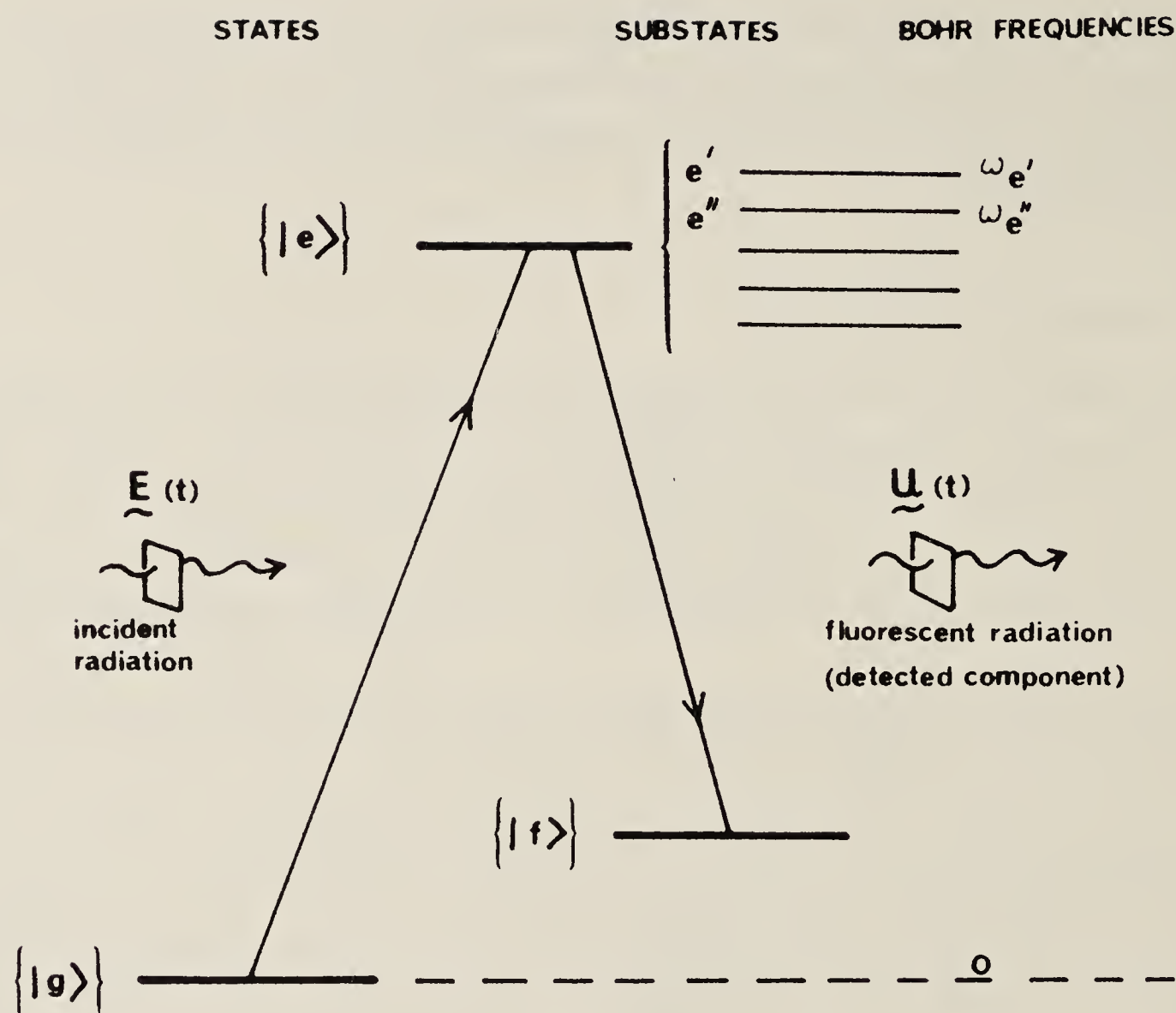


Figure 4. Illustration of the notation used in the theory of fluorescence.

eigenstates of energy and component of angular momentum, ( $\alpha, J, M_J$  or  $\alpha, F, M_F$ , for example). We then show how, by using expansions in terms of irreducible spherical tensors, the geometrical factors may be separated and all irrelevant quantum numbers eliminated.

Figure 4 shows the scheme we have in mind. The initial, excited, and final states ( $g, e, f$ , respectively) may each have structure, and we use primes to distinguish substates. The substates have been shown explicitly only for the excited state: the superposition-states of the analysis will be formed from these. When summations over  $g$  and  $f$  occur, these will describe incoherent processes.

We describe the light fields classically by  $\mathbf{E}(t)$  for the incident light and by  $\mathbf{U}(t)$  for that component of the fluorescent light that is detected. It is supposed that the spectrum of  $\mathbf{E}(t)$  is sufficiently broad to extend uniformly over the complex of transitions from the  $|g\rangle$  to the  $|e\rangle$ , making due allowance for Doppler broadening of the absorption line.  $\mathbf{e}$  and  $\mathbf{u}$  are unit vectors corresponding to  $\mathbf{E}$  and  $\mathbf{U}$ .

The following expression can be obtained by first-order perturbation theory for the intensity of fluorescent light at time  $t$  from  $N$  atoms supposed



initially to be distributed uniformly over the states  $|g\rangle$ :

$$\begin{aligned}
 I(t) = G \int_{-\infty}^t \int_{-\infty}^t dt'_0 dt_0 E^*(t'_0) E(t_0) \\
 \times \sum_{\substack{e, e' \\ f, g}} \langle g | \mathbf{e}^* \cdot \hat{\mathbf{D}} | e' \rangle \exp [(i\omega_{e'} - \tfrac{1}{2}\Gamma)(t - t'_0)] \langle e' | \mathbf{u}^* \cdot \hat{\mathbf{D}} | f \rangle \\
 \times \langle f | \mathbf{u} \cdot \hat{\mathbf{D}} | e \rangle \exp [(-i\omega_e - \tfrac{1}{2}\Gamma)(t - t_0)] \langle e | \mathbf{e} \cdot \hat{\mathbf{D}} | g \rangle
 \end{aligned} \quad (9)$$

The constant  $G$  is the accumulation  $(\mu_0/4\pi)(N\omega^4/8\pi c\hbar^2 r^2)$ , where  $\omega$  is the (average) optical frequency and  $r$  is the (average) distance from the sample. Equation (9) may easily be interpreted. Reading from right to left, the matrix element  $\langle e | \mathbf{e} \cdot \hat{\mathbf{D}} | g \rangle$ , together with a factor  $(i/\hbar) dt_0 E(t_0)$  is the increment of probability amplitude of  $|e\rangle$  which is created in time interval  $dt_0$  by the interaction Hamiltonian  $-\mathbf{E}(t_0) \cdot \hat{\mathbf{D}}$ ;  $\hat{\mathbf{D}}$  is the operator representing electric dipole moment. Next, the exponential term represents the evolution of  $|e\rangle$  from  $t_0$  to  $t$  (Bohr frequency  $\omega_e$ , amplitude damping coefficient  $\frac{1}{2}\Gamma$ ). Then the matrix element  $\langle f | \mathbf{u} \cdot \hat{\mathbf{D}} | e \rangle$ , together with factors from  $G$ , gives the element of electric field polarized along  $\mathbf{u}$  at distance  $r$  in emission from  $|e\rangle$ . Summation over the  $|e\rangle$  and integration over  $t_0$  gives the total field. The terms next following from right to left are the Hermitian conjugate expressions, which, correspondingly summed and integrated, give the complex conjugate field. The product gives the intensity. The prime on  $e'$  exhibits the possibility of interference between channels.

### 2.2.1. The Pulse Approximation

If the field  $E(t_0)$  were specified the integrations could be carried out, but in fact the measurable properties of light fields are expressible in terms of the statistically averaged quantities  $\Phi_{\alpha\beta}(t_0, \tau) = \langle E_\alpha^*(t_0 + \tau) E_\beta(t_0) \rangle$  (subscripts denote space components), and the observed  $I(t)$  will similarly be the result of a statistically averaged equation (9). For the broadband light that we have postulated it will be a good approximation to write  $\langle E^*(t'_0) E(t_0) \rangle = \Phi(t_0) \delta(\tau)$ , where  $\tau = t'_0 - t$ .  $\Phi(t_0)$  is the statistically averaged intensity of the field  $\mathbf{E}$  at time  $t_0$ . Inserting  $\Phi(t_0) \delta(\tau)$  in Eq. (9), we may carry out one of the time integrations and the equation has then been brought to the form used in Section 1, Eq. (5). What we have done here is to justify the so-called “pulse approximation.”

It should be understood that, since the above treatment rests on a first-order perturbation theory, it does not incorporate stimulated emission, but this does not mean that it cannot be used for the irradiation of atoms by laser light. The first point to notice is that we have specialized to broadband light, so that there is, in this approximation, no temporal coherence. The

second point to notice is that, in the context of quantum beats, the light is detected *after* the irradiation has ceased: Thus the observed fluorescence arises from spontaneous emission. However, both strong and weak light fields may, by optical pumping, change the distribution of population over the substates of  $|g\rangle$ . This can be taken into account, if necessary, by incorporating a weighting factor in the summation over  $g$ .

### 2.2.2. Excitation and Monitoring Operators

To return to Eq. (9), it may now be observed that the summed expression may be written as the trace of the product of two operators:

$$\sum_{\substack{e, e' \\ f, g}} \langle \dots \rangle = \text{Tr} \{ \hat{\rho}(\mathbf{e}, t, t_0) \hat{L}(\mathbf{u}) \} \quad (10)$$

with

$$\hat{\rho}(\mathbf{e}, t, t_0) = \sum_g |e\rangle\langle e| \mathbf{e} \cdot \hat{\mathbf{D}} |g\rangle \exp [(-i\omega_{ee'} - \Gamma)(t - t_0)] \langle g| \mathbf{e}^* \cdot \hat{\mathbf{D}} |e'\rangle \langle e'| \quad (11)$$

$$\hat{L}(\mathbf{u}) = \sum_f \mathbf{u}^* \cdot \hat{\mathbf{D}} |f\rangle\langle f| \mathbf{u} \cdot \hat{\mathbf{D}} \quad (12)$$

$\hat{\rho}(\mathbf{e}, t)$  is the density operator of the excited states at time  $t$ . (Its matrix is not normalized to unity because of the damping coefficients.)  $\hat{L}(\mathbf{u})$  is called a "monitoring operator" for the emission of electric dipole radiation which leaves the atoms in the states  $|f\rangle$ . Equation (10) is often used when the density operator has been obtained for more complicated situations and by more elaborate methods.

For our purposes we wish to separate  $\hat{\rho}(t, t_0)$  into factors that represent the excited system at time  $t_0$  and the subsequent evolution from  $t_0$  to  $t$ , as follows:

$$\hat{\rho}(\mathbf{e}, t, t_0) = \hat{P}_e \hat{F}(\mathbf{e}) \hat{P}_{e'} \exp [(-i\omega_{ee'} - \Gamma)(t - t_0)] \quad (13)$$

with

$$\hat{F}(\mathbf{e}) = \sum_g \mathbf{e} \cdot \hat{\mathbf{D}} |g\rangle\langle g| \mathbf{e}^* \cdot \hat{\mathbf{D}} \quad (14)$$

an expression formally identical with that for  $\hat{L}(\mathbf{u})$ . We call  $\hat{F}(\mathbf{e})$  the excitation operator.  $\hat{P}_e, \hat{P}_{e'}$  are the projection operators  $|e\rangle\langle e|, |e'\rangle\langle e'|$ . This factorization has reduced the expression for the intensity, Eq. (2.1), to the form

$$I(t, t_0) = G \int_{-\infty}^t dt_0 \Phi(t_0) \text{Tr} \{ \hat{P}_e \hat{F}(\mathbf{e}) \hat{P}_{e'} \hat{L}(\mathbf{u}) \exp [(-i\omega_{ee'} - \Gamma)(t - t_0)] \} \quad (15)$$



We have already discussed the time dependence. We now concentrate on the geometrical factors which are to be found in the excitation and monitoring operators  $\hat{F}(\mathbf{e})$  and  $\hat{L}(\mathbf{u})$ .

### 2.2.3. Irreducible Spherical Tensor Operators

The summations over  $g$  and  $f$  that occur in  $\hat{F}$  and  $\hat{L}$  suggest that it may be possible to find a basis for these operators in which the summation is automatically carried out, and this is indeed the case. The basis that serves this purpose is that of the standard components of irreducible spherical tensor operators. The simplification that is obtained derives from the fact that the spin-1 light vector is a simpler object than the combination of atomic angular momenta that it couples. We can make use of this simplification in respect of those states that are effectively degenerate, as the  $g$  and  $f$  states are in our analysis, but it is of the essence of our problem that the nondegenerate excited states must be distinguished, so we must expect to find in our final equations the quantum numbers that differentiate these states from one another and factors that represent their projection on to the basis of the spherical tensors. Similar factors for the substates  $|g\rangle$  would arise if weighting factors on account of optical pumping were present. In what follows we shall suppose that the  $|g\rangle$  are equally weighted.

### 2.2.4. Quantum Beats at Hyperfine Frequencies

The construction of spherical tensor operators is explained in the article by K. Blum, Chapter 2 of this work. The operators are labeled by integers  $k, q$ . When formed from angular momentum states  $|J, M_J\rangle$  the values of  $k$  run from  $J + J'$  to  $|J - J'|$ , and the values of  $q$  from  $k$  to  $-k$ . Operators for the hyperfine states  $|F, M_F\rangle$  are constructed similarly. Tensors that represent the polarization of the light are formed from spherical unit vectors in three-dimensional physical space. The possible values of  $k$  are 2, 1, 0. Thus, the  $k, q$  component of the tensor that represents the incident light is

$$E_q^k = (2k + 1)^{1/2} \sum_{\mu, \mu'} \begin{pmatrix} 1 & 1 & k \\ -\mu & -\mu' & q \end{pmatrix} e_{-\mu} e_{-\mu'}^* \quad (16)$$

The  $e_\mu$  ( $\mu = 0, \pm 1$ ) are components of the vector  $\mathbf{e}$  along the unit vectors in the spherical basis. In terms of the Cartesian components of  $\mathbf{e}$ , the  $e_\mu$  are

$$e_0 = e_z, \quad e_{\pm 1} = \mp (e_x \pm ie_y)/2^{1/2} \quad (17)$$

For the  $k, q$  tensor component of the fluorescent light we shall use the symbol  $U_q^k$ , formed from the components of  $\mathbf{u}$ .

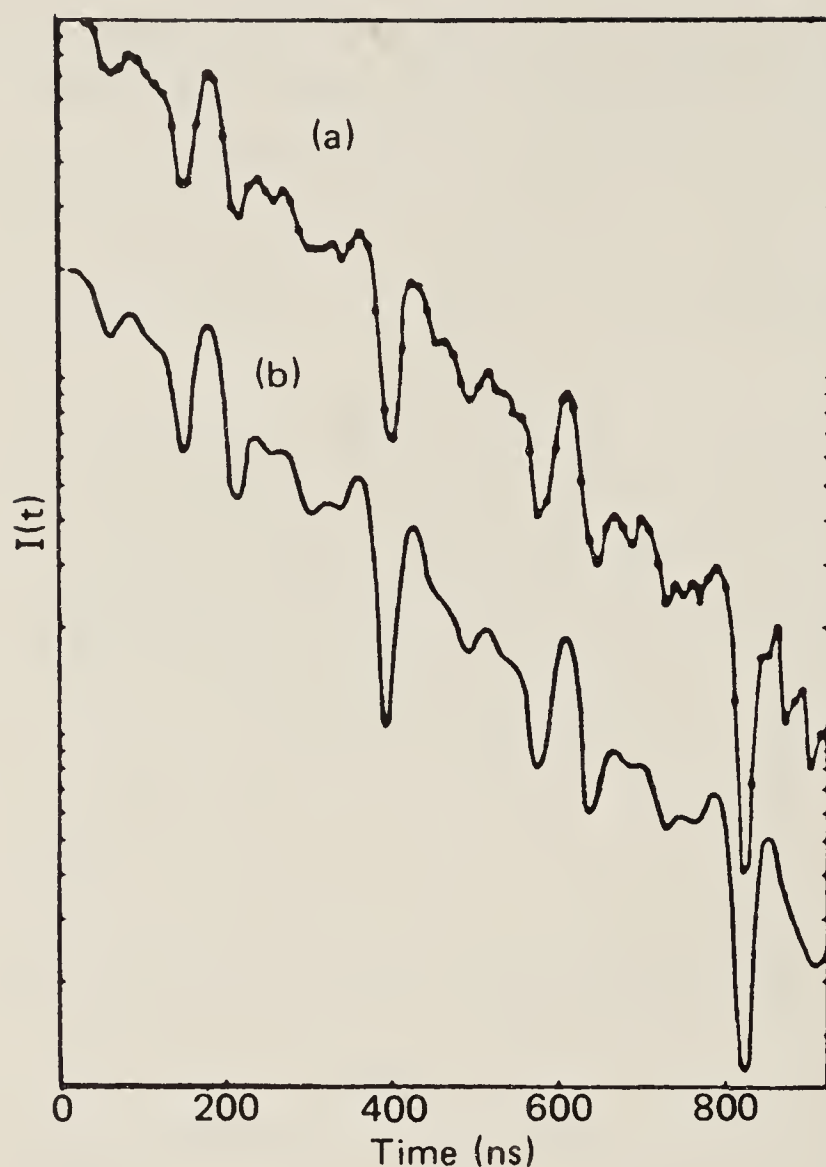


**Figure 5.** Quantum beats arising from hyperfine structure in  $9^2D_{3/2}$  of  $^{133}\text{Cs}$ .  $I(t)$  is plotted on a logarithmic scale. (a) Experimental points. (b) Evaluation of (18) for this case (from Deech *et al.*<sup>(36)</sup>).

The orthogonal properties of the tensor operators result in a separation of terms having the same value of  $k$ . Hence the expression for  $I(t, t_0)$  is reduced to a sum of nine terms only for each pair of states,  $|e\rangle, |e'\rangle$ , namely, for  $k = 2$ , five terms, for  $k = 1$ , three terms, and for  $k = 0$ , one term.

We give the result of the analysis for the case of atoms having hyperfine structure, in zero magnetic field. For this case the spherical tensor analysis is particularly appropriate, since the hyperfine structure of the states  $|g\rangle$  and  $|f\rangle$  is quite irrelevant to the problem of determining the hyperfine structure of the states  $|e\rangle$ . Equation (9) requires the summation over all these structures explicitly, whereas the corresponding expression in spherical tensor analysis contains no reference to the structures  $|g\rangle$  and  $|f\rangle$ . Moreover, we find in the spherical tensor expression no reference to the space-quantized hyperfine states  $|M_F\rangle$  for  $e, g$ , or  $f$ , since, the atom being in zero magnetic field, these are all degenerate. On the contrary, the  $|e\rangle$  in Eq. (9) would be the individual states labeled  $|J_e, F_e, M_{F,e}\rangle$ , and similarly for the  $|g\rangle$  and the  $|f\rangle$ .

The expression for the intensity in spherical tensor notation is

$$\begin{aligned}
 I(t, t_0) = & G |\langle J_e || \hat{\mathbf{D}} || J_g \rangle|^2 \times |\langle J_e || \hat{\mathbf{D}} || J_f \rangle|^2 \\
 & \times \sum_{\substack{k, q, \\ F_e, F'_e}} (-1)^{F'_e - F_e + q} E_q^k U_{-q}^k A^k(F_e, F'_e) B^k(F'_e, F_e) \\
 & \times \exp \{ [-i\omega(F_e, F'_e) - \Gamma](t - t_0) \}
 \end{aligned} \tag{18}$$



We distinguish the states  $e, e'$  by their hyperfine quantum numbers  $F_e, F'_e$ . The initial and final states appear specified only by their electronic quantum numbers,  $J_g$  and  $J_f$ .

In the first line of (18) we find the reduced matrix elements of the electric dipole operator between the  $|g\rangle$  and the  $|e\rangle$ , on the one hand, and between the  $|e\rangle$  and the  $|f\rangle$ , on the other.

In the second line we find the light tensors  $E_q^k$  and  $U_{-q}^k$ , defined by Eq. (16).

The quantities  $A^k, B^k$  in the second line are, effectively,  $6-j$  symbols which project the  $|e\rangle$  and the transition dipoles on to the  $k, q$  basis. They are

$$\begin{aligned}
 A^k(F_e, F'_e) &= (-1)^{3I+2J_g-J_e-F_e} \\
 &\times [(2F_e+1)(2F'_e+1)(2J_e+1)(2J_g+1)]^{1/2} \\
 &\times \left\{ \begin{matrix} k & J_e & J_e \\ I & F'_e & F_e \end{matrix} \right\} \left\{ \begin{matrix} k & J_e & J_e \\ J_g & 1 & 1 \end{matrix} \right\} \quad (19)
 \end{aligned}$$

$B^k(F_e, F'_e)$  is the same expression with  $J_g$  replaced by  $J_f$ . It is to be noticed that the quantity that occurs in Eq. (18) is  $B^k(F'_e, F_e)$ , not  $B^k(F_e, F'_e)$ .

The last line of Eq. (18) exhibits the modulation of the fluorescent light at the hyperfine frequencies  $\omega(F_e F'_e) = [E(F_e) - E(F'_e)]/\hbar$ , and radiative decay of the free atom at the rate  $\Gamma$ .

Details of the derivation of Eq. (18) have been given by Luypaert.<sup>(35)</sup> In Figure 5 we show experimental results for  $^{133}\text{Cs}$  which are compared, in the lower curve, with an evaluation of Eq. (18) for this case. [The numerical results were, in fact, checked against an evaluation of Eq. (15) and found to be identical.]

An example of the application of spherical tensors to Zeeman structures is to be found in Carrington and Corney.<sup>(37)</sup>

In Sections 2.2.5–2.2.7 we consider some characteristics of the multipoles and show how, by paying attention to the geometrical aspects of an experiment, we can select those multipoles that convey the information we require. The discussion is not limited to hyperfine structures: indeed, it applies to level-crossing and other atomic coherence effects, not solely to quantum beats.

### 2.2.5. Characteristics of the Multipoles

The multipoles  $k = 0, 1$  and  $2$  have the following interpretation:

(a)  $k = 0$ . A scalar quantity related to the excited state population. The  $k = 0$  component of the intensity is measurable, either by integrating the fluorescence over all directions, or by biasing the polarization components of the emission in some particular direction so as to represent a space average.

(b)  $k = 1$ . A vector part related to the degree of orientation in the excited state and therefore reflected in the content of circular polarization of the fluorescence.

(c)  $k = 2$ . A tensor part related to the degree of alignment in the excited state and therefore reflected in the content of linear polarization of the fluorescence.

The properties of the 6- $j$  symbols involving  $k$  and the quantum numbers  $F_e$  (for example) lead to the result that, for terms having  $k = 0$ ,  $F_e = F'_e$ . Modulation effects are therefore not to be expected either in the integrated light from the assembly or for those geometrical configurations that allow only the  $k = 0$  component to be recorded. Similarly, terms with  $|F_e - F'_e| = 2$  arise only in association with  $k = 2$ , and terms with  $|F_e - F'_e| = 1$  only with  $k = 1$ .

Terms with  $k = 0, 1$ , and  $2$  arise in Eq. (18) if circularly polarized light is used in the exciting and fluorescent beams, but with linearly polarized light one finds only  $k = 0$  or  $2$ . These results may be obtained as shown below.

### 2.2.6. Linearly Polarized Light

Recall that  $\mathbf{e}$  and  $\mathbf{u}$  are unit vectors along the polarization directions of the exciting and detected beams. Let these directions be chosen as principal axes of the tensors  $E$  and  $U$ , respectively. Then the only nonvanishing components of  $E$  and  $U$  are

$$E_0^k = (2k + 1)^{1/2} \begin{pmatrix} 1 & 1 & k \\ 0 & 0 & 0 \end{pmatrix} = (U')_0^k \quad (20)$$

where the prime on  $U$  reminds us that we are referring to  $U$  to a principal axis different from that of  $E$ . Referred to the same axis as that of  $E$ , we have

$$U_0^k = \sum_q R_{q0}^k (U')_q^k = R_{00}^k (U')_0^k \quad (21)$$

(since components of  $U'$  having  $q \neq 0$  are zero), where the  $R_{q0}^k$  are components of the matrix that describes a transformation of axes from  $\mathbf{e}$  to  $\mathbf{u}$ .

Looking back now to Eq. (18) we see that  $U_0^k$  is the only component of  $U^k$  that we need, since it is to couple with  $E_0^k$ , which is the only nonvanishing component of  $E^k$ . Finally, the only terms in (18) that do not vanish are those containing the factor

$$E_0^k U_0^k = (2k + 1) \begin{pmatrix} 1 & 1 & k \\ 0 & 0 & 0 \end{pmatrix}^2 P_k(\cos \theta) \quad (22)$$



where we have written  $P_k(\cos \theta)$ , the Legendre polynomial, as the rotation matrix element.  $\theta$  is the angle between  $\mathbf{e}$  and  $\mathbf{u}$ .

From the symmetry properties of the  $(3-j)$  symbol we learn that  $\begin{pmatrix} 1 & 1 & k \\ 0 & 0 & 0 \end{pmatrix}$  vanishes for  $k = 1$ . Equation (22) tells us, therefore, that the use of linear polarizers and analyzers cannot produce terms other than  $k = 0$  or 2. Moreover, we read from the  $P_k(\cos \theta)$  term that there is no angular dependence for  $k = 0$  and that the angular dependence for  $k = 2$  is as  $(3 \cos^2 \theta - 1)$ . If  $\theta$  is chosen to make this expression vanish ( $54.7^\circ$ ) the light reaching the detector will be represented by the  $k = 0$  terms only. With pulsed excitation the light will be unmodulated and will represent the decay of excited-state population. With steady-state excitation there will be no level-crossing effect.

### 2.2.7. Circularly Polarized Light

Let the directions of the principal axes of  $E$  and  $U$  now be chosen along the directions of propagation of the exciting and fluorescent beams. By this choice, again, the polarization vector of the light is one of the basis vectors ( $e_1$  or  $e_{-1}$  in this case), and the only nonvanishing components of the tensor are those with  $q = 0$ , namely,

$$E_0^k = (2k + 1)^{1/2} \begin{pmatrix} 1 & 1 & k \\ -1 & +1 & 0 \end{pmatrix} = (U')_0^k \quad (23)$$

As before we have

$$E_0^k U_0^k = (2k + 1) \begin{pmatrix} 1 & 1 & k \\ -1 & +1 & 0 \end{pmatrix}^2 P_k(\cos \theta) \quad (24)$$

The conclusion is that the fluorescent light may contain components  $k = 0$ , 1, and 2, but that, for  $\theta = 90^\circ$  the  $k = 1$  component will vanish because of the vanishing of  $P_1(\cos \theta) \equiv \cos \theta$ . This is an important result in relation to the study of hyperfine structures in  $S$  states. Electronic alignment ( $k = 2$ ) cannot exist in such states, so if modulation (or coherence) effects are to be studied one must select the  $k = 1$  component of fluorescence. Since this is zero for  $\theta = 90^\circ$  one must choose some geometrical configuration where, *not only* is the light circularly polarized, *but also* the exciting and fluorescent beams are at some angle other than  $90^\circ$ .

### 2.2.8. Density-Dependent Effects: Multipolar Damping Coefficients

The equations we have given so far relate to the fluorescence of an assembly of isolated atoms. As has been shown by (among others) D'yakonov and Perel',<sup>(38,39)</sup> Omont,<sup>(40)</sup> Happer and Mathur,<sup>(41)</sup> and Car-

rington *et al.*,<sup>(42)</sup> the method of expansion in multipoles is powerful also when the atomic density is increased to the point that other interactions occur. There are two important effects. First, when the atomic density increases or the vapor cell volume is large enough, radiation trapping may occur: The fluorescence from one excited atom may excite others before the radiation leaves the cell and is detected. This is particularly likely when the lower state of the fluorescence is the atomic ground state. It will be appreciated that this multiple scattering of radiation in all directions has the effects (i) of increasing the lifetime of the fluorescence, and (ii) of changing the polarization character of the light that escapes.

The second effect is that of collisions between atoms. In simple cases the same electronic excitation ( $J$ ) will be preserved, though it may be transferred from one atom to another, but the orientation or alignment of  $\mathbf{J}$  will become randomized (transfer between levels of different  $M_J$  or  $F$  or  $M_F$ ). In more complicated cases the excitation may be transferred to levels of different electronic excitation and the fluorescence may be lost to the detector.

The effects of radiation trapping and of the simple cases of collisions may be described formally by admitting the existence of different decay constants for the different multipoles. Thus, in Eq. (18),  $\Gamma$  is to be replaced by  $\Gamma^k$ . Three different damping constants, that is, three different lifetimes, make their appearance in the fluorescent light.  $\Gamma^0$  is not affected by collisions (in the simple cases) and, according to D'yakonov and Perel',<sup>(38)</sup> the effect of radiation trapping is expressed by the equation

$$\Gamma^0/\Gamma = \pi^{-1/2} \int_{-\infty}^{\infty} \exp(-t^2) \exp[(L/l_0) \exp(-t^2)] dt \quad (25)$$

an integral which is tabulated by Mitchell and Zemansky.<sup>(43)</sup>  $L$  is a characteristic dimension of the scattering cell and  $l_0$  is the mean free path of a photon whose wavelength is at the peak of the optical transition.  $\Gamma^0$  can be determined in the case of the field-free situation we have analyzed by setting polarizer and analyzer at  $54.7^\circ$  to one another. When a damping constant is determined from Hanle-effect experiments using linear polarizers it is  $\Gamma^2$  that is measured, but  $\Gamma^0$  can be determined directly at finite magnetic fields, as was shown by Gunn and Sandle,<sup>(44)</sup> by orienting the field in the (111) direction relative to Cartesian axes determined by the directions of linear polarizer and analyzer.

The decay constants  $\Gamma^0$  and  $\Gamma^2$  for mercury atoms in zero magnetic field were determined over a range of vapor densities by Deech and Baylis<sup>(45)</sup> by direct measurements of the decay of fluorescence. With an analyzer parallel to the polarizer, two exponential components were present, characterized by  $\Gamma^0$  and  $\Gamma^2$ . The former could be isolated by setting the analyzer at  $54.7^\circ$  with respect to the polarizer, and the latter evaluated



by subtraction. It was confirmed that the values of  $\Gamma^2$  obtained from these decay curves were in satisfactory agreement with values obtained from Hanle-effect experiments over the limited range of vapor density where reliable values could be obtained from both kinds of experiment. At low densities the subtraction procedure was impracticable. Values of  $\Gamma^2$  obtained from Hanle-effect experiments at these low densities tended towards the same limit at zero density as did values of  $\Gamma^0$ .

The general expression for the  $\Gamma^k$  in terms of  $\Gamma$ , the free-atom decay constant, is

$$\Gamma^k = \Gamma - C^k(\Gamma - \Gamma^0) + \Gamma_{(\text{coll})}^k \quad (26)$$

where

$$C^k = 1 \quad \text{for } k = 0$$

$$C^k = \frac{3}{10}(2J_e + 1)[6 + (-1)^k] \left\{ \frac{1}{J_e} \quad \frac{1}{J_e} \quad \frac{k}{J_g} \right\}^2 \quad \text{for } k = 1, 2$$

it being understood that this applies only when the initial and final states are the same ( $J_g = J_f$ ). Estimates of  $\Gamma_{(\text{coll})}^k$  can be made from expressions given in the literature cited.

In the so-called “quenching” collisions the energy of excitation is lost by transfer out of the original state to some different electronic state of either of the collision partners. Part of the energy may be lost as kinetic energy, or as vibrational energy if the colliding particle is a molecule of a foreign gas, or in a variety of other conceivable ways. The decay constant for the population of atoms in the initially excited state is, for these “quenching” collisions, represented by

$$\Gamma_{\text{total}}^0 = \Gamma^0 + \Gamma_{(\text{coll})}^0, \quad \text{where } \Gamma_{(\text{coll})}^0 \propto \nu \quad (27)$$

$\Gamma^0$  is determined by measuring the total decay constant as a function of density of the perturbing species,  $\nu$ , and extrapolating to zero density.

For some types of quenching collisions the reverse collisions contribute significantly to the population of the initially excited state. The decay of fluorescent light then ceases to follow a single exponential. It may be represented by a sum of exponential terms, each characterized by a different rate constant. An example is reported in a recent paper by Pendrill.<sup>(46)</sup> The rate constant of the dominant term tends to the  $\Gamma_{\text{total}}^0$  of the single-exponential decay at lower pressures. The rate constants of the other terms are related to the decay of the partner states and to the collisional rate constants. All these rate constants appear also in the equations describing sensitized fluorescence.

### 2.2.9. Experimental Techniques and Results

For details of the experimental realization of the foregoing analyses and for results that have been obtained we must refer the reader to Haroche's review,<sup>(25)</sup> to the original papers already cited, and to the article by R. G. Fowler, Chapter 26 of this work.

### 2.3. Superposition States of Mixed Parity

The modulation effects that have been described hitherto have been ascribed to the synchronous precessions of radiating atomic dipoles, motions that find quantum-mechanical expression in terms of coherent superpositions of states of different electronic orientation. It was supposed that the spontaneous decay constants for all states forming the superposition were identical. When this is not the case modulation can arise in the integrated intensity of the light received. Clearly, this can no longer be interpreted as a "searchlight effect" or as the spatial interference of components of different polarization, but it may be regarded as a temporal interference: radiation from each excited atom is periodically restrained and released by the coherent mixing of dipoles of different strengths oscillating at different frequencies. An example of such a situation is to be found in the superposition of states of opposite parity: the superposition of the  $2S$  and  $2P$  states of atomic hydrogen is a case in point. An early analysis of the effects to be expected by pulse excitation and by modulated excitation of these states was given by Series<sup>(47)</sup> and is represented in Figure 6. It was supposed that the atoms were in an electric field so that the eigenstates of the Hamiltonian for  $n = 2$  were superpositions of the  $S$  and  $P$  states. (For the purposes of the present argument we may neglect the spin.) The symmetry-breaking perturbation was the application of Lyman- $\alpha$  light which was to excite atoms from the ground state  $1S$  to the  $P$  components of the two nondegenerate  $2S$ - $2P$  superpositions. Modulation of the emitted Lyman- $\alpha$  light was to be expected at the frequency interval between the Stark-shifted  $S$ - $P$  levels.

The experimental realization of this kind of superposition-state has been achieved by Bashkin *et al.*,<sup>(48)</sup> by Sellin *et al.*,<sup>(49)</sup> by Andr <sup>(50)</sup> and co-workers, and most recently by van Wijngaarden *et al.*<sup>(51)</sup> These last authors allow a beam of hydrogen atoms in the metastable state  $2^2S_{1/2}$  to enter a region where they suddenly experience an electric field that is very accurately known. Atoms in pure  $S$  states as they enter the electric field are no longer in eigenstates of the atom in the field but are in superpositions of the  $S$ - $P$  eigenstates. They begin to radiate modulated Lyman- $\alpha$  light, which appears as a periodic spatial luminosity of the beam and which is measured by a movable detector. The modulation may be envisaged as a



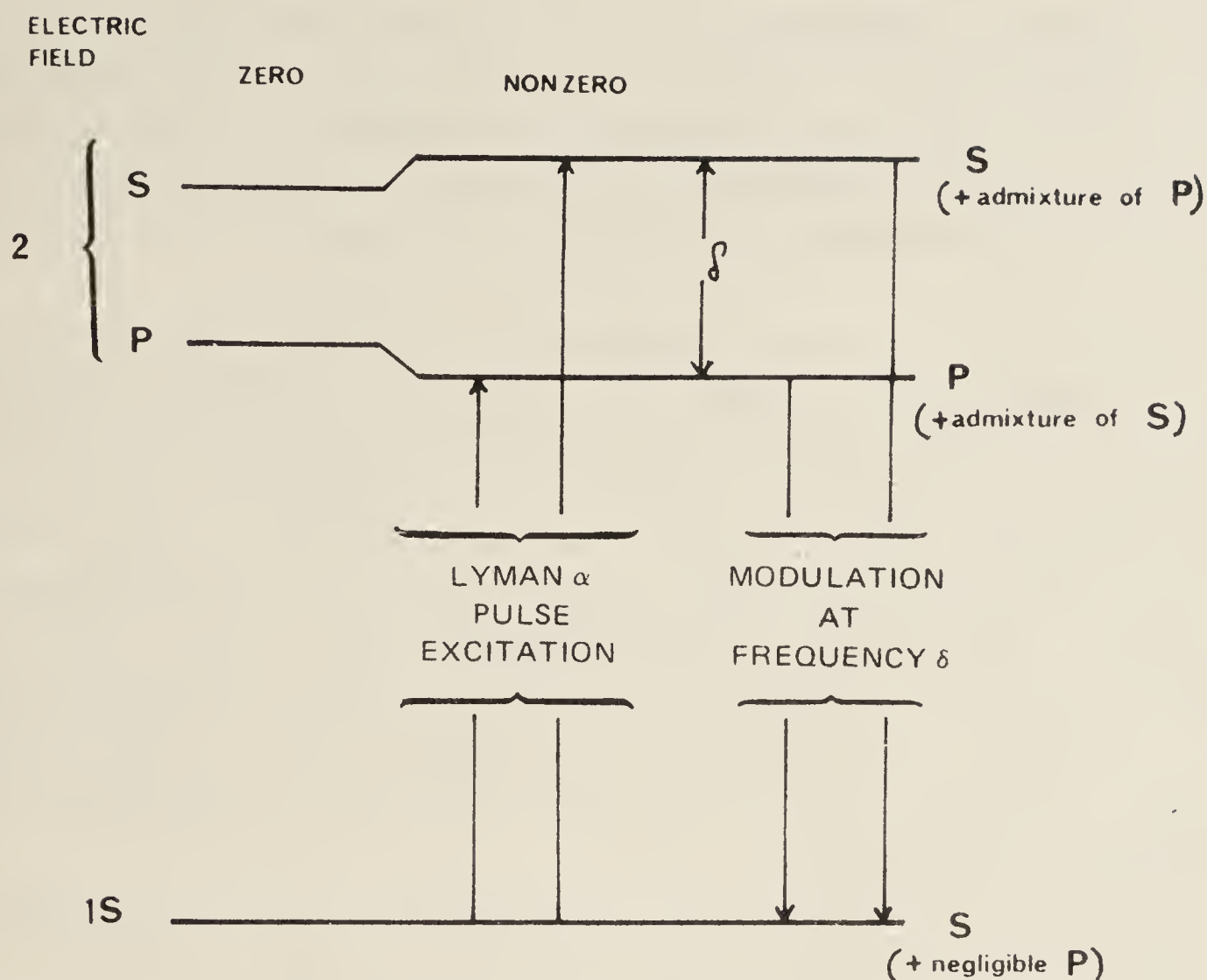


**Figure 6.** Representation of modulated fluorescence from superposition of  $S$  and  $P$  states in hydrogen.

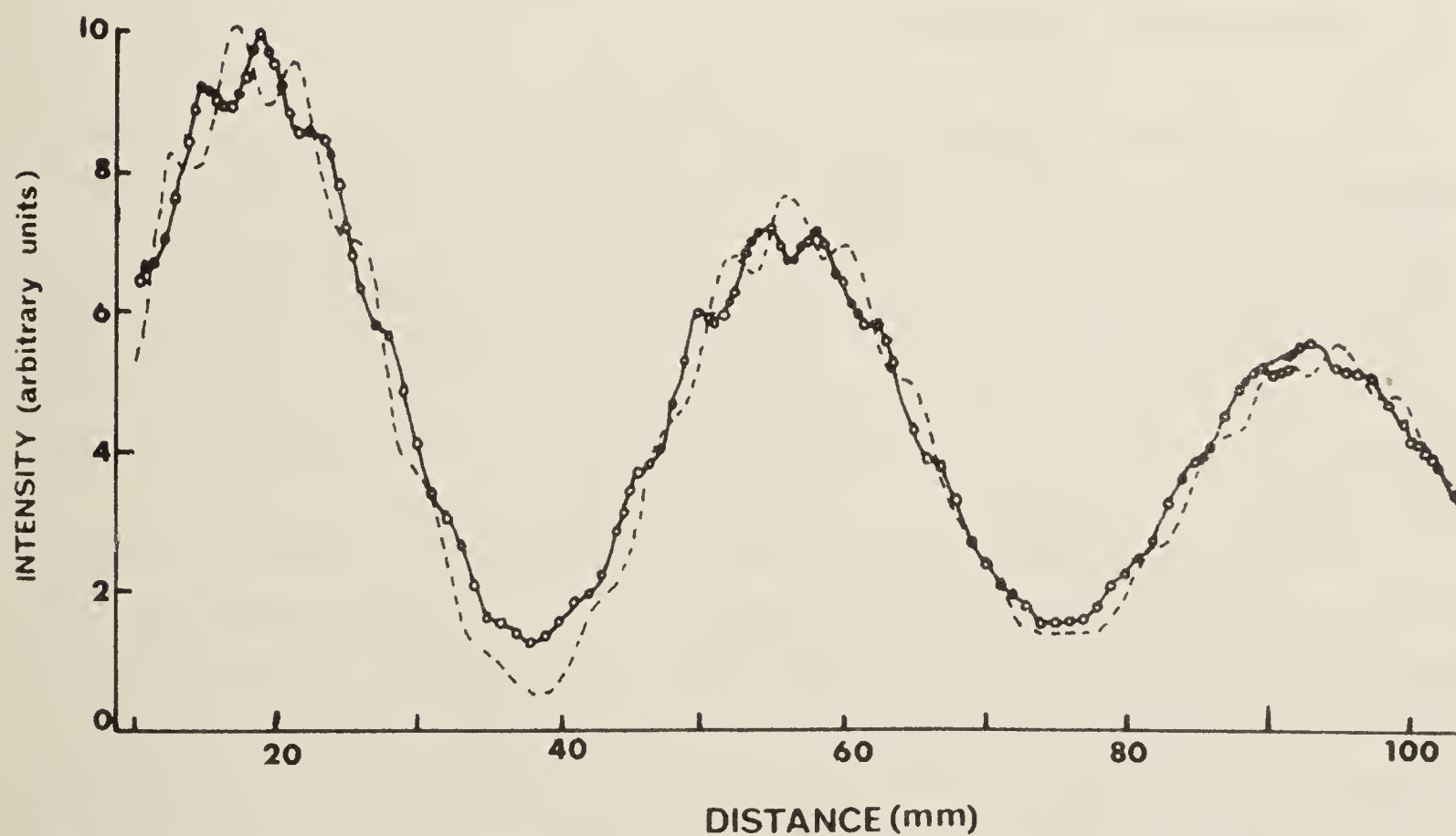


**Figure 7.** Modulated fluorescence from  $S$ - $P$  superposition states in hydrogen (from van Wijngaarden *et al.*<sup>(51)</sup>). The low-frequency modulation arises from  $S_{1/2}$ - $P_{1/2}$  superpositions; the high-frequency from  $S_{1/2}$ - $P_{3/2}$ . The broken curve represents the results of a theoretical analysis in which the onset of the field was supposed to be sudden. Closer agreement with the experimental curve was obtained when allowance was made for the fringing field.

periodic oscillation of population between pure  $S$  and  $P$  states, the latter being strongly radiative and the former metastable. The modulation frequencies that have been observed in this experiment (Figure 7) correspond to the whole complex of Bohr frequencies in the  $n = 2$  state, that is to say, the intervals between all the hyperfine components of  $2^2S_{1/2}$ ,  $2^2P_{1/2}$ , and  $2^2P_{3/2}$ .

The fascination of these experiments is that the modulation of the fluorescent light provides a direct record of the interval between the  $S$  and  $P$  states in hydrogen, which is the Lamb-shift interval (slightly modified by the electric field). No claim is made for the experiments that have been described that they give a value for the Lamb shift better than has been obtained by other methods, but it is hoped that the method—or something related to it—may be applied to hydrogenlike ions of high  $Z$  for which accurate values of the Lamb shift are needed. If the behavior of hydrogen under a symmetry-breaking pulse can be understood in detail, it will be possible to interpret with confidence the behavior of hydrogenlike ions under similar circumstances.

### 3. Pulsed (Stepped) Magnetic and Electric Fields

#### 3.1. Pulsed Magnetic Field

The transients observed in the intensity of fluorescence of atoms subjected to a pulse of some excitation process were analyzed in Section 2. Similar transients can be observed under conditions of constant excitation but following a sudden change in some physical quantity that affects the atomic structure. For example, a sudden change in the steady value of an electric or a magnetic field that determines the energies of the state of the atom gives rise to a transient in the intensity as it settles to a new steady-state value.

An early application was reported by Dehmelt.<sup>(52)</sup> A beam of circularly polarized sodium  $D$  light is passed through a cell containing sodium vapor, the dimensions and vapor density being such that about 50% absorption occurs. The intensity  $I + \Delta I$  of the transmitted beam is greater than the initial intensity  $I$  because the optical pumping process removes sodium atoms from those ground-state Zeeman sublevels which more strongly absorb the circularly polarized light. A sudden reversal of the magnetic field (about  $50 \mu T$  parallel to the optical beam) reverses the role of the ground-state sublevels. The intensity drops suddenly to  $I - \Delta I$  and then relaxes back to  $I + \Delta I$  with a lifetime dependent on the rate of the pumping process (proportional to  $I$ ) and of other relaxation processes such



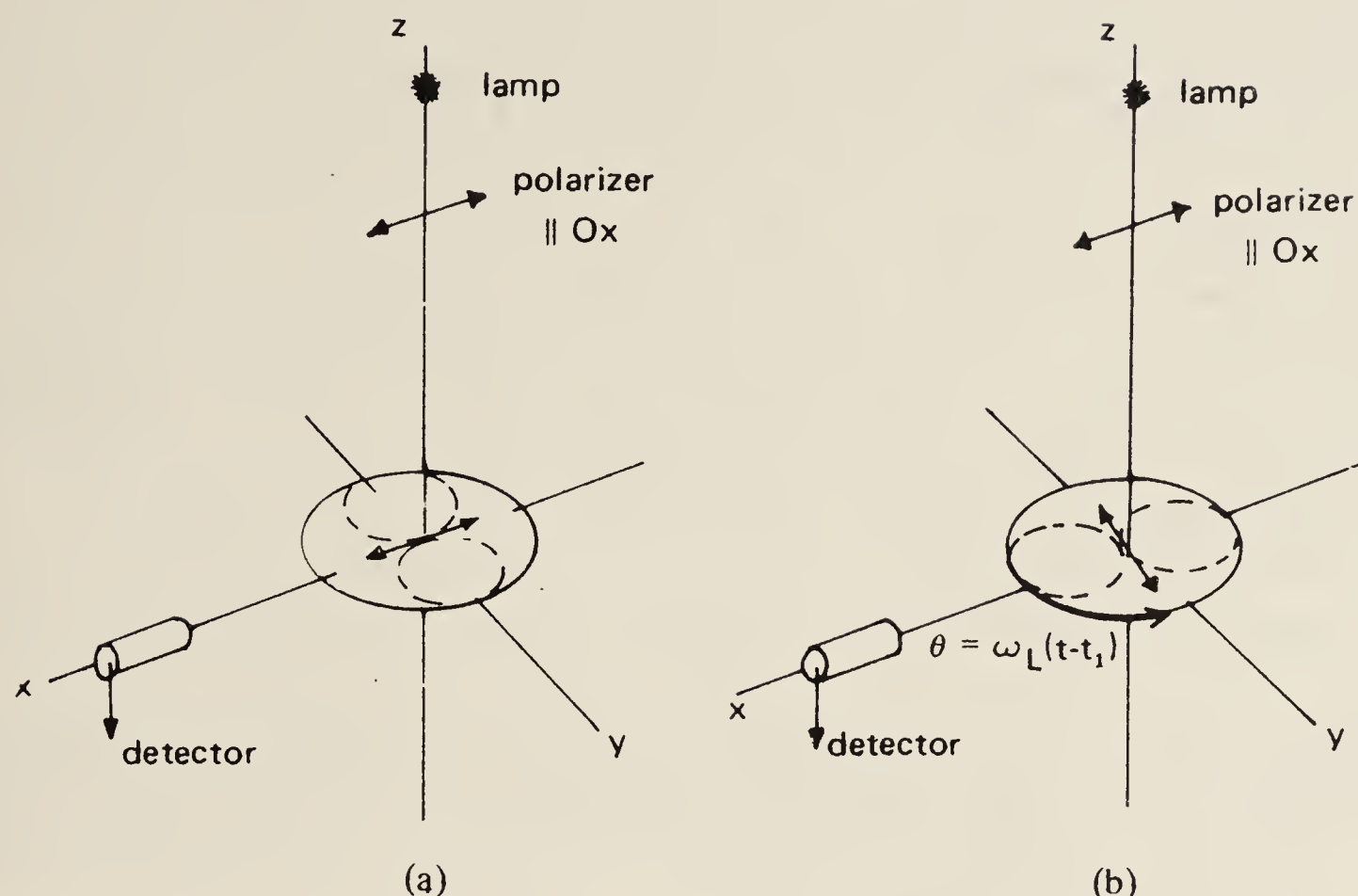


**Figure 8.** The stepped magnetic field experiment. (a) Magnetic field zero: Detector records zero intensity. (b) At time  $t$  the dipoles have precessed through  $\theta = \omega_L(t - t_1)$ . The intensity at the detector is modulated at the angular frequency  $2\omega_L = -2g\mu_B B/h$ .

as wall collisions and collisions between atoms of sodium and the buffer gas in the cell.

An application of the principle in the observation of resonance fluorescence was made by Dodd *et al.*<sup>(53)</sup> Here the resonance fluorescence of the  $6^1S_0 \leftrightarrow 6^3P_1$  (254 nm) line in mercury was observed. The method may readily be appreciated by appealing to a classical model. Consider the case of incident radiation, polarized parallel to the  $x$  axis, exciting a sample of atoms situated in a cell at the origin. This is illustrated in Figure 8. The dotted contour represents the polar distribution of fluorescent intensity in the  $x$ - $y$  plane appropriate to a  $J = 1 \leftrightarrow J = 0$  transition as in Figure 3a. Under conditions of zero magnetic field the axis of the equivalent dipole remains stationary in space. A detector placed along the  $x$  axis records zero intensity—the zero of the normal Hanle signal.

When a steady magnetic field  $B$  along the  $z$  axis is suddenly switched on at time  $t = t_1$ , all previously established equivalent classical dipoles (i.e., atoms excited with  $t_0 < t_1$ ), begin to precess about the  $z$  axis at the Larmor frequency  $\omega_L = -g\mu_B B/h$ ; at time  $t$  they lie at an angle to the detector given by  $\theta = \omega_L(t - t_1)$ . As these dipoles rotate, radiate, and decay, other dipoles are excited and rotate, their angle to the detector at time  $t$  being given by  $\theta = \omega_L(t - t_0)$ . Under the transient condition the intensity oscillates with frequency  $2\omega_L$ , damped with a mean lifetime  $\tau^{(2)} = 1/\Gamma^2$ , and

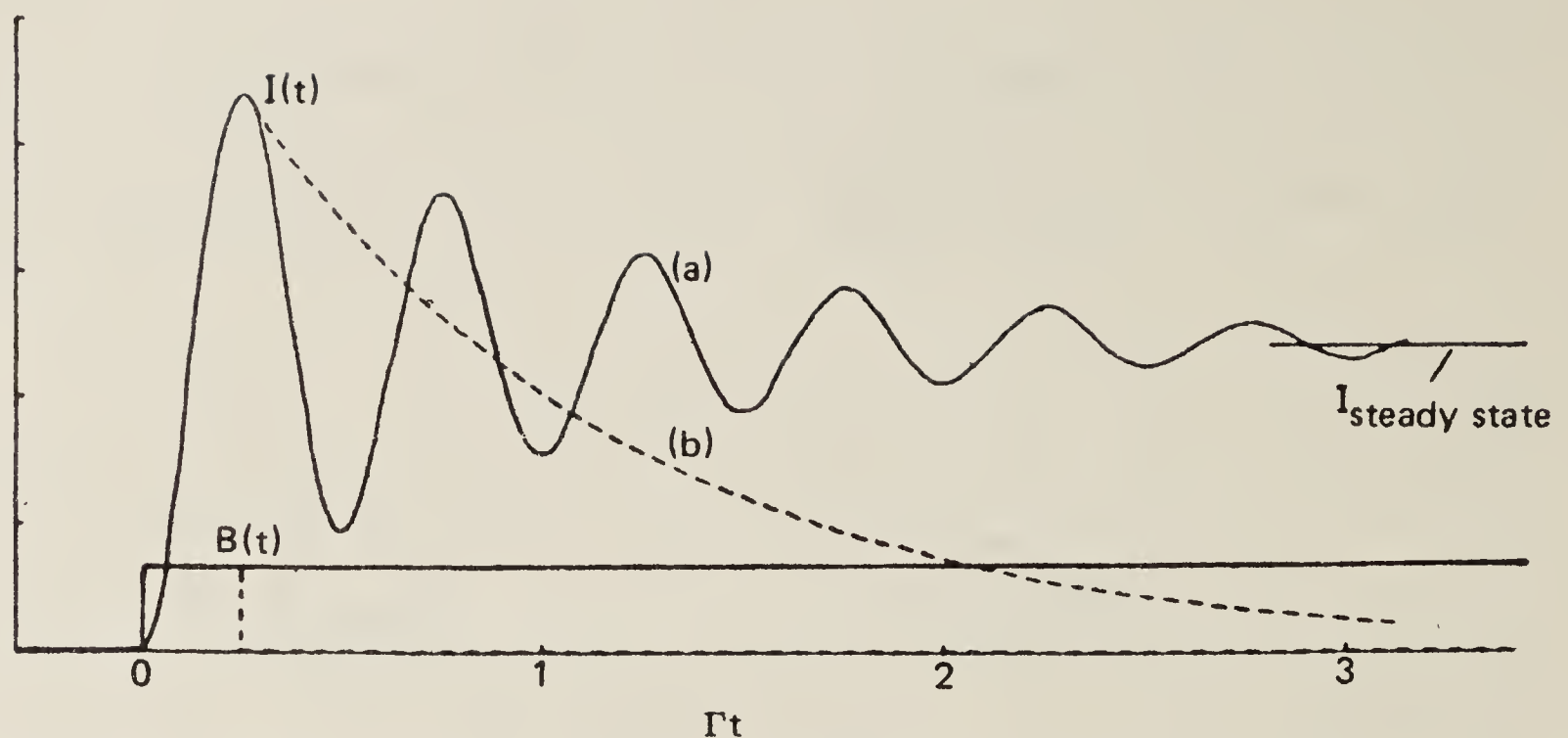


**Figure 9.** Predicted intensity in the stepped magnetic field experiment. (a) The modulation case: The magnetic field is such that two periods of modulation occur in one mean lifetime ( $4\pi/2\omega_L = \tau$ ). (b) The exponential case: The magnetic field is switched off after a time interval equal to a half period of modulation [ $(t_2 - t_1) = \pi/2\omega_L = \tau/4$ ].

settles to a new steady-state intensity appropriate to a point on the wings of the Hanle signal in the field  $B$ . If the magnetic field is suddenly switched off the intensity decays exponentially back to zero with the same mean lifetime. Figure 9 shows the two kinds of transients. The experiment yields the values of  $g$  and  $\tau^{(2)}$  independently (it is the product  $g\tau^{(2)}$  that is determined from the width of the Hanle curve).

A quantum-mechanical description of the above experiment can readily be given by adapting the theory in Sections 1 and 2. The intensity  $I(t, t_0)$  is calculated as before, the interaction with the field  $B$  being written into the Hamiltonian. The geometrical arrangement shown in Figure 8 generates alignment ( $k = 2$ ), the formation of a superposition state from  $J = 1$ ,  $M_J = \pm 1$ , and so leads to the expression

$$I(t, t_0) \propto \sin^2 \theta \exp [-\Gamma(t - t_0)] \quad (28)$$

where  $\theta = \omega_L(t - t_1)$  for  $t_0 \leq t_1$  and  $\theta = \omega_L(t - t_0)$  for  $t_0 \geq t_1$ . The intensity at time  $t$  is obtained by integrating over  $t_0$  from  $-\infty$ , through the discontinuity at  $t_1$ , up to  $t$ . The result is

$$I(t) \propto \frac{4\omega_L^2}{\Gamma^2 + 4\omega_L^2} - \frac{2\omega_L}{(\Gamma^2 + 4\omega_L^2)^{1/2}} \cos [2\omega_L(t - t_1) - \phi] \exp [-\Gamma(t - t_1)] \quad (29)$$

with  $\tan \phi = \Gamma/2\omega_L$ . The first term on the right is just the steady-state Hanle signal; the second is the damped oscillation of the transient signal. The exponential decay following sudden switching of the field to zero is obtained by introducing a further discontinuity at  $t_2 (> t_1)$ , and, for  $t > t_2$ ,



fixing  $\theta$  at the values reached at  $t = t_2$ . For a more complicated atomic system, the method of expansion in multipoles would lead to a generalization of Eq. (28). Transients of other kinds may be described by a generalization of Eq. (29).

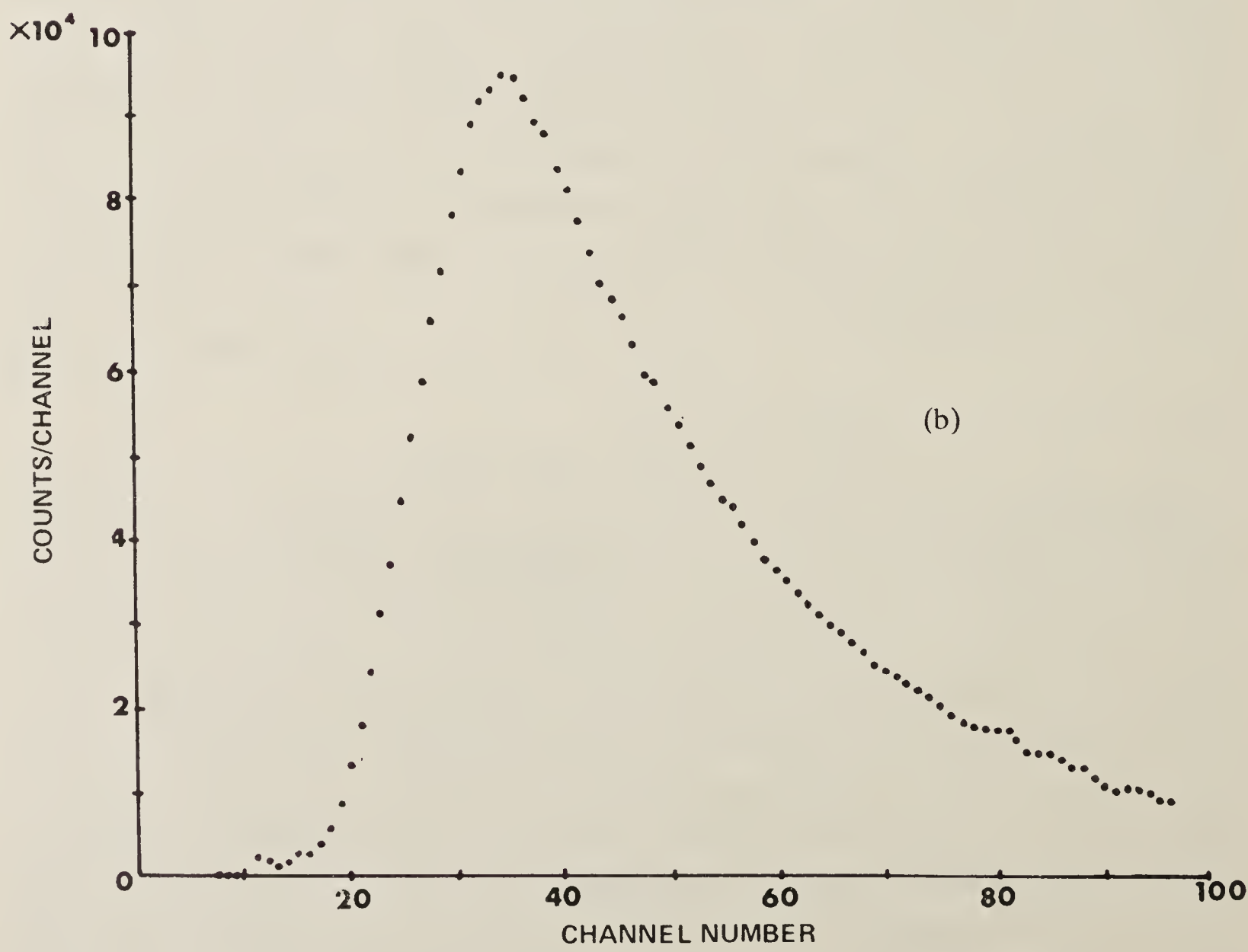
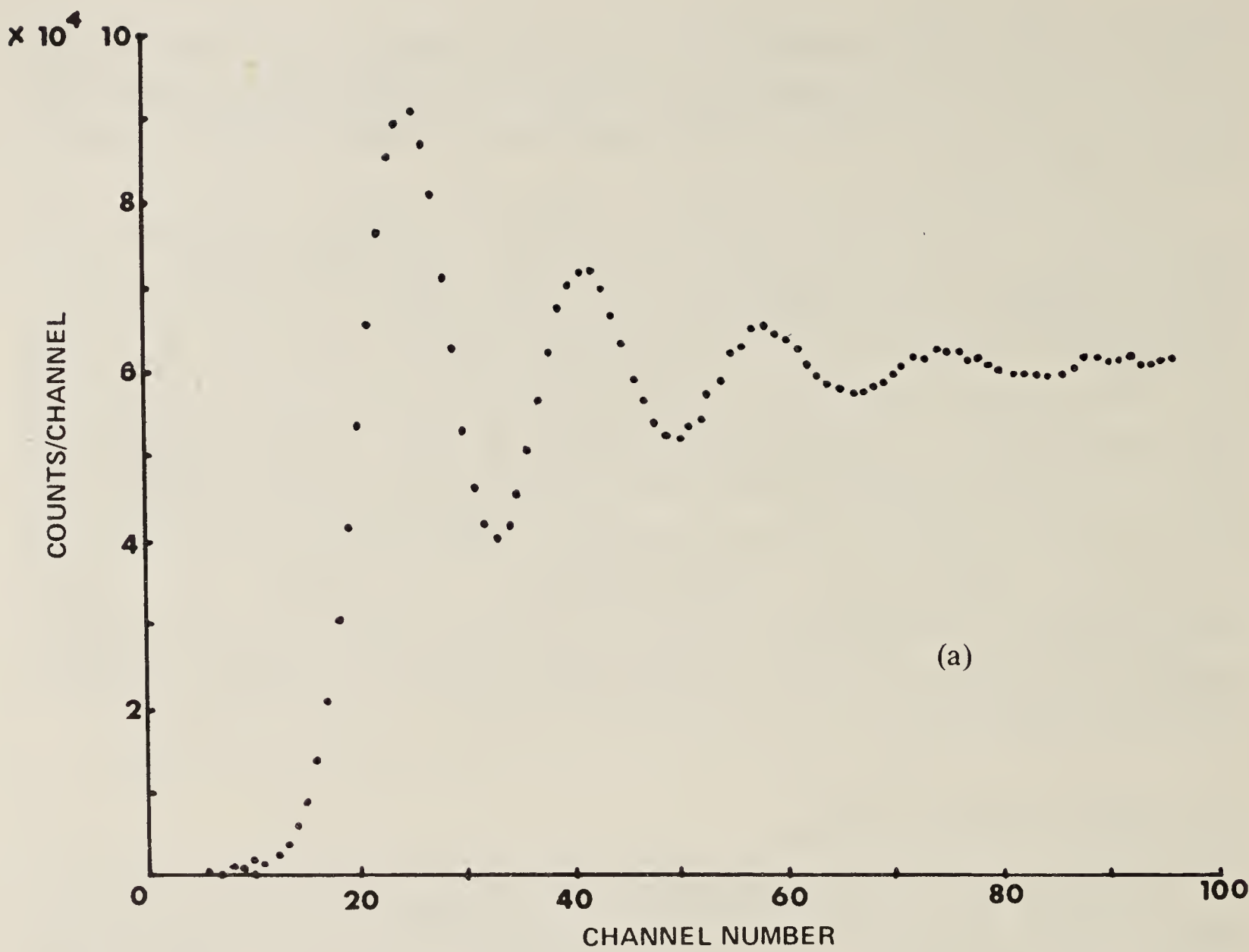
In the experiments of Dodd *et al.*<sup>(53)</sup> the detector recorded single photoelectric events and measured the time delay between the step of magnetic field and the arrival of the first photoelectron. Use of a time-to-pulse-height converter and a multichannel analyzer, with proper correction for "pulse pileup" and system linearity, yielded results for  $\tau^{(2)}$  with better than 1% accuracy. A typical result is shown in Figure 10. The method was used to study the variation of  $\tau^{(2)}$  with atomic density and thereby to check theories cited earlier for how this quantity is influenced by the phenomena of radiation trapping and atomic collisions. The technique was further developed by Piper and Sandle<sup>(54,55)</sup> to study the effects of cell geometry, atomic collisions, and isotopic constitution of the vapor in the resonance cell and in the lamp.

### 3.2. Pulsed Electric Field

The method is obviously applicable to the case where a step or pulse of electric field is applied to an atomic sample initially in a region free of electric and magnetic fields. In this case one obtains a measurement of the quadratic differential Stark coefficient rather than the Landé  $g$  coefficient. The principal advantage of the pulsed method is that, with an electric field applied for only a short time, the effects of discharge in the vapor are largely eliminated. An experiment of this kind has been performed by Sandle *et al.*<sup>(56)</sup> and is reported in the article by Kollath and Standage, Chapter 21 of this work.

### 3.3. Pulsed Radio-Frequency Field

In the traditional double-resonance method a radio-frequency magnetic field creates a coherent superposition of states from a pure state excited by appropriately polarized incident light. A transient experiment may obviously be developed by applying the rf field in a pulse. Pulses or steps of rf field have been extensively used in optical pumping experiments to study the relaxation of orientation in the ground state. We refer only to the early experiments of Dehmelt,<sup>(52)</sup> and of Cagnac and Brossel,<sup>(57)</sup> and a more recent paper of Gibbs and White.<sup>(58)</sup> These experiments are more concerned with relaxation processes than with atomic properties. Of more direct application to atomic properties, the method has been used by Jacobson<sup>(59)</sup> for a study of the nutational motion of aligned mercury atoms in the metastable  $6^3P_2$  state. In this case, Hg atoms were excited in a





resonance vessel by electron impact parallel to the static magnetic field, thus producing an alignment in the metastable state. The pulsed rf field, perpendicular to the steady field, disturbed this alignment. The transient character of the disturbance was monitored by absorption of linearly polarized light,  $\lambda = 546$  nm, corresponding to the transition  $6^3P_2$  to  $7^3S_1$ .

#### 4. Resolution within the Natural Width

By Fourier transformation of the time-resolved intensity variations we obtain spectra whose individual components are Lorentz curves centered on frequencies corresponding to the intervals  $\omega_{ee'}$  between excited levels, and whose widths, provided the vapor density is sufficiently low, depend inversely on the radiative lifetime of the excited states. (The full width at half-height is  $2\Gamma = 2/\tau$  if the lifetimes of the two levels are equal.)

It is possible to change the shape of the curves by biasing the signal in favor of a particular group of atoms. In particular, a bias in favor of the longer-lived atoms produces narrower curves. This can readily be shown analytically and has been demonstrated experimentally on a number of occasions. The technique has been applied in Mössbauer spectroscopy and in nuclear physics as well as in atomic physics. It appears to have been discovered independently by a number of different authors.

##### 4.1. Theory

A simple form of the quantum beat signal, Eq. (4), is

$$I(T) = (A + B \cos \omega_0 T) \exp(-\Gamma T) \quad (30)$$

where  $T$  is the time elapsed after the pulse and  $\omega_0$  is the interval between the excited states. The Fourier cosine transform of (30) is

$$I(\omega) = A\Gamma/(\Gamma^2 + \omega^2) + \frac{1}{2}B\Gamma/[\Gamma^2 + (\omega - \omega_0)^2] + \frac{1}{2}B\Gamma/[\Gamma^2 + (\omega + \omega_0)^2] \quad (31)$$

For  $\omega, \omega_0 > 0$  the second term gives the expected Lorentzian centered at  $\omega = \omega_0$ . The peak of  $I(\omega)$  is not exactly at  $\omega = \omega_0$  owing to overlap from the other terms, but this can be allowed for if necessary.

---

**Figure 10.** Typical experimental results in the stepped magnetic field experiment. (a) The modulation case:  $^{198}\text{Hg}$  in cell at  $-21.6^\circ\text{C}$  ( $5.7 \times 10^{17}$  atom  $\text{m}^{-3}$ );  $B = 190 \mu\text{T}$ ;  $7.78 \pm 0.02$  ns per channel. (b) The exponential case.  $^{198}\text{Hg}$  in cell at  $-11.4^\circ\text{C}$  ( $1.09 \times 10^{18}$  atom  $\text{m}^{-3}$ );  $B$  and time calibration as in (a) (from Dodd *et al.*<sup>(53)</sup>).

A biasing function  $f(T)$  can be introduced at the same time as the Fourier transform is calculated:

$$G(\omega) = \int_0^{\infty} I(T)f(T) \cos \omega T dT \quad (32)$$

Various forms of  $f(T)$  have been used. A simple form that corresponds to the experimental technique of delayed detection is the step function

$$f(T) = \begin{cases} 0, & T < T_1 \\ 1, & T \geq T_1 \end{cases} \quad (33)$$

This form of biasing, though easy to realize experimentally, introduces oscillatory structure (of period  $1/T_1$ ) into the wings of the spectral lines. It has been studied by Schenk *et al.*<sup>(60)</sup> and by Figger and Walther.<sup>(61)</sup>

An attractive function is the increasing exponential

$$f(T) = K e^{\gamma T}, \quad \gamma < \Gamma \quad (34)$$

which preserves the Lorentzian shape of the lines but narrows them from  $2\Gamma$  to  $2(\Gamma - \gamma)$ . It is, however, unrealistic to use a biasing function which increases indefinitely, and the function must be cut off at some time, which again introduces spurious oscillatory structure.

### *The Gaussian Biasing Function*

A biasing function that has greater appeal is the displaced Gaussian

$$f(T) = \exp [-(T-a)^2/b^2] \quad (35)$$

It is easy to show that, if the width,  $b$ , of the Gaussian is properly chosen in relation to the displacement of its peak,  $a$ , the oscillatory structure is suppressed. The required relation is

$$b = (2a/\Gamma)^{1/2} \quad (36)$$

With  $f(T)$  chosen according to Eqs. (35) and (36) the biased transform

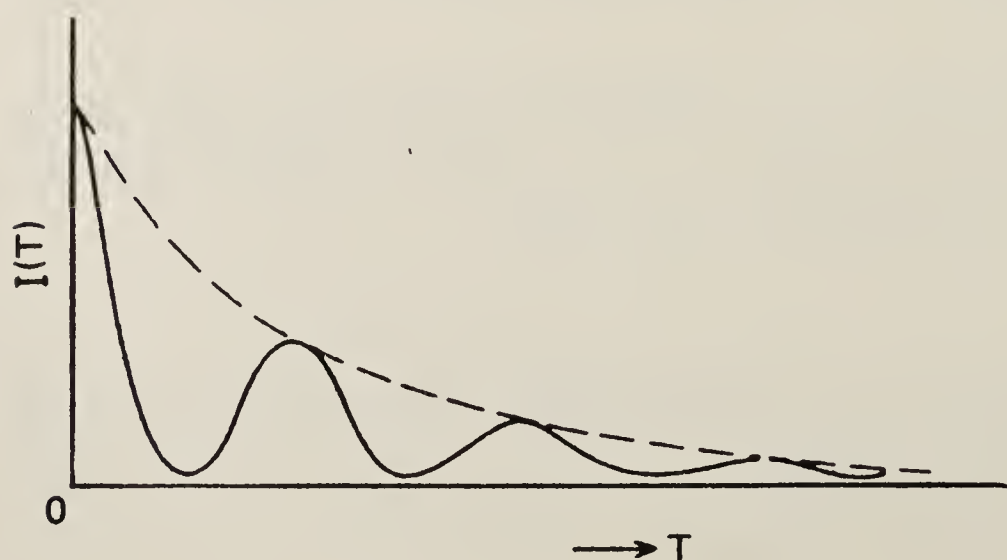


**Figure 11.** The function  $I(T)$ .



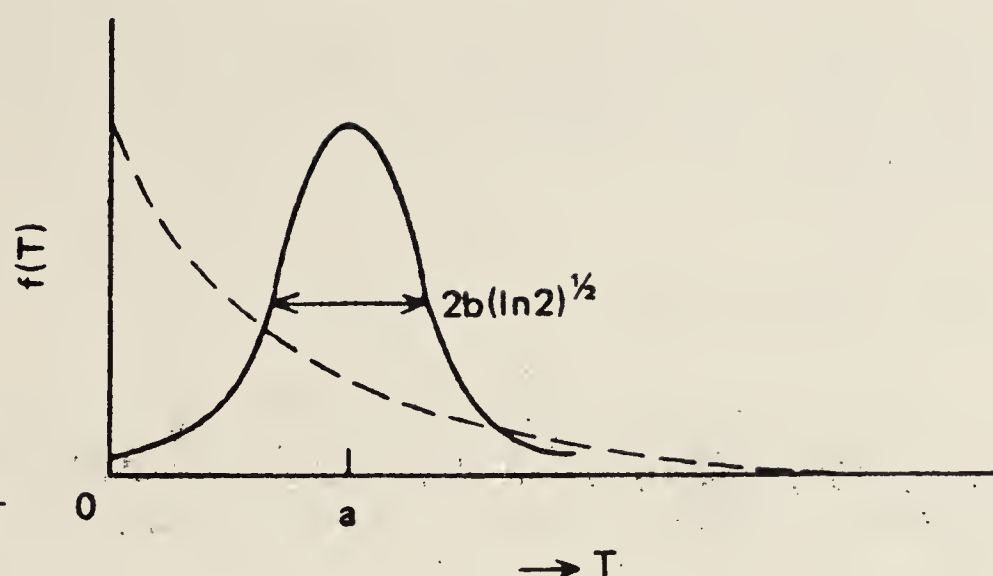


**Figure 12.** Gaussian biasing function,  $\exp [-(T-a)^2/b^2]$ .

$G(\omega)$  of  $I(T)$  [Eqs. (32) and (30)] becomes

$$G(\omega) = \frac{1}{2}b\pi^{1/2} \exp(-\Gamma^2 b^2/4) \{A \exp(-\omega^2 b^2/4) + \frac{1}{2}B \exp[-(\omega - \omega_0)^2 b^2/4] + \frac{1}{2}B \exp[-(\omega + \omega_0)^2 b^2/4]\} \quad (37)$$

This is to be compared with Eq. (31) with  $A = B = 1$ . The Lorentzians peaked at  $\omega = \pm \omega_0$  have been transformed into Gaussians whose full width at half-intensity is  $4(\ln 2)^{1/2}/b$ . The condition under which this is less than the width of the Lorentzian is

$$b > 2(\ln 2)^{1/2}/\Gamma = 1.67\tau \quad (38)$$

Figures 11–13 show the functions  $I(T)$ ,  $f(T)$ ,  $I(\omega)$ , and  $G(\omega)$ .

When  $b$  is chosen so that the widths are equal the height of the Gaussian is about 0.7 times the height of the Lorentzian. It will be noticed that the height of the Gaussian decreases exponentially with  $b^2$ , that is, with  $a$ , the time interval between the initiating pulse and the peak of the Gaussian. This implies a degradation of signal relative to noise and is the price one pays for the line-narrowing. On the other hand, the steeper fall of

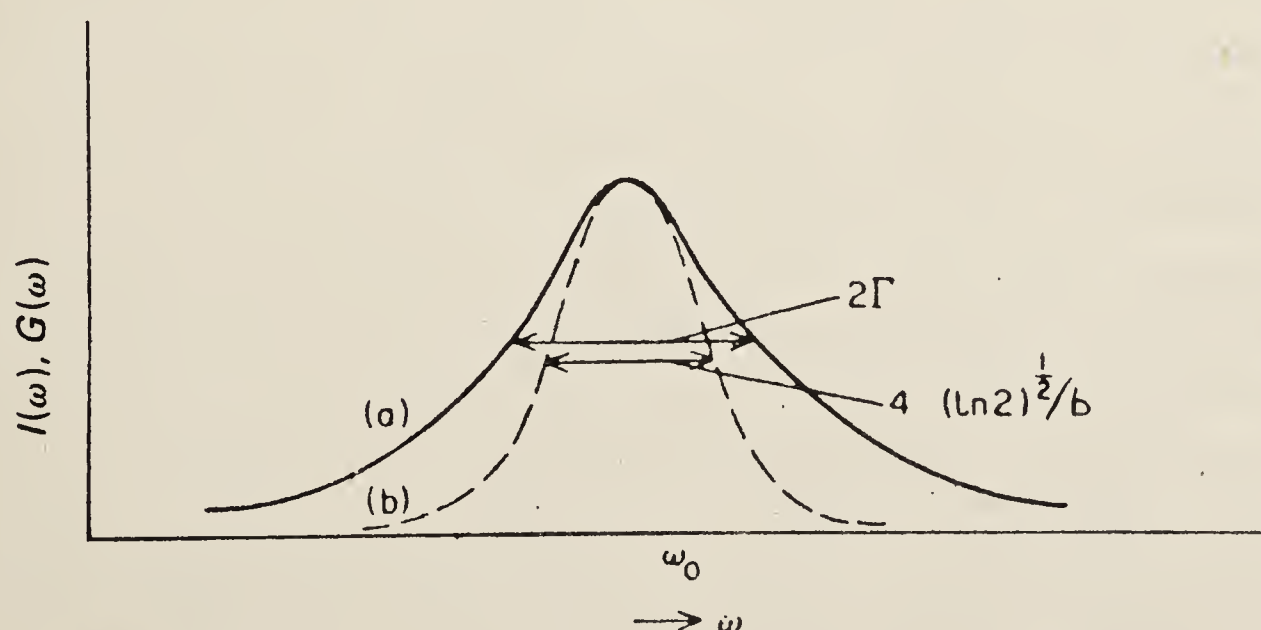


**Figure 13.** Narrowing achieved by biasing. (a) The unbiased transform,  $I(\omega)$  (b) The biased transform,  $G(\omega)$ .

the wings of the Gaussian relative to the Lorentzian gives an important advantage when one is trying to improve the resolution of overlapping spectral lines.

#### 4.2. *Practicalities and Examples*

The advantages gained by the technique of time-biasing have to be weighed against the increased uncertainties introduced by the degraded signal-to-noise ratio. If the problem were simply to obtain the best value for the center of a symmetrical line it could not be maintained that narrowing the width at the expense of increasing the uncertainty would lead to an improvement. On the other hand, if the problem is to find the relative positions of overlapping lines where the individual line profiles are not known with confidence, then improved resolution—even at the expense of signal-to-noise ratio—is to be preferred to an analysis based on profile synthesis, the alternative method. And although the Fourier-transformed signals of quantum beats are in principle Lorentzian curves, one cannot always rely on this on account of instrumental nonlinearities and unknown complicating factors. It is a matter of practical experience in general that the methods of profile analysis can lead to errors, and resolution of components, where possible, is to be preferred. A particular case, the hyperfine structure of  $3^2P_{3/2}$  in sodium, was studied in detail by Deech *et al.*<sup>(62)</sup> It was argued that the results obtained by line narrowing were more reliable than those obtained by profile analysis of experimental results obtained under comparable conditions.

An improvement in accuracy of an important spectroscopic interval, the Lamb shift in hydrogen, has been reported by Lundeen and Pipkin<sup>(63)</sup> in an application of the time-biasing technique. They measured electric dipole resonances between hyperfine components of  $2^2S_{1/2}$  and  $2^2P_{1/2}$  in a fast beam of hydrogen atoms. The complete pattern of resonances is complicated, but was simplified by a technique of state selection which very largely suppressed all but one of the transitions. Resonance curves are obtained by scanning the frequency of the rf field, so this is not strictly an experiment in which time-resolved signals are obtained, but the principles of time biasing still apply. Under ordinary conditions the width of the resonance curves is determined mainly by the inverse of the very short lifetime of the  $P$  states—the  $S$  states are metastable. In Lundeen and Pipkin's experiment a spectacular narrowing of the resonance curve was achieved by employing Ramsey's well-known two-field arrangement to elicit a time-biased signal. Atoms in a beam pass successively through two interaction regions before reaching the detector. The main part of the signal corresponds to atoms that undergo the transition from  $S$  to  $P$  in the first interaction region, and this resonance is broad. It does not depend on



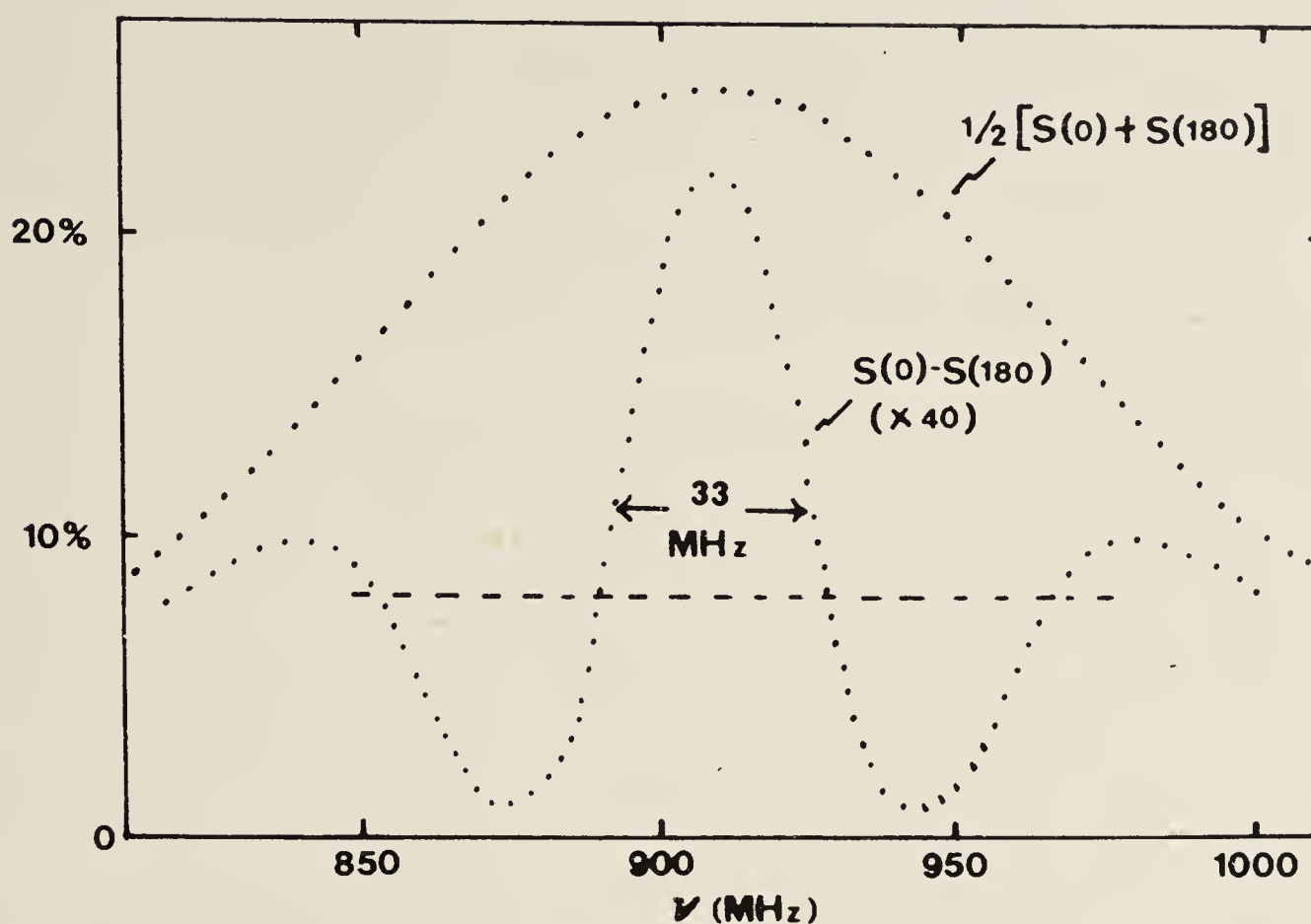


**Figure 14.** Lamb-shift resonance in H. The upper curve is typical of “ordinary” resonance curves, the lower shows the response of atoms that have interacted with the first field and have survived to interact with the second (from Lundeen and Pipkin<sup>(63)</sup>).

the phases of the rf fields. The total signal contains also the contribution from atoms that survive to interact with the field in the second region. The sign of this contribution depends on the relative phase of the fields, and the contribution is separated from the total signal by taking the difference between  $S(0)$  and  $S(180)$ , signals obtained with the fields in phase and in antiphase, respectively.

The narrowing achieved is seen by comparing the difference curve, which is the lower curve of Figure 14 with the upper curve, which is the average of  $S(0)$  and  $S(180)$  and so does not reflect the time biasing. The width of the difference curve is about three times less than the natural width of the  $P$  states and the authors claim to have gained a factor of 3 in precision over earlier measurements of the Lamb shift. It will be noticed that the signal-to-noise ratio in the time-biased curve is very high, notwithstanding the reduction in absolute signal strength. The oscillatory structure at the sides of the main peak will also be noticed: this reflects the spatial (and therefore the temporal) envelope of the rf fields.

### 4.3. Conceptual Problems

It is sometimes asked whether the narrowing of resonance curves below the “natural” width does not violate the uncertainty principle. Of

course it does not. Curves having the natural width are obtained by taking unweighted signals from all members of an assembly of atoms decaying by spontaneous emission of radiation. The narrowed curves are obtained by taking signals from a selected sample whose mean lifetime is longer than that of all members of the assembly. The relation between mean lifetime and spectral linewidth is simply the reciprocal relationship of Fourier transform pairs.

A more well-founded objection is to point out that all atoms, irrespective of how long they have survived in the excited state, have the same probability of decay. Does not this probability govern the spectral linewidth of the emitted radiation? How, then, can the linewidth be reduced by taking the light from a biased sample of atoms? Indeed, the spectral linewidth as determined by an ordinary spectrometer is independent of the time of observation after an exciting pulse. But the significant point is that the spectra obtained in an ordinary spectrometer are transforms of the amplitude of the light field correlated against itself, whereas the spectra we are concerned with here are transforms of the intensity of the light field correlated against a biasing function which we are free to choose. The lines are narrowed because we bias against the wings. The information to which we attach most weight is that which relates to the region near line center.

## 5. *Concluding Remarks*

We have attempted in this article to show how the time evolution of the intensity of fluorescent light from atoms reflects the dynamical processes in the atoms themselves. By implication, and by means of examples, we have shown how atomic parameters may be determined by measurements of fluorescent light, and we have shown how such determinations are free of Doppler broadening. We have shown also how the time-evolving intensity is related to the steady-state intensity and how the same atomic parameters enter into both, but we have not discussed the techniques in sufficient detail to assess their relative merits or to allow a critical comparison between them and alternative Doppler-free techniques such as radio-frequency optical double resonance, laser fluorescence or absorption from atomic beams, saturated absorption spectroscopy, multiple-photon laser spectroscopy, and others. Some comments on the relation between double resonance and the technique of modulated excitation were made in Section 1.4 and on certain advantages of the technique of pulsed electric fields in Section 3.2.

The impact of lasers on high-resolution spectroscopy has been explosive: several of the techniques just mentioned did not exist before lasers. The steady-state version of coherence spectroscopy (level-crossing



spectroscopy), however, did exist and a great deal of valuable work was accomplished using conventional light sources. As for time-resolved coherence spectroscopy, the principles were known and the pioneer experiments had been done in the prelaser age, but vastly more territory in this domain now lies open for exploration with lasers on account of their intensity, their tunability and the pulse technology that has been developed. The spectral purity offered by lasers is not useful in this work since the spectral range has to span the whole structure that is to be explored.

Level-crossing spectroscopy has been invigorated by lasers and many new structures have been explored both by this technique and also by time-resolved spectroscopy. The results have been gratifyingly in agreement. The choice of one or the other method is often determined by the equipment available to the experimenter—he or she requires magnetic fields and steady-state detection on the one hand, and short-pulse technology and counting techniques on the other. Where time-biasing is to be applied, time-resolved detection is essential (or, if atomic beams are used, space-resolved detection). It is sometimes useful to combine the two techniques, as when the intervals in zero field are uncomfortably large (time-resolution uncomfortably small) for pulse-counting but can be made manageable by the application of a magnetic field. Then, time-resolved measurements are made for a set of values of magnetic field, and for each field point an integration is made over time, incorporating a biasing function if required.<sup>(62)</sup> In this way one obtains a set of values of intensity as a function of magnetic field, which constitutes a level-crossing curve.

## Acknowledgments

The authors, in conclusion, wish to record their indebtedness to their colleagues and collaborators, many of whom have allowed their work to be quoted as examples to illustrate this text. They also wish to thank the authors specified in the figure legends and references for permission to use published material, and also the owners of copyright as follows: for Figures 1, 5, 7, 9, and 10, the Institute of Physics; for Figures 11, 12 and 13, the Rank Prize Funds and Academic Press; and for Figure 14; the American Institute of Physics.

## References

1. G. Breit, *Rev. Mod. Phys.* **5**, 91 (1933).
2. J. P. Barrat and C. Cohen-Tannoudji, *J. Phys. Radium* **22**, 329, 443 (1961).
3. C. Cohen-Tannoudji, Thesis, University of Paris (1962).

4. A. V. Durrant, *J. Phys. B* **5**, 133 (1972).
5. A. Corney and G. W. Series, *Proc. Phys. Soc. London* **83**, 213 (1964).
6. A. Corney, *J. Phys. B* **1**, 458 (1968).
7. T. Skalinski, A. Kopystynska, and K. Ernst, *Bull. Acad. Pol. Sci.* **13**, 851 (1965).
8. M. Broyer, J.-C. Lehmann, and J. Vigue, *J. Phys. (Paris)* **36**, 235 (1975).
9. A. Corney, B. P. Kibble, and G. W. Series, *Proc. R. Soc. London A* **293**, 70 (1966).
10. A. V. Durrant and B. Landheer, *J. Phys. B* **4**, 1200 (1971).
11. R. Q. Hackett and G. W. Series, *Opt. Commun.* **2**, 93 (1970).
12. W. W. Chow, M. O. Scully, and J. O. Stoner, *Phys. Rev. A* **11**, 1380 (1975).
13. J. L. Cojan, *Ann. Phys. (Paris)* **9**, 385 (1954).
14. M. F. H. Schuurmans, *J. Phys. (Paris)* **37**, 469 (1976); *Z. Phys.* **A279**, 243 (1976).
15. G. W. Series, *Proc. Phys. Soc. London* **91**, 432 (1967).
16. W. Hanle and G. Stanzel, *Z. Naturforsch.* **25a**, 309 (1970).
17. G. Stanzel, *Z. Phys.* **A270**, 361 (1974).
18. W. Siegmund and A. Scharmann, *Z. Phys.* **A276**, 19 (1976).
19. J. M. Hansen and H. W. Webb, *Phys. Rev.* **72**, 332 (1947).
20. R. van Traubenberg and S. Levy, *Z. Phys.* **44**, 549 (1927).
21. K. L. Hertel, *Phys. Rev.* **29**, 848 (1927).
22. I. Walerstein, *Phys. Rev.* **33**, 800 (1929).
23. W. Hanle, *Z. Phys.* **30**, 93 (1924).
24. W. Hanle, *Ergeb. Exakt Wiss.* **4**, 214 (1925).
25. S. Haroche, *High Resolution Laser Spectroscopy* (Ed. K. Shimoda), pp. 253–313. Springer, Berlin (1976).
26. E. B. Aleksandrov, *Opt. Spektrosk.* **17**, 957 (1964) [English transl. **18**, 522 (1964)].
27. J. N. Dodd, R. D. Kaul, and D. M. Warrington, *Proc. Phys. Soc. London* **84**, 176 (1964).
28. J. N. Dodd, W. J. Sandle, and D. Zissermann, *Proc. Phys. Soc. London* **92**, 497 (1967).
29. T. Hadeishi and W. A. Nierenberg, *Phys. Rev. Lett.* **14**, 891 (1965).
30. S. A. Bagaev, V. B. Smirnov, and M. P. Chaika, *Opt. Spektrosk.* **41**, 166 (1976) [English transl. *Opt. Spectrosc.* **41**, 98 (1976)].
31. S. Heron, R. W. P. McWhirter, and E. H. Rhoderick, *Proc. R. Soc. London A* **234**, 565 (1956).
32. G. C. King and A. Adams, *J. Phys. B* **7**, 1712 (1974).
33. G. C. King, A. Adams, and D. Cvejanovic, *J. Phys. B* **8**, 356 (1975).
34. D. A. Shaw, A. Adams, and G. C. King, *J. Phys. B* **8**, 2456 (1975).
35. R. Luypaert, Thesis, University of Reading (1976). See also R. Luypaert and J. Van Craen, *J. Phys. B* **10**, 3627 (1977).
36. J. S. Deech, R. Luypaert, and G. W. Series, *J. Phys. B* **8**, 1406 (1975).
37. G. G. Carrington and A. Corney, *J. Phys. B* **4**, 849 (1971).
38. M. I. D'yakonov and V. I. Perel', *Zh. Eksp. Teor. Fiz.* **47**, 1483 (1964). [English transl. *Sov. Phys. JETP* **20**, 997 (1965)].
39. M. I. D'yakonov and V. I. Perel', *Zh. Eksp. Teor. Fiz.* **48**, 345 (1965) [English transl. *Soviet Phys. JETP* **21**, 227 (1965)].
40. A. Omont, *J. Phys. (Paris)* **26**, 26 (1965).
41. W. Happer and B. S. Mathur, *Phys. Rev.* **163**, 12 (1967).
42. C. G. Carrington, D. N. Stacey, and J. Cooper, *J. Phys. B* **6**, 417 (1973).
43. A. C. G. Mitchell and N. W. Zemansky, *Resonance radiation and excited atoms*, Cambridge University Press, Cambridge (1934).
44. H. I. Gunn and W. J. Sandle, *J. Phys. B* **4**, L1 (1971).
45. J. S. Deech and W. E. Baylis, *Can. J. Phys.* **49**, 90 (1971).
46. L. R. Pendrill, *J. Phys. B* **10**, L469 (1977).
47. G. W. Series, *Phys. Rev.* **136**, A684 (1964).



48. S. Bashkin, W. S. Bickel, D. Fink, and R. K. Wangsness, *Phys. Rev. Lett.* **15**, 284 (1965).
49. I. A. Sellin, P. M. Griffin, and J. A. Biggerstaff, *Phys. Rev. A* **1**, 1553 (1970) (and earlier papers referenced there).
50. H. J. Andra, *Phys. Scr.* **9**, 257 (1974).
51. A. van Wijngaarden, E. Goh, G. W. F. Drake, and P. S. Farago, *J. Phys. B* **9**, 2017 (1976).
52. H. G. Dehmelt, *Phys. Rev.* **105**, 1487 (1957).
53. J. N. Dodd, W. J. Sandle, and O. M. Williams, *J. Phys. B* **3**, 256 (1970).
54. J. A. Piper and W. J. Sandle, *J. Phys. B* **3**, 1357 (1970).
55. J. A. Piper and W. J. Sandle, *J. Phys. B* **5**, 377 (1972).
56. W. J. Sandle, M. C. Standage, and D. M. Warrington, *J. Phys. B* **8**, 1203 (1975).
57. B. Cagnac and J. Brosset, *C.R. Acad. Sci.* **249**, 253 (1959).
58. H. M. Gibbs and C. W. White, *Phys. Rev.* **188**, 180 (1969).
59. E. Jacobson, *J. Phys. B* **8**, 869 (1975).
60. S. Schenk, R. C. Hilborn, and H. Metcalf, *Phys. Rev. Lett.* **31**, 189 (1973).
61. H. Figger and H. Walther, *Z. Phys.* **267**, 1 (1974).
62. J. S. Deech, P. Hannaford, and G. W. Series, *J. Phys. B* **7**, 1131 (1974).
63. S. R. Lundeen and F. M. Pipkin, *Phys. Rev. Lett.* **34**, 1368 (1975).





## Collisional and Radiative Relaxation as an Eigenvalue Problem

Attention is drawn to some recent studies of excited Cs atoms in collision with ground state atoms. The multi-exponential decay of the populations of excited energy eigenstates is seen as the single-exponential decay of linear combinations of these populations. The notion of eigenstates of relaxation is explored.

L.R. Pendrill<sup>1</sup> has recently reported studies of the decay of populations of excited caesium atoms under the competing perturbations of radiative damping and collisions with atoms in ground states. He finds that the decay of population following selective, pulsed excitation cannot be represented by a single exponential but requires a sum of exponentials: terms must be added progressively as the vapour density increases. An interpretation is given in terms of collisional transfer to and from between the state first excited and close-lying 'partner' states. The progressive increase in number of terms required corresponds to the participation of additional partner-states, sequentially according to the relative magnitudes of the collisional transfer cross-sections.

Pendrill demonstrates that the dominant partner-states for the  $nD_{3/2}$  sequence ( $n = 8$  to  $14$ ) are, as expected, the corresponding  $nD_{5/2}$  states, whereas for  $nS_{1/2}$  the dominant partner-states are  $(n - 4)F$ . In both cases these collision partners are the closest lying of all other states, and the energy differences are very much smaller than  $kT$ . The identification of dominant partner-states relies heavily, but not entirely, on the fact that the decay of sensitized fluorescence from such partner-states can be interpreted by a sum of exponential terms *having the same rate constants* as the decay of fluorescence from the primarily excited state (direct fluorescence).

An analysis is given in terms of solutions of the well-known rate equations, which we shall summarise below. We wish to enlarge on the analogy which Pendrill draws between the variation of the rate constants (which we may regard as the imaginary part of the energy of the excitation) with density of perturbers and the more familiar variation of real energy eigenvalues under an external perturbation.

The rate equations for the populations  $N_1, N_2$  of a pair of excited states, 1 and 2, are

$$\begin{aligned}\dot{N}_1 &= -(\Gamma_1 + \gamma_{21})N_1 + \gamma_{12}N_2 \\ \dot{N}_2 &= \gamma_{21}N_1 - (\Gamma_2 + \gamma_{12})N_2\end{aligned}\quad (1)$$

where the  $\Gamma$  are free-atom radiative decay constants and the  $\gamma_{ij}$  are collisional transfer rates from  $j$  to  $i$ . These equations are approximate to the extent that smaller terms representing transfers to other states have been neglected. A mean collisional transfer cross-section  $\sigma_{ij}$  is introduced by means of the equation  $\gamma_{ij} = \sigma_{ij}N_G\bar{v}$ , where  $N_G$  is the number density of atoms in the ground state and  $\bar{v}$  the mean relative velocity.

The solutions  $N_1(t), N_2(t)$  of Eq. (1) are linear combinations of eigenfunctions  $N_{\pm}(t) = N_0 \exp(-\lambda_{\pm}t)$ , where the eigenvalues  $\lambda_+$  and  $\lambda_-$  are given by diagonalizing the square matrix of rate coefficients on the right-hand side of Eq. (1), the signs of all terms having first been changed. The eigenvalues are

$$\begin{aligned}\lambda_{\pm} &= \frac{1}{2}(\Gamma_1 + \Gamma_2 + \gamma_{12} + \gamma_{21}) \pm \frac{1}{2}[(\Gamma_1 - \Gamma_2)^2 + 2(\gamma_{21} - \gamma_{12})(\Gamma_1 - \Gamma_2) \\ &\quad + (\gamma_{12} + \gamma_{21})^2]^{\frac{1}{2}}\end{aligned}\quad (2)$$

The constant  $N_0$  turns out to be equal to the total number of atoms at time  $t = 0$ .

We concentrate attention first on  $\lambda_{\pm}$ . Limiting values are

a) for low vapour densities,  $(\gamma_{12} + \gamma_{21} \ll |\Gamma_1 - \Gamma_2|)$ ,

$$\begin{aligned}\lambda_- &= \Gamma_2 + \gamma_{12} = \Gamma_2 + \sigma_{12}(N_G\bar{v}) \\ \lambda_+ &= \Gamma_1 + \gamma_{21} = \Gamma_1 + \sigma_{21}(N_G\bar{v})\end{aligned}\quad (3)$$

b) for high vapour densities,  $(\gamma_{12} + \gamma_{21} \gg |\Gamma_1 - \Gamma_2|)$ ,

$$\begin{aligned}\lambda_- &= (g_1\Gamma_1 + g_2\Gamma_2)/(g_1 + g_2) = \bar{\Gamma} \\ \lambda_+ &= (g_1\Gamma_2 + g_2\Gamma_1)/(g_1 + g_2) + (\gamma_{12} + \gamma_{21}) = \tilde{\Gamma} + (\gamma_{12} + \gamma_{21})\end{aligned}\quad (4)$$

In (b) we have used the ratio of the statistical weights,  $g_1, g_2$  to replace the ratio  $\gamma_{12}/\gamma_{21} = (g_1/g_2) \exp(-\Delta E_{12}/kT) \approx g_1/g_2$ .

$\lambda_-$  is independent of the  $\gamma$  and therefore of  $N_G$ .  $\lambda_+$  differs from  $\lambda_-$  principally by  $(\gamma_{12} + \gamma_{21})$ , but additionally by  $\tilde{\Gamma} - \bar{\Gamma} = -(g_1 - g_2)\dagger(\Gamma_1 - \Gamma_2)/(g_1 + g_2)$ . While this term may be of order  $\bar{\Gamma}$  it will always be smaller and will sometimes be very much smaller. In any case it is negligible in this approximation. We shall, however, retain  $\bar{\Gamma}$  in  $\lambda_+$  and rewrite equations (4) as

$$\begin{aligned}\lambda_- &= \bar{\Gamma} \\ \lambda_+ &= \bar{\Gamma} + (\sigma_{12} + \sigma_{21})(N_G\bar{v})\end{aligned}\quad (5)$$

---

$\dagger \tilde{\Gamma} - \bar{\Gamma} = -(g_1 - g_2)(\Gamma_1 - \Gamma_2)/(g_1 + g_2)$



Figure 1 shows a plot of  $\lambda_{\pm}$  against  $N_G \bar{v}$ . The resemblance to plots of energy against an external perturbation is immediately obvious and stems from the fact that both cases represent the diagonalization of a  $2 \times 2$  matrix. Nevertheless it is instructive to apply to the present case of imaginary energy the ideas which are familiar in the case of plots of real energy eigenvalues.

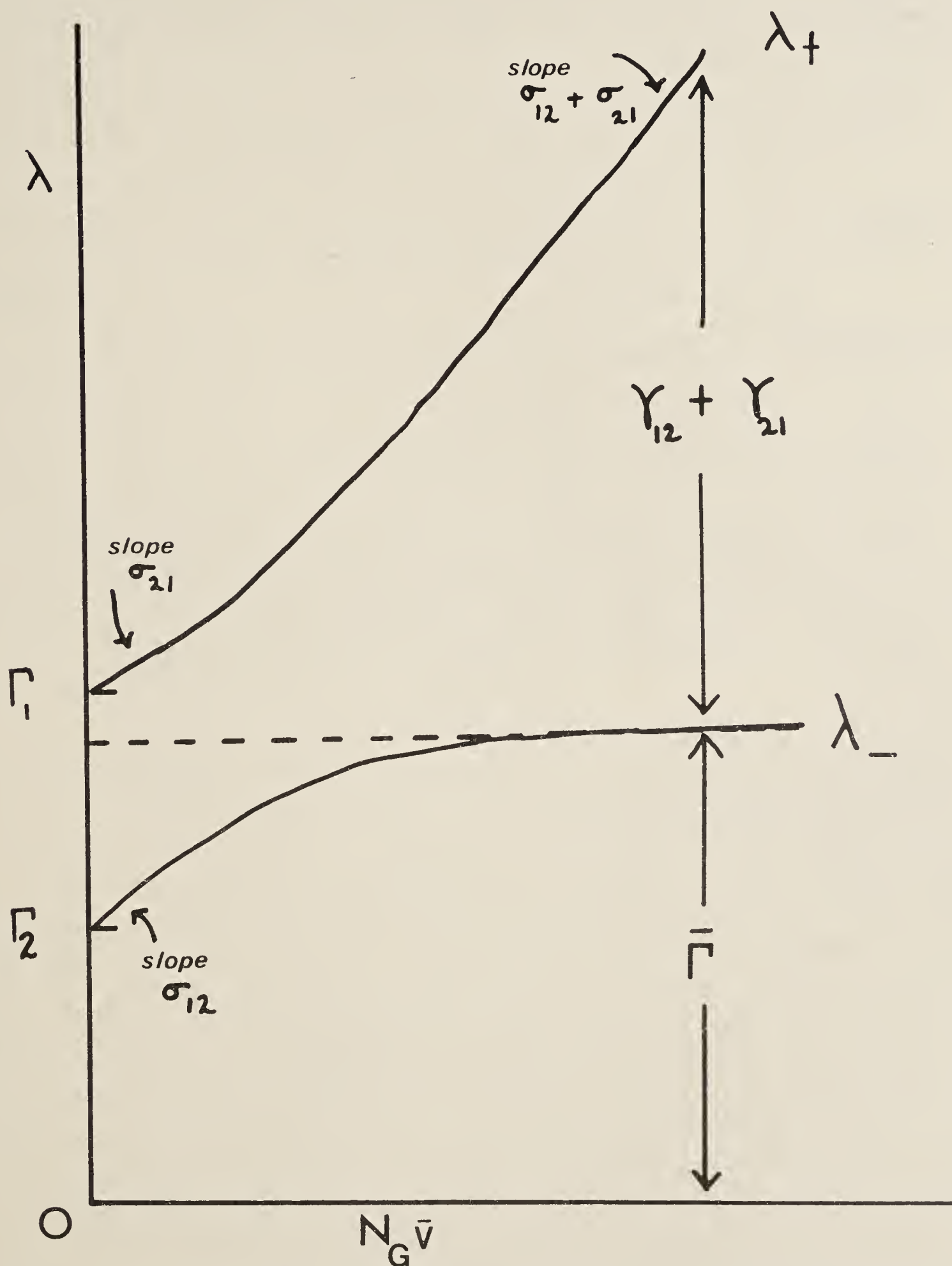


FIGURE 1. Plot of decay constants  $\lambda_{\pm}$  against  $N_G \bar{v}$ . Notice the similarity to plots of energy levels of states against the magnitude of a decoupling perturbation.

Recall that the eigenfunctions  $N_{\pm}(t)$  are those linear combinations of  $N_1(t)$  and  $N_2(t)$  whose decay can be represented by single exponential functions. In the low density regime the eigenfunctions correspond closely to the populations of states 1 and 2 and the eigenvalues tend to the radiative decay rates  $\Gamma_1$  and  $\Gamma_2$  as the density tends to zero. In the high density regime, on the other hand, the eigenfunctions correspond to complete mixing of the populations. Consider this regime in more detail. For initial excitation to  $N_2$  (i.e.,  $N_2(0) = N_0, N_1(0) = 0$ ) we find the solutions

$$N_1(t) = N_0 g_1 [\exp(-\lambda_- t) - \exp(-\lambda_+ t)] / (g_1 + g_2)$$

(sensitized fluorescence)

$$N_2(t) = N_0 [g_2 \exp(-\lambda_- t) + g_1 \exp(-\lambda_+ t)] / (g_1 + g_2)$$

(direct fluorescence) (6)

The eigenfunctions, in terms of  $N_1$  and  $N_2$ , are

$$N_-(t) = N_1(t) + N_2(t) = N_0 \exp(-\lambda_- t)$$

$$N_+(t) = N_2(t) - (g_2/g_1)N_1(t) = N_0 \exp(-\lambda_+ t) \quad (7)$$

The *sum* of the direct and sensitized fluorescence therefore decays at the rate  $\lambda_- = \bar{\Gamma}$ , the statistically averaged radiative decay rate, while the *difference* between the direct and sensitized fluorescence (weighted, in each case, by the reciprocals of the corresponding statistical weight) decays at the rate  $\lambda_+ = \bar{\Gamma} + (\gamma_{12} + \gamma_{21})$ , i.e. at a rate which exceeds  $\bar{\Gamma}$  by the sum of the collisional transfer rates.

We may give the following interpretation to the change in composition of the eigenfunctions between the low and high density regimes. The eigenfunctions in the low density regime represent relaxation arising predominantly from the stochastic interaction responsible for radiative decay (zero-point fluctuations of the radiation field). The *difference* in the radiative decay rates represents a differential effect of the perturbation between the two states. When the collisional relaxation is small in comparison with the radiative relaxation the effect of the collisions appears as a small admixture to the radiative eigenfunctions. As the collisional rates increase, affecting the two states equally (the two transfer rates are in the ratio of the statistical weights), the collisional interaction progressively breaks down the differential radiative interaction until, in the high density limit, the eigenfunctions represent pure states of the collisional interaction. In the one case ( $\lambda_+$ ) we find the sum of the collisional rates operating within the system, whereas in the other case ( $\lambda_-$ ) the collisional effects have been eliminated. The situation is analogous to, for example, the breakdown of hyperfine coupling in an atom by an external magnetic field.

We may take the analogy further by considering the slopes of the curves in



Figure 1. In the case of plots of energy against magnetic field, the negative slope ( $-\partial E/\partial B$ ) gives an effective magnetic moment whose value is a function of the field. The value may pass through zero: it is a measurable, physical property of atoms in eigenstates of the total Hamiltonian. Similarly, the slopes of our plots of  $\lambda_{\pm}$  against  $N_G \bar{\nu}$  are effective collisional cross-sections for physical states corresponding to the respective eigenfunctions. In the region of weak perturbation these cross-sections are  $\sigma_{12}$  and  $\sigma_{21}$ , respectively, i.e. cross-sections for transfer *out of* the states 2 and 1, which are good approximations to the eigenstates in this region. The cross-sections can be determined by fitting the direct fluorescence from states 2 and 1, respectively, to single exponential functions. In the region of strong perturbation the eigenvalue  $\lambda_-$  is independent of  $N_G \bar{\nu}$ : the effective collisional cross-section is zero. The eigenstate corresponding to  $\lambda_+$ , on the other hand, has an effective collisional cross-section  $\sigma_{12} + \sigma_{21}$ .

The experimental results reported by Pendrill for the  $nS, (n-4)F$  states could be represented by the equations we have been discussing. The plots of decay constants against  $N_G \bar{\nu}$  were curves similar to those in Figure 1 in which  $\Gamma_1 \neq \Gamma_2$ . For the  $nD_{3/2}, nD_{5/2}$  states, on the other hand, we have  $\Gamma_1 = \Gamma_2 = \Gamma$ , and the collisional perturbation acts on states which are degenerate under the radiative perturbation. In this case the eigenvalues simplify to  $\lambda_- = \Gamma$ ,  $\lambda_+ = \Gamma + \gamma_{12} + \gamma_{21}$  for all values of  $N_G \bar{\nu}$ : the 'repelling' curves degenerate into a pair of straight lines which intersect at  $N_G = 0$  and the 'mixing of states' is complete from the outset. The effective collisional cross-section is always zero for the eigenfunction  $N_-$  and always  $\sigma_{12} + \sigma_{21}$  for  $N_+$ . This situation was also explored experimentally by Pendrill.

G.W. SERIES

*J.J. Thomson Physical Laboratory,  
The University of Reading,  
Whiteknights,  
Reading RG6 2AF*

#### Reference

1. Pendrill, L.R., 1977. *J. Phys. B.* **10** (in press).





A SEMI-CLASSICAL APPROACH TO RADIATION PROBLEMS\*

G.W. SERIES

*J.J. Thomson Physical Laboratory, Whiteknights, Reading, England*

Received November 1977

Contents:

1. Introduction	3	4.1.3. Bessel functions of higher order	22
1.1. Quantized fields and classical fields	4	4.1.4. Validity of the approximation	22
1.2. Interaction of time-dependent magnetic fields with paramagnetic atoms	5	4.1.5. Evaluation of correction terms	23
2. Case A	6	5. The general problem	25
2.1. Exact solution	6	5.1. Condition of resonance	26
2.2. Zeeman effect in the transformed frame: the Rabi frequency	9	5.4. Shirley's method	26
2.3. Steady-state experiment	11	6. The Bloch-Siegert problem	27
2.3.1. Excitation to an eigenstate of $f_z$	11	6.1. Zeroth and first approximations: terms in $\omega_1^2$	27
2.3.2. Excitation to a superposition-state of $f_z$	13	6.2. Second approximation: terms in $\omega_1^4$	28
2.4. Use of irreducible spherical tensor operators	14	6.3. Third approximation: terms in $\omega_1^6$	29
3. Case B	15	6.4. Limit of strong, oscillating field	30
3.1. Exact solution	15	6.4.1. Additional small static field: zeroth approximation	30
3.2. Steady-state experiment	17	6.4.2. Additional small static field: terms in $\omega_0^3$	31
3.2.1. Excitation to an eigenstate of $f_z$	17	6.5. Results	32
3.2.2. Excitation to a superposition-state of $f_z$	17	6.6. Discussion: comments on other work	33
3.3. Modulated excitation to a superposition-state of $f_z$	18	7. Spontaneous emission	34
4. Approximations	19	7.1. The formalism	35
4.1. Case B with additional transverse magnetic field	19	7.2. Results: application to cycles of optical pumping	37
4.1.1. Zeroth approximation	20	7.3. Mechanism of spontaneous emission: radiation reaction	38
4.1.2. Hanle effect in the presence of an oscillating field	21	7.4. Concluding remarks on spontaneous emission	40
		References	41

\* Dedicated to Willis E. Lamb Jr. on the occasion of 65th birthday.

*Abstract:*

The article is mainly devoted to a detailed exposition of the method of solution of problems in magnetic resonance by transformations to rotating co-ordinate frames. The well-known method of transformation to a frame rotating at constant angular velocity has been extended to embrace modulated rotations, thereby allowing the elimination of oscillating fields of any strength. A detailed analysis of the Bloch–Siegert problem is given to illustrate the application of the techniques. Since the original work was carried out in relation to the study of excited atoms, the question naturally arose, how to deal with spontaneous emission? A general discussion of this question is given, and a technique is described which allows spontaneous emission to be included in semi-classical calculations of cycles of optical pumping.

## 1. Introduction

The major part of this article represents a development of the method of transformations to rotating co-ordinate frames as a technique for solving semi-classical equations of motion in quantum mechanics. The method had been developed from the classical theory of Larmor for studies in magnetic resonance, particularly for nuclear magnetic resonance and for resonance experiments on atomic beams, and was to hand when the optical-radio-frequency double resonance technique for excited atoms was introduced by Brossel and Bitter in the early nineteen fifties. In this context the two different kinds of resonance which were taking place simultaneously presented very different features: the optical resonance was induced by a broad-band radiation field where perturbation of the atoms was exceedingly weak compared with the resonance frequencies, whereas the radio-frequency field was monochromatic and interacted very strongly with the atoms. Both interactions could be treated by semi-classical methods, but the latter was particularly amenable to solution by the method of rotations.

Over the years my colleagues and I have applied this method to interpret a great variety of resonance phenomena in excited atoms. The extension from uniform rotations to frequency-modulated rotations led to the analysis of a whole new class of resonances, and the combination of uniform with frequency-modulated rotations has enabled quite complicated problems to be solved – in particular, the Bloch–Siegert effect has been analysed to cover shifts of the resonance as great as the resonance frequency itself.

The theoretical work has been published, as the occasion demanded, in the primary research literature, but a systematic account, including the more recent work on frequency-modulated rotations, is extant only in the form of lecture notes which I have prepared from time to time. I welcome the opportunity provided by the publication of this volume in honour of Willis Lamb to present as a whole the theory as it has been developed so far. The sphere of its application, atoms and fields and resonances, is a territory which Willis himself has explored with great distinction. We shall barely touch upon the subtleties which he has exposed with such success, but the elements we use are those which he also has used so often in the analysis of his experiments: atoms, classical fields, and Schrödinger's equation. We trust that he will give the work at least a qualified approval.

I must record, at the outset, that the shape of the theory as it is presented here owes much to discussions I have had with my collaborators in research: in particular to Professor J.N. Dodd, in the early days, and to Dr. D.T. Pegg, more recently. Dr. Pegg, and also Dr. B.J. Dalton have been kind enough to read the whole manuscript, and to give me the benefit of their comments.



### 1.1. Quantized fields and classical fields

There are those who consider that no analysis of interactions is worthwhile unless the fields are quantized; and this, notwithstanding the tremendous successes of semi-classical methods in treating electric and magnetic resonances in atomic and molecular beam experiments, in esr, in nmr, in optical pumping and indeed, in the functioning of lasers. True it is that quantized fields carry fluctuations, but these can be provided by other models if the phenomena to be interpreted require them. Here, for the most part, we shall be concerned with the analytical description of resonance experiments where the results (transition probabilities, line profiles, resonance conditions) obtained by semi-classical methods are identical with those obtained by quantized field methods in those cases where the comparisons have been properly and fairly made.

Our formal definition of “semi-classical” is this: a treatment in which, while the atoms are treated as quantum-mechanical systems, the fields which interact with the atoms are represented by c-numbers within the quantum mechanical analysis. This contrasts with the fully quantum-mechanical treatment in which atoms and fields are treated as one quantum-mechanical system.

That semi-classical and quantized field theories should lead to the same predictions when the fields are very strong is to be expected in terms of the necessity of correspondence between classical and quantum mechanics, for in such circumstances the change in quantum number ( $\Delta n = \pm 1$ ) is much smaller than the quantum number itself ( $n$ , the quantum number labelling the Fock state; the number of photons present in the field). This has been spelt out in detail in a number of publications, for example, by Stenholm [1]. When the fields are strong the dominant interactions are, of course, the *stimulated* absorption and emission processes.

It is perhaps, less widely appreciated that the semi-classical and quantum treatments agree in their predictions of the probability of *absorption* even when the fields are weak ( $n \ll 1$ ). This stems from the fact that, in both theories, the absorption coefficient is found to be proportional to the energy density of the stimulating field, in the one case,  $|E|^2$ , in the other,  $n\hbar\omega$ , with no restriction on the weakness of the field.

The probability of emission, on the other hand, is proportional to  $(n + 1)\hbar\omega$  for the quantum field theory, for the same stimulating field as before. In the semi-classical theory the probability is, again  $|E|^2$ . The “+1” contribution to the probability in the quantum field theory – commonly interpreted as *spontaneous emission* – is missing from the result of the semi-classical calculation if the field  $E$  is taken to represent the emission from a laboratory source. That this field needs to be supplemented to account for spontaneous emission by semi-classical theory is beyond question, but quantum field theory is not essential to meet the situation. A well-known thermodynamical argument, the equilibrium between atoms and radiation in a black-body cavity, for example, allows us to calculate the probability of spontaneous emission (Einstein  $A$ -coefficient) in terms of the probability of absorption (Einstein  $B$ -coefficient) which, as we have seen, can be calculated correctly by semi-classical methods. It will be recalled that the argument can be made without appealing to Planck’s law – we go to the limit of high temperatures and use the Rayleigh–Jeans law. By this route Planck’s constant is introduced into the  $A/B$  ratio through the photoelectric (interaction) equation,  $\epsilon = h\nu$ , not via the properties of the radiation field.

The need to supplement the “laboratory” field  $E$  by a term to account for spontaneous emission having been admitted, it is not difficult to find a field with the required properties. It needs to be isotropic and its temporal properties can be specified by an autocorrelation function or, alternatively, a power spectrum. An energy density of  $\frac{1}{2}h\nu$  per mode gives the required result. This



corresponds, of course, to the zero-point fluctuations of the quantized radiation field, but the derivation we have outlined is not based on that quantization.

A feature of this derivation, namely, that we need not specify the field analytically but only by its autocorrelation function, solves a problem that is present also for “weak” laboratory fields. We cannot measure the field from a conventional laboratory lamp, for example, though in the analysis we use a symbol to represent it. What is measurable about such fields are the components of a “coherency matrix”,  $\phi_{ij}(\tau) = \langle E_i(t)E_j^*(t + \tau) \rangle$ . Here, the suffixes refer to spatial components and the angle brackets indicate time averaging. The  $\phi_{ij}(\tau)$  may be determined by measurements made with photodetectors, polarizers and spectrometers. The interaction between fields and atoms is determined by calculating a scattering matrix for the  $\phi_{ij}$ . Symbols representing fields may enter the calculation, but there is no implication that these fields are measurable. The situation is quite analogous to the use of a wave function to represent an atom.

The approach outlined here is implied in the traditional semi-classical calculations of the interaction of light with atoms, for example, in text-book calculations of the Einstein  $B$ -coefficient. The “scattering matrix” point of view was explicitly taken by the present author [2] in a paper on the double scattering of resonance fluorescence. The auto-correlation method applied to spontaneous emission will be demonstrated in section 7. The merits of the method for fields at optical frequencies are not so apparent for fields at radio or microwave frequencies. This spectral region is characterised by the following features, (i) the fields used in experiments are usually monochromatic (to an extremely high degree), (ii) the fields are usually strong (in the sense  $n \gg 1$ ), and (iii) spontaneous emission is usually entirely negligible, not only because the fields are strong, but also because the probability for spontaneous emission, being proportional to the cube of the frequency, is many orders of magnitude smaller at these than at optical frequencies.

Additionally, the spectral structures studied are usually simpler at these frequencies than at optical frequencies: the latter are characterised by the very irregular distribution of energy levels between the ground states and ionization potentials of atoms, the former by Zeeman or hyperfine structures which are more regular. Indeed, we shall make much use of a model in which an atom is supposed to be characterised by a magnetic moment whose magnitude is independent of field strength, yielding a set of energy levels which, in an external magnetic field, are equally spaced. The bulk of this article has to do with the response of atoms characterised in this way to strong, monochromatic fields at radio or microwave frequencies.

### 1.2. Interaction of time-dependent magnetic fields with paramagnetic atoms

A special feature of the magnetic interaction is that rotations in physical space correspond to the establishment of additional magnetic fields on magnetic spin systems interacting with them. By a suitably chosen combination of rotations any specified time-dependent field can be reduced to a static field within any desired accuracy, and the quantum-mechanical problem correspondingly reduced to a solution of the evolution of an atomic state vector in a static magnetic field – the Zeeman effect. This is the path we shall follow. We remark, in passing, that the methods can be applied, in suitable cases, to electric dipole interactions, although the “rotations” are then in an abstract space, not in physical space [3]. We confess also to a preference for the interpretation of phenomena as “Zeeman effect in a transformed reference frame” rather than as “renormalization of the forward-scattering mass operator”, a form of expression to which adherents of field quantization have, on occasion, been led.



There are two configurations of fields for which the equation of motion of a paramagnetic atom in these fields can be solved exactly. These we refer to as case A and case B. Our approximate solutions for more complicated cases will rest upon the solutions for cases A and B.

The configuration for case A is that of a magnetic field *rotating uniformly* in a plane *perpendicular* to a static field. This is the arrangement of fields for the conventional magnetic resonance experiment. The analysis by the method of rotating co-ordinate frames, now extremely well known, was spelt out in classical and semi-classical terms in a review article in 1954 by Rabi, Ramsey and Schwinger [4].

The configuration for case B is that of a magnetic field *oscillating uniformly parallel* to a static field. The analysis by co-ordinate transformations for this case was given by Pegg and Series [5, 6] and used to study the Bloch–Siegert shift (section 6) and other phenomena which we shall meet later (section 4).

Our approach to the solution of these two basic situations will be to find the corresponding time-shift operators  $U(t, t_0)$  for the evolution of the atomic state vector in the interval  $t_0$  to  $t$ :

$$|t\rangle = U(t, t_0)|t_0\rangle. \quad (1)$$

$|t\rangle, |t_0\rangle$  are kets in the space of eigenkets of Hamiltonian operators describing the atom, and  $U$  is unitary.  $U$  will be derived as a function of operators representing rotations in physical space and the angular momentum operators of the atom. The role of the Larmor frequencies in the transformed frame will be evident.

## 2. Case A

### 2.1. Exact solution

The configuration of fields for this case is shown in fig. 1;

$$\mathbf{B}_A(t) = B_1 (\cos \omega t \mathbf{i} + \sin \omega t \mathbf{j}) + B_0 \mathbf{k}. \quad (2)$$

We represent the atom by its magnetic moment operator  $\hat{\mu}$  and angular momentum operator  $\hat{\mathbf{J}}$ :

$$\hat{\mu} = \gamma \hat{\mathbf{J}}, \quad (3)$$

where the gyromagnetic ratio,  $\gamma$ , is supposed to be independent of fields. The interaction Hamiltonian is then

$$\begin{aligned} \mathcal{H}_A(t) = -\hat{\mu} \cdot \mathbf{B}_A(t) = -\gamma \hat{\mathbf{J}} \cdot \mathbf{B}_A(t) = \omega_0 \hat{J}_z + \frac{1}{2}\omega_1(\hat{J}_x + i\hat{J}_y) \exp(-i\omega t) \\ + \frac{1}{2}\omega_1(\hat{J}_x - i\hat{J}_y) \exp(i\omega t), \end{aligned} \quad (4)$$

with  $\omega_0 = -\gamma B_0$ ,  $\omega_1 = -\gamma B_1$ .

It is required to integrate the Schrodinger equation of motion

$$i\hbar \frac{\partial}{\partial t} |t\rangle = \mathcal{H}_A(t) |t\rangle, \quad (5)$$

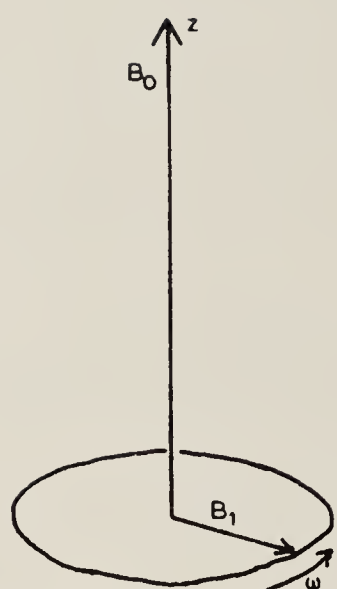
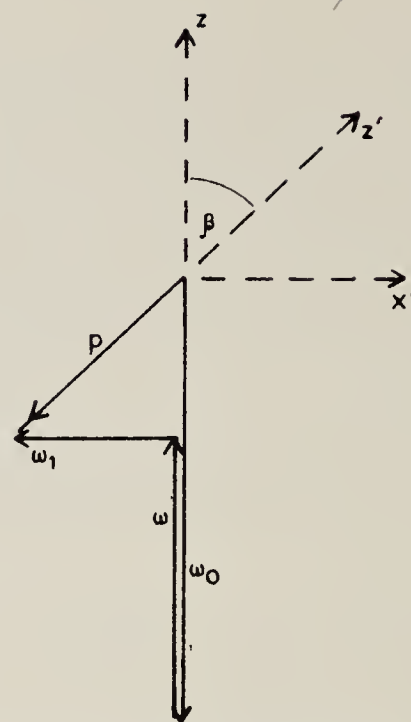


Fig. 1. Configuration of magnetic fields for case A.

Fig. 2. The fields of case A in the rotating frame, represented by their corresponding frequencies,  $\omega_i = -\gamma B_i$ .

in which we take  $\hbar = 1$ . Using (1) we have, equivalently,

$$i \frac{\partial}{\partial t} U_A(t, t_0) = \mathcal{H}_A(t) U_A(t, t_0). \quad (6)$$

The method of solution is

- make a co-ordinate transformation to eliminate the time-dependence of  $\mathcal{H}_A(t)$ ,
- integrate the equation of motion in the transformed frame, and
- apply the inverse co-ordinate transformation.

It is also convenient to diagonalize the Hamiltonian in the transformed frame.

It is apparent geometrically that the fields will be static in a frame  $(x', y', z)$  rotating about the  $z$ -axis with constant angular velocity,  $\omega$ . Transformation to this frame is achieved by use of the unitary operator

$$\hat{S}_A(t) \equiv \exp(i\hat{J}_z \omega t). \quad (7)$$

Denoting transformed states and operators by  $'$ , we have

$$|t'\rangle = \hat{S}_A(t) |t\rangle, \quad (8)$$

whence

$$U'_A(t, t_0) = \hat{S}_A(t) U_A(t, t_0) \hat{S}_A^{-1}(t_0). \quad (9)$$

If we write the equation of motion in the new frame

$$i \frac{\partial}{\partial t} U'_A(t, t_0) = \mathcal{H}'_A(t) U'_A(t, t_0), \quad (10)$$

we find, using (6), that

$$\mathcal{H}'_A(t) = \hat{S}_A(t) \mathcal{H}_A(t) \hat{S}_A^{-1}(t) - i \hat{S}_A(t) (\partial/\partial t) \hat{S}_A^{-1}(t). \quad (11)$$



The first term on the right corresponds to the purely geometrical aspect of the rotation which clearly leads to

$$\mathbf{B}'_A = B_0 \mathbf{k} + B_1 \mathbf{i}' \quad (12)$$

and

$$\hat{S}(t) \mathcal{H}_A(t) \hat{S}_A^{-1}(t) = -\gamma(\hat{J}_z B_0 + \hat{J}_{x'} B_1). \quad (13)$$

The second term on the right in (11) is readily evaluated as  $-\hat{J}_z \omega$ . It exhibits the effect of the rotation in simulating an additional magnetic field of magnitude  $-\omega/\gamma$  in the transformed frame. The net result is

$$\mathcal{H}'_A = (\omega_0 - \omega) \hat{J}_z + \omega_1 \hat{J}_{x'}. \quad (14)$$

It is to be noticed that we have used the operator  $\hat{S}_A(t)$  in the passive sense to achieve a rotation of co-ordinate axes. The ket  $|t\rangle$  describes the original atomic system, referred to the rotating frame, and the corresponding operators represent measurements made by instruments fixed in that frame. We shall continue to make this interpretation of the transformations. An alternative view (the active sense) is to regard  $\hat{S}_A(t)$  as inducing a transformation of the wave function, which then describes a set of atoms upon whose motion has been superimposed a rotation with respect to the laboratory frame. This view would lead to eq. (14), with  $\hat{J}_{x'}$  replaced by  $\hat{J}_x$ . The state vector and operators in the active sense are the same functions of  $(x, y, z)$  as the state vector and operators in the passive sense are of  $(x', y', z)$ .

We return now to eq. (14). The transformed Hamiltonian is independent of time but it does not commute with  $\hat{J}_z$ . It does, however, commute with  $\hat{J}_{z'}$ , where the  $z'$ -direction is related to the  $z$ -direction by a rotation through an angle  $\beta = \tan^{-1}[\omega_1/(\omega_0 - \omega)]$  about  $Oy'$  (see fig. 2). The rotation may be achieved by the operator

$$\mathcal{D}(\beta) \equiv \exp(i\beta \hat{J}_{y'}). \quad (15)$$

The transformed Hamiltonian and time-shift operators are

$$\mathcal{H}''_A = \mathcal{D}(\beta) \mathcal{H}'_A \mathcal{D}^{-1}(\beta) \quad (16)$$

and

$$U''_A = \mathcal{D}(\beta) U'_A \mathcal{D}^{-1}(\beta), \text{ respectively.} \quad (17)$$

Since  $\mathcal{D}$  is not time-dependent this transformation leaves the equation of motion invariant and we have

$$i \frac{\partial}{\partial t} U''_A(t, t_0) = \mathcal{H}''_A U''_A(t, t_0), \quad (18)$$

whence

$$U''_A(t, t_0) = \exp[-i\mathcal{H}''_A(t - t_0)]. \quad (19)$$

$\mathcal{H}''_A$  is diagonal in the basis of the eigenstates of  $\hat{J}_{z'}$ . Its eigenvalues are the Larmor frequencies in the field  $[(\omega_0 - \omega)^2 + \omega_1^2]^{1/2}$  (see fig. 2). We have reduced our problem to that of the Zeeman effect in a static field along  $Oz'$ . Before elaborating this we write the formal solution for  $U_A(t, t_0)$  obtained by applying to  $U''_A$ , eq. (19), the inverse transformations obtained from eqs. (17), (16), (9) and (7).

The result is

$$U_A(t, t_0) = \exp(-i\hat{J}_z\omega t)\mathcal{D}^{-1} \exp[-i(\mathcal{D}\mathcal{H}'_A\mathcal{D}^{-1})(t - t_0)]\mathcal{D} \exp(i\hat{J}_z\omega t_0). \quad (20)$$

Notice the effect of the time variables in this operator. The term on the right, in  $t_0$ , gives a reference phase marking the beginning of the interaction. The term on the left, in  $t$ , shows how the time evolution of the field is subsequently imposed on the wave function of the atom. The evolution from  $t_0$  to  $t$  at the Larmor frequency in the transformed frame is expressed by the middle term. The time-independent rotation operators,  $\mathcal{D}$  and its inverse, project the eigenstates of  $\hat{J}_z$  on those of  $\hat{J}_{z'}$  and, by virtue of the Larmor precession about  $Oz'$ , have the effect of inducing transitions between eigenstates of  $\hat{J}_z$ .

## 2.2. Zeeman effect in the transformed frame: the Rabi frequency

Eq. (16) may be written more explicitly in terms of a vector  $\mathbf{p} = p\mathbf{k}'$  which represents rotation at the Larmor frequency of the atom about  $Oz'$ . The components of  $\mathbf{p}$  along  $z$  and  $x'$  are:

$$p_z = \omega_0 - \omega, \quad p_{x'} = \omega_1, \quad (21)$$

so that

$$\mathcal{H}'_A = p_z\hat{J}_z + p_{x'}\hat{J}_{x'} = \mathbf{p} \cdot \hat{\mathbf{J}}, \quad (22)$$

$$\mathcal{H}''_A = p\hat{J}_{z'}, \quad \text{with } p = [(\omega_0 - \omega)^2 + \omega_1^2]^{1/2}. \quad (23)$$

Let the eigenstates of  $\hat{J}_{z'}$  be labelled  $\mu$ , with corresponding eigenvalues  $\mu\hbar$  ( $\hbar = 1$ ). The eigenvalues of  $\mathcal{H}''_A$  are  $q_\mu = \mu p$ . These are the Zeeman levels in the transformed frame. The frequency  $p$  was introduced into the solution of this problem by Rabi, and bears his name. (Sometimes the name "Rabi frequency" is given to  $\omega_1$ .)

In fig. 3 we see how the levels  $q_\mu$  are generated from the Zeeman levels of the atom in the laboratory frame. For illustration we chose the particular case of an atom having  $J = 1$  and label the eigenvalues of  $\hat{J}_z$  (laboratory frame) by  $m$ . The Zeeman levels in the field  $B_0$  are  $m\omega_0$ , represented in fig. 3(a). The transformation to the rotating frame generates the additional energy  $-m\omega$ , giving fig. 3(b). Notice that these are the Zeeman levels, seen in the transformed frame, under  $B_0$  alone. The consequences of adding  $B_1$  are: (i) that the levels are no longer linear, but hyperbolic functions

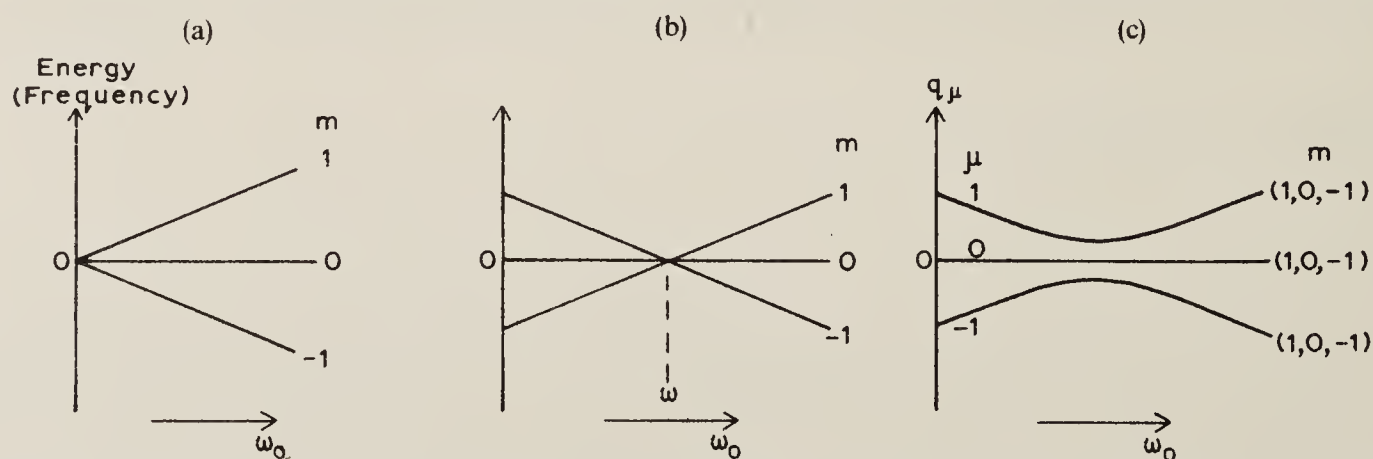


Fig. 3. Zeeman levels for  $J = 1$ , plotted against the frequency  $\omega_0$ . (a) Laboratory frame,  $\omega_1 = 0$ ; (b) Rotating frame,  $\omega_1 = 0$ ; (c) Rotating frame,  $\omega_1 \neq 0$ .



of  $\omega_0$ , as shown in fig. 3(c), (ii) that the eigenstates, now labelled by  $\mu$ , are linear superpositions of the eigenstates of the earlier figures according to

$$|\mu\rangle = \sum_m \mathcal{D}_{m\mu}^J(\beta) |m\rangle. \quad (24)$$

Hence, in the transformation back to the laboratory frame (subtract  $-m\omega$ ), each level of 3c is split into three levels, the result being shown in fig. 4.

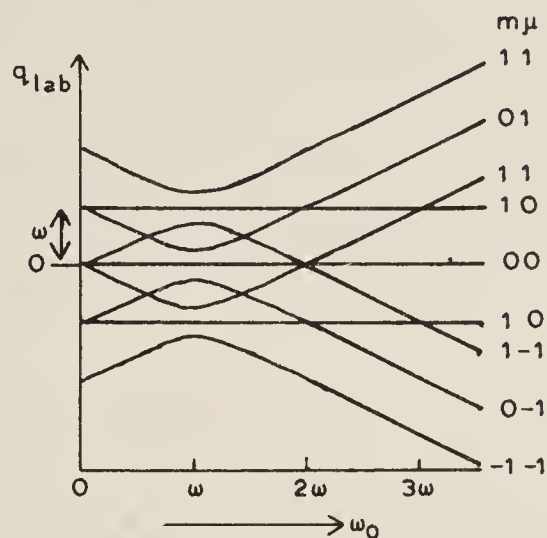


Fig. 4. Frequency diagram for  $J = 1$  in case A. Plot of  $q_{lab}$  against  $\omega_0$ .  $m, \mu$  label eigenstates of  $\hat{J}_z, \hat{J}_z'$ , respectively. ( $Oz$  is the axis of symmetry in the laboratory frame.) (By permission of the Royal Society.)

There are now  $(2J + 1)^2$  levels, each labelled by a different combination of the quantum numbers  $m$  and  $\mu$ . The equations of the levels are

$$q_{lab} = m\omega + \mu p \quad (25)$$

with  $m, \mu$  taking all the allowed values of component of  $\hat{J}$ .

Diagrams of which fig. 4 is an example were named "frequency diagrams" by Dodd and Series [7]. They are a generalisation of energy level diagrams to give a representation of time-dependent Hamiltonians. In a mathematical sense such diagrams display the possible combinations of frequencies which appear in the atomic wave function, but they have a physical reality also. For example, at the crossings of levels, which, for the case  $J = 1$ , occur in the region  $\omega_0 = \frac{1}{2}\omega, \frac{3}{2}\omega$ , the "level-crossing" phenomena of resonance fluorescence can be explored (see section 2.3.2). Frequency diagrams serve the purpose of exhibiting in a compact way the possibilities for the design and interpretation of experiments involving strong, oscillating fields. As to the condition of resonance, we shall, in section 2.3.1, derive the well known condition  $\omega_0 = \omega$  for a steady state experiment: here we wish to point out that this condition corresponds to the position of closest approach of the levels in the frequency diagram. For the symmetrical diagram which results from our assumption that  $\gamma$  is independent of the fields, the resonance condition may be written as  $\partial q / \partial \omega_0 = 0$ , or – since  $q^2$  is the quantity more directly related to the fields –  $\partial q^2 / \partial \omega_0 = 0$ . At resonance  $\beta = \pi/2$ ,  $p = \omega_1$ , its minimum value.

Diagrams of this sort have been obtained by authors who use different methods to analyse radiation interactions. The diagram for a 2-level system was first given by Autler and Townes [8].

Shirley, using Fourier and Floquet expansions (a technique to which we shall return in section 5.2) drew similar diagrams to represent the eigenvalues of a time-independent Hamiltonian which he constructed, by an analytical method, as an approximation to the time-dependent semi-classical Hamiltonian which was his starting point. But the more significant fact is that identical diagrams have been drawn by Cohen-Tannoudji and Haroche [9] in their theory of “dressed atoms”. Here, the starting point is the quantized field theory of radiation. The diagrams now appear as conventional energy-level diagrams of the quantum-mechanical system (atoms + fields). Shirley drew attention to a possible interpretation of his diagrams along these lines. The quantum numbers which label the system in the quantized field version are those of the atom ( $m$ ) and of the radiation field ( $n_k$  – where  $k$  labels the mode of the field). It is to be noticed, however, that the levels of these diagrams correspond to states which, being eigenstates of energy, cannot separately represent an atom subjected to an oscillating or rotating field. To represent such a physical system a linear superposition of states of different  $n_k$  but the same  $m$  is called for.

### 2.3. Steady-state experiment

#### 2.3.1. Excitation to an eigenstate of $\hat{J}_z$

Before developing the rotating-frame technique we shall give an example to show how the solution  $U_A(t, t_0)$  (eq. (20)) may be incorporated into the analysis of a resonance experiment.

Consider the fields of eq. (2) interacting with an assembly of atoms specified by eq. (3), but subject also to some isotropic, random process of relaxation which destroys the phase-coherence of the interaction, and some pumping mechanism which populates preferentially some particular eigenstate  $|n\rangle$  of  $\hat{J}_z$ . We might have in mind an electron spin resonance experiment in which thermal processes are responsible both for relaxation and for preferential population, or an optical pumping experiment in which excitation by broad-band light is responsible for the preferential population and radiative decay for the relaxation.

We describe the assembly of atoms by a density matrix  $\rho(t)$ . Consider first the evolution of the density matrix under the Hamiltonian  $\mathcal{H}_A$  (eq. (4)), that is, excluding the damping and regeneration. With  $\rho(t_0) = |n\rangle\langle n| \equiv \rho_n$ , the density matrix  $\rho^{(0)}(t)$  representing evolution under  $\mathcal{H}_A$  alone is given by

$$\rho^{(0)}(t) = U_A(t, t_0)\rho_n U_A^\dagger(t, t_0). \quad (26)$$

The complete equation of motion is

$$\dot{\rho}(t) = -i[\mathcal{H}_A, \rho] - \Gamma\rho + R\rho_n, \quad (27)$$

where  $-\Gamma\rho$  represents damping at the rate  $\Gamma$  and  $R\rho_n$  represents regeneration into  $|n\rangle$  at the rate  $R$ . The solution of eq. (27) is

$$\rho(t) = \rho^*(t, 0) + R \int_0^t \rho^*(t, t_0) dt_0, \quad (28)$$

with

$$\rho^*(t, t_0) = \rho^{(0)}(t, t_0) \exp -\Gamma(t - t_0), \quad (28a)$$



(notice that  $\rho^*$  is the solution of eq. (27) with  $R = 0$ ). The transient part of eq. (28),  $\rho^*$ , damps out in a time  $\gg \Gamma^{-1}$  so that the steady-state solution is given by the second term.

Let us write out  $\rho(t)$  more fully and consider particular features of it:

$$\rho(t) = R \int_0^t dt_0 U_A(t, t_0) \rho_n U_A^\dagger(t, t_0) \exp -\Gamma(t - t_0), \quad (29)$$

with  $U_A(t, t_0)$  given by eq. (20).

(i) Since we assumed  $\rho_n$  was diagonal in the eigenstates of  $\hat{J}_z$  (notice that the validity of eq. (29) does not rely on this assumption and that an interesting class of experiments arises for off-diagonal pumping), the terms  $\exp(\pm i\hat{J}_z \omega t_0)$  in  $U \rho_n U^\dagger$  will reduce to 1.

(ii)  $t_0$  will appear only in the factors  $\exp[\pm i\mu p(t - t_0)]$  of  $U$  and  $U^\dagger$ , and in  $\exp -\Gamma(t - t_0)$ .

(iii) Terms  $\exp(\pm i\hat{J}_z \omega t)$  will remain in  $U, U^\dagger$ .

From (i) and (ii) we conclude that the integration over  $t_0$  will yield denominators  $(\Gamma \pm i(\mu - \mu')p)$ . The frequencies  $p$  will not appear elsewhere. Taking note of (iii) we find that the result will be of the form

$$\rho_{mm',n}(t) = \sum_{\mu\mu'} [\exp -i(m - m')\omega t] \mathcal{D}_{m\mu}^{-1} \mathcal{D}_{\mu n} \mathcal{D}_{n\mu'} \mathcal{D}_{\mu'm'}^{-1} R / [\Gamma \pm i(\mu - \mu')p]. \quad (30)$$

We notice

(i) that the diagonal elements  $\rho_{mm}$  have no time-dependence;

(ii) that the off-diagonal elements are modulated at harmonics of the driving field. The number of possible harmonic frequencies is  $2J$ ;

(iii) that the magnitudes of the denominators,  $[\Gamma^2 + (\mu - \mu')^2 p^2]^{1/2}$ , are either independent of the fields (for  $\mu = \mu'$ ) or pass through minimum values (greatest degree of mixing between the  $m$ ) when  $(\mu - \mu')p$  passes through a minimum. Recall  $p = [(\omega_0 - \omega)^2 + \omega_1^2]^{1/2}$ .

Notice that these minima occur when  $\omega_0 = \omega$ , and that the value of  $p$  is then  $(\mu - \mu')\omega_1$ . This is the condition of resonance we mentioned in the last section. Notice also that this condition does not necessarily imply a maximum value for the  $\rho_{mm'}$ , since the matrix elements of  $\mathcal{D}$  also depend on the fields. The  $\rho_{mm'}$  are, however, symmetrical or antisymmetrical functions of  $(\omega_0 - \omega)$ . Some of these functions for  $J = 1$  are shown in fig. 5.

The resonances, then, correspond to terms in which  $\mu \neq \mu'$ . The widths of the resonances are governed largely by the denominators. Notice the occurrence of  $\omega_1^2$  in these denominators. When  $\mu - \mu' = 1$ , for example, the (denominator)<sup>2</sup> is  $[\Gamma^2 + \omega_1^2 + (\omega - \omega_0)^2]$ , whose value is double the value at resonance,  $(\Gamma^2 + \omega_1^2)$ , when  $(\omega - \omega_0)^2 = \Gamma^2 + \omega_1^2$ . The occurrence of  $\omega_1^2$  in this equation demonstrates the "power broadening" of the resonance.

With knowledge of the density matrix we are able to predict the results of any observation which may be made on the assembly of atoms by forming the corresponding monitoring operator  $M$  and calculating the Trace  $[M\rho]$ . For example, if the  $\rho$  of our calculation is the partial density matrix representing a set of excited states, the intensity of fluorescent light of polarization  $u$  emitted in radiative decay to a set of ground states  $|l\rangle$  is proportional to

$$\sum_l \sum_{m,m'} \rho_{mm'} \langle l|u \cdot P|m\rangle \langle m'|u^* \cdot P|l\rangle = \text{Tr} [M\rho], \quad (31)$$

where

$$M = \sum_l u^* \cdot P |l\rangle \langle l| u \cdot P. \quad (31a)$$

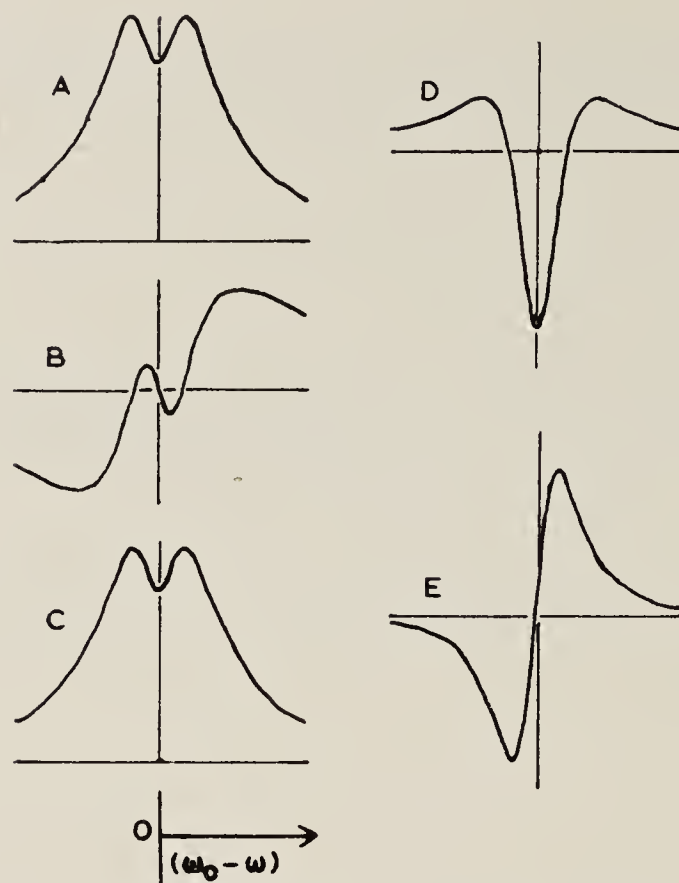


Fig. 5. Resonance functions for an aligned spin-system [7, 17, 18]. (By permission of the Royal Society.)

The intensity of the fluorescent light reflects the behaviour of those elements  $\rho_{mm'}$  which are selected by  $M$ .

### 2.3.2. Excitation to a superposition state of $\hat{J}_z$

This can be achieved if the pumping mechanism is not symmetrical about  $Oz$ , for example, excitation by light whose electric vector is perpendicular to  $Oz$ . In this case  $\rho(t_0)$  will contain off-diagonal elements  $|n\rangle\langle n'| \equiv \rho_{nn'}$  which enter eq. (29) in place of  $\rho_n$ . Under the assumption of broad-band excitation there will be no  $t_0$ -dependent phase factors, but the conclusion (i) following eq. (29) no longer applies;  $U\rho_{nn'}U^+$  will now provide a factor  $\exp i(n - n')\omega t_0$  in  $\rho(t_0)$  and hence in the integrand of eq. (29). Writing this as  $[\exp i(n - n')\omega t] \times [\exp -i(n - n')\omega(t - t_0)]$  we find that eq. (30) is replaced by

$$\rho_{mm'}(t) = \sum_{\substack{\mu\mu' \\ nn'}} \frac{\exp -i(m - m' - n + n')\omega t}{\Gamma \pm i(\mu - \mu')p \pm i(n - n')\omega} \mathcal{D}_{m\mu}^{-1} \mathcal{D}_{\mu n} \mathcal{D}_{n'\mu'} \mathcal{D}_{\mu'm'}^{-1} R_{nn'} \quad (32)$$

$R_{nn'}$  is the rate coefficient for  $\rho_{nn'}$ . The conclusions following (30) no longer apply. Instead, we have

- (i) the diagonal elements  $\rho_{mm}$  may be modulated;
- (ii) the number of possible modulation harmonics for the off-diagonal elements is now  $4J$ ;
- (iii) the denominators pass through minimum values, not only when  $p$  is a minimum but also when

$$(\mu - \mu')p = -(n - n')\omega. \quad (33)$$



Referring back to eq. (25) we see that eq. (33) is satisfied at the crossing of two levels in the frequency diagram. The present analysis shows that observation of the phenomena attendant upon these level-crossings is contingent on excitation to a superposition-state of  $\hat{J}_z$ . This is the well-known condition for observation of the Hanle effect: indeed, our analysis contains the Hanle effect as a trivial special case corresponding to zero amplitude of the rotating field.

The predictions of eqs. (30) and (32) were confirmed in a series of investigations by the author and his colleagues [10–13]. The systems chosen were the excited states  $6s6p\ ^3P_1$  of mercury and  $5s5p\ ^3P_1$  of cadmium, for which the density matrix was monitored by observations of fluorescent light, and the metastable state  $1s2s\ ^3S_1$  of helium, where the monitoring was by absorption of light. The unmodulated terms ( $m = m'$ ) had already been fully investigated in studies of magnetic resonance, and attention in these experiments was concentrated on the modulated terms. In relation to eq. (30), the four different modulated resonance functions predicted for alignment ( $k = 2$ : see section 2.4) were observed and studied under a wide range of variation of parameters, also the two identical modulated functions predicted for orientation ( $k = 1$ ). In relation to eq. (32) the additional level-crossing features, characterized by the higher harmonics, and contingent upon excitation with light whose electric vector was skew to  $\mathbf{B}_0$ , were also observed and showed the expected behaviour.

Corney's experiments, directed to investigating the *intervals* in the frequency diagram, were carried out by using modulated light to excite the atoms. The frequency of modulation,  $\nu$ , could be chosen to be very different from the frequency of the driving field,  $\omega$ . The analysis is similar to that worked out below in section 3.3. Resonances are predicted when the frequency  $\nu$  matches an interval in the diagram, and the details of line-shape are governed by the coefficients in eq. (32). The experiments vividly confirmed the details of the diagram.

#### 2.4. Use of irreducible spherical tensor operators

It has been common in recent years to obtain expressions for the observable quantities in resonance experiments in a form which, so far as possible, reflects the geometry of the experiment. By this means it is often possible to reduce the complexity of analytical expressions, in particular, of the density matrix. The underlying reason for this is that expansions in terms of eigenstates of  $\hat{J}_z$  are not necessarily the most economical.

Suppose the density operator is expressed in terms of the irreducible spherical tensor operators  $\hat{T}_q^k$  (e.g. [14]):

$$\hat{\rho}(t) = \sum_{kq} (-1)^q \rho_q^k(t) \hat{T}_{-q}^k. \quad (34)$$

The  $\hat{T}_q^k$  transform under rotations in the same way as the spherical harmonics. They are orthogonal, and normalised so that  $\text{trace}(\hat{T}_q^k \hat{T}_{-q}^{k'}) = (-1)^q \delta_{qq'} \delta_{kk'}$ .

They satisfy the commutator relations

$$[\hat{J}_0, \hat{T}_q^k] = q \hat{T}_q^k, \quad [\hat{J}_{\pm 1}, \hat{T}_{q\mp 1}^k] = \mp \left\{ \frac{1}{2}(k \mp q + 1)(k \pm q) \right\}^{1/2} \hat{T}_q^k. \quad (35)$$

With the initial density operator  $\hat{\rho}(t_0)$  given in this form (taking the place of  $\rho_n$  in eq. (26)) the operations of the  $U(t, t_0)$ , a series of rotations, are easily carried out. The rotation about the  $z$ -axis at time  $t_0$  preserves the values of  $k, q$  and introduces the factor  $q$  instead of  $(n - n')$ . The rotations  $\mathcal{D}(\beta)$  preserve the values of  $k$  but lead to linear combinations of the  $q$ . The evolution about the

axis  $Oz'$  is represented by terms in the density matrix  $\exp -iq'p(t - t_0)$ , where  $q'$  is representative of the values of  $q$  which are introduced under the rotation  $\mathcal{D}(\beta)$ . The inverse rotation generates a linear combination represented by  $q''$ , and rotation about the  $z$ -axis at time  $t$  introduces the frequencies  $-q''\omega$ .

Finally, eq. (32) is replaced by

$$\rho_{q''}^k(t) = \sum_{q,q'} [\exp -i(q'' - q)\omega t] \mathcal{D}_{q',q}^k \mathcal{D}_{q'',q'}^{-1,k} R_q^k / [\Gamma \pm q'p \pm iq\omega]. \quad (36)$$

The number of terms in the expression for  $\rho(t)$  is  $(2k + 1)^3$  for each value of  $k$ , with  $2J$  values of  $k$ . Thus, for  $J = 1$ , values of  $k$  are 0, 1, 2, with 1, 27, 125 terms for each, 153 in all. By contrast, the number of terms in  $\rho(t)$  expressed in the  $(m, m')$  basis for  $J = 1$  is  $3^6 = 729$ . The simplification in going to the  $(k, q)$  basis has been achieved by grouping the values of  $(m - m')$ ,  $(n - n')$ ,  $(\mu - \mu')$  according to their geometrical significance. This is formally achieved by the orthogonal properties of the  $\hat{T}_q^k$ .

The form (36) was derived and used by Gough [15, 16] in a series of papers describing the transfer of coherence in sensitized fluorescence. The simpler form, corresponding to eq. (30), was obtained by Pancharatnam [17, 18] who went on to give a geometrical model of alignment – a rotating ellipsoid – in generalisation of the model of a precessing magnet which is commonly used to illustrate the dynamics of oriented systems.

### 3. Case B

#### 3.1. Exact solution

We now turn to the second case whose solution may be obtained exactly, that for the configuration of fields represented in fig. 6:

$$\mathbf{B}_B(t) = (B_2 \cos \omega t + B_3)\mathbf{k}. \quad (37)$$

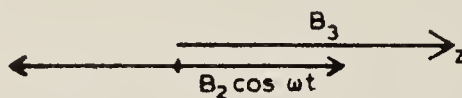


Fig. 6. Configuration of magnetic fields for case B. Notice that the  $z$ -axis has been chosen to be parallel, not perpendicular to the oscillating field.

Notice that we have chosen the  $z$ -axis in the direction of the oscillating field rather than perpendicular to it, as for case A. The distinction is important, and is likely to be overlooked, particularly in the special case  $B_3 = 0$ .

With  $\hat{\mu} = \gamma \hat{J}$  as before, we have

$$\mathcal{H}_B(t) = -\hat{\mu} \cdot \mathbf{B}_B(t) = -\gamma \hat{J} \cdot \mathbf{B}_B(t) \quad (38)$$

$$= (\omega_2 \cos \omega t + \omega_3) \hat{J}_z. \quad (39)$$

The transformation which eliminates the time-dependence is, in this case,

$$\hat{S}_B(t) \equiv \exp [i \hat{J}_z (r \omega t + a \sin \omega t)], \quad a = \omega_2 / \omega. \quad (40)$$



The integer  $r$  need not, at this stage, be specified. Its introduction allows us some freedom of choice later, when this transformation is used with a more complicated Hamiltonian.

The transformation (40) corresponds to a rotation round the  $z$ -axis at the uniform rate  $r\omega$ , together with a velocity-modulated rotation at the frequency  $\omega$ , whose amplitude is chosen so that the additional field generated in the velocity-modulated frame exactly annuls the oscillating field in the laboratory frame. The additional uniform rotation ( $r\omega$ ) will allow the residual field  $\omega_3$  to be cancelled to the nearest harmonic of  $\omega$ . At any time  $t$  the angle of rotation,  $\phi(t) = r\omega t + a \sin \omega t$ .

The Hamiltonian in the transformed frame is given formally by an equation similar to eq. (11), namely,

$$\begin{aligned}\mathcal{H}'_B &= \hat{S}_B(t) \mathcal{H}_B(t) \hat{S}_B^{-1}(t) - i \hat{S}_B(t) (\partial/\partial t) \hat{S}_B^{-1}(t) \\ &= \mathcal{H}_B(t) - (r\omega + \omega_2 \cos \omega t) \hat{J}_z = (\omega_3 - r\omega) \hat{J}_z.\end{aligned}\quad (41)$$

This is simpler than the corresponding Hamiltonian in case A since it commutes with  $\hat{J}_z$ . We integrate the equation of motion corresponding to (10) and obtain

$$U'_B(t, t_0) = \exp[-i \mathcal{H}'_B(t - t_0)], \quad (42)$$

whence, applying the transformation inverse to  $S_B(t)$ ,

$$U_B(t, t_0) = \hat{S}_B^{-1}(t) \exp[-i \mathcal{H}'_B(t - t_0)] \hat{S}_B(t_0), \quad (43)$$

with  $\hat{S}_B$  given by eq. (40). In fact, with our present form for  $\mathcal{H}_B$ , the term in  $r\omega$  in  $S_B$  cancels identically in  $U_B$ . Explicitly, we have

$$U_B(t, t_0) = \exp(-i \hat{J}_z a \sin \omega t) \exp[-i \omega_3 \hat{J}_z (t - t_0)] \exp(i \hat{J}_z a \sin \omega t_0). \quad (44)$$

In the first and last factors we use the expansion

$$\exp(ix \sin \omega t) = \sum_{s=-\infty}^{\infty} J_s(x) \exp(is\omega t), \quad (45)$$

where  $s$  is an integer and  $J_s$  a Bessel function of integral order. Eq. (44) may then be conveniently factorized as follows

$$\begin{aligned}U_B(t, t_0) &= \sum_s J_s(a \hat{J}_z) \exp[-i(\hat{J}_z \omega_3 + s\omega)t] \sum_p J_p(a \hat{J}_z) \exp[i(\hat{J}_z \omega_3 + p\omega)t_0] \\ &= U_B(t, 0) U_B^+(t_0, 0).\end{aligned}\quad (46)$$

The evolution of the wave function under  $\mathcal{H}_B$  is seen to be that of the eigenstates of  $\hat{J}_z$  in the field  $B_3$ , each characteristic frequency being augmented by a set of harmonics of the oscillating field. Eq. (46) makes explicit the frequency-modulation of the wave function.

The frequency diagram associated with  $U_B(t)$  is shown in fig. 7. In fig. 7(a) we see the set of subsidiary levels associated with a given eigenstate of  $\hat{J}_z$ ; in 7(b), the levels for two eigenstates ( $m$  and  $m'$ ) as a function of  $\omega_3$ . Each level is labelled by the two "quantum numbers"  $m$  and  $s$ ; each is associated with a coefficient  $J_s(am)$ . We may think of the levels as representing eigenvalues of "pseudo-states", each of which appear with amplitude  $J_s(am)$ . The equations for the levels are

$$q_{lab} = m\omega_3 + s\omega \quad (47)$$

which is to be compared with eq. (25), case A.

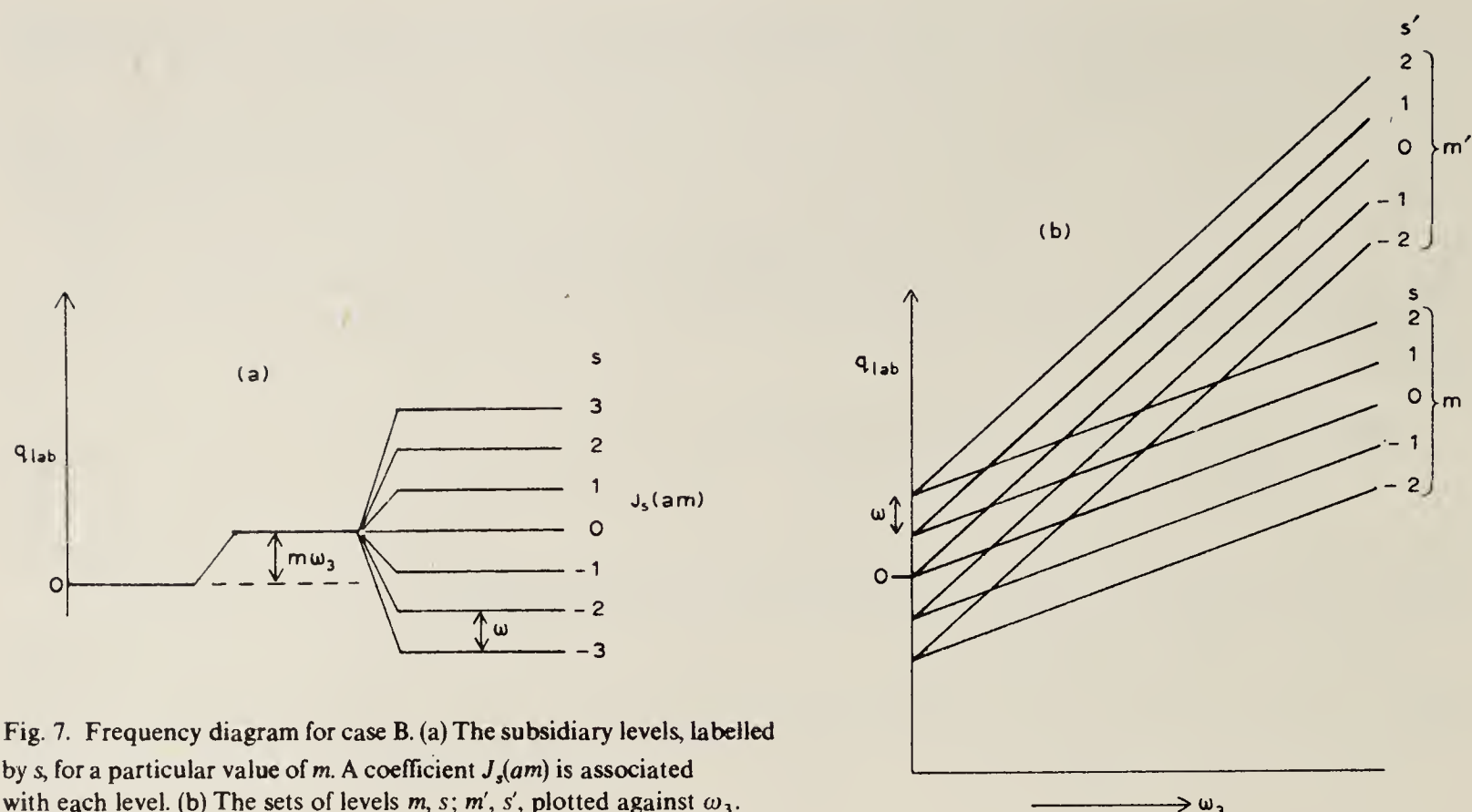


Fig. 7. Frequency diagram for case B. (a) The subsidiary levels, labelled by  $s$ , for a particular value of  $m$ . A coefficient  $J_s(am)$  is associated with each level. (b) The sets of levels  $m, s; m', s'$ , plotted against  $\omega_3$ .

### 3.2. Steady-state experiment

#### 3.2.1. Excitation to an eigenstate of $\hat{J}_z$

The equation of motion for the density matrix is identical with (27), save that  $\mathcal{H}_A$  is to be replaced by  $\mathcal{H}_B$ . Similarly,  $U_B$  (eq. (44)), replaces  $U_A$  in the solution, eq. (29). Since the initial density matrix is diagonal in eigenstates of  $\hat{J}_z$ , the product  $U_B(t, t_0)\rho_m U_B^\dagger(t, t_0)$  reduces to 1 and the result is trivial:

$$\rho(t) = (R/\Gamma)\rho_m, \quad (48)$$

i.e., there are no transitions and all off-diagonal elements are zero. (Since there are no transitions we need not distinguish between initial and final states,  $|n\rangle$  and  $|m\rangle$ , as before.)

#### 3.2.2. Excitation to a superposition-state of $\hat{J}_z$

This more interesting case may be achieved, as before, by a mechanism whose symmetry is different from that of the fields, e.g., by light of electric vector perpendicular to  $Oz$ . A population mechanism of this kind is known as “transverse pumping”. The configuration used for the Hanle effect is an example.

For the evaluation of  $U_B(t, t_0)\rho_{mm'}U_B^\dagger(t, t_0)$  in the modified eq. (29) we use the form (46). The result is

$$\begin{aligned} \rho_{mm'}(t) = R_{mm'} \sum_{ss'pp'} J_s(ma)J_{s'}(m'a)J_p(ma)J_{p'}(m'a) \exp[-i(s-s'-p+p')\omega t] \\ \times \int_0^t \exp\{-i[(m-m')\omega_3 + (p-p')\omega - i\Gamma](t-t_0)\} dt_0. \end{aligned} \quad (49)$$



The integration yields terms of the form

$$R_{mm'}/[(m - m')\omega_3 + (p - p')\omega - i\Gamma], \quad (50)$$

which implies resonance phenomena at values of  $\omega_3$  given by

$$(m - m')\omega_3 = -(p - p')\omega. \quad (51)$$

These phenomena may be classified with “level-crossing” effects as ordinarily studied, since the crossings of levels in fig. 7(b) satisfy eq. (51). But the present situation is to be distinguished from the ordinary “level-crossing” situation since the levels in the ordinary case represent eigenstates of a time-independent Hamiltonian, whereas here they represent pseudo-states of a time-dependent Hamiltonian. The resonances are Lorentzian, with widths determined by  $\Gamma$ : in fact, the full width at half-intensity is  $2\Gamma$ . The equivalent width in units of the magnetic field  $B_3$  is  $2\Gamma/\gamma$ . This is to be contrasted with a situation we shall explore in section 4.1.2.

### 3.3. Modulated excitation to a superposition-state of $\hat{J}_z$

As a further example of the significance of frequency diagrams we examine the possibility of resonances between the levels of fig. 7. Consider the effect of excitation by modulated, wide-band light of intensity

$$I(t) = I_0(1 + \cos vt), \quad (52)$$

whose electric vector is transverse to the magnetic fields of case B (fig. 8). The pumping term in the equation of motion is now

$$\rho_{mm'}(t_0) = R_{mm'}(1 + \cos vt_0). \quad (53)$$

$R_{mm'}$  depends on  $I_0$  and on electric dipole matrix elements, but is independent of  $t_0$ .  $\rho_{mm'}(t_0)$  replaces  $\rho_n$  in eq. (29), and  $U_B$  (eq. (46)) replaces  $U_A$ . The result for  $\rho(t)$  is similar to the result (49) and (50) except that

- (a) additional terms with the factors  $\exp \pm ivt$  appear in (49), and

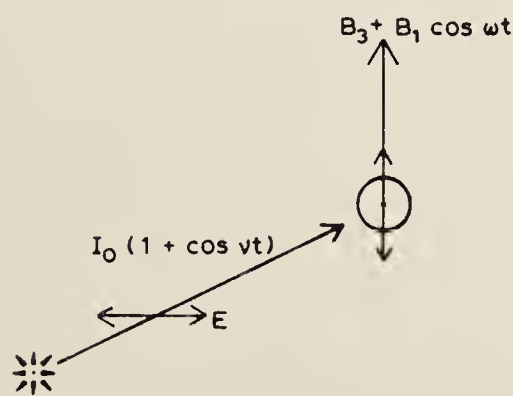


Fig. 8. Modulated excitation to a superposition-state of  $\hat{J}_z$ . The symmetry under the magnetic fields is broken by the electric vector of the light: the light is intensity-modulated.

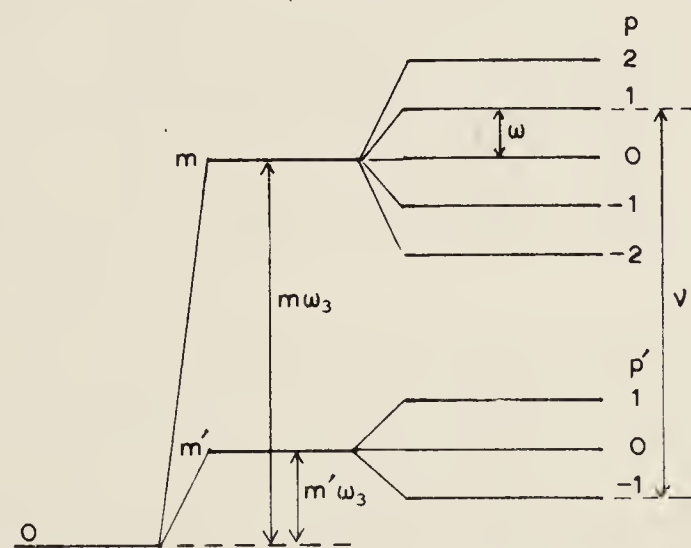


Fig. 9. Condition of resonance: the frequency of modulation of the light is matched to an interval in the frequency diagram.

(b) the factors resulting from the integration over  $t_0$  in these additional terms are of the form

$$R_{mm'}/[(m - m')\omega_3 + (p - p')\omega \pm \nu - i\Gamma]. \quad (54)$$

For these terms the condition of resonance is

$$(m - m')\omega_3 + (p - p')\omega = \mp \nu. \quad (55)$$

This condition may be read from the frequency diagram, fig. 9, as the requirement that the modulation frequency be matched to the interval between any pair of levels in the diagram. The tolerable amount of mismatch is given by the sum of the natural widths of the levels,  $2\Gamma$ .

It is to be noticed that the condition of transverse excitation was necessary only to exhibit the term  $(m - m')\omega_3$  in eq. (55). Resonances given by  $(p - p')\omega = \mp \nu$  may still be found when  $E$  is parallel to  $B$  (terms in  $m \neq m'$  vanish) or when  $\omega_3 = 0$ .

It is further to be noticed that all these resonances will be observed in the modulated response of the system, at the frequency  $\nu$ . If the system under study is an assembly of excited atoms, monitored by the fluorescent light, then the resonances will be seen in the amplitude of modulation of the fluorescent intensity. Resonances of this kind were explored by Chapman and Series [19]. They are characterised by the fact that the relative intensities of a series of resonances, given by different values of  $(p - p')$  in eq. (55), are proportional to products of Bessel functions as indicated in eq. (49). (The sums over  $s, s', p$  and  $p'$  may generally be simplified by use of the algebra of Bessel function expansions.)

## 4. Approximations

### 4.1. Case B with additional transverse magnetic field

This case, illustrated in fig. 10, does not lend itself to an exact solution. If the transverse field,  $B_0$ , is sufficiently small (more precisely, if  $\omega_0 = |\gamma B_0| \ll \omega$ ), we can treat it as an approximation to case B. If, on the other hand,  $\omega_0$  is comparable with  $\omega$ , and if, in addition,  $B_3$  is small or zero, the configuration will be recognised as the common arrangement for magnetic resonance studies. The fact that the time-dependent field is oscillating, not rotating, distinguishes this configuration from case A. We shall pursue this elaboration of case A in section 6.

To return to our present case, the fields of fig. 10 are

$$B(t) = (B_2 \cos \omega t + B_3)k + B_0i, \quad (B_0 \ll \omega/\gamma). \quad (56)$$

The transformation  $\hat{S}_B(t)$ , eq. (40), eliminates the oscillating field and leaves, in the transformed frame  $F'$ , a static field equivalent to  $(\omega_3 - r\omega)$ . (The rotation  $r\omega$  was incorporated into  $\hat{S}_B$  so that, by suitable choice of  $r$ ,  $(\omega_3 - r\omega)$  might always be made less than  $\omega/2$ .) In the frame  $F'$ ,  $B_0$  is seen as a velocity-modulated field rotating in the  $x'-y'$  plane. An expansion in terms of Bessel functions on the lines of eq. (45) shows that the component labelled  $-r$  is static: all other components are time-dependent. Formally, this may be expressed by evaluating the Hamiltonian in the transformed frame. The modified eq. (41) reads

$$\mathcal{H}'(t) = (\omega_3 - r\omega)\hat{J}_z + \frac{1}{2}\omega_0(\hat{J}_{x'} + i\hat{J}_{y'}) \exp \{ +i\phi(t) \} + \frac{1}{2}\omega_0(\hat{J}_{x'} - i\hat{J}_{y'}) \exp \{ -i\phi(t) \}, \quad (57)$$





Fig. 10. Configuration of magnetic fields for case B, with symmetry broken by an additional, transverse field.

where  $\phi(t) = r\omega t + a \sin \omega t$ . Use of

$$\exp \{ \pm i\phi(t) \} = \exp ( \pm ir\omega t ) \sum_{s=-\infty}^{\infty} J_s(a) \exp ( \pm is\omega t ) \quad (58)$$

yields

$$\begin{aligned} \mathcal{H}'(t) &= (\omega_3 - r\omega)\hat{J}_z + J_{-r}(a)\omega_0\hat{J}_{x'} + \frac{1}{2}\omega_0(\hat{J}_{x'} + i\hat{J}_{y'}) \sum_{s \neq -r} J_s(a) \exp \{ i(r+s)\omega t \} \\ &\quad + \frac{1}{2}\omega_0(\hat{J}_{x'} - i\hat{J}_{y'}) \sum_{s \neq -r} J_s(a) \exp \{ -i(r+s)\omega t \} \\ &= \mathcal{H}^{(0)} + \sum_{k \neq 0} [ \mathcal{H}^{(k)} \exp (ik\omega t) + \mathcal{H}^{(-k)} \exp (-ik\omega t) ], \quad (k = r + s). \end{aligned} \quad (59)$$

$\mathcal{H}^{(0)}$  represents the first two (time-independent) terms.

#### 4.1.1. Zeroth approximation

This entails the neglect of all the time-dependent terms in  $\mathcal{H}'(t)$ , leaving only  $\mathcal{H}^{(0)}$ . The legitimacy of this will be discussed in section 4.1.4. Meanwhile we notice that  $\mathcal{H}^{(0)}$  has the same form as  $\mathcal{H}'_A$ , the Hamiltonian of case A transformed to the rotating frame.

$$\mathcal{H}^{(0)} = (\omega_3 - r\omega)\hat{J}_z + J_{-r}(a)\omega_0\hat{J}_{x'}, \quad (60)$$

$$\mathcal{H}'_A = (\omega_0 - \omega)\hat{J}_z + \omega_1\hat{J}_{x'}. \quad (14)$$

By virtue of the exact correspondence between these equations we deduce that our present geometrical arrangement (fig. 10) has the consequences that a set of resonances is to be expected, under variation of  $\omega_3$  or  $\omega$ , centred on values of those variables which satisfy

$$\omega_3 = r\omega. \quad (61)$$

The detailed shape of the resonances may be ascertained from the density matrix, eq. (30), by substitution of  $r\omega$  for  $\omega$ ,  $\omega_3$  for  $\omega_0$ , and  $J_{-r}(a)\omega_0$  for  $\omega_1$ . It is to be noticed that the axis for quantization which generates the states  $|m\rangle$  is *parallel* to the oscillating field in the present case, *perpendicular* to the oscillating field in case A. We are prepared to find that the neglected terms may have a small effect on the positions and shapes of these resonances.

The Larmor frequency in the frame  $F'$  in the present case is

$$p' = \{(\omega_3 - r\omega)^2 + [J_{-r}(a)\omega_0]^2\}^{1/2}, \quad (62)$$

and the levels in this frame are given by  $\mu p'$ . The transform back to the laboratory frame is accomplished by the reverse frequency-modulated rotation, together with a counter-clockwise uniform rotation at the frequency  $r\omega$ , about the  $z$ -axis. In consequence, the frequencies  $mr\omega + s\omega$  must be added to  $\mu p'$ , with the result that the levels in the frequency diagram are given by

$$q_{\text{lab}} = (mr + s)\omega + \mu p'. \quad (63)$$

#### 4.1.2. Hanle effect in the presence of an oscillating field

This particularly interesting situation, a special case of our present analysis, is giving by setting  $\omega_3 = 0$  and studying the behaviour of the system as a function of  $\omega_0$ . We choose  $r = 0$  (to minimise  $\omega_3 - r\omega$ ) and obtain

$$q_{\text{lab}} = s\omega + \mu J_0(a)\omega_0. \quad (64)$$

We recall that the analysis is subject to the approximation  $\omega_0 \ll \omega$ , so the levels in fig. 11(a) are drawn only over a correspondingly limited range.

We notice the level-crossings in the region  $\omega_0 = 0$ , as in the Hanle effect, but the slopes of the

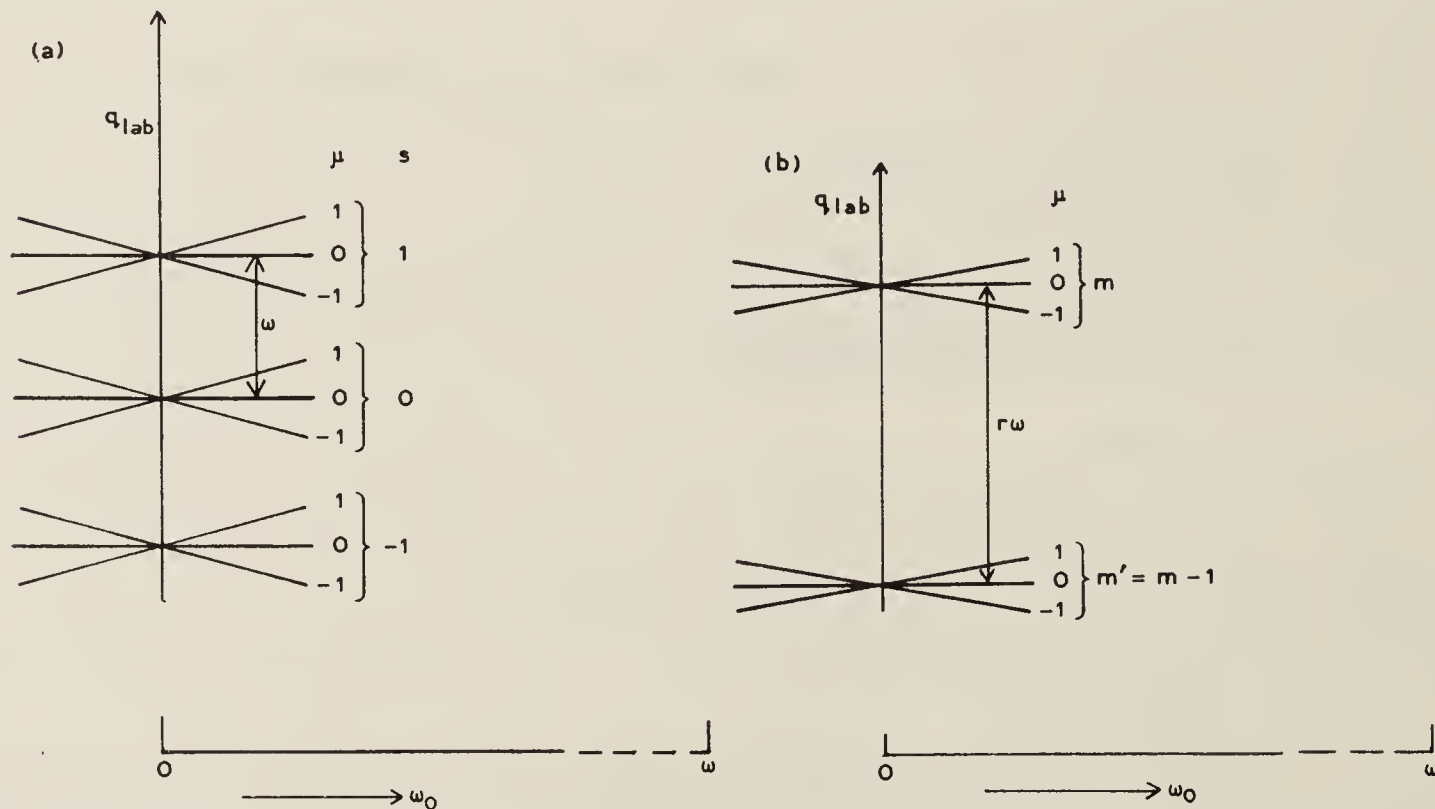


Fig. 11. Frequency diagram corresponding to the magnetic fields of fig. 10. (a)  $\omega_3 = 0$ . The level-crossing at  $\omega_0 = 0$  gives rise to a Hanle effect, but the slopes of the levels are  $\mu J_0(a)$  ( $a = \omega_2/\omega$ ) rather than  $\mu$ , and the Hanle curves are correspondingly broadened. (b)  $\omega_3 = r\omega$ . The level-crossings at  $\omega_0 = 0$  give rise to Hanle effects which can be monitored as modulated or unmodulated phenomena. The slopes of the levels are  $\mu J_{-r}(a)$ , and the Hanle curves are correspondingly broadened.



levels are now modified by the factor  $J_0(a)$  compared with the situation when the oscillating field is absent.

The response of the system is contained in  $\rho(t)$ , eq. (30), the  $m, m'$  quantization being parallel to the oscillating field. We concentrate on the resonance denominators

$$R/[\Gamma \pm i(\mu - \mu')p'] \quad (65)$$

which, in terms of the applied fields are

$$R/[\Gamma \pm i(\mu - \mu')J_0(a)\omega_0], \quad a = \omega_2/\omega. \quad (66)$$

The range of magnetic field ( $\omega_0$ ) required to scan a resonance is *increased*, in comparison with the Hanle effect in static fields, by the factor  $J_0^{-1}(a)$ . To secure non-zero values of  $(\mu - \mu')$  we must excite the system to superposition-states of the  $|\mu\rangle$ , which are eigenstates of the component of  $\mathbf{J}$  in the direction of the effective field in the frame  $F'$  – in our case, the direction of  $\mathbf{B}_0$ . This necessary condition can be secured, for example, by excitation with light whose electric vector is parallel to the oscillating field (or, equivalently, by unpolarized light travelling in that direction).

This “Hanle effect of dressed atoms” was first explored by Cohen-Tannoudji and Haroche [9] and interpreted by them by means of the quantum field theory of dressed atoms.

#### 4.1.3. Bessel functions of higher order

The appearance of the zero-order Bessel function in the last section was a consequence of taking  $r = 0$  which, in turn, resulted from the choice  $\omega_3 = 0$ . The higher order Bessel functions  $J_{-r}$ , make their appearance with fields  $\omega_3 = r\omega$ . Hanle-effect resonances occur, with widths increased by  $J_{-r}^{-1}(a)$ , under variation of  $\omega_0$  about zero. These phenomena were studied by Chapman [20], both in modulated and in unmodulated fluorescent light, under excitation by unpolarized light travelling in the direction of the oscillating field.

The possibility of modulation is exhibited by the factors  $\exp -i(m - m')\omega t$  in eq. (30), corresponding to  $\exp -i(m - m')r\omega t$  here. The frequency diagram in fig. 11(b), which illustrates eq. (63), shows levels separated by  $(m - m')r\omega$ . These represent terms in the wave function whose coherence is responsible for the modulation.

#### 4.1.4. Validity of the approximation

The Hamiltonian in the frame  $F'$  (in which the oscillating field  $B_2 \cos \omega t \mathbf{k}$  is completely suppressed) was

$$\mathcal{H}'(t) = \mathcal{H}^{(0)} + \sum_{k \neq 0} [\mathcal{H}^{(k)} \exp(ik\omega t) + \mathcal{H}^{(-k)} \exp(-ik\omega t)], \quad (67)$$

where the detailed form of the  $\mathcal{H}^{(\pm k)}$  may be read from eq. (59). We now examine the effect of the time-dependent terms. We shall follow closely the argument given in Pegg and Series [6]. Writing the time-dependent terms as  $V(t)$ , we have that the first-order correction arising from them is [21]

$$U^{(1)}(t, t_0) = -i \int_{t_0}^t U^{(0)}(t, \tau_1) V(\tau_1) U^{(0)}(\tau_1, t_0) d\tau_1, \quad (68)$$

with

$$U^{(0)}(t, t_0) = \exp[-i\mathcal{H}^{(0)}(t - t_0)]. \quad (69)$$

[These equations refer to the frame  $F'$ : we have dropped the prime to simplify the notation.] Taking matrix elements, we have

$$U_{\alpha\delta}^{(1)}(t, t_0) = -i \sum_{\beta\gamma} \exp \{ -i \mathcal{H}_{\alpha\beta}^{(0)} t \} \exp \{ i \mathcal{H}_{\gamma\delta}^{(0)} t_0 \} \sum_{k \neq 0} \mathcal{H}_{\beta\gamma}^{(k)} \int_{t_0}^t \exp [i \{ \mathcal{H}_{\alpha\beta}^{(0)} + k\omega - \mathcal{H}_{\gamma\delta}^{(0)} \} \tau_1] d\tau_1. \quad (70)$$

The integral is easily evaluated. It is then clear that first-order corrections are small if

$$| \mathcal{H}_{\beta\gamma}^{(k)} / (\mathcal{H}_{\alpha\beta}^{(0)} - \mathcal{H}_{\gamma\delta}^{(0)} + k\omega) | \ll 1 \quad (71)$$

for all possible  $\alpha, \beta, \gamma, \delta$ , and with  $k \neq 0$ . Moreover, if these corrections are of order  $\Delta$ , then the  $n$ th order corrections are of order  $\Delta^n$ , and the condition (71) ensures that the zero-order approximation is dominant.

To interpret (71), let us choose the basis states as eigenstates of  $\mathcal{H}^{(0)}$ . Then the off-diagonal components of  $\mathcal{H}^{(0)}$  (but not necessarily of  $\mathcal{H}^{(k)}$ ) vanish. The inequality (71) may then be written

$$\mathcal{H}_{\alpha\delta}^{(k)} / [k\omega - (\omega_\alpha^{(0)} - \omega_\delta^{(0)})] \ll 1. \quad (72)$$

The numerator and denominator may be varied independently, so we need two conditions to secure (72). The following are sufficient:

$$k\omega - (\omega_\alpha^{(0)} - \omega_\delta^{(0)}) \gtrsim \omega, \quad (73a)$$

$$\mathcal{H}_{\alpha\delta}^{(k)} \ll \omega, \text{ all } \alpha, \delta, \text{ with } k \neq 0. \quad (73b)$$

Condition (73b) is satisfied by the requirement that we have already specified: the amplitude of the driving field ( $\sim \omega_0$  in the case illustrated in fig. 10) must be  $\ll \omega$ . With this condition satisfied, (73a) is satisfied in regions of resonance. This may be read from fig. 3(c), which is precisely a diagram of the  $\omega_\alpha^{(0)}$  through the resonance region, that is, through the region where  $(\omega_3 - r\omega) = 0$  is satisfied under variation of  $\omega_3$  in this case (not  $\omega_0$ ). The equation is satisfied at the position of closest approach of the levels.

It is now clear why the rotation  $r\omega$  was incorporated into the transformation operator  $\hat{S}_B$ , eq. (40). An integer  $r$  can be chosen, for any given  $\omega_3$ , to make  $\omega_3 - r\omega < \frac{1}{2}\omega$ , and so satisfy condition (73a). As  $\omega_3$  is varied we pass from one resonance region to the next, and choose the next value of  $r$  accordingly. The resonance regions remain distinguishable so long as the amplitude of the driving field remains substantially less than  $\omega$ . Although this condition is sufficient, we note, in passing, that it will often be unnecessarily stringent.

#### 4.1.5. Evaluation of correction terms

It is straightforward to evaluate a correction (to second order in  $\omega_0/\omega$ ) for the neglected terms,  $\mathcal{H}^{(\pm k)}$ . Taking pairs of such terms, we have

$$\mathcal{H}^{(k)} + \mathcal{H}^{(-k)} = \frac{1}{2}\omega_0 J_{k-r}(a) \{ (\hat{J}_{x'} + i\hat{J}_{y'}) \exp(ik\omega t) + (\hat{J}_{x'} - i\hat{J}_{y'}) \exp(-ik\omega t) \}, \quad (74)$$

which corresponds to a rotation in the  $x'-y'$  plane of a field  $\omega_0 J_{k-r}(a)$ , clockwise or counter-clockwise according as  $k > 0$  or  $< 0$ . For a particular value of  $k$ , say  $l$ , let a transformation be made to a frame in which that particular rotating field is static, that is, a rotation about the  $z$ -axis at the uniform angular velocity  $-l\omega$ . The static field is then the vector sum of  $(\omega_3 - r\omega + l\omega)\mathbf{k}$  and  $J_{l-r}(a)\omega_0\mathbf{i}''$ . Let  $\mathbf{k}''$  be the direction of the resultant field (fig. 12). The magnitude of the resultant



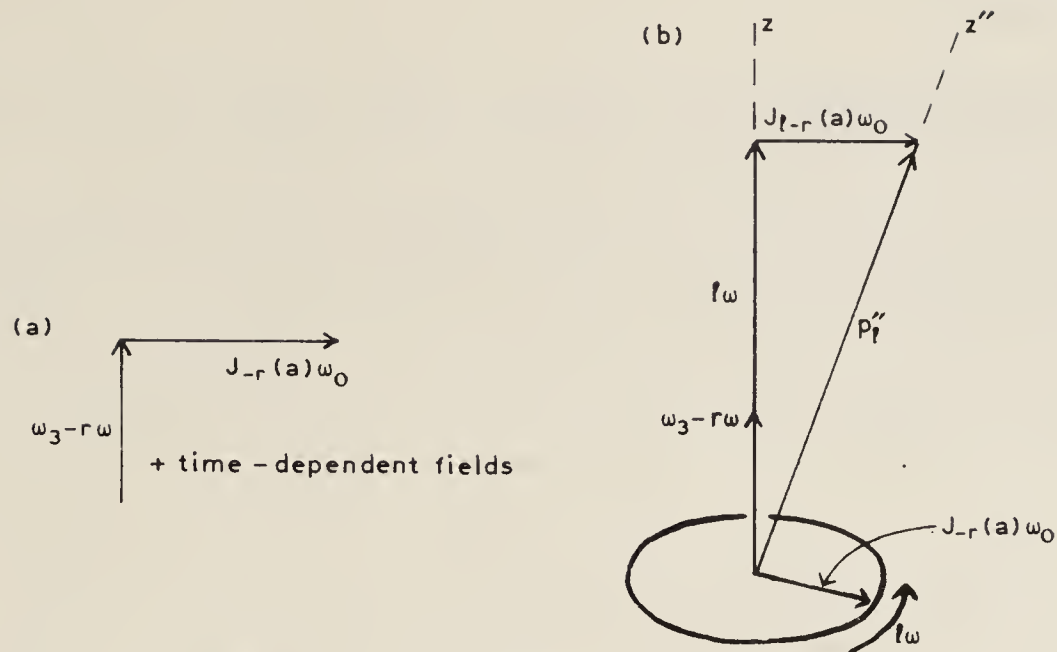


Fig. 12. Evaluation of corrections to the position of the resonance driven by the  $r$ th harmonic of the oscillating field (zero-order condition of resonance,  $\omega_3 = r\omega$ ). (a) Fields in the frame in which the harmonic  $-r$  is static. (b) Fields after transformation to the frame in which the perturbing field  $(l-r)$  is static. The harmonic  $-r$ , now rotating at the frequency  $l\omega$ , drives a resonance when  $l\omega = p_l''$ , approximately. (The fields have been labelled as frequencies, but the arrows have the sign of the fields.)

is

$$p_l'' = \{(\omega_3 - r\omega + l\omega)^2 + [J_{l-r}(a)\omega_0]^2\}^{1/2}. \quad (75)$$

Among the *rotating* fields in this frame is  $J_{-r}(a)\omega_0$  at the frequency  $l\omega$ . The component of this field in the plane perpendicular to  $\mathbf{k}''$  will drive the  $r$ th resonance when its frequency in this frame is equal to  $p_l''$ . The condition of resonance is therefore

$$l\omega = p_l'' = [\omega_3 - (r-l)\omega] \{1 + [\frac{1}{2}J_{l-r}(a)\omega_0/(\omega_3 - r\omega + l\omega)]^2\}, \quad (76)$$

that is,

$$r\omega = \omega_3 + \frac{1}{2}[J_{l-r}(a)\omega_0]^2/(\omega_3 - r\omega + l\omega). \quad (77)$$

In eq. (76) we have neglected terms in the binomial expansion of  $p_l''$  beyond the first two. We have also not taken account of the component of  $J_{-r}(a)\omega_0$  which is *out of* the plane normal to  $\mathbf{k}''$ : this has an effect in higher powers of  $\omega_0/\omega$  which can be calculated by the method of transformations if circumstances warrant it [22–24]. But the significant feature of eq. (76) is that, subject to the approximations mentioned here, the effect of the pair of terms  $\mathcal{H}^{(\pm l)} \exp(\pm il\omega t)$  on the  $r$ th resonance has been accounted for. The effect of the terms  $\mathcal{H}^{(\pm k)} \exp(\pm ikt)$  in eq. (59) is additive in this (second order) approximation, so that the condition of resonance becomes

$$r\omega = \omega_3 + \sum_{k \neq 0} \frac{1}{2}[J_{k-r}(a)\omega_0]^2/(\omega_3 - r\omega + k\omega). \quad (78)$$

The uncorrected condition of resonance was

$$r\omega = \omega_3. \quad (79)$$

The correction terms are described generically as “Bloch–Siegert shifts”, though the calculation originally made by these authors was of the perturbing effect of a counter-rotating field in connection with case A. We shall return to this in section 6.

## 5. The general problem

Case A represents the prototype of magnetic resonance experiments, but the configuration of fields, though convenient for purposes of analysis, is generally inconvenient to achieve experimentally. Moreover, more complicated arrangements of fields are sometimes used deliberately in order to achieve special effects (e.g. parametric resonances) or to study particular relaxation processes. The example of section 4.1.1 shows how the analysis of case A can be applied as a zeroth approximation in these more complicated situations, and 4.1.5 shows how case A may additionally be used to calculate corrections, subject to sufficiently small values of the time-dependent fields. Case B shows how an oscillating field of any magnitude may be eliminated.

For many situations it has been found possible, by combining the transformations A and B, to reduce the given problem to one in which the approximation demonstrated in 4.1.5 may legitimately be applied. The reduction procedure is first to identify the dominant perturbing field in relation to a contemplated case A-type of resonance (this corresponds to the selection of the terms  $\mathcal{H}^{(\pm 1)} \exp(\pm i\omega t)$  in 4.1.5). One then makes a transformation to a frame in which the corresponding field is static. Knowledge of this field and of the magnitude of the driving field for the resonance allows the frequencies  $q$  to be determined. From this the resonance condition can be found, as we explain in section 5.1. The procedure will have left uncompensated some small component of the driving field whose effect can be estimated by a combination of further transformations of types A and B or by the method of section 4.1.5. The transformation procedures can be applied, not only to determination of the shifts of resonance peaks, but also to the calculation of perturbed transition probabilities and line shapes.

The method of solution by transformations was considered by Ansbacher [25] as an attempt to find an integrable, time-dependent Hamiltonian  $\mathcal{H}_a$  which would approximate the given Hamiltonian as closely as possible. He described a variational procedure for finding the best values of the parameters of  $\mathcal{H}_a$  for any contemplated transformation, and a procedure for determining which of a number of contemplated transformations would provide the best approximation.

The most highly developed calculations by the method of rotational transformations have been carried out by D.T. Pegg. Pegg [24] remarks that the transformation (or series of transformations) to a reference frame in which an unwanted time-dependent component  $\mathcal{H}(t)$  of a Hamiltonian is eliminated is just a generalization (particularization) of the usual interaction representation, and can always be achieved by a unitary transformation  $\exp[i \int \mathcal{H}(t) dt]$  if all the terms in  $\mathcal{H}(t)$  commute with each other. It is this fact which underlies Ansbacher's work. The significance of the remark is that, although the transformations are formulated for magnetic interactions as rotations in physical space, they may be generalized to other (e.g., electric) interactions as rotations in an abstract space for suitably defined operators.

Pegg [23] gives a formal proof that the eigenvalues of a Hamiltonian  $\mathcal{H}^{(0)}$  obtained by transformation to a frame in which time-dependent fields can be neglected are the same as the eigenvalues of Shirley's Floquet matrix [26]. Since it is also the case that Shirley's eigenvalues are the same as those of the dressed atom of quantum field theory [9], it is clear that these different theories have a great deal in common.

In section 5.2 we give a brief account of Shirley's method. We go on to give, as an illustration of the semi-classical methods used in combination, a solution of the Bloch-Siegert problem to a high degree of approximation. We first give a more formal discussion of the condition of resonance.



### 5.1. Condition of resonance

In the discussion of case A, sections 2.2 and 2.3, we stated the condition of resonance as

$$\partial q^2 / \partial \omega_0 = 0, \quad (80)$$

a position corresponding to the minimum value of the static field in the transformed co-ordinate frame, and to the greatest mixing of eigenstates of  $\hat{J}_z$ . It is easy to show that this condition corresponds to the maximum value of the time-averaged transition probability for a spin- $\frac{1}{2}$  system (also for higher values of half-integral spins: for integral spins the condition corresponds to a minimum – see fig. 5 – but not an absolute minimum). The condition is satisfied for case A by

$$\text{driving frequency} = -\gamma (\text{static field}), \quad (81)$$

but eq. (81) is not, in general, strictly correct. In section 4.1.5 we showed how to derive a correction for the presence of additional time-dependent fields, but in the derivation we applied eq. (81) in a transformed frame. Even with neglect of residual time-dependent fields in this frame the equation gives the resonance position correctly only to terms in (driving field)<sup>2</sup>/(static field). For strong driving fields, the higher terms are clearly important. In such cases one must use the condition (80) for resonance under variation of the static field, and  $\partial q^2 / \partial \omega = 0$  for resonance under variation of  $\omega$ . These will not always give the same result.

### 5.2. Shirley's method

The method was formulated as a technique for solving problems expressed in terms of a semi-classical Hamiltonian of the form

$$\mathcal{H}(t) = \sum_k \mathcal{H}^{(k)} \exp(-ik\omega t). \quad (82)$$

The key to the solution is the observation that, by the application of Floquet's theorem to the Schrodinger equation of motion, the time-shift operator (or, alternatively, the wave function) can be expressed in the form

$$U(t, t_0) = \sum_{k,q} a_{kq} \exp(-ik\omega t) \exp[-iq(t - t_0)]. \quad (83)$$

(The  $k, q$  of eq. (83) are not to be confused with the  $k, q$  labels of the irreducible spherical tensor operators of section 2.4.) By a mathematical reduction Shirley showed that the frequencies  $q$  of eq. (83) are the eigenvalues of a time-independent Hamiltonian matrix of infinite rank, called the "Floquet Hamiltonian",  $\mathcal{H}_F$ , whose matrix elements can be derived from those of  $\mathcal{H}(t)$  as follows:

$$\langle \alpha, n | \mathcal{H}_F | \beta, m \rangle = \langle \alpha | \mathcal{H}^{(n-m)} | \beta \rangle + n\omega \delta_{\alpha\beta} \delta_{nm}. \quad (84)$$

The basis states of  $\mathcal{H}_F$  are labelled by  $\alpha, \beta$ , the atomic quantum numbers, and, in addition, by  $n, m$ , an infinite set of integers. It is not difficult to follow Shirley in making a correspondence between the term  $n\omega \delta_{\alpha\beta} \delta_{nm}$  of eq. (84) and the eigenvalues of a quantized field. The first term on the right, the matrix element of  $\mathcal{H}^{(n-m)}$ , clearly represents the interaction between the atom and the  $(n - m)$ th harmonic of the field. A correspondence with our techniques is to be seen in eq. (78) (correction to the zeroth approximation) where the second term on the right will be recognised as the contribution of second-order perturbation theory to the diagonalization of a Floquet matrix. Shirley introduced an equation equivalent to eq. (80) as the condition of resonance.

In applications of Shirley's method one approximates the infinite Floquet matrix by working with some finite portion of it – as much as is necessary to secure the required accuracy. In practice, the convergence of the eigenvalues as the working matrix is enlarged is sometimes too slow to be of practical use. For problems in which the dominant field is time-dependent this is, in fact, the case. In these circumstances it has proved advantageous – as we demonstrate in the next section – first to apply a rotational transformation to eliminate the dominant field. The problem in the transformed frame may then yield to Shirley's method with sufficiently rapid convergence.

## 6. The Bloch–Siegert problem

The most common configuration of fields for magnetic resonance experiments is

$$\mathbf{B}(t) = B_0 \mathbf{k} + 2B_1 \cos \omega t \mathbf{i}, \quad (85)$$

illustrated in fig. 13(a). Notice that the amplitude of the oscillating field has been written  $2B_1$  to allow an easier comparison with case A. The oscillating field may be decomposed into a rotating and a counter-rotating component, each of amplitude  $B_1$ , so that (85) corresponds to the situation of case A, with an additional counter-rotating field (fig. 13(b)).

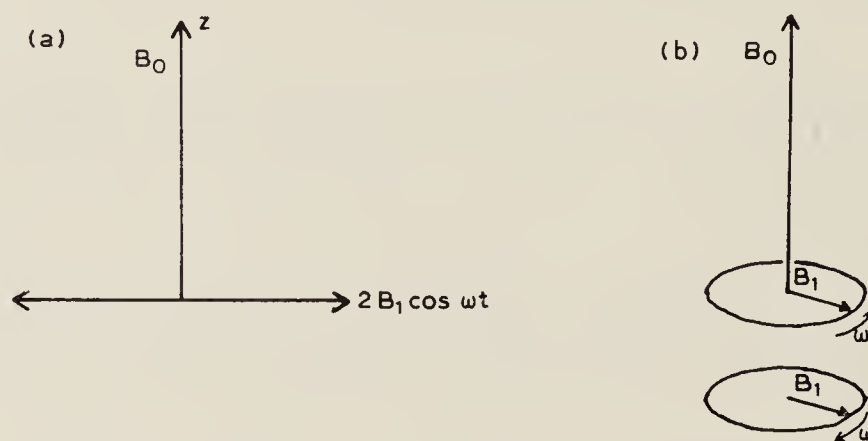


Fig. 13. (a) Fields for discussion of the Bloch–Siegert problem. (b) Resolution of the oscillating field into rotating and counter-rotating components.

The problem of determining the peak of the resonance in this configuration of fields has been approached by a number of authors in recent years, using a variety of methods. We summarise their work in section 6.3. The details of the solution given here are based on papers by Pegg [22, 23] and by Hannaford, Pegg and Series [27].

### 6.1. Zeroth and first approximations: terms in $\omega_1^2$

The zeroth condition of resonance is (case A)

$$\omega = \omega_0, \quad (86)$$

but this condition takes no account of the counter-rotating field. It is the correction due to this field which constitutes the Bloch–Siegert effect.



To calculate the effect of this field, we first make a transformation to a frame  $F'$  in which it is static. The required transformation is a counter-clockwise rotation of axes, leading to the situation shown in fig. 14a. This configuration is of the type treated in section 4.1.5. We remark that the field  $B_1$ , rotating at frequency  $2\omega$ , has a component perpendicular to  $Oz'$  which will drive a resonance under the condition (zero-order in this frame)

$$2\omega = p = [(\omega + \omega_0)^2 + \omega_1^2]^{1/2}, \quad (87)$$

which reduces to

$$\omega \approx \omega_0 + \frac{1}{2}\omega_1^2/(\omega + \omega_0) \approx \omega_0 + \frac{1}{4}\omega_1^2/\omega_0. \quad (88)$$

The second term on the right is the first approximation to the necessary correction for the counter-rotating field.

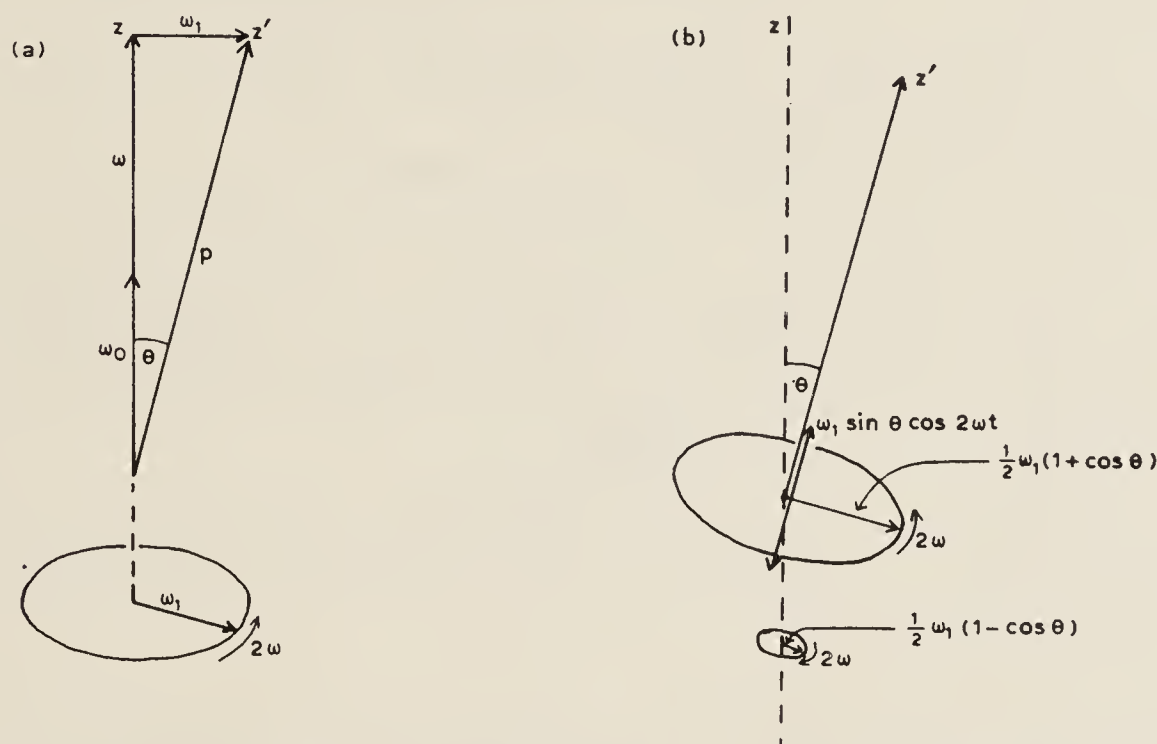


Fig. 14. (a) The fields of fig. 13(b) after transformation to the frame in which the counter-rotating field is static. (b) Resolution of the rotating field in (a) into components along and perpendicular to the resultant static field in this frame, in the direction of  $Oz'$ . (The fields have been labelled as frequencies, but the arrows have the sign of the fields.)

## 6.2. Second approximation: terms in $\omega_1^4$

We can obtain a better approximation by use of eq. (80) for this resonance, that is to say, we need to find  $q$ , or, equivalently, the Larmor frequency  $p'$  in the frame in which the driving field is static. The magnitude of the driving field is  $\frac{1}{2}B_1(1 + \cos \theta)$ , as shown by the resolution in fig. 14b. This configuration is equivalent to, and is in the same frame as, fig. 14a. To make the driving field static we need to transform to a frame rotating about  $Oz'$  at the frequency  $2\omega$ . We then find

$$\begin{aligned} p'^2 &= (p - 2\omega)^2 + [\tfrac{1}{2}\omega_1(1 + \cos \theta)]^2, \quad \tan \theta = \omega_1/(\omega + \omega_0) \\ &= (\omega_0 - \omega)^2 + \frac{2\omega_0\omega_1^2}{(\omega + \omega_0)} - \frac{\omega_1^4\omega_0}{2(\omega + \omega_0)^3} \dots, \end{aligned} \quad (89)$$

in which terms as far as  $\omega_1^4$  in the expansion have been kept. In deriving (89) the oscillating field along  $Oz'$  and the counter-rotating field of amplitude  $\frac{1}{2}B_1(1 - \cos \theta)$  have been ignored. The effect of these, as we show in the next section, is felt first in terms in  $\omega_1^6$ . Application of eq. (80) to (89) (recall  $q = \mu p'$ ) gives the resonance equation

$$\omega = \omega_0 + [\omega_1^2 \omega / (\omega + \omega_0)^2] + [\omega_1^4 (2\omega_0 - \omega) / 4(\omega + \omega_0)^4] \approx \omega_0 + [\omega_1^2 / 4\omega_0] + [\omega_1^4 / 64\omega_0^3] \quad (90)$$

The first form gives the condition of resonance correctly as far as  $\omega_1^4$ .

### 6.3. Third approximation: terms in $\omega_1^6$

The evaluation of  $p'$ , eq. (89) rests upon a transformation which makes the rotating field  $\frac{1}{2}B_1(1 + \cos \theta)$  static, i.e., a rotation about  $Oz'$  at the uniform angular velocity  $2\omega$ . There remain two perturbing fields,

(i)  $B_1 \sin \theta \cos 2\omega t$ , oscillating along  $Oz'$  and (ii)  $\frac{1}{2}B_1(1 - \cos \theta)$ , counter-rotating at the frequency  $2\omega$  in the plane perpendicular to  $Oz'$ .

The field (i) may be entirely eliminated if, in addition to the uniform rotation at velocity  $2\omega$  about  $Oz'$ , we superimpose a frequency-modulated rotation, effected by the transformation  $\hat{S}_B$ , eq. (40). In the transformed frame  $F''$  the field driving the resonance is static and its amplitude is multiplied by the factor  $J_0(\omega_1 \sin \theta / 2\omega)$ . Additionally a set of fields is generated, rotating at frequencies  $(2 + s)\omega$ , and with amplitudes  $\frac{1}{2}B_1(1 + \cos \theta)J_s(\omega_1 \sin \theta / 2\omega)$ . The counter-rotating field is represented in  $F''$  by a set of harmonics, the dominant harmonic being of amplitude  $\frac{1}{2}B_1(1 - \cos \theta)J_0(\omega_1 \sin \theta / 2\omega)$  and of frequency  $-4\omega$ .

At the level of  $\omega_1^6$ , terms appear in the following ways:

- (i) the expansion of  $(p - 2\omega)^2$  in eq. (89) yields such a term which was previously discarded;
- (ii) the square bracket in eq. (89) becomes  $[\frac{1}{2}\omega_1(1 + \cos \theta)J_0(\omega_1 \sin \theta / 2\omega)]^2$ , which yields terms in  $\omega_1^6$  through the  $\omega_1^4$  terms in  $(1 + \cos \theta)$  and in  $J_0$ ;
- (iii) the rotating fields yield terms in this order.

The additional terms under (i) and (ii) are readily evaluated by series expansions. The terms under (iii) may be evaluated by the procedure of 4.1.5, leading to eq. (78). The only fields which are significant at the level of  $\omega_1^6$  are those with amplitudes  $\frac{1}{2}B_1(1 - \cos \theta)J_0(\omega_1 \sin \theta / 2\omega)$  and  $\frac{1}{2}B_1(1 + \cos \theta)J_{\pm 1}(\omega_1 \sin \theta / 2\omega)$ . The correction due to the former, for example, is

$$\frac{1}{2}[\frac{1}{2}\omega_1(1 - \cos \theta)J_0(\omega_1 \sin \theta / 2\omega)]^2/p \quad (91)$$

with  $\tan \theta = \omega_1 / (\omega + \omega_0)$  and  $p \approx (\omega + \omega_0)$ . The factorisation in eq. (91) has been written to correspond exactly with that in eq. (78).

Taking account of all these terms, Pegg [23] obtained the following result for  $q^2$ , correct to  $\omega_1^6$ :

$$q^2 = \frac{1}{4}(\omega - \omega_0)^2 + \frac{2\omega_0 b^2}{\omega + \omega_0} - \frac{2\omega_0 b^4}{(\omega + \omega_0)^3} + \frac{8\omega_0(\omega^2 - 5\omega\omega_0 - 2\omega_0^2)b^6}{(\omega + \omega_0)^5(9\omega^2 - \omega_0^2)} \quad (92)$$

The eigenfrequencies,  $q$ , in his analysis, are explicitly for a spin- $\frac{1}{2}$  system. We have been calculating the corresponding Larmor frequency,  $p''$ , related to  $q$  by

$$q_{\pm} = \pm \frac{1}{2}p''. \quad (93)$$



Similarly, Pegg's  $b$  is the interaction matrix element related to  $\omega_1$  by

$$b = -\frac{1}{2}\omega_1. \quad (94)$$

The resonance condition obtained from eq. (92) by application of eq. (80) is

$$\omega = \omega_0 + \omega_1^2/4\omega_0 + \omega_1^4/64\omega_0^3 - 35\omega_1^6/2^{11}\omega_0^5, \quad (95)$$

or, expressing  $\omega_0$  in terms of  $\omega$ ,

$$\omega_0 = \omega - \omega_1^2/4\omega - 5\omega_1^4/64\omega^3 - 61\omega_1^6/2^{11}\omega^5. \quad (96)$$

A better expression is that obtained directly from eqs. (92) and (80), namely:

$$\begin{aligned} \omega_0 = \omega - \frac{4\omega b^2}{(\omega + \omega_0)^2} - \frac{4(2\omega_0 - \omega)b^4}{(\omega + \omega_0)^4} \\ - \frac{16(9\omega^5 - 126\omega^4\omega_0 + 82\omega^3\omega_0^2 + 42\omega^2\omega_0^3 - 23\omega\omega_0^4 - 8\omega_0^5)b^6}{(\omega + \omega_0)^6(9\omega^2 - \omega_0^2)^2} \end{aligned} \quad (97)$$

This is the expression on which the results of Pegg, Hannaford and Series were based.

#### 6.4. Limit of strong, oscillating field

Eq. (97) gives the peak of the resonance,  $\omega_0$ , to high accuracy ( $\sim 1\%$ ) for shifts of the resonance ( $\omega_0 - \omega$ ) greater than half the resonance frequency itself; such shifts are attained when  $\omega_1$  is nearly equal to  $\omega$ . To calculate the shifts for larger values of  $\omega_1$  it is expedient to approach the problem from the other end, that is to say, to regard the interaction with the oscillating field as dominant and to treat the static field as a small perturbation. The limiting problem is then precisely case B in its simplest form, section 3.1. The equations of 3.1 correspond to our present problem if we put  $B_3 = 0$ ,  $B_2 = 2B_1$ . Our field is now

$$\mathbf{B}(t) = 2B_1 \cos \omega t \mathbf{k}. \quad (98)$$

The physical situation is exactly that expressed by eq. (85), with  $B_0 = 0$ , but we find it expedient now to choose the  $z$ -axis, which will be the axis for rotations, parallel, rather than perpendicular to, the oscillating field. The eigenfrequencies of the Hamiltonian corresponding to eq. (98) are given by eq. (47):

$$q_{\text{lab}} = s\omega, \quad (99)$$

which are simply the harmonic frequencies corresponding to the Fourier expansion of the frequency-modulated Larmor precession.

##### 6.4.1. Additional small static field: zeroth approximation

The addition of the static field  $\mathbf{B}_0$  is expressed by

$$\mathbf{B}(t) = 2B_1 \cos \omega t \mathbf{k} + B_0 \mathbf{i}, \quad (100)$$

as in eq. (56). The frequency-modulated transformation then leads to the eigenfrequencies given in the zeroth approximation by eq. (64), namely

$$q_{\text{lab}} = \mu J_0(2\omega_1/\omega)\omega_0 + s\omega. \quad (101)$$

The condition of resonance  $\partial q^2/\partial\omega_0 = 0$  leads to

$$J_0(2\omega_1/\omega) = 0. \quad (102)$$

Since this equation is independent of  $\omega_0$  it gives insufficient information about the position of the resonance. It is to be recognised, however, that the right hand side of eq. (101) gives only the leading term in an expansion in powers of  $\omega_0$ : (the next term is given explicitly in eq. (105)). The resonance condition requires, then, in addition to (102), that  $\omega_0 = 0$ .

Inserting the numerical value of the argument which yields the first zero of  $J_0$ , we find the resonance equations

$$\omega_1/\omega = 1.2026; \quad \omega_0 = 0. \quad (103)$$

This solution is exact.

In establishing this result we have used the condition  $\partial q^2/\partial\omega_0 = 0$  rather uncritically. A justification is found in the work of Shirley and of Pegg who obtained the same result by working out the maximum value of the transition probability.

#### 6.4.2. Additional small static field: terms in $\omega_0^3$

The time-dependent terms in the transformed Hamiltonian yield contributions to the eigenfrequencies of order  $\omega_0^3$ . These are the terms  $\mathcal{H}^{(k)} \exp(ik\omega t)$  of eq. (59). Since, in the present application,  $r = 0$ ,  $k$  is to be identified with the  $s$  of eq. (101).

The contributions of these time-dependent terms, calculated to order  $\omega_0^2$ , are identically zero because the levels are "repelled" by equal amounts, in opposite directions, by co- and counter-rotating harmonic fields. This may be read from eq. (78) – the contributions from equal and opposite values of  $k$  cancel – or, diagrammatically, from fig. 11(a).

We need, therefore, to go to a higher order to find a correction to eq. (101), and this is most easily achieved by means of Shirley's technique. We construct a Floquet matrix (eq. (84)) based on the Hamiltonian appropriate to our problem, which is Hamiltonian in the transformed frame, namely eq. (59).  $\mathcal{H}^{(0)}$  gives the diagonal terms of the Floquet matrix

$$\langle ms | \mathcal{H}_F | ms \rangle = \langle m | \mathcal{H}^{(0)} | m \rangle + s\omega. \quad (104)$$

( $m$  here is the atomic quantum number and corresponds to Shirley's  $\alpha$ :  $s$  is our harmonic integer which corresponds to Shirley's  $n$ .) The  $\mathcal{H}^{(k)}$  of eq. (59) give the off-diagonal terms.

The diagonal terms correspond to the eigenfrequencies which we have obtained as the zeroth approximation, eq. (101): in this approximation the quantum number  $\mu$  may be identified with  $m$ .

The third order terms are evaluated from the off-diagonal elements by standard perturbation theory. Combining the result with the diagonal elements we have

$$q_\mu = \mu[\omega_0 J_0(2\omega_1/\omega) - (\omega_0^3/\omega^2)S(2\omega_1/\omega)] + s\omega, \quad (105)$$

where

$$S(2\omega_1/\omega) = \frac{1}{4} \sum_{\substack{\text{all } r \text{ and } s \\ \neq 0}} \left[ \frac{J_r J_{-s} J_{r-s}}{rs} - \frac{J_0 J_r^2}{r^2} \right]$$

The arguments of all the Bessel functions in (105) are  $(2\omega_1/\omega)$ .



The resonance condition may now be formed by using  $\partial q^2/\partial \omega_0 = 0$ , which yields

$$\omega_0 = \omega [J_0(2\omega_1/\omega)/3S(2\omega_1/\omega)]^{1/2} \quad (96)$$

Eq. (106) may be simplified to give the approximate result

$$\omega_0 = 2.14\omega(0.6013 - \omega_1/2\omega)^{1/2}. \quad (107)$$

The important point to notice about the procedure we have adopted in obtaining these results is that very poor convergence is obtained if Shirley's method is applied to the Hamiltonian describing the interactions in the laboratory frame. The zeroth-approximation, eq. (101), is obtained by this procedure as the power series expansion of the Bessel function. If, however, the strong, oscillating field is first transformed away, its effect in the zeroth approximation is obtained as an exact result, and the lesser interaction – the static field – may, with greater justification, be treated by standard perturbation theory.

### 6.5. Results

Eqs. (97) and (106) together represent a solution to the Bloch–Siegert problem which describes the shift of the peak of the resonance over the whole range from 0 to 100%, that is, from  $\omega_0 = \omega$  to  $\omega_0 = 0$ , as the amplitude of the oscillating field is increased. The results are shown in fig. 15, a plot of  $\omega_0/\omega$  against  $b/\omega$  ( $= |\frac{1}{2}\omega_1/\omega|$ ).

Successive approximations are shown by different curves in fig. 15. The solid curve, made up of the sections 1 and 2, represents eqs. (97) and (106) joined at the point where the separate curves intersect, as illustrated in the inset. The figure is taken from Hannaford, Pegg and Series [27], where a discussion of the accuracy of the formulae is given.

An experimental check of the formulae is very difficult for a variety of reasons, the most important being that the resonance line shape becomes grossly broadened and asymmetrical as the amplitude  $B_1$  is increased. A complete discussion of the line shape demands a specification of the relaxation processes, although Stenholm [28] has shown that the position of the peak is not very sensitive to the relaxation rate. Nevertheless, since the resonance under strong, oscillating fields is broad and distorted, it is difficult to locate the peak with any confidence.

An alternative approach is to make use of the “level-crossing” type of experiment. These rely on the resonance-like signals which are formed in the vicinity of degenerate eigenfrequencies (crossings in the frequency diagram) when the system under study is excited to a superposition-state (section 2.3.2). The breadth of the curves depends on the relaxation-width of the system (the  $\Gamma$  of eq. (27)) and on the slope of the crossing levels (eqs. (32) and (33)): the curves are not subject to power-broadening in the same way as the resonances associated with transitions (section 2.3.1).

In fig. 16 are shown the eigenfrequencies  $q_{\pm}$  for a two-level system. The position of the resonance is indicated  $R$ : there is a level-crossing at  $H$ , where  $\omega_0 = 0$  (Hanle effect), and also at  $C$ , where  $\omega_0 \neq 0$ . Eq. (101) describes the levels in the vicinity of  $H$ . Very thorough experimental tests showing excellent agreement with the theory have been carried out by Cohen-Tannoudji and Haroche and their colleagues [29, 30, and references given there].

The position of the crossing  $C$  can be found from the expressions we have obtained for  $q_{\pm}$  (eqs. (92) and (105)). Eq. (92) needs a little manipulation to obtain  $C$  for the smaller values of  $\omega_1$ , but eq. (105) yields immediately

$$\omega_0 = \omega [J_0(2\omega_1/\omega)/S(2\omega_1/\omega)]^{1/2} \quad (108)$$

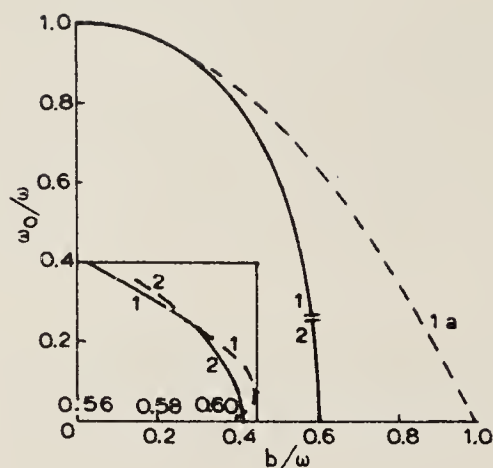


Fig. 15. Peak of the resonance,  $\omega_0$  (in units of  $\omega$ ), as a function of  $b/\omega$  ( $= |\frac{1}{2}\omega_1/\omega|$ ). Curve 1 is derived from eq. (97), curve 2 from eq. (106). Curve 1a represents the first approximation, eq. (88). The intercept  $(b/\omega)_0 = 0.6013$  is exact. The inset shows the crossing of curves 1 and 2 with an expanded scale of  $b/\omega$ . (By permission of the Institute of Physics.)

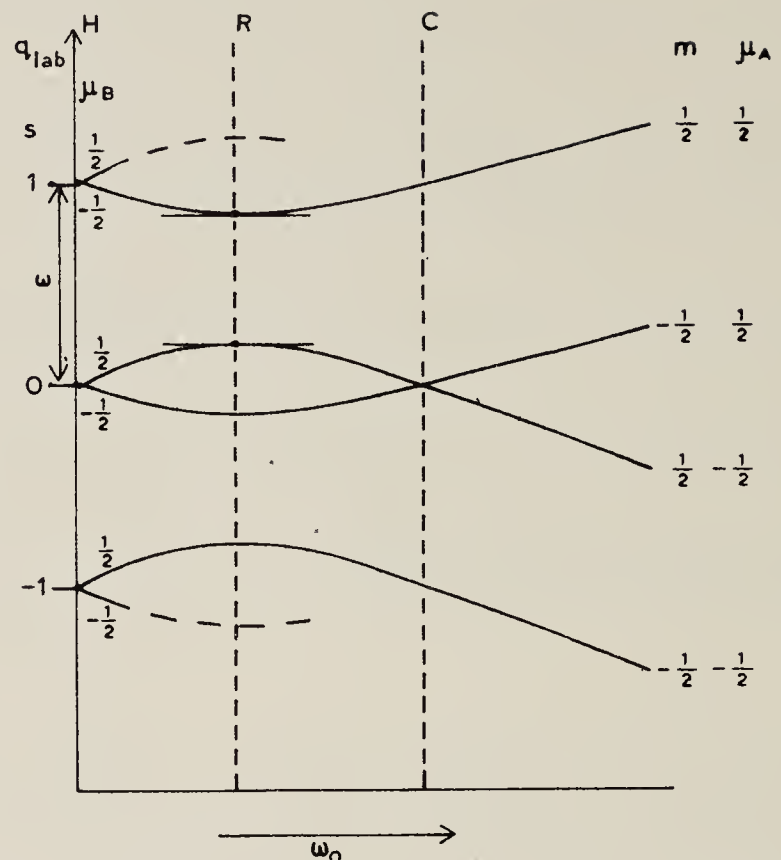


Fig. 16. Eigenfrequencies of a spin- $\frac{1}{2}$  system under the configuration of fields shown in fig. 13(a). The resonance  $R$  occurs at the value of  $\omega_0$  where  $\partial q/\partial \omega_0 = 0$ , shown by the horizontal tangent. The Hanle effect  $H$  occurs in the vicinity of  $\omega_0 = 0$ . A level-crossing effect occurs at  $C$ . Notice that  $R$  is nearer to  $H$  than to  $C$ . The quantum numbers on the right are those appropriate to case A; those on the left are appropriate to case B. In both cases, only representatives of the sets of levels are shown. The dominant levels are: on the left, those having  $s = 0$ ; on the right, those for which the value of  $\mu$  is the same as the value of  $m$ .

for the position of  $C$  when the oscillating field is strong. Eq. (108) was obtained by Cohen-Tannoudji, Dupont-Roc and Fabre [30] by the method of "dressed atoms" and agreed well with their experimental results. They also observed the position of  $C$  for smaller values of  $\omega_1$  and obtained excellent agreement with the theoretical values obtained from formulae which, though derived from the "dressed atom" theory, coincide with the expressions we have obtained by the method of transformations at all points where they have been tested.

#### 6.6. Discussion: comments on other work

We have chosen the Bloch-Siegert effect as an example to illustrate how the method of transformations may be applied systematically and successfully in a situation which is far more difficult to analyse than the conventional case A and the more sophisticated case B. Although we have concentrated attention on obtaining the eigenfrequencies and resonance conditions, it should not be overlooked that the transformations which we have used to obtain the eigenfrequencies may also be applied to find the evolution of the atomic density matrices, and therefore all details of whatever observable of the system is being monitored. Some of the alternative solutions which have been proposed calculate only the populations of the atomic states, whereas knowledge of



the density matrix allows a calculation of, for example, the precession of the magnetization.

By way of comparison with other work we have mentioned in particular the dressed-atom approach of Cohen-Tannoudji and Haroche [9] because the starting point of their work is the quantum field theory, and because they and their colleagues have tested their theory in a great variety of experimental situations. No differences have emerged between the predictions of that theory and of the method of transformations. Many other authors have attacked these problems in recent years. Stenholm has developed the continued-fraction method of solution in a series of papers based on semi-classical equations [28, 31–33, 35]. Both Stenholm [1] and Swain [36] have demonstrated the equivalence of the semi-classical and quantum field formulations. Swain also makes use of the continued fraction method [34, 37]. The starting point of Ahmad and Bullough's work [38] is the set of semi-classical equations describing the macroscopic magnetic moment of a system of atoms, the Bloch equations. They use algebraic methods to calculate the resonance condition as far as terms in  $\omega_1^{10}$ . Tsukada and Ogawa [39] have analysed resonances in a number of complicated configurations of fields, also starting from the Bloch equations. An iterative procedure based on phase-averaging of quantum electrodynamic equations has been used by Białynicka and Białynicka [40]. These authors claim to have obtained results which compare well with those of the other authors quoted. The most recent paper based entirely on quantum field theory is that of Yeh and Stehle [41], who use the formalism of resolvents and "walk diagrams". Their results do not differ from results obtained by semi-classical methods.

Significant differences between the predictions of semi-classical and quantum field theories have, in fact, been reported, but these have been shown to be due to errors and misapprehensions. So long as the fields are strong in the sense that simultaneous measurements of amplitude and phase might, if called for, be made – which are the conditions under which the vast majority of magnetic resonance experiments have been carried out – the two types of theory have given the same results. Although the correspondence between them in the limit of large photon number has been shown formally in the papers cited above, less attention has been paid to the equivalence of semi-classical and quantum field theories of *absorption* when the photon number is small, a point to which we referred in the Introduction. But in this limit of low photon number the theories differ in their predictions concerning the *emission* of radiation. Spontaneous emission requires special treatment in semi-classical theory. In the concluding section we deal with this problem.

## 7. Spontaneous emission

The work in this section is purely formal in the sense that we give a prescription for dealing with spontaneous emission by semi-classical methods. The method describes the phenomenon by the effects of an electric dipole operator,  $\mathcal{H}^s = -\mathbf{E}^s \cdot \mathbf{P}$ , a form which can conveniently be combined with, and treated similarly to, the interaction  $\mathcal{H}^{\text{lab}} = -\mathbf{E}^{\text{lab}} \cdot \mathbf{P}$ , where  $\mathbf{E}^{\text{lab}}$  is a field imposed on the atom from external sources and can be switched on and off.  $\mathbf{E}^s$  cannot be switched off.

In the introduction we outlined the argument, based on semi-classical radiation theory and classical thermodynamics, for the existence of the phenomenon of spontaneous emission. We are now concerned with the mechanism. Semi-classical theory yields the Einstein *B*-coefficient, and the *A*-coefficient may be derived from this without appealing to the quantized radiation field. The

power spectrum of  $E^s$  is chosen to secure for the  $A$ -coefficient the value so obtained. No direct physical interpretation can be given to  $E^s$  since it turns out to be a complex field, but a physical interpretation of the mechanism, based on classical concepts, is offered in subsection 7.3. Some further reflections are set down in 7.4.

### 7.1. The formalism

The operator

$$\mathcal{H}^s = -E^s \cdot P \quad (109)$$

is to represent a perturbation on atoms described by  $\mathcal{H}^0$ . The eigenstates of  $\mathcal{H}^0$  are  $|\alpha\rangle, |\beta\rangle, \dots$ , with eigenvalues  $\omega_\alpha, \omega_\beta, \dots$  ( $\hbar = 1$ , as before).

$E^s$  is a time-dependent field defined by equations such as

$$\langle E_i^s(t) E_j^{s*}(t + \tau) \rangle = \delta_{ij} \int_{-\infty}^{\infty} \rho_i(\omega) \exp(i\omega\tau) d\omega, \quad (110a)$$

$$\rho_i(\omega) = \rho_j(\omega) = \rho_k(\omega). \quad (110b)$$

The angle brackets represent time averaging, which will be taken to be equivalent to ensemble averaging. The spectral density,  $\rho(\omega)$ , will be specified later.

We now write down the equations of time-dependent perturbation theory for the amplitudes  $a_\alpha(t), a_\beta(t)$  of a particular pair of eigenstates of  $\mathcal{H}^0$ . For simplicity we shall include only these in our basis. We suppose  $\omega_\alpha > \omega_\beta$ . We work in the interaction representation. The equations are

$$\dot{a}_\alpha = iP_{\alpha\beta} E_c^s a_\beta(t) \exp(i\omega_{\alpha\beta}t), \quad (111)$$

$$\dot{a}_\beta = iP_{\alpha\beta} E_c^{s*} a_\alpha(t) \exp(-i\omega_{\alpha\beta}t), \quad (112)$$

with  $\omega_{\alpha\beta} = \omega_\alpha - \omega_\beta$ . The suffix  $c$  on  $E^s$  specifies that component of  $E^s$  which corresponds to an allowed electric dipole transition between the space-quantized states  $|\alpha\rangle$  and  $|\beta\rangle$ . Likewise  $P_{\alpha\beta}$  is a matrix element of a component of the vector operator  $P$ .

We make a formal integration of (112) and substitute the resulting equation in (111):

$$\dot{a}_\alpha = -|P_{\alpha\beta}|^2 \int_0^t a_\alpha(t') E_c^s(t) E_c^{s*}(t') \exp[i\omega_{\alpha\beta}(t - t')] dt'. \quad (113)$$

We now take  $a_\alpha(t')$  outside the integral as  $a_\alpha(t)$  and take it to the left hand side, which then becomes  $\partial(\ln a_\alpha)/\partial t$ . The justification for this step is that the change in the value of  $a_\alpha(t)$  is negligibly small in the coherence time of the perturbing field. This time is indeed very small since  $E^s$  will be seen to be equivalent to the zero-point fluctuations of quantum field theory. We recall also that, since we are working in the interaction representation, the high-frequency oscillations of the amplitudes have been factorised out.

We now take an ensemble average, replacing the amplitude  $a_\alpha$  by its geometric mean,  $b_\alpha$ ,

$$b_\alpha = \left[ \prod_{i=1}^n (a_\alpha^i) \right]^{1/n},$$



and  $\langle E_c^s(t)E_c^{s*}(t') \rangle$  by  $\int_{-\infty}^{\infty} \rho_c(\omega) \exp(i\omega\tau) d\omega$ , with  $\tau = t' - t$ . We then have, changing the order of integration,

$$\partial(\ln b_a)/\partial t = -|P_{\alpha\beta}|^2 \int_{-\infty}^{\infty} d\omega \rho_c(\omega) \int_{-\infty}^0 \exp\{i(\omega - \omega_{\alpha\beta})\tau\} d\tau. \quad (114)$$

The integral over  $\tau$  is the  $\zeta$ -function

$$\int_{-\infty}^0 \exp(ix\tau) d\tau = \pi\delta(x) - iP/x, \quad (115)$$

where  $P$  denotes that the principal value is to be taken in the subsequent integration. Carrying out the integration over  $\omega$  we arrive at

$$\partial(\ln b_a)/\partial t = -\pi|P_{\alpha\beta}|^2 \rho_c(\omega_{\alpha\beta}) + i|P_{\alpha\beta}|^2 P \int_{-\infty}^{\infty} d\omega \rho_c(\omega)/(\omega - \omega_{\alpha\beta}). \quad (116)$$

Solving for  $b_a(t)$ , we have:

$$b_a(t) = [\exp - i(L_a - \frac{1}{2}i\Gamma_a)(t - t_0)]b_a(t_0), \quad (117)$$

where

$$\Gamma_a = 2\pi|P_{\alpha\beta}|^2 \rho_c(\omega_{\alpha\beta}) \quad (118)$$

and

$$L_a = -|P_{\alpha\beta}|^2 P \int_{-\infty}^{\infty} d\omega \rho_c(\omega)/(\omega - \omega_{\alpha\beta}). \quad (119)$$

$L_a$  represents a level shift and  $\Gamma_a$  is the decay constant for population (to be equated in this context with the Einstein  $A$ -coefficient). It would be out of place here to discuss further the level shift. Let it suffice to remark that, with the choice of  $\rho_c(\omega)$  which we need for  $\Gamma_a$ ,  $L_a$  is the unrenormalised first-order Lamb shift.

To secure agreement with the Einstein  $A$ -coefficient

$$\begin{aligned} A_a &= \sum_{\beta} 4\omega_{\alpha\beta}^3 |P_{\alpha\beta}|^2 / 3c^3, & \omega_{\alpha\beta} > 0 \\ &= 0, & \omega_{\alpha\beta} < 0 \end{aligned} \quad (120)$$

we must have

$$\begin{aligned} \rho_c(\omega) &= 2\omega^3 / 3\pi c^3, & \omega > 0 \\ &= 0, & \omega < 0. \end{aligned} \quad (121)$$

A very significant quantity is the energy density per mode of the field, which may be obtained as follows. The spectral distribution of the energy in the electrical component of the field which drives the spontaneous emission is  $\rho_c/8\pi$ , by eq. (110a). The total energy in the range  $d\omega$  is  $(6\rho_c/8\pi) d\omega$  (three electrical and three magnetic components in the isotropic field, all contributing

equally). The energy per mode is given by dividing  $6\rho_c/8\pi$  by the density of modes,  $\omega^2/\pi^2c^3$ . The result is

$$(6/8\pi)(2\omega^3/3\pi c^3)(\pi^2 c^3/\omega^2) = \frac{1}{2}\omega, \quad (\text{i.e., } \frac{1}{2}\hbar\omega). \quad (122)$$

It is not surprising that our result is the same as that which quantum field theory interprets as the energy density per mode of the vacuum fluctuations. But our derivation of (122) is based on a value of the Einstein  $A$ -coefficient obtained from a thermodynamic equilibrium at high temperatures, not from field quantization.

Our field  $E^s$  is a mathematical, rather than a physical quantity. We draw attention to the fact that the field is complex, and also that, in taking matrix elements of the interaction  $\mathcal{H}^s$  we have, in eqs. (111) and (112), used the field and its complex conjugate. For a strictly  $c$ -number calculation we should have used the same quantity in both equations.

## 7.2. Results: application to cycles of optical pumping

Our result (117) for the time-dependence of the (ensemble-averaged) amplitude of the excited state constitutes a calculation of the time-shift operator for that state:

$$U_\alpha^s(t, t_0) = \exp - i(L^\alpha - \frac{1}{2}i\Gamma_\alpha)(t - t_0), \quad (123)$$

but we have not demonstrated the general validity of this operator; indeed, it must be used with caution because it is not unitary. Had we developed eqs. (111) and (112) in favour of the lower state,  $|\beta\rangle$ , we should have found a level shift  $L_\beta$ , but the damping constant  $\Gamma_\beta$  would have been zero on account of (121). However, the perturbation does, of course, induce transitions from  $|\alpha\rangle$  to  $|\beta\rangle$ , and the formalism allows us to calculate this. From equations (111) and (112) we can find the density matrix element for the ground state,  $\sigma_{\beta\beta}(t)$ , in terms of the corresponding quantity,  $\sigma_{\alpha\alpha}(t) = |b_\alpha(t)|^2$ , for the excited state. We make a formal integration of (112), as before, and then form the quantity  $\dot{a}_\beta(t)a_\beta^*(t)$ . On the right-hand side we find  $a_\alpha(t)a_\alpha^*(t')$ . Taking  $a_\alpha^*(t')$  outside the integral and making an ensemble average, we finally obtain

$$\dot{\sigma}_{\beta\beta}(t) = [2\pi|P_{\alpha\beta}|^2\rho_c(\omega_{\alpha\beta})]\sigma_{\alpha\alpha}(t) = \Gamma_\alpha\sigma_{\alpha\alpha}(t), \quad (124)$$

with

$$\sigma_{\alpha\alpha}(t) = \exp - \Gamma_\alpha(t - t_0)\sigma_{\alpha\alpha}(t_0), \quad (125)$$

– the latter equation being derived from (117).

Eqs. (124) and (125) together guarantee conservation of atoms in the process of spontaneous emission.

The procedures of this subsection may be generalised to embrace the situation commonly encountered in optical pumping experiments, when the ground and excited states have complicated hyperfine and Zeeman structures. One obtains equations, not only for the diagonal elements of the density matrix, but also for the off-diagonal elements within the ground and excited states. These equations are:

$$\dot{\sigma}_{\beta\beta'}(t) = 2\pi \sum_{\alpha\alpha'} \rho_c(\omega_{\alpha\beta}) P_{\beta\alpha} P_{\alpha'\beta'} \sigma_{\alpha\alpha'}(t), \quad (126)$$

$$\dot{\sigma}_{\alpha\alpha'}(t) = -i(\omega_{\alpha\alpha'} - i\Gamma_\alpha)\sigma_{\alpha\alpha'}(t), \quad (127)$$

$$\Gamma_\alpha = [2\pi\rho_c(\omega_{\alpha\beta})] \sum_{\beta'} |P_{\alpha\beta'}|^2. \quad (128)$$



Eq. (126) is subject to the condition that the change in  $m$ -quantum number be the same for the transitions  $\alpha \rightarrow \beta$ ,  $\alpha' \rightarrow \beta'$ . This condition implies that both transitions are driven by the same spectral component of  $E^s$ .

The equations here refer to the density matrix in the Schrödinger representation, not the interaction representation.

The energies of the sub-states are supposed to be so nearly equal that, for the purposes of calculating the decay constants, they are identical. Since, in addition, the  $|\alpha'\rangle$  have the same electronic configuration, they all decay at the same rate,  $\Gamma_\alpha$ .

Eqs. (126), (127), (128) allow one to deal with spontaneous emission by semi-classical methods in quite complicated experimental situations. When supplemented by terms representing the effect of a laboratory light source, introduced into the semi-classical equations of motion by the operator  $\mathcal{H}^{\text{lab}} = -\mathbf{E}^{\text{lab}} \cdot \mathbf{P}$ , the above equations become equivalent to the set of equations first introduced by Barrat and Cohen-Tannoudji [42, 43] to describe, with the use of quantized field formalism, a complete cycle of optical pumping. The present equations were used by the author [44] in a semi-classical calculation of the circulation of coherence, injected into the atomic system by a radio-frequency field, through many cycles of optical pumping induced by a laboratory light source.

### 7.3. Mechanism of spontaneous emission: radiation reaction

While the work in the foregoing subsections allows calculations involving spontaneous emission to be carried out within the semi-classical formalism, and notwithstanding the fact that the basic equations correspond closely with those of quantized field theory, the origin of the underlying field demands an explanation. In classical electromagnetism the damping of an oscillating charge is ascribed to radiation reaction. It is possible to obtain the Einstein  $A$ -coefficient and the first order Lamb shift by working with an operator equivalent of the reaction field  $E^r$ , as we now show.

It is well known that  $E^r$  is related to the third time-derivative of the displacement vector of the charge,  $\mathbf{r}$ , by the (non-relativistic) equation

$$\mathbf{E}^r = (2e/3c^3)\ddot{\mathbf{r}}. \quad (129)$$

It is also well known that this result can be obtained free of self-energy terms if one takes the symmetrised difference between the fields calculated from the retarded and advanced solutions of Maxwell's equations:

$$\mathbf{E}^r = \frac{1}{2}(\mathbf{E}^{\text{ret}} - \mathbf{E}^{\text{adv}}) = (2e/3c^3)\ddot{\mathbf{r}}. \quad (130)$$

Suppose then, that we form a perturbation operator

$$\mathcal{H}^r = -\mathbf{E}^r \cdot (e\mathbf{r}) = -(2e^2/3c^3)\mathbf{r} \cdot \ddot{\mathbf{r}}. \quad (131)$$

We regard the operator  $\ddot{\mathbf{r}}$  as acting, as does  $\mathbf{r}$ , in the space of the eigenstates of  $\mathcal{H}^0$ ,  $|\alpha\rangle, |\beta\rangle \dots |\varepsilon\rangle \dots$ . We are immediately aware of a possible ambiguity in the ordering of the two operators in (131): we have arbitrarily placed  $\ddot{\mathbf{r}}$  on the right. (The symmetrical combination would lead us to the result, zero.)

We notice next that  $\mathcal{H}^r$  has diagonal matrix elements:

$$\mathcal{H}_{\alpha\alpha}^r = -i(2e^2/3c^3) \sum_{\varepsilon} \omega_{\alpha\varepsilon}^3 |r_{\alpha\varepsilon}|^2. \quad (132)$$

But the radiative damping of the excited state  $|\alpha\rangle$  can be described by

$$\mathcal{H}_{\alpha\alpha}^d = -\frac{1}{2}i\Gamma_\alpha. \quad (133)$$

Identification of  $\mathcal{H}^d$  with  $\mathcal{H}^r$  leads to

$$\Gamma_\alpha = (4e^2/3c^3) \sum_\varepsilon \omega_{\alpha\varepsilon}^3 |r_{\alpha\varepsilon}|^2, \quad (134)$$

our previous result (eqs. (118), (120)), apart from the inconvenient fact that the sum over states in (134) includes states of *higher* as well as of *lower* energy. Nevertheless, the formal similarity of eqs. (134) to (120) encourages us to believe that the classical radiation reaction field may help us to a physical understanding of spontaneous emission without invoking the vacuum fluctuations of quantized field theory.

We are left in doubt on account of the arbitrary ordering of operators in eq. (131), and the occurrence of states of higher energy in eq. (134) is an embarrassment. A resolution of these problems can be effected by a symmetrisation based on eq. (130). Let  $\ddot{\mathbf{r}}$  be exhibited explicitly as a time-dependent operator, and let a Fourier analysis be made:

$$\ddot{\mathbf{r}}(t) = (2\pi)^{-1} \int_{-\infty}^{\infty} \ddot{\mathbf{r}}(t') dt' \int_{-\infty}^{\infty} \exp[-i\omega(t-t')] d\omega \quad (135)$$

$$= (2\pi)^{-1} \left[ \int_{-\infty}^0 \dots dt' \int_0^{\infty} \dots d\omega + \int_0^{\infty} \dots dt' \int_0^{\infty} \dots d\omega + \int_{-\infty}^0 \dots dt' \int_{-\infty}^0 \dots d\omega + \int_0^{\infty} \dots dt' \int_{-\infty}^0 \dots d\omega \right] \\ = I_1 + I_2 + I_3 + I_4. \quad (136)$$

$I_1$  and  $I_3$  refer to past times,  $I_2$  and  $I_4$  to future times. We associate  $I_1$  and  $I_3$  with “retarded” fields,  $I_2$  and  $I_4$  with “advanced” fields. One can show that  $I_1$  and  $I_3$ , and  $I_2$  and  $I_4$  are Hermitian-conjugate pairs: Hermitian conjugation has the effect of changing the sign of  $\omega$ . To keep the interaction in the domain of past times/positive frequencies (which is the same as future times/negative frequencies) we replace eq. (136) by

$$\ddot{\mathbf{r}}'(t) = I_1 + I_2^\dagger + I_3^\dagger + I_4 = 2(I_1 + I_4) = \ddot{\mathbf{r}}^{\text{ret}}(t) + \ddot{\mathbf{r}}^{\text{adv}}(t). \quad (137)$$

We then construct the perturbation operator

$$\mathcal{H}^s = -\frac{1}{2}(2e^2/3c^3) [\mathbf{r} \cdot \ddot{\mathbf{r}}^{\text{ret}} - \ddot{\mathbf{r}}^{\text{adv}} \cdot \mathbf{r}] \quad (138)$$

to echo eq. (130). This operator has diagonal matrix elements

$$\mathcal{H}_\alpha^s = L_\alpha - \frac{1}{2}i\Gamma_\alpha$$

with

$$L_\alpha = -(2e^2/3\pi c^3) \sum_\varepsilon \omega_{\alpha\varepsilon}^3 |r_{\alpha\varepsilon}|^2 P \int_0^{\infty} \frac{d\omega}{\omega - \omega_{\alpha\varepsilon}}, \quad (139)$$

and

$$\Gamma_\alpha = (4e^2/3c^3) \sum_\varepsilon \omega_{\alpha\varepsilon}^3 |r_{\alpha\varepsilon}|^2, \quad \omega_{\alpha\varepsilon} > 0. \quad (140)$$



The result for  $\Gamma_\alpha$ , that the sum-over-states no longer includes those of higher energy, is attributable to our having replaced  $I_2$  and  $I_3$  by their Hermitian conjugates. By this device we have obtained the correct form of the Einstein  $A$ -coefficient. Had we taken the Hermitian conjugates of  $I_1$  and  $I_4$  instead of  $I_2$  and  $I_3$  we should have obtained eq. (140) with the condition  $\omega_{\alpha\epsilon} < 0$ , that is to say, an equation describing the decay of the state  $|\alpha\rangle$  by spontaneous absorption. This is to be associated with time-reversal. Eq. (134), with no restriction on  $\omega_{\alpha\epsilon}$ , includes spontaneous absorption as well as spontaneous emission.

$L_\alpha$  is the first-order Lamb shift, the renormalised expression first obtained by Bethe [45] in 1947. The term arises here on account of the cut we made in the time-domain. The fact that the expression we have obtained is the *renormalised* level shift is gratifying in view of the fact that eq. (130) is free of self-energy. It is to be noticed that in eq. (139) there is no restriction on the sign of  $\omega_{\alpha\epsilon}$ , so that the equation gives a shift for ground states as well as for excited states.  $\Gamma_\alpha$ , on the other hand, is zero when  $|\alpha\rangle$  is the ground state.  $L_\alpha$  changes sign under the operation of time-reversal.

#### 7.4. Concluding remarks on spontaneous emission

The problems raised by theories of spontaneous emission appear to us to be quite profound. In section 7.1 we have given a technique for incorporating the process into semi-classical calculations, and in section 7.3 we have demonstrated connections between the behaviour of real atoms (decay constants and level-shifts) and the classical radiation reaction. (It has not been found possible to develop the equations of 7.3 to describe cycles of optical pumping.) In both sections we have taken arbitrary steps which, in effect, confine the spectrum of the interaction to positive frequencies. That some such steps are necessary is evident when it is recalled that the equation of motion of quantum mechanics, and the equations of classical electromagnetism, are time-symmetric. To describe the evolution of an atom in the process of radiating it is essential that the arrow of time be injected into the equations at some point. The arbitrary steps which we have taken have amounted to the replacement of the energy sink for the emitted radiation by a local field, or a local operator, acting on a potentially excited atom. It is remarkable that the interaction with the energy sink, which amounts to an interaction with all other matter in the universe, can be simulated in such simple ways.

It is not the intention of this section to give a balanced review of theories of spontaneous emission, but we mention, in passing, that the subject has received a great deal of attention from quantum field theorists in recent years. What has emerged is that the interpretation in terms of vacuum fluctuations, on the one hand, or of radiation reaction, on the other, is to some extent arbitrary, depending on the ordering of operators in the equations. But radiation reaction would appear to be an essential ingredient. A discussion, together with references, will be found in a recent article by Jaynes [46].

Versions of the absorber theory of radiation, adapted for quantized systems, have been offered in recent years by Hoyle and Narlikar [47], by Davies [48–50], and by Pegg [51]. In these theories there is no quantized field: direct interaction between the radiating atom and the “rest of the universe” is the mechanism of the energy sink. Pegg introduces a considerable simplification into these theories with the notion of “minimal perfect absorber” – a cavity surrounding the atom which is capable of absorbing all the radiation potentially emitted. He shows how the equations describing the interaction of the atom with such an absorber can be combined with the semi-classical terms which describe the interaction with a laboratory field to yield the full spontaneous + stimulated

interaction. To the present writer the appeal of these theories lies in the insight they offer into the mechanism of the complete radiative interaction.

## References

- [1] S. Stenholm, *J. Phys.* B6 (1973) 1650.
- [2] G.W. Series, *J. Phys.* B3 (1970) 84.
- [3] R.P. Feynman, F.L. Vernon and R.W. Hellwarth, *J. Appl. Phys.* 28 (1957) 49.
- [4] I.I. Rabi, J.F. Ramsey and J. Schwinger, *Rev. Mod. Phys.* 26 (1954) 167.
- [5] D.T. Pegg and G.W. Series, *J. Phys.* B3 (1970) L33.
- [6] D.T. Pegg and G.W. Series, *Proc. Roy. Soc.* A332 (1973) 281.
- [7] J.N. Dodd and G.W. Series, *Proc. Roy. Soc.* A263 (1961) 353.
- [8] S. Autler and C.H. Townes, *Phys. Rev.* 100 (1955) 703.
- [9] C. Cohen-Tannoudji and S. Haroche, *J. Phys. (Paris)* 30 (1969) 153.
- [10] J.N. Dodd, G.W. Series and M.J. Taylor, *Proc. Roy. Soc.* A273 (1963) 41.
- [11] B.P. Kibble and G.W. Series, *Proc. Roy. Soc.* A274 (1963) 213.
- [12] R.B. Partridge and G.W. Series, *Proc. Phys. Soc.* 88 (1966) 969.
- [13] A. Corney, *J. Phys.* B1 (1968) 458.
- [14] D.M. Brink and G.R. Satchler, *Angular momentum* (Oxford University Press, 1962).
- [15] W. Gough, *J. Phys.* B3 (1970) 1636.
- [16] R.S. Baker and W. Gough, *J. Phys.* B8 (1975) 552.
- [17] S. Pancharatnam, *Proc. Roy. Soc.* A330 (1972) 265.
- [18] S. Pancharatnam, *Proc. Roy. Soc.* A330 (1972) 271.
- [19] G.D. Chapman and G.W. Series, *J. Phys.* B3 (1970) 72.
- [20] G.D. Chapman, *J. Phys.* B3 (1970) L36.
- [21] A. Messiah, *Quantum mechanics II* (North-Holland, Amsterdam, 1961) p. 724.
- [22] D.T. Pegg, *J. Phys.* B6 (1973) 241.
- [23] D.T. Pegg, *J. Phys.* B6 (1973) 246.
- [24] D.T. Pegg, *J. Phys.* B10 (1977) 1027.
- [25] F. Ansbacher, *J. Phys.* B6 (1973) 1620.
- [26] J.N. Shirley, *Phys. Rev.* 138 (1965) B979.
- [27] P. Hannaford, D.T. Pegg and G.W. Series, *J. Phys.* B6 (1973) L222.
- [28] S. Stenholm, *J. Phys.* B5 (1972) 878.
- [29] C. Cohen-Tannoudji, J. Dupont-Roc and C. Fabre, *J. Phys.* B7 (1973) L214.
- [30] C. Cohen-Tannoudji, J. Dupont-Roc and C. Fabre, *J. Phys.* B6 (1973) L218.
- [31] S. Stenholm, *J. Phys.* B5 (1972) 890.
- [32] S. Stenholm, *J. Phys.* B6 (1973) 1097.
- [33] S. Stenholm, *J. Phys.* B6 (1973) 2390.
- [34] S. Swain, *Phys. Lett.* 46A (1974) 435.
- [35] S. Stenholm, *J. Phys.* B6 (1973) L240.
- [36] S. Swain, *J. Phys.* A6 (1973) L169.
- [37] S. Swain, *J. Phys.* B6 (1973) 1919.
- [38] F. Ahmad and R.K. Bullough, *J. Phys.* B7 (1974) L147.
- [39] N. Tsukada and T. Ogawa, *J. Phys.* B6 (1973) 1643.
- [40] Z. Bialynicka-Birula and I. Bialynicka-Birula, *Lett. Nuovo Cimento* (1976) 627.
- [41] S. Yeh and P. Stehle, *Phys. Rev.* A15 (1977) 213.
- [42] J.P. Barrat and C. Cohen-Tannoudji, *Journ. de Phys. et le Rad.* 22 (1961) 329 and 443.
- [43] J.P. Barrat and C. Cohen-Tannoudji, *Ann. Phys. (Paris)* 7 (1962) 426 and 469.
- [44] G.W. Series, *Proc. Phys. Soc.* 88 (1966) 957.
- [45] H.A. Bethe, *Phys. Rev.* 72 (1974) 339.
- [46] E.T. Jaynes, in: *Proc. Fourth Rochester Conf. on Coherence and quantum optics* (Plenum Press, New York, London, 1977).
- [47] F. Hoyle and J.V. Narlikar, *Action at a distance in physics and cosmology* (W.H. Freeman and Co., San Francisco, 1974).
- [48] P.C.W. Davies, *Proc. Camb. Phil. Soc.* 68 (1970) 751.
- [49] P.C.W. Davies, *J. Phys.* A4 (1971) 836.
- [50] P.W.C. Davies, *J. Phys.* A5 (1972) 1025.
- [51] D.T. Pegg, submitted for publication (1977).



## Forward Scattering and Polarization Spectroscopy

W. Gawlik<sup>1</sup> and G.W. Series

J.J. Thomson Physical Laboratory, The University of Reading, Whiteknights  
Reading RG6 2AF, U.K.

We recall some of the essential points concerning the forward scattering of radiation through a gas and show how the treatment that proved convenient for the analysis of optical pumping experiments can be used also for polarization spectroscopy with lasers. We distinguish between polarization spectroscopy as a saturation phenomenon and as a pumping phenomenon - the latter being realisable when the lower state is not single - and demonstrate how the long relaxation time of ground states allows polarization spectroscopy to be carried out with very weak light beams. We investigate some of the consequences of using strong beams: the decoupling of the hyperfine structure by the light and the manifestation of the Autler-Townes effect.

### 1. Forward Scattering

Two important points to notice about the forward scattering of monochromatic light through a gas are (i) the frequency of the forward scattered light is not Doppler-shifted with respect to the incident light, and (ii) the forward-scattered optical paths, for scattering from atoms in random positions, are all equal (see Fig.1).

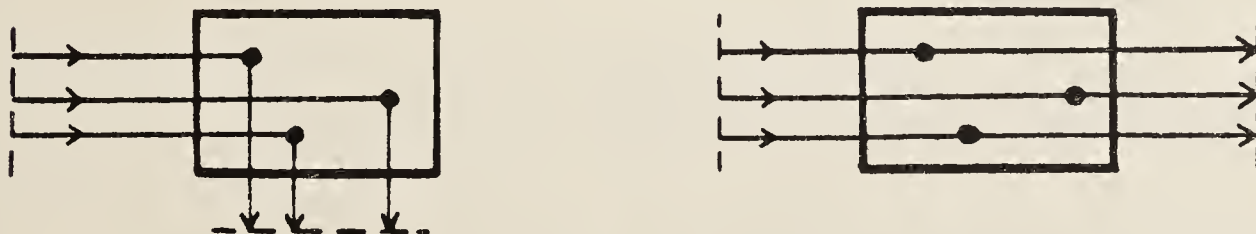


Fig.1 Lateral scattering: random paths between reference planes.

Forward scattering: equal paths.

These points, together with the principle of indistinguishability applied to atoms which return to their original state after the scattering process, secure that the forward-scattered light from different atoms is mutually coherent, and is coherent with the exciting light.

The properties of the atoms - which is our concern as spectroscopists - are reflected in the amplitude of the scattered light. To separate the forward-scattered light from the primary beam two methods have been used: (i) interferometric method based on beam splitting, which cancels the primary beam by introducing a controlled phase difference in that beam which does

<sup>1</sup> permanent address: Instytut Fizyki, Uniwersytetu Jagiellonskiego, ul. Reymonta 4, 30-059 Krakow, Poland.

not traverse the sample [1, 2, 3], (ii) polarization method (see figure 2) where the primary beam is rejected by a crossed polarizer [4, 5, 6, 7, 8].

With either technique it is sometimes useful to allow a small fraction of the primary light to be transmitted to heterodyne the scattered light. If all the primary light is transmitted the antiphase component of the scattered light appears as absorption, the quadrature component as dispersion.

Method (ii) will form the basis of our analysis. Although the scattered light is coherent with the primary light, it must be of different polarization in order to pass the analyser. It is, therefore, of the essence of this work that the scattering atoms introduce some asymmetry into the scattering process: the symmetry of the perturbation acting on the atoms must be different from the symmetry of the probe beam. While many different symmetry-breaking perturbations may be envisaged, we shall be concerned here with two: (i) external, longitudinal magnetic fields, and (ii) a counter-propagating 'pumping' beam, circularly polarized. When this is the same frequency as the probe beam there exists, of course, a velocity-selective interaction leading to narrow resonances. This is the basis of Doppler-free polarization spectroscopy [9]. We shall consider the two perturbations acting separately, and together.

### 1.1 Calculation of the Scattered Intensity

The object of the analysis is to relate the intensity of light which passes the crossed analyser (the signal) to the polarizability tensor of the medium, which is obtained by summing the polarizabilities of the atoms in a macroscopic volume. It is in the calculation of these polarizabilities that one finds the differences between optical pumping and laser saturation spectroscopy. The beam illustrated in figure 2 constitutes a probe beam. In simple cases it is so weak that its interaction with the atoms is linear, but we have found that non-linear interactions must also be reckoned with.

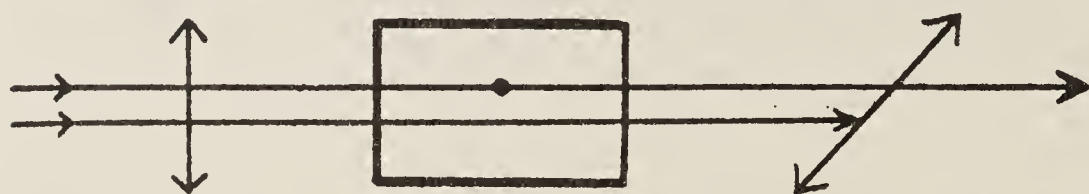


Fig.2 The primary beam is rejected but the scattered beam is transmitted if the polarization has been changed in the process of scattering.

Let the bulk medium be characterized by a polarizability tensor  $\chi$  or refractive indices  $n_{\pm} = n_{\pm}^r + in_{\pm}^i$ . We describe the tensor in a spherical basis with the z-axis in the direction of propagation of the light. Suffixes  $\pm$  on  $n$  refer to circularly polarized light. For small optical depth the intensity transmitted by the analyzer in Fig.2 is

$$I = \frac{1}{2} I_0 (\omega L/c)^2 [ (n_+^r - n_-^r)^2 + (n_+^i - n_-^i)^2 ],$$

where  $I_0$  is the intensity of the incident light and  $L$  is the length of the sample. In terms of the components of  $\chi$ , this becomes

$$I = \pi^2 I_0 (\omega L/c)^2 \{ [(\chi_{++}^r - \chi_{--}^r) - (\chi_{+-}^r - \chi_{-+}^r)]^2 + [(\chi_{++}^i - \chi_{--}^i) - (\chi_{+-}^i - \chi_{-+}^i)]^2 \}. \quad (1)$$



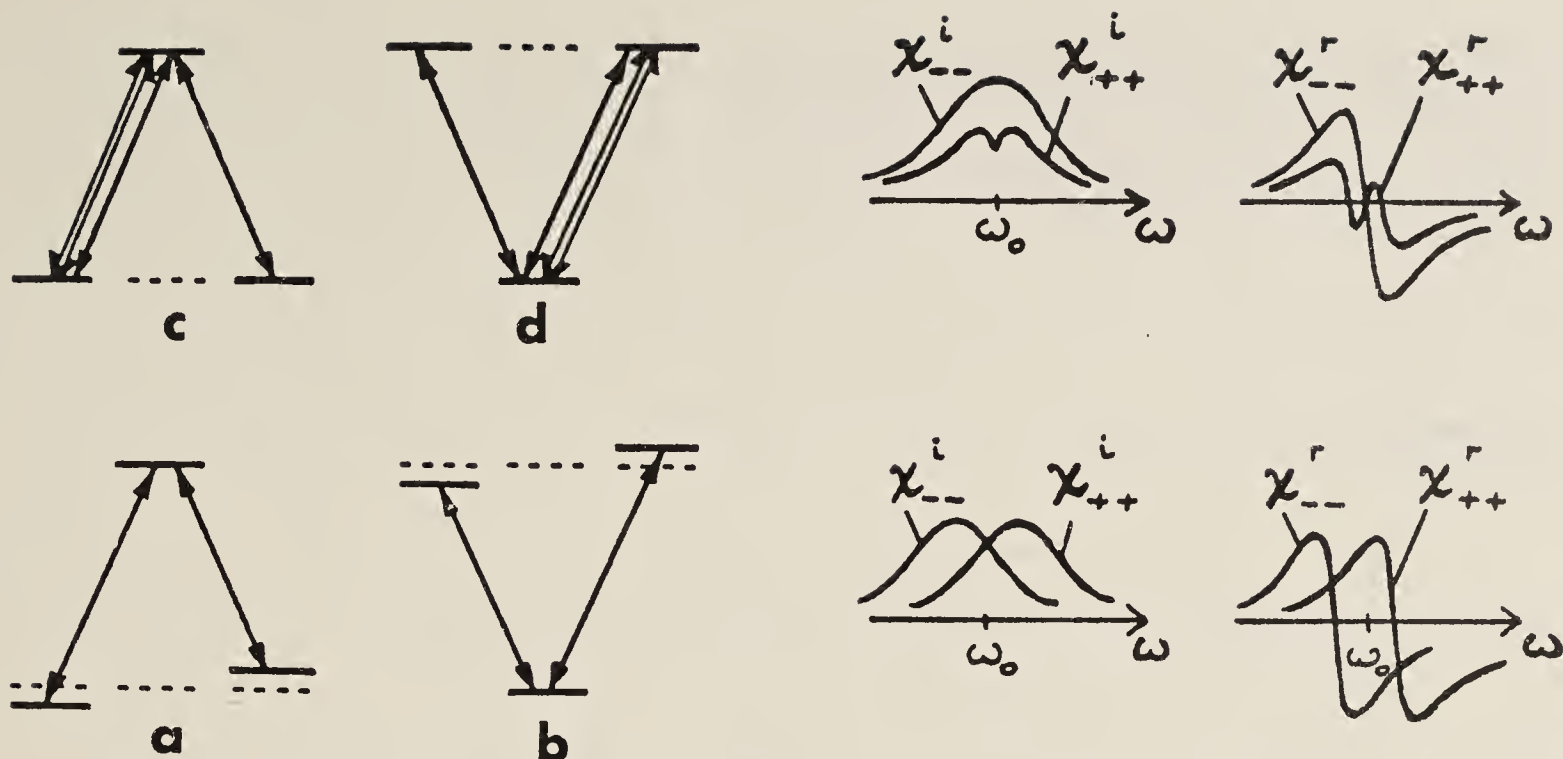


Fig.3 Three-level system interacting with a probe beam. In cases (a) and (b) there is a displacement of levels induced by an external electric or magnetic field. In cases (c) and (d) the levels remain degenerate but are unequally populated through the operation of a pumping beam (double lines). On the right of the transition diagrams are sketched the real and imaginary parts of the corresponding polarizability tensor, as a function of frequency

$\hat{\chi}$  will depend on the intensity and polarization of the pumping beam and, in the case of non-linear interactions with the probe beam, may be of rank higher than two, in which case the necessary summations must be carried out to contract it to a rank-2 tensor.

In contrast to saturated absorption spectroscopy, where a 2-level system provides an adequate model, the simplest atomic structure which will allow a discussion of the necessary asymmetries in polarization spectroscopy is a three-level structure of either of the types shown in Figs. 3(a) and (b) or (c) and (d).

## 2. Forward-Scattering Perturbed by a Magnetic Field.

In this section we treat the propagation of the probe beam in the presence of a longitudinal magnetic field (Fig.4).

If the probe beam is weak the  $\chi_{\pm\pm}$  are zero and  $I \propto |\chi_{+-} - \chi_{-+}|^2$ . These functions are Doppler-broadened, and  $I(B)$  is a Doppler-broadened Hanle curve [4]. If, however, the probe beam is strong enough to induce stimulated transitions between upper and lower levels (cases (a) and (b) of Fig.3), the

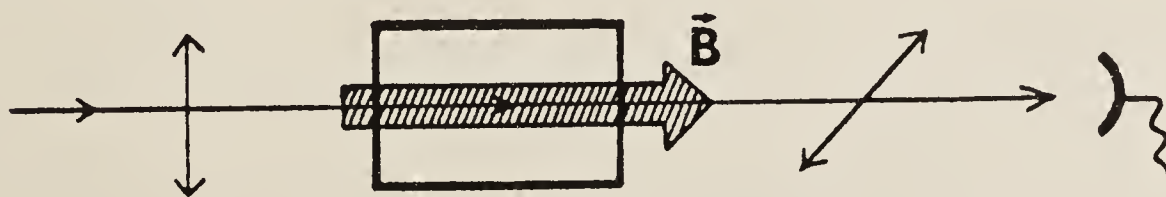


Fig.4 The forward-scattered signal attributable to the magnetic field  $B$  is recorded by the detector.

induced coherence between the lower levels or upper levels, as the case may be ('Zeeman coherence') generates non-vanishing values of  $\chi_{\pm}$  [6, 10, 11]. (Coherence of this kind may also be induced by transverse r.f. fields [4].) This Zeeman coherence gives rise to narrow resonances around  $B = 0$  superimposed on the broad background (see inset to Fig.10). The width of these resonances is determined by the relaxation constants of the levels involved.

### 3. Forward-Scattering Perturbed by a Counter-Propagating Pumping Beam

To induce the anisotropy in  $\hat{\chi}$  the polarization of the pumping beam needs to be different from that of the probe beam (Fig.5).

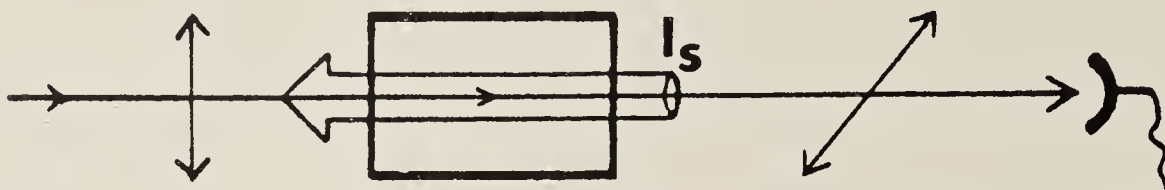


Fig.5 The forward-scattered signal attributable to the pumping beam  $I_s$  is recorded by the detector.

We consider the case when the pumping beam is circularly polarized, although other polarizations have been investigated [9, 12, 13]. The frequency of the pumping beam is taken to be the same as that of the probe beam.

The characteristics of the observed signals depend on the intensities of the two beams in relation to the relaxation rates of the levels involved. We use  $\Gamma$ ,  $\gamma$  for the relaxation rates of the upper and lower levels, respectively, in the absence of light, and  $\Gamma_+ = \Gamma/2 + aI_s$  for the power-broadened width of the optical transition. We use also the saturation parameters  $G_Y = (E_s \cdot D / \hbar \gamma)^2$  and  $G_\Gamma = (E_s \cdot D / \hbar \Gamma)^2$ .  $E_s$ ,  $I_s$  relate to the pumping beam.

It is not difficult to appreciate that, when the pumping beam is weak in the sense that stimulated emission is negligible ( $G_\Gamma \ll 1$ ), the induced anisotropy depends solely on the difference between the populations,  $N_+$ , of the sub-levels illustrated in Fig.3(c) or (d). The mechanisms responsible for maintaining these population differences are, however, quite different in the two cases and will be discussed further below. The signal detected by a weak probe beam is proportional to  $(N_+ - N_-)^2$  in both cases. Detailed calculation yields

$$I \propto G_Y^2 \frac{\Gamma_+^2}{4\delta^2 + \Gamma_+^2} \quad \text{for the } \Lambda\text{-system (Fig.3c),} \quad (2)$$

$$\text{and } I \propto G_\Gamma^2 \frac{\Gamma_+^2}{4\delta^2 + \Gamma_+^2} \quad \text{for the } V\text{-system (Fig.3d).} \quad (3)$$

Here,  $\delta$  is the frequency-offset from resonance. Notice that the equations predict a line-width of  $\Gamma_+$ , which tends to  $\frac{1}{2}\Gamma$  in the limit of weak pumping fields. This contrasts favourably with the value  $2\Gamma$ , the limiting line-width in saturation spectroscopy.

It is more especially important to notice the factors  $G_Y^2$ ,  $G_\Gamma^2$ , different in the two cases. The significance is that, in the frequently-encountered situation  $\gamma \ll \Gamma$ , the Doppler-free Lorentzian signals represented by (2) and



(3) are achieved with much weaker pumping beam intensities for the  $\Lambda$ -system than for the  $V$ -system. In the  $\Lambda$ -system the main effect of the pumping beam is to re-distribute the population between the sub-levels of the ground state - optical pumping. The dynamics of the re-distribution is determined by  $G_\gamma$ , the ratio between the perturbation due to the pumping beam and the relaxation of the lower states.

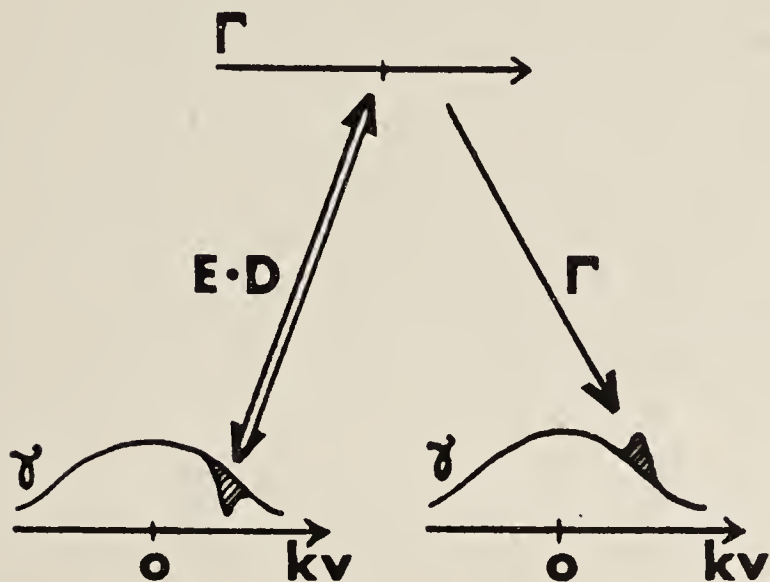


Fig.6 Population difference to be sustained against relaxation from the ground states.

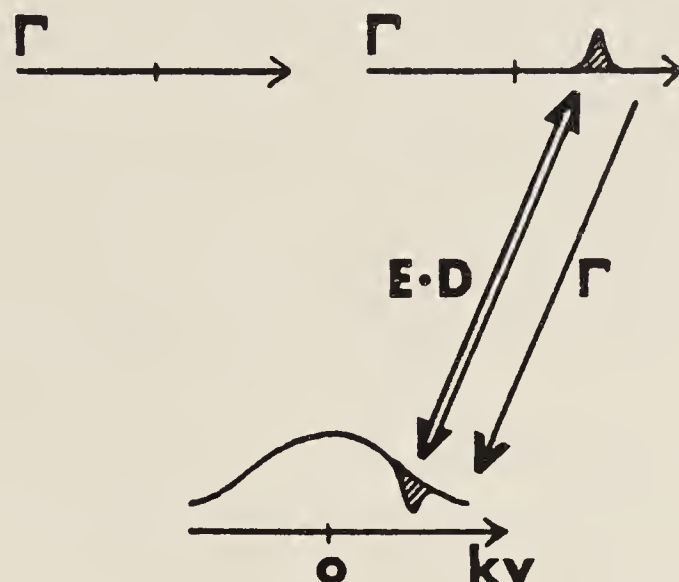


Fig.7 Population difference to be sustained against relaxation from the excited state.

In the  $V$ -system, on the other hand, the population difference on which the signal depends is between the upper state sub-levels. To sustain this population difference the pump beam must work against the relaxation of the upper states. If this is faster than that of the lower state, the intensity of the pumping beam needs to be correspondingly greater.

We distinguish the two mechanisms by the terms 'paramagnetic' and 'diamagnetic'. 'Paramagnetic polarization spectroscopy' (PPS) is represented by the  $\Lambda$ -system, 'diamagnetic polarization spectroscopy' (DPS) by the  $V$ -system. In PPS the signal depends on the existence of lower state structures, in DPS, on excited state structures.

In general, we shall find structure both in the upper and in the lower states, so that, in principle, we might expect both mechanisms to contribute to the signal. However, since PPS generally requires far weaker pump intensities, this will generally be the dominant mechanism. DPS will be the operative mechanism when  $J = 0$  in the lower state, or, with  $J \neq 0$ , when the population difference is destroyed by additional perturbations (r.f. fields, field gradients, depolarizing collisions). Some early analyses of polarization spectroscopy [9, 14] were carried through under the approximation  $G_\gamma \gg 1$ . This represents, effectively, the pure DPS case. Our conclusion is that analyses of this type are not representative of polarization spectroscopy. It will generally be the case that the appropriate mechanism for the interpretation of the signal will be PPS. Our analysis has been concerned with the dispersive as well as with the absorptive components of  $\chi$ . Saturated absorption spectroscopy concerns itself with the absorptive components only. The possibility that optical pumping effects might be important in this kind of work has recently been pointed out also by other investigators [15, 16].

## 4. Experimental Studies

We have studied forward-scattering and polarization spectroscopy in sodium vapour in the neighbourhood of the D-lines, which offer themselves as examples of the general case, having Zeeman structure in both upper and lower levels. The vapour, without buffer gas, was contained in a closed cell with strain-free windows at a vapour density of  $10^{11} \text{ cm}^{-3}$ . Stray magnetic fields were cancelled to within a few mG. Both probe and pumping beams were taken from a single-mode, tunable dye laser, line-width about 10 MHz. The probe beam followed a path through the vapour in exact opposition to the pumping beam, constrained by diaphragms to travel along the inner region of the pumping beam where the intensity was uniform. Crystal polarizers of high quality were used: a Babinet-Soleil compensator was employed to secure exact circular polarization of the pumping beam. For most experiments the polarizer and analyzer in the probe beam were exactly crossed to avoid heterodyning the forward-scattered light with the probe beam itself. No modulation was employed. The signal was recorded with a photo-multiplier.

### 4.1 Polarization Spectrum with Weak Beams

A high-resolution polarization spectrum of the  $\text{NaD}_1$  line is shown in Fig.8. Of the nine resonances shown, four are the allowed transitions between the hyperfine levels  $F = 1, 2$  in the lower and upper states; the remaining resonances are 'crossovers'. The pump intensity indicated in the legend corresponds to  $G_p \sim 0.1$ ,  $G_y \sim 100$ , so that the DPS contribution to the signals is negligible. The probe intensity was very much weaker.

### 4.2 Intensity of the Probe Beam

If the purpose of the probe beam is to monitor the asymmetry introduced by the pumping beam, its intensity must be much less. In Fig.9a it is 50 times weaker, and the resonances appear as simple near-Lorentzians. In Fig.9b the intensity of the probe beam has been increased by a factor 50 (though it is still very weak by the standards of saturation spectroscopy). Structure appears in the spectrum, and the relation between signal strength and beam intensity is strongly non-linear. These effects are due to the pumping action

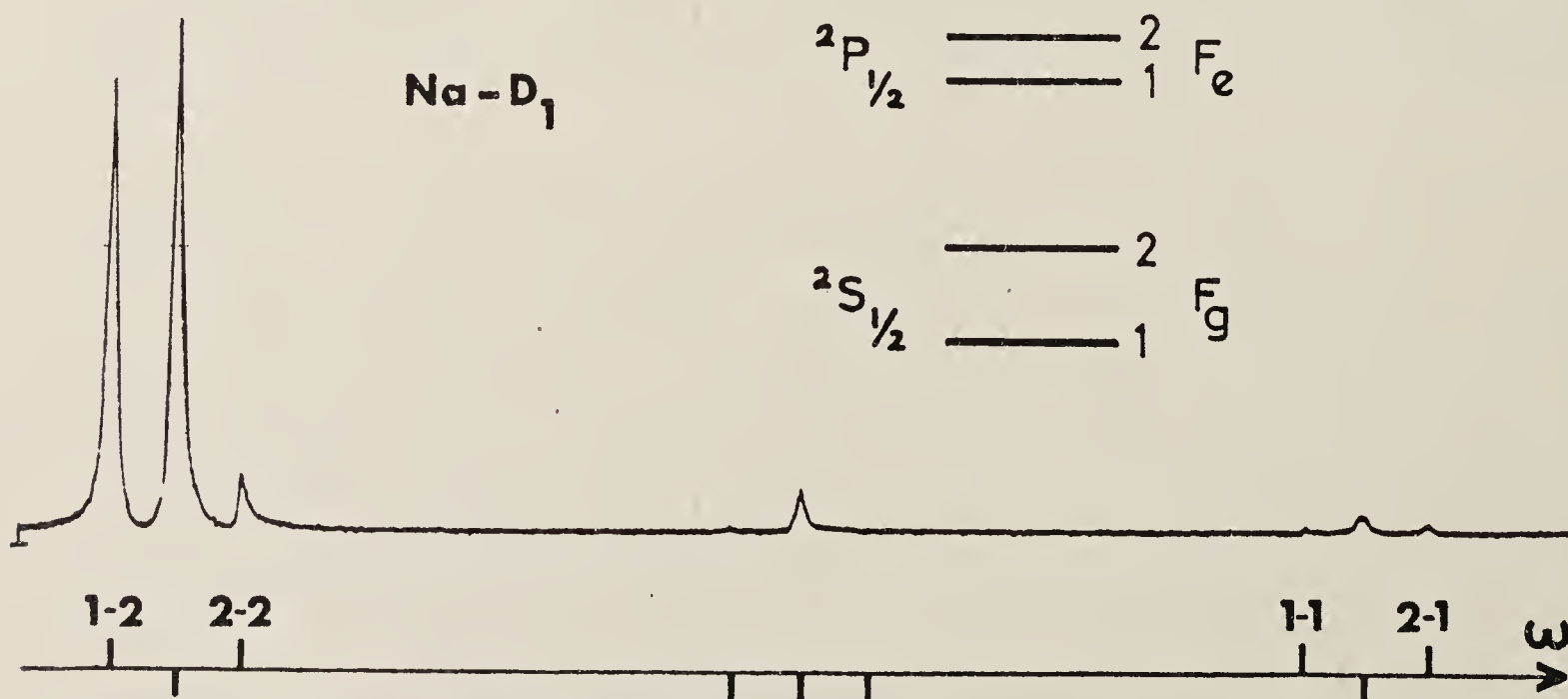


Fig.8 High resolution polarization spectrum of Na  $D_1$  line. The intensity of the pumping beam was  $25 \mu\text{W mm}^{-2}$ . On the frequency scale below, hyperfine components are marked  $F_e$ - $F_g$ . Crossovers are marked below the line.



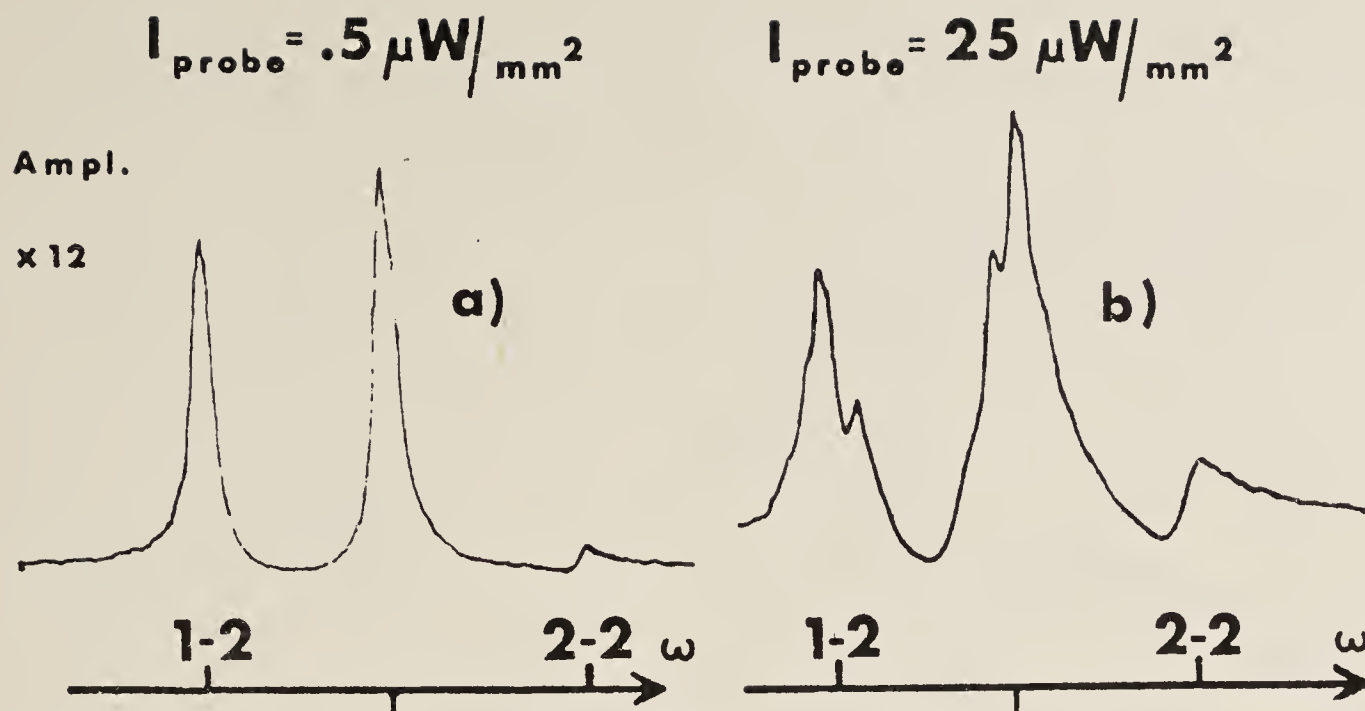


Fig.9 The effect of increasing the intensity of the probe beam.

of the probe beam: it tends to equalise the populations of levels of the same  $|m|$ , and in this way acts in opposition to the circularly-polarized pumping beam.

The strong probe beam, however, also induces coherence between Zeeman levels [6, 11], and hence generates non-vanishing components  $\chi_{\pm\mp}$ . The resulting contributions to the signal are zero if the levels are degenerate, but not if the degeneracy is removed by a magnetic field. This will be the subject of the next section.

An analysis of the signal to be expected for the  $\Lambda$ -system of Fig.3(c) yields the result

$$I \propto G_Y' G_Y^2 \left[ \frac{1}{4\delta^2 + \Gamma_+^2} \right] \left[ 1 - CG_Y' \frac{1}{4\delta^2 + \Gamma_+^2} \right]$$

where  $G_Y' = (E_{\text{probe}} \cdot D / \hbar \gamma)^2$  and  $C$  is a constant. This reproduces the important features of Fig.9b, the dip in the line, and the non-linear dependence on the intensity of the probe beam.

#### 4.3 Interference Between Polarization and Alignment in the Presence of a Longitudinal Magnetic Field

A strong probe beam ( $G_Y \approx 1$ : transverse linear polarization) propagating alone in the vapour generates (through stimulated emission) coherences between Zeeman levels of the ground state. Though the intensity transmitted through a crossed analyzer is zero if no other perturbations are applied to the vapour, a signal, illustrated in the inset to Fig.10, does appear when a longitudinal magnetic field is applied [6]. It should be noticed that this signal is narrow in relation to the Doppler width (about 500 G). In Fig.10c we see the signal, at fixed magnetic field, as a function of frequency. There is no velocity-selection: the signal is Doppler-broadened. The narrow polarization spectroscopy signal induced by a counter-propagating pumping beam with zero magnetic field is seen in Fig.10b: in this experiment the probe beam was not negligibly weak, though not as strong as in Fig.9b.

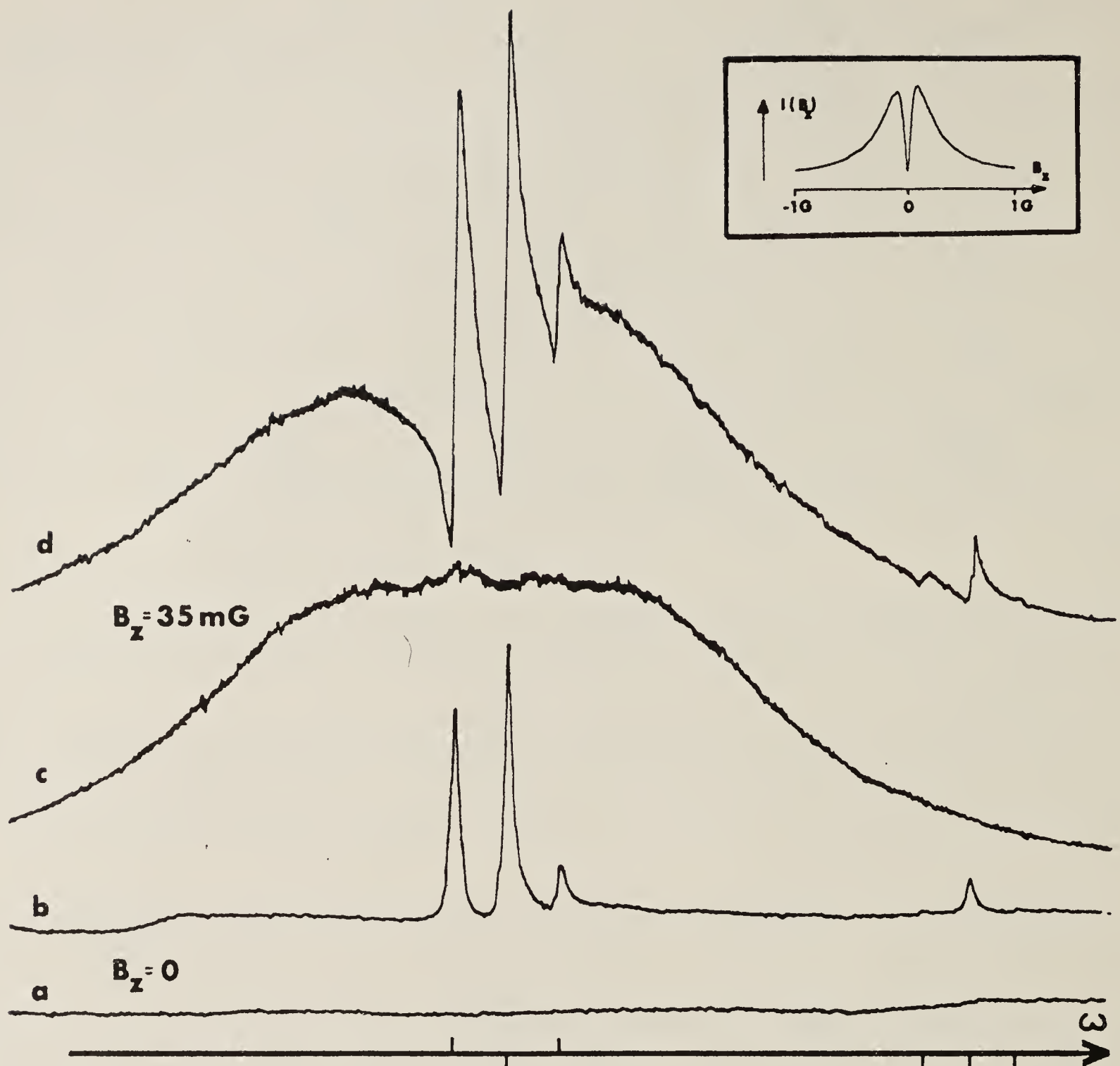
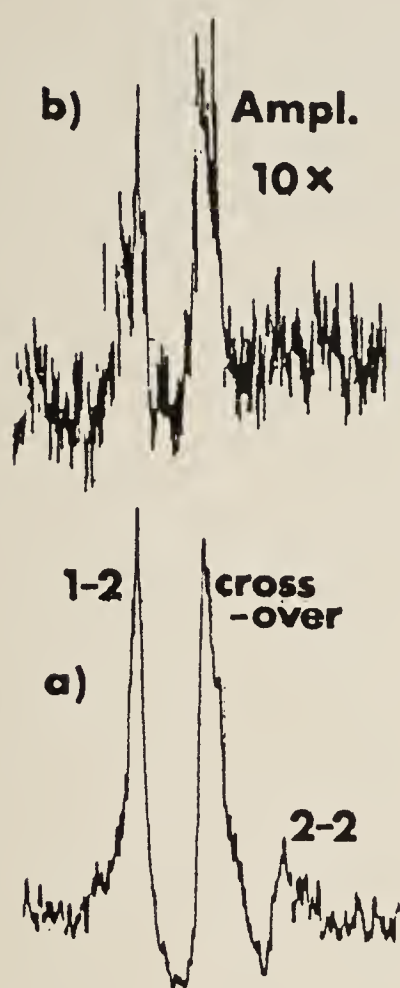


Fig.10 Interference between polarization and alignment: strong probe beam.  
a) No magnetic field. No pumping beam. Null signal recorded on probe beam.  
b) No magnetic field. Pumping beam. Polarization signal.  
c) Magnetic field. No pumping beam. Alignment signal.  
d) Magnetic field and pumping beam simultaneously applied.  
In the inset is shown the dependence of probe signal on magnetic field for fixed laser frequency near resonance [6]. [This is a ground-state Hanle effect]

In Fig.10d we see the interference between the polarization induced by the pumping beam and the alignment induced by the strong probe beam in the presence of the very weak longitudinal magnetic field. It is important to appreciate that effects of this kind can manifest themselves in polarization spectroscopy.



#### 4.4 Signal Attributable to Ground-State Population Differences: Direct Demonstration



In Fig.11a is to be seen a polarization spectrum taken with weak pumping and probe beams. The signal persists, as shown in Fig.11b, when the beams are spatially separated. Since the time which the atoms would have taken, a few  $\mu$ s, to have travelled the distance between the beams is very much longer than the lifetime of the excited state, it is clear that the signals cannot be attributed to any population of the excited state resulting from the operation of the pumping beam. They must result from a net polarization of the ground state.

Fig.11 a) Pumping and probe beams coincident.  
b) Probe beam displaced laterally by 2 mm.

#### 4.5 Coherent Background: Transition from Dispersive to Absorptive Signal

In Fig.12 is to be seen the effect of adding a coherent background to the polarization signal, a device used to increase the signal strength by heterodyning [10]. It can be achieved by rotation of the analyzer with respect to the polarizer in the probe beam. When polarizer and analyzer are crossed ( $0^\circ$  in the Fig.) the signal is due to the modulus of  $\hat{\chi}$ , differential dispersion and absorption. With rotation of the analyzer by a few degrees one sees the effect of interference between the signal and a transmitted component of the primary beam. The result is a series of dispersion-shaped resonances. Differential absorption now plays a minor role. At a rotation angle of  $90^\circ$  (analyzer parallel to polarizer), only that component of the signal is seen, the absorptive component of  $\hat{\chi}$ , which is in phase or antiphase with the strong, primary beam. The variations of the dispersive component, being in quadrature, result in this case in variations of the net scattered field which contribute negligibly to the detected signal.

The observation of Doppler-free, absorptive signals, in circumstances (as above) when the pumping beam is too weak to saturate the transition indicates again that it is inequalities of population in the ground, rather than in the excited state which are responsible for the observed effects (see also [16]).

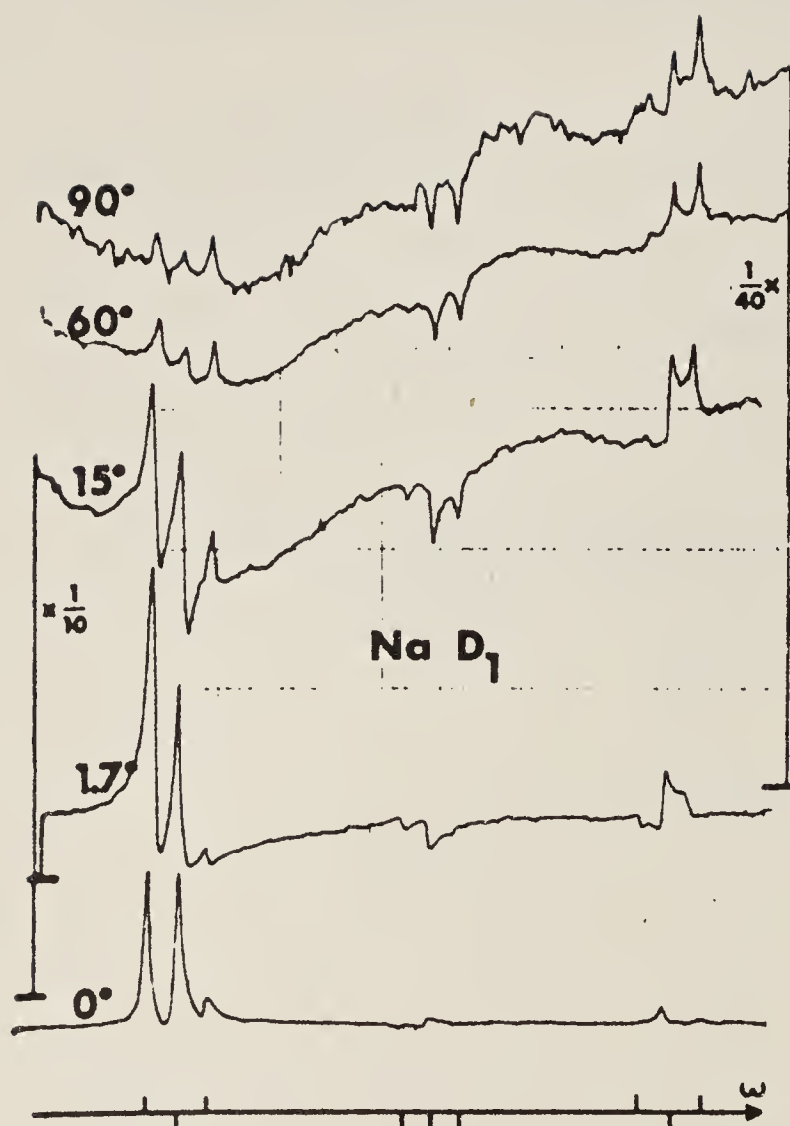


Fig.12 Polarization spectrum of Na D<sub>1</sub> line with coherent background introduced by rotation of the analyzer in the probe beam. The angle 0° represents analyzer crossed with polarizer. The intensities of the pumping and probe beams were unchanged throughout.

#### 4.6 Decoupling of Hyperfine Structure by the Pumping Beam, and Autler-Townes Effect

Finally, we report the effect of increasing the intensity of the pumping beam. In Fig.13 B is to be seen a resolved hyperfine structure under a moderately weak pumping beam ( $G_T = (E_g \cdot D / \hbar \Gamma)^2 = 0.6$ ). In part A of the figure the spectra are shown for increasing values of  $G_T$  up to 130. It is to be noticed that the first effect of increasing the intensity is that the lines are broadened until the resolution is lost: the interaction with the pumping beam has de-coupled the hyperfine structure.

At the higher intensities a new structure develops; a doubling of the line which becomes more symmetrical. The peaks move apart as  $G_T$  is increased. We believe this is a manifestation of Autler-Townes effect. In the inset, C, we have plotted the observed separation of the peaks as a function of  $(I_g)^{1/2}$ . The broken line on the same graph is a plot of the Rabi frequency of the strongest Zeeman hyperfine component,  $F_g = 3, m = 3 \rightarrow F_g = 2, m = 2$ . The observed signals are a blend of all the Zeeman hyperfine components of the D<sub>1</sub> line which originate from the  $F = 2$  ground level, which have a variety of Rabi frequencies. Moreover, averaging over velocities leads to a more complicated situation than in the case of simple resonances. For these reasons we do not expect the experimental points in Fig.13C to lie on the broken line, but we interpret the fact that they lie near the line as evidence that the observed splitting is a manifestation of the Autler-Townes effect.



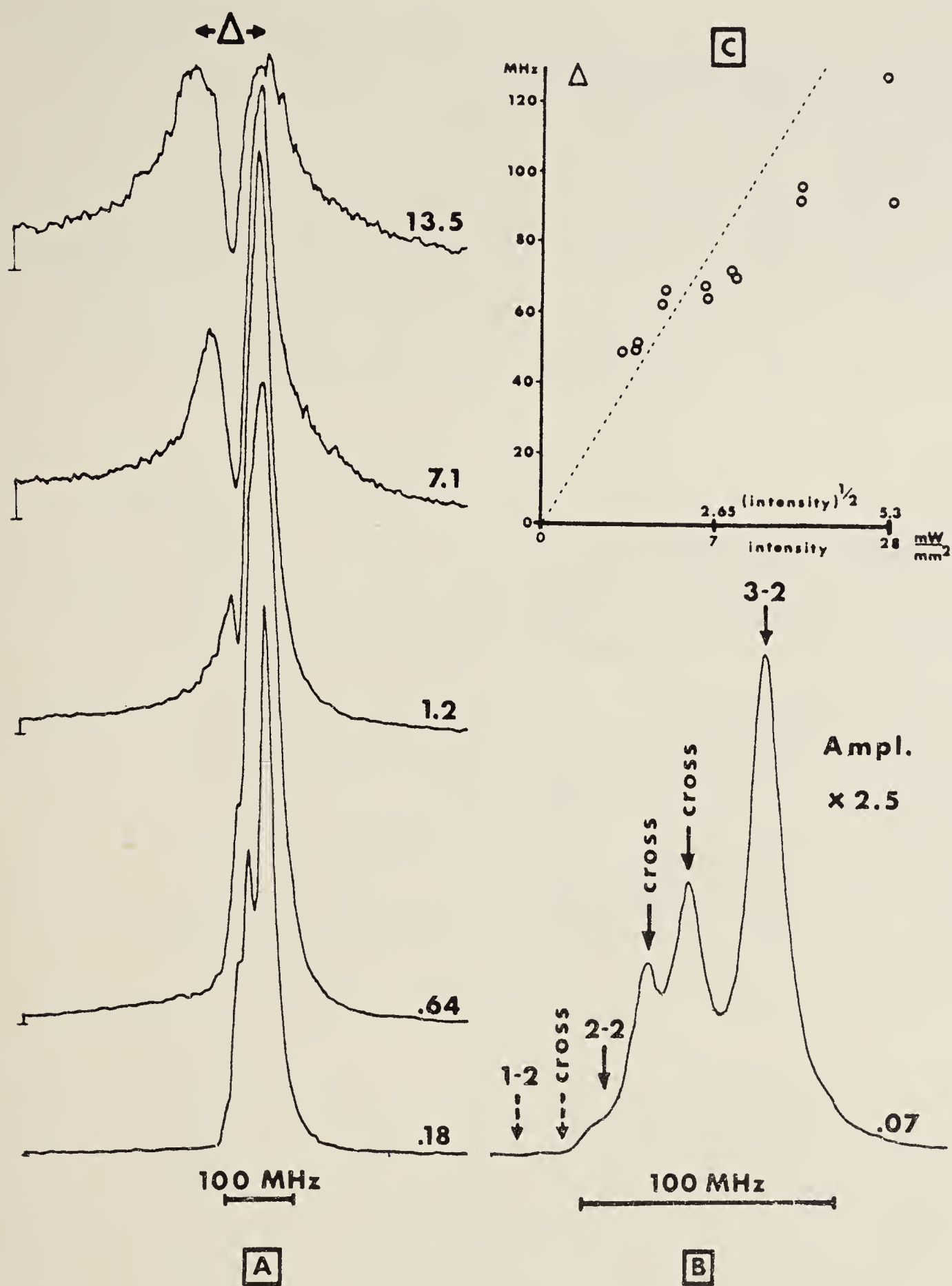


Fig.13 A. Polarization spectra of part of Na D<sub>2</sub> line under the indicated pump beam intensities (mW mm<sup>-2</sup>).

B. The hyperfine structure ( $F_e - F_g$ ) shown resolved at the lowest intensity.

C. Separation of peaks observed at high intensity plotted against  $I_s^{1/2}$  (see text).

## 5. Conclusions

We have investigated polarization spectroscopy from the point of view adopted in previous studies of the forward-scattering of resonance radiation. We are convinced of the importance, in the interpretation of the signals, of lower-state population changes arising from optical pumping. We regard polarization spectroscopy as a velocity-selective optical pumping technique, rather than as a variant of saturated absorption spectroscopy. We have demonstrated the complications that may arise from too strong a probe beam, or pumping beam, or from a longitudinal magnetic field. (We have observed, but not reported here, the destruction of the signals by static and r.f. transverse magnetic fields.) We believe polarization spectroscopy to be a most sensitive and delicate technique, but it is our experience that the signals need to be interpreted with especially great care and circumspection.

## References

1. R.L. Fork and L.C. Bradley, Appl. Opt. 3, 137 (1964).
2. C. Borde, G. Camy and B. Decomps, "Laser Spectroscopy II", Springer, Berlin, Heidelberg, N. York (1975).
3. R. Schieder, Opt. Commun. 26, 113 (1978).
4. A. Corney, B.P. Kibble and G.W. Series, Proc. Roy. Soc. 293A, 70 (1966).
5. A.V. Durrant and B. Landheer, J. Phys. B 4, 1200 (1971).
6. W. Gawlik, J. Kowalski, R. Neumann and F. Träger, Opt. Commun. 12, 400 (1974).
7. W. Winiarczyk, Acta Phys. Polon. A52, 157 (1977).
8. L.N. Novikov, Opt. Spektrosk. 24, 866 (1968); Opt. Spectrosc. 24, 465 (1968).
9. C. Wieman, and T.W. Hänsch, Phys. Rev. Lett. 36, 1170 (1976)
10. G.W. Series, Proc. Phys. Soc. 88, 995 (1966).
11. W. Gawlik, J. Phys. B 10, 2561 (1977).
12. V. Stert and R. Fischer, Appl. Phys. 17 151 (1978).
13. J.C. Keller and C. Delsart, Opt. Commun. 20, 147 (1977).
14. M. Sargent, Phys. Rev. A14, 524 (1976).
15. M. Pinard, C.G. Aminoff and F. Laloë, to be published in Phys. Rev. A. (Feb. 1979).
16. M.S. Feld and D.E. Murnick, Proceedings of this Conference.



## Determination of lifetimes and hyperfine structures of the 8, 9 and 10 $^2D_{3/2}$ states of $^{133}\text{Cs}$ by quantum-beat spectroscopy

J S Deech, R Luypaert and G W Series

J J Thomson Physical Laboratory, Whiteknights, University of Reading, RG6 2AF

Received 20 January 1975

**Abstract.** The states were studied by selective detection of the fluorescence generated in atoms of the vapour by stepwise excitation, using as sources a conventional caesium lamp for the first step from the ground state and a pulsed, tunable laser for the second. The techniques of delayed coincidence counting were applied to measure the time distribution of intensity of the fluorescent light. The observed modulation, representing in each case a superposition of the hyperfine intervals, showed a characteristic period which was interpreted as the reciprocal of the magnetic interaction constant  $a$  for the states in question. The relative simplicity of the modulation patterns is a consequence of the negligibly small quadrupole interaction in  $^{133}\text{Cs}$ . With the polarizer oriented at  $\cos^{-1} 3^{-1/2}$  to the analyser the modulation was suppressed, leaving a simple exponential decay from which the lifetime of the population,  $\tau$ , could be determined.

The results are  $a = 3.92 \pm 0.07$ ,  $2.32 \pm 0.04$ ,  $1.51 \pm 0.02$  MHz and  $\tau = 148 \pm 3$ ,  $208 \pm 2$ ,  $310 \pm 3$  ns for the 8, 9 and 10  $^2D_{3/2}$  states, respectively. The values for  $a$  agree with those of Svanberg *et al.* Values of  $\tau$  have not previously been reported.

### 1. Introduction

With the advent of tunable lasers, studies of highly excited states of atoms may be undertaken by the techniques of fluorescence spectroscopy. Small structures in these states may be explored by radio-frequency resonance or by methods based on coherent excitation of the states. Among these latter methods is that of 'quantum-beat' spectroscopy, that is to say, the study of modulation in exponentially decaying fluorescent light following the excitation of atoms by a pulse. The term 'quantum-beat' is used because the effect is a consequence of the oscillatory time-dependent probability of emission of light which is the same for all atoms excited at the same instant: it is not an effect arising from interference in the light from different atoms. It was studied originally for Zeeman structures by Dodd *et al* (1964), by Aleksandrov (1964) and by Hadeishi and Nierenberg (1965) and more recently, for hyperfine structures by Haroche *et al* (1973) and for fine structures by Haroche *et al* (1974). The same phenomenon is observed in beam foil spectroscopy (Andr  1974).

The determination of structures in the alkalis is attractive because, being relatively simple atoms, they are good subjects for theoretical studies. A considerable number of measurements has been made of hyperfine structures in caesium. Early measurements of the ground states and excited P states have been followed recently by measurements on excited S and D states (see for example Gupta *et al* 1973, Svanberg *et al* 1973, Svanberg and Belin 1974, Tsekeris *et al* 1974). Our work provides confirmatory evidence for some values already reported, and additionally provides experimental values of some lifetimes

for which hitherto only theoretical estimates have been available. The states in question are 8, 9 and 10  $^2\text{D}_{3/2}$  of  $^{133}\text{Cs}$ . Studies of some S states will be reported separately.

Fluorescence from these states was generated by the method of stepwise excitation. The first step, from the ground state  $6^2\text{S}_{1/2}$  to the  $6^2\text{P}$  states, was accomplished by continuous irradiation of the vapour by a conventional caesium lamp, and the second step, from one or other of the  $6^2\text{P}$  states to the higher S or D states, by a pulsed, tunable laser.

The fluorescence was studied by measuring the distribution in time of photoelectrons following the laser pulse. Quantum-beat modulation was observed by placing a linear analyser either parallel or perpendicular to the polarizer in the laser beam: with the polarizer at  $\cos^{-1}(\frac{1}{3})^{1/2}$  the coherent component of the fluorescent light was suppressed and the time dependence was a simple exponential decay, giving the lifetime of the excited state.

The beat frequencies are a measure of the hyperfine intervals in zero magnetic field,  $|\Delta F| = 1$  or 2, where the  $F$  values range from 5 to 2. Because the quadrupole contribution in  $^{133}\text{Cs}$  is small the interval rule is obeyed to a very good approximation and the beat patterns, though often rather complicated (figures 3 and 4), represent the superposition of a relatively small number of oscillations rationally related to one another, the whole having a well-defined repetition period which is the reciprocal of the magnetic dipole interaction constant  $a$ . Hence a measurement of this period gives directly the value of  $a$  without the need for Fourier analysis.

The transitions studied are shown in figure 1.

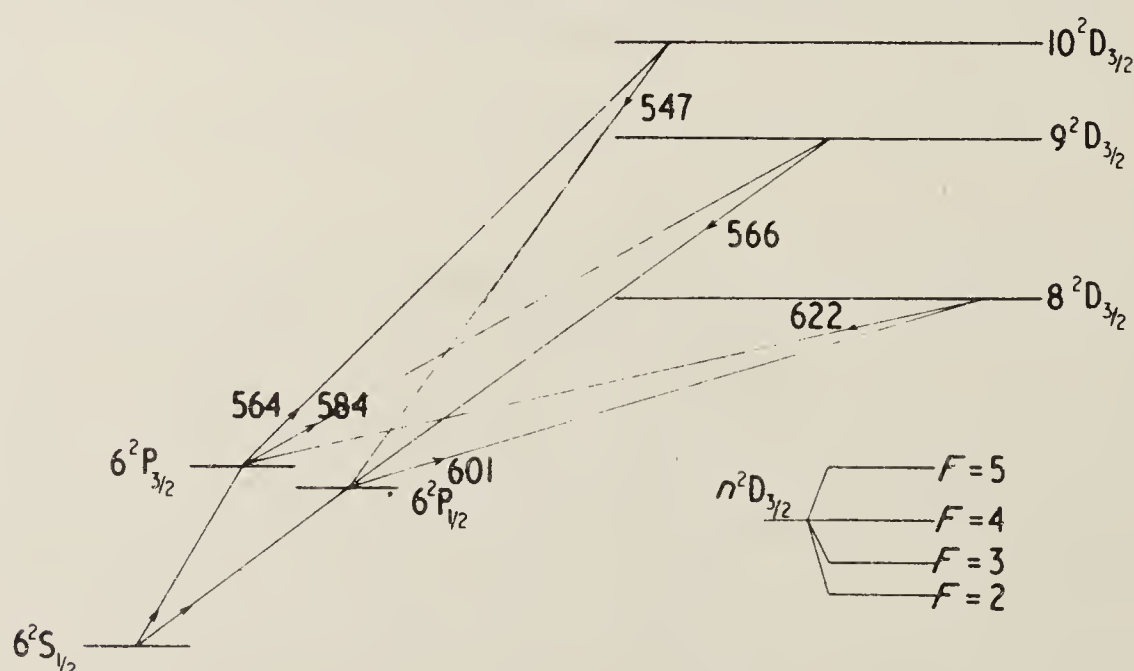


**Figure 1.** Term diagram and transitions studied (wavelengths in nm). The intervals are not to scale. Hyperfine structure of a typical  $\text{D}_{3/2}$  state is shown in the inset.

## 2. Description of the experiment

The disposition of apparatus is shown in figure 2. The fluorescence cell was cylindrical, 6.5 cm long, 3.5 cm diameter, with windows sealed parallel to one another as accurately as possible. By this construction parasitic light from the laser could be reduced to an acceptably low level. With caesium in the cell the temperature of the coldest part was thermostatically maintained at about 80 °C (vapour pressure  $10^{-4}$  Torr). The earth's magnetic field inside the cell was compensated to within 10 mG.



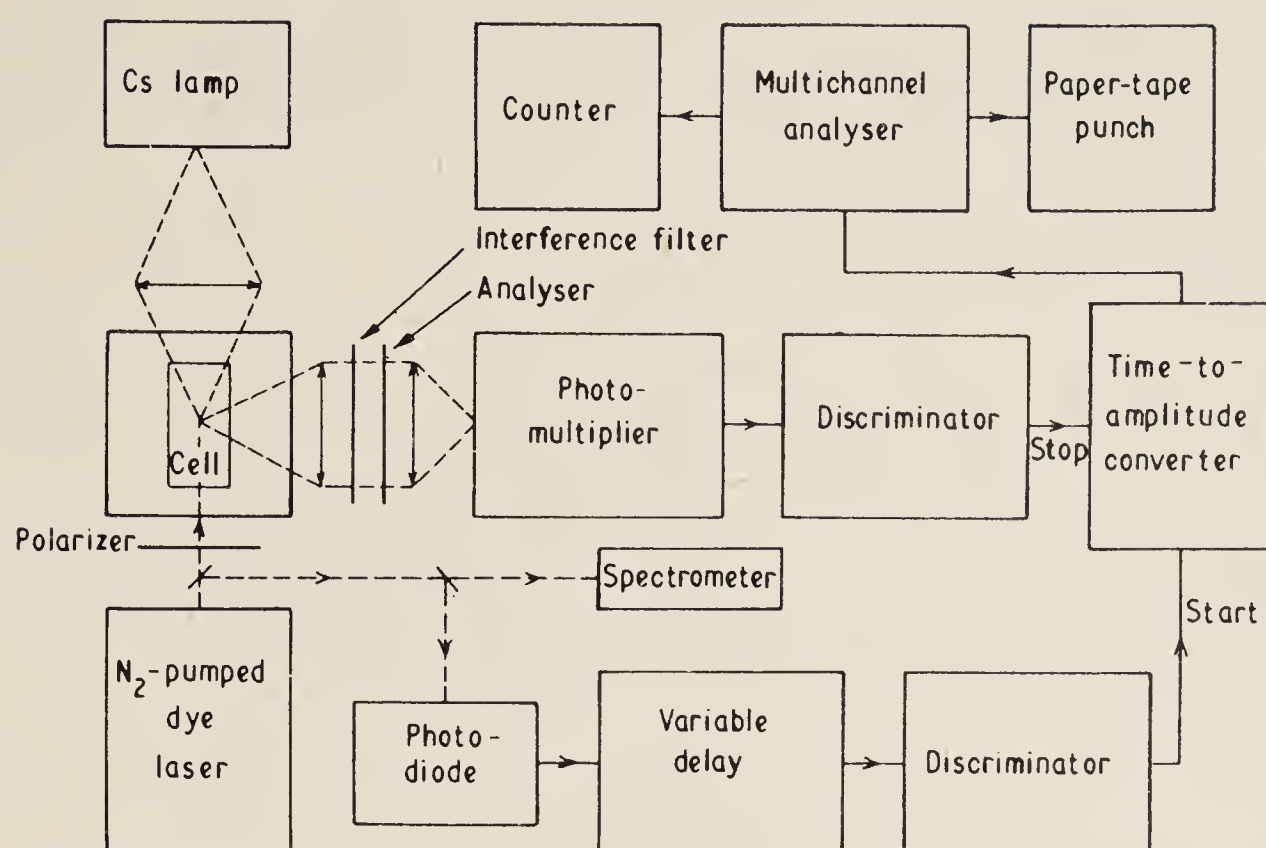


**Figure 2.** Arrangement of apparatus.

Incident radiation from the caesium lamp was unfiltered and unpolarized, and focused on the cell by a lens of large aperture. With the large amount of multiple scattering which must have occurred in the vapour, the first stage of excitation was substantially isotropic.

An AVCO model C5000 nitrogen laser was used to pump a dye laser. The dyes used in this work were rhodamine 6G for the 8D and 9D states and fluorescein disodium salt (FDS) for the 10D states. The dye laser produced flashes of about 5 ns duration, and the repetition rate normally used was 150 Hz. Rates up to 500 Hz were possible. Tuning was accomplished by rotation of a grating. A beam expander ( $10\times$ ) in front of the grating reduced the spectral line width to about 0.05 nm (5 GHz). The laser beam, about 2 mm in diameter, passed through a linear polarizer before entering the fluorescence cell. The desired wavelength was selected with the aid of an auxiliary spectrometer, and tuning to resonance monitored by measurement of the fluorescent intensity.

The fluorescent light in a wide angle cone perpendicular to the exciting beams was collected by an  $f/2.5$  lens. Before reaching the photomultiplier it passed through an interference filter of bandwidth 6 nm to select a transition of wavelength different from that of the laser light, and also a linear analyser. Its intensity was measured as a function of time following the laser pulse by the techniques of delayed coincidence counting.

As shown in figure 2 the time-to-amplitude converter is started by a pulse from the laser flash and stopped by a pulse from the fluorescent light. The delay introduced into the former line ensured that no signal could be recorded until after the termination of the laser flash. The multichannel analyser (100 channels) sorted and stored pulses from the time-to-amplitude converter to form the time-decay spectrum. The contents of the memory were transferred to paper tape at the end of a run.

The power output from the laser was controlled so that, with a repetition rate of 150 Hz, the count rate in the analyser was between 20 and 50 Hz. A pile-up correction was applied to the recorded counts (Coates 1968). A background correction was also applied: cooling of the photomultiplier reduced the background by a factor of 100. Examples of decay curves, plotted logarithmically with the numbers of counts corrected as described, are shown in figures 3, 4 and 5.

The multichannel analyser was calibrated for time against the variable delay generator which itself was calibrated against a quartz-controlled oscillator.

### 3. Theory

The time dependence of the fluorescent light in these experiments is almost independent of the first stage of the excitation process and of the properties of the intermediate P states. The excitation of these states from the ground states is at a uniform rate and is almost entirely isotropic on account of the multiple scattering in the cell. There may be some small residual anisotropy arising from this excitation and also by stimulated emission from the D states, and this might have some small effect on the relative intensities of different components of the quantum beats, but we find excellent agreement between our experimental results and an analysis which supposes that the  $|F, m_F\rangle$  components of the P states are statistically populated. These components form a set of ground states for the pulse excitation generated by the laser. We use the abbreviated notation  $\{|\mu\rangle\}$  for these P states. The observed fluorescence is from a set of excited D states  $\{|m\rangle\}$  to a set of lower P states  $\{|\mu'\rangle\}$  which, in our experiments, are different from the  $\{|\mu\rangle\}$ .

The expression for the intensity at time  $t$  following a pulse from a set of equally populated states  $\{|\mu\rangle\}$  is

$$I(t) = K \sum_{\substack{m, m' \\ \mu, \mu'}} \left( \frac{f_{m\mu} f_{\mu m'} g_{m'\mu'} g_{\mu' m}}{\Gamma - i\omega_{mm'}} \right) \exp(i\omega_{mm'} - \Gamma)t, \quad (1)$$

where  $f$  and  $g$  are electric dipole operators (Deech *et al* 1974 and earlier references given there).  $\Gamma$  is the decay constant of the states  $\{|m\rangle\}$  and the  $\omega_{mm'}$  are the Bohr frequencies†. Assumptions underlying equation (1) are: (i) that the duration of the pulse is short compared with  $\Gamma^{-1}$  and the  $\omega_{mm'}^{-1}$ ; (ii) that the spectrum of the exciting light is broad compared with the hyperfine structure  $\{|m\rangle\}$ ; and (iii) that the rate of excitation per atom is small compared with  $\Gamma$ . If (i) is violated the modulation is partially degraded but the periodicity remains unaltered. In our experiments the pulses were of duration about 5 ns and the periods that were actually measured ranged from 250 ns to 600 ns so that there was negligible degradation. Assumption (ii) was satisfied by a factor about  $10^3$ . Assumption (iii)—which is equivalent to ignoring stimulated emission—might not have been satisfied in our experiments. The consequential transfer of population from the  $\{|m\rangle\}$  to the  $\{|\mu\rangle\}$  would not have been important. There can have been no transfer of coherence at hyperfine frequencies since the coherence time of the laser light was too short.

The expression for  $I(t)$  in terms of multipole moments  $T_q^{(k)}$  is especially convenient for a discussion of the spatial properties of the fluorescent light. The  $(k, q)$  term in the expansion contains the factor  $E_q^{(k)} U_{-q}^{(k)}$ , the product of the multipole components of the light transmitted by polarizer and analyser, respectively (Carrington and Corney 1971). The time dependence of the  $(k, q)$  term appears as a sum similar to that in equation (1) with

$$\omega_{mm'} \equiv \omega(F, m_F) - \omega(F', m_{F'}), \quad (m_{F'} = m_F - q),$$

which is independent of the  $m_F$  since external fields are reduced to zero. The coherence that is observed is between states with  $m_F$  values differing by  $q$ .

† In Deech *et al* (1974),  $\omega_{mm'}$  should be defined as  $-(E_m - E_{m'})/\hbar$ .



### 3.1. Linear polarization

Choose the  $z$  axis of the spherical basis to be the direction of the electric vector of the incident light. Then the only non-vanishing components  $E_q^{(k)}$  are those having  $q = 0$ .  $E_0^{(0)}$  is a measure of the population of excited atoms,  $E_0^{(1)}$  is zero, and  $E_0^{(2)}$  is a measure of alignment in the excited states. Coherence is established between hyperfine states with the same value of  $m_F$ .

If the analyser tensor is first written with reference to an axis  $z'$  parallel to the electric vector of the transmitted light, again the only non-vanishing components are  $U_0^{(0)'}$  and  $U_0^{(2)'}$ . Under a rotation by the angle  $\theta$  which brings the  $z$  and  $z'$  axes into coincidence, the  $q = 0$  components are  $U_0^{(0)'}$  and  $\frac{1}{2}U_0^{(2)'}(3\cos^2\theta - 1)$  respectively. Hence the intensity of fluorescent light has a spherically symmetrical term with time dependence  $\exp(-\Gamma^{(0)}t)$ , while the modulated terms  $\exp(i\omega_{FF'} - \Gamma^{(2)})t$  depend on the relative orientation of polarizer and analyser as  $(3\cos^2\theta - 1)$ . (A similar discussion in relation to modulation at the Larmor frequency has been given by Gunn and Sandle 1971.) A distinction has been drawn here between the decay constant for population,  $\Gamma^{(0)}$ , and for alignment,  $\Gamma^{(2)}$ , though it was not expected that these would have different values in our experiments since multiple scattering of fluorescent light was not taking place (the lower state was not the ground state).

## 4. Results

The results were displayed as logarithmic plots of fluorescent intensity (number of counts, corrected for pile-up and background) against time (channel number, calibrated as described above). In figures 3, 4 and 5 the results are shown for fluorescence from  $9^2D_{3/2}$  with the angle  $\theta$  between polarizer and analyser having the values 0, 90°, 54° respectively, corresponding to the values 1,  $-\frac{1}{2}$  and 0 of the function  $\frac{1}{2}(3\cos^2\theta - 1)$ .

Complicated modulation is clearly seen under the envelope of an exponential decay. The stronger features of figure 3(a) are readily identified in figure 4(a) with opposite sign and with substantially reduced amplitude. In figure 5 the modulation has been very largely suppressed. The dependence of the modulation on  $\theta$  agrees satisfactorily with the theory when it is recalled that the fluorescent light was collected over a relatively large solid angle. Closer study of figures 3(a) and 4(a) shows that the pattern is repetitive with period rather less than 500 ns. This is evidence that the intervals in the hyperfine structure are rational multiples of a constant frequency and therefore obey the interval rule. Measurements of hyperfine structure in other levels of caesium (Violino 1969, Schmieder *et al* 1970) have shown that the ratio  $b/a$  of the electric quadrupole to the magnetic dipole interaction constant is of the order 1%, which supports our conclusion. It is shown in table 1 below that the fractional deviations from the interval rule are substantially smaller than the ratio  $b/a$ .

With the assumption that deviations from the interval rule may be neglected, a measurement of the recurrence period for any recognizable feature in figures 3(a) or 4(a) gives directly the value of  $1/a$ . It is not necessary to allow for displacement of peaks or troughs by overlap from neighbouring features since the pattern—under our assumption—is exactly repeated. It is to be noted, however, that the statistical uncertainty of the points is larger for the smaller values of  $\lg I$  so the best features to measure are the strongest peaks. Measurements from the experimental curves give  $1/a$  to an accuracy approaching 1 in 200. The hyperfine intervals themselves for the  $D_{3/2}$  states are  $5a$ ,

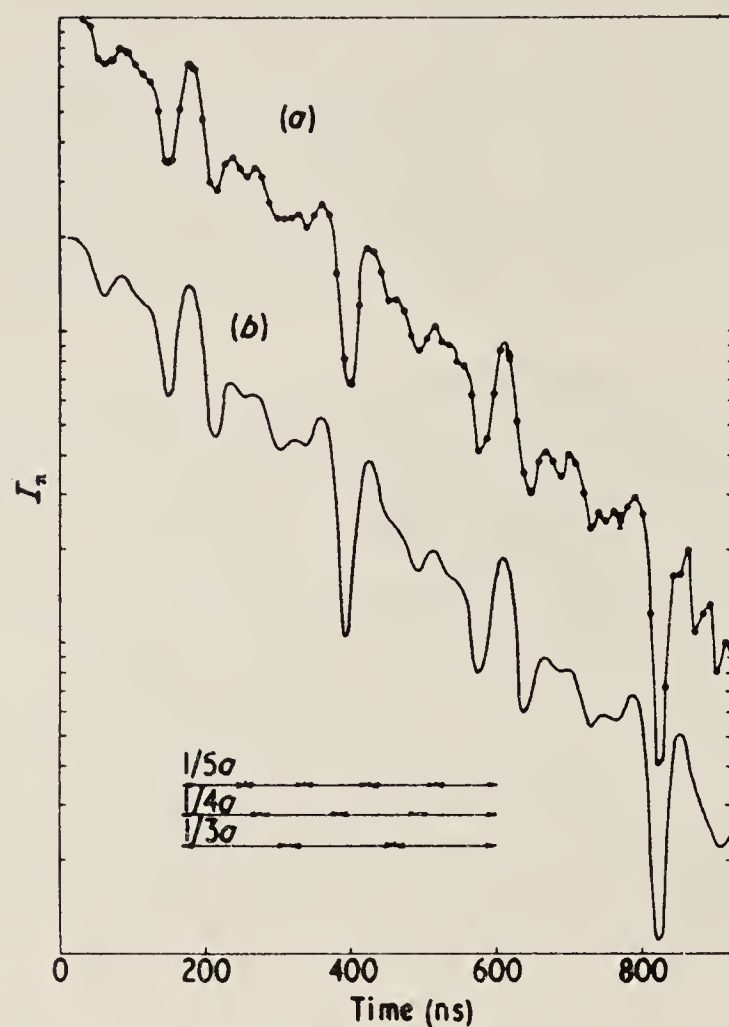


**Figure 3.** (a) Experimental decay spectrum for  $9\ ^2D_{3/2}:I_{\pi}$  (logarithmic scale) against time (arbitrary origin). The full curve has been drawn to join the experimental points with no attempt to smooth statistical fluctuations. Error bars where shown represent one standard deviation. (b) Theoretical curve calculated from equation (1) using experimental values of  $a$  and  $\Gamma$ . Periods corresponding to the intervals  $5a$ ,  $4a$  and  $3a$  are indicated.



**Figure 4.** (a) Similar to figure 3(a), with  $I_{\sigma}$  instead of  $I_{\pi}$ . (b) The corresponding theoretical curve.



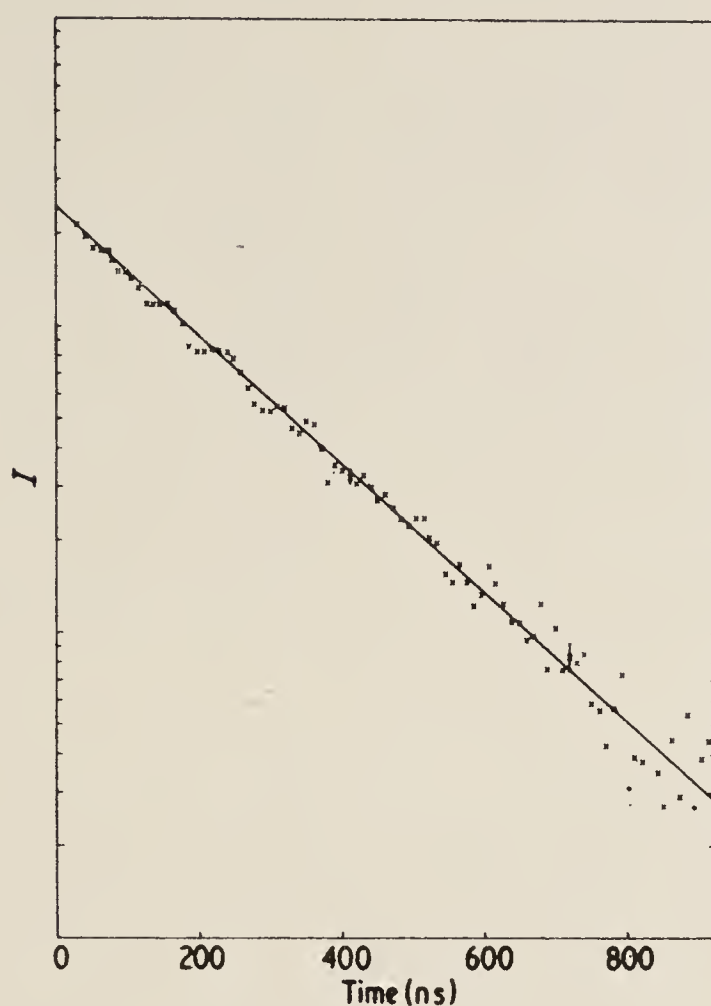


**Figure 5.** Experimental decay spectrum for  $9\ ^2D_{3/2}$  with  $\theta = 54^\circ$ . The straight line is the least squares fit to the points. Some residual modulation is to be seen, arising from departure from the ideal geometrical conditions.

**Table 1.** Deviations from the interval rule as fractions of  $b/a = x$ .

<i>F</i> values	5-4	4-3	3-2
Intervals	$5a(1 + x/7)$	$4a(1 - x/14)$	$3a(1 - 5x/21)$

$4a$  and  $3a$ . The corresponding periods can easily be recognized in recurring features of figures 3(a) and 4(a).

The decay constants  $\Gamma^{(0)}$  and the corresponding lifetimes were obtained by finding least squares fits to sets of points such as those shown in figure 5.

For comparison with the experimental curves, theoretical curves were calculated from equation (1) using experimental values of  $a$  and  $\Gamma$ . Such curves are shown in figures 3(b) and 4(b). The high degree of correlation between the theoretical and experimental curves is evidence that the theory of resonance fluorescence which is commonly used for single-step excitation using thermal sources is valid also in this more complicated situation. The correlation also justifies our neglect of the electric quadrupole interaction.

In table 2 below we compare our results with those of other observers and with theoretical calculations. Our values of  $a$  are based on a number of independent measurements of the period of the strongest recurring features in curves such as figures 3(a) and 4(a). The quoted errors are statistical and correspond to one standard deviation. The uncertainty in the time calibration is smaller than the statistical error by an order of magnitude.

Table 2. Values of *a* and  $\tau = 1/\Gamma^{(0)}$ .

Level	<i>a</i> (MHz)			<i>a</i> (this work)	$\tau$ (ns)		$\tau$ (this work)		
	This work	Other work	Theor	<i>a</i> (theor)	This work	Theor	$\tau$ (theor)		
8 <sup>2</sup> D <sub>3/2</sub>	3.92 ± 0.07	3.98 ± 0.12 <sup>a</sup>	5.12	1.02	0.76	2.04	148 ± 3	160	0.92
9 <sup>2</sup> D <sub>3/2</sub>	2.32 ± 0.04	2.37 ± 0.07 <sup>a</sup>	3.11	1.17	0.75	1.03	208 ± 2	240	0.88
10 <sup>2</sup> D <sub>3/2</sub>	1.51 ± 0.02	1.52 ± 0.03 <sup>b</sup>	2.03	0.76	0.75	1.04	310 ± 3	366	0.86

<sup>a</sup> Svanberg *et al* (1973).  
<sup>b</sup> Svanberg *et al* (1975).

5. Conclusion

Our measurements for *a* are in good agreement with those of Svanberg *et al* (1973) obtained at Columbia by the ‘level-crossing’ technique. Dr Svanberg, in private correspondence, has informed us that independent measurements made at Göteborg are also in agreement and that the sign of *a* has been determined by Stark effect measurements as being positive. The experimental values are not in agreement with values calculated from the Goudsmit–Fermi–Segre theory (Kopfermann 1958), but the experimental and theoretical values are in a constant ratio, to within the experimental error.

We believe these are the first reported measurements of the lifetimes of these states, though it was clear from the level-crossing experiments that the lifetimes could not be grossly different from those calculated by the method of Bates and Damgaard (1949) which are given in the last column but one of table 2. The experimental values are lower than the calculated values, and the fractional difference becomes progressively greater in the sequence 8D, 9D, 10D, contrary to what one might expect. In this connection we recall the well known anomaly in the intensity ratio of the members of the doublets of the principal series (Fermi 1930, Fulop and Stroke 1973).

Acknowledgments

We are indebted to Professor Happer and Dr Svanberg for comments on the measurements; also to Mr C H Smith and Mr A Keeling for valuable technical assistance. The work was supported by the Science Research Council. One of us (RL) expresses his thanks to the Vrije Universiteit Brussel for financial support.

References

Aleksandrov E B 1964 *Opt. Spectrosc.* **17** 522–3  
Andra H J 1974 *Phys. Scripta* **9** 257–80  
Bates D R and Damgaard A 1949 *Phil. Trans. R. Soc. A* **242** 101–22  
Carrington C G and Corney A 1971 *J. Phys. B: Atom. Molec. Phys.* **4** 849–68  
Coates P B 1968 *J. Phys. E: Sci. Instrum.* **1** 878–9  
Deech J S, Hannaford P and Series G W 1974 *J. Phys. B: Atom. Molec. Phys.* **7** 1131–47  
Dodd J N, Kaul R D and Warrington D M 1964 *Proc. Phys. Soc.* **84** 176–8



- Fermi E 1930 *Z. Phys.* **59** 680–6
- Fulop G F and Stroke H H 1973 *Atomic Physics* vol 3 (New York, London: Plenum Press) pp 543–52
- Gunn H I and Sandle W J 1971 *J. Phys. B: Atom. Molec. Phys.* **4** L1–4
- Gupta R, Happer W, Lam L K and Svanberg S 1973 *Phys. Rev. A* **8** 2792–813
- Hadeishi T and Nierenberg W A 1965 *Phys. Rev. Lett.* **14** 891–2
- Haroche S, Gross M and Silverman M P 1974 *Phys. Rev. Lett.* **33** 1063–6
- Haroche S, Paisner J A and Schawlow A L 1973 *Phys. Rev. Lett.* **30** 948–51
- Kopfermann H 1958 *Nuclear Moments* (New York: Academic Press)
- Schmieder R W, Lurio A, Happer W and Khadjavi A 1970 *Phys. Rev. A* **2** 1216–28
- Svanberg S and Belin G 1974 *J. Phys. B: Atom. Molec. Phys.* **7** L82–5
- Svanberg S, Tsekeris P and Happer W 1973 *Phys. Rev. Lett.* **30** 817–20
- 1975 *Phys. Rev. A* to be published
- Tsekeris P, Gupta R, Happer W, Belin G and Svanberg S 1974 *Phys. Lett.* **48A** 101–2
- Violino P 1969 *Can. J. Phys.* **47** 2095–9





## Optogalvanic Detection of Atomic Alignment

The cross sections leading to ionization of atoms in a discharge must depend to some extent on their alignment with respect to the direction of the current. This suggests the possibility of using optogalvanic signals to detect level crossing, quantum beat and other coherence effects. This possibility is to be distinguished from recent proposals by Beverini and Inguscio, which rely on changes of population between states involved in coupled transitions.

Optogalvanic spectroscopy is rapidly coming into vogue as a very sensitive technique for studying transitions between excited atomic states and, moreover, a technique in which tunable lasers find an obvious application. When atoms or ions in a gas discharge are irradiated by light which is in resonance with a transition frequency, the impedance of the discharge changes, and this change forms the basis for detecting the resonance. Although many different mechanisms may be invoked to explain the effect, depending on the particulars of the discharge, one mechanism that all discharges would be expected to share is that the probability of collisional ionization of an atom depends on its state of excitation; the redistribution of population brought about by optical irradiation therefore alters the electrical characteristics of the discharge. This mechanism is believed to be especially important when the states concerned are near an ionization limit: for lower-lying states the dominant mechanisms are known to be indirect and strongly correlated with the density of metastables.<sup>1</sup>

The purpose of this Comment is to draw attention to the possibility of finding optogalvanic signals arising from changes in the *alignment* of atoms or ions, rather than from changes in *population*. One could contemplate Hanle-effect and level-crossing experiments, quantum beats, resonances exhibited by modulated light and the whole range of coherence effects as candidates for detection by changes in the electric current of a gas discharge. The advantage would be that these effects are free of Doppler broadening and do not require stabilized, narrow-band lasers: a laser would be used simply as a quasimonochromatic light source, tuned to the electronic transition whose detailed structure was to be evidenced by the optogalvanic signal. It would not be necessary for the laser to induce nonlinear or saturation effects.

Consider the atoms in some excited state in a gas discharge, aligned by irradiation with linearly polarized light. The alignment might be in the upper state of the transition, induced by direct excitation from some isotropically populated state, or it might be in the lower state as a result of optical pumping. The key point is to accept that the cross section for collisional ionization from the aligned state must depend on the direction of the alignment axis in relation to any directional properties which may be possessed by the ionizing particles. One might think of a variety of mechanisms for ionization — charge exchange under collisions with randomly moving aligned ions or ionization following association with aligned atoms, for example — but we shall pursue the more universal situation where ionization results from collision with electrons. The directional property must then be the electron drift velocity corresponding to the current flow in the discharge. In principle, ionization resulting from electron impact must depend on whether the alignment is parallel or perpendicular to the direction of current flow. In a glow discharge at pressures of a few torr, one would expect only a very small effect because the directed motion of the electrons is superimposed on a random motion, but low-pressure, high-voltage discharges might be more favorable, and the use of thermionic cathodes with gases at very low pressures might be more favorable still. Indeed, the limiting case is already familiar: many years ago Descoubes<sup>2</sup> carried out level-crossing experiments in helium and Hadeishi and Nierenberg<sup>3</sup> observed quantum beats in cadmium vapor: in each case controlled beams of electrons were used to produce an alignment of the electronic structure of the atoms. The alignment was monitored through the anisotropy of the polarized fluorescence. The essence of the proposed experiment is the use of polarized light to produce an atomic alignment, which is to be monitored through the postulated anisotropy of the collisional ionization.

To be explicit concerning the design of an experiment, we give an example whose objective is to determine a Landé  $g$  factor by the method of quantum beats. Let us suppose that the state concerned is the upper state of the transition we shall use, and that the lower state either has  $J = 0$  or has a much longer lifetime than the state under investigation. We apply a magnetic field in a direction perpendicular to the current, strong enough to resolve the Zeeman levels against their homogeneous width. We irradiate the discharge with a short pulse of light, tuned to the transition frequency, linearly polarized with the electric vector in any direction in the plane perpendicular to the field. The duration of the pulse is to be much smaller than one period of Larmor precession. The induced alignment in the upper state will precess around the direction of the field and the atoms will present a periodically varying cross section to the current. The optogalvanic signal should exhibit an oscillatory component, modulated at twice the Larmor frequency, damped at the rate of relaxation of the alignment.

There is no doubt that alignment can survive in a gas discharge. Studies of the Hanle effect in neon were made some years ago by Decomps and Dumont<sup>4</sup> and by



Carrington and Corney,<sup>5</sup> and a variety of experiments on discharges in other gases have since been carried out.

Following another line of thought, we recall that the ionization of optically excited atoms by collisions with uncharged particles is a feature of the space-charge-limited diode detectors now commonly used in studies of Rydberg states. This, too, may be called an optogalvanic effect, and the measured currents could conceivably be influenced by controlling the alignment (or orientation) of the colliding particles.

Some proposals which, though rather different, are liable to be confused with ours have recently been made by Beverini and Inguscio.<sup>6</sup> They describe possibilities for obtaining r.f. double-resonance and level-crossing signals with optogalvanic detection, but their proposals depend on a redistribution of population between at least three states coupled by an optical and possibly also an r.f. field. Thus, in the r.f. double-resonance example which they cite, the changes in the optogalvanic signal depend, not on the reorientation of the atoms, which the r.f. field certainly brings about, but on the changes in the laser-induced population equilibrium resulting from r.f.-induced transfer of atoms between Zeeman states. Likewise, their argument for the possibility of observing level-crossing signals does not appeal to the perturbation of atomic alignment associated with removal of a degeneracy, but to the perturbation of population which occurs when two transitions, rather than one, are in resonance with the same beam of radiation. The Beverini-Inguscio proposals take no account of the effect we discuss in this Comment.

G.W. SERIES

*J.J. Thomson Physical Laboratory  
University of Reading  
Whiteknights, Reading, England*

#### Acknowledgements

I am grateful for the opportunity of discussions with E. Arimondo, L. Pendrill and S. Nakayama.

#### References

1. K.W. Meissner and K.F. Miller, *Phys. Rev.* **92**, 896 (1953); K.C. Smyth and P.K. Schenk, *Chem. Phys. Lett.* **55**, 466 (1978); E.F. Zalewski, R.A. Keller and R. Engleman, Jr., *J. Chem. Phys.* **70**, 1015 (1979).
2. J.P. Descoubes, in *Physics of the One- and Two-electron Atoms*, edited by Bopp and Kleinpoppen (North-Holland, Amsterdam, 1969) p. 341.
3. T. Hadeishi and W.A. Nierenberg, *Phys. Rev. Lett.* **14**, 891 (1965).
4. B. Decomps and M. Dumont, *IEEE J. Quant. Elec.* **4**, 916 (1968).
5. C.G. Carrington and A. Corney, *Opt. Comm.* **1**, 115 (1969); *J. Phys. B* **5**, 1001 (1972).
6. N. Beverini and M. Inguscio, *Nuov. Cim. Lett.* **20**, 10 (1980).





## Alignment Effects in Optogalvanic Spectroscopy

P. Hannaford\* and G.W. Series

J.J. Thomson Physical Laboratory, The University of Reading  
Whiteknights, Reading RG6 2AF, UK

### 1. Introduction

The principles of optogalvanic spectroscopy were recalled for us by Dr. Lawler at Rottach-Egern [1]. More recently, he has published an analysis of the mechanism for a discharge in helium [2]. The essentials of the technique are recalled in fig. 1. The current in a gas discharge is monitored while the discharge is irradiated with light. As the frequency of the light is tuned across some characteristic frequency of the atoms of the gas, changes may be detected in the discharge current. In favourable cases these changes provide a very sensitive monitor of the resonance, so that spectra may be plotted by recording the current as a function of the frequency of the light.

A number of mechanisms, all ultimately leading to changes in ionization, have been invoked to explain the optogalvanic effect, depending on the particular type of transition studied. But in all cases the primary mechanism has been the resonant transfer of atoms or ions between the states connected by the radiation, thus changing the distribution of population over the states, and hence the electrical characteristics of the discharge.

We report here a series of experiments which show that it may be possible to gain useful spectroscopic information by concerning ourselves with the polarization of the light rather than its frequency. We are interested in

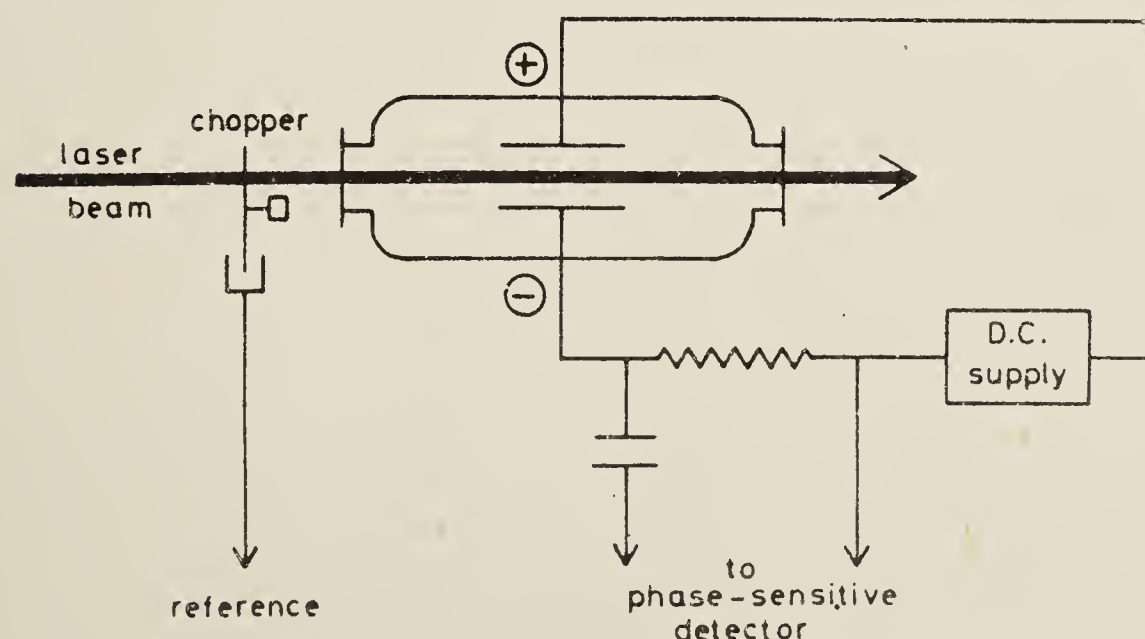


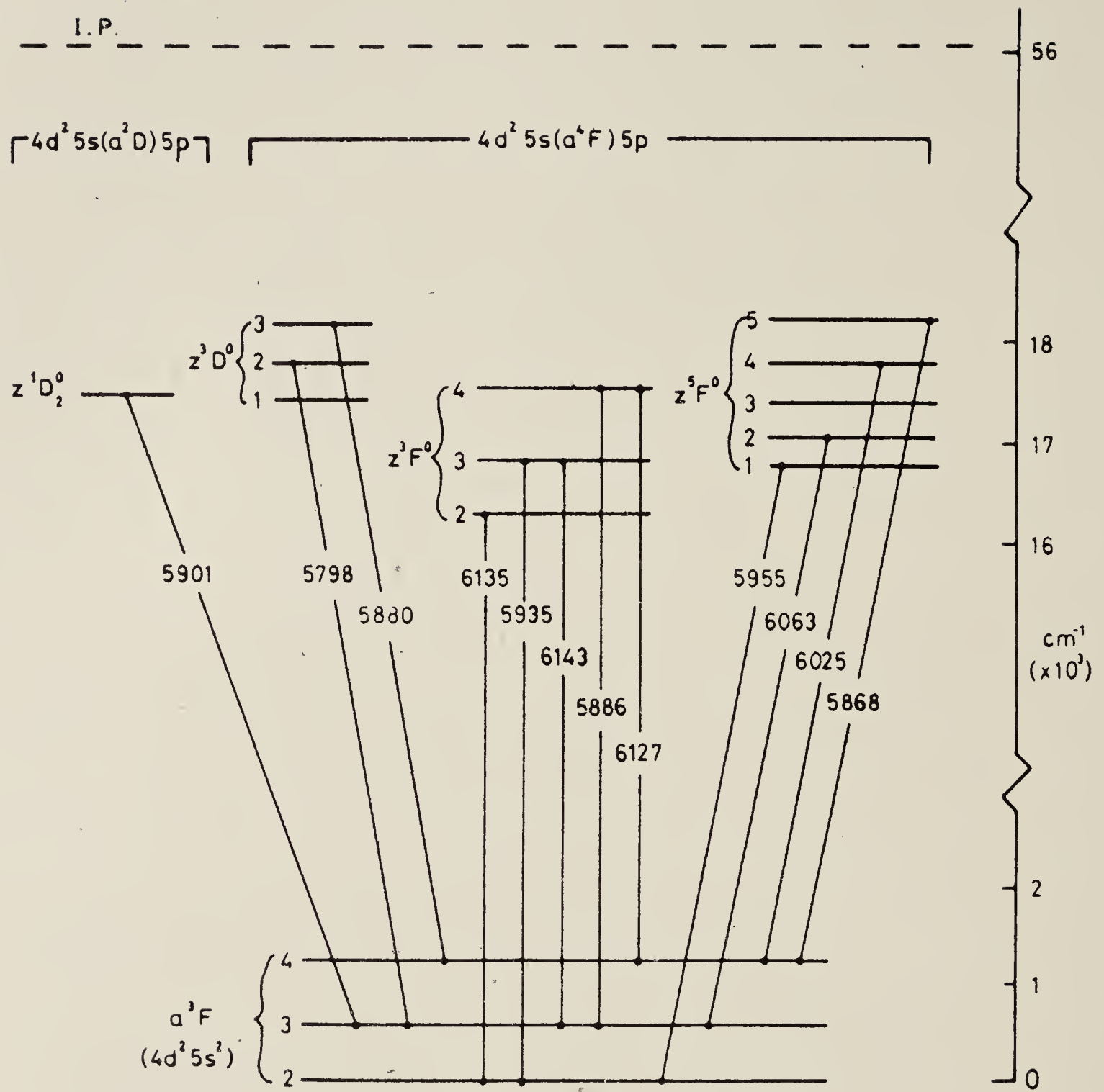
Fig. 1  
Arrangement  
for studying  
the opto-  
galvanic  
effect

\* On leave from CSIRO, Division of Chemical Physics, Clayton 3168, Australia









Zr I

Fig. 3 Transitions studied in Zr I

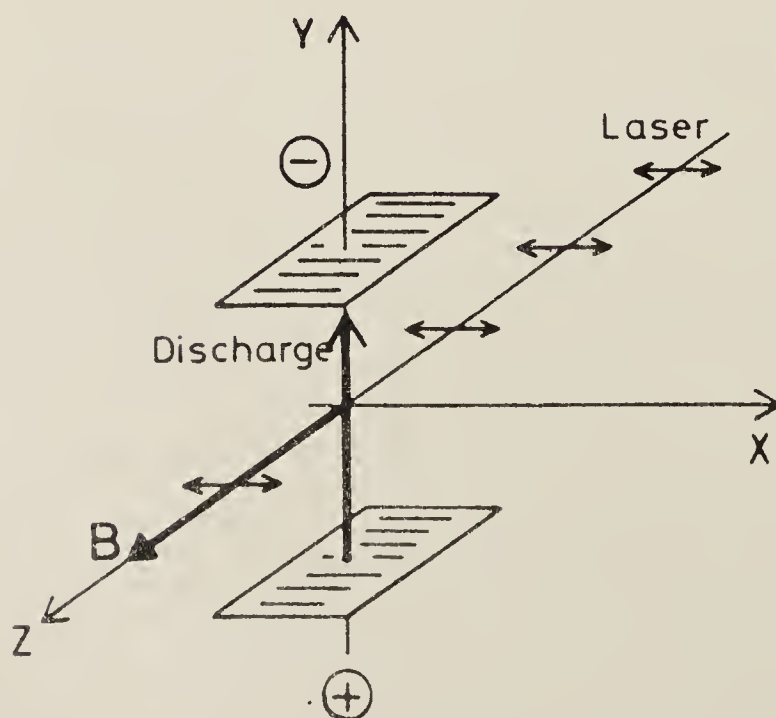


Fig. 4 Generation and monitoring of alignment



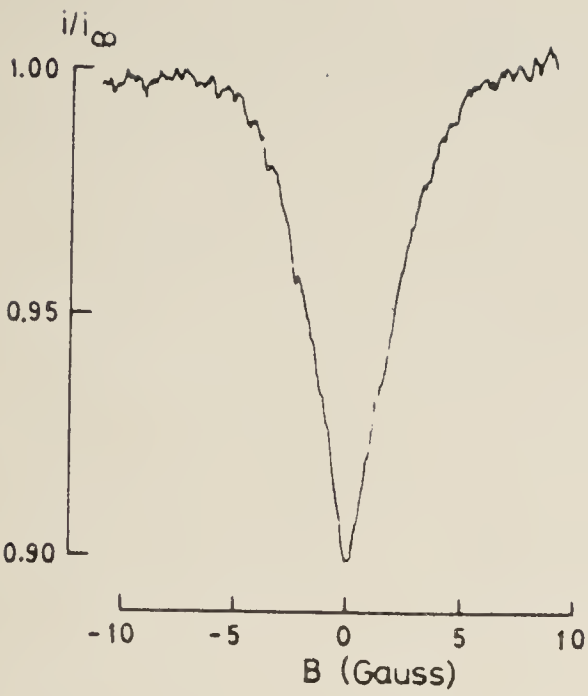


Fig. 5 Fractional optogalvanic signal,  $i/i_0$ , as function of magnetic field B. (0.8 torr neon. Laser power density:  $6\text{ W cm}^{-2}$ )

tion of the discharge current and with a discharge operated at 0.8 torr of neon and 5 mA current. The geometrical features of the resonance are summarised in Table 1.

The observed resonance is found to have some of the characteristics of a zero-field level-crossing signal: it is suppressed when the magnetic field is applied in the direction of polarization of the laser light, or in the case of circularly polarized light, when the magnetic field is along the axis of rotation of the electric vector, and it has an approximately Lorentzian-like shape with a width (FWHM 3.7 G) very much smaller than the Doppler width (400 G at 300 K). The resonance evidently represents a destruction of the atomic alignment by the applied magnetic field. There are

Table 1

Summary of geometrical features of observed resonance in the  $\text{Zr } 6127\text{ \AA}$  optogalvanic signal (0.8 torr Ne, laser power density:  $6\text{ W cm}^{-2}$ ). Directions are defined in Fig. 4.

Polarization vector	Direction of Magnetic field	Discharge current	Sign and fractional amplitude of resonance
Linear Y	Z	Y	+0.10
X	Z	Y	+0.09
Y	X	Y	+0.10
X	X	Y	<0.005
Y	Y	Y	<0.005
X	Y	Y	+0.09
Y	Z	X	+0.10
X	Z	X	+0.09
Circular (left or right)	Z	Y	<0.003
	X	Y	+0.06

several features, however, that distinguish this resonance from the normal linear Hanle effect that might be observed in an optogalvanic experiment.

(i) For an axial magnetic field (along Z), the sign and shape of the resonance remain fixed for any direction of the polarization vector. In particular, the resonance does not invert when the polarization vector is rotated by  $\pi/2$ . There is a small systematic difference of about 10% in the amplitude of the resonance when the polarization is nominally changed from vertical (Y) to horizontal (X), but this we believe to be some polarization artefact, as it persists when the discharge is rotated so that the current is in the horizontal polarization direction (X). Indeed, over the range of pressures used (0.5-3 torr) the ratio of the amplitudes for horizontal and vertical polarizations is invariant for any direction of the discharge current and for any position in the discharge. We conclude that the discharge current at these relatively high gas pressures is behaving as an isotropic probe.

(ii) The width of the resonance shown in Fig. 5 is a factor of about five greater than the width of the Hanle signal (0.7 G) measured in fluorescence under the same conditions. The fact that it is possible to observe the Hanle effect in fluorescence indicates that the alignment does survive in the discharge long enough to be monitored by fluorescent light. The width, sign and fractional amplitude (0.20) of the observed fluorescence Hanle signals are consistent with theoretical signals calculated from the known radiative lifetime of the  $z^3F_4^0$  level (520 ns), assuming a collisional depopulation cross section of about  $20 \text{ \AA}^2$ . Superimposed on the sharp Hanle signals, however, is a weak, broad resonance which does not invert when the polarization vector is rotated by  $\pi/2$  and which is not suppressed in the  $\pi$  fluorescence (analyser parallel to magnetic field). We identify this broad signal as the same resonance found in the optogalvanic experiment and conclude that it results from a change in the total population of the Zeeman sublevels when they become degenerate, rather than from the occurrence of an interference between the sublevels near zero field.

(iii) The resonance is found with different strengths in different transitions, most strongly in the transitions 6127, 6135 and 6143 Å (Table 2). The variation in strength over the different transitions is larger than can be explained by differences in the vector-coupling factors of the transitions. (The strengths of the calculated Hanle signals in fluorescent light are shown in the fifth column of Table 2.) In particular, the fractional amplitudes for transitions linked to the same upper level, such as the 6127 Å and 5886 Å transitions, can vary by more than an order of magnitude. From the results of Table 2 it is evident that the amplitude of the resonance is large when the Landé g-factors of the upper and lower levels are closely matched. This result was confirmed by extending our measurements to an additional zirconium transition at 6122 Å ( $a^1G_4 - y^1F_3$ ), for which the quantum numbers of the upper and lower levels are different, but for which  $S = 0$ ,  $L = J$  and hence  $g_{LS} = 1.00$  for both levels (Table 2).

(iv) The amplitude of the resonance is found to be strongly dependent upon the power density of the laser light and approaches zero at low power densities (Fig. 6). The reduction in amplitude with decreasing power density is accompanied by some narrowing of the resonance. The power densities of the laser are in the régime where some saturation in the population of the upper level is known to occur. It is clear that the resonance must be a non-linear effect which depends on partial saturation of the upper level by the laser light.



Table 2

Spectroscopic data and observed fractional amplitudes of resonance (at laser power densities of 2 and 6 W cm<sup>-2</sup>) for thirteen transitions in Zr I.

$\lambda(\text{\AA})$	Transition	<sup>a</sup> $\tau_2$	<sup>b</sup> $\Gamma_2^{(0)}$	<sup>c</sup> R	<sup>d</sup>		Fractional amplitude of resonance	
		(ns)	(G)		$g_1$	$g_2$	(2 W cm <sup>-2</sup> )	(6 W cm <sup>-2</sup> )
6135	$a^3F_2-z^3F_2^0$	500	0.34	0.45	0.66	0.67	0.066	0.089
5935	$a^3F_2-z^3F_3^0$	410	0.26	0.32	0.66	1.08	0.004	0.015
6143	$a^3F_3-z^3F_3^0$	410	0.26	0.47	1.06	1.08	0.076	0.097
5886	$a^3F_3-z^3F_4^0$	520	0.18	0.27	1.06	1.23	0.004	0.018
6127	$a^3F_4-z^3F_4^0$	520	0.18	0.48	1.24	1.23	0.072	0.100
5955	$a^3F_2-z^5F_1^0$	228	1.66	0.06	0.66	0.30	0.022	0.038
6063	$a^3F_3-z^5F_2^0$	288	0.42	0.04	1.06	0.95	0.011	0.015
6025	$a^3F_4-z^5F_4^0$	255	0.33	0.48	1.24	1.35	0.008	0.015
5868	$a^3F_4-z^5F_5^0$	220	0.37	0.24	1.24	1.40	<0.002	0.011
5798	$a^3F_3-z^3D_2^0$			0.04	1.06	1.09	0.041	0.061
5880	$a^3F_4-z^3D_3^0$	267	0.32	0.06	1.24	1.32	0.020	0.035
5901	$a^3F_3-z^1D_2^0$	540	0.22	0.04	1.06	0.96	0.003	0.014
6122	$a^1G_4-y^1F_3^0$			0.06	1.00	1.01	0.077	0.106

<sup>a</sup> Radiative lifetimes from ref. 8 and unpublished work of these authors.  
<sup>b</sup> Width of Hanle signal corresponding to  $\tau_2$ .  
<sup>c</sup> Strength of Hanle signal in fluorescent light, as a fraction of incoherent light, calculated for the J-values involved in the transition, and assuming no collisions.  
<sup>d</sup> Lande g-factors from ref. 9.

4. Discussion

The fact that the signals are observed under isotropic monitoring indicates that we are dealing with a change of total population in the excited state. The fact that the effects are non-linear in the intensity of the light indicates that stimulated emission plays a significant role in the process. The analysis of Feld et al. [5] would seem to describe the situation. Further evidence in support of Feld's analysis is that the observed resonances are more pointed than true Lorentzians, and could be interpreted as the superposition of Lorentzians of widths corresponding to the gT values of the states concerned.

An important feature of the resonances is the strong dependence of signal strength on the relative g-factors of the upper and lower levels. Conditions

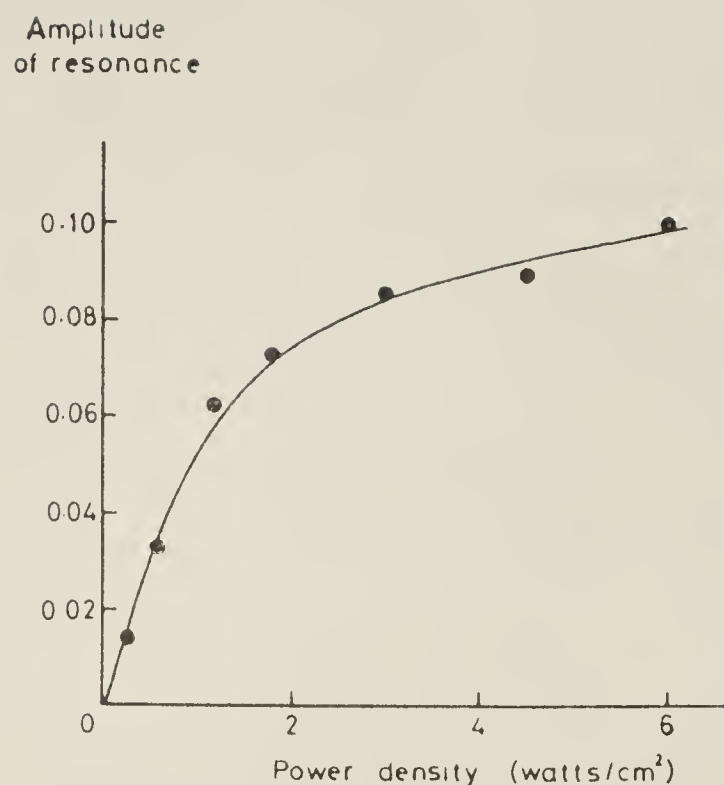


Fig. 6 Amplitude of resonance (fraction of optogalvanic signal) as function of laser power density. Conditions as in Fig. 5

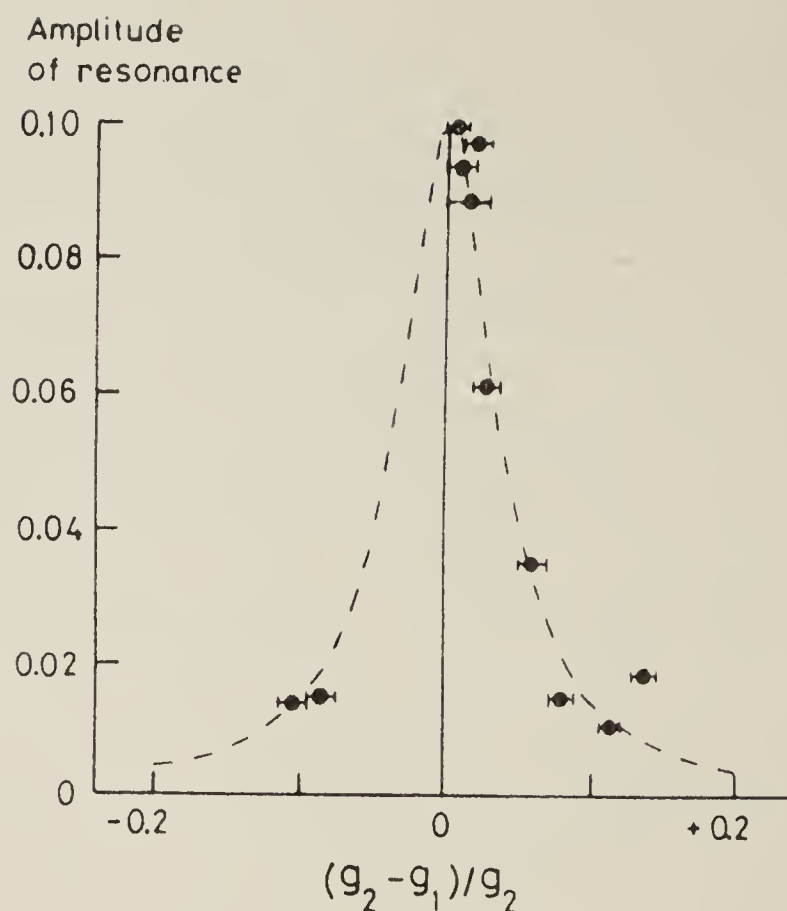


Fig. 7 Amplitude of resonance as function of  $g$ -mismatch for 11 transitions in Zr I. Conditions as in Fig. 5. The broken line is a Lorentzian with width parameter 0.08. The horizontal bars derive from rounding errors in quoted  $g$ -values

which favour strong signals are that the Larmor precessional frequencies in the upper and lower levels shall be as closely matched as possible: mismatch of the  $g$ -factors militates against efficient transfer of coherence round the optical pumping cycle.

The use of zirconium allowed a quantitative investigation of the significance of  $g$ -mismatch. In Fig. 7 we show the signal strength, for fixed laser power, for 11 of the transitions investigated, as a function of  $(g_2 - g_1)/g_2$ , where the suffixes 2 and 1 refer to upper and lower levels, respectively. The empirical evidence suggests a Lorentzian-like dependence. We have sketched out a theory which suggests a relationship proportional to

$\{[(g_2 - g_1)/g_2]^2 + (T_{12}/T_1)^2\}^{-1}$ , which effectively compares the relative dephasing  $(\omega_2 - \omega_1)T_1$  in the lifetime of the lower state with the phase evolution  $\omega_2 T_{12}$  in the lifetime of the electric dipole. The linewidth parameter of the Lorentzian shown in Fig. 7 (the broken line) would then be interpreted as  $T_2/T_1$ . The value obtained is not unreasonable. In support of this interpretation is adduced the fact that the experimental plot narrowed when the laser power density was reduced. Use of the data in Table 2 leads to the result that reduction of power by a factor 3 leads to a narrowing by 20%.

Finally we emphasise that the occurrence of phenomena attributable to isotropic monitoring of alignment reported in the latter part of this paper does not preclude the existence of the effect suggested in the first part.



It is our intention to continue our investigations into the régime where directed motion of the electrons may be expected to predominate.

It is a pleasure to acknowledge the contribution made by Dr. S. Nakayama in the early stages of this work.

### References

1. J.E. Lawler: In Laser Spectroscopy IV, ed. by H. Walther, K.W. Rothe, Springer Series in Optical Sciences, Vol. 21 (Springer Berlin, Heidelberg, New York 1979)
2. J.E. Lawler: Phys. Rev. A22, 1025 (1980)
3. G.W. Series: Comments At. Mol. Phys. X, 199 (1981)
4. H. Beverini and M. Inguscio: Nuov. Cim. Lett. 20, 10 (1980)
5. M.G. Feld, A. Sanchez, A. Javan and B.J. Feldman: 'Spectroscopie sans largeur Doppler...', CNRS No.217, Paris (1974)
6. B. Decomps, M. Dumont and M. Ducloy, in Laser Spectroscopy of Atoms and Molecules, ed. by H. Walther, Topics in Applied Physics, Vol. 2 (Springer Berlin, Heidelberg, New York 1976)
7. 'Excitation Electronique d'une Vapeur Atomique', CNRS No. 162, Paris (1976)
8. E. Biémont, N. Grevesse, P. Hannaforde and R.M. Lowe, Astrophys. J., In press (1981)
9. C.E. Moore, 'Atomic Energy Levels', NSRDS-NBS 35 (1971)





LETTER TO THE EDITOR

## Observation of level-crossing effects in optogalvanic spectroscopy

P Hannaford<sup>†</sup> and G W Series

J J Thomson Physical Laboratory, University of Reading, Whiteknights, Reading RG6 2AF, England

Received 12 August 1981

**Abstract.** Optogalvanic signals arising from a group of transitions in Zr I have been studied under irradiation of a cold cathode glow discharge with polarised laser light. The signals increase with the application of a magnetic field of a few gauss crossed with the symmetry axis of the polarisation, but the change is not related to the direction of current in the discharge. The occurrence of these magnetic resonances depends on at least partial saturation of the optogalvanic signals. The empirical evidence leads to the conclusion that the resonances result from changes of occupation probability in the excited state upon removal of degeneracy by the magnetic field—a non-linear, level-crossing effect.

The optogalvanic effect is the change in impedance of a gas discharge caused by irradiation of the plasma by light whose frequency matches a transition frequency in the atoms or ions which constitute the plasma (Penning 1928). With the advent of tunable lasers the effect has become a potentially important spectroscopic technique: changes in the discharge current indicate atomic resonances as the frequency of the laser is swept through them (Goldsmith and Lawler 1981). The mechanism of the effect depends on some change in the plasma leading to ionisation. The primary change is a resonant transfer of atoms between the states connected by the radiation.

We report here the first experimental evidence of level-crossing effects monitored by the optogalvanic method. The evidence lies in the changes that are observed in the optogalvanic signal when the zero-field degeneracy of Zeeman levels is removed by a small magnetic field. It is known that in non-linear interactions between light and atoms the removal of degeneracy can affect the population distribution (Decomps *et al* 1976, see also Feld *et al* 1974). The possibility of using this mechanism for detecting level crossings by optogalvanic means was pointed out by Beverini and Inguscio (1980). Our experiments were in fact undertaken as a preliminary to a study of an alternative mechanism depending on changes of alignment rather than of population (Series 1981), but for the discharges we first investigated, in which the gas pressure was of the order of 1 Torr, we found that the effects based on population changes dominate.

The experiments were carried out on zirconium atoms, sputtered from a cold cathode of zirconium metal into a discharge maintained in neon at pressures in the range 0.5–3 Torr. A convenient feature of zirconium is that more than twenty transitions based on the ground or metastable states, and providing a wide range of  $J$  values, Landé  $g$  factors and transition probabilities, lie within the tuning range of rhodamine 6G.

<sup>†</sup> On leave from CSIRO Division of Chemical Physics, Clayton 3168, Australia.

The discharge was irradiated with polarised light from a cw tunable laser at a power density of a few  $\text{W cm}^{-2}$ , distributed over all modes. We tuned the laser to resonance for the transition under investigation: there was then, in the excited state, an atomic polarisation which reflected the polarisation of the light. The stray magnetic field was reduced to less than 0.1 G. The laser was run multi-mode, but stably. The overall laser band width used was about 10 GHz and the width of individual modes, 5–7 MHz, was greater than the pressure-broadened width of the excited levels, about 1–2 MHz, but much less than the Doppler width, about 600 MHz. The interval between longitudinal modes of the laser was 390 MHz.

The optogalvanic signal was detected by chopping the laser beam at low frequency and using phase-sensitive detection to record the change in current through the discharge. For a discharge current of 5 mA (DC) the optogalvanic signal on strong transitions is typically found to be  $0.3 \mu\text{A}$ . Positive signals (enhancement of the current arising from increased population of the upper states) were observed in all cases except three, these being transitions based on metastable states.

Most of our experiments were carried out with linearly polarised light with the magnetic field applied transversely to the electric vector. In some experiments circularly polarised light was used and the magnetic field applied transversely to the direction of propagation of the light. For both configurations the optogalvanic signal increases in magnitude as the field is increased in either sense from zero up to a few gauss (figure 1). In neither case was there a change in the optogalvanic signal when the field was applied parallel to the symmetry axis.

For larger magnetic fields there is a direct effect of the field on the charge carriers in the discharge. This can be identified by observing the current under irradiation of different transitions and with different polarisations. The effects reported here are not attributable to this direct effect.

We have also been alert to the possibility that the signals might depend on the direction of the polarisation axis of the light in relation to the discharge current. While

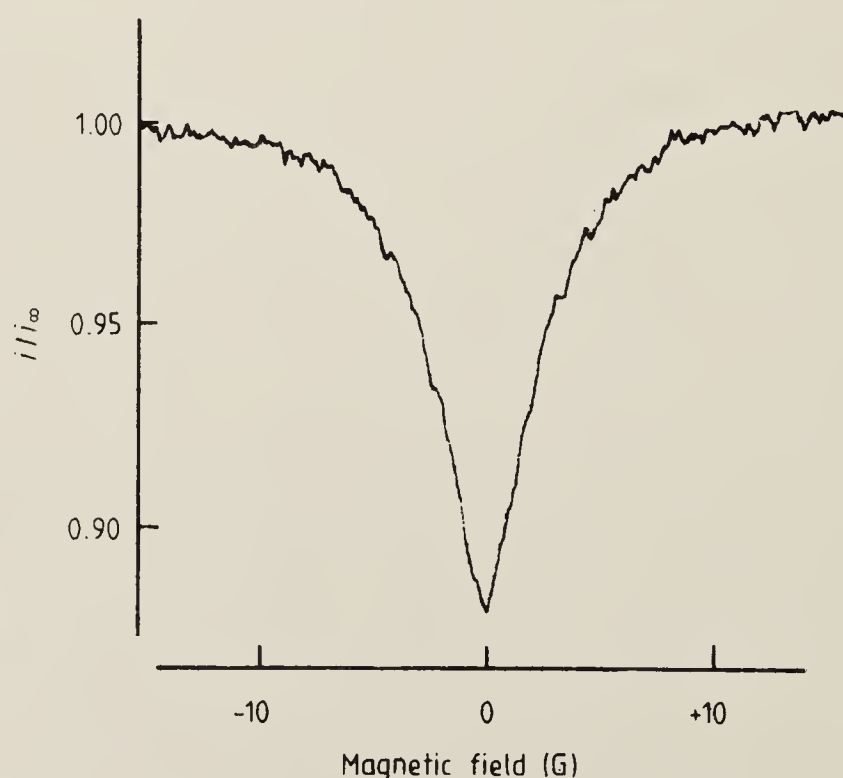


**Figure 1.** Optogalvanic current, as fraction of the current at high field, plotted against magnetic field. Transition Zr I 612.7 nm, 0.8 Torr neon. Laser power density =  $3 \text{ W cm}^{-2}$ . Geometry: laser beam 0z, linear polarisation 0x, magnetic field 0z, discharge current 0y. (The amplitude of the dip is called the resonance strength  $S$ .)



we believe that such an effect will appear at sufficiently low particle densities, we obtained no certain evidence of its occurrence in the present experiments.

Magnetic resonance signals such as in figure 1 were obtained for the stronger transitions and studied under variation of discharge current and pressure, and laser power. Additionally, the signal strength, obtained by switching the magnetic field on and off, was measured for twenty transitions, including the twelve based on the ground term and listed in table 1. (The quantity, resonance strength  $S$ , in table 1 is defined as the signal strength—base to peak height—divided by the optogalvanic signal at high field.) Furthermore, for comparison, we observed the Hanle effect in fluorescence for some of the transitions. The general characteristics of the signals are summarised below.

(i) The sense of the signals (we call them resonances) is always to increase with magnetic field, irrespective of the direction of polarisation of the light with respect to the discharge current and irrespective of the position of the light beam in the discharge. This is to be contrasted with observations of the Hanle effect in fluorescence where the sense of the signal depends on the relative orientations of the polarisation vectors in the exciting and monitoring beams.

(ii) The shape of the resonances is not Lorentzian: it appears to be more pointed. For some transitions which exhibit a weak resonance (e.g. 595.5 nm) the pointed component appears to be standing on a broad base.

(iii) The width of the resonances falls in the range 3–7 G, according to the transition. While this is very much less than the Doppler width ( $\sim 400$  G) it is, nevertheless, appreciably greater than the width of the Hanle resonance (0.7 G for the transition 612.7 nm at 0.8 Torr) measured in fluorescence under the same conditions. It

**Table 1.** Spectroscopic data and observed resonance strengths  $S$  for twelve transitions in Zr I (0.8 Torr Ne, laser power density  $3\text{ W cm}^{-2}$ ).

$\lambda$ (nm)	Transition	$\tau_2^a$ (ns)	$\Gamma_2^{(0)b}$ (G)	$f^a$	$P$	$S$	Width (FWHM) (G)
4d <sup>2</sup> 5s <sup>2</sup> –4d <sup>2</sup> 5s (a <sup>4</sup> F)5p							
613.5	a <sup>3</sup> F <sub>2</sub> –z <sup>3</sup> F <sub>2</sub> <sup>o</sup>	500	0.34	0.0106	–0.59	0.092	6.5
593.5	a <sup>3</sup> F <sub>2</sub> –z <sup>3</sup> F <sub>3</sub> <sup>o</sup>	410	0.26	0.0018	0.49	0.002	
614.3	a <sup>3</sup> F <sub>3</sub> –z <sup>3</sup> F <sub>3</sub> <sup>o</sup>	410	0.26	0.0113	–0.61	0.103	5.0
588.6	a <sup>3</sup> F <sub>3</sub> –z <sup>3</sup> F <sub>4</sub> <sup>o</sup>	520	0.18	0.0011	0.44	0.009	
612.7	a <sup>3</sup> F <sub>4</sub> –z <sup>3</sup> F <sub>4</sub> <sup>o</sup>	520	0.18	0.0096	–0.62	0.113	4.5
595.5	a <sup>3</sup> F <sub>2</sub> –z <sup>5</sup> F <sub>1</sub> <sup>o</sup>	230	1.66	0.003 <sup>c</sup>	0.10	0.023	3.0
606.3	a <sup>3</sup> F <sub>3</sub> –z <sup>5</sup> F <sub>2</sub> <sup>o</sup>	290	0.42	0.003 <sup>c</sup>	0.17	0.007	
602.5	a <sup>3</sup> F <sub>4</sub> –z <sup>5</sup> F <sub>4</sub> <sup>o</sup>	255	0.33	0.006 <sup>c</sup>	–0.62	0.022	
586.8	a <sup>3</sup> F <sub>4</sub> –z <sup>5</sup> F <sub>5</sub> <sup>o</sup>	220	0.37	0.0007	0.42	0.015	
579.8	a <sup>3</sup> F <sub>3</sub> –z <sup>3</sup> D <sub>2</sub> <sup>o</sup>	250	0.42	0.004 <sup>c</sup>	0.17	0.034	4.0
588.0	a <sup>3</sup> F <sub>4</sub> –z <sup>3</sup> D <sub>3</sub> <sup>o</sup>	270	0.32	0.007 <sup>c</sup>	0.20	0.050	3.5
4d <sup>2</sup> 5s <sup>2</sup> –4d <sup>2</sup> 5s (a <sup>2</sup> D)5p							
590.1	a <sup>3</sup> F <sub>3</sub> –z <sup>1</sup> D <sub>2</sub> <sup>o</sup>	540	0.22	0.0007 <sup>c</sup>	0.17	0.006	

<sup>a</sup> Radiative lifetimes ( $\tau_2$ ) and oscillator strengths ( $f$ ) from Biemont *et al* (1981) and unpublished work of these authors.  
<sup>b</sup> Calculated width of Hanle signal corresponding to  $\tau_2$ .  
<sup>c</sup> Derived from  $\tau_2$  using approximate branching ratios from Corliss and Bozman (1962).

was noticed, however, that the narrow Hanle fluorescence signals were superimposed on a weak, broad resonance of width similar to that of the optogalvanic resonances. This resonance did not invert (as do the Hanle resonances) when the polariser was rotated by  $\pi/2$ . Moreover, a resonance of this kind was observed also in the  $\pi$  component of the fluorescent light.

(iv) The width of the resonances decreases with pressure (for the 612.7 nm transition the reduction was from 5 G at 1.5 Torr to 4 G at 0.5 Torr). The width is insensitive to discharge current over the range 2–10 mA. The strength,  $S$ , of the resonances decreases strongly with pressure but is insensitive to discharge current.

(v) For different transitions  $S$  varies greatly. For example,  $S_{612.7}$  at a power density of  $3 \text{ W cm}^{-2}$  exceeds  $S_{588.6}$  by more than an order of magnitude, even though these transitions have the same upper level.

(vi) For the strongest transitions (613.5, 614.3, 612.7 nm) the width, in units of magnetic field, varies inversely as the  $g$  value (for these transitions the  $g$  values of the upper and lower states are approximately equal). In units of frequency, the width, therefore, is approximately the same for each: about 7 MHz. It will be noticed that this is about the same as the spectral line width of a single mode of the laser. The transition 595.5 nm, for which the  $g$  values of upper and lower states are 0.30 and 0.66 respectively, is anomalous not only in its shape (see (ii) above), but also in that the width (based on  $g = 0.30$ ) is about 1 MHz.

(vii)  $S$  depends strongly on the power density of the laser light: indeed, the magnetic resonance signals appear only with the onset of saturation of the optogalvanic signals themselves. (This contrasts with the linear Hanle effect, where the interference signal is always a constant fraction of the field-independent fluorescence.)

With increasing power density  $S$  tends to a limiting value,  $S_\infty$ . This limit is approached more rapidly for transitions of high  $f$  value (table 1).

For those transitions for which  $S_\infty$  could be measured (613.5, 614.3, 612.7, 595.5, 579.8 and 588.0 nm) the values of  $S_\infty$  correlate with values of  $|P|$ , where  $P$  is a polarisation parameter given by

$$\left\{ \begin{matrix} 2 & 1 & 1 \\ J_1 & J_2 & J_2 \end{matrix} \right\} / \left\{ \begin{matrix} 0 & 1 & 1 \\ J_1 & J_2 & J_2 \end{matrix} \right\}$$

(suffixes 1 and 2 refer to lower and upper states, respectively): high values of  $S_\infty$  are associated with high values of  $|P|$ .

(viii) the onset of saturation of  $S$  is accompanied by some power broadening of the resonances.

We have set out the experimental findings in some detail because an interpretation of them must go beyond any theoretical analyses which have so far come to our notice. In particular, the articles by Feld *et al* (1974) and by Decomps *et al* (1976) solve the optical pumping equations only to fourth order in the amplitudes, which is sufficient for lower-state, but not for upper-state populations.

The empirical evidence allows the following conclusions to be drawn. While it must be the case that atomic polarisation in the upper state is induced by the irradiation (we shall speak of *alignment* since linearly polarised light was used for most of the experiments), it cannot be true that the magnetic signals depend solely on the perturbation of this alignment by the magnetic field, as in the Hanle effect. Since the signal does not depend on the direction of the discharge current the atomic property being monitored must be the total population of a set of Zeeman levels. Further evidence that



it is the magnetically perturbed *population*, not the perturbed *alignment* that is being detected is provided by the weak background signal seen in all polarisations of fluorescence.

The effect must be non-linear, not simply in the intensity of the laser light, but also in the strength of the atomic interaction. This is shown by the dependence of the magnetic resonance signal on partial saturation in the optogalvanic signal, and also by the correlations between the signal strength and the values of  $f$  and  $|P|$  for the transition. The non-linearity suggests that stimulated emission must play a significant role in interpretation. This conclusion is supported by the evidence concerning the width of the resonance in relation to the width of the Hanle resonance measured in fluorescence: the latter monitors the alignment of the upper state and reflects its width. The greater width of the optogalvanic resonances reflects the shorter correlation time of the coupling between the lower and upper states. The theories already referred to show how 'hole-burning' and atomic interference effects in non-linear interactions can lead to changes of occupation probability for atoms of given velocity, and hence, after integration over velocities, to changes of total population.

The characteristic pointed shape of the resonances, whose width in frequency units corresponds approximately with the spectral width of individual modes of the laser, suggests that the intrinsic shape of the magnetic resonances for these relatively long-lived upper levels is being obscured by folding with the laser profile, although the anomalously narrow width associated with the transition 595.5 nm conflicts with this interpretation.

In a first report of this work (Hannaford and Series 1981) we pointed to a correlation between  $S$  and the  $g$  mismatch of the upper and lower states of the transition. Such a correlation indeed exists for the group of transitions based on the ground term, but we have found exceptions in the transitions 592.5, 599.5, 612.5 and 614.0 nm based on metastable levels. It is our present opinion that the correlation with  $f$  and  $|P|$  is more significant.

We have concentrated here on the characteristics and interpretation of the phenomenon, but its potential as a spectroscopic method will not be overlooked. Although our observations relate only to the removal of zero-field degeneracies it is to be expected that optogalvanic effects will signal level crossings in general, and perhaps in circumstances where fluorescence signals are impossible to obtain. Moreover, although we do not expect to find quantum beats associated with the phenomenon, we would expect to find resonances associated with modulation of the laser light at a frequency matching an interval between levels.

It is a pleasure to acknowledge the help of Mr C H Smith in technical matters and the contribution made by Dr S Nakayama in the early stages of this work. We are grateful to the Science and Engineering Research Council for financial support for the project in general, and in the form of a Visiting Fellowship for one of us (PH).

## References

- Beverini N and Inguscio M 1980 *Nuov. Cim. Lett.* **29** 10–12  
 Biémont E, Grevesse N, Hannaford P and Lowe R M 1981 *Astrophys. J.* **248** 867–73  
 Corliss C H and Bozman W R 1962 *NBS Monograph* No 53 (Washington, DC: US Govt Printing Office)  
 Decomps B, Dumont M and Ducloy M 1976 *Laser Spectroscopy of Atoms and Molecules* ed H Walther (Berlin: Springer) pp 283–347

Feld M S, Sanchez A, Javan A and Feldman B J 1974 *Colloques Internationaux du CNRS* No 217 (Paris: CNRS) pp 87-104

Goldsmith J E M and Lawler J E 1981 *Contemp. Phys.* **22** 235-48

Hannaford P and Series G W 1981 *Laser Spectroscopy* vol 5, ed B Stoicheff and T Oka (Berlin: Springer)

Penning F M 1928 *Physica* **8** 137-40

Series G W 1981 *Comment. At. Mol. Phys.* **10** 199-201



## MULTIMODE SATURATION RESONANCES IN OPTOGALVANIC SPECTROSCOPY: APPLICATION TO THE DETERMINATION OF LANDE $g$ -FACTORS IN ZIRCONIUM

P. HANNAFORD \* and G.W. SERIES

*J.J. Thomson Physical Laboratory, University of Reading,  
Whiteknights, Reading RG6 2AF, England*

Received 29 January 1982

Resonances corresponding to the matching of laser mode intervals with Larmor precessional frequencies have been observed in the discharge current for four transitions in the spectrum of atomic Zr, introduced into a gas discharge by cathodic sputtering. Signals were observed for lower as well as for upper levels. The measured  $g$ -factors for the states  $4d^25s(a^4F)5p^3F_{2,3,4}$  and  $4d^25s(a^2P)5p^3P_2$  are systematically higher than values given in the literature.

### 1. Introduction

In a recent paper [1] we reported the observation of zero-field level-crossing saturation resonances in the optogalvanic signals from some transitions in zirconium when the zero-field degeneracies of the Zeeman levels were removed by a small magnetic field. The technique has latterly been extended to level-crossing saturation resonances at finite magnetic fields, and the results used to determine hyperfine structures in excited and ground levels of atomic yttrium [2]. In this paper we report the observation of additional saturation resonances which appear in the optogalvanic signals from zirconium when the exciting laser is run multimode and the Zeeman splitting in either the upper ( $2g_2\beta B$ ) or the lower level ( $2g_1\beta B$ ) is equal to a multiple of the mode separation of the laser. Under these conditions, for one and the same velocity group of atoms, the  $\sigma^+$  transition is excited by one mode of the laser and the  $\sigma^-$  transition excited by another mode. When the transitions are completely or partially saturated, their simultaneous excitation can lead to a reduction in the overall number of atoms excited, and hence to a reduction in the magnitude of the optogalvanic signal.

Multimode saturation resonances, similar to those reported here but observed in *fluorescence*, have previously been reported for transitions in neon by Fork, Hargrove and Pollack [3], by Decamps and Dumont [4] and by Dumont [5]. In those experiments the coherence time of the multimode helium-neon laser was long compared with the lifetimes of the neon levels and the neighbouring laser modes could act coherently on the same neon atoms, thus giving rise to a Zeeman coherence effect in addition to the "hole-burning" population effect [5]. In the present optogalvanic experiment the coherence time of the multimode tunable laser is short compared with the lifetimes of the zirconium levels, and under such conditions the multimode saturation resonances originate entirely from the population effect. Thus the profiles of these multimode resonances are determined purely by the convolution of the profiles of individual modes of the laser. This contrasts with the zero-field and finite-field level-crossing saturation resonances for which there are contributions from both the Zeeman coherence effect, which is characterized by the sum of the pressure-broadened widths of the levels, and the population effect [6,1,2].

The detection of multimode saturation resonances by means of the optogalvanic effect offers a new Doppler-free spectroscopic technique for determining Landé  $g$ -factors in both excited and ground atomic

\* On leave from CSIRO Division of Chemical Physics, Clayton 3168, Australia.

levels, and in this paper we report the application of the technique to the  $4d^25s(a^4F)5p^3F_{2,3,4}$  and  $4d^25s(a^2P)5p^3P_2$  levels in Zr I.

## 2. Experimental

The experimental arrangement is similar to that described previously [1] and only the essential features are recalled here.

The zirconium atoms are sputtered from a cathode of naturally occurring zirconium metal (89% even isotopes, 11%  $^{91}\text{Zr}$ ) into a discharge maintained in neon or argon at a pressure of about 1 Torr. The atoms are excited with linearly polarized light from a c.w. tunable laser and subjected to a magnetic field crossed with the polarization vector of the light. Stray magnetic fields are reduced to less than 20 mG. The laser is run multimode (free-running) at a power density of typically  $30\text{ mW mm}^{-2}$  distributed over all modes. The width of individual modes of the laser is 5–7 MHz, which is greater than the pressure-broadened width (about 1–2 MHz) of the excited Zr levels, but much less than the Doppler width ( $\approx 600$  MHz) of the transitions. The separation of the longitudinal laser modes is nominally 390 MHz.

The zirconium transitions chosen for investigation are listed in table 1. Each was found to yield a strong zero-field saturation resonance ( $S \approx 0.10$ ) [1]. The optogalvanic current was large ( $\approx 0.2\text{ }\mu\text{A}$ ) for the first three transitions, but relatively small ( $\approx 0.2\text{ nA}$ ) for the 614.0 nm transition which is based on a meta-

stable  $a^3P_2$  level at  $4186\text{ cm}^{-1}$ . The 614.0 nm transition was included for investigation because of the large difference in  $g$ -factors of the upper and lower levels  $^\ddagger$ . The radiative lifetimes of the upper levels of the four transitions range from 280 ns for the  $z^3P_2^0$  level to about 500 ns for the three  $z^3P^0$  levels [9].

## 3. Results and interpretation

Table 2 lists the multimode saturation resonances we observed in the four transitions studied. That their occurrence does indeed demand multimode operation of the laser was established by the observation that, when the laser was stabilised so that the time between mode hops was appreciably lengthened, the resonances vanished.

For the transition at 612.7 nm we observed resonances for two values of magnetic field in the ratio 2 : 1. When converted to frequency using the  $g$ -values, either of the upper or of the lower level (these are closely equal: see table 1), we obtain 400 MHz and 805 MHz, respectively. Comparing these values with the nominal value of the mode separation of the laser, we have no hesitation in identifying these resonances as adjacent-mode and next-but-one adjacent-mode (first- and second-mode) saturation resonances. The strength of these multimode resonances ( $S \approx 0.06$ ) is

$^\ddagger$  The  $g$ -factor for the lower ( $a^3P_2$ ) level is significantly lower than the LS-coupling value (table 1) because of very strong perturbation by the nearby  $a^1D_2$  level [7,8].

Table 1  
Lande  $g$ -factors of upper ( $g_2$ ) and lower ( $g_1$ ) levels of Zr I transitions used in this investigation

$\lambda$ (nm)	Transition	$g_1$			$g_2$		
		LS <sup>a)</sup>	Moore [10]	BDG [7]	LS <sup>a)</sup>	Moore [10]	This work
	<u><math>4d^25s^2-4d^25s(a^4F)5p</math></u>						
612.7	$a^3F_4-z^3F_4^0$ (1241–17556 cm <sup>-1</sup> )	1.250	1.24	1.24987(6)	1.250	1.23	1.25(1)
614.3	$a^3F_3-z^3F_3^0$ (570–16844 cm <sup>-1</sup> )	1.083	1.06	1.08331(9)	1.083	1.08	1.09(1)
613.5	$a^3F_2-z^3F_2^0$ (0–16297 cm <sup>-1</sup> )	0.667	0.66	0.66981(4)	0.667	0.67	0.696(3)
	<u><math>4d^25s^2-4d^25s(a^2P)5p</math></u>						
614.0	$a^3P_2-z^3P_2^0$ (4186–20467 cm <sup>-1</sup> )	1.500 <sup>b)</sup>	1.25	1.26472(5)	1.500	1.47	1.51(1)

<sup>a)</sup> Calculated from  $g^{LS} = 1 + [J(J+1) + S(S+1) - L(L+1)]/2J(J+1)$ .

<sup>b)</sup> Intermediate coupling value = 1.26520 [7].



Table 2  
Positions and splittings of observed multi-mode saturation resonances in Zr I

$\lambda$ (nm)	Transition	Positions		Splittings (G)
		(G)	(MHz) <sup>a)</sup>	
612.7	$a^3F_4^0-z^3F_4^0$	114.5(0.5); 230(2)	400(2); 805(7)	
614.3	$a^3F_3-z^3F_3^0$	131.5(0.5)	399(2)	
613.5	$a^3F_2-z^3F_2^0$	$\left\{ \begin{array}{l} 206.5(1.0) \\ 214.5(1.0) \end{array} \right.$	$[387(2)]^*$ 402(2)	$\left. \vphantom{\left\{ \begin{array}{l} 206.5(1.0) \\ 214.5(1.0) \end{array} \right.}} \right\} 8.0(1.0)$
614.0	$a^3P_2-z^3P_2^0$	$\left\{ \begin{array}{l} 95.0(1.0) \\ 113.5(1.0) \end{array} \right.$	$[336(3)]^*$ 402(4)	$\left. \vphantom{\left\{ \begin{array}{l} 95.0(1.0) \\ 113.5(1.0) \end{array} \right.}} \right\} 18.5(1.0)$

<sup>a)</sup> Calculated with use of lower-level *g*-factors of Büttgenbach et al. (table 1).  
\* Clearly, the lower-level *g*-factors are not appropriate for these resonances. See text.

about one-half that of the zero-field resonance. The profiles of the resonances (fig. 1) appear to be less pointed than the zero-field resonance [1], a characteristic which is consistent with an interpretation based on the population effect only [6].

The transitions at 613.5 and 614.0 nm each show two closely-spaced resonances, certainly not standing in the 2 : 1 relationship. In each case the two components are of approximately equal strength. In each case we associate these resonances with the upper

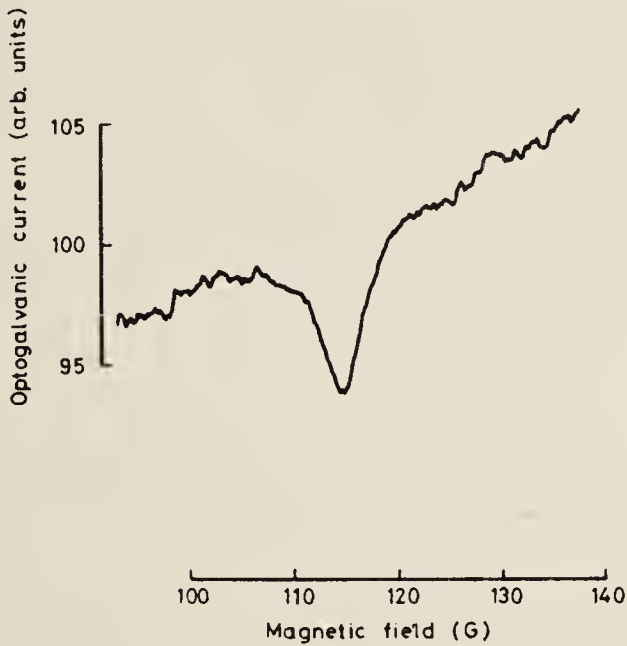


Fig. 1. First-mode saturation resonance in the optogalvanic signal for the 612.7 nm ( $a^3F_4-z^3F_4^0$ ) transition in Zr I. Discharge: 1 Torr argon, 5 mA. Laser power density = 30 mW mm<sup>-2</sup>. Geometry: laser beam Oz, linear polarization Ox, magnetic field Oz. The sloping background near the resonance is attributed to the direct effect of the magnetic field on the optogalvanic current.

and lower levels of the transition. Use of the lower level *g*-factors (which are known accurately from atomic beam work) to convert field to frequency identifies the higher-field resonance in each case with the Zeeman splitting of the lower level, and allows the calculation of the upper level *g*-factors by combining the measured values of the fields for the low-field resonances with the value 401 ± 2 MHz for the mode separation of the laser, obtained as a weighted mean derived from the five frequencies given in table 2 (excluding the starred values). There was no means available to us for making a direct measurement of this mode separation. The splitting observed for the transition at 613.5 nm is noteworthy in that the *g*-values reported in the literature for the upper and lower levels are sufficiently close that no splitting might have been expected.

The transition at 614.3 nm showed only one resonance, which we interpret as the unresolved superposition of the resonances to be expected from Zeeman splittings in the upper and in the lower levels. There was no evidence of asymmetry in the resonance profile. Likewise, for the transition at 612.7 nm the two resonances observed are interpreted as superpositions associated with upper and lower levels. We looked especially for evidence of additional broadening in the second-mode resonance, but found none. The width (FWHM) of all these resonances was about 8 MHz, which is close to that of the zero-field resonance measured under the same conditions. We conclude that, for these two transitions, the *g*-factors in the upper and lower levels must be same to within 1%.

The upper-level *g*-factors found in this investiga-

tion are systematically higher, by 0.01 to 0.04, than the values given in Moore's tables [10], which were taken from the early data of Sancho [11] and Kiess and Kiess [12]. Similar differences are found when the values in Moore's tables are compared with the accurate atomic-beam magnetic resonance results of Büttgenbach et al. [7]. Our  $g$ -factors are essentially the same as the LS-coupling values (table 1) for all levels except  $z^3F_2^0$ , for which our result exceeds the LS-value by  $0.029 \pm 0.003$ . Such a difference is not unexpected in view of the fact that there are three odd-parity  $J = 2$  levels ( $z^5F_2^0$ ,  $z^3D_2^0$ ,  $z^1D_2^0$ ) nearby that could perturb the  $z^3F_2^0$  level. (Each of these levels has a  $g$ -value that is higher than the  $z^3F_2^0$  value and lower than their respective LS-coupling values.)

#### 4. Discussion

The main objectives of this work were to search for multimode saturation resonances by the optogalvanic technique and to apply the phenomenon to determine Lande  $g$ -factors. The accuracy of the measurements could have been improved with better knowledge of the mode separation of the laser and with better calibration of the magnetic fields. The sensitivity and resolution could have been improved by modulating the magnetic field in addition to chopping the laser beam, a technique which we applied in the optogalvanic detection of level-crossings in  $^{89}\text{Y}$  [2]. The detection of saturation resonances by optogalvanic means seems well suited for studying atomic levels in highly refractory elements, such as

zirconium, which are difficult to vaporize by thermal means.

In carrying out this work we have greatly benefited from daily contacts with Professors J.R. Brandenberger and J.N. Dodd, and Dr. L. Frasinski, whose help we gratefully acknowledge. We are also greatly appreciative of help in technical matters from Mr. C.H. Smith and in the construction of discharge tubes from Mr. K. Sumpter. The work has been generously supported by the Science and Engineering Research Council.

#### References

- [1] P. Hannaford and G.W. Series, *J. Phys. B* 14 (1981) L661.
- [2] P. Hannaford and G.W. Series, in preparation.
- [3] R.L. Fork, L.E. Hargrove and M.A. Pollack, *Phys. Rev. Lett.* 12 (1964) 705.
- [4] B. Decomps and M. Dumont, *C.R. Acad. Sci., Ser. B* 265 (1967) 249.
- [5] M. Dumont, *Phys. Rev. Lett.* 28 (1972) 1357.
- [6] J.N. Dodd, in preparation.
- [7] S. Büttgenbach, R. Dicke and H. Gebauer, *Phys. Lett.* 58A (1976) 56.
- [8] S. Büttgenbach, R. Dicke, H. Gebauer, R. Kuhn and F. Träber, *Z. Phys.* 286 (1978) 125.
- [9] E. Biemont, N. Grevesse, P. Hannaford and R.M. Lowe, *Astrophys. J.* 248 (1981) 867.
- [10] C.E. Moore, *Atomic energy levels*, NSRDS-NBS 35 (1971).
- [11] P.M. Sancho, *Anal. Soc. Esp. de Física y Química (Madrid)* 30 (1932) 867.
- [12] C.C. Kiess and H.K. Kiess, *Bur. Std. J. Research* 6 RP 296 (1931) 621.



# Determination of Hyperfine Structures in Ground and Excited Atomic Levels by Level-Crossing Optogalvanic Spectroscopy: Application to $^{89}\text{Y}$

P. Hannaford<sup>(a)</sup> and G. W. Series

J. J. Thomson Physical Laboratory, University of Reading, Whiteknights, Reading RG6 2AF, England

(Received 9 February 1982)

This new technique in optogalvanic spectroscopy yields Doppler-free resonances when degeneracies in atomic energy levels are removed by a magnetic field, and also when the interval between levels matches the mode spacing of the laser.  $g_J$  factors and magnetic hyperfine interaction constants were determined for lower and upper levels of the transition at 619.2 nm in YI. The value  $A = (+)89.6(9)$  MHz for the upper level  $4d5s(a^3D)5p^2D_{3/2}^0$  is new; the remaining determinations agree with published values.

PACS numbers: 32.60.+i, 32.80.Bx, 32.90.+a

The change in impedance of a gas discharge caused by irradiation of the plasma with laser light tuned to some atomic transition (the optogalvanic effect) has become an important and sensitive technique for detecting atomic transitions in laser spectroscopy.<sup>1</sup> It has recently been demonstrated that a change in the optogalvanic signal accompanies the removal, by a small magnetic field, of the *zero-field degeneracy* of Zeeman levels.<sup>2</sup> We report here the location of *level crossings at finite fields* by the observation of changes in the optogalvanic signal as a function of applied magnetic field. The direction of the magnetic field must be crossed with (or oblique to) the direction of polarization of the laser light.

We apply the phenomenon as a new Doppler-free technique to the determination of hyperfine structures in both ground and excited atomic levels. The experiments were carried out on the  $4d5s^2-^2D_{3/2}-4d5s(a^3D)5p^2D_{3/2}^0$  619.2-nm transition in atomic yttrium.

The laser is tuned to some frequency within the Doppler absorption profile of the transition. Both upper and lower states have hyperfine structures much smaller than the Doppler width: Both structures undergo decoupling in the magnetic field, and crossings between hyperfine levels occur for the upper and for the lower states. At values of the magnetic field where crossings occur between levels differing by  $\pm 2$  in  $m$  quantum number, the

laser light coherently couples one lower level with a pair of upper levels or one upper level with a pair of lower levels. The coherence is lost as the degeneracy is removed and the total population of the upper level changes provided the interaction is nonlinear.<sup>3,4</sup> The change of total population leads to a change in optogalvanic signal.<sup>2,5,6</sup> Two types of interaction have been distinguished as contributing to the change of population: A "population effect" whose width depends on the spectral width of the laser if that is larger than the homogeneous width of the atomic transitions (as it is in our experiments) and a "Zeeman coherence effect," whose width represents the combined homogeneous widths of the upper and lower levels. In our experiments we did not undertake an analysis of the line profile into these components, but we obtained evidence of their separate contributions.

The 619.2-nm yttrium line was chosen for initial investigation because it is a relatively strong transition based on the ground state and lying within the tuning range of rhodamine 6 G, and because the Zeeman energy-level structure is particularly convenient: Over the range of magnetic fields 0–120 G, two crossings having  $|\Delta m| = 2$  occur in the ground levels and two in the excited levels. Furthermore, the optogalvanic signals were found to show a strong zero-field level-crossing resonance. The spectroscopic data for the system are summarized in Table I.

The yttrium atoms were sputtered from a cathode of naturally occurring yttrium (100% <sup>89</sup>Y) into a discharge maintained in argon at a pressure

of about 1 Torr. The discharge current was about 5 mA and the optogalvanic signals typically 10  $\mu$ A in the sense of enhancing the discharge current. Stray magnetic fields were reduced to less than 20 mG. The laser was a cw tunable laser running multimode at a power density of about 30 mW mm<sup>-2</sup> distributed over all modes. The width of the individual modes (5–7 MHz) was greater than the pressure-broadened width of the upper level ( $\approx 2$  MHz) but much less than the Doppler width ( $\approx 600$  MHz). The separation of longitudinal modes was determined to be  $401 \pm 2$  MHz.<sup>13</sup> The resonances were detected by modulating the magnetic field in addition to chopping the laser beam, and by tuning the phase-sensitive detector to the difference of the two modulation frequencies.

Six resonances, of which one is illustrated in Fig. 1, were found between 0 and 160 G, and a question of identification arises. We shall show later that the four resonances below 150 G correspond to the positions of the level crossings and serve to determine the values of  $|A/g_J|$  ( $A$  is the magnetic dipole hyperfine interaction constant). The two resonances above 150 G, which were weaker than the other four, derive from interaction of the atoms with more than one longitudinal mode of the laser and are similar to the multimode saturation resonances found in the optogalvanic signals from transitions in Zr.<sup>13</sup> Taken together, the six resonances (i) provide internal checks on the interpretation and (ii) determine separately the  $A$  and  $g_J$  factors of the upper and lower states.

We draw attention to the steepness of the cen-

TABLE I. Spectroscopic data for the 619.2-nm transition in <sup>89</sup>YI ( $I = \frac{1}{2}$ ).

	Term	Wave number (cm <sup>-1</sup> )	Radiative lifetime (ns)	$g_J$	$A$ (MHz)
Ground state (a)	$4d5s^2 2D_{3/2}$	0	...	0.798(2) <sup>b</sup> 0.799 27(1.1) <sup>c</sup> 0.800(8) <sup>d</sup>	-57.217(15) <sup>e</sup> (-)57.2(5) <sup>d</sup>
Excited state (z)	$4d5s(a^3D)5p^2D_{3/2}^0$	16 146	175(10) <sup>a</sup>	0.797(3) <sup>b</sup> 0.801(8) <sup>d</sup>	$\approx (+)100$ <sup>f</sup> (+)89.6(9) <sup>d</sup>

<sup>a</sup>Ref. 7.

<sup>b</sup>Ref. 8.

<sup>c</sup>Ref. 9.

<sup>d</sup>This work.

<sup>e</sup>Ref. 10.

<sup>f</sup>Estimated (Ref. 11) from measured hyperfine splitting in  $z^2D_{5/2}^0$  state assuming  $A(z^2D_{3/2}^0)/A(z^2D_{5/2}^0)$  to be the same as that of the corresponding states in scandium (Ref. 12).





FIG. 1. Field-dependent optogalvanic signal showing the level-crossing  $B_1^a$  in the lower ( $a^2D_{3/2}$ ) state of the transition 619.2 nm in  $^{89}\text{Y}$ . Magnetic field modulation. The derivative signal appears on a sloping background, representing the direct effect of the magnetic field on the discharge current. The amplitude of the level-crossing signal represents a change of about 1.5% in the optogalvanic current.

tral portion of the experimental curve in Fig. 1, which, considered in relation to the outer portions, echoes the characteristically pointed shape of the zero-field resonances in Zr.<sup>2</sup> This feature is consistent with the superposition of a narrow Zeeman-coherence resonance on a broader population-effect resonance. The full width at half height is about 7 G (8 MHz), which is comparable with the width of individual modes of the laser, but very much less than the Doppler width.

We identify the first four resonances in Table II as two related pairs of level-crossing resonances because the ratio of the fields at which these resonances occur is 0.748 for the first pair and 0.743 for the second, and these values are satisfactorily close to the value  $5^{1/2}/3 = 0.745$  predicted by the Breit-Rabi formula for  $|\Delta m| = 2$  level

crossings in systems having  $J = \frac{3}{2}, I = \frac{1}{2}$ . The values of  $|A/g_J|$  deduced from the positions of the first pair of resonances are essentially the same as the accurately known value of  $|A/g_J|$  for the  $a^2D_{3/2}$  ground state<sup>9,10</sup> (Table II), and we identify this pair,  $B_1^a$  and  $B_2^a$ , as level crossings arising from the ground state. The second pair of resonances,  $B_1^z$  and  $B_2^z$ , we attribute to level crossings in the  $z^2D_{3/2}^0$  excited state. This interpretation was confirmed by the results of *fluorescence studies* under the same conditions: Each member of the second pair of resonances could be analyzed into two superimposed components, one of which inverted with change through  $\pi/2$  of the polarizer. This behavior is characteristic of the fluorescence from excited atoms *aligned* by irradiation with linearly polarized light. The component which did not invert under rotation of the polarizer is attributable to the effect of irradiation on the *combined population* of the crossing levels.

We identify the pair of high-field resonances (near 150 G) as multimode saturation resonances because the fields at which they occur correspond to Zeeman splittings which match very closely the mode separation of the laser ( $401 \pm 2$  MHz). (This analysis was performed by using our determined values of  $|A/g_J|$  and  $g_J$  factors obtained from other sources<sup>8,9</sup>.) The first member of this pair,  $B_3^z$ , arises from the splitting of the  $F = 1, m = \pm 1$  levels in the excited state, and the second,  $B_3^a$ , from the splitting of the corresponding levels in the ground state. The identification of these resonances as multimode saturation resonances is further supported by the observation that they vanish when the laser is stabilized so as to lengthen appreciably the time between mode hops. Addi-

TABLE II. Observed positions of level crossing (LC) and multimode (MM) saturation resonances in the 619.2-nm optogalvanic signal from  $^{89}\text{Y}$ .

Position (G)	Ratio	$ A/g_J $ (MHz)		$\Delta\nu^b$ (MHz)	Identification <sup>c</sup>
		This work	ABMR <sup>a</sup>		
57.2(5) }	0.748(8)	71.6(6)	71.59(2)		LC $B_1^a$
76.5(5) }		71.4(4)	71.59(2)		LC $B_2^a$
89.2(5) }	0.743(7)	111.7(6)	...		LC $B_1^z$
120(1) }		112.0(9)	...		LC $B_2^z$
150.5(1.0)				399(3)	MM $B_3^z$
157(1)				401(5)	MM $B_3^a$

<sup>a</sup>Atomic-beam magnetic resonance studies; Refs. 9 and 10.

<sup>b</sup>Frequency of Zeeman splitting at position of observed resonance; determined with use of  $|A/g_J|$  values from column 3 and  $g_J$  factors from Refs. 8 and 9.

<sup>c</sup>Superscript  $a$  refers to ground state, and  $z$  to excited state.

tional multimode resonances corresponding to  $|\Delta m_J| = 2$  within the  $F = 2$  complexes would have been expected at higher fields, but this region was not explored. Resonances  $|\Delta m_J| = 2$  between  $F = 1$  and  $F = 2$  were expected near 145 G (lower level) and 119 G (upper level). There was, indeed, evidence of a weak resonance near 145 G, but this was not investigated in detail. The resonance near 119 G would have been obscured by the level crossing  $B_2^z$ .

From the measured positions of the six identified resonances (Table II) we determine the  $A$  factors of the excited and ground levels directly by setting the Breit-Rabi expression for the splitting of the Zeeman  $F = 1, m = \pm 1$  levels at  $B_3$  equal to the mode separation of the laser, i.e.,  $A[4x_3 - (1 - x_3 + x_3^2)^{1/2} + (1 + x_3 + x_3^2)^{1/2}] = 401$  MHz, where  $x_3 = 5^{1/2}B_3/4B_1$  or  $3B_3/4B_2$ . We note that the  $A$  factors determined in this way depend only on the ratio of pairs of magnetic field values and on the frequency difference between adjacent modes of the laser. In particular, they do not rely on prior knowledge of  $g_J$ , and the accuracy is determined by the accuracy with which ratios of magnetic field values have been measured, not absolute values.

Mean values of the  $A$  factors, together with the  $g_J$  factors which the analysis also yields, are presented in Table I. The sign of the  $A$  factor for the  $a^2D_{3/2}$  ground state is known to be negative from atomic-beam magnetic resonance studies.<sup>10</sup> As for the  $z^2D_{3/2}^0$  excited state, we note that in scandium, for which the term structure closely resembles that of yttrium, the  $A$  factor of the corresponding  $3d4s(a^3D)4p^2D_{3/2}^0$  level has opposite sign to the  $3d4s^2D_{3/2}$  ground level; also note that the fine-structure splitting of the yttrium  $z^2D_{3/2, 5/2}^0$  states is inverted, whereas that for the  $a^2D_{3/2, 5/2}$  states is normal. The  $A$  factor for the yttrium  $z^2D_{3/2}^0$  level is therefore very likely to be positive.

Our  $A$  factor for the  $a^2D_{3/2}$  ground state is in good agreement with the very accurate atomic-beam magnetic resonance result of Fricke, Kopfermann, and Penselin<sup>10</sup> (Table I). The value for the  $z^2D_{3/2}^0$  state appears to be the first reported measurement for that level. It is fairly close to

a value estimated by Kuhn and Woodgate<sup>11</sup> from their measured  $A$  factor for the  $z^2D_{5/2}^0$  state, assuming a value of  $A(z^2D_{3/2}^0)/A(z^2D_{5/2}^0)$  found for the corresponding states in scandium.<sup>12</sup>

We conclude that level-crossing optogalvanic spectroscopy offers a new high-resolution spectroscopic technique for determining hyperfine structures in both excited and ground atomic levels. When the exciting laser is run multimode and the frequency separation of the modes is known accurately, the technique can yield hyperfine interaction constants independently of the Landé  $g_J$  factors, and only relative values of the magnetic fields need to be determined accurately.

It is a pleasure to acknowledge stimulating conversations with and practical help from Professor J. R. Brandenberger, Professor J. N. Dodd, and Dr. L. Frašinski, and also from Mr. C. H. Smith and Mr. K. Sumpter. The work has been generously supported by the Science and Engineering Research Council (U.K.).

<sup>(a)</sup>On leave from Division of Chemical Physics, Commonwealth Scientific and Industrial Research Organization, Clayton 3168, Australia.

<sup>1</sup>J. E. M. Goldsmith and J. E. Lawler, *Contemp. Phys.* **22**, 235 (1981).

<sup>2</sup>P. Hannaford and G. W. Series, *J. Phys. B* **14**, L661 (1981).

<sup>3</sup>B. Decomps, M. Dumont, and M. Ducloy, in *Laser Spectroscopy of Atoms and Molecules*, edited by H. Walther (Springer, Berlin, 1976), p. 283.

<sup>4</sup>C. Cohen-Tannoudji, in *Frontiers in Laser Spectroscopy*, edited by R. Balian, S. Haroche, and S. Liberman (North-Holland, Amsterdam, 1977), p. 3.

<sup>5</sup>N. Beverini and M. Inguscio, *Lett. Nuovo Cimento* **29**, 10 (1980).

<sup>6</sup>J. N. Dodd, to be published.

<sup>7</sup>P. Hannaford and R. M. Lowe, to be published.

<sup>8</sup>J. R. McNally and G. R. Harrison, *J. Opt. Soc. Am.* **35**, 584 (1945).

<sup>9</sup>S. Penselin, *Z. Phys.* **154**, 231 (1959).

<sup>10</sup>G. Fricke, H. Kopfermann, and S. Penselin, *Z. Phys.* **154**, 218 (1959).

<sup>11</sup>H. Kuhn and G. K. Woodgate, *Proc. Phys. Soc., London, Sect. A* **63**, 830 (1950).

<sup>12</sup>H. Kopfermann and E. Rasmussen, *Z. Phys.* **92**, 82 (1934).

<sup>13</sup>P. Hannaford and G. W. Series, to be published.



# Laser spectroscopy\*

G W SERIES

Raman Visiting Professor, Indian Academy of Sciences, Bangalore 560 080

**Abstract.** Lasers arrived in 1960, but systematic spectroscopy with lasers had to wait for the discovery of the tunable variety, nearly ten years later. Then came an explosion of activity out of which some representative examples are assembled here. Doppler-free techniques and their application to the fine structure of hydrogen are important instances of ultra-high resolution work using highly-stabilised lasers and of the contributions of laser spectroscopy to fundamental physics. Measurement of the *frequency* of visible light leads inexorably to the fixing of a value for the speed of light and to the declaration that an independent standard of length shall no longer be necessary. The tunable variety of short-pulse laser extends the bounds of quantum-beat spectroscopy, while the combination of ion-detectors with tunable lasers allows the study of very highly excited, bound states and resonant structures above the series limit for atoms in strong magnetic fields. The review concludes with an account of a newly-discovered, Doppler-free effect, not yet fully understood.

## 1. Introduction

It was the invention of *tunable* lasers towards the end of the nineteen sixties<sup>(1)</sup> that brought lasers into the service of spectroscopy. The reader will recall that 'optical masers' had already been in existence for nearly a decade<sup>(2)</sup>, but that, during those years, the lasers that were available emitted light of some fixed frequency, determined by the energy level structure of whatever kind of atom or ion or molecule formed the 'active medium' of that particular laser. And what kind of spectroscopy can be done with a set of randomly-assorted, fixed-frequency oscillators?

It must be said at once that there is, indeed, one branch of spectroscopy, and a very important branch, that *can* be done with a strong monochromatic source of light of no particular frequency (though the bluer the better), and that is Raman spectroscopy. A new lease of life was granted to Raman spectroscopy by the powerful lasers that came to birth in the nineteen sixties, particularly the argon ion laser, but that is a story we shall not concern ourselves with here. CARS (coherent anti-Stokes Raman scattering) was born in the nineteen sixties, together with the new science of nonlinear optics, but we are concerned with the systematic study of the spectral properties of matter, particularly atoms and molecules, and for that we can take the decade of the nineteen seventies as cradling the new science.

Recall what remarkable sources of light these lasers are: even a small inexpensive helium-neon laser is many thousands of times brighter than the Sun (power per unit area, per unit solid angle, per unit spectral range). They come continuous-wave,

---

\*This paper is based on lectures delivered by the author during his stay in India from October 1982–February 1983. This has since been published in *Contemp. Phys.* (1984) **25**, 3–29.

a few milliwatts of power, or pulsed, up to terawatts, with pulse duration down below picoseconds, if that's what you want. They come relatively crude in spectral purity, say, a few terahertz bandwidth, to the most refined, a few tenths of a kilohertz. And now, since about 1970, *tunable*. For some spectroscopic applications you need simply a bright, directional beam of light, and spectral purity is of no great importance. For others, spectral purity is of the highest importance. We shall give examples of both types of work. But whether spectral purity is needed, or brightness, to be able to change the wavelength continuously over an extended spectral range is a facility which converts a phenomenon of science into a science of phenomena.

## 2. Tunable dye lasers

The diagram (figure 1) will remind you of the *essential elements* of a tunable dye laser. We see light from an external source (usually a fixed-frequency laser) exciting broad-band fluorescence in a dye (in solution), the axially-emitted light being trapped between mirrors so that standing-waves may be formed for all wavelengths which lie within the resolution-band-width of the prism (or grating, which is more conventionally used). Actually, this spectral range is relatively coarse—typically 0.1 nm—and hundreds of thousands of discrete wavelengths satisfying the standing wave condition  $n\lambda/2 = \text{cavity length}$  may fall within it. It is usually desirable to reduce the number of these longitudinal modes, as they are called, to a few or to one in order to produce something approaching a monochromatic light source. This is done by introducing additional subsidiary cavities into the principal cavity (the space between the mirrors): only those modes survive which satisfy the standing wave condition for all the cavities simultaneously.

Of course, the laser emission does not come from the *spontaneously*-emitted fluorescent light, but from the *stimulated* emission resulting from the interaction between the standing waves in the cavity and the dye molecules which have been excited by the external source, provided a sufficient excess of them has been transferred to the upper state of the transition.

The tuning is achieved by rotating the prism to select radiations within the fluorescence-band of the dye, and the cavity-lengths must also be changed in proper co-

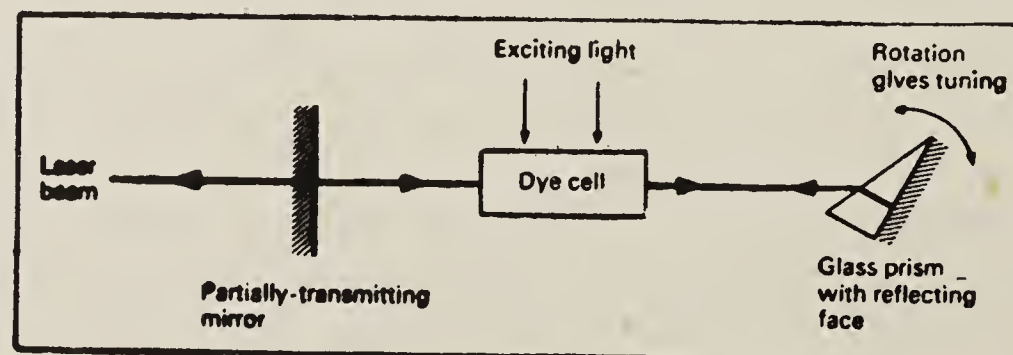


Figure 1. Schematic diagram of a tunable dye laser. Only the essential elements are illustrated here. See text.



ordination. The technical requirements for securing this for a single-mode laser are, as will be understood, very demanding.

### 3. Early applications to atomic hydrogen: Doppler-free techniques

The overall spectral width even of a multimode dye laser is substantially smaller than the width of spectral lines emitted from ordinary laboratory sources, so that as spectroscopic probes, tunable lasers offer themselves naturally for application in high resolution spectroscopy. In this field, the dominant contribution to the intrinsic width of spectral lines is Doppler broadening, resulting from the random motion of atoms in a light source. The elimination of Doppler broadening has been one of the major successes of laser spectroscopy. Of the variety of 'Doppler-free'-techniques which are commonly in use to-day, we shall describe two which were applied in the early nineteen seventies by Hänsch and Schawlow and their young colleagues at Stanford University to the study of that most important spectrum: the spectrum of atomic hydrogen<sup>(3)</sup>. For hydrogen more than for any other atom (since its mass is least) the problem of Doppler broadening is most severe: it has been, historically, the greatest obstacle to the spectral resolution of fine structure in the lines of the visible spectrum.

#### 3.1 Saturated absorption spectroscopy

At the top of figure 2 is a representation of an atom—one of an assembly in a gas in thermal equilibrium—moving with velocity  $v$  obliquely to a beam of laser light whose frequency, measured in the laboratory frame, is  $\omega$ . In the frame of the atom

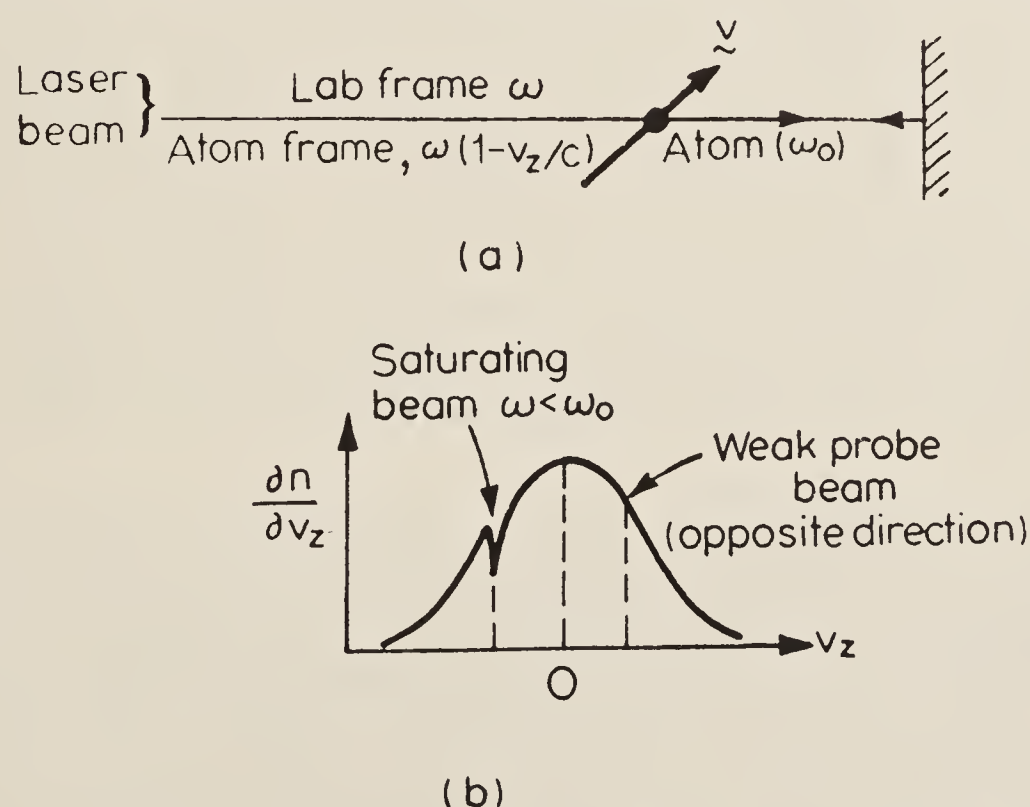


**Figure 2.** Diagram to illustrate velocity-selection by saturated absorption. (a) First-order Doppler effect for an atom moving obliquely to a laser beam. (b) Distribution of atoms by  $v_z$ , and showing the 'hole' burnt in the ground-state distribution by a laser beam tuned to resonance with obliquely-moving atoms, and sufficiently strong to excite a significant number of them.

# SATURATION SPECTROMETER

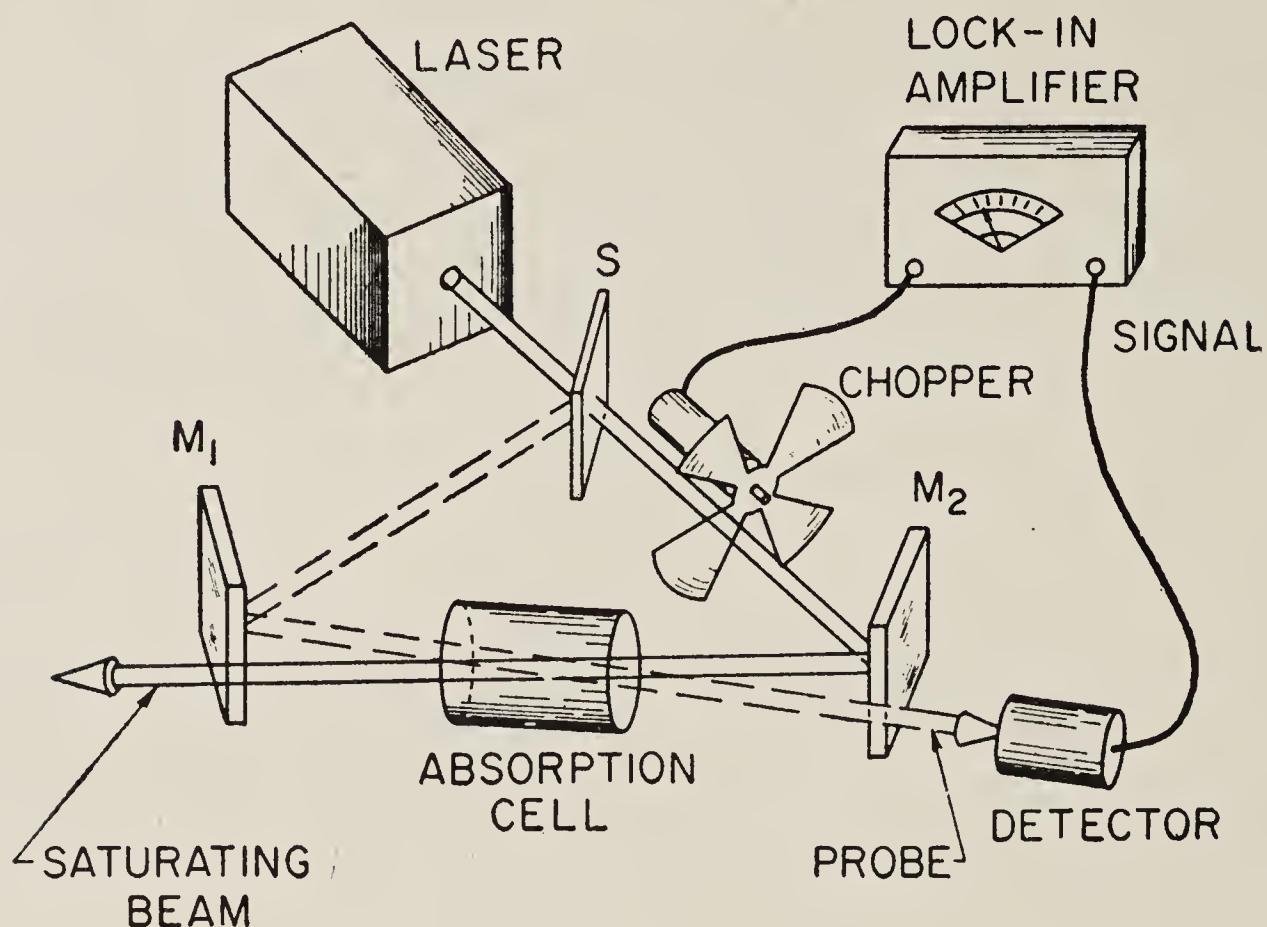


Figure 3. Schematic diagram of a saturation spectrometer, after Hänsch (ref. 3d).

the frequency appears to be  $\omega(1 - v_z/c)$  (first-order Doppler effect), where  $v_z$  is the component of  $v$  in the direction of the laser beam. Notice also that, for light travelling in the opposite sense, the frequency appears to be  $\omega(1 + v_z/c)$ . (The term of second order in the expansion,  $\frac{1}{2}(v_z/c)^2$ , is positive for both beams).

Now consider the one-dimensional velocity-distribution of atoms, a Gaussian, represented in the lower part of the figure. If the laser beam is tuned to an absorption resonance for obliquely moving atoms, and if it is sufficiently strong to excite a sufficient number of them (partial or complete saturation in absorption), the distribution will be depleted, as shown in the figure, for a range of velocities depending on the homogeneous width of the transition, the so-called 'natural' or radiative width, increased possibly by some pressure broadening, and by laser power broadening. But this width is typically about 100 times smaller than the width of the velocity distribution. One commonly speaks of 'burning a hole' in the velocity distribution.

The counter-propagating beam, of course, interacts with a different set of atoms, *unless the laser is tuned to that particular set which is moving transversely to the beam* ( $v_z \approx 0$ ), in which case both beams interact with the same atoms. Now, regard the counter-propagating beam as a probe of the velocity-distribution by measuring its intensity after it has traversed the gas. When the laser is tuned to the peak of the distribution the detector of the probe beam will register *increased* intensity. The spectral width over which this occurs will be the width of the 'hole' (approximately), many times narrower than the spectral width of the distribution, which is the Doppler width. We speak of a 'velocity-selective' technique, by which Doppler broadening has been eliminated.



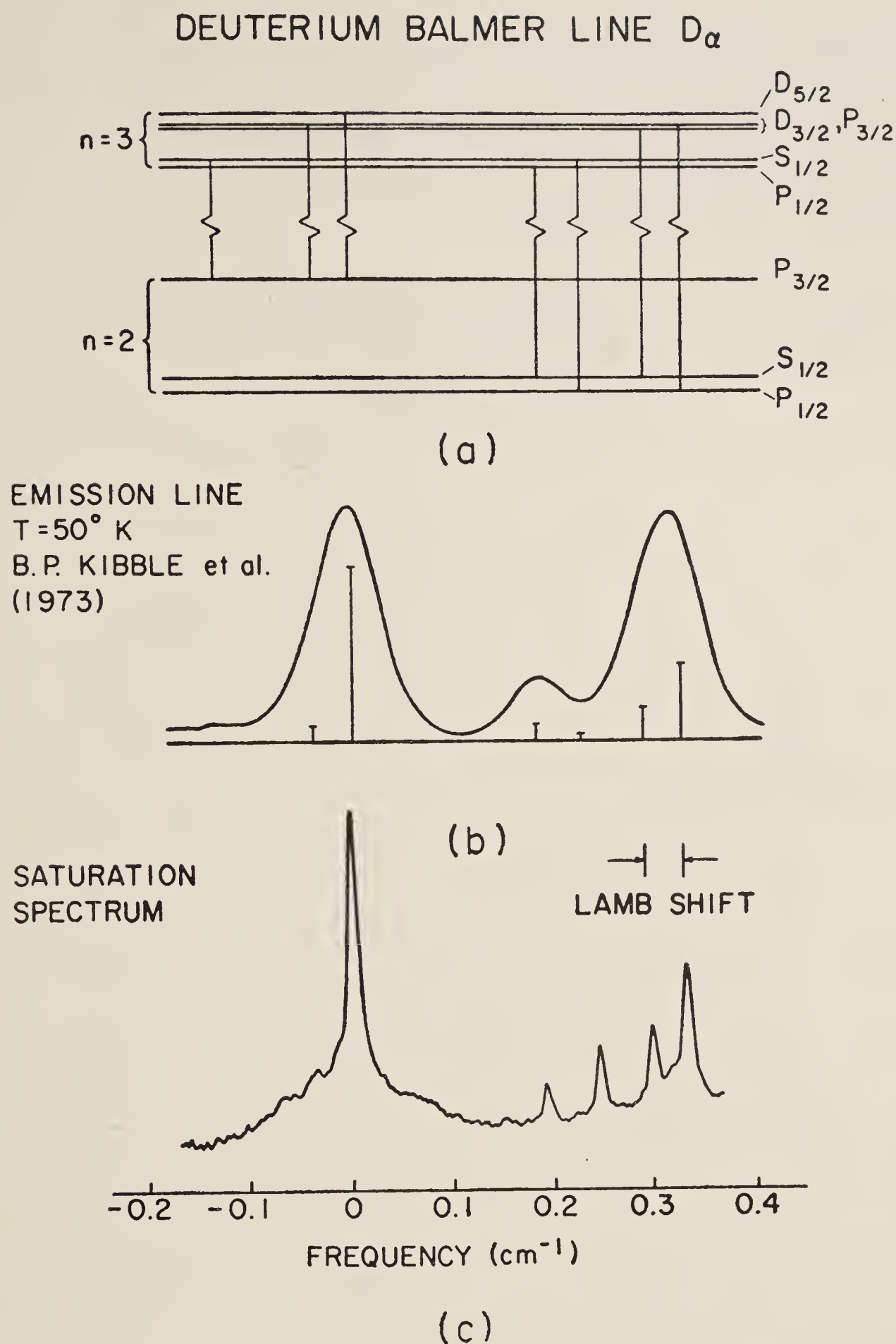


**Figure 4.** Fine structure of the Balmer- $\alpha$  line of atomic hydrogen (deuterium) (ref. 3d). (a) Term diagram showing fine structure of the levels  $n = 2$  and 3 and allowed transitions. (b) The experimental profile from a light source cooled by liquid helium, and the seven theoretically predicted components (ref. 4). (c) An early experimental result obtained by the saturation technique (ref. 3d).

3.1a *Application to hydrogen.* At the top of figure 4 is shown the theoretical fine structure of the famous Balmer- $\alpha$  line of atomic hydrogen, wavelength 656 nm, according to the Dirac theory supplemented by the 'Lamb-shift' corrections of quantum electrodynamics.

The middle part of the figure shows the spectral profile obtained in the most sophisticated of the many attempts to reduce Doppler broadening by cooling the light source—an experiment carried out by Kibble and colleagues<sup>(4)</sup> in 1972 in which an electrical discharge in hydrogen was cooled by liquid helium. Notice that only three resolved peaks are to be seen in the spectrum, whereas the theory predicts the occurrence of seven fine structure components.

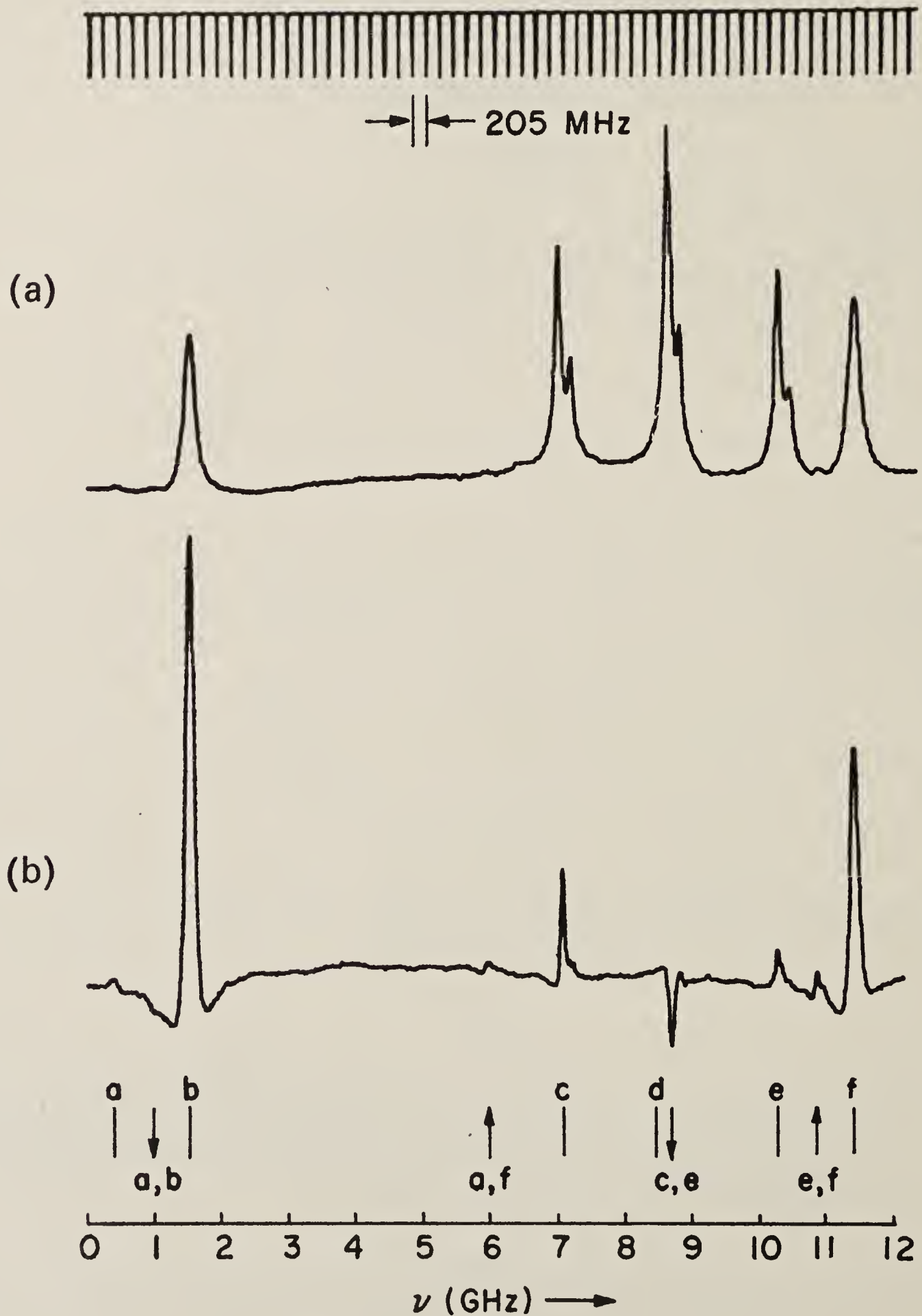


Figure 5. Velocity-selective spectra of the Balmer- $\alpha$  line (J. E. M. Goldsmith, Thesis, Stanford University, 1979). (a) Saturation spectrum obtained with stabilized, continuous dye laser. (b) Spectrum obtained by 'polarization spectroscopy'.



At the bottom of the figure is to be seen one of the first spectra obtained by the group at Stanford using saturated absorption spectroscopy. We notice immediately the increased sharpness of the peaks (though certainly not by as large a factor as we might have expected). We also notice that the relative heights of the peaks do not correspond with the predicted intensities of the components indicated in the middle part of the figure (in fact one of the peaks is called a 'crossover resonance': it occurs half-way between two others, and is a phenomenon frequently encountered in velocity-selective spectroscopy). This example serves to illustrate the point that in experiments relying on strong light fields, nonlinear effects are to be expected.

Figure 5 shows the improvement in reducing the width of the lines with development of the technique. The details need not concern us, but the implications of this reduction are far-reaching and take us into the realm of the fundamental constants of physics.

**3.1b The Rydberg constant: fundamental constants of physics.** It will be appreciated that the narrower the line, the more accurately can its wavelength be measured in relation to the primary standard of length. On the other hand, the wavelengths of the components of spectral lines of hydrogen can be related very easily to the energy levels predicted by Bohr's theory,  $-R/n^2$ , where  $R$  is the Rydberg constant,  $me^4/2\hbar^2$ , by making additions or subtractions corresponding to the fine-structure corrections to Bohr's theory. One can confidently use the theoretical values for these corrections since the fine-structure intervals have all been verified experimentally by radio-frequency spectroscopy. When these corrections have been made, we have a new, experimental determination of the combination of constants  $(me^4/4\pi\hbar^3c)(4\pi\epsilon_0)^{-2}$ . (The formula is here quoted in units of reciprocal length).

When 'recommended values' of the fundamental constants are prepared, the procedure is to use all available precision measurements of combinations of constants such as  $e/m$ ,  $h/e$ , and so on, including the Rydberg constant—in toto, an over-determined set—and to find least-squares solutions for values of the individual constants. In this procedure, the Rydberg constant has traditionally been the cornerstone: the most accurately-measured 'input' datum. But this position had been eroded in recent years, owing to improved values of other data. Now, with laser determinations of the Rydberg, its position of pre-eminence has been restored. The most recent determination by laser spectroscopy<sup>(5)</sup> (in this experiment velocity-selection was secured by an atomic beam, not by saturated absorption) has yielded the value  $R_\infty = 10\,973\,731.521(11)\text{ m}^{-1}$ , an accuracy of 1 part in  $10^9$ .

### *3.2 Two-photon spectroscopy*

Superficially, the experimental arrangement for this technique is similar to that used in saturated absorption spectroscopy, but the Doppler effect is eliminated in a way which allows *all* atoms in the sample to participate, irrespective of their velocity.

Consider atoms in a gas in random motion irradiated, as before, by opposing beams of laser light. In the atom frame the frequency of the light appears to be shifted, as before, by the factor  $(1 \pm v_z/c)$  figure (6a). But now, suppose the atoms absorb one photon from each beam. The increase in energy is  $\hbar\omega[(1 - v_z/c) + (1 + v_z/c)]$

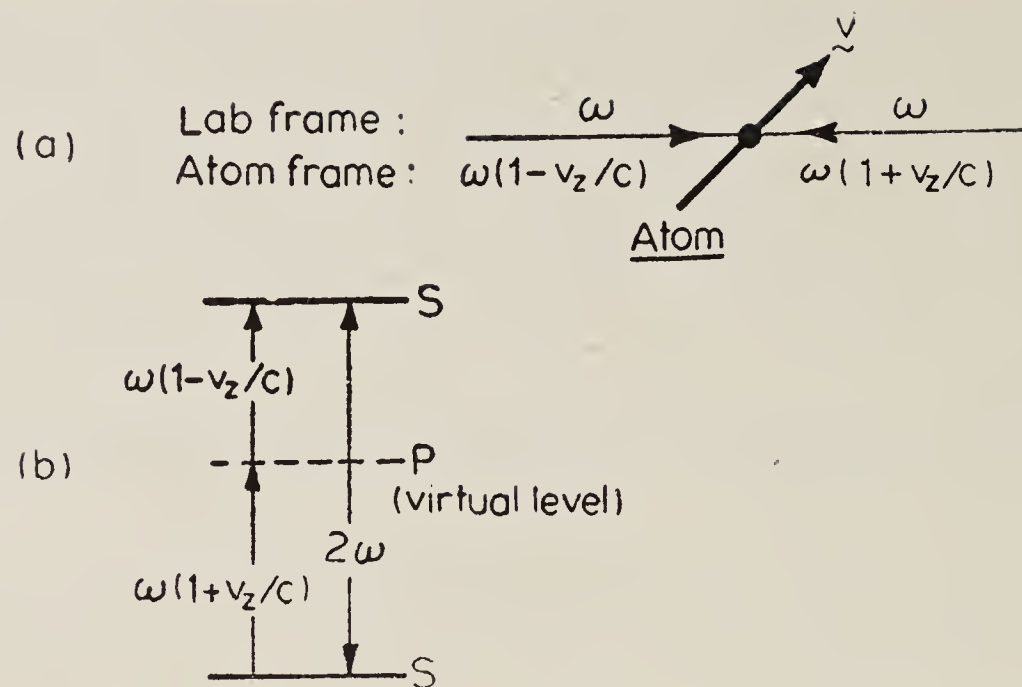


**Figure 6.** Two-photon absorption: elimination of Doppler effect in first-order. (a) Doppler-shifted frequencies seen by an atom moving transversely to a laser beam. (b) Absorption of one photon from each beam results in an increase of energy which is the same (to first-order in  $v_z/c$ ) for all atoms, independently of  $v_z$ .

$=2\hbar\omega$ , independent of  $v_z$  (to first order in  $v_z/c$ ). The possibility exists, therefore, for resonant absorption of light by all atoms in the assembly to a state energetically  $2\hbar\omega$  above the ground state. The selection rules governing this process are, of course, different from those governing a one-photon transition: in particular, the initial and final states must be of the same parity. The resonant absorption is detected by observing some convenient fluorescent radiation from the atoms, indicating spontaneous decay of the excited state.

**3.2a. Application to H: Lamb shift in the ground state.** Hänsch and his colleagues applied this technique to the study of the Lyman- $\alpha$  transition ( $n=1 \rightarrow 2$ ) in atomic hydrogen. The primary interest was to determine the Lamb shift of the ground state. Whereas the shift of the  $2S_{1/2}$  level can be determined by measuring the intervals  $2S_{1/2} - 2P_{1/2}$  or  $2S_{1/2} - 2P_{3/2}$  (which, of course, has been done by radio-frequency spectroscopy), there is no convenient level near to  $1S_{1/2}$  against which to determine its position. Two-photon spectroscopy allows the position of  $1S_{1/2}$  relative to  $2S_{1/2}$  to be obtained by measuring the wavelength of the Lyman- $\alpha$  transition.

They did not determine this wavelength against an external standard: rather, they used the special property of  $H$  that the  $n = 1 \rightarrow 2$  interval is, on Bohr's theory, exactly four times the  $n = 2 \rightarrow 4$  interval. They took a saturated absorption spectrum of the Balmer- $\beta$  line, using a laser tunable in the blue, and with this light, frequency-doubled, were able to excite the two-photon spectrum of Lyman- $\alpha$ . Figure 8 shows the two spectra, together with calibration fringes from which the spectral interval between components of Balmer- $\beta$  and Lyman- $\alpha$  could be determined. Knowing the frequency of Balmer- $\beta$  by use of the previously-measured Rydberg constant, and applying corrections for the fine structure of Balmer- $\beta$ , the wavelength of Lyman- $\alpha$  could be found and the Lamb shift of the ground state (its true position relative to the position predicted by Dirac's theory) determined. The value obtained,  $8161 \pm 29$  MHz, was about 40 times more accurate than the value Herzberg had obtained twenty years earlier by conventional spectroscopy. The importance of the new mea-



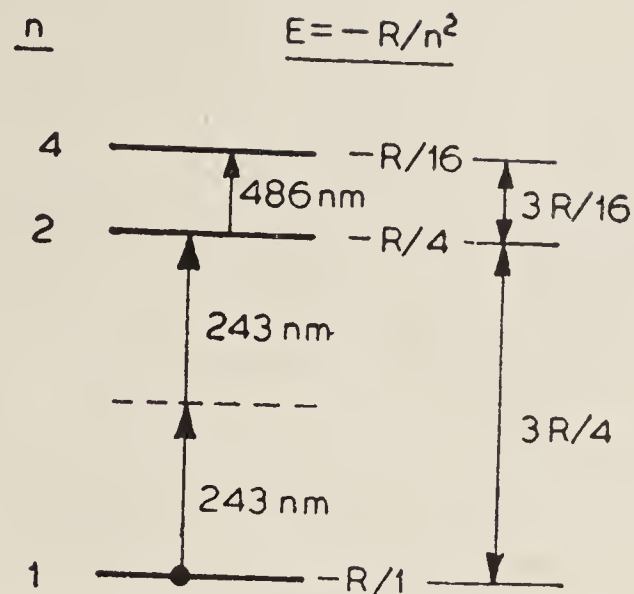


Figure 7. Energy levels of hydrogen disregarding fine structure and Lamb shifts.

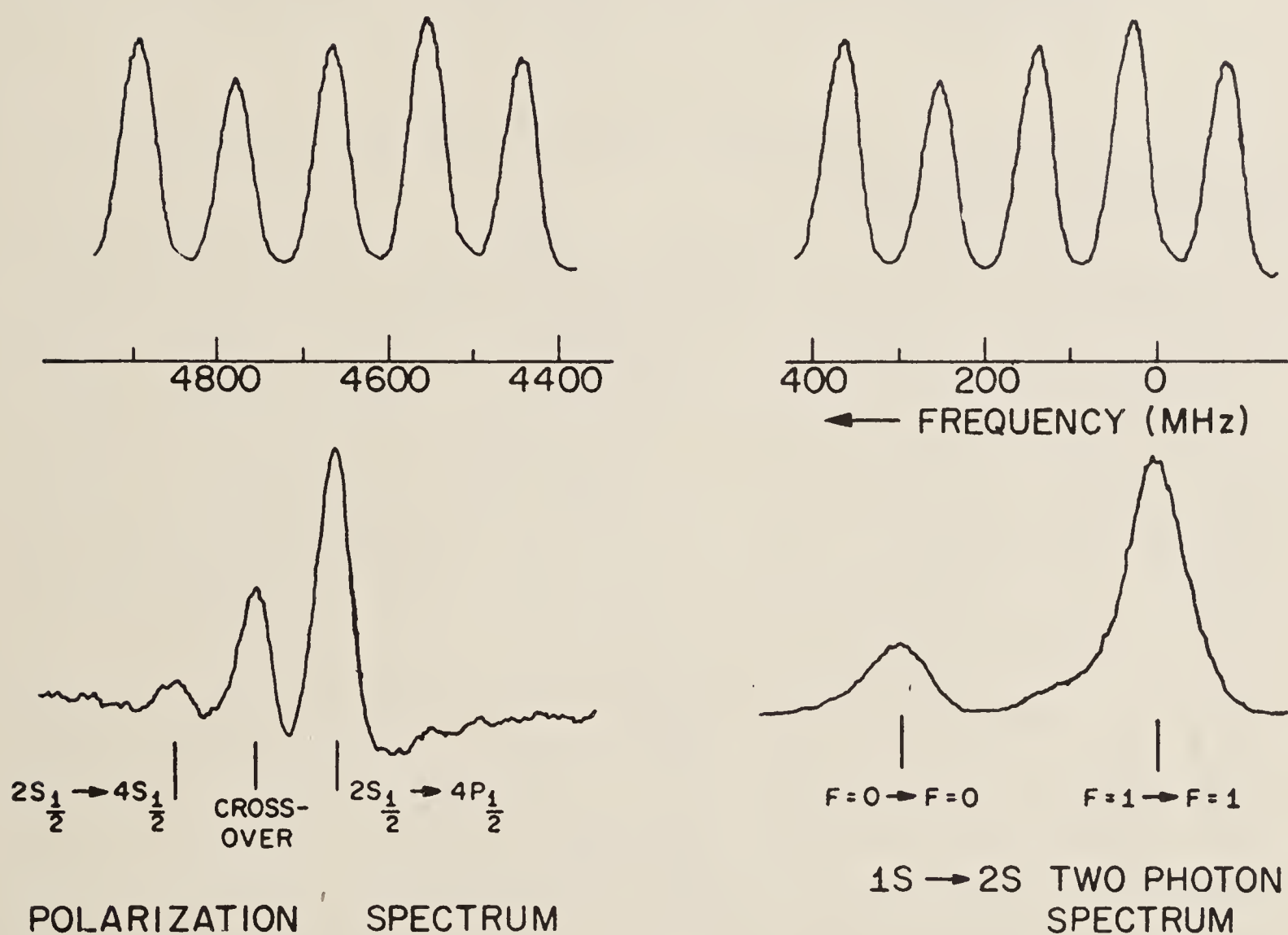


Figure 8. Simultaneous scan of velocity-selective (polarization) spectrum of Balmer- $\beta$  and two-photon spectrum of Lyman- $\alpha$  (C. Wieman, Thesis, Stanford University, 1976). Wavelength markers, seen at the top, are obtained by means of an interferometer, and used to construct the scale of frequency. The two peaks seen in the Lyman- $\alpha$  spectrum represent hyperfine structure, arising mainly from the structure in the ground state.

surement will be realised when it is recalled that the Lamb shift in the ground state is the largest of all such shifts in hydrogen.

The reader will have noticed two peaks in the Lyman- $\alpha$  spectrum. This is hyperfine structure whose magnitude may be read from the frequency scale: about  $4 \times 350$  MHz. It arises from the splitting of the ground state. This is the interval

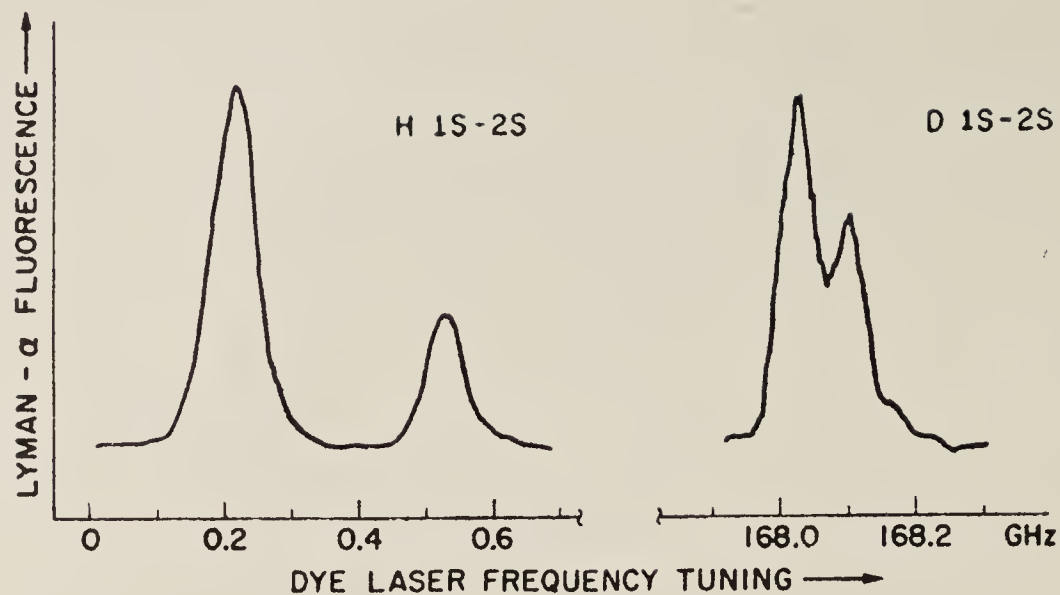


Figure 9. Isotope shift between hydrogen and deuterium in Lyman- $\alpha$  (S. A. Lee, Thesis, Stanford University, 1975). The hyperfine structure is different in the two cases (ref. 3c).

that forms the basis of the hydrogen maser: it corresponds to the famous 21 cm line of the radio-astronomers.

**3.2b Application to H and D: isotope shift.** In figure 9 is seen the two-photon spectrum of Lyman- $\alpha$  for hydrogen compared with the similar spectrum for deuterium: the two were taken in succession by tuning the laser over a range of about 700 GHz. Both spectra show hyperfine structure, different in the two cases, but the more significant feature is that the experiment allows a measurement of *displacement* between the two. This is the spectroscopic isotope shift which, in the case of hydrogen, is almost entirely due to the difference in nuclear *masses*. We recall that the Rydberg constant which governs the two spectra contains as factor the reduced electron mass,  $mM/(m + M)$ , where  $M$  is the nuclear mass. The measured isotope shift between hydrogen and deuterium is simply related to the ratio (electron mass)/(proton mass), and can be used to determine this ratio.

The first measurement of Hänsch and his colleagues yielded a value for the ratio  $m/M_p$  about as good as the value obtained from determinations by mass spectroscopy. But the two-photon determination is, in principle, capable of refinement by many orders of magnitude because the radiative line width of the transition (determined by the reciprocal of the radiative lifetime of the metastable upper state) is only about 10 Hz. Many technical difficulties remain to be overcome before this limit is approached, but an improvement in accuracy of the measurement of the isotope shift by a few orders of magnitude would establish the laser spectroscopic method as competitive with other high precision measurements of  $m_e/M_p$  which are at present being undertaken <sup>(3e)</sup>. Work on the spectroscopic method is continuing at Stanford.

Three important quantities of atomic physics—the Rydberg constant, the Lamb shift of the ground state of H, and the  $m/M_p$  ratio—yielded to the new spectroscopic techniques within a few years of their invention. This impressive tally gave enormous encouragement to those physicists and chemists whose eyes were beginning to open to the possibilities of spectroscopy with tunable lasers.



#### 4. The frequency of visible light

We break away from tunable lasers for a while to review some remarkable work that has been accomplished using fixed-frequency lasers, namely, to measure the *frequency* of visible light. The reader may have remarked that the word *wavelength* has generally been used till now in this article to characterize the radiation from a laser.

Measurement of frequency at a level comparable with the reproducibility of the primary standard of frequency (say, a few parts in  $10^{13}$ ) demands a highly stable

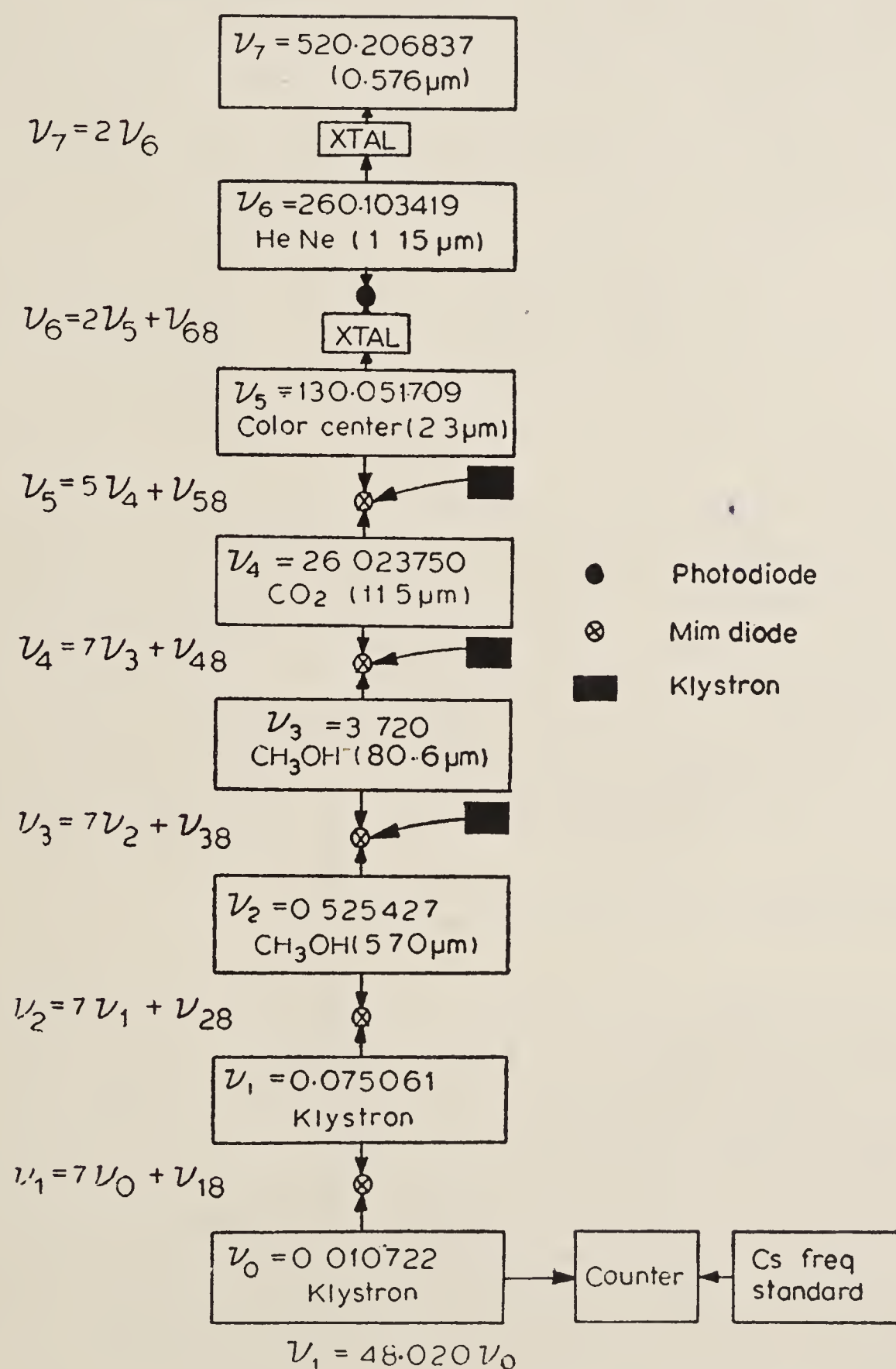


Figure 10. Proposed chain of highly stable laser and klystron oscillators linking visible light (576 nm; 520 THz) with the primary standard of frequency (0.00919 THz). (From Evenson, in Laser Spectroscopy V).

source. Narrow, Doppler-free resonances in selected molecules have been used to energise elaborate electronic feed-back mechanisms which control the cavity length of lasers and lock the frequency of radiation from the laser to that of the molecular transition. Figure 10 indicates schematically how a carefully-chosen set of such stabilised lasers might be used to construct a chain linking the highest frequency oscillator (orange light has a frequency about  $5 \times 10^{14}$  Hz) to the primary standard (the caesium clock, about  $10^{10}$  Hz). At the lower end of the chain are klystrons, then a variety of lasers through the infrared, to the visible. The standard techniques of frequency comparison are used: frequency multipliers (nonlinear crystals in the optical region) and nonlinear mixers which produce a beat at a directly measurable (GHz) frequency between the higher frequency oscillator and some harmonic of the oscillator next below it. The frequency of each oscillator is related to the frequency of the next by relations such as  $f_{\text{higher}} = nf_{\text{lower}} \pm f_{\text{beat}}$ , where  $n$  is an integer. If all the oscillators could be made to work at the same time (a very demanding technical operation) the frequency of visible light could be determined with an accuracy limited only by the reproducibility of the primary standard.

A number of such chains have been proposed<sup>(6a)</sup> and some will, no doubt, shortly be put into operation. Lasers in the near infrared have already been linked directly with the primary standard. For the visible, it has not yet proved possible to run the chains with all elements linked simultaneously and the full accuracy attainable by phase-locked operation of a complete chain has not yet been achieved: nevertheless, the reported frequency of 473 THz (wavelength 633 nm) for radiation from a helium-neon laser, locked onto a particular absorption feature in the spectrum of molecular iodine, has been quoted with an accuracy of 1.6 parts in  $10^{10}$  (ref. 6b). The success of this work depends very largely on being able to construct nonlinear devices capable of producing a measurable (THz) beat frequency from the mixing of different laser beams: such detectors have been realised in the junction between extremely fine-tipped tungsten wires and the oxide layer on a flat, nickel base—a modern version of the ‘cat’s whisker’ rectifiers used in early wireless receivers. The reader should reflect on the stability required of independently-operating lasers if their difference in frequency is to be measurable at all.

#### 4.1 *The speed of light and the standard of length*

If the *frequency* of light from a laser be measured against the primary standard, and also the *wavelength* against the primary standard of *length*, we have a determination of the speed of light. But in this latter measurement, the differences in the nature of radiations being compared is to be understood: the laser light very highly monochromatic (frequency uncertainty, a few kHz) and the light from the krypton standard (a specially-constructed, but essentially conventional gas discharge tube) exceedingly impure by comparison (frequency spread, hundreds of MHz). The uncertainty in the determination of wavelength of the laser light arises not from shortcomings of the technique of comparison but from the uncertainty of the standard of length itself.

In these circumstances the obvious course of action for those concerned with measurements of length at the highest level of accuracy was to abandon the krypton



source and to replace it by a stabilized laser source. Internationally agreed wavelengths for light from iodine-stabilized and methane-stabilized helium-neon lasers have been in use in standards laboratories for over a decade.

And now, with measurements of *frequency* available with accuracy several orders of magnitude better than the *wavelengths* could possibly be determined against the metre (the krypton standard), the next logical step has been accepted: *fix the value of the speed of light* at some agreed number (chosen to secure consistency with wavelength determinations, admittedly crude) and abandon the notion of a primary standard of length. Henceforward, distances at the highest level of accuracy will be measured by reference to a primary standard of time (or frequency) and by use of a fixed number,  $299\,792\,458\text{ ms}^{-1}$ , the agreed speed of light in free space, to convert a time interval to a length interval. It is planned that international agreements on these lines be adopted at the Conference Générale des Poids et Mesures in October 1983.

This does not imply that scales and length gauges are to be abandoned. They will continue to be used for purposes for which they were made—day-to-day comparisons of like with like. But, lest there be some disquiet at the abandonment of an independent standard of length, let us recall that this does conform with current practice in navigation (radar) and in surveying (geodimeter), and that astronomers have been measuring distances in light-years for a century. The primary purpose of meteorological standards is to satisfy a practical need.

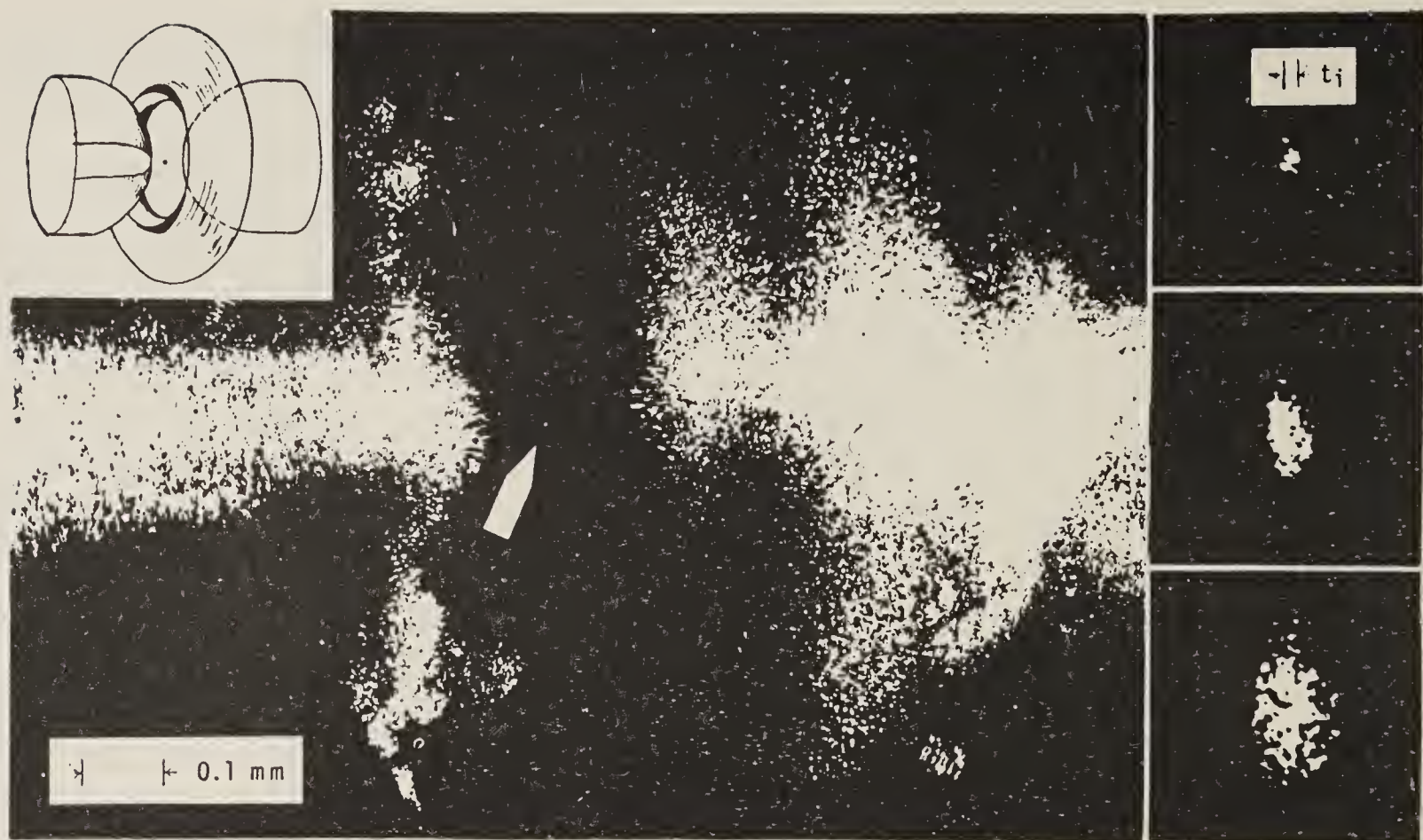
#### 4.2 *Frequency standards: outlook for the future*

Some remarkable experiments that have actually been performed with highly stabilized, tunable lasers point to the possibility of a frequency standard of the future several orders of magnitude more sharply defined than is the caesium clock. The reproducibility of this, the present standard, of the order of 1 part in  $10^{13}$ , depends on the ratio of the frequency (about 10 GHz) to the resonance line-width. This is the inverse of the interaction time (of the order of ms) between the Cs atoms in the beam and the r.f. fields which drive the resonance. Experiments on the fluorescence of single ions under irradiation by laser light have demonstrated continuous interaction for times of the order of 100 seconds. If the laser could be locked on to the atomic resonance we can envisage a frequency standard with a spectral purity some small fraction of 1 Hz at a frequency above  $10^{14}$  Hz; reproducible therefore at a level approaching parts in  $10^{18}$ .

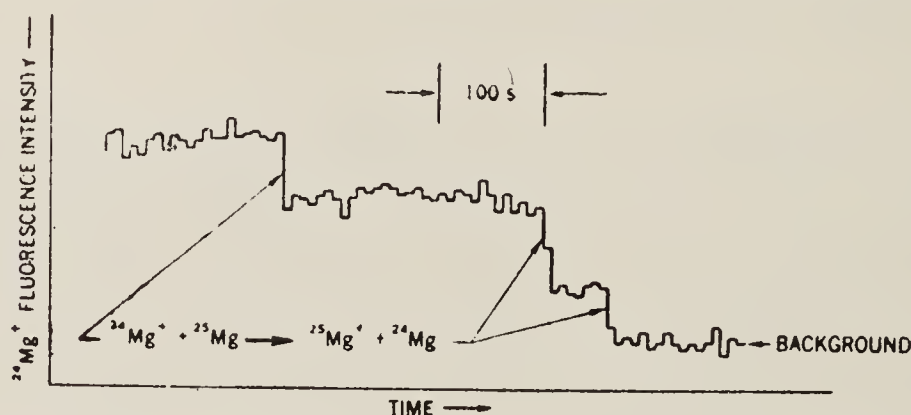
Let us not speculate too freely, but look at what already has been achieved. Figure 11 is a photograph of *fluorescence from a single ion*. The ion is confined in a radio-frequency quadrupole trap illustrated in the upper part of the figure and irradiated with laser-light: the irregular patches in the photograph represent light scattered from the stainless steel of the trap.

Figure 12 provides evidence that it is indeed single ions that are responsible for the fluorescence, and indicates the time intervals over which such fluorescence has been observed. (The two figures have deliberately been chosen to illustrate different experiments—fig. 11 represents  $\text{Ba}^+$  and fig. 12,  $\text{Mg}^+$ —in order to emphasize that the phenomenon is reproducible). In figure 12 the fluorescence intensity from  $^{24}\text{Mg}^+$  is plotted against time. The level of intensity changes abruptly from time to time as





**Figure 11.** Fluorescence from a single ion of  $\text{Ba}^+$ . The white arrow points to the image of an ion trapped in the r.f. quadrupole apparatus sketched in the inset. The irregular image represents light scattered from the apparatus. (From Dehmelt, ref. 7).



**Figure 12.** Fluorescence from 3, 2 and 1 ions of  $^{24}\text{Mg}^+$ . (From Wineland and Itano, ref. 7.)

the fluorescing ions collide with  $^{25}\text{Mg}$  neutral atoms and themselves become neutralised. Fluorescence does not occur from  $^{25}\text{Mg}^+$  ions because their resonance line is displaced from that of  $^{24}\text{Mg}^+$ . The different levels of intensity can, therefore, be associated with small, discrete numbers of ions, the lowest level above background corresponding to one ion.

There are many interesting features to these experiments. A parallel can be drawn between the oscillations of single ions bound to the trap and the vibrations of nuclei in a diatomic molecule: a spectrum of vibrational side-bands to the electronic transition can be calculated and the laser tuned to the side-bands—that is to say, the laser can be made to interact with moving ions, and kinetic energy can be exchanged between the ions and the laser field, leading to *cooling* of the ions. Temperatures of millidegrees K have been reported. It is important to reduce the kinetic energy because one of the anticipated limitations to the work lies in frequency shifts attributable to the second-order Doppler effect.



The initiatives for this work came from Professor Dehmelt in Seattle, whose work is illustrated in fig. 11. Figure 12 is taken from a publication of Wineland and colleagues. Recent accounts can be found in reference<sup>(7)</sup>.

## 5. Quantum beats

We move away now from the realm of highly stable, highly-monochromatic lasers to realms where we need, principally, a bright light. The directional property is important because we often need to control polarization. For the required spectral selectivity a multimode pulsed laser is usually adequate. The property of tunability is exploited fully.

The phenomenon of quantum beats was known and studied even before lasers were invented. It relates to the possibility of making evident, under carefully controlled conditions, slow precessional motions of electrons in atoms or molecules by observing pulsations of fluorescent light. Indeed, the analogy with a searchlight beam is helpful. Just as an observer sees a sequence of flashes of light as a searchlight beam swings round, so a detector of fluorescent light will register pulsations as the non-isotropic dipole—radiation pattern from an assembly of atoms swings round if the electrons in different atoms are caused to precess in synchronism.

The analogy brings out the importance of the directional element which must be injected into the assembly of atoms in the process of excitation. Suppose that the atoms are excited by a short pulse of linearly polarized light. The electrons (on a classical view) are set into oscillatory motion parallel to the electric vector of the light, and will precess if they are subjected to a torque. Such a torque may arise from an external field—in which case beats are observed at twice the Larmor frequency—or from an internal field (spin-orbit or hyperfine coupling), in which case the beat frequencies are the spin-orbit or hyperfine intervals.

The quantum interpretation of the phenomenon is illustrated by figure 13. Atoms represented by their energy-level diagram are excited by a short pulse (of light, or electrons, or other perturbation) to a *coherent superposition* of energy eigenstates. They decay to some lower state, the same for all components of the superposition, by the ordinary, spontaneous radiative process. The probability *amplitudes* for the distinguishable transitions are coherent, and the Bohr frequencies for these transitions are different. Since all atoms in the assembly are prepared in the same way the total

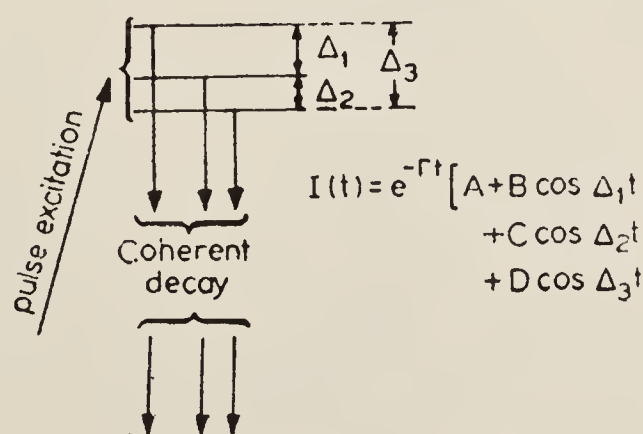


Figure 13. 'Quantum beats' are found in the light spontaneously emitted from atoms excited to a superposition-state by a short pulse of light or other form of excitation.

emission will exhibit interference between the radiations of different frequency, that is to say, will exhibit beats. The term 'quantum beat' was introduced to emphasize that the interference depends on coherence within the wave function for each individual atom, and does not originate in differences in the excitation of different atoms in the assembly.

The beat does not replace the exponential character of the decay: rather, the exponential enters as envelope to the modulation.

A word about spatial symmetries. The states are defined with reference to some hamiltonian possessing some spatial symmetry—for example, it may represent atoms in an external magnetic field. The essence of excitation to a superposition-state is that the symmetry of the exciting perturbation should be different from that of the hamiltonian. Moreover, the symmetry of that component of the light which is detected must be different from that of the hamiltonian. A conventional arrangement for the observation of Larmor beats, for example, would be that polarizers perpendicular to the magnetic field be inserted in the exciting and detected light beams.

### 5.1 *Spin-orbit structure in Na*

We turn now to the first of our examples: the D-doublets in atomic sodium<sup>(8)</sup>. Haroche and his colleagues excited a sequence of doublets  $n(D_{5/2} - D_{3/2})$  by irradiating Na vapour with two pulsed lasers, the first of which, tuned to the resonance line, established a population in the  $3P_{3/2}$  state and the second—whose frequency was chosen according to which doublet in the  $nD$  sequence was to be excited, prepared atoms in a coherent superposition of the  $3/2, 5/2$  states. The resulting fluorescent light showed modulation at the frequency of the doublet intervals (figure 14).

It is to be noticed how the frequency decreases systematically as  $n$  increases. This, of course, is to be expected. What is surprising to those who visualize the excited

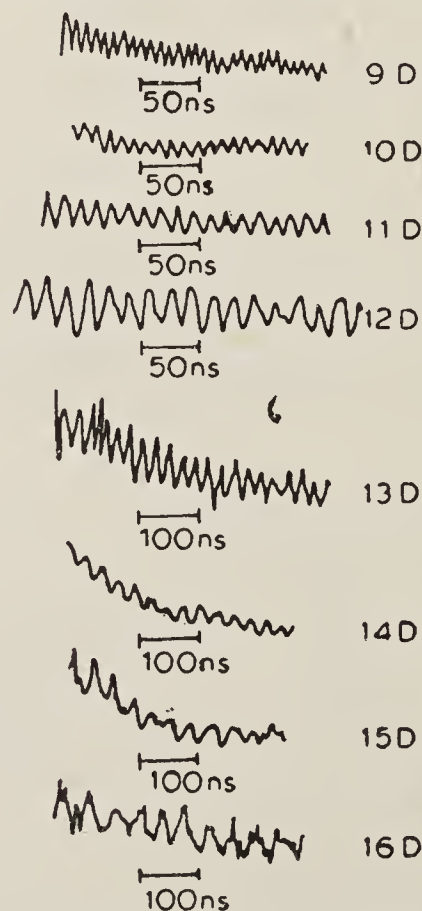


**Figure 14.** Fine-structure quantum beats observed from double-D levels in sodium. (From Fabre, Gross and Haroche, ref. 8.)



states of Na as a model of hydrogen-like behaviour is to know that the doublet structure in Na is inverted compared with H; a fact demonstrated in these experiments by studying the changes in the quantum beats resulting from the application of a small electric field to the atoms.

## 5.2 Hyperfine structure in Cs

This structure was studied by colleagues in the author's laboratory<sup>(9)</sup>. The  $nD_{3/2}$  states were excited in stepwise fashion,  $6S_{1/2}-6P_{1/2}-nD_{3/2}$ , the first step being achieved by continuous irradiation of atoms in a sealed cell by an ordinary Cs lamp. The second step was achieved by irradiation of the vapour by a pulsed, tunable laser. The pulse duration needs to be shorter than the period of any modulation one hopes to observe. In this case the pulses were about 6 ns long. Figure 15 exhibits the quantum beats in a plot of logarithm of the fluorescent intensity against time. The modulation is here more complicated than in the previous example because there are four hyperfine levels in each case, not two. Although the pattern looks complicated, it is repetitive, and a repeat interval can easily be read from the time axis. The inverse of this gives directly the hyperfine coupling constant. The case of caesium is uncharacteristically simple because the hyperfine coupling is almost entirely magnetic in character, resulting in intervals which are multiples of the coupling constant. In a more general

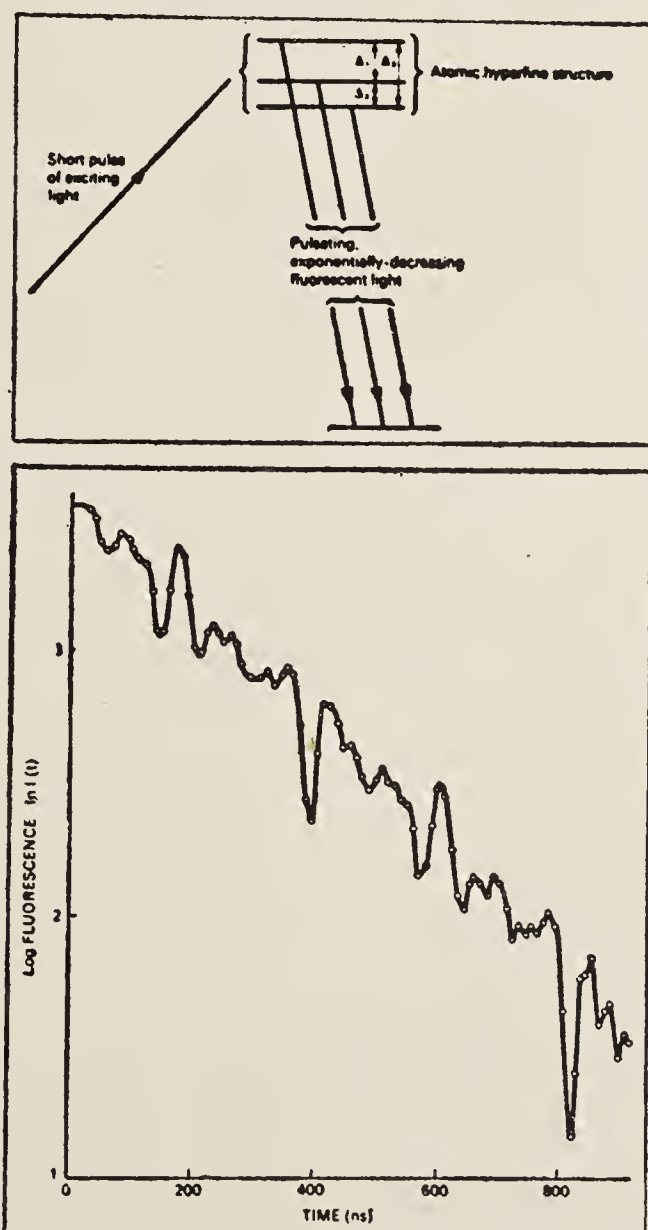


Figure 15. Hyperfine-structure quantum beats observed from the  $9^2D_{3/2}$  state in  $^{133}\text{Cs}$ . (ref. 9.)

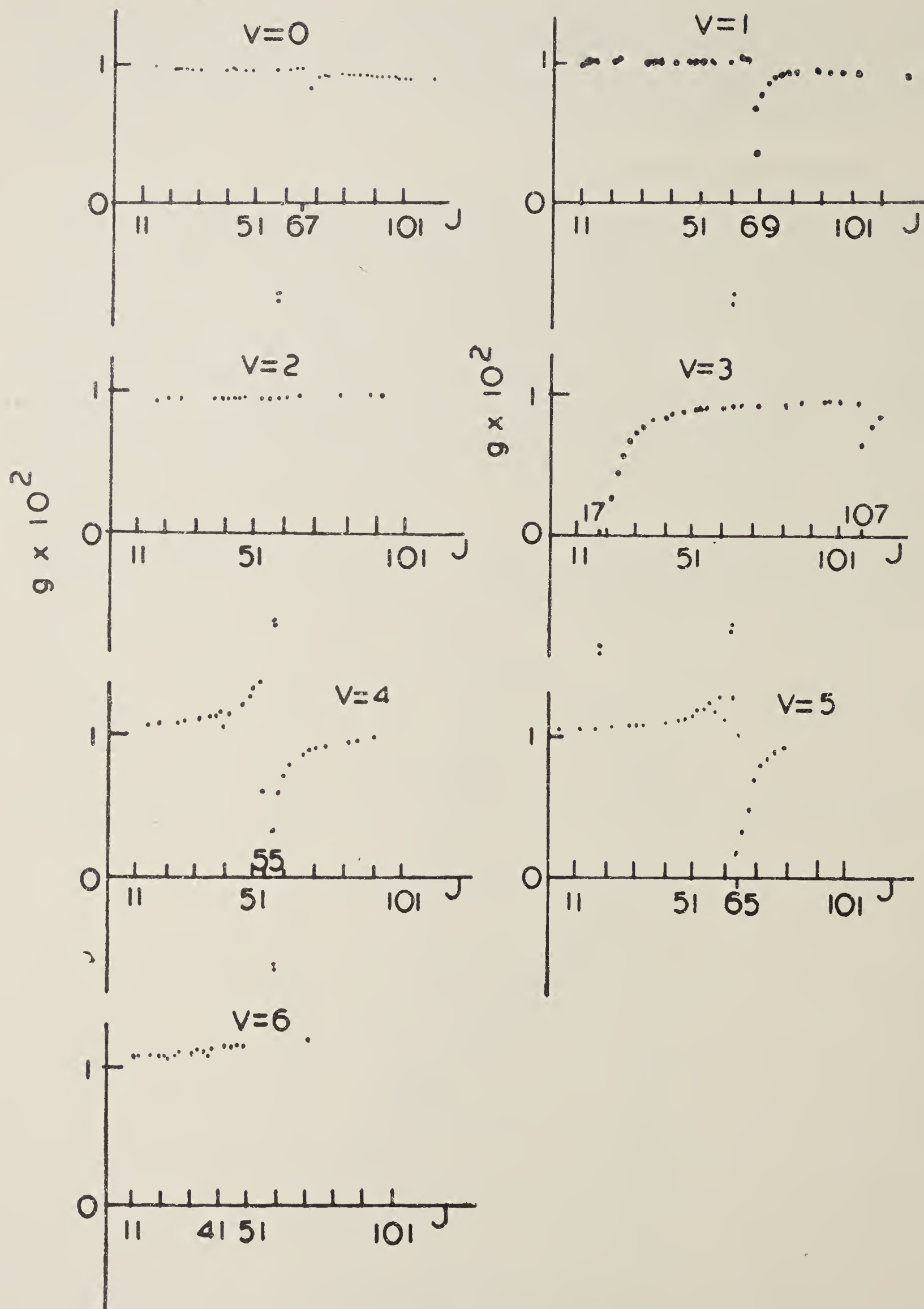


Figure 16. Gyromagnetic ratios of vibrational states in the  $B^3\Sigma_u^-$  state of  $\text{Se}_2$ , plotted against rotational quantum number. The Larmor frequencies were determined by the method of quantum beats. (ref. 10.)



case the hyperfine intervals can be determined by taking the Fourier transform of the fluorescence decay curve.

### 5.3 Larmor precession in $\text{Se}_2$

This final example, the work of Lehmann and colleagues<sup>(10)</sup>, is from a molecular spectrum, that of  $\text{Se}_2$ . A tunable, pulsed laser allowed the excitation of molecules to individual rotational states of the electronic state described as  $\text{B}^3 \Sigma_u^-$ . A magnetic field of known strength induced precession at the Larmor frequency which was determined by measuring the period of the beats in the fluorescent light. With knowledge of the field and the frequency, the Landé g-factor was computed for each level.

Figure 16 shows the remarkable result of this experiment. For each vibrational state the g-factor is plotted against the rotational quantum number. The figure shows how, for some vibrational states, the g-factor is practically the same for all rotational states, whereas for others the variation with rotational quantum number is profound. Here is an immense amount of detailed information to test whatever theories of coupling and potential curve-crossing might be adduced for this excited, molecular state.

Our examples illustrate the diversity of structures to which the technique of quantum beats have been applied. Two things in particular have been brought to this work by the use of tunable lasers: an intensity of light sufficient to excite transitions of very low oscillator strength (states of medium-high quantum number in the atoms; individual rotational transitions in the molecule), and the ability, through the tuning, to study a particular kind of structure over a long sequence of states. Such systematic information is far more valuable than the equivalent amount of information gathered haphazardly.

## 6. Detection by ion formation

As one tries to extend the range of study to states of higher principal quantum number, the progressive reduction in oscillator strength reaches a point where the number of atoms that can be excited is too low for detection by the observation of fluorescent light. Beyond that point, detection by ion formation has been successfully used. The method succeeds because single ions can be detected with higher efficiency than single photons.

Among the methods that have been used to produce ions from bound states are ionization by an electric field, ionization by collision, ionization by collision with amplification, and photo-ionization.

Highly excited atoms are very sensitive to electric fields and are ionized in fields of a few  $\text{V cm}^{-1}$ : the minimum field required for ionization increases with binding energy, and also depends on the angular momentum state. Good discrimination between different states is provided by measuring the ion signal as a function of field<sup>(11)</sup>.

Again, highly excited atoms undergoing collisions at thermal energies are readily

ionized. Ion-collecting plates incorporated into a vessel containing an atomic vapour provide a simple means of recording the excitation of atoms. Thus, for example, the higher members of series spectra can be recorded as ion signals as the vapour is irradiated by laser light progressively tuned across the spectral region near the series limit.

A modification of the apparatus allows the ion current to be amplified within the vapour cell itself. A hot cathode is introduced into the cell to form a conventional diode with a space-charge-limited current of electrons. If, now, ions are formed in a low-pressure vapour within the cell, the ions, by interacting with the space charge, strongly perturb the electron current, giving a signal which is very much greater than the current of ions alone would have been. This technique, though not new to the laser era, has been successfully used in a number of studies of series spectra near the ionization limit<sup>(12,13)</sup>.

Finally, excited atoms are frequently detected through their absorption of light whose quantum energy is sufficient to ionize them. Perhaps the most spectacular example of this is a recent experiment on positronium, when the  $2S$  state, excited from the ground state,  $1S$ , by 2-photon absorption, was identified by the ionization produced when a third photon was absorbed<sup>(14)</sup>.

### 6.1 Rydberg atoms in magnetic fields

The energies of highly excited atoms can generally be expressed by the Rydberg formula,  $E = -R/n^{*2}$ , where  $n^*$  increases by integral values as one proceeds up the series of terms. Such atoms are commonly called 'Rydberg atoms'. The behaviour of such atoms in magnetic fields has been the subject of an important branch of laser spectroscopy, where the method of detection has generally been one of those just described.

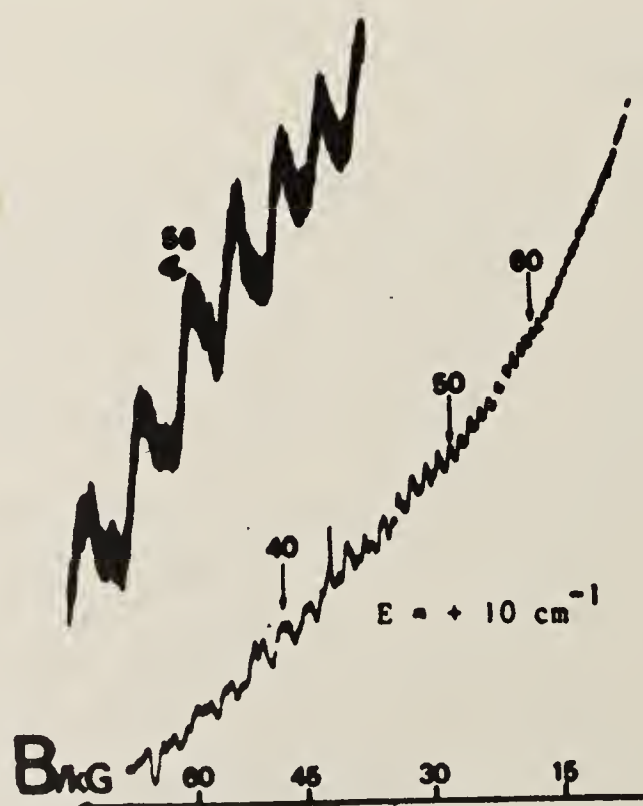


Figure 17. Resonances  $10 \text{ cm}^{-1}$  above the ionization limit in Cs subjected to strong magnetic fields. (From Gay and Delande, in *Laser Spectroscopy V*, p. 286.)



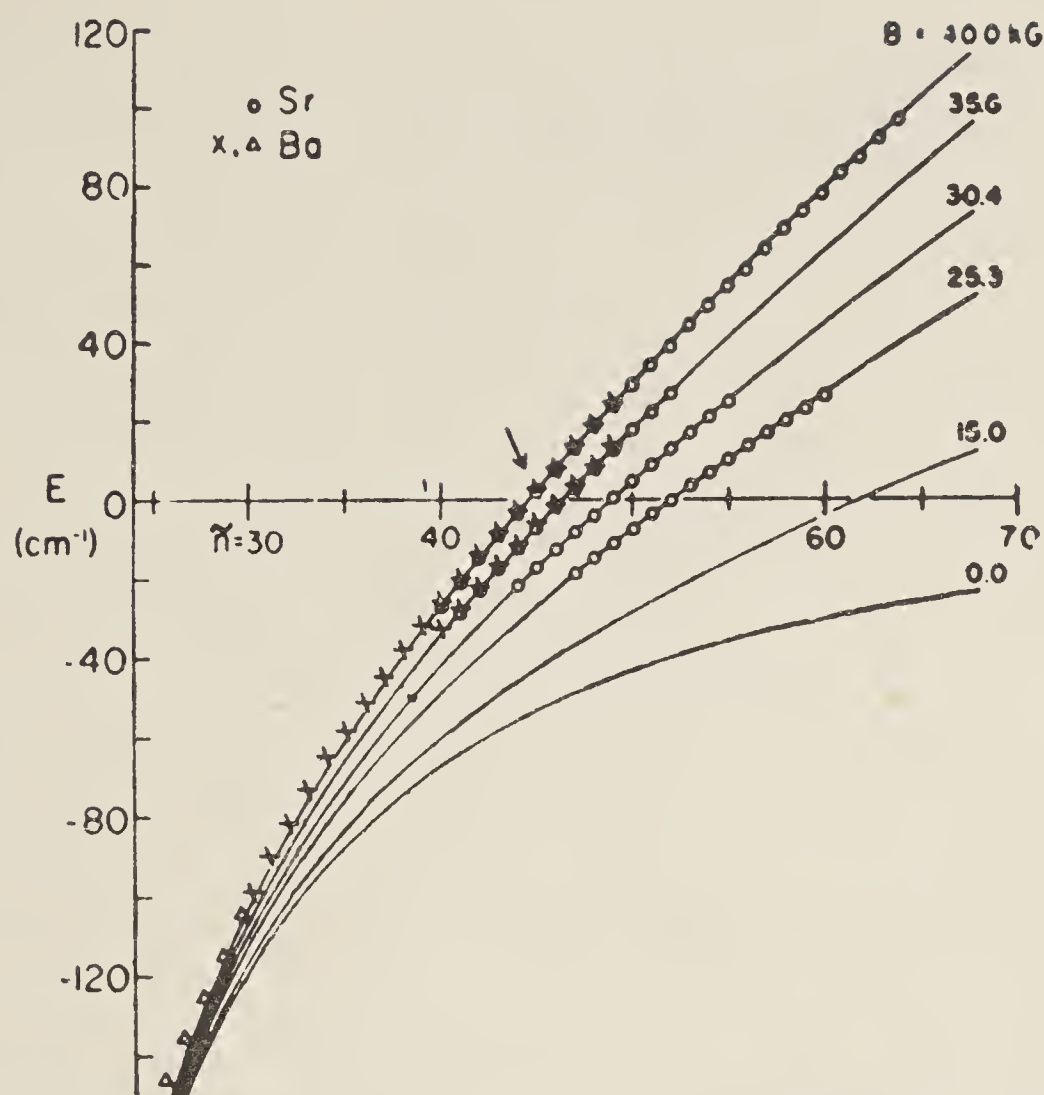


Figure 18. Resonances below and above the threshold in Sr(circles) and in Ba(crosses-peaks and triangles-dips) subjected to strong magnetic fields. (From Fonck, Tracy, Wright and Tomkins in *Phys. Rev. Lett.*, **40**, 1366.)

It has been found that the bound states, which, for a free atom, converge to a limit at the ionization threshold, break into a regularly-spaced sequence which extends from some distance below the threshold to a distance above it which depends on the field strength.

Although the regularities seen in figures 17 and 18 are striking, the complete picture is complicated and much effort has been made to attempts at interpretation. The binding of an electron to an atom subjected to a magnetic field represents a balance between forces of different symmetry: the spherical symmetry of the Coulomb force and the helical symmetry of the magnetic field. Thus, when an electron is energetic enough to escape from the atomic core, it may still be constrained in a plane by the magnetic field but be free to escape perpendicularly to the field. The periodic structure to be seen in the figures represents the energy of modified Landau orbits<sup>(15)</sup>.

## 6.2 Stark effect of close-lying levels

States in the intermediate range of principal quantum number ( $n \sim 10$  to  $20$ ) are sufficiently close-lying in energy to be brought into interaction with one another by the application of electric fields of a few  $\text{kV cm}^{-1}$ . Kleppner and his colleagues<sup>(16)</sup> displayed beautiful spectra of these interactions in a study of sodium atoms excited by a tunable laser and detected by the method of electric field ionization.

In figure 19 are to be seen their spectra of Na in the neighbourhood of  $n = 15$  (vertical axis) for values of electric field plotted on the horizontal axis. The maxi-

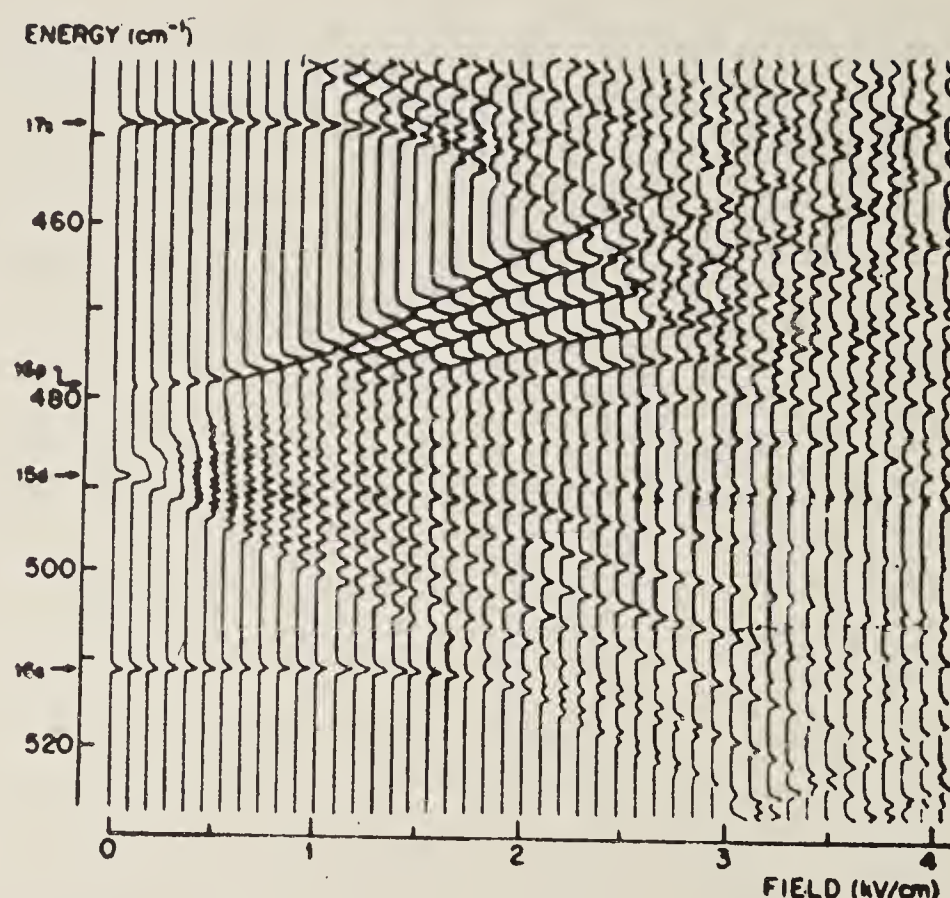


Figure 19. Stark effect in the spectrum of Na in the neighbourhood of  $n = 15$  (ref. 16.)

mum electric field used was  $4 \text{ kV cm}^{-1}$ . In fields as low as this the lower level of the transition is not greatly affected and the spectra are, effectively, plots of the upper levels in the electric field. The levels diverge linearly in low field (since levels of the same  $n$  having opposite parity lie close together) but begin to interact with levels of different  $n$ , (16s, for example), as the field is increased. Analysis of the Stark effect in these circumstances has called for a great deal of new theoretical work.

### 6.3 Super-radiance, millimetre-wave spectroscopy and maser action

Super-radiance in the optical regime is co-operative spontaneous emission from an assembly of atoms interacting with one another through their radiation fields and subject to constraints imposed by the time constants which characterise the sample. It is a directional emission determined by the shape of the sample. In that the radiating system consists of many atoms rather than one, the radiation rate is greatly increased over the single-atom rate.

Alkali vapours in which atoms are excited to Rydberg states by short pulses of laser light have provided systems in which super-radiance has been explored. A particularly interesting aspect of these studies has been to investigate the initiation of the super-radiance. The favoured interpretation appears to be that the initiation requires some quantum-statistical fluctuation, but that classical radiation theory is adequate to describe the subsequent evolution of the fluorescence<sup>(17)</sup>.

In the laboratory of Haroche and his colleagues experiments on super-radiance led into millimeter-wave resonance studies of alkali atoms in excited states. Atoms in collimated beams passing through a cavity tuned for millimeter waves were excited by pulsed laser light to particular states and sampled further along the beam by the technique of electric field ionization, whereby it could be ascertained whether transitions had been induced by the field in the cavity. Resonance frequencies were



determined for a large number of transitions between states of adjacent principal quantum number, for  $n$  in the region 30–40. Many such intervals were accurately measured and formulae have been established which allow these intervals to be used as spectroscopic standards in the millimetre-wave region and in the far infra-red.

Going beyond this, Haroche and his colleagues have studied the behaviour of atoms interacting with the thermally excited field in a tuned, microwave cavity and have shown that even a few atoms, excited to the upper state of a transition between two Rydberg levels, and within a millimeter-wave cavity tuned to the transition frequency, can constitute a Rydberg atom maser. The fundamental physics involved in understanding and interpreting these experiments extends from atomic theory, through radiation interactions to the quantum aspects of thermodynamics<sup>(18)</sup>.

## 7. Opto-galvanic spectroscopy

The opto-galvanic effect investigated in the late nineteen thirties and early nineteen forties by Prof. Joshi and his colleagues at the Banaras Hindu University<sup>(19)</sup>, has received a new lease of life with the coming of tunable lasers. The effect is this: irradiate a gas discharge with light whose frequency matches that of some transition in the atoms or ions (or molecules) of the discharge, and the discharge current changes. Naturally; because the electrical characteristics of the discharge depend on the balance between all the ionizing and radiative processes in the plasma, and if you transfer atoms from a particular state to some other state where the cross-section for ionization by electron impact (or by some other process) is most probably different, then you would expect to find a change in the electrical characteristics. Most frequently you do find such a change: the effect is quite sensitive. But the details of the phenomenon depend on the particular case, and although the general picture is easy to grasp, one would not expect to find any universal connection between the intensity of the light and the resulting change in impedance.

As a spectroscopic method the technique is straightforward<sup>(20)</sup>: illuminate the discharge with light from a tunable laser and observe changes of current as a function of frequency. It is customary to chop the laser beam and to observe the current with phase-sensitive detection. The optogalvanic signals can be positive or negative. Strong signals are represented by changes of discharge current of about 1%.

Among the many recent applications of the optogalvanic method are a number that have successfully used the saturated absorption and two-photon techniques described in section 3 to obtain Doppler-free spectra. Rather than show examples of this kind of spectroscopy we shall illustrate the optogalvanic method by a new discovery.

### 7.1 *Level-crossing effects and multimode resonances in opto-galvanic spectroscopy*

In this section I shall describe some very recent work carried out in my laboratory by my Australian colleague Dr. P. Hannaford. In one sense it was an experiment that failed: we did not discover the effect we were looking for. But on the way we found something else which forms the basis for yet another kind of Doppler-free spectroscopy, and which may find applications in high-resolution spectroscopy.



The original intention was to see whether the optogalvanic signal depended on the direction of polarization of light used to irradiate the discharge; that is, on whether the polarization vector was parallel or perpendicular to the discharge current. There is reason to believe that, when the gas pressure is low enough, such effects will appear, because atoms excited by polarized light are not spherically symmetrical, and the ionization cross-section will surely depend on the alignment of atoms relative to the discharge current.

We applied a magnetic field, variable over a few gauss about zero, in order to be able to change the orientation of the atoms. We *did* observe changes, but they did not behave as we expected them to behave and we convinced ourselves that the effect we had observed was *not* what we were looking for.

Let me now describe more precisely the experimental arrangements. We had chosen zirconium atoms as suitable for study partly because about twenty transitions from the ground and low-lying states of this element lie within the tuning range of Rhodamine 6 G, the commonest dye used in tunable lasers, and partly for reasons connected with the supposed mechanism of the optogalvanic effect. Zirconium in the form of metal formed the electrodes in our gas discharge and was sputtered into the vapour phase. The discharge was carried by an inert gas, usually neon at a pressure about 1 torr. We irradiated the discharge with light from a c-w laser, tuned to resonance with some particular transition. We could see the fluorescent light from the track of the laser light through the cell.

With the laser frequency fixed and the light linearly polarized in a known direction we applied a small magnetic field to the discharge tube, parallel to the laser beam. It is important to notice that the electric vector of the light was crossed with the magnetic field: the electric dipole transitions allowed by this configuration were the  $\sigma^+$  and  $\sigma^-$  Zeeman transitions ( $\Delta m = \pm 1$ ).

The changes of optogalvanic current that were recorded as a function of field are to be seen in figure 20. The reduction of current by (typically) 10% of the whole optogalvanic signal took place over a range of a few gauss on either side of zero: this is the region where Zeeman levels become degenerate. We believe that this degeneracy is the cause of the effect, as will be explained below. Moreover, it was established that the effect required an intensity of laser light sufficient to induce at least partial saturation of the transition: it does not occur unless the optogalvanic signal is nonlinear in the intensity of the light.

The width of the magnetic signal is especially to be noted and compared with Doppler-broadened Zeeman components of spectral lines—typically, 500 gauss. The new effect allows the position of degeneracy of energy levels to be determined to much higher accuracy, free of Doppler broadening.

We were anxious to demonstrate the possibility of using the effect as a spectroscopic tool, and did so by carrying out similar experiments on yttrium. This element has nuclear spin, and its electronic states have hyperfine structure. For the ground state and for a conveniently excited upper state the hyperfine structure is decoupled by fields of the order of 150 gauss, and over the range from zero to 150 gauss some of the hyperfine levels cross. For many years such ‘level-crossings’ have been determined by the techniques of linear fluorescence spectroscopy: the method is well-known as a basis for determining the magnitude of hyperfine coupling constants. A condition



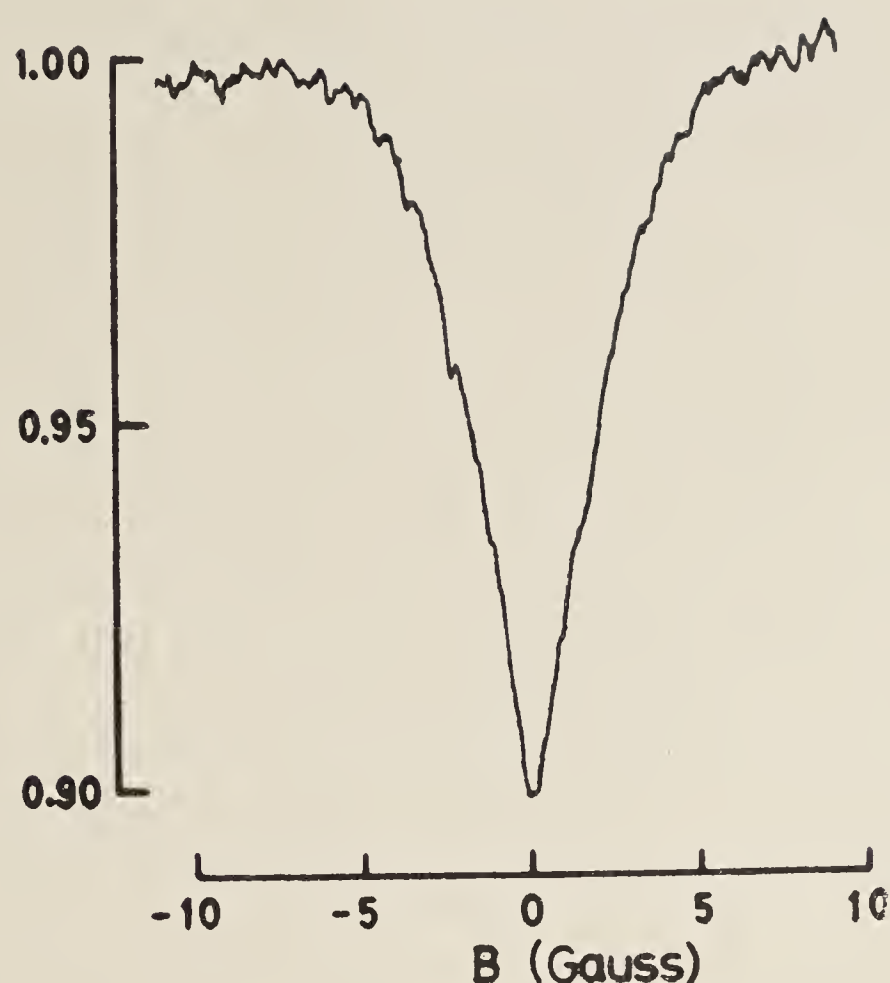


Figure 20. Magnetic scanning of the optogalvanic signal in Zr (612.7nm) in the region near  $B = 0$  (ref. 21.)

operative in the geometrical configuration we were using is that the  $m$ -quantum numbers of the crossing levels should differ by 2. Here we were able to locate level-crossings in yttrium in the lower states as well as in the upper and to determine the coupling constants. (The linear fluorescence method locates level-crossings in the upper states only.) The lower state hyperfine structure had been accurately measured by radio-frequency resonance methods, but the structure of the upper state had previously only been roughly estimated. Our determination of the lower state structure was in agreement with the previous measurements. Our determination of the upper state structure furnished a new piece of spectroscopic information and established the magnetic opto-galvanic phenomenon as a valid spectroscopic tool.

To complete the investigation we looked for and discovered resonances, both in zirconium as well as in yttrium, in lower states as well as in upper, when the spectral interval between neighbouring longitudinal modes of the laser (about 400 MHz) exactly matched an interval between Zeeman levels. The resonances disappeared when the laser was tuned so that only one longitudinal mode was generated: their occurrence depended on the simultaneous emission of several modes. We used these resonances to obtain a precise value for the mode spacing of the laser by measuring the magnetic field where the resonances occurred in states of zirconium for which Landé  $g$ -values are accurately known. Knowledge of this frequency then allowed us to determine unknown  $g$ -values.

**7.1a Interpretation of the phenomenon.** Although a complete explanation undoubtedly requires a detailed analysis of the interaction between high-intensity laser beams and atoms in a gas discharge, nevertheless it is possible to gain some understanding

by considering how the population changes induced by the laser depend on the fact that some saturation of the transition was taking place.

Suppose, when the laser is tuned to a transition, the light interacts with a group of  $N$  atoms, and that the light is strong enough to excite the maximum number, approximately  $1/2 N$ , to the excited state. If the levels are non-degenerate (we consider two upper levels, as in figure 21),  $1/2 N$  will be excited from one velocity group and  $1/2 N$  from a *different* velocity group, since the Doppler-shifted frequency of the light must match the transition frequency in the frame of the atom. The total number of excited atoms will, therefore, be approximately  $N$  when the levels are non-degenerate. But when the levels are degenerate, both transitions are excited by light of the same frequency, so that only one velocity group interacts with the laser. The number of atoms excited cannot exceed  $N/2$ , so the optogalvanic signal is smaller at a position of degeneracy than otherwise. This was the experimental observation, and this interpretation is called the 'population effect'.

Similarly for the multimode resonances: when the spectral interval between modes of the laser exactly matches a Zeeman interval, both modes are in resonance with one particular velocity group of atoms, but when the mode interval does not match a Zeeman interval the laser interacts with more than one group of atoms.

But there is a more subtle mechanism that can cause changes of population as the magnetic field is varied, a mechanism that invokes changes of alignment as an

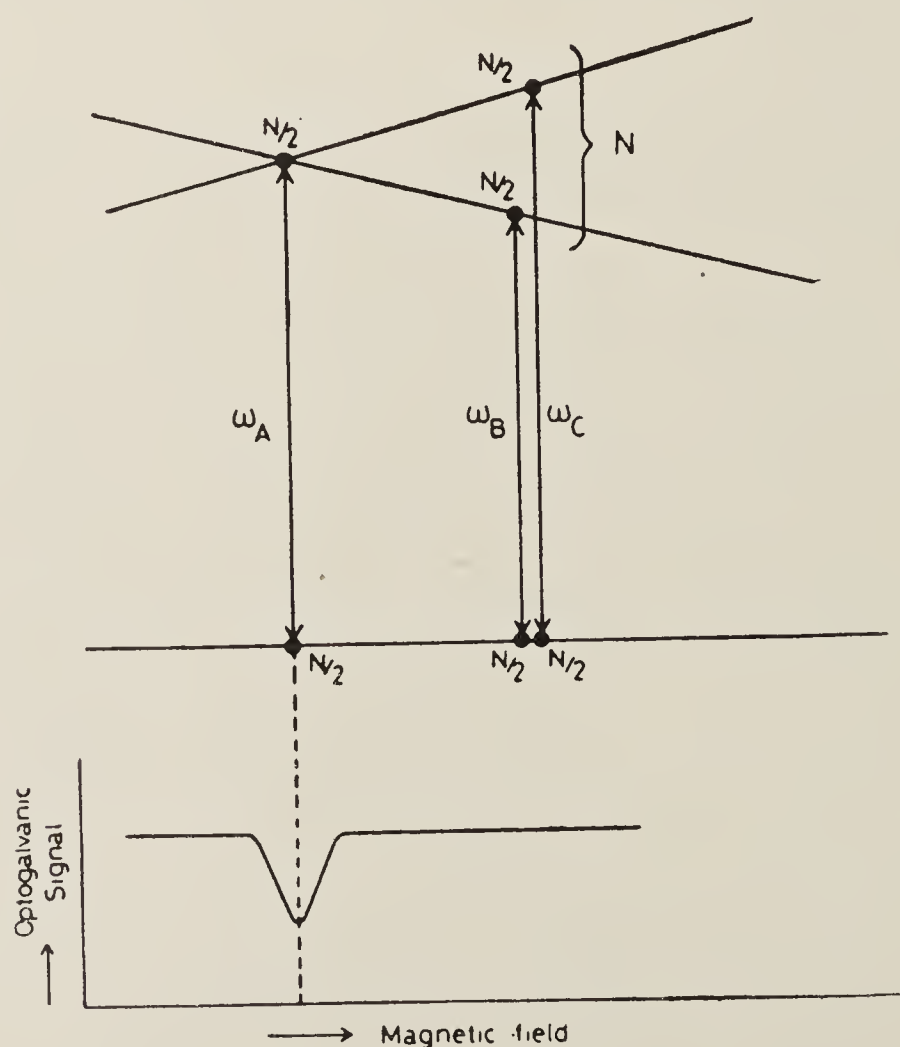


**Figure 21.** Diagram to illustrate reduction of the optogalvanic signal at a position of degeneracy.  $A$ ,  $B$ ,  $C$  are different velocity-groups, each of  $N$  atoms, which interact with the laser when the Doppler-shifted frequencies,  $\omega_A$ ,  $\omega_B$ ,  $\omega_C$  are in resonance with transition frequencies in the atoms. At the position of degeneracy, only group  $A$  is excited, while away from the degeneracy groups  $B$  and  $C$  are excited, leading to a larger number of excited atoms (it is supposed that all the transition frequencies lie well within the Doppler profile.)



intermediate step (the reader will realise that partial saturation implies a multi-step interaction). The polarized light undoubtedly generates alignment of the charge distribution within the atoms, and this alignment is destroyed at a certain rate under the impact of other particles in the discharge. Moreover, the direction of alignment rotates if a magnetic field is applied (magnetic precession), and the mean angle of rotation depends on the magnetic field and on the mean lifetime of the atoms as determined by the collision rate. The atoms continue to interact with the polarized light as they rotate, and the probability of excitation depends on the direction of their alignment with respect to the polarization vector of the light—hence the number of atoms excited will depend on the magnetic field and on the mean lifetime against collisions. The conclusion is that the optogalvanic signal depends on the magnetic field through this mechanism also, and that the widths of those contributions to the magnetic signals which depend on this effect (called the Zeeman coherence effect) should depend inversely on the lifetimes of the atoms in the upper and lower states. The width of the 'population effect' contribution, on the other hand, depends inversely on the coherence time of the interaction between the laser and the electric dipole which it induces in the atom—a time generally substantially shorter than the lifetime of the atoms in stationary states.

Much remains to be done to explain the line-shape in detail and other aspects of the effect. In the meantime, its application in spectroscopy must rest on the detailed phenomenological studies which have already been made<sup>(21)</sup>.

## **8. Conclusion and Acknowledgement**

This review of laser spectroscopy began with an account of some early experiments and now well-established techniques and has concluded with a recently-discovered and imperfectly understood phenomenon. The new life infused into spectroscopy by the invention of dye lasers has led to an explosion of activity, only a fraction of which has been touched upon here. Readers interested to discover more might care to refer to a series of volumes published by Springer<sup>(22)</sup>, the proceedings of biennial conferences in Laser Spectroscopy begun in 1973. The sixth conference took place in Interlaken in 1983.

It is with deep appreciation that I acknowledge the generosity of the Indian Academy of Sciences which invited me to India and gave me the opportunity of visiting a number of Universities and Institutes where, as Raman Visiting Professor, I gave the lectures on which this article is based.

The following houses have kindly permitted the reproduction of the figures indicated: North-Holland and the Italian Physical Society: Figs. 3, 4 and 14; Springer: Figs. 10, 11, 12 and 17; Institute of Physics: Figs. 15 and 20; Commission des Publications Françaises de Physique and Editions de Physique: Fig. 16, American Institute of Physics: Figs. 18 and 19.

December, 1982.



## References

1. *Topics in Applied Physics*, Vol. 1, *Dye Lasers*, ed: F. P. Schafer, Springer (1973).
- 2a. Schawlow, A. L. and Townes, C. H., *Phys. Rev.*, **112**, 1940, (1958)
- b. Maiman, T. H., *Nature*, **187**, 493, (1960); *Phys. Rev.*, **123**, 1145 and 1151, (1961).
- c. Javan, A., Bennett, W. R. and Herriott, D. R., *Phys. Rev. Lett.*, **6**, 106, (1961).
- 3a. Hänsch, T. W., Nayfeh, M. H., Lee, S. A., Curry, S. M. and Shahin, I. S., *Phys. Rev. Lett.*, **32**, 1336, (1974).
- b. Hänsch, T. W., Lee, S. A., Wallenstein, R. and Wieman, C., *Phys. Rev. Lett.*, **34**, 307, (1975).
- c. Lee, S. A., Wallenstein, R. and Hänsch, T. W., *Phys. Rev. Lett.*, **35**, 1262, (1975).
- d. Hänsch, T. W., *Proc. Intern. School of Physics Enrico Fermi*, Course LXIV, ed. N. Bloembergen (North-Holland, Amsterdam, 1977).
- e. Van Dyck, R. S., Moore, F. L. and Schwinberg, P. B., *Bull. Am. Phys. Soc.*, **28**, 791 (1983).
4. Kibble, B. P., Rowley, W. R. C., Shawyer, R. E. and Series, G. W., *J. Phys.*, **B6**, 1079, (1973).
5. Amin, S. R., Caldwell, C. D. and Lichten, W., *Phys. Rev. Lett.*, **47**, 1234, (1981).
- 6a. Baird, K. M., *Phil. Trans. Roy. Soc., Lond. A* (in press), (1982). (Discussion Meeting on New Techniques in Optical and Infrared Spectroscopy).
- b. Jennings, D. A., Pollock, C. R., Petersen, F. R., Drullinger, R. E., Evenson, K. M. and Wells, J. S., *Opt. Lett.*, **8**, 136 (1983).
7. Dehmelt, H. G. in *Laser Spectroscopy V* (ed: McKellar, Oka and Stoicheff), p. 358, Berlin: Springer, (1981).
8. Haroche, S., Gross, M. and Silverman, M., *Phys. Rev. Lett.*, **33**, 1063, (1974).  
   Fabre, C., Gross, M. and Haroche, S., *Opt. Commun.*, **13**, 393, (1975).  
   Haroche, S., in *High Resolution Laser Spectroscopy*, ed: K. Shimoda, Springer, p. 300, (1976).
9. Deech, J. S., Luybaert, R. and Series, G. W., *J. Phys.*, **B8**, 1406, (1975).
10. Gouedard, G. and Lehmann, J. C., *de Phys. Lett.*, **40**, L119, (1979).
11. Fabre, C., Haroche, S. and Goy, P., *Phys. Rev.*, **A18**, 229, (1978).  
   Ducas, T. W., Littman, M. G., Freeman, R. R. and Kleppner, D., *Phys. Rev. Lett.*, **35**, 366. (1975).
12. Harvey, K. C. and Stoicheff, B. P., *Phys. Rev. Lett.*, **38**, 537, (1977).
13. Pendrill, L. R. and Niemax, K., *J. Phys.*, **B13**, L461, (1980).
14. Chu, S. and Mills, A. P., *Phys. Rev. Lett.*, **48**, 1335, (1982).
15. Fano, U., *J. Phys.*, **B13**, L519, (1980).
16. Littman, M. G., Zimmerman, M. L., Ducas, T. W., Freeman, R. R. and Kleppner, D., *Phys. Rev. Lett.*, **36**, 788, (1976).
17. Macgillivray, J. C. and Feld, M. S., *Contemp. Phys.*, **22**, 299, (1981).  
   Vrehen, Q. H. F. and Schuurmans, M. H. F., *Phys. Rev. Lett.*, **42**, 224, (1979).
18. Haroche, S., Goy, P., Raimond, J. M., Fabre, C. and Gross, M., *Philos. Trans. Roy. Soc., Lond. A* (in press), (1982). (Discussion Meeting on New Techniques in Optical and Infrared Spectroscopy).
19. See text and references below.
20. Goldsmith, J. E. M. and Lawler, J. E., *Contemp. Phys.*, **22**, 235, (1981).
21. Hannaford, P. and Series, G. W., *J. Phys.* **B14**, L661, (1981); *Opt. Commun.*, **41**, 427-30, (1982); *Phys. Rev. Lett.*, **48**, 1326, (1982).
22. *Laser Spectroscopy* (1973) and *Laser Spectroscopy II-V* (1975, 77, 79, 81). Various eds. Springer (Heidelberg), Proceedings of Biennial Conferences.
19. So far as I have been able to discover, the first studies of the changes of the electrical characteristics of a discharge under irradiation by light were made by Penning, F. M., *Physica*, **8**, 137, (1928), whose interest was in the changes brought about in the population of *meta-stable* atoms. It would appear that Joshi and his collaborators discovered the 'light-effect' independently, and not in connection with the role of metastable atoms. Apart from a passing reference to the effect by Joshi (*Curr. Sci.*, **8**, 548, (1939)), the first specific account is by Joshi, S. S. and Narasimhan, V., *Curr. Sci.*, **9**, 535, (1940). A further account, with a suggested interpretation, is given by Joshi, S. S. and Deo, P. G., *Nature*, **151**, 561, (1943). Details of this work are reported by Deo in *Proc. Indian Acad. Sci.*, **A19**, 117, (1944). Various aspects of the phenomenon are reported in these three journals over the next few years.



BASIC QUANTUM MECHANICS OF ATOMIC STRUCTURES AND TRANSITIONS

G. W. SERIES

J. J. THOMSON PHYSICAL LABORATORY  
UNIVERSITY OF READING  
READING RG6 2AF

1. PRELIMINARIES

To set up a problem in mechanics one needs to specify:

- (a) the system, as, for example, point particles, specified by properties which determine their inertia (mass, spin) and their interactions (charge, magnetic moment). These properties are supposed to remain constant during the motion that is being analysed and the particles are, in that context, elementary particles. But for interactions in some other energy range one may make a different choice of elementary particle. For example, atomic nuclei, of specified spin, are 'elementary particles' in the context of atomic spectroscopy (energy range eV), but in the energy range MeV they are composite particles.
- (b) the geometry, as, for example, position vectors relative to some origin in three-dimensional physical space - but, frequently, one makes a transformation to a co-ordinate system moving with the centre of mass of the 'system'. Four-vectors are used in relativistic problems.
- (c) the field of force, commonly specified by a potential function of the position vectors. Such functions exist for electromagnetic forces, but not for all conceivable types of force.
- (d) the law of motion, as, for example, in classical mechanics, Newton's second law.

To solve a problem in mechanics one generally needs to integrate a differential equation: therefore, initial or boundary conditions

need to be specified. For example, to know the position of a particle as a function of time, after integration of the laws of motion in classical dynamics, one needs to know, for some initial time, where the particle is and where it is going (ordinary language); i.e. its position and velocity - strictly, momentum - (formal language).

Quantum mechanics admits that the specification of initial conditions required by classical mechanics may not be possible. Its fundamental law of motion can be expressed in a form very similar to Newton's second law, but it provides relations between average values of dynamical variables, not between the actual values of the dynamical variables of a system. These averages can be taken over the many members of an assembly of systems subject to the same preparation, or over the behaviour of one system repeatedly investigated by the same procedures.

### 1.1 The Hamiltonian Function (Classical Mechanics)

The law of motion in classical mechanics may be formulated in a variety of ways: one which is well adapted to the motion of interacting particles is based on the hamiltonian function. This is an expression for the total energy of the system expressed in particular variables, namely, the positions and momenta of the constituent particles. One must be careful with 'momenta': it is not always 'm $\dot{x}$ '. There is a formal definition, 'based on the prior specification of positional coordinates for each particle ( $q_i$ ) and the total kinetic energy of the system,  $T$ , in terms of the  $\dot{q}_i$ . Then, associate with each  $q_i$  a quantity

$$p_i = \partial T(\dot{q}_i, \dot{q}_j, \dots) / \partial \dot{q}_i \quad (1)$$

The  $p_i$  are called the momenta conjugate to the  $q_i$ . These  $q_i$  need not be Cartesian (rectangular) coordinates. They may, for example, be the spherical coordinates ( $r, \theta, \phi$ ) of each particle. Having defined the  $p_i$ , the velocities may be eliminated from  $T$  in favour of the  $p_i$ . A simple example leading to familiar expressions is that of a point particle, of mass  $m$ , specified by Cartesian coordinates  $x, y, z$ . Then  $T = \frac{1}{2}m(\dot{x}^2 + \dot{y}^2 + \dot{z}^2)$ ;  $p_x = m\dot{x}$ , etc;  $T = (p_x^2 + p_y^2 + p_z^2)/2m$ .

The hamiltonian function is

$$H = T + V \quad (\text{sum of kinetic and potential energies})$$

$$= \sum_N T(p_i^N, \dots, p_i^M, \dots) + V(q_i^N, \dots, q_i^M, \dots), \quad (2)$$

where  $N, M, \dots$  label the particles and the  $q_i^N, p_i^N$  are the coordinates



$q_i$  and momenta  $p_i$  of the particles  $N$ , etc.  $T$  will contain also the inertial parameters (e.g. mass) and  $V$  the interaction parameters (e.g. charge).

Use of the hamiltonian function in classical dynamics lends itself to the determination of constants of the motion which, in quantum theory, correspond to the quantum numbers that are used to label stationary states (see below). The hamiltonian formulation of quantum mechanics lends itself to the determination of these quantum numbers.

More complete discussions of the hamiltonian formalism are to be found in texts quoted in the References.

## 1.2 The Hamiltonian Operator (Quantum Mechanics)

The hamiltonian operator is a mathematical object used in quantum mechanics, constructed with an eye on the hamiltonian function of classical mechanics.

The hamiltonian operator operates in the space of a set of basis vectors or basis functions which, together, define a space called Hilbert space. It is important not to confuse Hilbert space with three-dimensional physical space.

The basis vectors or basis functions are usually obtained by setting up an eigenvalue equation for the hamiltonian operator and solving for its eigenvectors or eigenfunctions. Schrödinger's wave equation is an eigenvalue equation based on the hamiltonian operator, and the wave-function solutions of Schrödinger's equation form a set of eigenfunctions on which the hamiltonian operator can operate. But for many purposes Schrödinger's equation is too elaborate. It is an equation for a quantity,  $\psi$ , which is a function of coordinates in three-dimensional physical space,  $\psi(r, \theta, \phi)$ , for example. Now, those particular  $\psi$  which are eigenfunctions of the hamiltonian operator are given labels: for example  $\psi_\alpha$  is the eigenfunction corresponding to the eigenvalue  $E_\alpha$ . If one is only interested in the eigenvalue, the fact that  $\psi$  is a function of  $r, \theta, \phi$  is irrelevant: only the  $\alpha$  is relevant.

Here one sees the advantage of Dirac's notation. He introduced the symbol  $|\alpha\rangle$  and called it a ket. (The symbol  $\langle\alpha|$ , called bra, bears a relation to  $|\alpha\rangle$  similar to that between a complex number and its conjugate complex number). The kets are commonly thought of as vectors in a Hilbert space. The eigenvalue equation

$$H|\alpha\rangle = E_\alpha|\alpha\rangle \quad (3)$$

(H stands for hamiltonian operator, E for energy), defines a set of vectors  $|\alpha\rangle$  which are shown in mathematical texts to be orthogonal to one another, and to 'span' the whole space in which the operators work which represent the variables of a dynamical system.

To sum up:

$|\alpha\rangle$  is a vector in Hilbert space. One can apply to it the operators of quantum mechanics.

$\psi_\alpha(r, \theta, \phi)$  is, on the one hand, a function of the space variables  $r, \theta, \phi$ : on the other, a function to which one can apply the operators of quantum mechanics.  $\psi_\alpha(r, \theta, \phi)$  is a component of  $|\alpha\rangle$  on a set of basis vectors,  $|r, \theta, \phi\rangle$ .

To form the hamiltonian operator one must know how to form the operators corresponding to the positions and momenta of the interacting particles. Quantum mechanics permits a diversity of ways of doing this, but, whichever way is chosen, there is a constraint operating between the position operators  $q_i$  and the conjugate momentum operators  $p_i$  of each particle, expressed by

$$p_i q_i - q_i p_i = -i\hbar \quad (4)$$

We say ' $p_i$  does not commute with  $q_i$ ; their commutator is  $-i\hbar$ '.

(Notice that  $p_i^N q_j^N - q_j^N p_i^N = 0$ ;  $p_i^N q_i^M - q_i^M p_i^N = 0$ . These pairs of operators do commute. Here, we are concerned, in the one case, with components along different directions for the same particle or, in the other, with components along the same direction for different particles.) The constraint (4) is the underlying feature of quantum mechanics that distinguishes it from classical mechanics.

There is a tricky point to notice here: to form the hamiltonian operator one must work with coordinates based on a rectangular Cartesian system. It does not come out correctly if you use curvilinear coordinates.

You may use the rule:

- (a) classical variables  $q_i \rightarrow$  q.m. operators, 'multiply by  $q_i$   
classical variables  $p_i \rightarrow$  q.m. operators,  $-i\hbar \partial / \partial q_i$



or you may use the rule

- (b) classical variables  $p_i \rightarrow$  q.m. operators, 'multiply by  $p_i$ '  
 classical variables  $q_i \rightarrow$  q.m. operators,  $i\hbar\partial/\partial p_i$ .

Both rules satisfy the constraint (4). The first rule will lead you to Schrödinger's equation. This is the route we shall follow. The second rule will lead you to the so-called 'p-representation'. Whereas the wave functions you obtain from Schrödinger's equation are useful in specifying the distribution of electronic charge in atoms over coordinate space, the p-representation is more useful in specifying the distribution in momentum, which finds its application in interpreting experiments on Compton scattering, for example. Bearing in mind the relation  $p = \hbar k$  ( $k = 2\pi/\lambda$ ), you will appreciate that the p-representation is the Fourier transform of the q-representation.

### 1.3 Schrödinger's Equation

So then, for a particle of mass  $m$  whose position is specified by the Cartesian coordinates  $x, y, z$ , the hamiltonian operator is

$$H \equiv -\frac{\hbar^2}{2m} \left( \frac{\partial^2}{\partial x^2} + \frac{\partial^2}{\partial y^2} + \frac{\partial^2}{\partial z^2} \right) + V(x, y, z) \quad (5)$$

and the eigenvalue equation

$$H\psi(x, y, z) = E\psi(x, y, z) \quad (6)$$

is Schrödinger's equation for this particle.

## 2. ATOMS: SYSTEMS OF MANY PARTICLES

### 2.1 Internal and External Coordinates

It is usually convenient to distinguish between the motion of an atom as a whole and its internal motion and structure. This is conveniently done in quantum mechanics, as in classical mechanics, by introducing  $\underline{s}_i$  which give the positions of the electrons relative to the nucleus. We proceed thus:

Let  $\underline{r}$ ,  $\underline{r}_i$  be the position vectors of the nucleus and electrons (i) relative to a fixed origin. Let  $\underline{R}$  be the position vector of the centre of mass, so that

$$(M + Nm)\underline{R} = M\underline{r} + m\sum \underline{r}_i; \quad \text{and} \quad \underline{s}_i = \underline{r}_i - \underline{r}.$$

(M: mass of nucleus; m: mass of electron; N electrons)

Let  $\underline{p}_i, \underline{P}$  be momenta conjugate to  $\underline{s}_i, \underline{R}$ . The kinetic energy written in terms of the original coordinates and velocities is

$$T = \frac{1}{2}m\sum_i \dot{\underline{s}}_i^2 + \frac{1}{2}M\dot{\underline{R}}^2 \quad (7)$$

and in terms of the transformed coordinates and their conjugate momenta is

$$T = \frac{1}{2m'} \sum_i \underline{p}_i^2 + \frac{1}{M} \sum_{i \neq j} \underline{p}_i \cdot \underline{p}_j + \frac{1}{2(M+Nm)} \underline{P}^2 \quad (8)$$

with  $m' = mM/(m + M)$  (reduced mass).

Now, the potential energy term for an isolated atom will involve the  $\underline{s}_i$ , not  $\underline{R}$ . In such circumstances we find that Schrödinger's equation factorises:

$$\psi(\underline{r}, \underline{r}_i) = \psi_1(\underline{R})\psi_2(\underline{s}_i), \quad (9)$$

where  $\psi_1(\underline{R})$  satisfies the equation for a free particle of mass  $(M + Nm)$ :  
 $[-\hbar^2/2(M + Nm)]\nabla^2\psi_1(\underline{R}) = E_f\psi_1(\underline{R}); \quad \psi_1(\underline{R}) = e^{\pm i\mathbf{k} \cdot \underline{R}}; \quad E_f = \hbar^2 k^2/2(M + Nm),$   
(10)

and  $\psi_2(\underline{s}_i)$  satisfies the equation we would have set up for an atom at rest, save that the kinetic energy operator is now  $\frac{1}{2m'}\sum_i \underline{p}_i^2 + \frac{1}{M}\sum_{i \neq j} \underline{p}_i \cdot \underline{p}_j$  instead of  $\frac{1}{2m}\sum_i \underline{p}_i^2$ . We learn from this:

(i) The motion of the atom as a whole should not be overlooked. It is taken care of by the factor  $\exp(\pm i\mathbf{k} \cdot \underline{R})$ . This is an important factor in the quantum theory of the Doppler effect.

(ii) The internal structure can be calculated by using a co-ordinate system based on the position of the nucleus, provided that the electron mass is replaced by the reduced mass.

(iii) There is an additional term, representing coupling between the motions of the electrons, which may have some implications.

In fact, (ii) and (iii) give rise to displacements of energy levels between isotopes of the same element, 'isotope shifts'. (ii) is easy to calculate and is called the 'normal' mass effect. (iii) is difficult to calculate and is called the 'specific' mass effect.



## 2.2 Energy Eigenfunctions as Basis Functions

The eigenfunctions  $\psi_\alpha$  of Schrödinger's equation form a set of orthogonal, basis functions, and any function of the space coordinates can be expressed in terms of this basis set. The quantum-mechanical state of the system may correspond to one of the  $\psi_\alpha$ , in which case its energy is the corresponding eigenvalue  $E_\alpha$ . Such states are called 'stationary states' or 'energy eigenstates'. But, in general, the state of the system will not correspond to one of the  $\psi_\alpha$ . Suppose its state is represented by some function  $\phi$ . Then, writing

$$\phi = \sum_{\alpha} a_{\alpha} \psi_{\alpha}, \quad (11)$$

we speak of the particle as being in a coherent superposition of energy eigenstates, with amplitudes  $a_{\alpha}$ . In this case the energy does not have a definite value, but the weighted average over many measurements of its energy in the state represented by  $\phi$  is obtained by integration over the space variables:

$$\begin{aligned} E_{av} &= \iiint \phi^* H \phi dx dy dz \\ &= \sum_{\alpha} |a_{\alpha}|^2 E_{\alpha} \end{aligned} \quad (12)$$

This comes from (6) and (11), and uses the property that the  $\psi_{\alpha}$  are orthogonal.  $\phi$  is supposed to be normalised, that is

$$\iiint |\phi|^2 dx dy dz = 1, \quad (13)$$

and similarly for the  $\psi_{\alpha}$ .

## 2.3 Dirac Notation

The equations we have just written may be expressed more economically using the Dirac notation. Instead of (6) we have

$$H|> = E|>, \quad (14)$$

instead of (11),

$$|> = \sum_{\alpha} a_{\alpha} |\alpha> \quad (15)$$

and instead of (12),

$$E_{av} = \langle H |> = \sum_{\alpha} |a_{\alpha}|^2 E_{\alpha}. \quad (16)$$

This last equation comes from

$$H|\alpha\rangle = E_\alpha |\alpha\rangle \quad (\text{Eigenvalue equation})$$

$$\text{and } \langle\alpha|\alpha\rangle = 1, \quad (\text{normality}) \quad (17)$$

together with (15). The coefficients  $a_\alpha$  are the components of  $|\psi\rangle$  on  $|\alpha\rangle$ , written  $\langle\alpha|\psi\rangle$ . In Schrödinger notation,  $a_\alpha = \iiint \psi_\alpha^* \psi dx dy dz$ , sometimes called the 'overlap' or 'projection' of  $\psi$  on  $\psi_\alpha$ .

### 3. THE EQUATION OF MOTION: STATIONARY STATES

#### 3.1 Schrödinger Picture, Heisenberg Picture, Interaction Picture

The law of motion in quantum mechanics is usually based on the hamiltonian operator, though not necessarily so.

Thus, the hamiltonian operator appears in two contexts:

(i) in the formulation of the law of motion, when the evolution of a system needs to be determined as a function of time, and

(ii) as the energy operator, from which the average value of the total energy may be determined.

The quantum-mechanical law of motion is

$$i\hbar \frac{\partial}{\partial t} |\psi\rangle = H |\psi\rangle \quad (18)$$

$$\text{or } i\hbar \frac{\partial}{\partial t} \psi(t) = H \psi(t), \quad (19)$$

where  $H$  is the hamiltonian operator. In the Dirac form,  $t$  expresses the time-dependence of  $|\psi\rangle$ . If we use the expansion (15), then the coefficients  $a_\alpha$  are functions of  $t$ . This is the Schrödinger form of the equation of motion. We speak of the 'Schrödinger picture'. We use (18) and (15), and the orthogonality of the basis vectors  $|\alpha\rangle$  to form and then solve differential equations for the  $a_\alpha(t)$ .

But there are other procedures. Instead of working with time-independent basis vectors  $|\alpha\rangle$  we may work with the corresponding time-dependent vectors

$$|\alpha, t\rangle \equiv |\alpha\rangle \exp(-iE_\alpha t/\hbar) = |\alpha\rangle \exp(-i\omega_\alpha t). \quad (20)$$

(We write  $\omega_\alpha$  for  $E_\alpha/\hbar$ ).



These vectors are solutions of (18) with initial condition  $|t = 0\rangle = |\alpha\rangle$ .

We then write the expansion

$$|t\rangle = \sum_{\alpha} a_{\alpha} |\alpha\rangle \exp(-i\omega_{\alpha} t) \quad (21)$$

instead of  $|t\rangle = \sum_{\alpha} a_{\alpha}(t) |\alpha\rangle$ . equivalent to (15).

In equation (21) the coefficients  $a_{\alpha}$  are independent of time. This is called the Heisenberg picture, and is often used for demonstrating the formal similarities between classical and quantum mechanics.

It will be realised that the time-dependences of the coefficients  $a_{\alpha}(t)$  in the Schrödinger picture contain the factors  $\exp(-i\omega_{\alpha} t)$ .

These factors occur because we are using a basis of stationary states that are eigenstates of the hamiltonian operator  $H$ . But, in many problems, we don't know the eigenstates or the eigenvalues of the full hamiltonian, only of part of it. We often proceed then as follows:

Let  $H = H_0 + H'$ , and let us suppose that we know the eigenstates  $|\alpha^0\rangle$  and eigenvalues  $E^0$  of  $H_0$ . As basis states we use  $|\alpha^0\rangle \exp(-i\omega_{\alpha}^0 t)$ . The solution of the equation of motion under the complete hamiltonian  $H$  may then be written:

$$|t\rangle = \sum_{\alpha} a_{\alpha}(t) |\alpha^0\rangle \exp(-i\omega_{\alpha}^0 t). \quad (22)$$

In this equation the coefficients  $a_{\alpha}(t)$  vary with time on account of the additional part of the hamiltonian,  $H'$ . If this is small in relation to  $H_0$ , the  $a_{\alpha}(t)$  will vary only slowly with time compared with the fast oscillations represented by  $\exp(-i\omega_{\alpha}^0 t)$ . This often allows useful approximations in solving the differential equations for the  $a_{\alpha}(t)$ . We call this the 'interaction picture'. It is intermediate between the Schrödinger and Heisenberg pictures. The interaction picture is often used in solving problems concerned with the interaction between radiation and atoms.

### 3.2 Quantum labels for stationary states

Everyone is familiar with the fact that energy levels are labelled with quantum numbers. Some of these numbers (for example,

angular momentum quantum numbers) tell us about the dynamical 'variables' of the system when it is in the state having that particular energy. Others (for example, parity) tell us about mathematical properties of the wave function.

Why should energy levels be labelled with quantum numbers?

In the case of the dynamical variables, the quantum labels represent those quantities which, in the classical sense, are constants of the motion. The angular momentum of an isolated system is a case in point. For a classical system, the total angular momentum of an isolated system is a constant of the motion. Correspondingly, it is always possible (in principle) to label an atomic energy level with a definite value of a quantum number representing total angular momentum (conventionally, J, or F if the nuclear spin is non-zero). This can be understood by reference to the law of motion of the average value (mean value; expectation value) of any operator  $\hat{A}$ :

$$i\hbar \frac{d}{dt} \langle \hat{A} \rangle = \langle [\hat{A}, H] \rangle + i\hbar \left\langle \frac{\partial \hat{A}}{\partial t} \right\rangle, \quad (23)$$

which may be deduced from equation (18).

(The notation  $[\hat{A}, H]$  means 'the commutator of  $\hat{A}$  and  $H$ ', namely  $\hat{A}H - H\hat{A}$ ). If  $\hat{A}$  does not depend explicitly on time, the last term is zero. If, in addition,  $\hat{A}$  commutes with  $H$  (that is, if  $\hat{A}H = H\hat{A}$ ), then

$\frac{d}{dt} \langle \hat{A} \rangle = 0$  and  $\langle \hat{A} \rangle$  is independent of time. It is a constant of the motion. Thus, those dynamical variables whose corresponding operators commute with the hamiltonian operator are constants of the motion in the sense that the mean of their values,  $\langle \hat{A} \rangle$ , is a constant.

Now, if an operator  $\hat{A}$  commutes with  $H$ , then the eigenstates of  $H$  are also eigenstates of  $\hat{A}$ . (Formal proofs are found in texts on quantum mechanics.) This means that a stationary state - an energy eigenstate - is also an eigenstate of  $\hat{A}$ . States of given energy, then, can properly and usefully be labelled with eigenvalues of  $\hat{A}$ . We speak of good quantum numbers.

Further, it is shown in texts on quantum mechanics that, for an isolated system, the operator corresponding to the component of total angular momentum in a given direction ( $\hat{J}_z$ ) commutes with  $H$ . Therefore energy levels can be labelled with eigenvalues of  $\hat{J}_z$ . Similarly for the operator  $\hat{J}^2$ .

Notice the reservation, for an isolated system. If an atom is in an external field the above arguments do not necessarily hold.



For example, the 'J' labels which distinguish the energy levels of an atomic multiplet are no longer applicable if the atom is in a magnetic field strong enough to break down the spin-orbit coupling.

The proof that  $\hat{J}_z$  commutes with H depends on showing the close connection between  $\hat{J}_z$  and the mathematical operation, 'rotation round the z-axis'. One can show that a rotation of coordinates through the angle  $\phi$  is equivalent to multiplication of the wave function by  $\exp(-i\hat{J}_z\phi)$ . This is a piece of mathematical manipulation that doesn't alter the physical situation (remember: the system is isolated). It is a 'symmetry operation'. So, we have established a connection between quantum labels, constants of the motion, and symmetry operations.

Among the symmetry operations of special importance in atomic structure theory is the parity operation, symbol  $\hat{P}$ , which is defined as changing the sign of the space variables in a function on which it operates:

$$\hat{P}\psi(q) = \psi(-q). \quad (24)$$

For any hamiltonian H which commutes with  $\hat{P}$ , the eigenfunctions of H can be labelled additionally with a symbol indicating the eigenvalue of parity. The eigenvalues of  $\hat{P}$  are  $\pm 1$ , and these are the labels often used. Hamiltonian operators for atoms commute with  $\hat{P}$ , and atomic energy levels are often given a parity label, but the usual convention is the following:

for parity eigenvalue +1, the parity label is omitted;  
for parity eigenvalue -1, the symbol <sup>0</sup> (superscript 0 for odd)

is usually written after the other labels. These labels are especially important when we consider radiative transitions between stationary states.

#### 4. INTERACTIONS IN FREE ATOMS: CENTRAL FIELD APPROXIMATION

##### 4.1 Binding to the Nucleus

The dominant interaction between the particles which constitute an atom is the electrostatic attraction between the positively-charged nucleus and the negatively-charged electrons. The main features of this are exemplified in text books by investigating the properties of a so-called 'hydrogen atom' consisting of an infinitely heavy point nucleus carrying a unit charge e, to which is bound an object called an 'electron' - a particle specified by its mass m and charge -e. (We take e to be a positive quantity - the magnitude of

charge.) Of course, the actual hydrogen atom is more complicated than this in that the nucleus has finite mass, spin, magnetic moment and extension in space. For deuterium, the nucleus has, additionally, an electric quadrupole moment. These physical properties are distributed over the nucleus in a way which may be predictable by models of the nucleus, and which may be, up to a point, determined experimentally. Furthermore, the electron itself has additional properties: spin and magnetic moment.

Elementary treatments of the fictitious hydrogen atom are generally based on solutions of Schrödinger's equation, but this equation does not satisfy the special theory of relativity - it is not invariant under a Lorentz transformation. The solutions so obtained may be patched up to make up for the deficiencies of the model and for the deficiencies of Schrödinger's equation, but a more fundamental approach is to use a wave equation which does satisfy the requirements of special relativity: Dirac's equation. We shall come back to this, and we shall point out that this also is deficient - it requires supplementation by terms deriving from a more profound understanding of quantum electrodynamics (QED). This will form the subject of another set of lectures.

To return to our fictitious hydrogen atom in the context of Schrödinger's equation: it serves as a useful starting point for understanding atomic structure and the labelling of atomic energy levels: therefore we recall some of its features.

#### 4.2 Fictitious Hydrogen Atom

It is effectively a one-particle problem since the nuclear mass is taken to be infinite and the atom to be at rest. There are three space coordinates - those of the electron relative to the nucleus,  $r, \theta, \phi$ .

The sole contribution to the potential energy is the electrostatic interaction  $V = -e^2/r$ ; (additional <sup>factor</sup>  $1/4\pi\epsilon_0$  in S.I.).

The wave function factorises:  $R(r)\theta(\theta)\phi(\phi)$

The requirements that the wave function must be single-valued, continuous and vanish at infinity determine the acceptable solutions.

The acceptable solutions for  $\theta, \phi$  are spherical harmonic functions characterised by two integers (commonly called  $m$  and  $\ell$ , with  $|m| \leq \ell$ ). These functions do not depend on  $V$  for the reason that  $V$  in this problem does not depend on  $\theta$  or  $\phi$  - not because of the particular form of the  $r$ -dependence of  $V$ .

$\ell$  and  $m$  can be given a physical interpretation by using the explicit form of the wave functions to verify that they are eigen-



functions, not only of the energy operator, but also of the operators representing 'component of angular momentum along the polar axis' ( $\hat{L}_z$ ) and 'square of total angular momentum' ( $\hat{L}^2$ ). For the function

$\Theta_{\ell}^{m\phi}$  these eigenvalues are  $m\hbar$  and  $\ell(\ell + 1)\hbar^2$ . Notice that the  $r, \theta, \phi$  dependence, which is required for the operations of differentiation ( $\hat{L}_z \equiv -i\hbar \partial/\partial \phi$ ), does not appear in the results.

The wave equation for  $R(r)$  has acceptable solutions only under the condition  $E = -R/n^2$ , where  $R$  (Rydberg constant)  $= me^4/2\hbar^2$ , (additional factor  $(1/4\pi\epsilon_0)^2$  in S.I.).  $n$  has allowed values  $1, 2 \dots \infty$ .  $R(r)$  is characterized by this integer  $n$ , also by the  $\ell$  which occur in the associated angular factors.  $0 \leq \ell \leq (n - 1)$ .

$n$  has the following physical interpretation: the number of nodes in the function  $R_{n\ell}$  is  $(n - \ell - 1)$ . Therefore  $n$  has something to do with the shell structure of a many-electron atom.

Notice that the energy eigenvalues are exactly those predicted by Bohr's theory, although the break with classical mechanics is made in an entirely different way in Bohr's theory than in the modern form of quantum theory. The explanation for this lies in an appreciation of the high symmetries underlying the problem and in the specialised form of the Coulomb potential.

Notice also that the energy eigenvalues depend on  $n$  but not on  $\ell$ , although the radial eigenfunctions depend also on  $\ell$ . Neither do the energy eigenvalues depend on  $m$ . The whole set of angular functions characterised by all the values of  $\ell$  and  $m$  which go with a given  $n$  (there are  $n^2$  such functions) have the same energy eigenvalue. The solutions of the wave equation for the Coulomb potential are degenerate in  $\ell$  and degenerate in  $m$ . The  $m$ -degeneracy arises because of the rotational invariance of the hamiltonian of a free atom. The  $\ell$ -degeneracy is a consequence of the special form of the potential.

#### 4.3 Many-electron Atom: Central Field

It is common, even in high-brow books on atomic structure, to continue the fiction that atomic nuclei and electrons are point particles having charge and mass and no other properties (save that electrons are deemed to obey Fermi-Dirac statistics). This is not unreasonable if one is interested in the gross structure of spectra and the classification of states, since electrostatic forces are so strong. We shall preserve this fiction for a little longer and write a hamiltonian corresponding to a nucleus and  $N$  electrons interacting under electrostatic forces only. We also preserve the fiction that the nucleus is infinitely heavy and that we are dealing

with static atoms. There are then  $3N$  coordinates in the hamiltonian - the space coordinates of the electrons (labelled  $i, j$ ) relative to the nucleus:

$$H = \sum_i \left[ \frac{p_i^2}{2m} - \frac{Ze^2}{r_i} \right] + \sum_{i < j} \frac{e^2}{r_{ij}} ; (i, j = 1 \dots N). \quad (25)$$

Schrödinger's equation for the system is

$$\left\{ \sum_i \left[ -\frac{\hbar^2}{2m} \nabla_i^2 - \frac{Ze^2}{r_i} \right] + \sum_{i < j} \frac{e^2}{r_{ij}} \right\} \psi(\dots r_i \theta_i \phi_i \dots) = E \psi(\dots r_i \theta_i \phi_i \dots). \quad (26)$$

$$(r_{ij} = |r_j - r_i|)$$

Notice that  $\psi$  is a function of the  $3N$  coordinates  $\dots r_i \theta_i \phi_i \dots$ .

Just as, for hydrogen, the number of quantum numbers was the same as the number of coordinates, so also, here, the number of quantum numbers will be  $3N$ . (It will be useful at a later stage to construct other numbers which are combinations of these.) All the acceptable solutions of (26) will be functions of these coordinates. The different solutions will be distinguished from one another by different combinations of the quantum numbers. Each particular solution will be a member of the basis set of functions. Each particular solution will be orthogonal to every other in the sense

$$\begin{aligned} \int \dots \int_{3N} \psi_{\alpha}^*(\dots r_i \theta_i \phi_i \dots) \psi_{\beta}(\dots r_i \theta_i \phi_i \dots) d \dots dr_i d\theta_i d\phi_i d \dots \\ = 0, (\alpha \neq \beta) \\ = 1, (\alpha = \beta) \end{aligned}$$

The condition, ' $=1, (\alpha = \beta)$ ' is easily secured by suitable choices of numerical constants multiplying the functions. This is normalisation.

But equation (26) is not factorisable, as is the case for hydrogen, because of the non-central terms involving  $r_{ij}$ . These terms make up a very large part of the potential energy, and it would be quite inappropriate to treat them as perturbations, in the general case. But, with some knowledge of electron shell structures (derived, say, from X-ray spectra), we are aware that the resultant of the electrostatic force on any given electron coming from the remaining electrons is directed approximately radially: the 'other electrons' may be regarded, in a 'zeroth' approximation, as constituting



spherical shells of charge. So, then, let us represent the terms  $\Sigma e^2/r_{ij}$  by  $U(r_i) + [\Sigma e^2/r_{ij} - U(r_i)]$ . The term  $U(r_i)$  is central in  $r_i$  and represents a spherical average of  $\Sigma e^2/r_{ij}$ . The term in square brackets is not central, but it will be very much smaller than  $\Sigma e^2/r_{ij}$ .

If, now, in this zeroth approximation, we neglect the term<sup>above</sup> in square brackets, (26) becomes

$$\sum_i \left[ -\frac{\hbar^2}{2m} \nabla_i^2 - \frac{Ze^2}{r_i} + U(r_i) - E \right] \psi^0 = 0, \quad (27)$$

and this is factorisable into  $3N$  functions, each of the form  $R_i \Theta_i \Phi_i$ . The angular functions are spherical harmonics just as in the case of H: only the  $R_i$  functions are different, and so also the energy eigenvalues.

<sup>and m</sup> Because the angular functions are the same, the quantum numbers  $l$  have the same range of values and have the same interpretation. The physical meaning of the approximation is that each electron is moving in a spherical potential independently of the others, with angular momentum specified by the quantum numbers which label its spherical harmonic wave function.

But because  $\left[ -\frac{Ze^2}{r_i} + U(r_i) \right]$  is no longer Coulombic, the eigenvalues of energy are no longer  $-R/n^2$ , as for hydrogen. Rather, they are functions of  $n$  and  $l$ . To the extent that we can attribute the experimentally observed energy differences from the ground state to the excitation of one electron (as, for example, in term diagrams of the alkali atoms), we can make a correspondence with hydrogen in the following way:

let  $E$  be the experimentally-determined energy measured from the first ionisation potential. Define  $n^*$  by

$$E = -R/n^{*2} = -R/(n - \epsilon)^2. \quad (28)$$

Then  $n^*$  is called the 'effective quantum number' corresponding to the corresponding hydrogenic quantum number  $n$ .  $\epsilon$  is called the 'quantum defect'.

Within a series of energy levels (terms), characterised by successive values of  $n$ ,  $\epsilon$  is approximately constant, but is a function of  $l$ .  $\epsilon$  is a weak function of  $n$ : thus, one writes  $\epsilon(n, l)$ .

While the alkali metals furnish the readiest examples for this interpretation of theory, one may also use the model to interpret series of terms in the spectra of many-electron atoms. Each term in the series is associated with a set of quantum numbers, among which the  $n$  of one set takes successive integral values - all the other numbers remaining unchanged. Formula (28) is again applied. The series of terms is called a Rydberg series.

Notice that, although one commonly speaks of 'one electron being excited to successive quantum states', one should strictly think of the excitation of the whole atom to a sequence of states in which one of the quantum numbers is taking successive integral values. It is not correct to associate a particular electron with a particular state. The electrons are indistinguishable.

The indistinguishability of electrons finds expression in the way in which one constructs a wave function for the whole atom out of the set of one-electron functions which are the solutions of (27). We first need to introduce the notion of electron spin and its bearing on the statistics. Its bearing on the dynamics will come at a later stage.

#### 4.4 Electron Spin and Electron Spin Quantum Numbers

Admit the evidence which forces the ascription of an additional dynamical 'variable' to the electron, spin, and to the proportionality between this variable and a magnetic moment. (Evidence: doublet structure in alkali spectra, anomalous Zeeman effect, Stern-Gerlach experiment). The eigenvalues of the operator  $\hat{s}_z$  are  $\pm \frac{1}{2}\hbar$ , and of the operator  $\hat{s}^2$ ,  $\frac{3}{4}\hbar^2$ . Correspondingly, we need two new eigenfunctions, - call them  $s_+$  and  $s_-$ . With this notation, + and - are 'quantum numbers (quantum labels)'.

For the electron labelled  $i$  in (27), the eigenfunction  $R_i \Theta_i \Phi_i$  needs to be multiplied by a function  $s_i$  which is not a function of a space variable, but is like a Dirac ket. The Hilbert space spanned by the functions  $R_i \Theta_i \Phi_i$  is now extended by the space spanned by  $s_+$  and  $s_-$ . To specify a particular eigenfunction out of the set we need, in addition to value of  $n, l, m$ , one of the two labels  $s_+$  or  $s_-$  - a set of four quantum numbers.

#### 4.5 Pauli's Exclusion Principle: Dirac's principle of Anti-symmetry

The elementary form of Pauli's principle is familiar: in an assembly of electrons, no two may have the same set of quantum numbers. But this is to ascribe quantum numbers to electrons, not to states.



It is better to think in terms of the occupation of cells. A 'cell' is labelled by a set of four quantum numbers. The number of electrons which may occupy each cell is either 1 or 0. This is a principle additional to the commutation rule  $pq - qp = -i\hbar$ , and may not be deduced from it. The evidence for it lies everywhere in the quantum theory of electrons: in particular, the shell structure of atoms, the band structure of solids.

Embracing Pauli's principle, but going beyond it, is Dirac's principle: the total wave function for a system of electrons is antisymmetrical (in the sense, changes sign) under the interchange of the symbols which label any pair.

Consider again the solutions of (27), extended by the spin functions. A solution is the product of all the one-electron functions  $R_i \Theta_i \Phi_i S_i$ . Such a function we shall call a spin-orbital. If, for each spin-orbital, we choose a different set of quantum numbers, we shall have satisfied Pauli's principle, but not Dirac's.

#### 4.6 Determinantal Wave Functions

Consider the function

$$U = (N!)^{-\frac{1}{2}} \begin{vmatrix} u_1(1) & u_1(2) & \dots & u_1(N) \\ u_2(1) & u_2(2) & \dots & u_2(N) \\ \vdots & \vdots & \ddots & \vdots \\ u_N(1) & u_N(2) & \dots & u_N(N) \end{vmatrix} \quad (29)$$

where the  $u_\alpha$  are spin-orbitals. The suffixes  $\alpha$  stand for a set of quantum numbers. The labels (i), as in  $u_\alpha(i)$ , stand for the co-ordinates of the electron labelled i.

Each term in the expansion of the determinant is a product of spin orbitals and is a solution of (27). So also is the complete expansion, being a sum of such terms with alternating coefficients  $\pm 1$ , and because (27) is a linear differential equation.

Pauli's principle is satisfied if the label  $\alpha$  for each row is different, for then, in each term of the expansion, no set of quantum labels will occur more than once. If two or more rows carry the same quantum label, the determinant will be identically zero. But, additionally, Dirac's principle will be satisfied, because interchange of any two columns (electron labels) changes the sign of the determinant.

$(N!)^{\frac{1}{2}}$  is a normalising factor for U.

Wave-functions such as  $U$ , therefore, satisfy all the general principles of quantum mechanics and form the starting point for atomic structure calculations. Let us recapitulate what is needed in order to write down, in detail, such an equation as (29). We need to specify:

- (i) the number of electrons,  $N$ ,
- and (ii)  $N$  sets of quantum numbers,  $n, \ell, m, s$ .

These quantum numbers are commonly grouped into sets in which  $(n, \ell)$  is common to members of a set. Such a set is called the electron configuration.

For example, neutral sodium atoms have  $N = 11$ . The electron configuration of the second excited P-state of sodium is  $(1s)^2(2s)^2(2p)^64p$ .

In this notation we are using the convention that  $s$  stands for  $\ell = 0$ ,  $p$  for  $\ell = 1$ , and so on. The superscript 6 in  $(2p)^6$  means that 6 electrons have  $n = 2$ ,  $\ell = 1$ . The six states (cells) occupied by these six electrons differ from one another in the remaining numbers,  $m = 0, \pm 1$ ;  $s = \pm$ .

#### 4.7 Self-consistent Wave Functions

Having established the form of the function, and having recognised that only the  $R_i$  factors in the  $u(i)$  need to be determined, and that these depend on the potentials  $U(r_i)$  in (27), a self-consistent method is applied. If a function  $U^0(r_i)$  is chosen, the  $R_i$  may be determined, hence the total wave function  $U$  of (29). From this one may calculate a distribution of electron charge, and hence a potential  $U^1(r_i)$ . This will generally differ from  $U^0(r_i)$ . A correction to  $U^0$  is applied, and the procedure repeated until  $U^1$  differs from  $U^0$  only by a tolerable amount. Wave-functions so determined are called Hartree-Fock functions.

In contemporary work a similar procedure is used, based on Dirac's relativistic wave equation. One refers to RHF (relativistic Hartree-Fock) calculations.

### 5. INTERACTIONS IN FREE ATOMS: NEXT APPROXIMATIONS

#### 5.1 Electrostatic Non-central Forces: Electron Correlation

The foregoing sections have been written in the context of central forces: equation (27), instead of the more complete



equation (26). The term  $H_1 = \left[ \sum_{i>j} e^2/r_{ij} - U(r_i) \right]$  in the

hamiltonian has been neglected. Here we consider the implications of this term in relation to (a) energy eigenvalues and (b) the labelling of energy eigenstates.

As for energy eigenvalues, the totality of the contributions arising from the interactions between all the electrons in a closed shell ( $n\ell$ ) and an external electron is independent of the  $m$  and  $s_i$  values within the shell: these interactions therefore lead to a shift of energy of the whole configuration. It remains to consider the effect of  $H_1$  for electrons in incompletely closed shells.

Physically, the electron-electron repulsion constitutes a torque on the motion of each electron due to the other. Hence the individual orbital angular momenta are perturbed, though the total orbital angular momentum remains constant. Mathematically,  $\sum e^2/r_{ij}$  commutes with  $\hat{\tilde{L}} = \sum_i \hat{\tilde{\ell}}_i$ , but the  $\hat{\tilde{\ell}}_i$  are correlated.

Thus, the total orbital angular momentum provides good quantum numbers. The eigenvalues of  $\hat{\tilde{L}}^2$  and  $\hat{\tilde{L}}_z$  can be used as labels for the energy eigenstates and energy levels.<sup>2</sup> Moreover, the total angular momentum,  $\hat{\tilde{J}}$ , constituted of electron spin as well as orbital angular momentum:

$$\hat{\tilde{J}} = \sum_i \hat{\tilde{\ell}}_i + \sum_i \hat{\tilde{s}}_i = \hat{\tilde{L}} + \hat{\tilde{S}}, \quad (30)$$

also commutes with the total hamiltonian. So, therefore, does  $\hat{\tilde{S}}$ .

In this approximation (we have not yet incorporated spin-orbit interaction) we use quantum numbers  $L, M_L$ ;  $S, M_S$ ;  $J, M_J$  to label energy levels. The labels  $L, S, J$  mean that the states are eigenstates of  $\hat{\tilde{L}}^2$ , etc, with eigenvalues  $L(L+1)\hbar^2$ , etc. The labels  $M_L$  etc. means that the states are eigenstates of  $\hat{\tilde{L}}_z$  etc. with eigenvalues  $M_L\hbar$  etc.

The  $M$ -labels are generally not required for isolated atoms, for then the energy does not depend on the  $M$ . Neither does the energy depend on  $J$  so long as spin-orbit interactions are excluded. Under electrostatic interactions alone, therefore, energy levels are distinguished by  $L$  and  $S$ . We speak of terms as, for example, the triplet D term - meaning,  $L = 2$ ,  $S = 1$ . This has a different energy from the singlet D term, for which  $L = 2$ ,  $S = 0$ .

If the interactions are between electrons having the same ( $n\ell$ ), then the ( $n\ell$ ) also remain good quantum numbers, but not the  $m$  or the

$s_{\pm}$ . But if the electrons are in different configurations, then the  $(nl)$  values lose their status as good quantum numbers to the extent that the perturbation energy  $\langle nl | H_1 | n' l' \rangle$  is, or is not, a significant fraction of  $(E_{nl} - E_{n' l'})$ : (first order perturbation theory). If the perturbation energy is significant we speak of configuration mixing.

## 5.2 Spin-orbit Interaction: Single Electron

So far we have taken account only of electrostatic forces between atomic nuclei and electrons. In non-relativistic treatments we must write in explicitly the magnetic property of electrons, that they have a dipole moment proportional to the spin.

We write the operator equation

$$\hat{\mu}_e = -g_e \beta \hat{S}, \quad (31)$$

where  $\beta$  is the Bohr magneton ( $e\hbar/2m$ ) and  $g_e$  is a numerical factor (Landé g-factor) to be determined. (Notice the minus sign. It takes care of the negative sign of the charge on the electron.  $\beta$  is a positive quantity.  $g_e$  is a positive number. Contrast (31) with (40), the corresponding equation for nuclei. The convention we are using here is not followed by all authors.)

The first experiments (1% accuracy) gave  $g_e = 2$ . This was supported by Dirac's relativistic wave equation applied to the electron specified by  $-e$  and  $m$  only: such a particle must possess also spin and magnetic moment, with  $g_e = 2$ , exactly.

Experiments of higher accuracy (Nafe, Nelson, Rabi; Phys. Rev. 1947) showed that this relation is not exact. The theory of QED provides a theoretical foundation for the difference. The 'g-factor anomaly' is an exceedingly important area of current research, and will be dealt with in other lectures.

From a non-relativistic standpoint, the property  $\hat{\mu}_e$  requires additional terms in the hamiltonian, so far neglected. The magnetic dipole experiences a magnetic field attributable (in the frame of the electron) to the motion of charged particles round it (nucleus + other electrons). The perceived magnetic field acting on the electron labelled  $i$  is  $\xi(r_i) \hat{L}_i \cdot \hat{S}_i$ , where  $\xi(r_i)$  is a function which may (in principle) be ascertained.  $\xi$  will, of course, contain the value of  $g_e$ .

proportional to  $L_i$ . The interaction hamiltonian may be written



The interaction

$$H_2 = \sum_i \xi(r_i) \hat{\mathbf{l}}_i \cdot \hat{\mathbf{s}}_i \quad (32)$$

summed over all the electrons in a complete shell ( $nl$ ) is zero.

For a single electron outside closed shells, as, for example, in alkali atoms,  $H_2$  represents a perturbation of the orbital angular momentum. The field (proportional to  $\hat{\mathbf{l}}$ ) exerts a torque on the electron magnetic moment (proportional to  $\hat{\mathbf{s}}$ ), and, reciprocally. Let us discuss this a little more fully than we did for the electrostatic case. In classical mechanics, analysis of coupled angular momenta yields the result that the coupled system undergoes precessional motion round an axis along the vector resultant of the angular momenta. In quantum mechanics motion of this kind is seen as the time-evolution of a state vector that is a coherent superposition of eigenstates of the resultant angular momentum. Thus, define an operator

$$\hat{\mathbf{j}} = \hat{\mathbf{l}} + \hat{\mathbf{s}}, \quad (33)$$

a dynamical variable of the coupled system, to represent the total angular momentum. The eigenstates of the hamiltonian (32) are also eigenstates of  $\hat{\mathbf{j}}^2$  and of  $\hat{j}_z$ , with eigenvalues  $j(j+1)\hbar^2$ ,  $m_j\hbar$ . For a single electron  $j$  takes the values  $\frac{1}{2}, \frac{3}{2}, \frac{5}{2}, \dots$

It is easy to work out the eigenvalues of  $H_2$  for a single electron if we suppose the average value of  $\xi(r_i)$ , for a specified spin-orbital, to have been evaluated. Call it  $a/\hbar$ . Then

$$H_2 = (a/\hbar) \hat{\mathbf{l}} \cdot \hat{\mathbf{s}} = \frac{a}{2\hbar} (\hat{\mathbf{j}}^2 - \hat{\mathbf{l}}^2 - \hat{\mathbf{s}}^2), \quad (34)$$

by use of (33). The eigenstates of  $H_2$  bear the labels  $j, l, s$ ; the eigenvalue is  $\frac{a\hbar}{2} [j(j+1) - l(l+1) - s(s+1)]$ . For a given orbital  $l$  has a specific value, and  $s(s+1)$  is  $3/4$ .  $j$  may take the values  $l \pm \frac{1}{2}$ . The difference between the two eigenvalues is

$$\Delta \equiv E_{l+\frac{1}{2}} - E_{l-\frac{1}{2}} = \frac{a\hbar}{2} \left[ (l+\frac{1}{2})(l+\frac{3}{2}) - (l-\frac{1}{2})(l+\frac{1}{2}) \right] = a\hbar(l+\frac{1}{2}). \quad (35)$$

The Bohr frequency corresponding to this difference is  $\Delta$ . An atom which has been prepared in a superposition-state of  $(l \pm \frac{1}{2})$  will precess at the angular frequency  $a(l+\frac{1}{2})$ . This precession may be detected physically in a number of ways - by the generation of an e.m.f. in a coil (in principle) or by the observation of modulated, fluorescent light (which has been accomplished, in fact).

### 5.3 Spin-orbit Interaction: Many Electrons

The hamiltonian is now

$$H_2 = \sum_i \xi(r_i) \hat{\mathbf{l}}_i \cdot \hat{\mathbf{s}}_i \quad (36)$$

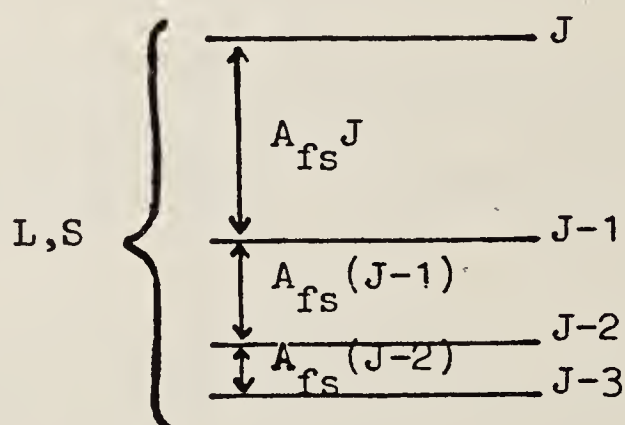
If we assume that the perturbation due to this interaction is small compared to the energy differences between terms (specified by  $L, S$ ), then we can work with the average of  $H_2$  for each term (first order perturbation theory). We can then show that

$$\bar{H}_2 = (A_{fs}/\hbar) \hat{\mathbf{L}} \cdot \hat{\mathbf{S}} \quad (37)$$

where  $A_{fs}$  can be evaluated. The eigenvalues of (37) are  $\frac{1}{2}A_{fs}\hbar[J(J+1) - L(L+1) - S(S+1)]$ , whence

$$\Delta(J, J-1) \equiv E_J - E_{J-1} = A_{fs}\hbar J. \quad (38)$$

This is known as the interval rule. It implies that the  $J$ -degeneracy of terms is broken by the spin-orbit interaction according to the following diagram.



If then, such a structure can be established experimentally, the interval rule may be applied to determine  $J$ -values. If the interval rule is not obeyed, the spin-orbit interaction is not small compared to other energy differences.



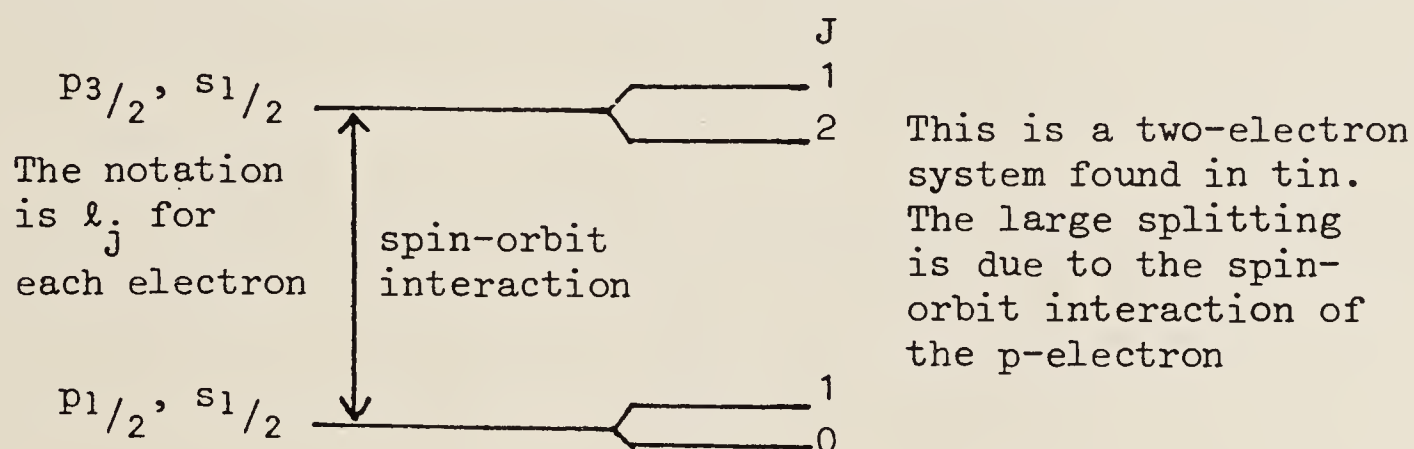
## 5.4 Coupling Schemes: j-j Coupling

We must consider the possibility that the total spin-orbit interaction for a number of valence electrons is greater than the electrostatic  $H_1$  interaction. In such cases the LSJ coupling scheme is inappropriate. We should first choose labels for the single electrons ( $\ell_i s_i j_i$ ) and evaluate the sum of the corresponding <sup>spin-orbit</sup> energies

$$\Delta E_2 = \sum_i (\Delta E_2)_i \quad (39)$$

The energy levels are labelled with the set of single-electron quantum numbers.  $J$  is still a good quantum number, but the levels are degenerate in  $J$ .

The average of  $H_1$  is now evaluated, and is different for different  $J$ , though these differences are small compared with the differences between the groups which differ in  $j$ . This is called 'j-j' coupling. An example of a level structure is shown below. Notice that  $L$  and  $S$  do not appear in the description of levels.



## 5.5 Coupling Schemes: General

The L,S,J scheme (electrostatic interactions greatest) is named after Russell and Saunders, who first explained it. It is very commonly used to label energy levels, although it is not always justified, and the ascription of values of  $L$  and  $S$  is, to that extent, doubtful.

The j-j scheme (magnetic interactions greatest) is likewise clear-cut only exceptionally.

Other schemes are used, for example, when the electrostatic interactions between the electrons in a partially-filled shell are strong (LS coupling between these), but the interaction between these and an electron in a different shell is weak. Then an appropriate scheme is (LSK) $jJ$ , where  $K$  is written for the ' $J$ ' of the shell.

Further breakdown of these coupling schemes occurs when hyper-

fine interactions (see later) become comparable with the interactions  $H_1$  and  $H_2$  of the preceding sections. An example is to be found in the spectrum of lithium.

## 6. NUCLEAR EFFECTS

To this point in our discourse the nucleus has been represented as a point mass, carrying electric charge. We now address the consequences of a more realistic description of nuclei. These consequences, in terms of incremental energy, are - apart from some exceptional cases - small in relation to the energy intervals we have so far considered. To that extent, the quantum numbers already allocated remain 'good', but we need to introduce additional quantum numbers to describe additional degrees of freedom for a complete description of the internal structure of the atom. However, the consequences in terms of inertia are not small: the total angular momentum, and hence the response to external torques can be grossly affected by the inertial properties of nuclei. Landé g-factors (see Zeeman effect) can be grossly changed, so also can the geometrical factors which govern the interaction with light. Transitions that were forbidden can become allowed (weakly). The polarization of scattered light can be affected (strongly).

The additional structure and the small energy increments are different for different isotopes of the same element. Hence, the spectra of mixtures of isotopes are richer in structure than the spectra of single nuclear species. It is customary to treat these latter effects under the name 'hyperfine structure' - this will be our usage. But some authors include multiple-isotope effects under 'hyperfine structure'.

### 6.1 Hyperfine Structure

Nuclei of odd mass number, and some nuclei of even mass number ( $^2\text{H}$  is a well-known example) carry spin and magnetic and electric multipole moments. Of these, the magnetic dipole moment and the electric quadrupole moment are most important, but higher moments (for example, magnetic octupole moment, electric hexadecapole moment) may be responsible for small measurable contributions to energy intervals in determinations at the highest accuracy.

### 6.2 Magnetic Dipole Interaction

To the extent that this interaction is small compared with nuclear excitation energies (an extremely well-satisfied condition) the nuclear spin  $\hat{I}$  is a constant of the motion,  $I$  is a good quantum number, and we write the magnetic moment

$$\hat{\mu}_I = g_I \mu_N \hat{I}, \text{ (operator equation).} \quad (40)$$



$\mu_N$  is the nuclear magneton,  $e\hbar/2(\text{proton mass})$ , a positive quantity.  
 $g_I$  is found to be sometimes positive, sometimes negative.

To the extent that the interaction is small compared with the separation of electronic states (this condition is not always well-satisfied),  $J$  is also a good quantum number. The magnetic field acting on the nucleus by virtue of the motion of the electronic charge (orbital contribution) and the proximity of the electronic magnetic dipoles (spin contribution) is proportional to  $\underline{J}$ :

$$\hat{B}_{el} \propto \underline{\hat{J}}. \quad (\text{operator equation}) \quad (41)$$

The interaction hamiltonian may be written

$$H_{mag} = (A/\hbar) \underline{\hat{I}} \cdot \underline{\hat{J}}. \quad (42)$$

The development follows as for L-S coupling: define

$$\underline{\hat{F}} = \underline{\hat{I}} + \underline{\hat{J}}, \quad (43)$$

(compare (30) and (33)). Label states with  $F, M_F$ .

The eigenvalues of (42) are

$$E_{mag} = \frac{A\hbar}{2} [F(F+1) - J(J+1) - I(I+1)] \quad (44)$$

One deduces an interval rule

$$\Delta(F, F-1) \equiv E_F - E_{F-1} = A\hbar F \quad (45)$$

similar to (38).  $A$  contains  $g_I$ . Notice that this interval rule is simply a consequence of the cosine coupling  $\underline{\hat{I}} \cdot \underline{\hat{J}}$ .

### 6.3 Electric Quadrupole Interaction

If the distribution of electric charge in the nucleus is not spherically symmetrical, it may be represented by an expansion in spherical harmonics. It is generally argued that the first moment (electric dipole) must be zero on the grounds that nuclear states must have a definite parity (nuclear hamiltonian invariant under the parity operation), but this is a matter for experimental verification. It is essentially the same problem as whether magnetic monopoles exist. If evidence for the ~~latter~~ were to be found, the ~~former~~ could not be ruled out.

Nuclear electric quadrupole moments do exist and are defined as the expectation value,  $Q$ , of the second moment of the charge

distribution about the symmetry axis, which is the direction of  $\hat{\mathbf{I}}$ . This charge distribution interacts with the gradient of electric field due to the electron charge distribution which has symmetry axis  $\hat{\mathbf{J}}$ . The hamiltonian is

$$H_{el} = eQ \left\langle \frac{\partial^2 V_e}{\partial z^2} \right\rangle \left[ \frac{3(\hat{\mathbf{I}} \cdot \hat{\mathbf{J}})^2 / \hbar^4 + \frac{3}{2}(\hat{\mathbf{I}} \cdot \hat{\mathbf{J}}) / \hbar^2 - I(I+1)J(J+1)}{2I(2I-1)J(2J-1)} \right] \quad (46)$$

and the eigenvalue for the state  $|IJF\rangle$  is

$$E_{el} = \frac{B\hbar}{4} \frac{\frac{3}{2} K(K+1) - 2I(I+1)J(J+1)}{I(2I-1)J(2J-1)} \quad (47)$$

where  $B\hbar = eQ \left\langle \frac{\partial^2 V_e}{\partial z^2} \right\rangle$  and  $K = F(F+1) - J(J+1) - I(I+1)$

Significant points to notice are

- (i) there can be no quadrupole interaction unless both  $I$  and  $J$  are greater than  $\frac{1}{2}$ ;
  - (ii) the formula (46) represents a distortion of the interval rule;
- and (iii)  $Q$  can be determined from the deviations from the interval rule provided it is possible to evaluate

$\left\langle \frac{\partial^2 V_e}{\partial z^2} \right\rangle$ . This is quite a difficult matter

because, even if the electronic wave functions for a spherical nucleus are known, these are distorted by the non-spherical nucleus and so depend on  $Q$ . Corrections for these effects are associated with the name of Sternheimer.

#### 6.4 Parameterisation of Hyperfine Structure

Although we have set down the physical basis of the incremental  $E_{mag}$  (44) and  $E_{el}$  (47) in relation to the nuclear properties  $g_I$  and  $Q$ , it will be appreciated that the quantities immediately deducible from spectroscopic measurements are the magnetic dipole A-factor and the electric quadrupole B-factor. Our definitions give these in units of angular frequency (radians/sec), but they are frequently given in other units.  $A$  and  $B$  may be regarded as parameters in <sup>two</sup> terms of which hyperfine intervals are expressed. If more than ~~three~~ intervals are measured, the parameterisation may be inadequate. Then one has to consider the possibility that higher moments are in question. But it must also be asked whether the structure is being



distorted by the technique of measurement.

### 6.5 Isotope Effects - Mass

We have already shown (section 2.1) how the effect of finite nuclear mass makes itself felt in atomic spectra by

- (i) a 'normal' effect - easy to calculate,
- and (ii) a 'specific' effect - difficult to calculate.

These differences (relative to infinite mass) make themselves felt between different isotopes of the same element as a second order effect.

The most important element, in relation to fundamental constants, is H. Here, there is no specific effect. Recall that the normal effect is the replacement of  $m$  by  $mM/(m + M)$ , where  $M$  is the nuclear mass. It follows that measurement of the isotope shift between H and D is an important source of information on the electron/proton and electron/deuteron mass ratios.

### 6.6 Isotope Effects - Volume

The spherically-averaged charge distribution is different for different isotopes of the same element, and the central-field energy reflects this distribution. Experimentally-determined differences between corresponding lines in the spectra of different isotopes, when corrected for mass effects, are interpreted as 'volume' or 'field' effects. They are a significant source of information on nuclear structure. Particularly important information comes from muonic atoms, where a negative muon has replaced an electron. The muon, being heavier than the electron, penetrates more deeply into the nuclear charge distribution.

### 6.7 Isotopic Anomalies in Hyperfine Structure

For different isotopes it is sometimes possible to measure directly the ratio of the  $g_I$  factors (in molecular beam experiments, for example) to an accuracy much greater than absolute determination of the  $g_I$ . These ratios are sometimes found to differ from the ratios of the corresponding  $A$  factors, which is at first sight surprising since the factors in  $A$  which relate to the magnetic field generated by the electron distribution should be the same for different isotopes. The effect was interpreted by A. Bohr and V. Weisskopf as a consequence of the distribution of magnetic moment over the nuclear volume, a distribution which differs between isotopes. Again, this 'hyperfine anomaly' furnishes material for testing theories of nuclear structure.

The effects we have mentioned - mass, volume, distribution of moments - enter again in QED calculations at the most detailed level of comparison between theory and experiment.

## 7. ZEEMAN EFFECT

The effects arising from the application of external fields are important, not simply because the measurable energy shifts furnish important information about the atoms, but also because the interaction with polarized radiation is different for states of different  $m_J$  or  $m_F$  (eigenstates of  $\hat{J}_z$  or  $\hat{F}_z$ ) belonging to a group of states having the same total angular momentum ( $J$  or  $F$ ). Such fields may be electric (Stark effect) or magnetic (Zeeman effect). We concentrate on the latter.

The polarization selection rules may, of course, be deduced from the fully quantum-mechanical theory of the interaction between radiation and matter, but it is helpful to regard them from two other points of view: (i) as expressions of the conservation of components of angular momentum between radiation and matter (photons have spin 1), and (ii) as expressions of the underlying classical interactions. We elaborate the latter point.

Distinguish between electric dipole and magnetic dipole interactions (or interactions of higher polarity). As example, we choose electric dipole. The oscillating field interacts with the electrons as charged particles, and the response is primarily that of the orbital motion of the electrons. If there is no electron spin ( $S = 0$ ; singlet states) and no nuclear spin ( $I = 0$ ), the response of the atom is that of classical charged particles under an applied field. Hence, the polarization rules of the Zeeman effect may easily be understood: for example, the spectral components whose frequency does not change are those corresponding to charged particles oscillating parallel to the applied magnetic field. For this component of motion the field exerts no torque - hence, no change is found in the frequency of the emitted light. If  $S$  or  $I$  are not zero, the orbital motion experiences a torque and electrons which may have been excited to oscillate parallel to the applied field will no longer do so: fluorescent light will be depolarized. The rules are:  $\Delta M = 0$  (called a  $\pi$ -transition);  $\Delta M = \pm 1$  (called  $\sigma_{\pm}$ -transitions.  $\sigma_{+}$  is  $\Delta M = +1$  in absorption). This notation is universal for electric dipole transitions, but some authors interchange  $\pi$  and  $\sigma$  for magnetic dipole transitions.

### 7.1 Energy Eigenvalues

Magnetic fields remove the degeneracy of the set of  $m_F$  belonging



to a given F. (We shall continue the discussion in the context of Zeeman effect of hyperfine structure.) The energy differences are given by the eigenvalues of the energy operator

$$H_Z = -\hat{\underline{\mu}} \cdot \underline{B}, \quad (48)$$

where  $\underline{B}$  is the externally-applied magnetic field.  $\hat{\underline{\mu}}$  is the magnetic moment operator for the whole atom, and consists of the sum of the operators for all the electron orbital and spin components, together with that for the nuclear magnetic moment. The extent to which we have to take the components separately depends on the eigenvalues of (48) in relation to the corresponding binding energies. We shall proceed on the assumption that the eigenvalues are small compared with the energy intervals between states of different J: then, the constituents of J are not uncoupled, and  $\hat{\underline{\mu}}$  is represented by  $\hat{\underline{\mu}}_J + \hat{\underline{\mu}}_I$ . By use of (31) (generalised for J) and (40), the energy operator becomes

$$H_Z = (g_J \beta \hat{\underline{J}} - g_I \mu_N \hat{\underline{I}}) \cdot \underline{B} \quad (49)$$

which has to be added to the hyperfine operators  $H_{\text{mag}}$  (equ. 42) and  $H_{\text{el}}$  (equ. 46). But if we could have made the further assumption that the eigenvalues were small compared with the hyperfine intervals ( $E_{\text{mag}} + E_{\text{el}}$ ) (equations (44) and (47)), then we could have written

$$H_Z = g_F \beta \hat{\underline{F}} \cdot \underline{B} \quad (50)$$

using, for convenience but not from necessity, the Bohr magneton  $\beta$ .

It is convenient (but not essential) to choose a z-axis in the direction of  $\underline{B}$ . Then, in (50) we find the operator  $\hat{F}_z$ . The most convenient set of basis states for the evaluation of (50) is the set labelled by fixed values of J, I, F, with values of  $M_F$  - to label eigenstates of  $\hat{F}_z$  - running from -F to F. The eigenvalues of  $H_Z$  are then, clearly,

$$E(M_F) = g_F \beta B M_F \quad (51)$$

Evaluation of (49) in this representation yields

$$g_F = g_J \frac{F(F+1) + J(J+1) - I(I+1)}{2F(F+1)} - g_I \left( \frac{\mu_N}{\beta} \right) \frac{F(F+1) - J(J+1) + I(I+1)}{2F(F+1)} . \quad (52)$$

Equation (52) simply expresses the fact that, when  $\underline{J}$  and  $\underline{I}$  are strongly coupled, the time-averaged magnetic moment of the whole atom is the sum of the components of  $\underline{\mu}_J$  and  $\underline{\mu}_I$  in the direction of  $\underline{F}$ .

Further, because  $g_J$  and  $g_I$  are of order unity, and because  $(\mu_N/\beta) = (m/M) \approx 10^{-3}$ , it is often legitimate to neglect the  $g_I$  term in (52). Contrast this with

$$\underline{\hat{F}} = \underline{\hat{J}} + \underline{\hat{I}} . \quad (53)$$

$\langle \underline{J} \rangle$  and  $\langle \underline{I} \rangle$  have comparable magnitudes. The magnetism of the nucleus may often be neglected in considering the interaction of atoms with external magnetic fields, but the inertia may not be neglected.

Equation (51) expresses the weak field Zeeman effect of hyperfine structure. The approximation on which it is based is frequently violated in laboratory experiments and the  $M_F$  labelling is not then useful. We recall the strong field situation - Zeeman splittings large compared with hyperfine intervals. In this case we have to take  $H_Z$  together with  $H_{\text{mag}}$  and  $H_{\text{el}}$ . The best representation to choose is that in which equation (49) is diagonal, namely, the eigenstates of  $\hat{J}_z$  and  $\hat{I}_z$ , labelled by  $M_J$  and  $M_I$ . The eigenvalues of (49) are  $g_J \beta M_J \hbar - g_I \mu_N M_I \hbar$  but the second term is very small and may often be neglected. The diagonal elements of  $H_{\text{mag}}$  and  $H_{\text{el}}$ , however, are significant, being intermediate in size between  $g_J \beta M_J \hbar$  and  $g_I \mu_N M_I \hbar$ . To evaluate them one needs the diagonal elements of  $\underline{\hat{I}} \cdot \underline{\hat{J}} = \hat{I}_x \hat{J}_x + \hat{I}_y \hat{J}_y + \hat{I}_z \hat{J}_z$ . In this representation only  $\hat{I}_z \hat{J}_z$  has diagonal elements. Its eigenvalues are  $M_I M_J \hbar^2$ . In writing the result we shall simplify by supposing  $H_{\text{el}}$  to be zero. Then:

$$E(M_J, M_I) = g_J \beta M_J \hbar + A \hbar M_J M_I (-g_I \mu_N M_I \hbar B). \quad (54)$$

We have neglected the off-diagonal components of  $\underline{\hat{I}} \cdot \underline{\hat{J}}$ .

We frequently have to deal with the intermediate case, when the Zeeman energies are neither very small nor very large compared with the hyperfine intervals. What set of basis states should we use for this case? Any set of basis states which spans the Hilbert space will serve our purpose. The energy operator must again embrace the



hyperfine as well as the Zeeman hamiltonians:

$$H_{\text{total}} = H_{\text{mag}} + H_{\text{el}} + H_Z \quad (55)$$

- the terms on the RHS are spelt out in equations (42), (46) and (49).

The good quantum numbers are  $I$  and  $J$ . With each of these is associated  $(2I + 1)$ ,  $(2J + 1)$  component states, and this is the number of basis states we need for the  $(F, M_F)$  as well as for the  $(M_J, M_I)$  representation. If we use  $|F, M_F\rangle$  states the matrix of  $H_{\text{total}}$  is diagonal for  $H_{\text{mag}}$  and  $H_{\text{el}}$  but not for  $H_Z$ . If we use  $|M_J, M_I\rangle$  states the matrix of  $H_Z$  is diagonal, but not that of  $H_{\text{mag}}$  or  $H_{\text{el}}$ . For either choice the matrix of  $H_{\text{total}}$  contains off-diagonal components and to find the energy eigenvalues we must diagonalise the matrix. These energy eigenvalues are physically observable quantities and are the same, whichever set of states we use.

The diagonalisation of a square matrix sounds formidable, but such a matrix may be factorised by grouping together entries having the same value of  $M_F$  (if the one representation is used) or  $M_J + M_I$  (if the other). These numbers, total  $M$ , are eigenvalues of the operator proportional to the component of total magnetic moment along the field. The field exerts no torque on this component, hence it is a constant of the motion, and total  $M$  is a good quantum number for all values of the field. It is a useful label for energy levels plotted as a function of the field. A level labelled  $M = M_F$  in weak fields is labelled with the same value of  $M = M_J + M_I$  in strong fields. The number of levels bearing the value  $M=0$  (or  $M=\frac{1}{2}$ ) is the same as the number of different values of  $F$ . This is the number of rows and columns in the largest matrix that needs to be diagonalised. We speak of levels with the same value of  $M$  as interacting with one another.

An example of the Zeeman structure of hyperfine levels is given in the next section.

## 8. HYDROGEN

The special importance of atomic hydrogen lies in its simplicity, as a composite particle: a two-body problem, capable, in classical terms, of exact solution. And while this is true in quantum physics, up to a point, contemporary experimental physics poses problems for the theorist that go beyond that point. Contemporary theoretical physics does not go as far as we could wish in predicting the energy-level structure of H.

The difficulties lie in two categories: problems with fundamental theory - quantum electrodynamics, and problems concerning the particles - the proton is not a simple, point particle. QED will form the subject of other lectures. As to the particles, there are other two-body systems, and some of these are simpler: positronium, for instance.

In this lecture we shall not be concerned with difficulties at this level. But when we speak of H, it is to be realised that the ideas and equations will be applicable, with minor and obvious changes, to many other systems, in particular (i) the isotopes of hydrogen, (ii) the one-electron ions of the elements,  $\text{He}^+$ ,  $\text{Li}^{++}$ ..., (iii) positronium,  $e^+e^-$ , (iv) muonium,  $\mu^+e^-$ . The differences, so far as they concern us here, lie first in the masses of the particles; these are easy to cope with: the reduced mass formulae apply. Secondly, differences lie in particle spin and g-factors, so the hyperfine structures are different. The common feature of these systems is, of course, the Coulomb field, which is the dominant interaction, and this we now take into consideration.

### 8.1 Consequences of the Coulomb Field

We recall that Bohr's theory predicts energy levels  $E_n = -R/n^2$  and that Schrödinger's equation, with the Coulomb potential, yields the same result. Corrections can be applied to take account of the relativistic variation of electron mass with velocity, and spin-orbit interaction. Remarkably, these together yield the same result for energy eigenvalues as the Dirac theory, to which we now turn.

### 8.2 Dirac Theory: Relativistic Wave Equation

Schrödinger's equation is not acceptable in the context of special theory (is not invariant in form under the Lorentz transformation). This is obvious because it relates second-order space derivatives such as  $\partial^2/\partial x^2$  to the energy, which is represented by the first-order time derivative  $\partial/\partial t$ . The difficulty is overcome in Dirac's wave equation, which is based on the hamiltonian

$$H_D = (\underline{\alpha} \cdot \underline{\hat{p}})c + \beta m_0 c^2 - eV(r) \quad (56)$$

for a particle of rest mass  $m_0$ , charge  $-e$ , in a static potential  $V(r)$ .  $\underline{\hat{p}}$  is the operator  $-i\hbar \underline{\text{grad}}$ . The three components of  $\underline{\alpha}$  and  $\beta$  are operators represented by four-by-four matrices. The space derivatives in (56) now appear in first order. The kinetic energy part of  $H_D$  represents the relativistic form of the energy of a free particle,  $(p^2 c^2 + m_0^2 c^4)^{1/2}$ : the operators  $\underline{\alpha}$  and  $\beta$  were invented by Dirac to enable the square root to be taken.



Since  $\alpha$  and  $\beta$  are represented by four-by-four matrices, the wave functions on which they operate must have four components.

Analysis of Dirac's equation for charged particles in an electromagnetic field shows that such particles must be possessed of two-valued spin and associated magnetic moment of magnitude  $q\hbar/2M_0$ , (charge  $q$ , rest mass  $M_0$ ). This applies to protons no less than to electrons - but for protons there is additional magnetic moment arising from the strong nuclear force. Leaving aside for the moment these properties of the hydrogen nucleus, we return to the problem of the electron in a central, electrostatic field.

The quantum numbers for the energy eigenstates are, in addition to  $s$  (spin), the total angular momentum,  $j$ , and an integer,  $n$ , which has the same significance as in the non-relativistic case. But the energy eigenvalues are degenerate in  $s$ : they depend only on  $n$  and  $j$ :

$$E_{n,j} = m_0 c^2 \left[ 1 + \frac{\alpha^2 Z^2}{\left\{ n - (j + \frac{1}{2}) + [(j + \frac{1}{2})^2 - \alpha^2 Z^2]^{\frac{1}{2}} \right\}^2} \right]^{-\frac{1}{2}}$$

$$= m_0 c^2 - \frac{RZ^2}{n^2} \left[ 1 + \frac{\alpha^2 Z^2}{n} \left( \frac{1}{j + \frac{1}{2}} - \frac{3}{4n} \right) + \dots \right], \quad (57)$$

where  $n = 1, 2, 3, \dots$ ,

$j = \frac{1}{2}, \frac{3}{2}, \dots, (n - \frac{1}{2})$ ,

$\alpha = (e^2/\hbar c)(4\pi\epsilon_0)^{-1}$ , the fine structure constant,

$R = (m_e^4/2\hbar^2)(4\pi\epsilon_0)^{-2}$ , the Rydberg constant,

and  $Ze$  is the charge on the nucleus ( $e > 0$ ).

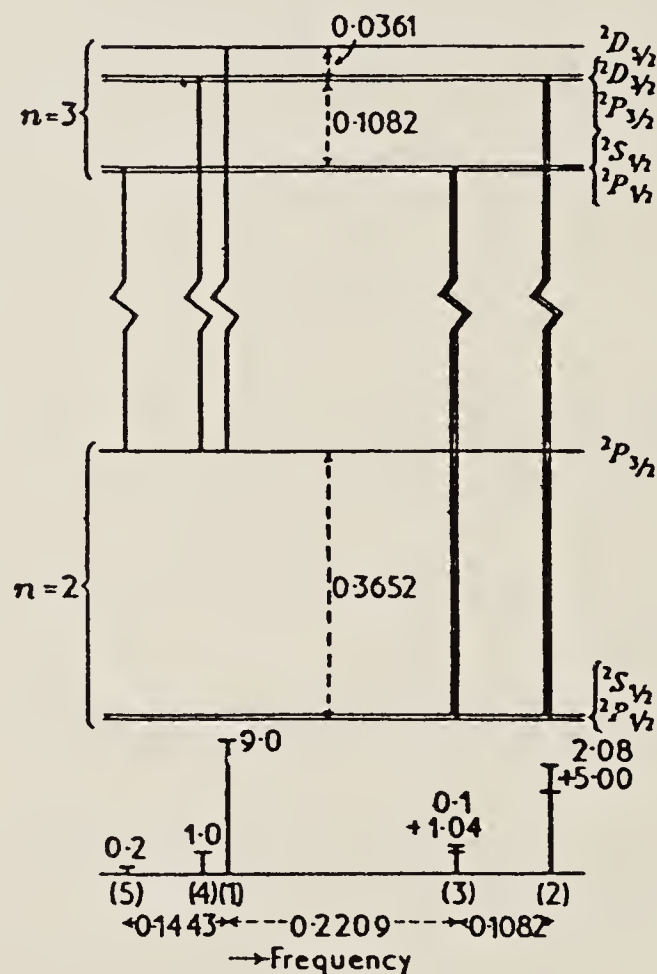
It will be noticed that  $E_{n,j}$  includes the rest-mass energy,  $m_0 c^2$ .

In the context of Dirac's theory we can separate an orbital quantum number  $\ell$  as before:  $\ell = j \pm \frac{1}{2}$  (subject to  $\ell < n$ ).

The dominant term in  $E_{n,j}$ , apart from  $m_0 c^2$ , is the Bohr term,  $-RZ^2/n^2$ . The remaining terms in the expansion are of order  $\alpha^2$  ( $\sim 10^{-4}$ ) for  $Z = 1$ , but become appreciable for large  $Z$ . These are the Sommerfeld-Dirac fine structure terms (Sommerfeld obtained equation (57) from the old form of quantum theory, many years earlier than Dirac, but Sommerfeld's quantum numbers had different physical interpretations.)

The fine structure terms embrace both the dependence of mass on velocity and the spin-orbit interaction. Further, the multiplet structure (set of  $J$  within a given  $L, S$ ) which, in alkali spectra, is distinct from the term structure (set of  $L, S$  within a given electron configuration  $n, l$ ) is here interwoven with it. This arises from the degeneracy in  $l$  which is an accident of the Coulomb potential.

The figure below shows the energy diagram for the fine structure states belonging to  $n = 2$  and  $n = 3$ . The set of allowed transitions between these states constitutes one of the most studied lines in atomic spectra: the first member of the Balmer series, Balmer  $\alpha$ , 656 nm.



Intervals in  $\text{cm}^{-1}$

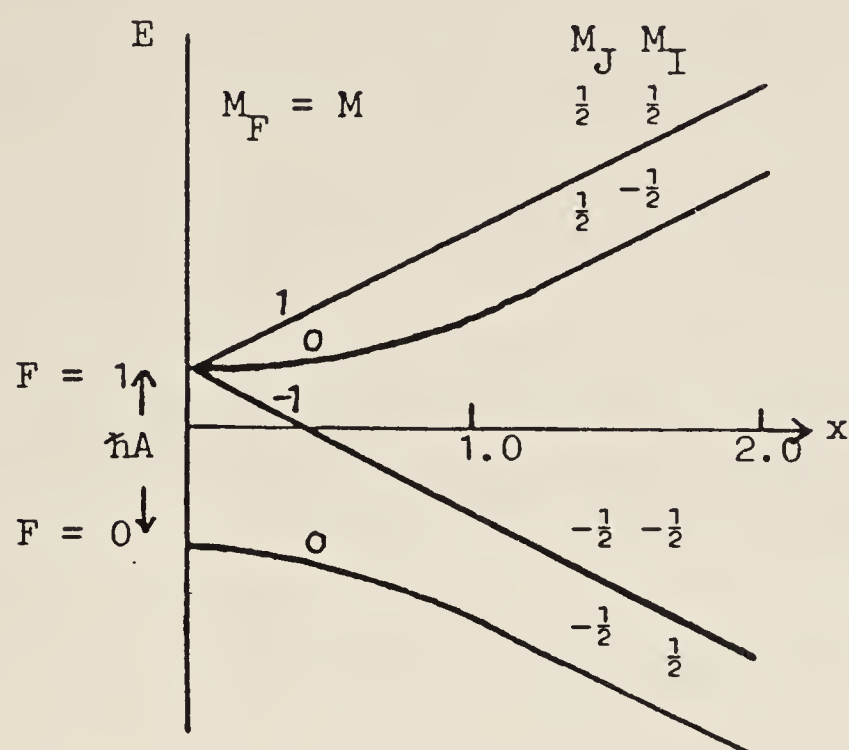
Notice particularly that all levels save the top one in each set are double, corresponding to the two values of  $l$  which belong to every  $j$  (subject to  $l < n$ ).

### 8.3 Hyperfine Structure and Zeeman Effect in $n = 1$

This hyperfine interval and its structure is of the greatest importance in laboratory and astronomical spectroscopy. It forms the basis of the hydrogen maser. It forms the famous 1400 MHz (21 cm) line of the radio astronomers.



We show below the energy eigenvalues for H as a function of magnetic field. The comments are to be read in the context of sections 6 and 7.



Dependence of energy on  $x = (g_J\beta - g_I\mu_N)B/\hbar A$ , where B is the flux density of the magnetic field.

The ground state of H is  $1^2S_{1/2}$ , with  $I = 1/2$ . Hence there are two hyperfine levels, labelled  $F = 1$  and  $0$ . The level  $F = 1$  is three-fold degenerate in zero magnetic field.

Notice that:

- the zero-field interval is  $F\hbar A$ , with  $F = 1$ ;
- the magnetic field is conveniently expressed in terms of a dimensionless variable  $x$ , scaled in relation to  $\hbar A$ ;
- $M_F$  numbers are used in the weak field;  $M_J$ ,  $M_I$  numbers in the strong field region of the diagram;
- for any level, the value of  $M = M_F = M_J + M_I$  remains unchanged as the field varies.
- the total M numbers  $\pm 1$  occur once only; the secular determinants are one-by-one; the energy is a linear function of  $x$ ;
- the total M number  $0$  occurs twice; the secular determinant

is two-by-two; the energy is a quadratic function of  $x$ .

- the diagram has been drawn for  $g_I > 0$ . For  $g_I < 0$  the levels would have been reflected in the axis of  $x$  and the sign on all the  $M$ -numbers would have been changed.
- in the high field region of the diagram the ordering of the  $M_I$  numbers is inverted between  $M_J = \frac{1}{2}$  and  $M_J = -\frac{1}{2}$ .

These sections summarise the energy-level structure of hydrogen as it was believed to be (except that some spectroscopists had expressed reservations) in the period up to, and immediately following World War II. Then came the famous experiment of Lamb and Retherford. But that is another story.

## 9. INTERACTION WITH RADIATION: TRANSITIONS

### 9.1 Preliminaries

A second great achievement of Dirac was to discover how to apply the formal mathematics of quantum theory (non-commuting operators) to radiation, and thus to a closed system consisting of atoms + radiation, allowing the exchange of energy between the two subsystems. The theory is called the quantized field theory. It is enormously successful, but it has serious difficulties, some mathematical, such as those arising from the infinitely-many degrees of freedom required by the field, some conceptual, such as the notion of zero-point fluctuations of the field. There is an alternative theory whose predictions coincide with those of the quantized field theory in the following situations:

- (i) when the radiation field is strong, as is normal in radio-frequency spectroscopy and common in laser spectroscopy. The mathematical condition is that, in the interchange of energy between atom and radiation, the change in the number of photons must be small compared with  $n$ , the number of photons per mode;
- (ii) in absorption processes - even when the energy density of the field is small ( $n \ll 1$ ).

This alternative theory is the so-called 'semi-classical' theory. The field is treated as an ordinary algebraic quantity, not an operator, but the atoms are quantized. In this theory special care has to be taken to describe the spontaneous emission of radiation, but this can be done by appealing to the Einstein equilibrium between



atoms and black-body radiation (A- and B- coefficients). The semi-classical theory, with spontaneous emission treated in this way, should not be confused with the 'neo-classical theory' developed by E. Jaynes and his colleagues.

## 10. SEMI-CLASSICAL THEORY

One writes a hamiltonian for the unperturbed atom,  $H_0$ , and one supposes the energy eigenvalues are known and a suitable labelling has been chosen. We shall use the notation  $|i\rangle, |j\rangle, \dots$ ;  $E_i = \hbar\omega_i, \dots$ . If one wants to take account of the fact that excited states have a finite lifetime owing to spontaneous emission one can do this by adding to the energy  $E_j$  an imaginary component  $-\frac{1}{2}i\hbar\Gamma_j$ . This introduces a damping factor  $\exp(-\frac{1}{2}\Gamma_j t)$  into the time-dependent wave function. The probability of occupation then decays at the rate  $\Gamma_j$ , corresponding to a mean lifetime  $\tau_j = 1/\Gamma_j$ .

To  $H_0$  is added a hamiltonian  $H'(t)$  representing the interaction of the atom with a radiation field. If we are thinking of electric dipole transitions we write

$$H'(t) = -\underline{E}(t) \cdot \hat{\underline{P}} \quad (58)$$

and for magnetic dipole transitions

$$H'(t) = -\underline{B}(t) \cdot \hat{\underline{\mu}} = \underline{B}(t) \cdot (\gamma \hat{\underline{J}}). \quad (59)$$

We can use the same formalism for interactions of higher polarity.  $\hat{\underline{P}}$  and  $\hat{\underline{\mu}}$  are operators representing electric and magnetic dipole moments, respectively.

The total hamiltonian is  $H_0 + H'(t)$ , and this is used in the equation of motion

$$i\hbar \frac{\partial}{\partial t} |t\rangle = \left[ H_0 + H'(t) \right] |t\rangle. \quad (60)$$

We choose a suitable basis for  $|t\rangle$  and work according to one of the 'pictures' outlined in section 3.1. There results a set of differential equations for the probability amplitudes  $a_j(t)$  for the occupation of the state  $|j\rangle$  under given initial conditions - for example,  $a_i = 1$ , all  $a_j = 0$  at  $t = 0$ . These equations are of the form

$$a_j(t) = (-i/\hbar) \sum_i \int_0^t \langle j | H'(t') | i \rangle a_i(t') dt', \quad (61)$$

and can generally not be solved without approximations. But certain general points can be made from (61). We shall investigate resonance, transition matrix elements and rate processes.

### 10.1 Resonance

Suppose we work in the interaction picture. The basis vectors then carry the intrinsic time-variation and the matrix element in (61) will contain a factor  $\exp(i\omega_{ij}t)$ . Resonance occurs when this factor is obliterated by a Fourier component  $\exp(i\omega t)$  of  $H'(t)$ , namely when

$$\omega_{ij} \equiv \omega_j - \omega_i = \omega, \quad (62)$$

that is to say, when

$$E_j - E_i = \hbar\omega. \quad (63)$$

The classical phenomenon of resonance is equivalent to the quantum concept of energy balance.

If the damping factors are written into the basis vectors one obtains a resonance denominator for the interaction,

$[\omega_{ij} - \omega + \frac{1}{2}i(\Gamma_i + \Gamma_j)]$ . This is an approximate expression based on a first-order perturbation solution of the equations.

### 10.2 Transition Matrix Elements. Rate Processes

We have concentrated on the time-dependence of (61). Now let us look at the time-independent factors. Write

$$H'(t) = -(\underline{e}^0 \cdot \hat{\underline{P}}) \int_{-\infty}^{\infty} \underline{E}_{\omega} \exp(-i\omega t) d\omega, \quad (64)$$

where  $\underline{e}^0$  is a unit vector in the direction of  $\underline{E}(t)$ .

The occupation probability  $|a_j|^2$  will be proportional to  $|\langle j | \underline{e}^0 \cdot \hat{\underline{P}} | i \rangle|^2$  and to some integral involving  $|\underline{E}_{\omega}|^2$ . Thus, the probability of transition will depend on the non-vanishing of the transition matrix element, in the shape of its modulus squared. It will also depend in some way on the spectral distribution of the intensity of the light. If this is known it may be possible to carry



out the integration.

In many cases of interest  $|E_\omega|^2$  is approximately constant over the resonance region. In this case the integral over frequencies leads to the result (in first order of perturbation theory) that  $|a_j|^2$  depends linearly on time and on  $|E(\omega_{ij})|^2$ . Taking the limit  $t \rightarrow 0$  to secure the legitimacy of first order perturbation theory, we find an expression for the rate of the transition:

$$\Gamma_{ji} = (2\pi/\hbar^2) |\langle j | \hat{e}^0 \cdot \hat{P} | i \rangle|^2 |E(\omega_{ij})|^2. \quad (65)$$

This is Fermi's Golden Rule. It is important to notice that the transition rate is independent of time. This result is a direct consequence of the assumption that the spectral distribution of  $|E_\omega|^2$  is wide compared with the resonance width of the transition,  $(\Gamma_j + \Gamma_i)$ , the broad-band approximation.

Fermi's Golden Rule is a consequence of linking something with sharply defined energy (in this case, our atom, in the transition  $i \rightarrow j$ ) with another system having a continuum of energy states (in this case, broad-band light having a wide spread of independent Fourier components). One finds the same result in the analysis of photoionisation: here, the light can be monochromatic but the atom has a continuum of states corresponding to the ejection of an electron with kinetic energy of any amount within a wide range.

When transition rates are independent of time we speak of rate processes. The characteristic equation is  $dN/dt = -\Gamma N$ . A rate process taking place over a finite time leads to exponential changes of population:  $N(t) = N(0)\exp - \Gamma t$ .

When the transition matrix element is identically zero we say that there is a selection rule prohibiting the transition. The most important rule for electric dipole transitions arises from the fact that the parity of  $\hat{P}$  is odd. In order, therefore, that the matrix element should not vanish the states  $|i\rangle$  and  $|j\rangle$  must have opposite parity - Laporte's rule.

For magnetic dipole transitions the operator  $\hat{e}^0 \cdot \hat{P}$  above must be replaced by  $\hat{e}^0 \cdot \hat{J}$ . The parity selection rule is that the states must be of the same parity because the parity of  $\hat{J}$  is even.

### 10.3 Selection Rules

Apart from the parity selection rule (preceding paragraph) selection rules involving angular momentum quantum numbers exist and can be understood in terms of conservation of angular momentum between

atoms and light, and coupling schemes.

Dipole radiation:  $\Delta J = 0, \pm 1$ , but  $J = 0 \rightarrow J' = 0$  is forbidden;  
(for hyperfine structure, read F for J).  
Zeeman transitions:  $\Delta m = 0, \pm 1$ .

Electric dipole radiation:  $\Delta l_i = \pm 1$ ,  $\Delta l_{\text{other}} = 0$ .

$\Delta S = 0$ ,  $\Delta L = 0, \pm 1$ : to the extent that  
Russell-Saunders coupling is valid.

Electric quadrupole radiation:  $\Delta l_i = 0, \pm 2$ ,  $\Delta l_{\text{other}} = 0$ .

Parity: even to even or odd to odd.

$\Delta J = 0, \pm 1, \pm 2$ , but  $J = 0 \rightarrow J' = 0$ ;  $J = 0 \rightarrow J' = 1$   
and  $J = \frac{1}{2} \rightarrow J' = \frac{1}{2}$  are forbidden.

Zeeman transitions:  $\Delta m = 0, \pm 1, \pm 2$ .

It is possible for magnetic dipole and electric quadrupole transition matrix elements to be non-vanishing between the same pairs of states. Interesting interference effects have been observed, for example, in the Zeeman components of such transitions.

#### 10.4 Stimulated and Spontaneous Emission.    Lifetime.    Natural Line-width

The procedure we outlined in section 10.2 is satisfactory for calculating absorption rates, which may be written

$$\Gamma_{ji} = B_{ji} \rho(\omega_{ij}) \quad (66)$$

where  $\rho$  is the energy density of unpolarized, isotropic radiation.  
 $B_{ji}$  is Einstein's B-coefficient, whose value is

$$B_{ji} = \frac{\pi e^2}{3\epsilon_0 \hbar^2} \frac{1}{g_i} \sum_{m_j, m_i} \sum_s |\langle m_j | \hat{r}_s | m_i \rangle|^2 \quad (67)$$

The dipole operator  $\hat{P}$  has been replaced by  $\sum_s -e\hat{r}_s$ , where  $s$  labels the electrons in a many-electron atom. Moreover, we have summed over the Zeeman states  $m_i, m_j$  of the lower and upper levels, supposing them to be degenerate.  $g_i$  is the multiplicity ( $2J + 1$ ) of the lower level.

The line of argument which led us to (67) also provides an expression for  $B_{ij}$ , the coefficient of stimulated emission from



$|j\rangle$  to  $|i\rangle$ . Clearly, we have to interchange the labels  $i$  and  $j$ .  
 We obtain the result  $B_{ij} = \frac{g_i}{g_j} B_{ji}$ . (68)

Einstein's well-known discussion of equilibrium between atoms and back-body radiation gives

$$A_{ij}/B_{ji} = \pi^2 c^3 / \hbar \omega_{ij}^3 \quad (69)$$

where  $A_{ij}$  is the rate coefficient for the spontaneous decay of an atom from  $|j\rangle$  to  $|i\rangle$ :

$$dN_j/dt = -A_{ij} N_j. \quad (70)$$

If the atom in state  $|j\rangle$  can decay to a number of lower states  $|i\rangle$ ,

$$\Gamma_j = \sum_i A_{ij} \quad (71)$$

where  $\Gamma_j$  is the decay constant previously used, equal to  $1/\tau_j$ ,  $\tau_j$  being the mean lifetime.

The spectrum of light emitted in the decay from  $|j\rangle$  to  $|i\rangle$  is centred on  $\omega_{ij}$  but has a Lorentz distribution represented by the function

$$I(\omega) = \frac{\text{const}}{(\omega - \omega_{ij})^2 + (\Gamma_{ij}/2)^2} \quad (72)$$

where  $\Gamma_{ij} = \Gamma_i + \Gamma_j$ . The full width at half-intensity, called the natural line-width, is  $\Gamma_{ij}$  (see the figure at the end of section 13).

These results follow from the Fourier analysis of an exponentially decaying oscillation. They represent the squared modulus of the expression for resonance denominator given in the text following equation (63).

The broad-band field corresponding to the function  $\underline{E}(t)$  is described in quantum field theory as 'zero-point field', whose spectrum is that of black-body radiation at absolute zero.

## 10.5 Monochromatic Radiation Fields

Such fields - of which the fields used in radio-frequency magnetic resonance experiments are a good example - are to be strongly contrasted with broad-band fields, since the atomic response is quite

different. Instead of an exponential response we have a sinusoidal response. The 'rate constant' is not a constant, it is a sinusoidal function of time.

We quote the result, calculated by time-dependent methods, for the probability  $P_{ji}(T)$  of finding an atom in state  $|j\rangle$  after a lapse of time  $T$ , given that it was initially in state  $|i\rangle$  and that it is irradiated by a field  $2B_1 \cos \omega t = B_1(\exp - i\omega t + \exp i\omega t)$ : (We are contemplating a magnetic dipole transition, but the analysis holds for all such interactions.)

$$P_{ji}(T) = \frac{|b_{ji}|^2}{p^2} \sin^2 \frac{1}{2} pT, \quad (73)$$

where  $|b_{ji}|^2 = |\langle j|H|i\rangle|^2$ ,  $p^2 = (\omega - \omega_{ij})^2 + |b_{ji}|^2$ ,

with  $H' = -\hat{\mu} \cdot B_1$ .

If both states are subject to damping with the same rate constant  $\Gamma$ , but the population is being replenished by injection into  $|i\rangle$  at a uniform rate,  $R$ , the steady-state population of  $|j\rangle$  is

$$N_j = \frac{(\frac{1}{2}R/\Gamma) |b_{ij}|^2}{(\omega - \omega_{ij})^2 + |b_{ij}|^2 + \Gamma^2} \quad (74)$$

Equation (74) describes a Lorentzian resonance curve having a maximum at the frequency  $\omega = \omega_{ij}$ . The peak of the resonance is proportional to  $|b_{ij}|^2$ , that is, to  $B_1^2$  - the energy density in the field. The width of the curve in the limit of small  $B_1$  is  $2\Gamma$  - representing the sum of the widths of the two states. But the width increases as  $B_1$  increases. This is called 'power broadening'. Notice also that the process depends on the existence of the matrix element  $\langle j|\hat{\mu} \cdot \hat{e}^0|i\rangle$ , where  $\hat{e}^0$  is a unit vector in the direction of the stimulating field.

A subtle point to notice in equation (74) is that resonance occurs for  $\omega = \omega_{ij}$ , not for  $\omega = \omega_{ji}$ . The sign is important:  $\omega_{ij} = -\omega_{ji}$ , and  $\omega$  must change likewise if the transition  $j \rightarrow i$  is to be in resonance. Both frequencies are present in  $\cos \omega t$ , as  $\exp(\pm i\omega t)$ . But only the one or the other is needed to drive the transition in each direction and the inactive component perturbs the resonance. This inactive component is not present if a rotating magnetic field is used, in the conventional magnetic resonance arrangement. The perturbation of the resonance caused by use of an oscillating field



is called the Bloch-Siegert effect. In the context of precision measurements this perturbation may not be ignored.

## 11. QUANTIZED FIELD THEORY

### 11.1 Formalism

A field is quantized by first making a Fourier expansion. The harmonically oscillating fields which form the orthogonal basis for such an expansion are regarded as quantum harmonic oscillators and, for each mode of specified polarization and frequency  $\omega$ , one defines a pair of conjugate variables related to the electric and magnetic components, and writes an expression for the energy density of the field in terms of these variables. One can then define energy eigenstates labelled by  $n$ , where the energy eigenvalues are  $(n + \frac{1}{2})\hbar\omega$ . The operators associated with field amplitudes do not commute with the energy operator, so no definite amplitude may be ascribed to a field of given energy. The field operators connect states which differ in  $n$  by one unit, so one speaks of 'annihilation' or 'creation' operators, meaning the absorption or emission of one photon, energy  $\hbar\omega$ , from the field.

In interaction with atoms, both factors in the interaction operator  $-\hat{\mathbf{E}} \cdot \hat{\mathbf{P}}$  are operators:  $\hat{\mathbf{P}}$  operates as before on the atomic eigenstates and  $\hat{\mathbf{E}}$  on the field eigenstates. A time-dependent calculation shows how, in an atomic transition  $|i\rangle \rightarrow |j\rangle$  the state of the field mode labelled  $\omega$  may change from  $|n\rangle$  to  $|n-1\rangle$ , indicating that energy  $\hbar\omega$  has passed from the field to the atom.  $\omega = \omega_{ij}$  indicates resonance and the conservation of energy.

Some interactions are multi-step, and for such interactions energy need not be conserved at each step. For example, one may be interested in a transition from  $|i\rangle$  to  $|k\rangle$  where the matrix element  $\langle k|P|i\rangle$  is zero but  $\langle j|P|i\rangle$  and  $\langle k|P|j\rangle$  are non-vanishing. For such a transition the field can change in two steps, either the same mode or two different modes. Suppose the latter, the modes being labelled 1,2. Then, energy  $\hbar\omega_1$  may be absorbed from the field in the first transition and  $\hbar\omega_2$  in the second, with  $\omega_1 + \omega_2 = \omega_{ik}$ , but  $\omega_1 \neq \omega_{ij}$ ,  $\omega_2 \neq \omega_{ik}$ . This would be called a 'two-photon transition'. Energy is conserved overall: so also is angular momentum and parity.

The double step from  $|i\rangle$  to  $|k\rangle$  may occur by two different routes:  $i \rightarrow j \rightarrow k$ , and  $i \rightarrow j' \rightarrow k$ . Then, interference effects may show up.

Processes such as these are commonly called 'multiphoton processes', but they can be analysed also by the semiclassical method.

## 12. PRESSURE BROADENING AND SHIFT OF SPECTRAL LINES

The interaction of atoms with radiation may be perturbed by the proximity of other atoms of the same kind, or of different species, or of electrons, or of ions. The perturbation results in a broadening of the spectral lines and possibly also a displacement and distortion of the line profile. The effects arising from the species listed above have different characteristics, and the literature on the subject is vast and controversial. Nevertheless, some general remarks may be helpful.

### 12.1 Impact Approximation

If the interaction with the perturber is strong and takes place in a time short compared with the mean time between such interactions (collisions), it is legitimate to take the view that the interaction with radiation is abruptly terminated. The Fourier analysis of a terminated wave train discloses a spread of frequencies, but the spectrum must be averaged over random times between collisions. There results a spectral distribution of Lorentz form (equation 72), where the width parameter is now

$$\Gamma'_{ij} = \Gamma_{ij} + 2/T_c. \quad (75)$$

$T_c$  is the mean time between collisions. We have, further,

$$1/T_c = N\sigma\bar{v}, \quad (76)$$

where  $N$  is the number density of perturbers,  $\bar{v}$  is the mean relative velocity of the particles, and  $\sigma$  the cross-section for the interaction. The study of line-broadening is a means of determining these cross-sections.

### 12.2 Interaction Potentials.    Scattering Matrix

More thorough studies are based on the formulation of an interaction potential  $V(\underline{r})$  between the perturber and the radiating system. Since  $\underline{r}$  is a function of time the analysis demands time-dependent quantum theory. One calculates the evolution of the radiating system under the perturbation. Suppose  $U(t, t_0)$  is an operator (time-displacement operator) which describes the evolution the system:

$$|t\rangle = U(t, t_0)|t_0\rangle \quad (77)$$

Then  $U(\infty, -\infty)$  describes the whole interaction. This operator is called a scattering operator,  $S$ , which - if its matrix elements can



be calculated and properly averaged - allows all details of the perturbation to be predicted.

The results are often expressed in the form of a complex energy,  $(d + i\omega)\hbar$ . The spectral line shape corresponding to this would be

$$I(\omega) \propto \frac{1}{(\omega - \omega_{ij} + d)^2 + \omega^2} \quad (78)$$

The equation describes a Lorentz profile, shifted from the resonance position  $\omega_{ij}$  by the amount  $d$ , and of width (full width at half-height)  $2\omega$ .

### 13. DOPPLER BROADENING OF SPECTRAL LINES

Whereas the broadening associated with radiative damping ( $\Gamma_{ij}$ , equation (72)) and the broadening arising from interactions with other particles ( $\omega$ , equation (78)) is represented by equations in which the wave-functions are supposed to represent the perturbed, internal structure of a representative atom - and is, for that reason, termed homogeneous broadening - the broadening of spectral lines associated with the random motion of different atoms in an assembly, Doppler broadening, is termed inhomogeneous broadening. The distinction can be maintained insofar as there is negligible overlap between the wave functions associated with different nuclei.

The quantum-mechanical analysis of Doppler broadening must incorporate the wave function of the centre-of-mass,  $\exp(-ikR)$ , where  $R = vt$ , but it is common to describe the motion by classical trajectories.

The outline of the classical analysis is this: the frequency of light from an atom moving with velocity  $v_z$  in the line of sight (z-direction), as detected by a stationary observer, is shifted by the factor  $(1 + v_z/c)$  owing to the Doppler effect in first order. For an assembly of radiating atoms in thermal equilibrium (at temperature  $T$ ) there will be a Gaussian distribution of  $v_z$ :

$$N(v_z) = N\beta\pi^{-\frac{1}{2}} \left[ \exp - (\beta^2 v_z^2) \right] \quad \beta^2 = M/2kT. \quad (79)$$

Frequencies  $\omega_o$  will be shifted to  $\omega' = \omega_o(1 + v_z/c)$ . Hence

$$N(\omega) = (N/\Delta\pi^{\frac{1}{2}}) \left[ \exp - (\omega_o - \omega')^2/\Delta^2 \right], \quad (80)$$

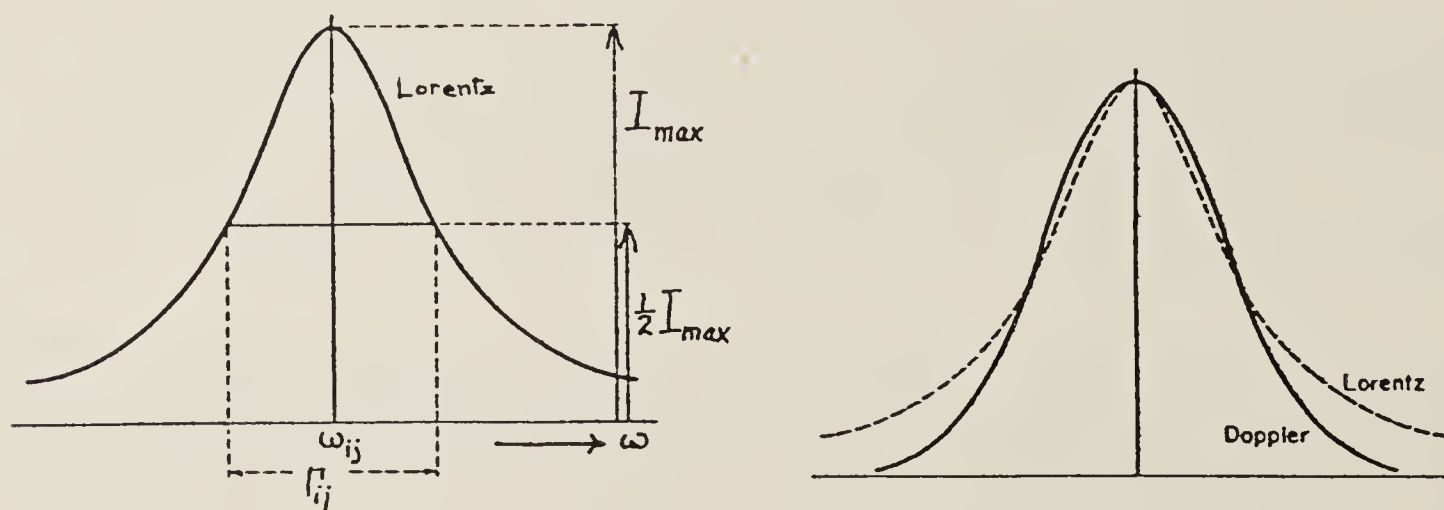
with  $\Delta^2 = 2kT\omega_o^2/Mc^2$ .

The distribution of intensity in the spectral line  $\omega_0$  will follow the Gaussian function of  $(\omega_0 - \omega)$  if the width parameter  $\Delta \gg$  (homogeneous broadening parameters). But a distribution which folds the two distributions can be written and used for all values of the parameters:

$$I(\omega) = \text{const} \int_{-\infty}^{\infty} \frac{\exp-(\omega_0 - \omega')^2 / \Delta^2}{(\omega - \omega')^2 + (\gamma/2)^2} d\omega', \quad (81)$$

where  $\gamma = \Gamma_{ij} + 1/T_c$  (equation (75)) or  $2w$  (equation (78)). The right-hand side of equation (81) is known as the Voigt profile for spectral lines. It is a function of  $\omega$ , symmetrical about  $\omega_0$ , and reflects the Lorentzian or Gaussian constituent functions to a greater or lesser degree according to the relative magnitudes of  $\gamma$  and  $\Delta$ .

The figure on the right, below, contrasts the Lorentz line-shape with the Doppler (Gaussian) shape. On the left is a Lorentz profile illustrating the parameters of equation (72).



This discussion by no means exhausts the possibilities for describing spectral line shapes, but it covers many situations. It will be clear that an analysis of spectral line profiles furnishes important information about the environment of radiating atoms.

### References

- Corney, A., 1977, "Atomic and Laser Spectroscopy", University Press, Oxford.
- Dicke, R. H. and Wittke, J. P., 1960, "Introduction to Quantum Mechanics", Addison-Wesley, Reading, Mass.
- Slater, J. C., 1960, "Quantum Theory of Atomic Structure", McGraw Hill, New York, London. (2 vols.)
- Woodgate, G. K., 1970, "Elementary Atomic Structure", McGraw Hill, London, New York.



# The Ubiquity of Alpha: The Fundamental Atomic Constants\*

G W SERIES

Raman Visiting Professor, Indian Academy of Sciences, Bangalore 560 080

**Abstract.** The fine structure constant, alpha, turns up again and again in connection with the determination of the fundamental atomic constants. But its evaluation from spectroscopic measurements is inextricably bound up with questions concerning the validity of the theory of quantum electrodynamics. Evaluations from independent knowledge of other atomic constants turn on measuring, with high precision, a great variety of quantities which are combinations of constants, and which invariably require reference back to the maintained units of the SI system—significantly not the same thing as the defined units. Time and again new physics has come from the recognition of small discrepancies.

Josephson's discovery of the quantized voltage drop across two superconductors brought the physics of condensed matter into the arena of the atomic constants, while von Klitzing's recent discovery of the quantized Hall resistance in semiconductors has illuminated the picture with a new view of alpha.

## 1. Atomic hydrogen and the fine structure constant

I was first introduced to Bohr's theory of the hydrogen atom by a fellow-undergraduate, in my first year at the University—though nowadays, I believe, Bohr's theory is, as often as not, taught in high schools. My imagination was caught by this first insight into the long-standing problem of the connection between the structure of atoms and the spectra of the light they emit, and into this bold and controversial solution of that other problem: the stability of atoms.

Do you recall the expression for the speed of an electron  $v_1$  round the proton in the orbit  $n = 1$  of Bohr's theory? It is simply  $e^2/\hbar$ , or, to be more careful with units,  $(e^2/\hbar)(\mu_0 c^2/4\pi)$  in the *Système Internationale*. ( $e$  is the fundamental charge,  $\hbar$  is Planck's constant divided by  $2\pi$  (the Dirac constant),  $\mu_0$  is the permeability of vacuum defined as  $4\pi \cdot 10^{-7}$  henries per metre, and  $c$  is the speed of light in free space). It is more interesting to make the expression for  $v_1$  dimensionless by quoting it in relation to the speed of light:

$$v_1/c = (e^2/\hbar c)(\mu_0 c^2/4\pi). \quad (1)$$

There we have it, this remarkable dimensionless quantity which is the subject of our discourse, universally given the symbol  $\alpha$ , and whose numerical value is close to  $1/137$ .

It became possible to make an experimental determination of  $\alpha$  a few years later, with the development by Sommerfeld of a relativistic version of Bohr's theory.

---

\*A lecture first given at the Raman Research Institute, Bangalore, on 3 February 1983.

## *G W Series*

The relativistic energy of the stationary state labelled by the quantum numbers (integers)  $n$  and  $k$  was calculated to be

$$E_{n,k} = -\frac{R}{n^2} \left[ 1 + \frac{\alpha^2}{n} \left( \frac{1}{k} - \frac{3}{4n} \right) + \dots \right]. \quad (2)$$

The first term inside the bracket, 1, (when multiplied by  $-R/n^2$ ), is the expression for the energy derived by Bohr. For a given value of  $n$ , the principal quantum number, the second term gives us a set ( $k = 1, 2, 3, \dots, (n-1)$ ) of small corrections to the energy, the consequences of the relativistic variation of mass with velocity of the electron as it moves round the nucleus in one or other of the quantized orbits of different ellipticity (different  $k$ ). Because  $\alpha$  is small, this second term is very small, of order  $10^{-5}$ . Now, since the frequencies of the lines in the spectrum are given by the theory as

$$\nu = (E_{n,k} - E_{n',k'})/h, \quad (3)$$

a study of the spectrum allows, in principle, an experimental determination of  $\alpha$ . But  $\alpha$  enters only in the 'fine structure' of the spectral lines. The gross structure—predicted by Bohr's theory—is interpreted simply by specifying sets of two different values,  $n, n'$ , of the principal quantum number:

$$\nu = (E_n - E_{n'})/h. \quad (3a)$$

Thus, the famous Balmer series, for example, has  $n = 2, n' = 3, 4, 5, \dots$ . But with the relativistic theory, each single frequency represented by equation (3a) becomes a set of frequencies represented by (3), that is to say, each line of the gross structure is predicted to be possessed of a fine structure of closely-spaced components. If, therefore, these components could be resolved and each associated unambiguously with a set of values of the integers  $n, n', k, k'$ , then equations (2) and (3) would enable  $\alpha$  to be determined.

Alas, this was not possible at the time when Bohr and Sommerfeld published their respective theories, and it has only very recently become possible with the application of highly-stabilised, tunable lasers to the study of the hydrogen spectrum. The difficulty has always been that the Doppler broadening of spectral lines—especially serious in the case of hydrogen—has prevented adequate resolution of the fine structure. But the spectrum of ionised helium, which is similar to that of hydrogen and to which the Bohr/Sommerfeld theory may also be applied, is less subject to Doppler broadening, and an experimental value for  $\alpha$  was indeed obtained from measurements of fine structure in the spectrum of  $\text{He}^+$ , by Paschen, in 1916.

A better value was obtained from measurements of x-ray spectra. The x-ray spectra of all the elements, it will be recalled, are hydrogen-like because they arise from the *absence* of one electron from otherwise complete shells, whereas the spectrum of hydrogen is attributable to the *presence* of one electron. Just as the hydrogen spectrum has fine structure, so also have x-ray spectra. The *K*-series of x-ray lines



## *The ubiquity of alpha*

are doublets, and the frequency interval within each doublet can be predicted by use of equation (3) with a simple modification of equation (2) to take account of the shells of electrons surrounding the 'hole'. This approach gave a more reliable experimental value of  $\alpha$  even in the early days, and, with refinements, it survived into the nineteen-fifties.

### **2. $\alpha$ : the coupling constant of the electromagnetic field**

We have seen  $\alpha$ , then, as having entered physics with Bohr, but as having established itself as an important and universal atomic constant with Sommerfeld. Their theories, though milestones in the history of physics, are obsolete today. We shall return to the successor theories—Dirac's theory and quantum electrodynamics, in both of which  $\alpha$  finds an important place—but we should notice that this remarkable quantity is no longer thought of simply as a feature of relativistic atomic theory, but plays a rôle of greater importance in the overall structure of modern physical theory. It is a measure of the strength of the coupling between charged particles and the fields which they generate, and with which they interact. Consider the potential energy between two particles, distance  $r$  apart, each bearing the fundamental charge:

$$V(r) = (e^2/r) \mu_0 (c^2/4\pi) = K^2/r. \quad (4)$$

The dimensionless form of the coupling constant,  $K^2$ , is obtained by dividing it by the universal constants  $\hbar$  and  $c$  to yield

$$K^2/\hbar c = (e^2/\hbar c) (\mu_0 c^2/4\pi) \equiv \alpha. \quad (5)$$

We should notice how this important electromagnetic quantity is built up from attributes of matter ( $e$ ) and of radiation ( $c$ ) in the context of quantum theory ( $\hbar$ ).

In a similar way coupling constants are defined for the other interactions known to physics, and, since these are all dimensionless, it is sensible to compare them one with another, so that one may say, for example, 'the hadronic interaction is much stronger than the electromagnetic interaction'.

### **3. Numerical values of atomic constants**

It is time now to turn our attention to the numerical values of the quantities we have been thinking about:  $e$ ,  $\hbar$ ,  $c$ ,  $\alpha$ . A set of reliable, experimental determinations of these quantities would provide a check of the theories which provide a relationship between them. If we are interested in  $\alpha$  we are led inevitably into that area of physics which deals with the determination of a consistent set of values of the fundamental atomic constants.

Millikan's oil-drop experiment for the determination of  $e$ , Michelson's rotating mirror device for the measurement of  $c$ , Millikan's photoelectric determination of  $e/h$ —these belong to history. In contemporary science there is a very large body

of highly skilled experimental work and extremely sophisticated theory upon which the 'received' values of the constants depends. The ingredients of this work are:

- (i) a set of experiments in which physical quantities can be measured to very high accuracy—nowadays, a few parts in  $10^8$  is typical;
- (ii) very reliable theories, by which the quantities measured can be related to the fundamental constants; and
- (iii) a set of laboratory standards of physical quantities, against which the measurements are to be made.

The number of high-precision experiments which can be carried out is greater than the number of constants to be ascertained, and the sets of self-consistent values of constants which are published from time to time represent least-squares evaluations of all the available data, weighted according to estimates of accuracy and reliability. Not everything goes smoothly in these evaluations. Discrepancies and inconsistencies appear, and these signal defects in some theory or unsuspected errors in some experiment. These problems and their resolution—we shall see examples later on—make the study of fundamental constants a fascinating area of physics, made up of a great diversity of techniques and skills.

We shall shortly give examples of the type of experiment which contributes to these evaluations, but first there is a very important point to be made in relation to point (iii) above—laboratory standards.

#### **4. Maintained standards and measurements of high precision**

What one aims at in making a physical measurement is to relate it to the base units of the SI system. But the units *as maintained* are to be distinguished from the units *as defined*. The objective of standards laboratories is to provide for their clients instruments calibrated to represent the *defined* units. But in this task they apply the instrument to their own *maintained* version of the physical quantity in question—a standard mass, a standard frequency, a standard current, or whatever. And, as we shall see, there can be significant uncertainties in the relation between the maintained standards and the defined units. Indeed, the ratios (maintained unit/SI defined unit)—which may differ from 1 by as much as a few parts in  $10^6$  for electrical quantities—are among the unknowns, to be determined from the least squares evaluations of the best values of fundamental constants.

Before we move on to consider the accuracy of standards, let us pause to look at some physical quantities which, today, can be measured with very high precision.

#### **5. Defined units and maintained standards**

It is instructive to contemplate the very different accuracy capabilities of the standards of physical quantities maintained to establish the SI system, that is, the accu-



## *The ubiquity of alpha*

racy with which different realisations of the same unit agree with one another:

time:	a few parts in	$10^{13}$
length:	„	$10^9$
mass:	„	$10^7$
electric current:	„	$10^6$

Let us recall the definitions of the units of these quantities and reflect on how they are realised in practice.

(i) *Mass*: The prototype kilogram is a physical object kept in a cellar under a glass cover. It is a shaped mass of a platinum-iridium alloy, exposed to air. Is it stable? Does it absorb molecules from the air which surrounds it? Does it evaporate? How should we know if it did? Though the guardians of the prototype will be able to reassure us up to a point on questions such as these, at what point will their reassurance fail to carry conviction as we make ever-more exacting demands on the constancy and reproducibility of our standards? It is recognised by experts that there is a pressing need for a new definition of the unit of mass that shall not be so singular and open to mischance as that precious, vulnerable piece of metal in the Bureau des Poids et Mesures at Sèvres.

(ii) *Length*: When this lecture was delivered the unit of length adopted by international agreement, the defined unit, was based on the wavelength of a particular orange radiation from krypton atoms, and the realisation of this unit was prescribed in terms of the light issuing from a krypton gas discharge lamp of a conventional type. The unit as maintained in standards laboratories had the advantage over the unit of mass that krypton atoms (of the specified isotope) are the same everywhere and available in all countries. It served well for twenty years or so, but it has not proved adequate for the demands of metrology and spectroscopy in the era of stabilised lasers. The accuracy capability of a standard based on the wavelength of light is limited by the spectral purity of the chosen radiation, and stabilised lasers provide radiation of much greater spectral purity than do gas-discharge lamps. Measurements of the wavelength of light from such lasers were limited, not by the characteristics of the object being measured nor by the technique of measurement, but by the 'bluntness' of the standard of length itself. This state of affairs was intolerable for those concerned with precision measurement, and workers in standards laboratories, having made many determinations, as accurately as possible, of the wavelengths of the radiations from selected types of stabilised laser, agreed on values for these wavelengths, to be used as working standards for the time being. And, further, towards the end of the nineteen seventies it became possible to measure, for radiations from one and the same laser (in the near infra-red) both the *wavelength*, against the working standard of length, and the *frequency*, against the primary standard of frequency. The position then was that a value for the speed of light was obtained (wavelength multiplied by frequency) whose *accuracy* was limited by the shortcomings of the primary standard of length, but whose *precision* was much higher. Discussions over the next few years in those international committees of



experts who determine the basis of our metrology led to the adoption, in October 1983, of a new definition of the metre:

‘the metre is the length equal to the distance travelled in free space by light during a period of  $1/299\,792\,458$  seconds.’

The entirely new basis for this definition will be appreciated: it has the effect of abolishing an independent standard for length and of fixing exactly the value of the speed of light in free space. There will no longer be any sense in doing an experiment to measure the speed of light, but if the objective were to be stated as to make a determination of length, then exactly the same experiment might be devised as was to have been devised for the speed of light determination. Scales and rulers need not be abolished: they will continue to be used for the purposes for which they were made. Comparisons of lengths at the highest levels of precision will continue to be made by the interferometric techniques which have served metrology so well in the past. But the primary standard for length measurements will be the primary standard for time.

(iii) *Time*: The second is defined in terms of an atomic standard, as was the krypton-based metre, whence the term ‘quantum metrology’. The second is the duration of 9 192 631 770 periods of the radiation corresponding to the transition between the two hyperfine levels in the ground state of the caesium-133 atom. Caesium ‘clocks’ are to be found in all standards laboratories. Since the measurement of frequency has a higher accuracy capability than any other physical measurement, it is common practice to reduce the measurement of physical quantities, where possible, to a measurement of frequency. But the present limiting accuracy of a few parts in  $10^{13}$  is unlikely to endure for more than another decade or two. Developments in the laser spectroscopy of single ions are pointing the way towards the replacement of the caesium standard by one several orders of magnitude better in stability and reproducibility. But this lies in the future. For the time being we must continue to cherish the caesium clock.

(iv) *Electric current*: While the krypton-based metre and the caesium-based second were defined with an eye to their laboratory realisation, this can hardly be said of the ampere:

‘that constant current which, if maintained in two *straight, parallel* conductors, of *infinite length*, of *negligible circular cross-section*, and placed 1 metre apart in vacuum, would produce between these conductors a force equal to  $2 \cdot 10^{-7}$  Newton per metre of length.’

Infinitely long wires of negligible circular cross-section are encountered less frequently in laboratories than are krypton atoms or caesium atoms. How remote is this definition from a laboratory experiment! What elaborate integrations come between a current balance and the definition of the unit of current! Nevertheless, the current balance, in one form or another, is the traditional method of realising, in the laboratory, a current which can be directly related to the SI definition.

The current balance used for many years at the National Physical Laboratory (U.K.), illustrated in figure 1, generated, with 1 amp flowing through the coils, a force which was balanced by about 4 g weight. The mass of the coils themselves,



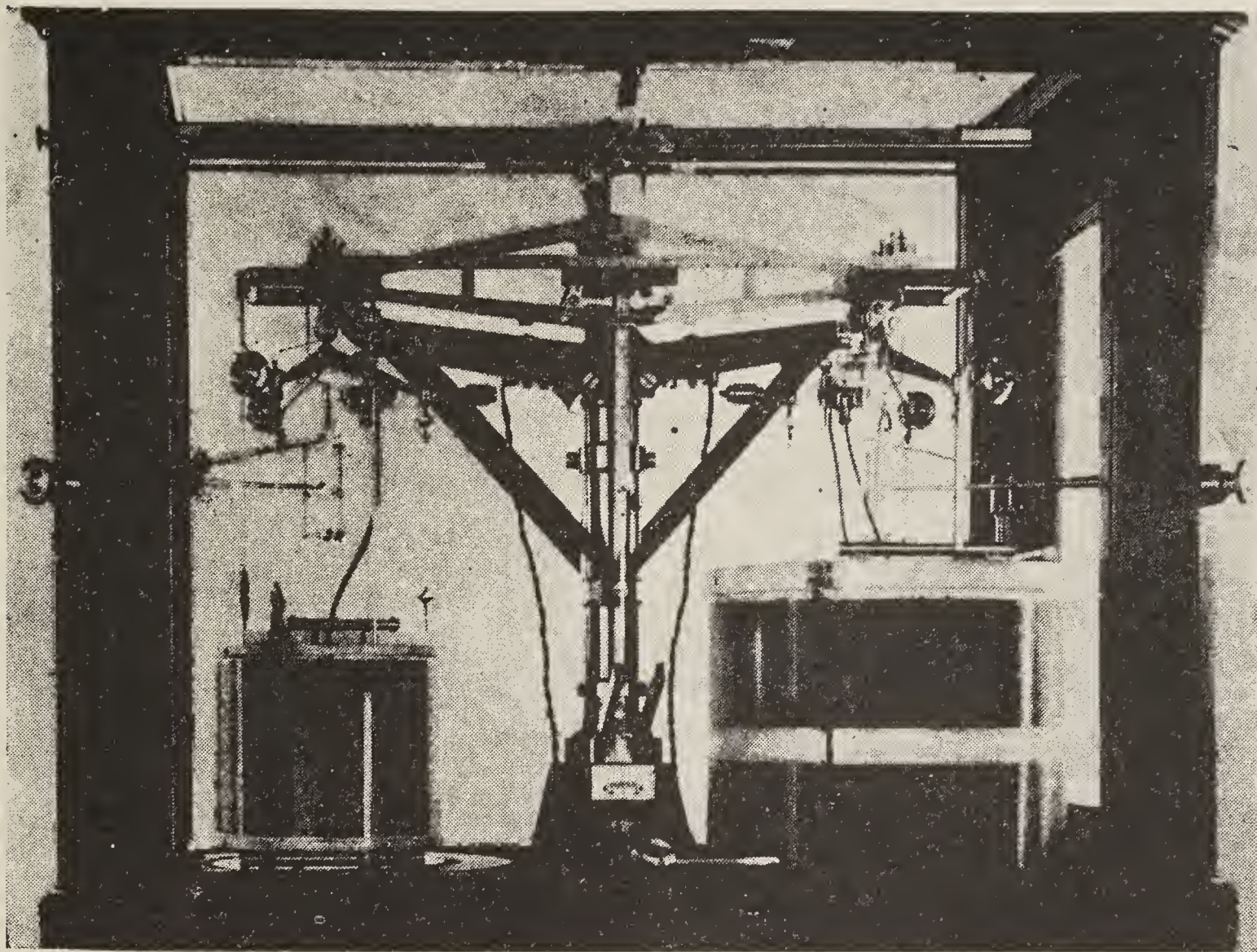


**Figure 1.** Current balance for the determination of the ampère, used at the National Physical Laboratory, Teddington (UK). On the left-hand side the outer coil has been removed to show the inner coil. Forces generated on the two sides of the balance act additively and are counterbalanced by weights.

on their formers, was about 10 kg. Consider then the problems of constructing and using the balance if one were aiming at an accuracy of 1 in  $10^6$  for the determination of current: one would require a sensitivity to  $10\mu\text{g}$ , that is, a relative mass sensitivity of 1 in  $10^9$ . And consider further the effects arising from ohmic heating of the coils during the passage of current—thermal expansion, convection currents, and so forth. Though the SI system embraces electricity by way of the definition of the ampère, it is not surprising that the maintained electrical standards are normally quantities other than electric current.

(v) *Capacitance and resistance:* In the late nineteen fifties a remarkable theorem in electrostatics was proved by Lampard (1957) in the Australian Standards Laboratory and developed into a standard capacitor by his colleague Thompson (1959). The cross-capacitance between a pair of parallel cylinders in proximity to another pair, parallel to the first pair, is  $(10^7/4\pi^2c^2) \ln 2$  farad per metre (this formula incorporates the defined quantity  $\mu_0 = 4\pi \cdot 10^{-7} \text{ h m}^{-1}$ ). For the theorem to hold the cylinders need not be of circular cross-section, but in its metrological application they are circular. The capacitance is rather small—about  $2 \text{ pF m}^{-1}$ , but the arrangement has served for two decades as a practical standard of capacitance and, by extension with use of a.c. bridge networks, of resistance. The values of the maintained standards of these electrical quantities are simply dependent, then, on the measurement



of a length—the displacement of an electrode which shields one cylinder from its partner (figure 2).

(vi) *Electric potential*: The maintained standard of voltage was, for many years, the Weston cadmium-mercury cell, but this suffered from the disadvantage of unpredictable drifts of the order of a few parts in  $10^6$  per year. The situation changed with the discovery in the early nineteen sixties of the a.c. Josephson effect. A highly reproducible voltage standard is obtained by irradiating a ‘weak’ junction between two superconducting wires by e-m waves of some suitable frequency  $\nu$ , usually in the GHz range. (A ‘weak’ junction means that a very thin, insulating film separates the two conductors). The current-voltage characteristic of such a junction is not linear, but shows discrete steps in the voltage whose separation  $V$  satisfies the equation

$$2eV = h\nu. \quad (6)$$

This simple relationship has been very thoroughly tested for different pairs of superconductors and for different types of junction and has been found to be reliable at a level of accuracy limited only by the accuracy of the voltage standards then available. By using equation (6) as the basis of a maintained standard of voltage—a further extension of quantum metrology—the problem of drifts was avoided. The agreed value of the constant relating voltage to frequency is

$$2e/h = 483\,594 \text{ GHz per volt.}$$

Notwithstanding the advantages secured by reducing the measurement of voltage to that of frequency, use of this number leaves open the possibility of a systematic difference between the maintained and defined units of voltage in the *Système International*.

With resistance referred to a calculable capacitance and voltage to a frequency,

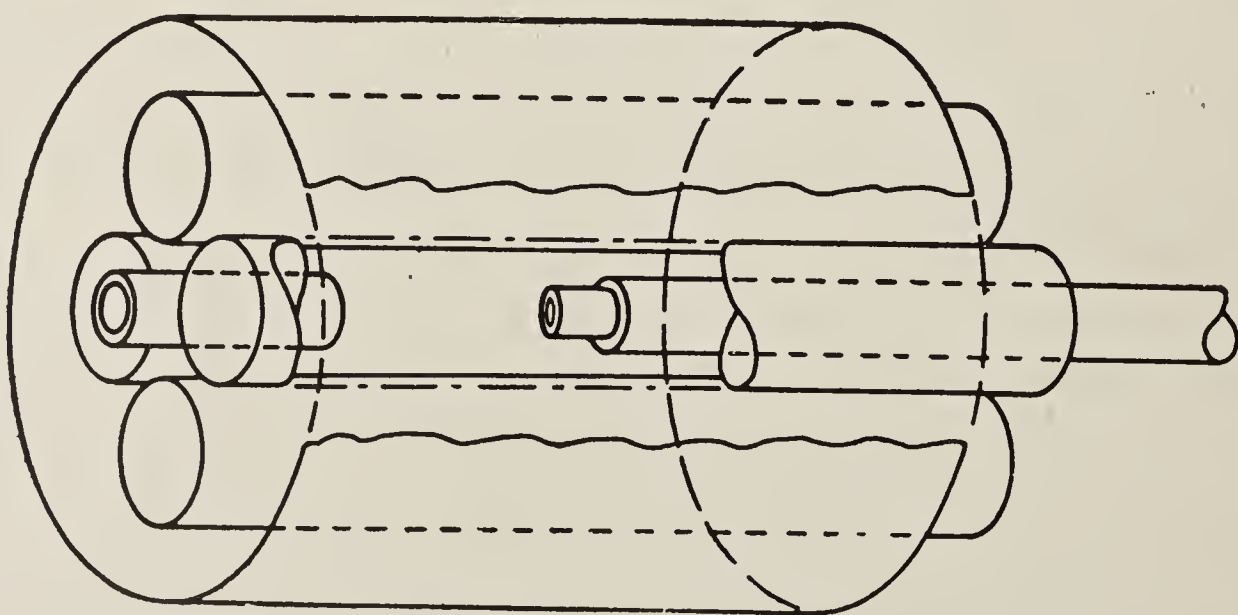


**Figure 2.** The Lampard capacitor.

A pair of the diametrically-opposed cylinders forms the plates of the capacitor. The other pair is earthed to the outer shield, as are the two portions of the central guard cylinder. Movement of the right-hand portion of the guard cylinder through a distance measured interferometrically brings about a calculable change of capacitance.



## *The ubiquity of alpha*

the use of the current balance is avoided. But the uncertainties which remain in determining the value of an electric current at the level of parts in  $10^6$  are well illustrated by the problem of  $\gamma_p'$  which, we shall see, will bring us back to the ubiquitous  $\alpha$ .

### 6. $\gamma_p$ and the ampère

$\gamma_p$  is the symbol used for the gyromagnetic ratio of protons, defined by the relation

$$\omega_p = \gamma_p B, \quad (7)$$

in which  $\omega_p$  is the precessional frequency of protons in a uniform magnetic field of induction  $B$ .  $\gamma_p$  enters our discussion because it brings the measurement of electric current into relationship with a measurement of frequency by one of the two paths linking current with magnetic field. And 'the problem of  $\gamma_p'$ ', which is related to 'the problem of the ampère', arises because the two paths give significantly different values for  $\gamma_p$ .

In these experiments it is not free protons that are used but protons bound in water molecules enclosed in a spherical container. That the protons are not free matters not at all: they act simply as objects whose response to magnetic fields is reproducible and accurately measurable. The symbol  $\gamma_p'$  is generally used for protons in a sphere of water, while  $\gamma_p$  is used for free protons. But since free protons are of no interest to us here we shall use  $\gamma_p$  for protons in the water sample. The two relationships between current and magnetic field are

- (i) the direct, in which a current is used to generate a magnetic field, as in a solenoid:

$$B = AI, \quad (8)$$

where  $A$  is a geometrical factor, and

- (ii) the inverse, in which a wire carrying a current in a magnetic field experiences a force:

$$B = A'/I, \quad (9)$$

where  $A'$  depends on the force as well as on the length of the wire.

Now, suppose we carry out a free precession experiment on our protons and determine  $\gamma_p$  from a measurement of the precessional frequency in a field  $B_l$  (the suffix  $l$  is to indicate 'low') related to the measured current  $I_m$  (maintained units) by equation (8). Let us admit that  $I_m$  may not be the true (SI defined) current  $I$ , but that

$$I_m = I/K. \quad (10)$$

It follows that the measured quantity  $(\gamma_p)_{m,l}$  will be related to the true  $\gamma_p$  by

$$(\gamma_p)_{m,l} = K\gamma_p. \quad (11)$$

In a second experiment we determine  $(\gamma_p)_{m,h}$  by measuring its precession frequency in a high field,  $B_h$ , whose value is determined by measuring the force on a wire carrying the current  $I_{m,h}$  (maintained units). Because of the inverse relationship between  $B_h$  and  $I_{m,h}$  in this experiment, we find

$$(\gamma_p)_{m,h} = \gamma_p / K. \quad (12)$$

'The problem of  $\gamma_p$ ' is that the quantities  $(\gamma_p)_{m,l}$  and  $(\gamma_p)_{m,h}$  have been found to be significantly different. Nevertheless, we may obtain the true value by taking the geometric mean of the high-field and low-field determinations:

$$\gamma_p = [(\gamma_p)_{m,h} (\gamma_p)_{m,l}]^{1/2}. \quad (13)$$

We also have

$$K = [(\gamma_p)_{m,l} / (\gamma_p)_{m,h}]^{1/2} \quad (14)$$

which turns out to be  $1 - (6.5 \pm 0.5) \cdot 10^{-6}$ , using the best experimental results available in 1980 (Cohen 1980). This figure is to be compared with the results of a set of determinations of  $K$  by the current balance method, reported from five different standards laboratories between 1958 and 1970,  $1 - (0.4 \pm 3.1) \cdot 10^{-6}$ . The discrepancy between these two sets of figures is 'the problem of the ampère'.

## 7. $\gamma_p$ , the Josephson effect, and $\alpha$

Having seen  $\gamma_p$  in its relationship with electrical standards we may indeed be surprised to find it playing a rôle in a set of measurements which yield the fine structure constant in a new and important way. We left  $\alpha$  in the hands of the spectroscopists, refining their measurements of hydrogenic fine structure and calling upon the successors of Sommerfeld's theory, namely, Dirac's theory and quantum electrodynamics to deliver up a value of  $\alpha$ . Some detail of this will appear below. Meanwhile, the point has to be taken that reliance on a theory of QED is an essential part of spectroscopic determinations if values at the level of parts in  $10^6$  are to be achieved. But QED itself, like all theories, is open to challenge, and spectroscopic determinations which call upon QED for their justification cannot then be invoked in support of its validity.

It was, therefore, of the greatest importance when it was realised that the Josephson determinations of  $2e/h$  could be combined with measurements of  $\gamma_p$  (and other reliably-measured constants) to furnish a value for  $\alpha$  *independent of the theory of QED*. The significant relationship is:

$$\alpha^{-1} = \left[ \frac{1}{4R_\infty} \cdot \frac{c}{(\Omega_{BI}/\Omega)} \cdot \frac{\mu_p}{\mu_B} \cdot \frac{(2e/h)_{BI}}{(\gamma_{p,l})_{BI}} \right]^{1/2}, \quad (15)$$

in which the least accurately known quantity is  $\gamma_{p,l}$ . The Rydberg constant,  $R_\infty = (m_e e^4 / 4\pi \hbar^3 c) (\mu_0 c^2 / 4\pi)^2$  has always been one of the most accurately known



## *The ubiquity of alpha*

physical constants (now at the level of parts in  $10^9$ ), and  $\mu_p/\mu_B$ —the ratio of proton magnetic moment to Bohr magneton ( $e\hbar/2m_e$ ) is known to better than 1 in  $10^7$ . A smaller uncertainty attached to  $c$ , even before it was given a fixed value. The suffix BI on three of the quantities means that the measurements were made against electrical standards maintained at the Bureau International des Poids et Mesures, and referred back to a particular year (1969). The factor  $\Omega_{\text{BI}}/\Omega$  is the ratio of the maintained ohm to the SI defined ohm, a quantity reliably known to about 2 parts in  $10^7$ . Finally, it is an important feature of this equation that the uncertainty in the value of the maintained ampère cancels out in the last fraction, where the Josephson coefficient is divided by  $\gamma_{p,l}$ —the low-field measurement. So we arrive at the simplified version of equation (15):

$$\alpha^{-1} = C(\gamma_{p,l})^{-1/2}, \quad (15a)$$

where  $C$  is a constant which does not depend on quantum electrodynamics and whose value is known to a degree of accuracy such that the uncertainty deduced for  $\alpha$  is dominated by the error bars in the experimental determination of  $\gamma_{p,l}$ .

Thus, for the first time, was macroscopic physics brought into determinations of  $\alpha$ , and a value derived from equation (15) that could be compared with spectroscopic determinations relying in one way or another on QED. It is time for us now to return to these determinations, to be reminded of the diversity of avenues to  $\alpha$  which hydrogen and other simple systems provide.

### 8. Return to hydrogen and $\alpha$ , with QED

The contemporary situation is shown in figure 3.

On the left of the figure the energy levels of Bohr's theory will be recognised:  $E = -R/n^2$ ; we show the levels for  $n = 1, 2$  and  $3$ . The structure on the right shows the principal features predicted by Dirac's relativistic wave equation, supplemented by QED. And for  $n = 1$  the hyperfine structure is shown also: this is not negligible for the other levels, and it is taken into account in high precision work, but it is not shown in the figure.

The fine structure intervals have been very fully explored by radio-frequency spectroscopy, and it is clear that a value for  $\alpha$  can be obtained by equating the experimentally-determined intervals (generally the  $P_{3/2}$ — $P_{1/2}$  interval in  $n = 2$ ) to a theoretical expression involving  $R$  as well as  $\alpha$ , and subject to uncertainties (represented by the question marks) as to the validity of the theory (if that is under scrutiny) and as to numerical coefficients in the theoretical expressions. Only the leading terms are shown in the figure—the actual expressions are power series in  $\alpha$  obtained from perturbation expansions in which the coefficients become increasingly difficult to calculate as higher terms are taken.

The gross intervals are scaled by the Rydberg constant, which is determined from laser spectroscopic measurements of wavelengths of, for example, the first member of Balmer's series,  $n = 3 \rightarrow 2$ . When corrected for Dirac and QED displacements of the levels the experimental values give the Bohr intervals ( $5R/36$  for  $n = 3 \rightarrow 2$ ),

### G W Series

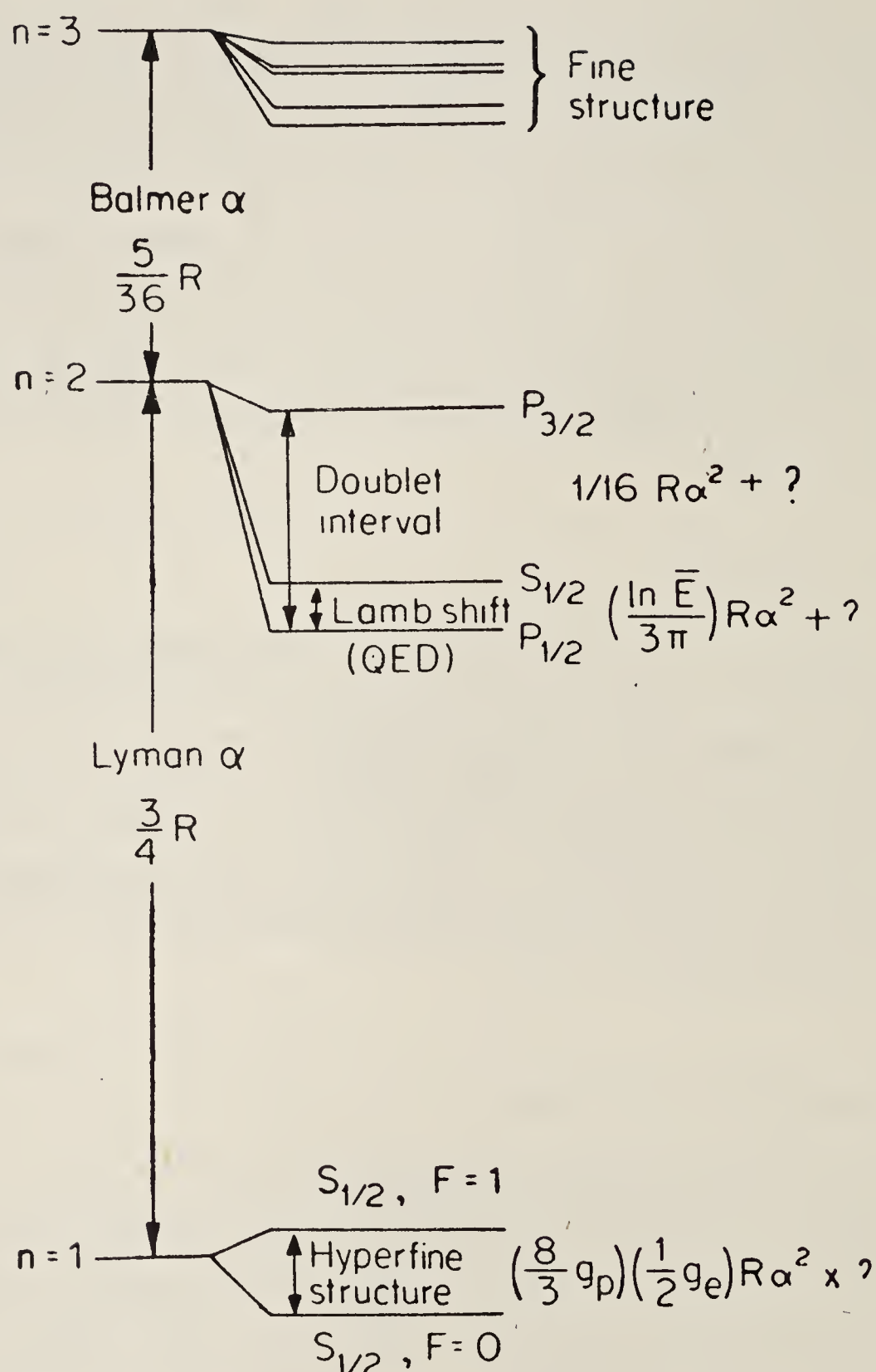


Figure 3. Energy levels of hydrogen (not to scale).

On the left are the energy levels given by Bohr's theory. 'Balmer  $\alpha$ ' and 'Lyman  $\alpha$ ' indicate the transitions for the first members of the well-known series of lines in the spectrum of atomic hydrogen. On the right are shown the fine-structure levels for  $n = 2$  and 3 and the hyperfine levels for  $n = 1$ . The symbols  $P_{1/2}, S_{1/2} \dots$  are standard spectroscopic notation representing the quantum numbers which label the energy levels. Relativistic quantum theory (Dirac theory) supplemented by QED (Lamb shift) leads to expressions for the intervals involving  $R$  and  $\alpha$  as shown.  $\bar{E}$  is an average energy appearing in the formula for the Lamb shift.  $g_p$  and  $g_e$ , the Landé  $g$ -factors of proton and electron, are measurable quantities appearing in the hyperfine formula. The question marks represent uncertainties of the QED evaluations, and also, in the hyperfine formula, uncertainties concerning the structure of the proton.

and hence the value of the Rydberg constant. But it is to be realised that this will be the value for the particular isotope under investigation, and that a 'reduced mass' correction needs to be applied before  $R_\infty$  is obtained.

The evaluations of  $R$  and  $\alpha$  from gross structure and fine structure measurements are thus, in a sense, interwoven. But the determination of  $R$  involves the fine struc-



ture only as a correction, and the very high accuracy with which  $R$  is known is not degraded by uncertainties in the fine structure. This accurate value of  $R$ , taken into the fine structure formulae, allows the determination of  $\alpha$  with uncertainties arising from the experimental error bars and from the theory, not from the Rydberg constant.

The hyperfine structure in the ground state is another matter. Its experimental value—the frequency of oscillation of the hydrogen maser—is probably the most accurately-determined interval known to spectroscopy. Its theoretical value involves not only standard hyperfine structure theory (the Fermi formula) with QED corrections, but also some assumptions concerning the structure of the proton. But with plausible assumptions as to this structure, and with knowledge of  $R$  and of the Landé  $g$ -factor of the proton, a high-precision value of  $\alpha$  can be extracted.

For a long period in the nineteen fifties and early nineteen-sixties the values of  $\alpha$  determined from the fine and hyperfine structures differed by substantially more than the sum of the estimated uncertainties in both. It was a period of anxiety and of much soul-searching, and in the opinion of many atomic physicists the mystery at the heart of the proton was the strongest candidate for the resolution of the discrepancy. But they were wrong. In 1962 came ‘the Josephson  $\alpha$ ’, whose value sided with the hyperfine  $\alpha$  and recoiled from the fine-structure  $\alpha$ . With the spotlights on the latter there were found, on the experimental side, a small systematic error whose elimination pushed the value of  $\alpha$  a little way towards the other determinations, and a mistake (wrong sign) in the evaluation of a particular term contributing to one of the numerical coefficients in the formula. When this was corrected the three determinations—Josephson, fine, and hyperfine—were substantially in agreement. The history of the fundamental constants is too long, and the discovered errors too numerous for practitioners in the field to rest content with agreement at any level of accuracy. Comparisons continue to be made, and in the assessment of precision measurements with a view to obtaining a consistent set of values for the atomic constants, the ‘with QED’ and ‘without QED’ evaluations are still critically compared—the latter depending heavily on measurements of  $\gamma_p$ .

Hydrogen is not the only simple system to provide values for  $\alpha$ . Deuterium, of course, provides independent fine-structure values, but the hyperfine structure of deuterium has not played such an important role as has that of hydrogen because of the more complicated nature of the nucleus. The hyperfine structures of positronium and of muonium, on the other hand, have been very closely studied. It is argued that the positively-charged member of these systems is simpler than the proton, which is true, but the experimental difficulties are greater. Fine-structure intervals in helium, a two-electron system, have also contributed values for  $\alpha$  with the aid of very highly-developed theoretical studies. But the most accurate measurements and the most highly-developed calculations have been carried out for free electrons. The Landé  $g$ -factor of free electrons (and of positrons) is not exactly 2 (as the Dirac theory predicts) but is greater according to the expression given in table 1. Very highly-developed experimental techniques (van Dyck *et al* 1979; Newman *et al* 1980) determine  $g-2$  rather than  $g$  itself, and accuracies of a few parts in  $10^8$  are claimed for this quantity. Calculations to this level of accuracy, based on the theory, require the evaluation and summation of a very large number of terms, and



**Table 1.** Physical quantities which can be determined with precision, typically, of a few parts in  $10^8$ .

$c$	The speed of light in vacuum. (But see section 5).
$R_\infty$	$= (m_e e^4 / 2 \hbar^2) (\mu_0 c^2 / 4 \pi)^2$ . The Rydberg constant for an infinitely heavy nucleus. Determinations of $R_\infty$ are usually made in units of reciprocal length. In this case the expression is to be divided by $\hbar c$ . Laser spectroscopic experiments have given $R_\infty$ to an accuracy of 1 in $10^9$ .
$1 + m_e/m_p$	Electron/nuclear mass ratios obtained from mass spectrometry. $m_e$ — electron mass $m_p$ — proton mass $m_d$ — deuteron mass $m_\alpha$ — $\alpha$ -particle mass
$1 + m_e/m_d$	
$1 + m_e/m_\alpha$	
$\mu_p/\mu_B$	
$\mu_p/\mu_N$	The ratio, proton magnetic moment, $\mu_p$ , to Bohr magneton, $\mu_B = e\hbar/2m_e c$ . The ratio, proton magnetic moment to nuclear magneton, $\mu_N = e\hbar/2m_p c$ . This ratio, and the foregoing, are determined as the ratio of two frequencies by magnetic resonance experiments. In the case of $\mu_p/\mu_N$ the experiment is not at present capable of accuracy at the level of parts in $10^8$ . It will be noticed that, by combining these two ratios, a determination of $m_e/m_p$ may be obtained.
$g_{e-}$ $g_{e+}$ $g_\mu$	The Lande $g$ -factors of the free electron, the free positron and the free muon. The theory of quantum electrodynamics gives an expression for these $g$ -factors as a power series in $\alpha$ : $2[1 + \alpha/2\pi + C_4 (\alpha/\pi)^2 + C_6 (\alpha/\pi)^3 + C_8 (\alpha/\pi)^4 + \dots]$ . $C_4$ and $C_6$ have been calculated reliably, $C_8$ with less certainty. (The values of these constants are not the same for the muon as for the electron).
$2e/\hbar$	A ratio characteristic of the a.c. Josephson effect described in § 5 (vi).

comparisons of experiment with theory in this area are regarded as tests of the theory rather than as determinations of  $\alpha$ .

## 9. The quantized Hall resistance

This last chapter in our story brings a contribution from an entirely unexpected source: semiconductor physics. In recent years particular attention has been given to the flow of electrons in a two-dimensional sheet, as, for example, within the inversion layer between the silicon and silicon dioxide in a metal-oxide-semiconductor (MOS) field effect transistor. This is essentially a two-dimensional flow because layers of this kind are so thin that movement of electrons out of the layer is energetically impossible, the quantized energy eigenvalues for motion in that direction being too widely separated.

The Hall effect on such a junction is investigated (at low temperatures) by applying a uniform magnetic field normal to the layer, as in figure 4: measurements are made of the voltage appearing transversely, as well as parallel, to the flow of current in the layer.

It was found by von Klitzing, Dorda and Pepper (1980) that, for certain regions of magnetic field, the longitudinal resistance  $R_{||}$  drops to zero (figure 5), and that, in these regions the transverse resistance  $R_{\perp} = V_y/I_x$  presents a plateau. The values of  $R_{\perp}$  at these plateaux were soon demonstrated to have the simple form  $h/e^2 i$ , where  $i$  was an integer taking values 1, 2, 3... for the successive values of  $R_{\perp}$ . Measurements carried out in different laboratories verified that the phenomenon did not depend on the particular sample nor on a particular geometrical configuration, and that the values of  $h/e^2$  obtained in these experiments—simply a comparison between  $R_{\perp}$



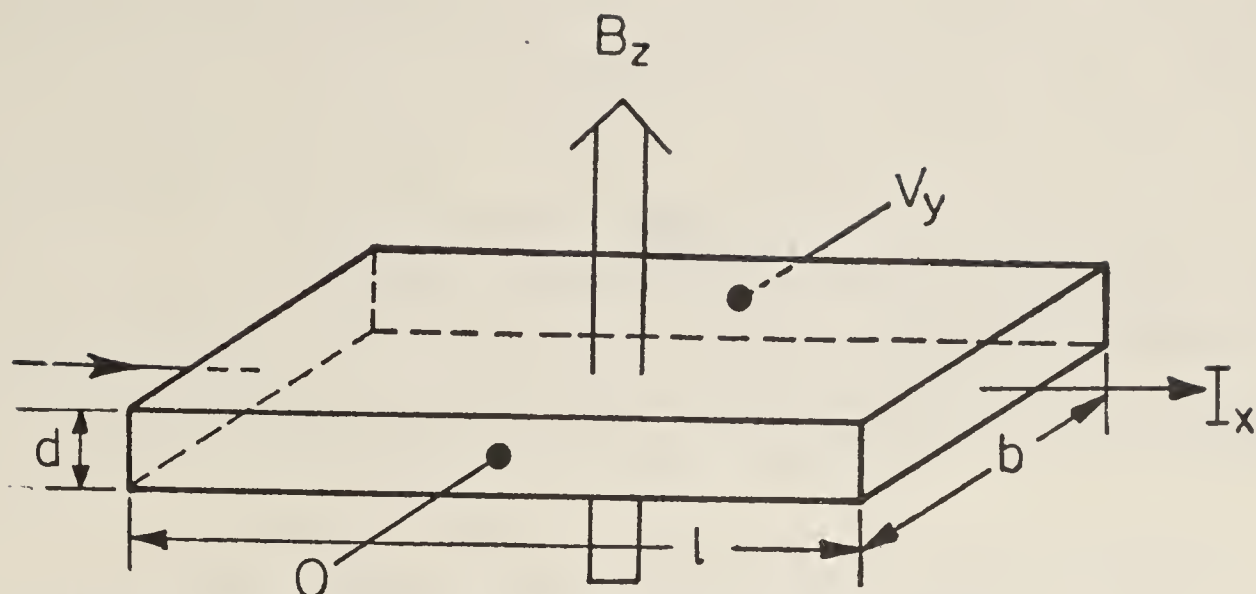


Figure 4. Notation for the representation of the Hall effect.

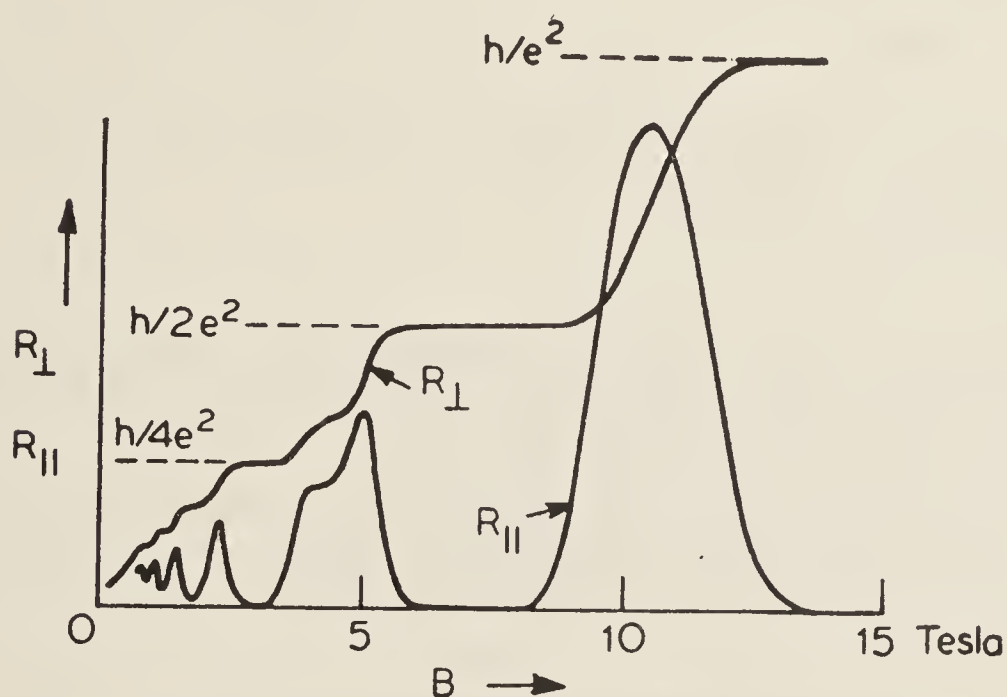


Figure 5. Variation of the transverse ( $R_{\perp}$ ) and parallel ( $R_{\parallel}$ ) resistances with magnetic field, for a sample of a gallium-arsenide-aluminium heterostructure at low temperature (after von Klitzing 1982). Notice the plateaux in  $R_{\perp}$  at those values of  $B$  where  $R_{\parallel}$  drops to zero. The plateaux are not evenly spaced in  $B$  because the spin magnetic moment of the electrons as well as the orbital motion interacts with the field.

and a 'maintained' standard resistor calibrated against a Lampard capacitor—agreed with the best values obtained by the methods we have already described. But  $h/e^2$  is essentially the fine structure constant, for the  $c$  and  $\mu_0$  which enter into its definition are fixed numbers. (Although  $c$  was not fixed in 1980, its value was known so much more accurately than the other quantities that the uncertainty in  $c$  was quite irrelevant). So surprising were these results that it was not at first recognised that semiconductor physics might have some contribution to make to the study of the fundamental atomic constants.

The theory of the effect has proved difficult and is still incomplete. And further experimental studies have revealed plateaux of  $R_{\perp}$  at non-integral (but still, simple fractional) values of  $i$ , as, for example,  $1/3$ . This semiconductor work has not yet, therefore, been taken into the realm of physical constants with the same confidence as has the Josephson effect. But the promise is undoubted, and not only in relation

to the value of  $\alpha$ . For the reproducibility and universality of the effect establish its claim to find a place in standards laboratories in providing a working standard of resistance, a new recruit in the field of quantum metrology, in place of standards derived from the Lampard capacitor. It would be, indeed, a more attractive standard, in that the value of  $h/e^2$ , about 26,000 ohm, is closer to everyday electrical quantities than is the picofarad magnitude of the Lampard capacitor.

Notwithstanding the deep-lying difficulties of the theory I shall risk the charge of superficiality by presenting a simple version, referring to figure 4. Let us proceed first to calculate  $R_{\perp}$  as in the familiar calculation of the Hall coefficient.

$I_x = (nev_x) bd$  where  $n$  is the number of carriers per unit *volume* and  $v_x$  is the drift velocity in the direction of the applied voltage.

$$V_y = (Bev_x)/(e/b) = Bbv_x.$$

$$R_{\perp} = V_y/I_x = B/ned. \quad (16)$$

Now, since we are to consider two-dimensional flow, let us introduce  $n_A = nd$ , the number of carriers per unit *area*. Then

$$R_{\perp} = B/n_A e. \quad (17)$$

This result is general. We need a condition which defines a plateau. We shall suppose that the plateaux occur at those values of magnetic field for which the area is exactly filled with  $i = 1, 2, 3 \dots$  layers of electrons.

We need, then, to calculate the area occupied by an electron as it undergoes cyclotron motion in the  $x$ - $y$  plane. Let us write an equation to represent the quantization of this motion:

$$ma^2\omega_c = \hbar, \text{ (quantization of angular momentum),} \quad (18)$$

where  $\omega_c$  is the cyclotron frequency,  $eB/m$ , in the field  $B$ , and  $a$  the radius of the orbit. From these equations we might deduce that  $\pi a^2 = \hbar/2eB$  is the area in the  $x$ - $y$  plane occupied by an electron in a quantized orbit. Actually, this picture gives too classical a representation of the electron. A more formal argument based on the uncertainty relations for motion in a plane leads to the expression

$$2\pi a^2 = \hbar/eB \quad (19)$$

for the area per electron.

The same result is obtained from a more quantum-statistical definition of the condition for a plateau: that the occurrence of plateaux coincides with the filling of the states available to electrons in  $i = 1, 2, 3 \dots$  quantized Landau levels. In this energy-level picture the distribution of electrons over energy is supposed to condense into a function which peaks at the Landau energies  $(n + 1/2)\hbar\omega_c$ , each peak having a degeneracy factor per unit area of  $eB/\hbar$ , the inverse of equation (19).

Either interpretation leads to the density

$$n_A = i(eB/\hbar), \quad (20)$$



## *The ubiquity of alpha*

when the area is saturated, in the one interpretation, or when the states are filled, in the other. Combining (20) with (17) we have

$$R_1 = h/e^2 i, \quad (21)$$

the 'quantized Hall resistance'.

Among the many interesting features of this expression is the fact that it does not depend on the mass of the charged particle: thus, the effect of the lattice, represented by the use of effective mass rather than free mass, cancels out.

We conclude by quoting a value for  $\alpha^{-1}$  given in a recent account of a determination based on the quantized Hall effect (Tsui *et al* 1982):

$$\alpha^{-1} = 137.035\,968 \text{ (23),}$$

which may be compared with a recent determination based on  $\gamma_p$  (Williams and Olsen 1979):

$$\alpha^{-1} = 137.035\,963 \text{ (15)}$$

and with a recent 'with QED' result (Cohen 1980):

$$\alpha^{-1} = 137.035\,973 \text{ (??).}$$

Many years ago Eddington, in speculations on the nature of the physical universe, having appreciated that a dimensionless constant of the electromagnetic field must have some very important rôle to fulfil in fundamental theory, supposed that the value of  $\alpha^{-1}$  might be an integer. We can say now, with complete confidence, that whatever the rôle of  $\alpha$  may be (and, indeed, it finds an important place with other coupling constants in the grand unified theory) Eddington's supposition is untenable. But that the value of  $\alpha$  is small is of the utmost importance to us and to physical theory, for if it were not so it would not be possible to entertain a theory of electrically-charged matter without taking fully into account, from the outset, the coupling of matter to radiation, and this we know we need not do.

And so our thought leads us back to Bohr's theory, and to the realisation that here, in semi-conductor physics, we have a laboratory determination of the speed of the electron in Bohr's first orbit. For did we not write

	$v_1 = e^2/\hbar (\mu_0 c^2/4\pi),$	equation (1)
and	$R_1 = h/e^2 i,$	equation (21)?
So, then	$v_1 = (1/R_1) \cdot (i\mu_0 c^2/2).$	

And since  $\mu_0$  and  $c$  are fixed numbers, a measurement of  $R_1$  leads us directly back into the heart of Bohr's atom.

Bohr orbits and Landau orbits, 70 years apart; hidden in each we find this remarkable number, this ubiquitous alpha. Truly, there are more things in  $h$  and  $e$ , Horatio, than are dreamt of in your philosophy!

## Acknowledgements

I am deeply grateful to the Indian Academy of Sciences, through whose generosity this lecture came to be devised and delivered: also to the officers of the Academy.

in particular to Dr. S. Varadarajan and Professor S. Ramaseshan, for their consideration and thoughtfulness during my tenure of the Raman Visiting Professorship of the Academy in 1982/3, and to Professor V. Radhakrishnan, Director of the Raman Research Institute in Bangalore and my host during that period, whose kindness and support were never-failing.

Figures 1 and 2 are reproduced by permission of the National Physical Laboratory, through the kind offices of Dr. B. Petley.

## References

- Cohen, E. R., *Atomic masses and fundamental constants* (eds.) Jerry A. Nolen Jr. and Walter Benenson, pp. 525-40. Plenum Press, N.Y. and London (1980).
- Lampard, D. G., *Proc. IEEE* **C104**, 271, (1957).
- Newman, D. E., Sweetman, E., Conti, R. S. and Rich, A., *Atomic masses and fundamental constants* (eds.) Jerry A. Nolen Jr. and Walter Benenson, pp. 183-7. Plenum Press. N.Y. and London (1980).
- Thompson, A. M., *Proc. IEEE* **B106**, 307, (1959).
- Tsui, D. C., Gossard, A. C., Field, B. F., Cage, M. E. and Dziuba, R. F., *Phys. Rev. Lett.* **48**, 3, (1982).
- van Dyck, R. S., Schwinberg, P. B. and Dehmelt, H. G., *Phys. Rev. Lett.* **38**, 310, (1977).
- von Klitzing, K. *Europhysics News*, **13**, 2, (1982).
- von Klitzing, K., Dorda, G. and Pepper, M., *Phys. Rev. Lett.* **45**, 494, (1980).
- Williams, E. R. and Olsen, P. T., *Phys. Rev. Lett.* **42**, 1575, (1979).











